

TUMOR MICRO-ENVIRONMENT AND DRUG RESISTANCE

EDITED BY: Wei Zhao, Zhe-Sheng Chen, Liwu Fu and Yong Song
PUBLISHED IN: Frontiers in Cell and Developmental Biology and
Frontiers in Oncology



frontiers

Frontiers eBook Copyright Statement

The copyright in the text of individual articles in this eBook is the property of their respective authors or their respective institutions or funders. The copyright in graphics and images within each article may be subject to copyright of other parties. In both cases this is subject to a license granted to Frontiers.

The compilation of articles constituting this eBook is the property of Frontiers.

Each article within this eBook, and the eBook itself, are published under the most recent version of the Creative Commons CC-BY licence.

The version current at the date of publication of this eBook is CC-BY 4.0. If the CC-BY licence is updated, the licence granted by Frontiers is automatically updated to the new version.

When exercising any right under the CC-BY licence, Frontiers must be attributed as the original publisher of the article or eBook, as applicable.

Authors have the responsibility of ensuring that any graphics or other materials which are the property of others may be included in the CC-BY licence, but this should be checked before relying on the CC-BY licence to reproduce those materials. Any copyright notices relating to those materials must be complied with.

Copyright and source acknowledgement notices may not be removed and must be displayed in any copy, derivative work or partial copy which includes the elements in question.

All copyright, and all rights therein, are protected by national and international copyright laws. The above represents a summary only. For further information please read Frontiers' Conditions for Website Use and Copyright Statement, and the applicable CC-BY licence.

ISSN 1664-8714

ISBN 978-2-88974-184-7

DOI 10.3389/978-2-88974-184-7

About Frontiers

Frontiers is more than just an open-access publisher of scholarly articles: it is a pioneering approach to the world of academia, radically improving the way scholarly research is managed. The grand vision of Frontiers is a world where all people have an equal opportunity to seek, share and generate knowledge. Frontiers provides immediate and permanent online open access to all its publications, but this alone is not enough to realize our grand goals.

Frontiers Journal Series

The Frontiers Journal Series is a multi-tier and interdisciplinary set of open-access, online journals, promising a paradigm shift from the current review, selection and dissemination processes in academic publishing. All Frontiers journals are driven by researchers for researchers; therefore, they constitute a service to the scholarly community. At the same time, the Frontiers Journal Series operates on a revolutionary invention, the tiered publishing system, initially addressing specific communities of scholars, and gradually climbing up to broader public understanding, thus serving the interests of the lay society, too.

Dedication to Quality

Each Frontiers article is a landmark of the highest quality, thanks to genuinely collaborative interactions between authors and review editors, who include some of the world's best academicians. Research must be certified by peers before entering a stream of knowledge that may eventually reach the public - and shape society; therefore, Frontiers only applies the most rigorous and unbiased reviews.

Frontiers revolutionizes research publishing by freely delivering the most outstanding research, evaluated with no bias from both the academic and social point of view. By applying the most advanced information technologies, Frontiers is catapulting scholarly publishing into a new generation.

What are Frontiers Research Topics?

Frontiers Research Topics are very popular trademarks of the Frontiers Journals Series: they are collections of at least ten articles, all centered on a particular subject. With their unique mix of varied contributions from Original Research to Review Articles, Frontiers Research Topics unify the most influential researchers, the latest key findings and historical advances in a hot research area! Find out more on how to host your own Frontiers Research Topic or contribute to one as an author by contacting the Frontiers Editorial Office: frontiersin.org/about/contact

TUMOR MICRO-ENVIRONMENT AND DRUG RESISTANCE

Topic Editors:

Wei Zhao, City University of Hong Kong, Hong Kong, SAR China

Zhe-Sheng Chen, St. John's University, United States

Liwu Fu, Sun Yat-Sen University, China

Yong Song, Nanjing University, China

Citation: Zhao, W., Chen, Z.-S., Fu, L., Song, Y., eds. (2022). Tumor Micro-Environment and Drug Resistance. Lausanne: Frontiers Media SA.
doi: 10.3389/978-2-88974-184-7

Table of Contents

- 06** *CKS1B as Drug Resistance-Inducing Gene—A Potential Target to Improve Cancer Therapy*
Wenwen Shi, Qiudi Huang, Jiacui Xie, He Wang, Xiyong Yu and Yi Zhou
- 13** *VWCE Functions as a Tumor Suppressor in Breast Cancer Cells*
Dan Zhang, Lili Wan, Fan Yang, Wenlan Liu, Litao Liu, Shengnan He and Ni Xie
- 27** *The Role of Autophagy in Gastric Cancer Chemoresistance: Friend or Foe?*
Jing-Li Xu, Li Yuan, Yan-Cheng Tang, Zhi-Yuan Xu, Han-Dong Xu, Xiang-Dong Cheng and Jiang-Jiang Qin
- 44** *Lactic Acidosis Interferes With Toxicity of Perifosine to Colorectal Cancer Spheroids: Multimodal Imaging Analysis*
Barbora Pavlatovská, Markéta Macháľková, Petra Brisudová, Adam Pruška, Karel Štěpka, Jan Michálek, Tereza Nečasová, Petr Beneš, Jan Šmarda, Jan Preisler, Michal Kozubek and Jarmila Navrátilová
- 62** *Dihydroartemisinin Sensitizes Esophageal Squamous Cell Carcinoma to Cisplatin by Inhibiting Sonic Hedgehog Signaling*
Wei Cui, Tingting Fang, Zhaocheng Duan, Dongfang Xiang, Yanxia Wang, Mengsi Zhang, Fangzheng Zhai, Xiang Cui and Lang Yang
- 76** *EGCG Enhanced the Anti-tumor Effect of Doxorubicine in Bladder Cancer via NF- κ B/MDM2/p53 Pathway*
Ke-Wang Luo, Xiao-hong Zhu, Ting Zhao, Jin Zhong, Han-chao Gao, Xin-Le Luo and Wei-Ren Huang
- 87** *Tumor-Associated Macrophages in Pancreatic Ductal Adenocarcinoma: Origin, Polarization, Function, and Reprogramming*
Sen Yang, Qiaofei Liu and Quan Liao
- 111** *Mechanism and Molecular Network of RBM8A-Mediated Regulation of Oxaliplatin Resistance in Hepatocellular Carcinoma*
Rong Liang, Jinyan Zhang, Zhihui Liu, Ziyu Liu, Qian Li, Xiaoling Luo, Yongqiang Li, Jiazhou Ye and Yan Lin
- 123** *Estrogen Receptor α Mediates Doxorubicin Sensitivity in Breast Cancer Cells by Regulating E-Cadherin*
Xiaoqing Wan, Jiaxin Hou, Shurong Liu, Yanli Zhang, Wenqing Li, Yanru Zhang and Yi Ding
- 133** *Cell-Free DNA: Hope and Potential Application in Cancer*
Yan-yan Yan, Qiao-ru Guo, Feng-hua Wang, Rameshwar Adhikari, Zhuang-yan Zhu, Hai-yan Zhang, Wen-min Zhou, Hua Yu, Jing-quan Li and Jian-ye Zhang
- 146** *Adaptive Mechanisms of Tumor Therapy Resistance Driven by Tumor Microenvironment*
Peijie Wu, Wei Gao, Miao Su, Edouard C. Nice, Wenhui Zhang, Jie Lin and Na Xie
- 169** *Identification of an Immune-Related Risk Signature Correlates With Immunophenotype and Predicts Anti-PD-L1 Efficacy of Urothelial Cancer*
Pengju Li, Shihui Hao, Yongkang Ye, Jinhuan Wei, Yiming Tang, Lei Tan, Zhuangyao Liao, Mingxiao Zhang, Jiaying Li, Chengpeng Gui, Jiefei Xiao, Yong Huang, Xu Chen, Jiazheng Cao, Junhang Luo and Wei Chen

- 180** *Advances in Drug Resistance of Esophageal Cancer: From the Perspective of Tumor Microenvironment*
Siyuan Luan, Xiaoxi Zeng, Chao Zhang, Jiajun Qiu, Yushang Yang, Chengyi Mao, Xin Xiao, Jianfeng Zhou, Yonggang Zhang and Yong Yuan
- 190** *CARD-Associated Risk Score Features the Immune Landscape and Predicts the Responsiveness to Anti-PD-1 Therapy in IDH Wild-Type Gliomas*
Depei Li, Wanming Hu, Xiaoping Lin, Ji Zhang, Zhenqiang He, Sheng Zhong, Xia Wen, Peiyu Zhang, Xiaobing Jiang, Hao Duan, Chengcheng Guo, Jian Wang, Jing Zeng, Zhongping Chen, Yonggao Mou and Ke Sai
- 205** *Cabozantinib Reverses Topotecan Resistance in Human Non-Small Cell Lung Cancer NCI-H460/TPT10 Cell Line and Tumor Xenograft Model*
Zi-Ning Lei, Qiu-Xu Teng, Pranav Gupta, Wei Zhang, Silpa Narayanan, Dong-Hua Yang, John N. D. Wurpel, Ying-Fang Fan and Zhe-Sheng Chen
- 216** *Extracellular Matrix Proteins Confer Cell Adhesion-Mediated Drug Resistance Through Integrin α_v in Glioblastoma Cells*
Qi Yu, Weikun Xiao, Songping Sun, Alireza Sohrabi, Jesse Liang and Stephanie K. Seidlits
- 233** *Girdin Knockdown Increases Gemcitabine Chemosensitivity to Pancreatic Cancer by Modulating Autophagy*
Sheng Wang, Wei Feng, Wulin Wang, Xiaoman Ye, Hao Chen and Chunzhao Yu
- 246** *Targeting c-Jun in A549 Cancer Cells Exhibits Antiangiogenic Activity In Vitro and In Vivo Through Exosome/miRNA-494-3p/PTEN Signal Pathway*
Chen Shao, Yingying Huang, Bingjie Fu, Shunli Pan, Xiaoxia Zhao, Ning Zhang, Wei Wang, Zhe Zhang, Yuling Qiu, Ran Wang, Meihua Jin and Dexin Kong
- 260** *Lansoprazole Alone or in Combination With Gefitinib Shows Antitumor Activity Against Non-small Cell Lung Cancer A549 Cells in vitro and in vivo*
Xiaoxia Zhao, Ning Zhang, Yingying Huang, Xiaojing Dou, Xiaolin Peng, Wei Wang, Zhe Zhang, Ran Wang, Yuling Qiu, Meihua Jin and Dexin Kong
- 274** *The Role of Tumor-Stroma Interactions in Drug Resistance Within Tumor Microenvironment*
Yanghong Ni, Xiaoting Zhou, Jia Yang, Houhui Shi, Hongyi Li, Xia Zhao and Xuelei Ma
- 303** *Salubrinal Exposes Anticancer Properties in Inflammatory Breast Cancer Cells by Manipulating the Endoplasmic Reticulum Stress Pathway*
Andrew Alsterda, Kumari Asha, Olivia Powrozek, Miroslava Repak, Sudeshna Goswami, Alexandra M. Dunn, Heidi C. Memmel and Neelam Sharma-Walia
- 318** *Markers and Reporters to Reveal the Hierarchy in Heterogeneous Cancer Stem Cells*
Amrutha Mohan, Reshma Raj Rajan, Gayathri Mohan, Padmaja Kollenchery Puthenveetil and Tessy Thomas Maliekal

- 337 Tumor Immune Microenvironment Components and Checkpoint Molecules in Anaplastic Variant of Diffuse Large B-Cell Lymphoma**
Tianqi Xu, Jia Chai, Kaijing Wang, Qingge Jia, Yixiong Liu, Yingmei Wang, Junpeng Xu, Kangjie Yu, Danhui Zhao, Jing Ma, Linni Fan, Qingguo Yan, Shuangping Guo, Gang Chen, Qiongrong Chen, Hualiang Xiao, Fang Liu, Chubo Qi, Rong Liang, Mingyang Li and Zhe Wang
- 348 Hypoxia-Related Gene FUT11 Promotes Pancreatic Cancer Progression by Maintaining the Stability of PDK1**
Wenpeng Cao, Zhirui Zeng, Runsang Pan, Hao Wu, Xiangyan Zhang, Hui Chen, Yingjie Nie, Zijiang Yu and Shan Lei
- 363 Linking Tumor Microenvironment to Plasticity of Cancer Stem Cells: Mechanisms and Application in Cancer Therapy**
Xiaobo Zheng, Chune Yu and Mingqing Xu
- 371 The Tumor Microenvironment Factors That Promote Resistance to Immune Checkpoint Blockade Therapy**
Bonnie L. Russell, Selisha A. Sooklal, Sibusiso T. Malindisa, Lembelani Jonathan Daka and Monde Ntwasa
- 388 Transcriptomic Analysis Identified ARHGAP Family as a Novel Biomarker Associated With Tumor-Promoting Immune Infiltration and Nanomechanical Characteristics in Bladder Cancer**
Chen Yang, Siqi Wu, Zezhong Mou, Quan Zhou, Zheyu Zhang, Yiling Chen, Yuxi Ou, Xinan Chen, Xiyu Dai, Chenyang Xu, Na Liu and Haowen Jiang
- 408 PAK1 Mediates Bone Marrow Stromal Cell-Induced Drug Resistance in Acute Myeloid Leukemia via ERK1/2 Signaling Pathway**
Banban Li, Ruinan Jia, Wei Li, Ying Zhou, Dongmei Guo, Qingliang Teng, Shenghong Du, Mingying Li, Wěi Li, Tao Sun, Daoxin Ma, Min Ji and Chunyan Ji
- 423 LINC00261 Suppresses Cisplatin Resistance of Esophageal Squamous Cell Carcinoma Through miR-545-3p/MT1M Axis**
Lijun Wang, Xiaojun Wang, Pengwei Yan, Yatian Liu and Xuesong Jiang
- 434 Inhibition of miR-185-3p Confers Erlotinib Resistance Through Upregulation of PFKL/MET in Lung Cancers**
Ke Li, Xinling Zhu and Conghu Yuan
- 444 Identification of a Novel Immune Landscape Signature for Predicting Prognosis and Response of Endometrial Carcinoma to Immunotherapy and Chemotherapy**
Jinhui Liu, Yichun Wang, Jie Mei, Sipei Nie and Yan Zhang
- 463 Surface PEGylated Cancer Cell Membrane-Coated Nanoparticles for Codelivery of Curcumin and Doxorubicin for the Treatment of Multidrug Resistant Esophageal Carcinoma**
Yi Gao, Yue Zhu, Xiaopeng Xu, Fangjun Wang, Weidong Shen, Xia Leng, Jiyi Zhao, Bingtuan Liu, Yangyun Wang and Pengfei Liu
- 476 Long Non-coding RNA MAFG-AS1 Promotes Cell Proliferation, Migration, and EMT by miR-3196/STRN4 in Drug-Resistant Cells of Liver Cancer**
Tianming Chen, Bin Huang and Yaozhen Pan



CKS1B as Drug Resistance-Inducing Gene—A Potential Target to Improve Cancer Therapy

Wenwen Shi¹, Qiudi Huang¹, Jiabei Xie¹, He Wang², Xiyong Yu¹ and Yi Zhou^{1*}

¹ Key Laboratory of Molecular Target and Clinical Pharmacology, The State Key Laboratory of Respiratory Disease, School of Pharmaceutical Sciences and The Fifth Affiliated Hospital, Guangzhou Medical University, Guangzhou, China, ² Center of Cancer Research, The Second Affiliated Hospital, Guangzhou Medical University, Guangzhou, China

Cancer is a threat to human health and life. Although previously centered on chemical drug treatments, cancer treatment has entered an era of precision targeted therapy. Targeted therapy entails precise guidance, allowing the selective killing of cancer cells and thereby reducing damage to healthy tissues. Therefore, the need to explore potential targets for tumor treatment is vital. Cyclin-dependent kinase regulatory subunit 1B (CKS1B), a member of the conserved cyclin kinase subunit 1 (CKS1) protein family, plays an essential role in cell cycling. A large number of studies have shown that CKS1B is associated with the pathogenesis of many human cancers and closely related to drug resistance. Here, we describe the current understanding of the cellular functions of CKS1B and its underlying mechanisms, summarize a recent study of CKS1B as a target for cancer treatment and discuss the potential of CKS1B as a therapeutic target.

Keywords: drug resistance, therapeutic target, cell cycling, human cancers, CKS1B

OPEN ACCESS

Edited by:

Zhe-Sheng Chen,
St. John's University, United States

Reviewed by:

Xuejun Li,
Peking University, China
Yanfang Chen,
Wright State University, United States

*Correspondence:

Yi Zhou
zhouyi0264@gzhmu.edu.cn

Specialty section:

This article was submitted to
Molecular and Cellular Oncology,
a section of the journal
Frontiers in Oncology

Received: 12 July 2020

Accepted: 28 August 2020

Published: 25 September 2020

Citation:

Shi W, Huang Q, Xie J, Wang H, Yu X
and Zhou Y (2020) CKS1B as Drug
Resistance-Inducing Gene—A
Potential Target to Improve Cancer
Therapy. *Front. Oncol.* 10:582451.
doi: 10.3389/fonc.2020.582451

INTRODUCTION

In recent years, the incidence of cancer has increased annually. According to national cancer statistics released by the National Cancer Center in 2019, in 2015, 3.929 million new malignant tumors were diagnosed in individuals 0–47 years of age in China, corresponding to an incidence of 285.83/100,000. The cumulative incidence of cancer is 21.44%, with lung cancer ranking first in incidence and mortality. Lung cancer is the most common malignant tumor in the world (11.6%) and the leading cause of cancer-related death (18.4%) (1). According to the latest report from the International Agency for Research on Cancer (IARC), there are ~9.63 million lung cancer patients worldwide. In 2018, there were an estimated 2,093,876 new cases of lung cancer and ~1,761,007 deaths due to lung cancer worldwide. Eighty percent of new lung cancer patients have been diagnosed with non-small-cell lung cancer (NSCLC) (2), which exhibits no clinically significant outcomes or symptoms at an early stage. By the time a patient is diagnosed with NSCLC, the optimal treatment period has typically already passed. Seventy-five percent of NSCLC cases are diagnosed as advanced NSCLC, which is associated with a 5-years survival rate of <15% (3, 4). During tumor development, tumor cell growth is uncontrolled, changing the genome, damaging healthy cells due to invasion of the tumor into nearby tissues and transferring tumor cells to distant tissues. In such cases, only non-surgical treatment options are available to patients. Although targeted drug therapy and immunotherapy have good curative effects, chemotherapy remains the preferred treatment for cancer patients in the clinical. However, due to the development of chemotherapy resistance in cancers, the vast majority of patients have a poor prognosis.

CYCLIN-DEPENDENT KINASE REGULATORY SUBUNIT 1 (CKS1B)

Malignant tumors are caused by dysregulation of the cell cycle and impaired cell differentiation. Regulation of the cell cycle depends on interactions among cyclins, cyclin-dependent kinase (CDK) and its inhibitors. CKS1B, the protein encoded by the CKS1 gene on human chromosome 1q21, has a molecular weight of 9 kDa and is highly functionally conserved (5). In early coimmunoprecipitation studies, scholars found that CKS1 tightly bound CDK from yeast, human cells, and frog eggs. Therefore, this protein was named cell cycle-dependent protease regulatory subunit (6). CDKs are a family of proteases related to the cell cycle that can degrade CDK substrates and proteins regulated by upstream CDKs. The Cdc kinase subunit (CKS) protein has been isolated and shown to inhibit fission and germination yeast cyclin-dependent kinase 1 (CDK1) gene mutations (7, 8). Two homologs of the yeast CKS gene, CKS1 and CKS2 (9), have been found in mammalian cells. Biochemical and genetic analyses suggest that CKS may play a key role in cell cycle regulation (10).

UPREGULATION OF CKS1B IN HUMAN CANCERS

Various genetic and biochemical experiments in different species have demonstrated the primary functions of CKS1 in normal cell division and growth. The deletion of CKS1 led to mitotic arrest, which eventually decreased cell viability. Due to mitotic retardation, the overexpression of CKS1 produced another abnormal phenotype (11, 12). Functional analysis of CKS1 has shown that (i) CKS1 is essential for maintaining cell viability and that (ii) significant changes in its expression significantly affect the cell division cycle (5). CKS1B, a member of the CKS/Suc1 small protein family, can bind and regulate the function of cyclin-dependent protein kinase catalytic subunits (13, 14). Studies have shown that CKS1B promotes cell growth, invasion, metastasis, and chemical resistance (15, 16). In addition, CKS1B is necessary for normal cell division and growth (5). High CKS1B expression has been shown in many cancers, such as hepatocellular carcinoma (15), colon cancer (17), lung cancer (18), oral squamous cell carcinoma (19), breast cancer (20), and retinoblastoma (RB) (14), among others. Studies have also identified CKS1B as one of 70 high-risk genes whose expression is inversely proportional to the survival of patients newly diagnosed with multiple myeloma (MM) (21). High nuclear expression of CKS1B is also a poor prognostic factor in patients with relapsed/refractory MM (22). These findings provide compelling evidence that CKS1B represents a powerful candidate therapeutic gene (23). Analyses using data from public databases have led to the same conclusion. A study using the public database GENT2 (<http://gent2.appex.kr/gent2/>) to analyze the expression levels of CKS1B in various cancer types revealed that CKS1B expression levels in brain, colon, bone, ovarian, pancreatic, liver, and lung cancer samples were significantly increased compared with those in healthy tissue samples (24). Kaplan-Meier estimates of event-free survival (left panel), metastasis-free survival (middle panel),

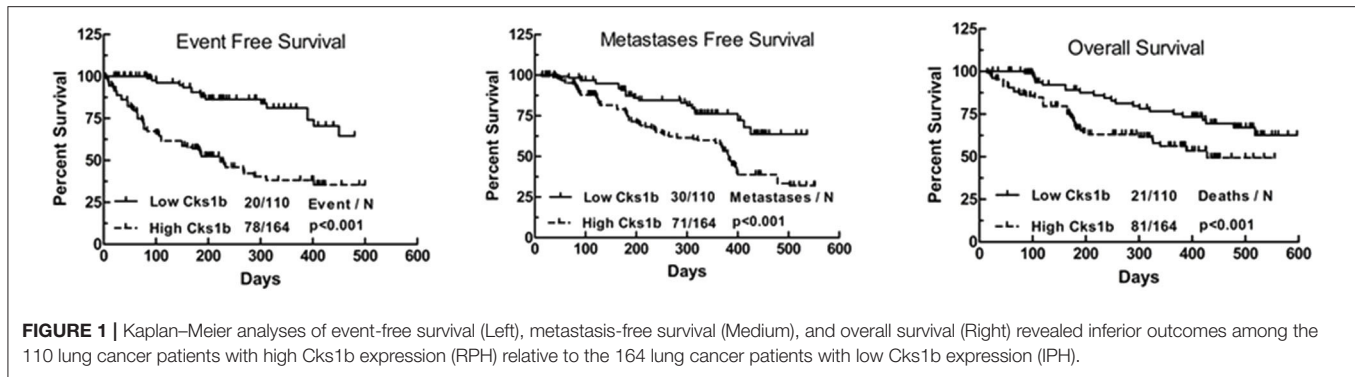
and overall survival (right panel) found that recurrent primary human (RPH) lung cancer patients with CKS1B overexpression showed decreased survival compared to that of incipient primary human (IPH) lung cancer patients (**Figure 1**) (25).

CKS1B PARTICIPATES IN REGULATION OF THE CELL CYCLE

The CKS1 protein, which is encoded by the human CKS1B gene, consists of 79 amino acids and is a member of the CKS/SUC1 protein family. CKS1 can regulate the mitotic cycle in eukaryotes (26). In mammalian cells, P27 and P21 control the cell cycle from G1 phase to S phase and are essential proteins for phase transformation. The P27kip1 protein, a member of the CIP/kip family, inhibits most CDKs and arrests the cell cycle in S phase (27). CKS1B is an indispensable regulatory unit of the SCFskp² ubiquitin ligase complex that can promote the binding of SCF to the cyclin inhibitor P27^{Kip1}, after which phosphorylated P27 and p21 are recognized by the SCF/skp2 complex and catalyze multiple surface connections. The recognition and degradation of a ubiquitinated chain by the 26S protease promotes transition of the cell cycle from G1 to S phase (28, 29). CKS1B has three protein-binding sites, including an S-phase kinase-associated protein 2 (SKP2)-binding site and a CDK-binding site, the latter of which plays an important role in the ubiquitination process regulated by CKS1B (**Figure 2**). As a ubiquitin-regulating protein, CKS1B can specifically bind the SCF/SKP2 complex, which contains SKP1, Cullin1, F-box proteins, and the ubiquitin ligase E3-SKP2 (30).

CKS1B IS A DRUG RESISTANCE-INDUCING GENE

Tumor resistance can be induced by many stimuli, among which gene mutation is of increasing concern. Studies showed that erlotinib, gefitinib, afatinib, and other epidermal growth factor receptor-tyrosine kinase inhibitors (EGFR-TKIs) could effectively improve the objective response rate and overall survival of NSCLC patients with EGFR mutations (including the deletion of exon 19 and the single point mutation L858R in exons 18-21). However, sustained EGFR-TKI treatment can lead to secondary resistance, and more 50% of secondary resistance is caused by the T790M secondary mutation in the catalytic pyrolysis region of the EGFR tyrosine kinase domain. In addition, HER2/neu (ErbB2), EGFR (ErbB1), HER3 (ErbB3), and HER4 (ErbB4) are members of the ErbB receptor-tyrosine kinase (RTK) family, and the oncogenic mutation patterns of EGFR and HER2 provide attractive options for targeted NSCLC therapy. Preclinical studies *in vitro* and *in vivo* models and human tissues have shown that overexpression of HER2 can lead to drug resistance to EGFR-TKIs and erlotinib resistance in mice and patients. Clinical studies have found that the current treatments for MM are ineffective in killing cells that specifically express CKS1B, leading to poor patient prognosis (23, 31). Studies have shown that overexpression of CKS1B promoted drug resistance in MM



cells (31). In addition, *in vitro* proliferation experiments showed that CKS1 overexpression significantly enhanced the proliferation of liver cancer cells (15). Wang et al. observed that CKS1B overexpression in lung cancer cells achieved through lentiviral infection enhanced drug resistance by inhibiting cisplatin (CDDP)- and doxorubicin (DOX)-induced apoptosis, supporting the critical role of CKS1B in lung cancer progression (25). Furthermore, CKS1B upregulation is a predictor of poor prognosis and aggressive disease in many other malignancies (32–34). CKS1B has been identified as a ubiquitin-like protein system resistance gene that can selectively induce resistance to ubiquitin-like protein synthesis inhibitors but no other antitumor drugs. Furthermore, research has shown that CKS1B induces resistance to ubiquitin-like protein synthesis inhibitors such as bortezomib by inhibiting expression of the SCF/SKP2 substrate p21.

CKS1B ACTIVATES STAT3 AND MEK/ERK THROUGH SKP2- AND P27KIP1-INDEPENDENT PATHWAYS

From cell surface receptors to transcription factors, members of the MEK/ERK signaling pathway, including the prosurvival proteins myeloid cell leukemia 1 and caspase-9, are involved in gene regulation (35) and protein activity regulation (36). Many diseases, such as cancer, human immunodeficiency virus infection (37), cardiac hypertrophy (38), and Parkinson's disease (39), result from aberrant regulation of the MEK/ERK signaling pathway. In particular, current research on the drugs used to treat cancer are focused on the ERK pathway (40). Moreover, a previous study demonstrated the potential of inactivating the MEK/ERK signaling pathway as a therapeutic target and an effective cancer treatment (41). Furthermore, the downregulation of CKS1B could inhibit the proliferation, migration, invasion, and angiogenesis of RB cells through inactivation of the MEK/ERK signaling pathway (14).

CKS1 is an important component of the SCF-Skp2 ubiquitin ligase complex, which degrades the CDK inhibitors p27Kip1, p21Cip1, and p130/Rb2. Interestingly, in addition to its influence on cell growth and survival through the regulation of p27Kip1, CKS1B leads to cell death in the presence of the

p27Kip1 locus and inhibits the growth of MM cells. This observation indicates that CKS1B promotes cell proliferation independent of p27Kip1- and SKP2-associated mechanisms (16). Shi et al. determined that CKS1B upregulation activated the STAT3 and MEK/ERK pathways, whereas SKP2 knockdown or p27Kip1 overexpression activated, rather than suppressed, the STAT3 and MEK/ERK pathways, suggesting that the effects of SKP2 overexpression and p27 Kip1 inhibition on STAT3 and MEK/ERK were opposite those of CKS1B overexpression (Figure 2). Furthermore, MM cell death and growth inhibition induced by CKS1B knockout were partially eliminated by activation of the STAT3 and MEK/ERK/BCL2 signaling pathways (31). In addition, CKS1B downregulation inhibited RB cell proliferation, invasion, migration, and angiogenesis by blocking the MEK/ERK signaling pathway.

CKS1B INDUCES DRUG RESISTANCE THROUGH TARGETING HEAT SHOCK PROTEIN 90 (HSP90)

Previous studies showed that Hsp90 overexpression was induced in MM cells by the activation of STAT3 and MAPK signaling, which was essential for tumor cell survival. Overexpression of Hsp90 has been observed in many cancer types, and it is speculated that abnormal Hsp90 signaling must be maintained for the survival of malignant cells (42). Some components of the growth and survival pathways associated with tumor cells are Hsp90 clients, so Hsp90 is believed to maintain the functional expression of oncoproteins while enabling transformed cells to tolerate unbalanced signaling. These characteristics make Hsp90 a potential target for the development of anticancer drugs (43, 44). Wang et al. first reported that CKS1B uses the Hsp90 and MEK1/2 pathways in lung cancer cells to develop chemical resistance (Figure 2) (25). CKS1B upregulates Hsp90 independently through SKP2 and p27. In contrast, the Hsp90 inhibitor PU-H71 could inhibit the substrate protein AKT in CKS1B-overexpressing (OE) H358 cells, indicating that CKS1B mainly activates Hsp90 to resist CDDP. Furthermore, a proteomic study demonstrated that Cks1 could bind Hsp90 and its cochaperone in Ramos lymphoma cells (45).

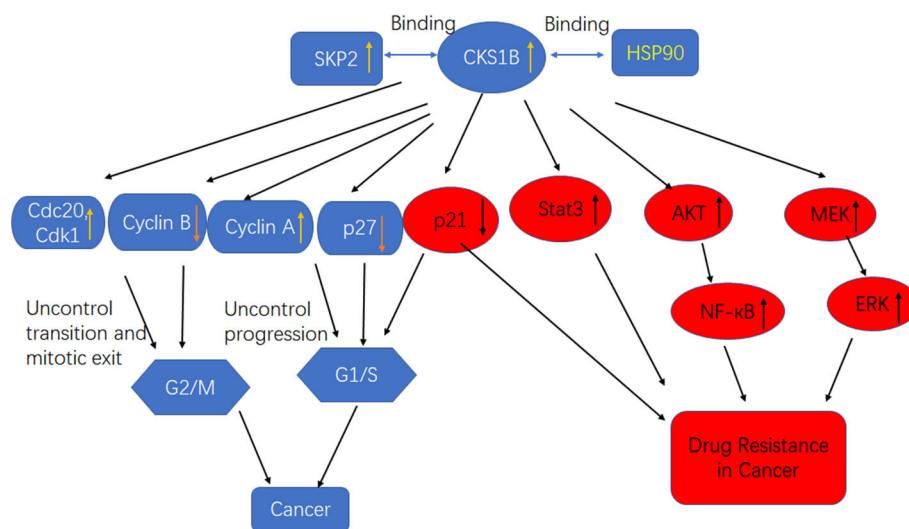


FIGURE 2 | High CKS1B promotes cancer progression or cancer drug resistance through multiple pathways.

STATUS OF RESEARCH ON CKS1B TARGETING IN CANCER

Use of Non-coding RNA to Target Cks1B for Cancer Treatment

Use of Mirnas to Target Cks1B for Cancer Treatment

MicroRNAs (miRNAs) are small non-coding RNA oligonucleotides ~21–23 nucleotides in length that can regulate genes at the posttranscriptional level with functions in various biological processes (46, 47). The dysregulation of miRNAs can lead to a variety of diseases, including developmental disorders, neurological diseases, and cancer. Abnormal miRNA and mRNA expression has been noted in many cancers (48–52). Therefore, a comprehensive analysis of miRNA and mRNA expression should be performed to enhance our understanding of miRNAs and mRNAs during tumorigenesis. Many databases and target prediction tools have recently been used to identify potential targets for miRNAs. However, the identification of miRNA targets is faced with enormous challenges.

Some studies have used bioinformatics methods to screen miRNAs that target CKS1B via TargetScan 7.2 and microRNA.org. In a bioinformatics analysis, several miRNAs targeting CKS1B (miR-125a, miR-1258, miR-197, miR-181a-1, miR-361, and miR-485) were predicted. Among mimics of these miRNAs, miR-1258 mimics inhibited the mRNA and protein expression of CKS1B in colorectal cancer (CRC) cells compared to cells treated with only negative control (NC) mimics. In addition, experiments have shown that miR-1258 exerts a tumor-suppressive effect through immediately downregulation of the oncogenic CKS1B gene in CRC (24). Other studies have shown that miR-204 negatively regulates the expression of CKS1B in gastric cancer (53). Yu Fujita found that miR-197 was downregulated in platinum-resistant NSCLC specimens, leading to *in vitro* and *in vivo* chemical resistance, tumorigenicity, and increased lung metastasis. Mechanistic studies have shown that

the miR-197-mediated CKS1B/STAT3 axis plays a role in tumor progression and is regulated by multiple oncogenes (Bcl-2, c-Myc, and cyclin D1) and that PD-L1 is a putative biomarker of this axis. In addition, we demonstrated that miR-197 mimics could cause highly resistant PD-L1 cells to become sensitive to chemotherapy. Ting La's study showed that miR-27b-3p targets CKS1B, resulting in a decrease in p27Kip1 mediation by Skp2. The coding region for miRNA-27b-3p is embedded in an intron spanning the open reading frames of three genes on chromosome 9 and is activated by p53 transcription. The results of Ting La's study showed that miRNA-27b-3p is an important regulator of cancer cell dormancy in response to p53 and suggest that the manipulation of miRNA-27b-3p may represent a new therapeutic approach to improve cancer treatment outcomes (54).

Use of Long Non-coding RNAs (Lncnas) Targeting CKS1B for Cancer Treatment

LncRNAs, which are present at lower cellular concentrations and exhibit higher tissue specificity than protein-encoding RNAs, participate in cell differentiation, proliferation, and apoptosis under different conditions. Furthermore, the differential expression of several lncRNAs shown in subjects with cancer suggests that lncRNAs can be used as biomarkers in the treatment of malignant tumors (55, 56). Metastasis-associated lung adenocarcinoma transcript 1 (MALAT1) is a novel lncRNA that was initially found to be overexpressed in patients with NSCLC at high risk for metastasis (57). The upregulation of MALAT1 is related to cancer cell proliferation and metastasis and the malignant development of esophageal squamous cell carcinoma (ESCC) (58, 59). MALAT1 has even been suggested as a predictor of poor prognosis in patients with midthoracic ESCC who have undergone radical resection (57, 60). In addition, experiments have revealed that CKS1 expression is positively regulated by MALAT1. This study not only elaborated on the function of the MALAT1/CKS1 pathway in regulating

radiosensitivity in ESCC but also suggests a new adjunct strategy to increase the efficacy of radiation therapy in the treatment of ESCC (61).

Use of Natural Medicines Targeting Cks1B for Tumor Treatment

Due to their low selectivity, radiotherapy and drug therapies currently used for clinical cancer treatment not only damage tumor cells but also kill healthy cells to varying degrees. Furthermore, they elicit many adverse reactions, and their long-term use leads to drug resistance. The development of drug resistance is one of the causes of chemotherapy failure. Therefore, much research has been devoted to identifying natural active antitumor ingredients from various organisms and natural compounds with antitumor activity. 3-O-(Z)-coumaric acid (3-COA), an oleanolic acid and active ingredient in the leaves of *Elaeagnus oldhamii* Maxim, was shown to mimic the antitumor activity of a specific inhibitor of Hsp90 (PU-H71) against A549 lung cancer cells. In H358 CKS1b-OE cells and relapsed lung cancer, PU-H71 has antitumor activity alone or in combination with CDDP or DOX, which it achieves by inhibiting Hsp90. This observation suggests that 3-COA is a novel inhibitor of Hsp90. 3-COA, as a new type of antitumor drug, exhibited excellent antitumor activity alone or in combination with CDDP against chemically resistant or non-resistant lung cancer through the Hsp90/MEK signaling pathway. Therefore, 3-COA might be a candidate compound for reversing drug resistance in the clinical treatment of lung cancer (25).

Nedd8 Inhibition Overcame Cks1B-Induced Drug Resistance in MM by Upregulating p21

MLN4924, a new and selective ubiquitin-like inhibitor with a structure similar to the energy-supply molecule ATP/AMP, is involved in the process of ubiquitin-like modification and selectively inhibits a ubiquitin-like activating enzyme (NEDD8-activating enzyme, NAE), thereby inhibiting the function of NEDD8 from a ubiquitin-like molecule-activating enzyme to a ubiquitin-like molecule-binding enzyme. Zhou et al. showed that CKS1B-OE cells were resistant to bortezomib but sensitive to

MLN4924. Furthermore, the treatment of CKS1B-OE cells with MLN4924 reduced cell proliferation and clone formation and induce senescence by upregulating p21 in MM (23).

CONCLUSION

As is a member of the Cks/Suc1 family of proteins, CKS1B plays an important role in the regulation of cell cycle progression. Increased CKS1B expression is involved in tumor initiation, maintenance, and progression and positively correlated with poor prognosis. Furthermore, CKS1B accelerates chemotherapeutic resistance in many types of cancers, while a decrease in CKS1B makes these tumor cells sensitive to chemotherapeutic drugs, suggesting that CKS1B is a promising treatment target in cancers. Recently, researchers found some drugs that reverse tumor resistance; these drugs include miRNA- and lncRNA-based drugs, natural medicines, and ubiquitin-like inhibitors but have not undergone clinical trial. The molecular mechanism by which CKS1B interacts with its binding targets remains unknown. Thus, more work to further understand the primary mechanisms underlying the function of CKS1B and its regulation is needed.

AUTHOR CONTRIBUTIONS

YZ, XY, JX, WS, QH, and HW contributed equally to the design, analysis, and interpretation of data. YZ and HW drafted the paper. All authors read and approved the final manuscript.

FUNDING

This study was supported by 2018 High-level university academic backbone and training program in Guangzhou Medical University (B185004199), 2018 Guangdong Key discipline construction project of pharmacy (Q185031010), 2019 Undergraduate laboratory open project (C195015003), 2018 Construction of scientific research teaching and academic improvement project in Guangzhou Medical University (B185004025), and 2017 University innovation and strengthening program (Q17024031).

REFERENCES

- Bray F, Ferlay J, Soerjomataram I, Siegel RL, Torre LA, Jemal A. Global cancer statistics 2018: GLOBOCAN estimates of incidence and mortality worldwide for 36 cancers in 185 countries. *CA Cancer J Clin.* (2018) 68:394–424. doi: 10.3322/caac.21492
- Torre LA, Bray F, Siegel RL, Ferlay J, Lortet-Tieulent J, Jemal A. Global cancer statistics, 2012. *CA Cancer J Clin.* (2015) 65:87–108. doi: 10.3322/caac.21262
- Lin A, Wei T, Meng H, Luo P, Zhang J. Role of the dynamic tumor microenvironment in controversies regarding immune checkpoint inhibitors for the treatment of non-small cell lung cancer (NSCLC) with EGFR mutations. *J Mol Cancer.* (2019) 18:139. doi: 10.1186/s12943-019-1062-7
- Taylor MD, LaPar DJ, Isbell JM, Kozower BD, Lau CL, Jones DR. Marginal pulmonary function should not preclude lobectomy in selected patients with non-small cell lung cancer. *J Thorac Cardiovasc Surg.* (2014) 147:738–44. doi: 10.1016/j.jtcvs.2013.09.064
- Krishnan A, Nair SA, Pillai MR. Loss of cks1 homeostasis deregulates cell division cycle. *J Cell Mol Med.* (2010) 14:154–64. doi: 10.1111/j.1582-4934.2009.00698.x
- Lan Y, Zhang Y, Wang J, Lin C, Ittmann MM, Wang F. Aberrant expression of Cks1 and Cks2 contributes to prostate tumorigenesis by promoting proliferation and inhibiting programmed cell death. *Int J Cancer.* (2008) 123:543–51. doi: 10.1002/ijc.23548
- Hadwiger JA, Wittenberg C, Mendenhall MD, Reed SI. The *Saccharomyces cerevisiae* CKS1 gene, a homolog of the *Schizosaccharomyces pombe* suc1+ gene, encodes a subunit of the Cdc28 protein kinase complex. *J Mol Cell Biol.* (1989) 9:2034–41. doi: 10.1128/MCB.9.5.2034
- Hayles J, Beach D, Durkacz B, Nurse P. The fission yeast cell cycle control gene cdc2: isolation of a sequence suc1 that suppresses cdc2 mutant function. *Mol Gen Genet.* (1986) 202:291–3. doi: 10.1007/BF00331653
- Richardson HE, Stueland CS, Thomas J, Russell P, Reed SI. Human cDNAs encoding homologs of the small p34Cdc28/Cdc2-associated protein of

- Saccharomyces cerevisiae* and *Schizosaccharomyces pombe*. *J Genes Dev.* (1990) 4:1332–44. doi: 10.1101/gad.4.8.1332
10. Tsai YS, Chang HC, Chuang LY, Hung WC. RNA silencing of Cks1 induced G2/M arrest and apoptosis in human lung cancer cells. *J IUBMB Life.* (2005) 57:583–9. doi: 10.1080/15216540500215531
 11. Basi G, Draetta G. p13suc1 of *Schizosaccharomyces pombe* regulates two distinct forms of the mitotic cdc2 kinase. *J Mol Cell Biol.* (1995) 15:2028–36. doi: 10.1128/MCB.15.4.2028
 12. Hindley J, Phear G, Stein M, Beach D. Suc1+ encodes a predicted 13-kilodalton protein that is essential for cell viability and is directly involved in the division cycle of *Schizosaccharomyces pombe*. *J Mol Cell Biol.* (1987) 7:504–11. doi: 10.1128/MCB.7.1.504
 13. Stella F, Pedrazzini E, Baialardo E, Fantl DB, Schutz N, Slavutsky I. Quantitative analysis of CKS1B mRNA expression and copy number gain in patients with plasma cell disorders. *J Blood Cells Mol Dis.* (2014) 53:110–7. doi: 10.1016/j.bcmd.2014.05.006
 14. Zeng Z, Gao ZL, Zhang ZP, Jiang HB, Yang CQ, Yang J, et al. Downregulation of CKS1B restrains the proliferation, migration, invasion and angiogenesis of retinoblastoma cells through the MEK/ERK signaling pathway. *Int J Mol Med.* (2019) 44:103–14. doi: 10.3892/ijmm.2019.4183
 15. Lee EK, Kim DG, Kim JS, Yoon Y. Cell-cycle regulator Cks1 promotes hepatocellular carcinoma by supporting NF- κ B-dependent expression of interleukin-8. *J Cancer Res.* (2011) 71:6827–35. doi: 10.1158/0008-5472.CAN-10-4356
 16. Zhan F, Colla S, Wu X, Chen B, Stewart JP, Kuehl WM, et al. CKS1B, overexpressed in aggressive disease, regulates multiple myeloma growth and survival through SKP2- and p27Kip1-dependent and -independent mechanisms. *J Blood.* (2007) 109:4995–5001. doi: 10.1182/blood-2006-07-038703
 17. Wang X, Xu J, Ju S, Ni H, Zhu J, Wang H. Livin gene plays a role in drug resistance of colon cancer cells. *J Clin Biochem.* (2010) 43:655–60. doi: 10.1016/j.clinbiochem.2010.02.004
 18. Zolota VG, Tzelepi VN, Leotsinidis M, Zili PE, Panagopoulos ND, Dougenis D, et al. Histologic-type specific role of cell cycle regulators in non-small cell lung carcinom. *J Surg Res.* (2010) 164:256–65. doi: 10.1016/j.jss.2009.03.035
 19. Kitajima S, Kudo Y, Ogawa I, Bashir T, Kitagawa M, Miyauchi M, et al. Role of Cks1 overexpression in oral squamous cell carcinomas: cooperation with Skp2 in promoting p27 degradation. *J Am J Pathol.* (2004) 165:2147–55. doi: 10.1016/S0002-9440(10)63264-6
 20. Slotky M, Shapira M, Ben-Izhak O, Linn S, Futerman B, Tsalic M, et al. The expression of the ubiquitin ligase subunit Cks1 in human breast cancer. *J Breast Cancer Res.* (2005) 7:R737–44. doi: 10.1186/bcr1278
 21. Shaughnessy JJ, Zhan F, Burington BE, Huang Y, Colla S, Hanamura I, et al. A validated gene expression model of high-risk multiple myeloma is defined by deregulated expression of genes mapping to chromosome 1. *J Blood.* (2007) 109:2276–84. doi: 10.1182/blood-2006-07-038430
 22. Chen MH, Qi C, Reece D, Chang H. Cyclin kinase subunit 1B nuclear expression predicts an adverse outcome for patients with relapsed/refractory multiple myeloma treated with Bortezomib. *J Hum Pathol.* (2012) 43:858–64. doi: 10.1016/j.humpath.2011.07.013
 23. Huang J, Zhou Y, Thomas GS, Gu Z, Yang Y, Xu H, et al. NEDD8 inhibition overcomes CKS1B-induced drug resistance by upregulation of p21 in multiple myeloma. *J Clin Cancer Res.* (2015) 21:5532–42. doi: 10.1158/1078-0432.CCR-15-0254
 24. Hwang JS, Jeong EJ, Choi J, Lee YJ, Jung E, Kim SK, et al. MicroRNA-1258 inhibits the proliferation and migration of human colorectal cancer cells through suppressing CKS1B expression. *J Genes.* (2019) 10:110912. doi: 10.3390/genes10110912
 25. Wang H, Sun M, Guo J, Ma L, Jiang H, Gu L, et al. 3-O-(Z)-coumaroyloleanolic acid overcomes Cks1b-induced chemoresistance in lung cancer by inhibiting Hsp90 and MEK pathways. *Biochem Pharmacol.* (2017) 135:35–49. doi: 10.1016/j.bcp.2017.03.007
 26. Egan EA, Solomon MJ. Cyclin-stimulated binding of Cks proteins to cyclin-dependent kinases. *J Mol Cell Biol.* (1998) 18:3659–67. doi: 10.1128/MCB.18.7.3659
 27. Martinsson-Ahlzen HS, Liberal V, Grunenfelter B, Chaves SR, Spruck CH, Reed SI. Cyclin-dependent kinase-associated proteins Cks1 and Cks2 are essential during early embryogenesis and for cell cycle progression in somatic cells. *J Mol Cell Biol.* (2008) 28:5698–709. doi: 10.1128/MCB.01833-07
 28. Ganoth D, Bornstein G, Ko TK, Larsen B, Tyers M, Pagano M, et al. The cell-cycle regulatory protein Cks1 is required for SCF(Skp2)-mediated ubiquitinylation of p27. *J Nat Cell Biol.* (2001) 3:321–4. doi: 10.1038/35060126
 29. Spruck C, Strohmaier H, Watson M, Smith AP, Ryan A, Krek TW, et al. A CDK-independent function of mammalian Cks1: targeting of SCF(Skp2) to the CDK inhibitor p27Kip1. *Mol Cell.* (2001) 7:639–50. doi: 10.1016/S1097-2765(01)00210-6
 30. Pines J. Cell cycle: reaching for a role for the Cks proteins. *J Curr Biol.* (1996) 6:1399–402. doi: 10.1016/S0960-9822(96)00741-5
 31. Shi L, Wang S, Zangari M, Xu H, Cao TM, Xu C, et al. Over-expression of CKS1B activates both MEK/ERK and JAK/STAT3 signaling pathways and promotes myeloma cell drug-resistance. *J Oncotarget.* (2010) 1:22–33. doi: 10.18632/oncotarget.105
 32. Kawakami K, Enokida H, Tachiwada T, Nishiyama K, Seki N, Nakagawa M. Increased SKP2 and CKS1 gene expression contributes to the progression of human urothelial carcinoma. *J Urol.* (2007) 178:301–7. doi: 10.1016/j.juro.2007.03.002
 33. Liu Z, Fu Q, Lv J, Wang F, Ding K. Prognostic implication of p27Kip1, Skp2 and Cks1 expression in renal cell carcinoma: a tissue microarray study. *J Exp Clin Cancer Res.* (2008) 27:51. doi: 10.1186/1756-9966-27-51
 34. Shapira M, Ben-Izhak O, Slotky M, Goldin O, Lahav-Baratz S, Hershko DD. Expression of the ubiquitin ligase subunit cyclin kinase subunit 1 and its relationship to S-phase kinase protein 2 and p27Kip1 in prostate cancer. *J Urol.* (2006) 176:2285–9. doi: 10.1016/j.juro.2006.07.051
 35. Zassadowski F, Rochette-Egly C, Chomienne C, Cassinat B. Regulation of the transcriptional activity of nuclear receptors by the MEK/ERK1/2 pathway. *Cell Signal.* (2012) 24:2369–77. doi: 10.1016/j.cellsig.2012.08.003
 36. Gao N, Budhraj A, Cheng S, Liu EH, Huang C, Chen J, et al. Interruption of the MEK/ERK signaling cascade promotes dihydroartemisinin-induced apoptosis *in vitro* and *in vivo*. *Apoptosis.* (2011) 16:511–23. doi: 10.1007/s10495-011-0580-6
 37. Lieske NV, Tonby K, Kvale D, Dyrholm-Riise AM, Tasken K. Targeting tuberculosis and HIV infection-specific regulatory T cells with MEK/ERK signaling pathway inhibitors. *PLoS ONE.* (2015) 10:e0141903. doi: 10.1371/journal.pone.0141903
 38. Ren J, Zhang N, Liao H, Chen S, Xu L, Li J, et al. Caffeic acid phenethyl ester attenuates pathological cardiac hypertrophy by regulation of MEK/ERK signaling pathway *in vivo* and *in vitro*. *Life Sci.* (2017) 181:53–61. doi: 10.1016/j.lfs.2017.04.016
 39. Liu C, Lee WC, Huang BM, Chia YC, Chen YC, Chen Y. 16-Hydroxycyclocloda-3 C, 13-dien-15, 16-olide inhibits the proliferation and induces mitochondrial-dependent apoptosis through Akt, mTOR, and MEK-ERK pathways in human renal carcinoma cells. *Phytomedicine.* (2017) 36:95–107. doi: 10.1016/j.phymed.2017.09.021
 40. Xie C, Li Y, Li LL, Fan XX, Wang YW, Wei CL, et al. Identification of a new potent inhibitor targeting KRAS in non-small cell lung cancer cells. *Front Pharmacol.* (2017) 8:823. doi: 10.3389/fphar.2017.00823
 41. Cyprian FS, Al-Farsi HF, Vranic S, Akhtar S, Al Moustafa EA. Epstein-barr virus and human papillomaviruses interactions and their roles in the initiation of epithelial-mesenchymal transition and cancer progression. *Front Oncol.* (2018) 8:111. doi: 10.3389/fonc.2018.00111
 42. Whitesell L, Lindquist SL. HSP90 and the chaperoning of cancer. *J Nat Rev Cancer.* (2005) 5:761–72. doi: 10.1038/nrc1716
 43. Workman P. Combinatorial attack on multistep oncogenesis by inhibiting the Hsp90 molecular chaperone. *J Cancer Lett.* (2004) 206:149–57. doi: 10.1016/j.canlet.2003.08.032
 44. Zhang H, Burrows F. Targeting multiple signal transduction pathways through inhibition of Hsp90. *J Mol Med.* (2004) 82:488–99. doi: 10.1007/s00109-004-0549-9
 45. Khattar V, Fried J, Xu B, Thottassery JV. Cks1 proteasomal degradation is induced by inhibiting Hsp90-mediated chaperoning in cancer cells. *Cancer Chemother Pharmacol.* (2015) 75:411–20. doi: 10.1007/s00280-014-2666-7
 46. Tomczak K, Czerwinski P, Wiznerowicz M. The Cancer Genome Atlas (TCGA): an immeasurable source of knowledge. *J Contemp Oncol.* (2015) 19:A68–77. doi: 10.5114/wo.2014.47136

47. Deng M, Bragelmann J, Schultze JL, Perner S. Web-TCGA: an online platform for integrated analysis of molecular cancer data sets. *J BMC Bioinform.* (2016) 17:72. doi: 10.1186/s12859-016-0917-9
48. Guo WG, Zhang Y, Ge D, Zhang YX, Lu CL, Wang Q, et al. Bioinformatics analyses combined microarray identify the desregulated microRNAs in lung cancer. *J Eur Rev Med Pharmacol Sci.* (2013) 17:1509–16.
49. Song F, Yang D, Liu B, Guo Y, Zheng H, Li L, et al. Integrated microRNA network analyses identify a poor-prognosis subtype of gastric cancer characterized by the miR-200 family. *J Clin Cancer Res.* (2014) 20:878–89. doi: 10.1158/1078-0432.CCR-13-1844
50. Lin L, Lin Y, Jin Y, Zheng C. Microarray analysis of microRNA expression in liver cancer tissues and normal control. *J Gene.* (2013) 523:158–60. doi: 10.1016/j.gene.2013.02.055
51. Feng J, Huang C, Diao X, Fan M, Wang P, Xiao Y, et al. Screening biomarkers of prostate cancer by integrating microRNA and mRNA microarrays. *J Genet Test Mol Biomarkers.* (2013) 17:807–13. doi: 10.1089/gtmb.2013.0226
52. Shrestha S, Hsu SD, Huang WY, Huang HY, Chen W, Weng SL, et al. A systematic review of microRNA expression profiling studies in human gastric cancer. *J Cancer Med.* (2014) 3:878–88. doi: 10.1002/cam4.246
53. Shrestha S, Yang CD, Hong HC, Chou CH, Tai CS, Chiew MY, et al. Integrated microRNA-mRNA analysis reveals mir-204 inhibits cell proliferation in gastric cancer by targeting CKS1B, CXCL1, and GPRC5A. *Int J Mol Sci.* (2017) 19:87. doi: 10.3390/ijms19010087
54. La T, Liu GZ, Farrelly M, Cole N, Feng YC, Zhang YY, et al. A p53-responsive miRNA network promotes cancer cell quiescence. *Cancer Res.* (2018) 78:6666–79. doi: 10.1158/0008-5472.CAN-18-1886
55. Sugihara H, Ishimoto T, Miyake K, Izumi D, Baba Y, Yoshida N, et al. Noncoding RNA expression aberration is associated with cancer progression and is a potential biomarker in esophageal squamous cell carcinoma. *Int J Mol Sci.* (2015) 16:27824–34. doi: 10.3390/ijms161126060
56. Lin CY, Xu HM. Novel perspectives of long non-coding RNAs in esophageal carcinoma. *Carcinogenesis.* (2015) 36:1255–62. doi: 10.1093/carcin/bgv136
57. Cao X, Zhao R, Chen Q, Zhao Y, Zhang B, Zhang Y, et al. MALAT1 might be a predictive marker of poor prognosis in patients who underwent radical resection of middle thoracic esophageal squamous cell carcinoma. *Cancer Biomark.* (2015) 15:717–23. doi: 10.3233/CBM-150513
58. Wang W, Zhu Y, Li S, Chen X, Jiang G, Shen Z, et al. Long noncoding RNA MALAT1 promotes malignant development of esophageal squamous cell carcinoma by targeting beta-catenin via Ezh2. *J Oncotarget.* (2016) 7:25668–82. doi: 10.18632/oncotarget.8257
59. Peng Y-T, Wu W-R, Chen L-R, Kuo K-K, Tsai C-H, Huang Y-T, et al. Upregulation of cyclin-dependent kinase inhibitors CDKN1B and CDKN1C in hepatocellular carcinoma-derived cells via goniiothalamine-mediated protein stabilization and epigenetic modifications. *J Toxicol Rep.* (2015) 2:322–32. doi: 10.1016/j.toxrep.2015.01.010
60. Ji P, Diederichs S, Wang W, Boing S, Metzger R, Schneider PM, et al. MALAT-1, a novel noncoding RNA, and thymosin beta4 predict metastasis and survival in early-stage non-small cell lung cancer. *J Oncogene.* (2003) 22:8031–41. doi: 10.1038/sj.onc.1206928
61. Li Z, Zhou Y, Tu B, Bu Y, Liu A, Kong J. Long noncoding RNA MALAT1 affects the efficacy of radiotherapy for esophageal squamous cell carcinoma by regulating Cks1 expression. *J Oral Pathol Med.* (2017) 46:583–90. doi: 10.1111/jop.12538

Conflict of Interest: The authors declare that the research was conducted in the absence of any commercial or financial relationships that could be construed as a potential conflict of interest.

Copyright © 2020 Shi, Huang, Xie, Wang, Yu and Zhou. This is an open-access article distributed under the terms of the Creative Commons Attribution License (CC BY). The use, distribution or reproduction in other forums is permitted, provided the original author(s) and the copyright owner(s) are credited and that the original publication in this journal is cited, in accordance with accepted academic practice. No use, distribution or reproduction is permitted which does not comply with these terms.



VWCE Functions as a Tumor Suppressor in Breast Cancer Cells

Dan Zhang, Lili Wan, Fan Yang, Wenlan Liu, Litao Liu, Shengnan He and Ni Xie*

Health Science Center, Biobank Shenzhen Second People's Hospital, The First Affiliated Hospital of Shenzhen University, Shenzhen, China

Breast cancer remains a leading cause of cancer-related death, for which the majority of deaths result from metastases. Von Willebrand factor C and EGF domain (VWCE) is a member of the Von Willebrand factor (VWF) gene family; however, its function, regulatory mechanism, and clinical value in breast cancer remain unclear. In the present study, we sought to elucidate the role of VWCE in breast cancer metastasis. We examined the expression of VWCE in breast cancer tissues and normal control tissues of 50 breast cancer patients. We found that VWCE expression was downregulated in breast cancer cells and tissues compared to normal breast epithelial cells or the adjacent normal tissues. To explore the role of VWCE in human breast cancer development, we introduced a VWCE-overexpressing or control lentiviral vector into the breast cancer MDA-MB-453 and MDA-MB-231 lines *in vitro*. The overexpression of VWCE inhibited the proliferation, migration, invasion, and chemoresistance of the breast cancer cell lines. More importantly, the forced expression of VWCE suppressed tumor formation and metastasis in nude mice. iTRAQ-based quantitative proteomic analysis revealed that VWCE overexpression induced a 10-fold decrease in the level of WD-repeat domain 1 (WDR1) protein expression. Rescue experiments further verified that WDR1 was a downstream molecule of VWCE, and WDR1 overexpression reversed the above effects of VWCE overexpression on tumor growth. Therefore, VWCE may represent a novel tumor suppressor, for which its deregulation promotes breast cancer progression *via* the upregulation of WDR1.

Keywords: breast cancer cells, Von Willebrand factor C and EGF domain, tumor suppressor, WD-repeat domain 1, metastasis

OPEN ACCESS

Edited by:

Wei Zhao,
Chengdu Medical College, China

Reviewed by:

Leli Zeng,
Sun Yat-sen University, China
Chenxi Zhang,
Nanjing Chest Hospital, China

*Correspondence:

Ni Xie
xn100@szu.edu.cn

Specialty section:

This article was submitted to
Molecular and Cellular Oncology,
a section of the journal
Frontiers in Oncology

Received: 23 July 2020

Accepted: 30 September 2020

Published: 22 October 2020

Citation:

Zhang D, Wan L, Yang F, Liu W, Liu L,
He S and Xie N (2020) VWCE
Functions as a Tumor Suppressor in
Breast Cancer Cells.
Front. Oncol. 10:586342.
doi: 10.3389/fonc.2020.586342

INTRODUCTION

Breast cancer is the most common type of cancer affecting women worldwide and the leading cause of cancer-related death in women (1). Moreover, metastasis is the leading cause of death in breast cancer patients, accounting for 90% of breast cancer mortality (2). Although significant progress has been made in breast cancer research over the past decade, our understanding of metastasis remains limited and it is not yet possible to prevent and provide targeted treatment for metastases (3). Therefore, there is an urgent need to elucidate the potential molecular pathways and associated mechanisms that contribute to the progression of breast cancer metastasis.

VWCE is a member of the Von Willebrand factor (VWF) gene family (4), also called URG11. Previous studies have demonstrated that VWF gene polymorphisms play an important role in a variety of physiological and pathological processes, including embryonic development, angiogenesis, physiological hemostasis, genetic hereditary diseases, and malignant tumors (5–12). In addition, the role of VWCE has been studied in several types of tumors. For example, VWCE has been found to be highly expressed in hepatocellular carcinoma, gastric cancer, pancreatic cancer, and lung cancer, and is associated with increased invasion and metastasis of these tumor cells (13–18). It has also been found that the N-terminal VWC domain of VWCE binds to bone morphogenetic proteins (BMPs) with a high affinity (10), which have been linked to the transformation of breast cancer subtypes (11). Notably, BMP signal transduction mediated by a new peptide agonist, P123, leads to the reversal of the epithelial-mesenchymal transition process in human breast cancer stem cells and inhibits self-renewal and growth, thereby slowing the invasion and metastasis of breast cancer (12). However, to date, there have been no reports on the role of VWCE in breast cancer. In this study, the expression and function of VWCE in breast cancer cells are studied, and the possible anti-tumor mechanisms are further explored.

MATERIALS AND METHODS

Patient Tissue Specimens

This study was approved by the clinical research medical ethics committee of the First Affiliated Hospital of Shenzhen University. After obtaining written informed consent, breast cancer tissues and matched adjacent non-cancerous tissues were collected from 50 patients at the First Affiliated Hospital of Shenzhen University (The Second People's Hospital of Shenzhen, Shenzhen 518037, China). All tumor specimens were obtained from new patients who were not treated prior to surgery (study period: 2017–2018); Tissues were fixed in RNAlater and stored at -80°C until further use (19). Pathology reports were provided by the Shenzhen Second People's Hospital Cancer Center.

Cell Lines

Five breast cancer cell lines with different hormone receptor profiles were used in this study: 1) MCF7; 2) BT-474; 3) SK-BR-3; 4) MDA-MB-231; and 5) MDA-MB-453. In addition, MCF-10A cells are normal breast epithelial cells, used as a control. All cell lines were purchased from the Chinese Science Shanghai Institute of Cell Biology and cultured in L-15/1640/Dulbecco's modified Eagle medium (DMEM; Gibco, Carlsbad, CA, USA) supplemented with 10% fetal bovine serum (Gibco) at 37°C in a humidified atmosphere with 5% CO_2 .

Quantitative Real-Time PCR

Quantitative real-time RT-PCR (qRT-PCR) was performed using SYBR Premix Ex TaqTM II (TaKaRa), and the expression of

β -actin was used as an internal control. The assay was conducted in triplicate using the following primer sets: VWCE forward, 5'-ACG GAA ATG TGG CAT TCA GCAAAG-3', VWCE reverse, 5'-CGGGCTTGTAGGTAAAGTCTGTGT-3', product size 179 bp; β -actin (used as the internal primer) forward, 5'-GATCATTGC TCCTCCTGAGC-3', reverse, 5'-ACTCCTGCTTGCTGATCCAC-3', product size 101 bp. Amplification was carried out in 20 μl reaction systems, comprised of SYBR Green Mix (16.4 μl), cDNA (2 μl), and 0.8 μl of the forward and reverse primer (10 μM) under the following conditions: 95°C pre-denaturation for 30 s, followed by 40 cycles of denaturation at 95°C for 5 s, and annealing/extension at 60°C for 34 s. All reactions were conducted in duplicate. The relative expression of VWCE was calculated using the $2^{-\Delta\Delta\text{CT}}$ method.

Western Blot

We randomly selected six pairs of tissues that were lysed along with the six breast cell lines using 500 μl of the cell lysate (100 μl containing RIPA buffer with 1 μl phenylmethylsulfonyl fluoride). The total protein concentration was determined by the BCA method, and 20 μg of each protein sample was separated by 10% sodium dodecyl sulfate-polyacrylamide gel electrophoresis. Proteins were transferred to polyvinylidene fluoride membranes using the semi-dry method. The membranes were blocked with 5% bovine serum albumin, treated with a rabbit anti-human VWCE polyclonal antibody (1:500 dilution) (Sigma Aldrich, St. Louis, MO, USA) and GAPDH polyclonal antibody (1:5,000 dilution) (CST, USA) and β -tubulin polyclonal antibody (1:5,000 dilution) (Abcam, Cambridge, UK) overnight at 4°C , washed three times with TBST for 10 min each, and treated with horse radish peroxidase (HRP)-labeled goat anti-Rabbit IgG at room temperature for 1 h. The immunocomplexes were then visualized by chemiluminescent imaging.

Immunohistochemical Analysis

A total of 87 paraffin-embedded breast cancer tissues and the corresponding adjacent tissue microarray were purchased from Alenabio (Xi'an, China). Briefly, after deparaffinization and rehydration, tissue slides were subjected to antigen retrieval by boiling in citrate buffer (10 mM, pH 6.0) and immersed in 30% hydrogen peroxide (H_2O_2) to quench the endogenous peroxidase activity. After washing in phosphate-buffered saline, the slides were incubated with an anti-VWCE antibody (1:500, Sigma-Aldrich) overnight at 4°C , followed by an HRP-conjugated goat anti-rabbit IgG antibody (sc-2030; Santa Cruz Biotechnology, Dallas, TX, USA) at room temperature. The samples were then stained with a freshly prepared DAB solution (Dako Pure Chemicals, Glostrup, Denmark) and counterstained with hematoxylin. All of the stained sections were assessed for the degree of immunostaining and scored by two pathologists. Five fields of vision were randomly selected under the microscope. The presence of brown staining in the cytosol was considered to be positive for VWCE expression, regardless of the intensity. The sections were scored as follows: 0 points, 0 positively stained cells; 1 point, < 25% of the cells were stained positive; 2 points, 25%–50% of the cells were stained positive; 3 points, 50%–75%

of the cells were stained positive; and 4 points, > 75% of the cells were stained positive. Moreover, the staining intensity was divided into four groups: 0, negative; 1, weak positive; 2, moderate positive; and 3, strong positive. The score for each tissue was the product of the two integrals. The results were determined as follows: I (0), II (1–4), III (5–8), and IV (9–12), where I was considered to be negative and II, III, and IV were considered to be positively stained.

Cell Transfection

Cells were plated approximately 24 h prior to transfection to achieve 80%–90% confluence at the time of transfection. Each cell line was transfected with VWCE and WDR1-overexpressing lentiviral vectors and a corresponding negative control virus, respectively, using transfection reagent (GENE, Shanghai, China) according to the manufacturer's instructions.

CCK8 Assay

The cell suspensions were adjusted to 2,000 cells/ml and seeded into 96-well plates at 100 µl per well. After an incubation for 6–8 h to ensure cell adherence, the cell growth rate was determined using Cell Counting Kit-8 (CCK-8; CCK8: medium, 1:10). After an incubation at 37°C for 2 h, the light absorbance at 450 nm was measured for each sample. The OD (450) value was taken as the absorbance value at Day 0. Cell absorbance values were recorded on days 1, 2, 3, and 4.

Colony Formation Assay

Cell suspensions were adjusted to 1,500 cells/ul and seeded into six-well plates at 1 µl/well. After cultivation for 7–10 days, the medium was removed, and the cells were fixed with 4% paraformaldehyde (1 ml) at 37°C for 15 min, and then cells were stained with 0.1% crystal violet at room temperature for 20 min and washed with water 2–3 times prior to imaging (20).

Transwell Migration Assay

To assess the level of cellular migration, cells in the logarithmic growth phase were routinely harvested by digestion and centrifugation. The cells were resuspended in serum-free medium, and adjusted to 1×10^5 /ml. Then, 200 µl of each suspension was added to the upper Transwell chamber, whereas 500 µl medium containing serum was added to the lower chamber. After 24 h, the non-migrated cells on the upper surface of the filters were wiped off using a cotton swab. Migratory cells on the lower membrane surface were fixed with 4% paraformaldehyde for 15 min, stained with 1% crystal violet for 20 min, washed with single distilled water, and dried. Cells were then visualized with an OLYMPUS IX71 Inverted Microscope and the number of migratory cells was counted. Data were presented as the means \pm standard deviations of the results from three independent experiments.

Wound-Healing Assay

The cells were planted in a six-well plate at a certain density, and the cells were incubated in a medium containing 0.5% FBS at 37°C (21). They reached a monolayer confluence of about 80%, using a 10 µl pipette. The suction tip scrapes the cell monolayer

to prepare the wound. After the wound appears, wash twice with PBS to remove the separated cells and replace it with fresh serum-free medium. The wound area is photographed under an inverted microscope within a specified time. Use image software to quantify and analyze the width of the gap. The average wound size represents the level of relative cell migration (22).

Drug Resistance Clonogenic Assay

The cells were treated with a single dose of docetaxel for one week. The resistant clones were fixed in 4% paraformaldehyde and stained with 0.1% crystal violet and counted.

Cell Cycle Analysis

After the cells grow to 70%–80%, digest and centrifuge to collect the cells, add pre-cooled ethanol to fix. The cells were washed with pre-chilled PBS and resuspended with 500 µl of PBS containing staining buffer, 10 µl RNase A and 25 µl propidium iodide. The cell suspension was evaluated by flow cytometry.

iTRAQ-Based Proteomics Analysis

iTRAQ-based proteomics analyses were performed in MDA-MB-231 cells. Briefly, the cells were dissolved in lysis buffer and labeled with iTRAQ-labeling reagents. After 2D LC and tandem mass spectrometry analyses, protein identification and relative iTRAQ quantification were performed with ProteinPilot™ Software 4.2 (AB SCIEX) using the Paragon™ algorithm for peptide identification. Results with iTRAQ ratio cut-off values of 1.2 and 0.8 for the fold-change and number of cut-off values of three quantifiable peptides for in-protein abundance were accepted.

Construction of a Breast Cancer Xenograft

BALB/c-nude mice (4–5 weeks of age; 18–20 g) were purchased from the Center of Experimental Animals of Guangdong province, China, and housed in a sterile environment. For the tumor formation experiment, a total of 16 four-week-old female BALB/c-nude mice were randomly divided into two groups ($n = 8$ /group): 1) MDA-MB-231 cells (8×10^6) with the stable expression of VWCE or a control vector were subcutaneously injected into the right flanks of the nude mice, respectively. The tumor volume was determined using the eq. $V = 0.5 \times D \times d^2$ (V , volume; D , longitudinal diameter; d , latitudinal diameter). The developing tumors were observed over the next 33 days.

Construction of a Xenograft Metastasis Model

MDA-MB-231 cells stably expressing luciferase (referred to as MDA-MB-231-luc) were transfected to express VWCE. In the lung metastasis experiment, with a density of 1×10^6 MDA-MB-231 cells expressing luciferase overexpressing VWCE were suspended in 100 µl PBS and injected into the tail vein of six-week-old BALB/c nude mice. Six weeks later, IVIS-200 camera system was used to analyze the metastatic disease of mice by bioluminescence imaging to detect the expression of luciferase, the nude mice were dissected, and lung tissues were collected. For the histological examination, pulmonary tissues were fixed in 10% neutral-buffered formalin and embedded in paraffin. Then,

four resections were prepared for H&E staining and an immunohistological assay. E-cadherin was detected using an anti-E-cadherin antibody. All experimental animal procedures were approved by the Institutional Animal Care and Use Committee of The Second People's Hospital of ShenZhen, China.

Database Analysis

The BRCA datasets and expression of the target genes VWCE by mRNA sequencing were downloaded from The Cancer Genome Atlas (TCGA) dataset. The expression data between breast cancer tissues and adjacent normal breast tissues were compared using the edgeR package in R. Use the website (<http://www.kmplot.com>) to identify the prognosis of VWCE in breast cancer patients.

Statistical Analysis

Data were presented as the means of the results from at least three independent experiments. Correlations between the level of VWCE expression and various clinicopathological parameters were analyzed using a χ^2 test. Differences between VWCE-overexpression and the negative control of the lentivirus-transfected cells in the CCK-8 assay were analyzed by a one-way analysis of variance (ANOVA). All other data were analyzed using independent sample *t*-tests. All statistical analyses were performed using the SPSS 21.0 software package (SPSS Statistics Inc., Chicago, IL, USA), and a threshold of $p < 0.05$ was defined as significant for all tests.

RESULTS

VWCE Is Down-Regulated in Breast Cancer Tissues and Cells

We first analyzed the level of VWCE expression in breast cancer tissues and cultured the breast cancer cell lines using qRT-PCR, immunohistochemistry, and Western blot. The level of VWCE mRNA expression was lower in moderately invasive cells (MCF-7 and BT474) than in non-tumorigenic MCF-10A cells, and was the lowest in highly invasive cancer cell lines (MDA-MB-453, SKBR-3, and MDA-MB-231), as assessed by reverse transcription-PCR (**Figure 1A**). Similarly, using qRT-PCR, we assessed the level of VWCE mRNA expression in 50 human breast cancer specimens relative to 50 normal breast tissue samples, and VWCE mRNA is highly expressed in normal tissues adjacent to the tumor (**Figure 1B**); However, in contrast, the expression in breast cancer tissue is lower. The level of VWCE mRNA expression in breast cancer tissues and matched adjacent non-cancerous tissues ($n = 50$) was assessed by qRT-PCR analysis. In most patients, there was a positive fold-change in the level of VWCE expression (**Figure 1C**).

We next examined the level of VWCE protein expression in breast cancer cell lines (**Figure 1D**) and tumor tissues (**Figure 1E**), which was consistent with our VWCE mRNA expression data. In order to examine the level of VWCE protein expression in human breast cancer, we performed an immunohistochemical analysis of the purchased tissue microarray, which consisted of 87 breast cancer tissues and 87 matched normal breast tissue

samples. Staining was performed using VWCE specific antibodies, and at least two pathologists scored the staining intensity. Quantification of the mean of the tumor-adjacent normal breast tissues exhibited a significantly higher level of VWCE expression than that of the breast cancer tissues (**Figure 1F**). These data are consistent with our results regarding the level of VWCE mRNA expression. The positive expression rate of VWCE among the tested breast cancer and adjacent normal tissues was 39.08% (34/87) and 59.77% (52/87), respectively.

We also used the TCGA datasets to examine the level of VWCE mRNA expression in 1,079 human breast cancer specimens relative to the 113 normal breast tissues (**Figure 1G**). Data from the same tissue sample but from different vials was averaged. The gene expression data was generated *via* RNAseq. We further confirmed that VWCE exhibited lower levels of expression in breast cancer tissues compared to the adjacent normal tissues in breast cancer patients.

VWCE Overexpression Inhibits the Proliferation of Breast Cancer Cells

We next transfected MDA-MB-453 and MDA-MB-231 cells with a VWCE-overexpressing lentivirus and control virus to analyze the role of VWCE of proliferation in breast cancer cells. The efficacy of transfection was examined by a Western blot analysis (**Figure 2A**). As expected, the level of VWCE protein expression in the cells of the experimental groups exhibited significantly higher levels of VWCE expression compared to those in the negative control groups. VWCE overexpression significantly inhibited the proliferation of MDA-MB-453 and MDA-MB-231 cells compared with the negative control groups ($p < 0.05$), as determined by a cancer cell colony formation assay (**Figure 2B**). Moreover, the CCK-8 assay showed that the ectopic expression of VWCE significantly inhibited MDA-MB-453, and MDA-MB-231 cell proliferation in a time-dependent manner, compared with the negative control transfection groups ($p < 0.001$) (**Figure 2C**). In addition, to further assess the effect of VWCE overexpression on tumorigenicity *in vivo*, we subcutaneously injected MDA-MB-231-GFP and MDA-MB-231-VWCE cells into nude mice. Intriguingly, as shown in **Figures 2D, E**, the tumors formed by MDA-MB-231-VWCE cells were significantly smaller than that of the control cells. The average tumor weight of the VWCE-transfected cells in the inoculated mice was significantly decreased compared with that of the control cells on Day 30 (**Figure 2F**). These results suggest that VWCE inhibits tumor growth. To investigate whether cells expressing VWCE are less proliferating *in vivo*, we took immunohistochemical staining of Ki67 (a marker of cell proliferation) from tumors of nude mice. Tumors expressing VWCE showed Ki67 staining significantly lower than controls expressing GFP (**Figure 2G**). These indicating that VWCE may acts as a tumor suppressor *in vivo*, supporting a role for VWCE in the regulation of tumor growth *via* its effects on cellular proliferation.

VWCE Overexpression Inhibits the Cellular Migration of Breast Cancer Cells

To investigate the function of VWCE in breast cancer, we first transfected the MDA-MB-231 and MDA-MB-453 cell lines using a control and VWCE expression vector, and verified VWCE expression by Western blot and qRT-PCR. We then

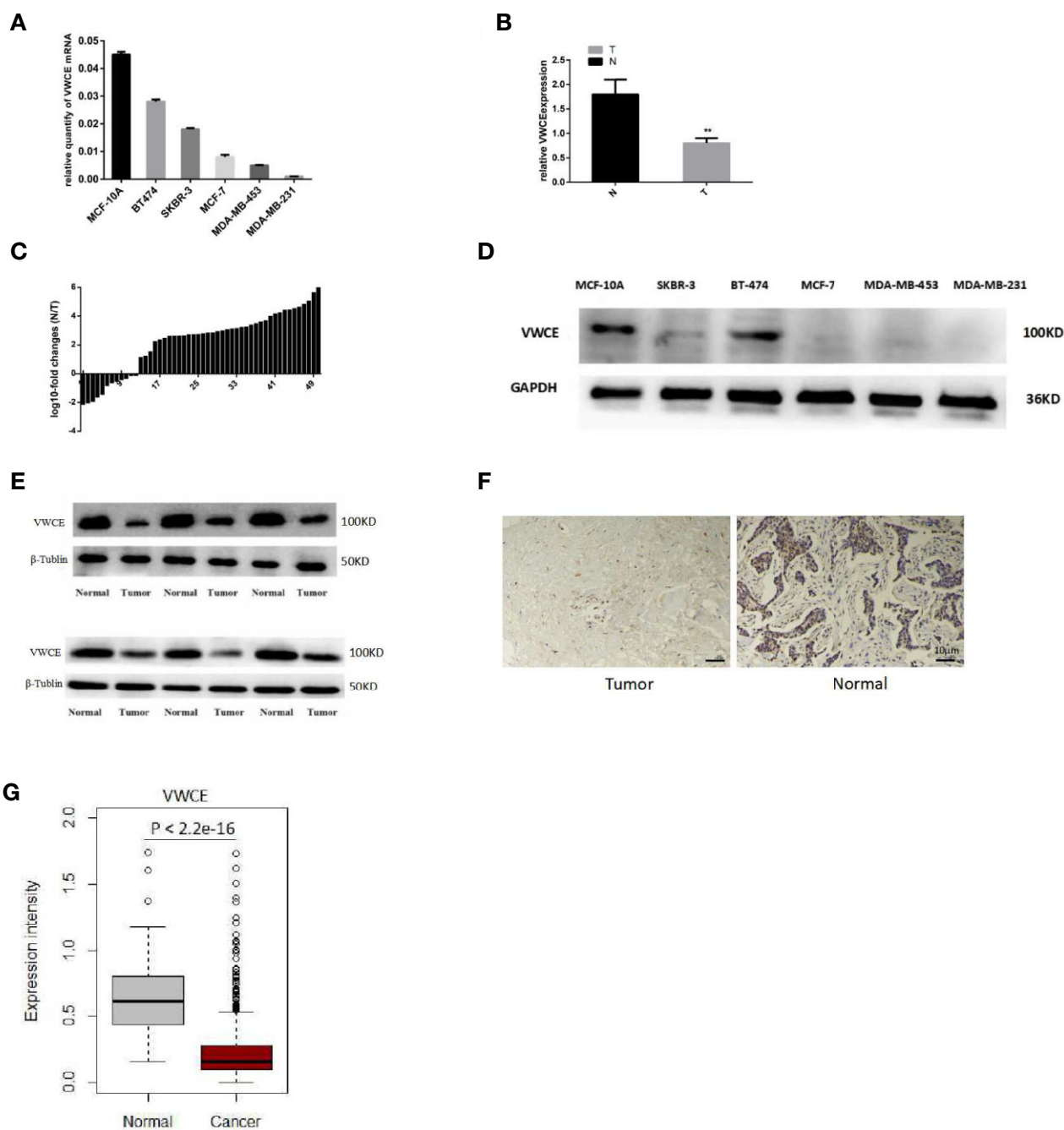


FIGURE 1 | Down-regulation of Von Willebrand factor C and EGF domain (VWCE) in breast cancer tissues and breast cancer cell lines. **(A)** Quantitative real-time RT (RT-PCR) analysis of VWCE expression in five breast cancer cell lines (MCF-7, BT474, SKBR-3, MDA-MB-231, and MDA-MB-453) and a normal breast cell line (MCF-10A). **(B)** qRT-PCR analysis of VWCE mRNA expression in breast cancer tissues and matched normal control tissues. T, tumor; N, normal. **(C)** The expression of VWCE was analyzed in samples from 50 breast cancer patients. The height of the columns in the chart represents log₁₀-transformed fold-changes (normal and cancer tissue) in VWCE expression. **(D)** Western blot analysis of VWCE protein expression in the five breast cancer cell lines and in MCF-10A cells. **(E)** Western blot analysis of VWCE protein expression in fresh breast cancer and adjacent non-tumor tissues. **(F)** Representative immunohistochemical staining of VWCE protein expression in breast cancer (right) and matched non-tumor tissues (left) (scale bar = 10 μ M). **(G)** The level of VWCE mRNA expression was compared between the tumor and normal group of TCGA breast cancer. ** $P < 0.01$.

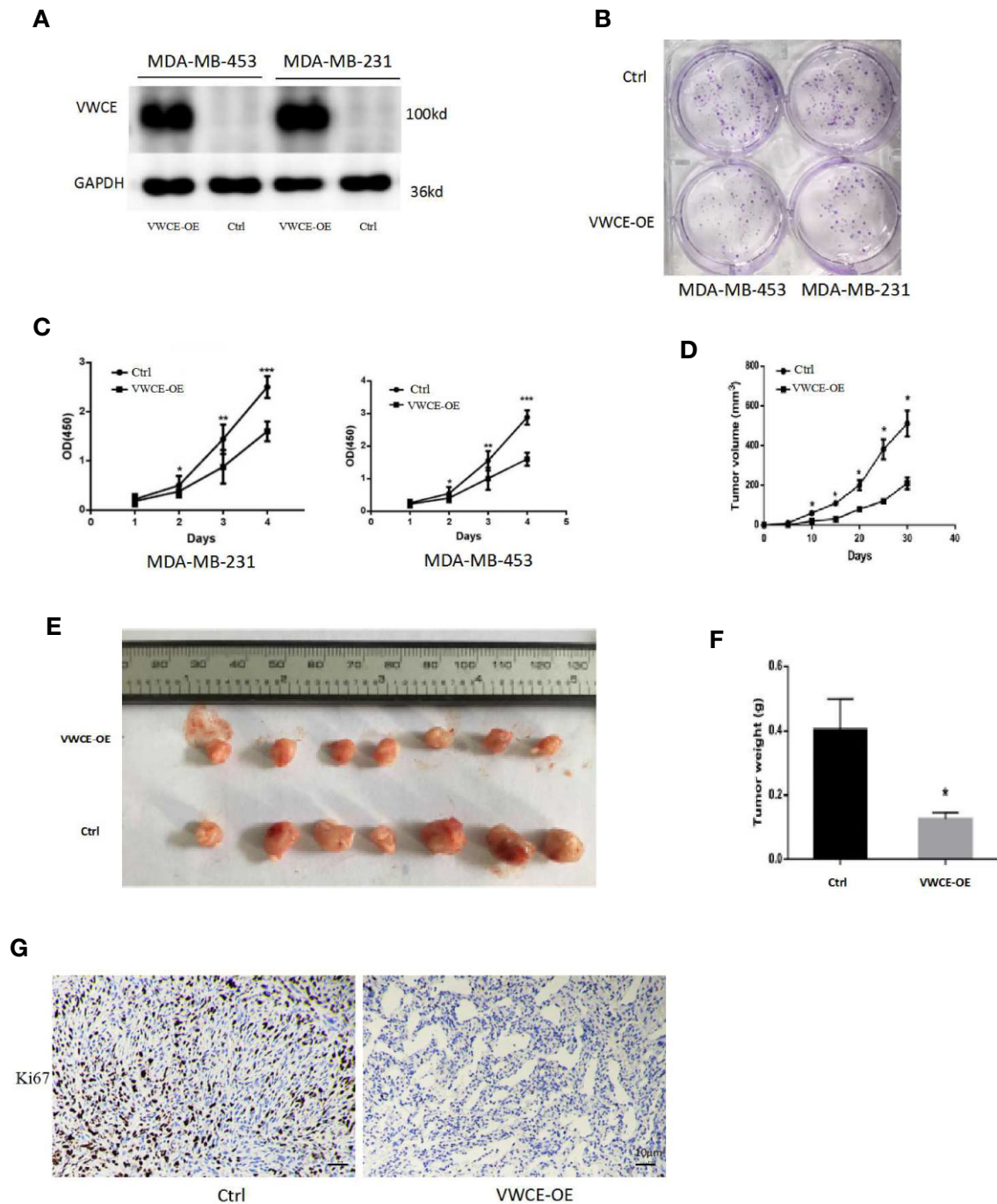


FIGURE 2 | Von Willebrand factor C and EGF domain (VWCE) inhibits breast cancer cell proliferation. **(A)** Western blot analysis of VWCE protein expression in MDA-MB-453 and MDA-MB-231 cells stably transfected with a VWCE-overexpressing or negative control lentivirus. GAPDH was used as a loading control. **(B)** A plate cell colony formation assay of the ectopic expression of VWCE on MDA-MB-453 and MDA-MB-231 cells. **(C)** CCK8 analysis of the effects of the ectopic expression of VWCE on the proliferation of MDA-MB-453 and MDA-MB-231 cells. Experiments were performed in triplicate and data are presented as means \pm standard deviations; * $p < 0.05$, ** $p < 0.01$, and *** $p < 0.001$, compared to the control, respectively. **(D)** The tumor growth curves were measured after a subcutaneous injection of the MDA-MB-231-Control and MDA-MB-231-VWCE. The tumor volume was calculated every five days. Error bars indicate standard deviation (Student's *t*-test; * $P < 0.05$; $n = 5$). **(E)** Photographs of the dissected tumors from nude mice. **(F)** The weight of tumors from mice with MDA-MB-231-Control and MDA-MB-231-VWCE implantation. Error bars indicate standard deviation (Student's *t*-test; * $P < 0.05$, $n = 5$). **(G)** Cellular proliferation in VWCE-expressing vs. control tumors. Paraffin-embedded tissue sections of the primary tumors from mice injected with MDA-MB-231-Control and MDA-MB-231-VWCE cells were immunostained with an anti-Ki67 antibody. Photomicrographs were taken at 20 \times magnification; scale bars = 10 μ M.

investigated the effect of VWCE on breast cancer cell metastasis. Transwell assays with or without matrix gel showed that VWCE suppressed the migration and invasion ability of MDA-MB-231 and MDA-MB-453 cells (**Figure 3A**). Moreover, while the overexpression of VWCE robustly accelerated wound closure in all of the analyzed breast cancer cell lines, cell motility was also effected (**Figure 3B**). VWCE overexpression also reduced the number of metastatic nodules when MDA-MB-231 cells were injected into the tail veins of mice (**Figure 3C**). To further confirm the effect of VWCE on breast cancer metastasis, we injected MDA-MB-231 breast cancer cells overexpressed with VWCE into the nude mice through the tail vein. The histological analysis of the lung tissue of nude mice was carried out. Lung tissue was extracted and sectioned (**Figures 3D, E**). H&E staining showed that the lungs of mice injected with VWCE overexpressing breast cancer cells had almost no metastasis (**Figure 3F**). In contrast, the lungs of mice injected with vehicle-controlled breast cancer cells were severely infiltrated by metastatic foci. Further pathological examination of lung

metastases in mice carrying MDA-MB-231 xenografts overexpressing VWCE showed that the larger ones were observed in nude mice with control MDA-MB-231-luc xenografts compared with local invasive metastases, these metastases are smaller and separate. These results suggest that VWCE can inhibit the metastasis of breast cancer cells *in vivo* and is an important regulator of breast cancer cell invasion and metastasis *in vivo*.

VWCE Overexpression Induces the Reversal of EMT to MET in Aggressive Breast Cancer Cells

We next examined the expression of EMT markers, a characteristic used to define the aggressiveness of breast cancer cells. We selected two breast cancer cell lines that represent the mesenchymal phenotype, MDA-MB-231 and MDA-MB-435 cells, to elucidate the mechanism by which VWCE mediates its anticancer effects. We found that VWCE-overexpression resulted in a significant downregulation of the mesenchymal markers, vimentin, ZEB1, and ZEB2 in both MDA-MB-231 and

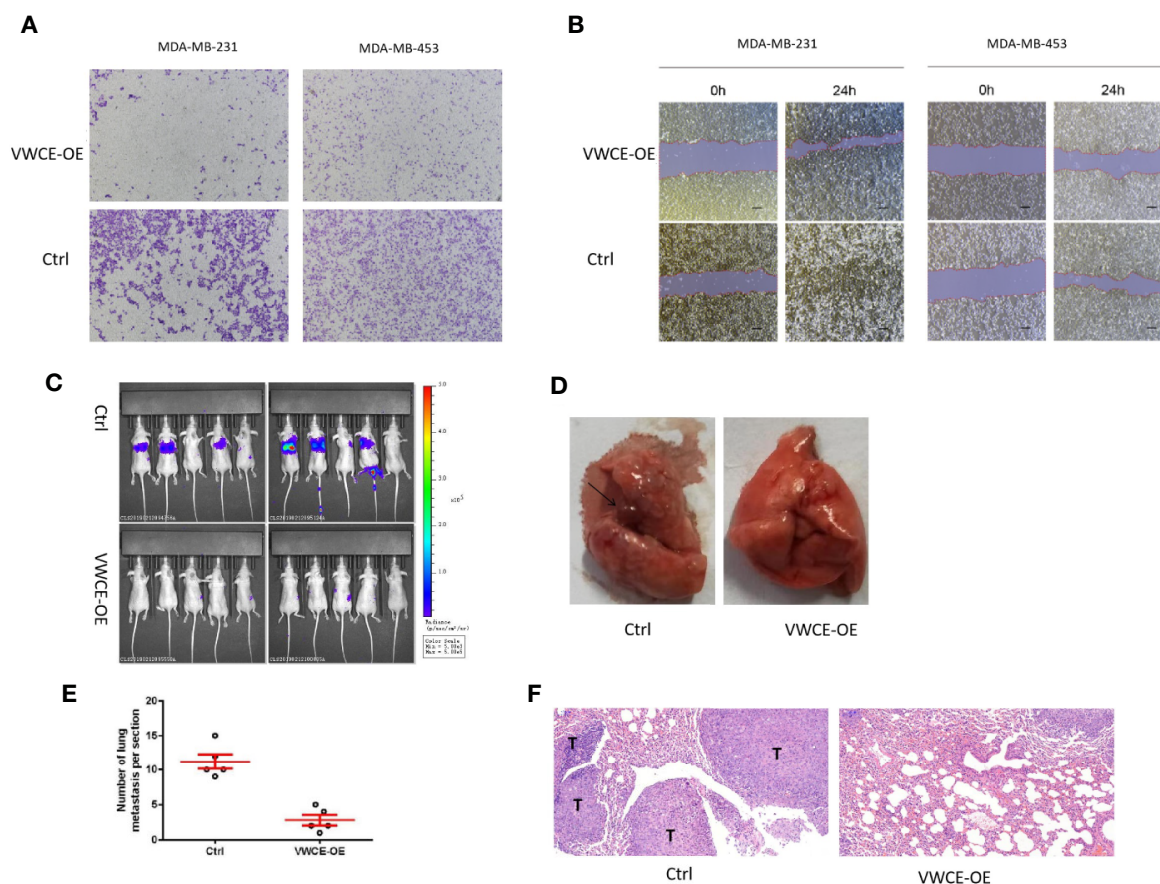


FIGURE 3 | Von Willebrand factor C and EGF domain (VWCE) inhibited the cell migration of breast cancer cells. **(A)** The invasion ability of MDA-MB-231 and MDA-MB-453 cells infected with either the VWCE-overexpression or vector control lentivirus detected by a transwell assay (scale bar = 100 μ m). **(B)** The impact of stably up-regulated VWCE expression on cellular invasion in MDA-MB-231 and MDA-MB-453 breast cancer cell lines by a wound healing assay. **(C)** *In vivo* imaging of the control and the VWCE-OE group in the metastatic model was created by tail vein injection. **(D)** The black arrows indicate lung metastatic lesions. **(E)** lung metastases were counted, quantification of lung metastasis in VWCE-overexpression mice compared to control mice. **(F)** Lung tissues were photographed, fixed, and stained with hematoxylin and eosin (H&E); scale bar: 100 μ m.

MDA-MB-453 cells with the concomitant highly significant upregulation of the epithelial marker, E-cadherin, in both the cell lines (**Figures 4A, B**). These results suggest an effective switch from the MET phenotype of breast cancer cells following VWCE overexpression. We also conducted an immunohistochemical analysis to study the *in vivo* effects of VWCE on MET in our

xenograft model (**Figure 4C**). Immunostaining for EMT markers confirmed the reversal of EMT by VWCE, in which VWCE-overexpression in the treated tumors had upregulated E-cadherin and decreased vimentin. These results suggest that VWCE overexpression reverses the EMT that occurs during lung metastasis of breast cancer *in vivo*.

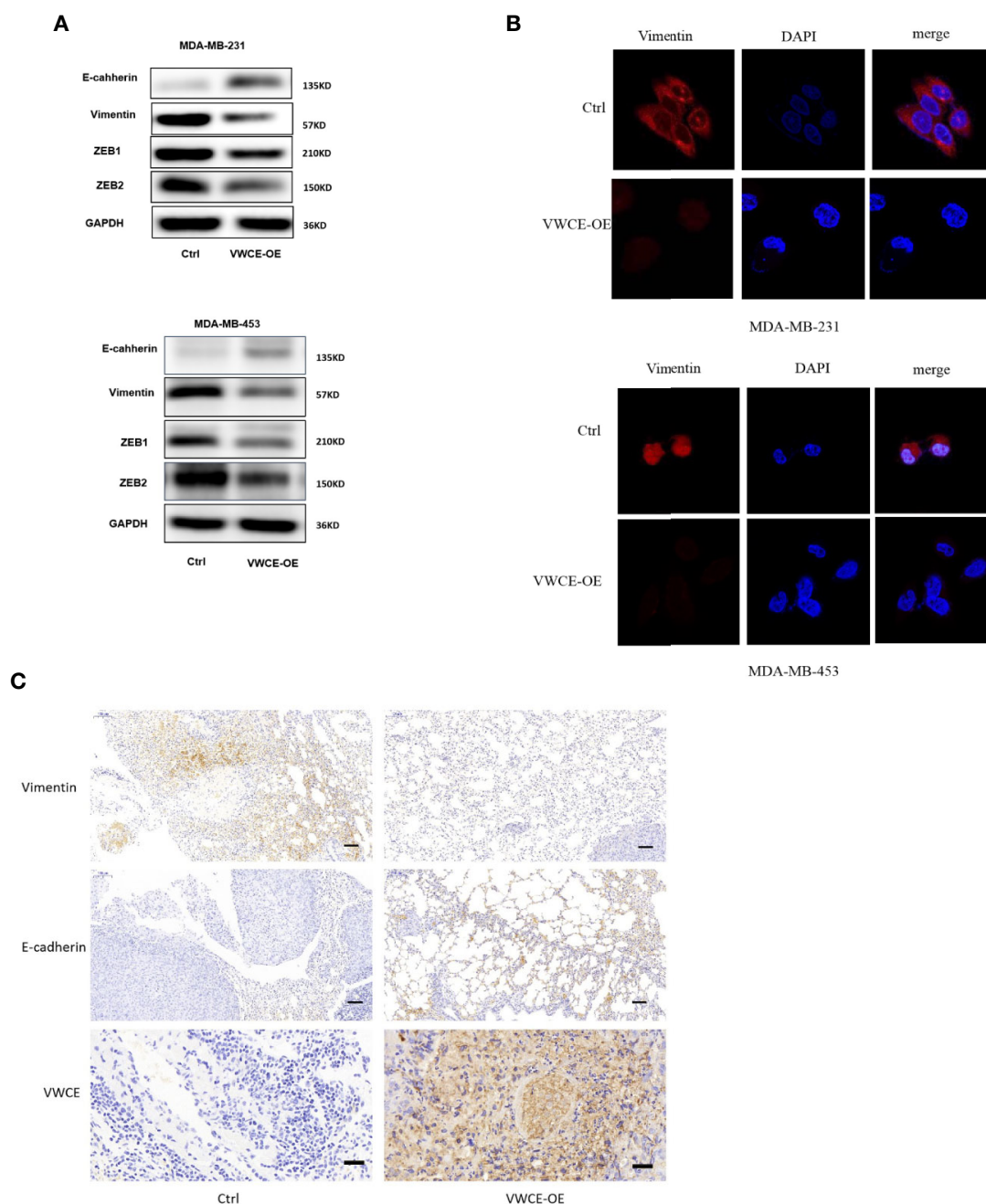


FIGURE 4 | Von Willebrand factor C and EGF domain (VWCE) causes the reversal of EMT to MET in aggressive breast cancer cells. **(A)** EMT molecule markers were determined by Western blot. **(B)** Vimentin expression were evaluated by immunofluorescence in MDA-MB-231 and MDA-MB-453 cells treated by VWCE-overexpression or a control vector.(scale bar =100 μ M) **(C)** Representative E-cadherin, vimentin, and VWCE expression in the lung metastases of a nude mouse model by immunohistochemistry (scale bar =100 μ M).

VWCE Overexpression Causes Cell Cycle Arrest at the G1 Phase and Inhibits Chemoresistance in Breast Cancer Cells

We used flow cytometry to evaluate whether VWCE regulates cell cycle progression in MDA-MB-231 cells treated with a control or VWCE-expressing vector. VWCE induced cell cycle arrest at the G0/G1 phase in MDA-MB-231 cells after 48 h of treatment (**Figure 5A**). The percentage of cells in the G0/G1 phase in the control and VWCE-expressing groups was 41%, and 54%, respectively (**Figure 5B**; $P < 0.01$). Overcoming resistance to chemotherapy is one of the fundamental issues affecting clinical treatment. Therefore, we examined the effect of VWCE on chemoresistance. We selected Docetaxel (DOC, taxus chemotherapy drug) to assess the chemoresistance of breast cancer cell lines by a colony formation assay. Compared with the control cells, the VWCE-OE cells exhibited lower cell viability under DOC treatment. In the colony formation assays, VWCE-OE cells exhibited a reduced capacity compared to the control cells to form colonies upon DOC treatment (**Figure 5C**). Finally, these results showed that the overexpression of VWCE inhibits chemoresistance.

Overexpression of WDR1 Partially Reverses the Tumor-Suppressor Role of VWCE in Breast Cancer Cells

In order to explore the possible mechanism of the function of VWCE in breast cancer, the total protein of two groups (MDA-MB-231-Control and MDA-MB-231-VWCE cells) was extracted for iTRAQ analysis to identify the VWCE of breast cancer cell lines. The differentially expressed protein (DEP) between the overexpression group and the control group. A total of 6163 proteins were detected using iTRAQ. Compared with the NC group, the expression levels of 101 proteins in the VWCE group were significantly different. The layered clustering heat map of differentially expressed proteins is shown in **Figure 6A**. The David database was used to classify the DEPs' identified biological processes (BP), cellular components (CC), and molecular functions (MF) (**Figure 6B**). In the BP category, protein phosphorylation/oxidation-reduction process/signal transduction/metabolic processes were over-represented. In the CC category, the nucleus/integral component of the membrane/membrane/intracellular were highlighted. In the MF category, protein binding/ATP binding/nucleic acid binding/zinc ion

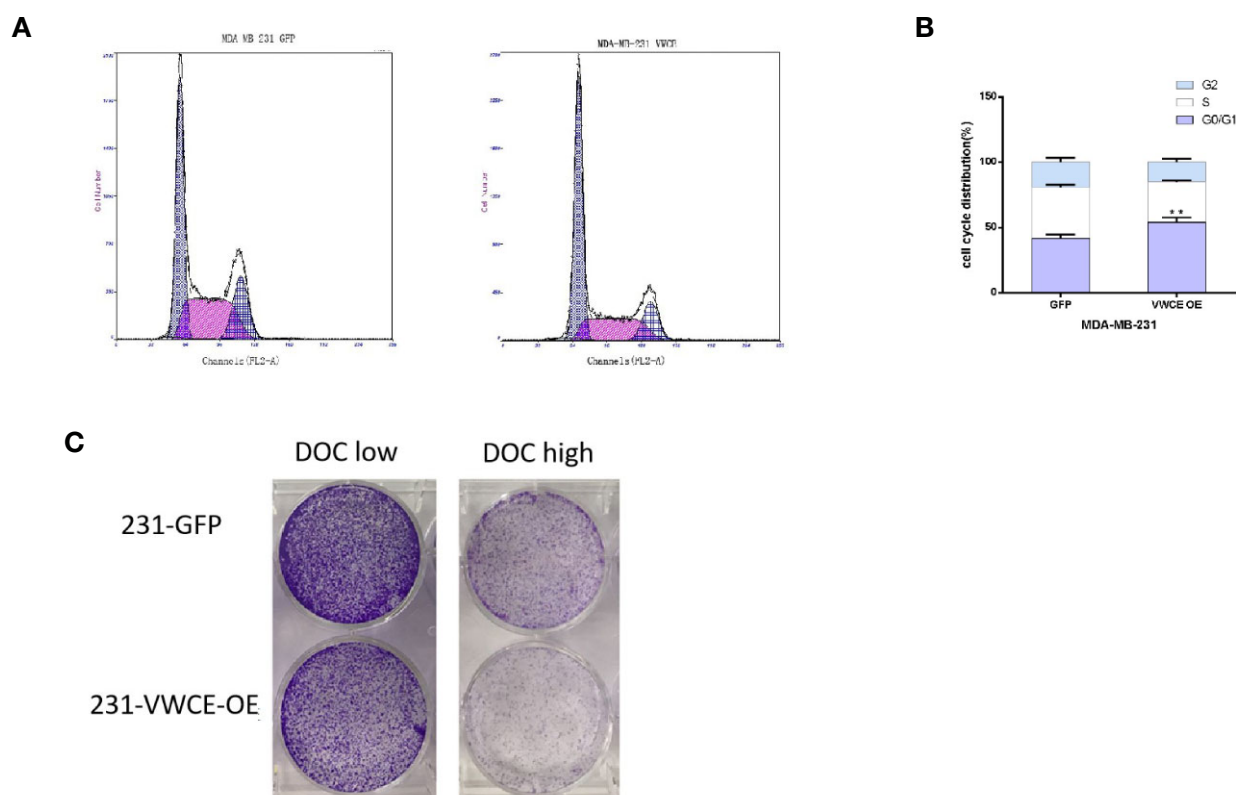


FIGURE 5 | Von Willebrand factor C and EGF domain (VWCE) causes cell cycle arrest at the G1 phase and inhibits chemoresistance in breast cancer cells. Overexpression of VWCE inhibits cell cycle progression in MD-MBA-231 cells. **(A, B)** Flow-cytometry analysis showed that the overexpression of VWCE significantly causes a G0/G1 phase cell cycle arrest in MD-MBA-231 cells. $^{**}P < 0.01$. **(C)** Clone formation in the control or over-expressing VWCE cells following treatment with DOC (2.5 nM) and DOC (5 nM) for five days.

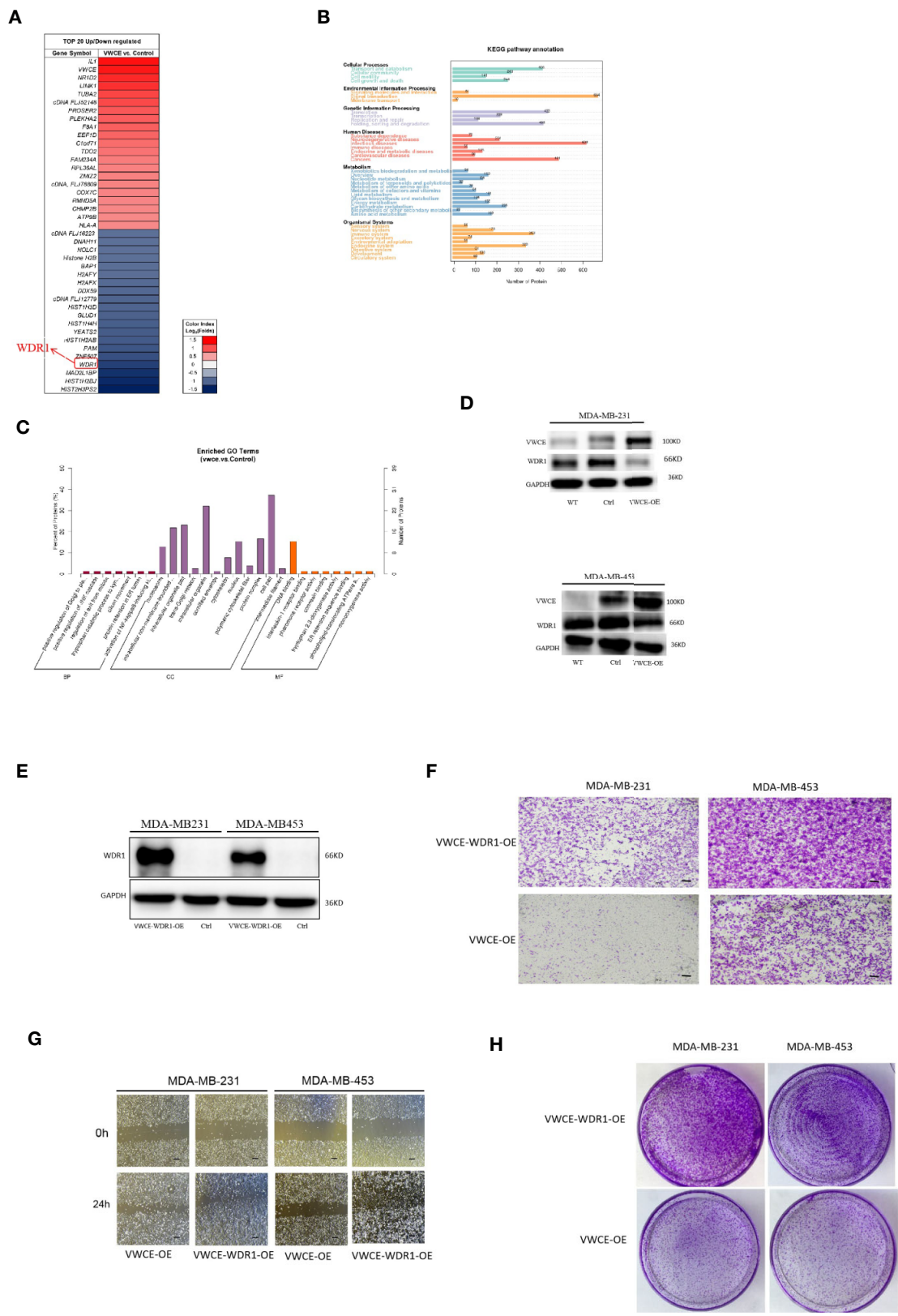


FIGURE 6 | Continued

FIGURE 6 | Overexpression of WDR1 partially reversed the tumor-suppressor role of Von Willebrand factor C and EGF domain (VWCE) in breast cancer cells. Identification of differentially-expressed proteins (DEPs) between VWCE overexpression and control groups using an iTRAQ-based proteomic analysis. **(A)** A heat map showing the DEPs between VWCE overexpression (231-VWCE) and control (231-Control) groups of breast cancer cell lines. Blue represents lower levels of protein expression and red represents higher levels of expression compared to the control. **(B)** A KEGG pathway analysis of the DEPs. **(C)** A GO analysis of the DEPs. **(D)** Relative expression of VWCE and WDR1 in MDA-MB-231 and MDA-MB-453 cell lines by Western blot. **(E)** Western blot analysis of WDR1 protein expression in MDA-MB-453-VWCE, and MDA-MB-231-VWCE cells were stably transfected with the WDR1-overexpressing or negative control lentiviruses. GAPDH was used as a loading control. **(F)** The impact of WDR1 overexpression on cell invasion in MDA-MB-453 and MDA-MB-231 cell lines using a transwell assay (scale bar = 100 μ M). **(G)** The impact of WDR1 overexpression on cell migration in MDA-MB-453 and MDA-MB-231 cell lines using a wound healing assay (scale bar = 100 μ M). **(H)** The impact of WDR1 overexpression on cellular proliferation in MDA-MB-453 and MDA-MB-231 cell lines using a plate cell colony formation assay.

binding were over-represented. In the analysis of the KEGG pathway, the top five pathways included signal transduction, infectious diseases, cancers, translation, as well as folding, sorting, and degradation, in which WDR1 was the prior participant without exception (**Figure 6C**). Consequently, based on the combined results of proteomics, GO, and KEGG pathway analyses, we selected WDR1 as the downstream target of VWCE for further validation with *in vitro* assays. To explore how VWCE and WDR1 influenced each other in breast cancer cells, a Western blot was performed. The results showed that the overexpression of VWCE decreased the level of WDR1 protein expression (**Figure 6D**). A WDR1-overexpressing lentivirus and the control virus were then transfected into VWCE-MDA-MB-453 and VWCE-MDA-MB-231 cells. The transfection efficacy was confirmed by a Western blot analysis (**Figure 6E**). We then carried out a transwell assay under VWCE and WDR1-overexpression. The results show that the mean cell number in the MDA-MB-231-VWCE-WDR1 group that moved to the lower chamber was significantly increased compared to the MDA-MB-231-VWCE group. Similarly, in the MDA-MB453-VWCE-WDR1 group, the mean number of cells that moved to the lower chamber was significantly increased compared to the MDA-MB453-VWCE group (**Figure 6F**). The wound healing assay revealed that the relative mobility from 0 h to 24 h in the OE-WDR1 group was increased in the MDA-MB-231 and MDA-MB453 cells lines (**Figure 6G**). The wound healing assay showed that the overexpression of WDR1 partially reversed the suppressive role of VWCE on tumor migration in MDA-MB-231 and MDA-MB-453 breast cancer cell lines. In the transwell assay, WDR1 overexpression partially reversed the suppressor role of VWCE on tumor invasion in the MDA-MB-231 and MDA-MB-453 breast cancer cell lines. In the colony formation assay, there was an increased number of cell colonies in the OE-WDR1 group in the presence of TMZ (**Figure 6H**). Thus, WDR1 overexpression partially reversed the tumor proliferation suppressor role of VWCE in the MDA-MB-231 and MDA-MB-453 breast cancer cell lines.

VWCE Expression Is Associated With Breast Cancer Clinicopathology and Survival

Next, the association between the level of VWCE expression and clinical characteristics was further assessed. A tissue microarray (TMA) for both an immunohistochemical and statistical analysis of the clinicopathological data for the 87 breast cancer patients included in the array indicated that the level of VWCE expression was significantly correlated with the histological

grade ($p < 0.001$) of the tumor, but not with the age of the patient or type of breast cancer (**Table 1**). Finally, according to the microarray data from 3,955 breast cancer patients, the results of the Kaplan-Meier Plotter analysis (www.kmplot.com) showed that a higher VWCE (242957_at) abundance correlated with a better overall survival (OS). A higher VWCE (242957_at) abundance was correlated with a better OS based on the microarray data from 360 triple negative breast cancer patients (**Figure 7A**). A higher VWCE (242957_at) abundance was also correlated with a better OS based on the microarray data from 970 breast cancer patients (**Figure 7B**). Based on these results, we concluded that the down-regulation of VWCE was associated with TNBC progression and may serve as a novel prognostic biomarker for TNBC.

DISCUSSION

Here, we found that normal breast tissue samples exhibited a higher level of VWCE expression than breast cancer tissues. For the first time, we have fully revealed the potential role of VWCE in breast cancer progression, and found that VWCE is associated with the inhibition of breast cancer metastasis (e.g., tumor cell growth, migration, invasion, and epithelial-interstitial transformation [EMT]). Moreover, VWCE inhibits the growth and migration of cancer cells by limiting the expression of WD-repeat domain 1 (WDR1). WDR1 is highly conserved across all eukaryotes, and has been shown to act together with ADF/cofilin

TABLE 1 | Association of VWCE protein expression and clinicopathologic characteristics.

Clinicopathologic variables	Number of cases	VWCE expression		p
		High	Low	
All cases	87	34	53	
Gender				
Female	87	34	53	
Age				
≤ 60	40	11	29	0.333
> 60	47	15	22	
Histopathological grade				
Low (G1+G2)	61	13	48	0.001
High (G3+G4)	26	21	5	
Histotypes				
Invasive ductal carcinoma	74	29	45	1.000
Invasive lobular carcinoma	13	5	8	

* $P < 0.05$ by χ^2 test.

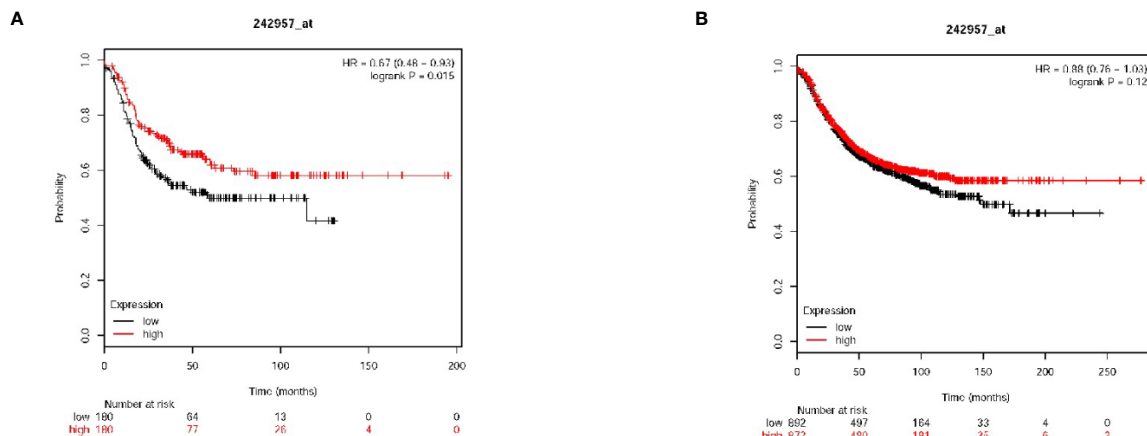


FIGURE 7 | Von Willebrand factor C and EGF domain (VWCE) expression is associated with breast cancer clinicopathology and survival. Kaplan-Meier survival plots demonstrating the good prognostic effect of VWCE overexpression in breast cancer patients. **(A)** Overall survival (OS) rate for triple negative breast cancer patients with low VWCE expression (n=180) compares to those with high VWCE expression (n=180), **(B)** OS rate for breast cancer patients with low VWCE expression (n=497) compares to those with high VWCE expression (n=480).

to promote actin dynamics in various actin-based processes, including cell migration and cytokinesis (23–25). Thus, our findings suggest that VWCE may be a novel tumor suppressor that limits breast cancer progression by regulating WDR1 expression.

The findings of this study show that VWCE is significantly downregulated in breast cancer. Importantly, VWCE expression was significantly associated with the OS of breast cancer patients. Together, these findings indicate that VWCE may represent a useful prognostic biomarker for breast cancer. Recently, the upregulation of VWCE has been found in prostate cancer (26); however, its biological role in breast cancer remains unknown. In the current study, we have demonstrated for the first time, that VWCE is down-regulated in breast cancer and inhibits the proliferation, migration, invasion and metastasis of breast cancer cells both *in vitro* and *in vivo*. Breast cancers differ somewhat from other cancers. VWCE is also called Upregulated gene 11 (URG11), a gene upregulated by Hepatitis B Virus X protein (HBx) (27). URG11 mRNA and protein were observed in HB x Ag-positive compared to HB x Ag-negative HepG2 cells (14). Antibodies to URG11 were detectable in serum samples from patients with HBV associated cirrhosis and HCC, but not in serum samples from uninfected individuals (28), but the reason is unclear. It suggests that this gene may be related to inflammation. Hepatocellular carcinoma, gastric cancer and lung cancer are all cancers related to inflammation, while breast cancer is not very related to inflammation. This means that the role of VWCE in breast cancer is different from that of other inflammation-related tumors. This indicates that VWCE plays a vital role in breast cancer.

Abnormal WDR1 expression has been reported to be associated with breast cancer metastasis (29). Moreover, a WDR1 deletion was found to result in defective E-cadherin distribution (30, 31). In these studies, WDR1 was identified as an oncogene for the development of oncogenic breast cancer. In

the present study, we demonstrated that VWCE down-regulates the expression of WDR1 using proteomic techniques. Importantly, the overexpression of WDR1 could effectively block the ability of VWCE to inhibit proliferation and metastasis. The findings of our study provide solid evidence that VWCE inhibits breast cancer proliferation and metastasis by targeting WDR1. We will further investigate the effect of VWCE on WDR1 in subsequent genetic studies.

The EMT process also plays an important role in both tumor cell metastasis and chemical resistance (32, 33). In addition, VWCE promotes tumor cell migration and invasion through EMT, as VWCE overexpression leads to decreased levels of N-cadherin, vimentin, and the EMT-induced transcription factor, ZEB1, as well as elevated E-cadherin levels, indicating a significant inhibition of EMT processes. WDR1 enhances the effect of MRTF-A-induced breast cancer cell migration by promoting the expression of EMT markers and migration markers by RhoA-MRTF (34). WDR1-mediated actin dynamics are required for membrane-associated adhesive junction remodeling in tumor cells. Based on the above results, VWCE appears to mediate WDR1-mediated disruption of actin dynamics, and cytoskeletal reorganization may be a target for tumor therapy intervention.

Notably, VWCE overexpression inhibited the proliferation and metastasis of mouse breast cancer cells, suggesting that VWCE is a potential therapeutic target for breast cancer. Interestingly, our mechanical and functional data allow us to better understand the functional role of WDR1 in human breast cancer. Moreover, its expression can positively regulate cellular proliferation, migration, invasion, and metastasis. In addition, WDR1, a direct functional target of VWCE in breast cancer, may represent an attractive therapeutic target since it can be precisely targeted with specific antibodies. The main hypothesis we can draw from this study is that an increased level of VWCE as a regulator of WDR1 may represent a therapeutic strategy for

breast cancer; however, this attractive assumption requires further validation in animal models.

In conclusion, this study found that VWCE is a potent tumor suppressor in breast cancer, and its growth inhibition is mediated in part by the expression of its downstream target gene, WDR1. Using cell culture and animal models, the functional characterization of the role of VWCE revealed that the loss of its expression is an important event in the progression of breast cancer.

DATA AVAILABILITY STATEMENT

The original contributions presented in the study are publicly available. This data can be found here: The ProteomeXchange Consortium (<http://proteomecentral.proteomexchange.org>) with the dataset identifier PXD021733.

ETHICS STATEMENT

The studies involving human participants were reviewed and approved by: Clinical research medical ethics committee of the First Affiliated Hospital of Shenzhen University. The patients/participants provided their written informed consent to

participate in this study. The animal study was reviewed and approved by Clinical research medical ethics committee of the First Affiliated Hospital of Shenzhen University.

AUTHOR CONTRIBUTIONS

NX designed the study. DZ performed most of the experiments. LW performed part of the experiments. WL made some suggestions and help on the study. DZ and LL analyzed the data. DZ prepared and wrote manuscript. SH and FY guided the preliminary experiments and revised the manuscript. All authors contributed to the article and approved the submitted version.

FUNDING

This project was supported by the Natural Science Foundation of National (81972003), the Natural Science Foundation of Guangdong (2016A030313029, 2017A030313668), the Sanming Project of Medicine in Shenzhen (SZSM201612031), and the Shenzhen Municipal Government of China (JCYJ20170817171808368, JCYJ20170818085657917, JCYJ20180507184647104, KQTD20170810160226082).

REFERENCES

- Bray F, Ferlay J, Soerjomataram I, Siegel RL, Torre LA, Jemal A. Global cancer statistics 2018: GLOBOCAN estimates of incidence and mortality worldwide for 36 cancers in 185 countries. *CA Cancer J Clin* (2018) 68:394–424. doi: 10.3322/caac.21492
- Kennecke H, Yerushalmi R, Woods R, Cheang MC, Voduc D, Speers CH, et al. Metastatic behavior of breast cancer subtypes. *J Clin Oncol* (2010) 28:3271–7. doi: 10.1200/JCO.2009.25.9820
- Chaffer CL, Weinberg RA. A perspective on cancer cell metastasis. *Science* (2011) 331:1559–64. doi: 10.1126/science.1203543
- Zhou YF, Eng ET, Zhu J, Lu C, Walz T, Springer TA. Sequence and structure relationships within von Willebrand factor. *Blood* (2012) 120:449–58. doi: 10.1182/blood-2012-01-405134
- Malukiewicz-Wisniewska G, Kotschy M. Von Willebrand factor in subretinal fluid. *Eur J Ophthalmol* (2001) 11:361–5. doi: 10.1177/112067210101100408
- Szpera-Gozdziewicz A, Majcherek M, Boruckiowski M, Gozdziwicz T, Dworacki G, Wicherek L, et al. Circulating endothelial cells, circulating endothelial progenitor cells, and von Willebrand factor in pregnancies complicated by hypertensive disorders. *Am J Reprod Immunol* (2017) 77. doi: 10.1111/aji.12625
- Sheldon TJ, Miguel-Aliaga I, Gould AP, Taylor WR, Conklin D. A novel family of single VWC-domain proteins in invertebrates. *FEBS Lett* (2007) 581:5268–74. doi: 10.1016/j.febslet.2007.10.016
- Kirschbaum M, Jenne CN, Veldhuis ZJ, Sjollem KA, Lenting PJ, Giepmans B, et al. Transient von Willebrand factor-mediated platelet influx stimulates liver regeneration after partial hepatectomy in mice. *Liver Int* (2017) 37:1731–7. doi: 10.1111/liv.13386
- Fiebig JE, Weidauer SE, Qiu LY, Bauer M, Schmieder P, Beerbaum M, et al. The clip-segment of the von Willebrand domain 1 of the BMP modulator protein Crossveinless 2 is preformed. *MOLECULES* (2013) 18:11658–82. doi: 10.3390/molecules181011658
- Zhang JL, Huang Y, Qiu LY, Nickel J, Sebald W. von Willebrand factor type C domain-containing proteins regulate bone morphogenetic protein signaling through different recognition mechanisms. *J Biol Chem* (2007) 282:20002–14. doi: 10.1074/jbc.M700456200
- Chapellier M, Maguer-Satta V. BMP2, a key to uncover luminal breast cancer origin linked to pollutant effects on epithelial stem cells niche. *Mol Cell Oncol* (2016) 3:e1026527. doi: 10.1080/23723556.2015.1026527
- Bosukonda A, Carlson WD. Harnessing the BMP signaling pathway to control the formation of cancer stem cells by effects on epithelial-to-mesenchymal transition. *Biochem Soc Trans* (2017) 45:223–8. doi: 10.1042/BST20160177
- Fan R, Li X, Du W, Zou X, Du R, Zhao L, et al. Adenoviral-mediated RNA interference targeting URG11 inhibits growth of human hepatocellular carcinoma. *Int J Cancer* (2011) 128:2980–93. doi: 10.1002/ijc.25624
- Lian Z, Liu J, Li L, Li X, Tufan NL, Clayton M, et al. Upregulated expression of a unique gene by hepatitis B x antigen promotes hepatocellular growth and tumorigenesis. *Neoplasia* (2003) 5:229–44. doi: 10.1016/S1476-5586(03)80055-6
- Tong GD, Zhang X, Zhou DQ, Wei CS, He JS, Xiao CL, et al. Efficacy of early treatment on 52 patients with preneoplastic hepatitis B virus-associated hepatocellular carcinoma by compound Phyllanthus Urinaria L. *Chin J Integr Med* (2014) 20:263–71. doi: 10.1007/s11655-013-1320-7
- Peng W, Zhang J, Liu J. URG11 predicts poor prognosis of pancreatic cancer by enhancing epithelial-mesenchymal transition-driven invasion. *Med Oncol* (2014) 31:64. doi: 10.1007/s12032-014-0064-y
- Du R, Xia L, Sun S, Lian Z, Zou X, Gao J, et al. URG11 promotes gastric cancer growth and invasion by activation of beta-catenin signalling pathway. *J Cell Mol Med* (2010) 14:621–35. doi: 10.1111/j.1582-4934.2008.00622.x
- Liu ZL, Wu J, Wang LX, Yang JF, Xiao GM, Sun HP, et al. Knockdown of Upregulated Gene 11 (URG11) Inhibits Proliferation, Invasion, and beta-Catenin Expression in Non-Small Cell Lung Cancer Cells. *Oncol Res* (2016) 24:197–204. doi: 10.3727/096504016X14648701447850
- Florrell SR, Coffin CM, Holden JA, Zimmermann JW, Gerwels JW, Summers BK, et al. Preservation of RNA for functional genomic studies: a multidisciplinary tumor bank protocol. *Mod Pathol* (2001) 14:116–28. doi: 10.1038/modpathol.3880267

20. Sharma C, Wang HX, Li Q, Knoblich K, Reisenbichler ES, Richardson AL, et al. Protein Acyltransferase DHHC3 Regulates Breast Tumor Growth, Oxidative Stress, and Senescence. *Cancer Res* (2017) 77:6880–90. doi: 10.1158/0008-5472.CAN-17-1536
21. Zhang F, Zhang H, Wang Z, Yu M, Tian R, Ji W, et al. P-glycoprotein associates with Anxa2 and promotes invasion in multidrug resistant breast cancer cells. *Biochem Pharmacol* (2014) 87:292–302. doi: 10.1016/j.bcp.2013.11.003
22. Yan M, Wang J, Ren Y, Li L, He W, Zhang Y, et al. Over-expression of FSIP1 promotes breast cancer progression and confers resistance to docetaxel via MRP1 stabilization. *Cell Death Dis* (2019) 10:204. doi: 10.1038/s41419-018-1248-8
23. Bamburg JR. Proteins of the ADF/cofilin family: essential regulators of actin dynamics. *Annu Rev Cell Dev Biol* (1999) 15:185–230. doi: 10.1146/annurev.cellbio.15.1.185
24. Ono S. Regulation of actin filament dynamics by actin depolymerizing factor/cofilin and actin-interacting protein 1: new blades for twisted filaments. *Biochemistry-US* (2003) 42:13363–70. doi: 10.1021/bi034600x
25. Okada K, Blanchoin L, Abe H, Chen H, Pollard TD, Bamburg JR. Xenopus actin-interacting protein 1 (XAip1) enhances cofilin fragmentation of filaments by capping filament ends. *J Biol Chem* (2002) 277:43011–6. doi: 10.1074/jbc.M203111200
26. Sun C, Zhang G, Cheng S, Qian H, Li D, Liu M. URG11 promotes proliferation and induced apoptosis of LNCaP cells. *Int J Mol Med* (2019) 43:2075–85. doi: 10.3892/ijmm.2019.4121
27. Lian Z, Liu J, Li L, Li X, Clayton M, Wu MC, et al. Enhanced cell survival of Hep3B cells by the hepatitis B x antigen effector, URG11, is associated with upregulation of beta-catenin. *Hepatology* (2006) 43:415–24. doi: 10.1002/hep.21053
28. Tong GD, Zhou DQ, He JS, Xiao CL, Liu XL, Zhou XZ, et al. Preneoplastic markers of hepatitis B virus-associated hepatocellular carcinoma and their significance in clinical settings. *Zhonghua Gan Zang Bing Za Zhi* (2007) 15:828–32.
29. Lee JH, Kim JE, Kim BG, Han HH, Kang S, Cho NH. STAT3-induced WDR1 overexpression promotes breast cancer cell migration. *Cell Signal* (2016) 28:1753–60. doi: 10.1016/j.cellsig.2016.08.006
30. Xu J, Wan P, Wang M, Zhang J, Gao X, Hu B, et al. AIP1-mediated actin disassembly is required for postnatal germ cell migration and spermatogonial stem cell niche establishment. *Cell Death Dis* (2015) 6:e1818. doi: 10.1038/cddis.2015.182
31. Chu D, Pan H, Wan P, Wu J, Luo J, Zhu H, et al. AIP1 acts with cofilin to control actin dynamics during epithelial morphogenesis. *Development* (2012) 139:3561–71. doi: 10.1242/dev.079491
32. Morris HT, Machesky LM. Actin cytoskeletal control during epithelial to mesenchymal transition: focus on the pancreas and intestinal tract. *Br J Cancer* (2015) 112:613–20. doi: 10.1038/bjc.2014.658
33. Fischer KR, Durrans A, Lee S, Sheng J, Li F, Wong ST, et al. Epithelial-to-mesenchymal transition is not required for lung metastasis but contributes to chemoresistance. *NATURE* (2015) 527:472–6. doi: 10.1038/nature15748
34. Xiang Y, Liao XH, Yao A, Qin H, Fan LJ, Li JP, et al. MRTF-A-miR-206-WDR1 form feedback loop to regulate breast cancer cell migration. *Exp Cell Res* (2017) 359:394–404. doi: 10.1016/j.yexcr.2017.08.023

Conflict of Interest: The authors declare that the research was conducted in the absence of any commercial or financial relationships that could be construed as a potential conflict of interest.

Copyright © 2020 Zhang, Wan, Yang, Liu, Liu, He and Xie. This is an open-access article distributed under the terms of the Creative Commons Attribution License (CC BY). The use, distribution or reproduction in other forums is permitted, provided the original author(s) and the copyright owner(s) are credited and that the original publication in this journal is cited, in accordance with accepted academic practice. No use, distribution or reproduction is permitted which does not comply with these terms.



The Role of Autophagy in Gastric Cancer Chemoresistance: Friend or Foe?

Jing-Li Xu^{1,2,3†}, Li Yuan^{1,2,3†}, Yan-Cheng Tang^{4†}, Zhi-Yuan Xu^{1,2}, Han-Dong Xu^{1,2,3}, Xiang-Dong Cheng^{1,2*} and Jiang-Jiang Qin^{1,2*}

¹ Institute of Cancer and Basic Medicine, Chinese Academy of Sciences, Hangzhou, China, ² Cancer Hospital of the University of Chinese Academy of Sciences, Zhejiang Cancer Hospital, Hangzhou, China, ³ The First Clinical Medical College of Zhejiang Chinese Medical University, Hangzhou, China, ⁴ School of Chinese Medicine, Hong Kong Baptist University, Kowloon Tsai, Hong Kong, China

OPEN ACCESS

Edited by:

Wei Zhao,
Chengdu Medical College, China

Reviewed by:

Jing Zhou,
Guangxi Medical University, China
Chuanbin Yang,
Jinan University, China

*Correspondence:

Xiang-Dong Cheng
chengxd516@126.com
Jiang-Jiang Qin
zylysitu@hotmail.com

[†] These authors have contributed
equally to this work

Specialty section:

This article was submitted to
Molecular and Cellular Oncology,
a section of the journal
Frontiers in Cell and Developmental
Biology

Received: 26 October 2020

Accepted: 12 November 2020

Published: 03 December 2020

Citation:

Xu J-L, Yuan L, Tang Y-C, Xu Z-Y,
Xu H-D, Cheng X-D and Qin J-J
(2020) The Role of Autophagy
in Gastric Cancer Chemoresistance:
Friend or Foe?
Front. Cell Dev. Biol. 8:621428.
doi: 10.3389/fcell.2020.621428

Gastric cancer is the third most common cause of cancer-related death worldwide. Drug resistance is the main inevitable and vital factor leading to a low 5-year survival rate for patients with gastric cancer. Autophagy, as a highly conserved homeostatic pathway, is mainly regulated by different proteins and non-coding RNAs (ncRNAs) and plays dual roles in drug resistance of gastric cancer. Thus, targeting key regulatory nodes in the process of autophagy by small molecule inhibitors or activators has become one of the most promising strategies for the treatment of gastric cancer in recent years. In this review, we provide a systematic summary focusing on the relationship between autophagy and chemotherapy resistance in gastric cancer. We comprehensively discuss the roles and molecular mechanisms of multiple proteins and the emerging ncRNAs including miRNAs and lncRNAs in the regulation of autophagy pathways and gastric cancer chemoresistance. We also summarize the regulatory effects of autophagy inhibitor and activators on gastric cancer chemoresistance. Understanding the vital roles of autophagy in gastric cancer chemoresistance will provide novel opportunities to develop promising therapeutic strategies for gastric cancer.

Keywords: gastric cancer, autophagy, chemoresistance, ncRNAs, natural products, inhibitor and activator

INTRODUCTION

Gastric cancer is one of the most common gastrointestinal tumors in the world, with more than one million new cases every year, and remains the third leading cause of cancer-related deaths (Fitzmaurice et al., 2019; Thrift and El-Serag, 2019). For patients with early gastric cancer, surgical resection is the best treatment option. However, more than 60% of patients have developed local or distant metastasis at diagnosis, which causes that most of the patients do not have the opportunity to receive surgical treatment (Yuan et al., 2020). Hence, chemotherapy-based comprehensive treatment is the main choice for most patients with middle- and late-stage gastric cancer (Zhang et al., 2020). However, poor or even no response to chemotherapy is frequently observed in the treatment of gastric cancer patients due to the intrinsic or acquired drug resistance, which becomes the most detrimental cause of treatment failure and low survival rate (Biagioni et al., 2019).

Autophagy, as a major intracellular degradation system in eukaryotic cells that degrades and clears defective or aging organelles, can be divided into three major forms according to the

different mechanisms of clearing intracellular components: macroautophagy, microautophagy, and chaperone-mediated autophagy (Galluzzi and Green, 2019). Among them, macroautophagy (hereafter autophagy) is the most common and intensively studied form (Amaravadi et al., 2019; Abdrakhmanov et al., 2020). Previous studies have shown that autophagy plays a double-edged sword role at different stages of tumorigenesis. At the early stage, autophagy plays a “tumor-suppressor” function, which can stabilize the genome, protect the damaged tissues and cells, and suppress tumor occurrence, proliferation, invasion, and metastasis (Høyer-Hansen and Jäättelä, 2008). On the contrary, once the tumor is formed, autophagy plays an oncogenic function that provides cancer cells with needed survival contexts, such as nutrition to resist stress (especially after chemotherapy treatment) (Kimmelman and White, 2017). The specific roles of autophagy in tumors depend on tumor type and tumor heterogeneity, which is regulated by multiple proteins and non-coding RNAs (ncRNAs) (Jiang et al., 2020; Perez-Montoyo, 2020).

Traditional medicine (TM) has been widely used in China, South Korea, and Japan for thousands of years to treat various diseases, usually in the form of decoctions with 2–15 kinds of herbs (Qin et al., 2017; Hempen and Hummelsberger, 2020). Numerous TM decoctions or natural products derived from medical herbs have been proven to have anticancer activities (Li et al., 2013; Qin et al., 2013; Yang et al., 2019; Yuan et al., 2019). Also, dietary natural products have been shown to regulate autophagy and thus enhance the chemosensitivity of cancer cells (Emanuele et al., 2018; Dutta et al., 2019). Some antibiotics, anti-inflammatory drugs, anesthetics, etc. have been shown to regulate autophagy to exert anticancer effects (Zhu et al., 2013; Jiang et al., 2019; Moon et al., 2019; Petroni et al., 2020).

The roles of autophagy in gastric cancer progression, metastasis, and prognosis have been extensively discussed in several recent reviews (Qian and Yang, 2016; Cao et al., 2019; Zhang F. et al., 2019). Herein, we provide a review focusing on the relationship between autophagy and chemotherapy resistance in gastric cancer. We comprehensively discuss the roles and molecular mechanisms of multiple proteins and newly identified ncRNAs including miRNAs and long non-coding RNAs (lncRNAs) in autophagy and gastric cancer chemotherapy resistance, as well as their potential as therapeutic targets for gastric cancer precise medicine. We also summarize the natural products and other drugs that exhibit regulatory effects on autophagy and chemotherapy resistance. Summarizing the process of autophagy in detail and classifying the different roles of autophagy in gastric chemoresistance will provide a comprehensive understanding of autophagy and develop promising therapeutic strategies for gastric cancer.

OVERVIEW OF AUTOPHAGY

Autophagy is a common, complex, physiological and pathological, and highly conserved self-metabolic process (Galluzzi and Green, 2019). During certain extreme conditions like starvation, hypoxia, or other environmental stresses,

autophagy is also an indispensable process to provide energy for cell regeneration and cell survival, which functions as a cytoprotective mechanism. However, autophagic cell death, also called type II-programmed cell death, may be accompanied by excessive autophagy (Qi et al., 2020). Here, we summarize the latest updates on the process and related signaling pathways of autophagy.

Process of Autophagy

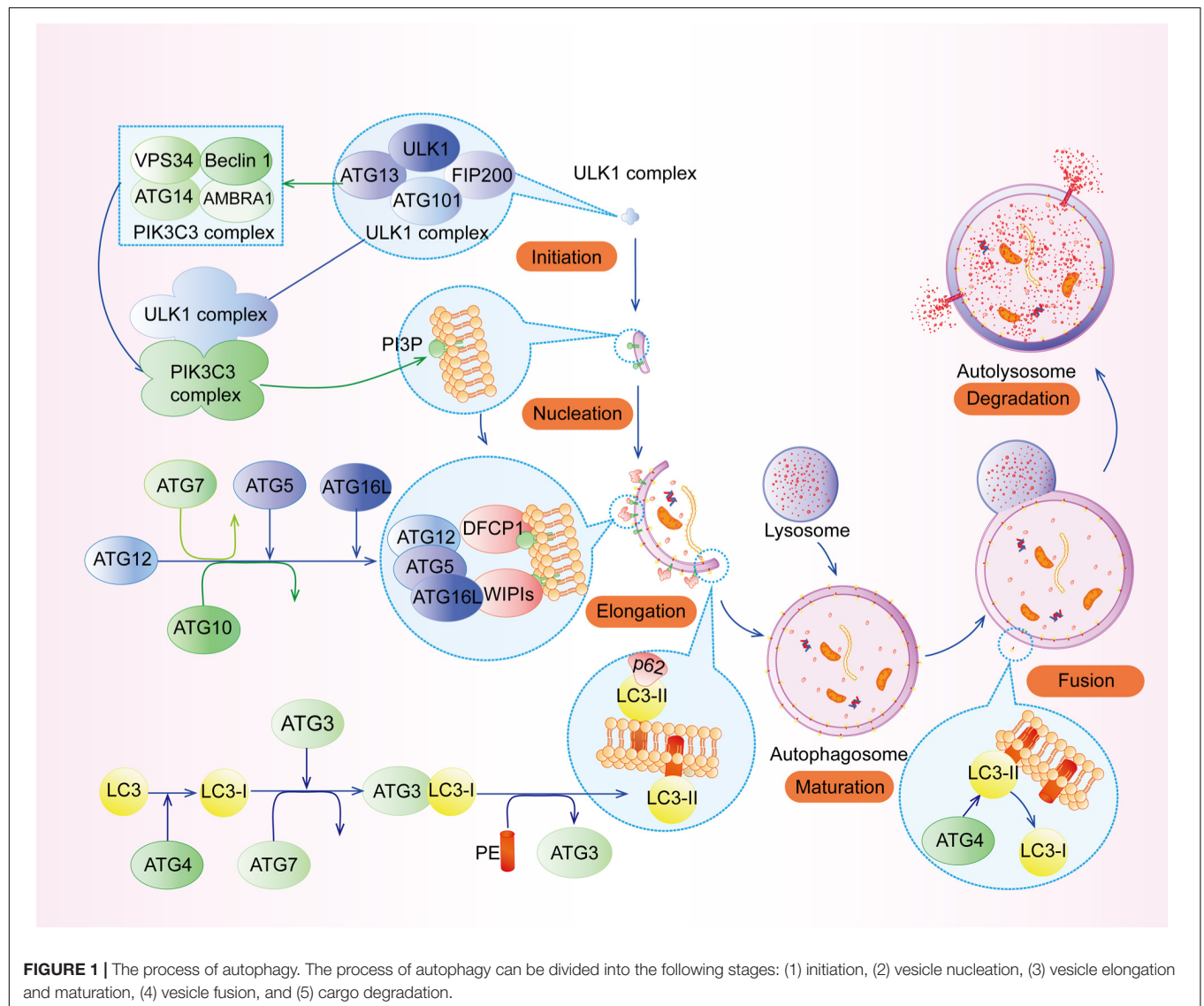
The process of autophagy can be divided into the following stages (**Figure 1**): (1) initiation, (2) vesicle nucleation, (3) vesicle elongation and maturation, (4) vesicle fusion, and (5) cargo degradation (Levy et al., 2017). Each stage of autophagy is regulated by a variety of autophagy-related genes (ATGs) such as ATG5, ATG7, ATG12, ATG16L1, and their complexes, etc. (Levine and Kroemer, 2019).

Initiation and Nucleation

Upon nutrient deficiency, hypoxia, and inflammation, autophagy is initiated by the unc-51-like kinase 1 (ULK1) complex (**Figure 2A**), composing of ULK1, FIP200 (FAK family kinase-interacting protein of 200 kDa, also known as ATG17), ATG13, and ATG101. Specifically, the intrinsically disordered region (IDR) of ATG13 interacts with ULK1 and FIP200 to form a pre-autophagosomal structure (PAS) (Hollenstein and Kraft, 2020), while its HORMA (Hop1, Rev7, and MAD2) domain forms a dimer with ATG101's HORMA domain (Kim B. W. et al., 2018). In addition, the N-terminal 640 residues (NTD) of FIP200, shaping like a letter C with the presence of ATG13, has an intimate interaction with C-terminal IDR of ATG13 and C-terminal early autophagy targeting/tethering (EAT) domain of ULK1, ensuring the successful initiation of autophagy (Shi et al., 2020). Following the activation of ULK1 complex, the class III phosphatidylinositol 3-kinase (PI3KC3) complex, which consists of vacuolar protein sorting 34 (VPS34, also known as PI3KC3), ATG14, the activating molecule in BECN1-regulated autophagy protein 1 (AMBRA1), and the scaffold protein Beclin-1, generates phosphatidylinositol 3-phosphate (PI3P) at an endoplasmic reticulum (ER) subdomain named omegasome (Young et al., 2019; Sanchez-Martin et al., 2020). Subsequently, PI3P recruits certain effector proteins, including WIPIs (WD repeat domain phosphoinositide-interacting proteins) (**Figure 2B**), which can bind ATG16L1 (Bakula et al., 2017).

Elongation and Maturation

ATG5-ATG12 complex interacts with ATG16L1 to form the ATG12-ATG5-ATG16L1 complex, the crucial element for autophagosome elongation (Lystad et al., 2019). ATG12-ATG5-ATG16L1 complex cooperating with ATG7 and ATG3 recruits LC3 (microtubule-associated protein 1 light chain 3 alpha) to lipid phosphatidylethanolamine (PE) (Lystad et al., 2019). This type of LC3 is called LC3-II, which can elongate and close membranes in the outer surfaces of the autophagosome membrane and bind with cargo receptors such as p62 to select proteins or organelles (Zhang X. et al., 2019). In addition, recent studies have highlighted that TRAPP III-specific proteins (TRAPPC11) are necessary for the close of isolation membranes



and recruitment of WIPI4-ATG2 to isolation membranes with the presence of ATG9, perhaps due to its carboxy-terminus, while TRAPPC12 is downstream of TRAPPC11 (Stanga et al., 2019). Interestingly, Guardia et al. (2020) have found that ATG9A (human ATG9), a homotrimer with four transmembrane helices, interacts with ATG2 at C-terminal platform domain of ATG9A (1-723 construct and 1-522 construct) to transfer lipids from ATG2 to ATG9A, and then ATG9A can induce the autophagosome membrane curvature for the further processes of autophagy.

Fusion and Degradation

After the formation and maturation of the autophagosome, most of the proteins in the outer membrane are dissociated, including ATG proteins. Then, the autophagosome fuses with the lysosome (Figure 2C) to form autolysosome in the perinuclear region (Lőrincz and Juhász, 2020). In this special area, SNAREs (soluble N-ethylmaleimide-sensitive factor attachment protein

receptors), Syntaxin17, and SNAP29 located at autolysosome and VAMP8 located at lysosome play indispensable roles in this process (Diao et al., 2015). The localization of Syntaxin17-SNAP29 complex is regulated by vesicle-associated membrane protein 2 (LAMP2), while localization of Syntaxin17 is also regulated by LC3 due to its LC3-interacting region (LIR) (Corona and Jackson, 2018). However, recent research has found that LAMP2 can regulate this fusion without the function of Syntaxin17 in human cardiomyocytes (Chi et al., 2019). There are many other regulators of autolysosome fusion, including RAB7, NRBF2, PLEKHM1, TECPR1, RUFY4, and so on (Reggiori and Ungermann, 2017; Cai et al., 2020). At the same time, LC3-II located on outer surfaces of the membrane can be disconnected from PE by ATG4 for recycling, but internal LC3-II is degraded with cargoes and p62 by lysosomal enzymes (Nakayama et al., 2017). Finally, products of decomposition can be recycled and provided for cell growth.

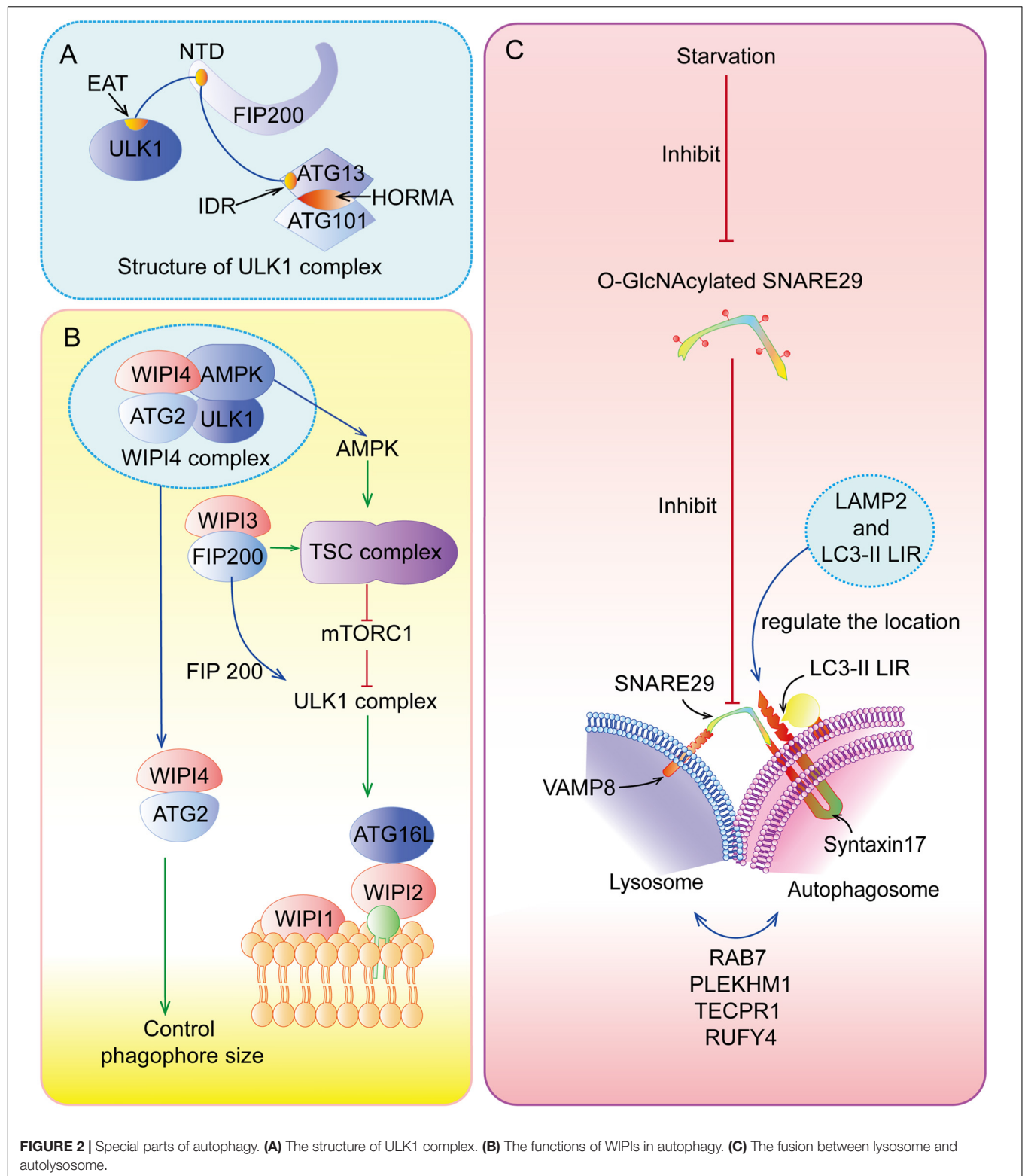


FIGURE 2 | Special parts of autophagy. **(A)** The structure of ULK1 complex. **(B)** The functions of WIPIs in autophagy. **(C)** The fusion between lysosome and autolysosome.

Signal Pathways Regulating Autophagy

Mammalian target of rapamycin (mTOR) complex 1 (mTORC1, made up of mTOR, Raptor, Deptor, mLST8, and PRAS40) and mTOR complex 2 (mTORC2, composed of mTOR, Rictor,

Deptor, mLST8, Sin1, and PRA5/Protor-1) have a common central kinase, mTOR, a conserved serine/threonine protein kinase, which plays important roles in multiple biological processes involving in cell growth, such as regulating autophagy

(Murugan, 2019). Previous studies have shown that multiple signaling pathways, such as PI3K/AKT, MAPK (mitogen activated kinase-like protein), AMPK (protein kinase AMP-activated catalytic subunit alpha 1, also known as PRKAA1) (Figure 3), p53, and PTEN (phosphatase and tensin homolog) pathways, can regulate mTORC1 and autophagy (Figure 4).

PI3K/AKT Pathway

The pro-oncogenic class-I PI3K (PI3KC1) can catalyze the phosphorylation of phosphatidylinositol-4,5-bisphosphate (PI-4,5-P₂) into phosphatidylinositol-3,4,5-trisphosphate (PIP₃), which binds both AKT and phosphoinositide-dependent protein kinase 1 (PDK1), resulting in the AKT phosphorylation at Thr308 by PDK1 (Parikh et al., 2012). The complete activation of AKT, in turn, activates its downstream mTORC1, contributing to the suppression of autophagy (Figure 3). In addition, phosphorylated AKT can phosphorylate the Ser939 and Thr1462 residues of TSC2 to block the formation of TSC1 (TSC complex subunit 1)/TSC2 complex, an inhibitor of Ras homolog enriched in the brain (Rheb). TSC1/TSC2 complex acts as a guanosine triphosphatase (GTPase)-activating protein (GAP), which can promote Rheb-GTP into Rheb-GDP; the former can activate mTORC1 while the latter cannot (Fawal et al., 2015; Yu et al., 2017). Besides, AKT can also be phosphorylated by mTORC2 at Ser473 and then the activated AKT promotes its downstream regulator, causing the inhibition of autophagy (Li et al., 2018).

MAPK Pathway

MAPKs play indispensable roles in many cellular processes, including cell growth, proliferation as well as autophagy (Anerillas et al., 2020). There are many subtypes of MAPKs whose upstream regulators are different, including mitogen-activated protein 3 kinases (MAPKKKs) and mitogen-activated protein 2 kinases (MAPKKs) (Gomez-Osuna et al., 2020). c-Jun N-terminal kinase (JNK) and extracellular signal-regulated kinase (ERK) are two classical and important types of MAPKs (Anerillas et al., 2020). Under various stresses (Figure 3), JNK can phosphorylate and activate BCL-2, leading to the dissociation of Beclin-1, a crucial member of PI3KC3, from BCL-2 and the subsequent induction of autophagy (Fan et al., 2016; Cheng et al., 2019). On one hand, the activated ERK1 and ERK2 can induce autophagy through Ras-Raf (MAPKKK)-MEK (MAPKK)-ERK signal pathway (Panda et al., 2015). On the other hand, the phosphorylated ERK1/2 can block the TSC1/TSC2 complex, leading to the increased expression of Rheb-GTPase to induce mTORC1, which can result in the inhibition of autophagy (Pattingre et al., 2003; Ranek et al., 2019).

AMPK Pathway

AMPK pathway is a key pathway to preserve energy balance and coordinate metabolism in eukaryotic cells, which is extensively involved in the regulation of autophagy, apoptosis, epithelial-mesenchymal transition (EMT), etc. (Carling, 2017; Zhang et al., 2018). Under the depletion of nutrients and energy with the increasing AMP/ATP ratio, LKB1 (liver kinase B1), a tumor suppressor kinase, stimulates the activation of AMPK, which subsequently promotes the formation of TSC1/TSC2 complex to

inactivate mTORC1 and induce autophagy (Figure 3) (Bakula et al., 2017). Moreover, AMPK can inhibit mTORC1 by directly phosphorylating Raptor (Barroso-Chinea et al., 2020). Under the undernourished condition, AMPK can directly phosphorylate ULK1 at Ser317, S467, S555, S574, S637, and Ser777 by separating mTORC1 from ULK1 and stimulate autophagy (Zachari and Ganley, 2017), whereas mTORC1 can block the function of AMPK by phosphorylating ULK1 under the glucose abundant condition (Mao and Klionsky, 2011).

p53 Pathway

The p53 tumor suppressor participates in multiple cellular biological processes, including cell cycle arrest, apoptosis, senescence, proliferation, DNA repair, and autophagy (Qin et al., 2018; Hafner et al., 2019). However, the mechanisms of nuclear p53 and cytoplasmic p53 are different. With the expression of nuclear p53 stimulated by starvation conditions, the activated AMPK induces autophagy through the TSC1/TSC2 complex and mTOR pathway (Figure 4) (Hu et al., 2019; Gao et al., 2020). Chollat-Namy et al. (2019) have found that p53 upregulates the expression of its downstream targets Sestrin-1 and Sestrin-2, which further activate AMPK through phosphorylating AMPK at Thr172, subsequently leading to the dephosphorylation of mTORC1 at S2448 and the induction of autophagy. Damage-regulated autophagy modulator (DRAM) and death-associated protein kinase 1 (DAPK1) are other important downstream targets of p53 and have been reported to induce autophagy (Crichton et al., 2006; Zhou et al., 2016; Hu et al., 2019). At the same time, the activated DAPK1 can, in turn, stimulate and stabilize p53, forming a positive feedback loop (Hu et al., 2019). In contrast, cytoplasmic p53 inhibits autophagy through blocking AMPK, TIGAR (TP53-induced glycolysis and apoptosis regulator), and Beclin-1, whose underlying mechanisms need to be further studied (Mrakovcic and Fröhlich, 2018).

PTEN Pathway

The tumor suppressor PTEN has been found to act as a negative endogenous regulator of the PI3K/AKT pathway, which can hydrolyze PIP₃ back to PIP₂, resulting in the induction of autophagy (Figure 4) (Sun et al., 1999; Gao et al., 2018). It has also been reported that PTEN can play the role of autophagy catalysator through the AKT/mTOR pathway (Chen et al., 2015; Gao et al., 2018). PTEN regulates autophagy in PTEN/AKT/FOXO3a/ATG7 axis in non-small-cell lung cancer (NSCLC) cells, independent of mTOR and Beclin-1 (Cai et al., 2018). Specifically, the overexpression of PTEN inhibits AKT activity, which leads to the increased ATG7 expression through FOXO3a (Cai et al., 2018). Chen et al. (2015) have found that the phosphorylation of PTEN at Ser113 makes PTEN located in the nucleus, resulting in the activation of the MAPK8/JNK1-MAPK9/JNK2-sestrin2-AMPK pathway to facilitate autophagy. Furthermore, upon mitochondria damage, the accumulated PINK1 (PTEN induced putative kinase 1) can induce autophagy by blocking the release of cytochrome c, which needs further investigations (Boosani et al., 2019).

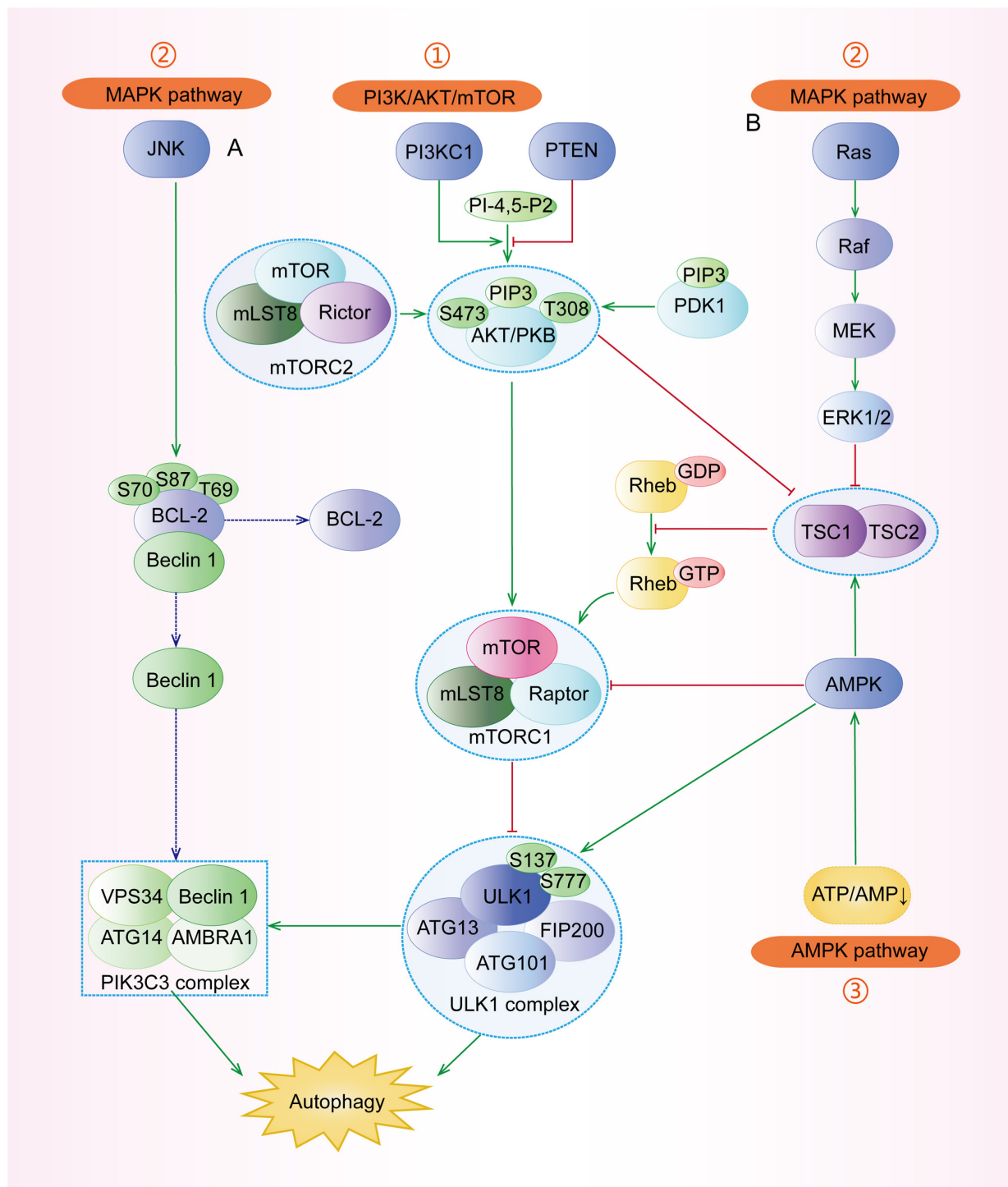


FIGURE 3 | The major signaling pathways involved in the regulation of autophagy. (1) PI3K/AKT pathway: under stresses, the activated PI3KC1 makes PI-4,5-P2 into PIP3 and then activates AKT with the help of PDK1. The activated AKT, directly and indirectly, activates mTORC1 (composed of mTOR, mLST8, and Raptor) to inhibit ULK1 complex and autophagy. Specifically, the indirect pathway includes the TSC1/TSC2 complex and Rheb-GTP. (2) MAPK pathway: the major regulators include the JNK pathway and the ERK pathway. (A) JNK can separate the conjunction of Beclin-1 and BCL-2 by phosphorylating BCL-2 at Thr69, Ser70, and Ser87, and then Beclin-1 participates in the assembly of PIK3C3 complex to induce autophagy. (B) ERK has dual roles in autophagy. The successively activated Ras-Raf-MEK-ERK1/2 can directly induce autophagy. Besides, the activated ERK1/2 can block the TSC1/TSC2 complex and regulate its downstream to inhibit autophagy. (3) AMPK pathway: Under some conditions with the increasing AMP/ATP ratio, the activated AMPK promotes the formation of the TSC1/TSC2 complex to inactivate mTORC1 and regulates its downstream regulators. AMPK can also phosphorylate ULK1 at Ser317, Ser777, S467, S555, S574, and S637 to stimulate autophagy.

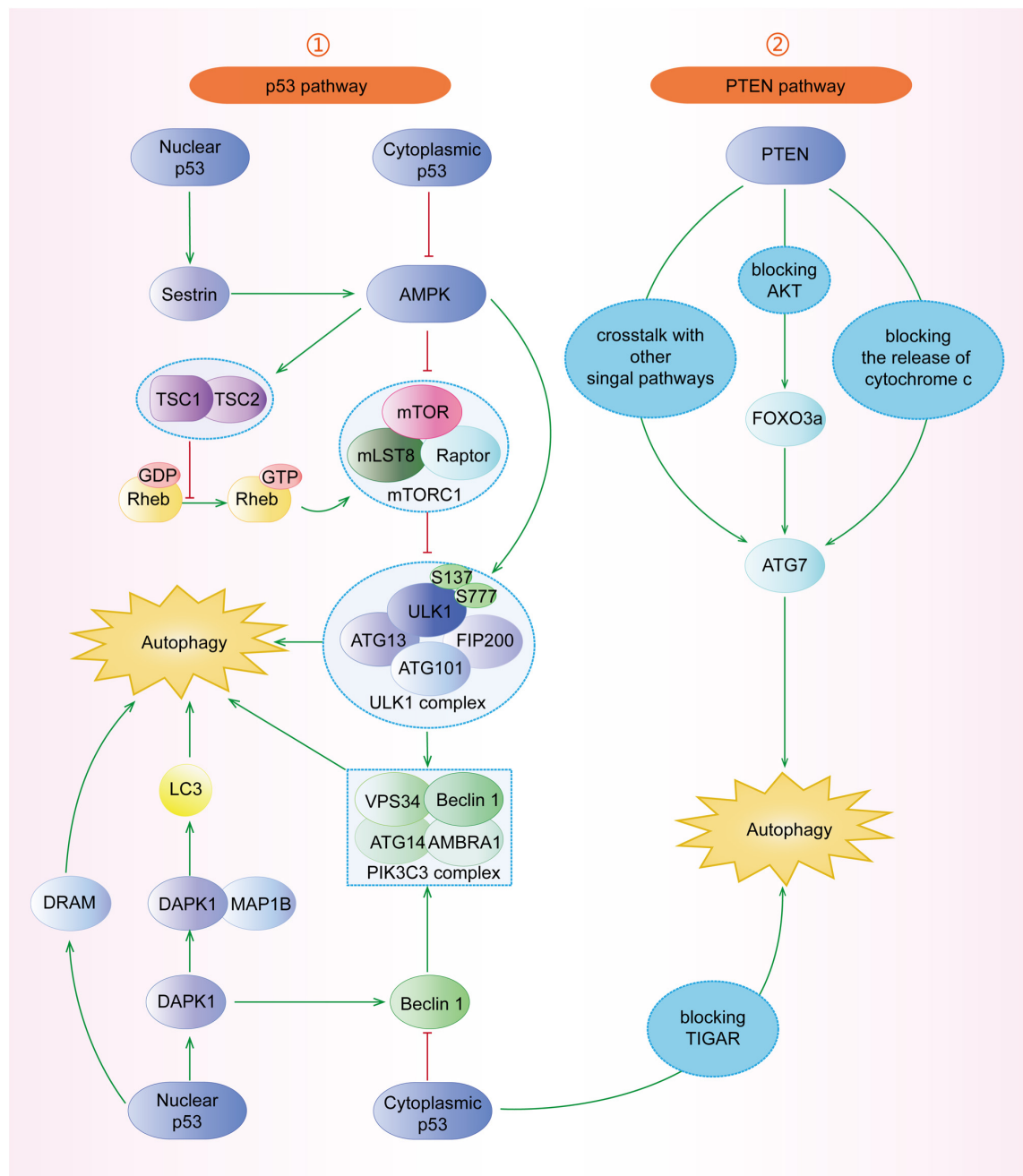


FIGURE 4 | The roles of p53 and PTEN signaling pathways in the regulation of autophagy. (1) p53 pathway: nuclear p53 can induce autophagy through Sestrin1/Sestrin2-AMPK-TSC1/TSC2 complex-mTOR. DRAM is a downstream target of p53 facilitating autophagy. Furthermore, p53 can induce DAPK1 to phosphorylate Beclin-1 or bind to MAP1B to inhibit autophagy. However, cytoplasmic p53 blocks AMPK, TIGAR, and Beclin-1 to inhibit autophagy. (2) PTEN pathway: PTEN has crosstalk with other signal pathways. PTEN can induce autophagy through the PTEN/AKT/FOXO3a/Atg7 pathway, independent of mTOR and Beclin-1. Additionally, PTEN blocks the release of cytochrome c to induce autophagy.

DUAL ROLES OF AUTOPHAGY IN CHEMORESISTANCE OF GASTRIC CANCER

Autophagy functions as a double-edged sword for chemoresistance of gastric cancer. On one hand, autophagy can

protect gastric cancer cells from the cytotoxicity of chemotherapy drugs and contribute to the formation of chemoresistance (Russi et al., 2019). On the other hand, it can reverse chemoresistance by promoting apoptosis and/or inhibiting EMT (Nie et al., 2020). The main reason is that autophagy is regulated by multiple proteins and/or ncRNAs and thus plays different roles in gastric

cancer chemoresistance (Tsai et al., 2020; Zeng et al., 2020). Therefore, if properly applied, targeting autophagy may be an important strategy for the prevention and treatment of chemoresistance. In this section, we provide a summary of the regulation of autophagy by various proteins (Table 1) and ncRNAs (Table 2) as well as its different roles in gastric cancer chemoresistance (Figure 5).

Key Regulatory Proteins in Autophagy-Mediated Gastric Cancer Chemoresistance

Several proteins have shown regulatory effects on autophagy-mediated gastric cancer chemoresistance (Figure 5A) by (i) inducing both autophagy and chemoresistance; (ii) inhibiting autophagy but inducing chemoresistance; or (iii) inhibiting both autophagy and chemoresistance. Based on the modulatory effects of these proteins on autophagy and chemoresistance, developing their inhibitors or activators and combining these compounds with autophagy inhibitors or activators have been emerging as a promising strategy to overcome chemotherapy resistance.

Regulatory Proteins Inducing Both Autophagy and Chemoresistance

It has recently been reported that several proteins (Table 1) can induce autophagy by regulating autophagy regulatory genes, such as Beclin-1, ATG12, ATG5, p62, LC3-I, LC3-II, and so on. Nie et al. (2020) have reported that wiskott-aldrich syndrome protein family member 3 (WASF3) is an obstacle for the sensitivity of gastric cancer to oxaliplatin (OXA). It has been found that WASF3 overexpression induces autophagy by increasing ATG12 level and causes OXA resistance in gastric cancer cells, while interference with WASF3 can reverse OXA resistance *in vitro* (Nie et al., 2020). Chen et al. (2019) have demonstrated that the expression of polo-like kinase 1 (PLK1) is significantly increased in cisplatin (DDP)-resistant SGC-7901/DDP cells, whereas PLK1 knockdown inhibits autophagy, increases apoptosis, and restores the chemosensitivity of DDP-resistant cells. Aquaporins (AQPs) are a family of small integral membrane proteins; among them, AQP3 is highly expressed in gastric cancer tissues (Moosavi and Elham, 2020). Dong et al. (2016) have shown that the upregulation of AQP3 increases the expression of ATG5 and Beclin-1, decreases the expression of p62, induces autophagy, and causes DDP resistance, while the application of autophagy inhibitor chloroquine (CQ) can reverse DDP resistance. DJ-1, also known as Parkinson's disease associated protein 7 (PARK7), is highly expressed in several types of cancer and has been proposed as a chemoresistance-related factor (Jin, 2020). Indeed, DJ-1 is highly expressed in gastric cancer tissues and Epirubicin (EPI)-resistant gastric cancer cells, and EPI treatment can increase the expression of DJ-1 in a dose-dependent manner (Pan et al., 2018). Pan et al. (2018) have reported that the overexpression of DJ-1 significantly increases LC3-II level, induces autophagy, and attenuates EPI-induced apoptosis, while DJ-1 knockdown can reduce autophagy and increase apoptosis, thereby reversing EPI resistance in MGC803 and SGC7901 gastric cancer cells.

Some regulatory proteins have been found to induce autophagy and chemoresistance by regulating the PI3K/AKT/mTOR signaling pathway (Table 1). Tetraspanin 9 (TSPAN9), a member of four transmembrane protein superfamily that plays an important role in tumor progression, has shown regulatory effects on proliferation, migration, invasion, and autophagy (Qi et al., 2019, 2020). Qi et al. (2020) have reported that the protein level of TSPAN9 is increased in 5-fluorouracil (5-FU)-resistant gastric cancer cells, which inhibits the catalytic activity of PI3K through binding to PIK3R3 (p55) and promotes autophagy, whereas knockdown of p55 can enhance the sensitivity of gastric cancer cells to 5-FU. The cluster of differentiation 133 (CD133), an important stemness-related marker has also been related to autophagy (Liu Y. C. et al., 2020b). Lu et al. (2019) have reported that the expression level of CD133 and the percentage of CD133-positive cells are increased in DDP-resistant gastric cancer cells, promoting cancer stem cell (CSC) properties of DDP-resistant cells. Further studies have shown that CD133 can increase autophagy and the stemness of gastric cancer cells via activating the PI3K/AKT/mTOR signaling pathway, causing DDP resistance of gastric cancer cells *in vivo* and *in vitro* (Lu et al., 2019).

The regulatory proteins of the AMPK pathway have been shown to induce autophagy and chemoresistance (Table 1). Xiao et al. (2020) have suggested that tripartite motif containing 14 (TRIM14) is significantly up-regulated in 5-FU- and OXA-resistant gastric cancer tissues and cell lines. Further studies have shown that TRIM14 can promote autophagy and induce chemoresistance by activating the AMPK/mTOR pathway *in vivo* and *in vitro* while silencing TRIM14 provides the opposite effects (Xiao et al., 2020). Pei et al. (2018) have found that metadherin (MTDH) expression in gastric cancer tissues is significantly increased and positively correlated with 5-FU resistance. Further mechanism studies have suggested that MTDH can promote AMPK phosphorylation, upregulate ATG5 expression, activate autophagy, and consequently induce 5-FU resistance (Pei et al., 2018).

Regulatory Proteins Inhibiting Autophagy but Inducing Chemoresistance

Embryonic stem cell-expressed Ras (ERas) is a novel member of the Ras protein family and is highly expressed in gastric, colorectal, and breast cancer (Suárez-Cabrera et al., 2018; Tian et al., 2019). Tian et al. (2019) have found that ERas overexpression significantly increases the phosphorylation level of mTOR (Ser2448) and its substrate (ULK1-Ser757), as well as AKT-Ser473, activates the AKT/mTOR pathway, blocks autophagic flux in gastric cancer cells, suppresses DDP-induced apoptosis, and induces DDP resistance. In contrast, silencing ERas has been found to increase autophagic flux and enhance the sensitivity of gastric cancer cells to DDP *in vitro* (Tian et al., 2019).

Chemokine C-C motif ligand 2 (CCL2), is a well-known cytokine belonging to the CC chemokine family 9, which can affect drug sensitivity in both paracrine and autocrine manners (Hao et al., 2020). CCL2 expression has been related to tumor invasion, metastasis, and drug resistance (Zhong et al., 2018;

Dutta et al., 2020; Hao et al., 2020). Xu et al. (2018b) have found that DPP-resistant gastric cancer cell lines, such as BGC823/DDP cells and SGC7901/DDP cells secrete more CCL2 to maintain DDP resistance. It has further been found that CCL2 overexpression increases the expression of p62 by activating PI3K/AKT/mTOR signaling pathway, whilst the increased expression of p62, in turn, activates the transcription of CCL2, inhibits autophagy, and forms a positive feedback loop to maintain drug resistance (Xu et al., 2018b).

Rab5a, also known as RAB5, is a member of the Rab family of small GTPases and is involved in the autophagy process by blocking autophagosome-lysosome fusion (Lu et al., 2014). Xu et al. (2018a) have shown that Rab5a expression level is positively associated with drug resistance in gastric cancer cells. It has been found that Rab5a overexpression increases the phosphorylation level of mTOR, decreases the LC3-II/I ratio, and increases p62 expression level, thereby inhibiting autophagy

and inducing DDP resistance, whereas Rab5a knockdown can facilitate autophagy and reverse DDP resistance *in vitro* (Xu et al., 2018a).

Regulatory Proteins Inhibiting Both Autophagy and Chemoresistance

O-6-methylguanine-DNA methyltransferase (MGMT) is a type of suicide DNA damage repair enzymes, and DNA damage repair disorders have been reported to induce autophagy (Balvers et al., 2015; Abdu et al., 2020). Lei et al. (2020) have found that the high expression of MGMT is significantly correlated with the low expression of ATG4B and the favorable prognosis of gastric cancer. DDP can inhibit MGMT expression in a dose- and time-dependent manner and the low expression of MGMT can, in turn, induce autophagy and cisplatin resistance. Overexpression of MGMT can inhibit autophagy and reverse DDP resistance *in vivo* and *in vitro* (Lei et al., 2020).

TABLE 1 | Key regulatory proteins in autophagy-mediated chemoresistance of gastric cancer.

Protein	Expression in GC	Effects on autophagy	Chemotherapy	Effects on chemosensitivity	Downstream pathways	References
WASF3	NA	Inducing	OXA	Decreasing	ATG12	Nie et al., 2020
PLK1	Up	Inducing	DDP	Decreasing	CDC25C, cyclin B1, LC3-I, LC3-II	Chen et al., 2019
AQP3	Up	Inducing	DDP	Decreasing	Atg5, Beclin-1, P62	Dong et al., 2016
DJ-1	Up	Inducing	EPI	Decreasing	LC3-I, LC3-II	Pan et al., 2018
TSPAN9	Up	Inducing	5-FU	Decreasing	PI3K/AKT/mTOR	Qi et al., 2020
CD133	Up	Inducing	DDP	Decreasing	PI3K/AKT/mTOR	Lu et al., 2019
TRIM14	Up	Inducing	5-FU, OXA	Decreasing	AMPK/mTOR	Xiao et al., 2020
MTDH	Up	Inducing	5-FU	Decreasing	AMPK/ATG5	Pei et al., 2018
ERAS	Up	Inhibiting	DDP	Decreasing	AKT/mTOR	Tian et al., 2019
CCL2	Up	Inhibiting	DDP	Decreasing	PI3K/AKT/mTOR, SQSTM1	Xu et al., 2018b
RAB5A	Up	Inhibiting	DDP	Decreasing	mTOR	Xu et al., 2018a
MGMT	NA	Inhibiting	DDP	Increasing	ATG4B	Lei et al., 2020
CISD2	Down	Inhibiting	5-FU	Increasing	AKT/mTOR	Sun et al., 2017

5-FU, 5-fluorouracil; DDP, cisplatin; EPI, epirubicin; GC, gastric cancer; OXA, oxaliplatin; NA, not applicable.

TABLE 2 | Key regulatory non-coding RNAs in autophagy-mediated chemoresistance of gastric cancer.

Biomarker	Expression in GC	Effects on autophagy	Chemotherapy	Effects on chemosensitivity	Downstream pathways	References
miR-874	Down	Inhibiting	DDP	Increasing	ATG16L1	Huang et al., 2018
miR-30a	Down	Inhibiting	DDP	Increasing	MDR1, P-gp	Du et al., 2018
miR-181a	Down	Inhibiting	DDP	Increasing	MTMR3	Lin et al., 2017
miR-23b-3p	Down	Inhibiting	DDP, VCR, 5-FU	Increasing	ATG12, HMGB2	An et al., 2015
miR-148a-3p	Down	Inhibiting	DDP	Increasing	RAB12, mTORC1	Li et al., 2017
miR-495-3p	Down	Inhibiting	ADM, DDP, 5-FU, VCR	Increasing	GRP78/mTOR	Chen et al., 2018
miR-361-5p	NA	Inhibiting	DOC	Increasing	PI3K/AKT/mTOR, FOXM1	Tian et al., 2018
miR-21	NA	Inhibiting	DDP	Decreasing	PI3K/AKT/mTOR, Beclin-1, LC3	Gu et al., 2020
HOTTIP	Up	Inhibiting	DDP	Decreasing	miR-216a-5p, BCL-2, Beclin-1	Zhao et al., 2020
MALAT1	Up	Inducing	DDP, VCR	Decreasing	miR-30b, ATG5, miR-23b-3p, ATG12	YiRen et al., 2017; Xi et al., 2019
HULC	NA	Inducing	DDP	Decreasing	FoxM1	Xin et al., 2019

5-FU, 5-fluorouracil; ADM, adriamycin; DDP, cisplatin; DOC, docetaxel; GC, gastric cancer; VCR, vincristine; NA, not applicable.

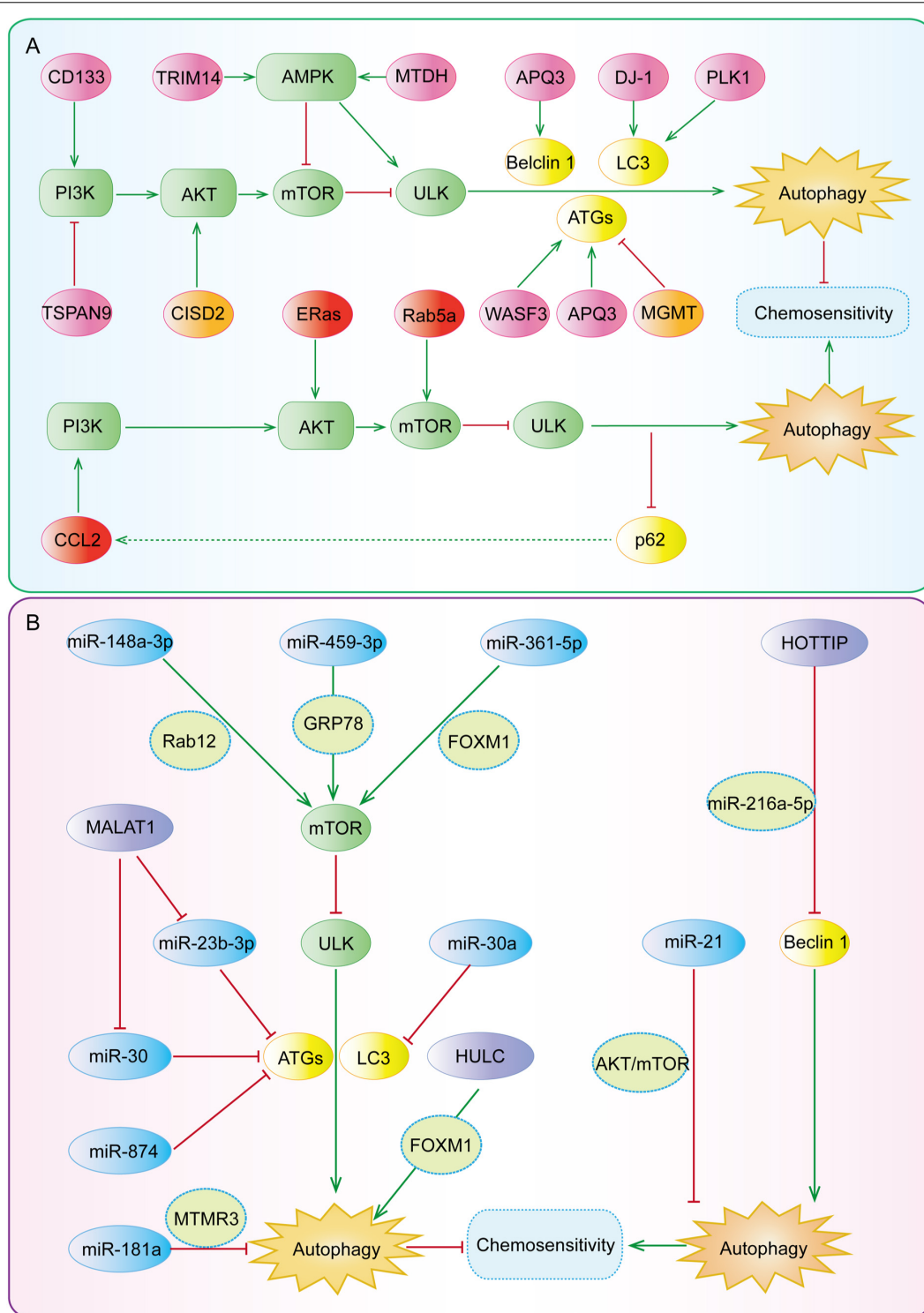


FIGURE 5 | The key regulatory nodes in autophagy-mediated gastric cancer chemoresistance. Various regulatory nodes, including several **(A)** proteins and **(B)** ncRNAs, are involved in the regulation of autophagy, thereby enhancing or reversing the chemotherapy resistance of gastric cancer.

CDGSH iron sulfur domain 2 (CISD2) is a survival gene and plays an important role in the redox reaction, longevity, tumorigenesis, and tumor progression (Li et al., 2019;

Nobili et al., 2020). Sun et al. (2017) have shown that CISD2 is significantly down-regulated in gastric cancer tissues and drug-resistant cell lines, which contributes to the resistance of

gastric cancer cells to 5-FU. Further studies have found that CISD2 overexpression antagonizes 5-FU-induced autophagy by increasing the phosphorylation levels of AKT (S473) and mTOR (Ser2448), consequently reversing the reduction of p-MTOR and p-AKT by 5-FU and enhancing the sensitivity of MKN1 and BGC823 cells to 5-FU (Sun et al., 2017).

Regulatory Effects of miRNAs on Autophagy-Mediated Gastric Cancer Chemoresistance

MiRNAs, as a kind of highly conserved short ncRNAs, have a length of 18–25 nucleotides, regulate the expression of many genes, and participate in the development of human cancer and drug resistance (Poursheikhani et al., 2020; Ratti et al., 2020). miRNA-mediated autophagy (Figure 5B) has been found to play a role in chemoresistance in gastric cancer by regulating autophagy-related genes or signaling pathways (Jamali et al., 2020).

To date, many miRNAs, including miR-874, miR-30, miR-181a, miR-23b-3p, miR-148a-3p, miR-495-3p, miR-361-5p, and miR-21 have been involved in the regulation of autophagy and chemoresistance in gastric cancer (as summarized in Table 2). Among them, the expression of miR-874, miR-30, miR-181a, and miR-23b-3p are down-regulated in drug-resistant gastric cancer cell lines and gastric cancer tissues (An et al., 2015; Lin et al., 2017; Du et al., 2018; Huang et al., 2018). Huang et al. (2018) have found that miR-874 inhibits autophagy by down-regulating ATG16L1, thus enhancing the sensitivity of gastric cancer cells to DDP *in vitro* and *in vivo*. Du et al. (2018) have reported that miR-30a up-regulates the expression of P-gp and MDR1, decreases the LC3-II/I ratio, inhibits autophagy, and reverses DDP resistance. Lin et al. (2017) have shown that miR-181a directly targets the 3'-UTR of myotubularin related protein 3 (MTMR3), decreases the mRNA and protein levels of MTMR3,

inhibits autophagy, and increases the sensitivity of gastric cancer cells to DDP. An et al. (2015) have demonstrated that miR-23b-3p directly targets ATG12 and high-mobility group box 2 (HMGB2), inhibits autophagy, and increases the sensitivity of gastric cancer cells to DDP, vincristine (VCR), and 5-FU.

It has been found that both miR-148a-3p and miR-495-3p are lowly expressed in drug-resistant gastric cancer cell lines and tumor tissues (Li et al., 2017; Chen et al., 2018). Li et al. (2017) have found that miR-148a-3p down-regulates the expression of A-kinase anchoring protein 1 (AKAP1) and RAB12 (RAB12, member RAS oncogene family) and reduces the inhibitory effects of RAB12 on mTORC1, thereby inhibiting autophagy and reversing the resistance of gastric cancer cells to DDP. Chen et al. (2018) have reported that miR-495-3p directly targets glucose regulated protein 78 (GRP78) at the post-transcriptional level, activates mTOR signaling, inhibits autophagy, and reverses multidrug resistance (MDR) in gastric cancer. Tian et al. (2018) have suggested that miR-361-5p negatively regulates the expression of FOXM1, which further causes an increase in the expression of p-AKT and mTOR, the inhibition of autophagy, and the enhanced sensitivity of gastric cancer cells to Docetaxel (DOC) *in vitro*. Gu et al. (2020) have found that miR-21 overexpression can increase the phosphorylation of AKT and mTOR, inhibit autophagy, and induce DDP resistance. It has been further demonstrated that the knockdown of miR-21 can promote autophagy and then sensitize DDP-resistant gastric cancer cell lines to DDP (Gu et al., 2020).

Regulatory Effects of lncRNAs on Autophagy-Mediated Gastric Cancer Chemoresistance

lncRNAs are the transcripts of more than 200 nucleotides, accounting for 80–90% of all ncRNAs, and regulate gene expression at the pre-transcriptional, transcriptional, and

TABLE 3 | Modulatory effects of autophagy inhibitor and activators on gastric cancer chemoresistance.

Compounds	Source	Effects on autophagy	Chemotherapy	Effects on chemosensitivity	Downstream pathways	References
Genipin	Natural products from TM	Inducing	OXA	Increasing	p53, DRAM	Kim et al., 2020
Tanshinone IIA	Natural products from TM	Inducing	ADM	Increasing	LC3-II, P62	Xu Z. et al., 2018
Liquiritin	Natural products from TM	Inducing	DDP	Increasing	LC3B, Beclin-1, p62	Wei et al., 2017
DSGOST	Prescription from TM	Inducing	DDP	Increasing	LC3-II, ATG5, Beclin-1, Bcl2, AMPK α /ULK1	Kim T. W. et al., 2018
Cucurbitacin B	Natural products from edible plants	Inducing	DDP	Increasing	CIP2A/PP2A/mTORC1	Dandawate et al., 2020
Phloretin	Natural products from edible plants	Inducing	ADM	Increasing	ERK1/2, MAP, LC3B II, Beclin-1	You et al., 2020
Tunicamycin	Antibiotic	Inducing	ADM, VCR	Increasing	LC3-I, LC3-II	Wu et al., 2018
Indomethacin	NSAIDs	Inhibiting	OXA	Increasing	LC3-II, LC3-II, p62, NBR1	Vallecillo-Hernandez et al., 2018
Propofol	Anesthetic	Inhibiting	DDP	Increasing	MALAT1, miR-30e, ATG5	Zhang Y.F. et al., 2020

ADM, adriamycin; DDP, cisplatin; OXA, oxaliplatin; TM, traditional medicine; VCR, vincristine.

post-transcriptional levels (Yuan et al., 2020). Therefore, lncRNAs widely participate in various physiological and pathological processes of organisms (Yuan et al., 2020). LncRNAs have been found to regulate autophagy and drug resistance (**Figure 5B**) by acting as a competing endogenous RNA (ceRNA) or directly binding to proteins to modulate their expression and functions (as summarized in **Table 2**).

It has been found that the expression levels of HOTTIP (HOXA distal transcript antisense RNA), MALAT1 (metastasis associated lung adenocarcinoma transcript 1), and HULC (hepatocellular carcinoma up-regulated long non-coding RNA) are elevated in chemotherapy-resistant gastric cancer cell lines and tumor tissues (YiRen et al., 2017; Xin et al., 2019; Zhao et al., 2020). Zhao et al. (2020) have indicated that HOTTIP may function as a ceRNA of miR-216a-5p, increasing the expression level of BCL-2 and decreasing the expression level of Beclin-1. Further studies have shown that HOTTIP overexpression inhibits autophagy and induces DDP resistance in gastric cancer while the silencing of HOTTIP increases the sensitivity of gastric cancer cells to DDP (Zhao et al., 2020). YiRen et al. (2017) have reported that MALAT1 acts as a ceRNA against miR-23b-3p and attenuates the inhibitory effects of miR-23b-3p on ATG12, leading to autophagy induction and VCR resistance in gastric cancer cells. Moreover, Xi et al. (2019) have found that MALAT1 can competitively bind to miR-30 and promote the expression of ATG5, thus inducing autophagy and DDP resistance. Xin et al. (2019) have shown that HULC can stabilize FoxM1 by inhibiting its ubiquitination and induce autophagy and DDP resistance. It has further been observed that intervening HULC can suppress autophagy and then reduce the resistance of gastric cancer cells to DDP *in vitro* (Xin et al., 2019).

MODULATORY EFFECTS OF AUTOPHAGY INHIBITORS AND ACTIVATORS ON GASTRIC CANCER CHEMORESISTANCE

Given the importance of autophagy in chemotherapy resistance, the development of autophagy inhibitors or activators may provide a new opportunity for the treatment of human cancer, especially for those with drug resistance (Mele et al., 2020). FDA has approved the clinical application of CQ and its derivative hydroxychloroquine (HCQ), which can inhibit autophagy by blocking autophagosome fusion and degradation (Liu T. et al., 2020a). At present, there are several clinical studies on the treatment of multiple tumors with HCQ alone or in combination with chemotherapy. Various natural products from TM, medicinal plants, or microorganisms, such as flavonoids, alkaloids, terpenoids, coumarins, etc. have been reported as potential autophagy inhibitors and activators and MDR reversal agents (as summarized in **Table 3**) (Sato et al., 2019; Liu S. et al., 2020; Nazim et al., 2020).

Effects of Autophagy Activators on Gastric Cancer Chemoresistance

Genipin, a natural product derived from traditional Chinese medicine (TCM) *Gardenia jasminoides*, has shown anti-angiogenic, anti-proliferative, anti-inflammatory, and anticancer activities (Jo et al., 2019; Zhang C. et al., 2020; Zhou et al., 2020). Kim et al. (2020) have found that genipin can increase the expression of p53 and DRAM, induce apoptosis and autophagy, and enhance the sensitivity of AGS and MKN45 gastric cancer cell lines to OXA. Tanshinones are a group of abietane diterpenes from the TCM Danshen and have exhibited anticancer activities *in vitro* and *in vivo* (Li M. et al., 2020). Xu Z. et al. (2018) have reported that tanshinone IIA can reduce the expression of multidrug resistance protein 1 (MRP1) and inhibit the efflux of adriamycin (ADM). Besides, the combination of tanshinone IIA with ADM can induce autophagy, thus promoting cell apoptosis and enhancing the sensitivity of gastric cancer cells to ADM (Xu Z. et al., 2018). Liquiritin is the main medicinal component of TCM licorice. Wei et al. (2017) have found that liquiritin increases Beclin-1 expression, inhibits p62 expression, triggers autophagy and apoptosis, and then reverses DDP resistance *in vitro* and *in vivo*.

Danggui-Sayuk-Ga-Osuyu-Saenggang-Tang (DSGOST) is a traditional Korean herbal medicine (Kim T. W. et al., 2018). DSGOST is similar to TCM Danggui-Sini-Jia-Wuzhuyu-Shengjian-Tang and is commonly used in treating patients with Raynaud's phenomenon caused by multiple chemotherapy drugs (Kim T. W. et al., 2018). Kim T. W. et al. (2018) have reported that DSGOST can cause the dissociation of the Beclin-1-Bcl2 complex, activate the AMPK/ULK1 pathway, increase the autophagy flux, induce autophagy and apoptosis, and enhance the sensitivity of gastric cancer cell lines AGS and SNU-638 to DDP.

The dietary natural products, cucurbitacin B and phloretin have recently been found to exert anticancer activities and reverse chemotherapy resistance (Hsiao et al., 2019; Dandawate et al., 2020). Xu et al. (2020) have shown that cucurbitacin B induces autophagy and apoptosis and reverses the sensitivity of DDP-resistant cells to DDP. The mechanisms of action studies have indicated that cucurbitacin B inhibits CIP2A (cancerous inhibitor of protein phosphatase 2A), subsequently reactivating PP2A (protein phosphatase 2A) and enhancing PP2A-dependent mTORC1 inactivation (Xu et al., 2020). You et al. (2020) have found that phloretin inhibits the phosphorylation of ERK1/2 and MAPK p38 and increases the expression of LC3B II and Beclin-1, thus inducing autophagy and enhancing the sensitivity of gastric cancer cells to ADM *in vitro*.

Abnormal glycosylation has been widely regarded as an important sign of cancer and is significantly associated with tumor development, progression, metastasis, and chemoresistance (Liu et al., 2018; Liu T. et al., 2020a). As an effective glycosylation inhibitor, tunicamycin has been initially identified as a natural antibiotic and anticancer compound (Liu Y. C. et al., 2020b; Santos-Laso et al., 2020). Wu et al. (2018) have suggested that tunicamycin inhibits N-glycosylation to aggravate ER stress, induces autophagy, and increases the sensitivity of gastric cancer cells to ADM and VCR.

Effects of Autophagy Inhibitors on Gastric Cancer Chemoresistance

Indomethacin, a common non-steroidal anti-inflammatory drug (NSAID), has been reported as a coadjutant of anticancer drugs with satisfactory efficacy (López-Contreras et al., 2019; Seetha et al., 2020). Vallecillo-Hernandez et al. (2018) have found that indomethacin can induce the accumulation of p62 and neighbor of BRCA1 (NBR1), impair lysosomal function, inhibit autophagic degradation, and increase OXA-induced cell death in AGS cells. Propofol, a sedative widely used in surgery, has shown efficacy in several types of cancer, such as pancreatic cancer (Wang et al., 2020), gastric cancer (Liu F. et al., 2020), colon cancer (Liu F. et al., 2020), papillary thyroid carcinoma (Li Y. et al., 2020), and so on. Zhang et al. have demonstrated that propofol in combination with DDP inhibits the expression of lncRNA MALAT1 and enhances the inhibitory effects of miR-30e on ATG5 and autophagy, thereby increasing the sensitivity of gastric cancer cells to DDP *in vivo* and *in vitro* (Zhang Y.F. et al., 2020).

CONCLUSION AND FUTURE DIRECTION

Overall, this review provides compelling evidence for the dual roles of autophagy in the chemoresistance of gastric cancer. Autophagy can protect cancer cells from chemotherapy and participate in the formation of MDR, while it can also promote apoptosis and kill MDR cancer cells. Therefore, the development of autophagy inhibitors or activators may be an important way to reverse drug resistance and enhance chemosensitivity. The combination of autophagy modulators and chemotherapy drugs will also bring new hope for the treatment of human cancer. For instance, it is exciting to note that the combination of autophagic inhibitor HCQ and gemcitabine or nab-paclitaxel can significantly improve the overall response rate of cancer patients (Karasic et al., 2019).

The dual roles of autophagy in drug resistance are mainly regulated by different proteins and ncRNAs. Proteins and ncRNAs can monitor autophagy by regulating autophagy regulatory proteins and/or autophagy regulatory signaling pathways. In the fields of drug resistance and autophagy in gastric cancer, researchers have focused on PI3K/AKT and MAPK pathways. More studies on other autophagy-related pathways (p53, MAPK, or PTEN pathways) are expected in the future. The development of small-molecule inhibitors or activators targeting key regulatory nodes in the process of autophagy may provide an alternative treatment for patients with cancer. For example, SBI-0206965, as a small molecule inhibitor of ULK1, has been

found to enhance daunorubicin sensitivity in acute myeloid leukemia (Qiu et al., 2020). Besides, the ULK1 activator LYN-1604, which can induce autophagy-related cell death through the ULK complex, shows significant anticancer activity in triple-negative breast cancer (Ouyang et al., 2017). Therefore, further strengthening the research on the role of different proteins and ncRNAs in regulating autophagy-mediated gastric cancer chemoresistance will be beneficial to the development of promising drugs for gastric cancer therapy.

Many natural products from TM and edible plants have shown preventive and therapeutic efficacy in human cancer by targeting multiple signaling pathways and inducing cell cycle arrest and apoptosis (Koh et al., 2020). Accumulating evidence has demonstrated the modulatory effects of these anticancer natural products on autophagy and chemosensitivity. Thus, using natural products alone or in combination with autophagy modulators and/or chemotherapy drugs may exhibit promising efficacy in human cancer, especially in drug-resistant cancer. Nevertheless, further studies are warranted to identify the specific molecular targets of these natural products and examine the efficacy and safety of these strategies in clinically relevant cancer models.

AUTHOR CONTRIBUTIONS

J-JQ and X-DC conceptualized the manuscript. J-LX, LY, Y-CT, Z-YX, and H-DX collected the literature, wrote the manuscript, and made the figures. J-JQ edited and made significant revisions to the manuscript. All authors read and approved the final manuscript.

FUNDING

This study was supported by Natural Science Foundation of Zhejiang Province (LY18H290006), National Natural Science Foundation of China (81903842 and 81973634), and Program of Zhejiang Provincial TCM Sci-tech Plan (2018ZY006 and 2020ZZ005).

ACKNOWLEDGMENTS

We thank the current and former members of our laboratories and collaborators for their contributions to the publications cited in this review article. The research field in autophagy is rapidly growing, and we apologize for not being able to cite all the recent publications, due to space limitation.

REFERENCES

- Abdrakhmanov, A., Gogvadze, V., and Zhivotovsky, B. (2020). To eat or to die: deciphering selective forms of autophagy. *Trends Biochem. Sci.* 45, 347–364. doi: 10.1016/j.tibs.2019.11.006
- Abdu, K., Aiertza, M. K., Wilkinson, O. J., Senthong, P., Craggs, T. D., Povey, A. C., et al. (2020). Synthesis of oligodeoxyribonucleotides containing a tricyclic thio analogue of O(6)-methylguanine and their recognition by MGMT and
- At11. *Nucleos. Nucleot. Nucl. Acids* 39, 1108–1121. doi: 10.1080/15257770.2020.1764971
- Amaravadi, R., Kimmelman, A., and Debnath, J. (2019). Targeting autophagy in cancer: recent advances and future directions. *Cancer Discov.* 9, 1167–1181. doi: 10.1158/2159-8290.Cd-19-0292
- An, Y., Zhang, Z., Shang, Y., Jiang, X., Dong, J., Yu, P., et al. (2015). miR-23b-3p regulates the chemoresistance of gastric cancer cells by targeting ATG12 and HMGB2. *Cell Death Dis.* 6:e1766. doi: 10.1038/cddis.2015.123

- Anerillas, C., Abdelmohsen, K., and Gorospe, M. (2020). Regulation of senescence traits by MAPKs. *Geroscience* 42, 397–408. doi: 10.1007/s11357-020-00183-3
- Bakula, D., Müller, A., Zuleger, T., Takacs, Z., Franz-Wachtel, M., Thost, A., et al. (2017). WIP1 and WIP4 β -proteins are scaffolds for LKB1-AMPK-TSC signalling circuits in the control of autophagy. *Nat. Commun.* 8:15637. doi: 10.1038/ncomms15637
- Balvers, R. K., Lamfers, M. L., Kloeze, J. J., Kleijn, A., Berghauer Pont, L. M., Dirven, C. M., et al. (2015). ABT-888 enhances cytotoxic effects of temozolomide independent of MGMT status in serum free cultured glioma cells. *J. Transl. Med.* 13:74. doi: 10.1186/s12967-015-0427-y
- Barroso-Chinea, P., Luis-Ravelo, D., Fumagallo-Reading, F., Castro-Hernandez, J., Salas-Hernandez, J., Rodriguez-Nuñez, J., et al. (2020). DRD3 (dopamine receptor D3) but not DRD2 activates autophagy through mTORC1 inhibition preserving protein synthesis. *Autophagy* 16, 1279–1295. doi: 10.1080/15548627.2019.1668606
- Biagioni, A., Skalamera, I., Peri, S., Schiavone, N., Cianchi, F., Giommoni, E., et al. (2019). Update on gastric cancer treatments and gene therapies. *Cancer Metast. Rev.* 38, 537–548. doi: 10.1007/s10555-019-09803-7
- Boosani, C., Gunasekar, P., and Agrawal, D. K. (2019). An update on PTEN modulators - a patent review. *Exp. Opin. Ther. Pat.* 29, 881–889. doi: 10.1080/13543776.2019.1669562
- Cai, C. Z., Yang, C., Zhuang, X. X., Yuan, N., Wu, M.-Y., Tan, J.-Q., et al. (2020). NRBF2 is a RAB7 effector required for autophagosome maturation and mediates the association of APP-CTFs with active form of RAB7 for degradation. *Autophagy* 1–19. doi: 10.1080/15548627.2020.1760623
- Cai, J., Li, R., Xu, X., Zhang, L., Lian, R., Fang, L., et al. (2018). CK1 α suppresses lung tumour growth by stabilizing PTEN and inducing autophagy. *Nat. Cell Biol.* 20, 465–478. doi: 10.1038/s41556-018-0065-8
- Cao, Y., Luo, Y., Zou, J., Ouyang, J., Cai, Z., Zeng, X., et al. (2019). Autophagy and its role in gastric cancer. *Clin. Chim. Acta* 489, 10–20. doi: 10.1016/j.cca.2018.11.028
- Carling, D. (2017). AMPK signalling in health and disease. *Curr. Opin. Cell Biol.* 45, 31–37. doi: 10.1016/j.ccb.2017.01.005
- Chen, J., Zhang, P., Chen, W., Li, D., Wu, X., Deng, R., et al. (2015). ATM-mediated PTEN phosphorylation promotes PTEN nuclear translocation and autophagy in response to DNA-damaging agents in cancer cells. *Autophagy* 11, 239–252. doi: 10.1080/15548627.2015.1009767
- Chen, S., Wu, J., Jiao, K., Wu, Q., Ma, J., Chen, D., et al. (2018). MicroRNA-495-3p inhibits multidrug resistance by modulating autophagy through GRP78/mTOR axis in gastric cancer. *Cell Death Dis.* 9:1070. doi: 10.1038/s41419-018-0950-x
- Chen, Z., Chai, Y., Zhao, T., Li, P., Zhao, L., He, F., et al. (2019). Effect of PLK1 inhibition on cisplatin-resistant gastric cancer cells. *J. Cell Physiol.* 234, 5904–5914. doi: 10.1002/jcp.26777
- Cheng, C. Y., Tseng, H. H., Chiu, H. C., Chang, C. D., Nielsen, B. L., and Liu, H. J. (2019). Bovine ephemeral fever virus triggers autophagy enhancing virus replication via upregulation of the Src/JNK/AP1 and PI3K/Akt/NF- κ B pathways and suppression of the PI3K/Akt/mTOR pathway. *Vet. Res.* 50:79. doi: 10.1186/s13567-019-0697-0
- Chi, C., Leonard, A., Knight, W., Beussman, K., Zhao, Y., Cao, Y., et al. (2019). LAMP-2B regulates human cardiomyocyte function by mediating autophagosome-lysosome fusion. *Proc. Natl. Acad. Sci. U.S.A.* 116, 556–565. doi: 10.1073/pnas.1808618116
- Chollat-Namy, M., Ben Safta-Saadoun, T., Haferssas, D., Meurice, G., Chouaib, S., Thiery, J., et al. (2019). The pharmacological reactivation of p53 function improves breast tumor cell lysis by granzyme B and NK cells through induction of autophagy. *Cell Death Dis.* 10:695. doi: 10.1038/s41419-019-1950-1
- Corona, A. K., and Jackson, W. T. (2018). Finding the middle ground for autophagic fusion requirements. *Trends Cell Biol.* 28, 869–881. doi: 10.1016/j.tcb.2018.07.001
- Crichton, D., Wilkinson, S., O'Prey, J., Syed, N., Smith, P., Harrison, P., et al. (2006). DRAM, a p53-induced modulator of autophagy, is critical for apoptosis. *Cell* 126, 121–134. doi: 10.1016/j.cell.2006.05.034
- Dandawate, P., Subramaniam, D., Panovich, P., Standing, D., Krishnamachary, B., Kaushik, G., et al. (2020). Cucurbitacin B and I inhibits colon cancer growth by targeting the Notch signaling pathway. *Sci. Rep.* 10:1290. doi: 10.1038/s41598-020-57940-9
- Diao, J., Liu, R., Rong, Y., Zhao, M., Zhang, J., Lai, Y., et al. (2015). ATG14 promotes membrane tethering and fusion of autophagosomes to endolysosomes. *Nature* 520, 563–566. doi: 10.1038/nature14147
- Dong, X., Wang, Y., Zhou, Y., Wen, J., Wang, S., and Shen, L. (2016). Aquaporin 3 facilitates chemoresistance in gastric cancer cells to cisplatin via autophagy. *Cell Death Discov.* 2:16087. doi: 10.1038/cddiscovery.2016.87
- Du, X., Liu, B., Luan, X., Cui, Q., and Li, L. (2018). miR-30 decreases multidrug resistance in human gastric cancer cells by modulating cell autophagy. *Exp. Ther. Med.* 15, 599–605. doi: 10.3892/etm.2017.5354
- Dutta, P., Paico, K., Gomez, G., Wu, Y., and Vadgama, J. V. (2020). Transcriptional Regulation of CCL2 by PARP1 is a driver for invasiveness in breast cancer. *Cancers* 12, 1317. doi: 10.3390/cancers12051317
- Dutta, S., Mahalanobish, S., Saha, S., Ghosh, S., and Sil, P. C. (2019). Natural products: an upcoming therapeutic approach to cancer. *Food Chem. Toxicol.* 128, 240–255. doi: 10.1016/j.fct.2019.04.012
- Emanuele, S., Notaro, A., Palumbo Piccionello, A., Maggio, A., Lauricella, M., D'Anneo, A., et al. (2018). Sicilian litchi fruit extracts induce autophagy versus apoptosis switch in human colon cancer cells. *Nutrients* 10:1490. doi: 10.3390/nu10101490
- Fan, J., Liu, Y., Yin, J., Li, Q., Li, Y., Gu, J., et al. (2016). Oxygen-Glucose-Deprivation/Reoxygenation-induced autophagic cell death depends on JNK-mediated phosphorylation of Bcl-2. *Cell Physiol. Biochem.* 38, 1063–1074. doi: 10.1159/000443057
- Fawal, M. A., Brandt, M., and Djouder, N. (2015). MCRC1 binds and couples Rheb to amino acid-dependent mTORC1 activation. *Dev. Cell* 33, 67–81. doi: 10.1016/j.devcel.2015.02.010
- Fitzmaurice, C., Abate, D., Abbasi, N., Abbastabar, H., Abd-Allah, F., Abdel-Rahman, O., et al. (2019). Global, regional, and national cancer incidence, mortality, years of life lost, years lived with disability, and disability-adjusted life-years for 29 cancer groups, 1990 to 2017: a systematic analysis for the global burden of disease study. *JAMA Oncol.* 5, 1749–1768. doi: 10.1001/jamaoncol.2019.2996
- Galluzzi, L., and Green, D. R. (2019). Autophagy-independent functions of the autophagy machinery. *Cell* 177, 1682–1699. doi: 10.1016/j.cell.2019.05.026
- Gao, A., Li, F., Zhou, Q., and Chen, L. (2020). Sestrin2 as a potential therapeutic target for cardiovascular diseases. *Pharmacol. Res.* 159:104990. doi: 10.1016/j.phrs.2020.104990
- Gao, S., Zhao, Z., Wu, R., Wu, L., Tian, X., and Zhang, Z. (2018). MiR-146b inhibits autophagy in prostate cancer by targeting the PTEN/Akt/mTOR signaling pathway. *Aging* 10, 2113–2121. doi: 10.18632/aging.101534
- Gomez-Osuna, A., Calatrava, V., Galvan, A., Fernandez, E., and Llamas, A. (2020). Identification of the MAPK Cascade and its Relationship with Nitrogen Metabolism in the Green Alga *Chlamydomonas reinhardtii*. *Int. J. Mol. Sci.* 21:3417. doi: 10.3390/ijms21103417
- Gu, Y., Fei, Z., and Zhu, R. (2020). miR-21 modulates cisplatin resistance of gastric cancer cells by inhibiting autophagy via the PI3K/Akt/mTOR pathway. *Anticancer Drugs* 31, 385–393. doi: 10.1097/cad.0000000000000886
- Guardia, C., Tan, X., Lian, T., Rana, M., Zhou, W., Christensen, E., et al. (2020). Structure of human ATG9A, the only transmembrane protein of the core autophagy machinery. *Cell Rep.* 31:107837. doi: 10.1016/j.celrep.2020.107837
- Hafner, A., Bulyk, M., Jambhekar, A., and Lahav, G. (2019). The multiple mechanisms that regulate p53 activity and cell fate. *Nat. Rev. Mol. Cell Biol.* 20, 199–210. doi: 10.1038/s41580-019-0110-x
- Hao, Q., Vadgama, J. V., and Wang, P. (2020). CCL2/CCR2 signaling in cancer pathogenesis. *Cell Commun. Signal.* 18:82. doi: 10.1186/s12964-020-00589-8
- Hempfen, C. H., and Hummelsberger, J. (2020). [Traditional Chinese medicine (TCM)-what is myth and what is the state of evidence today?]. *Bundesgesundheitsblatt Gesundheitsforschung Gesundheitsschutz* 63, 570–576. doi: 10.1007/s00103-020-03132-9
- Hollenstein, D. M., and Kraft, C. (2020). Autophagosomes are formed at a distinct cellular structure. *Curr. Opin. Cell Biol.* 65, 50–57. doi: 10.1016/j.ccb.2020.02.012
- Høyer-Hansen, M., and Jäättelä, M. (2008). Autophagy: an emerging target for cancer therapy. *Autophagy* 4, 574–580. doi: 10.4161/auto.5921
- Hsiao, Y. H., Hsieh, M. J., Yang, S. F., Chen, S. P., Tsai, W. C., and Chen, P. N. (2019). Phloretin suppresses metastasis by targeting protease and inhibits cancer stemness and angiogenesis in human cervical

- cancer cells. *Phytomedicine* 62:152964. doi: 10.1016/j.phymed.2019.152964
- Hu, W., Chen, S., Thorne, R., and Wu, M. (2019). TP53. TP53 Target Genes (DRAM, TIGAR), and Autophagy. *Adv. Exp. Med. Biol.* 1206, 127–149. doi: 10.1007/978-981-15-0602-4_6
- Huang, H., Tang, J., Zhang, L., Bu, Y., and Zhang, X. (2018). miR-874 regulates multiple-drug resistance in gastric cancer by targeting ATG16L1. *Int. J. Oncol.* 53, 2769–2779. doi: 10.3892/ijo.2018.4593
- Jamali, Z., Taheri-Anganeh, M., Shabaninejad, Z., Keshavarzi, A., Taghizadeh, H., Razavi, Z. S., et al. (2020). Autophagy regulation by microRNAs: novel insights into osteosarcoma therapy. *IUBMB Life* 72, 1306–1321. doi: 10.1002/iub.2277
- Jiang, H., Wang, H., Zou, W., Hu, Y., Chen, C., and Wang, C. (2019). Sufentanil impairs autophagic degradation and inhibits cell migration in NCI-H460 in vitro. *Oncol. Lett.* 18, 6829–6835. doi: 10.3892/ol.2019.10997
- Jiang, S., Liu, Y., Xu, B., Zhang, Y., and Yang, M. (2020). Noncoding RNAs: New regulatory code in chondrocyte apoptosis and autophagy. *Wiley Interdiscip. Rev. RNA* 11, e1584. doi: 10.1002/wrna.1584
- Jin, W. (2020). Novel Insights into PARK7 (DJ-1), a potential anti-cancer therapeutic target, and implications for cancer progression. *J. Clin. Med.* 9:1256. doi: 10.3390/jcm9051256
- Jo, M. J., Jeong, S., Yun, H. K., Kim, D. Y., Kim, B. R., Kim, J. L., et al. (2019). Genipin induces mitochondrial dysfunction and apoptosis via downregulation of Stat3/mcl-1 pathway in gastric cancer. *BMC Cancer* 19:739. doi: 10.1186/s12885-019-5957-x
- Karasic, T. B., O'Hara, M. H., Loaiza-Bonilla, A., Reiss, K. A., Teitelbaum, U. R., Borazanci, E., et al. (2019). Effect of gemcitabine and nab-paclitaxel with or without hydroxychloroquine on patients with advanced pancreatic cancer: a phase 2 randomized clinical trial. *JAMA Oncol.* 5, 993–998. doi: 10.1001/jamaoncol.2019.0684
- Kim, B. R., Jeong, Y. A., Kim, D. Y., Kim, J. L., Jeong, S., Na, Y. J., et al. (2020). Genipin increases oxaliplatin-induced cell death through autophagy in gastric cancer. *J. Cancer* 11, 460–467. doi: 10.7150/jca.34773
- Kim, B. W., Jin, Y., Kim, J., Kim, J. H., Jung, J., Kang, S., et al. (2018). The C-terminal region of ATG101 bridges ULK1 and PtdIns3K complex in autophagy initiation. *Autophagy* 14, 2104–2116. doi: 10.1080/15548627.2018.1504716
- Kim, T. W., Lee, S. Y., Kim, M., Cheon, C., Jang, B. H., Shin, Y. C., et al. (2018). DSGOST regulates resistance via activation of autophagy in gastric cancer. *Cell Death Dis.* 9:649. doi: 10.1038/s41419-018-0658-y
- Kimmelman, A. C., and White, E. (2017). Autophagy and tumor metabolism. *Cell Metab.* 25, 1037–1043. doi: 10.1016/j.cmet.2017.04.004
- Koh, Y. C., Ho, C. T., and Pan, M. H. (2020). Recent advances in cancer chemoprevention with phytochemicals. *J. Food Drug Anal.* 28, 14–37. doi: 10.1016/j.jfda.2019.11.001
- Lei, Y., Tang, L., Hu, J., Wang, S., Liu, Y., Yang, M., et al. (2020). Inhibition of MGMT-mediated autophagy suppression decreases cisplatin chemosensitivity in gastric cancer. *Biomed Pharmacother* 125:109896. doi: 10.1016/j.biopha.2020.109896
- Levine, B., and Kroemer, G. (2019). Biological functions of autophagy genes: a disease perspective. *Cell* 176, 11–42. doi: 10.1016/j.cell.2018.09.048
- Levy, J. M. M., Towers, C. G., and Thorburn, A. (2017). Targeting autophagy in cancer. *Nat. Rev. Cancer* 17, 528–542. doi: 10.1038/nrc.2017.53
- Li, B., Wang, W., Li, Z., Chen, Z., Zhi, X., Xu, J., et al. (2017). MicroRNA-148a-3p enhances cisplatin cytotoxicity in gastric cancer through mitochondrial fission induction and cyto-protective autophagy suppression. *Cancer Lett.* 410, 212–227. doi: 10.1016/j.canlet.2017.09.035
- Li, J., Duan, H., Xuan, F., Zhao, E., and Huang, M. (2019). CDGSH iron sulfur domain 2 deficiency inhibits cell proliferation and induces cell differentiation of neuroblastoma. *Pathol. Oncol. Res.* 26, 1725–1733. doi: 10.1007/s12253-019-00753-7
- Li, M., Gao, F., Zhao, Q., Zuo, H., Liu, W., and Li, W. (2020). Tanshinone IIA inhibits oral squamous cell carcinoma via reducing Akt-c-Myc signaling-mediated aerobic glycolysis. *Cell Death Dis.* 11:381. doi: 10.1038/s41419-020-2579-9
- Li, X., Yang, X., Liu, Y., Gong, N., Yao, W., Chen, P., et al. (2013). Japonicone A suppresses growth of Burkitt lymphoma cells through its effect on NF-kappaB. *Clin. Cancer Res.* 19, 2917–2928. doi: 10.1158/1078-0432.CCR-12-3258
- Li, Y., Wang, Y., Zou, M., Chen, C., Chen, Y., Xue, R., et al. (2018). AMPK blunts chronic heart failure by inhibiting autophagy. *Biosci. Rep.* 38:BSR20170982. doi: 10.1042/bsr20170982
- Li, Y., Zeng, Q. G., Qiu, J. L., Pang, T., Wang, H., and Zhang, X. X. (2020). Propofol suppresses migration, invasion, and epithelial-mesenchymal transition in papillary thyroid carcinoma cells by regulating miR-122 expression. *Eur. Rev. Med. Pharmacol. Sci.* 24, 5101–5110. doi: 10.26355/eurrev_202005_21203
- Lin, Y., Zhao, J., Wang, H., Cao, J., and Nie, Y. (2017). miR-181a modulates proliferation, migration and autophagy in AGS gastric cancer cells and downregulates MTMR3. *Mol. Med. Rep.* 15, 2451–2456. doi: 10.3892/mmr.2017.6289
- Liu, B., Pan, S., Xiao, Y., Liu, Q., Xu, J., and Jia, L. (2018). LINC01296/miR-26a/GALNT3 axis contributes to colorectal cancer progression by regulating O-glycosylated MUC1 via PI3K/AKT pathway. *J. Exp. Clin. Cancer Res.* 37:316. doi: 10.1186/s13046-018-0994-x
- Liu, F., Qiu, F., Fu, M., Chen, H., and Wang, H. (2020). Propofol reduces epithelial to mesenchymal transition, invasion and migration of gastric cancer cells through the MicroRNA-195-5p/Snail Axis. *Med. Sci. Monit.* 26:e920981. doi: 10.12659/msm.920981
- Liu, H., Ma, L., Lin, J., Cao, B., Qu, D., Luo, C., et al. (2020a). Advances in molecular mechanisms of drugs affecting abnormal glycosylation and metastasis of breast cancer. *Pharmacol. Res.* 155:104738. doi: 10.1016/j.phrs.2020.104738
- Liu, H., Xie, S., Fang, F., Kalvakolanu, D. V., and Xiao, W. (2020b). SHQ1 is an ER stress response gene that facilitates chemotherapeutics-induced apoptosis via sensitizing ER-stress response. *Cell Death Dis.* 11:445. doi: 10.1038/s41419-020-2656-0
- Liu, S., Zhang, J., Yang, H., Zhang, Q., and Chen, M. (2020). Pectolinarigenin flavonoid exhibits selective anti-proliferative activity in cisplatin-resistant hepatocellular carcinoma, autophagy activation, inhibiting cell migration and invasion. G2/M phase cell cycle arrest and targeting ERK1/2 MAP kinases. *J. Buon.* 25, 415–420.
- Liu, T., Zhang, J., Li, K., Deng, L., and Wang, H. (2020a). Combination of an autophagy inducer and an autophagy inhibitor: a smarter strategy emerging in cancer therapy. *Front. Pharmacol.* 11:408. doi: 10.3389/fphar.2020.00408
- Liu, Y. C., Yeh, C. T., and Lin, K. H. (2020b). Cancer stem cell functions in hepatocellular carcinoma and comprehensive therapeutic strategies. *Cells* 9:1331. doi: 10.3390/cells9061331
- López-Contreras, F., Muñoz-Urbe, M., Pérez-Laines, J., Ascencio-Leal, L., Rivera-Dictter, A., Martín-Martín, A., et al. (2019). Searching for drug synergy against cancer through polyamine metabolism impairment: insight into the metabolic effect of indomethacin on lung cancer cells. *Front. Pharmacol.* 10:1670. doi: 10.3389/fphar.2019.01670
- Lórin, P., and Juhász, G. (2020). Autophagosome-lysosome fusion. *J. Mol. Biol.* 432, 2462–2482. doi: 10.1016/j.jmb.2019.10.028
- Lu, R., Zhao, G., Yang, Y., Jiang, Z., Cai, J., and Hu, H. (2019). Inhibition of CD133 overcomes cisplatin resistance through inhibiting PI3K/AKT/mTOR signaling pathway and autophagy in CD133-positive gastric cancer cells. *Technol. Cancer Res. Treat.* 18:1533033819864311. doi: 10.1177/1533033819864311
- Lu, Y., Dong, S., Hao, B., Li, C., Zhu, K., Guo, W., et al. (2014). Vacuolin-1 potently and reversibly inhibits autophagosome-lysosome fusion by activating RAB5A. *Autophagy* 10, 1895–1905. doi: 10.4161/auto.32200
- Lystad, A. H., Carlsson, S. R., and Simonsen, A. (2019). Toward the function of mammalian ATG12-ATG5-ATG16L1 complex in autophagy and related processes. *Autophagy* 15, 1485–1486. doi: 10.1080/15548627.2019.1618100
- Mao, K., and Klionsky, D. J. (2011). AMPK activates autophagy by phosphorylating ULK1. *Circ. Res.* 108, 787–788. doi: 10.1161/RES.0b013e3182194c29
- Mele, L., Del Vecchio, V., Liccardo, D., Prisco, C., Schwerdtfeger, M., Robinson, N., et al. (2020). The role of autophagy in resistance to targeted therapies. *Cancer Treat Rev.* 88:102043. doi: 10.1016/j.ctrv.2020.102043
- Moon, H. J., Park, S. Y., Lee, S. H., Kang, C. D., and Kim, S. H. (2019). Nonsteroidal anti-inflammatory drugs sensitize CD44-overexpressing cancer cells to Hsp90 inhibitor through autophagy activation. *Oncol. Res.* 27, 835–847. doi: 10.3727/096504019x15517850319579
- Moosavi, M. S., and Elham, Y. (2020). Aquaporins 1, 3 and 5 in different tumors, their expression, prognosis value and role as new therapeutic targets. *Pathol. Oncol. Res.* 26, 615–625. doi: 10.1007/s12253-019-00646-9
- Mrakovcic, M., and Fröhlich, L. F. (2018). p53-Mediated molecular control of autophagy in tumor cells. *Biomolecules* 8:14. doi: 10.3390/biom8020014

- Murugan, A. K. (2019). mTOR: Role in cancer, metastasis and drug resistance. *Semin. Cancer Biol.* 59, 92–111. doi: 10.1016/j.semcancer.2019.07.003
- Nakayama, S., Karasawa, H., Suzuki, T., Yabuuchi, S., Takagi, K., Aizawa, T., et al. (2017). p62/sequestosome 1 in human colorectal carcinoma as a potent prognostic predictor associated with cell proliferation. *Cancer Med.* 6, 1264–1274. doi: 10.1002/cam4.1093
- Nazim, U. M., Yin, H., and Park, S. Y. (2020). Downregulation of c-FLIP and upregulation of DR-5 by cantharidin sensitizes TRAIL-mediated apoptosis in prostate cancer cells via autophagy flux. *Int. J. Mol. Med.* 46, 280–288. doi: 10.3892/ijmm.2020.4566
- Nie, Y., Liang, X., Liu, S., Guo, F., Fang, N., and Zhou, F. (2020). WASF3 knockdown sensitizes gastric cancer cells to oxaliplatin by inhibiting ATG12-mediated autophagy. *Am. J. Med. Sci.* 359, 287–295. doi: 10.1016/j.amjms.2020.02.007
- Nobili, A., Krashia, P., and D'Amelio, M. (2020). Cisd2: a promising new target in Alzheimer's disease(†). *J. Pathol.* 251, 113–116. doi: 10.1002/path.5436
- Ouyang, L., Zhang, L., Fu, L., and Liu, B. (2017). A small-molecule activator induces ULK1-modulating autophagy-associated cell death in triple negative breast cancer. *Autophagy* 13, 777–778. doi: 10.1080/15548627.2017.1283470
- Pan, X. K., Su, F., Xu, L. H., Yang, Z. S., Wang, D. W., Yang, L. J., et al. (2018). DJ-1 Alters Epirubicin-induced Apoptosis via modulating epirubicin activated autophagy in human gastric cancer cells. *Curr. Med. Sci.* 38, 1018–1024. doi: 10.1007/s11596-018-1978-y
- Panda, P. K., Mukhopadhyay, S., Das, D. N., Sinha, N., Naik, P. P., and Bhutia, S. K. (2015). Mechanism of autophagic regulation in carcinogenesis and cancer therapeutics. *Semin. Cell Dev. Biol.* 39, 43–55. doi: 10.1016/j.semcdb.2015.02.013
- Parikh, C., Janakiraman, V., Wu, W. I., Foo, C. K., Kljavin, N. M., Chaudhuri, S., et al. (2012). Disruption of PH-kinase domain interactions leads to oncogenic activation of AKT in human cancers. *Proc. Natl. Acad. Sci. U.S.A.* 109, 19368–19373. doi: 10.1073/pnas.1204384109
- Pattingre, S., Bauvy, C., and Codogno, P. (2003). Amino acids interfere with the ERK1/2-dependent control of macroautophagy by controlling the activation of Raf-1 in human colon cancer HT-29 cells. *J. Biol. Chem.* 278, 16667–16674. doi: 10.1074/jbc.M210998200
- Pei, G., Luo, M., Ni, X., Wu, J., Wang, S., Ma, Y., et al. (2018). Autophagy facilitates metadherin-induced chemotherapy resistance through the AMPK/ATG5 pathway in gastric cancer. *Cell Physiol. Biochem.* 46, 847–859. doi: 10.1159/000488742
- Perez-Montoyo, H. (2020). Therapeutic potential of autophagy modulation in cholangiocarcinoma. *Cells* 9:614. doi: 10.3390/cells9030614
- Petroni, G., Bagni, G., Iorio, J., Duranti, C., Lottini, T., Stefanini, M., et al. (2020). Clarithromycin inhibits autophagy in colorectal cancer by regulating the hERG1 potassium channel interaction with PI3K. *Cell Death Dis.* 11:161. doi: 10.1038/s41419-020-2349-8
- Poursheikhani, A., Bahmanpour, Z., Razmara, E., Mashouri, L., Taheri, M., Morshedi Rad, D., et al. (2020). Non-coding RNAs underlying chemoresistance in gastric cancer. *Cell Oncol.* doi: 10.1007/s13402-020-00528-2 [Epub ahead of print].
- Qi, Y., Lv, J., Liu, S., Sun, L., Wang, Y., Li, H., et al. (2019). TSPAN9 and EMILIN1 synergistically inhibit the migration and invasion of gastric cancer cells by increasing TSPAN9 expression. *BMC Cancer* 19:630. doi: 10.1186/s12885-019-5810-2
- Qi, Y., Qi, W., Liu, S., Sun, L., Ding, A., Yu, G., et al. (2020). TSPAN9 suppresses the chemosensitivity of gastric cancer to 5-fluorouracil by promoting autophagy. *Cancer Cell Int.* 20:4. doi: 10.1186/s12935-019-1089-2
- Qian, H. R., and Yang, Y. (2016). Functional role of autophagy in gastric cancer. *Oncotarget* 7, 17641–17651. doi: 10.18632/oncotarget.7508
- Qin, J., Wang, W., and Zhang, R. (2017). Novel natural product therapeutics targeting both inflammation and cancer. *Chin. J. Nat. Med.* 15, 401–416. doi: 10.1016/S1875-5364(17)30062-6
- Qin, J. J., Jin, H. Z., Huang, Y., Zhang, S. D., Shan, L., Voruganti, S., et al. (2013). Selective cytotoxicity, inhibition of cell cycle progression, and induction of apoptosis in human breast cancer cells by sesquiterpenoids from *Inula linearifolia* Turcz. *Eur. J. Med. Chem.* 68, 473–481. doi: 10.1016/j.ejmech.2013.07.018
- Qin, J. J., Li, X., Hunt, C., Wang, W., Wang, H., and Zhang, R. (2018). Natural products targeting the p53-MDM2 pathway and mutant p53: recent advances and implications in cancer medicine. *Genes Dis.* 5, 204–219. doi: 10.1016/j.gendis.2018.07.002
- Qiu, L., Zhou, G., and Cao, S. (2020). Targeted inhibition of ULK1 enhances daunorubicin sensitivity in acute myeloid leukemia. *Life Sci.* 243:117234. doi: 10.1016/j.lfs.2019.117234
- Ranek, M. J., Kokkonen-Simon, K. M., Chen, A., Dunkerly-Eyring, B. L., Vera, M. P., Oeing, C. U., et al. (2019). PKG1-modified TSC2 regulates mTORC1 activity to counter adverse cardiac stress. *Nature* 566, 264–269. doi: 10.1038/s41586-019-0895-y
- Ratti, M., Lampis, A., Ghidini, M., Salati, M., Mirchev, M. B., Valeri, N., et al. (2020). MicroRNAs (miRNAs) and long non-coding RNAs (lncRNAs) as new tools for cancer therapy: first steps from bench to bedside. *Target Oncol.* 15, 261–278. doi: 10.1007/s11523-020-00717-x
- Reggiori, F., and Ungermann, C. (2017). Autophagosome maturation and fusion. *J. Mol. Biol.* 429, 486–496. doi: 10.1016/j.jmb.2017.01.002
- Russi, S., Verma, H. K., Laurino, S., Mazzone, P., Storto, G., Nardelli, A., et al. (2019). Adapting and surviving: intra and extra-cellular remodeling in drug-resistant gastric cancer cells. *Int. J. Mol. Sci.* 20:3736. doi: 10.3390/ijms20153736
- Sanchez-Martin, P., Lahuerta, M., Viana, R., Knecht, E., and Sanz, P. (2020). Regulation of the autophagic PI3KC3 complex by laforin/malin E3-ubiquitin ligase, two proteins involved in Lafora disease. *Biochim. Biophys. Acta Mol. Cell Res.* 1867:118613. doi: 10.1016/j.bbamcr.2019.118613
- Santos-Laso, A., Izquierdo-Sanchez, L., Rodrigues, P. M., Huang, B. Q., Azkargorta, M., Lapitz, A., et al. (2020). Proteostasis disturbances and endoplasmic reticulum stress contribute to polycystic liver disease: new therapeutic targets. *Liver Int.* 40, 1670–1685. doi: 10.1111/liv.14485
- Sato, E., Ohta, S., Kawakami, K., Ikeda, M., Takahashi, T., Kobayashi, S., et al. (2019). Tetrandrine increases the sensitivity of human lung adenocarcinoma PC14 cells to Gefitinib by Lysosomal Inhibition. *Anticancer Res.* 39, 6585–6593. doi: 10.21873/anticancer.13874
- Seetha, A., Devaraj, H., and Sudhandiran, G. (2020). Indomethacin and juglone inhibit inflammatory molecules to induce apoptosis in colon cancer cells. *J. Biochem. Mol. Toxicol.* 34:e22433. doi: 10.1002/jbt.22433
- Shi, X., Yokom, A., Wang, C., Young, L., Youle, R., and Hurley, J. (2020). ULK complex organization in autophagy by a C-shaped FIP200 N-terminal domain dimer. *J. Cell Biol.* 219:e201911047. doi: 10.1083/jcb.201911047
- Stanga, D., Zhao, Q., Milev, M., Saint-Dic, D., Jimenez-Mallebrera, C., and Sacher, M. (2019). TRAPPC11 functions in autophagy by recruiting ATG2B-WIPI4/WDR45 to preautophagosomal membranes. *Traffic* 20, 325–345. doi: 10.1111/tra.12640
- Suárez-Cabrera, C., de la Peña, B., González, L. L., Page, A., Martínez-Fernández, M., Casanova, M. L., et al. (2018). The Ras-related gene ERAS is involved in human and murine breast cancer. *Sci. Rep.* 8:13038. doi: 10.1038/s41598-018-31326-4
- Sun, H., Lesche, R., Li, D., Liliental, J., Zhang, H., Gao, J., et al. (1999). PTEN modulates cell cycle progression and cell survival by regulating phosphatidylinositol 3,4,5-trisphosphate and Akt/protein kinase B signaling pathway. *Proc. Natl. Acad. Sci. U.S.A.* 96, 6199–6204. doi: 10.1073/pnas.96.11.6199
- Sun, Y., Jiang, Y., Huang, J., Chen, H., Liao, Y., and Yang, Z. (2017). Cisd2 enhances the chemosensitivity of gastric cancer through the enhancement of 5-FU-induced apoptosis and the inhibition of autophagy by AKT/mTOR pathway. *Cancer Med.* 6, 2331–2346. doi: 10.1002/cam4.1169
- Thrift, A. P., and El-Serag, H. B. (2019). Burden of gastric cancer. *Clin. Gastroenterol. Hepatol.* 18, 534–542. doi: 10.1016/j.cgh.2019.07.045
- Tian, H., Wang, W., Meng, X., Wang, M., Tan, J., Jia, W., et al. (2019). ERas enhances resistance to cisplatin-induced apoptosis by suppressing autophagy in gastric cancer cell. *Front. Cell Dev. Biol.* 7:375. doi: 10.3389/fcell.2019.00375
- Tian, L., Zhao, Z., Xie, L., and Zhu, J. (2018). MiR-361-5p suppresses chemoresistance of gastric cancer cells by targeting FOXM1 via the PI3K/Akt/mTOR pathway. *Oncotarget* 9, 4886–4896. doi: 10.18632/oncotarget.23513
- Tsai, C. Y., Lin, T. A., Huang, S. C., Hsu, J. T., Yeh, C. N., Chen, T. C., et al. (2020). Is adjuvant chemotherapy necessary for patients with deficient mismatch repair gastric cancer? autophagy inhibition matches the mismatched. *Oncologist* 25, e1021–e1030. doi: 10.1634/theoncologist.2019-0419
- Vallecillo-Hernandez, J., Barrachina, M. D., Ortiz-Masia, D., Coll, S., Esplagues, J. V., Calatayud, S., et al. (2018). Indomethacin disrupts autophagic flux by

- p>inducing lysosomal dysfunction in gastric cancer cells and increases their sensitivity to cytotoxic drugs.
- Sci. Rep.*
- 8:3593. doi: 10.1038/s41598-018-21455-1
- Wang, H., Jiao, H., Jiang, Z., and Chen, R. (2020). Propofol inhibits migration and induces apoptosis of pancreatic cancer PANC-1 cells through miR-34a-mediated E-cadherin and LOC285194 signals. *Bioengineered* 11, 510–521. doi: 10.1080/21655979.2020.1754038
- Wei, F., Jiang, X., Gao, H. Y., and Gao, S. H. (2017). Liquiritin induces apoptosis and autophagy in cisplatin (DDP)-resistant gastric cancer cells in vitro and xenograft nude mice in vivo. *Int. J. Oncol.* 51, 1383–1394. doi: 10.3892/ijo.2017.4134
- Wu, J., Chen, S., Liu, H., Zhang, Z., Ni, Z., Chen, J., et al. (2018). Tunicamycin specifically aggravates ER stress and overcomes chemoresistance in multidrug-resistant gastric cancer cells by inhibiting N-glycosylation. *J. Exp. Clin. Cancer Res.* 37:272. doi: 10.1186/s13046-018-0935-8
- Xi, Z., Si, J., and Nan, J. (2019). LncRNA MALAT1 potentiates autophagy-associated cisplatin resistance by regulating the microRNA-30b/autophagy-related gene 5 axis in gastric cancer. *Int. J. Oncol.* 54, 239–248. doi: 10.3892/ijo.2018.4609
- Xiao, F., Ouyang, B., Zou, J., Yang, Y., Yi, L., and Yan, H. (2020). Trim14 promotes autophagy and chemotherapy resistance of gastric cancer cells by regulating AMPK/mTOR pathway. *Drug Dev. Res.* 81, 544–550. doi: 10.1002/ddr.21650
- Xin, L., Zhou, Q., Yuan, Y. W., Zhou, L. Q., Liu, L., Li, S. H., et al. (2019). METase/lncRNA HULC/FoxM1 reduced cisplatin resistance in gastric cancer by suppressing autophagy. *J. Cancer Res. Clin. Oncol.* 145, 2507–2517. doi: 10.1007/s00432-019-03015-w
- Xu, J., Chen, Y., Yang, R., Zhou, T., Ke, W., Si, Y., et al. (2020). Cucurbitacin B inhibits gastric cancer progression by suppressing STAT3 activity. *Arch. Biochem. Biophys.* 684:108314. doi: 10.1016/j.abb.2020.108314
- Xu, W., Shi, Q., Qian, X., Zhou, B., Xu, J., Zhu, L., et al. (2018a). Rab5a suppresses autophagy to promote drug resistance in cancer cells. *Am. J. Transl. Res.* 10, 1229–1236.
- Xu, W., Wei, Q., Han, M., Zhou, B., Wang, H., Zhang, J., et al. (2018b). CCL2-SQSTM1 positive feedback loop suppresses autophagy to promote chemoresistance in gastric cancer. *Int. J. Biol. Sci.* 14, 1054–1066. doi: 10.7150/ijbs.25349
- Xu, Z., Chen, L., Xiao, Z., Zhu, Y., Jiang, H., Jin, Y., et al. (2018). Potentiation of the anticancer effect of doxorubicin drug-resistant gastric cancer cells by tanshinone IIA. *Phytomedicine* 51, 58–67. doi: 10.1016/j.phymed.2018.05.012
- Yang, L. Q., Li, R. Y., Yang, X. Y., Cui, Q. F., Wang, F. Y., Lin, G. Q., et al. (2019). Co-administration of shexiang baixin pill and chemotherapy drugs potentiated cancer therapy by vascular-promoting strategy. *Front. Pharmacol.* 10:565. doi: 10.3389/fphar.2019.00565
- YiRen, H., YingCong, Y., Sunwu, Y., Keqin, L., Xiaochun, T., Senrui, C., et al. (2017). Long noncoding RNA MALAT1 regulates autophagy associated chemoresistance via miR-23b-3p sequestration in gastric cancer. *Mol. Cancer* 16:174. doi: 10.1186/s12943-017-0743-3
- You, Q., Xu, J., Zhu, Z., Hu, Z., and Cai, Q. (2020). Phloretin flavonoid exhibits selective antiproliferative activity in doxorubicin-resistant gastric cancer cells by inducing autophagy, inhibiting cell migration and invasion, cell cycle arrest and targeting ERK1/2 MAP pathway. *J. Buon.* 25, 308–313.
- Young, L. N., Goerdeler, F., and Hurley, J. H. (2019). Structural pathway for allosteric activation of the autophagic PI 3-kinase complex I. *Proc. Natl. Acad. Sci. U.S.A.* 116, 21508–21513. doi: 10.1073/pnas.1911612116
- Yu, Y., Hou, L., Song, H., Xu, P., Sun, Y., and Wu, K. (2017). Akt/AMPK/mTOR pathway was involved in the autophagy induced by vitamin E succinate in human gastric cancer SGC-7901 cells. *Mol. Cell Biochem.* 424, 173–183. doi: 10.1007/s11010-016-2853-4
- Yuan, L., Xu, Z. Y., Ruan, S. M., Mo, S., Qin, J. J., and Cheng, X. D. (2020). Long non-coding RNAs towards precision medicine in gastric cancer: early diagnosis, treatment, and drug resistance. *Mol. Cancer* 19:96. doi: 10.1186/s12943-020-01219-0
- Yuan, L., Zhang, K., Zhou, M. M., Wasan, H. S., Tao, F. F., Yan, Q. Y., et al. (2019). Jiedu sangen decoction reverses epithelial-to-mesenchymal transition and inhibits invasion and metastasis of colon cancer via AKT/GSK-3 β signaling pathway. *J. Cancer* 10, 6439–6456. doi: 10.7150/jca.32873
- Zachari, M., and Ganley, I. G. (2017). The mammalian ULK1 complex and autophagy initiation. *Essays Biochem.* 61, 585–596. doi: 10.1042/ebc20170021
- Zeng, X., Wang, H. Y., Bai, S. Y., Pu, K., Wang, Y. P., and Zhou, Y. N. (2020). The roles of microRNAs in multidrug-resistance mechanisms in gastric cancer. *Curr. Mol. Med.* doi: 10.2174/1566524020066200226124336 [Epub ahead of print].
- Zhang, C., Wang, N., Tan, H. Y., Guo, W., Chen, F., Zhong, Z., et al. (2020). Direct inhibition of the TLR4/MyD88 pathway by geniposide suppresses HIF-1 α -independent VEGF expression and angiogenesis in hepatocellular carcinoma. *Br. J. Pharmacol.* 177, 3240–3257. doi: 10.1111/bph.15046
- Zhang, F., Chen, C., Hu, J., Su, R., Zhang, J., Han, Z., et al. (2019). Molecular mechanism of *Helicobacter pylori*-induced autophagy in gastric cancer. *Oncol. Lett.* 18, 6221–6227. doi: 10.3892/ol.2019.10976
- Zhang, X., Wang, L., Ireland, S. C., Ahat, E., Li, J., Bekier, M. E., et al. (2019). GORASP2/GRASP55 collaborates with the PtdIns3K UVRAG complex to facilitate autophagosome-lysosome fusion. *Autophagy* 15, 1787–1800. doi: 10.1080/15548627.2019.1596480
- Zhang, X., Xie, K., Zhou, H., Wu, Y., Li, C., Liu, Y., et al. (2020). Role of non-coding RNAs and RNA modifiers in cancer therapy resistance. *Mol. Cancer* 19:47. doi: 10.1186/s12943-020-01171-z
- Zhang, Y., Fan, Y., Huang, S., Wang, G., Han, R., Lei, F., et al. (2018). Thymoquinone inhibits the metastasis of renal cell cancer cells by inducing autophagy via AMPK/mTOR signaling pathway. *Cancer Sci.* 109, 3865–3873. doi: 10.1111/cas.13808
- Zhang, Y. F., Li, C. S., Zhou, Y., and Lu, X. H. (2020). Propofol facilitates cisplatin sensitivity via lncRNA MALAT1/miR-30e/ATG5 axis through suppressing autophagy in gastric cancer. *Life Sci.* 244:117280. doi: 10.1016/j.lfs.2020.117280
- Zhao, R., Zhang, X., Zhang, Y., Zhang, Y., Yang, Y., Sun, Y., et al. (2020). HOTTIP predicts poor survival in gastric cancer patients and contributes to cisplatin resistance by sponging miR-216a-5p. *Front. Cell Dev. Biol.* 8:348. doi: 10.3389/fcell.2020.00348
- Zhong, B., Li, Y., Liu, X., and Wang, D. (2018). Association of mast cell infiltration with gastric cancer progression. *Oncol. Lett.* 15, 755–764. doi: 10.3892/ol.2017.7380
- Zhou, H., Yuan, M., Yu, Q., Zhou, X., Min, W., and Gao, D. (2016). Autophagy regulation and its role in gastric cancer and colorectal cancer. *Cancer Biomark* 17, 1–10. doi: 10.3233/cbm-160613
- Zhou, S., Sun, Y., Zhao, K., Gao, Y., Cui, J., Qi, L., et al. (2020). miR-21/PTEN pathway mediates the cardioprotection of geniposide against oxidized low-density lipoprotein-induced endothelial injury via suppressing oxidative stress and inflammatory response. *Int. J. Mol. Med.* 45, 1305–1316. doi: 10.3892/ijmm.2020.4520
- Zhu, J. X., Qin, J. J., Jin, H. Z., and Zhang, W. D. (2013). Japonicones Q-T, four new dimeric sesquiterpene lactones from *Inula japonica* Thunb. *Fitoterapia* 84, 40–46. doi: 10.1016/j.fitote.2012.09.026

Conflict of Interest: The authors declare that the research was conducted in the absence of any commercial or financial relationships that could be construed as a potential conflict of interest.

Copyright © 2020 Xu, Yuan, Tang, Xu, Xu, Cheng and Qin. This is an open-access article distributed under the terms of the Creative Commons Attribution License (CC BY). The use, distribution or reproduction in other forums is permitted, provided the original author(s) and the copyright owner(s) are credited and that the original publication in this journal is cited, in accordance with accepted academic practice. No use, distribution or reproduction is permitted which does not comply with these terms.



Lactic Acidosis Interferes With Toxicity of Perifosine to Colorectal Cancer Spheroids: Multimodal Imaging Analysis

Barbora Pavlatovská¹, Markéta Machálková², Petra Brisudová¹, Adam Pruška^{3†}, Karel Štěpka⁴, Jan Michálek⁴, Tereza Nečasová⁴, Petr Beneš^{1,5}, Jan Šmarda¹, Jan Preisler², Michal Kozubek⁴ and Jarmila Navrátilová^{1,5*}

¹ Department of Experimental Biology, Faculty of Science, Masaryk University, Brno, Czechia, ² Department of Chemistry, Faculty of Science, Masaryk University, Brno, Czechia, ³ Department of Chemistry and Applied Biosciences, ETH Zurich, Zurich, Switzerland, ⁴ Centre for Biomedical Image Analysis, Faculty of Informatics, Masaryk University, Brno, Czechia, ⁵ Center for Biological and Cellular Engineering, International Clinical Research Center, St. Anne's University Hospital, Brno, Czechia

OPEN ACCESS

Edited by:

Wei Zhao,
Chengdu Medical College, China

Reviewed by:

Giacomo Domenici,
Instituto de Biologia e Tecnologia
Experimental (IBET), Portugal
Xin-ying Li,
Nanjing University, China

*Correspondence:

Jarmila Navrátilová
jnavratilova@sci.muni.cz

†ORCID:

Adam Pruška
orcid.org/0000-0002-5304-2541

Specialty section:

This article was submitted to
Molecular and Cellular Oncology,
a section of the journal
Frontiers in Oncology

Received: 08 July 2020

Accepted: 20 October 2020

Published: 04 December 2020

Citation:

Pavlatovská B, Machálková M, Brisudová P, Pruška A, Štěpka K, Michálek J, Nečasová T, Beneš P, Šmarda J, Preisler J, Kozubek M and Navrátilová J (2020) Lactic Acidosis Interferes With Toxicity of Perifosine to Colorectal Cancer Spheroids: Multimodal Imaging Analysis. *Front. Oncol.* 10:581365. doi: 10.3389/fonc.2020.581365

Colorectal cancer (CRC) is a disease with constantly increasing incidence and high mortality. The treatment efficacy could be curtailed by drug resistance resulting from poor drug penetration into tumor tissue and the tumor-specific microenvironment, such as hypoxia and acidosis. Furthermore, CRC tumors can be exposed to different pH depending on the position in the intestinal tract. CRC tumors often share upregulation of the Akt signaling pathway. In this study, we investigated the role of external pH in control of cytotoxicity of perifosine, the Akt signaling pathway inhibitor, to CRC cells using 2D and 3D tumor models. In 3D settings, we employed an innovative strategy for simultaneous detection of spatial drug distribution and biological markers of proliferation/apoptosis using a combination of mass spectrometry imaging and immunohistochemistry. In 3D conditions, low and heterogeneous penetration of perifosine into the inner parts of the spheroids was observed. The depth of penetration depended on the treatment duration but not on the external pH. However, pH alteration in the tumor microenvironment affected the distribution of proliferation- and apoptosis-specific markers in the perifosine-treated spheroid. Accurate co-registration of perifosine distribution and biological response in the same spheroid section revealed dynamic changes in apoptotic and proliferative markers occurring not only in the perifosine-exposed cells, but also in the perifosine-free regions. Cytotoxicity of perifosine to both 2D and 3D cultures decreased in an acidic environment below pH 6.7. External pH affects cytotoxicity of the other Akt inhibitor, MK-2206, in a similar way. Our innovative approach for accurate determination of drug efficiency in 3D tumor tissue revealed that cytotoxicity of Akt inhibitors to CRC cells is strongly dependent on pH of the tumor microenvironment. Therefore, the effect of pH should be considered during the design and pre-clinical/clinical testing of the Akt-targeted cancer therapy.

Keywords: perifosine, Akt kinase, tumor environment, lactic acidosis, alkalization, signal co-registration, mass spectrometry imaging, colorectal cancer

INTRODUCTION

Colorectal carcinoma (CRC) is the fourth most common cause of cancer death in Western countries (1, 2). More than 1.8 million new cases of CRC were diagnosed in 2018 (3). Accumulation of several genetic mutations including those affecting the PI3K/Akt pathway has been described during CRC development (1, 4–6). Akt transduces signals regulating multiple biological processes, such as cell proliferation, survival, growth, angiogenesis, migration and epithelial-mesenchymal transition in CRC as well as other cancers (6, 7). Therefore, targeting Akt has been suggested as a potential therapeutic strategy in cancer diseases (1, 5, 6, 8).

One of the most promising Akt inhibitors, perifosine, is a synthetic alkyl phospholipid that targets signal transduction pathways at the cell membrane by preventing correct localization of the Akt kinase, thus precluding its phosphorylation (9–12). Perifosine was shown to effectively target the PI3K/Akt pathway both in preclinical models and in clinical trials (10, 11). However, clinical studies resulted in disappointing response rates of common solid tumors to perifosine as a single agent, while combination with another therapies seemed to be more effective (13–15).

One of the factors contributing to the late recognition of insufficient cytotoxicity of drugs, occurring often in up to the third phase of clinical trials, is the model used for *in vitro* tests. Although it is well known that cells cultured in monolayer do not mimic the real environment, they are still widely used in preclinical research (16). Model dimensionality directly affects features of tumor-specific environment and as a result cell proliferation, differentiation, protein expression and response to cellular stimuli. *In vivo*, real tumors exhibit also increased expression of extracellular matrix proteins, increased stiffness, more natural cell-to-cell contacts, interstitial flow, stromal and immune cells, and gradients of nutrients, oxygen and pH. The efforts to define pH of the *in vivo* growing tumor (17) and manipulations of extracellular pH to support therapy have been performed on 2D and 3D models in the past (18–22). Moreover, the intercapillary distance is relatively large in tumor tissues, and this contributes to reduced transport of drugs. For these reasons, the 3D tumor models are considered to be more suitable for drug testing (16, 23–28). Acquisition of drug resistance followed by chemotherapy failure is frequently associated with establishment of acidic tumor-specific microenvironment (19, 29–33). Interestingly, tumor alkalization may restore drug efficacy and reduce cancer invasion (29, 34). Extracellular acidosis might result from dysregulated tumor metabolism, increased glycolytic activity or poor vascular perfusion (35, 36). As a result, the pH of

the tumor microenvironment may reach the values ranging from 6.2 to 6.9. Furthermore, colorectal tumors could be exposed to a wide range of intraluminal pH (5.9 – 8.1) depending on their localization in the intestinal tract, patient diet, and activity of intestinal microflora (37–41). This fact is mostly overlooked in CRC research.

Limited drug penetration into tumor tissue might lead to chemotherapy failure and drug resistance. The matrix-assisted laser desorption/ionization time-of-flight mass spectrometry imaging (MALDI TOF MSI) has been used to localize the distribution of drugs in colon, ovarian, breast or pancreatic tissue (42–45). Cell apoptosis and proliferation markers can be detected by immunohistochemistry (IHC) (46, 47). Since the 3D models emerge as a valuable tool for high-throughput drug screening and nanomedicine research (23, 48, 49), an efficient workflow for spatial co-localization of drug distribution with IHC-detectable biological response is essential for the correct interpretation of the results. Therefore, we have recently introduced the IHC-compatible MALDI mass spectrometry (MS) protocol employing fiducial markers for co-localization of signals. Quantification of MS and IHC signals in equidistant layers from the spheroid boundary to its center has been used to obtain information about the effects of drugs on cell proliferation, apoptosis, metabolism and other processes (50). Since the MALDI MSI analysis setting does not modify the protein epitopes (51), MS and IHC can be performed on the same spheroid section.

This work aims to clarify the effect of specific features of the CRC tumor and colon microenvironment on perifosine distribution and cytotoxicity. Using 2D and 3D CRC models, we observed that perifosine cytotoxicity was strongly pH dependent. Perifosine penetration into cells was pH-dependent in 2D but was rather low and not influenced by extracellular pH in 3D settings.

METHODS

Cell Cultures and Chemicals

HT-29 and HCT-116 human adenocarcinoma cells (ATCC®, HTB-38™) were obtained from LGC Standards (Teddington, UK). Cells were cultivated in humidified 5% CO₂ at 37°C in DMEM (Sigma-Aldrich, St. Louis, Missouri, USA) with 10% fetal bovine serum (FBS) (Invitrogen, Paisley, UK), 2 mM L-glutamine, 100 U/mL penicillin and 100 U/mL streptomycin (Lonza, Basel, Switzerland). Adherent cells were harvested with trypsin (Biosera, Nuaille, France) and counted using the Bürker chamber (Assistent, Sondheim vor der Rhön, Germany). The cells were treated with a stock solution of 5 mM perifosine (Sigma-Aldrich, St. Louis, Missouri, USA) in 50% ethanol (VWR International, Monroeville, Pennsylvania, USA).

pH of Culture Media

Conditions of eight different culture media mimicking the tumor microenvironment (normal pH/normoxia, acidic pH/normoxia, normal pH/hypoxia, acidic pH/hypoxia and each of

Abbreviations: ATP, adenosine triphosphate; calcein-AM, calcein-acetoxymethyl; CRC, colorectal cancer; DHB, 2,5-dihydroxybenzoic acid; DMEM, Dulbecco's Modified Eagle's Medium; DMSO, dimethyl sulfoxide; FBS, fetal bovine serum; IHC, immunohistochemistry; IQR, interquartile range; ITO, indium tin oxide; LA, lactic acid; LSCM, laser scanning confocal microscopy; MALDI TOF MS, matrix-assisted laser desorption/ionization time-of-flight mass spectrometry imaging; MSI, mass spectrometry imaging; MTT, 3-(4,5-dimethylthiazol-2-yl)-2,5-diphenyltetrazolium bromide; NaL, sodium lactate; per.-treated, perifosine-treated; PBS, phosphate-buffered saline; pHe, extracellular pH; PI3K, phosphoinositide 3-kinase; pKa, dissociation constant; RPMI, Roswell Park Memorial Institute; SD, standard deviation.

them with alkalization) were simulated by pH modulation of RPMI 1640 media (Sigma-Aldrich, St. Louis, Missouri, USA) by lactic acid (LA) and sodium bicarbonate (NaHCO_3). As a control, normal pH 7.4 was maintained by the addition of 20 mM sodium lactate (NaL) excluding the effect of lactate alone on drug efficacy (52). The pH of the culture media was determined by the HydroDish® HD24 (PreSens, Freiburg, Germany) at 37°C, 5% CO_2 after 24 h in wells without the cells (**Table 1**). These pH values of conditioned media were used for description of all experiments. For hypoxic cell culture (1% O_2), the BioSpherix I-Glove cell culture chamber (BioSpherix, New York, USA) was used. Furthermore, the presence of hypoxic conditions (1% O_2) in this chamber was verified by the optical oxygenic probe WTW-FDO 925, WTW Multi 3410 (WTW—measuring and analytical technology, Prague, Czechia). The up-regulation of carbonic anhydrase IX level finally proved the exposition of cells to hypoxia (not shown).

To determine alterations of pH during cultivation of cells grown in monolayers, we monitored pH in real-time using the HydroDish® HD24 plates. The cells (2×10^5 cells/mL) were cultivated in media supplemented with NaL, LA and NaHCO_3 in concentrations described in **Table 1**. The experiments were performed in normoxia and hypoxia for 48 h.

Three-Dimensional Cell Culture Models

For multicellular spheroid formation, the HT-29 and HCT-116 cells were seeded at a density of 5×10^4 cells/mL on the agar-coated (1% agar in 1× PBS) 12-well plate (Costar®, Corning Incorporate, Kennebunk, Maine, USA) in DMEM supplemented with 2 mM L-glutamine and lacking FBS. Cells were incubated on a rotary shaker (Orbital Shaker, NB-101SRC, N-BIOTEK, Korea) at 75 rpm in a humidified 5% CO_2 atmosphere at 37°C for 3 h, after which FBS was added at a 1% concentration. The next day, FBS was supplied to a final concentration of 10%, and the spheroids were cultivated for another 5 days at 60 rpm (51).

Cell Proliferation and Viability

MTT Assay

Cell metabolic activity was measured using the MTT assay. Briefly, cell suspension (2×10^5 cells/mL) was seeded to the 24-well plates (Costar®, Corning Incorporate, Kennebunk, Maine,

USA) and cells were pre-treated in culture media with various pH (pH 6.6, 7.3, 7.4, and 7.9) for 72 h. Next, the depleted media were replaced with fresh ones, and the cells were treated with perifosine (final concentration 10 and 20 μM). Control cells were treated with 50% ethanol as a solvent. The medium was removed, and 500 μL of 10% MTT (5 mg/mL) in RPMI was added for 1 h. Then, harvested cells were centrifuged, the supernatant removed, and 150 μL of dimethyl sulfoxide (DMSO) was added to dissolve formazan crystals. Optical density was measured as a difference at two wavelengths (570–650 nm). For the MTT assay on 3D models, spheroids were treated with 20 μM perifosine or 50% ethanol in different culture media (pH 6.6, 7.4 for 72 h, pH 8.1 for 48 h). Spheroids were loosened by trypsin, pellets were collected by centrifugation and 200 μL of 10% MTT (5 mg/mL) in RPMI medium was added for 2.5 h. Optical density was determined as described for the 2D cell culture.

ATP Assay

The cells were treated with perifosine as described for the MTT assay. Quantification of cellular ATP was performed in cells cultured in 24-well plates using the ATP assay kit (Cayman Chemicals, Ann Arbor, Michigan, USA) as described earlier (53). The ATP concentration was subtracted from the calibration curve. The 3D models were disintegrated by trypsin and subjected to ATP assay using the same procedure.

Quantification of the Cell Cycle by Flow Cytometry

The cells (2×10^5 cells/mL) were seeded to the 6-wells plates (Costar®, Corning Incorporate, Kennebunk, Maine, USA) and left in various culture media for three days. Next, the depleted media were replaced with fresh ones and the cells were treated with perifosine (20 μM) for 24 h and harvested using trypsin. For detection of cells with fragmented DNA, the samples were processed by the citrate-modified cell cycle analysis, using flow cytometry (FACSVerse, BD, Andover, Massachusetts, USA) as described previously (54). The cell populations were quantified using FACSuite software (BD, Andover, Massachusetts, USA).

Live/Dead Cells Staining and LSCM Analysis

Viability of cells up to 100 μm from the spheroid surface was determined using the calcein-AM/propidium iodide live/dead cells staining. Experiments were performed in 12-well plates. Spheroids were treated with perifosine in different culture media (pH 6.6 and 7.4 for 72 h, pH 8.1 for 48 h). Next, 1 μM calcein-AM (ChemCruz, Santa Cruz Biotechnology, Santa Cruz, California, USA) and 3 μM propidium iodide (Cayman Pharma, Neratovice, Czech Republic) were added for 1 h. Subsequently, spheroids were washed in 1×PBS, and emitted fluorescence was detected by laser scanning confocal microscopy (LSCM) (TCS SP8, Leica Microsystems, Wetzlar, Germany). The wavelength for the calcein excitation was 488 nm, and the detection window was set to 500–550 nm. The propidium iodide was excited with 552 nm laser, and the emission was detected in the range of 590–670 nm. Cell viability was finally determined as the ratio of dead and live cells using TissueQuest software (TissueGnostics, Wien, Austria).

TABLE 1 | pH of the modified culture media.

The environment	Abbreviation	Concentration of chemicals	pH
Lactic acid	LA	20 mM	6.6
Lactic acid with sodium bicarbonate	LA + NaHCO_3	20 + 20 mM	7.3
Sodium lactate	NaL	20 mM	7.4
Sodium lactate with sodium bicarbonate	NaL + NaHCO_3	20 + 20 mM	7.9
Sodium bicarbonate	NaHCO_3	80 mM	8.1

The culture media were prepared by pH alteration of RPMI media using 20 mM lactic acid to decrease the pH or 20 mM/80 mM NaHCO_3 to increase the pH. As a control, 20 mM sodium lactate was used. The pH was measured by the HydroDish® HD24 at 37°C, 5% CO_2 after 24 h in wells without the cells.

Determination of pH Using the SNARF-5F Probe

For determination of the extracellular pH up to 15 μm from the spheroid surface (pHe), the cell-impermeant pH indicator, carboxy SNARF[®]-5F dye (S23922, Thermo Fisher Scientific, Waltham, Massachusetts, USA) was used. For calibration data, RPMI medium alone or supplemented with either LA or NaHCO_3 was prepared. pH values in these media were determined by HydroDish[®] HD24 plates (PreSens, Regensburg, Germany) in 37 °C, 5% CO_2 . Then, the SNARF-5F dye was added into calibration media (22 μM final concentration). Fluorescence emissions of this probe at 520–580 and 630–700 nm were simultaneously recorded in two channels of the confocal microscope in response to 488-nm laser excitation. Ratios of these fluorescence signals were calculated for each pH and plotted against the respective pH. All fluorescence measurements were performed at 37°C, 5% CO_2 . Fluorescence images of the samples were acquired using Leica Application Suite X (LAS X) software (Leica Microsystems, Wetzlar, Germany). For pHe determination, the spheroids were exposed to the cultivation media with or without LA (pH 6.6) or NaHCO_3 (pH 8.1) for three days. Then, the spheroids were loaded with SNARF[®]-5F dye (22 μM final concentration) for 4 h, and emitted fluorescence was measured. To eliminate autofluorescence, the spheroid without SNARF-5F loading was used as a control.

Gel Electrophoresis and Immunoblotting

Cells (2×10^5 cells/mL) were seeded in various culture media for 72 h. Then, the depleted media were replaced with fresh ones, and the cells were treated with perifosine for 24 and 48 h or left untreated. The cells were collected, lysed, and processed for gel electrophoresis followed by immunoblotting as described (55). The blots were probed with phospho-Akt, total Akt-, cleaved caspase 8-, cleaved PARP- (CST4060, CST4691, CST9496, CST5625, Cell Signaling Technology, Beverly, Massachusetts, USA) and α -tubulin-specific (ab7291, Abcam, Cambridge, UK) antibodies. For developing, goat anti-rabbit or anti-mouse secondary antibody conjugated to peroxidase (Cell Signaling Technology, Beverly, Massachusetts, USA) and standard ECL procedure with Immobilon Western Chemiluminescent HRP Substrate (Millipore, Burlington, Billerica, Massachusetts, USA) were used.

Treatment of Spheroids in the Floating Media

Spheroids were transferred to the 12-well plate with fresh RPMI media and treated with 20 μM perifosine for 6, 24, 48, and 72 h to determine perifosine penetration. To analyze the effect of microenvironment on perifosine penetration, the spheroids were treated with 20 μM perifosine in media with pH adjusted to either 6.6 or 8.1 for 72 and 48 h, respectively. As a control, the standard culture medium with pH 7.4 was used. Finally, all the spheroids were collected in cryomolds with warm gelatine and frozen at -80°C . Next, the sectioned tissue was processed for the perifosine analysis (MALDI MS) followed by cleaved caspase 8 determination (IHC) (briefly described in the **Supplementary**

Data Sheet 1), full description in (51). Unless otherwise stated, experiments were performed under floating conditions.

Treatment of Spheroids in the Collagen Matrix

Collagen was used for the culture of epithelial cancer cells in 3D setting. Compared to Matrigel, its composition is well defined, can be used in translational medicine and is easy to prepare (56). To better mimic *in vivo* conditions, glycated collagen has been used (57). Collagen glycation results in its stiffening, significantly altering its biological properties and was previously associated with cancer progression (57, 58).

For matrix preparation, collagen I (Sigma-Aldrich, St. Louis, Missouri, USA) was non-enzymatically glycosylated with glucose (Sigma-Aldrich, St. Louis, Missouri, USA, final concentration 100 mM) for five days at 4°C and then mixed with 3× concentrated cultivation medium in a 2:1 ratio (59). The pH was set to 7 or 8 using 1 M NaOH. The spheroids were embedded in 300 μL of this matrix and left at 37°C until solidified, then covered by 50 μL of culture medium and treated with perifosine for 48 h. Subsequently, the medium was removed, whole collagen matrix blocks were fixed by 4% paraformaldehyde for 24 h and dehydrated in 30% solution of sucrose (Sigma-Aldrich, St. Louis, Missouri, USA) for 7 days. Blocks were transferred to warm gelatine and frozen at -80°C . Finally, the spheroids were sectioned and subjected to MALDI MS and IHC analyses.

MALDI TOF MS of 2D and 3D Cell Cultures

MALDI MSI settings and the workflow for detection of the perifosine spatial distribution in 3D were fully described by Machálová et al., 2019 (51). For an overview, see the **Supplementary Data Sheet 1, Methodology**.

Perifosine Detection in Cell Culture Monolayers

Cells (2×10^5 cells/mL) cultivated in different tumor environments for 72 h were treated with perifosine (20 μM) for 2 h. Then, 6×10^5 cells in 100 μL of 1×PBS was cytocentrifuged (Rotofix 32A, HETTICH Zentrifugen, Tuttlingen, Germany, 1,000 rpm/5 min) on 4 positions of an indium tin oxide (ITO) conductive glass slide. The diameter of each spot was approximately 5 mm. The samples were covered by sublimated 2,5-dihydroxybenzoic acid (DHB, 0.24 mg/cm²) and dried in a desiccator for at least 30 min. Perifosine in spots of cytocentrifuged cells was measured using MALDI MSI (see the **Supplementary Data Sheet 1, Methodology**). However, since the imaging mode was not employed to obtain spatial information, but rather to automatically measure selected areas of all 4 spots at once, the laser beam diameter was set to a relatively large value of 70–80 μm and the pixel size was 200 μm . To obtain maximum information from the 200- μm pixel area, a total number of 1,000 laser shots were summed within the pixel, with random movement of the laser firing 200 shots/position. The number of pixels measured from each cytocentrifuged spot was approximately 40 to control the pixel-to-pixel reproducibility. The cytocentrifugation experiment was performed in duplicates the same day (2 glass slides) and in triplicates during a longer period.

Spatial Distribution, Co-Localization, and Quantification of MALDI MSI and IHC Signal in Spheroid Sections

The signals of perifosine from MALDI MSI and antibodies specific for Ki-67 and cleaved caspase 8 from IHC were obtained. The IHC protocol is described in **Supplementary Data Sheet 1**. The signals were co-localized and quantified. Then, the respective intensities of both MS and IHC modalities were evaluated along equidistant layers (“peels”) starting from the spheroid boundary. Since sections may contain areas with no tissue and therefore no meaningful signal, we used interactive thresholding to exclude these gaps from further analysis. The same threshold was used for all samples to be compared. Semiautomatic co-registration of MALDI MSI and IHC signals and the “peeling” analysis were also described by our group recently (50, 51).

Statistical Data Analysis

Distributions of the collected data were described in boxplots, showing medians (a thick mark), interquartile range (box bounding) and range (the whiskers of boxplots correspond to the minimum and maximum values). Statistical comparison for viability assays was performed using a two-sample t-test. In the case of non-normal distribution of data (tested via Shapiro-Wilk test), a log transformation was applied before the test. All experiments were performed at least in triplicate. For statistical evaluation of signal co-registration, the protocol presented in (51) was followed. The conclusions drawn from MALDI MS and IHC co-registration were based on at least three independent observations.

RESULTS

Acidosis Decreases the Intracellular Level and Cytotoxicity of Perifosine on CRC Cells in Monolayers

Cytotoxicity of drugs used to eliminate tumor cells *in vivo* can be significantly affected by specific features of the tumor, especially by acidosis and hypoxia. Therefore, *in vitro* culture conditions were optimized to mimic the corresponding values of tumor pH and hypoxia *in vivo*. The pH of cell culture media in the wells during cell cultivation was monitored by the PreSens method. After 24 h of cultivation in normoxia, the pH of the original culture medium and NaL-enriched medium was 7.4, while the pH of the LA-supplemented medium was 6.6. The decrease of pH induced by LA could be reversed by NaHCO₃ (20 mM) back to the normal pH value 7.3. On the contrary, in control wells with NaL, addition of NaHCO₃ resulted in an increase of pH to 7.9 (**Figure 1A**). After 48 h, slight acidification of the NaL- and NaHCO₃-supplemented medium was detected, presumably due to cellular metabolism (**Figure 1A**). These results verified that the cells in our cultures were exposed to physiological pH values within the range of those found either in the intestinal tract or in the extracellular space of tumors.

Then, we investigated the effect of extracellular acidosis and hypoxia on cytotoxicity of perifosine to HT-29 cells. We found

that cytotoxicity of perifosine used in clinically relevant 10 and 20 μ M concentrations (60, 61) for 24 h was suppressed by both acidosis alone and acidosis associated with hypoxia, as assessed by the MTT and ATP assays (**Figures 1B, C**). Less severe acidosis (pH 6.8 and higher) was not detrimental to perifosine efficacy (**Supplementary Image 1A**). Both controls and perifosine-induced cells exposed to acidic conditions pH 6.6 were still live and metabolically active, as verified by strong decrease of their metabolic activity after inhibition of glucose uptake and oxidative phosphorylation (OXPHOS) (**Supplementary Image 1B**). Addition of NaHCO₃ to the medium supplemented with LA (pH 7.3) restored perifosine efficacy, both in normoxia and hypoxia (**Figures 1B, C**). No difference in perifosine cytotoxicity was observed in the medium alone and the medium supplemented with NaL (**Supplementary Image 2**). Further alkalization of the NaL medium to a value 7.9 did not improve perifosine efficacy (**Figures 1B, C**). To confirm that the effect of media pH on cytotoxicity of perifosine is not cell line specific, we performed similar experiments using HCT-116 cells. We confirmed that cytotoxicity of perifosine on these cells was reduced by acidosis as well, although to a lesser extent than to HT-29 cells. Perifosine efficacy to HCT-116 cells exposed to hypoxia was affected by the fact that their survival in hypoxic conditions is limited (**Supplementary Image 3**). The importance of the pH for perifosine cytotoxicity was verified by the cell cycle analysis (**Figures 1D, E**). Frequency of the perifosine-treated cells with fragmented (subG0/G1) DNA presumably undergoing apoptosis significantly differed in acidic (pH 6.6) and other conditions (pH 7.3, 7.4, 7.9), both in normoxia and hypoxia (**Figures 1D, E, Supplementary Table 1**). Again, we verified that there was no difference in the perifosine cytotoxicity in media containing or lacking NaL. This indicates that lactate alone did not affect cytotoxicity of perifosine (data not shown). For complete information on the frequency of the cells detected in all phases of the cell cycle see **Supplementary Table 1**.

To confirm the role of pH in regulation of the perifosine ability to induce apoptosis, intracellular levels of cleaved PARP and caspase 8 were determined by immunoblotting. Compared to acidic conditions, elevated levels of cleaved PARP and cleaved caspase 8 were detected in HT-29 cells exposed to perifosine at pH 7.4 and normoxia. Alkalization of the LA-containing medium increased the levels of cleaved PARP and caspase 8 after treatment with perifosine (**Supplementary Image 4**). To confirm that perifosine inhibits the Akt activity under these conditions, the level of phospho-Akt (Ser473) was also determined. The decrease of the phospho-Akt protein was detected in normal, acidic and alkaline conditions. Similar results were obtained for the cells cultivated in hypoxia (**Supplementary Image 4**).

Since acidosis can limit the uptake of drugs by cells, we assessed the intracellular level of perifosine in HT-29 cells exposed to normoxia/hypoxia combined with either normal conditions or acidosis by MALDI MSI. Suitability of MALDI MSI for detection of perifosine was verified by laser capture microdissection followed by offline liquid extraction coupled to liquid chromatography with electrospray ionization mass spectrometry (51). Interestingly, the intracellular level

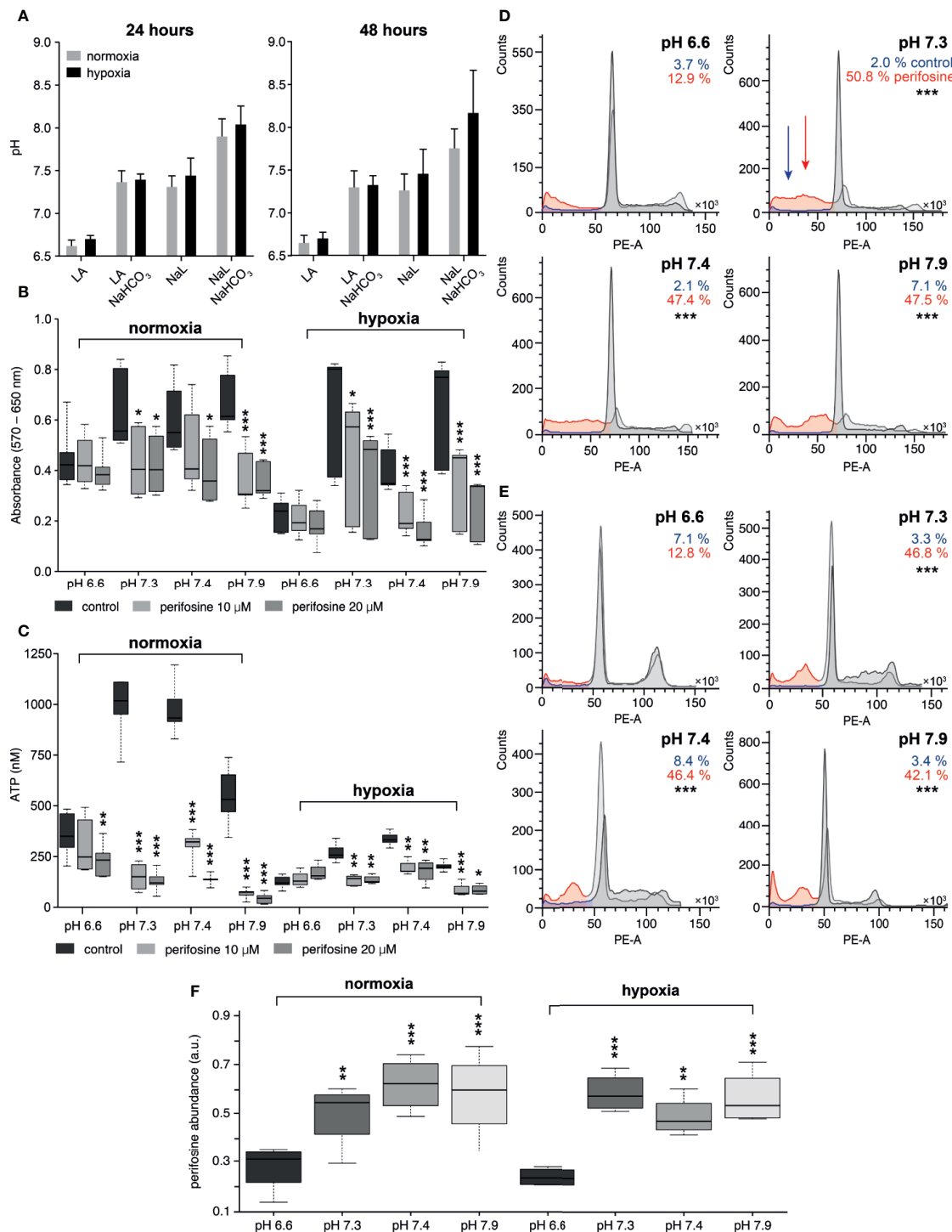


FIGURE 1 | The effect of the tumor-specific environment on perifosine cytotoxicity in 2D cell cultures. **(A)** The pH of conditioned media in normoxia and hypoxia; acidic media (LA), control conditions (Nal), alkalinized media (LA+NaHCO₃ and Nal+NaHCO₃). Results are presented as an average with standard deviation. **(B, C)** The effect of the pH on the perifosine cytotoxicity evaluated by MTT and ATP assays. Significant difference (*) in both absorbance and ATP value between controls and perifosine-induced samples is shown. **(D, E)** The frequency (%) of the cells in the subG0/G1 phase of the cell cycle in **(D)** normoxia and **(E)** hypoxia; control (blue) and perifosine-treated cells (red); statistically significant difference (*) between the cells treated in acidosis and other conditions is shown. **(F)** The level of perifosine determined in the cells cultivated in various tumor-specific environments using MALDI MSI; the significant increase of perifosine abundance between acidic (pH 6.6) and other conditions (*) are highlighted. Results are presented in boxplots showing median, interquartile range, minimum and maximum values; significant difference of all experiments was evaluated by t-test; * $p < 0.05$, ** $p < 0.01$, *** $p < 0.001$.

of perifosine in cells exposed to acidosis was lower than in cells cultivated in normal pH (**Figure 1F**). This effect was reverted by alkalization of the culture medium up to 7.3 or 7.9 (**Figure 1F**). A similar effect of pH on the intracellular level of perifosine was found in hypoxia (**Figure 1F**).

Perifosine Cytotoxicity and Spreading Through the Spheroids Are Limited

To test perifosine cytotoxicity in the 3D models, spheroids of HT-29 cells were treated with perifosine for 48 or 72 h. Cytotoxicity was assessed by the MTT assay performed either on intact or the trypsin-dissociated spheroids (**Supplementary Image 5**). Compared to the trypsin-dissociated spheroids, the intact spheroids exhibited only a minor decrease of viability after treatment with perifosine. This results from poor penetration of MTT into the spheroids, as verified by the bright-field microscopy of the spheroid sections (**Supplementary Image 5**). Therefore, for further experiments, the spheroids were dissociated into a suspension of individual cells before starting the MTT assays.

Next, we analyzed the perifosine distribution in the spheroids treated with perifosine for 6, 24, 48, and 72 h using MALDI MSI (**Figure 2**). The MS images of perifosine spots inside the spheroid and their quantification by peeling analysis are shown in **Figures 2A, B**. The MS imaging of the perifosine distribution revealed some perifosine signals in the gelatine surrounding the spheroid boundary (**Figure 2**). As reported previously, this perifosine signal can be explained by increased perifosine ionization in gelatine compared to biological tissue (51). Therefore, only perifosine signal within the spheroid section was quantified by peeling analysis. After 6 h, perifosine penetrated approximately 50 μm from the spheroid surface. During incubation prolonged

to 72 h, perifosine penetrated up to the maximum distance of 200 μm . The statistical analysis of the MS signal revealed a very heterogeneous distribution of perifosine within spheroids, not only from the spheroid periphery to its central part but also within the same peel—within the same distance from the spheroid boundary (**Figure 2B**).

To investigate the effect of perifosine on the biological response of the cells forming the spheroids, we co-localized its spatial distribution with markers of proliferation and apoptosis detected by IHC. Using the protocol for the co-localization of the MALDI MSI and fluorescence IHC data (50, 51), the distributions of Ki-67 (**Figure 3**) and cleaved caspase 8 (**Figure 4**) were examined. The distribution of Ki-67 and cleaved caspase 8 obtained by LSCM is depicted in **Figures 3A** and **4A** respectively, and the resulting graphs of both proteins and perifosine signals median values from the spheroid boundary towards its center are shown in **Figures 3B** and **4B**. The differences between median values of IHC signal in the control and the perifosine-induced spheroids are shown in **Figures 3C** and **4C**. This workflow allowed us to make the following conclusions for Ki-67 distribution. First, in each time interval, independently of perifosine induction, the highest abundance of the Ki-67 signal appeared within 200 μm from the spheroid boundary with a strong decline toward the spheroid center (**Figures 3A, B**). Second, analysis of differences between the Ki-67 median values in control and the perifosine-treated spheroids (**Figure 3C**) revealed increase of the Ki-67 abundance in the perifosine-free regions of the spheroids treated with the drug for 6 and 24 h. In the 24 h interval, the Ki-67 signal was stronger in the entire induced spheroid section, while in 48 and 72 h intervals, an abundance of Ki-67 diminished in the perifosine-exposed regions within the distance of 50 μm

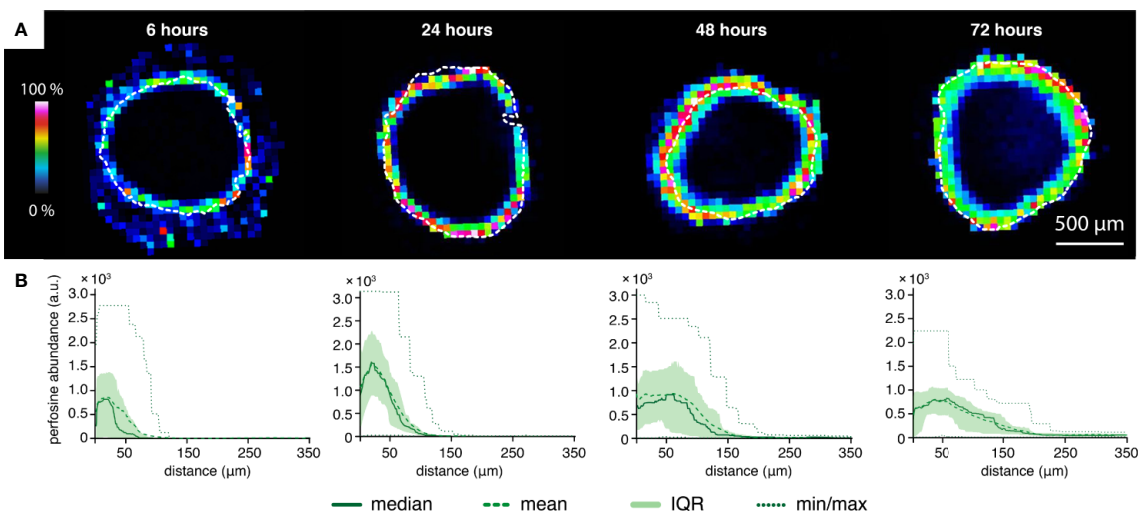


FIGURE 2 | The time-dependent peeling analysis of the perifosine penetration into the spheroids obtained by MALDI MSI. **(A)** MALDI MSI of perifosine distribution in the spheroid sections during the 6, 24, 48, and 72 h of treatment co-localized with the spheroid boundary detected by optical microscopy (white dashed line). **(B)** The distribution of perifosine abundance across the respective distances. The median and mean abundance in the peels are represented by the solid and dashed lines, respectively. Minimum and maximum values are represented by the dotted lines, the area of the interquartile range (IQR, i.e. values between the 25th and 75th quantiles) is highlighted in green. The zero at the X-axis coincides with the outer edge of the spheroid, while the Y-axis shows the peel abundance of perifosine.

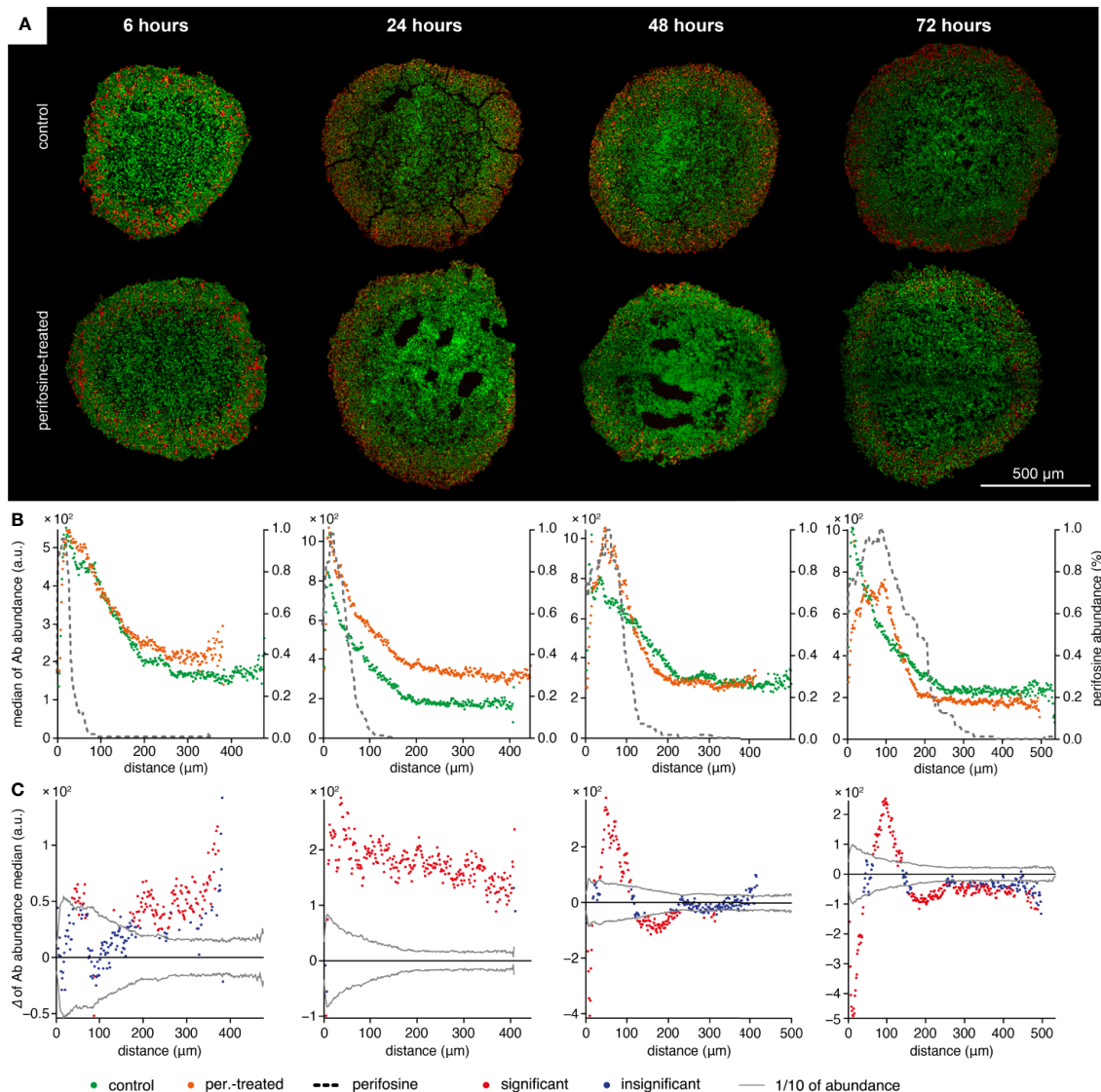


FIGURE 3 | The time-dependent co-localization of the perifosine and Ki-67 spatial distribution in the spheroids. **(A)** IHC images showing the signal of Ki-67 (red) and nuclei (green) for control and perifosine-treated (20 μ M) spheroids. **(B)** Peeling analysis of Ki-67 and perifosine distributions within the spheroid sections. Distribution of the Ki-67 (median per peel) for control (●) and perifosine-treated (●) spheroids are depicted. The perifosine signal was re-scaled using min-max normalization and its distribution is marked by the dashed line. **(C)** Differences between the median values of Ki-67 abundance in the control and the perifosine-treated spheroids. The median value of the control spheroid was subtracted from the median value of the induced spheroid in each peel. The zero at the X-axis coincides with the outer edge of the spheroid. The significant (●) and insignificant (●) differences of medians for $p < 0.05$ are distinguished.

from their boundary. This region of Ki-67 down-regulation adjoined to the area of 50–100 μ m from the spheroid boundary with elevated Ki-67 abundance (Figures 3B, C).

In contrast to the spheroid boundary, the increase of cleaved caspase 8 was detected in the spheroid center, both in controls and in perifosine-treated spheroids (Figures 4A, B). This may result from unfavorable conditions in the central zone of the spheroid. This gradient of cleaved caspase 8 distribution was not observed in the spheroids treated with perifosine for 72 h (Figures 4A, B). In each time interval tested, the level of cleaved caspase 8 was elevated in the perifosine-positive areas

(Figures 4A–C). Surprisingly, cleaved caspase 8 was upregulated also in the perifosine-free regions of the spheroid treated with perifosine for 24 h (Figure 4B). The possible explanation of this phenomenon is discussed in more detail below (Discussion section, paragraph 3).

Acidosis Decreases Efficacy of Perifosine on HT-29 Spheroids

The spheroids were placed into the control medium (pH 7.4) or the medium supplemented with either NaHCO_3 (80 mM, pH 8.1) or LA (20 mM, pH 6.6). The pH on the spheroid surface

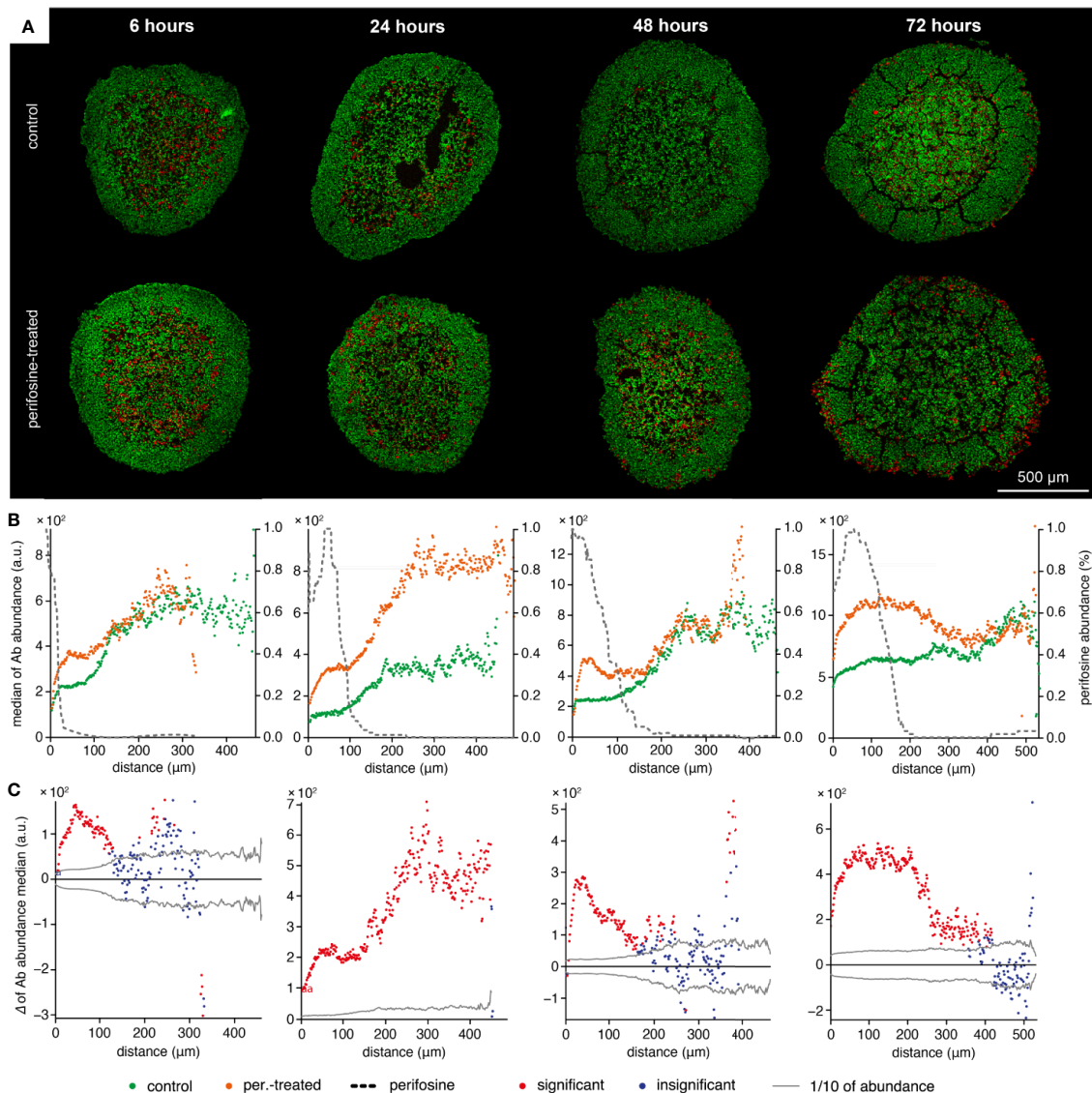


FIGURE 4 | The time-dependent co-localization of the perifosine and the cleaved caspase 8 spatial distribution. **(A)** IHC images showing the signal of cleaved caspase 8 (red) and nuclei (green) for control and perifosine-treated (20 μ M) spheroids. **(B)** Peeling analysis of cleaved caspase 8 and perifosine distributions within the spheroid sections. Distribution of the cleaved caspase 8 (median per peel) for control (●) and perifosine-treated (●) spheroids are depicted. The perifosine signal was re-scaled using min-max normalization, and its distribution is marked by the dashed line. **(C)** Differences between the median values of cleaved caspase 8 abundance in the control and the perifosine-treated spheroids. The median value of the control spheroid was subtracted from the median value of the induced spheroid in each peel. The zero at the X-axis coincides with the outer edge of the spheroid. The significant (●) and insignificant (●) differences of medians for $p < 0.05$ are distinguished.

was determined using cell-impermeable, ratiometric pH indicator SNARF-5F and LSCM analysis (**Supplementary Image 6A**). Even though cultivated in the medium with pH 7.4, the pHe on the surface of the spheroids (up to 15 μ m from the boundary) reached the value 6.3. Similar acidification of the spheroid surface to the value of 7.3 and 5.2 was detected for the spheroids exposed to the medium with pH 8.1 and 6.6, respectively (**Supplementary Image 6B**). It documents that the spheroid-forming cells maintain lower pHe on its surface, compared to the pH of the culture media.

To analyze the efficacy of perifosine in different intraluminal pH, the spheroids were cultivated in media with pH 6.6 or 7.4 and treated with perifosine for 72 h. Control spheroids were left untreated in both environments. The calcein-AM/propidium iodide staining showed that though acidic conditions induced some cell death even in the controls, perifosine did not cause further increase of the dead/live cell ratio. This suggests that perifosine is not efficient under acidic conditions (**Figures 5A, B**). Results of ATP and MTT assays confirmed that the efficacy of perifosine is reduced in acidic tumor environment (**Figure 5B**).

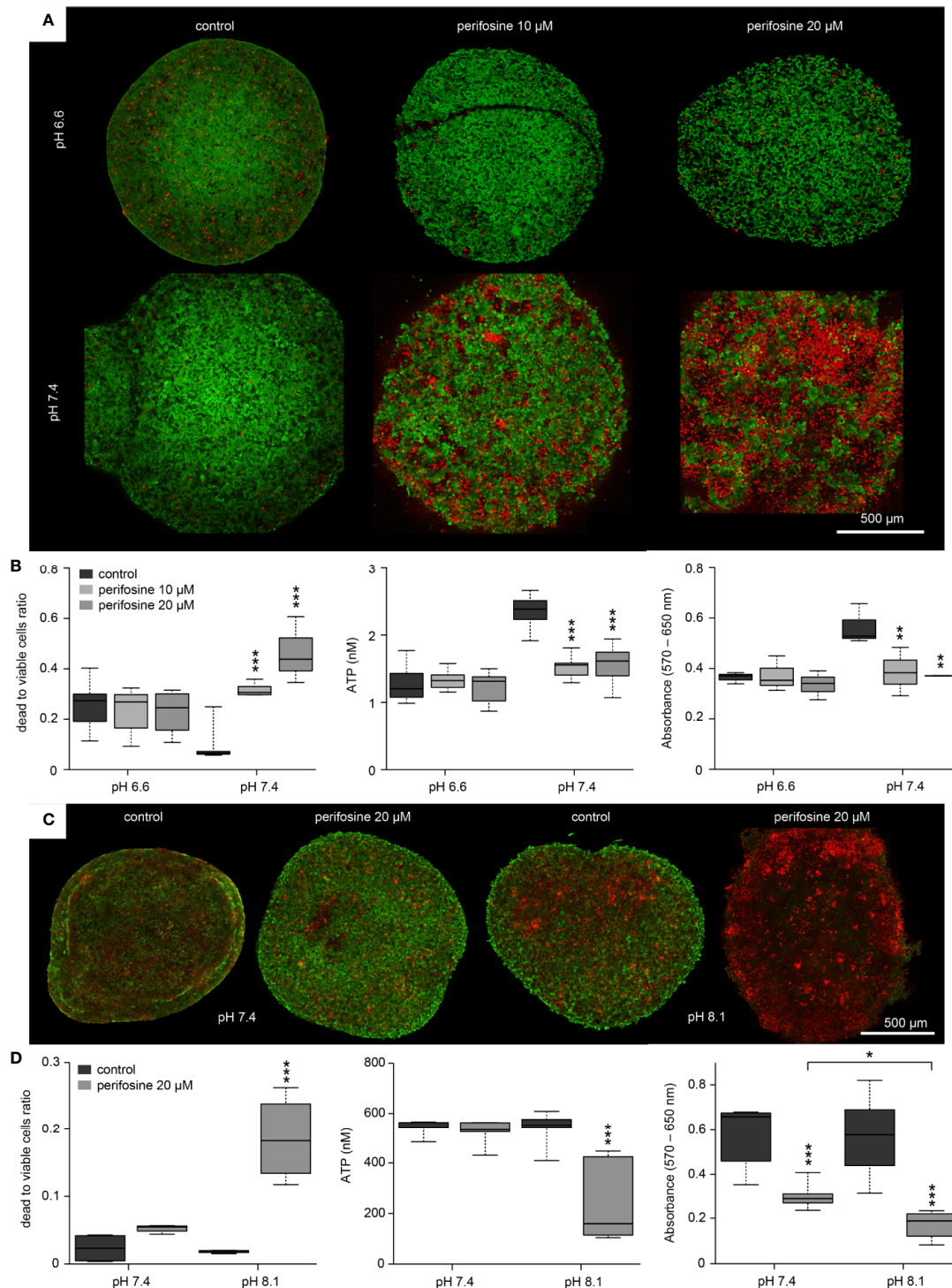


FIGURE 5 | The effect of the tumor-specific environment on cytotoxicity of perifosine to 3D cell cultures. **(A, C)** Images of the control and perifosine-treated (20 μ M) spheroids in either acidic, normal, or alkaline media obtained by LSCM after 72 **(A)** and 48 h **(C)**; living cells were dyed using calcein-AM (green) and dead cells using propidium-iodide (red). **(B, D)** Cytotoxicity of perifosine in different tumor-specific environments was calculated as a ratio of dead and living cells after calcein-AM/propidium iodide staining (left), as a change in ATP level (middle) and by MTT assay (right). Results are presented in boxplots showing median, interquartile range, minimum and maximum values; significant difference (*) between controls and perifosine-induced and perifosine-induced samples respectively were evaluated by t-test; * $p < 0.05$, ** $p < 0.01$, *** $p < 0.001$.

Compared to pH 7.4, further alkalization of the environment to pH 8.1 for 48 h increased the frequency of dead cells in the perifosine-treated spheroids as documented by the calcein-AM/propidium iodide staining, ATP and MTT assays (Figures 5C, D). Spheroids treated in alkalosis for more than 48 h were excluded from analyses due to loss of compactness. We conclude that acidosis significantly decreases cytotoxicity of perifosine to HT-29 cells grown both in the monolayers and in the 3D cultures. Similar results were observed also for the HCT-116 spheroids (Supplementary Image 7). This indicates that the modulatory effect of the tumor environment on perifosine efficacy is not cell-line-specific.

To further demonstrate the pH-dependency of the perifosine cytotoxicity, we co-localized perifosine distribution with the

cleaved caspase 8-positive areas in the spheroids exposed to normal and acidic conditions (Figures 6A–C). We found elevation of the cleaved caspase 8 in the perifosine-treated spheroids only in normal pH, not in the acidosis (Figures 6A–C). Then, we compared the level of cleaved caspase 8 in the perifosine-treated spheroids grown in pH 6.6 and 7.4. In acidic conditions, abundance of this apoptotic marker in the perifosine-rich regions was lower, while in the perifosine-free area located 200 μ m and more from the spheroid boundary, apoptosis was more pronounced (Figure 6D). The same phenomena was observed also in the control spheroids grown in acidosis, where the effect of perifosine was excluded (Figure 6B).

Finally, we wondered if alkalization of the culture medium can contribute to the perifosine toxicity on spheroids. Therefore,

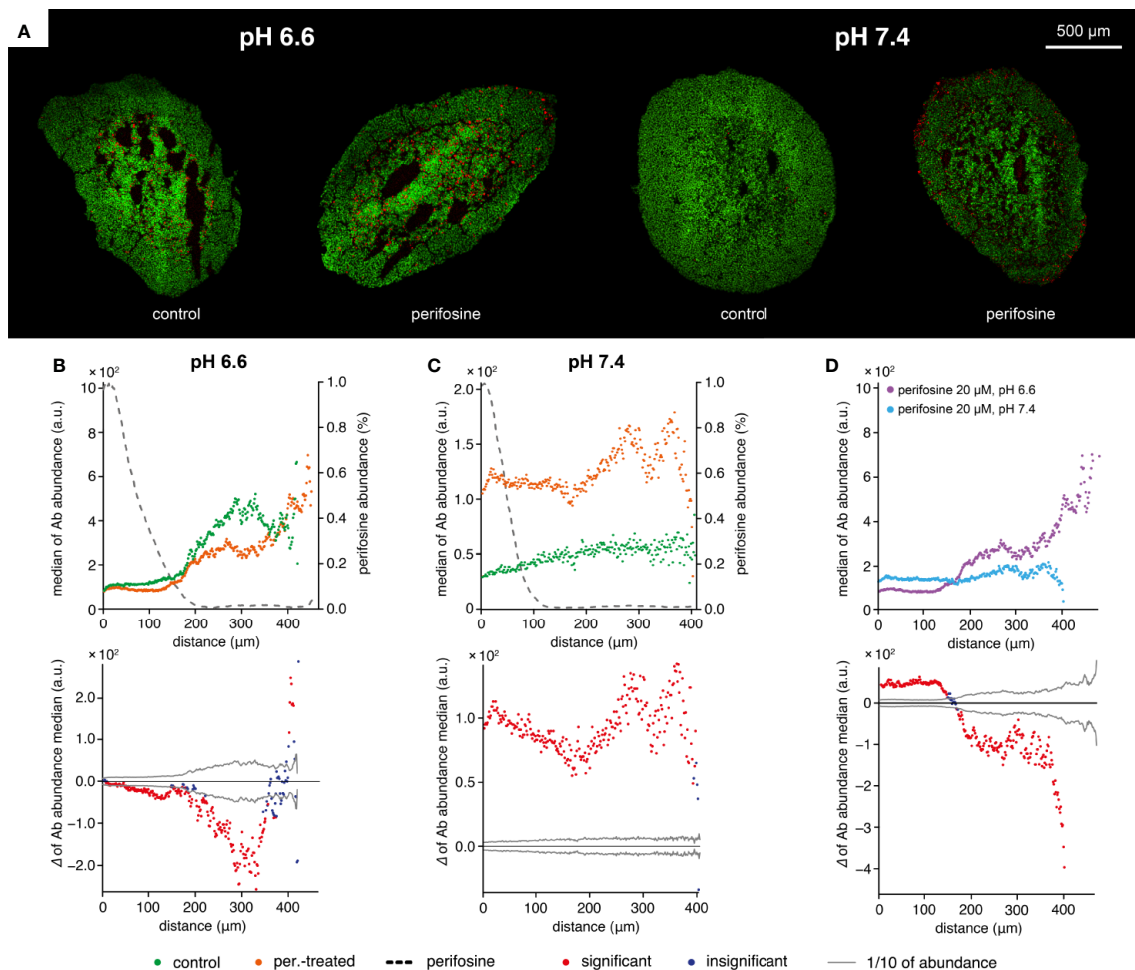


FIGURE 6 | The effect of acidosis on perifosine and cleaved caspase 8 signal abundance and co-localization. **(A)** IHC images showing the signal of cleaved caspase 8 (red) and nuclei (green) for control and perifosine-treated (20 μ M) spheroids after 72 h. **(B, C)** Peeling analysis of cleaved caspase 8 and perifosine distributions within the spheroid sections in acidic pH 6.6 **(B)** or normal pH 7.4 **(C)** conditions; distribution of cleaved caspase 8 (median per peel) in the control (●) and perifosine-treated (●) spheroid sections; the perifosine signal was re-scaled using min-max normalization and its distribution is marked by the dashed line (upper part); differences between the median values of cleaved caspase 8 abundance in the control spheroid and perifosine-treated spheroid (lower part). **(D)** Comparison of the cleaved caspase 8 distributions (median per peel) in the perifosine-treated spheroids in acidosis (●) and normal (●) media. Differences between the median values of cleaved caspase 8 abundance in the spheroids treated in acidic and normal media (bottom). The median value of the spheroid treated in acidic media was subtracted from the median value of the spheroid treated in normal media. The zero at the X-axis coincides with the outer edge of the spheroid. The significant (●) and insignificant (●) differences of medians for $p < 0.05$ are distinguished.

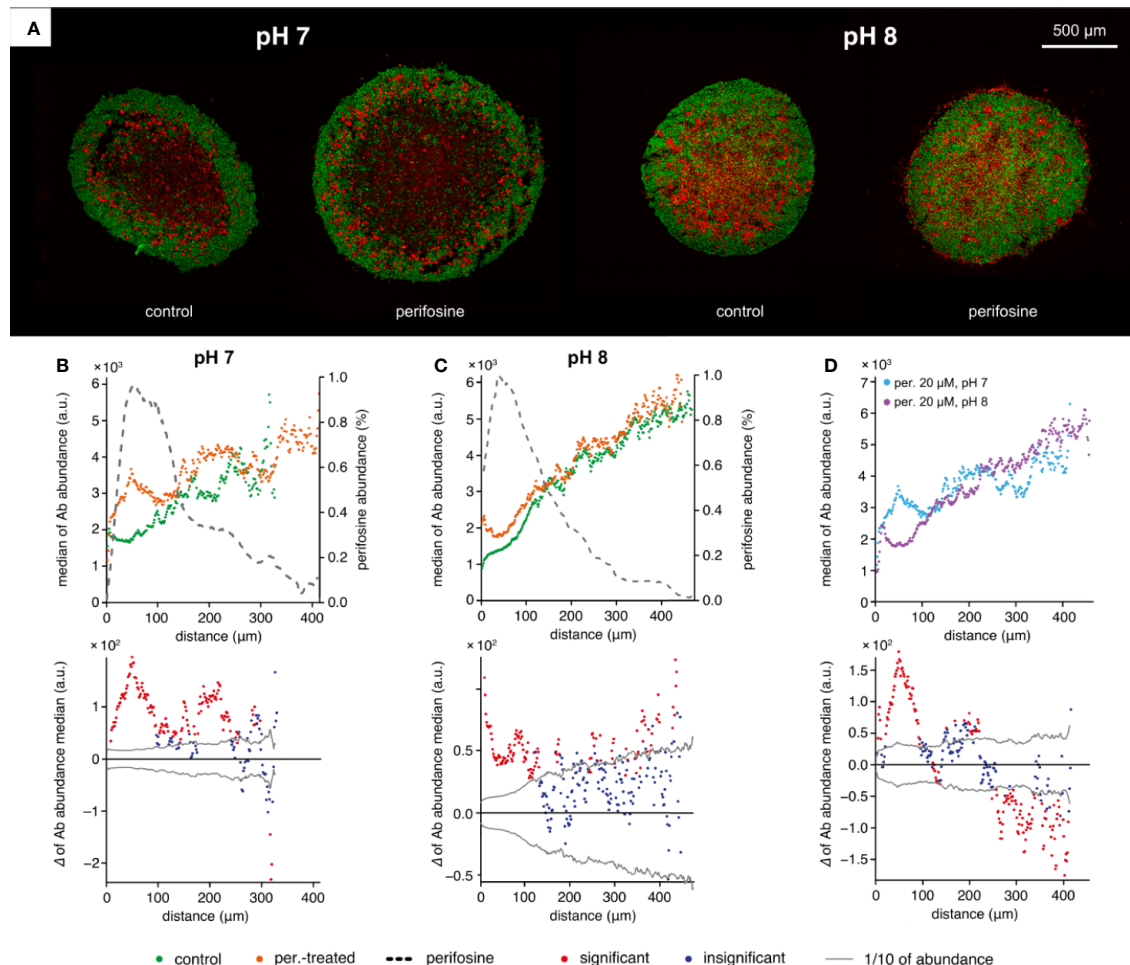


FIGURE 7 | The effect of alkaline conditions on perifosine and cleaved caspase 8 abundance and co-localization in the collagen matrix. **(A)** IHC images showing the signal of cleaved caspase 8 (red) and nuclei (green) for control and perifosine-treated (20 μ M) spheroids embedded in collagen matrix after 48 h. **(B, C)** Peeling analysis of cleaved caspase 8 and perifosine distributions within the spheroid sections in normal **(B)** or alkaline **(C)** conditions; distribution of cleaved caspase 8 (median per peel) in the control (●) and perifosine-treated (●) spheroid sections; the perifosine signal was re-scaled using min-max normalization and its distribution is marked by the dashed line (upper part); differences between the median values of cleaved caspase 8 abundance in the control spheroid and perifosine-treated spheroid (lower part). The median value of the control spheroid was subtracted from the median value of the treated spheroid in each peel. **(D)** Comparison of the cleaved caspase 8 distributions (median per peel) in the perifosine-treated spheroids in pH 7 (●) and alkaline pH 8 (●) media; differences between the median values of cleaved caspase 8 abundance in the spheroids treated in normal and alkaline media (bottom). The median value of the spheroid treated in alkaline media was subtracted from the median value of the spheroid treated in normal media. The zero at the X-axis coincides the outer edge of the spheroid. The significant (●) and insignificant (●) differences of medians for $p < 0.05$ are distinguished.

we assessed the distribution of cleaved caspase 8 and perifosine in spheroids exposed to media with pH 7.4 and 8.1 for 48 h. We did not detect any further upregulation of cleaved caspase 8 in the spheroids grown at pH 8.1 compared to pH 7.4 in fluidic conditions (**Supplementary Image 8**). To verify that the cleaved caspase 8-positive cells were not lost during the cultivation in these conditions, the spheroids were embedded and treated in collagen matrix with pH adjusted to 7 and 8 for 48 h. Elevation of cleaved caspase 8 in the perifosine-exposed regions compared to controls was detected in both pH 7 and pH 8 (**Figures 7A–C**). However, elevation of extra-spheroidal pH from 7 to 8 did not further increase the level of cleaved caspase 8; instead, a significant decrease was observed in the perifosine-rich

area (**Figures 7B–D**). No difference between perifosine penetration into spheroids exposed to pH 7 and 8 was detected (**Figures 7B, C**). Compared to fluidic conditions (**Supplementary Image 8**), the perifosine signal at the boundary of embedded spheroids was weaker and its penetration was slightly more efficient (**Figure 7B**).

DISCUSSION

Drug distribution in tumor tissue is important for its clinical efficacy. Only drugs capable of reaching high and homogeneous intratumoral concentrations can significantly reduce tumor

growth and angiogenesis (62). Spatial heterogeneity and incomplete drug penetration into tumor tissue facilitate the evolution of multidrug resistance (62, 63). Therefore, uneven intratumoral distribution highlights the need for studies addressing spatial drug distribution within tumors (64). We assessed the perifosine distribution in spheroids derived from colorectal carcinoma cells using MALDI MSI. The perifosine-positive regions were spread within the maximum distance of 200–300 μm from the spheroid boundary with the spheroids $\sim 1,000$ μm in diameter, as found in the longest time interval tested (72 h). Within these perifosine-positive regions, the cells were exposed to concentration gradients of this drug. Perifosine concentration variations were determined not only in the direction from the spheroid boundary to its central part, but also within peels. This shows that cells growing at the same distance from the spheroid boundary are exposed to various concentrations of perifosine, as depicted in the graphs of perifosine descriptive statistics (interquartile range, min/max values per peel). This irregular spread of perifosine might result in the development of compartments, in which the cells are exposed to lower dose of perifosine than its effective therapeutic concentration (65). Cells of these compartments might develop resistance to perifosine more frequently, due to stepwise accumulation of mutations (65).

No perifosine was detected deeper than 200 μm from spheroid boundary either in 6 h or in the 24 h time intervals. We investigated whether the perifosine-free regions overlap with the areas of dead cells that might originate from poor supply of oxygen and nutrients in deeper cellular layers (66). Using multi-modal imaging and co-localization workflow, we verified the presence of proliferating cells in the perifosine-free compartments of the perifosine-induced spheroids. Thus, we excluded the possibility that the perifosine-free regions overlap with the areas lacking viable cells. Inability of perifosine to reach tumor cells that are distant from the spheroid boundary suggests mechanism for development of the drug-resistance (44, 64, 67).

As reported previously, maximum inter-vessel distance in human colorectal carcinomas reached 1,000 μm (68). Given the maximum distance of perifosine penetration (200–300 μm) in our experiments, we hypothesize that the perifosine-free regions can be also found in *in vivo* growing tumors. Perifosine penetration into the collagen-embedded spheroids was investigated as well. In contrast to the spheroids exposed to perifosine in fluidic conditions, the maximum perifosine level at the boundary of the collagen embedded spheroids was lower, presumably due to its non-specific binding to the collagen matrix (69). Interestingly, perifosine was detected in the center of the collagen-embedded spheroids, even though at a very low level. Thus, the presence of an extra-tumoral matrix might influence drug distribution within the spheroid.

Determination of drug efficacy in the 3D models might be complicated by the natural presence of apoptotic regions originating from hypoxia, nutrient shortage and/or acidosis. To distinguish the perifosine-induced apoptosis from apoptosis caused by a hostile tumor microenvironment, the precise perifosine distribution in spheroids must be determined. Distributions of the apoptotic regions in the perifosine-treated

spheroid and untreated controls need to be compared as well. In the normal pH, the spheroids exhibited regions with both the presence of perifosine and up-regulated markers of apoptosis in each time interval tested. The apoptotic signal was also elevated in the perifosine-free area after 24 h of treatment. This result might be explained by the bystander effect. The bystander effect refers to cell death, altered growth or senescence of cells that had not been directly exposed to ionizing radiation or genotoxic chemicals, such as adriamycin, actinomycin D or mitomycin C, but accepted the medium-soluble or plasma factors (death ligands, inflammatory cytokines, and reactive oxygen species) excreted from the exposed cells. The intercellular signaling between the cells undergoing apoptosis and their neighborhood might reduce the survival rate even in cells, which were not directly exposed (70–75). Thus, perifosine might induce expression of soluble death ligands inducing apoptosis in the perifosine-free areas (71). The level of cleaved caspase 8 detected in spheroid cultivated in the LA-enriched media was lower than in the normal media providing further evidence that acidosis contributes to reduction of the perifosine cytotoxicity.

Ki-67 is strongly associated with cell proliferation and prognosis in CRC patients (76, 77). Therefore, we were interested in the Ki-67 level/distribution in the spheroids treated with perifosine. Surprisingly, increased level of Ki-67 was found in the perifosine-rich areas (in 24 h interval up to 100 μm from the spheroid boundary, in 48 and 72 h intervals 50–150 μm from the spheroid boundary) or localized in the perifosine-free regions (6 and 24 h intervals, 150 μm from spheroid boundary and deeper) in the perifosine-treated spheroids. The mechanism underlying this phenomenon needs to be further investigated. The chemotherapy-induced apoptosis might alleviate solid stress and favor the supply of oxygen and nutrients to the tumor cells resulting in the proliferation of drug-resistant cells or cells localized in the drug-free layers (78, 79). Indeed, the perifosine-treated spheroids are less compact than the controls and their periphery is composed of loosely attached cells. Therefore, perifosine might improve the supply of nutrients to the spheroid cells (**Supplementary Image 9**). The chemotherapy-induced cell proliferation has been observed previously and might contribute to chemotherapy failure (79, 80). However, perifosine downregulates Ki-67 during 48 and 72 h, and this effect is spatially restricted to the most peripheral cell layers 0–50 μm from the spheroid boundary. This indicates that perifosine should be administered for an extended period of time to decrease cell proliferation marked by Ki-67.

Perifosine penetration into spheroids is limited, as documented by spheroids derived from HT-29 cells. An inverse relationship between drug penetration and its binding to cellular components was reported (81). Perifosine accumulates in the cell membranes, thus, it belongs to the group of drugs with strong binding to cellular macromolecules, similar to doxorubicin, daunomycin, actinomycin D, and others (64, 82). Therefore, the slow delivery of perifosine to the inner cells of spheroids might be attributable to its efficient binding to cells in the outer layers (83).

Analysis of perifosine distribution, cell proliferation, and apoptosis reveals great heterogeneity in perifosine uptake and phenotypic response even within the same layer. This is exemplified in **Figures 3** and **4**, showing both cleaved caspase 8 and Ki-67 elevated at the distance of 50 μm from the spheroid boundary in the spheroids treated with perifosine for 48 h. The spheroids were derived from cell lines comprising of mixtures of phenotypically distinct subpopulations (84–87). These cell subpopulations might respond variously to drug application, for example, they might uptake perifosine with different efficacy. Also, even the cells with similar perifosine accumulation might respond dissimilarly, inducing either apoptosis or drug-resistant phenotype (84, 85, 88).

Drug efficacy may be seriously hampered by the tumor microenvironment. Acidosis, hypoxia, and nutrient shortage are common factors affecting chemotherapy effectiveness (30, 31, 89, 90). We have also previously reported increased cytotoxicity of the disulfiram/copper complex in acidosis and tetrathiomolybdate in low-glucose conditions (54, 55). It is well established that in tumors, acidosis can result from poor perfusion and accumulation of lactate in deep tumor layers (30, 91). Besides, as often neglected in CRC, colorectal tumors can be localized in colon regions with various intraluminal pH values (92). Using multiple assays, we proved that pH less than 6.7 significantly interferes with perifosine efficacy, both in cells in monolayers as well as spheroids. Elevation of extratumoral pH potentiated cytotoxicity of perifosine. However, the levels of cleaved caspase 8 in the spheroids exposed to perifosine in pH 7.4 and 8.1 in fluidic conditions or 7 and 8 in the collagen matrix, respectively, were comparable. The interpretation of this observation requires further experiments, but presumably the caspase 8-independent apoptotic and pro-death signaling pathway might be activated by perifosine in the spheroids exposed to highly alkaline conditions. In cellular monolayers, acidosis also interfered with intracellular accumulation of perifosine, both in normoxia and hypoxia. The mechanism behind the pH-dependent perifosine accumulation remains to be elucidated. We hypothesize that perifosine can be internalized by the phospholipid translocase activity or raft- and dynamin-mediated endocytosis (9, 93). Since especially the translocase activity strongly depends on ATP and the ATP level is decreased in cells exposed to acidosis, the absence of the translocase activity in the ATP-depleted acidic compartments might result in the lower accumulation of perifosine. However, the lack of perifosine accumulation in cells exposed to acidic pH cannot easily explain the loss of its cytotoxicity; the active form of the major perifosine target, the Akt kinase, is decreased to a similar extent in normal and acidic pH (**Supplementary Image 4**).

The untreated controls in pH 6.6 differed from those at pH 7.3, 7.4 and 7.9 in MTT and ATP level. It can be explained by the lower proliferation rate of cells cultivated in acidosis compared to those exposed to more alkaline conditions. The slower proliferation of these cells can result from the acidosis-induced “anti-Warburg” metabolic effects, starvation response and mTORC1 inhibition (94, 95).

The Akt kinase exerts its anti-apoptotic effect through multiple mechanisms, such as stimulation of glycolysis and glucose metabolism, regulation of the Bcl-2 proteins, and hexokinase activity (96–99). We hypothesize that the metabolism of cells

exposed to acidosis might not be sensitive to the Akt kinase inhibition, as acidosis directs energy generation from the Akt-dependent glucose metabolism and glycolysis toward aerobic respiration (30, 94, 100, 101) and glutamine utilization (102). Likewise, during the preparation of this manuscript, Barnes et al. reported that lactic acidosis interferes with cytotoxicity of another Akt inhibitor, uprosertib, in colon cancer cells (30). They suggest the ability to utilize lactate as a carbon source, decoupled glycolysis from the Citrate cycle, and enhanced oxidative metabolism as possible mechanisms of resistance of CRC cells to Akt inhibition in acidosis (30). Furthermore, the induction of chronic autophagy belongs to the survival adaptation of cells exposed to acidic conditions (103). Since protective autophagy is curtailed by the Akt signaling, cells in acidosis might benefit from Akt inhibition (104). Apart from this, in normal pH, phosphorylated Akt activates mTORC1, the master regulator of cellular proliferation and NF κ B, whose aberrant activation leads to tumorigenic potential of cancer cells (105, 106). However, acidosis reduces both mTORC1 activity and the efficacy of its inhibitor, rapamycin (107). Moreover, in low pH, NF κ B regulation is diverted from Akt kinase to alternative ASIC1-ROS-ERK-I κ B α axis (108). Thus, decreased efficacy of Akt inhibitors in low pH might be explained by pH-dependent regulation of signaling pathways linked to this kinase. Limited efficacy of the Akt inhibitors to cells grown in acidosis was shown by our group also for the other Akt inhibitor, MK-2206 (**Supplementary Image 10**). Therefore, the effect of the tumor-specific microenvironment should be considered in design and preclinical studies of Akt inhibitors in CRC therapy.

CONCLUSIONS

Our experiments confirmed the critical role of perifosine spatial distribution for the evaluation of its efficacy in spheroids. Distribution of perifosine inside the spheroids was found to be very heterogeneous, and the depth of penetration was time-dependent. Changes in the Ki-67 and cleaved caspase 8 distribution resulting from perifosine administration were interpreted in the context of 3D objects. We document that the drug-induced pro-apoptotic effect might be associated with increased proliferation of the drug-resistant cells as a result of changes in cellular density and presumably, nutrient supplementation. Moreover, the suppressive effect of acidosis on cytotoxicity of perifosine to cancer cells growing in monolayers and spheroids and its reversibility by alkalization was highlighted. As lactic acidosis interferes with cytotoxicity of the other Akt kinase inhibitors, external tumor pH should be considered in further design of the Akt-targeted treatment strategy.

DATA AVAILABILITY STATEMENT

The raw data supporting the conclusions of this article will be made available by the authors, without undue reservation.

AUTHOR CONTRIBUTIONS

JN, JP, and MK contributed to the conception of the study. BP, MM, PBr, AP, and JN performed the experiments. BP and JN wrote the manuscript. KŠ, JM, and MK developed the fiducial-marker-based co-registration workflow and performed the image analysis. TN was responsible for the statistical evaluation. AP helped significantly with graphic processing. PBe helped formulate clear conclusions with constructive discussion and JŠ contributed to the final coherence of text and by language skills. All authors contributed to the article and approved the submitted version.

FUNDING

This work was supported by the Grant Agency of Masaryk University (MUNI/G/0974/2016 and MUNI/A/1127/2019) and the Ministry of Education, Youth and Sports of the Czech

Republic (MEYS CR) under the projects CEITEC 2020 (LQ1601), TRANS-MED (LQ1605), the core facility CELLIM of CEITEC supported by the Czech-BioImaging large RI project (LM2018129 funded by MEYS CR) and ERDF (No. CZ.02.1.01/0.0/0.0/16_013/0001775).

ACKNOWLEDGMENTS

The authors would like to thank John B. Smith for proofreading the manuscript.

SUPPLEMENTARY MATERIAL

The Supplementary Material for this article can be found online at: <https://www.frontiersin.org/articles/10.3389/fonc.2020.581365/full#supplementary-material>

REFERENCES

- Pandurangan AK. Potential Targets for Prevention of Colorectal Cancer: A Focus on PI3K/Akt/mTOR and Wnt Pathways. *Asian Pac J Cancer Prev* (2013) 14:2201–5. doi: 10.7314/apjcp.2013.14.4.2201
- Mármol I, Sánchez-de-Diego C, Dieste AP, Cerrada E, Yoldi MJR. Colorectal carcinoma: A general overview and future perspectives in colorectal cancer. *Int J Mol Sci* (2017) 18(1):197. doi: 10.3390/ijms18010197
- World Cancer Research Fund International. *Colorectal cancer statistics* (2018). Available at: http://www.wcrf.org/cancer_statistics/data_specific_cancers/colorectal_cancer_statistic.s.php (Accessed July 7, 2020).
- Foley TM, Payne SN, Pasch, Cheri A, Foley TM, Payne SN, et al. Dual PI3K/mTOR Inhibition in Colorectal Cancers with APC and PIK3CA Mutations. *Mol Cancer Res MCR* 2017; (2017) 15:317–27. doi: 10.1158/1541-7786.MCR-16-0256
- Haydon AM, Jass JR. Emerging pathways in colorectal-cancer development. *Lancet Oncol* (2002) 3:83–8. doi: 10.1016/S1470-2045(02)00649-6
- Li D, Wang G, Jin G, Yao K, Zhao Z, Bie L, et al. Resveratrol suppresses colon cancer growth by targeting the AKT/STAT3 signaling pathway. *Int J Mol Med* (2019) 43(1):630–40. doi: 10.3892/ijmm.2018.3969
- Suman S, Kurisetty V, Das TP, Vadodkar A, Ramos G, Lakshmanaswamy R, et al. Activation of AKT signaling promotes epithelial-mesenchymal transition and tumor growth in colorectal cancer cells. *Mol Carcinog* (2013) Suppl 1:E151–60. doi: 10.1002/mc.22076
- Coant N, García-Barros M, Zhang Q, Obeid LM, Hannun YA. AKT as a key target for growth promoting functions of neutral ceramidase in colon cancer cells. *Oncogene* (2018) 37(28):3852–63. doi: 10.1002/mc.22076
- Muñoz-Martínez F, Torres C, Castany S, Gamarro F. The anti-tumor alkylphospholipid perifosine is internalized by an ATP-dependent translocase activity across the plasma membrane of human KB carcinoma cells. *Biochim Biophys Acta - Biomembr* (2008) 1778(2):530–40. doi: 10.1016/j.bbmem.2007.10.017
- Richardson PG, Eng C, Kolesar J, Hideshima T, Anderson KC. Perifosine, an oral, anti-cancer agent and inhibitor of the Akt pathway: mechanistic actions, pharmacodynamics, pharmacokinetics, and clinical activity. *Expert Opin Drug Metab Toxicol* (2012) 8(5):623–33. doi: 10.1517/17425255.2012.681376
- Kaley TJ, Panageas KS, Mellinghoff IK, Nolan C, Gavrilovic IT, DeAngelis LM, et al. Phase II trial of an AKT inhibitor (perifosine) for recurrent glioblastoma. *J Neurooncol* (2019) 144(2):403–7. doi: 10.1007/s11060-019-03243-7
- Ebrahimi S, Hosseini M, Shahidsales S, Maftouh GA, Ferns S, Ghayour-Mobarhan M, et al. Targeting the Akt/PI3K signaling pathway as a potential therapeutic strategy for the treatment of pancreatic cancer. *Curr Med Chem* (2017) 24(13):1321–31. doi: 10.2174/0929867324666170206142658
- Gills JJ, Dennis PA. Perifosine: Update on a novel Akt inhibitor. *Curr Oncol Rep* (2009) 11(2):102–10. doi: 10.1007/s11912-009-0016-4
- Becher OJ, Gilheeny SW, Khakoo Y, Lyden DC, Haque S, De Braganca KC, et al. A phase I study of perifosine with temsirolimus for recurrent pediatric solid tumors. *Pediatr Blood Cancer* (2017) 64(7):e26409. doi: 10.1002/pbc.26409
- Shen JS, Xu L, Zhao Q. Perifosine and ABT-737 synergistically inhibit lung cancer cells in vitro and in vivo. *Biochem Biophys Res Commun* (2016) 473(4):1170–6. doi: 10.1016/j.bbrc.2016.04.035
- Kapalczyńska M, Kolenda T, Przybyła W, Zajackowska M, Teresiak A, Filas V, et al. 2D and 3D cell cultures – a comparison of different types of cancer cell cultures. *Arch Med Sci* (2018) 14(4):910–9. doi: 10.5114/aoms.2016.63743
- Zhang X, Lin Y, Gillies RJ. Tumor pH and Its Measurement. *J Nucl Med* (2010) 51(8):1167–70. doi: 10.2967/jnumed.109.068981
- Mehta G, Hsiao AY, Ingram M, Luker GD, Takayama S. Opportunities and challenges for use of tumor spheroids as models to test drug delivery and efficacy. *J Control Release* (2012) 164(2):192–204. doi: 10.1016/j.jconrel.2012.04.045
- Wojtkowiak JW, Verduzco D, Schramm KJ, Gillies RJ. Drug resistance and cellular adaptation to tumor acidic pH microenvironment. *Mol Pharm* (2011) 8(6):2032–8. doi: 10.1021/mp200292c655
- Swietach P, Hulikova A, Patiar S, Vaughan-Jones RD, Harris AL. Importance of intracellular pH in determining the uptake and efficacy of the weakly basic chemotherapeutic drug, doxorubicin. *PLoS One* (2012) 7(4):1–9. doi: 10.1371/journal.pone.0035949
- Saggar JK, Yu M, Tan Q, Tannock IF. The tumor microenvironment and strategies to improve drug distribution. *Front Oncol* (2013) 3:154:154. doi: 10.3389/fonc.2013.00154
- Nunes AS, Barros AS, Costa EC, Moreira AF, Correia IJ. 3D tumor spheroids as in vitro models to mimic in vivo human solid tumors resistance to therapeutic drugs. *Biotechnol Bioeng* (2019) 116(1):206–26. doi: 10.1002/bit.26845
- Edmondson R, Broglie JJ, Adcock AF, Yang L. Three-Dimensional Cell Culture Systems and Their Applications in Drug Discovery and Cell-Based Biosensors. *Assay Drug Dev Technol* (2014) 12(4):207–18. doi: 10.1089/adt.2014

24. Huh D, Hamilton GA, Ingber DE. From 3D cell culture to organs-on-chips. *Trends Cell Biol* (2011) 21(12):745–54. doi: 10.1016/j.tcb.2011.09.005
25. Tibbitt MW, Anseth KS. Hydrogels as extracellular matrix mimics for 3D cell culture. *Biotechnol Bioeng* (2009) 103(4):655–63. doi: 10.1002/bit.22361
26. Senavirathna LK, Fernando R, Maples D, Zheng Y, Polf JC, Ranjan A. Tumor spheroids as an in vitro model for determining the therapeutic response to proton beam radiotherapy and thermally sensitive nanocarriers. *Theranostics* (2013) 3(9):687–91. doi: 10.7150/thno
27. Niero EL, Rocha-Sales B, Lauand C, Cortez BA, De Souza MM, Rezende-Teixeira P, et al. The multiple facets of drug resistance: One history, different approaches. *J Exp Clin Cancer Res* (2014) 33(1):1–14. doi: 10.1186/1756-9966-33-37
28. Souza AG, Silva IBB, Campos-Fernandez E, Barcelos LS, Souza JB, Marangoni K, et al. Comparative Assay of 2D and 3D Cell Culture Models: Proliferation, Gene Expression and Anticancer Drug Response. *Curr Pharm Des* (2018) 24(15):1689–94. doi: 10.2174/1381612824666180404152304
29. Alessandra L. Manipulating pH in Cancer Treatment : Alkalizing Drugs and Alkaline Diet. *J Complement Med Alt Healthcare* (2017) 2(1):1–5. doi: 10.19080/JCMAH.2017.02.555580
30. Barnes EME, Xu Y, Benito A, Herendi L, Siskos AP, Aboagye EO, et al. Lactic acidosis induces resistance to the pan-Akt inhibitor uposertib in colon cancer cells. *Br J Cancer* (2020) (March):1–11. doi: 10.1038/s41416-020-0777-y
31. Ibrahim-Hashim A, Estrella V. Acidosis and cancer: from mechanism to neutralization. *Cancer Metastasis Rev* (2019) 2019:38.1–2: 149–155. doi: 10.1007/s10555-019-09787-4
32. Roma-Rodrigues C, Mendes R, Baptista PV, Fernandes AR. Targeting tumor microenvironment for cancer therapy. *Int J Mol Sci* (2019) 20(4):840. doi: 10.3390/ijms20040840
33. Pellegrini P, Serviss JT, Lundbäck T, Bancaro N, Mazurkiewicz M, Kolosenko I, et al. A drug screening assay on cancer cells chronically adapted to acidosis. *Cancer Cell Int* (2018) 18(1):1–15. doi: 10.1186/s12935-018-0645-5
34. De Milito A, Fais S. Tumor acidity, chemoresistance and proton pump inhibitors. *Future Oncol* (2005) 1(6):779–86. doi: 10.2217/14796694.1.6.779
35. Neugent ML, Goodwin J, Sankaranarayanan I, Yetkin CE, Hsieh MH, Kim JW. A new perspective on the heterogeneity of cancer glycolysis. *Biomol Ther* (2018) 26(1):10–8. doi: 10.4062/biomolther.2017.210
36. Lin J, Xia L, Liang J, Han Y, Wang H, Oyang L, et al. The roles of glucose metabolic reprogramming in chemo- and radio-resistance. *J Exp Clin Cancer Res* (2019) 38(1):1–13. doi: 10.1186/s13046-019-1214-z
37. Holma R, Osterlund P, Sairanen U, Blom M, Rautio M, Korpela R. Colonic methanogenesis in vivo and in vitro and fecal pH after resection of colorectal cancer and in healthy intact colon. *Int J Colorectal Dis* (2012) 27(2):171–8. doi: 10.1007/s00384-011-1323-4
38. McDougall CJ, Wong R, Scudera P, Lesser M, DeCossé JJ. Colonic mucosal pH in humans. *Dig Dis Sci* (1993) 38(3):542–5. doi: 10.1007/BF01316512
39. Rose C, Parker A, Jefferson B, Cartmell E. The characterization of feces and urine: A review of the literature to inform advanced treatment technology. *Crit Rev Environ Sci Technol* (2015) 45(17):1827–79. doi: 10.1080/10643389.2014.1000761
40. Tian L, Bae YH. Cancer nanomedicines targeting tumor extracellular pH. *Colloids Surfaces B Biointerf* (2012) 99:116–26. doi: 10.1016/j.colsurfb.2011.10.039
41. Zhou ZH, Song JW, Li W, Liu X, Cao L, Wan LM, et al. The acid-sensing ion channel, ASIC2, promotes invasion and metastasis of colorectal cancer under acidosis by activating the calcineurin/NFAT1 axis. *J Exp Clin Cancer Res* (2017) 36(1):1–12. doi: 10.1186/s13046-017-0599-9
42. Walch A, Rauser S, Deininger SO, Höfler H. MALDI imaging mass spectrometry for direct tissue analysis: A new frontier for molecular histology. *Histochem Cell Biol* (2008) 130(3):421–34. doi: 10.1007/s00418-008-0469-9
43. Buck A, Halbritter S, Späth C, Feuchtinger A, Aichler M, Zitzelsberger H, et al. Distribution and quantification of irinotecan and its active metabolite SN-38 in colon cancer murine model systems using MALDI MSI. *Anal Bioanal Chem* (2015) 407(8):2107–16. doi: 10.1007/s00216-014-8237-2
44. Giordano S, Zucchetti M, Decio A, Cesca M, Fuso Nerini I, Maiezza M, et al. Heterogeneity of paclitaxel distribution in different tumor models assessed by MALDI mass spectrometry imaging. *Sci Rep* (2016) 6:1–12. doi: 10.1038/srep39284
45. Liu X, Flinders C, Mumenthaler SM, Hummon AB. MALDI Mass Spectrometry Imaging for Evaluation of Therapeutics in Colorectal Tumor Organoids. *J Am Soc Mass Spectrom* (2018) 29(3):516–26. doi: 10.1007/s13361-017-1851-4
46. Penault-Llorca F, Radosevic-Robin N. Ki67 assessment in breast cancer: an update. *Pathology* (2017) 49(2):166–71. doi: 10.1016/j.pathol.2016.11.006
47. Natalino RJM, Antoneli CBG, Ribeiro K de CB, Campos AHJFM, Soares FA. Immunohistochemistry of apoptosis-related proteins in retinoblastoma. *Pathol Res Pract* (2016) 212(12):1144–50. doi: 10.1016/j.prp.2016.09.010
48. Mardhian DF, Vrynas A, Storm G, Bansal R, Prakash J. FGF2 engineered SPIONs attenuate tumor stroma and potentiate the effect of chemotherapy in 3D heterospheroidal model of pancreatic tumor. *Nanotheranostics* (2020) 4(1):26–39. doi: 10.7150/ntno.38092
49. Wang Z, Li W, Jing H, Ding M, Fu G, Yuan T, et al. Generation of hepatic spheroids using human hepatocyte-derived liver progenitor-like cells for hepatotoxicity screening. *Theranostics* (2019) 9(22):6690–705. doi: 10.7150/thno.34520
50. Michálek J, Štěpka K, Kozubek M, Navrátilová J, Pavlatovská B, Machálková M, et al. Quantitative Assessment of Anti-Cancer Drug Efficacy from Coregistered Mass Spectrometry and Fluorescence Microscopy Images of Multicellular Tumor Spheroids. *Microsc Microanal* (2019) 25(6):1311–22. doi: 10.1017/S1431927619014983
51. Machálková M, Pavlatovská B, Michálek J, Pruška A, Štěpka K, Nečasová T, et al. Drug Penetration Analysis in 3D Cell Cultures Using Fiducial-Based Semiautomatic Coregistration of MALDI MSI and Immunofluorescence Images. *Anal Chem* (2019) 91(21):13475–84. doi: 10.1021/acs.analchem.9b02462
52. Michl J, Park KC, Swietach P. Evidence-based guidelines for controlling pH in mammalian live-cell culture systems. *Commun Biol* (2019) 2(1):1–12. doi: 10.1038/s42003-019-0393-7
53. Navrátilová J, Karasová M, Kohutková Lánová M, Jiráková L, Budková Z, Pacherník J, et al. Selective elimination of neuroblastoma cells by synergistic effect of Akt kinase inhibitor and tetrathiomolybdate. *J Cell Mol Med* (2017) 21(9):1859–69. doi: 10.1111/jcmm.13106
54. Navrátilová J, Hankeová T, Beneš P, Šmarda J. Low-glucose conditions of tumor microenvironment enhance cytotoxicity of tetrathiomolybdate to neuroblastoma cells. *Nutr Cancer* (2013) 65(5):702–10. doi: 10.1080/01635581.2013.789118
55. Navrátilová J, Hankeová T, Beneš P, Šmarda J. Acidic pH of tumor microenvironment enhances cytotoxicity of the disulfiram/Cu2+ complex to breast and colon cancer cells. *Chemotherapy* (2013) 59(2):112–20. doi: 10.1159/000353915
56. Jabaji Z, Sears CM, Brinkley GJ, Lei NY, Joshi VS, Wang J, et al. Use of collagen gel as an alternative extracellular matrix for the in vitro and in vivo growth of murine small intestinal epithelium. *Tissue Eng - Part C Methods* (2013) 19(12):961–9. doi: 10.1089/ten.TEC.2012.0710
57. Bansode S, Bashtanova U, Li R, Clark J, Müller KH, Puszkarska A, et al. Glycation changes molecular organization and charge distribution in type I collagen fibrils. *Sci Rep* (2020) 10(1):1–13. doi: 10.1038/s41598-020-60250-9
58. Schröter D, Höhn A. Role of Advanced Glycation End Products in Carcinogenesis and their Therapeutic Implications. *Curr Pharm Des* (2019) 24(44):5245–51. doi: 10.2174/1381612825666190130145549
59. Vicens-Zygmunt V, Estany S, Colom A, Montes-Worboys A, Machahua C, Sanabria AJ, et al. Fibroblast viability and phenotypic changes within glycated stiffened three-dimensional collagen matrices. *Respir Res* (2015) 16(1):1–15. doi: 10.1186/s12931-015-0237-z
60. Floryk D, Thompson TC. Perifosine induces differentiation and cell death in prostate cancer cells. *Cancer Lett* (2008) 266(2):216–26. doi: 10.1016/j.canlet.2008.02.060
61. Crul M, Rosing H, de Klerk G, Dubbelman R, Traiser M, Reichert S, et al. and pharmacological study of daily oral administration of perifosine (D-21266) in patients with advanced solid tumours. *Eur J Cancer* (2002) 38(12):1615–21. doi: 10.1016/s0959-8049(02)00127-2

62. Torok S, Rezeli M, Kelemen O, Vegvari A, Watanabe K, Sugihara Y, et al. Limited tumor tissue drug penetration contributes to primary resistance against angiogenesis inhibitors. *Theranostics* (2017) 7(2):400–12. doi: 10.7150/thno.16767
63. Dheda K, Lenders L, Magombedze G, Srivastava S, Raj P, Arning E, et al. Drug-penetration gradients associated with acquired drug resistance in patients with tuberculosis. *Am J Respir Crit Care Med* (2018) 198(9):1208–19. doi: 10.1164/rccm.201711-2333OC
64. Jang SH, Wientjes MG, Lu D, Au JLS. Drug delivery and transport to solid tumors. *Pharm Res* (2003) 20(9):1337–50. doi: 10.1023/a:1025785505977
65. Moreno-Gamez S, Hilla AL, Rosenbloom DIS, Petrov DA, Nowak MA, Pennings PS. Imperfect drug penetration leads to spatial monotherapy and rapid evolution of multidrug resistance. *Proc Natl Acad Sci U S A* (2015) 112(22):E2874–83. doi: 10.1073/pnas.1424184112
66. Lazzari G, Couvreur P, Mura S. Multicellular tumor spheroids: A relevant 3D model for the: In vitro preclinical investigation of polymer nanomedicines. *Polym Chem* (2017) 8(34):4947–69. doi: 10.1039/C7PY00559H
67. Tannock IF, Lee CM, Tunggal JK, Cowan DSM, Egorin MJ. Limited Penetration of Anticancer Drugs Through Tumor Tissue. *Clin Cancer Res* (2002) 8:878–84.
68. Folarin AA, Konerding MA, Timonen J, Nagl S, Pedley RB. Three-dimensional analysis of tumour vascular corrosion casts using stereomicroscopy and micro-computed tomography. *Microvasc Res* (2010) 80(1):89–98. doi: 10.1016/j.mvr.2010.03.007
69. Zhang Y, Lukacova V, Reindl K, Balaz S. Quantitative characterization of binding of small molecules to extracellular matrix. *J Biochem Biophys Methods* (2006) 67(2–3):107–22. doi: 10.1016/j.jbbm.2006.01.007
70. Di X, Bright AT, Bellott R, Gaskins E, Robert J, Holt S, et al. A chemotherapy-associated senescence bystander effect in breast cancer cells. *Cancer Biol Ther* (2008) 7(6):682–90. doi: 10.4161/cbt.7.6.5861
71. Wang R, Zhou T, Liu W, Zuo L. Molecular mechanism of bystander effects and related abscopal/cohort effects in cancer therapy. *Oncotarget* (2018) 9(26):18637–47. doi: 10.18632/oncotarget.24746
72. Jin C, Wu S, Lu X, Liu Q, Qi M, Lu S, et al. Induction of the bystander effect in Chinese hamster V79 cells by actinomycin D. *Toxicol Lett* (2011) 202(3):178–85. doi: 10.1016/j.toxlet.2011.02.002
73. Rugo RE, Almeida KH, Hendricks CA, Jonnalagadda VS, Engelward BP. A single acute exposure to a chemotherapeutic agent induces hyper-recombination in distantly descendant cells and in their neighbors. *Oncogene* (2005) 24(32):5016–25. doi: 10.1038/sj.onc.1208690
74. Kadhim M, Salomaa S, Wright E, Hildebrandt G, Belyakov OV, Prise KM, et al. Non-targeted effects of ionising radiation-Implications for low dose risk. *Mutat Res - Rev Mutat Res* (2013) 752(2):84–98. doi: 10.1016/j.mrrev.2012.12.001
75. Mukherjee D, Coates PJ, Lorimore SA, Wright EG. Responses to ionizing radiation mediated by inflammatory mechanisms. *J Pathol* (2014) 232(3):289–99. doi: 10.1002/path.4299
76. Xiong DD, Lin XG, He RQ, Pan DH, Luo YH, Dang YW, et al. Ki67/MIB-1 predicts better prognoses in colorectal cancer patients received both surgery and adjuvant radio-chemotherapy: A meta-analysis of 30 studies. *Int J Clin Exp Med* (2017) 10(2):1788–804.
77. Melling N, Kowitz CM, Simon R, Bokemeyer C, Terracciano L, Sauter G, et al. High Ki67 expression is an independent good prognostic marker in colorectal cancer. *J Clin Pathol* (2016) 69(3):209–14. doi: 10.1136/jclinpath-2015-202985
78. Sagar JK, Tannock IF. Chemotherapy rescues hypoxic tumor cells and induces their reoxygenation and repopulation - An effect that is inhibited by the hypoxia-activated prodrug TH-302. *Clin Cancer Res* (2015) 21(9):2107–14. doi: 10.1158/1078-0432.CCR-14-2298
79. Rasbridge SA, Gillett CE, Seymour AM, Patel K, Richards MA, Rubens RD, et al. The effects of chemotherapy on morphology, cellular proliferation, apoptosis and oncoprotein expression in primary breast carcinoma. *Br J Cancer* (1994) 70(2):335–41. doi: 10.1038/bjc.1994.303
80. Hultman I, Haegblom L, Rognmo I, Edqvist JJ, Blomberg E, Ali R, et al. Doxorubicin-provoked increase of mitotic activity and concomitant drain of G0-pool in therapy-resistant BE(2)-C neuroblastoma. *PLoS One* (2018) 13(1):1–16. doi: 10.1371/journal.pone.0190970.
81. Erlanson M, Daniel-Szolgay E, Carlsson J. Relations between the penetration, binding and average concentration of cytostatic drugs in human tumour spheroids. *Cancer Chemother Pharmacol* (1992) 29(5):343–53. doi: 10.1007/BF00686002
82. Van Der Luit AH, Vink SR, Klarenbeek JB, Perrissoud D, Solary E, Verheij M, et al. A new class of anticancer alkylphospholipids uses lipid rafts as membrane gateways to induce apoptosis in lymphoma cells. *Mol Cancer Ther* (2007) 6(8):2337–45. doi: 10.1158/1535-7163
83. Durand RE. Slow penetration of anthracyclines into spheroids and tumors: a therapeutic advantage? *Cancer Chemother Pharmacol* (1990) 26(3):198–204. doi: 10.1007/BF02897199
84. Slack MD, Martinez ED, Wu LF, Altschuler SJ. Characterizing heterogeneous cellular responses to perturbations. *Proc Natl Acad Sci U S A* (2008) 105(49):19306–11. doi: 10.1073/pnas.0807038105
85. Singh DK, Ku CJ, Wichaidit C, Steininger RJ, Wu LF, Altschuler SJ. Patterns of basal signaling heterogeneity can distinguish cellular populations with different drug sensitivities. *Mol Syst Biol* (2010) 6(369):1–10. doi: 10.1038/msb.2010.22
86. Jeppesen M, Hagel G, Vainer B, Harling H, Thastrup O, Jorgensen LN, et al. Spheroid culture of primary colorectal cancer cells from liver metastases as an in vitro model of patient tumors [abstract]. In: Proceedings of the 105th Annual Meeting of the American Association for Cancer Research; 2014 Apr 5–9; San Diego, CA. *Philadelphia (PA): AACR; Cancer Res* (2014) 74(19 Suppl). doi: 10.1158/1538-7445.AM2014-2020 Abstract nr 2020.
87. árnaðóttir SS, Jeppesen M, Lamy P, Bramsen JB, Nordentoft I, Knudsen M, et al. Characterization of genetic intratumor heterogeneity in colorectal cancer and matching patient-derived spheroid cultures. *Mol Oncol* (2018) 12(1):132–47. doi: 10.1002/1878-0261.12156
88. Kam Y, Das T, Tian H, Foroutan P, Ruiz E, Martinez G, et al. Sweat but no gain: Inhibiting proliferation of multidrug resistant cancer cells with ersatzdrugs. *Int J Cancer* (2015) 136(4):E188–96. doi: 10.1002/ijc.29158
89. Mahoney BP, Raghunand N, Baggett B, Gillies RJ. Tumor acidity, ion trapping and chemotherapeutics: I. Acid pH affects the distribution of chemotherapeutic agents in vitro. *Biochem Pharmacol* (2003) 66(7):1207–18. doi: 10.1016/s0006-2952(03)00467-2
90. Lindner K, Borchardt C, Schöpp M, Bürgers A, Stock C, Hussey DJ, et al. Proton pump inhibitors (PPIs) impact on tumour cell survival, metastatic potential and chemotherapy resistance, and affect expression of resistance-relevant miRNAs in esophageal cancer. *J Exp Clin Cancer Res* (2014) 33(1):1–12. doi: 10.1186/s13046-014-0073-x
91. Corbet C, Feron O. Tumour acidosis: From the passenger to the driver's seat. *Nat Rev Cancer* (2017) 17(10):577–93. doi: 10.1038/nrc.2017.77
92. Yilmaz B, Li H. Gut microbiota and iron: The crucial actors in health and disease. *Pharmaceuticals* (2018) 11(4):98. doi: 10.3390/ph11040098
93. Van Der Luit AH, Budde M, Verheij M, Van Blitterswijk WJ. Different modes of internalization of apoptotic alkyl-lysophospholipid and cell-rescuing lysophosphatidylcholine. *Biochem J* (2003) 374(Pt 3):747–53. doi: 10.1042/BJ20030179
94. Chen JLY, Lucas JE, Schroeder T, Mori S, Wu J, Nevins J, et al. The genomic analysis of lactic acidosis and acidosis response in human cancers. *PLoS Genet* (2008) 4(12):e1000293. doi: 10.1371/journal.pgen.1000293
95. Chen JLY, Merl D, Peterson CW, Wu J, Liu PY, Yin H, et al. Lactic acidosis triggers starvation response with paradoxical induction of TXNIP through MondoA. *PLoS Genet* (2010) 6(9):e1001093. doi: 10.1371/journal.pgen.1001093
96. Elstrom RL, Bauer DE, Buzzai M, Karnauskas R, Harris MH, Plas DR, et al. Akt stimulates aerobic glycolysis in cancer cells. *Cancer Res* (2004) 64(11):3892–9. doi: 10.1158/0008-5472.CAN-03-2904
97. Franke TF. PI3K/Akt: Getting it right matters. *Oncogene* (2008) 27(50):6473–88. doi: 10.1038/onc.2008.313
98. Coloff JL, Mason EF, Altman BJ, Gerriets VA, Liu T, Nichols AN, et al. Akt requires glucose metabolism to suppress Puma expression and prevent apoptosis of leukemic T cells. *J Biol Chem* (2011) 286(7):5921–33. doi: 10.1074/jbc.M110.179101
99. Majewski N, Nogueira V, Bhaskar P, Coy PE, Skeen JE, Gottlob K, et al. Hexokinase-mitochondria interaction mediated by Akt is required to inhibit apoptosis in the presence or absence of Bax and Bak. *Mol Cell* (2004) 16(5):819–30. doi: 10.1016/j.molcel.2004.11.014

100. Dietl K, Renner K, Dettmer K, Timischl B, Eberhart K, Dorn C, et al. Lactic Acid and Acidification Inhibit TNF Secretion and Glycolysis of Human Monocytes. *J Immunol* (2010) 184(3):1200–9. doi: 10.4049/jimmunol.0902584
101. Wu H, Ying M, Hu X. Lactic acidosis switches cancer cells from aerobic glycolysis back to dominant oxidative phosphorylation. *Oncotarget* (2016) 7 (26):40621–9. doi: 10.18632/oncotarget.9746
102. Corbet C, Draoui N, Polet F, Pinto A, Drozak X, Riant O, et al. The SIRT1/HIF2 α axis drives reductive glutamine metabolism under chronic acidosis and alters tumor response to therapy. *Cancer Res* (2014) 74(19):5507–19. doi: 10.1158/0008-5472.CAN-14-0705
103. Wojtkowiak JW, Rothberg JM, Kumar V, Schramm KJ, Haller E, Proemsey JB, et al. Chronic autophagy is a cellular adaptation to tumor acidic pH microenvironments. *Cancer Res* (2012) 72(16):3938–47. doi: 10.1158/0008-5472.CAN-11-3881
104. Seiwert N, Neitzel C, Stroh S, Frisan T, Audebert M, Toulany M, et al. AKT2 suppresses pro-survival autophagy triggered by DNA double-strand breaks in colorectal cancer cells. *Cell Death Dis* (2017) 8(8):e3019. doi: 10.1038/cddis.2017.418
105. Xu F, Na L, Li Y, Chen L. Roles of the PI3K/AKT/mTOR signalling pathways in neurodegenerative diseases and tumours. *Cell Biosci* (2020) 10(1):1–12. doi: 10.1186/s13578-020-00416-0
106. Shankar E, Weis M, Avva J, Shukla S, Shukla M, Sreenath S, et al. Complex Systems Biology Approach in Connecting PI3K-Akt and NF- κ B Pathways in Prostate Cancer. *Cells* (2019) 8(3):201. doi: 10.3390/cells8030201
107. Faes S, Duval AP, Planche A, Uldry E, Santoro T, Pythoud C, et al. Acidic tumor microenvironment abrogates the efficacy of mTORC1 inhibitors. *Mol Cancer* (2016) 15(1):1–11. doi: 10.1186/s12943-016-0562-y
108. Chen B, Liu J, Ho T-T, Ding X, Mo Y-Y. ERK-mediated NF- κ B activation through ASIC1 in response to acidosis. *Oncogenesis* (2016) 5(12):e279–e279. doi: 10.1038/oncsis.2016.81

Conflict of Interest: The authors declare that the research was conducted in the absence of any commercial or financial relationships that could be construed as a potential conflict of interest.

Copyright © 2020 Pavlatovská, Machálková, Brisudová, Pruška, Štěpka, Michálek, Nečasová, Beneš, Šmarda, Preisler, Kozubek and Navrátilová. This is an open-access article distributed under the terms of the Creative Commons Attribution License (CC BY). The use, distribution or reproduction in other forums is permitted, provided the original author(s) and the copyright owner(s) are credited and that the original publication in this journal is cited, in accordance with accepted academic practice. No use, distribution or reproduction is permitted which does not comply with these terms.



Dihydroartemisinin Sensitizes Esophageal Squamous Cell Carcinoma to Cisplatin by Inhibiting Sonic Hedgehog Signaling

Wei Cui^{1*}, Tingting Fang¹, Zhaoheng Duan¹, Dongfang Xiang², Yanxia Wang², Mengsi Zhang², Fangzheng Zhai¹, Xiang Cui^{3*} and Lang Yang^{4*}

¹ Department of Pharmacology, Shenyang Pharmaceutical University, Shenyang, China, ² Institute of Pathology and Southwest Cancer Center, Southwest Hospital, Third Military Medical University (Army Medical University), Chongqing, China, ³ Department of Breast and Thyroid Surgery, Southwest Hospital, Third Military Medical University (Army Medical University), Chongqing, China, ⁴ Department of Gastroenterology, The Seventh Medical Center, Chinese PLA General Hospital, Beijing, China

OPEN ACCESS

Edited by:

Liwu Fu,
Sun Yat-sen University, China

Reviewed by:

Dongmei Zhang,
Jinan University, China
Zhi Shi,
Jinan University, China

*Correspondence:

Wei Cui
cuiwei@syphu.edu.cn
Lang Yang
yanglang2009@126.com
Xiang Cui
xiangcui84@163.com

Specialty section:

This article was submitted to
Molecular and Cellular Oncology,
a section of the journal
Frontiers in Cell and Developmental
Biology

Received: 20 August 2020

Accepted: 19 November 2020

Published: 10 December 2020

Citation:

Cui W, Fang T, Duan Z, Xiang D,
Wang Y, Zhang M, Zhai F, Cui X and
Yang L (2020) Dihydroartemisinin
Sensitizes Esophageal Squamous Cell
Carcinoma to Cisplatin by Inhibiting
Sonic Hedgehog Signaling.
Front. Cell Dev. Biol. 8:596788.
doi: 10.3389/fcell.2020.596788

Platinum-based regimens have been routinely used in the clinical treatment of patients with esophageal squamous cell carcinoma (ESCC). However, administration of these drugs is frequently accompanied by drug resistance. Revealing the underlying mechanisms of the drug resistance and developing agents that enhance the sensitivity to platinum may provide new therapeutic strategies for the patients. In the present study, we found that the poor outcome of ESCC patients receiving platinum-based regimens was associated with co-expression of Shh and Sox2. The sensitivity of ESCC cell lines to cisplatin was related to their activity of Shh signaling. Manipulating of Shh expression markedly changed the sensitivity of ESCC cells to platinum. Continuous treatment with cisplatin resulted in the activation of Shh signaling and enhanced cancer stem cell-like phenotypes in ESCC cells. Dihydroartemisinin (DHA), a classic antimalarial drug, was identified as a novel inhibitor of Shh pathway. Treatment with DHA attenuated the cisplatin-induced activation of the Shh pathway in ESCC cells and synergized the inhibitory effect of cisplatin on proliferation, sphere and colony formation of ALDH-positive ESCC cells *in vitro* and growth of ESCC cell-derived xenograft tumors *in vivo*. Taken together, these results demonstrate that the Shh pathway is an important player in cisplatin-resistant ESCC and DHA acts as a promising therapeutic agent to sensitize ESCC to cisplatin treatment.

Keywords: cisplatin resistance, esophageal squamous cell carcinoma, Shh pathway, dihydroartemisinin, cancer stem cell

INTRODUCTION

Esophageal cancer with esophageal squamous cell carcinoma (ESCC) as its main histological type is the eighth most common form of cancer worldwide, and has been demonstrated to be one of the most difficult malignancies to be cured (Arnold et al., 2015). Platinum-based chemotherapy is commonly used for the treatment of patients with unresectable ESCC (Nakajima and Kato, 2013; Rubenstein and Shaheen, 2015). However, the treatment efficacy is diminished due to the

occurrence of platinum resistance (Galanski, 2006; Aichler et al., 2014). Insight into the molecular underpinnings of platinum resistance would benefit the development of novel therapeutic strategies for ESCC patients. Recently, several molecules or signaling pathways have been reported to be involved in the platinum resistance, including sirtuin type 1 (SIRT1) (Cao et al., 2015), multidrug resistance protein 2 (MRP2) (Yamasaki et al., 2011), 14-3-3 σ (Lai et al., 2016), leptin and AKT signaling (Bain et al., 2014; Li et al., 2014). Nevertheless, none of them has been used as an indicator to predict the response to platinum or a target to sensitize cancer cells to platinum for patients with ESCC in clinical practice.

Sonic hedgehog (Shh) signaling plays an important role in embryonic development, cell proliferation, tissue polarity, and carcinogenesis (Merchant, 2012; Athar et al., 2014). Once Shh protein binds to its receptor patched 1 (PTCH1), smoothened (SMO) is released from the inhibitory combination of PTCH1 and activates downstream Gli transcriptional factors (Glis). So the target genes of Glis were activated, including *SOX2* (Rimkus et al., 2016) and *PTCH1* (Xie et al., 1998). It has been well demonstrated that the activation of Shh signaling was involved in the development and progression of many types of cancer (Cui et al., 2010; Yoo et al., 2011; Wang et al., 2012; Duan et al., 2015), including ESCC (Berman et al., 2003; Yang et al., 2012). Moreover, the critical roles of Shh pathway in maintaining cancer stem cells (CSCs) and drug resistance have also been well-illustrated (Chase et al., 2010; Zahreddine et al., 2014; Rimkus et al., 2016). Thus, Shh signaling might also been involved in platinum resistance in ESCC.

Dihydroartemisinin (DHA) is a derivative of artemisinin isolated from a traditional Chinese medicine *Artemisia annua*, and has been used as classical antimalarial drug worldwide. In the recent years, DHA has also been reported to have anti-cancer properties in several types of cancer, including ESCC (Efferth, 2017a; Luo et al., 2019). Moreover, it has been reported that DHA can sensitize cisplatin to cisplatin-resistant ovarian cancer cells by inhibiting mTOR (Feng et al., 2014). DHA exerts anti-tumor effects in a multi-specific manner, in which it inhibits important tumor-related signaling pathways, such as Wnt/ β -catenin, AMPK, PI3K/AKT, and so on (Efferth, 2017a). However, whether DHA could reverse cisplatin resistance in ESCC and its underlying mechanism need to be elucidated.

In this study, we demonstrated that Shh pathway was a key player of the cisplatin resistance in ESCC and DHA could inhibit Shh pathway to sensitize ESCC to cisplatin, suggesting that DHA may serve as a promising agent combined with cisplatin in ESCC treatment.

MATERIALS AND METHODS

Cell Lines and Cell Culture

Human ESCC cell lines TE-1, EC109, and KYSE150 were obtained from Cell Bank of the Chinese Academy of Sciences (Shanghai, China). Human ESCC cell line KYSE510 was obtained from German Collection of Microorganisms and Cell Cultures (Germany). All cells were routinely cultured in RPMI-1640 or

MEM medium supplemented with 10% fetal bovine serum (FBS) and maintained at 37°C in 5% CO₂ and 100% humidity. For continuous treatment cells, the 1/2 and 1/4 IC₅₀ concentrations of cisplatin were continuously given to cell lines for 2–3 weeks, and then cells were collected for next investigation.

Patients and Tissue Specimens

A total of 59 ESCC patients who received platinum-based regimens were enrolled between Jan 2006 and Dec 2007 from Southwest Hospital (Chongqing, China). The enrolled patients met the following eligibility criteria: histological or cytological confirmation of esophageal squamous cell carcinoma, presence of measurable disease, no second malignancies, and availability of adequate diagnostic tumor tissues. The clinicopathologic features of these patients are summarized in **Supplementary Table S1**. Overall survival (OS) was defined as the time between the onset of chemotherapy and the date of the last follow up or death from any cause. Ethical oversight and approval were obtained from the Institutional Review Board of Southwest Hospital, and written informed consent was obtained from all patients.

Immunohistochemistry

Immunohistochemical staining was performed on formalin-fixed, paraffin-embedded ESCC sections (4 μ m) using Dako REALTM EnVision™ detection System (Code K5007; Dako, Glostrup, Denmark) as previously described (Liu et al., 2017). Briefly, the sections were pretreated by 0.3% H₂O₂ and antigen retrieval was performed according to the manufacturer's instructions. The slides were incubated with mouse anti-human Shh (1:100; Cell Signaling Technology, United States) or Sox2 (1:100; Cell Signaling Technology, United States) at 4°C overnight. The secondary antibody (1:400; Jackson ImmunoResearch, United States) was added for incubation at 37°C for 30 min. All slides were evaluated independently by two pathologists in a blind manner. The intensity of immunohistochemical staining and the proportion of positively stained tumor cells was evaluated as previously described (Liu et al., 2017). Briefly, the staining intensity was scored with “0” (no staining), “1” (weakly positive), “2” (moderately positive), and “3” (strongly positive). The staining average percentage of positive cells was scored as: 0 = 0%, 1 = 1–25%, 2 = 26–50%, 3 = 51–75%, and 4 = 76–100%. The expression levels of detected proteins were reported by multiplication of staining density and average percentage of positive cells. It was defined as high expression if calculation of the scores more than 4 or 2 for Shh and Sox2, respectively, and the cut-off was derived from X-tile analysis, other tumor tissues were considered as low expression.

Compounds and Reagents

Dihydroartemisinin (DHA) and cisplatin (CDDP) were obtained from Sigma, United States. These agents were dissolved in DMSO to 100 mM and stored at –20°C. Before treatment, the stock solution was diluted to different concentrations. The final concentration of DMSO in cultures was 0.1% (v/v) or less. MTT (3-(4,5-dimethylthiazol-2-yl)-2,5-diphenyl tetrazolium bromide) was purchased from Sigma, United States. The primary antibodies against Shh, PTCH1, Gli1, Nanog, Sox2,

Oct4, P-gp, ALDH1A1, Tubulin, and β -actin were listed in **Supplementary Table S2**.

Cell Viability Assay

The *in vitro* cell viability was determined by MTT assay. The cells (/mL) were seeded into 96-well culture plates at 5×10^3 cells/well in 100 μ L DMEM containing 10% FBS. After incubation overnight, the cells were treated with various concentrations of agents for 48 h. Then 10 μ L MTT solution (2.5 mg/mL in PBS) was added to each well, and the plates were incubated for an additional 4 h at 37°C. After centrifugation (2,500 rpm, 10 min), the medium with MTT was aspirated, and replaced with 100 μ L DMSO. The optical density of each well was measured at 570 nm with a Molecular Devices M5 Reader.

Transient Transfection

For transiently silencing Shh, the Shh Silencer Select Validated siRNA was purchased from Life Technologies, United States (Catalog #AM16708). For overexpression of Shh, human Shh full-length cDNA was cloned into the pCMV expression vector. The Shh siRNA and pCMV-Shh (2 μ g/ μ L) was transiently transfected into TE-1 or KYSE-510 cells by Lipofectamine 2000 (Invitrogen) according to the manufacturer's instructions. Transfection efficiency was verified by western blotting.

ALDEFLUOR Assay and Flow Cytometry

An ALDEFLUOR kit (Stem Cell Technologies, Canada) was used to isolate tumor cells with ALDH enzymatic activity according to the manufacturer's instruction. Briefly, ESCC cells were suspended in ALDEFLUOR assay buffer containing ALDH substrate, then treated with BODIPY-aminoacetaldehyde (BAAA) and incubated for 40 min at 37°C. Diethylaminobenzaldehyde (DEAB), a specific ALDH inhibitor, was used as a negative control. 7-Amino-actinomycin D (7-AAD) staining solution (BD Pharmingen, United States) was used to exclude dead cells. Cells with intact plasma membranes were sorted for experiments.

Western Blot Analysis

ESCC cells or FACS-sorted ALDH^{high} cells were gathered after pre-treatment for the indicated time periods as described previously (Liu et al., 2017). Western blotting was performed as previously described (Wang et al., 2014). Briefly, equal amounts of total protein extracts from cultured cells or tissues were fractionated by 8–12% SDS-PAGE and then electrically transferred onto polyvinylidene difluoride (PVDF) membranes. Mouse or rabbit primary antibodies and appropriate horseradish peroxidase (HRP)-conjugated secondary antibodies were used to detect the designated proteins. The bound secondary antibodies on the PVDF membrane were reacted with ECL detection reagents (Pierce; Rockford, United States) and detected by a ChemiDocXRS system (Bio-Rad). β -actin or Tubulin were used as loading control.

Quantitative RT-PCR Analysis

Total RNA was isolated from cells using RNeasy Mini Kits (Qiagen) as described in the product insert. The RNA was

reverse transcribed with RevertAid First Strand cDNA Synthesis Kits (Thermo Fisher Scientific) and PCR was done using iQ SYBR Green Supermix and the CFX96 Real-Time PCR Detection System (Bio-Rad). Primers used in this study were listed in **Supplementary Table S3**. The expression of each gene was determined using the $2^{-\Delta\Delta CT}$ method. Results were normalized against *GAPDH*. All experiments were performed in triplicate, and results were plotted as the mean \pm s.d.

Real-Time Cell Analysis (RTCA)

The RTCA assay was performed as previously described (Wang et al., 2015). A chemotactic signal for movement was provided by inoculating 30,000–50,000 TE-1 cells in serum-free medium in the upper chamber and supplying RPMI-1640 with 10% FBS in the lower chamber. Cell index (electrical impedance) was monitored every 5 min for the duration of the experiment. The cell index represents the capacity of cell migration, and the slope of the curve was related to the migration velocity of tumor cells.

Colony Formation Assay

One hundred viable FACS-sorted ALDH^{high} TE-1 cells per well were seeded in each well of 24-well plates and cultured in DMEM containing 10% FBS. After incubation for 2 weeks, the colonies were stained with crystal violet and the colonies containing more than 50 cells were counted.

Tumorsphere Formation Assay

FACS-sorted ALDH^{high} cells were seeded in 6-well ultra-low attachment plates (Corning, NY) at 500 cells/well with or without the indicated treatments in serum-free DMEM/F-12 medium supplemented with B27 (1 \times , Invitrogen), 20 ng/mL human recombinant bFGF (PeproTech), 20 ng/mL EGF (PeproTech), 10 ng/mL leukemia inhibitory factor (Chemicon) and 4 U/L insulin (Sigma). After culture for 2 weeks, spheres were counted under a phase contrast microscope, and pictures were taken by AF6000 and DFC350FX (Leica).

Immunofluorescence Confocal Microscopy

FACS-sorted ALDH^{high} cells were seeded on cover slides and cultured in DMEM containing 10% FBS for 7 days with or without treatment. The cells were then fixed and blocked by preimmune goat serum. Primary mouse anti-human Gli1 (1:100, Cell Signaling, United States) was added to the cells and incubated at 4°C overnight. Secondary goat anti-mouse IgG conjugated with Cy5 (1:500, Cell Signaling, United States) was added to the cells and incubated at 37°C for 30 min. DAPI was used to stain the nuclei. Cells were then observed under laser confocal microscopy (Zeiss, Germany).

Determination of Combination Index

TE-1 or KYSE-510 cells were treated with different concentrations of DHA alone, cisplatin alone, or the two agents in combination. The cell viability was measured by MTT assay. The nature of the drug interaction was analyzed by using the combination index (CI) according to the method of

Chou and Talalay (1984). A CI value lower than 0.90 indicates synergism; a CI value between 0.90 and 1.10 indicates an additive effect; and a CI value higher than 1.10 indicates antagonism. Data analysis was performed using Calcsyn software (Biosoft, Oxford, United Kingdom).

Mouse Xenograft Tumor Study

For tumorigenesis assessment, viable TE-1 cells ($1 \times 10^6/100 \mu\text{L}$ PBS per mouse), as confirmed by trypan blue staining, were subcutaneously injected into the right flank of 7- to 8-week-old female BALB/c mice. When the average tumor volume reached 100 mm^3 , the mice were randomly divided into four treatment groups, including control (saline only, $n = 4$), DHA (25 mg/kg/5 days/week, i.p.; $n = 4$), CDDP (4 mg/kg/week, i.p.; $n = 4$), and the combination ($n = 4$). The dosage of CDDP and DHA was designed based on the clinical equivalent dose. Tumor size was measured once every 3 days with a caliper (calculated volume = $\text{shortest diameter}^2 \times \text{longest diameter}/2$). The body weight was also measured once every 3 days to assess gross toxicity. After 35 days, the mice were sacrificed and the tumors were excised and stored at -80°C until western blot analysis. These studies were performed in strict accordance with the recommendations in the Guide for the Care and Use of Laboratory Animals of the National Institutes of Health. The protocol was approved by the Committee on the Ethics of Animal Experiments of the Shenyang Pharmaceutical University.

Statistical Analysis

Differences between experimental groups were evaluated by one-way ANOVA with Turkey's *post-hoc* test using the SPSS11.5 software package for Windows (SPSS, Chicago, IL). Survival curves were constructed using the Kaplan–Meier method. Statistical significance was based on a *P*-value of 0.05 ($P < 0.05$, two-tailed test).

RESULTS

Activation of the Shh Pathway Is Associated With Poor Outcome of ESCC Patients Receiving Platinum-Based Regimens

In order to investigate whether the activation of Shh signaling was correlated to platinum resistance of ESCC, we first used immunohistochemistry (IHC) to measure the expression of Shh and Sox2, where Shh is a ligand and Sox2 is a target in canonical Shh signaling (Rimkus et al., 2016), in paraffin-embedded tumor tissues from 59 ESCC patients who were treated with platinum-based regimens. The Shh protein was mainly detected in the membrane and cytoplasm and Sox2 staining was mainly existed in nuclei in ESCC cells (Figure 1A). The cases with high expression of Shh and Sox2 were 26/59 (44.1%) and 25/59 (42.4%), respectively. The cases with both Shh and Sox2 high expression were 18/59 (30.5%). There was a positive relationship between Shh and Sox2 expression ($P < 0.05$, Figure 1B). Analysis of the relationship between expression of

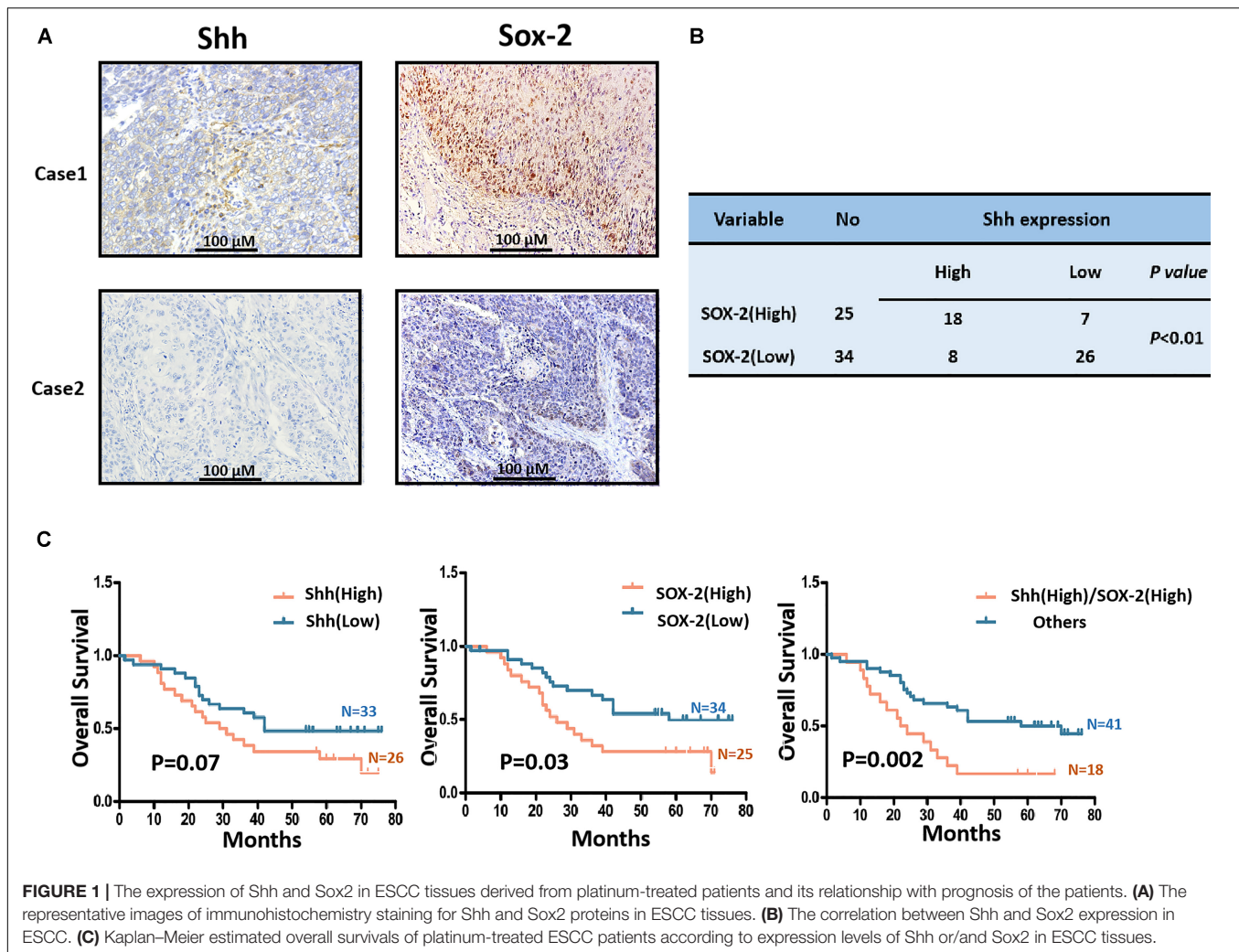
Shh and Sox2 and overall survival (OS) of the patients showed that the expression of Shh was marginally related to the OS of platinum-treated ESCC patients ($P = 0.07$, Figure 1C left), whereas Sox2 showed a significant correlation with the patients' OS ($P = 0.03$, Figure 1C middle). Importantly, we found that both Shh and Sox2 high expression group was much more strongly correlated with poor prognosis than the "other" group included either single- or double-lower Shh and Sox2 ($P = 0.002$, Figure 1C right). Taken together, these results suggest that the activation of Shh signaling is involved in efficacy of platinum-based treatments in ESCC patients.

The Activation of Shh Signaling Is Correlated With the Response of ESCC Cells to Cisplatin

To further confirm the correlation between Shh signaling and platinum sensitivity, we measured the expression levels of Shh and PTCH1, which is both a receptor and a downstream transcriptional target of Shh signaling, and the cytotoxic effect of cisplatin (CDDP) in four ESCC cell lines. TE-1 and EC109 cells expressed Shh and PTCH1 at a relatively higher levels than that in KYSE510 and KYSE150 cells (Figure 2A), suggesting that TE-1 and EC109 cells had a higher innate Shh signaling activity than that of KYSE510 and KYSE150 cells. In accordance with the expression levels of Shh and PTCH1, the IC_{50} values of TE-1 and EC109 cells on cisplatin were significantly higher than that of KYSE510 and KYSE150 cells, implying that the Shh signaling activity was negatively correlated with the sensitivity of ESCC cells to cisplatin ($R = 0.9$; Figure 2B). These results were confirmed by manipulating the expression of Shh in ESCC cells. Transient transfection with siRNA targeted Shh markedly reduced the expression of Shh and PTCH1 (Figure 2C left upper panel) and significantly increased cisplatin-induced cytotoxicity (Figure 2C left lower panel) in TE-1 cells. Inversely, overexpression of Shh in KYSE510 cells resulted in a significant upregulation of PTCH1 expression (Figure 2C right upper panel) and reduction of cisplatin-induced cytotoxicity (Figure 2C right lower panel). These results suggest that the Shh pathway plays a key role in the sensitivity of ESCC cells to cisplatin.

Continuous Cisplatin Treatment Activates Shh Signaling and Induces Cancer Stem-Like Properties in ESCC Cells

To further clarify the linkage of cisplatin resistance to the activation of Shh signaling pathway, we continuously treated ESCC cells with cisplatin to observe the activation status of Shh pathway in TE-1 and KYSE510 cell lines. As shown in Figure 3A, continuous cisplatin treatment resulted in a significant nuclear translocation of Gli1 in TE-1 and KYSE510 cells, which represented the activation of Shh signaling. Consistent with the activation of the Shh pathway, the expression of the downstream transcriptional target PTCH1 was markedly increased at the mRNA and protein levels in both cell lines (Figures 3A,B). It is well known that Shh signaling is involved in the maintenance of cancer stem cell (CSC) traits, such as self-renewal and drug



resistance (Ruiz i Altaba et al., 2002). Thus, we next observed the effect of continuous treatment of cisplatin on CSC properties. The results showed that continuous cisplatin treatment induced the upregulation of CSC related transcription factors, including Nanog, Sox2, and Oct4 in TE-1 cells (**Figure 3C**) and increased the proportion of ALDH1 positive cells, i.e., ESCC stem cells (Yang et al., 2014; **Figure 3D**). Cisplatin-treated TE-1 cells also showed enhanced tumor sphere formation (**Figure 3E**) and increased migration capability (**Figure 3F**). These results indicate that continuous exposure of ESCC cells to cisplatin lead to the activation of Shh signaling and the accumulation of ESCC stem cells.

Dihydroartemisinin Suppresses the Activation of Shh Pathway and Attenuates the Cancer Stem-Like Traits in ESCC Cells

Dihydroartemisinin (DHA, **Figure 4A**), a sesquiterpene lactone isolated from the traditional Chinese herb *Artemisia annua*, was

reported to have antitumorigenic properties and has been tested in clinical trials as a new agent to treat various cancers (Odaka et al., 2014; Lucibello et al., 2015; Qin et al., 2015). We treated TE-1 cells with DHA and found that it significantly inhibited nuclear translocation of Gli1 (**Figure 4B**) and downregulated the transcription of the Shh target genes *PTCH1* and *MDR1* (**Figure 4C**). These results suggest that DHA might be a novel inhibitor of the Shh signaling pathway in ESCC cells. So we further observed whether overexpressing Shh would affect the roles of DHA in TE-1 cells. As shown in **Figure 4D**, overexpression of Shh significantly attenuated the DHA-induced cytotoxicity ($P < 0.05$), implying that the Shh signaling pathway was an important target of DHA in ESCC cells. Since Shh signaling is a classical cancer stem cell-related pathway, so we next examined whether DHA could affect the property of cancer stem cells. As shown in **Figure 4E**, DHA decreased the expression level of the stem cell-related transcription factors Sox2 and Oct4 in TE-1 cells. Furthermore, flow cytometry assay data indicated that DHA treatment also decreased the proportion of ALDH1 positive cells in TE-1 cells (**Figure 4F**).

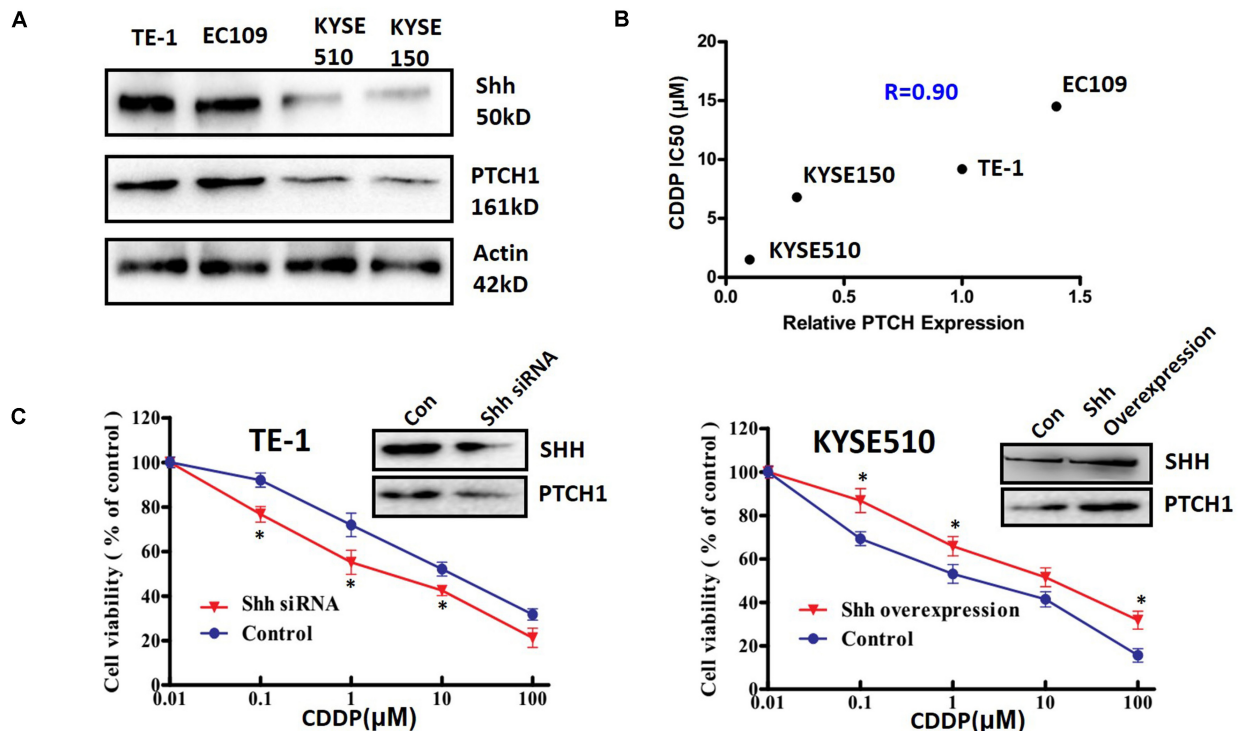


FIGURE 2 | The relationship between the Shh signaling pathway and the sensitivity to cisplatin in ESCC cell lines. **(A)** The expression of Shh and PTCH1 in ESCC cell lines. **(B)** The correlation between PTCH expression level and sensitivity to cisplatin (CDDP) in ESCC cell lines. IC₅₀ values were determined by the MTT method after treatment with CDDP for 48 h. **(C)** The effect of manipulating Shh expression on the cytotoxicity of CDDP in TE-1 and KYSE510 cells. The cells were transfected with specific siRNA in TE-1 cells (left panel) or pCMV-Shh vector in KYSE510 cells (right panel) for 48 h, and then treated with different concentrations of CDDP for another 48 h. All error bars are s.e.m. * $P < 0.05$, compared with control group.

These results identify DHA as a novel inhibitor of the Shh pathway with the ability to suppress the cancer stem-like properties in ESCC cells.

The Combination of Dihydroartemisinin and Cisplatin Synergistically Suppress the Cell Proliferation and the Stem Cell Properties in ESCC Cells

We next assessed the growth inhibitory effect of DHA in combination with cisplatin on ESCC cells. In TE-1 cells, which have high innate Shh signaling activity, the combination of DHA and cisplatin suppressed proliferation more effectively than DHA or cisplatin alone (**Figure 5A**). Combination analysis showed that DHA/cisplatin together led to a strong synergistic antiproliferative effect on TE-1 cells with a minimal combination index (CI) of 0.506 (**Figure 5B**). However, in KYSE-510 cells, which have lower innate Shh activity, the combination of DHA and cisplatin did not have a synergistic antiproliferative effect (minimal CI = 1.411; see **Supplementary Figure S1**). The above results demonstrate that the synergistic effect of DHA and cisplatin is associated with the Shh signaling activity in ESCC cells.

In view of the relationship between Shh signaling and the cancer stem cell property, we further verified the synergistic effect of DHA and cisplatin on ESCC stem cells. As shown in **Figures 5C–F**, cisplatin alone inhibited sphere and colony formation of ALDH⁺ TE-1 cells. In comparison to cisplatin, DHA at equal effective concentrations (calculated by IC₅₀) displayed an enhanced inhibitory effect. Importantly, the combination of DHA and cisplatin had an obvious synergistic anti-self renewal effect on ALDH⁺ TE-1 cells, that is which exhibited stronger inhibitory effect on sphere and colony formation than DHA and cisplatin alone (**Figures 5E,F**). These results indicated that DHA and cisplatin synergistically inhibit the proliferation of bulk cells and the self-renewal of cancer stem cells in ESCC cells.

To further explore the effect of the cisplatin/DHA combination on ESCC stem cells, we analyzed the levels of cancer stem cell markers. The results showed that cisplatin alone upregulated the expression of Sox2, Oct4, and ALDH1A1 at the mRNA and protein levels. The combination of DHA and cisplatin inhibited the upregulation of Sox2, Oct4, and ALDH1A1 induced by continuous cisplatin treatment (see **Supplementary Figures S2A,B**). Taken together, our results indicate that the combination of DHA and cisplatin synergistically suppresses the ESCC stem cell properties.

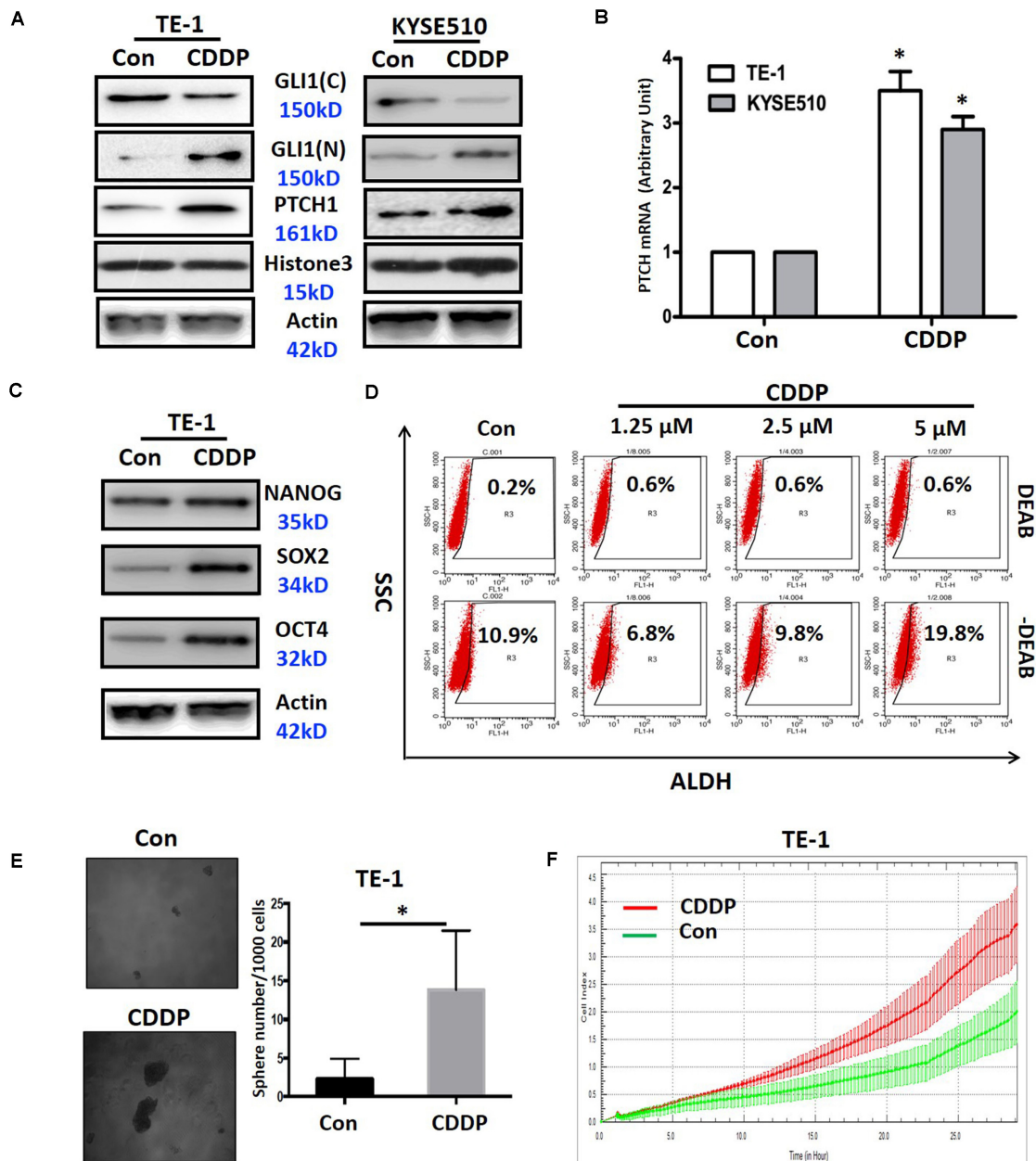


FIGURE 3 | The effects of cisplatin on activation of the Shh pathway and related biological functions. **(A)** The protein expression of Gli1 (nuclear and cytoplasmic) and PTCH1 in TE-1 and KYSE510 cells continuously treated with cisplatin (CDDP). Histone3 and β -actin expression were used as nuclear and total loading controls, respectively. **(B)** The mRNA expression of PTCH1 in TE-1 and KYSE510 cells continuously treated with CDDP. *GAPDH* expression was used as a control. * $P < 0.05$, compared with control group cells. **(C)** The expression of the cancer stem cell-related transcription factors Nanog, Sox2, and Oct4 in TE-1 cells after continuous exposure to CDDP. β -actin expression was used as a loading control. **(D)** The percentages of ALDH1 positive cells in TE-1 cells after continuous exposure to CDDP. **(E)** Sphere formation after continuous exposure to CDDP in TE-1 cells. * $P < 0.05$, compared with control group. **(F)** The effect of continuous exposure to CDDP on cell migration in TE-1 cells.

DHA Enhances Cellular Enrichment of Cisplatin and Blocks Cisplatin-Induced Activation of Shh Signaling in TE-1 Cells

The reduction of drug accumulation in the cells is a common mechanism for anticancer drugs (Fletcher et al., 2016).

Considering the synergistic action of DHA in combination with cisplatin, we next used HPLC to examine whether DHA could enhance the enrichment of cisplatin in TE-1 cells. As shown in **Figure 6A**, the cisplatin in cell culture medium was detected by HPLC as a clear peak. Incubation of TE-1 cells with DHA resulted in a 35.4% increase of cellular cisplatin

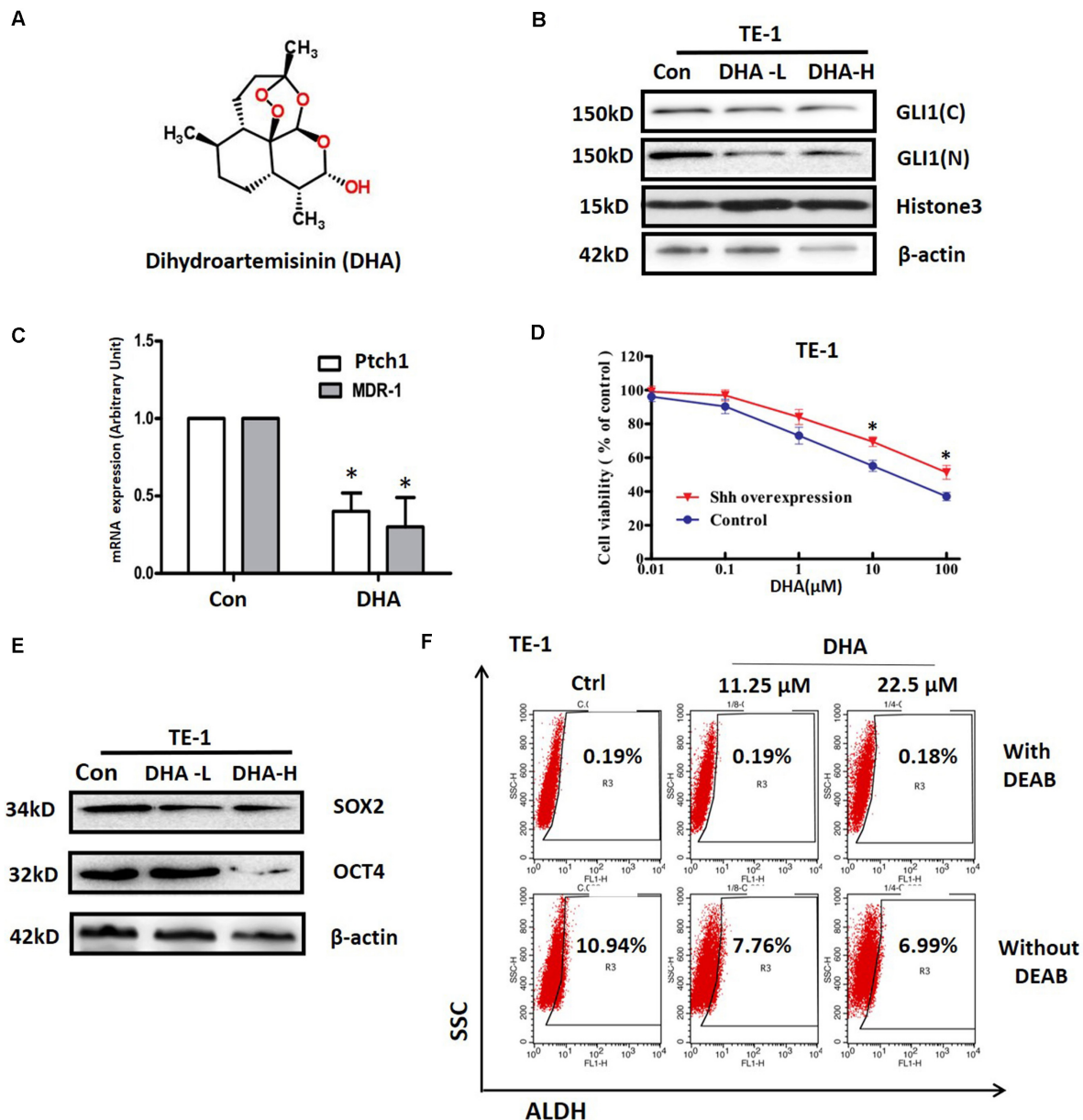


FIGURE 4 | The effects of DHA on activation of Shh pathway and stemness in ESCC cells. **(A)** The structure of DHA. **(B)** The effect of DHA at 2 μ M (low concentration, DHA-L) and 20 μ M (high concentration, DHA-H) on expression of Gli1 in the nucleus and cytoplasm in TE-1 cells. Histone3 and β -actin expression were used as nuclear and total loading controls, respectively. **(C)** The effect of DHA on the expressions of *PTCH* and *MDR1* at mRNA level in TE-1 cells. * $P < 0.05$, compared with DMSO treated group cells. **(D)** Effect of DHA on the viability of TE-1 cells with or without Shh overexpression vector transfection. The cells were transfected with Shh overexpression or mock vector (control) for 48 h, and then treated with different concentrations of DHA for another 48 h. **(E)** The effects of DHA on the expression of Sox2 and Oct4 proteins in TE-1 cells. β -actin expression was used as a loading control. **(F)** The effect of DHA on the proportion of ALDH1 positive cells in TE-1 cells. All error bars are s.e.m. * $P < 0.05$, compared with control group.

(Figure 6B), which suggests that DHA promotes cellular enrichment of cisplatin. In order to further investigate the mechanisms underlying the synergistic action, we investigated the effect of cisplatin alone, DHA alone, or the cisplatin/DHA combination on Shh signaling. As shown in Figure 6C, cisplatin single treatment upregulated the mRNA levels of the Shh signaling target genes *Gli1*, *PTCH1*, and *MDR1*, a

gene that promotes cisplatin efflux in ALDH + TE-1 cells, whereas these effects were completely blocked by DHA (Figure 6C). A similar pattern was also observed at the protein level. DHA in combination with cisplatin caused an obvious downregulation of *PTCH1* and *Pgp* as compared to cisplatin single treatment (Figure 6D). We also assessed the nuclear location of Gli1 by using confocal microscopy. As shown in

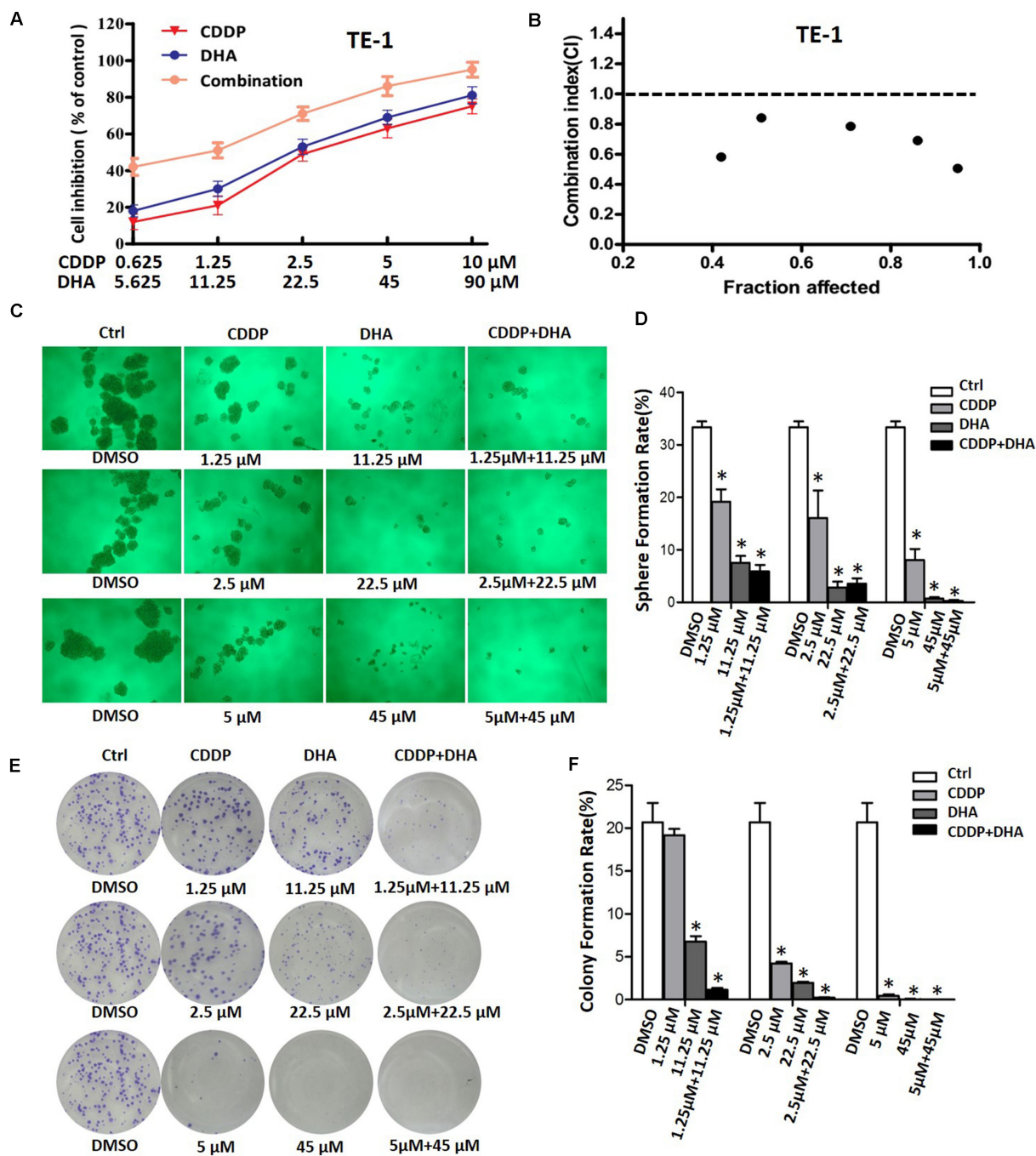


FIGURE 5 | The effects of DHA, cisplatin, and their combination on cell viability and sphere and colony formation. **(A)** Growth curves of TE-1 cells after treatment with DHA, cisplatin (CDDP), and their combination. **(B)** Analysis of the combination of DHA and CDDP in TE-1 cells. The cells were treated by using various concentrations of DHA and CDDP, either alone or in a fixed ratio for 48 h. The combination index was analyzed using the Calcsyn program. **(C)** Representative images for sphere formation of ALDH+ TE-1 cells after treatment with DHA, CDDP, and DHA + CDDP at designated concentrations for 24 h. **(D)** Bar graph of sphere formation efficiency of ALDH+ TE-1 cells after treatment with DHA or/and CDDP. * $P < 0.05$, compared with DMSO treated group. **(E)** Representative images of colony formation of ALDH+ TE-1 cells after treatment with DHA, CDDP and DHA + CDDP at designated concentrations for 24 h. **(F)** Bar graph of colony formation efficiency of ALDH+ TE-1 cells after treatment with DHA or/and CDDP. * $P < 0.05$, compared with DMSO treated group.

Figure 6E, cisplatin treatment led to the accumulation of Gli1 in nuclei, and this co-treatment with DHA blocked the nuclear translocation of Gli1 in TE-1 cells. The above data demonstrate

that DHA synergistically enhances the anti-tumor effect of cisplatin in ESCC cells by blocking cisplatin-induced activation of Shh signaling.

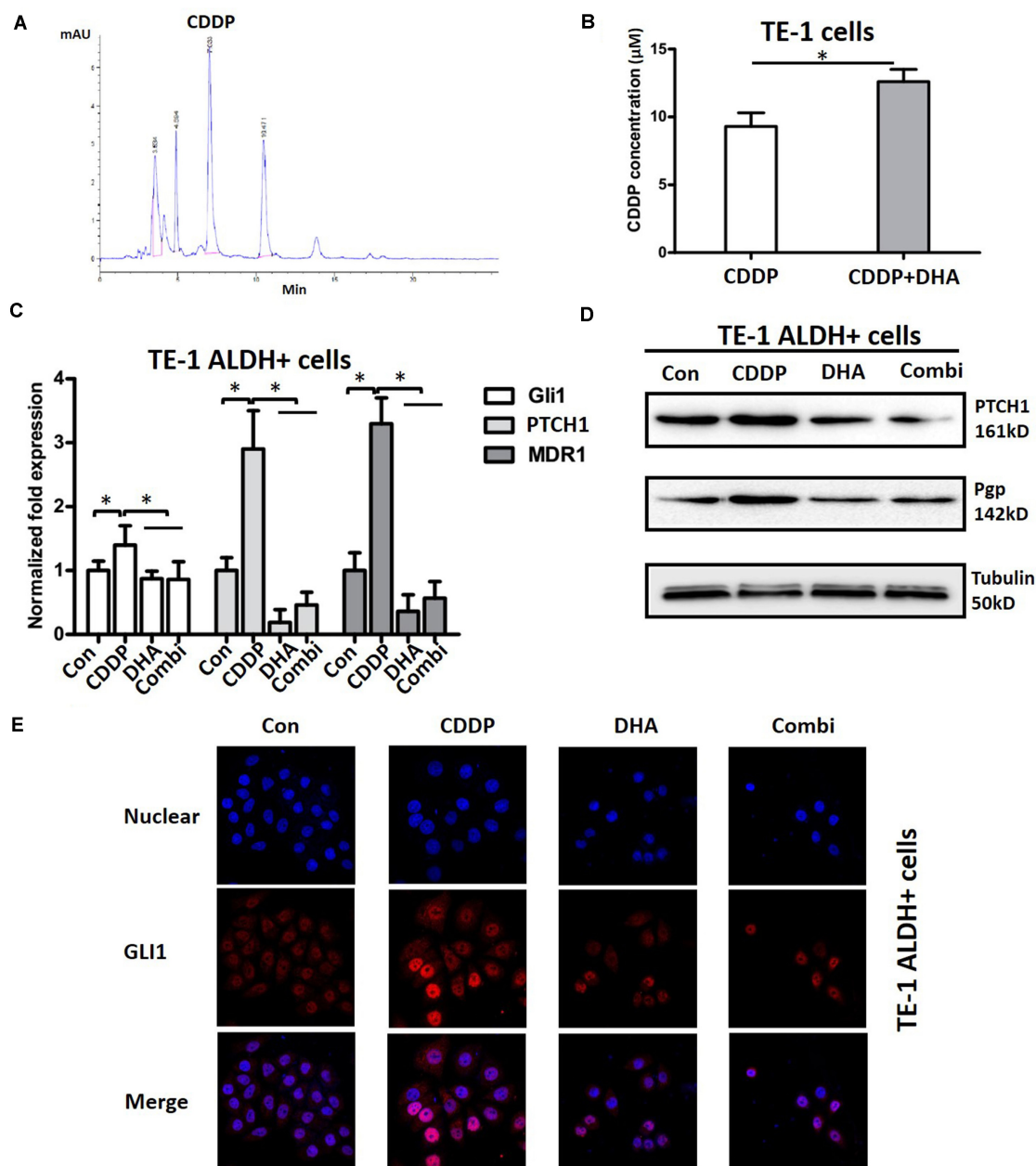


FIGURE 6 | The effects of DHA on the cellular cisplatin content and cisplatin-induced activation of the Shh pathway. **(A)** Representative HPLC trace showing the cisplatin (CDDP) peak. **(B)** Analysis of the cellular concentration of CDDP in TE-1 cells with or without DHA. **(C)** The expression of *Gli1*, *PTCH1*, and *MDR1* mRNAs in ALDH + TE-1 cells after treatment with DHA (11.25 μM) or/and CDDP (1.25 μM) for 24 h. **P* < 0.05, compared with CDDP treated group. **(D)** The expression of *PTCH1* and P-gp proteins in ALDH + TE-1 cells after treatment with DHA (11.25 μM) or/and CDDP (1.25 μM) for 24 h. Tubulin expression was used as a loading control. **(E)** The effect of DHA or/and CDDP on Gli1 nuclear translocation in ALDH + TE-1 cells. **P* < 0.05 for DHA plus CDDP compared with the DMSO plus CDDP.

DHA Combined With Cisplatin Synergistically Retards Tumor Growth *in vivo* by Inhibiting Shh Signaling

Next we assessed the effects of the combination strategy of DHA and cisplatin *in vivo*. BALB/c nude mice bearing TE-1 xenografts were treated with cisplatin, DHA, or cisplatin plus DHA. As shown in **Figure 7A**, cisplatin or DHA single

administration resulted in a moderate inhibition of tumor growth, with inhibition rates of 56.8 and 43.6%, respectively. Compared to the single treatments, cisplatin plus DHA treatment displayed a much more obvious inhibition of tumor growth (inhibition rate 84.2%), which confirmed our *in vitro* results. Additionally, the gross toxicity data showed that cisplatin group had a significant decrease in the body weights of the mice, whereas DHA group had not, as compared to control

group. Importantly, the body weights of mice treated with the combination of cisplatin and DHA showed a weak increase when compared with cisplatin alone (**Figure 7B**). The effects of DHA, cisplatin and the combination of cisplatin and DHA on Shh signaling was confirmed by testing the expression levels of nuclear Gli1, PTCH1, and Sox2 in tumor cells obtained from xenografts (**Figure 7C**). Xenografts treated with cisplatin alone exhibited increased expression levels of nuclear Gli1, PTCH1, and Sox2, which suggests that Shh signaling was activated. However, treatment with the combination of cisplatin and DHA led to an inhibition of Shh activity. These results indicate that DHA combined with cisplatin synergistically retarded tumor growth by overcoming cisplatin-induced activation of Shh signaling *in vivo*.

DISCUSSION

Platinum derivatives, the best known of which is cisplatin, are currently employed as a key component in the first-line standard of care for the clinical treatment of patients with ESCC (Nakajima and Kato, 2013; Rubenstein and Shaheen, 2015). Despite the unresolved issues regarding its mechanism of action, treatment with platinum-based drugs is generally associated with high rates of clinical response. However, accumulating evidence now suggests that malignant cells continuously exposed to cisplatin will activate adaptive responses that render them less susceptible to the antiproliferative and cytotoxic effects of the drug, and will eventually resume proliferation (Galluzzi et al., 2014). Therefore, the vast majority of cisplatin-treated ESCC patients are destined to experience the emergence of acquired cisplatin resistance and tumor recurrence.

Delineation of the molecular mechanisms whereby ESCC cells progressively lose their sensitivity to cisplatin will pave the way for rationally designed and hopefully long-lasting combinations of targeted therapies. In the present study, we found that the Shh signaling activity was increased in the tumors of platinum-treated ESCC patients with poor survival. Furthermore, the activation of Shh signaling was negatively correlated with the sensitivity of ESCC cell lines to cisplatin. Interestingly, continuous treatment of ESCC cells with cisplatin also resulted in the activation of Shh signaling along with the enhanced cancer stem cell property. Importantly, our results indicate that inhibition of Shh signaling by DHA could be a strategy to overcome acquired resistance to cisplatin. Overall, our results have important implications for clinical oncology and ESCC biology.

Feedback activation of oncogenic pathways is considered as an important mechanism to mediate acquired drug resistance in tumors. Recently, several studies have shown that feedback activation of oncogenic pathways is also involved in the cisplatin resistance in ESCC. Myers et al. (2015) reported that IGF signaling, together with the MAPK or PI3K/AKT signaling pathways, was activated in cisplatin-resistant ESCC patients, and inhibition of the IGF or/and MAPK and PI3K/AKT signaling pathways could sensitize ESCC cells to cisplatin. Based on clinical pathological and *in vitro* data, Sugimura et al. (2012) demonstrated that the interleukin-6/STAT3 prosurvival pathway

was activated in ESCC cells by cisplatin treatment, and inhibition of that feedback pathway by let-7c restored sensitivity to cisplatin. Here, we found for the first time that the Shh signaling pathway was activated in cells continuously exposed to cisplatin compared to the parental cells, and this activation resulted in an enhanced migratory capability and cancer stem cell characteristics, which suggests a novel biological role of the Shh signaling pathway in cisplatin resistance. Furthermore, the relationship between Shh activity and outcome in cisplatin-treated ESCC patients implies that Shh pathway activity might serve as a predictive biomarker for cisplatin treatment.

Besides feedback activation of oncogenic pathways, the classical mechanisms of cisplatin resistance are widely recognized to include increased DNA repair, altered cellular accumulation of drug and increased drug inactivation (Amable, 2016). Here, we found that the Shh signaling pathway is involved in cisplatin resistance. Two lines of evidence suggest how Shh signaling may be linked to the classical resistance mechanisms. First, MDR1 is considered to be involved in the process of altered cellular cisplatin accumulation and increased cisplatin inactivation (Sims-Mourtada et al., 2007), and *MDR1* is also recognized as a target gene of the Shh signaling pathway (Kudo et al., 2012). Consistent with previous reports, our results showed that inhibition of *MDR1* expression by DHA enhanced the enrichment of cellular cisplatin. Secondly, Kudo and his co-workers demonstrated that inhibition of the Shh pathway by shRNA led to the downregulation of three genes essential to nucleotide excision repair (*ERCC1*, *XPD*) and base excision repair (*XRCC1*) (Kudo et al., 2012), which mediated cisplatin resistance by increasing DNA repair. These published results indicate that the Shh signaling pathway might also be involved in other cisplatin resistance mechanisms.

The essential role of the Shh signaling pathway in ESCC cisplatin resistance in our studies and the limitation of an FDA-approved Shh inhibitor prompted us to identify a novel Shh inhibitor. In the current study, we identified DHA as a novel inhibitor of the Shh signaling pathway. Our results indicated that DHA inhibits the nuclear translocation of Gli1, one of the key transcription factors in the Shh signaling pathway, and suppresses the transcription of *PTCH* and *MDR1* which are target genes of the Shh pathway. Furthermore, overexpression of Shh ligand resulted in decreased sensitivity of ESCC cells to DHA. The above results demonstrate the inhibitory role of DHA in the Shh signaling pathway. Consistent with the Shh activity data, our functional studies also indicated that DHA reduced the expression level of cancer stem cell transcription factors and inhibited ALDH activity, which is recognized as an ESCC stem cell marker. However, the detailed mechanism by which DHA inhibits the Shh signaling pathway needs to be further elucidated.

Although the cisplatin resistance mechanisms in ESCC have been a subject of considerable interest, the development of therapeutic strategies that reverse cisplatin resistance has remained a challenge in clinical oncology. The cisplatin-induced increase of Shh activity and the inhibitory action of DHA on the Shh pathway prompted us to evaluate a combination strategy to

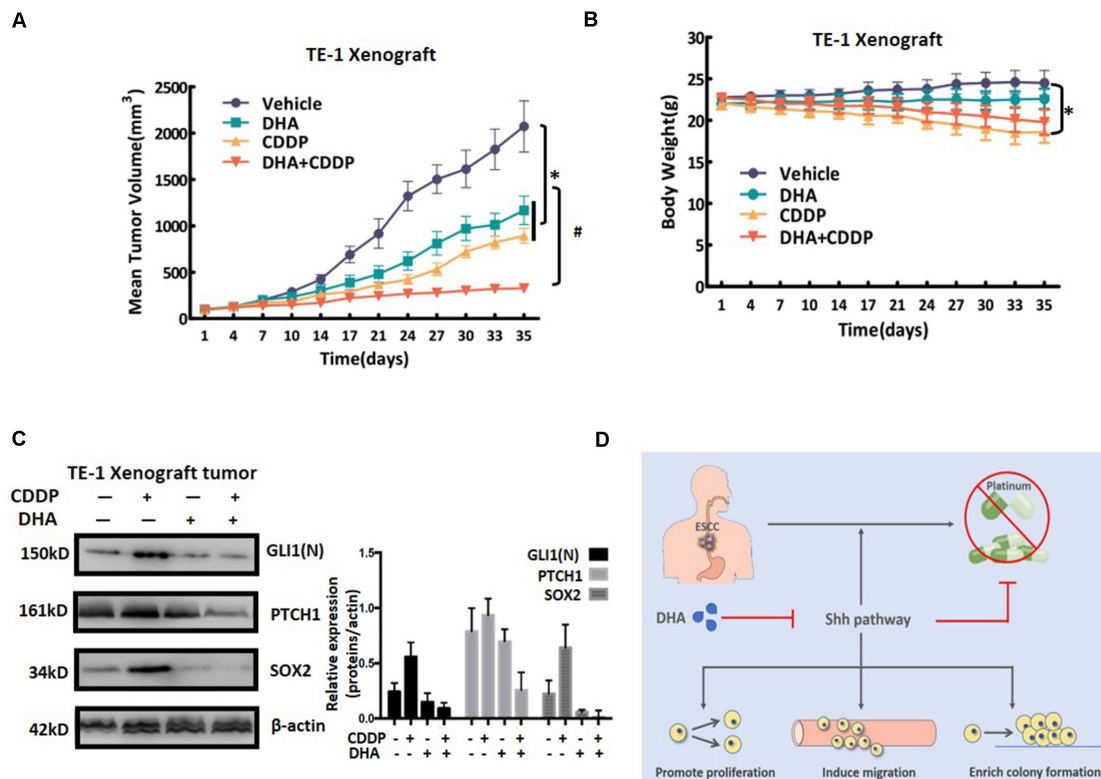


FIGURE 7 | The anti-tumor effect of DHA and cisplatin on TE-1-derived xenografts in mice. **(A)** The effect of administration of DHA alone, cisplatin (CDDP) alone or the DHA/CDDP combination on the tumor volumes. Tumor volumes are expressed as mean \pm SD ($n = 4$ per group). **(B)** The average body weight of each group is expressed as mean \pm SD ($n = 4$ per group). **(C)** The expression levels of nuclear Gli1, PTCH1, and Sox2 were detected by western blot. Proteins were extracted from the tumor tissues of mice in the four groups. The expression levels of nuclear Gli1, PTCH1, and Sox2 were detected by western blot. Proteins were extracted from the tumor tissues of mice in the four groups. **(D)** Schematic of the mechanism by which Shh pathway activation results in cisplatin resistance in ESCCs and reversing resistance by novel Shh pathway inhibitor DHA. All error bars are s.e.m. * $P < 0.05$ for DHA alone, CDDP alone or the combination treatment compared with the vehicle control. # $P < 0.05$ for the combination treatment compared with single administration of DHA and CDDP.

overcome cisplatin resistance *in vitro* and *in vivo*. Our results showed that DHA in combination with cisplatin displayed a synergistic inhibitory effect *in vitro* and *in vivo* on TE-1 ESCC cells, which have relatively high Shh activity. The combination also synergistically inhibited the characteristics of ESCC stem cells. Given the limited capacity of cisplatin to control ESCC and the important role of the Shh pathway in the cisplatin resistance of patients, this work lays the foundation for a promising therapeutic strategy.

It should be noted that several clinical studies have demonstrated the combination of DHA or its derivatives and chemotherapy agents could obtain a promising efficacy in various tumor patients (Efferth, 2017b). The advantage of these combinations might be explained by the following fact: (1) DHA owns a known safety profile and pharmacokinetic characteristics (Efferth, 2017b); (2) Multiple action to suppress drug-resistant signaling pathways, such as Wnt, Shh, Stat3 and NF- κ B pathways (Efferth, 2017b; Chaib et al., 2019). However, a recent study indicated that Artesunate, a DHA derivatives, could induce hepatotoxicity when combined with temozolomide in the treatment for glioblastoma (Efferth, 2017b). Thus, optimizing dose should be

addressed when combined chemotherapy agents with DHA in treatment for cancer.

CONCLUSION

In conclusion, we provide evidence that activation of the Shh pathway is related to cisplatin resistance in ESCC and also to predicted poor overall survival of ESCC patients treated with cisplatin. Combining DHA with cisplatin suppressed the Shh signaling pathway, and thus synergistically inhibited cell growth and the characteristics of cancer stem cells *in vitro* and *in vivo* (see Figure 7D; Cui et al., 2020). Our findings not only elucidate a novel mechanism for cisplatin resistance, but also provide a promising therapeutic strategy to overcome cisplatin resistance in ESCC.

DATA AVAILABILITY STATEMENT

All datasets generated for this study are included in the article/Supplementary Material, further inquiries can be directed to the corresponding authors.

ETHICS STATEMENT

The studies involving human participants were reviewed and approved by the Institutional Review Board of Southwest Hospital. The patients/participants provided their written informed consent to participate in this study. The animal study was reviewed and approved by Committee on the Ethics of Animal Experiments of the Shenyang Pharmaceutical University.

AUTHOR CONTRIBUTIONS

WC, XC, and LY: conceptualization, writing—original draft preparation, and writing—review and editing. TF, ZD, and DX: methodology. YW and MZ: validation. TF: formal analysis. TF, ZD, DX, and XC: investigation. TF and ZD: data curation. WC: supervision and project administration. WC and LY: funding acquisition. All authors have read and agreed to the published version of the manuscript.

FUNDING

This work was financially supported by the National Natural Science Foundation of China (Nos. 81372339, 81102028, and 81402460), the Natural Science Foundation of Liaoning Province

(No. 20180550076), the Program for Innovative Talents in Liaoning (No. LR2019068), Youth Foundation of Shenyang Pharmaceutical University (ZQN2015022).

ACKNOWLEDGMENTS

This manuscript has been released as a pre-print at Research Square.

SUPPLEMENTARY MATERIAL

The Supplementary Material for this article can be found online at: <https://www.frontiersin.org/articles/10.3389/fcell.2020.596788/full#supplementary-material>

Supplementary Figure 1 | The effect of CDDP, DHA, and combination on cell growth of KYSE-510 cells.

Supplementary Figure 2 | The effect of CDDP, DHA, and combined treatment on the expressions of Sox-2, Oct4, and ALDH1A1 in TE-1 ALDH⁺ cells.

Supplementary Table 1 | The clinicopathological parameters of ESCC patients.

Supplementary Table 2 | The information for antibodies used in this study.

Supplementary Table 3 | The primer sequences for qRT-PCR analyses.

REFERENCES

- Aichler, M., Motschmann, M., Jütting, U., Luber, B., Becker, K., Ott, K., et al. (2014). Epidermal growth factor receptor (EGFR) is an independent adverse prognostic factor in esophageal adenocarcinoma patients treated with cisplatin-based neoadjuvant chemotherapy. *Oncotarget* 5, 6620–6632. doi: 10.18632/oncotarget.2268
- Amable, L. (2016). Cisplatin resistance and opportunities for precision medicine. *Pharmacol. Res.* 106, 27–36. doi: 10.1016/j.phrs.2016.01.001
- Arnold, M., Soerjomataram, I., Ferlay, J., and Forman, D. (2015). Global incidence of oesophageal cancer by histological subtype in 2012. *Gut* 64, 381–387. doi: 10.1136/gutjnl-2014-308124
- Athar, M., Li, C., Kim, A. L., Spiegelman, V. S., and Bickers, D. R. (2014). Sonic hedgehog signaling in basal cell nevus syndrome. *Cancer Res.* 74, 4967–4975. doi: 10.1158/0008-5472.can-14-1666
- Bain, G. H., Collie-Duguid, E., Murray, G. I., Gilbert, F. J., Denison, A., McKiddie, F., et al. (2014). Tumour expression of leptin is associated with chemotherapy resistance and therapy-independent prognosis in gastro-oesophageal adenocarcinomas. *Br. J. Cancer* 110, 1525–1534. doi: 10.1038/bjc.2014.45
- Berman, D. M., Karhadkar, S. S., Maitra, A., Montes, De Oca, R., Gerstenblith, M. R., et al. (2003). Widespread requirement for Hedgehog ligand stimulation in growth of digestive tract tumours. *Nature* 425, 846–851. doi: 10.1038/nature01972
- Cao, B., Shi, Q., and Wang, W. (2015). Higher expression of SIRT1 induced resistance of esophageal squamous cell carcinoma cells to cisplatin. *J. Thorac. Dis.* 7, 711–719.
- Chaib, I., Cai, X., Llige, D., Santarpia, M., Jantus-Lewintre, E., Filipiska, M., et al. (2019). Osimertinib and dihydroartemisinin: a novel drug combination targeting head and neck squamous cell carcinoma. *Ann. Transl. Med.* 7:651. doi: 10.21037/atm.2019.10.80
- Chase, D. M., Mathur, N., and Tewari, K. S. (2010). Drug discovery in ovarian cancer. *Recent Pat Anticancer Drug Discov.* 5, 251–260. doi: 10.2174/157489210791760472
- Chou, T. C., and Talalay, P. (1984). Quantitative analysis of dose-effect relationships: the combined effects of multiple drugs or enzyme inhibitors. *Adv. Enzyme Regul.* 22, 27–55. doi: 10.1016/0065-2571(84)90007-4
- Cui, W., Wang, L. H., Wen, Y. Y., Song, M., Li, B. L., Chen, X. L., et al. (2010). Expression and regulation mechanisms of Sonic Hedgehog in breast cancer. *Cancer Sci.* 101, 927–933. doi: 10.1111/j.1349-7006.2010.01495.x
- Cui, W., Fang, T., Duan, Z., Xiang, D., Wang, Y., Zhang, M., et al. (2020). Dihydroartemisinin sensitizes esophageal squamous cell carcinoma to cisplatin by inhibiting Sonic Hedgehog signaling. *Res. Square*.
- Duan, Z. H., Wang, H. C., Zhao, D. M., Ji, X. X., Song, M., Yang, X. J., et al. (2015). Cooperatively transcriptional and epigenetic regulation of sonic hedgehog overexpression drives malignant potential of breast cancer. *Cancer Sci.* 106, 1084–1091. doi: 10.1111/cas.12697
- Efferth, T. (2017a). From ancient herb to modern drug: artemisia annua and artemisinin for cancer therapy. *Semin Cancer Biol.* 46, 65–83. doi: 10.1016/j.semcancer.2017.02.009
- Efferth, T., Schöttler, U., Krishna, S., Schmiedek, P., Wenz, F., and Giordano, F. A. (2017b). Hepatotoxicity by combination treatment of temozolomide, artesunate and Chinese herbs in a glioblastoma multiforme patient: case report review of the literature. *Arch. Toxicol.* 91, 1833–1846. doi: 10.1007/s00204-016-1810-z
- Feng, X., Li, L., Jiang, H., Jiang, K., Jin, Y., and Zheng, J. (2014). Dihydroartemisinin potentiates the anticancer effect of cisplatin via mTOR inhibition in cisplatin-resistant ovarian cancer cells: involvement of apoptosis and autophagy. *Biochem. Biophys. Res. Commun.* 444, 376–381. doi: 10.1016/j.bbrc.2014.01.053
- Fletcher, J. I., Williams, R. T., Henderson, M. J., Norris, M. D., and Haber, M. (2016). ABC transporters as mediators of drug resistance and contributors to cancer cell biology. *Drug Resist Updat.* 26, 1–9. doi: 10.1016/j.drug.2016.03.001
- Galanski, M. (2006). Recent developments in the field of anticancer platinum complexes. *Recent Pat Anticancer Drug Discov.* 1, 285–295. doi: 10.2174/15748920677442287
- Galluzzi, L., Vitale, I., Michels, J., Brenner, C., Szabadkai, G., Harel-Bellan, A., et al. (2014). Systems biology of cisplatin resistance: past, present and future. *Cell Death Dis.* 5:e1257. doi: 10.1038/cddis.2013.428

- Kudo, K., Gavin, E., Das, S., Amable, L., Shevde, L. A., and Reed, E. (2012). Inhibition of Gli1 results in altered c-Jun activation, inhibition of cisplatin-induced upregulation of ERCC1, XPD and XRCC1, and inhibition of platinum-DNA adduct repair. *Oncogene* 31, 4718–4724. doi: 10.1038/ncr.2011.610
- Lai, K. K., Chan, K. T., Choi, M. Y., Wang, H. K., Fung, E. Y., Lam, H. Y., et al. (2016). 14-3-3 σ confers cisplatin resistance in esophageal squamous cell carcinoma cells via regulating DNA repair molecules. *Tumour Biol.* 37, 2127–2136. doi: 10.1007/s13277-015-4018-6
- Li, B., Tsao, S. W., Chan, K. W., Ludwig, D. L., Novosyadlyy, R., Li, Y. Y., et al. (2014). Id1-induced IGF-II and its autocrine/endocrine promotion of esophageal cancer progression and chemoresistance—implications for IGF-II and IGF-IR-targeted therapy. *Clin. Cancer Res.* 20, 2651–2662. doi: 10.1158/1078-0432.ccr-13-2735
- Liu, Q., Cui, X., Yu, X., Bian, B. S., Qian, F., Hu, X. G., et al. (2017). Cripto-1 acts as a functional marker of cancer stem-like cells and predicts prognosis of the patients in esophageal squamous cell carcinoma. *Mol. Cancer* 16:81.
- Lucibello, M., Adanti, S., Antelmi, E., Dezi, D., Ciafrè, S., Carcangiu, M. L., et al. (2015). Phospho-TCTP as a therapeutic target of Dihydroartemisinin for aggressive breast cancer cells. *Oncotarget* 6, 5275–5291. doi: 10.18632/oncotarget.2971
- Luo, H., Vong, C. T., Chen, H., Gao, Y., Lyu, P., Qiu, L., et al. (2019). Naturally occurring anti-cancer compounds: shining from Chinese herbal medicine. *Chin. Med.* 14:48.
- Merchant, J. L. (2012). Hedgehog signalling in gut development, physiology and cancer. *J. Physiol.* 590, 421–432. doi: 10.1113/jphysiol.2011.220681
- Myers, A. L., Lin, L., Nancarrow, D. J., Wang, Z., Ferrer-Torres, D., Thomas, D. G., et al. (2015). IGFBP2 modulates the chemoresistant phenotype in esophageal adenocarcinoma. *Oncotarget* 6, 25897–25916. doi: 10.18632/oncotarget.4532
- Nakajima, M., and Kato, H. (2013). Treatment options for esophageal squamous cell carcinoma. *Expert Opin. Pharmacother* 14, 1345–1354.
- Odaka, Y., Xu, B., Luo, Y., Shen, T., Shang, C., Wu, Y., et al. (2014). Dihydroartemisinin inhibits the mammalian target of rapamycin-mediated signaling pathways in tumor cells. *Carcinogenesis* 35, 192–200. doi: 10.1093/carcin/bgt277
- Qin, G., Zhao, C., Zhang, L., Liu, H., Quan, Y., Chai, L., et al. (2015). Dihydroartemisinin induces apoptosis preferentially via a Bim-mediated intrinsic pathway in hepatocarcinoma cells. *Apoptosis* 20, 1072–1086. doi: 10.1007/s10495-015-1132-2
- Rimkus, T. K., Carpenter, R. L., Qasem, S., Chan, M., and Lo, H. W. (2016). Targeting the sonic hedgehog signaling pathway: review of smoothened and GLI inhibitors. *Cancers (Basel)* 8:22. doi: 10.3390/cancers8020022
- Rubenstein, J. H., and Shaheen, N. J. (2015). Epidemiology, diagnosis, and management of esophageal adenocarcinoma. *Gastroenterology* 149, 302–317. doi: 10.1053/j.gastro.2015.04.053
- Ruiz i Altaba, A., Sánchez, P., and Dahmane, N. (2002). Gli and hedgehog in cancer: tumours, embryos and stem cells. *Nat. Rev. Cancer* 2, 361–372. doi: 10.1038/nrc796
- Sims-Mourtada, J., Izzo, J. G., Ajani, J., and Chao, K. S. (2007). Sonic Hedgehog promotes multiple drug resistance by regulation of drug transport. *Oncogene* 26, 5674–5679. doi: 10.1038/sj.onc.1210356
- Sugimura, K., Miyata, H., Tanaka, K., Hamano, R., Takahashi, T., Kurokawa, Y., et al. (2012). Let-7 expression is a significant determinant of response to chemotherapy through the regulation of IL-6/STAT3 pathway in esophageal squamous cell carcinoma. *Clin. Cancer Res.* 18, 5144–5153. doi: 10.1158/1078-0432.ccr-12-0701
- Wang, L., Chen, G., Chen, K., Ren, Y., Li, H., Jiang, X., et al. (2015). Dual targeting of retinoid X receptor and histone deacetylase with DW22 as a novel antitumor approach. *Oncotarget* 6, 9740–9755. doi: 10.18632/oncotarget.3149
- Wang, L. H., Li, Y., Yang, S. N., Wang, F. Y., Hou, Y., Cui, W., et al. (2014). Gambogic acid synergistically potentiates cisplatin-induced apoptosis in non-small-cell lung cancer through suppressing NF- κ B and MAPK/HO-1 signaling. *Br. J. Cancer* 110, 341–352. doi: 10.1038/bjc.2013.752
- Wang, Y. F., Chang, C. J., Lin, C. P., Chang, S. Y., Chu, P. Y., Tai, S. K., et al. (2012). Expression of hedgehog signaling molecules as a prognostic indicator of oral squamous cell carcinoma. *Head Neck.* 34, 1556–1561. doi: 10.1002/hed.21958
- Xie, J., Murone, M., Luoh, S. M., Ryan, A., Gu, Q., Zhang, C., et al. (1998). Activating smoothened mutations in sporadic basal-cell carcinoma. *Nature* 391, 90–92. doi: 10.1038/34201
- Yamasaki, M., Makino, T., Masuzawa, T., Kurokawa, Y., Miyata, H., Takiguchi, S., et al. (2011). Role of multidrug resistance protein 2 (MRP2) in chemoresistance and clinical outcome in esophageal squamous cell carcinoma. *Br. J. Cancer* 104, 707–713. doi: 10.1038/sj.bjc.6606071
- Yang, L., Ren, Y., Yu, X., Qian, F., Bian, B. S., Xiao, H. L., et al. (2014). ALDH1A1 defines invasive cancer stem-like cells and predicts poor prognosis in patients with esophageal squamous cell carcinoma. *Mod. Pathol.* 27, 775–783. doi: 10.1038/modpathol.2013.189
- Yang, L., Wang, L. S., Chen, X. L., Gatalica, Z., Qiu, S., Liu, Z., et al. (2012). Hedgehog signaling activation in the development of squamous cell carcinoma and adenocarcinoma of esophagus. *Int. J. Biochem. Mol. Biol.* 3, 46–57.
- Yoo, Y. A., Kang, M. H., Lee, H. J., Kim, B. H., Park, J. K., Kim, H. K., et al. (2011). Sonic hedgehog pathway promotes metastasis and lymphangiogenesis via activation of Akt, EMT, and MMP-9 pathway in gastric cancer. *Cancer Res.* 71, 7061–7070. doi: 10.1158/0008-5472.can-11-1338
- Zahreddine, H. A., Culjkovic-Kraljic, B., Assouline, S., Gendron, P., Romeo, A. A., Morris, S. J., et al. (2014). The sonic hedgehog factor GLI1 imparts drug resistance through inducible glucuronidation. *Nature* 511, 90–93. doi: 10.1038/nature13283

Conflict of Interest: The authors declare that the research was conducted in the absence of any commercial or financial relationships that could be construed as a potential conflict of interest.

Copyright © 2020 Cui, Fang, Duan, Xiang, Wang, Zhang, Zhai, Cui and Yang. This is an open-access article distributed under the terms of the Creative Commons Attribution License (CC BY). The use, distribution or reproduction in other forums is permitted, provided the original author(s) and the copyright owner(s) are credited and that the original publication in this journal is cited, in accordance with accepted academic practice. No use, distribution or reproduction is permitted which does not comply with these terms.



EGCG Enhanced the Anti-tumor Effect of Doxorubicine in Bladder Cancer via NF- κ B/MDM2/p53 Pathway

Ke-Wang Luo^{1,2}, Xiao-hong Zhu¹, Ting Zhao¹, Jin Zhong¹, Han-chao Gao³, Xin-Le Luo^{1*} and Wei-Ren Huang^{2*}

¹ Key Laboratory, People's Hospital of Longhua, The Affiliated Hospital of Southern Medical University, Shenzhen, China, ² Key Laboratory of Medical Programming Technology, Shenzhen Second People's Hospital, The First Affiliated Hospital of Shenzhen University, Shenzhen, China, ³ Department of Nephrology, Shenzhen Longhua District Central Hospital, Affiliated Central Hospital of Shenzhen Longhua District, Guangdong Medical University, Shenzhen, China

OPEN ACCESS

Edited by:

Liwu Fu,
Sun Yat-sen University, China

Reviewed by:

Dexin Kong,
Tianjin Medical University, China
Zui Pan,
University of Texas at Arlington,
United States

*Correspondence:

Wei-Ren Huang
pony8980@163.com
Xin-Le Luo
luoxinlesz@163.com

Specialty section:

This article was submitted to
Molecular and Cellular Oncology,
a section of the journal
Frontiers in Cell and Developmental
Biology

Received: 14 September 2020

Accepted: 17 November 2020

Published: 23 December 2020

Citation:

Luo K-W, Zhu X-h, Zhao T, Zhong J,
Gao H-c, Luo X-L and Huang W-R
(2020) EGCG Enhanced the
Anti-tumor Effect of Doxorubicine in
Bladder Cancer via
NF- κ B/MDM2/p53 Pathway.
Front. Cell Dev. Biol. 8:606123.
doi: 10.3389/fcell.2020.606123

Doxorubicin (DOX), the first-line chemotherapy for bladder cancer, usually induces side effects. We previously demonstrated that green tea polyphenol EGCG had potent anti-tumor effect in bladder cancer via down regulation of NF- κ B. This study aimed to investigate the additive/synergistic effect EGCG and DOX against bladder cancer. Our results demonstrated that the combined use of DOX and EGCG inhibited T24 and SW780 cell proliferation. EGCG enhanced the apoptosis induction effect of DOX in both SW780 and T24 cells and resulted in significant differences. Besides, EGCG promoted the inhibitory effect of DOX against bladder cancer cell migration. In addition, the *in vivo* results demonstrated that DOX in combination with EGCG showed the most potent anti-tumor effects among DOX, EGCG and DOX+EGCG treatment groups. Further mechanistic studies determined that the combination of DOX and EGCG inhibited phosphorylated NF- κ B and MDM2 expression, and up-regulated p53 expression in tumor, as assessed by western blot and immunohistochemistry. Western blot in SW780 cells also confirmed that the combined use of EGCG and DOX caused significant increase in p53, p21, and cleaved-PARP expression, and induced significant inhibition in phosphorylated NF- κ B and MDM2. When NF- κ B was inhibited, the expression of p53 and p-MDM2 were changed, and the combination of DOX and EGCG showed no obvious effect in transwell migration and cell viability. In conclusion, the novel application of chemotherapy DOX and EGCG demonstrated potent anti-tumor, anti-migration and anti-proliferation effects against bladder cancer. EGCG enhanced the anti-tumor effect of DOX in bladder cancer via NF- κ B/MDM2/p53 pathway, suggesting the potential clinical application against bladder cancer patients.

Keywords: MDM2, p53, NF- κ B, bladder cancer, doxorubicine, EGCG

INTRODUCTION

Despite significant advances in cancer research, cancer remains a worldwide health problem, with an estimated 9.6 million deaths in 2018. Bladder cancer ranks 9th of incidence and caused about 430,000 new cases annually worldwide (Antoni et al., 2017). It is estimated that ~549,939 persons are diagnosed with bladder cancer worldwide each year (Stewart and Wild, 2014). Therefore, novel therapeutic strategies and more effective combinations for bladder cancer treatment are still needed.

Doxorubicin (DOX), a first-line chemotherapy for bladder cancer, inhibits cell proliferation by directly interfering with DNA synthesis and transcription, with a broad anti-tumor spectrum (Chen et al., 2018). It is reported that DOX could regulate the expression of p53 to exert its antitumor effect. Lu et al. found that DOX increased p53 expression in A549 cells, and thereby promoted cell apoptosis and necrosis (Lu et al., 2014). Doxorubicin was demonstrated to be effective in induction of apoptosis in prostate cancer, by activating p53-mediated pathway to exert their anti-cancer effects by causing DNA damage and initiating cell cycle arrest in cancer cells (Yang et al., 2016). Though DOX was widely used in the treatment of bladder and other cancers, the drug could cause immune function declines and induce severe cardiac toxicity with long-term application (Renu et al., 2018). Therefore, it is of great importance to find combined treatment plans with synergistic antitumor efficacy or reducing the side effects of doxorubicin.

Epigallocatechin-3-gallate (EGCG), the most bioactive polyphenol from *Camellia sinensis*, has been demonstrated to have various biological activities, including anti-oxidation, anti-cancer and others (Gan et al., 2018). EGCG was found to be effective in improving liver and pancreatic β -cell functions in iron-overloaded β -thalassemia mice by diminishing redox iron and free radicals (Koonyosying et al., 2018). Besides, numerous literatures also reported the anti-cancer effect of EGCG. It was demonstrated that tea polyphenol EGCG was effective in decreasing the risk of several cancer types, including stomach, prostate, and lung cancers (Lin and Liang, 2000). Treatment with EGCG resulted in significant down-regulation of tumor burden in breast, bladder, and prostate cancers (Yang et al., 2009). EGCG was also clarified to be effective in inhibiting metastasis or angiogenesis, or promoting apoptosis in leukemia, breast, prostate cancer cells (Gan et al., 2018). We previously found that treatment with green tea aqueous extract resulted in obviously inhibition of 4T1 breast tumor by induction of apoptosis, and EGCG was shown to be the most abundant ingredient in green tea (Luo et al., 2014). We also demonstrated that EGCG suppressed the bladder cancer SW780 tumor growth by down regulation of NF- κ B (Luo et al., 2017). Recently, varieties of studies investigated the effects of EGCG in combination with chemotherapies as adjuvant agent. Wang et al. found that EGCG enhanced cisplatin sensitivity and increased the drug accumulation of cisplatin in ovary cancer by regulating expression of the copper and cisplatin influx transporter CTR1 (Wang et al., 2015); Chen et al. determined that EGCG synergistically enhanced DOX anticancer effects involving autophagy inhibition in hepatocellular carcinoma as

a chemotherapeutic augmentor (Chen et al., 2014). EGCG is naturally derived and can be used as a preventive or sensitizer in the prevention and treatment of cancer, and could inhibit bladder cancer proliferation and migration by down regulation of NF- κ B. DOX is a first-line chemotherapy drug for bladder cancer, but usually induces side effects. This study aims to investigate the synergistic/additive anti-tumor effect of DOX and EGCG in bladder cancer and determine the underlying mechanisms, when DOX in a much lower dose than clinic use.

During the process of cancer propagation, Murine double minute-2 (MDM2) plays an important role, which serves as a negative regulator of p53 and thereby limits cell cycle arrest and apoptosis (Zhao et al., 2018). It is reported that MDM2 can bind to p53 and block the p53 signaling pathway, and could also promote the degradation of p53; when p53 is activated, in turn, it also inhibits the transcriptional expression of MDM2 (Thomasova et al., 2012). Besides, NF- κ B can promote the expression of oncogene MDM2, which in turn inhibits the activation of p53 (Zhuang et al., 2014). We previously found that EGCG was effective in down-regulated the expression of NF- κ B and inhibited bladder tumor growth (Luo et al., 2017); while DOX could regulate the expression of p53 to exert its antitumor effect. Thus, we hypothesize that tea polyphenol EGCG could work synergistically with DOX in inhibiting bladder cancer cells proliferation and migration via NF- κ B/MDM2/p53 pathway.

The present study aimed to investigate the combined use of DOX and EGCG against tumor growth, proliferation, and migration in bladder cancer. We hypothesize that tea polyphenol EGCG can work synergistically with DOX in inhibiting bladder cancer cells proliferation and migration. Here, we assessed the apoptosis-induction and anti-migration abilities of the combination of DOX and EGCG *in vitro*, and then further evaluated the anti-tumor activities of DOX and EGCG in mice *xenograft* model. Besides, the protein expression of NF- κ B, p53, and MDM2 were also evaluated both *in vitro* and *in vivo* after treatment. Immunohistochemistry and western blot were used to determine the underlying mechanism of anti-metastasis activities of DOX+EGCG.

MATERIALS AND METHODS

Cells and Reagents

Bladder cancer SW780 and T24 cells were cultured in DMEM medium containing 10% (v/v) fetal bovine serum and 1% penicillin-streptomycin (Life technology, United States) at 37°C in 5% CO₂ humidified incubator. MTT and Doxorubicine (DOX) were obtained from Sigma, USA. Transwell plates were from Corning Incorporated, United States. Annexin V-FITC kit was purchased from BD Pharmingen, United States. NF- κ B, NF- κ B p65 (p-NF- κ B), MDM2, Phospho-MDM2 (p-MDM2), p53, p21, Bcl-2, and PARP were purchased from Cell signaling technology, United States. Alanine transaminase (ALT), Creatine kinase (CK), and aspartate transaminase (AST) kits were obtained from Stanbio, United States. NF- κ B inhibitor (SC75741) was purchased from Selleck, United States.

Cell Viability Assay

Cells (1×10^4 /well) were seeded in 96-well plates (Corning, United States) and incubated with DOX (0, 0.05, 0.1, 0.2, 0.4, and $0.8 \mu\text{M}$) and EGCG (0, 12.5, $25 \mu\text{M}$) for 48 h. Following incubation, MTT (30 μl /well) was added and the plate was incubated for additional 4 h. Then, the absorbance of each sample was measured at 540 nm as a reference with the microplate reader (Thermo Multiskan GO, United States).

Annexin V Double Staining

SW780 cells were treated with EGCG ($100 \mu\text{M}$) and/or DOX ($0.1 \mu\text{M}$) for 24 h, and T24 cells were treated with EGCG ($200 \mu\text{M}$) and/or DOX ($0.1 \mu\text{M}$) for 24 h. Then, the cells were harvested and washed with cold PBS. After stained with Annexin V-FITC and PerCP for 15 min in dark at room temperature, the fluorescent signal was assessed by flow cytometry (FACSARIA II, Becton Dickinson). Positioning of quadrants on annexin-V plots was performed to distinguish living cells (FITC-/PerCP-), early apoptotic cells (FITC+/PerCP-), and late apoptotic or necrotic cells (FITC+/PerCP+).

Cell Migration Assays

The efficacy of EGCG and/or DOX against SW780 and T24 cell migration *in vitro* were assessed by scratch wound healing and transwell migration assays.

In scratch wound healing assay, cells (1×10^5 /well) were seeded in 24-well plates. After incubated in FBS-free medium for 24 h, cells were scraped with crosses using yellow pipette tips, and then added with full medium (with 10% FBS) with EGCG and/or DOX. SW780 cells were treated with EGCG ($12.5 \mu\text{M}$) and/or DOX ($0.1 \mu\text{M}$) for 24 h, and T24 cells were treated with EGCG ($25 \mu\text{M}$) and/or DOX ($0.1 \mu\text{M}$) for 24 h. Then each well was photographed under a microscope (Olympus IX73). The percentages of open wound area were measured and calculated using the TScratch software.

During transwell migration assay, cells (2×10^4 /well) were added into transwell upper chambers with 100 μl medium containing EGCG and DOX (with 1% FBS). And the concentration of EGCG and DOX were the same as the dose in scratch wound assay. Then 500 μl full DMEM medium (with 10% FBS) was added in the lower chamber. Cells were allowed to migrate from the upper layer through the chamber membrane to the lower well for 24 h incubation at 37°C . Later, cells were fixed with 100% methanol and stained with 0.1% crystal violet for 10 min. Stained membranes were photographed using microscope (Olympus IX73), and the migrated rates were assessed by manual counting of the cells in chamber membrane.

Nude Mice Tumor Model

BALB/c mice (female, 6–8 weeks) were purchased from Vital River Laboratory Animal Technology Co. Ltd, Beijing, and were kept under pathogen-free conditions in Guangdong Medical University. The animal experiments were carried out under the permission of the animal ethical and welfare committee. The sensitive cell line SW780 was chosen for animal study. Cells (3×10^6 in 0.2 ml PBS) were subcutaneously (s.c.) inoculated at the back of mice. After the tumor size reached

to 80–100 mm^3 , the mice were randomly grouped ($n = 7$): control group (saline, i.p., injected everyday), EGCG group (50 mg/kg EGCG, i.p., injected everyday), DOX group (2 mg/kg DOX, i.p., injected once) and EGCG+DOX group (50 mg/kg EGCG, i.p., injected everyday, and 2 mg/kg DOX, i.p., injected once). Treatments were initiated after the tumor size reached 80–100 mm^3 , and lasted for 3 weeks. During treatment, the body weight and tumor volume of each mouse was measured twice a week. At day 28, mice were sacrificed, and the tumors were removed for quantification of tumor burden and immunohistochemistry staining. The tumors were also cut up and lysed for protein analysis. The effect of treatments on hemato-biochemical markers were assessed by measuring the activities of liver or heart related enzymes (ALT, AST, and CK) in the plasma using assay kits purchased from Stanbio Co. Ltd.

Western Blot Analysis

Tumors were cut into pieces, grinded, and lysed in lysis buffer. Cells treated with EGCG ($100 \mu\text{M}$) and/or DOX ($0.1 \mu\text{M}$) were also lysed in lysis buffer. After protein concentration measured, protein samples (20 μg) were electrophoresed in 10 % SDS-PAGE gel and transferred to PVDF membrane (Millipore, United States). After blocking with 10% non-fat milk, the membranes were washed with PBS-T, and then incubated with primary antibodies for 24 h at 4°C . After washing, the membrane was incubated with secondary antibodies for 1 h. Finally, visualization of protein bands was performed using the ECL substrate reagent kit (GE Healthcare) on a Gel Doc XR imaging system (Bio-RAD, United States).

Immunohistochemistry

Tumor tissues were fixed with 10% formalin solution for 7 days at room temperature. Then the samples were paraffin embedded, sectioned longitudinally at $3 \mu\text{m}$. After the sections dewaxing in xylene, 100, 95, 80, and 70% ethanol and running water for 1 min, respectively, the sections were blocked with BSA solution for 20 min. Then the sections were probed with primary antibody at 4°C overnight. After washing, the sections were incubated with secondary antibody for 1 h at room temperature. The sections were washed 3 times with PBS for 5 min each time, and incubated with streptavidin-biotin peroxidase at room temperature for 30 min. Finally, the sections were colored with DAB for 5 min, stained with hematoxylin and mounted. The stained sections were examined and photographed using an Olympus IX73 microscope (Japan).

Statistical Analysis

All data were expressed as mean \pm SD/SEM. Statistical analysis was performed using one way ANOVA, with $p < 0.05$ as regarded statistically significant.

RESULTS

Effect of the Combined Use of EGCG and DOX on Bladder Cancer SW780 and T24 Cell Viability

MTT assay was performed to assess the effect of EGCG in combination with DOX at different concentrations on cell viability of bladder cancer SW780 and T24 cells, and then the effective doses of DOX and EGCG would be chosen for further studies when the synergistic index (CI) was lower than 1. As shown in **Figure 1**, the combination of EGCG and DOX inhibited cell viability significantly. The inhibition rate of the combination of EGCG and DOX was higher than DOX alone at various concentrations. The combination of DOX and EGCG demonstrated additive or synergistic cytotoxic effects, especially at the doses of 0.1 μ M DOX plus 25 μ M EGCG in T24 cells, which produced an inhibition of 21.8% cell viability, while DOX and EGCG alone caused inhibition rates of 12.3 and 5.2 %, respectively. Besides, the combined use of DOX (0.1 μ M) and EGCG (12.5 μ M) on SW780 cells also demonstrated additive cytotoxic effects, which produced an inhibition of 22.1% cell viability, while DOX and EGCG alone caused inhibition rates of 12.1 and 8.6%, respectively. Since the combination of DOX (0.1 μ M) and EGCG (12.5 μ M, 25 μ M) has the best additive/synergistic inhibition capacity of cell viability in SW780 and T24 cells, respectively, such dose of combination was selected in further studies.

EGCG Enhanced the Apoptosis Induction Effect of DOX in SW780 and T24 Cells

Annexin-V FITC/Per CP staining showed that treatments of EGCG, DOX, and EGCG plus DOX, resulted in significant apoptosis induction efficacies in bladder cancer SW780 and T24 cells (**Figure 2**). The percentage of apoptotic cells upon treatment with 0.1 μ M of DOX was found to be 12.52 and 9.95% in SW780 and T24 cells, while DOX plus EGCG caused an increasing of 42.94 and 33.69% of apoptotic cells in SW780 and T24 cells, respectively. Significant differences were shown between DOX+EGCG and EGCG groups, and DOX+EGCG and DOX groups, indicating EGCG enhanced the apoptosis induction effect of DOX in bladder cancer.

EGCG Promoted the Anti-migration Effect of DOX in SW780 and T24 Cells

To determine the efficacy of EGCG and/or DOX against cancer cell migration *in vitro*, the scratch wound healing and transwell migration assays were introduced. As shown in **Figure 3A**, treatment of EGCG at 25 μ M resulted in no obvious effect in inhibition of T24 cell migration and invasion, and DOX (0.1 μ M) alone induced significant decrease of T24 cell metastasis. The inhibition effect of DOX in cell migration and invasion was enlarged when in combination with EGCG, and significant differences were shown between DOX+EGCG and DOX (**Figures 3C,D**). Besides, similar results were also shown in SW780 cell migration and invasion when treated with EGCG, DOX and DOX+EGCG. In **Figure 3F**, no significant

difference was shown in EGCG and DOX treatment alone in SW780 cell migration, and the combination of EGCG and DOX caused significant increase of open wound area, indicating that DOX+EGCG treatment demonstrated synergistic effect in SW780 cell migration. Furthermore, the combined use of EGCG and DOX showed better effect in SW780 cell invasion than individual treatment, the cell invasion was inhibited to 56.2%, and significantly differences were shown to individual treatments (**Figure 3H**).

EGCG Enhanced the Anti-tumor Effect of DOX in Nude Mice Tumor Model

To evaluate the activity of EGCG and/or DOX on tumor growth *in vivo*, a subcutaneous tumor model in nude mice was employed. No significant body weight loss was found in all treatment groups (**Figure 4A**). Besides, hemato-biochemical markers test showed that no obvious difference was shown on plasma activities of heart specific (CK) and liver related (AST and ALT) enzymes between untreated control and treatment groups (**Figure 4B**). As shown in **Figure 4C**, the tumor volume were decreased in EGCG and DOX individual treatment group, however no significant difference was shown. The combination of EGCG and DOX demonstrated significant inhibition of tumor volume from day 23, when compared with untreated control. In addition, tumor weights were decreased in all treatment groups, and significant difference was only shown in DOX+EGCG treatment group (by 76.8%) when compared with control (**Figure 4D**). These results clarified that EGCG enhanced the anti-tumor effect of DOX in bladder cancer, and the combination of DOX and EGCG showed the best anti-tumor effects among the treatment groups.

The Combination of EGCG and DOX Inhibited NF- κ B, p53, and MDM2 Expression in Tumor

In order to evaluate the protein expression of NF- κ B, p53, and MDM2 in tumor, the western blot and immunohistochemistry were performed. As shown in **Figure 5A**, treatment of EGCG, DOX, and DOX+EGCG in nude mice resulted in obviously increase in p53, and inhibition of phosphorylated NF- κ B and MDM2 in protein. Semi-quantitative analysis demonstrated that EGCG promoted the effect of DOX in increase of p53 expression and decrease of p-NF- κ B and p-MDM2 expression, and the combination DOX+EGCG showed the best result among treatment groups. Significant differences were shown between DOX+EGCG and individual treatments. In addition, similar results were also shown in immunohistochemistry that p-NF- κ B and p-MDM2 were down regulated, and p53 was up regulated in DOX+EGCG group, and significant differences were shown when compared with control (**Figure 5B**).

EGCG and DOX Regulated the Protein Expressions

In order to evaluate the expression of NF- κ B, p53, MDM2, and other related proteins in bladder cancer SW780 cells, the western blot was performed. As shown in **Figure 5C**, EGCG treatment induced no obvious effect in p53 and p21 expression, while the

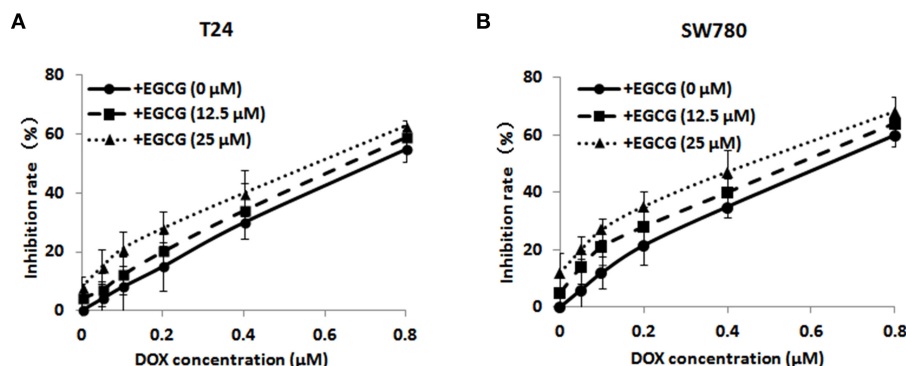


FIGURE 1 | The effects of EGCG in combination of various doses of DOX on bladder cancer T24 (A) and SW780 (B) cell viability. Cells were incubated with EGCG (0, 12.5, and 25 μM) in the presence of various concentrations of EGCG (0, 0.05, 0.1, 0.2, 0.4, and 0.8 μM) after 48 h treatment. Data were expressed as mean \pm SD ($n = 3$).

combined use of EGCG and DOX caused significant increase in p53 and p21 expression, and significant differences were shown to EGCG and DOX individual treatments. There was no obvious change shown in NF- κ B and MDM2 expression among treatment groups, however the activated phosphorylated NF- κ B and phosphorylated MDM2 was down-regulated significantly in EGCG and DOX individual groups, and the combination group of DOX+EGCG enlarged the inhibition and showed the best result among three treatment groups. Besides, EGCG, DOX and DOX+EGCG treatment resulted in significant decreasing in Bcl-2 expression, and significant increase of cleaved-PARP, indicating the activation of apoptosis.

The Combination of EGCG and DOX Showed no Obvious Effect on Transwell Migration and Cell Viability When NF- κ B Was Inhibited

In order to confirm the importance of NF- κ B and NF- κ B/MDM2/p53 pathway in EGCG+DOX induced migration and proliferation inhibition, SC75741 (NF- κ B inhibitor) was added in SW780 cells, and then the cells were harvested for transwell and MTT assays. As shown in **Figure 6A**, when SC75741 was added, the NF- κ B was blocked, and expression of p-MDM2 was decreased and p53 was up-regulated. Besides, the combination of DOX+EGCG showed no obvious effect in transwell migration when NF- κ B inhibited, which worked effectively in normal SW780 cells. The cell viability analysis in **Figure 6C** showed similar results that DOX+EGCG treatment led to no difference in cell viability in NF- κ B inhibited SW780 cells, when compared with control.

DISCUSSION

Green tea is the most popular beverage consumed worldwide, and EGCG is the most abundant and bioactive tea Polyphenol. EGCG has been widely consumed as health-promoting food ingredients and showed chemotherapeutic efficacies in cancer

prevention and treatment. In this study, we aim to investigate the additive/synergistic effect of EGCG in combination with DOX against bladder cancer both *in vitro* and *in vivo*.

In the present study, we demonstrated that treatment of EGCG in combination with DOX resulted in dose-dependent inhibition of cell viability in T24 and SW780 cells *in vitro* (**Figure 1**). The combination of DOX (0.1 μM) and EGCG (12.5 μM , 25 μM) has the best additive/synergistic inhibition effect of cell viability in SW780 and T24 cells, respectively, and these dose of combination was selected in further studies. In order to determine whether the anti-proliferative effect of EGCG and DOX was associated with apoptosis induction, Annexin V assay was employed. The results showed that DOX plus EGCG caused significant increases of percentage of apoptotic cells in bladder cancer T24 and SW780 cells, when compared to the individual treatment of DOX or EGCG (**Figure 2**), indicating the synergistic effect of EGCG to DOX on apoptosis induction. The findings were in line with the results in head and neck cancer that EGCG exhibited synergistic apoptosis induction effects in combination with chemotherapy erlotinib (Haque et al., 2015). EGCG was also demonstrated to be effective in reducing cell viability and migration in oral cancer when combined with 5-fluorouracil (Pons-Fuster López et al., 2019). In addition, the combination of DOX and EGCG showed greater level inhibition of cell migration on T24 and SW780 cells, when compared with individual treatment of DOX or EGCG, as assessed by scratch wound healing and transwell migration assays (**Figure 3**). These results indicated that EGCG enhanced the inhibitory effect of DOX on cell migration in bladder cancer T24 and SW780 cells, which was in line with Flores-Pérez's finding that EGCG enhanced cisplatin-induced inhibition in cell migration and sensitize A549 cells to chemotherapy (Flores-Pérez et al., 2016). Moreover, the selected doses of EGCG and DOX for migration and invasion assays were non-cytotoxic doses, and the cell viability was about 80%. This non-cytotoxic doses of DOX+EGCG showed remarkable anti-migration effects to bladder cancer cells, revealing that EGCG could be added as an effective supplement for bladder cancer prevention and treatment.

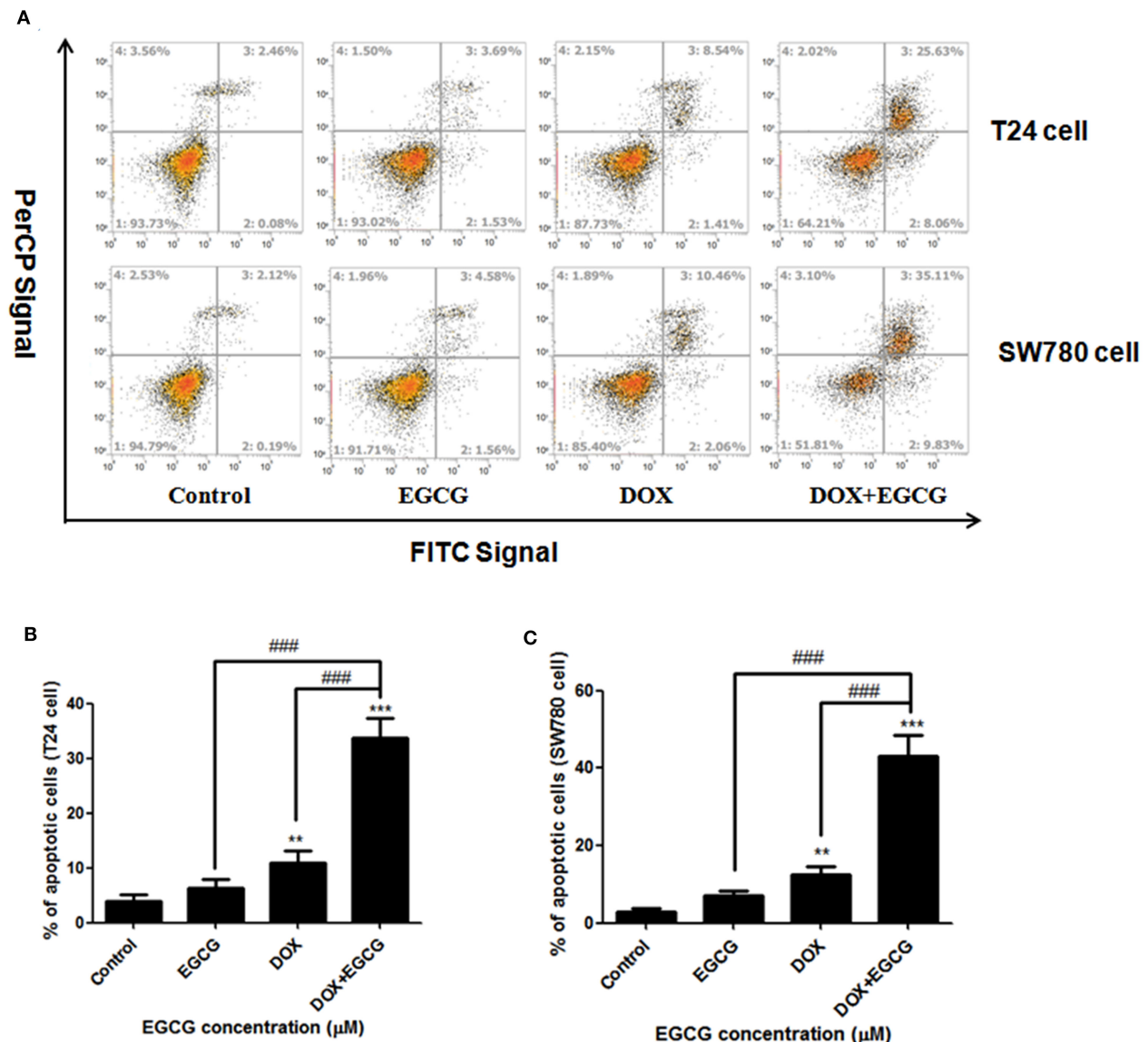


FIGURE 2 | EGCG enhanced the apoptosis induction effect of DOX in SW780 and T24 cells. **(A)** Flow cytometry images. **(B)** Quantitative analysis of the percentage of apoptotic cells of EGCG and/or DOX on bladder cancer T24 cells **(B)** and SW780 cells **(C)**, after 24 h incubation. The percentage of total apoptotic cells was defined as the sum of early and late apoptotic cells. Data were presented as mean + SD ($n = 3$). $**p < 0.01$ and $***p < 0.001$, as compared with untreated control. $###p < 0.001$, as compared between groups indicated.

In addition to *in vitro* studies, the *in vivo* anti-tumor effects of DOX and EGCG were evaluated in a xenograft mouse model. No obvious toxicity was shown to the mice after treatment, as assessed by the body weight and hemato-biochemical markers (AST, ALT, and CK). Administration of EGCG (50 mg/kg) and DOX (2 mg/kg) was able to decrease the tumor volume and tumor weight in mice bearing SW780 tumors. The combination of EGCG and DOX demonstrated significant inhibition of tumor volume from day 23, and also caused significant inhibition of tumor weight (**Figures 4C,D**).

The finding suggested that DOX and EGCG could work together against tumor growth, and showed better anti-tumor effect when compared with DOX or EGCG alone. It is demonstrated that EGCG/gelatin-doxorubicin gold nanoparticles enhanced the therapeutic efficacy of doxorubicin for prostate cancer treatment (Tsai et al., 2016). A recent preclinical study revealed that EGCG attenuated DOX-induced cardiotoxicity in rats (Saeed et al., 2015). Besides, reports also showed that EGCG could work as an adjuvant in cancer treatment to enhance the efficacy of chemotherapy, such as EGCG inhibited DNA repair and

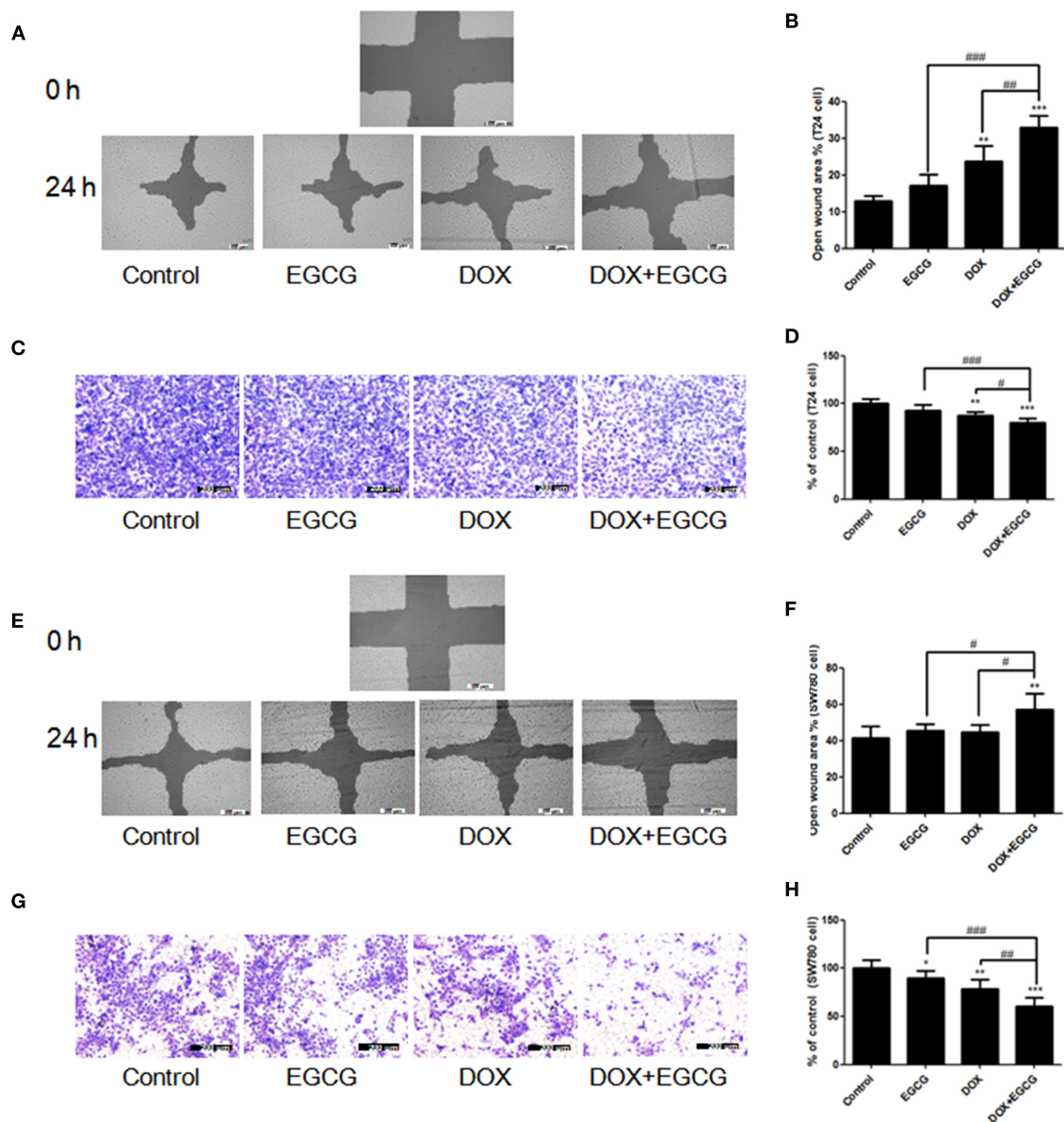


FIGURE 3 | EGCG promoted the anti-migration effects of DOX in T24 and SW780 cells. The efficacy of EGCG and/or DOX against bladder cancer cell migration *in vitro* were assessed by scratch wound healing and transwell migration assays. **(A,E)** Representative images of the wounded cell monolayers of T24 cells **(A)** and SW780 cells **(E)**. **(B,F)** Quantitative analysis of the anti-migration activity of EGCG and/or DOX in T24 **(B)** and SW780 cells **(F)**, as assessed by scratch wound healing assay. Data were expressed as the percentage of open wound area from baseline cultures without treatment. **(C,G)** Representative images of the stained migrated T24 **(C)** and SW780 cells **(G)** in filters in transwell migration assay. **(D,H)** Quantitative analysis of the transwell migration activity of EGCG and/or DOX in T24 cells **(D)** and SW780 cells **(H)**. The migrated cells were quantified by manual counting and represented as a percentage of control values. Data were presented as mean + SD ($n = 3$). * $p < 0.05$, ** $p < 0.01$, and *** $p < 0.001$, as compared with untreated control. # $p < 0.05$, ## $p < 0.01$, and ### $p < 0.001$, as compared between groups indicated.

enhanced cisplatin sensitivity in human cancer cells both *in vitro* and *in vivo* (Heyza et al., 2018), and the 5-FU and EGCG co-loaded nanoparticles could sustained drug release, and enhanced cellular uptake, thus exhibited superior anti-tumor activity and pro-apoptotic efficacy *in vivo* against colon cancer (Wang et al., 2019).

In our study, the *in vivo* doses of EGCG and DOX were 50 and 2 mg/kg, respectively, which were based on the clinical

dose of DOX and our previous study of EGCG. The clinical dose of DOX on bladder cancer patient was about 60 mg for a 60 kg adult per month, which was equivalent to a single dose of 12.3 mg/kg for mouse per month. We chose the dose of 2 mg/kg of DOX in combination study *in vivo*, which was much lower than the clinical dose transfer to mouse, and would not induce severe side effects. Besides, we previously found that EGCG at 100 mg/kg (i.p., injected daily) decreased the

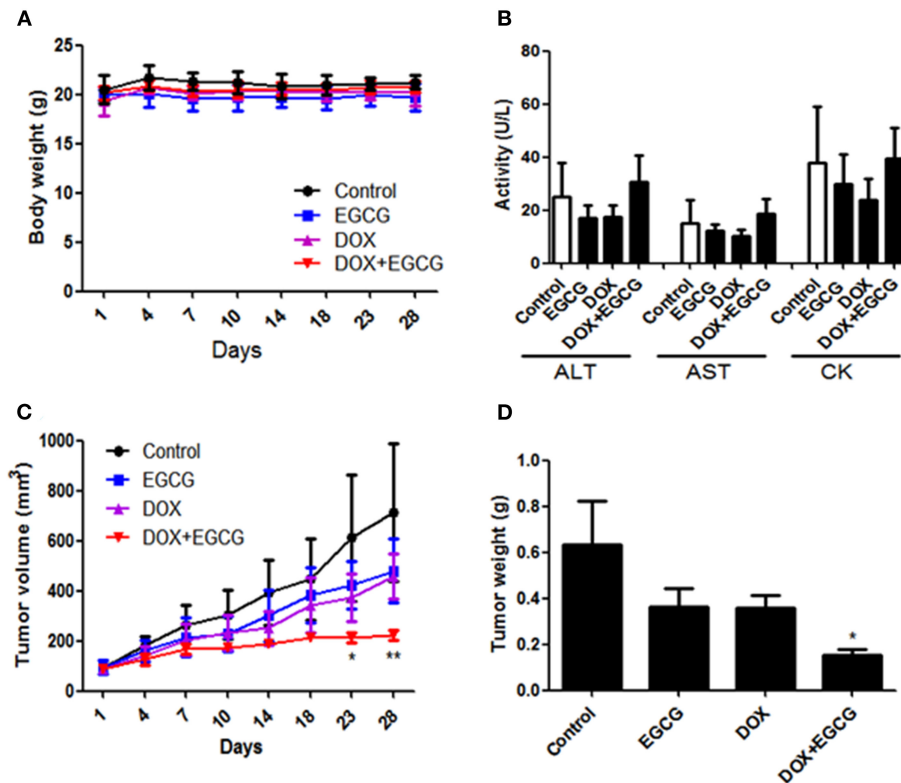
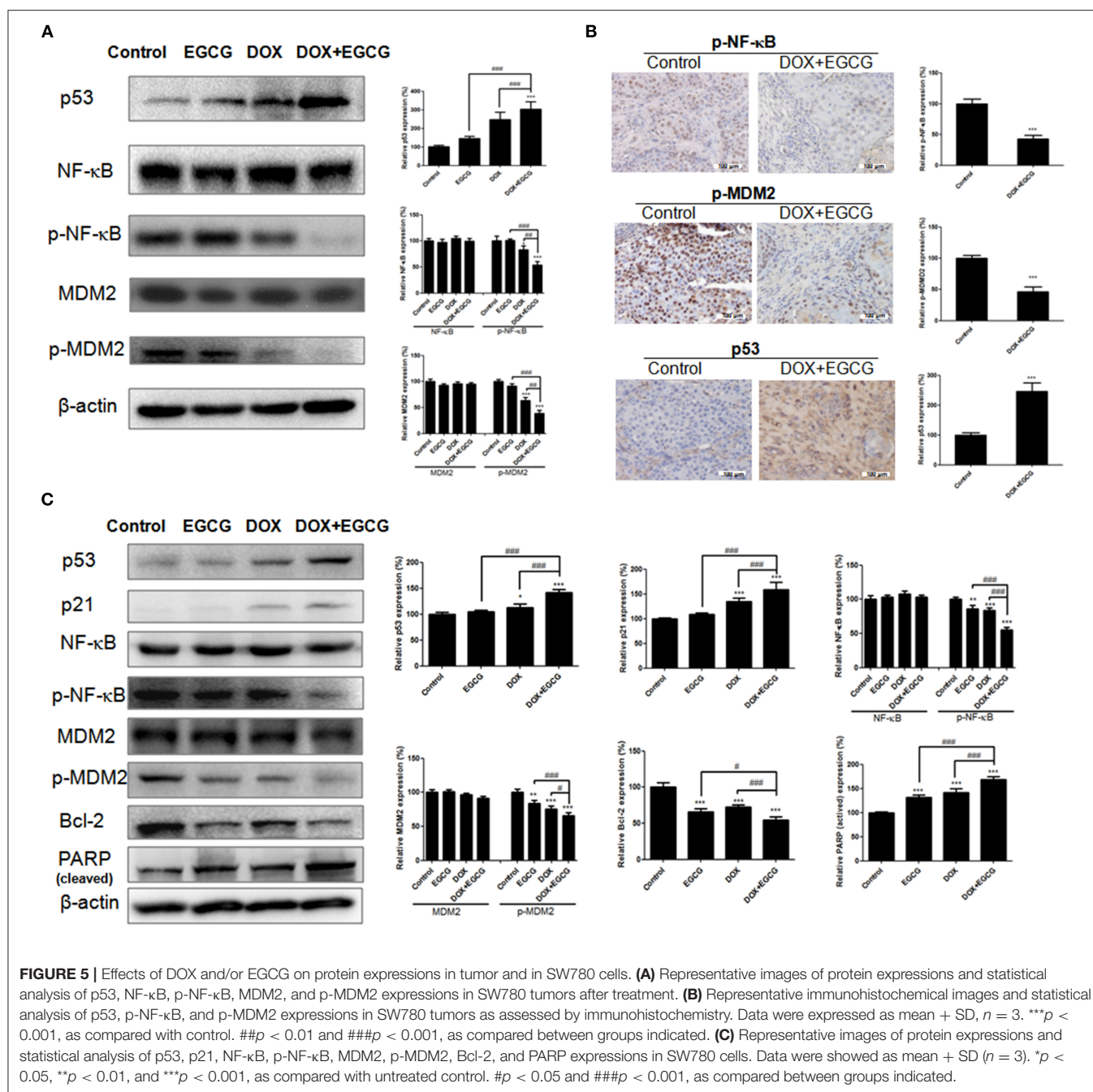


FIGURE 4 | EGCG enhanced the anti-tumor effect of DOX in SW780 nude mice xenograft tumor model. **(A)** No significant body weight loss of mice was found during EGCG treatment period. **(B)** Evaluation of the hemato-biochemical markers (ALT, AST, and CK) of mice plasma after treated with EGCG and/or DOX. **(C)** Quantitative analysis of the tumor volume in each group during treatment. Tumor volume was assessed by caliper and calculated as the length * width * width * 0.5. The combination of DOX+EGCG demonstrated significant inhibition of tumor volume from day 23, when compared with untreated control. **(D)** Graph showed the tumor weight from different group. Data were expressed as mean \pm SEM, $n = 7$. * $p < 0.05$ and ** $p < 0.01$, as compared with control.

tumor volume by 68.4% in mice bearing SW780 tumors, while EGCG at the dose of 50 mg/kg showed no obvious inhibition in bladder tumor (Luo et al., 2017). In order to investigate the additive/synergistic effect of EGCG and DOX, we adopt the ineffective dose of EGCG (50 mg/kg) and much lower than clinical dose of DOX (2 mg/kg) in the combination study. Thus, if the combination was work, it means the ineffective dose of EGCG plus DOX could work synergistically, and enhance the anti-tumor effect of DOX. On the other hand, the dose of DOX (2 mg/kg) was much lower than clinical dose transferred to mouse, and the unwanted side effects could be lowered. The *in vivo* animal study demonstrated that the combination of EGCG and DOX showed significant inhibition in bladder tumor, while the individual treatments exhibited no obvious effect. That indicates EGCG can synergistically enhance the action of DOX in inhibiting the bladder tumor growth, as adjuvant therapy in bladder cancer treatment.

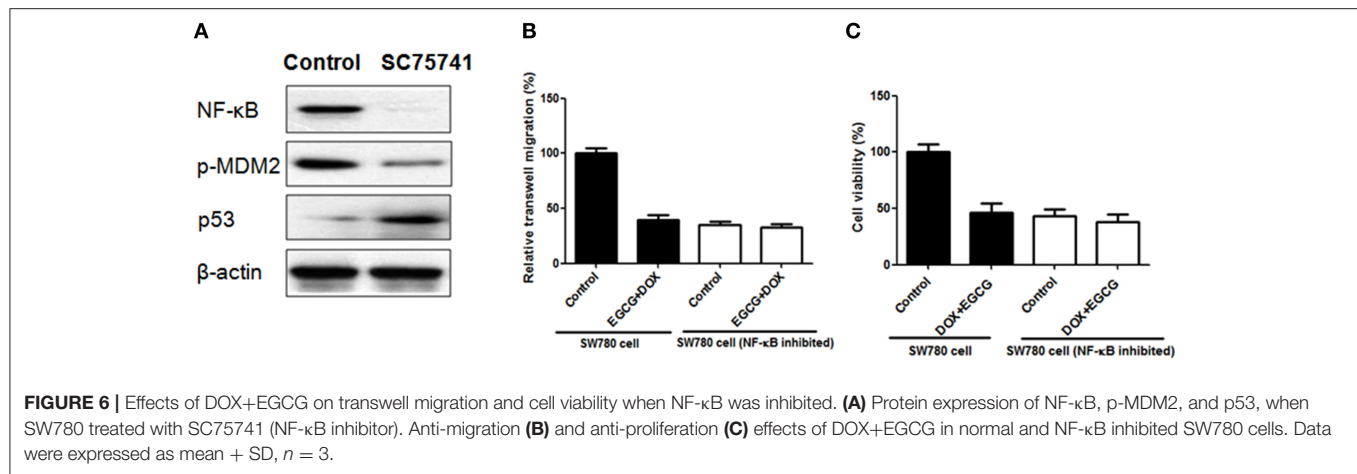
To gain insight into the underlying mechanism of DOX+EGCG induced anti-tumor efficacies, western blot and immunohistochemistry were employed. As shown in **Figure 5C**, treatment of DOX+EGCG in nude mice resulted in significant increase in p53, and obvious inhibition of

phosphorylated NF- κ B and MDM2, with significant differences to individual treatment of EGCG or DOX. Similar results were also shown in immunohistochemistry analysis that the combination of DOX and EGCG was effective in down-regulation of p-NF- κ B and p-MDM2, and up-regulation of p53 (**Figure 5B**). The *in vivo* animal results and protein analysis in tumor indicated that the combination of DOX and EGCG showed the best anti-tumor effect and the strongest protein regulation in p53, p-NF- κ B, and p-MDM2, among three treatment groups of DOX, EGCG, and DOX+EGCG. In addition, protein expressions of p53, p21, NF- κ B, MDM2, PARP, and Bcl-2 were also tested in SW780 cells. As shown in **Figure 5C**, DOX was effective in up-regulation of p53 and p21, and the increases were enlarged when DOX combined with EGCG, with significant difference to DOX. Treatment of DOX alone resulted in activation of NF- κ B and MDM2, and the combination of DOX+EGCG caused strongest decrease on p-NF- κ B and p-MDM2 among three treatment groups. Similar results were also found on the effect of PARP and Bcl-2, DOX+EGCG showed better effect than DOX treatment alone. The result was in agreement with Pan's finding that treatment of mice with EGCG markedly attenuated cisplatin



induced mitochondrial oxidative stress and damages through decreasing NF- κ B (Pan et al., 2015). Besides, the *in vitro* findings in proteins were completely in line with the *in vivo* result that DOX+EGCG showed the best result in suppression p-NF- κ B and p-MDM2, and increasing p53, which suggested that EGCG could work synergistically with DOX as an adjuvant reagent. EGCG was the most abundant and bioactive polyphenol from green tea, which showed efficacies in cancer prevention and treatment of tumors, as an efficient natural preventive agent or adjuvant sensitizer in combination therapy (Kallifatidis et al., 2016). We previously found that EGCG suppressed the

bladder cancer SW780 tumor growth by down regulation of NF- κ B (Luo et al., 2017). Moreover, it was demonstrated that NF- κ B could promote the expression of oncogene MDM2, which in turn inhibit the activation of p53 (Zhuang et al., 2014). Jin et al. found that EGCG promoted p53 accumulation and activity via inhibition of MDM2 in human lung cancer cells (Jin et al., 2013). Same findings were also shown in human prostate carcinoma LNCaP cells that EGCG induced apoptosis via stabilization of p53, downregulation of MDM2 protein, and negative regulation of NF- κ B activity, thereby decreasing the expression of Bcl-2 (Hastak et al., 2003). Our



results demonstrated that EGCG was effective in suppressing the phosphorylation of NF-κB, inhibiting the expression of MDM2, and activating the downstream proteins of Bcl-2 and PARP, and then promoted the apoptosis induction, which might contribute to the synergistic effect of combination with DOX against bladder cancer proliferation and migration. In addition, DOX up-regulated the expression of p53, worked together with EGCG, and then amplified the anti-tumor effect in bladder cancer via NF-κB/MDM2/p53 pathway. Once NF-κB was inhibited in bladder cancer cells, the expression of p-MDM2 was decreased and p53 was up-regulated, and the combination of DOX+EGCG showed no obvious effect in SW780 cell migration and proliferation (Figure 6), indicating the importance of NF-κB/MDM2/p53 pathway played in DOX+EGCG induced effects.

Our results have clearly demonstrated that the combination of DOX and EGCG worked together in decreasing the phosphorylation of NF-κB and MDM2, and increasing the expression of p53, and showed significant anti-proliferation and anti-migration effects both *in vitro* and *in vivo*. This finding sheds light on the combination of DOX+EGCG on tumor inhibition in bladder cancer, and provides clear directions for mechanism study. Besides, the effective dose of EGCG worked synergistically with DOX and enhanced the apoptosis induction and anti-migration effects of DOX without obvious cytotoxic to cells, indicating that EGCG could be a safe and natural supplement for bladder cancer prevention and treatment in combined with DOX. In addition, EGCG also got other comprehensive benefits, such as anti-oxidation, cardiovascular protective effects, which made EGCG a good candidate for combination therapy in cancer treatment and comprehensive health care.

In conclusion, our results present the first evidence on the anti-tumor effect of DOX and EGCG against bladder cancer via NF-κB/MDM2/p53 pathway. More detailed molecular mechanisms, for instance, genomic and proteomic responses

underlying the DOX+EGCG-induced bladder cancer cell apoptosis and anti-metastasis remain to be elucidated. Besides, further investigation on primary cultured bladder cancer cells, patient-derived xenografts model or clinical investigations were needed to determine the clinical efficacy of EGCG in combination with DOX. Our observation holds promise for further studies to develop EGCG as a potential anti-tumor adjuvant in combination with DOX against bladder cancer.

DATA AVAILABILITY STATEMENT

The raw data supporting the conclusions of this article will be made available by the authors, without undue reservation.

ETHICS STATEMENT

The animal study was reviewed and approved by Animal Ethics Committee of Shenzhen Second People's Hospital.

AUTHOR CONTRIBUTIONS

K-WL provided the idea and wrote the manuscript. K-WL, X-hZ, TZ, JZ, and H-cG involved in cell culture, flow cytometry experiments, western blot, transwell migration assay, animal study, and immunochemistry assays. X-LL and W-RH designed the work and revised the manuscript. All authors contributed to the article and approved the submitted version.

FUNDING

This work was supported by Shenzhen Longhua District Science and Technology Innovation Fund (201801), Shenzhen Municipal Science and Technology program of China (JCYJ20160425100840929), and the Natural Science Foundation of Guangdong province (2019A1515011009).

REFERENCES

- Antoni, S., Ferlay, J., Soerjomataram, I., Znaor, A., Jemal, A., and Bray, F. (2017). Bladder cancer incidence and mortality: a global overview and recent trends. *Eur. Urol.* 71, 96–108. doi: 10.1016/j.eururo.2016.06.010
- Chen, C., Lu, L., Yan, S., Yi, H., Yao, H., Wu, D., et al. (2018). Autophagy and doxorubicin resistance in cancer. *Anticancer Drugs* 29, 1–9. doi: 10.1097/CAD.0000000000000572
- Chen, L., Ye, H. L., Zhang, G., Yao, W. M., Chen, X. Z., and Zhang, F. C., et al. (2014). Autophagy inhibition contributes to the synergistic interaction between EGCG and doxorubicin to kill the hepatoma Hep3B cells. *PLoS ONE* 9:e85771. doi: 10.1371/journal.pone.0085771
- Flores-Pérez, A., Marchat, L. A., Sánchez, L. L., Romero-Zamora, D., Arechaga-Ocampo, E., and Ramírez-Torres, N., et al. (2016). Differential proteomic analysis reveals that EGCG inhibits HDGF and activates apoptosis to increase the sensitivity of non-small cells lung cancer to chemotherapy. *Proteomics Clin. Appl.* 10, 172–182. doi: 10.1002/prca.201500008
- Gan, R. Y., Li, H. B., Sui, Z. Q., and Corke, H. (2018). Absorption, metabolism, anti-cancer effect and molecular targets of epigallocatechin gallate (EGCG): an updated review. *Crit. Rev. Food Sci. Nutr.* 58, 924–941. doi: 10.1080/10408398.2016.1231168
- Haque, A., Rahman, M. A., Chen, Z. G., Saba, N. F., Khuri, F. R., and Shin, D. M., et al. (2015). Combination of erlotinib and EGCG induces apoptosis of head and neck cancers through posttranscriptional regulation of Bim and Bcl-2. *Apoptosis* 20, 986–995. doi: 10.1007/s10495-015-1126-0
- Hastak, K., Gupta, S., Ahmad, N., Agarwal, M. K., Agarwal, M. L., and Mukhtar, H. (2003). Role of p53 and NF-kappaB in epigallocatechin-3-gallate-induced apoptosis of LNCaP cells. *Oncogene* 22, 4851–4859. doi: 10.1038/sj.onc.1206708
- Heyza, J. R., Arora, S., Zhang, H., Conner, K. L., Lei, W., and Floyd, A. M., et al. (2018). Targeting the DNA repair endonuclease ERCC1-XPF with green tea polyphenol epigallocatechin-3-gallate (EGCG) and its prodrug to enhance cisplatin efficacy in human cancer cells. *Nutrients* 10:1644. doi: 10.3390/nu10111644
- Jin, L., Li, C., Xu, Y., Wang, L., Liu, J., and Wang, D., et al. (2013). Epigallocatechin gallate promotes p53 accumulation and activity via the inhibition of MDM2-mediated p53 ubiquitination in human lung cancer cells. *Oncol. Rep.* 29, 1983–1990. doi: 10.3892/or.2013.2343
- Kallifatidis, G., Hoy, J. J., and Lokeshwar, B. L. (2016). Bioactive natural products for chemoprevention and treatment of castration-resistant prostate cancer. *Semin. Cancer Biol.* 40–41, 160–169. doi: 10.1016/j.semcancer.2016.06.003
- Koonyosying, P., Kongkarnka, S., Uthairatibull, C., Svasti, S., Fucharoen, S., and Srithairatanakool, S. (2018). Green tea extract modulates oxidative tissue injury in beta-thalassemic mice by chelation of redox iron and inhibition of lipid peroxidation. *Biomed Pharmacother.* 108, 1694–1702. doi: 10.1016/j.biopha.2018.10.017
- Lin, J. K., and Liang, Y. C. (2000). Cancer chemoprevention by tea polyphenols. *Proc. Natl. Sci. Coun. Repub. China B.* 24:1e13
- Lu, J. H., Shi, Z. F., and Xu, H. (2014). The mitochondrial cyclophilin D/p53 complexation mediates doxorubicin-induced non-apoptotic death of A549 lung cancer cells. *Mol. Cell Biochem.* 389, 17–24. doi: 10.1007/s11010-013-1922-1
- Luo, K. W., Ko, C. H., Yue, G. G., Lee, J. K., Li, K. K., and Lee, M., et al. (2014). Green tea (*Camellia sinensis*) extract inhibits both the metastasis and osteolytic components of mammary cancer 4T1 lesions in mice. *J. Nutr. Biochem.* 25, 395–403. doi: 10.1016/j.jnutbio.2013.11.013
- Luo, K. W., Wei Chen, N. I., Lung, W. Y., Wei, X. Y., Cheng, B. H., and Cai, Z. M., et al. (2017). EGCG inhibited bladder cancer SW780 cell proliferation and migration both *in vitro* and *in vivo* via down-regulation of NF-κB and MMP-9. *J. Nutr. Biochem.* 41:56–64. doi: 10.1016/j.jnutbio.2016.12.004
- Pan, H., Chen, J., Shen, K., Wang, X., Wang, P., and Fu, G., et al. (2015). Mitochondrial modulation by epigallocatechin 3-Gallate ameliorates cisplatin induced renal injury through decreasing oxidative/nitrative stress, inflammation and NF-kB in mice. *PLoS ONE* 10:e0124775. doi: 10.1371/journal.pone.0124775
- Pons-Fuster López, E., Gómez García, F., and López Jornet, P. (2019). Combination of 5-Flourouracil and polyphenol EGCG exerts suppressive effects on oral cancer cells exposed to radiation. *Arch Oral Biol.* 101, 8–12. doi: 10.1016/j.archoralbio.2019.02.018
- Renu, K., Abilash, V. G., Tirupathi Pichiah P. B., and Arunachalam, S. (2018). Molecular mechanism of doxorubicin-induced cardiomyopathy - an update. *Eur. J. Pharmacol.* 818, 241–253. doi: 10.1016/j.ejphar.2017.10.043
- Saeed, N. M., El-Naga, R. N., El-Bakly, W. M., Abdel-Rahman, H. M., Salah ElDin, R. A., and El-Demerdash, E. (2015). Epigallocatechin-3-gallate pretreatment attenuates doxorubicin-induced cardiotoxicity in rats: a mechanistic study. *Biochem. Pharmacol.* 95, 145–155. doi: 10.1016/j.bcp.2015.02.006
- Stewart, B. W., and Wild, C. P. (2014). *2014 World Cancer Report*. Chapter 1.1. IARC Nontional Publication.
- Thomasova, D., Mulay, S. R., Bruns, H., and Anders, H. J. (2012). p53-independent roles of MDM2 in NF-κB signaling: implications for cancer therapy, wound healing, and autoimmune diseases. *Neoplasia* 14, 1097–1101. doi: 10.1593/neo.121534
- Tsai, L. C., Hsieh, H. Y., Lu, K. Y., Wang, S. Y., and Mi, F. L. (2016). EGCG/gelatin-doxorubicin gold nanoparticles enhance therapeutic efficacy of doxorubicin for prostate cancer treatment. *Nanomedicine* 11, 9–30. doi: 10.2217/nnm.15.183
- Wang, R., Huang, J., Chen, J., Yang, M., Wang, H., and Qiao, H., et al. (2019). Enhanced anti-colon cancer efficacy of 5-fluorouracil by epigallocatechin-3-gallate co-loaded in wheat germ agglutinin-conjugated nanoparticles. *Nanomedicine* 1:102068. doi: 10.1016/j.nano.2019.102068
- Wang, X., Jiang, P., Wang, P., Yang, C. S., Wang, X., and Feng, Q. (2015). EGCG enhances cisplatin sensitivity by regulating expression of the copper and cisplatin influx transporter CTR1 in ovary cancer. *PLoS ONE* 10:e0125402. doi: 10.1371/journal.pone.0125402
- Yang, C. S., Wang, X., Lu, G., and Picinich, S. C. (2009). Cancer prevention by tea: animal studies, molecular mechanisms and human relevance. *Nat. Rev. Cancer* 9:429e439. doi: 10.1038/nrc2641
- Yang, M. C., Lin, R. W., Huang, S. B., Huang, S. Y., Chen, W. J., Wang, S., et al. (2016). BIM directly antagonizes Bcl-xL in doxorubicin-induced prostate cancer cell apoptosis independently of p53. *Cell Cycle* 15, 394–402. doi: 10.1080/15384101.2015.1127470
- Zhao, K., Yang, Y., Zhang, G., Wang, C., Wang, D., Wu, M., et al. (2018). Regulation of the Mdm2-p53 pathway by the ubiquitin E3 ligase MARCH7. *EMBO Rep.* 19, 305–319. doi: 10.15252/embr.201744465
- Zhuang, C., Miao, Z., Wu, Y., Guo, Z., Li, J., and Yao, J., et al. (2014). Double-edged swords as cancer therapeutics: novel, orally active, small molecules simultaneously inhibit p53-MDM2 interaction and the NF-κB pathway. *J. Med. Chem.* 57, 567–577. doi: 10.1021/jm401800k

Conflict of Interest: The authors declare that the research was conducted in the absence of any commercial or financial relationships that could be construed as a potential conflict of interest.

Copyright © 2020 Luo, Zhu, Zhao, Zhong, Gao, Luo and Huang. This is an open-access article distributed under the terms of the Creative Commons Attribution License (CC BY). The use, distribution or reproduction in other forums is permitted, provided the original author(s) and the copyright owner(s) are credited and that the original publication in this journal is cited, in accordance with accepted academic practice. No use, distribution or reproduction is permitted which does not comply with these terms.



Tumor-Associated Macrophages in Pancreatic Ductal Adenocarcinoma: Origin, Polarization, Function, and Reprogramming

Sen Yang[†], Qiaofei Liu[†] and Quan Liao^{*}

Department of General Surgery, Peking Union Medical College Hospital, Peking Union Medical College, Chinese Academy of Medical Sciences, Beijing, China

OPEN ACCESS

Edited by:

Liwu Fu,
Sun Yat-sen University, China

Reviewed by:

Qingbin Cui,
The University of Toledo Medical
Center, United States
Zhi-Xiang Xu,
The University of Alabama
at Birmingham, United States

*Correspondence:

Quan Liao
lqpumc@126.com

[†]These authors share first authorship

Specialty section:

This article was submitted to
Molecular and Cellular Oncology,
a section of the journal
Frontiers in Cell and Developmental
Biology

Received: 16 September 2020

Accepted: 19 November 2020

Published: 11 January 2021

Citation:

Yang S, Liu Q and Liao Q (2021)
Tumor-Associated Macrophages
in Pancreatic Ductal
Adenocarcinoma: Origin, Polarization,
Function, and Reprogramming.
Front. Cell Dev. Biol. 8:607209.
doi: 10.3389/fcell.2020.607209

Pancreatic ductal adenocarcinoma (PDAC) is a highly lethal malignancy. PDAC is only cured by surgical resection in its early stage, but there remains a relatively high possibility of recurrence. The development of PDAC is closely associated with the tumor microenvironment. Tumor-associated macrophages (TAMs) are one of the most abundant immune cell populations in the pancreatic tumor stroma. TAMs are inclined to M2 deviation in the tumor microenvironment, which promotes and supports tumor behaviors, including tumorigenesis, immune escape, metastasis, and chemotherapeutic resistance. Herein, we comprehensively reviewed the latest researches on the origin, polarization, functions, and reprogramming of TAMs in PDAC.

Keywords: tumor-associated macrophages, pancreatic ductal adenocarcinoma, polarization, reprogramming, origin

INTRODUCTION

Pancreatic ductal adenocarcinoma takes a proportion of 85% in pancreatic cancer cases and is still one of the most malignant tumors with 5-year overall survival of less than 10% (Foucher et al., 2018). Fewer than 20% of patients are candidates for curative surgery since the overwhelming proportion of patients with PDAC have presented locally advanced or distant metastatic disease (Singhi et al., 2019). PDAC is a well-known inflammatory cancer. Distinctive to acute inflammations, immune activity in a tumor microenvironment is extremely repressive, and chronic substimulation by that immunity results in further growth and proliferation of tumor cells. The immune suppression in the tumor microenvironment enables tumor cells to escape

Abbreviations: ADCC, antibody-dependent cell-mediated cytotoxicity; ADM, acinar-to-ductal metaplasia; Arg1, arginase-1; α KG, α -ketoglutarate; BMDMs, bone marrow-derived macrophages; CCL, chemokine (C-C motif) ligand; CSFs, colony-stimulating factors; CTGF, connective tissue growth factor; DAMPs, damage-associated molecular patterns; EGFR, epidermal growth factor receptor; EMT, epithelial-mesenchymal transition; ERM, ezrin-radixin-moesin; ET, endothelin; ETAR, endothelin receptor A; ETBR, endothelin receptor B; EVs, extracellular vesicles; FR- β , folate receptor β ; HGBM1, high mobility group box 1; HIF, hypoxia-inducible factors; HSCs, hematopoietic stem cells; IRF4, interferon regulatory factor 4; MDSCs, myeloid-derived suppressor cells; MIP-3 α , macrophage inflammatory protein-3 α ; MMPs, matrix metalloproteinases; NACRT, neoadjuvant chemoradiotherapy; NK, natural killer; NNC, nitrosamine-4-(methylnitrosamino)-1-(3-pyridyl)-1-butanone; NSAIDs, non-steroidal anti-inflammatory drugs; PanIN, pancreatic intraepithelial neoplasia; PDAC, pancreatic ductal adenocarcinoma; PDPK1, 3-phosphoinositide-dependent protein kinase 1; PGE, prostaglandin E; PGK1, phosphoglycerate kinase 1; PRRs, pattern recognition receptors; RIP1, receptor-interacting serine/threonine-protein kinase 1; SUCNR1, succinate receptor 1; TAMs, tumor-associated macrophages; TCA cycle, tricarboxylic acid cycle; TREM-1, triggering receptor expressed on myeloid cells-1.

from the immune surveillance and elimination by the antitumor immunity system, which plays a pivotal role in multiple solid tumors including PDAC (von Ahrens et al., 2017). Nevertheless, immune components in PDAC are complicated and an intricate cross talk connecting tumor cells and stromal cells leaves the single immune targets invalid in immunotherapy; therefore, it is imperative to find effective strategies to incite significant and extensive alteration in a pancreatic tumor microenvironment (Morrison et al., 2018; Bear et al., 2020). Macrophages in the tumor stroma, called TAMs, are one of the most abundant immune cell populations in the tumor microenvironment. TAMs can be differentiated into subsets with distinctive phenotypes and functions, which is called macrophage polarization. The traditional view offers a dichotomy concerning macrophage polarization, the M1 and M2 type. M1 macrophages are pro-inflammatory, while M2 is anti-inflammatory, which corresponds to the antitumor and protumor in the tumor microenvironment (Lankadasari et al., 2019). Although TAMs always have a dynamically changeable status in PDAC, they are inclined to M2 deviation with protumor effects, such as promoting tumorigenesis, forming the immunosuppression, accelerating metastasis, inducing chemotherapeutic resistance, and so on. According to the above, impeding M2 macrophage formation is of vital significance in hindering PDAC development, improving antitumor immunity and even clinical therapy. Currently, a growing body of reports on TAMs in PDAC has been published; herein, we comprehensively reviewed the origin, polarization, roles (Figure 1), and reprogramming (Figure 2) of TAMs in pancreatic cancer.

THE ROLE OF TAMs IN PDAC

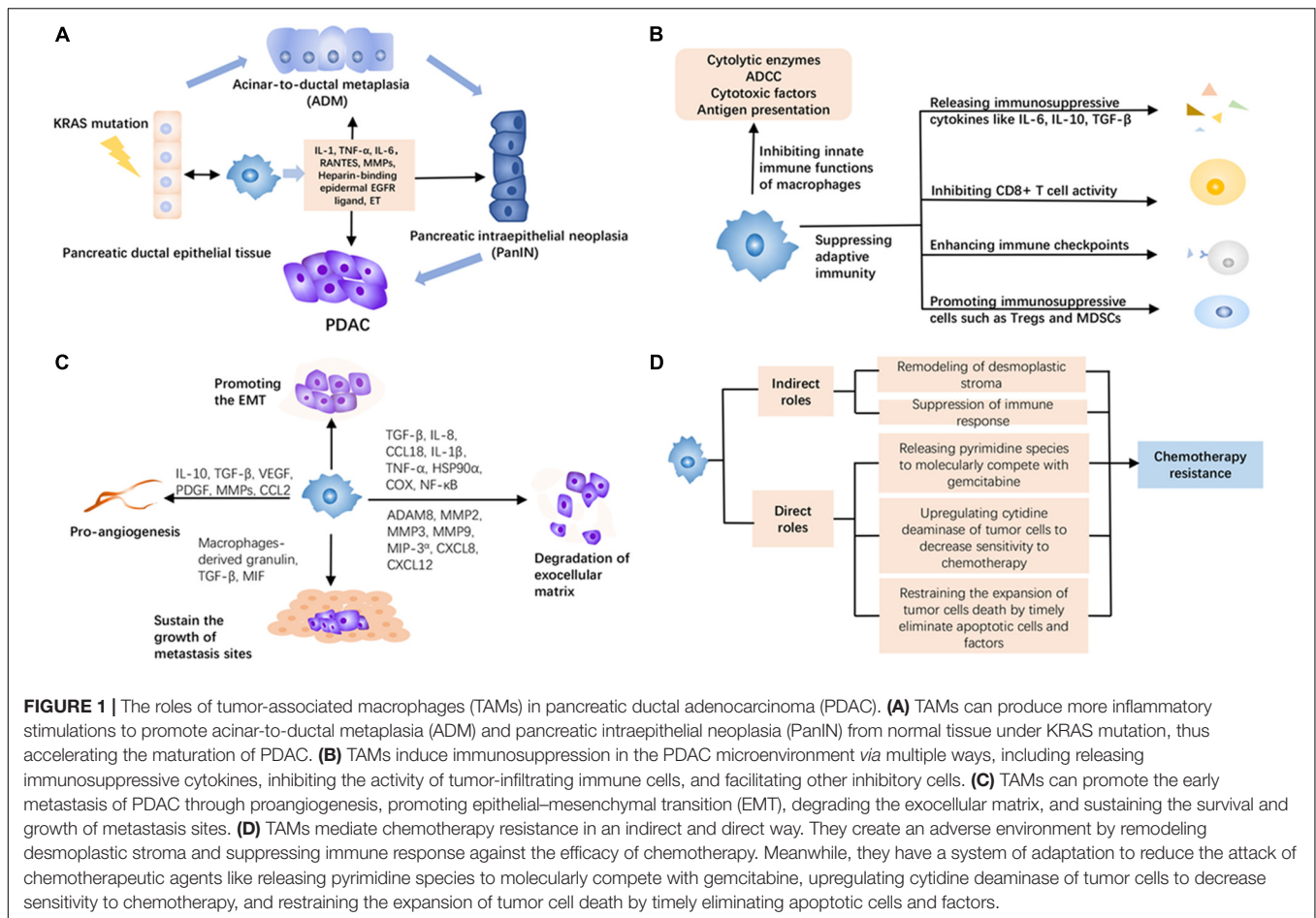
Promoting Tumorigenesis

Numerous researches on tumor evolution make the consistent opinion that maturation of PDAC requires a long-standing and persistent precancerous state. ADM and PanIN are acknowledged as indispensable precancerous processes. Acinar cells with high plasticity have undergone differentiation to a progenitor-like cell type with ductal characteristics under external stress, termed as ADM. Subsequently, cells following ADM in response to oncogenic signaling are precursors for PanIN lesions, which can further progress to PDAC (Storz, 2017). More than 90% of clinical PDAC cases have been detected as KRAS mutations, frequently occurring in the threshold of precancerous lesions, to accelerate the ADM and PanIN (Hong et al., 2012; Kamisawa et al., 2016). Featuring as fibrous inflammation incorporating immune cells, fibroblasts, extracellular matrix, vessels, and nerves, the initiation of PDAC depends on the intricate and consecutive interactions between epithelial cells and stroma (Zhang Y. et al., 2019). Macrophages are recruited and accumulated at the early stage of pancreatic precancerous lesions, which can be regarded as one of the earliest immune cell responses (Liu et al., 2016). Bidirectional signaling between the epithelium and macrophages has been recently noted. Epithelial KRAS promoted protumorigenic expression patterns in macrophages which in turn augmented cancerous phenotypes in the epithelium

(Bishehsari et al., 2018). In pancreatic tumorigenesis, oncogenic KRAS augment the sensitivity to carcinogenic stimulation by multiple steps and offer an incentive to the accomplishment of ADM and the formation of PanIN, which are engined by various stress, such as inflammation (Carrer et al., 2019; Nishikawa et al., 2019). Among the related inflammatory pathways, the activation of STAT3 serves as a significant tumorigenic pathway, actuated by macrophage-derived pro-inflammatory cytokines, such as IL-6 and IL-10, increasing the sensitivity of acinar cells to reprogram under inflammatory stimuli. Activation of the JAK-STAT3 pathway requires the facilitation of YAP1 and TAZ signaling (Gruber et al., 2016). The ADM induction has also underlined another two macrophage-derived pro-inflammatory cytokines, RANTES (CCL5) and TNF- α , via a NF- κ B-dependent manner and PI3K/Akt/IKK signaling pathway, engaging in survival, proliferation, and degradation of the extracellular matrix (Huang et al., 2015). The ET axis in the ductal and stromal cells has been proposed to have a potential role in the initiation and progression of PDAC at the background of mutant KRAS, promoted by various inflammatory stimuli in the environment. Especially, ET-1 binds to its dual receptors, ETAR and ETBR, interconnecting the interactions among epithelial cells, TAMs, CAFs, and other immune cells (Gupta et al., 2020). Besides, TAMs predominantly enhance the expression of heparin-binding EGFR ligand in pre-neoplastic lesions to facilitate ADM (Kumar et al., 2015). Fibrous inflammation activates MMPs to remodel the tumor microenvironment and MMP inhibitors remarkably decelerate pancreatitis-induced ADM (Liou et al., 2013). Furthermore, TAM-derived IL-6 induces the phosphorylation of PDPK1-mediated PGK1 threonine (T) 243 in tumor cells, to facilitate a PGK1-catalyzed reaction toward glycolysis by altering substrate affinity, which upholds PDAC initiation in a metabolic regulation way. Neutralization of macrophage-derived IL-6 or inhibition of PGK1 T243 phosphorylation or PDPK1 in tumor cells markedly abrogates macrophage-promoted glycolysis, proliferation, and tumorigenesis (Zhang Y. et al., 2018). It is remarkably observed that the elimination of TAM populations in pancreatic lesions by the immunomodulatory agent pomalidomide successfully turns the microenvironment from immunosuppressive to immune-responsive, which prevents ADM transformation and PanIN formation (Zhang Y. et al., 2017; Bastea et al., 2019). The mutilation of NSAIDs has been evidenced as effective in tumor precaution, such as aspirin, celecoxib, diclofenac, diflunisal, and ibuprofen. On the contrary, the result from several large cohort studies has refuted the view that regular use of NSAIDs was not associated with future risk of pancreatic cancer in participants (Khalaf et al., 2018). However, it should be noted that regular aspirin application ablated the risk of PDAC among participants with higher systemic inflammation induced by diabetes and hyperglycemia in contrast to local inflammation. This put forward a viewpoint into inflammatory response in the tumor microenvironment.

Immune Escape

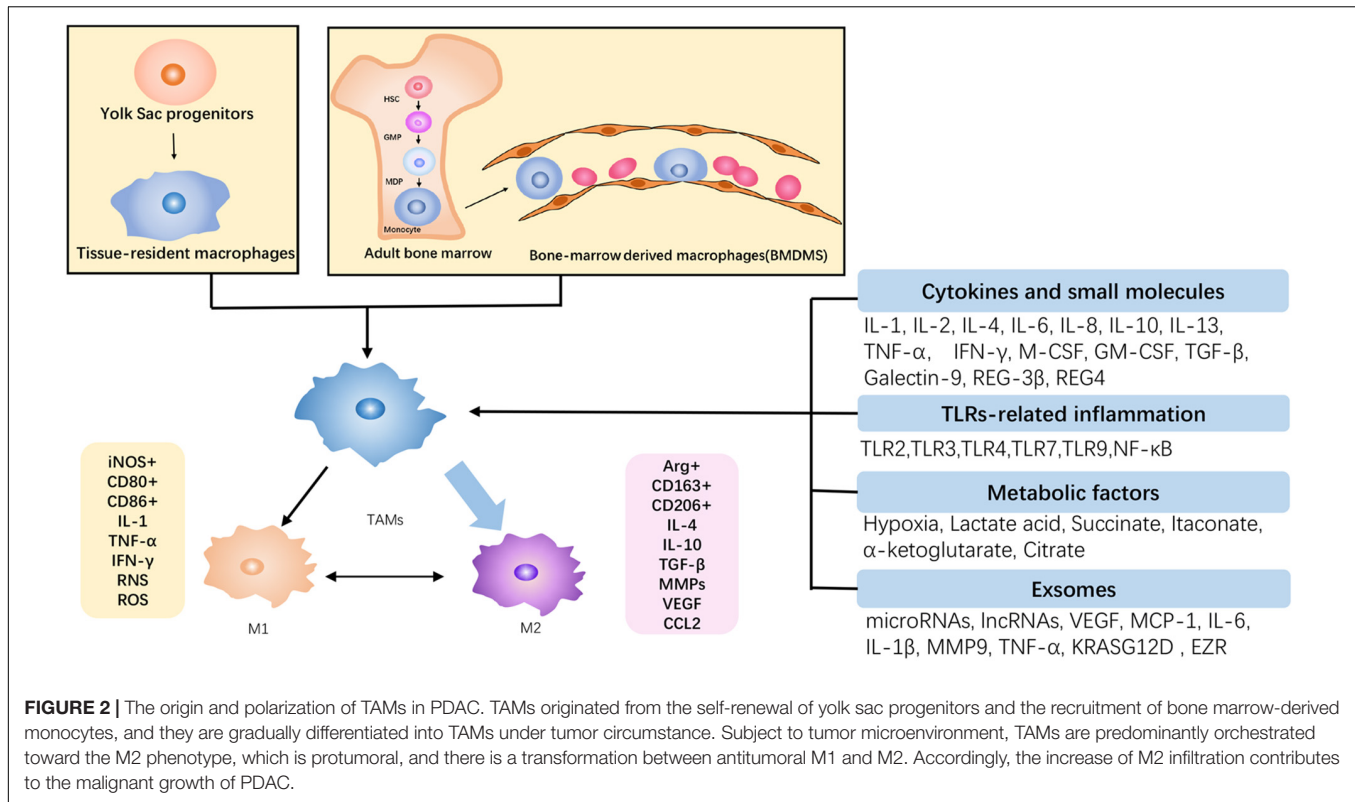
As the front line of innate immune defense, macrophages play significant roles in tumor immunity, including the direct tumor-killing effect by releasing cytolytic enzymes, triggering



ADCC via surface Fc receptors on the macrophages, secreting cytotoxic factors such as TNF, and presenting of tumor antigens to activate specific T-cell immune response. In the initial phase, macrophages can implement their innate immune functions to eliminate tumor cells, while these direct roles will be covered by tumor cells. For instance, phagocytosis is impaired resulting from tumor cells hijacking “not-eat me” labeling such as CD47-SIRPα to evade the attack of macrophages (Michaels et al., 2018). Indeed, phagocytosis depends on the promotion of the homeobox protein VentX via regulating a series of the signaling cascade, which was previously correlated with the immune function of macrophages and the M1 orientation of TAMs (Wu et al., 2011; Le et al., 2018, 2020). Additionally, tumoricidal factors produced by activated macrophages such as TNF-α and NO can be invalidated. Tumor cells can inhibit NF-κB and further downregulate its downstream genes *Tnf* and *iNOS* by upregulating the expression of GDF-15, ultimately leading to a reverse hampering to the production of these cytokines (Ratnam et al., 2017). Such tumor immune microenvironment hinders macrophages to implement their immune surveillance, in a way that directly weakens the immune system.

One crucial mechanism concerning the PDAC microenvironment is relying on a panel of immunosuppressive

cytokines produced by M2-type TAMs, containing IL-10, TGF-β, IL-6, PGE, CCL2, CCL17, CCL20, and others, which inhibit immune cell activity like CD8⁺ T cells and convert the inflammatory response into calmness (Principe et al., 2016; Daley et al., 2017; Eriksson et al., 2019). Immune checkpoints refer to the co-stimulatory and inhibitory signals of immune cells capable of curbing immune response, frequently adopted by tumor cells to suppress surrounding immune elimination (Martinez-Bosch et al., 2018). TAMs aggravate the signaling of immune checkpoints, such as the increased secretion of CTLA-4, PD-L1, which undermined immune recognition by T cells and enhanced immune tolerance (Mantovani et al., 2017). On the other hand, the upregulation of CTLA4 and PD-L1 on T cells and tumor cells also regresses the recruitment and infiltration of TAMs (Zhang Y. et al., 2017). Immune checkpoints on macrophages can likewise lessen immune functions of immune cells incorporating themselves. Macrophage-expressed PD-1 is influential to its phagocytic potency against tumor cells, to induce the immune tolerance of innate and adaptive immunity (Gordon et al., 2017). Other immunosuppressive components have functional connections with TAMs, such as Treg, their immunosuppressive induction dependent on TAM assistance. TAMs participate in the differentiation and maturation of Treg cells from CD4⁺ T lymphocytes, thus



enriching the Treg population. The study of Zhou et al. (2018) has found that TAM-derived exosomes carry out multiple miRNAs including miR-29a-3p and miR-21-5 to stimulate T cells, causing a rise in the Treg differentiation ratio *via* STAT3 activation. Certainly, immune checkpoints of T cells such as PD1/PD-L1 subject to TAMs equally induce the differentiation and functional maturation of Treg cells (Seo and Pillarisetty, 2017). In summary, the immunosuppressive roles of TAMs consist of producing inhibitory cytokines, diminishing the effector of tumor-infiltrating lymphocytes, and promoting immunosuppressive cells.

Metastasis

Tumor-associated macrophages infiltration accelerates tumor growth and metastasis, emerging as malignant outcomes and adverse prognosis (Lankadasari et al., 2019). PDAC growth relies on the delivery of nutrients and oxygen, owing to the aerobic glycolysis of tumor cells. Based on the demand, angiogenesis is a critical pathological behavior for tumor cells to exempt from scant nutrients and oxygen (Daniel et al., 2019). A visible aggregation of massive macrophages was reported to occur in the hypoxic area of PDAC and a large proportion of them surrounds intertumoral vessels, implicating the essential association between TAMs and angiogenesis. However, stromal pressure has been increasingly elevated as the expansion of tumor entity, resulting in vascular collapse up to an absence of large diameter vessels in pancreatic cancer (Li S. et al., 2019). Despite the shortage of vessels in PDAC, a high level of pro-angiogenic factors like VEGFA promotes the increased

risk of early metastasis (Rigamonti et al., 2014). Exuberant angiogenesis exerts the prometastasis in PDAC as common as other solid tumors, which remains the therapeutic target. Tumor metastasis depends on the stromal degradation and the loss of intercellular connections, which can be realized by TAMs *via* secreting matrix proteins and proteases such as serine proteases, MMPs, and cathepsins (Cui et al., 2016). Especially, pancreatic tumor cell migration rate can be enhanced through TAMs regulating the expression of ADAM8 and MMP9, conducive to breach the basement membrane and accrete the invasiveness (Puolakkainen et al., 2014). Notably, MMP9 is an essential factor, which enhances the degradation of the extracellular matrix protein laminin, as a major component of blood vessels, which directly manipulates the disintegration of the vessel wall for extravasation (Knapinska et al., 2017; Tekin et al., 2020). Likewise, MMP9 overproduction can be induced by CAF-derived IL-33 *via* the IL-33-ST2-NF-κB-MMP9 axis (Andersson et al., 2018). Additionally, several chemokine signals help tumor cells to penetrate blood vessels. These chemokines like CXCL8 and CXCL12 collaboratively aggravate invasion and angiogenesis in pancreatic cancer, *via* their corresponding receptors, CXCR2 and CXCR4 (Matsuo et al., 2009). Meanwhile, these signals could also drive macrophages to M2 polarization (Pausch et al., 2020; Zhang et al., 2020). Moreover, TAM-induced inflammation also promotes EMT in PDAC, which is defined as a phenotypic switch from epithelial to mesenchymal phenotype cell through gradually vanishing cell polarity and intercellular connections, consequently enhancing tumor cell migration and invasion. Pancreatic cancer cells following co-culture with M2

macrophages showed the upregulation of mesenchymal markers vimentin and Snail coupled with downregulating the epithelial marker E-cadherin (Liu et al., 2013). However, EMT in PDAC is irrespective of TAM polarization, and both pro- and antitumor phenotype can contribute to the conversion (Helm et al., 2014). Apart from these M2-type cytokines such as TGF- β , IL-8, and CCL18 (Meng et al., 2015; Chen S. J. et al., 2018), emerging evidence has revealed that the pro-inflammatory activation by TAMs is capable of EMT promotion, such as the release of IL-1 β and TNF- α , and the activation of COX and NF- κ B (Chen et al., 2019). Interestingly, pancreatic cancer cells after EMT can secrete HSP90 α to mediate M2 polarization, while M2 macrophages overproducing HSP90 α actuate pancreatic tumorigenesis. It is like a reciprocal loop due to the coordination of tumor microenvironment constitution (Fan et al., 2019). Loose cells and leaking blood vessels allow free tumor cells into the bloodstream and spread throughout distant organs. The colonization of metastatic tumor cells at distant organs critically requires the support of surrounding non-cancerous stromal components, especially TAMs appearing as a surge in the metastatic site (Costa-Silva et al., 2015). Nielsen et al. (2016) have demonstrated that a specific granulin by TAMs can activate stellate cells into α SMA⁺ myofibroblasts with a high yield of periostin, sustaining the survival of metastatic cells. Simultaneously, normal resident macrophages can be educated by PDAC cells to protumoral and prometastatic phenotype. Activating TGF- β signaling of liver-resident macrophages is induced through PDAC cell-derived exosomes, thus constituting the pre-metastatic niche by activating HSCs and remodeling ECM and exosome-derived migration inhibitory factor (MIF) as a well-known mediator of liver inflammation and fibrosis (Costa-Silva et al., 2015).

Chemotherapy Resistance

Clonal selection for a resistant population belongs to one of the numerous tumor cell-autonomous responses, for their adaptation to a stressful environment. TAMs promote resistance, while gemcitabine treatment in turn attracts abundant TAM infiltration (Liu et al., 2016; Liu Q. et al., 2020). Pharmacological depletion of TAMs overthrows chemoresistance like gemcitabine, leading to an obvious improvement of PDAC therapy (Céspedes et al., 2016). Dense stroma is conceived as a key factor to hinder medicine delivery, and TAMs promote stroma formation by activating cancer-related fibroblasts (Zhang D. et al., 2018). The existence of TAMs influences antitumoral drug delivery, biophysically creating an impenetrable medium to hamper the pharmacokinetic motion of gemcitabine (Buchholz et al., 2020). TAMs directly induce the resistance of PDAC to gemcitabine and the apoptosis of PDAC cells has been minimized upon incubation with a TAM-conditioned medium (Xian et al., 2017). The present understanding of TAMs to chemotherapy resistance remains not illuminated. TAMs are capable of the upregulation of cytidine deaminase to decrease their sensitivity to gemcitabine by accelerating the metabolism of gemcitabine (Binenbaum et al., 2018). Meanwhile, a sphere of pyrimidine species is liberated by TAMs to molecularly compete with gemcitabine, thus influencing drug uptake and metabolism and largely reducing the efficacy of

chemotherapy (Halbrook et al., 2019). The immunosuppressive cytokine TGF- β 1 secreted by TAMs can upregulate CTGF and HMGB1 by virtue of regressing Gfi-1 expression (Xian et al., 2017). The hypothesis has been evidenced by D'Errico et al. (2019) that the timely phagocytosis and clearance of TAMs to apoptotic cells and related factors prevent further expansion of cellular apoptosis and contribute to chemoresistance to gemcitabine, which is associated with the 14-3-3 ζ /Axl signaling. In research on hepatic carcinoma, TREM-1 expressing TAMs exhibited as the fundamental bridge to enhance CCR6⁺ Foxp3⁺ Treg accumulation, which disabled targeting PD-1 therapy, while the blockade on TREM-1⁺ TAMs revived the therapeutic activity (Wu et al., 2019). It provides us with a novel insight to consider therapeutic resistance by targeting TREM-1⁺ TAMs in pancreatic cancer. Although the mechanism concerning TAMs inducing tumor chemotherapy resistance is still obscure, TAM amounts are paralleling with chemotherapy resistance, which implicates the significance of TAMs as a target to chemotherapy resistance.

THE ORIGIN AND RECRUITMENT OF TAMs IN PDAC

Traditional researches on the monocyte-macrophage system hold the dichotomous concept, tissue-resident macrophages and BMDMs. Tissue-resident macrophages have a dual identity in disease development: they trigger an inflammatory response by PRRs and recruit inflammatory cells to elicit the inflammation cascade; it delineates the limit of inflammation, tranquilizes the immune system, and repairs damaged tissues (Ginhoux and Guillemins, 2016). Nonetheless, tissue-resident macrophages cannot offset consumption and acquire rapid replenishing by BMDMs to sustain pathogen challenge and energize inflammation until further explosion (Zhu et al., 2017). Macrophages in the tumor microenvironment are heterogeneous and its origin has been controversial until now. It has been historically insisted that mature tissue-resident macrophages are merely from BMDMs, whereas accumulative advances have proposed the yolk sac progenitors seeding tissues during the fetal and embryonal period as the major origin of such macrophages in healthy tissues, which acclaims its self-renewal rather than replenishment of peripheral circulation monocytes (Ginhoux et al., 2016; Mantovani et al., 2017). Zhu et al. (2017) found that TAMs in PDAC do not always originate from HSCs, but can also proliferate and differentiate from self-renewing embryonic precursors, which casts doubt about the immunological dogma of TAM derived from circulating monocytes. Tracing the origin of tumor macrophages has inspired the study of the phenotype and function of multisource macrophages. The accumulation of Ly6C^{hi} circulating inflammatory monocytes in glioma contributes to an increase in tumor incidence and shortened survival expectancy, while inherent macrophages and microglia do not (Chen et al., 2017). As for PDAC tumorigenesis, BMDMs focused on antigen presentation and self-renewal TAMs are inclined to a profibrotic phenotype, implicating their role in the constitution of the extracellular matrix (Zhu et al., 2017). Furthermore, macrophage recruitment is a complex multistage

process with the involvement of multiple cytokines, signal transmission, and cellular interaction. Chemoattractants like CCL2, CCL5, VEGF, and CSF-1 attract circulating monocytes in a gradient of concentration (Nielsen and Schmid, 2017). The CCL2/CCR2 axis particularly displays irreplaceability to recruit macrophages from bone marrow to tumor lesion. In post-resection patients of PDAC, CCL2/CCR2 chemokine signals can be prognostic of reduced survival (Sanford et al., 2013). The blockade of the CCL2/CCR2 axis has been employed in PDAC researches for reducing the TAM population, which accomplishes significant tumor regression (Long et al., 2016). A recent study has revealed a novel approach to aggregating macrophages: the neurotransmitter receptor unit, gamma-aminobutyric acid type A receptor pi subunit (GABRP), can ultimately induce the CXCL5 and CCL20 to mediate the recruitment of TAMs in pancreatic cancer *via* the activation NF- κ B signaling by interacting with KCNN4 to trigger Ca^{2+} entry (Jiang et al., 2019).

INFLAMMATORY CYTOKINES, CSFS, AND SOLUBLE SMALL MOLECULES ON TAM POLARIZATION

Chronic inflammatory cytokines have a positive relationship with poor prognosis in PDAC patients, and these cytokines coordinating with immunosuppressive cells induce immune suppression in the local surrounding of cancers (Farajzadeh Valilou et al., 2018; Feng L. et al., 2018). In the conventional polarization theory, alternatively activated macrophages depend on IL-4 and IL-13 through their share receptor IL-4R α , and then actuate JAK/STAT6 to ignite marker gene explication. Their productions fluctuate in different phases. In the precancerous phase PanIN, those mutant cells have taken the major responsibility of secreting them (Liou et al., 2017). Pancreatic stellate cells (PSCs) become the sustainable and principal supplier of IL-4/IL-13, attributing to the histopathological feature of an ample fibrous matrix (Xue et al., 2015). Targeting the SH2 domain of STAT6 by phosphopeptide mimetic PM37 enables to repress IL4/IL13-mediated STAT6 phosphorylation and downregulates M2 polarization markers (Rahal et al., 2018). Besides, the activation of IL-4/IL-13 signaling can be managed by the adaptive factor c-MYC, which relays the impulse to their downstream mediators of transcription-6 and PPAR γ to undergo M2 reprogramming, with the elevated expression of VEGF, MMP9, HIF-1 α , and TGF- β (Pello et al., 2012). Another typical member IL-10, as a product of M2 macrophages, can also act on IL-10R of TAMs in turn, to enhance M2-like gene appearance by the JNK/STAT3 pathway, which forms a feedback loop (Fu et al., 2017). IL-6 is a cytokine with both pro-inflammatory and anti-inflammatory roles, diversely performing in different diseases. IL-6-induced macrophage seems to appear as an immune-tolerant type *via* equally activating JAK/STAT3 pathway, and co-stimulation with CSF1 can induce the expression of Arg1 involving the PPAR γ -dependent transcriptional activation of HIF-2 α (Wang Q. et al., 2018). Recently, IL-8 has been found to have a novel role in gemcitabine-induced infiltration of macrophages, which suggests

the significant role of IL-8 in TAM-related chemotherapy resistance (Deshmukh et al., 2018). Acute inflammatory cytokines are previously reckoned as M1-like activators, such as IL-1 β , TNF- α , and IFN γ , which are exemplified classically in multiple tumor models. In acute inflammation, differentiation of CD4 $^{+}$ T cells toward Th1 and Th17 cells relies on IL-1 β signaling, favorable to pathogen elimination (Bent et al., 2018). However, it is in a subactivated state in chronic inflammation or tumor, promoting tumorigenesis through its downstream signals and cytokines and creating M2 tendency. IL-1 β can also be produced by M2 macrophages and M2-derived IL-1 β enhances the synthesis of HIF-1 α through cyclooxygenase-2, ultimately facilitating EMT and metastasis (Zhang J. et al., 2018). TNF- α as a typical representative of pro-inflammatory cytokines carries the core duty in acute inflammation by triggering cell apoptosis and activating the NF- κ B signaling pathway. M2-type macrophages and tumor cells are qualified to release TNF- α in a low concentration (Farajzadeh Valilou et al., 2018). TNF- α inducing cell death leaves a massive cell debris to the tumor microenvironment that can be recognized by macrophages and thus actuated the orientation toward M2 type (Chen et al., 2019). As a soluble dimeric cytokine in charge of tumor immune surveillance and cytotoxicity, IFN γ endows macrophages polarized toward an M1 state of enhancing pro-inflammatory reaction and resisting to immune tolerance (Ivashkiv, 2018). However, co-stimulation of IFN γ and IL-21 provides conditions for protumorigenic M2 macrophages, which further expedite the tumor progression (Chen et al., 2016). Undoubtedly, adequate supplementation of these cytokines is advantageous to M1 deviation. Recent studies have reported that elevation of TNF- α and IL-2 in tissues by transfecting oncolytic adenovirus loaded with TNF- α and IL-2 sequence into T cells modulates host tumor immune status and orchestrates TAMs toward the M1 type (Watanabe et al., 2018). The remarkable antitumor efficacy of exogenous IFN γ administration has also been witnessed in pancreatic cancer, coupled with the reversing ratio of M1/M2 (Zhang et al., 2020). Accordingly, their specific efficacy is concentration dependent, with double roles for tumor progression. Phenotypes of TAMs are synthetically determined by assorted stimulations rather than one certain way, and the transformation from M1 to M2 implicates a dynamic variation of the macrophage phenotype, which is fundamentally attributed to the overall ambiance of the tumor microenvironment.

Colony-stimulating factors have decisive impacts on the cytogenesis of HSCs at different developmental stages, as essential stimulators for the generation of blood cells (Metcalf, 2013). Notably, CSF-1 (M-CSF) and CSF-2 (GM-CSF) are two critical cytokines to regulate the circulated reservoir of monocytes/macrophages (Jeannin et al., 2018), which shoulder different functions of body needs. CSF-1 has been reckoned as an adverse prognostic factor, and its serum level keeps the same pace with tumor progression in multiple tumor models (Ławicki et al., 2016). CSF-1 is engaged in the development, morphology, survival, and function of TAMs, under a stable and persistent production of a relatively high level, which is recognized by CSF-1R to activate molecule adaptors PI3K and Grb2, to phosphorylate the PI3K/Akt and MAPK pathways

(Bencheikh et al., 2019; Evrard et al., 2019). Macrophages stimulated by CSF-1 exhibit immunoregulatory properties, tending to repress inflammation, and repair damaged tissue. Thus, they hamper the tumor-killing immune effect during tumor progression, significantly overproducing IL-10 while decreasing IL-12 (Jeannin et al., 2018). A recent study has revealed that CSF-1 can induce macrophages to express granulin to exclude cytotoxic CD8⁺ T cells from stroma, while genetic depletion of granulin impedes the formation of stroma and increasingly restores antitumor immunity (Quaranta et al., 2018). TREM-1⁺ macrophages inducing chemotherapy resistance may be in a CSF-1-dependent antitumor mechanism (Shen and Sigalov, 2017). Furthermore, CSF-1R blockade significantly undermines the population of TAMs to a large degree, thereby reducing/diminishing M2-like TAM infiltration, but it has no definite effect on tumor cells (Pyonteck et al., 2013). Anti-CSF-1 therapy alters the tumor immune microenvironment by removing macrophages and reducing M2 infiltration, which is a useful therapeutic target in pancreatic cancer treatment. IL-34 has been identified as an alternative ligand for CSF-1R, but IL-34-activated macrophages produce more IL-10 and CCL17, compared to the mode of CSF-1 action (Lin et al., 2008; Boulakirba et al., 2018). Distinctive to CSF-1, CSF-2 has a lower basal circulation level under homeostasis, but its level surges rapidly during infection or inflammation (Zhan et al., 2019). CSF-2 is the product of activated state under pathological conditions which can bring about the prosperity of the macrophage population, and thus, serves as a potent immune enhancer in inflammation or infection diseases (Wang et al., 2016; Grasse et al., 2018; Venet and Monneret, 2018). Similarly, boosting immunity by CSF-2 can be successfully replicated in some neoplastic diseases, as an immune adjuvant for promoting antitumor immunity (Oh et al., 2017; Yan et al., 2017). Nevertheless, CSF-2 analogous to pro-inflammatory cytokines can promote epithelial and stromal interactions to accelerate tumorigenesis (Waghray et al., 2016). A remarkable rise in CSF-2 has been measured after exposure to tobacco-specific nitrosamine 4-(methylnitrosamino)-1-(3-pyridyl)-1-butanone (NNK), which effectively augments the level of cyclic AMP response element-binding protein (CREB) to accelerate pancreatic tumorigenesis (Srinivasan et al., 2018). Likewise, chemotherapy resistance is induced by CSF-2 *via* mediating the differentiation of monocytes into MDSCs, as well as hampering the tumoricidal effect of T cells (Takeuchi et al., 2015). Recent cohort analysis has proposed the highest elevated level of TGF- β 1 and CSF-2 following gemcitabine treatment, suggesting their contributions to immunosuppression and chemotherapy resistance. The subsequent dual blockade of two cytokines has improved the chemotherapeutic efficacy by hampering M2-polarized TAMs and prospering CD8⁺ T cells (Liu Q. et al., 2020). Comparative research on the respective macrophage-associated functions of CSF-1 and CSF-2 has been conducted, concluding that CSF-1-macrophages are preferentially converted from Ly6C^{hi} monocytes into MHC-II^{hi} TAMs, while GM-CSF only fine-tunes the MHC-II^{hi} phenotype without significantly affecting the TAM populations (Van Overmeire et al., 2016). Although the directing action of CSF-2 is not significant, the immunosuppressive tumor

microenvironment created by CSF-2 is deeply influential to TAM reprogramming. Pro-inflammatory macrophages activated and summoned by CSF-2 can be converted to M2-like macrophages, educated by immunosuppressive circumstances (Zhan et al., 2019). The immune function of CSF-2 is likely dose dependent. A relatively high level of endogenous or exogenous CSF-2 contributes to the amplification of M2-like suppressor cells, while a low dose of CSF-2 acts as an immune adjuvant (Parmiani et al., 2007). Despite CSF-1 and CSF-2 distinctively influencing macrophages, the unique properties of the tumor immune microenvironment lead tumor-infiltrating macrophages toward the protumoral phenotype. To sum up, the role of CSFs mainly focuses on promoting the proliferation, survival, and maturation of monocytes/macrophages, and their abundance provides basic conditions for macrophage polarization.

Lectin exhibits a specific affinity toward specific glycan structures to form a relatively strong complex, which is detected in multiple tumors and a useful detective tool for cancer diagnosis (Silva, 2019). It undertakes diversified functions such as signal transmission during the ontogenetic process, which plays a crucial role in PDAC progression. Galectin-9, a β -galactoside-binding lectin, switches the protumor M2 polarization leading to suppressed T-cell cytokine secretion, and its serum concentration can discriminate PDAC and serves as a prognostic for stage IV patients (Seifert et al., 2020). Macrophages highly expressing dectin 1, as the receptor of galectin-9, and their activation can reprogram tolerogenic macrophages to suppress adaptive immunity (Daley et al., 2017). The potential risk factor for PDAC regenerating islet-derived 3 β (REG3 β) acquires an increase in serum and pancreatic juice of PDAC patients. The presence of REG3 β triggers M2 polarization through the activation of the STAT3 signaling pathway, while its deficiency led to a decrease in the M2/M1 ratio in the tumor area (Folch-Puy, 2013). Another REG family member, REG4, secreted by PDAC cells, promotes TAM polarization to M2, *via* a signaling transmission of the EGFR/AKT/CREB pathway (Ma et al., 2016). These small molecules secreted from tumor cells modulate the microenvironment which is advantageous to the survival and progression of tumor cells. These signaling molecules facilitate the communication between tumor cells and stroma while complicating the network of cell cross talk, which renders it harder to break the stabilization of the tumor microenvironment. The underlying network constituted by assorted cytokines and small molecules leaves an open question, and its potential influence on tumor requires further investigation.

TLRS-RELATED INFLAMMATION ON TAM POLARIZATION

Cancer-related inflammation as the seventh hallmark of cancer is categorized as unresolved inflammation. TLRs belonging to PRRs are extensively expressed on dendritic cells, macrophages, endothelial cells, and tumor cells. The non-specific recognition of TLRs consolidates the initial immune defense with multiple agonists to trigger an inflammatory response. The double face of TLRs in tumor development includes anti- and protumoral

roles. On one aspect, the recognition of tumor-derived antigens reignites the agitation of innate and adaptive immunity for the enforcement of immune surveillance. Recent advances in TLR-related studies have suggested that TLR activation may indeed represent a relevant antitumor pathway, allowing to convert immune tolerance to antitumor immune response (Pradere et al., 2014). Moreover, the high expression of TLR9 in PDAC implies prolonged survival and superior prognosis (Leppänen et al., 2017). However, chronic inflammation mediated by TLRs is undoubtedly competent to incite tumorigenesis, which is exactly proved by an increased risk of carcinogenesis in patients with chronic inflammation, indicated by the relationship of hepatocellular carcinoma and chronic hepatitis, colorectal cancer and inflammatory bowel disease, gastric cancer, and *Helicobacter pylori* infections (Diakos et al., 2014). Certainly, systemic or local chronic inflammation aggravates the risk of PDAC (Padoan et al., 2019). T2DM and chronic pancreatitis have been identified as the risk factors for pancreatic tumorigenesis (Andersen et al., 2017). Emerging evidence has revealed the conservative role of TLRs in pancreatic cancer progression. In precursor lesions of early pancreatic cancer, PanIN, the aberrant expression of TLR2, TLR4, and TLR9 was also detected in PDAC (Leppänen et al., 2018). Constitutive activation of IRAK4, the downstream effector of TLRs, predicts poor prognosis and chemoresistance in PDAC (Zhang D. et al., 2017). Subsequently, the stimulation of TLRs can actuate some adverse protumoral signaling pathways, such as TLR2, TLR4, and TLR9, which activate signaling pathways and anti-apoptotic Bcl-xL expression in terms of tumor cell activation and proliferation in pancreatic cancer (Grimmig et al., 2016). Likewise, TLR7/TLR8 overexpressing pancreatic tumor cells promote the expression of NF- κ B and COX-2, increasing cancer cell proliferation and reducing chemosensitivity (Grimmig et al., 2015). The influences of the TLR signaling pathway activations are pleiotropic in cancer progression, one key regulation of TAMs infiltrating in the stroma of PDAC. TLR activation switches on macrophage polarization to portray the image of a macrophage phenotype. A previous study has reported that macrophages exposed to TLR7/TLR9 ligands deviated into the M2 state as well as decreased antigen presentation (Celhar et al., 2016). As far as the related mechanisms are concerned, TLR-mediated macrophage differentiation requires an intricate regulatory network to actuate marker gene expression. A recent study has proposed that the CD14 antigen, a glycosyl-phosphatidylinositol (GPI)-linked glycoprotein, may incorporate in the signal transmission of TLR-mediated macrophage polarization (Cheah et al., 2015). Additionally, the phenotype of TAMs likewise complies with mitochondrial dynamics. FAM73b, a mitochondrial outer membrane protein, is involved in TLR-regulated mitochondrial morphology from fusion to fission, mediating M1 conversion *via* the CHIP-IRF1 axis (Gao et al., 2017). STAT3 as the downstream effector can be stimulated by TLR activations, which is imperative to M2 orchestration. Tumor cell-released autophagosomes (TRAPs), a type of LC3-II + double-membrane exocellular vesicles, depend on TLR4-mediated MyD88-p38-STAT3 signaling (Wen et al., 2018). Resistin with a significant

role in insulin resistance has been reported to be secreted by macrophages and it activates the STAT3 signaling pathway by TLR4 and CAPI1, which can aggravate cancer progression (Zhang M. et al., 2019). Moreover, tumor-secreted cathepsin K (CTSK) could stimulate TLR4 to switch to M2 polarization relying on the mTOR signaling activation (Li R. et al., 2019). Profiling experiments showed that the transcription factor CUX1 is an important modulator of the TAM phenotype by participating in NF- κ B inflammatory signal activation (Kühnemuth et al., 2015).

Cellular debris and contents can be recognized by the corresponding PRRs on immune cells to trigger cancer-related inflammation, which is identified as DAMPs including HMGB1, hot shock protein, hyaluronan, fibrinogen, nucleic acid fragments, and so on (Patidar et al., 2018; Miller-Ocuin et al., 2019; Zhang B. et al., 2019). After NACRT, DAMP overproduction acquired a purposeful immune response and longer survival of PDAC patients (Murakami et al., 2017). The immune-activating capability of DAMPs may be applied to cancer therapy as a vaccine approach, to increase the probability of evoking broader and all-embracing cytotoxic and memory T-cell responses (Lybaert et al., 2018). This reflects the antitumor effect of the early inflammatory response in tumors. However, sustained activation of the immune system has an opposite effect and the restraining of DAMPs is beneficial from a long-standing perspective. Using nucleic acid-binding polymers (NABPs) to reduce nucleic acid-mediated TLR activation can combat pancreatic cancer growth and metastasis (Naqvi et al., 2018). Moreover, although the pancreas is not exposed to massive microbes like the gut, whose lesions are closely associated with microbial lives, recent advances have offered a bright insight into the role of microorganisms in pancreatic tumors. The oncogenic role of microbial dysbiosis has been acknowledged in pancreatic cancer, especially influential to immune status and contracture. Microbiomes affect the development of pancreatic cancer, including inflammation and immunomodulation *via* innate and adaptive immunity (Wang et al., 2019; Wei et al., 2019). Depletion of the gut microbiome led to a series of alterations in the tumor immune microenvironment, incorporating the diminution of MDSC infiltration and the reorientation toward the M1-like phenotype and promoting the tumoricidal effects of T cells. It is possible in a TLR-dependent manner, and the absence of TLR-related signals makes it invalid to induce immunosuppressive macrophages by PDAC-bacterial extracts (Pushalkar et al., 2018). According to the above, TLR activation strikes the immune system by triggering an inflammatory response, but it will be ultimately converted to an immunosuppressive type, under the coordination of tumor cells and anti-inflammatory regulation of the body. The dual outcome of TLRs in PDAC can be witnessed: early antitumor and late protumor. The suggested application of TLR activation and inactivation targeting their different functional phases is an effective and promising strategy during PDAC therapy. Given the adaptability and conversion of long-term TLR stimulation, whether it will promote the development of PDAC remains a question, which requires more profound investigations.

METABOLIC FACTORS ON TAM POLARIZATION

The unique metabolism characteristics are one of the seven hallmarks of cancer. In particular, the tumor microenvironment is famous for the deficiency of oxygen supply and nutrients, which render settling cells to alter their metabolic methods. Changes in metabolic conditions regulate cellular expression of some characteristic genes to adapt to external stress, which is known as metabolic reprogramming. Macrophages in the tumor microenvironment indeed undergo metabolic reprogramming, with preferential amplification of adaptive genes. Generally, differentiation to the M2 phenotype is conducive to their survival in such hypoxic-, acid-, and glucose-deficient pancreatic cancer stroma. The environmental factors can guide TAMs toward its survivable differentiation. Hypoxia inducing cellular variation is a research hotspot in the recent medical domain, and hypoxia commonly occurs in many solid tumors and mediates the biological behavior of tumor cells (Semenza, 2012; Moreno Roig et al., 2018). Previous data have revealed a decrease in tissue partial oxygen pressure in PDAC, with median pO_2 0–5.3 mmHg compared to surrounding normal tissues at pO_2 24.3–92.7 mmHg (Koong et al., 2000). Considerable reviews have summarized the role of hypoxia in PDAC progression and proposed the significance of targeting hypoxia (Semenza, 2012; Daniel et al., 2019). The inhibition of hypoxia synergistically reinforced the tumoricidal efficacy of gemcitabine, as well as significantly prolonged the survival in KPC mice after tumor resection, which indicated a series of stromal alterations, incorporating increased vasculature and decreased fibrillar collagen, and the infiltration of immune-responsive macrophages and neutrophils (Miller et al., 2015). It should be affirmed that hypoxia affects dynamic alterations of macrophages in the tumor microenvironment. Macrophages in hypoxic areas show a more dominant alternative activation, which might illuminate a positive effect of tumor hypoxia on the M2 tendency (Wang X. et al., 2018). The gene expression profile of hypoxic macrophages varies including low expression of MHC-II, as well as strengthened hypoxic adaptations such as VEGFA, LDHA, and uPAR (Henze and Mazzone, 2016; Chen X. et al., 2018). Hypoxia recruits TAM precursors from bone marrow to tumor lesion, through multiple mechanisms such as releasing chemoattractants like CCL2, CCL5, CXCL12, VEGFA, and endothelin and liberating some cellular contents like DAMPs from the hypoxic dying cell (Li et al., 2016). The stabilization of hypoxia-inducible factors HIF-1 α and HIF-2 α has been detected in hypoxic macrophages of PDAC as tumor progression (Talks et al., 2000). HIF-1 α has a more dominating part of hypoxia-inducing TAM polarization than HIF-2 α . External hypoxic stimulations trigger its subsequent signaling molecules by inducing changes of HIF-1 α , commonly like PI3Ky, Akt, mTOR, c-myc, and so on, translationally and transcriptionally modulating marker genes (Attri et al., 2018). Certainly, Th1 and Th2 cytokines are involved in the stabilization of HIF-1 α , which aggregately regulates the fate of macrophages (Riera-Domingo et al., 2020). Nevertheless, its role in tumor remains to correlate with malignancy and poor prognosis,

resulting from a protumoral property of hypoxic macrophages. Ren et al. (2018) have found that miR-301a-3p-rich exosomes by tumor cells trigger HIF-1 α stabilization to polarize macrophages to the M2 type, to promote malignant behaviors of PDAC. On the contrary, the irradiated tumors after low-dose radiation manifest the observation of TAMs toward an M1 phenotype due to downmodulating HIF-1 α (Nadella et al., 2018). HIF-1 α participates in the differentiation of immunosuppressive MDSCs into TAMs by enhancing the PD-L1 ligand, Arg1, and NOS2, actually serving as the significant intermediate to realize the poor immune status (Zhang J. et al., 2018; Wu et al., 2019). Apart from macrophage-mediated immunosuppression, the significant effect occurring in TAMs is pro-angiogenic by HIF stabilization. The significance of vascular growth for tumor growth and early metastasis is universally acknowledged. Hypoxia can upregulate the expression and release of VEGFA in TAMs *via* HIF-1 α and its downstream effectors. The lack of macrophages or VEGFA expression can both remarkably reduce vascular density and tumor progression (Li S. et al., 2019). Additionally, hypoxic macrophage can produce the matrix metalloproteinase MMP9 to degrade thick and dense matrix in a HIF-1 α -dependent way, facilitating the formation and extension of blood vessels in solid tumors (Riera-Domingo et al., 2020). More than influential on macrophages, the hypoxia state can alter multiple normal physiological processes of pancreatic tissue, thus fostering the environment beneficial to tumor progression, as diverse as the tumorigenesis, growth, immune evasion, metastasis, and so on.

The adjustment of glucose metabolism is simultaneously initiated under the hypoxic circumstance, defined as the Warburg effect, resulting in an accumulation of lactic acid in the tumor microenvironment (Lundahl et al., 2017). The differences in M1 and M2 macrophages lie in metabolic preferences: the energy supply of M1 macrophages is apt for glycolysis, whereas M2 macrophages are dependent on the TCA cycle. However, there is an inversion in the tumor microenvironment wherein M2 differentiation and glycolysis are equally predominant, seemingly contradictory to the above metabolic theory (Penny et al., 2016). There is an underlying mechanism deserving investigation to explain the disagreement under inflammation and tumor. Because of the uncoupling glycolysis and the TCA cycle, lactate acid acts as the primary circulating TCA substrate in most tissues and tumors, which is a distinctive approach of energy generation (Hui et al., 2017). The enriched lactate acid can inhibit various immune cell activities, contributing to the suppression of immune surveillance (Anderson et al., 2017; Dehne et al., 2017). The activation of the M2 phenotype is an indispensable link in the immunosuppressive tumor microenvironment, and high levels of lactate acid offer an impetus to TAMs toward M2 polarization (Ohashi et al., 2017; Zhang and Li, 2020). Nrf2 signaling is activated by lactate to skew the M2-like orientation in PDAC (Feng R. et al., 2018). There is an interesting feedback loop found by Ye et al. where CCL18 secreted by TAMs induces a glycolytic type in PDAC cells and, conversely, VCAM-1 produced by the tumor cells to mediate M2 deviation (Ye et al., 2018). On account of glucose metabolism having impacts on PDAC progression, recent related researches have proposed the anticancer role of metabolic regulation drugs,

especially some diabetes medicines, such as metformin, which effectively alleviates the M2 polarization of TAMs, as well as reduces tumor cell invasion at normal but not high-glucose levels (Karnevi et al., 2014).

Furthermore, the TCA cycle as the primary metabolic pathway manages the transformation of multiple substances like sugars, fatty acids, nucleic acids, and proteins. The halt of the cycle leads to the accumulation and consumption of their components, creating the disbalance in metabolism, which affects the tumor microenvironment. Endogenous metabolites govern the specific procedure of inflammatory response, such as succinate regulating the IL-1 β /HIF-1 α inflammatory signaling axis. The amassment of succinate as the key part of the TCA cycle offers anti-inflammatory cues for immune cells like macrophages (Lampropoulou et al., 2016). In the tumor microenvironment, cancer cells secreted succinate to stimulate succinate receptor (SUCNR1) of TAMs, which actuates the macrophages to M2 tendency by triggering the PI3K-HIF-1 α axis (Wu et al., 2020). Activated macrophages are commonly observed in the induction of itaconate, which has recently been reckoned as a regulator on macrophage metabolic reprogramming toward the anti-inflammatory type. Itaconate mitigates the oxidation of succinate by mediating succinate dehydrogenase, thereby leading to anti-inflammatory conversion *via* the accumulation of its succinate (Lampropoulou et al., 2016). Besides, itaconate can directly modify the protein KEAP1 *via* alkylation of cysteine residues, enabling Nrf2 to upregulate its downstream antioxidant and anti-inflammatory genes (Mills et al., 2018). The rise in itaconate production reprograms the phenotype of macrophages whether in tumor progression or inflammatory response. Glutaminolysis by α KG plays a significant role in M2 differentiation, involved in fatty acid oxidation and Jmjd3-dependent manner (Liu et al., 2017). Citrate accumulation is the most remarkable change in TCA cycle alteration and can take account for macrophage metabolic reprogramming, for which autologous nitric oxide (NO) is responsible. Apart from mitochondrial aconitase inhibited by macrophage-produced NO, macrophages render pyruvate away from pyruvate dehydrogenase under a NO-dependent and HIF-1 α -independent manner, thereby promoting glutamine-based anaplerosis (Palmieri et al., 2020). Especially in tumor development, the change in metabolic conditions modulates the intracellular metabolic process and thus affects certain gene expression. Accumulative evidence leaves us to witness metabolism reprogramming not merely in macrophages but in all immune cells. Further explorations on metabolic reprogramming provide us with a new insight on macrophage polarization.

EXOSOMES ON TAM POLARIZATION

Extracellular vesicles are often used as an important carrier of intercellular communication, shuttling between tumor cells and stromal cells of local or distant microenvironments. EVs are categorized according to their sizes and biogenesis mechanism, including exosomes, microvesicles, exosomes, apoptotic bodies, and oncosomes (Becker et al., 2016). Crucial message molecules

enveloped by EVs are secreted into the microenvironment, which is discharged to regulate the gene expression of target cells following the recognition of the surface proteins and receptors on target cells. Notably, exosomes with diameters of less than 100 nm undertake the intermediate carrier to engage in cell communication, originally introduced by Johnstone et al. in 1987 at culturing sheep reticulocytes *in vitro* (Johnstone et al., 1987). Depending on exosomes' transportation, tumor cells achieve cell-to-cell communication with macrophages, particularly affecting their phenotype. Exosomes from tumor cells package assorted proteins and chemokines with immunomodulatory capability, including CSF-1, CCL2, and TGF- β , to promote M2-like characterization of TAMs (Park et al., 2019). Multiple RNAs with regulatory functions including microRNAs, long non-coding RNAs, circular RNAs, and so on, are carried into target macrophages to enhance M2 feature gene expression (Chen X. et al., 2018; Hsieh et al., 2018; Wu et al., 2019). Furthermore, DAMPs as inflammation triggers are subject to exosome transportation, engaging in reprogramming TAMs. One of the DAMPs, KRAS^{G12D} protein, is induced by oxidative stress from tumor cells and enveloped into exosomes then captured by macrophages through an AGER-dependent mechanism, which orchestrates M2 differentiation through STAT3-dependent fatty acid oxidation (Dai et al., 2020). Previous findings demonstrate that proteins packaged into exosomes can maintain their activity following uptake by recipient cells. Membrane surface tyrosine kinase receptors traveled to macrophages as the fluxion of exosomes, such as the IL-6 receptor, highly enriched in exosomes from breast cancer cells, shaping macrophages toward alternatively activated phenotype by activating the STAT3 signaling of macrophages (Ham et al., 2018). Intrinsic compositions of exosomes have impacts on the intercellular cross talk. Linton et al. (2018) have observed that the exosomes from APC-1 (an ascites-derived metastatic pancreatic cancer cell line) exhibit a difference in composition with less metastatic PDAC cancer cell lines and normal pancreatic epithelial cell lines. Exosomes from APC-1 can overexpress the adhesion molecule ICAM-1 and fatty acid AA, which is conducive to their fusion faculty with target macrophages. Therefore, alterations in exosomes in content and composition have been taking place as the tumor progresses; hence, exosomes have a promising application of early detection. Glypican-1 (GPC1) as a cell membrane proteoglycan abundant in exosomes from cancer cells is capable of indicating the tumor burden and reflecting the prognosis of pre- and post-surgical patients, which can be applied into early detection of pancreatic cancer (Melo et al., 2015). Owing to their tropism of action, exosomes have the potential as therapeutic targets to be employed in targeted therapy of PDAC. Targeting the signaling vehicle, exosomes can effectively be a promising approach to convert TAMs' adverse characteristics. By successful transfection of a plasmid with miR-155 and miR-125b to pancreatic cancer cells, M1-directed reprogramming of macrophages was elicited in the basement of altered exosome content leading to differential communication (Su et al., 2016). EZR, a member of the ERM family, in charge of cell proliferation, morphogenesis, migration, and adhesion and mediating plasma membrane signaling transduction, can modulate the polarization

of macrophages to the M2 phenotype. However, the knockdown of EZR TAMs into the M1 phenotype provides a potential candidate to reprogram macrophages by modulating molecular pattern on EVs (Chang et al., 2020). Label molecules of exosomes are recognized by target cells and then initiate its related regulation toward the selected cells. Removal or masking of label molecules is a promising approach to remold the exosome-based communication, which remodels the immunophenotype and immune structure of the tumor microenvironment, beneficial to immunotherapy of PDAC. Simultaneously, exosomes are non-immunogenic nanosized vesicles that have received significant attention as an efficient drug delivery system. Since exosomes carry similar surface receptors of tumor cells and stromal cells such as immune cells and fibroblasts, they can be effectively recognized and uptaken by surrounding cells in tumor stroma. A comparative analysis parallelly compared the drug delivery efficiency of exosomes from pancreatic cancer cells, pancreatic stellate cells, and macrophages, showing that macrophage-derived exosomes have the highest activity of antitumor efficacy (Kanchanapally et al., 2019). In conclusion, exosomes have broad research prospects and may become useful drug transport materials and therapeutic targets in the future.

POTENTIAL TARGETS TO REGULATE TAMs

With the development of deep research on the mononuclear macrophage system, conventional dualism has been advanced into macrophage activation theory, which provides us the accurate cognition of macrophage behavior in inflammation and tumor progression. Emerging advance on macrophage adjustment has been proposed, such as blockade of CSF-1/CSF-1R, CD40 agonists, and so on, which are favorable to re-educate TAMs to M1 from the M2 state (Table 1). An increasing number of approaches to target macrophages make it effective to repress tumor progression and present an excellent application in tumor treatment (Figure 3).

Anti-CSF-1/CSF-1R

CSF-1/CSF-1R signaling has undergone relatively explicit investigation so far, the well-known fact that CSF-1 can attract, polarize, and sustain TAMs infiltrating in the tumor microenvironment, especially in PDAC with affluent stroma. The blockade of CSF-1/CSF-1R activation can be a promising approach in pancreatic cancer therapy *via* reducing the TAM population, using combinative partners of standard treatment and immunotherapeutic agents (Cannarile et al., 2017). The data from Zhu et al. (2014) have shown that inhibiting CSF-1R signaling depletes CD206^{hi} TAMs and reprograms the remaining macrophages to immune-active M1 type, paralleling with enhanced antitumor interferon, promoting T-cell infiltration, and preventing tumor progression. Depletion of TAMs by the CSF inhibitor has conspicuously enhanced the tumoricidal activity of radiation, indicative of its association with promoting adaptive immunity (Jones et al., 2018). However, CSF-1R inhibition may not deplete CD206^{hi} TAMs activated by IL-4

and GM-CSF, indicating that patients with IL-4 and GM-CSF overexpression may not benefit from CSF-1R blocking therapy (Pradel et al., 2016). Classical small molecule inhibitors of the CSF-1 pathway are PLX-3397, BLZ945, and ARRY-382, widely adopted in preclinical experimental researches of multiple tumors (Cannarile et al., 2017). The monoclonal CSF-1R antibody RG7155 blocks receptor dimerization, thereby improving objective clinical responses and increasing the CD8⁺ T-cell amounts (Ries et al., 2014). Another report from Candido et al. (2018) of the selective CSF-1R inhibitor AZD7507 in genetic PDAC model mice has underlined its profound antitumoral effect and T-cell activation, not subject to PD1 inhibition, particularly in the squamous subtype with abundant TAM infiltration. The reactivation of T cells is the core part, but overactivated immune checkpoint signals consume these T cells' activity, gradually depriving the antitumor effect (Jones et al., 2018). Besides, growing recruitment of CXCR2⁺ neutrophils was incited by fibroblasts reactively overproducing corresponding chemokines from CSF-1R inhibition (Kumar et al., 2017). These adverse alterations create a big challenge to the administration of anti-CSF-1, and thus, shortcomings of monotherapy must be rectified in combination with other therapeutic methods. For instance, dual inhibition of PI3K- γ and CSF-1R by a nanomicelle encapsulating the PI3K- γ inhibitor BEZ 235 and CSF-1R-siRNA has been reported to largely diminish M2 macrophage infiltration and remove the immune blockade in the tumor microenvironment of PDAC (Li et al., 2020). A triple combination of anti-CSF-1R, anti-PD-1, and PDAC vaccine (GVAX) contributes to the conversion of exhausted PD-1⁺ T cells to CD137⁺ activated effector T cells, intriguing the vigorous antineoplastic immunity (Saung et al., 2018). Anti-CSF-1 is an effective adjuvant therapy applied to realistic practice and obtains a curative effect combined with other therapeutic regimens. On the basis of preclinical investigation, these classical and novel inhibitors have undergone clinical examinations to test their clinical therapeutic values. Nevertheless, some adverse effects of this method need to be overcome in future clinical applications.

CD40 Agonists

The application of targeting CD40 in cancer immunotherapy recently can be foreseen as the development of tumor immunity research, through irritating Th1 immunity *via* maturing dendritic cells and driving M2 to M1. CD40 is a cell surface molecular receptor of the TNF receptor family and expressed on a wide range of leukocytes including monocytes/macrophages, B cells, and dendritic cells, being responsible for antitumor immunity activation. In PDAC, tumor cells are CD40-negative, whereas stromal cells express CD40, particularly TAMs. Progressively, CD40 activation has been thought to resort to macrophages to regress and counteract tumor. A study from Beatty's group (Beatty et al., 2011) explores the efficacy of CD40 agonists in both humans and mice. Systemic CD40 activation abolished tumor-induced immunosuppression and incited T-cell-dependent antineoplastic immunity in PDAC. Interestingly, depletion of macrophages obscured the previous antitumor effect by CD40 agonists, which underlines the significance of macrophages in the application

TABLE 1 | Potential targets to reprogram TAMs polarization.

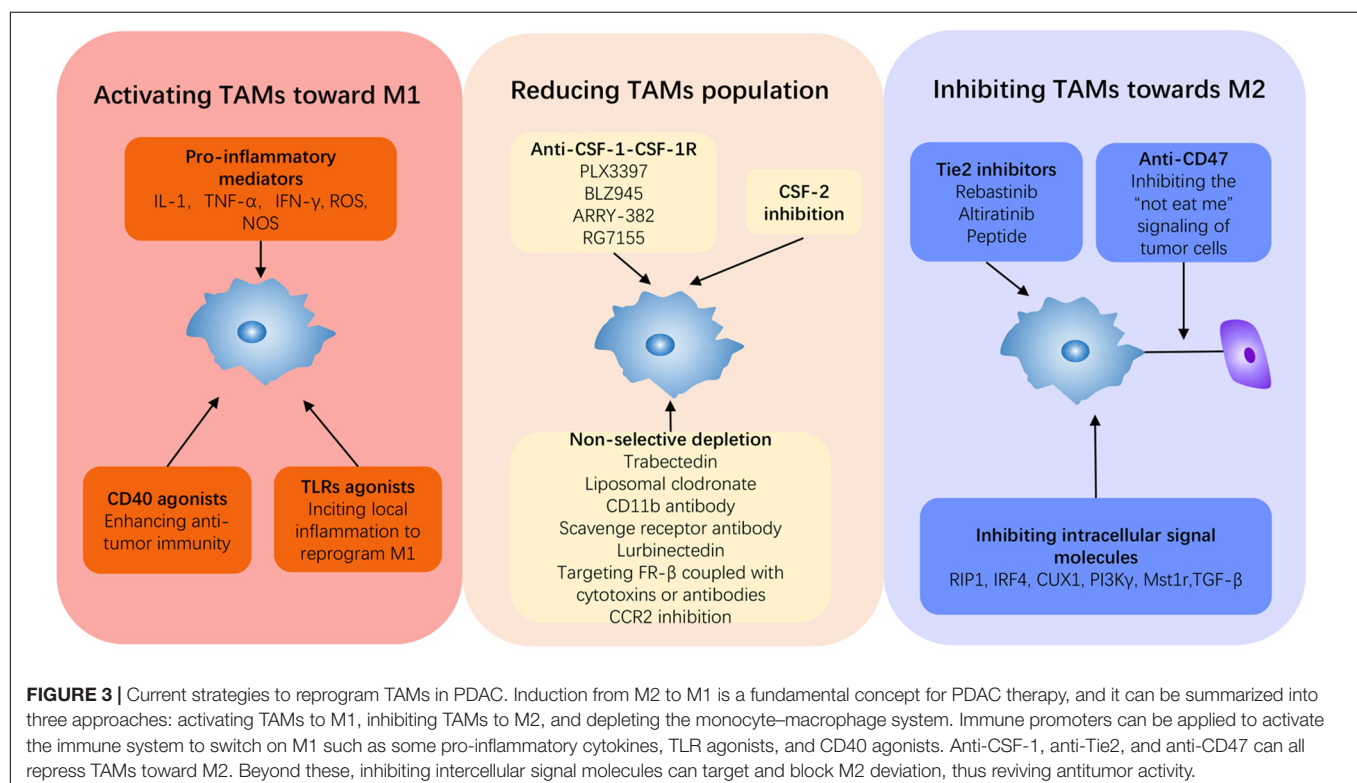
Potential targets	Therapeutic Effects	References
Blocking CSF-1/CSF-1R signaling		
CSF-1R inhibitors/CSF-1 neutralizing antibodies	Decreasing CD206 ^{hi} TAMs	Pradel et al., 2016; Ries et al., 2014
	Supporting anti-tumoral IFN responses and T cell activities	
	Overcoming immunosuppression	
	Enhancing antigen presentation	
Anti-CSF-1/CSF-1R/CTLA4 and PD1 antagonists	Enhancing responses to checkpoint immunotherapy	Zhu et al., 2014
	Promoting CD8 ⁺ T cells anti-tumoral activity	
Anti-CSF-1 + Radiation	Reducing TAMs recruitment after radiation	Jones et al., 2018
	Increasing the ratio of M1/M2	
	Promoting cytotoxic CD8 ⁺ T lymphocytes infiltration	
Anti-CSF-1R/Anti-PD-1/GVAX	Increases PD-1 ⁺ CD137 ⁺ T lymphocytes and PD-1 ⁺ OX40 ⁺ CD4 ⁺ T lymphocytes in the tumor microenvironment	Saung et al., 2018
	Promoting expression of IFN- γ .	
Activating CD40		
CD40 agonist	Activating TCR signals and promoting T lymphocytes efficacy and increasing activity and longevity of T cells	Long et al., 2016; Stromnes et al., 2019
	Reprogramming TAMs to M1 and inhibiting M2 polarization	
	Promoting PDAC sensitivity to chemotherapy	
CD40 agonist/T cell-inducing vaccine/anti-PD-1	Achieving the optimal T cell activation	Ma et al., 2019
	Promotes the development of functional T cell memory	
	Reducing M2 macrophages and MDSCs while increasing M1 and DCs	
Anti-Tie2+		
Anti-Tie2 + /Anti-VEGFR2	Lessening the relapse of pancreatic tumor	Piao et al., 2016; Harney et al., 2017; Arai et al., 2019
	Reducing the accumulation of anti-angiogenesis therapy	
	Enhancing anti-angiogenesis therapy	
Anti-CD-47		
Anti-CD47	Improving macrophages to scavenge PDAC cells	Michaels et al., 2018; Pan et al., 2019
	Increasing the ratio of M1/M2	
	Reconstituting T cells in a more active direction	
Activating Toll-like receptors		
Activating TLR3, 4, 7, 8 and 9	Recalibrating the immune status of tumor cells and immune cells	Wanderley et al., 2018
	Promoting M1 polarization while inhibiting M2 deviation	
R848-loaded β -cyclodextrin nanoparticles	Activating the M1 phenotype by activating TLR7 and TLR8	Rodell et al., 2018
SC1	Promoting a systemic release of IFN α	Vascotto et al., 2019
	Resulting in the activation of circulating immune cells	
	Creating the circumstance apt to M1 polarization	
Phagocytosis-activating ligand/TLR agonist/anti-CD40 antibody	Achieving eighty percent recovery in the murine model of the aggressive pancreatic tumor	Caisová et al., 2018
Peptide-pulsed DCs/TLR3 agonist/poly-ICLC	Inducing a measurable tumor-specific T cell population in patients with advanced pancreatic cancer	Mehrotra et al., 2017
Quantum dot (QD) pulsed-DC vaccines/TLR9 agonists	Reversing macrophage polarization	Liu F. et al., 2020
	Boosting antigen-specific T-cell immunity	
	Eliciting a potent response to the innate and adaptive immune system	
	Breaking out the immunosuppressive barrier	
Targeting the intercellular signaling molecules		
Inhibiting RIP1	Enhancing the efficacy of the checkpoint receptor PD-1 and the costimulatory ligand ICOS based immunotherapies	Wang W. et al., 2018

(Continued)

TABLE 1 | Continued

Potential targets	Therapeutic Effects	References
Inhibiting IRF4	Reprogramming the state of macrophage toward an MHCII ^{hi} TNF α ⁺ IFN γ ⁺ immunogenic phenotype	Bastea et al., 2019
Inhibiting CUX1	Creating the immune responsive environment upregulating the expression of IL-1 α Activating IFN γ ⁺ CD4 ⁺ and CD8 ⁺ T lymphocytes population	Kühnemuth et al., 2015; Liu F. et al., 2020
Activating PI3K γ	Reprogramming TAMs toward M1 tendency	Gunderson et al., 2016; Kaneda et al., 2016
Inhibiting Mst1r	Abolishing CD8 ⁺ T-cell-mediated tumor suppression Lessening the accumulation of MRC1 ⁺ Arg ⁺ macrophages in the PDAC microenvironment Transforming M1 polarization in the orthotopic model	Babicky et al., 2019
Depletion and inhibition of recruitment of TAMs		
Diphtheria toxin	Exhausting macrophages to establish the TAMs-deficient mice models in experiments	Zhang Y. et al., 2017
Trabectedin	Inducing the apoptosis of monocytes and macrophages via activating the caspase 8 apoptotic pathway Promoting infiltrating T cells anti-tumor phenotype	Germano et al., 2013; Borgoni et al., 2018
Liposomal Clodronate	Eliminating CD11b + macrophages in the pancreas and other organs including liver, lung, and spleen Effectively hampering PDAC progression	Griesmann et al., 2017
Lurbinectedin	Triggering caspase-dependent apoptosis of monocytes and macrophages via constituting lurbinectedin-DNA adducts Accomplishing TAMs depletion thus leading to cytidine deaminase downregulation in PDAC, alleviating the chemoresistance	Céspedes et al., 2016
Folate Receptor β (FR- β)	Being a potential address label for transporting therapeutic pharmacological molecules into macrophages to exclusively attack macrophages to reduce their population	Hu et al., 2019
CCR2 inhibition + FOLFIRINOX	The local tumor control has been achieved in 32 of 33 patients (97%).	Nywening et al., 2016

GVAX, the pancreatic cancer vaccine; R848-loaded β -cyclodextrin nanoparticles, TLR7 and TLR8 agonist; SC1, TLR7 agonist; RIP1, Receptor-interacting protein 1 (RIP1) kinase; FR- β , Folate receptor β .



of CD40 activation. Despite acting as a T-cell activation pathway, CD40 activation does exert its antitumor mechanism by reactivating macrophages to change the immune status of the tumor microenvironment. The activation of CD40, along with the elevated production of IFN γ and CCL2, drives a subset of Ly6C⁺CCR2⁺ macrophage infiltration (Long et al., 2016), as well as upregulates MHC class II molecules and the co-stimulatory molecule CD86 (Beatty et al., 2011). Besides, a recent study has pointed out that agonistic anti-CD40 reprograms the TAM phenotype to antitumoral and accumulates intratumoral population as well as increases longevity of TCR-engineered T cells (Stromnes et al., 2019). A phase I study of 22 patients with chemotherapy-naïve advanced PDAC revealed the excellent tolerance of CD40 agonist allied with gemcitabine, by reviving T-cell functions and reawaking the antitumor activity in patients with PDAC (Beatty et al., 2013). CD40 agonists augment antitumor immunity in PDAC in a non-redundant manner, which is effective in immune checkpoint blockade (Rech et al., 2018). The triple combination of T-cell-inducing vaccine, CD40 agonist, and anti-PD-1 significantly disarms the functionality of multiple suppressor cell populations by achieving the optimal T-cell activation, shown by an expansion of MHCII^{hi} CD86^{hi} CD11b⁺ F4/80⁺ and declines in the population of Arg1-expressed macrophages and immature MDSCs (Ma et al., 2019). The administration of CD40 agonists stimulates the immune state of the tumor site, and CD40-activated macrophages may promote the delivery of chemotherapy in the destructed stroma (Vonderheide, 2020). Visibly, the appearance of macrophages plays a significant role in CD40 activation treatment, but the specific mechanism of macrophages is worthy of further investigation.

Tie2 Inhibitors

Tie2 is a tyrosine kinase receptor and Tie2-expressing macrophages have been generally reckoned as a predictive marker of poor prognosis in multiple cancers, attributed to the influence to angiogenesis, vascular remodeling in tumor entity, and macrophage differentiation (Matsubara et al., 2013; Mao et al., 2017; Yang et al., 2018). Tie2⁺ macrophage infiltration after chemotherapy indicates the possibility of tumor recurrence. Especially, TAMs with high expression of Tie2 aggregate around tumor blood vessels and are selectively activated into M2-like subpopulations following chemotherapy, which promote tumor blood vessel reconstruction and recurrence in a VEGFA-dependent manner (Hughes et al., 2015). The molecule marker Tie2 can be counted as a unique feature of M2-like macrophages, involved in angiogenesis *via* the ang2–Tie2 axis. Accordingly, the elimination of Tie2⁺ macrophages can acquire excellent therapeutic benefits. Rebastinib is a potent and selective inhibitor of the Tie2 receptor tyrosine kinase. The preclinical validation on the administration of rebastinib in breast carcinoma and pancreatic neuroendocrine tumor has revealed that rebastinib inhibits Ang2/Tie2 signaling *via* multiple pathways (Harney et al., 2017). Targeting Ang2/Tie2 not only suppresses the angiogenesis of Tie2⁺ macrophages but also modifies the immunosuppressive tumor microenvironment,

which consolidates the antitumor therapy. Long-standing anti-VEGFA therapy leads to the upregulation of Ang2 production and enhanced infiltration by Tie2-expressing macrophages, which reduce the efficacy of targeting VEGFA in PDAC (Rigamonti et al., 2014). The dual blockade of VEGF and Tie2 significantly enhanced the prevention of tumor progression (Arai et al., 2019). Given that anti-Tie2 effectively complements the anti-angiogenesis of anti-VEGFA therapy, current strategies have focused on combining different strengths. Altiratinib, a novel balanced inhibitor of MET/TIE2/VEGFR2, exhibits a latent capacity of auxiliary treatment in glioblastoma, by virtue of their pleiotropic inhibitions among tumor growth, invasiveness, angiogenesis, and myeloid cell infiltration (Piao et al., 2016). A new peptide designed for ang2/VEGFR, a fusion protein of AS16 and IgG Fc fragment, can significantly reduce tumor volume, blood vessel density, and tumor-related macrophages (Zhu et al., 2018). Moreover, Zhang L. et al. (2019) designed a dual-responsive amphiphilic peptide to modify the small peptide T4 as a Tie2 inhibitor, endowing it with endurance in circulation and specifically targeting the tumor site. The nanoformulation can hamper the Tie2 signaling activation in Tie2⁺ macrophages and endothelial cells to exert its antitumor role. Thus, the Ang2/Tie2 axis is expected to be an effective therapeutic target of cancer immune therapy.

Anti-CD47

As the first line of defense against pathogenic insults, macrophages can rapidly scavenge cell debris or pathogenic microorganism *via* an inflammation cascade. Dying cells secrete a biochemical agent, called a “find-me” signal, drawing phagocytes to their vicinity and being engulfed after recognition at the earliest stage of apoptosis, while the “not-eat-me” signals of healthy cells are identified to avoid phagocytosis. The mechanism is frequently hijacked by tumor cells to counteract phagocytosis, leading to the proliferation of tumor cells. Signal regulatory protein alpha (SIRP α)–CD47 is a classical molecule match to prohibit the phagocytosis of macrophages in tumor immune escape. Additionally, CD47-mediated protection against phagocytosis prolongs the retention of exosomes in the extracellular environment, favorable for tumor cells to modulate the tumor microenvironment (Kamerkar et al., 2017). In engulfment assays, blocking CD47 by a monoclonal antibody *in vitro* improves macrophages to scavenge PDAC cells, retarding metastatic progression and prolonging survival (Michaels et al., 2018). Anti-CD47 significantly alters the structure of TAMs in tumor stroma, with a rise in the ratio of M1/M2, simultaneously reconstituting T cells in a more active direction (Pan et al., 2019). Several microRNAs like miR-340 and miR128 in pancreatic cancer cells inversely correlated with CD47 expression and can negatively regulate it, which is a chance to be a molecular means of anti-CD47 (Xi et al., 2020a,b). Recently, Liu et al. have revealed the close relationship between the central carbon metabolism and the antitumor activity of macrophages, where alteration of the metabolic state in macrophages by the TLR9 agonist CpG induces phagocytosis to CD47-positive tumor cells (Liu et al., 2019). Targeting the CD47–SIRP α axis results in a functional skewing of macrophages toward an M1-like phenotype in tumor

models, thus contributing to antitumor immune response, and it has promising clinical prospective in PDAC therapy.

TLR Agonists

As we mentioned above, the inflammatory response is a double-edged sword in the development of pancreatic tumors. It is greatly convincing by adequate researches that inciting controlled and limited inflammatory response reactivates the immune system suppressed by the tumor microenvironment, thus enabling it to perform antitumor functions. Activation of TLR signaling using TLR agonists alters the immunosuppressive structure in the PDAC microenvironment, especially reorienting TAMs to induce immunogenic inflammation. Prakash et al. (2016) provided experimental evidence that TLR4 activation by LPS recalibrates the immune status of tumor cells and immune cells, particularly bringing antitumor potentials back to macrophages. The role of the classical antineoplastic agent paclitaxel has been broadened by the novel finding of reprogramming M2-polarized macrophages to M1-like phenotype *via* the TLR4 signaling pathway, apart from impeding the cell cycle (Wanderley et al., 2018). Similarly, activations of TLR3, TLR7, TLR8, and TLR9 prominently revive the innate immune cell functions in the tumor microenvironment, as potential immunologic adjuvants in cancer chemotherapy (Silva et al., 2015; Liu Z. et al., 2020). Related advancements put forward the availability of TLR reactivation in tumor therapy, but some tumor cell types are not sensitive to TLR agonist, just like mice bearing Pros1-expressed tumor do not show sensitiveness to TLR agonists (Ubil et al., 2018). Moreover, current compounds are not well tolerated during intravenous administration and restrained in disease conditions despite being suitable for topical use. Novel nanomaterials are introduced to improve drug delivery, strengthen efficacy, and reduce side effects. R848-loaded β -cyclodextrin nanoparticles offered efficient drug delivery to TAMs, as a potent driver of the M1 phenotype by activating TLR7 and TLR8 (Rodell et al., 2018). Likewise, TLR7/8 agonists effectually activated antitumoral inflammation by utilizing a nanoemulsion-based immunotherapeutic platform, steering the M2 toward the M1 phenotype and restoring the immunogenicity of the stromal environment (Kim et al., 2019). Vascotto et al. (2019) provided the preclinical characterization of SCI1, a novel synthetic agonist with exquisite specificity for TLR7, and demonstrated that it induces a systemic release of IFN α , resulting in the activation of circulating immune cells and affording the circumstance apt for M1 polarization. Some natural compounds similar to TLR agonists are capable of reorienting immunosuppressive M2 to pro-inflammatory M1, such as cryptotanshinone acting on the TLR7/MyD88/NF- κ B signaling pathway (Han et al., 2019) and the linear 3-O-methylated galactan WCCP-N-b targeting TLR2 signaling and suppressing STAT6 activation (Meng et al., 2019). Synergistic administration with TLR agonists has been adapted to conspicuously enhance both innate and adaptive immunity, comprising chemotherapy, immune checkpoint inhibitors, immune adjuvants, and radiotherapy. The alliance of phagocytosis-activating ligand, TLR agonist, and anti-CD40 antibody achieved 80% recovery in the murine

model of aggressive pancreatic tumor (Caisová et al., 2018). TLR7/8 ligands along with radiotherapy contribute to a profound systemic antitumor immune reaction, coordinated by macrophages and dendritic cells and executed by NK and cytotoxic T cells (Schölch et al., 2015). It is worth noting that dendritic cell (DC) vaccines exhibit a great capacity for cancer immunotherapy, which is available for combination therapy of TLR agonists. A clinical trial verified the safety of vaccination with peptide-pulsed DCs in combination with the TLR3 agonist poly-ICLC, which induced a measurable tumor-specific T-cell population in patients with advanced pancreatic cancer (Mehrotra et al., 2017). Specifically, Liu F. et al. (2020) designed quantum dot (QD)-pulsed DC vaccines integrated with TLR9 agonists to reverse macrophage polarization, which elicited a potent response to the innate and adaptive immune system and ameliorated the immunosuppression of the tumor microenvironment. Taken together, TLR agonists significantly provide an expansive immune effect and systematically alter the immune state, particularly to intensify the tumoricidal activity of immune cells. The transformation of the tumor immune structure is the basis of the antitumor execution and the premise of immunoadjuvant therapy for tumors. A wide variety of TLR agonists have been designed to make this approach clinically possible, but the ambiguous relationship between inflammation and tumor remains an important factor affecting treatment outcomes, which is worthy of further discussion and investigation. However, it should be also noticed that aberrant long-term activation of TLRs in PDAC also could promote tumor growth and attenuate the efficacy of immunotherapy or conventional treatments.

The Adjustments to Intracellular Signaling Molecules

Macrophage polarization is subject to the intricate regulation of multiple cellular signaling pathways. As researches further developed, the accurate grasp of polarization signaling pathways has transferred the therapeutic focus from extracellular ligand-receptor blockade to intracellular signaling regulation, more precisely, directly, and obviously. The inflammatory signaling pathways represented by NF- κ B have a great influence on macrophage phenotype differentiation, owing to the release of various inflammatory cytokines depending on it. As was stated above, TLR-dependent inflammatory response triggers a new round of immune turbulence, which improves the immune capacity to eliminate tumor cells. The RIP1 is a serine/threonine-protein kinase, a putative master upstream regulator of TLR signaling, driving NF- κ B and MAP kinase signaling in response to inflammatory stimuli. In TAMs, the persistent abnormal activation can lead to an M2-like differentiation, which mediated the immune tolerance in the tumor microenvironment. As shown by the study of Wang W. et al. (2018), RIP1 signaling in macrophages serves as a master regulator of immune tolerance in PDAC and the inhibition can enhance the efficacy of the checkpoint receptor PD-1 and the co-stimulatory ligand ICOS-based

immunotherapies *via* reprogramming the state of macrophage toward an MHCII^{hi}TNF α ⁺IFN γ ⁺ immunogenic phenotype in a STAT1-dependent manner. IRF4 is a crucial transcriptional factor for TAM alternative activation, while its inhibition creates the immune-responsive environment to combat immunosuppression and fibrosis in PDAC, with the upregulation of IL-1 α and the activation of the population of IFN γ ⁺CD4⁺ and CD8⁺ T lymphocytes (Bastea et al., 2019). Additionally, CUX1, the transcriptional factor suppressing M1 deviation, has been implicated to have the potential to regulate TAM polarization (Kühnemuth et al., 2015). The deprivation of oxygen and nutrients initiates metabolic reprogramming in TAMs, which involves the intersection molecule PI3K γ . The blockade of PI3K γ in PDAC-bearing mice reprograms TAMs to stimulate CD8⁺ T-cell-mediated tumor suppression and to inhibit tumor cell invasion, metastasis, and desmoplasia (Kaneda et al., 2016). The activation of B-cell signaling has also been discovered to engage in PI3K γ -dependent M2 macrophage reprogramming and inhibiting BTK leads to M1 induction (Gunderson et al., 2016). Mst1r overexpression by KRAS aberration contributed to the increase of ADM and the acceleration of PanIN, as well as resulted in the accumulation of MRC1⁺Arg⁺ macrophages in the PDAC microenvironment. Certainly, the suppression of Mst1 expression transforms M1 polarization in the orthotopic model, providing further rationale for targeting Mst1r as a therapeutic strategy (Babicky et al., 2019). Manipulation of cellular signals makes it possible to precisely target tumors, but widespread suppression of certain signaling pathways may contribute to disorders in cellular biological processes. Various effective therapeutic targets have been identified, but specific reagents are still under development. Additionally, RNA vaccines and targeted drug delivery have promoted the clinical development of such drugs. Despite numerous restrictions to face, the therapeutic strategy can be progressed and enriched, with broad prospects and practical significance.

Depletion and Inhibition of Recruitment of TAMs

Studies to date have illustrated the interrelationship between poor prognosis and amounts of TAMs infiltrating pancreatic tumor stroma. Except for orchestrating M2 toward M1, another therapeutic strategy is to diminish the circulating load of the mononuclear macrophage system by inhibiting cytogenesis or promoting cell death. Until now, the pharmacological depletion of TAMs has prevailed in experimental researches, but has not been clinically employed. Cytotoxic agents such as liposomal clodronate, trabectedin, and diphtheria toxin have been reported to systematically remove macrophages. Several studies have used diphtheria toxin to exhaust macrophages to establish TAM-deficient mice models, for the sake of investigating the role of TAMs in pancreatic cancer progression (Zhang Y. et al., 2017), but it lacks clinical values in cancer treatment. Trabectedin, a natural alkaloid derived initially from a Caribbean tunicate, with effective anticancer properties, has

been approved for the therapy of ovarian cancer and soft-tissue sarcomas. Recent data have demonstrated that trabectedin induced the apoptosis of monocytes and macrophages in assorted surroundings by activating the caspase-8 apoptotic pathway (Germano et al., 2013). In the experimental research on pancreatic cancer, treatment with trabectedin significantly diminished the amounts of TAMs, which promote and trigger the infiltrating T-cell antitumor phenotype (Borgoni et al., 2018). However, the benefit of single-agent trabectedin is not significant and it is currently being studied in combination with other chemotherapeutic drugs. Liposomal clodronate is a common macrophage-depletion agent in pancreatic cancer experiment researches. The impact of liposomal clodronate is non-specific, which can eliminate CD11b⁺ macrophages in the pancreas and other organs including the liver, lung, and spleen (Griesmann et al., 2017). Like other macrophage-targeted agents, the effect is not obvious as a single administration. Additionally, specific antibodies against monocyte/macrophage surface molecules have the competence of TAM depletion. CD11b is a surface molecule universally expressed on the cell membrane of bone marrow-derived immune cells. CD11b⁺ macrophages are dominant in pancreatic cancer stroma, and the neutralized antibody anti-CD11b can effectively reduce TAM infiltration, which presents a better outcome (Chen C. C. et al., 2018). Antibodies scavenging receptors have demonstrated their counteraction of pancreatic cancer, further indicating the great potential targeting the TAM population (Neyen et al., 2013). Lurbinectedin (PM01183) is a novel antitumor agent with a broad panel of antitumor activity, including lung, ovarian, colorectal, and gastric carcinoma xenograft, which constitutes lurbinectedin–DNA adducts to eventually trigger caspase-dependent apoptosis. Its antitumor activity correlates with the depletion of TAMs in different tumor models. In the combination treatment of lurbinectedin and gemcitabine, lurbinectedin significantly accomplished TAM depletion thus leading to cytidine deaminase downregulation in PDAC, which aggravates the damage strength by gemcitabine (Céspedes et al., 2016). FR- β is exclusively overexpressed by TAMs in any kind of cancer entity. The FR- β ⁺ macrophages infiltrating perivascular regions were observed in the tumor tissues of PDAC patients, explicitly correlating with tumor angiogenesis and high incidence of metastasis (Kurahara et al., 2012). FR- β has been perceived as a potential address label for transporting therapeutic pharmacological molecules into macrophages. Targeting FR- β coupled with cellular cytotoxins or antibodies can exclusively attack macrophages to reduce their population (Hu et al., 2019). Reducing the macrophage population can alleviate the accelerative influence of TAMs on tumor progression, being a favorable strategy allied with other therapeutic approaches. The realistic efficacy has been demonstrated by a recent study on the union of radiation, macrophage depletion, and anti-PD-L1 (Jones et al., 2018). Indeed, the clinical significance of reducing the TAM population has been enlightened in clinical application. A phase 1b study has verified the effectiveness and safety of the combination of targeting TAMs by CCR2 inhibition and FOLFIRINOX in locally advanced and borderline resectable pancreatic cancer. Eventually, imaging results have demonstrated local tumor control achieved

in 32 of 33 patients (97%), along with less side effects (Nywening et al., 2016). Accordingly, targeting TAMs obviously facilitates the antitumor effect of chemotherapy, which can be developed into a potent therapeutic method.

DISCUSSION AND FUTURE PERSPECTIVE

Tumor-associated macrophages emerge to have multiple functions from the initiation phase to the mature stage of PDAC, including tumorigenesis, immune evasion, metastasis, and chemoresistance. Current researches have emphasized TAM polarization defined as an educated phenotype of macrophages in line with surrounding immune conditions, almost accepted by all modulations from various environmental factors in PDAC stroma. There is no denying that extensive cross talk has been constructed among stromal cells. Various signal molecules constitute an intricate network to collectively engage in the construction of TAM differentiation, which establishes a stable and substantial foundation for supporting tumor progression. In other words, others can substitute the blockade in one pathway, which makes it in a dilemma to break the steady state of the tumor microenvironment. Therefore, therapeutic effects are attenuated in response to targeting alone macrophage treatment by enhancing other aspects, such as augmented immune checkpoints and increased tumor-associated neutrophils (Zhu et al., 2014). Current views advocate combination therapy, for instance, in alliance with anti-PD1/PD-L1. Reprogramming the M2 phenotype of TAMs can effectively alter the immune state of the tumor microenvironment and revive the antitumor activity of the immune system. Compared to non-selective depletion of macrophages, re-education of TAMs to antitumoral orientation not only restores their immune pattern but also destroys immunosuppression of the PDAC tumor microenvironment, equal to internally disintegrate the network constituted by tumor cells and stromal cells. However, the present approaches to promote TAMs toward M1 have some limitations, which due to the complicated regulated network, repolarization can be counteracted by underlying mechanisms worthy of further investigations. M2 orientation of TAMs is endowed by overall characteristics of the tumor microenvironment, with involvements of multiple pathways, and reprogramming TAMs must depend on the integrated alterations

of the tumor microenvironment. Nonetheless, a new tumor microenvironment will be reinstituted with the restabilization of the environment, which renders it to eliminate tumor cells as thoroughly as possible. Tumor cells create a cradle advantageous to their growth and regulating tumor microenvironments is just to exorcise the shelter to effectively attack against tumor cells. As it is known to all, TAMs shoulder the chief responsibility of establishing the tumor microenvironment, thus targeting them to acquire radical alterations. Hence, it is greatly convincing that targeting TAM therapy has promising development prospects. Furthermore, recent advancement in nanotechnology has persistently updated nanotargeted drug delivery systems, which has promoted directed TAM treatment more effectively and precisely (Yang et al., 2020). The introduction of new nanomaterials in pancreatic cancer therapy has promoted traditional drug delivery and pharmacological efficacy. Especially, vesicle transport as the major intercellular communication approach can be better applied to improve the conversion rate of TAMs, superior to single antibody or receptor blockade, being the future development direction.

Taken together, the polarization of TAMs acts as a key link in the tumor microenvironment and exerts significant roles in PDAC progression, but more underlying mechanisms require further explorations. More comprehensive immunotherapeutic modes are hopefully developed to participate in PDAC treatment, and TAMs are a potential target to fundamentally overthrow the immunosuppressive constitution in pancreatic cancer. Reprogramming TAMs to recalibrate tumor immunity has a better prospect of clinic therapy in the future.

AUTHOR CONTRIBUTIONS

QL provided significant guidance for the review. SY and QFL drafted the manuscript and illustrated the figures for the manuscript. All authors approved the final manuscript.

FUNDING

This project was supported by funds granted by the National Natural Science Foundation of China (81673023, 81872501, and 81502068) and Beijing Natural Science Foundation of China (7172177).

REFERENCES

- Andersen, D. K., Korc, M., Petersen, G. M., Eibl, G., Li, D., Rickels, M. R., et al. (2017). Diabetes, pancreatogenic diabetes, and pancreatic cancer. *Diabetes* 66, 1103–1110. doi: 10.2337/db16-1477
- Anderson, K. G., Stromnes, I. M., and Greenberg, P. D. (2017). Obstacles posed by the tumor microenvironment to t cell activity: a case for synergistic therapies. *Cancer cell* 31, 311–325. doi: 10.1016/j.ccell.2017.02.008
- Andersson, P., Yang, Y., Hosaka, K., Zhang, Y., Fischer, C., Braun, H., et al. (2018). Molecular mechanisms of IL-33-mediated stromal interactions in cancer metastasis. *JCI Insight* 3:e122375. doi: 10.1172/jci.insight.122375
- Arai, H., Battaglin, F., Wang, J., Lo, J. H., Soni, S., Zhang, W., et al. (2019). Molecular insight of regorafenib treatment for colorectal cancer. *Cancer Treat. Rev.* 81:101912. doi: 10.1016/j.ctrv.2019.101912
- Attri, K. S., Mehla, K., and Singh, P. K. (2018). Evaluation of macrophage polarization in pancreatic cancer microenvironment under hypoxia. *Methods Mol. Biol.* 1742, 265–276. doi: 10.1007/978-1-4939-7665-2_23
- Babicky, M. L., Harper, M. M., Chakedis, J., Cazes, A., Mose, E. S., Jaquish, D. V., et al. (2019). MST1R kinase accelerates pancreatic cancer progression via effects on both epithelial cells and macrophages. *Oncogene* 38, 5599–5611. doi: 10.1038/s41388-019-0811-9
- Bastea, L. I., Liou, G.-Y., Pandey, V., Fleming, A. K., von Roemeling, C. A., Doeppler, H., et al. (2019). Pomalidomide alters pancreatic macrophage populations to generate an immune-responsive environment at precancerous

- and cancerous lesions. *Cancer Res.* 79, 1535–1548. doi: 10.1158/0008-5472.CAN-18-1153
- Bear, A. S., Vonderheide, R. H., and O'Hara, M. H. (2020). Challenges and opportunities for pancreatic cancer immunotherapy. *Cancer Cell* [Epub ahead of print] doi: 10.1016/j.ccell.2020.08.004
- Beatty, G. L., Chiorean, E. G., Fishman, M. P., Saboury, B., Teitelbaum, U. R., Sun, W., et al. (2011). CD40 agonists alter tumor stroma and show efficacy against pancreatic carcinoma in mice and humans. *Science* 331, 1612–1616. doi: 10.1126/science.1198443
- Beatty, G. L., Torigian, D. A., Chiorean, E. G., Saboury, B., Brothers, A., Alavi, A., et al. (2013). A phase I study of an agonist CD40 monoclonal antibody (CP-870,893) in combination with gemcitabine in patients with advanced pancreatic ductal adenocarcinoma. *Clin. Cancer Res.* 19, 6286–6295. doi: 10.1158/1078-0432.Ccr-13-20
- Becker, A., Thakur, B. K., Weiss, J. M., Kim, H. S., Peinado, H., and Lyden, D. (2016). Extracellular vesicles in cancer: cell-to-cell mediators of metastasis. *Cancer Cell* 30, 836–848. doi: 10.1016/j.ccell.2016.10.009
- Bencheikh, L., Diop, M. B. K., Rivière, J., Imanci, A., Pierron, G., Souquere, S., et al. (2019). Dynamic gene regulation by nuclear colony-stimulating factor 1 receptor in human monocytes and macrophages. *Nat. Commun.* 10:1935. doi: 10.1038/s41467-019-09970-9
- Bent, R., Moll, L., Grabbe, S., and Bros, M. (2018). Interleukin-1 Beta-A friend or foe in malignancies? *Int. J. Mol. Sci.* 19:E2155. doi: 10.3390/ijms19082155
- Binenbaum, Y., Fridman, E., Yaari, Z., Milman, N., Schroeder, A., Ben David, G., et al. (2018). Transfer of miRNA in macrophage-derived exosomes induces drug resistance in pancreatic adenocarcinoma. *Cancer Res.* 78, 5287–5299. doi: 10.1158/0008-5472.CAN-18-0124
- Bishehsari, F., Zhang, L., Barlass, U., Preite, N. Z., Turturro, S., Najor, M. S., et al. (2018). KRAS mutation and epithelial-macrophage interplay in pancreatic neoplastic transformation. *Int. J. Cancer* 143, 1994–2007. doi: 10.1002/ijc.31592
- Borgoni, S., Iannello, A., Cutrupi, S., Allavena, P., D'Incalci, M., Novelli, F., et al. (2018). Depletion of tumor-associated macrophages switches the epigenetic profile of pancreatic cancer infiltrating T cells and restores their anti-tumor phenotype. *Oncoimmunology* 7, e1393596. doi: 10.1080/2162402X.2017.1393596
- Boulakirba, S., Pfeifer, A., Mhaidly, R., Obba, S., Goulard, M., Schmitt, T., et al. (2018). IL-34 and CSF-1 display an equivalent macrophage differentiation ability but a different polarization potential. *Sci. Rep.* 8:256. doi: 10.1038/s41598-017-18433-4
- Buchholz, S. M., Goetze, R. G., Singh, S. K., Ammer-Herrmenau, C., Richards, F. M., Jodrell, D. I., et al. (2020). Depletion of macrophages improves therapeutic response to gemcitabine in murine pancreas cancer. *Cancers* 12, 1978. doi: 10.3390/cancers12071978
- Caisová, V., Uher, O., Nedbalová, P., Jochmanová, I., Kvardová, K., Masáková, K., et al. (2018). Effective cancer immunotherapy based on combination of TLR agonists with stimulation of phagocytosis. *Int. Immunopharmacol.* 59, 86–96. doi: 10.1016/j.intimp.2018.03.038
- Candido, J. B., Morton, J. P., Bailey, P., Campbell, A. D., Karim, S. A., Jamieson, T., et al. (2018). CSF1R(+) macrophages sustain pancreatic tumor growth through T cell suppression and maintenance of key gene programs that define the squamous subtype. *Cell Rep.* 23, 1448–1460. doi: 10.1016/j.celrep.2018.03.131
- Cannarile, M. A., Weissner, M., Jacob, W., Jegg, A. M., Ries, C. H., and Rüttinger, D. (2017). Colony-stimulating factor 1 receptor (CSF1R) inhibitors in cancer therapy. *J. Immunother. Cancer* 5:53. doi: 10.1186/s40425-017-0257-y
- Carrer, A., Trefely, S., Zhao, S., Campbell, S. L., Norgard, R. J., Schultz, K. C., et al. (2019). Acetyl-CoA metabolism supports multistep pancreatic tumorigenesis. *Cancer Discov.* 9, 416–435. doi: 10.1158/2159-8290.Cd-18-0567
- Celhar, T., Pereira-Lopes, S., Thornhill, S. I., Lee, H. Y., Dhillon, M. K., Poidinger, M., et al. (2016). TLR7 and TLR9 ligands regulate antigen presentation by macrophages. *Int. Immunol.* 28, 223–232. doi: 10.1093/intimm/dxv066
- Céspedes, M. V., Guillén, M. J., López-Casas, P. P., Sarno, F., Gallardo, A., Álamo, P., et al. (2016). Lurbinectedin induces depletion of tumor-associated macrophages, an essential component of its in vivo synergism with gemcitabine, in pancreatic adenocarcinoma mouse models. *Dis. Model. Mech.* 9, 1461–1471. doi: 10.1242/dmm.026369
- Chang, Y.-T., Peng, H.-Y., Hu, C.-M., Huang, S.-C., Tien, S.-C., and Jeng, Y.-M. (2020). Pancreatic cancer-derived small extracellular vesicle Ezrin regulates macrophage polarization and promotes metastasis. *Am. J. Cancer Res.* 10, 12–37.
- Cheah, M. T., Chen, J. Y., Sahoo, D., Contreras-Trujillo, H., Volkmer, A. K., Scheeren, F. A., et al. (2015). CD14-expressing cancer cells establish the inflammatory and proliferative tumor microenvironment in bladder cancer. *Proc. Natl. Acad. Sci. U.S.A.* 112, 4725–4730. doi: 10.1073/pnas.1424795112
- Chen, C.-C., Chen, L.-L., Li, C.-P., Hsu, Y.-T., Jiang, S.-S., Fan, C.-S., et al. (2018). Myeloid-derived macrophages and secreted HSP90 α induce pancreatic ductal adenocarcinoma development. *Oncoimmunology* 7, e1424612. doi: 10.1080/2162402X.2018.1424612
- Chen, S. J., Lian, G. D., Li, J. J., Zhang, Q. B., Zeng, L. J., Yang, K. G., et al. (2018). Tumor-driven like macrophages induced by conditioned media from pancreatic ductal adenocarcinoma promote tumor metastasis via secreting IL-8. *Cancer Med.* 7, 5679–5690. doi: 10.1002/cam4.1824
- Chen, X., Zhou, J., Li, X., Wang, X., Lin, Y., and Wang, X. (2018). Exosomes derived from hypoxic epithelial ovarian cancer cells deliver microRNAs to macrophages and elicit a tumor-promoted phenotype. *Cancer Lett.* 435, 80–91. doi: 10.1016/j.canlet.2018.08.001
- Chen, M.-M., Xiao, X., Lao, X.-M., Wei, Y., Liu, R.-X., Zeng, Q.-H., et al. (2016). Polarization of tissue-resident TFH-Like cells in human hepatoma bridges innate monocyte inflammation and M2b macrophage polarization. *Cancer Discov.* 6, 1182–1195. doi: 10.1158/2159-8290.cd-16-0329
- Chen, Q., Wang, J., Zhang, Q., Zhang, J., Lou, Y., Yang, J., et al. (2019). Tumour cell-derived debris and IgG synergistically promote metastasis of pancreatic cancer by inducing inflammation via tumour-associated macrophages. *Br. J. Cancer* 121, 786–795. doi: 10.1038/s41416-019-0595-2
- Chen, Z., Feng, X., Herting, C. J., Garcia, V. A., Nie, K., Pong, W. W., et al. (2017). Cellular and molecular identity of tumor-associated macrophages in glioblastoma. *Cancer Res.* 77, 2266–2278. doi: 10.1158/0008-5472.CAN-16-2310
- Costa-Silva, B., Aiello, N. M., Ocean, A. J., Singh, S., Zhang, H., Thakur, B. K., et al. (2015). Pancreatic cancer exosomes initiate pre-metastatic niche formation in the liver. *Nat. Cell Biol.* 17, 816–826. doi: 10.1038/ncb3169
- Cui, R., Yue, W., Lattime, E. C., Stein, M. N., Xu, Q., and Tan, X.-L. (2016). Targeting tumor-associated macrophages to combat pancreatic cancer. *Oncotarget* 7, 50735–50754. doi: 10.18632/oncotarget.9383
- Dai, E., Han, L., Liu, J., Xie, Y., Kroemer, G., Klionsky, D. J., et al. (2020). Autophagy-dependent ferroptosis drives tumor-associated macrophage polarization via release and uptake of oncogenic KRAS protein. *Autophagy* 16, 2069–2083. doi: 10.1080/15548627.2020.1714209
- Daley, D., Mani, V. R., Mohan, N., Akkad, N., Ochi, A., Heindel, D. W., et al. (2017). Dectin 1 activation on macrophages by galectin 9 promotes pancreatic carcinoma and peritumoral immune tolerance. *Nat. Med.* 23, 556–567. doi: 10.1038/nm.4314
- Daniel, S. K., Sullivan, K. M., Labadie, K. P., and Pillarisetty, V. G. (2019). Hypoxia as a barrier to immunotherapy in pancreatic adenocarcinoma. *Clin. Transl. Med.* 8:10. doi: 10.1186/s40169-019-0226-9
- Dehne, N., Mora, J., Namgaladze, D., Weigert, A., and Brüne, B. (2017). Cancer cell and macrophage cross-talk in the tumor microenvironment. *Curr. Opin. Pharmacol.* 35, 12–19. doi: 10.1016/j.coph.2017.04.007
- D'Errico, G., Alonso-Nocelo, M., Vallespinos, M., Hermann, P. C., Alcalá, S., García, C. P., et al. (2019). Tumor-associated macrophage-secreted 14-3-3 ζ signals via AXL to promote pancreatic cancer chemoresistance. *Oncogene* 38, 5469–5485. doi: 10.1038/s41388-019-0803-9
- Deshmukh, S. K., Tyagi, N., Khan, M. A., Srivastava, S. K., Al-Ghadhban, A., Dugger, K., et al. (2018). Gemcitabine treatment promotes immunosuppressive microenvironment in pancreatic tumors by supporting the infiltration, growth, and polarization of macrophages. *Sci. Rep.* 8:12000. doi: 10.1038/s41598-018-30437-2
- Diakos, C. I., Charles, K. A., McMillan, D. C., and Clarke, S. J. (2014). Cancer-related inflammation and treatment effectiveness. *Lancet Oncol.* 15, e493–e503. doi: 10.1016/S1470-2045(14)70263-3
- Eriksson, E., Milenova, I., Wenthe, J., Moreno, R., Alemany, R., and Loskog, A. (2019). IL-6 signaling blockade during CD40-mediated immune activation favors antitumor factors by reducing TGF- β , collagen Type I, and PD-L1/PD-1. *J. Immunol.* 202, 787–798. doi: 10.4049/jimmunol.1800717
- Errard, D., Szturz, P., Tijeras-Raballand, A., Astorgues-Xerri, L., Abitbol, C., Paradis, V., et al. (2019). Macrophages in the microenvironment of head and

- neck cancer: potential targets for cancer therapy. *Oral Oncol.* 88, 29–38. doi: 10.1016/j.oraloncology.2018.10.040
- Fan, C. S., Chen, L. L., Hsu, T. A., Chen, C. C., Chua, K. V., Li, C. P., et al. (2019). Endothelial-mesenchymal transition harnesses HSP90 α -secreting M2-macrophages to exacerbate pancreatic ductal adenocarcinoma. *J. Hematol. Oncol.* 12:138. doi: 10.1186/s13045-019-0826-2
- Farajzadeh Valilou, S., Keshavarz-Fathi, M., Silvestris, N., Argentiero, A., and Rezaei, N. (2018). The role of inflammatory cytokines and tumor associated macrophages (TAMs) in microenvironment of pancreatic cancer. *Cytokine Growth Factor Rev.* 39, 46–61. doi: 10.1016/j.cytogfr.2018.01.007
- Feng, L., Qi, Q., Wang, P., Chen, H., Chen, Z., Meng, Z., et al. (2018). Serum levels of IL-6, IL-8, and IL-10 are indicators of prognosis in pancreatic cancer. *J. Int. Med. Res.* 46, 5228–5236. doi: 10.1177/0300060518800588
- Feng, R., Morine, Y., Ikemoto, T., Imura, S., Iwahashi, S., Saito, Y., et al. (2018). Nrf2 activation drive macrophages polarization and cancer cell epithelial-mesenchymal transition during interaction. *Cell Commun. Signal.* 16, 54. doi: 10.1186/s12964-018-0262-x
- Folch-Puy, E. (2013). REG3 β contributes to the immunosuppressive microenvironment of pancreatic cancer. *Oncoimmunology* 2, e26404. doi: 10.4161/onci.26404
- Foucher, E. D., Ghigo, C., Chouaib, S., Galon, J., Iovanna, J., and Olive, D. (2018). Pancreatic ductal adenocarcinoma: a strong imbalance of good and bad immunological cops in the tumor microenvironment. *Front. Immunol.* 9:1044. doi: 10.3389/fimmu.2018.01044
- Fu, X.-L., Duan, W., Su, C.-Y., Mao, F.-Y., Lv, Y.-P., Teng, Y.-S., et al. (2017). Interleukin 6 induces M2 macrophage differentiation by STAT3 activation that correlates with gastric cancer progression. *Cancer Immunol.* 66, 1597–1608. doi: 10.1007/s00262-017-2052-5
- Gao, Z., Li, Y., Wang, F., Huang, T., Fan, K., Zhang, Y., et al. (2017). Mitochondrial dynamics controls anti-tumour innate immunity by regulating CHIP-IRF1 axis stability. *Nat. Commun.* 8:1805. doi: 10.1038/s41467-017-01919-0
- Germano, G., Frapolli, R., Belgiovine, C., Anselmo, A., Pesce, S., Liguori, M., et al. (2013). Role of macrophage targeting in the antitumor activity of trabectedin. *Cancer cell* 23, 249–262. doi: 10.1016/j.ccr.2013.01.008
- Ginhoux, F., and Williams, M. (2016). Tissue-resident macrophage ontogeny and homeostasis. *Immunity* 44, 439–449. doi: 10.1016/j.immuni.2016.02.024
- Ginhoux, F., Schultze, J. L., Murray, P. J., Ochando, J., and Biswas, S. K. (2016). New insights into the multidimensional concept of macrophage ontogeny, activation and function. *Nat. Immunol.* 17, 34–40. doi: 10.1038/ni.3324
- Gordon, S. R., Maute, R. L., Dulken, B. W., Hutter, G., George, B. M., McCracken, M. N., et al. (2017). PD-1 expression by tumour-associated macrophages inhibits phagocytosis and tumour immunity. *Nature* 545, 495–499. doi: 10.1038/nature22396
- Grasse, M., Meryk, A., Miggitsch, C., and Grubeck-Loebenstien, B. (2018). GM-CSF improves the immune response to the diphtheria-component in a multivalent vaccine. *Vaccine* 36, 4672–4680. doi: 10.1016/j.vaccine.2018.06.033
- Griesmann, H., Drexel, C., Milosevic, N., Sipos, B., Rosendahl, J., Gress, T. M., et al. (2017). Pharmacological macrophage inhibition decreases metastasis formation in a genetic model of pancreatic cancer. *Gut* 66, 1278–1285. doi: 10.1136/gutjnl-2015-310049
- Grimmig, T., Matthes, N., Hoeland, K., Tripathi, S., Chandraker, A., Grimm, M., et al. (2015). TLR7 and TLR8 expression increases tumor cell proliferation and promotes chemoresistance in human pancreatic cancer. *Int. J. Oncol.* 47, 857–866. doi: 10.3892/ijo.2015.3069
- Grimmig, T., Moench, R., Kreckel, J., Haack, S., Rueckert, F., Rehder, R., et al. (2016). Toll Like Receptor 2, 4, and 9 signaling promotes autoregulative tumor cell growth and VEGF/PDGF expression in human pancreatic cancer. *Int. J. Mol. Sci.* 17:2060. doi: 10.3390/ijms17122060
- Gruber, R., Panayiotou, R., Nye, E., Spencer-Dene, B., Stamp, G., and Behrens, A. (2016). YAP1 and TAZ control pancreatic cancer initiation in mice by direct up-regulation of JAK-STAT3 signaling. *Gastroenterology* 151, 526–539. doi: 10.1053/j.gastro.2016.05.006
- Gunderson, A. J., Kaneda, M. M., Tsujikawa, T., Nguyen, A. V., Affara, N. I., Ruffell, B., et al. (2016). Bruton tyrosine kinase-dependent immune cell cross-talk drives pancreas cancer. *Cancer Discov.* 6, 270–285. doi: 10.1158/2159-8290.CD-15-0827
- Gupta, S., Prajapati, A., Gulati, M., Gautam, S. K., Kumar, S., Dalal, V., et al. (2020). Irreversible and sustained upregulation of endothelin axis during oncogene-associated pancreatic inflammation and cancer. *Neoplasia* 22, 98–110. doi: 10.1016/j.neo.2019.11.001
- Halbrook, C. J., Pontious, C., Kovalenko, I., Lapienyte, L., Dreyer, S., Lee, H.-J., et al. (2019). Macrophage-released pyrimidines inhibit gemcitabine therapy in pancreatic cancer. *Cell Metab.* 29, 1390.e6–1399.e6. doi: 10.1016/j.cmet.2019.02.001
- Ham, S., Lima, L. G., Chai, E. P. Z., Muller, A., Lobb, R. J., Krumeich, S., et al. (2018). Breast cancer-derived exosomes alter macrophage polarization via gp130/STAT3 signaling. *Front. Immunol.* 9:871. doi: 10.3389/fimmu.2018.00871
- Han, Z., Liu, S., Lin, H., Trivett, A. L., Hannifin, S., Yang, D., et al. (2019). Inhibition of murine hepatoma tumor growth by cryptotanshinone involves TLR7-dependent activation of macrophages and induction of adaptive antitumor immune defenses. *Cancer Immunol.* 68, 1073–1085. doi: 10.1007/s00262-019-02338-4
- Harney, A. S., Karagiannis, G. S., Pignatelli, J., Smith, B. D., Kadioglu, E., Wise, S. C., et al. (2017). The selective Tie2 inhibitor rebastinib blocks recruitment and function of Tie2 macrophages in breast cancer and pancreatic neuroendocrine tumors. *Mol. Cancer Therap.* 16, 2486–2501. doi: 10.1158/1535-7163.MCT-17-0241
- Helm, O., Held-Feindt, J., Grage-Griebenow, E., Reiling, N., Ungefroren, H., Vogel, I., et al. (2014). Tumor-associated macrophages exhibit pro- and anti-inflammatory properties by which they impact on pancreatic tumorigenesis. *Int. J. Cancer* 135, 843–861. doi: 10.1002/ijc.28736
- Henze, A. T., and Mazzone, M. (2016). The impact of hypoxia on tumor-associated macrophages. *J. Clin. Invest.* 126, 3672–3679. doi: 10.1172/jci84427
- Hong, S. M., Vincent, A., Kanda, M., Leclerc, J., Omura, N., Borges, M., et al. (2012). Genome-wide somatic copy number alterations in low-grade PanINs and IPMNs from individuals with a family history of pancreatic cancer. *Clin. Cancer Res.* 18, 4303–4312. doi: 10.1158/1078-0432.Ccr-12-1075
- Hsieh, C. H., Tai, S. K., and Yang, M. H. (2018). Snail-overexpressing cancer cells promote M2-Like polarization of tumor-associated macrophages by delivering MiR-21-abundant exosomes. *Neoplasia* 20, 775–788. doi: 10.1016/j.neo.2018.06.004
- Hu, Y., Wang, B., Shen, J., Low, S. A., Putt, K. S., Niessen, H. W. M., et al. (2019). Depletion of activated macrophages with a folate receptor-beta-specific antibody improves symptoms in mouse models of rheumatoid arthritis. *Arthritis. Res. Ther.* 21, 143. doi: 10.1186/s13075-019-1912-0
- Huang, X., Li, X., Ma, Q., Xu, Q., Duan, W., Lei, J., et al. (2015). Chronic alcohol exposure exacerbates inflammation and triggers pancreatic acinar-to-ductal metaplasia through PI3K/Akt/IKK. *Int. J. Mol. Med.* 35, 653–663. doi: 10.3892/ijmm.2014.2055
- Hughes, R., Qian, B.-Z., Rowan, C., Muthana, M., Keklikoglou, I., Olson, O. C., et al. (2015). Perivascular M2 macrophages stimulate tumor relapse after chemotherapy. *Cancer Res.* 75, 3479–3491. doi: 10.1158/0008-5472.CAN-14-3587
- Hui, S., Ghergurovich, J. M., Morscher, R. J., Jang, C., Teng, X., Lu, W., et al. (2017). Glucose feeds the TCA cycle via circulating lactate. *Nature* 551, 115–118. doi: 10.1038/nature24057
- Ivashkiv, L. B. (2018). IFN γ : signalling, epigenetics and roles in immunity, metabolism, disease and cancer immunotherapy. *Nat. Rev. Immunol.* 18, 545–558. doi: 10.1038/s41577-018-0029-z
- Jeannin, P., Paolini, L., Adam, C., and Delneste, Y. (2018). The roles of CSFs on the functional polarization of tumor-associated macrophages. *FEBS J.* 285, 680–699. doi: 10.1111/febs.14343
- Jiang, S. H., Zhu, L. L., Zhang, M., Li, R. K., Yang, Q., Yan, J. Y., et al. (2019). GABRP regulates chemokine signalling, macrophage recruitment and tumour progression in pancreatic cancer through tuning KCNN4-mediated Ca(2+) signalling in a GABA-independent manner. *Gut* 68, 1994–2006. doi: 10.1136/gutjnl-2018-317479
- Johnstone, R. M., Adam, M., Hammond, J. R., Orr, L., and Turbide, C. (1987). Vesicle formation during reticulocyte maturation. association of plasma membrane activities with released vesicles (exosomes). *J. Biol. Chem.* 262, 9412–9420.
- Jones, K. I., Tiersma, J., Yuzhalin, A. E., Gordon-Weeks, A. N., Buzzelli, J., Im, J. H., et al. (2018). Radiation combined with macrophage depletion promotes

- adaptive immunity and potentiates checkpoint blockade. *EMBO Mol. Med.* 10:e9342. doi: 10.15252/emmm.201809342
- Kamerkar, S., LeBleu, V. S., Sugimoto, H., Yang, S., Ruivo, C. F., Melo, S. A., et al. (2017). Exosomes facilitate therapeutic targeting of oncogenic KRAS in pancreatic cancer. *Nature* 546, 498–503. doi: 10.1038/nature22341
- Kamisawa, T., Wood, L. D., Itoi, T., and Takaori, K. (2016). Pancreatic cancer. *Lancet* 388, 73–85. doi: 10.1016/s0140-6736(16)00141-0
- Kanchanapally, R., Deshmukh, S. K., Chavva, S. R., Tyagi, N., Srivastava, S. K., Patel, G. K., et al. (2019). Drug-loaded exosomal preparations from different cell types exhibit distinctive loading capability, yield, and antitumor efficacies: a comparative analysis. *Int. J. Nanomed.* 14, 531–541. doi: 10.2147/ijn.S191313
- Kaneda, M. M., Cappello, P., Nguyen, A. V., Ralainirina, N., Hardamon, C. R., Foubert, P., et al. (2016). Macrophage PI3K γ drives pancreatic ductal adenocarcinoma progression. *Cancer Discov.* 6, 870–885. doi: 10.1158/2159-8290.CD-15-1346
- Karnevi, E., Andersson, R., and Rosendahl, A. H. (2014). Tumour-educated macrophages display a mixed polarisation and enhance pancreatic cancer cell invasion. *Immunol. Cell Biol.* 92, 543–552. doi: 10.1038/icb.2014.22
- Khalaf, N., Yuan, C., Hamada, T., Cao, Y., Babic, A., Morales-Oyarvide, V., et al. (2018). Regular use of aspirin or non-aspirin nonsteroidal anti-inflammatory drugs is not associated with risk of incident pancreatic cancer in two large cohort studies. *Gastroenterology* 154, 1380.e5–1390.e5. doi: 10.1053/j.gastro.2017.12.001
- Kim, S.-Y., Kim, S., Kim, J.-E., Lee, S. N., Shin, I. W., Shin, H. S., et al. (2019). Lyophilizable and multifaceted toll-like receptor 7/8 agonist-loaded nanoemulsion for the reprogramming of tumor microenvironments and enhanced cancer immunotherapy. *ACS Nano* 13, 12671–12686. doi: 10.1021/acsnano.9b04207
- Knapinska, A. M., Estrada, C. A., and Fields, G. B. (2017). The roles of matrix metalloproteinases in pancreatic cancer. *Prog. Mol. Biol. Transl. Sci.* 148, 339–354. doi: 10.1016/bs.pmbts.2017.03.004
- Koong, A. C., Mehta, V. K., Le, Q. T., Fisher, G. A., Terris, D. J., Brown, J. M., et al. (2000). Pancreatic tumors show high levels of hypoxia. *Int. J. Radiat. Oncol. Biol. Phys.* 48, 919–922. doi: 10.1016/s0360-3016(00)00803-8
- Kühnemuth, B., Mühlberg, L., Schipper, M., Griesmann, H., Neesse, A., Milosevic, N., et al. (2015). CUX1 modulates polarization of tumor-associated macrophages by antagonizing NF- κ B signaling. *Oncogene* 34, 177–187. doi: 10.1038/onc.2013.530
- Kumar, S., Torres, M. P., Kaur, S., Rachagani, S., Joshi, S., Johansson, S. L., et al. (2015). Smoking accelerates pancreatic cancer progression by promoting differentiation of MDSCs and inducing HB-EGF expression in macrophages. *Oncogene* 34, 2052–2060. doi: 10.1038/onc.2014.154
- Kumar, V., Donthireddy, L., Marvel, D., Condamine, T., Wang, F., Lavilla-Alonso, S., et al. (2017). Cancer-associated fibroblasts neutralize the anti-tumor effect of CSF1 receptor blockade by inducing PMN-MDSC infiltration of tumors. *Cancer Cell* 32, 654.e5–668.e5. doi: 10.1016/j.ccell.2017.10.005
- Kurahara, H., Takao, S., Kuwahata, T., Nagai, T., Ding, Q., Maeda, K., et al. (2012). Clinical significance of folate receptor β -expressing tumor-associated macrophages in pancreatic cancer. *Ann. Surg. Oncol.* 19, 2264–2271. doi: 10.1245/s10434-012-2263-0
- Lampropoulou, V., Sergushichev, A., Bambouskova, M., Nair, S., Vincent, E. E., Loginicheva, E., et al. (2016). Itaconate links inhibition of succinate dehydrogenase with macrophage metabolic remodeling and regulation of inflammation. *Cell Metab.* 24, 158–166. doi: 10.1016/j.cmet.2016.06.004
- Lankadasari, M. B., Mukhopadhyay, P., Mohammed, S., and Harikumar, K. B. (2019). TAMing pancreatic cancer: combat with a double edged sword. *Mol. Cancer* 18, 48. doi: 10.1186/s12943-019-0966-6
- Lawicki, S., Głżewska, E. K., Sobolewska, M., Będkowska, G. E., and Szmikowski, M. (2016). Plasma levels and diagnostic utility of macrophage colony-stimulating factor, matrix metalloproteinase-9, and tissue inhibitor of Metalloproteinases-1 as new biomarkers of breast cancer. *Ann. Lab. Med.* 36, 223–229. doi: 10.3343/alm.2016.36.3.223
- Le, Y., Gao, H., Bleday, R., and Zhu, Z. (2018). The homeobox protein VentX reverts immune suppression in the tumor microenvironment. *Nat. Commun.* 9:2175. doi: 10.1038/s41467-018-04567-0
- Le, Y., Gao, H., Richards, W., Zhao, L., Bleday, R., Clancy, T., et al. (2020). VentX expression in tumor-associated macrophages promotes phagocytosis and immunity against pancreatic cancers. *JCI Insight* 5:e137088. doi: 10.1172/jci.insight.137088
- Leppänen, J., Helminen, O., Huhta, H., Kauppila, J. H., Isohookana, J., Haapasaari, K.-M., et al. (2017). High toll-like receptor (TLR) 9 expression is associated with better prognosis in surgically treated pancreatic cancer patients. *Virchows Archiv.* 470, 401–410. doi: 10.1007/s00428-017-2087-1
- Leppänen, J., Helminen, O., Huhta, H., Kauppila, J. H., Isohookana, J., Haapasaari, K.-M., et al. (2018). Toll-like receptors 2, 4 and 9 and hypoxia markers HIF-1 α and CAIX in pancreatic intraepithelial neoplasia. *APMIS* 126, 852–863. doi: 10.1111/apm.12894
- Li, M., Li, M., Yang, Y., Liu, Y., Xie, H., Yu, Q., et al. (2020). Remodeling tumor immune microenvironment via targeted blockade of PI3K- γ and CSF-1/CSF-1R pathways in tumor associated macrophages for pancreatic cancer therapy. *J. Control. Release* 321, 23–35. doi: 10.1016/j.jconrel.2020.02.011
- Li, N., Li, Y., Li, Z., Huang, C., Yang, Y., Lang, M., et al. (2016). Hypoxia inducible factor 1 (HIF-1) recruits macrophage to activate pancreatic stellate cells in pancreatic ductal adenocarcinoma. *Int. J. Mol. Sci.* 17:799. doi: 10.3390/ijms17060799
- Li, R., Zhou, R., Wang, H., Li, W., Pan, M., Yao, X., et al. (2019). Gut microbiota-stimulated cathepsin K secretion mediates TLR4-dependent M2 macrophage polarization and promotes tumor metastasis in colorectal cancer. *Cell Death Differ.* 26, 2447–2463. doi: 10.1038/s41418-019-0312-y
- Li, S., Xu, H. X., Wu, C. T., Wang, W. Q., Jin, W., Gao, H. L., et al. (2019). Angiogenesis in pancreatic cancer: current research status and clinical implications. *Angiogenesis* 22, 15–36. doi: 10.1007/s10456-018-9645-2
- Lin, H., Lee, E., Hestir, K., Leo, C., Huang, M., Bosch, E., et al. (2008). Discovery of a cytokine and its receptor by functional screening of the extracellular proteome. *Science* 320, 807–811. doi: 10.1126/science.1154370
- Linton, S. S., Abraham, T., Liao, J., Clawson, G. A., Butler, P. J., Fox, T., et al. (2018). Tumor-promoting effects of pancreatic cancer cell exosomes on THP-1-derived macrophages. *PLoS One* 13:e0206759. doi: 10.1371/journal.pone.0206759
- Liou, G. Y., Bastea, L., Fleming, A., Döppler, H., Edenfield, B. H., Dawson, D. W., et al. (2017). The presence of Interleukin-13 at pancreatic ADM/PanIN lesions alters macrophage populations and mediates pancreatic tumorigenesis. *Cell Rep.* 19, 1322–1333. doi: 10.1016/j.celrep.2017.04.052
- Liou, G.-Y., Döppler, H., Necela, B., Krishna, M., Crawford, H. C., Raimondo, M., et al. (2013). Macrophage-secreted cytokines drive pancreatic acinar-to-ductal metaplasia through NF- κ B and MMPs. *J. Cell Biol.* 202, 563–577. doi: 10.1083/jcb.201301001
- Liu, C. Y., Xu, J. Y., Shi, X. Y., Huang, W., Ruan, T. Y., Xie, P., et al. (2013). M2-polarized tumor-associated macrophages promoted epithelial-mesenchymal transition in pancreatic cancer cells, partially through TLR4/IL-10 signaling pathway. *Lab Invest.* 93, 844–854. doi: 10.1038/labinvest.2013.69
- Liu, F., Sun, J., Yu, W., Jiang, Q., Pan, M., Xu, Z., et al. (2020). Quantum dot-pulsed dendritic cell vaccines plus macrophage polarization for amplified cancer immunotherapy. *Biomaterials* 242:119928. doi: 10.1016/j.biomaterials.2020.119928
- Liu, Q., Wu, H., Li, Y., Zhang, R., Kleeff, J., Zhang, X., et al. (2020). Combined blockade of TGF- β 1 and GM-CSF improves chemotherapeutic effects for pancreatic cancer by modulating tumor microenvironment. *Cancer Immunol. Immunother.* 69, 1477–1492. doi: 10.1007/s00262-020-02542-7
- Liu, Z., Xie, Y., Xiong, Y., Liu, S., Qiu, C., Zhu, Z., et al. (2020). TLR 7/8 agonist reverses oxaliplatin resistance in colorectal cancer via directing the myeloid-derived suppressor cells to tumoricidal M1-macrophages. *Cancer Lett.* 469, 173–185. doi: 10.1016/j.canlet.2019.10.020
- Liu, M., O'Connor, R. S., Trefely, S., Graham, K., Snyder, N. W., and Beatty, G. L. (2019). Metabolic rewiring of macrophages by CpG potentiates clearance of cancer cells and overcomes tumor-expressed CD47-mediated 'don't-eat-me' signal. *Nat. Immunol.* 20, 265–275. doi: 10.1038/s41590-018-0292-y
- Liu, P.-S., Wang, H., Li, X., Chao, T., Teav, T., Christen, S., et al. (2017). α -ketoglutarate orchestrates macrophage activation through metabolic and epigenetic reprogramming. *Nat. Immunol.* 18, 985–994. doi: 10.1038/ni.3796
- Liu, Q., Li, Y., Niu, Z., Zong, Y., Wang, M., Yao, L., et al. (2016). Atorvastatin (Lipitor) attenuates the effects of aspirin on pancreatic cancerogenesis and the chemotherapeutic efficacy of gemcitabine on pancreatic cancer by promoting M2 polarized tumor associated macrophages. *J. Exp. Clin. Cancer Res.* 35:33. doi: 10.1186/s13046-016-0304-4

- Long, K. B., Gladney, W. L., Tooker, G. M., Graham, K., Fraietta, J. A., and Beatty, G. L. (2016). IFN γ and CCL2 cooperate to redirect tumor-infiltrating monocytes to degrade fibrosis and enhance chemotherapy efficacy in pancreatic carcinoma. *Cancer Discov.* 6, 400–413. doi: 10.1158/2159-8290.CD-15-1032
- Lundahl, M. L. E., Scanlan, E. M., and Lavelle, E. C. (2017). Therapeutic potential of carbohydrates as regulators of macrophage activation. *Biochem. Pharmacol.* 146, 23–41. doi: 10.1016/j.bcp.2017.09.003
- Lybaert, L., Vermaelen, K., De Geest, B. G., and Nuhn, L. (2018). Immunoen지니어링 through cancer vaccines - a personalized and multi-step vaccine approach towards precise cancer immunity. *J. Control. Release* 289, 125–145. doi: 10.1016/j.jconrel.2018.09.009
- Ma, H. S., Poudel, B., Torres, E. R., Sidhom, J. W., Robinson, T. M., Christmas, B., et al. (2019). A CD40 agonist and PD-1 antagonist antibody reprogram the microenvironment of nonimmunogenic tumors to allow t-cell-mediated anticancer activity. *Cancer Immunol. Res.* 7, 428–442. doi: 10.1158/2326-6066.Cir-18-0061
- Ma, X., Wu, D., Zhou, S., Wan, F., Liu, H., Xu, X., et al. (2016). The pancreatic cancer secreted REG4 promotes macrophage polarization to M2 through EGFR/AKT/CREB pathway. *Oncol. Rep.* 35, 189–196. doi: 10.3892/or.2015.4357
- Mantovani, A., Marchesi, F., Malesci, A., Laghi, L., and Allavena, P. (2017). Tumour-associated macrophages as treatment targets in oncology. *Nat. Rev. Clin. Oncol.* 14, 399–416. doi: 10.1038/nrclinonc.2016.217
- Mao, L., Wang, Y., Wang, D., Han, G., Fu, S., and Wang, J. (2017). TEMs but not DKK1 could serve as complementary biomarkers for AFP in diagnosing AFP-negative hepatocellular carcinoma. *PLoS One* 12:e0183880. doi: 10.1371/journal.pone.0183880
- Martinez-Bosch, N., Vinaixa, J., and Navarro, P. (2018). Immune evasion in pancreatic cancer: from mechanisms to therapy. *Cancers* 10:6. doi: 10.3390/cancers10010006
- Matsubara, T., Kanto, T., Kuroda, S., Yoshio, S., Higashitani, K., Kakita, N., et al. (2013). TIE2-expressing monocytes as a diagnostic marker for hepatocellular carcinoma correlates with angiogenesis. *Hepatology* 57, 1416–1425. doi: 10.1002/hep.25965
- Matsuo, Y., Ochi, N., Sawai, H., Yasuda, A., Takahashi, H., Funahashi, H., et al. (2009). CXCL8/IL-8 and CXCL12/SDF-1 α co-operatively promote invasiveness and angiogenesis in pancreatic cancer. *Int. J. Cancer* 124, 853–861. doi: 10.1002/ijc.24040
- Mehrotra, S., Britten, C. D., Chin, S., Garrett-Mayer, E., Cloud, C. A., Li, M., et al. (2017). Vaccination with poly(IC:LC) and peptide-pulsed autologous dendritic cells in patients with pancreatic cancer. *J. Hematol. Oncol.* 10:82. doi: 10.1186/s13045-017-0459-2
- Melo, S. A., Luecke, L. B., Kahlert, C., Fernandez, A. F., Gammon, S. T., Kaye, J., et al. (2015). Glypican-1 identifies cancer exosomes and detects early pancreatic cancer. *Nature* 523, 177–182. doi: 10.1038/nature14581
- Meng, F., Li, W., Li, C., Gao, Z., Guo, K., and Song, S. (2015). CCL18 promotes epithelial-mesenchymal transition, invasion and migration of pancreatic cancer cells in pancreatic ductal adenocarcinoma. *Int. J. Oncol.* 46, 1109–1120. doi: 10.3892/ijo.2014.2794
- Meng, Y., Qu, Y., Wu, W., Chen, L., Sun, L., Tai, G., et al. (2019). Galactan isolated from *Cantharellus cibarius* modulates antitumor immune response by converting tumor-associated macrophages toward M1-like phenotype. *Carbohydrate Polym.* 226:115295. doi: 10.1016/j.carbpol.2019.115295
- Metcalf, D. (2013). The colony-stimulating factors and cancer. *Cancer Immunol. Res.* 1, 351–356. doi: 10.1158/2326-6066.Cir-13-0151
- Michaels, A. D., Newhook, T. E., Adair, S. J., Morioka, S., Goudreau, B. J., Nagdas, S., et al. (2018). CD47 blockade as an adjuvant immunotherapy for resectable pancreatic cancer. *Clin. Cancer Res.* 24, 1415–1425. doi: 10.1158/1078-0432.Ccr-17-2283
- Miller, B. W., Morton, J. P., Pinese, M., Saturno, G., Jamieson, N. B., McGhee, E., et al. (2015). Targeting the LOX/hypoxia axis reverses many of the features that make pancreatic cancer deadly: inhibition of LOX abrogates metastasis and enhances drug efficacy. *EMBO Mol. Med.* 7, 1063–1076. doi: 10.15252/emmm.201404827
- Miller-Ocuin, J. L., Liang, X., Boone, B. A., Doerfler, W. R., Singhi, A. D., Tang, D., et al. (2019). DNA released from neutrophil extracellular traps (NETs) activates pancreatic stellate cells and enhances pancreatic tumor growth. *Oncoimmunology* 8:e1605822. doi: 10.1080/2162402X.2019.1605822
- Mills, E. L., Ryan, D. G., Prag, H. A., Dikovskaya, D., Menon, D., Zaslon, Z., et al. (2018). Itaconate is an anti-inflammatory metabolite that activates Nrf2 via alkylation of KEAP1. *Nature* 556, 113–117. doi: 10.1038/nature25986
- Moreno Roig, E., Yaromina, A., Houben, R., Groot, A. J., Dubois, L., and Vooijs, M. (2018). Prognostic role of hypoxia-inducible factor-2 α tumor cell expression in cancer patients: a meta-analysis. *Front. Oncol.* 8:224. doi: 10.3389/fonc.2018.00224
- Morrison, A. H., Byrne, K. T., and Vonderheide, R. H. (2018). immunotherapy and prevention of pancreatic cancer. *Trends Cancer* 4, 418–428. doi: 10.1016/j.trecan.2018.04.001
- Murakami, T., Homma, Y., Matsuyama, R., Mori, R., Miyake, K., Tanaka, Y., et al. (2017). Neoadjuvant chemoradiotherapy of pancreatic cancer induces a favorable immunogenic tumor microenvironment associated with increased major histocompatibility complex class I-related chain A/B expression. *J. Surg. Oncol.* 116, 416–426. doi: 10.1002/jso.24681
- Nadella, V., Singh, S., Jain, A., Jain, M., Vasquez, K. M., Sharma, A., et al. (2018). Low dose radiation primed iNOS+M1 macrophages modulate angiogenic programming of tumor derived endothelium. *Mol. Carcinogen.* 57, 1664–1671. doi: 10.1002/mc.22879
- Naqvi, I., Gunaratne, R., McDade, J. E., Moreno, A., Rempel, R. E., Rouse, D. C., et al. (2018). Polymer-mediated inhibition of pro-invasive nucleic acid DAMPs and microvesicles limits pancreatic cancer metastasis. *Mol. Ther.* 26, 1020–1031. doi: 10.1016/j.ymthe.2018.02.018
- Neyen, C., Plüddemann, A., Mukhopadhyay, S., Maniati, E., Bossard, M., Gordon, S., et al. (2013). Macrophage scavenger receptor promotes tumor progression in murine models of ovarian and pancreatic cancer. *J. Immunol.* 190, 3798–3805. doi: 10.4049/jimmunol.1203194
- Nielsen, S. R., Quaranta, V., Linford, A., Emeagi, P., Rainer, C., Santos, A., et al. (2016). Macrophage-secreted granulin supports pancreatic cancer metastasis by inducing liver fibrosis. *Nat. Cell Biol.* 18, 549–560. doi: 10.1038/ncb3340
- Nielsen, S. R., and Schmid, M. C. (2017). Macrophages as key drivers of cancer progression and metastasis. *Mediat. Inflamm.* 2017, 9624760. doi: 10.1155/2017/9624760
- Nishikawa, Y., Kodama, Y., Shiokawa, M., Matsumori, T., Marui, S., Kuriyama, K., et al. (2019). Hes1 plays an essential role in Kras-driven pancreatic tumorigenesis. *Oncogene* 38, 4283–4296. doi: 10.1038/s41388-019-0718-5
- Nywenning, T. M., Wang-Gillam, A., Sanford, D. E., Belt, B. A., Panni, R. Z., Cusworth, B. M., et al. (2016). Targeting tumour-associated macrophages with CCR2 inhibition in combination with FOLFIRINOX in patients with borderline resectable and locally advanced pancreatic cancer: a single-centre, open-label, dose-finding, non-randomised, phase 1b trial. *Lancet Oncol.* 17, 651–662. doi: 10.1016/s1470-2045(16)00078-4
- Oh, E., Oh, J.-E., Hong, J., Chung, Y., Lee, Y., Park, K. D., et al. (2017). Optimized biodegradable polymeric reservoir-mediated local and sustained co-delivery of dendritic cells and oncolytic adenovirus co-expressing IL-12 and GM-CSF for cancer immunotherapy. *J. Control. Release* 259, 115–127. doi: 10.1016/j.jconrel.2017.03.028
- Ohashi, T., Aoki, M., Tomita, H., Akazawa, T., Sato, K., Kuze, B., et al. (2017). M2-like macrophage polarization in high lactic acid-producing head and neck cancer. *Cancer Sci.* 108, 1128–1134. doi: 10.1111/cas.13244
- Padoan, A., Plebani, M., and Basso, D. (2019). Inflammation and pancreatic cancer: focus on metabolism. *Cytokine Immun.* 20:676. doi: 10.3390/ijms20030676
- Palmieri, E. M., Gonzalez-Cotto, M., Baseler, W. A., Davies, L. C., Ghesquière, B., Maio, N., et al. (2020). Nitric oxide orchestrates metabolic rewiring in M1 macrophages by targeting aconitase 2 and pyruvate dehydrogenase. *Nat. Commun.* 11:698. doi: 10.1038/s41467-020-14433-7
- Pan, Y., Lu, F., Fei, Q., Yu, X., Xiong, P., Yu, X., et al. (2019). Single-cell RNA sequencing reveals compartmental remodeling of tumor-infiltrating immune cells induced by anti-CD47 targeting in pancreatic cancer. *J. Hematol. Oncol.* 12:124. doi: 10.1186/s13045-019-0822-6
- Park, J. E., Dutta, B., Tse, S. W., Gupta, N., Tan, C. F., Low, J. K., et al. (2019). Hypoxia-induced tumor exosomes promote M2-like macrophage polarization of infiltrating myeloid cells and microRNA-mediated metabolic shift. *Oncogene* 38, 5158–5173. doi: 10.1038/s41388-019-0782-x
- Parmiani, G., Castelli, C., Pilla, L., Santinami, M., Colombo, M. P., and Rivoltini, L. (2007). Opposite immune functions of GM-CSF administered as vaccine

- adjuvant in cancer patients. *Ann. Oncol.* 18, 226–232. doi: 10.1093/annonc/mdl158
- Patidar, A., Selvaraj, S., Sarode, A., Chauhan, P., Chattopadhyay, D., and Saha, B. (2018). DAMP-TLR-cytokine axis dictates the fate of tumor. *Cytokine* 104, 114–123. doi: 10.1016/j.cyto.2017.10.004
- Pausch, T. M., Aue, E., Wirsik, N. M., Freire Valls, A., Shen, Y., Radhakrishnan, P., et al. (2020). Metastasis-associated fibroblasts promote angiogenesis in metastasized pancreatic cancer via the CXCL8 and the CCL2 axes. *Sci. Rep.* 10:5420. doi: 10.1038/s41598-020-62416-x
- Pello, O. M., De Pizzol, M., Mirolo, M., Soucek, L., Zammataro, L., Amabile, A., et al. (2012). Role of c-MYC in alternative activation of human macrophages and tumor-associated macrophage biology. *Blood* 119, 411–421. doi: 10.1182/blood-2011-02-339911
- Penny, H. L., Sieow, J. L., Adriani, G., Yeap, W. H., See Chi, Ee, P., et al. (2016). Warburg metabolism in tumor-conditioned macrophages promotes metastasis in human pancreatic ductal adenocarcinoma. *Oncoimmunology* 5:e1191731. doi: 10.1080/2162402X.2016.1191731
- Piao, Y., Park, S. Y., Henry, V., Smith, B. D., Tiao, N., Flynn, D. L., et al. (2016). Novel MET/TIE2/VEGFR2 inhibitor altiratinib inhibits tumor growth and invasiveness in bevacizumab-resistant glioblastoma mouse models. *Neuro-oncology* 18, 1230–1241. doi: 10.1093/neuonc/now030
- Pradel, L. P., Ooi, C.-H., Romagnoli, S., Cannarile, M. A., Sade, H., Rüttinger, D., et al. (2016). Macrophage susceptibility to emactuzumab (RG7155) treatment. *Mol. Cancer Therap.* 15, 3077–3086. doi: 10.1158/1535-7163.mct-16-0157
- Pradere, J. P., Dapito, D. H., and Schwabe, R. F. (2014). The Yin and Yang of toll-like receptors in cancer. *Oncogene* 33, 3485–3495. doi: 10.1038/ncr.2013.302
- Prakash, H., Nadella, V., Singh, S., and Schmitz-Winnenthal, H. (2016). CD14/TLR4 priming potentially recalibrates and exerts anti-tumor efficacy in tumor associated macrophages in a mouse model of pancreatic carcinoma. *Sci. Reports* 6:31490. doi: 10.1038/srep31490
- Principe, D. R., DeCant, B., Mascariñas, E., Wayne, E. A., Diaz, A. M., Akagi, N., et al. (2016). TGF β signaling in the pancreatic tumor microenvironment promotes fibrosis and immune evasion to facilitate tumorigenesis. *Cancer Res.* 76, 2525–2539. doi: 10.1158/0008-5472.Can-15-1293
- Puolakkainen, P., Koski, A., Vainionpää, S., Shen, Z., Repo, H., Kempainen, E., et al. (2014). Anti-inflammatory macrophages activate invasion in pancreatic adenocarcinoma by increasing the MMP9 and ADAM8 expression. *Med. Oncol.* 31:884. doi: 10.1007/s12032-014-0884-9
- Pushalkar, S., Hundeyin, M., Daley, D., Zambirinis, C. P., Kurz, E., Mishra, A., et al. (2018). The pancreatic cancer microbiome promotes oncogenesis by induction of innate and adaptive immune suppression. *Cancer Discov.* 8, 403–416. doi: 10.1158/2159-8290.Cd-17-1134
- Pyonteck, S. M., Akkari, L., Schuhmacher, A. J., Bowman, R. L., Sevenich, L., Quail, D. F., et al. (2013). CSF-1R inhibition alters macrophage polarization and blocks glioma progression. *Nat. Med.* 19, 1264–1272. doi: 10.1038/nm.3337
- Quaranta, V., Rainer, C., Nielsen, S. R., Raymant, M. L., Ahmed, M. S., Engle, D. D., et al. (2018). Macrophage-derived granulins drives resistance to immune checkpoint inhibition in metastatic pancreatic cancer. *Cancer Res.* 78, 4253–4269. doi: 10.1158/0008-5472.CAN-17-3876
- Rahal, O. M., Wolfe, A. R., Mandal, P. K., Larson, R., Tin, S., Jimenez, C., et al. (2018). Blocking Interleukin (IL)4- and IL13-Mediated phosphorylation of STAT6 (Tyr641) decreases M2 polarization of macrophages and protects against macrophage-mediated radioresistance of inflammatory breast cancer. *Int. J. Radiat. Oncol. Biol. Phys.* 100, 1034–1043. doi: 10.1016/j.ijrobp.2017.11.043
- Ratnam, N. M., Peterson, J. M., Talbert, E. E., Ladner, K. J., Rajasekera, P. V., Schmidt, C. R., et al. (2017). NF- κ B regulates GDF-15 to suppress macrophage surveillance during early tumor development. *J. Clin. Invest.* 127, 3796–3809. doi: 10.1172/jci91561
- Rech, A. J., Dada, H., Kotzin, J. J., Henao-Mejia, J., Minn, A. J., Twyman-Saint Victor, C., et al. (2018). Radiotherapy and CD40 activation separately augment immunity to checkpoint blockade in cancer. *Cancer Res.* 78, 4282–4291. doi: 10.1158/0008-5472.Can-17-3821
- Ren, B., Cui, M., Yang, G., Wang, H., Feng, M., You, L., et al. (2018). Tumor microenvironment participates in metastasis of pancreatic cancer. *Mol. Cancer* 17:108. doi: 10.1186/s12943-018-0858-1
- Riera-Domingo, C., Audigé, A., Granja, S., Cheng, W. C., Ho, P. C., Baltazar, F., et al. (2020). Immunity, hypoxia, and metabolism-the ménage à trois of cancer: implications for immunotherapy. *Physiol. Rev.* 100, 1–102. doi: 10.1152/physrev.00018.2019
- Ries, C. H., Cannarile, M. A., Hoves, S., Benz, J., Wartha, K., Runza, V., et al. (2014). Targeting tumor-associated macrophages with anti-CSF-1R antibody reveals a strategy for cancer therapy. *Cancer cell* 25, 846–859. doi: 10.1016/j.ccr.2014.05.016
- Rigamonti, N., Kadioglu, E., Keklikoglou, I., Wyser Rmili, C., Leow, C. C., and De Palma, M. (2014). Role of angiopoietin-2 in adaptive tumor resistance to VEGF signaling blockade. *Cell Rep.* 8, 696–706. doi: 10.1016/j.celrep.2014.06.059
- Rodell, C. B., Arlauckas, S. P., Cuccarese, M. F., Garriss, C. S., Li, R., Ahmed, M. S., et al. (2018). TLR7/8-agonist-loaded nanoparticles promote the polarization of tumour-associated macrophages to enhance cancer immunotherapy. *Nat. Biomed. Engin.* 2, 578–588. doi: 10.1038/s41551-018-0236-8
- Sanford, D. E., Belt, B. A., Panni, R. Z., Mayer, A., Deshpande, A. D., Carpenter, D., et al. (2013). Inflammatory monocyte mobilization decreases patient survival in pancreatic cancer: a role for targeting the CCL2/CCR2 axis. *Clin. Cancer Res.* 19, 3404–3415. doi: 10.1158/1078-0432.Ccr-13-0525
- Saung, M. T., Muth, S., Ding, D., Thomas, D. L., Blair, A. B., Tsujikawa, T., et al. (2018). Targeting myeloid-inflamed tumor with anti-CSF-1R antibody expands CD137+ effector T-cells in the murine model of pancreatic cancer. *J. Immunother. Cancer* 6, 118. doi: 10.1186/s40425-018-0435-6
- Schölch, S., Rauber, C., Weitz, J., Koch, M., and Huber, P. E. (2015). TLR activation and ionizing radiation induce strong immune responses against multiple tumor entities. *Oncoimmunology* 4:e1042201. doi: 10.1080/2162402x.2015.1042201
- Seifert, A. M., Reiche, C., Heiduk, M., Tannert, A., Meinecke, A.-C., Baier, S., et al. (2020). Detection of pancreatic ductal adenocarcinoma with galectin-9 serum levels. *Oncogene* 39, 3102–3113. doi: 10.1038/s41388-020-1186-7
- Semenza, G. L. (2012). Hypoxia-inducible factors: mediators of cancer progression and targets for cancer therapy. *Trends Pharmacol. Sci.* 33, 207–214. doi: 10.1016/j.tips.2012.01.005
- Seo, Y. D., and Pillarisetty, V. G. (2017). T-cell programming in pancreatic adenocarcinoma: a review. *Cancer Gene Ther.* 24, 106–113. doi: 10.1038/cgt.2016.66
- Shen, Z. T., and Sigalov, A. B. (2017). Novel TREM-1 inhibitors attenuate tumor growth and prolong survival in experimental pancreatic cancer. *Mol. Pharmacol.* 14, 4572–4582. doi: 10.1021/acs.molpharmaceut.7b00711
- Silva, A., Mount, A., Krstevska, K., Pejowski, D., Hardy, M. P., Owczarek, C., et al. (2015). The combination of ISCOMATRIX adjuvant and TLR agonists induces regression of established solid tumors in vivo. *J. Immunol.* 194, 2199–2207. doi: 10.4049/jimmunol.1402228
- Silva, M. L. S. (2019). Lectin biosensors in cancer glycan biomarker detection. *Adv. Clin. Chem.* 93, 1–61. doi: 10.1016/bs.acc.2019.07.001
- Singhi, A. D., Koay, E. J., Chari, S. T., and Maitra, A. (2019). Early detection of pancreatic cancer: opportunities and challenges. *Gastroenterology* 156, 2024–2040. doi: 10.1053/j.gastro.2019.01.259
- Srinivasan, S., Totiger, T., Shi, C., Castellanos, J., Lamichhane, P., Dosch, A. R., et al. (2018). Tobacco carcinogen-induced production of GM-CSF activates CREB to promote pancreatic cancer. *Cancer Res.* 78, 6146–6158. doi: 10.1158/0008-5472.Can-18-0579
- Storz, P. (2017). Acinar cell plasticity and development of pancreatic ductal adenocarcinoma. *Nat. Rev. Gastroenterol. Hepatol.* 14, 296–304. doi: 10.1038/nrgastro.2017.12
- Stromnes, I. M., Burrack, A. L., Hulbert, A., Bonson, P., Black, C., Brockenbrough, J. S., et al. (2019). Differential effects of depleting versus programming tumor-associated macrophages on engineered T cells in pancreatic ductal adenocarcinoma. *Cancer Immunol. Res.* 7, 977–989. doi: 10.1158/2326-6066.Cir-18-0448
- Su, M.-J., Aldawsari, H., and Amiji, M. (2016). Pancreatic cancer cell exosome-mediated macrophage reprogramming and the role of MicroRNAs 155 and 125b2 transfection using nanoparticle delivery systems. *Sci. Rep.* 6:30110. doi: 10.1038/srep30110
- Takeuchi, S., Baghdadi, M., Tsuchikawa, T., Wada, H., Nakamura, T., Abe, H., et al. (2015). Chemotherapy-derived inflammatory responses accelerate the formation of immunosuppressive myeloid cells in the tissue microenvironment of human pancreatic cancer. *Cancer Res.* 75, 2629–2640. doi: 10.1158/0008-5472.Can-14-2921

- Talks, K. L., Turley, H., Gatter, K. C., Maxwell, P. H., Pugh, C. W., Ratcliffe, P. J., et al. (2000). The expression and distribution of the hypoxia-inducible factors HIF-1 α and HIF-2 α in normal human tissues, cancers, and tumor-associated macrophages. *Am. J. Pathol.* 157, 411–421. doi: 10.1016/s0002-9440(10)64554-3
- Tekin, C., Abernethy, H. L., Waasdorp, C., Hooijer, G. K. J., de Boer, O. J., Dijk, F., et al. (2020). Macrophage-secreted MMP9 induces mesenchymal transition in pancreatic cancer cells via PAR1 activation. *Cell Oncol.* [Epub ahead of print] doi: 10.1007/s13402-020-00549-x
- Ubil, E., Caskey, L., Holtzhausen, A., Hunter, D., Story, C., and Earp, H. S. (2018). Tumor-secreted Pros1 inhibits macrophage M1 polarization to reduce antitumor immune response. *J. Clin. Invest.* 128, 2356–2369. doi: 10.1172/JCI97354
- Van Overmeire, E., Stijlemans, B., Heymann, F., Keirsse, J., Morias, Y., Elkrin, Y., et al. (2016). M-CSF and GM-CSF receptor signaling differentially regulate monocyte maturation and macrophage polarization in the tumor microenvironment. *Cancer Res.* 76, 35–42. doi: 10.1158/0008-5472.CAN-15-0869
- Vascotto, F., Petschenka, J., Walzer, K. C., Vormehr, M., Brkic, M., Strobl, S., et al. (2019). Intravenous delivery of the toll-like receptor 7 agonist SC1 confers tumor control by inducing a CD8 $^{+}$ T cell response. *Oncoimmunology* 8:1601480. doi: 10.1080/2162402X.2019.1601480
- Venet, F., and Monneret, G. (2018). Advances in the understanding and treatment of sepsis-induced immunosuppression. *Nat. Rev. Nephrol.* 14, 121–137. doi: 10.1038/nrneph.2017.165
- von Ahrens, D., Bhagat, T. D., Nagraath, D., Maitra, A., and Verma, A. (2017). The role of stromal cancer-associated fibroblasts in pancreatic cancer. *J. Hematol. Oncol.* 10:76. doi: 10.1186/s13045-017-0448-5
- Vonderheide, R. H. (2020). CD40 agonist antibodies in cancer immunotherapy. *Annu. Rev. Med.* 71, 47–58. doi: 10.1146/annurev-med-062518-045435
- Waghray, M., Yalamanchili, M., Dziubinski, M., Zeinali, M., Erkkinen, M., Yang, H., et al. (2016). GM-CSF mediates mesenchymal-epithelial cross-talk in pancreatic cancer. *Cancer Discov.* 6, 886–899. doi: 10.1158/2159-8290.Cd-15-0947
- Wanderley, C. W., Colón, D. F., Luiz, J. P. M., Oliveira, F. F., Viacava, P. R., Leite, C. A., et al. (2018). Paclitaxel reduces tumor growth by reprogramming tumor-associated macrophages to an M1 Profile in a TLR4-Dependent manner. *Cancer Res.* 78, 5891–5900. doi: 10.1158/0008-5472.CAN-17-3480
- Wang, Q., He, Z., Huang, M., Liu, T., Wang, Y., Xu, H., et al. (2018). Vascular niche IL-6 induces alternative macrophage activation in glioblastoma through HIF-2 α . *Nat. Commun.* 9:559. doi: 10.1038/s41467-018-03050-0
- Wang, W., Marinis, J. M., Beal, A. M., Savadkar, S., Wu, Y., Khan, M., et al. (2018). RIP1 kinase drives macrophage-mediated adaptive immune tolerance in pancreatic cancer. *Cancer cell* 34, 757.e–774.e. doi: 10.1016/j.ccell.2018.10.006
- Wang, X., Luo, G., Zhang, K., Cao, J., Huang, C., Jiang, T., et al. (2018). Hypoxic tumor-derived exosomal miR-301a mediates M2 macrophage polarization via PTEN/PI3K γ to promote pancreatic cancer metastasis. *Cancer Res.* 78, 4586–4598. doi: 10.1158/0008-5472.CAN-17-3841
- Wang, X., Dong, A., Xiao, J., Zhou, X., Mi, H., Xu, H., et al. (2016). Overcoming HBV immune tolerance to eliminate HBsAg-positive hepatocytes via pre-administration of GM-CSF as a novel adjuvant for a hepatitis B vaccine in HBV transgenic mice. *Cell. Mol. Immunol.* 13, 850–861. doi: 10.1038/cmi.2015.64
- Wang, Y., Yang, G., You, L., Yang, J., Feng, M., Qiu, J., et al. (2019). Role of the microbiome in occurrence, development and treatment of pancreatic cancer. *Mol. Cancer* 18, 173. doi: 10.1186/s12943-019-1103-2
- Watanabe, K., Luo, Y., Da, T., Guedan, S., Ruella, M., Scholler, J., et al. (2018). Pancreatic cancer therapy with combined mesothelin-redirected chimeric antigen receptor T cells and cytokine-armed oncolytic adenoviruses. *JCI Insight* 3:e99573. doi: 10.1172/jci.insight.99573
- Wei, M. Y., Shi, S., Liang, C., Meng, Q. C., Hua, J., Zhang, Y. Y., et al. (2019). The microbiota and microbiome in pancreatic cancer: more influential than expected. *Mol. Cancer* 18:97. doi: 10.1186/s12943-019-1008-0
- Wen, Z.-F., Liu, H., Gao, R., Zhou, M., Ma, J., Zhang, Y., et al. (2018). Tumor cell-released autophagosomes (TRAPs) promote immunosuppression through induction of M2-like macrophages with increased expression of PD-L1. *J. Immunother. Cancer* 6: 151. doi: 10.1186/s40425-018-0452-5
- Wu, J.-Y., Huang, T.-W., Hsieh, Y.-T., Wang, Y.-F., Yen, C.-C., Lee, G.-L., et al. (2020). Cancer-derived succinate promotes macrophage polarization and cancer metastasis via succinate receptor. *Mol. Cell* 77, 213.e5–227.e5. doi: 10.1016/j.molcel.2019.10.023
- Wu, Q., Zhou, W., Yin, S., Zhou, Y., Chen, T., Qian, J., et al. (2019). Blocking triggering receptor expressed on myeloid cells-1-positive tumor-associated macrophages induced by hypoxia reverses immunosuppression and anti-programmed cell death ligand 1 resistance in liver cancer. *Hepatology* 70, 198–214. doi: 10.1002/hep.30593
- Wu, X., Gao, H., Ke, W., Giese, R. W., and Zhu, Z. (2011). The homeobox transcription factor VentX controls human macrophage terminal differentiation and proinflammatory activation. *J. Clin. Invest.* 121, 2599–2613. doi: 10.1172/jci45556
- Xi, Q., Chen, Y., Yang, G. Z., Zhang, J. Y., Zhang, L. J., Guo, X. D., et al. (2020a). miR-128 regulates tumor cell CD47 expression and promotes anti-tumor immunity in pancreatic cancer. *Front. Immunol.* 11:890. doi: 10.3389/fimmu.2020.00890
- Xi, Q., Zhang, J., Yang, G., Zhang, L., Chen, Y., Wang, C., et al. (2020b). Restoration of miR-340 controls pancreatic cancer cell CD47 expression to promote macrophage phagocytosis and enhance antitumor immunity. *J. Immunother. Cancer* 8:e000253. doi: 10.1136/jitc-2019-000253
- Xian, G., Zhao, J., Qin, C., Zhang, Z., Lin, Y., and Su, Z. (2017). Simvastatin attenuates macrophage-mediated gemcitabine resistance of pancreatic ductal adenocarcinoma by regulating the TGF- β 1/Gli-1 axis. *Cancer Lett.* 385, 65–74. doi: 10.1016/j.canlet.2016.11.006
- Xue, J., Sharma, V., Hsieh, M. H., Chawla, A., Murali, R., Pandol, S. J., et al. (2015). Alternatively activated macrophages promote pancreatic fibrosis in chronic pancreatitis. *Nat. Commun.* 6:7158. doi: 10.1038/ncomms8158
- Yan, W.-L., Shen, K.-Y., Tien, C.-Y., Chen, Y.-A., and Liu, S.-J. (2017). Recent progress in GM-CSF-based cancer immunotherapy. *Immunotherapy* 9, 347–360. doi: 10.2217/imt-2016-0141
- Yang, W.-J., Hao, Y.-X., Yang, X., Fu, X.-L., Shi, Y., Yue, H.-L., et al. (2018). Overexpression of Tie2 is associated with poor prognosis in patients with gastric cancer. *Oncol. Lett.* 15, 8027–8033. doi: 10.3892/ol.2018.8329
- Yang, Y., Guo, J., and Huang, L. (2020). Tackling TAMs for cancer immunotherapy: it's nano time. *Trends Pharmacol. Sci.* 41, 701–714. doi: 10.1016/j.tips.2020.08.003
- Ye, H., Zhou, Q., Zheng, S., Li, G., Lin, Q., Wei, L., et al. (2018). Tumor-associated macrophages promote progression and the Warburg effect via CCL18/NF- κ B/VCAM-1 pathway in pancreatic ductal adenocarcinoma. *Cell Death Dis.* 9:453. doi: 10.1038/s41419-018-0486-0
- Zhan, Y., Lew, A. M., and Chopin, M. (2019). The pleiotropic effects of the GM-CSF rheostat on myeloid cell differentiation and function: more than a numbers game. *Front. Immunol.* 10:2679. doi: 10.3389/fimmu.2019.02679
- Zhang, B., Du, Y., He, Y., Liu, Y., Zhang, G., Yang, C., et al. (2019). INT-HA induces M2-like macrophage differentiation of human monocytes via TLR4-miR-935 pathway. *Cancer Immunol.* 68, 189–200. doi: 10.1007/s00262-018-2261-6
- Zhang, D., Li, L., Jiang, H., Knolhoff, B. L., Lockhart, A. C., Wang-Gillam, A., et al. (2017). Constitutive IRAK4 activation underlies poor prognosis and chemoresistance in pancreatic ductal adenocarcinoma. *Clin. Cancer Res.* 23, 1748–1759. doi: 10.1158/1078-0432.CCR-16-1121
- Zhang, D., Li, L., Jiang, H., Li, Q., Wang-Gillam, A., Yu, J., et al. (2018). Tumor-stroma IL1 β -IRAK4 feedforward circuitry drives tumor fibrosis, chemoresistance, and poor prognosis in pancreatic cancer. *Cancer Res.* 78, 1700–1712. doi: 10.1158/0008-5472.CAN-17-1366
- Zhang, J., Zhang, Q., Lou, Y., Fu, Q., Chen, Q., Wei, T., et al. (2018). Hypoxia-inducible factor-1 α /interleukin-1 β signaling enhances hepatoma epithelial-mesenchymal transition through macrophages in a hypoxic-inflammatory microenvironment. *Hepatology* 67, 1872–1889. doi: 10.1002/hep.29681
- Zhang, L., and Li, S. (2020). Lactic acid promotes macrophage polarization through MCT-HIF1 α signaling in gastric cancer. *Exp. Cell Res.* 388, 111846. doi: 10.1016/j.yexcr.2020.111846
- Zhang, L., Qi, Y., Min, H., Ni, C., Wang, F., Wang, B., et al. (2019). Cooperatively responsive peptide nanotherapeutic that regulates angiopoietin receptor Tie2 activity in tumor microenvironment to prevent breast tumor relapse after chemotherapy. *ACS Nano* 13, 5091–5102. doi: 10.1021/acsnano.8b08142
- Zhang, M., Yan, L., Wang, G.-J., and Jin, R. (2019). Resistin effects on pancreatic cancer progression and chemoresistance are mediated through its receptors CAP1 and TLR4. *J. Cell. Physiol.* 234, 9457–9466. doi: 10.1002/jcp.27631

- Zhang, M., Huang, L., Ding, G., Huang, H., Cao, G., Sun, X., et al. (2020). Interferon gamma inhibits CXCL8-CXCR2 axis mediated tumor-associated macrophages tumor trafficking and enhances anti-PD1 efficacy in pancreatic cancer. *J. Immunother. Cancer* 8:e000308. doi: 10.1136/jitc-2019-000308
- Zhang, Y., Crawford, H. C., Pasca, and di Magliano, M. (2019). Epithelial-stromal interactions in pancreatic cancer. *Annu. Rev. Physiol.* 81, 211–233. doi: 10.1146/annurev-physiol-020518-114515
- Zhang, Y., Velez-Delgado, A., Mathew, E., Li, D., Mendez, F. M., Flannagan, K., et al. (2017). Myeloid cells are required for PD-1/PD-L1 checkpoint activation and the establishment of an immunosuppressive environment in pancreatic cancer. *Gut* 66, 124–136. doi: 10.1136/gutjnl-2016-312078
- Zhang, Y., Yu, G., Chu, H., Wang, X., Xiong, L., Cai, G., et al. (2018). Macrophage-associated PGK1 phosphorylation promotes aerobic glycolysis and tumorigenesis. *Mol. Cell* 71, 201.e–215.e. doi: 10.1016/j.molcel.2018.06.023
- Zhou, J., Li, X., Wu, X., Zhang, T., Zhu, Q., Wang, X., et al. (2018). Exosomes released from tumor-associated macrophages transfer miRNAs that induce a Treg/Th17 cell imbalance in epithelial ovarian cancer. *Cancer Immunol. Res.* 6, 1578–1592. doi: 10.1158/2326-6066.Cir-17-0479
- Zhu, X., Yang, J., Gao, Y., Wu, C., Yi, L., Li, G., et al. (2018). The dual effects of a novel peptibody on angiogenesis inhibition and M2 macrophage polarization on sarcoma. *Cancer Lett.* 416, 1–10. doi: 10.1016/j.canlet.2017.10.043
- Zhu, Y., Herndon, J. M., Sojka, D. K., Kim, K.-W., Knolhoff, B. L., Zuo, C., et al. (2017). Tissue-resident macrophages in pancreatic ductal adenocarcinoma originate from embryonic hematopoiesis and promote tumor progression. *Immunity* 47, 323.e6–338.e6. doi: 10.1016/j.immuni.2017.07.014
- Zhu, Y., Knolhoff, B. L., Meyer, M. A., Nywening, T. M., West, B. L., Luo, J., et al. (2014). CSF1/CSF1R blockade reprograms tumor-infiltrating macrophages and improves response to T-cell checkpoint immunotherapy in pancreatic cancer models. *Cancer Res.* 74, 5057–5069. doi: 10.1158/0008-5472.Can-13-3723

Conflict of Interest: The authors declare that the research was conducted in the absence of any commercial or financial relationships that could be construed as a potential conflict of interest.

Copyright © 2021 Yang, Liu and Liao. This is an open-access article distributed under the terms of the Creative Commons Attribution License (CC BY). The use, distribution or reproduction in other forums is permitted, provided the original author(s) and the copyright owner(s) are credited and that the original publication in this journal is cited, in accordance with accepted academic practice. No use, distribution or reproduction is permitted which does not comply with these terms.



Mechanism and Molecular Network of RBM8A-Mediated Regulation of Oxaliplatin Resistance in Hepatocellular Carcinoma

Rong Liang¹, Jinyan Zhang¹, Zhihui Liu¹, Ziyu Liu¹, Qian Li¹, Xiaoling Luo², Yongqiang Li¹, Jiazhou Ye^{3*} and Yan Lin^{1*}

¹ Department of Medical Oncology, Guangxi Medical University Cancer Hospital, Nanning, China, ² Department of Experimental Research, Guangxi Medical University Cancer Hospital, Nanning, China, ³ Department of Hepatobiliary Surgery, Guangxi Medical University Cancer Hospital, Nanning, China

OPEN ACCESS

Edited by:

Wei Zhao,
Chengdu Medical College, China

Reviewed by:

Hong Shen,
Central South University, China
Na Xie,
Independent Researcher,
Chengdu, China

*Correspondence:

Yan Lin
linyanmgx@163.com
Jiazhou Ye
nnsz20013@163.com

Specialty section:

This article was submitted to
Molecular and
Cellular Oncology,
a section of the journal
Frontiers in Oncology

Received: 20 July 2020

Accepted: 03 December 2020

Published: 22 January 2021

Citation:

Liang R, Zhang J, Liu Z, Liu Z, Li Q,
Luo X, Li Y, Ye J and Lin Y (2021)
Mechanism and Molecular Network of
RBM8A-Mediated Regulation of
Oxaliplatin Resistance in
Hepatocellular Carcinoma.
Front. Oncol. 10:585452.
doi: 10.3389/fonc.2020.585452

RNA-binding motif protein 8A (RBM8A) is abnormally overexpressed in hepatocellular carcinoma (HCC) and involved in the epithelial-mesenchymal transition (EMT). The EMT plays an important role in the development of drug resistance, suggesting that RBM8A may be involved in the regulation of oxaliplatin (OXA) resistance in HCC. Here we examined the potential involvement of RBM8A and its downstream pathways in OXA resistance using *in vitro* and *in vivo* models. RBM8A overexpression induced the EMT in OXA-resistant HCC cells, altering cell proliferation, apoptosis, migration, and invasion. Moreover, whole-genome microarrays combined with bioinformatics analysis revealed that RBM8A has a wide range of transcriptional regulatory capabilities in OXA-resistant HCC, including the ability to regulate several important tumor-related signaling pathways. In particular, histone deacetylase 9 (HDAC9) emerged as an important mediator of RBM8A activity related to OXA resistance. These data suggest that RBM8A and its related regulatory pathways represent potential markers of OXA resistance and therapeutic targets in HCC.

Keywords: RNA-binding motif protein 8A, hepatocellular carcinoma, oxaliplatin, drug resistance, histone deacetylase 9, molecular network

INTRODUCTION

Hepatocellular carcinoma (HCC) is a highly lethal cancer: it is the fifth most common malignant tumor globally, and its mortality rate ranks third among all cancers (1). The advent of the targeted drug sorafenib opened the door to advanced HCC drug therapies, but first-line therapies are associated with relatively low rates of objective response and progression-free survival (2). Their inefficacy and elevated cost limit their clinical usefulness (3). The complexity of HCC means that it needs to be treated through multiple approaches, including systemic chemotherapy. Oxaliplatin (OXA)-based systemic chemotherapy is a widely used treatment for advanced HCC in Asia, where good efficacy has been achieved (4–6). Nevertheless, chemotherapy resistance has become a

tremendous obstacle to the further survival benefit of HCC patients. Identifying the molecules and pathways that give rise to such resistance is critical.

RNA-binding proteins (RBPs) regulate the maturation, translocation, and translation of RNA, making them important in cell development, differentiation, and metabolism (7). We previously showed that the RBP RNA-binding motif protein 8A (RBM8A) is expressed in HCC tumor tissues at higher levels than in normal liver tissues (8, 9). Overexpression of RBM8A is associated with poor overall and progression-free survival in HCC. RBM8A promotes proliferation, migration, and invasion in HCC by activating the epithelial-mesenchymal transition (EMT) (8). Previous studies have shown that EMT is closely related to the promotion of tumor cell metastasis and induction of chemotherapy resistance (10). However, the function of RBM8A in the regulation of chemotherapy resistance remains obscure. More specifically, it has not yet been characterized whether RBM8A is involved in the regulation of OXA resistance *via* initiating EMT in HCC.

The present study explored this hypothesis using a combination of *in vitro* and *in vivo* experiments as well as bioinformatics analyses. Our results identify RBM8A as a potential key factor in OXA resistance in HCC and provide numerous predictions to guide further studies into drug resistance mechanisms.

MATERIALS AND METHODS

Cell Lines and Cell Cultures

Human HCC cell lines (Bel7404, QGY-7703, SMMC-7721, MHCC97L, MHCC97H, HepG2, and SK-HEP-1) and a normal liver cell line (HL7702) were purchased from the Stem Cell Bank of the Chinese Academy of Sciences (Shanghai, China) and were cultured in Dulbecco's modified Eagle's medium (DMEM) with 10% fetal bovine serum (FBS; Invitrogen, Carlsbad, CA, USA) in a humidified atmosphere of 5% carbon dioxide at 37°C.

Establishment of OXA-Resistant HCC Cells

Bel7404 cells were suspended at a density of 1×10^5 cells/mL, cultured for 24 h, then exposed to an induction dose of OXA (8 μ M). After cell growth had stabilized, the drug concentration was increased to 8, 12, 18, 34, 46, 60, 76, 94, 114, and 136 μ M. Each dose was maintained for 15 days. Similarly, MHCC97H cells were suspended at a density of 1×10^5 cells/mL, cultured for 24 h, then exposed to an induction dose of OXA (6 μ M). After cell growth had stabilized, the drug concentration was increased to 6, 9, 13.5, 20.3, 30.4, 40.5, 55, 70, 86, and 102 μ M.

Establishment of Stable Cell Lines in Which RBM8A Was Overexpressed (OE) or Knocked Down (KD)

Our previous research showed that the short hairpin RNA (shRNA) with the sequence 5'-AGAGCATTCACAAACTGAA-3' can reduce endogenous levels of RBM8A by more than 80%

(8). Using this shRNA, we established two stable KD HCC cell lines, one sensitive to OXA (Bel7404-RBM8A-KD) and one resistant to OXA (Bel7404/OXA-RBM8A-KD). As described in our previous work (8), we obtained two stable OE HCC cell lines, one sensitive to OXA (MHCC97H-RBM8A-OE) and one resistant to OXA (MHCC97H/OXA-RBM8A-OE).

Total RNA Isolation and Quantitative Real-Time PCR (qRT-PCR)

Total RNA was isolated from parental cell lines (PCLs) and drug resistant (DR)-HCC cells using TRIzol reagent (Invitrogen, USA), then cDNA was reverse-transcribed from 1 mg of total RNA using PrimeScript RT Reagent (TaKaRa, Dalian, China) following the manufacturer's instructions. Quantitative real-time polymerase chain reaction (qRT-PCR) was performed using SYBR Premix Ex Taq (Takara). PCR primers are described in the **Supplementary Materials and Methods**.

Protein Extraction and Western Blot Analysis

Western blotting was performed as previously described (8) using antibodies against human RBM8A (catalog no. sc-32312, Santa Cruz Biotechnology, Santa Cruz, CA, USA), human actin (HRP-60008, Proteintech, Rosemont, IL, USA), and rabbit IgG (7074, Cell Signaling Technology, Danvers, MA, USA). Additional reagents are described in the **Supplementary Materials and Methods**.

Cell Counting Kit-8 Assay

Cell proliferation and half maximal inhibitory concentration (IC_{50}) were assessed using the Cell Counting Kit-8 (CCK-8) kit (Dojindo, Japan) according to the manufacturer's protocol. To measure IC_{50} , OXA was added to cultures at concentrations of 40, 80, 320, 640, and 1280 μ M, and 48 h later, 10 μ L of CCK8 per 100 μ L medium was added to the wells. The cells were then incubated at 37°C for another 2 h. Finally, the absorbance was measured at 450 nm using a microplate reader (5082Grodig, Tecan, Austria).

Flow Cytometry

Cells were collected and stained with an apoptosis detection kit based on phycoerythrin-conjugated annexin V (FXP018-100, 4A Biotech, Beijing, China) according to the manufacturer's instructions. Apoptosis was analyzed by flow cytometry (FACS Calibur, BD Biosciences, San Jose, CA, USA).

Wound-Healing Assay, Cell Migration, and Invasion Assays

Detailed methods are described in **Supplementary Materials and Methods**.

Xenograft Tumorigenesis in Nude Mice

Mouse studies were conducted according to the Guide for the Care and Use of Laboratory Animals and were approved by the Animal Care and Use Committee of the Affiliated Tumor Hospital of Guangxi Medical University, China. BALB/C nude

mice (5–6 weeks old, 18–22 g) were randomly divided into two groups of eight mice each. Bel7404/OXA-RBM8A-KD and Bel7404/OXA-NC cells (2×10^6 cells in 100 μ L of serum-free DMEM) were injected subcutaneously into nude mice. OXA at 10 mg/kg was injected around the tumor at 1, 2, 4, and 6 weeks after tumor cell injection. The tumor diameter was measured weekly with calipers, and the tumor volume was recorded. After six weeks, the mice were euthanized, and the tumor was removed, weighed, and photographed.

Immunohistochemical Staining

Hematoxylin & eosin (H&E) staining was performed to assess histopathology of tumors in nude mice, and slides were subsequently stained with a horseradish peroxidase kit (UltraTek, Scytek, Utah, USA) for immunohistochemistry. Immunostaining was performed as described (8) using primary antibodies against RBM8A (same as for western blots), E-cadherin, N-cadherin, Snail, ABCG2, ABCB1, ABCC1, or Ki-67 (9027, Cell Signaling Technology) and reagents from Fuzhou Maixin (Fuzhou, China).

Whole-Genome Microarrays

Total RNA was isolated from Bel7404/OXA-RBM8A-KD, Bel7404/OXA-RBM8A-NC, MHCC97H/OXA-RBM8A-OE, and MHCC97H/OXA-RBM8A-NC cells using an RNeasy Micro kit (Qiagen, Hilden, Germany) following the manufacturer's instructions. RNA integrity was assessed using a Bioanalyzer 2100 (Agilent, Santa Clara, CA, USA). Microarray analysis was performed using Affymetrix GeneChip Mouse Genome 430 2.0 Arrays. The arrays were hybridized, washed, and scanned according to the standard Affymetrix protocol. Raw data were normalized using the MAS 5.0 algorithm in GeneSpring 11.0 (Agilent).

Bioinformatics Analysis

Gene expression was profiled using the limma package in R (11–13). Weighted gene coexpression network analysis (WGCNA) (14) was used to analyze the differential expression profile matrix in cell samples, and gene modules showing coexpression were clustered. Among these module genes, the ClusterProfiler package in R (15) was used to analyze Gene Ontology (GO) functions (p value cutoff = 0.01, q value cutoff = 0.01) and Kyoto Encyclopedia of Genes and Genomes (KEGG) pathways (p value cutoff = 0.05, q value cutoff = 0.2).

Pivot regulators were defined as modulators exerting significant regulation over modules involved in RBM8A-induced resistance. In the pivot analysis, the background set was based on the interaction of transcription factors (TFs) with other proteins in the TRRUST v2 database (16). A network of interactions of long non-coding RNA (lncRNA) and microRNA (miRNA) with protein partners was constructed based on data in the RAID v2.0 database (17). Data on regulation of module genes and pivot TFs by RBM8A were obtained by searching databases with STRING v10.5 (18). The results about pivot regulators and KEGG pathways in the gene module were used to generate a comprehensive map of RBM8A regulation underlying OXA resistance in HCC.

Since qRT-PCR and Western blotting showed histone deacetylase 9 (HDAC9) to be the pivotal TF most closely

related to RBM8A-regulated OXA resistance in HCC, the HDAC9-module gene-KEGG signaling pathway was extracted. Finally, a potential mechanism by which the RBM8A-HDAC9 axis regulates drug resistance in HCC was identified.

Statistical Analyses

Data were analyzed using SPSS 17.0 (IBM, Chicago, IL, USA). All experiments in this study were repeated in triplicate unless otherwise specified. All results were expressed as mean \pm standard deviation (SD). Student's t test was used to analyze the statistical significance of differences between groups. Differences associated with $p < 0.05$ were considered significant.

RESULTS

Establishment of OXA-Resistant HCC Cell Lines and Analysis of RBM8A Expression

According to the qRT-PCR and Western blotting results, RBM8A showed the lowest expression in the normal human liver cell line HL7702 and was highly expressed in various human HCC cell lines. Among the HCC cell lines, Bel7404 cells showed the highest expression of RBM8A while MHCC97H cells showed the lowest (Figure 1A). To discover the potential relationship between RBM8A and oxaliplatin resistance in HCC, we first constructed OXA-resistant HCC cell lines. The schematic representation of the protocol used to obtain OXA-resistant HCC cells from the PCL (Figure 1B). The mesenchymal phenotype of DR-HCC cells is shown in Figure 1C. Expression of RBM8A was significantly higher in Bel7404/OXA and MHCC97H/OXA cells than in Bel7404 and MHCC97H PCLs, based on qRT-PCR and Western blotting (Figure 1D). These results indicate that the expression level of RBM8A may be related to OXA resistance in HCC.

High RBM8A Expression Promotes Tumor Progression and OXA Resistance of HCC Cells In Vitro

To study the specific role of RBM8A in regulating OXA resistance in HCC cells, we conducted phenotypic studies related to drug resistance. Knocking down RBM8A in Bel7404 cells, which normally express the protein at high levels, significantly reduced proliferation of PCLs and DR-HCC cells. Ectopic expression of RBM8A in MHCC97H cells, which normally express the protein at low levels, significantly enhanced proliferation of PCLs and DR-HCC cells (Figure 2A). The IC_{50} of OXA was significantly higher in DR-HCC cell lines than in PCLs. IC_{50} was highest in MHCC97H/OXA-RBM8A-OE cells. Knockdown of RBM8A in Bel7404/OXA cells significantly reduced IC_{50} , consistent with the proliferation results (Figure 2B). Flow cytometry showed that, regardless of the cell type, the apoptosis level was significantly lower in DR-HCC cell lines than in PCLs (Figures 2C, D). In Bel7404 cells with RBM8A knockdown, apoptosis levels were significantly higher in PCLs and DR-HCC cells than in control cells. Conversely, overexpressing RBM8A in MHCC97H cells led to

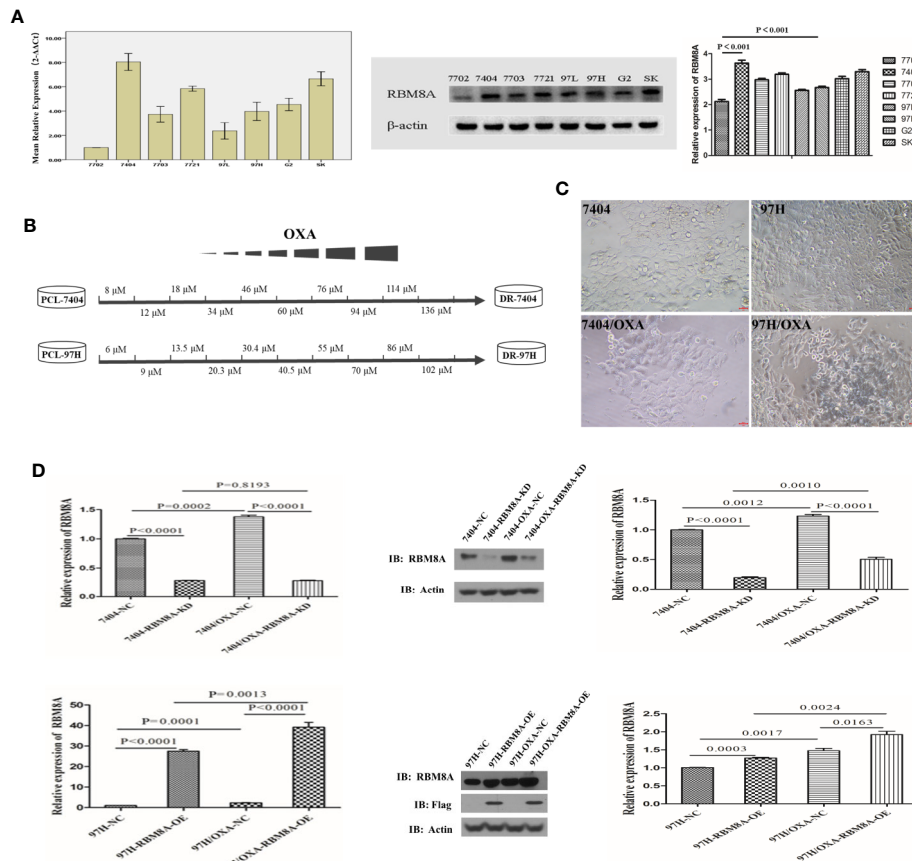


FIGURE 1 | Selection of OXA-resistant hepatocellular carcinoma (HCC) cells and establishment of cell lines in which RBM8A was overexpressed or knocked down. **(A)** Real time (RT)-PCR and western blot analysis of RBM8A expression in HCC cell lines. Western blot results were quantitated. **(B)** Schematic representation of the protocol used to obtain OXA-resistant HCC cells from the parental cell line (PCL). During concentration-elevation and intermittent induction treatment with OXA, each dose was maintained for 15 days. OXA-resistant cell lines were obtained by the end of 6 months. **(C)** Representative phase contrast images of Bel7404 PCLs and drug-resistant cells (DR-HCC cells, *left panels*) or MHCC97H PCLs and DR-HCC cells (*right panels*). Magnification, 20×. Scale bar, 20 μm. **(D)** Knockdown (KD) and overexpression (OE) efficiency of RBM8A in PCLs and DR-HCC cells based on RT-PCR and western blot analysis, compared with the negative control (NC). Western blot data were quantitated (*right panels*). Data were expressed as mean ± SD of three independent experiments, or were representative of three independent observations.

significantly lower apoptosis levels in PCLs and DR-HCC cells than in control cells.

In Bel7404 and MHCC97H cells, migration and invasion of the DR-HCC cell lines were significantly greater than those in the corresponding PCLs (**Figures 3A–C**). Drug-resistant Bel7404/OXA-RBM8A-KD cells showed significantly less migration and invasion than drug-resistant Bel7404/OXA-NC cells at 24 and 72 h. Conversely, MHCC97H/OXA-RBM8A-OE cells showed significantly greater migration and invasion than MHCC97H/OXA-NC cells at the same time points.

Overexpression of the ATP-binding cassette (ABC) membrane transport pump is one of the most important contributors to multidrug resistance (19). Thus, we explored the relationship between the expression of RBM8A and that of ABC subfamily G member 2 (ABCG2), ABC subfamily B member 1 (ABCB1) and ABC subfamily C member 1 (ABCC1) in PCLs and DR-HCC cells. Western blotting showed that ABCG2, ABCB1, and ABCC1 levels were significantly higher in Bel7404 and MHCC97H DR-HCC

cells than in the corresponding PCLs (**Figures 3D, E**). These three proteins were expressed at significantly lower levels in Bel7404/OXA-RBM8A-KD cells than in Bel7404/OXA-NC cells. Conversely, they were expressed at significantly higher levels in MHCC97H/OXA-RBM8A-OE cells than in MHCC97H/OXA-NC cells. Overall, our data indicate that RBM8A promotes proliferation, migration and invasion of HCC cells, while inhibiting OXA-induced apoptosis.

High RBM8A Expression Regulates OXA-Resistance via EMT in HCC In Vitro

Previous reports demonstrate that EMT processes contribute to tumor progression, cancer cell invasion, and therapy resistance (20). Using rhodamine-labeled fluoropeptide to track changes in the cytoskeleton, we found that OXA-resistant Bel7404 and MHCC97H cells were spindle-shaped and exhibited less cell-cell contact than the corresponding PCLs (**Figure 4A**). The ectopic expression of RBM8A in MHCC97H/OXA HCC cells

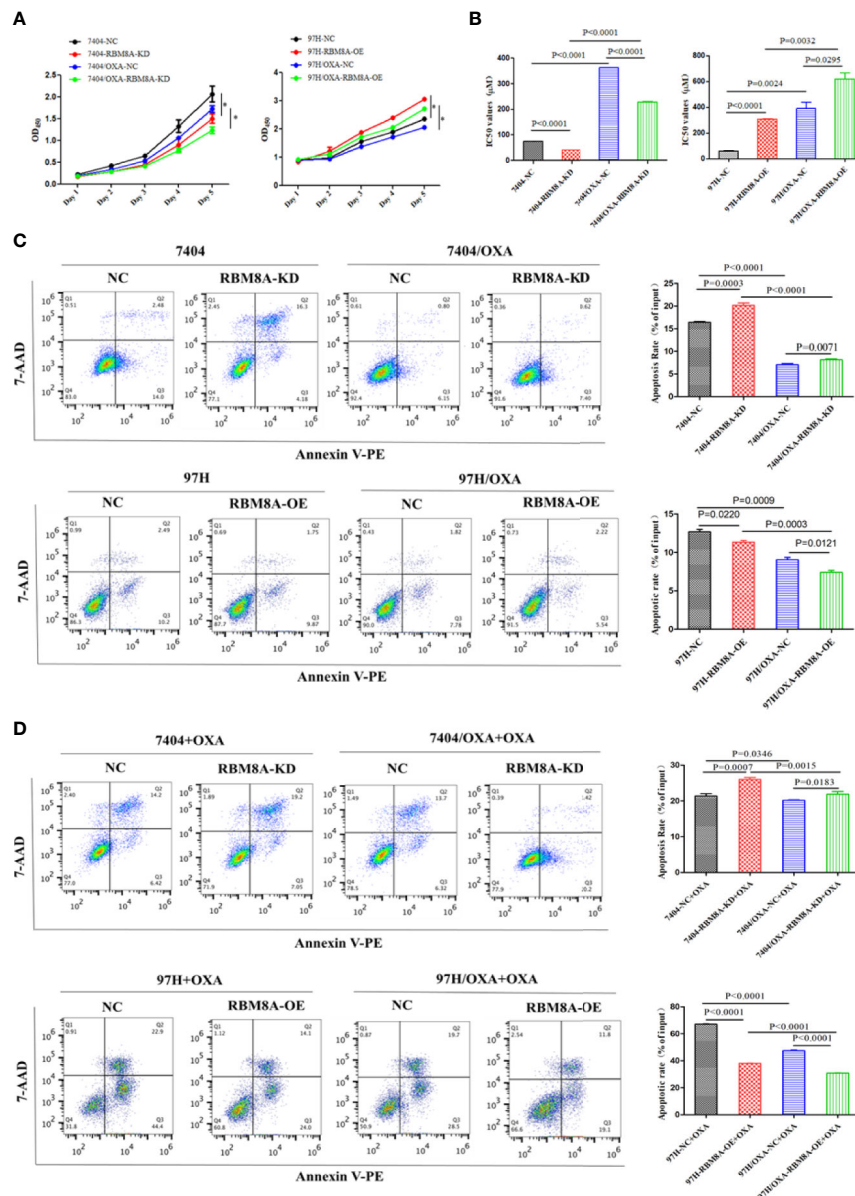


FIGURE 2 | Modulation of RBM8A expression affects proliferation, apoptosis and cell cycle progression in parental cell lines (PCLs) and drug-resistant (DR)-hepatocellular carcinoma (HCC) cells. **(A)** Cell proliferation measured using the Cell Counting Kit-8. * $P < 0.001$. **(B)** Half maximal inhibitory concentration (IC_{50}) of oxaliplatin (OXA) when cells were treated for 48 h. **(C)** Apoptosis determined by flow cytometry. Representative quadrant figures were presented on the left, and rates of apoptotic PCLs and DR-HCC cells were shown on the right. **(D)** Apoptosis in PCLs and DR-HCC cells at 48 h after OXA treatment.

induced loose cell contact and spindle-shaped morphology reminiscent of EMT, whereas RBM8A knockdown in Bel7404/OXA cells resulted in a dramatic shift in the cell morphology from loose cell growth to a tighter cell-cell adherence characteristic of epithelial cells. Furthermore, we sought to determine whether RBM8A levels were associated with epithelial and mesenchymal markers. OXA-resistant Bel7404 or MHCC97H cells showed lower expression of the epithelial protein E-cadherin than the corresponding PCLs, but higher expression of the mesenchymal proteins N-cadherin and Snail

(Figures 4B–D). Western blotting indicated that MHCC97H/OXA-RBM8A-OE cells, regardless of whether they had been treated with OXA, showed significantly lower levels of epithelial protein E-cadherin but higher levels of mesenchymal proteins N-cadherin and Snail than MHCC97H/OXA-NC cells. Conversely, Bel7404/OXA-RBM8A-KD showed significantly higher levels of E-cadherin and lower levels of N-cadherin and Snail than Bel7404/OXA-NC cells (Figures 4E, F). Further suppression of the EMT pathway using the EMT inhibitor C19 significantly reversed the proliferation, invasion and migration of RBM8A-

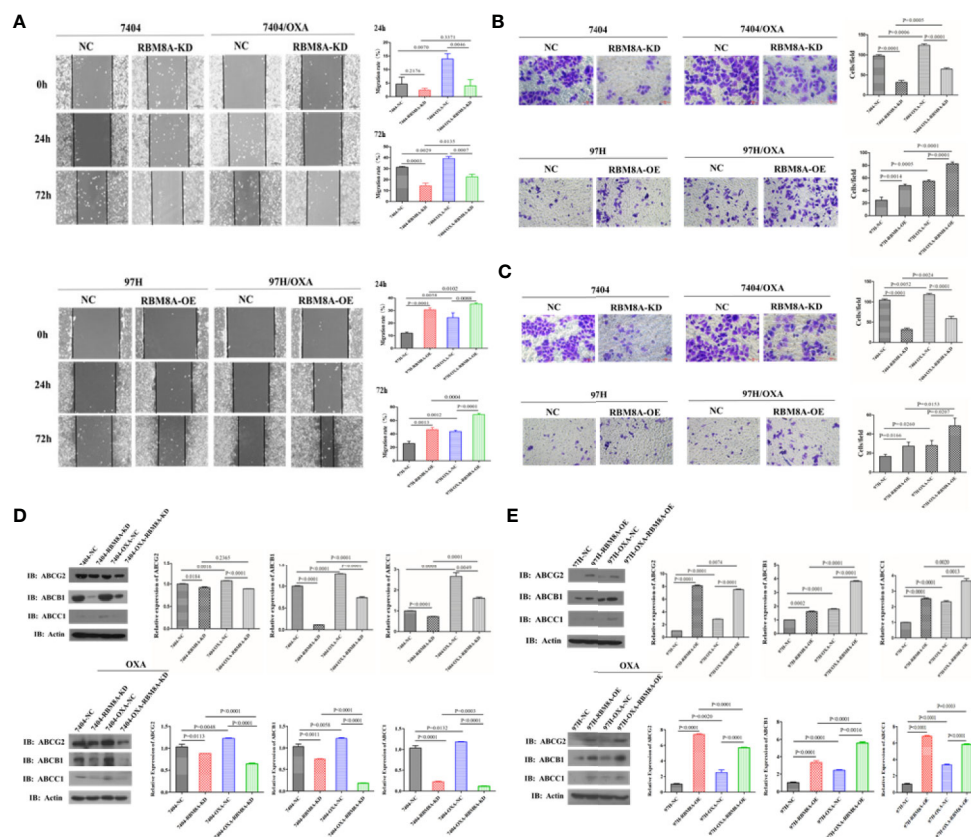


FIGURE 3 | Modulation of RBM8A expression affects the migratory and invasive potential of parental cell lines (PCLs) and drug-resistant (DR)-hepatocellular carcinoma (HCC) cells, as well as the expression of proteins related to drug resistance. **(A)** Wound-healing assay. The scraped areas were photographed at 0, 24, and 72 h after scraping. Migration efficiency was quantitated at 24 and 72 h after scraping (*right panel*). Magnification, 10 \times . Scale bar, 200 μ m. **(B)** Transwell assay. Representative examples of each experimental group are shown. Migration efficiency was quantitated at 24 and 72 h (*right panel*). Magnification, 40 \times . Scale bar, 50 μ m. **(C)** Matrigel-Transwell assay. Representative photographs and quantitation were shown. Data were either representative of three similar observations, or were shown as the mean \pm SD of three experiments. Magnification, 40 \times . Scale bar, 50 μ m. **(D)** Western blot analysis of PCL-Bel7404-NC, PCL-Bel7404-RBM8A-KD, DR-Bel7404-NC and DR-Bel7404-RBM8A-KD. Cells were analyzed without OXA treatment (*second row*) or with OXA treatment (*third row*). Data were representative of three similar observations or were shown as the mean \pm SD of three experiments. **(E)** Western blot analysis of PCL-MHCC97H-NC, PCL-MHCC97H-RBM8A-OE, DR-MHCC97H-NC and DR-MHCC97H-RBM8A-OE cells as in **(D)**.

enhanced PCLs and DR-HCC cells (**Figures 5A–D**). Taken together, these results and our previous studies indicate that the EMT pathway is one of the important mechanisms by which RBM8A regulates the malignant phenotype and OXA resistance of HCC.

RBM8A Regulates OXA Resistance in HCC Xenograft Models *via* the EMT

To evaluate *in vivo* the ability of RBM8A to promote OXA resistance in HCC through the EMT, nude mouse xenograft models were established using Bel7404/OXA-NC and Bel7404/OXA-RBM8A-KD cells. Tumor size, tumor formation rate, and body weight were lower in Bel7404/OXA-RBM8A-KD animals than in control mice (**Figures 6A, B**). Compared to Bel7404/OXA-RBM8A-NC tumors, Bel7404/OXA-RBM8A-KD tumors expressed lower levels of Ki-67, ABCG2, ABCB1, ABCC1, and the mesenchymal proteins N-cadherin and Snail, but higher levels of the epithelial protein E-cadherin (**Figures 6C, D**).

These data suggest that the reduction of RBM8A expression inhibits HCC growth and EMT processes, sensitizing HCC to OXA *in vitro*.

RBM8A Regulates the Transcription of Genes in OXA Resistance in HCC *via* a Network Involving Tumor-Associated TFs, ncRNAs, and Signaling Pathways Expression of Dysregulated Molecules Associated With RBM8A in OXA-Resistant HCC

The flow chart of the bioinformatics analysis is shown in **Supplementary Figure 1A**. Wayne mapping identified 8365 genes differentially expressed between Bel7404/OXA-NC and Bel7404/OXA-RBM8A-KD cells, as well as between MHCC97H/OXA-NC vs. MHCC97H/OXA-RBM8A-OE cells (**Supplementary Figure 1B**). These genes may be associated with RBM8A-mediated OXA resistance in HCC (**Supplementary Table S1**). WGCNA of these differentially expressed genes revealed patterns of

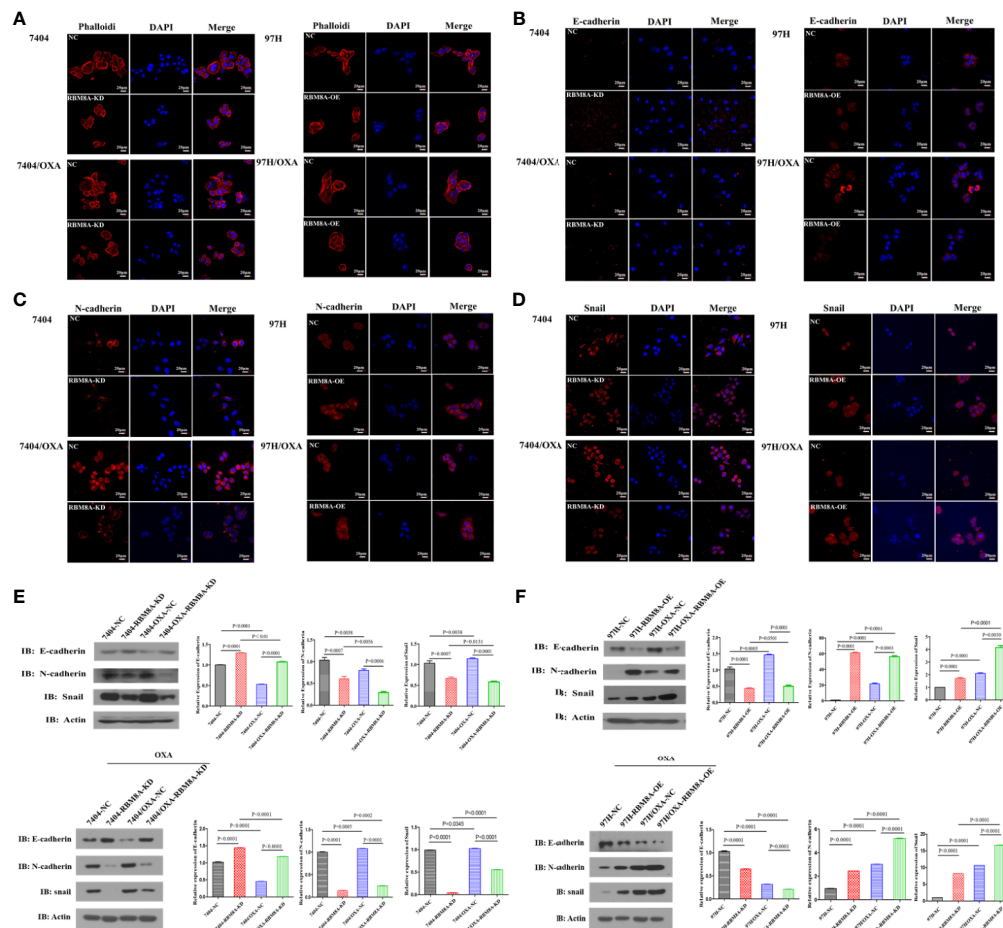


FIGURE 4 | Modulation of RBM8A expression affects the epithelial-mesenchymal transition (EMT) in parental cell lines (PCL) and drug-resistant (DR)-hepatocellular carcinoma (HCC) cells. **(A–D)** Immunofluorescence staining of the **(A)** cytoskeleton, **(B)** E-cadherin, **(C)** N-cadherin, and **(D)** Snail (all red). All confocal microscopy images show the merging with DAPI (blue) in PCLs and DR-HCC cells upon RBM8A knockdown or overexpression. Scale bar, 20 μ m. **(E)** Western blot analysis of E-cadherin, N-cadherin, and Snail in PCL-Bel7404 and DR-Bel7404 cells with or without RBM8A knockdown. Cells were analyzed without OXA treatment (*second row*) or with OXA treatment (*third row*). Data were expressed as the mean \pm SD of three independent experiments or were representative of three independent observations. **(F)** Western blot analysis of E-cadherin, N-cadherin, and Snail protein expression in PCL-MHCC97H and DR-MHCC97H cells with or without RBM8A overexpression as in **(E)**.

coexpression that we were able to organize into five modules of OXA resistance-related genes in HCC (**Supplementary Figures 1C–E**). Based on the association between gene modules and cells, we found that the fourth module positively correlated the most strongly with the Bel7404/OXA-RBM8A-KD phenotype, while the third module positively correlated strongly with the MHCC97H/OXA-RBM8A-OE phenotype (**Supplementary Figures 1F, G**).

Identification of the Biological Molecular Network of RBM8A in OXA-Resistant HCC

Exploring the functions and pathways involved in the relevant modules helps to establish molecular bridges between gene modules and disease pathology and pharmacology, potentially deepening understanding of the molecular mechanism. Therefore, we analyzed the enrichment of GO biological processes and KEGG pathways in the five modules. From these

results, we found that the potential functions of genes in the five modules were mainly related to mRNA splicing, ribonucleoprotein complex biogenesis, and ncRNA processing (**Supplementary Table S2**). RBM8A-related genes were involved mainly in the following KEGG pathways: PI3K-Akt signaling, MAPK signaling, viral carcinogenesis, mRNA surveillance, and cell cycle (**Supplementary Table S3**).

We used TF- and ncRNA-targeting regulatory genes as a background set for hypergeometric prediction analysis. The results identified 1663 ncRNAs and 38 TFs with regulatory influence over module genes, which we considered candidate pivotal regulators (**Supplementary Tables S4 and S5**). Among them, MALAT1, MYCN, HDAC9, FENDRR, and other key regulatory nodes showed significant regulatory influence over more than one module and thus were identified as core pivot regulators. These core pivot regulators may be driven by RBM8A

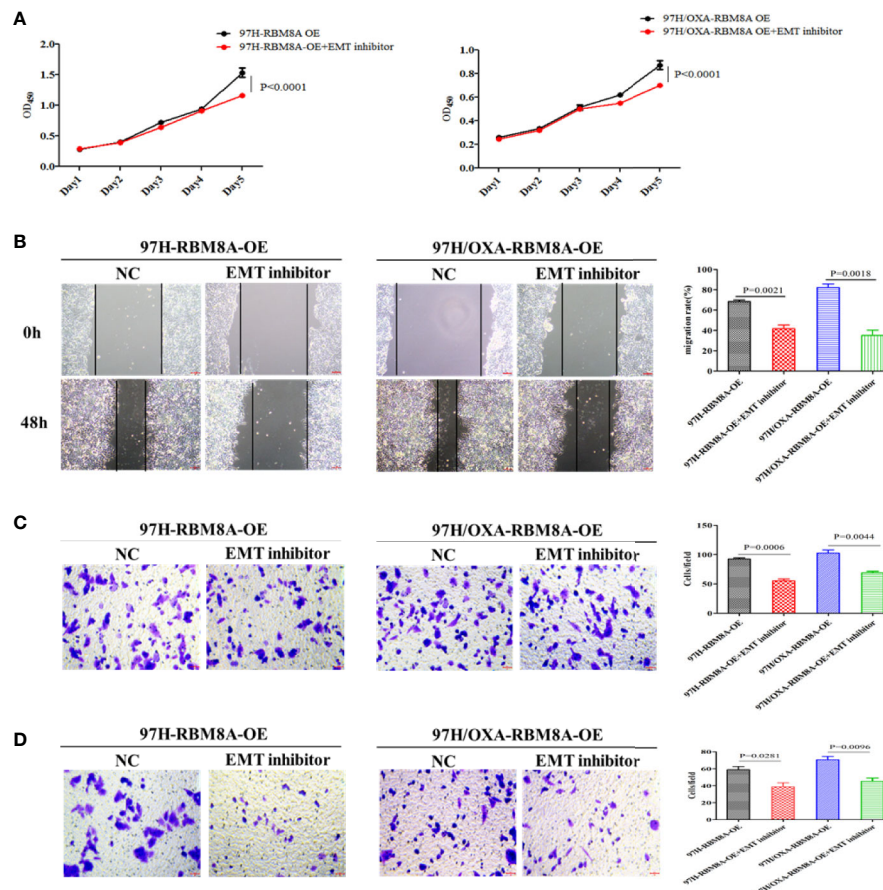


FIGURE 5 | Involvement of the epithelial-mesenchymal transition (EMT) in RBM8A-mediated proliferation, invasion and drug resistance of hepatocellular carcinoma (HCC) cells. **(A)** Cell proliferation was analyzed in PCL-MHCC97H-NC, PCL-MHCC97H-RBM8A-OE, DR-MHCC97H-NC and DR-MHCC97H-RBM8A-OE cells in the presence or absence of the EMT inhibitor C19 using the CCK8 assay. **(B)** Wound-healing assay with or without EMT inhibitor C19. The scraped areas were photographed at 0 and 48 h after scraping. Migration efficiency was quantitated at 48 h after scraping (right). **(C)** Transwell analysis with or without EMT inhibitor C19. **(D)** Matrigel-Transwell analysis with or without EMT inhibitor C19. Magnification, 40×. Scale bar, 50 μ m.

and may regulate genes and pathways related to OXA resistance in HCC. Based on the genes within the modules and the KEGG signaling pathways, we obtained a comprehensive map of RBM8A regulation of OXA resistance in HCC (**Figure 7A**).

Combining the WGCNA and hypergeometric predictions, we selected the following pivotal regulators with significant effects on the module genes: the lncRNAs MALAT1 and FENDRR, and the TFs MYC, STAT3, P53, E2F1, YY1, HDAC1, and HDAC9. qRT-PCR and Western blotting were used to verify the correlation between RBM8A and core pivotal regulator expression in HCC cell lines *in vitro* (**Figure 7B** and **Supplementary Figure 2**). HDAC9 expression was significantly higher in DR-HCC cells than in PCLs, and in both cell types, it was up- or down-regulated after RBM8A was overexpressed or knocked down, respectively. Thus, HDAC9 is closely related to RBM8A-regulated OXA resistance in HCC cells.

Based on the proposed downstream signaling network involving RBM8A and HDAC9 (**Figure 7C**), NFKB1 and TP53 are predicted to be direct target genes of HDAC9. In addition to

the NRAS oncogene, several cyclin-dependent kinase and MAPK family genes may also be involved. Enrichment analysis suggests that the module genes regulated by the RBM8A-HDAC9 axis participate mainly in the PI3K-Akt and MAPK pathways, which help control cell proliferation, inflammation, apoptosis, and the cell cycle.

DISCUSSION

RBM8A (also known as Y14) was identified only within the last decade and has since been shown to play roles in the formation, degradation, translation, and quality control of mRNA as a core component in the exon junction complex (21, 22). Abnormal expression of RBM8A may play an important role in activating signal transduction pathways that drive oncogenesis (9, 23). We found that RBM8A overexpression promoted proliferation, reduced apoptosis and increased the chemotherapeutic resistance of HCC cells to OXA, while RBM8A knockdown

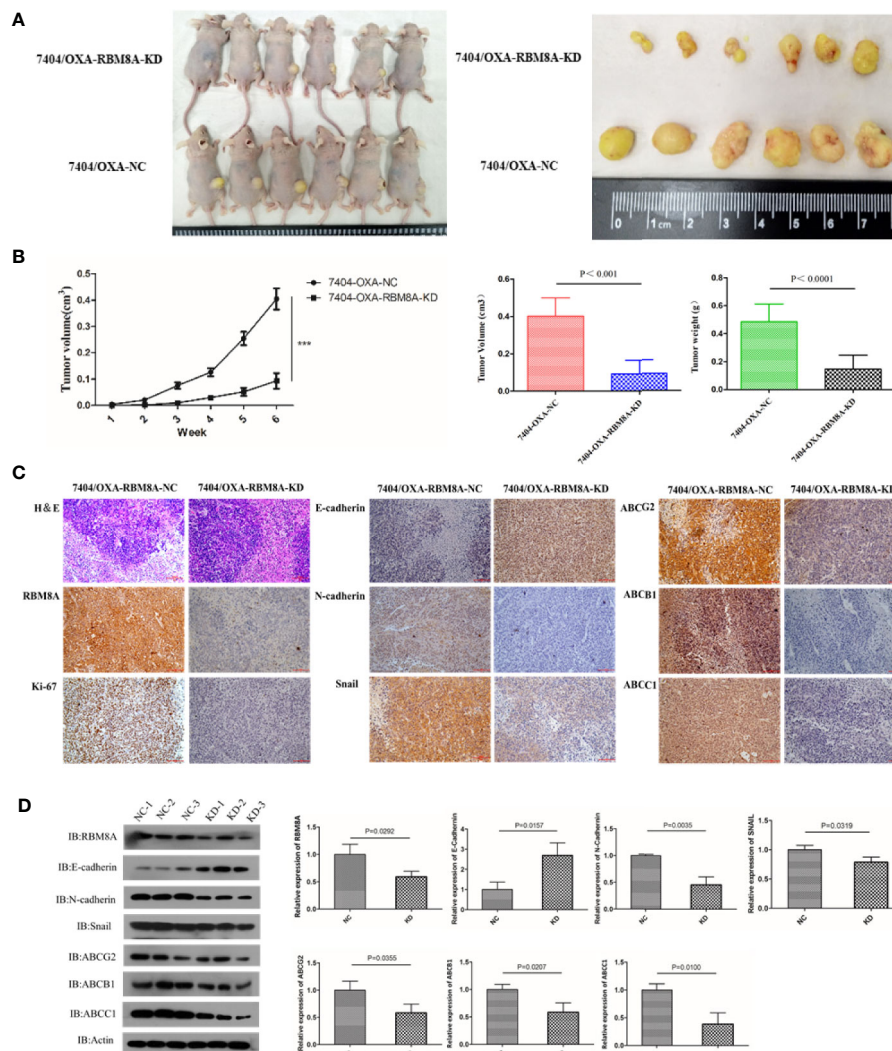


FIGURE 6 | Effects of RBM8A on drug-resistant (DR)-hepatocellular carcinoma (HCC) tumorigenesis *in vivo*. **(A)** Bel7404/OXA-RBM8A-KD and control cells were injected orthotopically into mammary fat pads of nude mice, which were then injected with OXA at 10 mg/kg around the tumor at 1, 2, 4, and 6 weeks. The growth of tumors was followed during a six-week period. Photographs of primary tumors are shown on the right. **(B)** Comparison of tumor volume in Bel7404/OXA-RBM8A-KD and Bel7404/OXA-RBM8A-NC animals. Mice injected with Bel7404/OXA-RBM8A-KD cells formed smaller ($p < 0.0001$) and lighter ($p = 0.0004$) tumors than mice injected with control cells (NC). $*** < 0.001$. **(C, D)** Immunohistochemical staining and western blotting of Bel7404/OXA-RBM8A-KD and Bel7404/OXA-RBM8A-NC tumors. Data were expressed as the mean \pm SD of three independent experiments or were representative of three independent observations. Magnification, 20 \times . Scale bar, 100 μ m.

reversed these effects, consistent with reports that the deletion of the RBM8A gene down-regulates Bcl-Xs, Bim, and Mcl-1, as well as several proapoptotic genes, including members of the Bcl-2 family, thereby inducing apoptosis (24).

Malignant tumors are often resistant to antitumor drugs, they show unlimited proliferative ability, and they eventually progress to local infiltration and distant metastasis (25). In our study, RBM8A overexpression further increased the migration and invasion of HCC cells, and this involved the promotion of the EMT, which is the first step in invasion and metastasis (20, 26). Consistently with our work, a previous study (27) reported that

OXA-resistant HCC cell lines showed higher incidence of a mesenchymal phenotype.

How HCC cells become resistant to OXA is complex. Several mechanisms have been proposed, including apoptosis escape, autophagy activation, drug excretion, and enhanced epigenetic transformation (28–32). Inactivation of multiple signaling pathways is thought to alter expression of genes involved in apoptosis and proliferation to confer resistance, and several cytokines also control one another through regulatory networks. The EMT process is also central to most models of drug resistance (25, 33–35). In order to take into account these

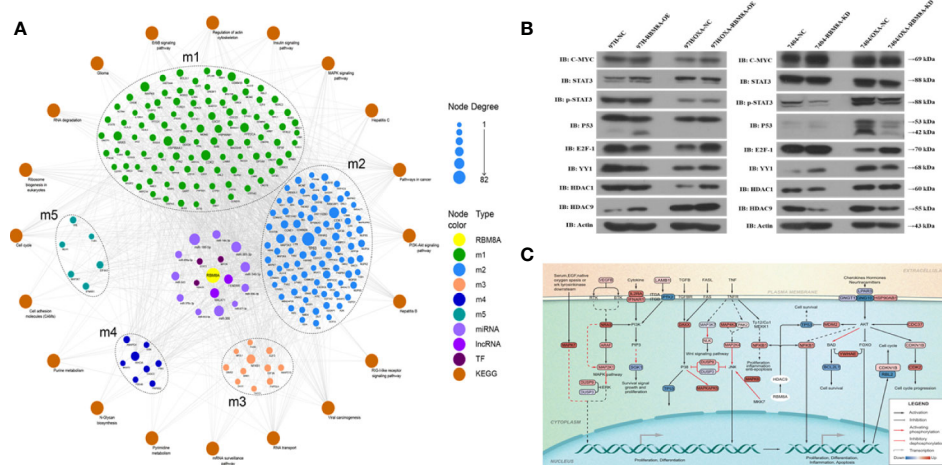


FIGURE 7 | Molecular network showing how RBM8A may regulate oxaliplatin (OXA) resistance in hepatocellular carcinoma (HCC). **(A)** Bioinformatics analysis integrating the regulatory information of RBM8A on module genes and pivot factors to construct a comprehensive overview of RBM8A-mediated OXA resistance in HCC. In this landscape, long non-coding RNAs (lncRNAs), microRNAs (miRNAs), and transcription factors (TFs) mediate the ability of RBM8A-regulated module genes and their downstream signaling pathways to confer drug resistance on HCC cells. **(B)** Western blot analysis of the expression of transcription factors MYC, STAT3, P53, E2F1, YY1, HDAC1, and HDAC9 in HCC cell lines. Western blotting revealed that, after overexpression or knockdown of RBM8A in parental cell lines (PCLs) and drug-resistant (DR)-HCC cells, HDAC9 expression regulated by RBM8A was associated with OXA resistance in HCC cells. **(C)** Bioinformatics analysis combined with quantitative real time PCR (qRT-PCR) and western blotting revealed that HDAC9 is the pivotal transcription factor most closely related to the RBM8A-mediated regulation of OXA resistance in HCC. The HDAC9-module gene-KEGG signaling pathway was extracted, and the potential mechanism by which the RBM8A-HDAC9 axis regulates drug resistance in HCC was identified.

multi-dimensional interactions, a comprehensive analysis combining experimental and bioinformatics approaches is needed. Using such an approach, we identified several TFs and ncRNAs as well as their corresponding metabolic pathways that may help RBM8A regulate OXA resistance in HCC (Figure 6 and Supplementary Tables S4 and S5).

Several of these TFs and ncRNAs have already been implicated in HCC growth and drug resistance, validating our approach. In MHCC97H/OXA cells, expression of most genes involved in cell death or apoptosis (including Ras, MAPK, and p53 pathway genes) is altered relative to OXA-sensitive cells (36), and genes encoding TFs and kinases are the most up-regulated. The ncRNAs miR-125 (35), miR-31 (37), H19 (38), and NR2F1 (39) have been linked to the development and progression of HCC and drug resistance. NF- κ B, PI3K/Akt, GSK3 β / β -catenin, and HIF-1 α signaling pathways have also been implicated in HCC chemoresistance (40–43).

We identified and validated HDAC9 as a key TF that likely helps RBM8A regulate OXA resistance in HCC. Abnormally high HDAC9 expression is closely related to proliferation, invasion, and metastasis of various tumor types (44–48), and it may up-regulate genes that participate in the oncogenic Ras, VEGF, MAPK, and EGFR signaling pathways (49). HDAC9 is known to regulate the transcription of tumor suppressor gene p53 (47), deacetylated FoxO1 (50), SOX9 (51), and transcriptional coactivator with PDZ-binding motif (TAZ) (52). Changes in HDAC inhibitors show promise as anticancer treatments (53, 54). Our study is one of the few to analyze HDAC9 in the context of HCC. Given that previous work has shown that HDAC9 can down-regulate miR-376a and

thereby promote cancer (55), future studies should identify genes, miRNAs and ncRNAs targeted by HDAC9 in drug-resistant HCC.

CONCLUSIONS

Our study shows that RBM8A can induce EMT in HCC cells, thereby affecting proliferation, apoptosis, migration, and invasion, as well as promoting OXA resistance. Gene array combined with bioinformatics analysis revealed that RBM8A has a wide range of transcriptional regulatory capabilities in drug-resistant HCC, including the ability to regulate several important tumor-related signaling pathways. In particular, HDAC9 was identified as an important mediator of RBM8A-induced OXA resistance. These data suggest that RBM8A and its related regulatory pathways represent potential markers of OXA resistance and potential therapeutic targets in HCC.

DATA AVAILABILITY STATEMENT

The raw data supporting the conclusions of this article will be made available by the authors, without undue reservation.

ETHICS STATEMENT

The animal study was reviewed and approved by Animal Care and Use Committee of the Affiliated Tumor Hospital of Guangxi Medical University.

AUTHOR CONTRIBUTIONS

RL, JY, and YL came up with the design and conception. The data analysis and visualization were conducted by JZ, ZHL, ZL, QL, XL, and YL. The original writing of the draft and its editing were by JY and YL. All authors contributed to the article and approved the submitted version.

FUNDING

This research was supported by the National Natural Science Foundation of China (NO. 81660498, 82060427 and 81803007), Guangxi Key Research and Development Plan (NO. GUIKEAB19245002), Guangxi Scholarship Fund of Guangxi Education Department, General Program of Guangxi Natural Science Foundation (NO. 2020GXNSFAA259080), Youth Talent Fund Project of Guangxi Natural Science Foundation (NO. 2018GXNSFBA281030, 2018GXNSFBA281091), Guangxi Medical and Health Appropriate Technology Development and Application Project (No. S2017101, S2018062), Guangxi Medical

University Training Program for Distinguished Young Scholars, Science and Technology Plan Project of Qingxiu District, Nanning (NO. 2020037, 2020038).

ACKNOWLEDGMENTS

This manuscript has been released as a pre-print at Research Square [+https://doi.org/10.21203/rs.3.rs-15789/v1+], Yan Lin, Rong Liang, Jinyan Zhang et al. Mechanism and molecular network of RBM8A-mediated regulation of oxaliplatin resistance in hepatocellular carcinoma *via* EMT, 03 March 2020, PREPRINT.

SUPPLEMENTARY MATERIAL

The Supplementary Material for this article can be found online at: <https://www.frontiersin.org/articles/10.3389/fonc.2020.585452/full#supplementary-material>

REFERENCES

- Siegel RL, Miller KD, Jemal A. Cancer statistics, 2018. *CA Cancer J Clin* (2018) 68:7–30. doi: 10.3322/caac.21442
- Cheng AL, Kang YK, Chen Z, Tsao CJ, Qin S, Kim JS, et al. Efficacy and safety of sorafenib in patients in the Asia-Pacific region with advanced hepatocellular carcinoma: a phase III randomised, double-blind, placebo-controlled trial. *Lancet Oncol* (2009) 10:25–34. doi: 10.1016/S1470-2045(08)70285-7
- Qin S, Kruger E, Tan SC, Cheng S, Wang N, Liang J. Cost-effectiveness analysis of FOLFOX4 and sorafenib for the treatment of advanced hepatocellular carcinoma in China. *Cost Eff Resour Alloc* (2018) 16:29. doi: 10.1186/s12962-018-0112-0
- Petrelli F, Coinu A, Borgonovo K, Cabiddu M, Ghilardi M, Lonati V, et al. Oxaliplatin-based chemotherapy: a new option in advanced hepatocellular carcinoma. a systematic review and pooled analysis. *Clin Oncol (R Coll Radiol)* (2014) 26:488–96. doi: 10.1016/j.clon.2014.04.031
- Qin S, Bai Y, Lim HY, Thongprasert S, Chao Y, Fan J, et al. Randomized, multicenter, open-label study of oxaliplatin plus fluorouracil/leucovorin versus doxorubicin as palliative chemotherapy in patients with advanced hepatocellular carcinoma from Asia. *J Clin Oncol* (2013) 31:3501–8. doi: 10.1200/JCO.2012.44.5643
- 2020CSCO原发性肝癌诊疗指南.
- Marx V. Profiling the dress codes of RNA-binding proteins. *Nat Methods* (2018) 15:655–8. doi: 10.1038/s41592-018-0117-9
- Liang R, Lin Y, Ye JZ, Yan XX, Liu ZH, Li YQ, et al. High expression of RBM8A predicts poor patient prognosis and promotes tumor progression in hepatocellular carcinoma. *Oncol Rep* (2017) 37:2167–76. doi: 10.3892/or.2017.5457
- Lin Y, Liang R, Qiu Y, Lv Y, Zhang J, Qin G, et al. Expression and gene regulation network of RBM8A in hepatocellular carcinoma based on data mining. *Aging (Albany NY)* (2019) 11:423–47. doi: 10.18632/aging.101749
- Dongre A, Weinberg RA. New insights into the mechanisms of epithelial-mesenchymal transition and implications for cancer. *Nat Rev Mol Cell Biol* (2019) 20:69–84. doi: 10.1038/s41580-018-0080-4
- Law CW, Chen Y, Shi W, Smyth GK. voom: Precision weights unlock linear model analysis tools for RNA-seq read counts. *Genome Biol* (2014) 15:R29. doi: 10.1186/gb-2014-15-2-r29
- Ritchie ME, Phipson B, Wu D, Hu Y, Law CW, Shi W, et al. limma powers differential expression analyses for RNA-sequencing and microarray studies. *Nucleic Acids Res* (2015) 43:e47. doi: 10.1093/nar/gkv007
- Smyth GK. Linear models and empirical bayes methods for assessing differential expression in microarray experiments. *Stat Appl Genet Mol Biol* (2004) 3:Article3. doi: 10.2202/1544-6115.1027
- Langfelder P, Horvath S. WGCNA: an R package for weighted correlation network analysis. *BMC Bioinf* (2008) 9:559. doi: 10.1186/1471-2105-9-559
- Yu G, Wang LG, Han Y, He QY. clusterProfiler: an R package for comparing biological themes among gene clusters. *OMICS* (2012) 16:284–7. doi: 10.1089/omi.2011.0118
- Han H, Cho JW, Lee S, Yun A, Kim H, Bae D, et al. TRRUST v2: an expanded reference database of human and mouse transcriptional regulatory interactions. *Nucleic Acids Res* (2018) 46:D380–380D386. doi: 10.1093/nar/gkx1013
- Yi Y, Zhao Y, Li C, Zhang L, Huang H, Li Y, et al. RAID v2.0: an updated resource of RNA-associated interactions across organisms. *Nucleic Acids Res* (2017) 45:D115–D115D118. doi: 10.1093/nar/gkw1052
- Szklarczyk D, Franceschini A, Wyder S, Forslund K, Heller D, Huerta-Cepas J, et al. STRING v10: protein-protein interaction networks, integrated over the tree of life. *Nucleic Acids Res* (2015) 43:D447–52. doi: 10.1093/nar/gku1003
- Muriithi W, Macharia LW, Heming CP, Echevarria JL, Nyachio A, Filho PN, et al. ABC transporters and the hallmarks of cancer: roles in cancer aggressiveness beyond multidrug resistance. *Cancer Biol Med* (2020) 17:253–69. doi: 10.20892/j.issn.2095-3941.2019.0284
- Dudas J, Ladanyi A, Ingruber J, Steinbichler TB, Riechmann H. Epithelial to Mesenchymal Transition: A Mechanism that Fuels Cancer Radio/Chemoresistance. *Cells* (2020) 9(2):428. doi: 10.3390/cells9020428
- Chuang TW, Chang WL, Lee KM, Tarn WY. The RNA-binding protein Y14 inhibits mRNA decapping and modulates processing body formation. *Mol Biol Cell* (2013) 24:1–13. doi: 10.1091/mbc.E12-03-0217
- Le Hir H, Saulière J, Wang Z. The exon junction complex as a node of post-transcriptional networks. *Nat Rev Mol Cell Biol* (2016) 17:41–54. doi: 10.1038/nrm.2015.7
- Chuang TW, Lu CC, Su CH, Wu PY, Easwaran S, Lee CC, et al. The RNA Processing Factor Y14 Participates in DNA Damage Response and Repair. *iScience* (2019) 13:402–15. doi: 10.1016/j.isci.2019.03.005
- Michelle L, Cloutier A, Toutant J, Shkreta L, Thibault P, Durand M, et al. Proteins associated with the exon junction complex also control the alternative splicing of apoptotic regulators. *Mol Cell Biol* (2012) 32:954–67. doi: 10.1128/MCB.06130-11
- Chaffer CL, San Juan BP, Lim E, Weinberg RA. EMT, cell plasticity and metastasis. *Cancer Metastasis Rev* (2016) 35:645–54. doi: 10.1007/s10555-016-9648-7

26. Yeldag G, Rice A, Del Río Hernández A. Chemoresistance and the Self-Maintaining Tumor Microenvironment. *Cancers (Basel)* (2018) 10(12):471. doi: 10.3390/cancers10120471
27. Ma JL, Zeng S, Zhang Y, Deng GL, Shen H. Epithelial-mesenchymal transition plays a critical role in drug resistance of hepatocellular carcinoma cells to oxaliplatin. *Tumour Biol* (2016) 37:6177–84. doi: 10.1007/s13277-015-4458-z
28. Ceballos MP, Rigalli JP, Ceré LI, Semeniuk M, Catania VA, Ruiz ML. ABC Transporters: Regulation and Association with Multidrug Resistance in Hepatocellular Carcinoma and Colorectal Carcinoma. *Curr Med Chem* (2019) 26:1224–50. doi: 10.2174/0929867325666180105103637
29. Du H, Yang W, Chen L, Shi M, Seewoo V, Wang J, et al. Role of autophagy in resistance to oxaliplatin in hepatocellular carcinoma cells. *Oncol Rep* (2012) 27:143–50. doi: 10.3892/or.2011.1464
30. Ohata Y, Shimada S, Akiyama Y, Mogushi K, Nakao K, Matsumura S, et al. Acquired Resistance with Epigenetic Alterations Under Long-Term Antiangiogenic Therapy for Hepatocellular Carcinoma. *Mol Cancer Ther* (2017) 16:1155–65. doi: 10.1158/1535-7163.MCT-16-0728
31. Wang N, Wang S, Li MY, Hu BG, Liu LP, Yang SL, et al. Cancer stem cells in hepatocellular carcinoma: an overview and promising therapeutic strategies. *Ther Adv Med Oncol* (2018) 10:1758835918816287. doi: 10.1177/1758835918816287
32. Zhang X, Xu P, Ni W, Fan H, Xu J, Chen Y, et al. Downregulated DYRK2 expression is associated with poor prognosis and Oxaliplatin resistance in hepatocellular carcinoma. *Pathol Res Pract* (2016) 212:162–70. doi: 10.1016/j.prp.2016.01.002
33. Banyard J, Bielenberg DR. The role of EMT and MET in cancer dissemination. *Connect Tissue Res* (2015) 56:1–11. doi: 10.3109/03008207.2015.1060970
34. Lohitesh K, Chowdhury R, Mukherjee S. Resistance a major hindrance to chemotherapy in hepatocellular carcinoma: an insight. *Cancer Cell Int* (2018) 18:44. doi: 10.1186/s12935-018-0538-7
35. Ren WW, Li DD, Chen X, Li XL, He YP, Guo LH, et al. MicroRNA-125b reverses oxaliplatin resistance in hepatocellular carcinoma by negatively regulating EVA1A mediated autophagy. *Cell Death Dis* (2018) 9:547. doi: 10.1038/s41419-018-0592-z
36. Yin X, Zheng SS, Zhang L, Xie XY, Wang Y, Zhang BH, et al. Identification of long noncoding RNA expression profile in oxaliplatin-resistant hepatocellular carcinoma cells. *Gene* (2017) 596:53–88. doi: 10.1016/j.gene.2016.10.008
37. Que KT, Zhou Y, You Y, Zhang Z, Zhao XP, Gong JP, et al. MicroRNA-31-5p regulates chemosensitivity by preventing the nuclear location of PARP1 in hepatocellular carcinoma. *J Exp Clin Cancer Res* (2018) 37:268. doi: 10.1186/s13046-018-0930-0
38. Yang Z, Lu Y, Xu Q, Tang B, Park CK, Chen X. HULC and H19 Played Different Roles in Overall and Disease-Free Survival from Hepatocellular Carcinoma after Curative Hepatectomy: A Preliminary Analysis from Gene Expression Omnibus. *Dis Markers* (2015) 2015:191029. doi: 10.1155/2015/191029
39. Huang H, Chen J, Ding CM, Jin X, Jia ZM, Peng J. LncRNA NR2F1-AS1 regulates hepatocellular carcinoma oxaliplatin resistance by targeting ABCC1 via miR-363. *J Cell Mol Med* (2018) 22:3238–45. doi: 10.1111/jcmm.13605
40. Fu X, Liu M, Qu S, Ma J, Zhang Y, Shi T, et al. Exosomal microRNA-32-5p induces multidrug resistance in hepatocellular carcinoma via the PI3K/Akt pathway. *J Exp Clin Cancer Res* (2018) 37:52. doi: 10.1186/s13046-018-0677-7
41. Ng L, Chow A, Man J, Yau T, Wan T, Iyer DN, et al. Suppression of Slit3 induces tumor proliferation and chemoresistance in hepatocellular carcinoma through activation of GSK3 β -catenin pathway. *BMC Cancer* (2018) 18:621. doi: 10.1186/s12885-018-4326-5
42. Qin Y, Liu HJ, Li M, Zhai DH, Tang YH, Yang L, et al. Salidroside improves the hypoxic tumor microenvironment and reverses the drug resistance of platinum drugs via HIF-1 α signaling pathway. *EBioMedicine* (2018) 38:25–36. doi: 10.1016/j.ebiom.2018.10.069
43. Qiu Y, Dai Y, Zhang C, Yang Y, Jin M, Shan W, et al. Arsenic trioxide reverses the chemoresistance in hepatocellular carcinoma: a targeted intervention of 14-3-3 η /NF- κ B feedback loop. *J Exp Clin Cancer Res* (2018) 37:321. doi: 10.1186/s13046-018-1005-y
44. Choi YW, Bae SM, Kim YW, Lee HN, Kim YW, Park TC, et al. Gene expression profiles in squamous cell cervical carcinoma using array-based comparative genomic hybridization analysis. *Int J Gynecol Cancer* (2007) 17:687–96. doi: 10.1111/j.1525-1438.2007.00834.x
45. Huang Y, Jian W, Zhao J, Wang G. Overexpression of HDAC9 is associated with poor prognosis and tumor progression of breast cancer in Chinese females. *Oncotargets Ther* (2018) 11:2177–84. doi: 10.2147/OTT.S164583
46. Zhang Y, Wu D, Xia F, Xian H, Zhu X, Cui H, et al. Downregulation of HDAC9 inhibits cell proliferation and tumor formation by inducing cell cycle arrest in retinoblastoma. *Biochem Biophys Res Commun* (2016) 473:600–6. doi: 10.1016/j.bbrc.2016.03.129
47. Zhao YX, Wang YS, Cai QQ, Wang JQ, Yao WT. Up-regulation of HDAC9 promotes cell proliferation through suppressing p53 transcription in osteosarcoma. *Int J Clin Exp Med* (2015) 8:11818–23.
48. Ávila-Moreno F, Armas-López L, Álvarez-Moran AM, López-Bujanda Z, Ortiz-Quintero B, Hidalgo-Miranda A, et al. Overexpression of MEOX2 and TWIST1 is associated with H3K27me3 levels and determines lung cancer chemoresistance and prognosis. *PloS One* (2014) 9:e114104. doi: 10.1371/journal.pone.0114104
49. Salgado E, Bian X, Feng A, Shim H, Liang Z. HDAC9 overexpression confers invasive and angiogenic potential to triple negative breast cancer cells via modulating microRNA-206. *Biochem Biophys Res Commun* (2018) 503:1087–91. doi: 10.1016/j.bbrc.2018.06.120
50. Chen J, Zhou Y, Zhuang Y, Qin T, Guo M, Jiang J, et al. The metabolic regulator small heterodimer partner contributes to the glucose and lipid homeostasis abnormalities induced by hepatitis C virus infection. *Metabolism* (2019) 100:153954. doi: 10.1016/j.metabol.2019.153954
51. Lapierre M, Linares A, Dalvai M, Duraffourd C, Bonnet S, Boulahtouf A, et al. Histone deacetylase 9 regulates breast cancer cell proliferation and the response to histone deacetylase inhibitors. *Oncotarget* (2016) 7:19693–708. doi: 10.18632/oncotarget.7564
52. Yang R, Wu Y, Wang M, Sun Z, Zou J, Zhang Y, et al. HDAC9 promotes glioblastoma growth via TAZ-mediated EGFR pathway activation. *Oncotarget* (2015) 6:7644–56. doi: 10.18632/oncotarget.3223
53. Falkenberg KJ, Johnstone RW. Histone deacetylases and their inhibitors in cancer, neurological diseases and immune disorders. *Nat Rev Drug Discov* (2014) 13:673–91. doi: 10.1038/nrd4360
54. Li ZY, Zhang C, Zhang Y, Chen L, Chen BD, Li QZ, et al. A novel HDAC6 inhibitor Tubastatin A: Controls HDAC6-p97/VCP-mediated ubiquitination-autophagy turnover and reverses Temozolomide-induced ER stress-tolerance in GBM cells. *Cancer Lett* (2017) 391:89–99. doi: 10.1016/j.canlet.2017.01.025
55. Zheng Y, Chen H, Yin M, Ye X, Chen G, Zhou X, et al. MiR-376a and histone deacetylation 9 form a regulatory circuitry in hepatocellular carcinoma. *Cell Physiol Biochem* (2015) 35:729–39. doi: 10.1159/000369733

Conflict of Interest: The authors declare that the research was conducted in the absence of any commercial or financial relationships that could be construed as a potential conflict of interest.

Copyright © 2021 Liang, Zhang, Liu, Liu, Li, Luo, Li, Ye and Lin. This is an open-access article distributed under the terms of the Creative Commons Attribution License (CC BY). The use, distribution or reproduction in other forums is permitted, provided the original author(s) and the copyright owner(s) are credited and that the original publication in this journal is cited, in accordance with accepted academic practice. No use, distribution or reproduction is permitted which does not comply with these terms.



Estrogen Receptor α Mediates Doxorubicin Sensitivity in Breast Cancer Cells by Regulating E-Cadherin

Xiaoqing Wan^{1,2}, Jiaxin Hou³, Shurong Liu¹, Yanli Zhang², Wenqing Li¹, Yanru Zhang¹ and Yi Ding^{2,4*}

¹ Laboratory of Molecular Oncology, Weifang Medical University, Weifang, China, ² Department of Pathophysiology, Weifang Medical University, Weifang, China, ³ School of Physical Education & Sports Science, Qufu Normal University, Qufu, China, ⁴ Key Laboratory of Applied Pharmacology, Weifang Medical University, Weifang, China

OPEN ACCESS

Edited by:

Zhe-Sheng Chen,
St. John's University, United States

Reviewed by:

Xiaozhuo Liu,
University at Buffalo, United States
Xingqi Li,
Stony Brook University, United States

*Correspondence:

Yi Ding
dingyi6767@163.com

Specialty section:

This article was submitted to
Molecular and Cellular Oncology,
a section of the journal
Frontiers in Cell and Developmental
Biology

Received: 15 July 2020

Accepted: 11 January 2021

Published: 04 February 2021

Citation:

Wan X, Hou J, Liu S, Zhang Y, Li W,
Zhang Y and Ding Y (2021) Estrogen
Receptor α Mediates Doxorubicin
Sensitivity in Breast Cancer Cells by
Regulating E-Cadherin.
Front. Cell Dev. Biol. 9:583572.
doi: 10.3389/fcell.2021.583572

Anthracyclines resistance is commonly seen in patients with estrogen receptor α (ER α) positive breast cancer. Epithelial-mesenchymal transition (EMT), which is characterized with the loss of epithelial cell polarity, cell adhesion and acquisition of new invasive property, is considered as one of the mechanisms of chemotherapy-induced drug resistance. In order to identify factors that associated with doxorubicin resistance, we performed *in vitro* and *in vivo* experiments using human and mouse breast cancer cell lines with different ER α status. Cell survival experiments revealed that ER α -positive cells (MCF-7 and MCF-7/ADR cell lines), were less sensitive to doxorubicin than ER α -negative (MDA-MB-231, MDA-MB-468) cells, and mouse mammary carcinoma cells (4T-1). The expression of E-cadherin reduced in low-invasive ER α -positive MCF-7 cells after treatment with doxorubicin, indicating epithelial mesenchymal transition. In contrast, the expression of E-cadherin was upregulated in high-invasive ER α -negative cells, showing mesenchymal-epithelial transition (MET). Moreover, it was found that the growth inhibition of 4T-1 cells by doxorubicin was positively correlated with the expression of E-cadherin. In a mouse breast cancer xenograft model, E-cadherin was overexpressed in the primary tumor tissues of the doxorubicin-treated mice. In ER α -positive MCF-7 cells, doxorubicin treatment upregulated the expression of EMT-related transcription factors Snail and Twist, that regulate the expression of E-cadherin. Following overexpression of ER α in ER α -negative cells (MDA-MB-231 and MDA-MB-468), doxorubicin enhanced the upregulation of Snail and Twist, decreased expression of E-cadherin, and decreased the sensitivity of cells to doxorubicin. In contrast, inhibition of ER α activity increased the sensitivity to doxorubicin in ER α -positive MCF-7 cells. These data suggest that the regulation of Snail and/or Twist varies depends on different ER α status. Therefore, doxorubicin combined with anti-estrogen receptor α therapy could improve the treatment efficacy of doxorubicin in ER α -positive breast cancer.

Keywords: breast cancer, estrogen receptor α , doxorubicin, chemoresistance, E-cadherin

INTRODUCTION

Breast cancer is the most commonly diagnosed cancer among women and the second leading cause of cancer-related death (Bray et al., 2018). Based on tumor ER α status, patients with breast cancer are classified as either estrogen receptor α (ER α) positive or ER α -negative. Nearly 70% of breast cancer patients are ER α -positive, and their tumor growth and development depend on estrogen. There is a significant difference in the sensitivity to chemotherapy between ER α -negative and ER α -positive tumors (Liedtke et al., 2008).

Anthracyclines, such as doxorubicin, used alone or in combination with paclitaxel are the first-line chemotherapeutic regimens for the treatment of breast cancer. Doxorubicin effectively inhibits the synthesis of nucleic acid by intercalating to DNA double helix, leading to tumor cell death. In patients without a pathologically complete response (pCR) after treatment with doxorubicin (i.e., the absence of residual invasive disease in the breast and in the axillary lymph nodes), the residual cancer burden was observed (Symmans et al., 2017). Defining the mechanisms of doxorubicin sensitivity of breast cancer cells may improve the treatment strategy for patients who fail to achieve a pCR.

Epithelial-mesenchymal transition (EMT) is considered to be the initiation and necessary process for tumor metastasis. EMT is a process of cell phenotypic change in which epithelial cells lose their adhesion molecules, such as E-cadherin, and acquire mesenchymal molecules such as N-cadherin and vimentin (Cano et al., 2000). EMT may lead to malignant tumor chemoresistance, particularly seen in pancreatic cancer (Arumugam et al., 2009; Zheng et al., 2015; Elaskalani et al., 2017), lung cancer (Fischer et al., 2015), hepatocellular carcinoma (Dai et al., 2016; Xu et al., 2016), breast cancer (Mallini et al., 2014; Hu et al., 2016; Lambies et al., 2019), and colon cancer (Liu et al., 2015). Several transcription factors such as Snail, Twist, Slug, ZEB, CarB-box-binding factor can regulate this process (Cano et al., 2000; Zhang and Ma, 2012; Lamouille et al., 2014; Jung et al., 2015; Zhang et al., 2015).

Clinically, ER α -negative breast cancer patients are more likely to acquire pCR than ER α -positive patients receiving neoadjuvant chemotherapy with anthracyclines, suggesting that ER α -negative breast tumors are more sensitive to anthracyclines (Liedtke et al., 2008). However, the mechanism of the difference in sensitivity of doxorubicin between ER α -positive and ER α -negative breast cancer patients is not well-understood. In this study, we investigated the role of ER α in doxorubicin sensitivity using five breast cancer cell lines with different ER α status both *in vitro* and *in vivo*.

Abbreviations: ER α , Estrogen receptor α ; DOX, Doxorubicin; EMT, Epithelial-mesenchymal transition; BC, Breast cancer; E2, estradiol; ICI, ICI182780; ox-ER, over-expression ER α ; pCR, pathologically complete response.

MATERIALS AND METHODS

Cell Culture

To compare the doxorubicin sensitivity between ER α -positive and ER α -negative breast cancer cells, ER α -positive human breast cancer cell lines (MCF-7 and MCF-7/ADR), ER α -negative human breast cancer cell lines (MDA-MB-231 and MDA-MB-468), and ER α -negative murine breast cancer cell 4T-1 were used in this study. MDA-MB-231, MDA-MB-468 and 4T-1 were obtained from the American Type Culture Collection (ATCC, USA). MCF-7/ADR cells was purchased from Bogu Biology Company (Shanghai, China). MDA-MB-231, MDA-MB-468, and 4T-1 cells were cultured in RPMI-1640 medium. MCF-7 cells were cultured in MEM medium with 0.01 mg/ml insulin. MCF-7/ADR cells were also cultured in RPMI-1640 medium with 0.86 μ M doxorubicin. All the media were supplemented with 10% (v/v) heat-inactivated fetal bovine serum (FBS, Gibco, Thermo Fisher Scientific, Waltham, MA), L-glutamine 1% (v/v), penicillin (100 U/ml) and streptomycin (100 U/ml, Solarbio, China). All cells were incubated in a humidified incubator with 5% CO₂ at 37°C. Doxorubicin (DOX, 25316-40-9, purity 98.0-102.0%) and ICI182780 (129453-61-8, purity \geq 98%) were obtained from Sigma-Aldrich.

MTT Assay

The MTT assay was used to assess the effect of DOX on cell viability. Tumor cells were seeded into 96-well plates with the density of 35~40% for 24 h, starved with 1% FBS medium for 12 h, and then incubated with different concentrations of DOX. After 24 or 48 h, 20 μ l 3-(4,5-dimethylthiazol-2-yl)-2,5-diphenyltetrazolium bromide (MTT, M8180, purity \geq 98%, Solarbio, China) at a concentration of 5 mg/ml was added into each well for 4 h. Medium/MTT mixture was removed and followed by adding 150 μ l of DMSO. The light absorbance was measured at 570 nm. The percentage of cell survival rate was calculated using the following formula: survival rate (%) = (OD of treated wells/OD of control well) \times 100 (OD, optical density).

Western Blot

Whole cell protein (25~60 μ g) extracted by RIPA lysis buffer from each sample was loaded into 8% or 10% polyacrylamide gel for electrophoresis as previously described (Cheng et al., 2018) followed by membrane transfer carried out at 300 mA for 1.5~2.5 h. Membranes were blocked with 5% non-fat milk in Tris-buffered saline solution (pH 7.4) containing 0.05% Tween-20 and incubated with primary antibodies overnight. The following primary antibodies were used. β -actin (20536-1-AP, Proteintech, China), E-cadherin (24E10, CST, USA), N-cadherin (ab18203, abcam, USA), Estrogen receptor α (ab32063, abcam, USA), Twist (ab49254, abcam, USA), and Snail (L70G2, CST, USA). After incubation with secondary antibodies (A0208, Beyotime, China), the membranes were treated with reagents from the ECL kits (P90719, Millipore, USA) and exposed to X-ray film (Kodak, USA) in darkness.

Immunofluorescence

Mouse 4T-1 cells were seeded in 24-well plates with the density of 2.5×10^4 for 24 h and then starved with 1% FBS

medium for 12 h. Afterward, cells were treated with DOX at different concentrations for 24 h, followed by fixation with 4% paraformaldehyde for 20 min at room temperature. After blocking with goat serum at 37°C for 1 h, cells were incubated with E-cadherin antibody (1:200, 24E10, CST, USA) overnight, and then with TRITC goat anti-rabbit IgG (1:300, ZF-0313, ZSGB-BIO, China) at 37°C for 1 h. After washing with PBS, cell nuclei were stained with DAPI (10 μ g/ml, C0065, Solarbio, China) for 10 min at room temperature, and photographed using a Leica fluorescence microscope.

Plasmid Transfection

Cells were seeded in 6-well plates at the density of 80~90% with the full medium except penicillin and streptomycin for 16 h. Afterward, ESR1 plasmids (2.5 μ g, GENE, China) and Lipofectamine 3000 (5 μ l, life technologies, USA) were diluted in 125 μ l Opti-MEM medium and mixed for 10 min then added to each well. Empty vector was used simultaneously as a negative control. Twelve hours later, the transfection mixture was replaced with fresh medium and protein was extracted after additional 12 h and detected using Western blot to verify the ER expression level in ESR1 plasmids-transfected cells.

Animal Studies

Six-week-old female BALB/c mice (Shandong University Animal Center, China) housed under specific pathogen free conditions were used for *in vivo* animal experiments. Murine breast cancer 4T-1 cells transfected with GFP (1×10^6 cells) were inoculated into the mammary fat pad of BALB/c mice. After 1 week, 12 mice were randomly divided into two groups. Six mice per group. Animals in the experimental group were given DOX treatment by intraperitoneal injection at a dose of 2.5 mg/kg, once a week. The mice in the other group received 0.9% NaCl as parallel control. After 4 weeks of treatment, the primary breast cancer lesions of both groups were collected and fixed in 10% neutral buffered formaldehyde. All animals used were under an approved protocol of the Institutional Animal Care and Use Committee of Weifang Medical University.

Immunohistochemistry (IHC)

A 4 μ m thick tissue sections were cut from the paraffin-embedded tissues. After dewaxing and rehydration, 3% hydrogen peroxide was used to block endogenous peroxidase. Non-specific binding was blocked with normal goat serum for 1 h at 37°C. Sections were incubated with anti-E-cadherin antibody (1:200, 24E10, CST) overnight at 4°C. The slides were incubated with Solution I (PV9001, Zsbio, China) for 40 min at 37°C and then incubated with Solution II (PV9001, Zsbio, China) for 40 min at 37°C according to the manufacturer's instruction. After washing with PBS, it was developed with DAB (CW0125, CWBIO, China). The slides were counterstained with Mayer's hematoxylin, washed, dehydrated, and the coverslips were mounted with neutral glue.

Statistical Analysis

Each experiment was repeated at least three times independently. Data statistics are expressed as the mean \pm SD of the specified

number of individual experiments. Statistical analysis was performed with GraphPad Prism software (version 5.01, San Diego, CA). ANOVA (parametric) test was used for multiple comparisons and Student's *t*-test was used for two-group comparisons. *P* < 0.05 was considered as statistically significant.

RESULTS

The Cytotoxic Effect of DOX Is Associated With Expression of ER α in Breast Cancer Cells

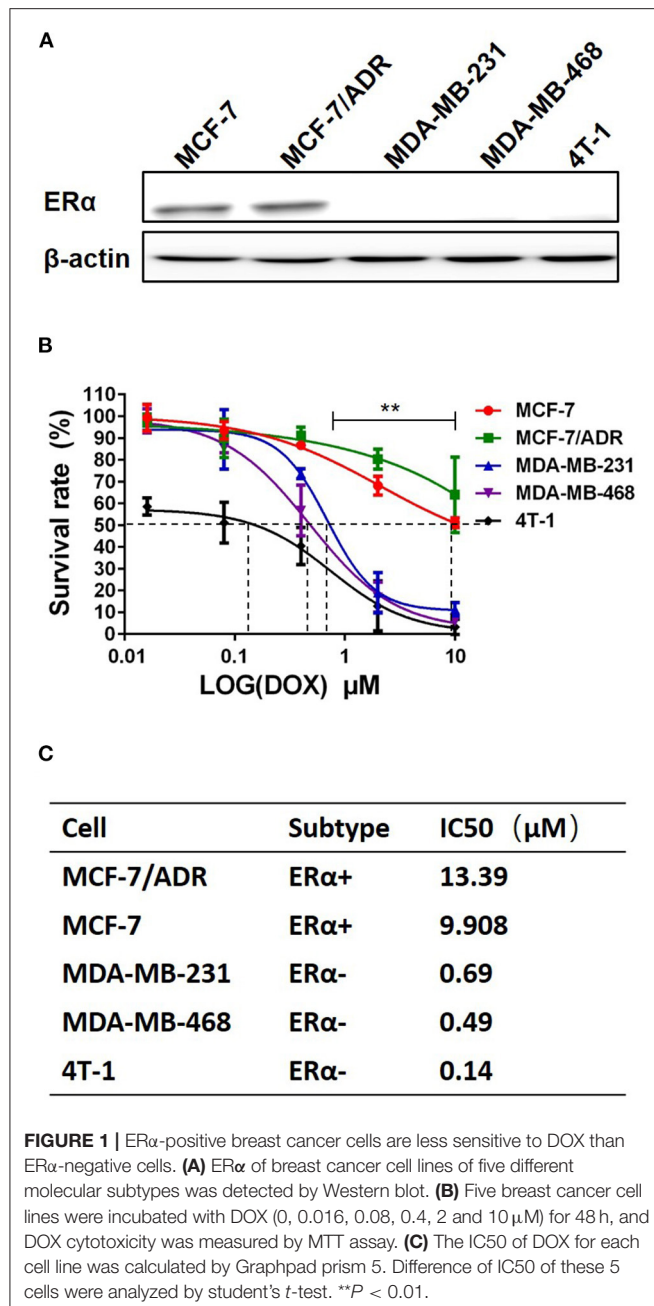
To study the cytotoxic effects of DOX on breast cancer cells, five breast cancer cell lines, including MCF-7, MCF-7/ADR, MDA-MB-231, MDA-MB-468 and 4T-1, were used. The ER α expression in these five breast cancer cell lines was examined by western blot to confirm the cell subtype. The expression of ER α was seen in MCF-7 and MCF-7/ADR cells, but not in MDA-MB-231, MDA-MB-468 and 4T-1 cells (**Figure 1A**). These cells were cultured and treated with DOX at different concentration (0–10 μ M) for 48 h. It was found that DOX inhibited cell survival in a dose-dependent manner. MCF-7 and MCF-7/ADR cells were less sensitive to DOX than MDA-MB-231, MDA-MB-468 and 4T-1 cells (**Figure 1B**). The IC₅₀ of DOX in MDA-MB-231, MDA-MB-468 and 4T-1 cells were 0.69, 0.49, and 0.14 μ M, respectively, which were lower than that in MCF-7 and MCF-7/ADR cells (9.908 and 13.39 μ M, respectively, **Figure 1C**). The difference of sensitivity to DOX between ER α -negative and ER α -positive breast cancer cells is statistically significant. This result suggests that different sensitivity of cells to DOX is associated with the presence or absence of ER α . ER α -negative cells are more sensitive to DOX than ER α -positive cells.

DOX Regulates EMT in Human Breast Cancer Cells

To address whether EMT is involved in sensitivity to DOX treatment in breast cancer cells, cells with different phenotypes and ER α expression were incubated with DOX and the related epithelial and mesenchymal phenotypic biomarkers were characterized using western blots.

In ER α -positive MCF-7 cells, E-cadherin was downregulated with 0.74 μ M DOX (Gu et al., 2016) incubation for 24 and 48 h, and N-cadherin was upregulated by DOX treatment for 24 and 48 h (**Figure 2A**). In contrast, in ER α -positive MCF-7/ADR, E-cadherin expression was too low to be detected with or without DOX incubation (**Figure 2A**). In ER α -negative MDA-MB-231 cells, E-cadherin couldn't be detected at 24 h with or without DOX, but was upregulated with DOX treatment for 48 h (**Figure 2B**). Interestingly, N-cadherin was upregulated at 24 h with DOX treatment, while no obvious difference at 48 h (**Figure 2B**). Similarly, in ER α -negative MDA-MB-468 cells, both E-cadherin and N-cadherin expression were upregulated in a dose-dependent manner with DOX incubation for 24 and 48 h (**Figure 2C**).

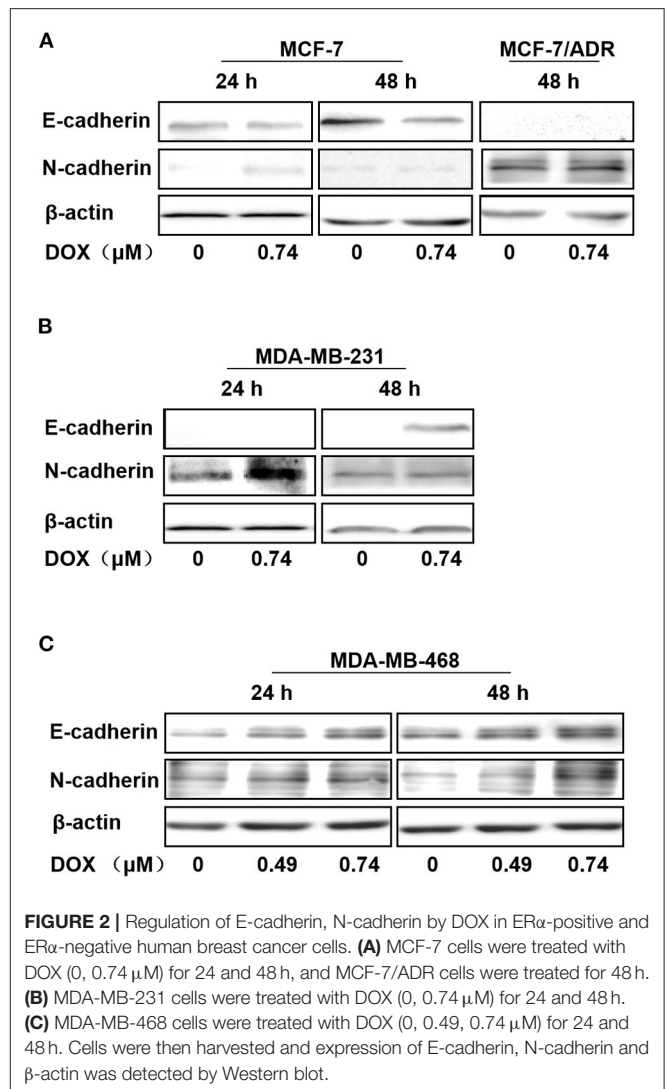
Therefore, N-cadherin expression was increased with DOX treatment in ER α -positive MCF-7, ER α -negative MDA-MB-231 and MDA-MB-468 cells, while E-cadherin was increased in



MDA-MB-231 and MDA-MB-468 cells and decreased in MCF-7 cells. E-cadherin was not detected in MCF-7/ADR cells even after 48 h incubation with DOX. These data suggest that DOX promotes EMT primarily in ER α positive cells and this may contribute to its chemo-resistance.

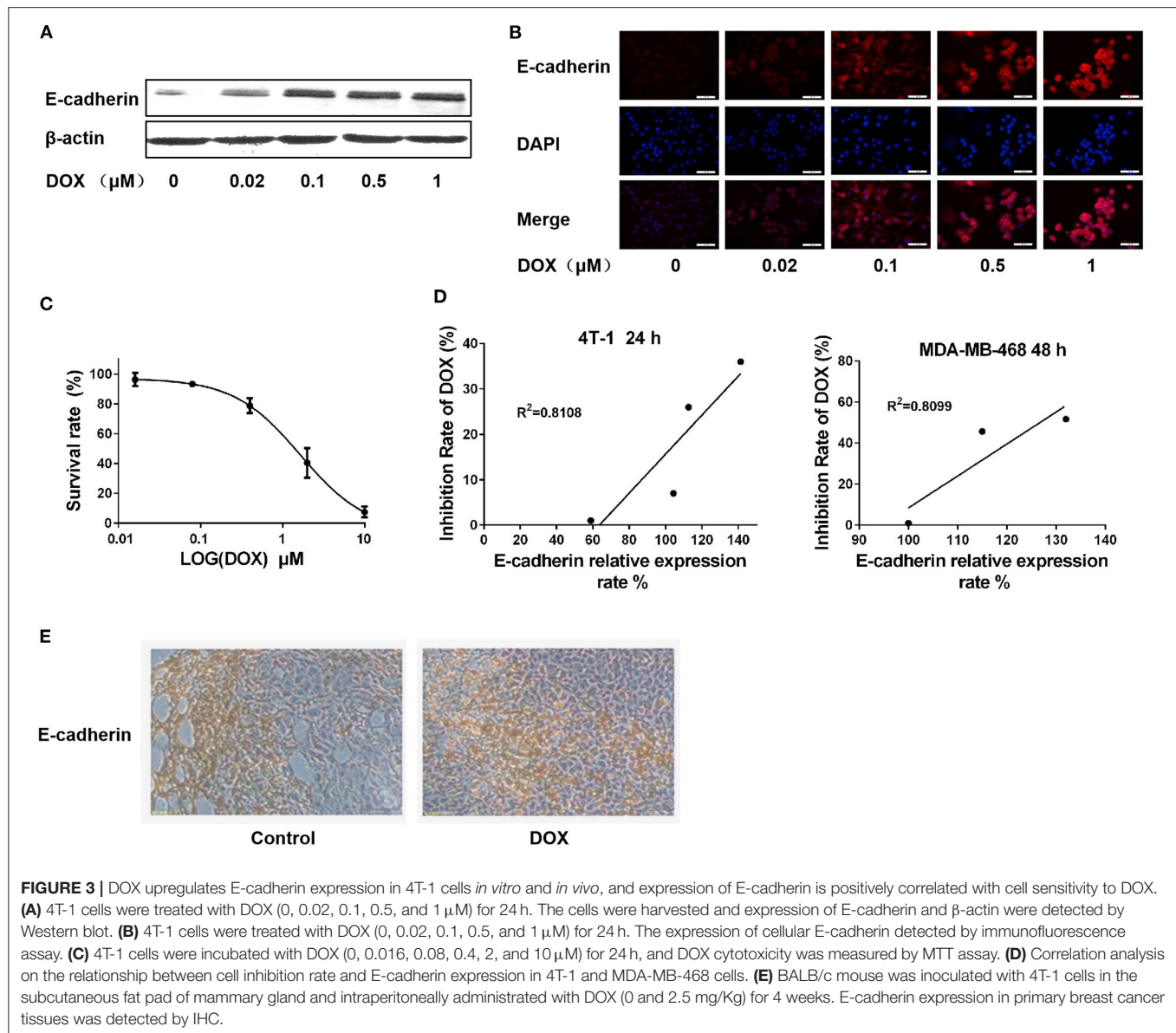
DOX Upregulates E-Cadherin Expression in Mouse ER α -Negative Breast Cancer Cells *in vitro* and *in vivo*

The mouse ER α -negative breast cancer 4T-1 cells were cultured and treated with different concentrations of DOX for 24 h.



The expression of E-cadherin was determined by western blot and immunofluorescence assay. Both western blot and immunofluorescence assay results revealed that E-cadherin was upregulated in a dose-dependent manner (**Figures 3A,B**), which is in consistent with results in the human ER α -negative breast cancer MDA-MB-231 and MDA-MB-468 cells.

The cytotoxic effect of DOX on 4T-1 cells was assessed by MTT assay. After 24 h of DOX incubation, the survival rate of 4T-1 cells was reduced in a dose-dependent manner (**Figure 3C**). The correlation between E-cadherin expression and DOX proliferation inhibition was analyzed in both mouse and human ER α -negative breast cancer cells (4T-1 and MDA-MB-468) to clarify whether the cytotoxicity of DOX on breast cancer cells is associated with expression of E-cadherin. The results showed that there was a significant positive correlation between the cytotoxicity of DOX and the expression of E-cadherin (**Figure 3D**) suggesting that the chemosensitivity of breast cancer cells to DOX is related to E-cadherin expression.



BALB/c mice were used for 4T-1 breast cancer model *in vivo* studies. After 4 weeks of intraperitoneal injection of DOX (2.5 mg/kg) or the same amount of physiological saline as a control, primary cancer tissues of each group was isolated, and E-cadherin expression was detected by IHC. Consistent with our *in vitro* results, the expression of E-cadherin in the DOX treatment group was higher than in the control group (Figure 3E).

DOX Upregulates the Expression of Snail and Twist in Breast Cancer Cells

Snail and Twist are key molecules regulating EMT process. The expression of both Snail and Twist were upregulated in ER α -positive MCF-7 cells treated with DOX (0.74 μ M) for 24 and 48 h (Figure 4A). In order to further delineate the findings in MCF-7 cells and MDA-MB-231 cells, these cells were transfected with

ER α (ESR1) plasmid or empty vector as a negative control. After treatment with or without DOX (0.74 μ M) for 24 or 48 h, the expression of the ER α was significantly increased in ER α (ESR1) plasmid transfected cells (Figure 4B).

Snail was upregulated by DOX treatment either in ER α overexpressing cells or controls (Figures 4B,C). After 48 h of DOX treatment, Snail increased in ER α overexpressing cells, and ER α overexpression enhanced DOX-induced Snail upregulation (Figures 4B,C). Similarly, Twist upregulation of ER α at 48 h and a synergistic effect of DOX and ER α on Twist expression was found (Figures 4B,D).

E-cadherin was upregulated in the presence of ER α and this effect was attenuated by DOX treatment for 24 and 48 h (Figure 4B). These data indicate that, DOX may promote EMT by upregulating Snail and Twist via an ER α related mechanism.

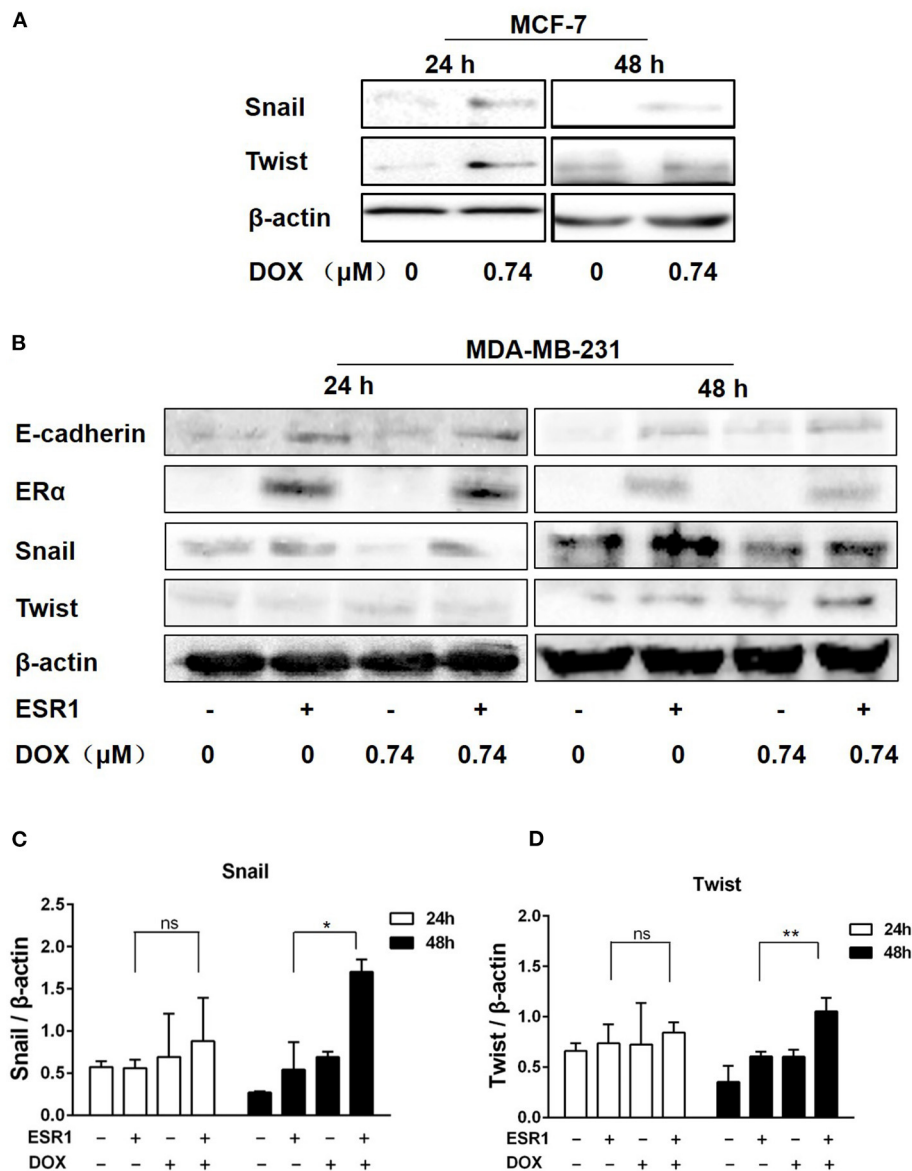


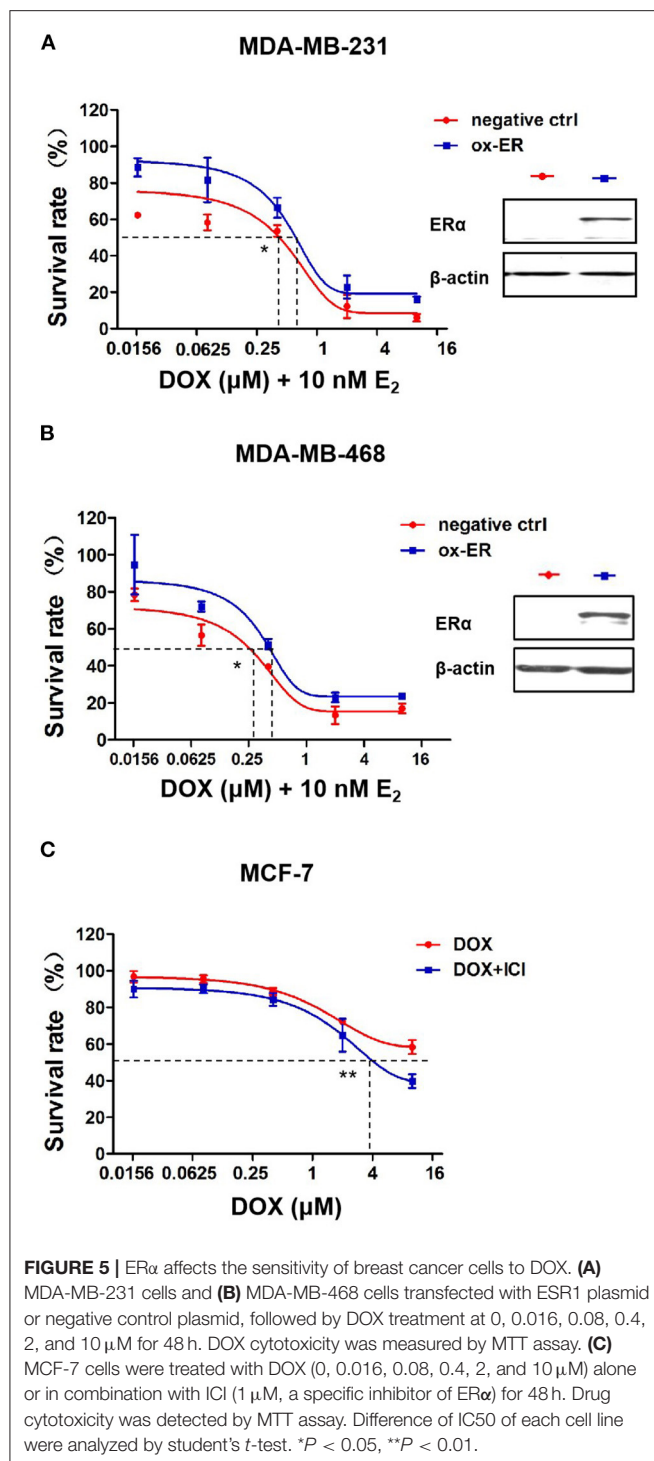
FIGURE 4 | DOX induced the expression of Twist and Snail in breast cancer cells. **(A)** MCF-7 cells were treated with DOX (0 and 0.74 μ M) for 24 and 48 h. Cells were then harvested and the expression of Snail, Twist and β -actin was determined by Western blot. **(B)** MDA-MB-231 cells were transfected with the ESR1 plasmid or the negative control plasmid, followed by treatment with DOX (0 and 0.74 μ M) for 24 and 48 h. Cells were then harvested and the expression of E-cadherin, ER α , Snail, Twist and β -actin was detected by Western blot. **(C,D)** The relative expression levels of Snail and Twist proteins were analyzed based on gray intensity. * $P < 0.05$ vs. ER α overexpressed cells without DOX. ** $P < 0.01$.

The Cytotoxic Effect of DOX Is Related to ER α Expression in Breast Cancer Cells

To identify the role of ER α in chemotherapeutic resistance to DOX, MDA-MB-231 and MDA-MB-468 cells were transfected with either an ER α plasmid or an empty vector as a negative control. After transfection, MDA-MB-231 and MDA-MB-468 cells were incubated with DOX plus 10 nM estradiol, an activator of ER α signaling. The cell survival rate is higher in the ER α overexpression group than that in the MDA-MB-231 (Figure 5A) and MDA-MB-468 cells (Figure 5B) after DOX treatment.

Furthermore, for MDA-MB-231 cells, the IC₅₀ of DOX in cells of the negative control group was 0.39 vs. 0.61 μ M in ER α overexpression group. And for MDA-MB-468 cells, the IC₅₀ of DOX in cells of the negative control group was 0.26 vs. 0.41 μ M in ER α overexpression group. The difference of IC₅₀ in each cell line is statistically significant.

By incubating MCF-7 ER α positive cells with 1 μ M ICI182780, a specific inhibitor of ER α , ER α signaling was inhibited and MCF-7 cells became more sensitive to DOX than cells without ICI182780 treatment (Figure 5C). These data suggest that ER α



plays an important role in mediating the chemo sensitivity of breast cancer cells to DOX treatment.

DISCUSSION

Patients with ER α -negative breast cancer are more sensitive to anthracyclines-based neoadjuvant chemotherapy than ER α -positive patients (Liedtke et al., 2008), but the mechanism

behind this response remains unclear. In this study, we have observed an association of DOX cytotoxicity with expression of EMT biomarkers in multiple breast cancer cells with different ER status.

DOX Resistance Is Positively Correlated With ER α and E-Cadherin Expression *in vitro* and *in vivo*

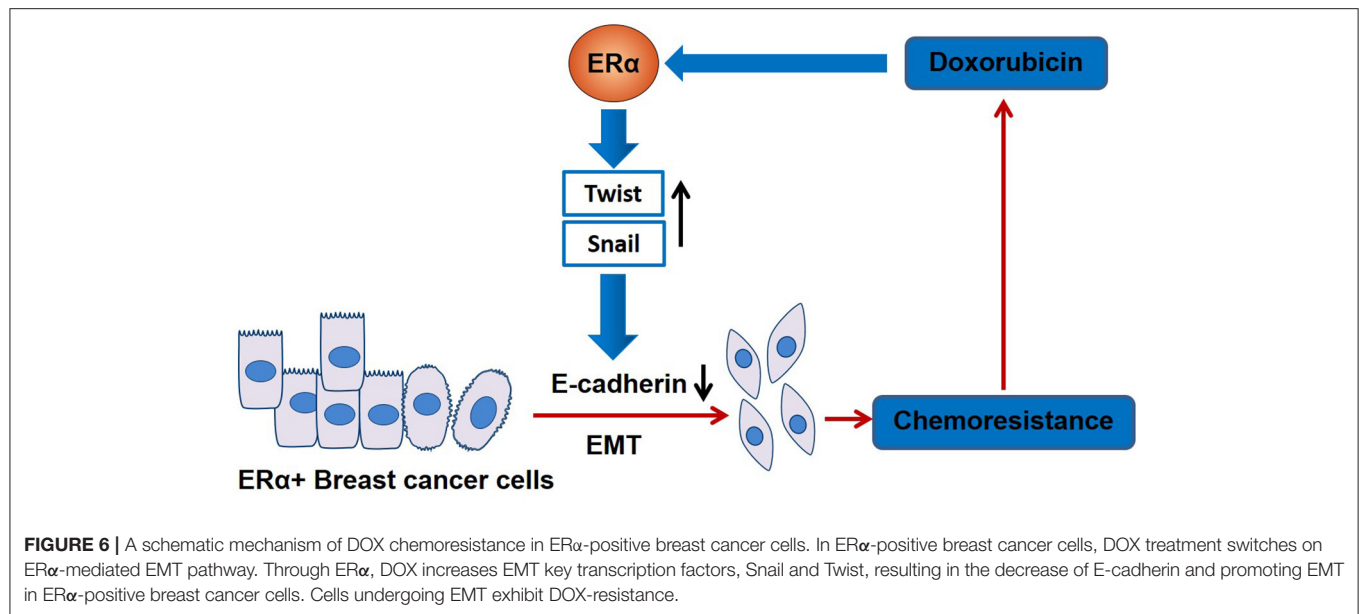
ER α -negative breast cancer cells (MDA-MB-231, MDA-MB-468 and 4T-1 cells) were more susceptible to the cytotoxic effect of DOX than ER α -positive (MCF-7 and MCF-7/ADR) cells. It was reported that although ER α -negative breast cancer has more mesenchymal characteristics and poorer prognosis than ER α -positive tumors (Tomaskovic-Crook et al., 2009), ER α -negative tumor subtypes are more likely to be benefited from DOX treatment than the other breast cancer subtypes.

The chemo-resistance of breast cancer cells to DOX depends in part on the expression of E-cadherin. Our study demonstrated that the expression of E-cadherin is downregulated by DOX treatment in MCF-7 cells. DOX-resistant MCF-7/ADR cells have very low level of E-cadherin. In contrast, E-cadherin was upregulated by DOX treatment in the DOX sensitive MDA-MB-231 and MDA-MB-468 human breast cancer cells. Similar upregulation of E-cadherin by DOX treatment was seen in the mouse 4T-1 cells.

Furthermore, we found a positive correlation between DOX cytotoxicity and expression of E-cadherin in 4T-1 cells, which is in consistent with the observations by Zhou et al. (2014) and Wang et al. (2017). In our BALB/c mouse tumor model, expression of E-cadherin was increased in primary tumor compared to controls. *In vitro* studies by other investigators have also shown that MCF-7 cells are more resistant to DOX and have mesenchymal characteristics after E-cadherin knockout (Zhou et al., 2014). These data suggest that E-cadherin may be a useful biomarker for determining the susceptibility of breast cancer to DOX therapy.

The Effect of DOX on E-Cadherin Expression Is Mediated by EMT-Related Transcription Factors in Breast Cancer Cells

EMT can increase migration and invasion potential of tumor cells by increasing expression of mesenchymal biomarkers, N-cadherin, vimentin and fibronectin and decreasing epithelial cell phenotype biomarkers like E-cadherin (Cano et al., 2000). Overexpression of E-cadherin in tumor cells prevents transcription of mesenchymal genes (Ohkubo and Ozawa, 2004; Solanas et al., 2008). Recent studies have shown that tumor cells undergoing EMT exhibit enhanced multidrug resistance (MDR) (Fischer et al., 2015; Zheng et al., 2015; Xu et al., 2016; El Amrani et al., 2019). In the current study, DOX reduced E-cadherin expression in MCF-7 cells. MCF-7 cells is more resistant to DOX than MDA-MB-231 cells. Notably, in MDA-MB-231 cells, we found that DOX increased the expression of E-cadherin suggesting that mesenchymal to epithelial transitions may contribute to chemical resistance to DOX.



Previous studies have shown that EMT-induced transcription factors, such as Twist, Snail and Zeb1, as well as some signaling pathways. Transforming growth factor beta, Wnt and Notch, can induce EMT and result in chemoresistance (Moreno-Bueno et al., 2008). E-cadherin is a key protein in the formation of adhesion junctions, and it is essential to maintain the epithelial phenotype by binding to neighboring cells (van Roy and Berx, 2008). In the current study, both Snail and Twist were upregulated by DOX treatment in MCF-7 cells. In MDA-MB-231 cells, Snail and Twist also increased after 48 h of DOX treatment.

The function of E-cadherin could be disrupted in tumor invasion and metastasis (Cano et al., 2000; Arumugam et al., 2009). There are several mechanisms involved in downregulation of E-cadherin during tumor progression such as transcription downregulation, mutation, and methylation (van Roy and Berx, 2008; Cui et al., 2018). EMT-induced transcription factors including Snail, Zeb1 and Zeb2, that can inhibit E-cadherin transcription (Moreno-Bueno et al., 2008). For example, the transcription factors Snail, E12/E47, Zeb1 and SIP1 bind to E-box elements at the proximal promoter site of E-cadherin leading to transcriptional inactivation of E-cadherin. Snail binds to partly overlapping promoter sequences and downregulates the expression of E-cadherin in breast cancer cells (Cano et al., 2000). Twist is possibly involved in EMT by repressing E-cadherin and promoting expression of N-cadherin.

Our data showed that DOX upregulated the expression of Snail and Twist to stimulate the transcriptional expression of E-cadherin and trigger the process of MET. Although DOX induced Snail and Twist expression consistently in MCF-7 cells and MDA-MB-231 cells, these cells showed different responses to DOX treatment in E-cadherin expression. We hypothesized that this might be due to the different expression of ER α and further investigated the role of ER α in DOX-induced Snail and Twist expression.

The Regulation of E-Cadherin Expression by Snail and Twist Is Associated With ER α in Breast Cancer Cells

Our studies demonstrate that DOX increases Snail and Twist expression, and this effect is significantly enhanced by ER α . We hypothesized that DOX treatment activates Snails and Twist signaling pathways and E-cadherin gene transcription is determined by ER α status in breast cancer cells. In the absence of ER α , Snail triggers E-cadherin gene transcription. However, in ER α -positive cells, ER α may be a cofactor of Snail, Twist or both to inhibit E-cadherin gene transcription, resulting in E-cadherin reduction and EMT. More research is warranted to support this result. It has been reported that ER α signaling is regulated by EMT-associated transcription factors (Ye et al., 2008, 2010; Al Saleh et al., 2011; Vesuna et al., 2012; Bouris et al., 2015). Vesuna et al. (2012) et al. found that Twist binds to the E-box in the ER α promoter, thereby inhibiting the expression of ER α . A Twist overexpressing MCF-7 cells mouse breast cancer model showed resistance to endocrine therapy with tamoxifen (ATM). And suppression of Twist can partially restore the function of ER α . Therefore, in ER α -positive breast cancer cells, DOX treatment can upregulate Snail and Twist leading to EMT, and suppress ER α expression can attenuate the sensitivity of cells to ER α therapy.

In clinical settings, patients with ER α -positive breast cancer and high expression of Twist and Snail usually indicate a high risk of tumor recurrence (van Nes et al., 2012). In addition, previous studies suggested that Twist can induce Snail, and the expression of Snail is an important biomarker indicating Twist activation (Ip et al., 1992; Smit et al., 2009). Therefore, the increase of Snail may be partially affected by increasing Twist. Other transcription factors such as Zeb1/2 and Slug can downregulate E-cadherin by direct binding to its promoter (Ye et al., 2010; Kurahara et al., 2012). In the case of Snail and Twist

upregulation, the upregulation of E-cadherin in MDA-MB-231 cells in response to DOX treatment may due to the effect of other transcription factors. The specific mechanism needs to be further explored.

In summary, our work suggests that DOX treatment promotes EMT leading to chemo-resistance in ER α -positive breast cancer through the ER α signaling pathway (Figure 6). This might be the reason why patients with ER α -negative breast cancer are easier in obtaining pCR than those with ER α -positive cancer after anthracycline-based chemotherapy. Therefore, therapeutic strategy using alternative chemotherapeutic drugs or combining an ER α -target inhibitor can benefit patients with ER α -positive breast cancer by avoiding drug resistance.

NOVELTY AND IMPACT

Anthracyclines, the first-line chemotherapeutic drugs for the treatment of breast cancer, are prone to drug resistance in patients with positive estrogen receptor α (ER α). However, the mechanism of drug resistance is largely unknown. We performed both *in vitro* and *in vivo* studies using breast cancer cells with different ER α status by overexpression and inhibition of ER α . It was found that doxorubicin treatment upregulates the expression of transcription factors that related to epithelial-mesenchymal transition (EMT), leading to different drug sensitivity depending on the ER α status of the cells. Our results suggest that ER α

could be a switch that regulates EMT or MET in the action of doxorubicin.

DATA AVAILABILITY STATEMENT

The raw data supporting the conclusions of this article will be made available by the authors, without undue reservation.

ETHICS STATEMENT

The animal study was reviewed and approved by Ethics Committee of Weifang Medical University.

AUTHOR CONTRIBUTIONS

YD designed and developed the study. XW, JH, SL, YanlZ, WL, and YanrZ performed experiments. XW and YD analyzed the data and wrote the manuscript. All authors reviewed and approved the final manuscript.

FUNDING

This work was supported by grants from The Project of Shandong Province Higher Educational Science and Technology Program (J13LK02), Shandong Co-Innovation Center of Classic TCM formula (2019KF203), Shandong University of Traditional Chinese Medicine.

REFERENCES

- Al Saleh, S., Al Mulla, F., and Luqmani, Y. A. (2011). Estrogen receptor silencing induces epithelial to mesenchymal transition in human breast cancer cells. *PLoS ONE* 6:e20610. doi: 10.1371/journal.pone.0020610
- Arumugam, T., Ramachandran, V., Fournier, K. F., Wang, H., Marquis, L., Abbruzzese, J. L., et al. (2009). Epithelial to mesenchymal transition contributes to drug resistance in pancreatic cancer. *Cancer Res.* 69, 5820–5828. doi: 10.1158/0008-5472.CAN-08-2819
- Bouris, P., Skandalis, S. S., Piperigkou, Z., Afratis, N., Karamanou, K., Aletras, A. J., et al. (2015). Estrogen receptor alpha mediates epithelial to mesenchymal transition, expression of specific matrix effectors and functional properties of breast cancer cells. *Matrix Biol.* 43, 42–60. doi: 10.1016/j.matbio.2015.02.008
- Bray, F., Ferlay, J., Soerjomataram, I., Siegel, R. L., Torre, L. A., and Jemal, A. (2018). Global cancer statistics 2018: GLOBOCAN estimates of incidence and mortality worldwide for 36 cancers in 185 countries. *CA Cancer J. Clin.* 68, 394–424. doi: 10.3322/caac.21492
- Cano, A., Perez-Moreno, M. A., Rodrigo, I., Locascio, A., Blanco, M. J., del Barrio, M. G., et al. (2000). The transcription factor snail controls epithelial-mesenchymal transitions by repressing E-cadherin expression. *Nat. Cell Biol.* 2, 76–83. doi: 10.1038/35000025
- Cheng, C. C., Shi, L. H., Wang, X. J., Wang, S. X., Wan, X. Q., Liu, S. R., et al. (2018). Stat3/Oct-4/c-Myc signal circuit for regulating stemness-mediated doxorubicin resistance of triple-negative breast cancer cells and inhibitory effects of WP1066. *Int. J. Oncol.* 53, 339–348. doi: 10.3892/ijo.2018.4399
- Cui, H., Hu, Y., Guo, D., Zhang, A., Gu, Y., Zhang, S., et al. (2018). DNA methyltransferase 3A isoform b contributes to repressing E-cadherin through cooperation of DNA methylation and H3K27/H3K9 methylation in EMT-related metastasis of gastric cancer. *Oncogene* 37, 4358–4371. doi: 10.1038/s41388-018-0285-1
- Dai, A., Ahn, K. S., Wang, L. Z., Kim, C., Deivasigamni, A., Arfuso, F., et al. (2016). Ascochlorin enhances the sensitivity of doxorubicin leading to the reversal of Epithelial-to-Mesenchymal Transition in Hepatocellular Carcinoma. *Mol. Cancer Ther.* 15, 2966–2976. doi: 10.1158/1535-7163.MCT-16-0391
- El Amrani, M., Corfiotti, F., Corvaisier, M., Vasseur, R., Fulbert, M., Skrzypczyk, C., et al. (2019). Gemcitabine-induced epithelial-mesenchymal transition-like changes sustain chemoresistance of pancreatic cancer cells of mesenchymal-like phenotype. *Mol. Carcinog.* 58, 1985–1997. doi: 10.1002/mc.23090
- Elaskalani, O., Razak, N. B., Falasca, M., and Metharom, P. (2017). Epithelial-mesenchymal transition as a therapeutic target for overcoming chemoresistance in pancreatic cancer. *World J. Gastrointest. Oncol.* 9, 37–41. doi: 10.4251/wjgo.v9.i1.37
- Fischer, K. R., Durrans, A., Lee, S., Sheng, J., Li, F., Wong, S. T., et al. (2015). Epithelial-to-mesenchymal transition is not required for lung metastasis but contributes to chemoresistance. *Nature* 527, 472–476. doi: 10.1038/nature15748
- Gu, X., Xue, J. Q., Han, S. J., Qian, S. Y., and Zhang, W. H. (2016). Circulating microRNA-451 as a predictor of resistance to neoadjuvant chemotherapy in breast cancer. *Cancer Biomark* 16, 395–403. doi: 10.3233/CBM-160578
- Hu, S.-H., Wang, C.-H., Huang, Z.-J., Liu, F., Xu, C.-W., and Li, X.-L. (2016). miR 760 mediates chemoresistance through inhibition of epithelial mesenchymal transition in breast cancer cells. *Eur. Rev. Med. Pharmacol. Sci.* 20, 5002–5008.
- Ip, Y. T., Park, R. E., Kosman, D., Yazdanbakhsh, K., and Levine, M. (1992). Dorsal-twist interactions establish snail expression in the presumptive mesoderm of the *Drosophila* embryo. *Genes Dev.* 6, 1518–1530. doi: 10.1101/gad.6.8.1518
- Jung, H. Y., Fattet, L., and Yang, J. (2015). Molecular pathways: linking tumor microenvironment to epithelial-mesenchymal transition in metastasis. *Clin. Cancer Res.* 21, 962–968. doi: 10.1158/1078-0432.CCR-13-3173
- Kurahara, H., Takao, S., Maemura, K., Mataka, Y., Kuwahata, T., Maeda, K., et al. (2012). Epithelial-mesenchymal transition and mesenchymal-epithelial transition via regulation of ZEB-1 and ZEB-2 expression in pancreatic cancer. *J. Surg. Oncol.* 105, 655–661. doi: 10.1002/jso.23020

- Lambies, G., Miceli, M., Martinez-Guillamon, C., Olivera-Salguero, R., Pena, R., Frias, C. P., et al. (2019). TGF β -activated USP27X deubiquitinase regulates cell migration and chemoresistance via stabilization of snail1. *Cancer Res.* 79, 33–46. doi: 10.1158/0008-5472.CAN-18-0753
- Lamouille, S., Xu, J., and Derynck, R. (2014). Molecular mechanisms of epithelial-mesenchymal transition. *Nat. Rev. Mol. Cell Biol.* 15, 178–196. doi: 10.1038/nrm3758
- Liedtke, C., Mazouni, C., Hess, K. R., Andre, F., Tordai, A., Mejia, J. A., et al. (2008). Response to neoadjuvant therapy and long-term survival in patients with triple-negative breast cancer. *J. Clin. Oncol.* 26, 1275–1281. doi: 10.1200/JCO.2007.14.4147
- Liu, Y., Du, F., Zhao, Q., Jin, J., Ma, X. I. N., and Li, H. (2015). Acquisition of 5-fluorouracil resistance induces epithelial-mesenchymal transitions through the Hedgehog signaling pathway in HCT-8 colon cancer cells. *Oncol. Lett.* 9, 2675–2679. doi: 10.3892/ol.2015.3136
- Mallini, P., Lennard, T., Kirby, J., and Meeson, A. (2014). Epithelial-to-mesenchymal transition: what is the impact on breast cancer stem cells and drug resistance. *Cancer Treat. Rev.* 40, 341–348. doi: 10.1016/j.ctrv.2013.09.008
- Moreno-Bueno, G., Portillo, F., and Cano, A. (2008). Transcriptional regulation of cell polarity in EMT and cancer. *Oncogene* 27, 6958–6969. doi: 10.1038/onc.2008.346
- Ohkubo, T., and Ozawa, M. (2004). The transcription factor Snail downregulates the tight junction components independently of E-cadherin downregulation. *J. Cell Sci.* 117, 1675–1685. doi: 10.1242/jcs.01004
- Smit, M. A., Geiger, T. R., Song, J. Y., Gitelman, I., and Peeper, D. S. (2009). A Twist-Snail axis critical for TrkB-induced epithelial-mesenchymal transition-like transformation, anoikis resistance, and metastasis. *Mol. Cell. Biol.* 29, 3722–3737. doi: 10.1128/MCB.01164-08
- Solanas, G., Porta-de-la-Riva, M., Agusti, C., Casagolda, D., Sanchez-Aguilera, F., Larriba, M. J., et al. (2008). E-cadherin controls beta-catenin and NF- κ B transcriptional activity in mesenchymal gene expression. *J. Cell Sci.* 121, 2224–2234. doi: 10.1242/jcs.021667
- Symmans, W. F., Wei, C., Gould, R., Yu, X., Zhang, Y., Liu, M., et al. (2017). Long-term prognostic risk after neoadjuvant chemotherapy associated with residual cancer burden and breast cancer subtype. *J. Clin. Oncol.* 35, 1049–1060. doi: 10.1200/JCO.2015.63.1010
- Tomaskovic-Crook, E., Thompson, E. W., and Thiery, J. P. (2009). Epithelial to mesenchymal transition and breast cancer. *Breast Cancer Res.* 11:21–23. doi: 10.1186/bcr2416
- van Nes, J. G., de Kruijf, E. M., Putter, H., Faratian, D., Munro, A., Campbell, F., et al. (2012). Co-expression of SNAIL and TWIST determines prognosis in estrogen receptor-positive early breast cancer patients. *Breast Cancer Res. Treat.* 133, 49–59. doi: 10.1007/s10549-011-1684-y
- van Roy, F., and Berx, G. (2008). The cell-cell adhesion molecule E-cadherin. *Cell. Mol. Life Sci.* 65, 3756–3788. doi: 10.1007/s00018-008-8281-1
- Vesuna, F., Lisok, A., Kimble, B., Domek, J., Kato, Y., van der Groep, P., et al. (2012). Twist contributes to hormone resistance in breast cancer by downregulating estrogen receptor- α . *Oncogene* 31, 3223–3234. doi: 10.1038/onc.2011.483
- Wang, W., Wang, L., Mizokami, A., Shi, J., Zou, C., Dai, J., et al. (2017). Down-regulation of E-cadherin enhances prostate cancer chemoresistance via Notch signaling. *Chin. J. Cancer* 36:35. doi: 10.1186/s40880-017-0203-x
- Xu, T., Zhang, J., Chen, W., Pan, S., Zhi, X., Wen, L., et al. (2016). ARK5 promotes doxorubicin resistance in hepatocellular carcinoma via epithelial-mesenchymal transition. *Cancer Lett.* 377, 140–148. doi: 10.1016/j.canlet.2016.04.026
- Ye, Y., Xiao, Y., Wang, W., Yearsley, K., Gao, J. X., and Barsky, S. H. (2008). ER α suppresses slug expression directly by transcriptional repression. *Biochem. J.* 416, 179–187. doi: 10.1042/BJ20080328
- Ye, Y., Xiao, Y., Wang, W., Yearsley, K., Gao, J. X., Shetuni, B., et al. (2010). ER α signaling through slug regulates E-cadherin and EMT. *Oncogene* 29, 1451–1462. doi: 10.1038/onc.2009.433
- Zhang, J., and Ma, L. (2012). MicroRNA control of epithelial-mesenchymal transition and metastasis. *Cancer Metastasis Rev.* 31, 653–662. doi: 10.1007/s10555-012-9368-6
- Zhang, P., Sun, Y., and Ma, L. (2015). ZEB1: at the crossroads of epithelial-mesenchymal transition, metastasis and therapy resistance. *Cell Cycle* 14, 481–487. doi: 10.1080/15384101.2015.1006048
- Zheng, X., Carstens, J. L., Kim, J., Scheible, M., Kaye, J., Sugimoto, H., et al. (2015). Epithelial-to-mesenchymal transition is dispensable for metastasis but induces chemoresistance in pancreatic cancer. *Nature* 527, 525–530. doi: 10.1038/nature16064
- Zhou, Y., Hu, Y., Yang, M., Jat, P., Li, K., Lombardo, Y., et al. (2014). The miR-106b~25 cluster promotes bypass of doxorubicin-induced senescence and increase in motility and invasion by targeting the E-cadherin transcriptional activator EP300. *Cell Death Differ.* 21, 462–474. doi: 10.1038/cdd.2013.167

Conflict of Interest: The authors declare that the research was conducted in the absence of any commercial or financial relationships that could be construed as a potential conflict of interest.

Copyright © 2021 Wan, Hou, Liu, Zhang, Li, Zhang and Ding. This is an open-access article distributed under the terms of the Creative Commons Attribution License (CC BY). The use, distribution or reproduction in other forums is permitted, provided the original author(s) and the copyright owner(s) are credited and that the original publication in this journal is cited, in accordance with accepted academic practice. No use, distribution or reproduction is permitted which does not comply with these terms.



Cell-Free DNA: Hope and Potential Application in Cancer

Yan-yan Yan^{1,2†}, Qiao-ru Guo^{2,3†}, Feng-hua Wang^{4†}, Rameshwar Adhikari⁵, Zhuang-yan Zhu¹, Hai-yan Zhang¹, Wen-min Zhou², Hua Yu^{6*}, Jing-quan Li^{3*} and Jian-ye Zhang^{1,2,3*}

¹ School of Medicine, Shanxi Datong University, Datong, China, ² Key Laboratory of Molecular Target and Clinical Pharmacology and the State Key Laboratory of Respiratory Disease, School of Pharmaceutical Sciences and the Fifth Affiliated Hospital, Guangzhou Medical University, Guangzhou, China, ³ The First Affiliated Hospital, Hainan Medical University, Haikou, China, ⁴ Guangzhou Institute of Pediatrics/Guangzhou Women and Children's Medical Center, Guangzhou Medical University, Guangzhou, China, ⁵ Research Centre for Applied Science and Technology, Tribhuvan University, Kirtipur, Nepal, ⁶ State Key Laboratory of Quality Research in Chinese Medicine, Institute of Chinese Medical Sciences, Avenida da Universidade, Taipa, China

OPEN ACCESS

Edited by:

Wei Zhao,
Chengdu Medical College, China

Reviewed by:

Hongming Miao,
Army Medical University, China
Yi-Chao Zheng,
Zhengzhou University, China

*Correspondence:

Jian-ye Zhang
jianyez@163.com
Jing-quan Li
lijingquan2008@163.com
Hua Yu
bcalecyyu@um.edu.mo

[†]These authors have contributed
equally to this work

Specialty section:

This article was submitted to
Molecular and Cellular Oncology,
a section of the journal
Frontiers in Cell and Developmental
Biology

Received: 08 December 2020

Accepted: 20 January 2021

Published: 22 February 2021

Citation:

Yan Y-y, Guo Q-r, Wang F-h,
Adhikari R, Zhu Z-y, Zhang H-y,
Zhou W-m, Yu H, Li J-q and Zhang J-y
(2021) Cell-Free DNA: Hope and
Potential Application in Cancer.
Front. Cell Dev. Biol. 9:639233.
doi: 10.3389/fcell.2021.639233

Cell-free DNA (cfDNA) is easily accessible in peripheral blood and can be used as biomarkers for cancer diagnostics, prognostics, and therapeutics. The applications of cfDNA in various areas of cancer management are attracting attention. In this review article, we discuss the potential relevance of using cfDNA analysis in clinical oncology, particularly in cancer screening, early diagnosis, therapeutic evaluation, monitoring disease progression; and determining disease prognosis.

Keywords: cell-free DNA (cfDNA), cancer, diagnosis, therapeutic effect evaluation, liquid biopsy

INTRODUCTION

Cell-free DNA (cfDNA) is released from cells into the circulatory system throughout the body. It was first discovered by Mandel and Métais in 1948 (Mandel and Metais, 1948). cfDNA can be found in plasma (Mandel and Metais, 1948) and other body fluids such as, cerebral spinal fluid (CSF) (Rhodes et al., 1994), pleural fluid (Sriram et al., 2012), urine (Sidransky et al., 1991; Zhang et al., 1999), saliva (Mithani et al., 2007; Wang et al., 2015), and others. Previous studies indicated that most of the plasma cfDNA molecules originate from the hematopoietic system in healthy individuals (Lui et al., 2002; Sun et al., 2015). However, in certain physiological or pathological conditions, such as pregnancy, organ transplantation, and cancers, the related/affected tissues could release additional DNA into peripheral circulation (Leon et al., 1977; Lo et al., 1997, 1998). Therefore, detection of cfDNA in peripheral blood could identify abnormalities of individuals in a noninvasive manner. In recent years, a variety of technologies have emerged based on the analysis of cfDNA for noninvasive prenatal testing (NIPT) (Lo et al., 1997, 2007; Hyett et al., 2005; Wong and Lo, 2015; Hudecova and Chiu, 2017; Bianchi and Chiu, 2018; Malan et al., 2018; Vivanti et al., 2019; Zhang J. et al., 2019), monitoring organ transplantation (Lo et al., 1998; Gielis et al., 2015; Gala-Lopez et al., 2018; Sherwood and Weimer, 2018), and detecting immune diseases (Zhang et al., 2014; Beranek et al., 2017; Dunaeva et al., 2018; Xu et al., 2018; Duvvuri and Lood, 2019), as well as cancers.

Analysis of protein biomarkers and nucleic acids has become very popular for cancer diagnosis (Huang et al., 2020), risk stratification, and molecular targeting therapeutics (Zhang D. et al., 2019; Wang et al., 2020). However, many biomarker studies are based on analysis of tumor tissues that are obtained from invasive surgical procedures and may not be accessible in some cases. New approaches with noninvasive procedure are urgently needed. cfDNA analysis has attracted

increasing attention because of its easy accessibility, noninvasive nature, and potential tumor specificity through quantitative detection or specific sequencing. In **Table 1**, we summarized several cfDNA applications in different diseases. Therefore, considerable efforts have been made to explore the potential application of cfDNA in clinical cancer management. The sensitivity of cfDNA analytic technologies has been greatly improved due to the advancement of molecular biology and next-generation sequencing (NGS) approaches. cfDNA analysis is widely used in various areas of cancer diagnostics and prognostics, as well as cancer drug resistance, and early screening.

Cancer patients usually have a high level of cfDNA in their serum or plasma as a result of cellular necrosis or apoptosis, because tumor cells divide faster than normal cells, and cfDNAs are released in a high proportion (Sorenson et al., 1994; Vasioukhin et al., 1994; Raja et al., 2018). The fraction of cfDNA that derived from tumor cells is named circulating tumor DNA (ctDNA) (Leon et al., 1977; Shu et al., 2017). In recent years, both cfDNA and ctDNA have gotten huge attention as novel blood biomarkers, as quantification and kinetic analysis of cfDNA (Diehl et al., 2008) and molecular profiling of ctDNA have suggested their predictive and prognostic values (Iizuka et al., 2006; Tokuhisa et al., 2007). Several liquid biopsy tests, designed for the identification of cancer-specific mutations, have been recommended as companion diagnostic (CDx) tests, by the European Medicines Agency (EMA) and Food and Drug Administration (FDA) of USA, to guide therapeutic decision making. Such tests include the cobas EGFR Mutation Test for non-small lung cancer or BRAC Analysis CDx for breast and

ovarian cancer. Epi proColon[®], based on the analyses of the methylation status of the SEPT9 gene, is the first and only FDA-approved blood-based test for the detection of colorectal cancer. The applications of cfDNA in cancer are shown in **Figure 1**.

cfDNA FOR CANCER DIAGNOSIS AND EARLY SCREENING

Analysis of cfDNA has become a promising noninvasive approach in cancer diagnosis (Haber and Velculescu, 2014; Siravegna et al., 2017). The applications of cfDNA-based cancer liquid biopsy in recent year are summarized in **Table 2**. cfDNA comes from fragmented DNA released by cells into the circulation, most commonly as a result of cell death. In healthy individuals, the blood cfDNA originates from germline DNA released by normal cells. In cancer patients, a portion of cfDNA comes from tumor cells, named circulating-tumor DNA (ctDNA), which may contain tumor-specific variations corresponding to the patient's tumor, such as mutated tumor suppressor genes or oncogenes (Wang et al., 2004), microsatellite instability (MSI) (Shaw et al., 2000), and DNA methylation (Fujiwara et al., 2005). Based on some quantitative studies, it is found that the concentration of cfDNA in healthy subjects is between 0 and 100 ng/ml of blood with an average of 30 ng/ml, whereas the concentration of cfDNA in the blood of cancer patients varies from 0 to 1,000 ng/ml, with an average of 180 ng/ml (Leon et al., 1977; Esposito et al., 2017; Phallen et al., 2017).

TABLE 1 | Summary of cfDNA applications in different diseases.

Disease	Marker(s)	Technical method	Clinical significance	Sample	References
Non-invasive prenatal testing (NIPT)	Fetal DNA	PCR, sequencing; Y-PCR assay	Trisomy 13, 18, or 21; fetal achondroplasia; dominant monogenic diseases; thalassemias; determination of fetal sex	Maternal plasma or serum	Lo et al., 1997; Wong and Lo, 2015; Hudecova and Chiu, 2017; Bianchi and Chiu, 2018; Malan et al., 2018; Vivanti et al., 2019; Zhang J. et al., 2019
Organ transplantation	Donor-specific DNA	PCR, Sequencing	Monitoring organ transplantation	Plasma of transplant recipients	Lo et al., 1998; Gielis et al., 2015; Gala-Lopez et al., 2018; Sherwood and Weimer, 2018
Immune diseases	Elevated levels of cfDNA; LINE-1 hypermethylation	Picogreen Kit; qPCR (quantitative real-time PCR); methylation-specific quantitative PCR, sequencing	Detecting and assessing systemic lupus erythematosus (SLE) disease activity and monitoring treatment; exacerbated psoriasis; relapsing remitting multiple sclerosis; autoimmune rheumatic diseases	Plasma or serum of patients	Zhang et al., 2014; Beranek et al., 2017; Dunaeva et al., 2018; Xu et al., 2018; Duvvuri and Lood, 2019
Cancer	Circulating tumor DNA	PCR; sequencing	Diagnosis; predicting response to therapy; indicating prognosis	Plasma and serum of cancer patients	Wan et al., 2017; Wang and Xu, 2019; Fares et al., 2020

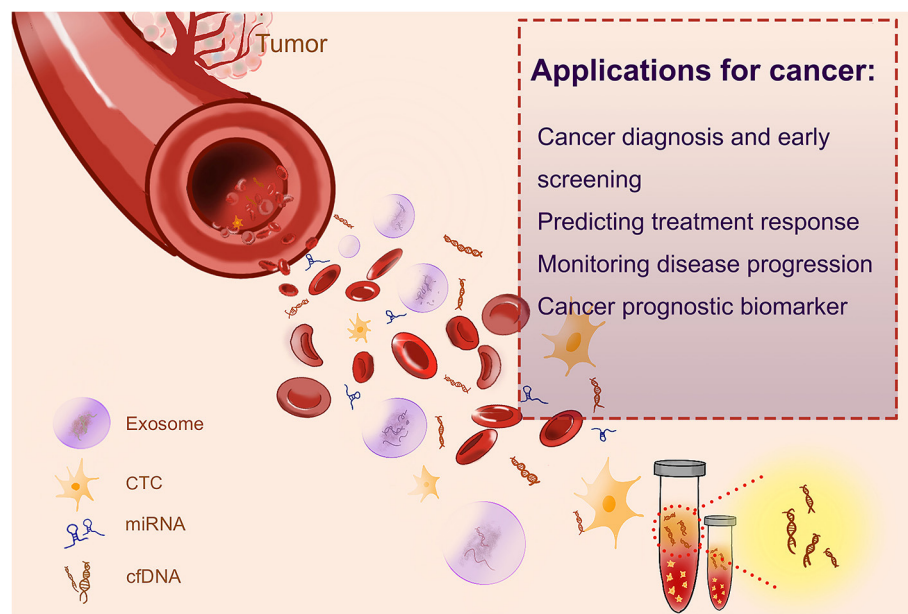


FIGURE 1 | The applications of cfDNA in cancer.

It is reported that the size (Kamat et al., 2006; Gorges et al., 2012) and stage (Nawroz et al., 1996; Bettegowda et al., 2014) of tumors are correlated with the blood level of ctDNA. There are 100–1,000 copies of ctDNA per 5 mL of blood in patients with stage IV or advanced tumors, and only 10 copies of ctDNA in those with early stage cancers (Bettegowda et al., 2014). Additional amount of ctDNA is also seen in patients with metastatic tumors. Quantification on patients with relapsed high-grade serous ovarian carcinoma (HGSOC) has indicated an increase of six copies of ctDNA per mL blood for an additional 1 cm³ of tumor (Parkinson et al., 2016).

Hematological Malignancies

Some studies analyzed the cfDNA in hematologic malignancies. TP53 (G249 T, G249A, T176C, C250 T, and T238 G) and nucleophosmin mut.A (a duplication of the TCTG at positions 956–959) mutations were found in cfDNA from patients with acute myelogenous leukemia (AML) and non-Hodgkin's lymphoma (NHL) (Hosny et al., 2009; Quan et al., 2015). The diagnosis of lymphomas in the central nervous system (CNS) is complex, and obtaining brain biopsy is of high risk of complications. Biomarkers in blood and cerebrospinal fluid could be potential tools for early diagnosis of lymphomas. Zorofchian et al. examined a patient with suspected CNS lymphoma by detecting MYD88 mutation (L265 P and V217 F) in the cerebrospinal fluid (CSF). They suggested that analysis of cfDNA in CSF could be a minimally invasive diagnostic tool for CNS lymphomas (Zorofchian et al., 2018). Other studies also proved the potential of detecting MYD88 mutation in CSF as well as in plasma (Fontanilles et al., 2017; Hiemcke-Jiwa et al., 2019). Patients with lymphoma showed a higher level of cfDNA in their plasma than did healthy subjects. Hohaus et al. (2009)

reported that the cfDNA level is different in patients with diffuse large B-cell lymphoma (DLBCL), mantle cell lymphoma (MCL), and Hodgkin's lymphoma (HL). Nucleosomal DNA (ncDNA) is another source of cfDNA. The changes of ncDNA corresponded with response to treatment, suggesting that ncDNA could be a valuable biomarker for hemopoietic cancer patients (Mueller et al., 2006). Taken together, cfDNA can be used for detecting gene mutation and chromosomal abnormalities. The level of blood cfDNA might serve as an important noninvasive diagnostic tool for patients with hemopoietic cancers.

Thyroid Cancer

Salvianti et al. adopted a quantitative real-time PCR (qPCR) approach based on quantification of two amplicons with different lengths (67 and 180 bp) to evaluate the integrity index 180/67. They reported that the cfDNA integrity index 180/67 can monitor cfDNA fragmentation in thyroid cancer. Thus, the cfDNA integrity index 180/67 could be used as a circulating biomarker for the diagnosis of thyroid nodules. The quantity of cfDNA is higher in patients affected by nodular thyroid diseases than in healthy individuals. Importantly, the cfDNA integrity index was higher in patients with cytologically diagnosed thyroid carcinoma (Thy4/Thy5) than in individuals with benign nodules (Thy2) (Salvianti et al., 2017).

Colorectal Cancer

It is reported that KRAS mutation can be identified using cfDNA. Wang et al. uncovered KRAS mutations (in codons 12, 13, and 61) in patients with stage I–IV colorectal cancer and found these mutations in blood samples. They showed that there are about 45% of concordance between the CRC tumor tissues and cfDNA. KRAS mutations are not found in cfDNA of healthy subjects

TABLE 2 | Summary of cfDNA-based cancer liquid biopsy studies.

Cancer type	Marker(s)	Technical method	Clinical significance	Sample	References
Hematological malignancies	Copies of circulating NPM mutation A (NPM mut.A) DNA; TP53 mutations; MYD88 p.L265P mutation	RT-PCR and sequencing analysis; direct sequencing and a PCR-restriction digestion analysis (RFLP); droplet digital PCR (ddPCR)	Diagnosis	Plasma; serum; cerebrospinal fluid (CSF)	Hosny et al., 2009; Quan et al., 2015; Zorofchian et al., 2018
Thyroid cancer	Cell-free DNA quantity and integrity index 180/67	Quantitative real-time PCR (qPCR)	Diagnosis	Plasma	Salvianti et al., 2017
Colorectal cancer	ALU115; dozens of DNA hypermethylation markers (e.g., SEPT9 and IKZF1, EMBP1, KCNQ5, CHST11, APBB1P, and TJP2)	qPCR; methylated CpG tandem amplification and sequencing (MCTA-Seq)	Diagnosis	Plasma	Bhangu et al., 2017; Li et al., 2019
	High cfDNA and ctDNA levels; methylated circulating DNA biomarkers (EYA4, GRIA4, ITGA4, MAP3K14-AS1, MSC)	ddPCR	Predicting response to therapy	Plasma	Barault et al., 2018; Lyskjaer et al., 2019
	High cfDNA levels; methylation levels of HMTF, HPP1/TPEF, hMLH1, TAC1, and SEPT9	ddPCR; quantitative methylation-specific PCR	Indicating prognosis	Plasma; serum	Wallner et al., 2006; Tham et al., 2014; Hamford et al., 2019
Gastric cancer	Mutations of cadherin (CDH1), phosphatidylinositol-4,5-bisphosphate 3-kinase catalytic subunit alpha (PIK3CA), ARID1A (AT-rich interactive domain 1A), epidermal growth factor receptor (EGFR), and phosphatase and tensin homolog deleted on chromosome 10 (PTEN); 5-hydroxymethylcytosine (5hmC)	Bidirectional sequencing; 5 hmC quantification	Diagnosis	Plasma	Samuels et al., 2004; Li et al., 2005, 2017; Velho et al., 2005; Kaurah et al., 2007; Heald et al., 2010; Wen et al., 2010; Corso et al., 2011, 2012; Liu et al., 2011; Lee et al., 2012; Zang et al., 2012; Chen et al., 2013
Hepatocellular carcinoma	RASSF1A promoter hypermethylation	Methylation-specific PCR	Diagnosis	Serum	Chan et al., 2008
	Post-radiotherapy (RT) cfDNA levels; mutation of BAX, CYP2B6 and HNF1A	RT-PCR; NGS	Predicting response to therapy	Plasma	Park et al., 2018; Alunni-Fabbroni et al., 2019
	Methylation of insulin-like growth factor-binding protein 7 (IGFBP7); higher level of circulating DNA	RT-PCR	Indicating prognosis	Serum; plasma	Ren et al., 2006; Li et al., 2018
HPV-positive metastatic cervical cancer	HPV cfDNA	Duplex digital droplet PCR (ddPCR)	Diagnosis; predicting response to therapy	Serum	Kang et al., 2017
Nasopharyngeal carcinoma	Epstein-Barr virus (EBV) DNA	PCR	Diagnosis	Plasma	Chan et al., 2017
Lung cancer	act-EGFR mutant allele frequency (MAF) and T790M/act-EGFR MAF ratio; 36 cancer-related genes; TP53, RB1, BRAF, KIT, NOTCH1-4, PIK3CA, PTEN, FGFR1, MYC, MYCL1, and MYCN	ddPCR; NGS	Predicting response to therapy	Plasma	Almodovar et al., 2018; Del Re et al., 2018; Guibert et al., 2019
	EGFR19del, L858R, and T790M; cfDNA concentration; KRAS mutation	ddPCR; RFLP-PCR; mutant-enriched PCR	Indicating prognosis	Plasma or serum	Ai et al., 2016; Yanagita et al., 2016

(Continued)

TABLE 2 | Continued

Cancer type	Marker(s)	Technical method	Clinical significance	Sample	References
Prostate cancer	Androgen receptor gene (AR) copy numbers (CN) and mutations; cfDNA concentration and mutations (BRCA2, PALB2); AR amplification, TMPRSS2-ERG fusion, PTEN gene deletion, NOTCH1 locus amplification along with genomic amplifications	dPCR and target sequencing; targeted cfDNA sequencing; whole-genome sequencing (WGS)	Predicting response to therapy	Plasma, urine	Xia et al., 2016; Goodall et al., 2017; Sumiyoshi et al., 2019
	Hypermethylation patterns of two genes (GSTP1 and APC)	Methylation-specific PCR	Indicating prognosis	Plasma	Hendriks et al., 2018
Breast cancer	ESR1 mutation	Digital PCR	Predicting response to therapy	Plasma	Beije et al., 2018
	cfDNA concentration and cfDNA integrity (cfDI); ALU-247, ALU-115, and cfDNA Integrity; methylation of KLK10, SOX17, WNT5A, MSH2, GATA3	RT-qPCR; quantitative methylation-specific PCR	Indicating prognosis	Plasma	Cheng et al., 2018; Hussein et al., 2019; Panagopoulou et al., 2019
Cervical cancer	Increased cfDNA allele fraction deviation (AFD)	Targeted deep sequencing	Predicting response to therapy	Plasma	Tian et al., 2019
Bladder carcinoma	Presence and dynamics of cfDNA	Ultra-deep multiplex polymerase chain reaction-based next-generation sequencing	Predicting response to therapy	Plasma	Christensen et al., 2019
Pancreatic cancer	ABL1, ATM, DNMT3A, FLT3, HNF1A, NRAS, and SMAD4	NGS; Library Preparation Kit	Predicting response to therapy	Plasma	Vietsch et al., 2017
	Pretreatment cfDNA fragment size of ≤ 167 bp (mode) and high pre-treatment cfDNA levels	Agilent 2100 Bioanalyzer and the Agilent High Sensitivity DNA chip	Indicating prognosis	Plasma	Lapin et al., 2018
Esophageal cancer	Mutations of TP53, PIK3CA, ERBB2	NGS; ddPCR	Predicting response to therapy	Plasma	Pasternack et al., 2018
Oral squamous cell carcinoma	Higher cfDNA levels	Quantitative spectrometry	Indicating prognosis	Plasma	Lin et al., 2018
Metastatic melanoma	Baseline cfDNA concentration	ddPCR	Indicating prognosis	Plasma	Valpione et al., 2018

(Wang et al., 2004). In the study of Anker et al. (1997), a high (86%) KRAS mutation in codon 12 was found in tumor tissue and blood. Thierry et al. (2014) reported an even higher (96%) mutation of KRAS in codons 12 and 13 in tumor tissues and blood, and the mutation of BRAF (V600E) reached 100%. Bhangu et al. (2017) found that the level of ALU115 in cfDNA could be an indicator of colorectal cancer (CRC).

Li et al. adopted a fully methylated molecule algorithm with the methylated CpG tandem amplification and sequencing (MCTA-Seq) method, to examine the blood sample of patients with CRC ($n = 147$) and healthy individuals ($n = 136$), as well as cancer and adjacent noncancerous tissues ($n = 66$). They found that a number of biomarkers of DNA hypermethylation including the known (e.g., SEPT9 and IKZF1) and the novel

(e.g. TJP2, EMBP1, APBB1IP, CHST11, and KCNQ5) genes were detected in cfDNA of CRC (Li et al., 2019).

Gastric Cancer

It was known that mutations in genes such as CDH1 (Kaurah et al., 2007; Corso et al., 2012; Chen et al., 2013), PIK3CA (Samuels et al., 2004; Li et al., 2005; Velho et al., 2005; Lee et al., 2012), ARID1A (AT-rich interactive domain 1A) (Zang et al., 2012), EGFR (Corso et al., 2011; Liu et al., 2011), and PTEN (Heald et al., 2010; Wen et al., 2010) existed in gastric cancer, providing potential circulating DNA for detection of gastric cancer. For example, a clinical correlation analysis of ctDNA in patients with gastric adenocarcinoma showed that PIK3CA is one of the most frequently affected character-altered

alterations, which can help to indicate clinically relevant genomic data for clinical diagnosis and treatment (Maron et al., 2019). Li et al. (2017) reported that 5 hmC of circulating cfDNA could specifically and sensitively separate gastric cancer patients from healthy subjects.

Hepatocellular Carcinoma

DNA methylation is involved in activating protooncogenes or inactivating tumor-suppressor genes. The study of Yeo et al. (2005) revealed that RASSF1A promoter hypermethylation in blood cfDNA is correlated with the size of hepatocellular carcinoma (HCC). Furthermore, patients with hypermethylated RASSF1A in cfDNA at the time of diagnosis or 1 year after tumor resection have shorter DFS (Chan et al., 2008). The detection of RASSF1A promoter methylation in cfDNA in the blood is 90% in HCC patients and only 10% in healthy subjects. The mean blood level of methylated RASSF1A in HCC patients is significantly higher than that in healthy individuals (Mohamed et al., 2012).

Virus-associated Cancer

cfDNA analysis has been used to screen diseases before clinical onset (Mao et al., 1994; Gormally et al., 2006; Phallen et al., 2017). cfDNA analysis has shown to be an effective way to screen the asymptomatic early-stage nasopharyngeal carcinoma caused by Epstein-Barr virus (EBV), as the viral cfDNA level is much higher than that of ctDNA. One study involved in screening of >20,000 asymptomatic subjects for EBV DNA in blood has led to the diagnosis of nasopharyngeal carcinoma in 34 individuals (Chan et al., 2017). Identification of these early diagnosed patients improved the 3-year progression-free survival (Chan et al., 2017). Circulating cfDNA of human papillomavirus (HPV) (HPV cfDNA) may be used as a unique tumor biomarker for HPV-associated malignancies, including cervical cancer (Kang et al., 2017).

cfDNA IN MONITORING DISEASE PROGRESSION AND PREDICTING TREATMENT RESPONSE IN CANCERS

Since access to longitudinal tumor tissues are limited, some studies chose to focus on the characterization of cfDNA for rapid, noninvasive monitoring for disease progression, treatment response, and disease relapse.

Hepatocellular Carcinoma

cfDNA is used as a prognostic biomarker in patients with advanced HCC. Park et al. examined the clinical significance of cfDNA in patients with HCC treated with radiotherapy (RT). They found that the level of post-RT cfDNA was negatively correlated with treatment outcome, indicating the potential of using post-RT cfDNA level as a predictor of treatment response and local control (LC) (Park et al., 2018). Alunni-Fabbroni et al. investigated the use of cfDNA and ctDNA in HCC patients to assess therapeutic response and clinical outcome. The level of cfDNA was shown to have a significant correlation with tumor metastases and patient survival. In addition, a dynamic study on cfDNA uncovered a trend of cfDNA level

with the clinical history of patients, suggesting its usefulness as a biomarker for monitoring treatment response. Twenty-eight variants were identified in different combinations at different time points using NGS-based analysis on ctDNA. Among these variants, BAX, CYP2B6, and HNF1A genes showed the highest frequency of mutation and a significant association with the clinicopathological characteristics of patients, indicating their possible roles as driver genes in the clinical setting (Alunni-Fabbroni et al., 2019). The relationship between the level of blood cfDNA and clinicopathological characteristics was investigated in other studies. It was found that HCC patients with a larger tumor size (≥ 5 cm) or vascular invasion often showed higher levels of blood cfDNA (Iizuka et al., 2006; Huang et al., 2012). Huang et al. (2012) investigated the dynamic change of the level of blood cfDNA in patients with stage I–IV HCC and found that the level of cfDNA decreases after removal of tumors.

Lung Cancer

The correlation between osimertinib treatment outcome and activating EGFR (act-EGFR) mutations and T790M in cfDNA was evaluated in patients with advanced non-small cell lung cancer (NSCLC). Thirty-four patients with NSCLC resistant to first- and second-generation EGFR-TKIs, who are positive for both act-EGFR and T790M in cfDNA at the time of progression, were enrolled in this study. Blood samples were collected at baseline and 3 months after osimertinib treatment. cfDNA was analyzed by droplet digital PCR, and the results were expressed as mutant allele frequency (MAF). At baseline, the MAF of act-EGFR was significantly higher than that of T790M ($p < 0.0001$). The act-EGFR MAF and ratio of T790M/act-EGFR MAF was significantly correlated with disease response ($p = 0.02$). The cutoff value of act-EGFR MAF and T790M/act-EGFR ratio was found to be 2.6% and 0.22, respectively. The PFS of patients with act-EGFR MAF of >2.6 and $<2.6\%$, was 10 months vs. not reached, respectively ($p = 0.03$), whereas patients with T790M/act-EGFR ≤ 0.22 had poorer PFS than those >0.22 (6 months vs. not reached, respectively, $p = 0.01$). act-EGFR MAF and T790M/act-EGFR MAF ratio are potential indicators of outcome in patients treated with osimertinib. The amount of activating EGFR mutations in circulating cfDNA is an indicator for monitoring osimertinib response (Del Re et al., 2018).

Mutation of tumor genes can be indicators of treatment response to immune checkpoint inhibitors (ICI) (Yuan et al., 2019). The study of Guibert et al. showed that sequencing of blood cfDNA can predict response to PD1 inhibitors in advanced NSCLC. The presence of a PTEN or STK11 mutation was correlated with early progression, while transversion mutations (Tv) in KRAS and TP53 predicted better outcomes. Patients with a low immune score (driver gene and/or PTEN or STK11 mutation and/or without KRAS or TP53 Tv) have a poor outcome with a median PFS of 2 months, compared with patients who have a high immune score (no driver gene, no PTEN or STK11, and with KRAS or TP53 Tv) and have a median PFS of 14 months ($p = 0.0001$, HR = 2.96). Another study showed that the change of allele fraction (AF) of ctDNA is correlated with clinical outcomes in 65 specimens, where the PFS is 14 months if AF decreases vs. 2 months if AF increases ($p < 0.0001$) (Guibert et al., 2019).

Almodovar et al. (2018) demonstrated that longitudinal cfDNA analysis in patients with small cell lung cancer (SCLC) can reveal insights into treatment efficacy and disease relapse.

Colorectal Cancer

Lyskjær et al. suggested that the level of cfDNA and ctDNA is correlated with the outcome of FOLFIRI treatment in metastatic colorectal cancer (mCRC). In their study, 24 patients with mCRC were enrolled and treated with FOLFIRI-based therapy. Blood was sampled before treatment, at days 7, 14, 21, and 60 after treatment and at progression, and the level of cfDNA and ctDNA was analyzed. Patients with a high level of pretreatment ctDNA or cfDNA (≥ 75 th percentile) had significantly shorter PFS than those with a low level of ctDNA or cfDNA. Despite an overall decline in ctDNA level from pretreatment to first CT scan, 7 patients were identified with temporary increases in ctDNA and these patients had shorter PFS and OS, which was coincident with growth of drug-resistant cells. This study indicated that increased level of ctDNA in the first cycle of FOLFIRI treatment was an indicator of progressive disease and poor survival. Therefore, monitoring the level of ctDNA as early as 1 week after treatment is important for early detection of treatment failure (Lyskjær et al., 2019).

Zitt et al. (2008) reported that the blood level of cfDNA decreased in patients who responded to chemoradiotherapy (responders, stage I–II), while the blood level of cfDNA increased in the nonresponders. The integrity index of cfDNA was lower after chemoradiotherapy (CRT) in responders when compared to nonresponders. In general, patients with CRC have 10 times higher integrity index than healthy individuals (Agostini et al., 2011). Sun et al. (2014) observed that the incidence of KRAS mutation at codon 12 in cfDNA decreased in responders.

Methylation test in liquid biopsy can be used in the absence of specific mutations of patients to monitor dynamic tumor burden. The selected biomarkers allowed monitoring tumor burden under different treatment regimens. Methylation test might be used to assess pharmacodynamics in clinical trials or in complementing conventional imaging analysis. Barault et al. (2018) reported that dynamics of methylation biomarkers was correlated with subjective tumor response and progression-free survival in patients with metastatic colorectal cancer.

Prostate Cancer

cfDNA analysis can be used as a useful tool for precision medicine in castration-resistant prostate cancer (CRpC). Sumiyoshi et al. (2019) analyzed the cfDNA from 41 patients with CRpC. Most AR aberrations at baseline diminished with effective treatments, whereas AR amplification or mutations emerged in some patients with disease progression.

Goodall et al. reported that cfDNA analysis could guide the treatment of using poly(ADP)-ribose polymerase (PARP) inhibitor olaparib in metastatic prostate cancer (mPC). A decrease in blood level of cfDNA is correlated with the treatment outcome of PARP inhibitor olaparib in the Phase II Trial of Olaparib in Patients with Advanced Castration Resistant Prostate Cancer (Goodall et al., 2017). Briefly, somatic mutations of DNA repair were detectable in cfDNA in tumor tissues. The

allele frequency of somatic mutations decreased selectively in responding patients (Chi-squared $p < 0.001$). Multiple subclonal aberrations revert somatic and germline mutations of DNA repair (BRCA2, PALB2) following response to olaparib treatment as disease progressed (Goodall et al., 2017).

To evaluate the tumor DNA fraction in urine cfDNA, Xia et al. developed an algorithm of Urine Genomic Abnormality (UGA) score which summed up the top 10 most significant segments with copy number changes. The UGA score is correlated with tumor burden, and the change in UGA score after stage-specific therapy reflected the status of disease progression and overall survival. The study demonstrated the potential clinical use of urine cfDNA in predicting treatment response and monitoring disease progression (Xia et al., 2016).

Breast Cancer

Monitoring gene mutations is important in clinics. Notably, ESR1 mutation is detected at a high frequency in cfDNA of ER-positive metastatic breast cancer (MBC) and rarely found at the early-stage cancer. ESR1 mutation is enriched at disease progression, suggesting a role of ESR1 in MBC (Beije et al., 2018). The presence of ESR1 mutation indicates the development of endocrine resistance, especially resistant to aromatase inhibitors (Spoerke et al., 2016). Beije et al. (2018) suggested that ESR1 mutation is more prevalent in tumor progression (42%) than before progression (11%) ($P = 0.04$).

Cervical Cancer

Tian et al. applied blood cfDNA analysis to evaluate the dynamic mutational change in 48 cancer driver genes in cervical cancer patients. They found that different treatments, including radiotherapy ($n = 14$), chemotherapy ($n = 22$), and surgery ($n = 15$), resulted in a significant decrease in the value of allele fraction deviation (AFD) (Wilcoxon, $p = 0.029$). The decrease of cfDNA AFD value was associated with reduced size of tumor in most patients. Progressive disease (metastasis) was detected in a subgroup of patients whose cfDNA AFD value did not reflect a reduction in tumor size. Also, a low AFD value at diagnosis followed by a later increased AFD value predicted disease relapse (Tian et al., 2019).

HPV ccfDNA could be used to select patients for HPV-type-specific T-cell-based immunotherapies. It might also have a value for evaluating antitumor activity of therapeutic drugs and long-term follow-up in patients with cervical cancer. Kang et al. proposed an approach to genotype and quantify HPV-circulating DNA in patients with HPV16- or HPV18-positive metastatic cervical cancer for potential disease monitoring and treatment decision making. In this retrospective study, HPV ccfDNA was detected in 100% (19 of 19) patients with HPV-positive metastatic cervical cancer but not in any of the 45 healthy blood donors. The HPV genotype harbored in the patients' tumors was correctly identified in 100% (87 of 87) of serial blood samples of nine patients who received TIL immunotherapy. In three patients who experienced objective cancer regression after TIL treatment, a transient HPV ccfDNA peak was observed 2–3 days after TIL infusion. Moreover, persistent clearance of HPV ccfDNA was

found in two patients who experienced complete response (CR) after TIL immunotherapy (Kang et al., 2017).

Bladder Carcinoma

Using Ultra-Deep Sequencing of Plasma Cell-Free DNA, Emil Christensen and his group evaluated early metastatic relapse and examined treatment efficacy of urothelial bladder carcinoma. They found that ctDNA positivity before or in the course of treatment indicated high-risk patients. The dynamic change of ctDNA is correlated with tumor recurrence (Christensen et al., 2019).

Pancreatic Cancer

Analysis of cfDNA can be applied to evaluate the mutational makeup of cancer lesions and monitor cancer progression at the molecular level with no need of invasively acquired tissues from primary or metastatic lesions. Vietsch et al. showed that incorporation of cfDNA analysis provides crucial insights into the molecular change of progression of colon and pancreatic cancer. They revealed that cfDNA collected at the time of progression harbored 3–5 new mutations not detected in cfDNA collected at the earlier time points (Vietsch et al., 2017).

Esophageal Cancer

Pasternack et al. (2018) found that detection of somatically altered cfDNA in patients with esophageal carcinoma in early stage is associated with postsurgical tumor recurrence.

cfDNA AS A PROGNOSTIC BIOMARKER FOR CANCER

cfDNA is attracting attention as a novel biomarker for predicting outcome in oncology and is able to predict overall survival in cancer patients.

Breast Cancer

Panagopoulou et al. revealed that elevated concentrations of blood cfDNA are correlated with nonresponse to pharmacotherapy, shorter progression-free survival (PFS), and increased incidence of death in metastatic breast cancer (MBC). The methylation of WNT5A was significantly correlated with large tumor size, poor prognosis, and advanced-stage disease with short overall survival in MBC patients (Panagopoulou et al., 2019). Hussein et al. (2019) suggested that both plasma ALU-247 and ALU-115 repeats were preoperative prognostic biomarkers for breast cancer. Schiavon et al. (2015) showed that metastatic breast cancer patients with ESR1 mutations in their ctDNA had substantially shorter PFS on subsequent aromatase inhibitor-based therapy. Cheng et al. (2018) found that the integrity and blood level of cfDNA can serve as attractive and independent prognostic biomarkers for MBC patients at baseline and in the course of systematic therapy. The cfDNA mutation has also been evaluated in MBC. Chandarlapaty et al. (2016) showed that ESR1 mutation was associated with poor outcome in patients with metastatic breast cancer who were previously treated with an aromatase inhibitor.

Lung Cancer

A prospective phase II trial evaluated cfDNA in patients with EGFR-mutant NSCLC treated with erlotinib until progression. Results indicated that the level of cfDNA is correlated with PFS. High level of cfDNA was defined as >55 EGFR mutation copies/mL compared with low level of cfDNA, which is <55 EGFR-mutant copies/mL. The median PFS of patients with high-level cfDNA ($n = 18$) was 9.3 months (95% CI, 6.3–14.8) vs. 14.0 months (95% CI, 9.2–20.1) for patients with low-level cfDNA ($n = 41$; $P = 0.08$) (Yanagita et al., 2016). Circulating cfDNA can be a predictive and prognostic biomarker in NSCLC. Several studies have assessed the predictive and prognostic value of cfDNA in NSCLC. A meta-analysis result demonstrated that NSCLC patients with high level of cfDNA were significantly associated with poor PFS. In addition, NSCLC patients who harbored EGFR mutation in cfDNA had a greater chance of response to EGFR-TKIs (Ai et al., 2016).

Hepatocellular Carcinoma

Li et al. reported that cfDNA of methylated insulin-like growth factor-binding protein 7 (IGFBP7) was associated with overall survival and early tumor recurrence. Therefore, IGFBP7 could be an independent prognostic factor in hepatitis B virus-associated hepatocellular carcinoma after hepatectomy (Li et al., 2018). Ren et al. investigated the association between blood cfDNA level and overall survival and disease-free survival in patients with stage I–IV HCC. They found that a high level of cfDNA was associated with poor overall survival (Ren et al., 2006).

Pancreatic Cancer

It was suggested that ctDNAs are shorter than cfDNA fragments originated from nonmalignant cells. Lapin et al. evaluated whether the size of cfDNA fragment and level of cfDNA had prognostic value in patients with advanced pancreatic cancer. Results indicated that both high cfDNA level and a cfDNA fragment size of ≤ 167 bp before treatment were associated with shorter PFS and OS (Lapin et al., 2018). Chen et al. suggested that cfDNA was a prognostic factor for OS and PFS in patients with pancreatic cancer. The presence of ctDNA, high level of cfDNA, mutation including Kras, ERBB2-exon17, and KrasG12V; and hypermethylation were associated with poor survival in pancreatic cancer (Chen et al., 2018).

Colorectal Cancer

The analysis of cfDNA before surgery can indicate prognosis, and analysis of cfDNA after surgery can predict recurrence. A high level of blood cfDNA in the pretreatment phase is significantly correlated with poor survival (Schwarzenbach et al., 2008; Spindler et al., 2015). A prospective multicenter phase III trial indicated that the level of cfDNA can be a prognostic biomarker for oxaliplatin-based chemotherapy in metastatic colorectal cancer. A high level of cfDNA was associated with poor outcome. The median PFS is 7.7 months for the cfDNA level above the upper limit of normal (ULN) and 8.3 months for the cfDNA level below ULN. The median OS is 16.6 months for a cfDNA level above ULN and 25.9 months for a cfDNA level below ULN (Hamfjord et al., 2019). Patients with locally advanced-stage

III–IV rectal cancer who had a high baseline cfDNA level showed short DFS (Schou et al., 2018).

The presence of methylation in HMTF and HPM1 genes in cfDNA in patients with stage I–IV colorectal cancer was associated with a poor OS (Wallner et al., 2006). Promoter methylation of three genes (HPM1, HMTF, and HMLH1) in blood cfDNA was positively correlated with tumor size. Also, methylation of HMTF and HPM1 genes was detected more frequently in metastatic CRC patients and in patients with high tumor stage (Philipp et al., 2012). The presence of a high level of TAC1 methylation 6–12 months after diagnosis was associated with early recurrence (Tham et al., 2014). The methylated status of the APC gene in cfDNA was associated with higher stage and older age. Moreover, patients with the unmethylated promoter of APC or RASSF1A genes showed better OS than patients with promoter hypermethylation (Matthaios et al., 2016).

Oral Squamous Cell Carcinoma

Lin et al. evaluated plasma cfDNA in 121 patients with oral squamous cell carcinoma (OSCC) and 50 matched controls using quantitative spectrometry. Results indicated that blood cfDNA was significantly increased in patients with OSCC compared to controls. The high level of blood cfDNA was correlated with large tumor size, cervical lymph node metastasis, and late stage. High level of blood cfDNA was associated with a poor prognosis of OSCC (Lin et al., 2018).

Prostate Cancer

Epigenetic biomarkers in circulating cfDNA can predict survival of castration-resistant prostate cancer patients. A high level of cfDNA and methylated GSTP1 and APC was observed in CRPC patients compared to healthy subjects. Moreover, the baseline level of cfDNA and methylated APC and GSTP1 before treatment can predict overall survival (Hendriks et al., 2018).

Melanoma

Valpione et al. (2018) revealed that the blood total cfDNA is a surrogate biomarker for tumor burden and can predict overall survival in patients with metastatic melanoma.

CONCLUSION

Analysis of cfDNA in liquid biopsy is a minimally invasive, low-cost, and promising alternative to tumor biopsy. Liquid biopsy

based on cfDNA can not only detect cancer recurrence more quickly than the current radiological imaging technology but also provide insights on the molecular evolution of minimal residual disease (MRD) in tumor progression through molecular characterization of cfDNA, which is of great significance for the prevention and treatment of tumor recurrence. The most common body fluid is blood. In addition, different body fluids will be selected for different detection targets. For example, saliva is often used in the detection of head and neck tumor, and cerebrospinal fluid is applied in the diagnosis of tumors of the central nervous system, urine in the case of urinary tract cancers, and pleural effusion for respiratory tract cancers. However, due to the very low concentration of cfDNA in blood or other samples, it has high requirements for sensitivity and detection limit of the detection method. The gold standard of cfDNA analysis, including quantitative PCR (qPCR) and digital PCR, is becoming mature. In recent years, the development of whole-genome sequencing and novel PCR-free biosensing approaches have also made some breakthroughs. In this article, we reviewed studies exploring cfDNA for diagnostic, therapeutic, and prognostic evaluation in various types of cancers. This study supports the idea that cfDNA analysis for cancer represents a potential research area and will have wide application in clinics.

AUTHOR CONTRIBUTIONS

Y-yY, Q-rG, and J-yZ conceived the review. Y-yY, F-hW, and Z-yZ searched the literature and drafted the manuscript. RA, H-yZ, and W-mZ critically appraised the literature. HY and J-qL edited the manuscript. All authors approved the final version of the manuscript.

FUNDING

This work is supported by the Finance Science and Technology project of Hainan province (ZDYF2020137), the Natural Science Foundation of Guangdong Province (2020A1515010605), the National Natural Science Foundation of China (81902152 and 81773888), the Social Development Foundation of Shanxi Province (201903D321021), and the Fund of Shanxi Province Higher Education Technology Innovation Project (2019L0753).

REFERENCES

- Agostini, M., Pucciarelli, S., Enzo, M. V., Del Bianco, P., Briarava, M., Bedin, C., et al. (2011). Circulating cell-free DNA: a promising marker of pathologic tumor response in rectal cancer patients receiving preoperative chemoradiotherapy. *Ann. Surg. Oncol.* 18, 2461–2468. doi: 10.1245/s10434-011-1638-y
- Ai, B., Liu, H., Huang, Y., and Peng, P. (2016). Circulating cell-free DNA as a prognostic and predictive biomarker in non-small cell lung cancer. *Oncotarget*. 7, 44583–44595. doi: 10.18632/oncotarget.10069
- Almodovar, K., Iams, W. T., Meador, C. B., Zhao, Z., York, S., Horn, L., et al. (2018). Longitudinal cell-free DNA analysis in patients with small cell lung cancer reveals dynamic insights into treatment efficacy and disease relapse. *J. Thorac. Oncol.* 13, 112–123. doi: 10.1016/j.jtho.2017.09.1951
- Alunni-Fabbroni, M., Ronsch, K., Huber, T., Cyran, C. C., Seidensticker, M., Mayerle, J., et al. (2019). Circulating DNA as prognostic biomarker in patients with advanced hepatocellular carcinoma: a translational exploratory study from the SORAMIC trial. *J. Transl. Med.* 17:328. doi: 10.1186/s12967-019-2079-9
- Anker, P., Lefort, F., Vasioukhin, V., Lyautey, J., Lederrey, C., Chen, X. Q., et al. (1997). K-ras mutations are found in DNA extracted from the plasma of patients with colorectal cancer. *Gastroenterology*. 112, 1114–1120. doi: 10.1016/s0016-5085(97)70121-5
- Barault, L., Amatu, A., Siravegna, G., Ponzetti, A., Moran, S., Cassingena, A., et al. (2018). Discovery of methylated circulating DNA biomarkers for

- comprehensive non-invasive monitoring of treatment response in metastatic colorectal cancer. *Gut*. 67, 1995–2005. doi: 10.1136/gutjnl-2016-313372
- Beije, N., Sieuwerts, A. M., Kraan, J., Van, N. M., Onstenk, W., Vitale, S. R., et al. (2018). Estrogen receptor mutations and splice variants determined in liquid biopsies from metastatic breast cancer patients. *Mol. Oncol.* 12, 48–57. doi: 10.1002/1878-0261.12147
- Beranek, M., Fiala, Z., Kremlacek, J., Andrys, C., Krejsek, J., Hamakova, K., et al. (2017). Changes in circulating cell-free DNA and nucleosomes in patients with exacerbated psoriasis. *Arch. Dermatol. Res.* 309, 815–821. doi: 10.1007/s00403-017-1785-5
- Bettegowda, C., Sausen, M., Leary, R. J., Kinde, I., Wang, Y., Agrawal, N., et al. (2014). Detection of circulating tumor DNA in early- and late-stage human malignancies. *Sci. Transl. Med.* 6:224ra24. doi: 10.1158/1538-7445.AM2014-5606
- Bhangu, J. S., Taghizadeh, H., Braunschmid, T., Bachleitner-Hofmann, T., and Mannhalter, C. (2017). Circulating cell-free DNA in plasma of colorectal cancer patients - A potential biomarker for tumor burden. *Surg. Oncol.* 26, 395–401. doi: 10.1016/j.suronc.2017.08.001
- Bianchi, D. W., and Chiu, R. W. K. (2018). Sequencing of circulating cell-free DNA during pregnancy. *N. Engl. J. Med.* 379, 464–473. doi: 10.1056/NEJMra1705345
- Chan, K. C., Lai, P. B., Mok, T. S., Chan, H. L., Ding, C., Yeung, S. W., et al. (2008). Quantitative analysis of circulating methylated DNA as a biomarker for hepatocellular carcinoma. *Clin. Chem.* 54, 1528–1536. doi: 10.1373/clinchem.2008.104653
- Chan, K. C. A., Woo, J. K. S., King, A., Zee, B. C. Y., Lam, W. K. J., Chan, S. L., et al. (2017). Analysis of plasma Epstein-Barr virus DNA to screen for nasopharyngeal cancer. *N. Engl. J. Med.* 377, 513–522. doi: 10.1056/NEJMoa1701717
- Chandraratnam, S., Chen, D., He, W., Sung, P., Samoil, A., You, D., et al. (2016). Prevalence of ESR1 mutations in cell-free DNA and outcomes in metastatic breast cancer: a secondary analysis of the BOLERO-2 clinical trial. *JAMA Oncol.* 2, 1310–1315. doi: 10.1001/jamaoncol.2016.1279
- Chen, L., Zhang, Y., Cheng, Y., Zhang, D., Zhu, S., and Ma, X. (2018). Prognostic value of circulating cell-free DNA in patients with pancreatic cancer: A systematic review and meta-analysis. *Gene*. 679, 328–334. doi: 10.1016/j.gene.2018.09.029
- Chen, Q. H., Deng, W., Li, X. W., Liu, X. F., Wang, J. M., Wang, L. F., et al. (2013). Novel CDH1 germline mutations identified in Chinese gastric cancer patients. *World J. Gastroenterol.* 19, 909–916. doi: 10.3748/wjg.v19.i6.909
- Cheng, J., Holland-Letz, T., Wallwiener, M., Surowy, H., Cuk, K., Schott, S., et al. (2018). Circulating free DNA integrity and concentration as independent prognostic markers in metastatic breast cancer. *Breast Cancer Res. Treat.* 169, 69–82. doi: 10.1007/s10549-018-4666-5
- Christensen, E., Birkenkamp-Demtroder, K., Sethi, H., Shchegrova, S., Salari, R., Nordentoft, I., et al. (2019). Early detection of metastatic relapse and monitoring of therapeutic efficacy by ultra-deep sequencing of plasma cell-free DNA in patients with urothelial bladder carcinoma. *J. Clin. Oncol.* 37, 1547–1557. doi: 10.1158/1538-7445.SABCS18-913
- Corso, G., Marrelli, D., Pascale, V., Vindigni, C., and Roviello, F. (2012). Frequency of CDH1 germline mutations in gastric carcinoma coming from high- and low-risk areas: metanalysis and systematic review of the literature. *BMC Cancer*. 12:8. doi: 10.1186/1471-2407-12-8
- Corso, G., Velho, S., Paredes, J., Pedrazzani, C., Martins, D., Milanezi, F., et al. (2011). Oncogenic mutations in gastric cancer with microsatellite instability. *Eur. J. Cancer*. 47, 443–451. doi: 10.1016/j.ejca.2010.09.008
- Del Re, M., Bordini, P., Rofi, E., Restante, G., Valleggi, S., Minari, R., et al. (2018). The amount of activating EGFR mutations in circulating cell-free DNA is a marker to monitor osimertinib response. *Br. J. Cancer*. 119, 1252–1258. doi: 10.1038/s41416-018-0238-z
- Diehl, F., Schmidt, K., Choti, M. A., Romans, K., Goodman, S., Li, M., et al. (2008). Circulating mutant DNA to assess tumor dynamics. *Nat. Med.* 14, 985–990. doi: 10.1038/nm.1789
- Dunaeva, M., Derksen, M., and Pruijn, G. J. M. (2018). LINE-1 hypermethylation in serum cell-free DNA of relapsing remitting multiple sclerosis patients. *Mol. Neurobiol.* 55, 4681–4688. doi: 10.1007/s12035-017-0679-z
- Duvvuri, B., and Lood, C. (2019). Cell-free DNA as a biomarker in autoimmune rheumatic diseases. *Front. Immunol.* 10:502. doi: 10.3389/fimmu.2019.00502
- Espósito, A., Criscitello, C., Trapani, D., and Curigliano, G. (2017). The emerging role of “liquid biopsies,” circulating tumor cells, and circulating cell-free tumor DNA in lung cancer diagnosis and identification of resistance mutations. *Curr. Oncol. Rep.* 19, 1. doi: 10.1007/s11912-017-0564-y
- Fares, J., Fares, M. Y., Khachfe, H. H., Sallhab, H. A., and Fares, Y. (2020). Molecular principles of metastasis: a hallmark of cancer revisited. *Signal Transduct. Target. Ther.* 5:28. doi: 10.1038/s41392-020-0134-x
- Fontanilles, M., Marguet, F., Bohers, E., Vailly, P. J., Dubois, S., Bertrand, P., et al. (2017). Non-invasive detection of somatic mutations using next-generation sequencing in primary central nervous system lymphoma. *Oncotarget*. 8, 48157–48168. doi: 10.18632/oncotarget.18325
- Fujiwara, K., Fujimoto, N., Tabata, M., Nishii, K., Matsuo, K., Hotta, K., et al. (2005). Identification of epigenetic aberrant promoter methylation in serum DNA is useful for early detection of lung cancer. *Clin. Cancer Res.* 11, 1219–1225. doi: 10.1016/S1040-6736(61)92729-5
- Gala-Lopez, B. L., Neiman, D., Kin, T., O’Gorman, D., Pepper, A. R., Malcolm, A. J., et al. (2018). Beta cell death by cell-free DNA and outcome after clinical islet transplantation. *Transplantation*. 102, 978–985. doi: 10.1097/TP.0000000000002083
- Gielis, E. M., Ledeganck, K. J., De Winter, B. Y., Del Favero, J., Bosmans, J. L., Claas, F. H., et al. (2015). Cell-free DNA: an upcoming biomarker in transplantation. *Am. J. Transplant.* 15, 2541–2551. doi: 10.1111/ajt.13387
- Goodall, J., Mateo, J., Yuan, W., Mossop, H., Porta, N., Miranda, S., et al. (2017). Circulating cell-free DNA to guide prostate cancer treatment with PARP inhibition. *Cancer Discov.* 7, 1006–1017. doi: 10.1158/2159-8290.CD-17-0261
- Gorges, T. M., Schiller, J., Schmitz, A., Schuetzmann, D., Schatz, C., Zollner, T. M., et al. (2012). Cancer therapy monitoring in xenografts by quantitative analysis of circulating tumor DNA. *Biomarkers*. 17, 498–506. doi: 10.3109/1354750X.2012.689133
- Gormally, E., Vineis, P., Matullo, G., Veglia, F., Caboux, E., Le Roux, E., et al. (2006). TP53 and KRAS2 mutations in plasma DNA of healthy subjects and subsequent cancer occurrence: a prospective study. *Cancer Res.* 66, 6871–6876. doi: 10.1158/0008-5472.CAN-05-4556
- Guibert, N., Jones, G., Beeler, J. F., Plagnol, V., Morris, C., Mourlanette, J., et al. (2019). Targeted sequencing of plasma cell-free DNA to predict response to PD1 inhibitors in advanced non-small cell lung cancer. *Lung Cancer*. 137, 1–6. doi: 10.1016/j.lungcan.2019.09.005
- Haber, D. A., and Velculescu, V. E. (2014). Blood-based analyses of cancer: circulating tumor cells and circulating tumor DNA. *Cancer Discov.* 4, 650–661. doi: 10.1158/2159-8290.CD-13-1014
- Hamfjord, J., Guren, T. K., Dajani, O., Johansen, J. S., Glimelius, B., Sorbye, H., et al. (2019). Total circulating cell-free DNA as a prognostic biomarker in metastatic colorectal cancer before first-line oxaliplatin-based chemotherapy. *Ann. Oncol.* 30, 1088–1095. doi: 10.1093/annonc/mdz139
- Heald, B., Mester, J., Rybicki, L., Orloff, M. S., Burke, C. A., and Eng, C. (2010). Frequent gastrointestinal polyps and colorectal adenocarcinomas in a prospective series of PTEN mutation carriers. *Gastroenterology*. 139, 1927–1933. doi: 10.1053/j.gastro.2010.06.061
- Hendriks, R. J., Dijkstra, S., Smit, F. P., Vandersmissen, J., Van de Voorde, H., Mulders, P. F. A., et al. (2018). Epigenetic markers in circulating cell-free DNA as prognostic markers for survival of castration-resistant prostate cancer patients. *Prostate*. 78, 336–342. doi: 10.1002/pros.23477
- Hiemcke-Jiwa, L. S., Leguit, R. J., Snijders, T. J., Bromberg, J. E. C., Nierkens, S., Jiwa, N. M., et al. (2019). MYD88 p.(L265P) detection on cell-free DNA in liquid biopsies of patients with primary central nervous system lymphoma. *Br. J. Haematol.* 185, 974–977. doi: 10.1111/bjh.15674
- Hohaus, S., Giachelia, M., Massini, G., Mansueto, G., Vannata, B., Bozzoli, V., et al. (2009). Cell-free circulating DNA in Hodgkin’s and non-Hodgkin’s lymphomas. *Ann. Oncol.* 20, 1408–1413. doi: 10.1093/annonc/mdp006
- Hosny, G., Farahat, N., and Hainaut, P. (2009). TP53 mutations in circulating free DNA from Egyptian patients with non-Hodgkin’s lymphoma. *Cancer Lett.* 275, 234–239. doi: 10.1016/j.canlet.2008.10.029
- Huang, W., Yan, Y., Liu, Y., Lin, M., Ma, J., Zhang, W., et al. (2020). Exosomes with low miR-34c-3p expression promote invasion and migration of non-small cell lung cancer by upregulating integrin $\alpha 2 \beta 1$. *Signal Transduct. Target. Ther.* 5, 39. doi: 10.1038/s41392-020-0133-y

- Huang, Z., Hua, D., Hu, Y., Cheng, Z., Zhou, X., Xie, Q., et al. (2012). Quantitation of plasma circulating DNA using quantitative PCR for the detection of hepatocellular carcinoma. *Pathol. Oncol. Res.* 18, 271–276. doi: 10.1007/s12253-011-9438-z
- Hudecova, I., and Chiu, R. W. (2017). Non-invasive prenatal diagnosis of thalassemias using maternal plasma cell free DNA. *Best Pract. Res. Clin. Obstet. Gynaecol.* 39, 63–73. doi: 10.1016/j.bpobgyn.2016.10.016
- Hussein, N. A., Mohamed, S. N., and Ahmed, M. A. (2019). Plasma ALU-247, ALU-115, and cfDNA Integrity as Diagnostic and Prognostic Biomarkers for Breast Cancer. *Appl. Biochem. Biotechnol.* 187, 1028–1045. doi: 10.1007/s12010-018-2858-4
- Hyett, J. A., Gardener, G., Stojilkovic-Mikic, T., Finning, K. M., Martin, P. G., Rodeck, C. H., et al. (2005). Reduction in diagnostic and therapeutic interventions by non-invasive determination of fetal sex in early pregnancy. *Prenat. Diagn.* 25, 1111–1116. doi: 10.1002/pd.1284
- Iizuka, N., Sakaida, I., Moribe, T., Fujita, N., Miura, T., Stark, M., et al. (2006). Elevated levels of circulating cell-free DNA in the blood of patients with hepatitis C virus-associated hepatocellular carcinoma. *Anticancer Res.* 26, 4713–4719. doi: 10.1016/S0166-6851(00)00331-5
- Kamat, A. A., Bischoff, F. Z., Dang, D., Baldwin, M. F., Han, L. Y., Lin, Y. G., et al. (2006). Circulating cell-free DNA: a novel biomarker for response to therapy in ovarian carcinoma. *Cancer Biol. Ther.* 5:1369–1374. doi: 10.4161/cbt.5.10.3240
- Kang, Z., Stevanovic, S., Hinrichs, C. S., and Cao, L. (2017). Circulating cell-free DNA for metastatic cervical cancer detection, genotyping, and monitoring. *Clin. Cancer Res.* 23, 6856–6862. doi: 10.1158/1078-0432.CCR-17-1553
- Kaurah, P., MacMillan, A., Boyd, N., Senz, J., De Luca, A., Chun, N., et al. (2007). Founder and recurrent CDH1 mutations in families with hereditary diffuse gastric cancer. *JAMA.* 297, 2360–2372. doi: 10.1001/jama.297.21.2360
- Lapin, M., Olteidal, S., Tjensvoll, K., Buhl, T., Smaaland, R., Garresori, H., et al. (2018). Fragment size and level of cell-free DNA provide prognostic information in patients with advanced pancreatic cancer. *J. Transl. Med.* 16, 300. doi: 10.1186/s12967-018-1677-2
- Lee, J., van Hummelen, P., Go, C., Palescandolo, E., Jang, J., Park, H. Y., et al. (2012). High-throughput mutation profiling identifies frequent somatic mutations in advanced gastric adenocarcinoma. *PLoS One.* 7:e38892. doi: 10.1371/journal.pone.0038892
- Leon, S. A., Shapiro, B., Sklaroff, D. M., and Yaros, M. J. (1977). Free DNA in the serum of cancer patients and the effect of therapy. *Cancer Res.* 37, 646–650.
- Li, F., Qiao, C. Y., Gao, S., Fan, Y. C., Chen, L. Y., and Wang, K. (2018). Circulating cell-free DNA of methylated insulin-like growth factor-binding protein 7 predicts a poor prognosis in hepatitis B virus-associated hepatocellular carcinoma after hepatectomy. *Free Radic. Res.* 52, 455–464. doi: 10.1080/10715762.2018.1443448
- Li, J., Zhou, X., Liu, X., Ren, J., Wang, J., Wang, W., et al. (2019). Detection of colorectal cancer in circulating cell-free DNA by methylated CpG tandem amplification and sequencing. *Clin. Chem.* 65:916–926. doi: 10.1373/clinchem.2019.301804
- Li, V. S., Wong, C. W., Chan, T. L., Chan, A. S., Zhao, W., Chu, K. M., et al. (2005). Mutations of PIK3CA in gastric adenocarcinoma. *BMC Cancer.* 5:29. doi: 10.1186/1471-2407-5-29
- Li, W., Zhang, X., Lu, X., You, L., Song, Y., Luo, Z., et al. (2017). 5-Hydroxymethylcytosine signatures in circulating cell-free DNA as diagnostic biomarkers for human cancers. *Cell Res.* 27, 1243–1257. doi: 10.1038/cr.2017.121
- Lin, L. H., Chang, K. W., Kao, S. Y., Cheng, H. W., and Liu, C. J. (2018). Increased Plasma circulating cell-free DNA could be a potential marker for oral cancer. *Int. J. Mol. Sci.* 19, 3303. doi: 10.3390/ijms19113303
- Liu, Z., Liu, L., Li, M., Wang, Z., Feng, L., Zhang, Q., et al. (2011). Epidermal growth factor receptor mutation in gastric cancer. *Pathology.* 43, 234–238. doi: 10.1097/PAT.0b013e328344e61b
- Lo, Y. M., Corbetta, N., Chamberlain, P. F., Rai, V., Sargent, I. L., Redman, C. W., et al. (1997). Presence of fetal DNA in maternal plasma and serum. *Lancet.* 350, 485–487. doi: 10.1016/S0140-6736(97)02174-0
- Lo, Y. M., Lun, F. M., Chan, K. C., Tsui, N. B., Chong, K. C., Lau, T. K., et al. (2007). Digital PCR for the molecular detection of fetal chromosomal aneuploidy. *Proc. Natl. Acad. Sci. U. S. A.* 104, 13116–13121. doi: 10.1073/pnas.0705765104
- Lo, Y. M., Tein, M. S., Pang, C. C., Yeung, C. K., Tong, K. L., and Hjelm, N. M. (1998). Presence of donor-specific DNA in plasma of kidney and liver-transplant recipients. *Lancet.* 351, 1329–1330. doi: 10.1016/S0140-6736(05)79055-3
- Lui, Y. Y., Chik, K. W., Chiu, R. W., Ho, C. Y., Lam, C. W., and Lo, Y. M. (2002). Predominant hematopoietic origin of cell-free DNA in plasma and serum after sex-mismatched bone marrow transplantation. *Clin. Chem.* 48, 421–427. doi: 10.1093/clinchem/48.3.421
- Lyskjaer, I., Kronborg, C. S., Rasmussen, M. H., Sorensen, B. S., Demuth, C., Rosenkilde, M., et al. (2019). Correlation between early dynamics in circulating tumour DNA and outcome from FOLFIRI treatment in metastatic colorectal cancer. *Sci. Rep.* 9, 11542. doi: 10.1038/s41598-019-47708-1
- Malan, V., Bussieres, L., Winer, N., Jais, J. P., Baptiste, A., Le Lorc'h, M., et al. (2018). Effect of cell-free DNA screening vs direct invasive diagnosis on miscarriage rates in women with pregnancies at high risk of trisomy 21: a randomized clinical trial. *JAMA.* 320, 557–565. doi: 10.1001/jama.2018.9396
- Mandel, P., and Metais, P. (1948). Nuclear acids in human blood plasma. *C. R. Seances Soc. Biol. Fil.* 142, 241–243.
- Mao, L., Hruban, R. H., Boyle, J. O., Tockman, M., and Sidransky, D. (1994). Detection of oncogene mutations in sputum precedes diagnosis of lung cancer. *Cancer Res.* 54, 1634–1637. doi: 10.1016/0304-3835(94)90050-7
- Maron, S. B., Chase, L. M., Lomnicki, S., Kochanny, S., Moore, K. L., Joshi, S. S., et al. (2019). Circulating Tumor DNA Sequencing Analysis of Gastroesophageal Adenocarcinoma. *Clin. Cancer Res.* 25, 7098–7112. doi: 10.1158/1078-0432.CCR-19-1704
- Matthaios, D., Balgkouranidou, I., Karayiannakis, A., Bolanaki, H., Xenidis, N., Amarantidis, K., et al. (2016). Methylation status of the APC and RASSF1A promoter in cell-free circulating DNA and its prognostic role in patients with colorectal cancer. *Oncol. Lett.* 12, 748–756. doi: 10.3892/ol.2016.4649
- Mithani, S. K., Smith, I. M., Zhou, S., Gray, A., Koch, W. M., Maitra, A., et al. (2007). Mitochondrial resequencing arrays detect tumor-specific mutations in salivary rinses of patients with head and neck cancer. *Clin. Cancer Res.* 13, 7335–7340. doi: 10.1158/1078-0432.CCR-07-0220
- Mohamed, N. A., Swify, E. M., Amin, N. F., Soliman, M. M., Tag-Eldin, L. M., and Elsherbiny, N. M. (2012). Is serum level of methylated RASSF1A valuable in diagnosing hepatocellular carcinoma in patients with chronic viral hepatitis C? *Arab J. Gastroenterol.* 13, 111–115. doi: 10.1016/j.ajg.2012.06.009
- Mueller, S., Holdenrieder, S., Stieber, P., Haferlach, T., Schalhorn, A., Braess, J., et al. (2006). Early prediction of therapy response in patients with acute myeloid leukemia by nucleosomal DNA fragments. *BMC Cancer.* 6:143. doi: 10.1186/1471-2407-6-143
- Nawroz, H., Koch, W., Anker, P., Stroun, M., and Sidransky, D. (1996). Microsatellite alterations in serum DNA of head and neck cancer patients. *Nat. Med.* 2, 1035–1037. doi: 10.1038/nm0996-1035
- Panagopoulou, M., Karagani, M., Balgkouranidou, I., Bizioti, E., Koukaki, T., Karamitrousis, E., et al. (2019). Circulating cell-free DNA in breast cancer: size profiling, levels, and methylation patterns lead to prognostic and predictive classifiers. *Oncogene.* 38, 3387–3401. doi: 10.1038/s41388-018-0660-y
- Park, S., Lee, E. J., Rim, C. H., and Seong, J. (2018). Plasma Cell-Free DNA as a Predictive Marker after radiotherapy for hepatocellular carcinoma. *Yonsei Med. J.* 59, 470–479. doi: 10.3349/ymj.2018.59.4.470
- Parkinson, C. A., Gale, D., Piskorz, A. M., Biggs, H., Hodgkin, C., Addley, H., et al. (2016). Exploratory analysis of TP53 mutations in circulating tumour DNA as biomarkers of treatment response for patients with relapsed high-grade serous ovarian carcinoma: a retrospective study. *PLoS Med.* 13:e1002198. doi: 10.1371/journal.pmed.1002198
- Pasternack, H., Fassunke, J., Plum, P. S., Chon, S. H., Hescheler, D. A., Gassa, A., et al. (2018). Somatic alterations in circulating cell-free DNA of oesophageal carcinoma patients during primary staging are indicative for post-surgical tumour recurrence. *Sci. Rep.* 8:14941. doi: 10.1038/s41598-018-33027-4
- Phallen, J., Sausen, M., Adleff, V., Leal, A., Hruban, C., White, J., et al. (2017). Direct detection of early-stage cancers using circulating tumor DNA. *Sci. Transl. Med.* 9, eaan2415. doi: 10.1126/scitranslmed.aan2415
- Philipp, A. B., Stieber, P., Nagel, D., Neumann, J., Spelsberg, F., Jung, A., et al. (2012). Prognostic role of methylated free circulating DNA in colorectal cancer. *Int. J. Cancer.* 131, 2308–2319. doi: 10.1002/ijc.27505
- Quan, J., Gao, Y. J., Yang, Z. L., Chen, H., Xian, J. R., Zhang, S. S., et al. (2015). Quantitative detection of circulating nucleophosmin mutations DNA in the

- plasma of patients with acute myeloid leukemia. *Int. J. Med. Sci.* 12:17–22. doi: 10.7150/ijms.10144
- Raja, R., Kuziora, M., Brohawn, P. Z., Higgs, B. W., Gupta, A., Dennis, P. A., et al. (2018). Early reduction in ctDNA predicts survival in patients with lung and bladder cancer treated with durvalumab. *Clin. Cancer Res.* 24, 6212–6222. doi: 10.1158/1078-0432.CCR-18-0386
- Ren, N., Ye, Q. H., Qin, L. X., Zhang, B. H., Liu, Y. K., and Tang, Z. Y. (2006). Circulating DNA level is negatively associated with the long-term survival of hepatocellular carcinoma patients. *World J. Gastroenterol.* 12, 3911–3914. doi: 10.3748/wjg.v12.i24.3911
- Rhodes, C. H., Honsinger, C., and Sorenson, G. D. (1994). Detection of tumor-derived DNA in cerebrospinal fluid. *J. Neuropathol. Exp. Neurol.* 53, 364–368. doi: 10.1097/00005072-199407000-00007
- Salvianti, F., Giuliani, C., Petrone, L., Mancini, I., Vezzosi, V., Pupilli, C., et al. (2017). Integrity and quantity of total cell-free DNA in the diagnosis of thyroid cancer: correlation with cytological classification. *Int. J. Mol. Sci.* 18, 1350. doi: 10.3390/ijms18071350
- Samuels, Y., Wang, Z., Bardelli, A., Silliman, N., Ptak, J., Szabo, S., et al. (2004). High frequency of mutations of the PIK3CA gene in human cancers. *Science*. 304:554. doi: 10.1126/science.1096502
- Schiavon, G., Hrebien, S., Garcia-Murillas, I., Cutts, R. J., Pearson, A., Tarazona, N., et al. (2015). Analysis of ESR1 mutation in circulating tumor DNA demonstrates evolution during therapy for metastatic breast cancer. *Sci. Transl. Med.* 7:313ra182. doi: 10.1126/scitranslmed.aac7551
- Schou, J. V., Larsen, F. O., Sorensen, B. S., Abrantes, R., Boysen, A. K., Johansen, J. S., et al. (2018). Circulating cell-free DNA as predictor of treatment failure after neoadjuvant chemo-radiotherapy before surgery in patients with locally advanced rectal cancer. *Ann. Oncol.* 29, 610–615. doi: 10.1093/annonc/mdx778
- Schwarzenbach, H., Stoehlmacher, J., Pantel, K., and Goekkurt, E. (2008). Detection and monitoring of cell-free DNA in blood of patients with colorectal cancer. *Ann. N. Y. Acad. Sci.* 1137, 190–196. doi: 10.1196/annals.1448.025
- Shaw, J. A., Smith, B. M., Walsh, T., Johnson, S., Primrose, L., Slade, M. J., et al. (2000). Microsatellite alterations plasma DNA of primary breast cancer patients. *Clin. Cancer Res.* 6, 1119–1124. doi: 10.1159/000007270
- Sherwood, K., and Weimer, E. T. (2018). Characteristics, properties, and potential applications of circulating cell-free dna in clinical diagnostics: a focus on transplantation. *J. Immunol. Methods*. 463, 27–38. doi: 10.1016/j.jim.2018.09.011
- Shu, Y., Wu, X., Tong, X., Wang, X., Chang, Z., Mao, Y., et al. (2017). Circulating tumor DNA mutation profiling by targeted next generation sequencing provides guidance for personalized treatments in multiple cancer types. *Sci. Rep.* 7, 583. doi: 10.1038/s41598-017-00520-1
- Sidransky, D., Von Eschenbach, A., Tsai, Y. C., Jones, P., Summerhayes, I., Marshall, F., et al. (1991). Identification of p53 gene mutations in bladder cancers and urine samples. *Science*. 252, 706–709. doi: 10.1126/science.2024123
- Siravegna, G., Marsoni, S., Siena, S., and Bardelli, A. (2017). Integrating liquid biopsies into the management of cancer. *Nat. Rev. Clin. Oncol.* 14, 531–548. doi: 10.1038/nrclinonc.2017.14
- Sorenson, G. D., Pribish, D. M., Valone, F. H., Memoli, V. A., Bzik, D. J., and Yao, S. L. (1994). Soluble normal and mutated DNA sequences from single-copy genes in human blood. *Cancer Epidemiol. Biomarkers Prev.* 3, 67–71. doi: 10.1007/BF00685912
- Spindler, K. L., Pallisgaard, N., Andersen, R. F., Brandslund, I., and Jakobsen, A. (2015). Circulating free DNA as biomarker and source for mutation detection in metastatic colorectal cancer. *PLoS One*. 10:e0108247. doi: 10.1371/journal.pone.0108247
- Spoerke, J. M., Gendreau, S., Walter, K., Qiu, J., Wilson, T. R., Savage, H., et al. (2016). Heterogeneity and clinical significance of ESR1 mutations in ER-positive metastatic breast cancer patients receiving fulvestrant. *Nat. Commun.* 7:11579. doi: 10.1038/ncomms11579
- Sriram, K. B., Relan, V., Clarke, B. E., Duhig, E. E., Windsor, M. N., Matar, K. S., et al. (2012). Pleural fluid cell-free DNA integrity index to identify cytologically negative malignant pleural effusions including mesotheliomas. *BMC Cancer*. 12:428. doi: 10.1186/1471-2407-12-428
- Sumiyoshi, T., Mizuno, K., Yamasaki, T., Miyazaki, Y., Makino, Y., Okasho, K., et al. (2019). Clinical utility of androgen receptor gene aberrations in circulating cell-free DNA as a biomarker for treatment of castration-resistant prostate cancer. *Sci. Rep.* 9:4030. doi: 10.1038/s41598-019-40719-y
- Sun, K., Jiang, P., Chan, K. C., Wong, J., Cheng, Y. K., Liang, R. H., et al. (2015). Plasma DNA tissue mapping by genome-wide methylation sequencing for noninvasive prenatal, cancer, and transplantation assessments. *Proc. Natl. Acad. Sci. U. S. A.* 112, E5503–E5512. doi: 10.1073/pnas.1508736112
- Sun, W., Sun, Y., Zhu, M., Wang, Z., Zhang, H., Xin, Y., et al. (2014). The role of plasma cell-free DNA detection in predicting preoperative chemoradiotherapy response in rectal cancer patients. *Oncol. Rep.* 31, 1466–1472. doi: 10.3892/or.2013.2949
- Tham, C., Chew, M., Soong, R., Lim, J., Ang, M., Tang, C., et al. (2014). Postoperative serum methylation levels of TAC1 and SEPT9 are independent predictors of recurrence and survival of patients with colorectal cancer. *Cancer*. 120, 3131–3141. doi: 10.1002/cncr.28802
- Thierry, A. R., Mouliere, F., El Messaoudi, S., Mollevi, C., Lopez-Crape, E., Rolet, F., et al. (2014). Clinical validation of the detection of KRAS and BRAF mutations from circulating tumor DNA. *Nat. Med.* 20, 430–435. doi: 10.1038/nm.3511
- Tian, J., Geng, Y., Lv, D., Li, P., Cordova, M., Liao, Y., et al. (2019). Using plasma cell-free DNA to monitor the chemoradiotherapy course of cervical cancer. *Int. J. Cancer*. 145, 2547–2557. doi: 10.1002/ijc.32295
- Tokuhisa, Y., Iizuka, N., Sakaida, I., Moribe, T., Fujita, N., Miura, T., et al. (2007). Circulating cell-free DNA as a predictive marker for distant metastasis of hepatitis C virus-related hepatocellular carcinoma. *Br. J. Cancer*. 97, 1399–1403. doi: 10.1038/sj.bjc.6604034
- Valpione, S., Gremel, G., Mundra, P., Middlehurst, P., Galvani, E., Girotti, M. R., et al. (2018). Plasma total cell-free DNA (cfDNA) is a surrogate biomarker for tumour burden and a prognostic biomarker for survival in metastatic melanoma patients. *Eur. J. Cancer*. 88, 1–9. doi: 10.1016/j.ejca.2017.10.029
- Vasioukhin, V., Anker, P., Maurice, P., Lyautey, J., Lederrey, C., and Stroun, M. (1994). Point mutations of the N-ras gene in the blood plasma DNA of patients with myelodysplastic syndrome or acute myelogenous leukaemia. *Br. J. Haematol.* 86:774–779. doi: 10.1111/j.1365-2141.1994.tb04828.x
- Velho, S., Oliveira, C., Ferreira, A., Ferreira, A. C., Suriano, G., Schwartz, S. Jr., et al. (2005). The prevalence of PIK3CA mutations in gastric and colon cancer. *Eur. J. Cancer*. 41:1649–1654. doi: 10.1016/j.ejca.2005.04.022
- Vietsch, E. E., Graham, G. T., McCutcheon, J. N., Javadi, A., Giaccone, G., Marshall, J. L., et al. (2017). Circulating cell-free DNA mutation patterns in early and late stage colon and pancreatic cancer. *Cancer Genet.* 218–219, 39–50. doi: 10.1016/j.cancergen.2017.08.006
- Vivanti, A. J., Costa, J. M., Rosefort, A., Kleinfinger, P., Lohmann, L., Cordier, A. G., et al. (2019). Optimal non-invasive diagnosis of fetal achondroplasia combining ultrasonography with circulating cell-free fetal DNA analysis. *Ultrasound Obstet. Gynecol.* 53, 87–94. doi: 10.1002/uog.19018
- Wallner, M., Herbst, A., Behrens, A., Crispin, A., Stieber, P., Goke, B., et al. (2006). Methylation of serum DNA is an independent prognostic marker in colorectal cancer. *Clin. Cancer Res.* 12, 7347–7352. doi: 10.1158/1078-0432.CCR-06-1264
- Wan, J. C. M., Massie, C., Garcia-Corbacho, J., Mouliere, F., Brenton, J. D., Caldas, C., et al. (2017). Liquid biopsies come of age: towards implementation of circulating tumour DNA. *Nat. Rev. Cancer*. 17, 223–238. doi: 10.1038/nrc.2017.7
- Wang, J., and Xu, B. (2019). Targeted therapeutic options and future perspectives for HER2-positive breast cancer. *Signal Transduct. Target. Ther.* 4, 34. doi: 10.1038/s41392-019-0069-2
- Wang, J. Y., Hsieh, J. S., Chang, M. Y., Huang, T. J., Chen, F. M., Cheng, T. L., et al. (2004). Molecular detection of APC, K-ras, and p53 mutations in the serum of colorectal cancer patients as circulating biomarkers. *World J. Surg.* 28, 721–726. doi: 10.1007/s00268-004-7366-8
- Wang, Y., Fang, Z., Hong, M., Yang, D., and Xie, W. (2020). Long-noncoding RNAs (lncRNAs) in drug metabolism and disposition, implications in cancer chemoresistance. *Acta Pharm. Sin. B*. 10, 105–112. doi: 10.1016/j.apsb.2019.09.011
- Wang, Y., Springer, S., Mulvey, C. L., Silliman, N., Schaefer, J., Sausen, M., et al. (2015). Detection of somatic mutations and HPV in the saliva and plasma of patients with head and neck squamous cell carcinomas. *Sci. Transl. Med.* 7:293ra104. doi: 10.1126/scitranslmed.aaa8507
- Wen, Y. G., Wang, Q., Zhou, C. Z., Qiu, G. Q., Peng, Z. H., and Tang, H. M. (2010). Mutation analysis of tumor suppressor gene PTEN in patients with

- gastric carcinomas and its impact on PI3K/AKT pathway. *Oncol. Rep.* 24:89–95. doi: 10.3892/or_00000832
- Wong, A. I., and Lo, Y. M. (2015). Noninvasive fetal genomic, methylomic, and transcriptomic analyses using maternal plasma and clinical implications. *Trends Mol. Med.* 21, 98–108. doi: 10.1016/j.molmed.2014.12.006
- Xia, Y., Huang, C. C., Dittmar, R., Du, M., Wang, Y., Liu, H., et al. (2016). Copy number variations in urine cell free DNA as biomarkers in advanced prostate cancer. *Oncotarget.* 7, 35818–35831. doi: 10.18632/oncotarget.9027
- Xu, Y., Song, Y., Chang, J., Zhou, X., Qi, Q., Tian, X., et al. (2018). High levels of circulating cell-free DNA are a biomarker of active SLE. *Eur. J. Clin. Invest.* 48:e13015. doi: 10.1111/eci.13015
- Yanagita, M., Redig, A. J., Paweletz, C. P., Dahlberg, S. E., O'Connell, A., Feeney, N., et al. (2016). A prospective evaluation of circulating tumor cells and cell-free DNA in EGFR-mutant non-small cell lung cancer patients treated with erlotinib on a phase II trial. *Clin. Cancer Res.* 22, 6010–6020. doi: 10.1158/1078-0432.CCR-16-0909
- Yeo, W., Wong, N., Wong, W. L., Lai, P. B., Zhong, S., and Johnson, P. J. (2005). High frequency of promoter hypermethylation of RASSF1A in tumor and plasma of patients with hepatocellular carcinoma. *Liver Int.* 25, 266–272. doi: 10.1111/j.1478-3231.2005.01084.x
- Yuan, M., Huang, L.-L., Chen, J.-H., Wu, J., and Xu, Q. (2019). The emerging treatment landscape of targeted therapy in non-small-cell lung cancer. *Signal Transduct. Target. Ther.* 4:61. doi: 10.1038/s41392-019-0099-9
- Zang, Z. J., Cutcutache, I., Poon, S. L., Zhang, S. L., McPherson, J. R., Tao, J., et al. (2012). Exome sequencing of gastric adenocarcinoma identifies recurrent somatic mutations in cell adhesion and chromatin remodeling genes. *Nat. Genet.* 44, 570–574. doi: 10.1038/ng.2246
- Zhang, D., Gao, M., Jin, Q., Ni, Y., and Zhang, J. (2019). Updated developments on molecular imaging and therapeutic strategies directed against necrosis. *Acta Pharm. Sin. B.* 9:455–468. doi: 10.1016/j.apsb.2019.02.002
- Zhang, J., Li, J., Saucier, J. B., Feng, Y., Jiang, Y., Sinson, J., et al. (2019). Non-invasive prenatal sequencing for multiple Mendelian monogenic disorders using circulating cell-free fetal DNA. *Nat. Med.* 25, 439–447. doi: 10.1038/s41591-018-0334-x
- Zhang, J., Tong, K. L., Li, P. K., Chan, A. Y., Yeung, C. K., Pang, C. C., et al. (1999). Presence of donor- and recipient-derived DNA in cell-free urine samples of renal transplantation recipients: urinary DNA chimerism. *Clin. Chem.* 45, 1741–1746. doi: 10.1093/clinchem/45.10.1741
- Zhang, S., Lu, X., Shu, X., Tian, X., Yang, H., Yang, W., et al. (2014). Elevated plasma cfDNA may be associated with active lupus nephritis and partially attributed to abnormal regulation of neutrophil extracellular traps (NETs) in patients with systemic lupus erythematosus. *Intern. Med.* 53, 2763–2771. doi: 10.2169/internalmedicine.53.2570
- Zitt, M., Muller, H. M., Rochel, M., Schwendinger, V., Zitt, M., Goebel, G., et al. (2008). Circulating cell-free DNA in plasma of locally advanced rectal cancer patients undergoing preoperative chemoradiation: a potential diagnostic tool for therapy monitoring. *Dis. Markers.* 25, 159–165. doi: 10.1155/2008/598071
- Zorofchian, S., Lu, G., Zhu, J. J., Duose, D. Y., Windham, J., Esquenazi, Y., et al. (2018). Detection of the MYD88 p.L265P mutation in the CSF of a patient with secondary central nervous system lymphoma. *Front. Oncol.* 8:382. doi: 10.3389/fonc.2018.00382

Conflict of Interest: The authors declare that the research was conducted in the absence of any commercial or financial relationships that could be construed as a potential conflict of interest.

Copyright © 2021 Yan, Guo, Wang, Adhikari, Zhu, Zhang, Zhou, Yu, Li and Zhang. This is an open-access article distributed under the terms of the Creative Commons Attribution License (CC BY). The use, distribution or reproduction in other forums is permitted, provided the original author(s) and the copyright owner(s) are credited and that the original publication in this journal is cited, in accordance with accepted academic practice. No use, distribution or reproduction is permitted which does not comply with these terms.



Adaptive Mechanisms of Tumor Therapy Resistance Driven by Tumor Microenvironment

Peijie Wu^{1,2†}, Wei Gao^{2†}, Miao Su², Edouard C. Nice³, Wenhui Zhang⁴, Jie Lin^{4*} and Na Xie^{2*}

¹ School of Basic Medical Sciences, Chengdu University of Traditional Chinese Medicine, Chengdu, China, ² State Key Laboratory of Biotherapy and Cancer Center, West China Hospital, and West China School of Basic Medical Sciences & Forensic Medicine, Sichuan University, and Collaborative Innovation Center for Biotherapy, Chengdu, China, ³ Department of Biochemistry and Molecular Biology, Monash University, Clayton, VIC, Australia, ⁴ Department of Medical Oncology, The Second Affiliated Hospital of Kunming Medical University, Kunming, China

OPEN ACCESS

Edited by:

Wei Zhao,
Chengdu Medical College, China

Reviewed by:

Longxiang Xie,
Henan University, China
Yunlong Lei,
Chongqing Medical University, China

*Correspondence:

Jie Lin
linjieshi@126.com
Na Xie
naxie@scu.edu.cn

[†] These authors have contributed
equally to this work

Specialty section:

This article was submitted to
Molecular and Cellular Oncology,
a section of the journal
Frontiers in Cell and Developmental
Biology

Received: 14 December 2020

Accepted: 05 February 2021

Published: 01 March 2021

Citation:

Wu P, Gao W, Su M, Nice EC,
Zhang W, Lin J and Xie N (2021)
Adaptive Mechanisms of Tumor
Therapy Resistance Driven by Tumor
Microenvironment.
Front. Cell Dev. Biol. 9:641469.
doi: 10.3389/fcell.2021.641469

Cancer is a disease which frequently has a poor prognosis. Although multiple therapeutic strategies have been developed for various cancers, including chemotherapy, radiotherapy, and immunotherapy, resistance to these treatments frequently impedes the clinical outcomes. Besides the active resistance driven by genetic and epigenetic alterations in tumor cells, the tumor microenvironment (TME) has also been reported to be a crucial regulator in tumorigenesis, progression, and resistance. Here, we propose that the adaptive mechanisms of tumor resistance are closely connected with the TME rather than depending on non-cell-autonomous changes in response to clinical treatment. Although the comprehensive understanding of adaptive mechanisms driven by the TME need further investigation to fully elucidate the mechanisms of tumor therapeutic resistance, many clinical treatments targeting the TME have been successful. In this review, we report on recent advances concerning the molecular events and important factors involved in the TME, particularly focusing on the contributions of the TME to adaptive resistance, and provide insights into potential therapeutic methods or translational medicine targeting the TME to overcome resistance to therapy in clinical treatment.

Keywords: therapeutic resistance, tumor microenvironment, adaptive resistance, exosome, immunotherapy, cancer-associated fibroblasts, vasculature system, hypoxia

INTRODUCTION

Cancer is a significant public health problem worldwide, with substantial incidence and mortality rates (Ferlay et al., 2019). There have been spectacular advances in the development and therapeutic application of treatment for tumors, including chemotherapy, radiotherapy, targeted therapy, and immunotherapy over the past several decades (Szakács et al., 2006). However, resistance to these therapies has been a major obstacle that restricts the effectiveness of cancer treatments and impacts patient survival (Liu et al., 2018). Therefore, most patients respond to therapies at an early stage, whereas patients at a later stage frequently display poor clinical outcomes with continuous treatment (Miller et al., 2019). A broad range of intrinsic mechanisms underlying how cancer cells escape from the cytotoxicity of tumor therapies have been revealed, including decreased

drug accumulation, altered drug metabolism, mutated or altered drug target and enhanced DNA repair capability, as well as inactivated cell death signaling (Assaraf et al., 2019; Milman et al., 2019; Valencia and Kadoch, 2019; Zhong and Virshup, 2020). Tumor cell heterogeneity, especially cancer stem-like cells (CSCs), is another cause leading to various resistance responses for multiple therapies (Housman et al., 2014; Steinbichler et al., 2018). Accordingly, multiple studies have addressed intracellular response, including genetic or epigenetic alterations, for cell survival under the death pressure induced by therapies (Cheng et al., 2020; Jiang W. et al., 2020; Long et al., 2020; Wang et al., 2020). New viewpoints and theories have proposed that tumor progression, especially when confronted with external pressure from various therapies, is a dynamic and complicated process that tightly interacts with the surrounding environment (Hanahan, 2014).

The tumor microenvironment (TME) is the extracellular environment in which tumors cells exist, and consists of carcinogenic cells, cancer-associated fibroblast (CAFs), immune cells [including T and B lymphocytes, tumor-associated macrophages (TAMs), and natural killer cells], the vasculature system, and the extracellular matrix (ECM; including secreted cytokine, chemokine, metabolites, and exosomes) (Quail and Joyce, 2013; Belli et al., 2018). It has been shown that the non-malignant cells in the TME are not just silent bystanders, but rather actively boost carcinogenesis by promoting excessive tumor initiation, malignant progression, metastasis, and therapeutic resistance (Mantovani et al., 2008; Grivennikov et al., 2010; Hanahan and Weinberg, 2011; Balkwill et al., 2012; Hanahan and Coussens, 2012). The transformed cancer cells are found to interact with stromal cells in the TME, which contribute extensively to tumor development and resistance. Additionally, hyperplasia, metabolic remodeling, malignant proliferation, and inhibition of apoptosis in tumor cells contribute to hypoxia, oxidative stress, and acidosis within the TME. These abnormal conditions further modulate the ECM to induce angiogenesis or mechanical stiffness, and ultimately result in metastasis and resistance (Schrader et al., 2011; Quail and Joyce, 2013; Maman and Witz, 2018; Lin et al., 2019). CAFs induce cancer progression as well as therapeutic resistance through the secretion of cytokines or chemokines, exosomes, and ECM remodeling factors (Shiga et al., 2015; Fu et al., 2016). Macrophages, adipocytes, and fibroblasts in the TME can also act as a sanctuary for tumor cells to escape immune elimination (Hui and Chen, 2015). Therefore, combination chemotherapy with drugs targeting the TME, such as immune cells and angiogenesis, has had success in clinical trials for overcoming drug resistance (Correia and Bissell, 2012; Jo et al., 2018).

Accordingly, an interesting concept has been proposed that the resistance of tumor cells to multiple therapies may be caused by both active (cell-autonomous) and adaptive (non-cell-autonomous) mechanisms. While numerous active mechanisms of therapeutic resistance have been summarized previously, here, we focus on the adaptive resistance to various therapies mainly dependent on the TME (**Figure 1**) (Holohan et al., 2013; Housman et al., 2014). Furthermore, the complex reciprocity between tumors and TME and its role in adaptive resistance

is discussed, with a perspective on prospects of overcoming therapeutic resistance.

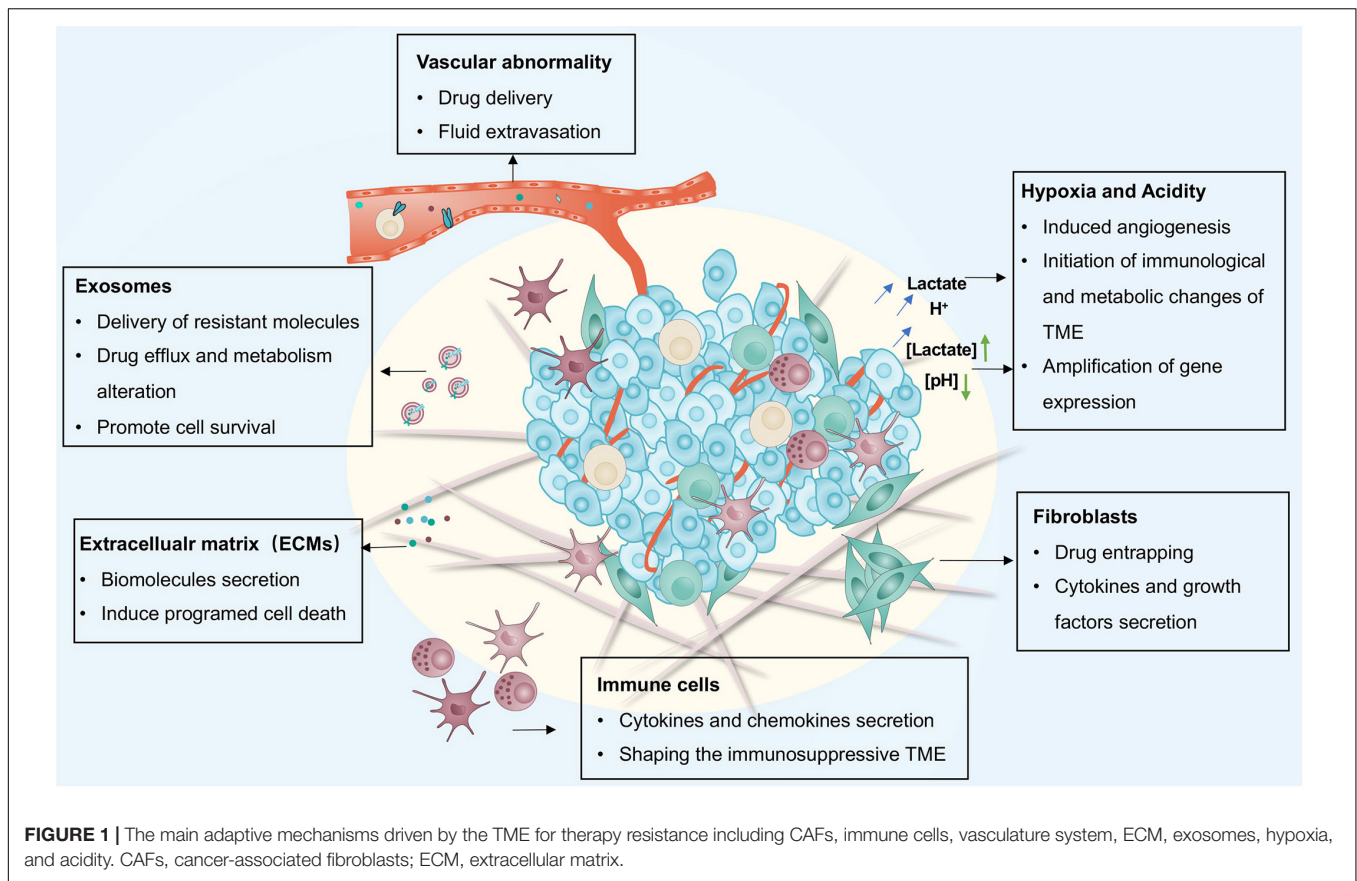
TME-DRIVEN ADAPTIVE MECHANISMS OF THERAPY RESISTANCE

The TME contains a wide variety of cell types including CAFs, immune cells, and vascular cells embedded in the ECM. The TME also contains exosomes, metabolites and cytokines that mediate heterocellular interactions. Moreover, the physical or chemical features, including hypoxia, acidity, and oxidative stress, all facilitate tumor progression and resistance.

Cancer-Associated Fibroblasts (CAFs)

Cancer-associated fibroblasts are a prevalent subpopulation of cells in the tumor stroma (Orimo et al., 2005; Räsänen and Vaheri, 2010). The conversion from quiescence to activation of fibroblasts provokes various oncogenic signals that facilitate tumor cells to escape therapies (Kalluri and Zeisberg, 2006). Co-culture of prostate tumor cells with CAFs attenuates doxorubicin cytotoxicity by obstructing DNA damage and suppressing ROS generation in tumor cells (Cheteh et al., 2017). CAFs may also be responsible for the resistance of therapy through secreting chemokines, growth factors, metabolites, and exosomes, causing resistance and recurrence (**Figure 2**) (Billottet et al., 2008; Kojima et al., 2010; Räsänen and Vaheri, 2010; Straussman et al., 2012). CAF-secreted PAI-1 activates the AKT and MAPK pathways in a paracrine way to reduce chemotherapy drug-induced DNA damage, ROS generation, and cell death in esophageal squamous cell carcinoma (ESCC) (Che et al., 2018). HGF secreted by CAFs can combine with the MET receptor to activate the PI3K-Akt and MAPK pathways, which is responsible for the resistance of BRAF inhibitors or EGFR inhibitors to glioblastoma, colon cancer, and melanoma (Thomasset et al., 1998; Luraghi et al., 2014; Fiori et al., 2019). In addition, CAF-derived paracrine signals including chemoattractant cytokines, metabolites, and exosomes induce the NF- κ B pathway, contributing to tumor cell resistance (Sun et al., 2012; Chan et al., 2016; Su et al., 2018; Zhang D. et al., 2018). Treatment with chemotherapeutic drugs upregulates WNT16B in CAFs, which mitigates the cytotoxic effects of drugs through the NF- κ B pathway in prostate cancer cells (Sun et al., 2012). Similarly, secreted IL-1 β and the constitutively expressed IL-1 receptor associated kinase 4 (IRAK4) induce the activation of the NF- κ B pathway both in CAFs and pancreatic cancer cells, alleviating the cytotoxicity of gemcitabine in pancreatic tumors (Zhang D. et al., 2018). IL-6 is another cytokine released by CAFs that promotes cisplatin resistance through the STAT3/NF- κ B pathway by upregulating CXCR7 in ESCC (Qiao et al., 2018).

Given the pivotal role of CSCs in therapeutic resistance, the CAFs strengthen stemness as a route of acquired resistance (Zhao, 2016; Fiori et al., 2017). The IL-6 and IL-8 released by CD10⁺GPR77⁺ CAFs can promote CSCs sustaining chemotherapy resistance in breast and lung tumors (Su et al., 2018). Meanwhile, chemotherapy-treated colorectal CAFs promote the self-renewal of CSCs by increasing the secretion of interleukin-17A (IL-17A) (Lotti et al., 2013). In addition,



TGF- β 2 secreted by CAFs cooperate with HIF-1 α derived from the hypoxic TME to activate the Hedgehog pathway, which promotes cancer cell stemness and resistance to chemotherapy (Tang et al., 2018). Moreover, ELF chemokines secreted by CAFs are also proven to induce the transformation of tumor cells to stem cells in breast and pancreatic tumors (Chan et al., 2016). The secretion of FGF5 by Hedgehog-activated CAFs in mouse models of breast cancer creates a supportive microenvironment for cancer cells by fostering a reversible stem-like phenotype. Indeed, inhibition of Hedgehog signaling by Smo inhibitors can hinder the transformation toward stemness status to recover the sensitivity of cancer cells to docetaxel (Cazet et al., 2018).

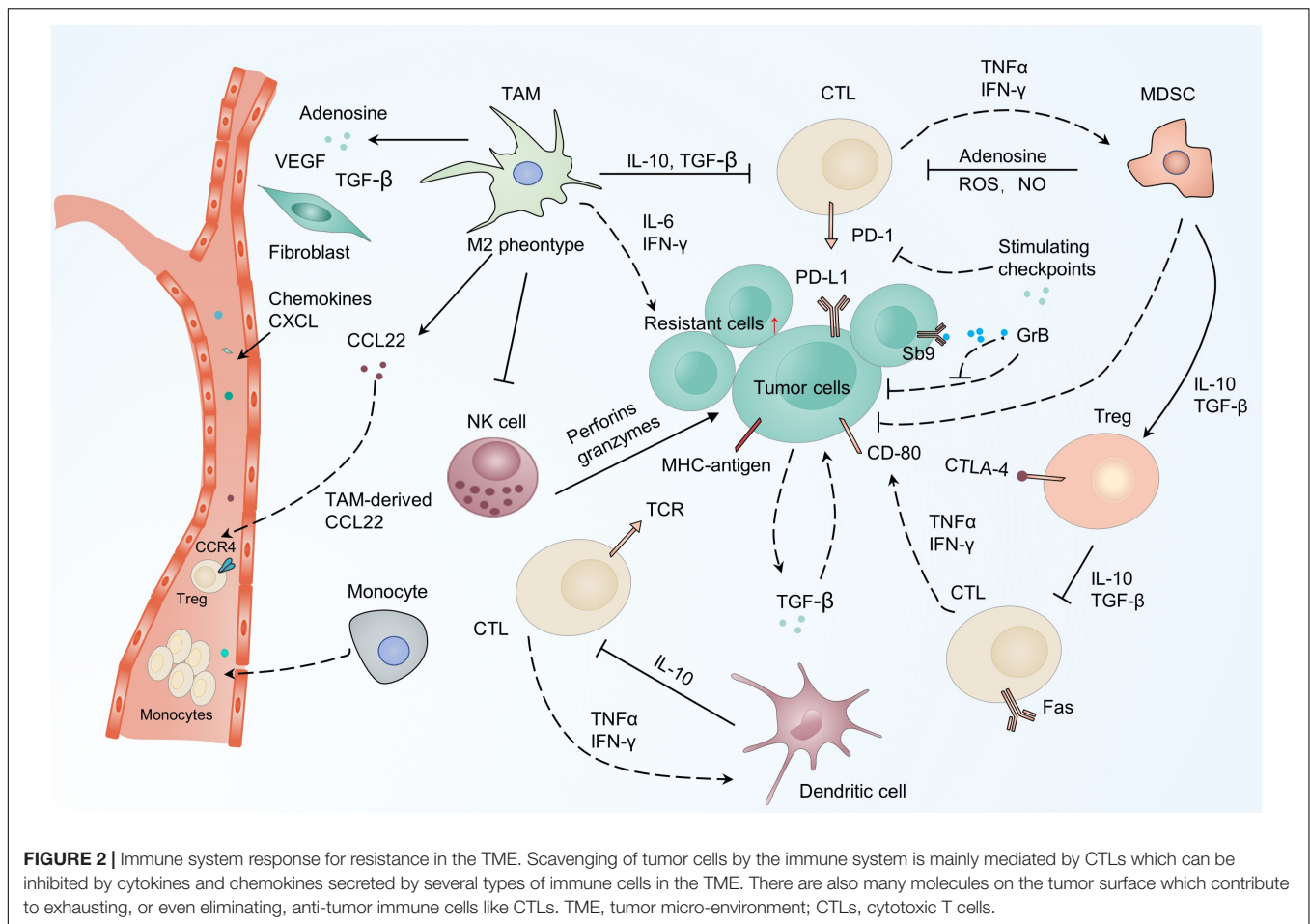
Furthermore, the complicated crosstalk between CAFs and tumor cells also contributes to resistance. For example, epithelial expression of platelet-derived growth factor (PDGF)-CC causes the CAFs to secrete STC1, IGFBP3, and HGF, which are responsible for the tamoxifen resistance in breast cancer (Roswall et al., 2018). To escape tumor treatment, the upregulated insulin receptor (IR) and insulin-like growth factor (IGF) 1 receptor (IGF1R) in cholangiocarcinoma (CCA) cancer cells promote the proliferation and activation of CAFs. CAF-secreted IGF2 provides a feedback pathway with IR/IGF1R to induce the resistance of cancer cells to erlotinib, a tyrosine kinase inhibitor (TKI). Hence, an IR/IGF1R inhibitor can improve the deleterious effect of erlotinib in xenografts models (Vaquero et al., 2018). Additionally, cancer cell-derived serum components,

such as lysophosphatidic acid (LPA) and proteases, are reported to stimulate CAFs remodeling for tumor cells survival (Park et al., 2008; Yarnold and Brotons, 2010; Mantoni et al., 2011; Calvo et al., 2013). The remodeled CAFs, however, exert paracrine actions on tumor resistance via secreted growth factors, including VEGF-A, TGF- β , and various cytokines. CAFs-tumor cell contact can also activate the NOTCH signaling pathway, facilitating stroma-mediated radiotherapy (Freund et al., 2010; Acosta et al., 2013).

In general, the above evidence has shed light on the adaptive mechanism that CAFs utilize with tumor cells for acquired resistance in many cancers including lung, breast, prostate, and glioblastoma. CAFs can interact with various TME factors including immune cells, tumor cells, and the ECM to participate in tumor cell resistance. The heterogeneous nature of CAFs and their multiple functions are interesting potential research directions as they offer a promising strategy for novel cutting-edge therapies directed at tumors and the TME.

Immune Cells

The immune cells in the TME mainly consist of B cells, effector and regulatory T cells, TAMs, myeloid-derived suppressor cells (MDSCs), natural killer cells (NKs) as well as dendritic cells (DCs) (Chen F. et al., 2015; Lei et al., 2020). These cells are crucial for tumorigenesis, exerting either promoting or antagonizing effects on tumors (Lei et al., 2020). Cytotoxic CD8⁺ T cells



(CTLs) are the primary lymphocytes for killing tumor cells. They secrete cytotoxic enzymes including perforin and granzyme, and can interact with the major histocompatibility complex I (MHC-I) (Tanaka et al., 1999; Jackaman et al., 2012; Martínez-Lostao et al., 2015; Wei et al., 2018; Zhong et al., 2020). The involvement of CTLs in tumor therapeutic resistance is proven by the strong association between the profile of CTLs in tumors and the chemotherapy outcomes (Figure 3) (Denkert et al., 2010; Halama et al., 2011; Chen and Chang, 2019). In ovarian cancer, CTLs can enhance the immunogenic action of IFN-β to abrogate CAF-mediated resistance to platinum-based chemotherapy (Wang et al., 2016). Indeed, the combination of cisplatin with immune checkpoint inhibitors (ICIs) have been shown to result in better clinical outcomes (Gandhi et al., 2018; Socinski et al., 2018). TAMs are one of the most abundant cells detected in solid tumors and are derived from circulating monocytes. They also play an important role in controlling the immunosuppressive mechanisms of the TME, contributing to tumor development and therapeutic resistance (Solinas et al., 2010; Ruffell and Coussens, 2015; Rähä and Puolakkainen, 2018; Salmaninejad et al., 2019; Saleh and Elkord, 2020). Evidence implicates TAMs in the secretion of cytokines including IL-6 and IFN in response to resistance (Jinushi et al., 2011; Salvagno et al., 2019). Blocking colony stimulating factor 1 receptor (CSF-1R) signaling to

regulate the polarization status of TAMs has been found to be an effective way of restoring the sensitivity of cisplatin involving IFN response (Salvagno et al., 2019). Accordingly, these promising results have encouraged the evaluation of combination therapy strategies targeting the immune system for tumor patients.

Growing evidence suggests that immunotherapy has shown dramatic efficacy in clinical outcomes (Wei et al., 2018; Cervantes-Villagrana et al., 2020). However, some cancer patients treated using this approach show limited response rates due to acquired resistance (O'Donnell et al., 2017; Sharma et al., 2017). It has been shown that acquired immune resistance may be achieved by three approaches: (i) increased levels of immunosuppressive cells and molecules; (ii) upregulation of immune checkpoints; and (iii) tumor mutation loads and loss of target antigens. For example, enhanced recruitment of immunosuppressive cells, such as TAMs and MDSCs, reduces the sensitivity of immunotherapy and enhances immunosuppression, leading to acquired resistance (Restifo et al., 2016; O'Donnell et al., 2017; Sharma et al., 2017). Maj et al. (2017) have demonstrated that apoptotic Tregs can upregulate the level of extracellular adenosine which can be correlated with acquired resistance to anti-PD-L1 mAb treatment in mice models. Moreover, the compensatory inhibitory mechanism also contributes to acquired resistance. For instance, increased

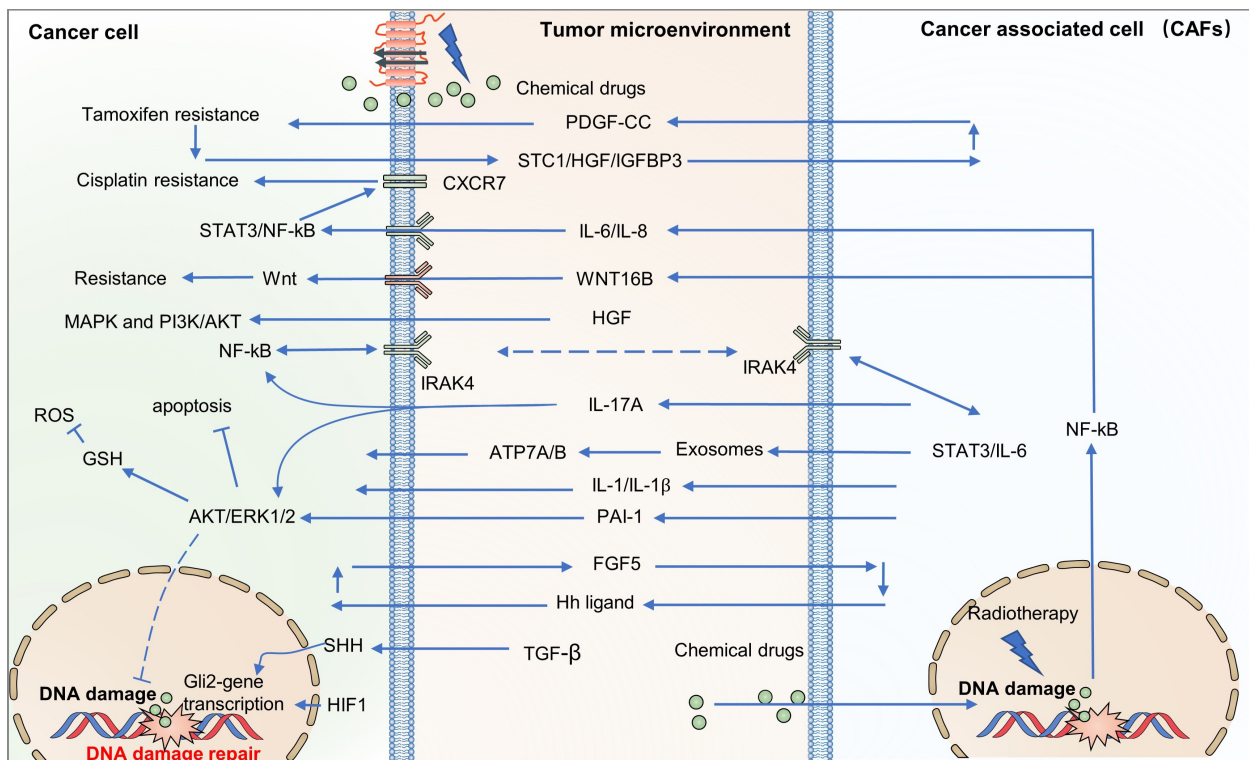


FIGURE 3 | CAFs drive resistance-related paracrine pathways in the TME. CAFs provide an adaptive response for resistance by secreting chemokines, growth factors, metabolites, and exosomes, which activate various signaling pathways in cancer cells, including PI3K-Akt/MAPK, NF-κB, and STAT3. PI3K-Akt, the phosphatidylinositol 3-kinase (PI3K)/protein kinase B (AKT) signaling pathway; MAPK, mitogen-activated protein kinase pathway; NF-κB, nuclear factor-κB; STAT3, signal transducer and activator of transcription 3.

CD4⁺TIM-3⁺ and CD8⁺TIM-3⁺ T cells in lung tumor biopsies has been related with resistance to anti-PD-1 mAb in both humans and mice (Koyama et al., 2016). Similarly, increased TIM-3 on CTLs has been reported in HNSCC following treatment with anti-PD-1 mAb (Shayan et al., 2017). The alteration of neoantigens may be another reason for acquired resistance, as manifested by the fact that loss of CD19 causes resistance following CD19-CAR-T cell therapy (Shalabi et al., 2018). Interestingly, the latest studies implicate that the serine protease inhibitor SerpinB9 (Sb9), expressed in CAFs, MDSCs, and TAMs, can promote tumor cell proliferation by combining with granzyme B (GrB) leading to resistance to immunotherapy (Mangan et al., 2017; Jiang L. et al., 2020; Yin et al., 2020).

Vasculature System

Numerous studies have shown that the responsiveness of tumors to therapy is affected by the vasculature system. Mechanically, the vasculature influences drugs transportation and sensitivity by controlling the supply of nutrients and oxygen, ultimately regulating tumor cell survival (Galmarini et al., 2000). The vasculature transports nutrients and oxygen, as well as other growth factors, to both normal and tumor tissue, and removes waste products following cellular metabolism, which can be involved in tumor relapse, metastasis, and resistance. Vessels in tumors are observed to be convoluted, branched, and

dilated, with excessive loops compared with normal tissues (Jain, 1988). In some cases, vessels cannot be transformed into capillaries, arterioles, or venules. Moreover, vessel walls are often discontinuous or absent compared with normal tissues leading to varying degrees of leakiness in different tumors (Benjamin et al., 1999; Carmeliet and Jain, 2000; Hashizume et al., 2000; Yonenaga et al., 2005; Trédan et al., 2007). Accordingly, blood flow in tumors becomes chaotic and variable (Carmeliet and Jain, 2000). In the tumor vascular network, the viscosity and geometric resistance of blood is increased, and the pressure between arterioles and venules is depressed (Sevick and Jain, 1989; Trédan et al., 2007). Further, in normal tissues, pressure is reduced via the lymphatic network. However, lymph vessels are found to be lacking or have reduced functionality in solid tumors compared with normal tissues, leading to higher interstitial pressure (Leu et al., 2000; Stohrer et al., 2000; Heldin et al., 2004; Trédan et al., 2007). This higher interstitial pressure can suppress the transportation and distribution of larger biological molecules, and diverts blood away from the center toward the periphery of the tumor (Salnikow et al., 2003; Heldin et al., 2004). Interestingly, even in the same tumor, the rate of blood flow or morphology of vessels may vary with space and time (Gillies et al., 1999; Vaupel, 2004). These aberrant vasculature systems, and the dimensional compression of vessels caused by the excessive proliferation of tumor cells, reduce the rate of blood flow and impair the nutrition

and oxygen supply to the tumor tissues (Padera et al., 2004). The insufficient supply of nutrients and oxygen as well as clearance of metabolic waste creates an acidic and hypoxic TME, which promotes therapeutic resistance (Tatum, 2006).

Further, the synergistic effect of various cell types in the TME, such as pericytes, endothelial cells, and bone marrow-derived progenitors, is the basis of tumor angiogenesis, which is reported to be sensitive to oxygen levels (Weis and Cheresh, 2011; Semenza, 2013). Mesenchymal stem cells (MSCs), TAMs, and CAFs all promote tumor angiogenesis by releasing various angiogenesis-related ligands. For instance, increased VEGFA is associated with poor prognosis in metastatic tumors such as lung, colon, and renal cell carcinomas (Hegde et al., 2013; Lee and Wu, 2015).

The delivery of drugs is also compromised by these aberrant vasculature systems (Durand, 2001). The infiltration gradient in the spatial distance from vascular components to tumor lesions is related to the distribution of drugs from the tissues to cancer cells. Microvascular density (MVD) is an important index for the clinical outcomes of carcinomas of the lung, breast, and liver (Trédan et al., 2007; Ariotti et al., 2015; Yuan et al., 2015). Growing evidence indicates that VEGF receptor inhibitor resistance is mainly caused by proangiogenic factors, suggesting that combination with anti-angiogenic agents may improve clinical outcomes compared with VEGF receptor inhibitors alone (Flaherty et al., 2015). In addition, the chemokine CXCR7 is reported to promote angiogenesis by increasing ERK1/2 phosphorylation (Yamada et al., 2015). Interestingly, the CXCL12-CXCR7 complex has been shown to mediate pro-angiogenesis, tumor growth, lung metastasis, and resistance (Yamada et al., 2015; Sun, 2016). Accordingly, anti-angiogenesis may be an effective therapy by specifically targeting tumor blood vessels.

Extracellular Matrix (ECM)

The ECM consists of fibrous protein (such as laminin, elastin, and collagen), proteoglycans, water, and microelements, weaving a complex fiber-based network to provide structural support and regulate cellular activities, including proliferation, communication, and adhesion (Watnick, 2012; Martino et al., 2014; McAndrews et al., 2015; Korneev et al., 2017; Walker et al., 2018). In tumors, both the composition and physical or chemical properties of the ECM are different, depending on the tumor tissue, resident cells, tumor staging, and therapeutic strategies (Shree et al., 2011; Correia and Bissell, 2012; Watnick, 2012; Klemm and Joyce, 2015; Sato et al., 2016; Korneev et al., 2017; Jo et al., 2018; Senthebane et al., 2018; Walker et al., 2018). The ECM contributes to tumor resistance by influencing drug delivery, facilitating the escape from immune surveillance, and manipulating the transmembrane signaling transduction process.

Drugs are usually transported to the tumor issues by the pressure of blood circulation through interstitial areas. In this process, drugs need to cross the physical and biochemical barriers of the TME. The desmoplastic stroma has been found to be a barrier responsible for drug resistance by impeding the delivery of anti-cancer drugs and affecting vascular systems in tumors (Olive et al., 2009). In interstitial spaces, the organization of

the ECM has been found to increase fluid pressure due to the barriers of the tumor mass, significantly suppressing the efficacy of drug delivery (Correia and Bissell, 2012; Maeda and Khatami, 2018). Moreover, excessive proliferation of cancer cells promotes fluid flux from the neoplasms toward the surroundings which impedes drug transportation (Chen Y. et al., 2019). Indeed, drug delivery efficiency has been demonstrated to be inhibited in the 3D cultured spheroids compared with the 2D monolayer owing to the density of the ECM cells (Jo et al., 2018). Furthermore, tumor cells within the collagen I matrix display obvious resistance when cells are exposed to 5-fluorouracil/oxaliplatin (Kanazawa et al., 2017; Jo et al., 2018; Matsunuma et al., 2019).

Besides influencing drug delivery, the ECM also plays an essential role in controlling cytokine activity, of which TGF- β is the most important. TGF- β induces the recruitment of fibroblasts to the tumor site and transformation to CAFs by regulating ECM matrix degradation (Itoh et al., 2017; Paauwe et al., 2018; Purcell et al., 2018). In addition, TGF- β along with HIF-1 can induce lysyl oxidase (LOX) which orchestrates ECM stiffness by inducing cross-linked collagen (Dauer et al., 2018; Zhao et al., 2018). ECM stiffness, in turn, can activate the TGF- β signaling pathway to form a bridge in the basement membrane and contribute to tumor cell evasion (Upagupta et al., 2018; Najafi et al., 2019). Indeed, genomic and transcriptomic analysis have demonstrated that the activated gene sets in response to TGF- β signaling are involved in regulating various pathophysiological processes including EMT, wound healing, angiogenesis, and dissemination (Hugo et al., 2016). On the other hand, TGF- β can regulate immune response by orchestrating the crosstalk of multiple cell types in the TME, including CAFs, lymphocytes, and endothelial cells (Korneev et al., 2017; Chakravarthy et al., 2018; Kesh et al., 2020). TGF- β can inhibit the proliferation and differentiation of anti-tumor T cells by increasing the expression of CD25 and Foxp3 (Löffek, 2018). Moreover, TGF- β induces the secretion of monocyte chemoattractant protein-1 (MCP-1) to upregulate the expression of mesenchymal markers and chemotactic factors (CCL-2, 7, 8, 13), which are associated with anti-PD-1 immune resistance (Díaz-Valdés et al., 2011; Sawa-Wejksza and Kandefer-Szerszeń, 2018).

Among the multiple TME factors that impact cancer cell therapy resistance, cell adhesion to the ECM has been considered as a key determinant (Eke and Cordes, 2015). In particular, cell adhesion-mediated drug resistance depends on interactions between integrins and ECM components such as collagen, fibronectin, and laminin (Grivennikov et al., 2010; Hanahan and Weinberg, 2011; Korneev et al., 2017; Arneth, 2019; Cassim and Pouyssegur, 2019). Integrin-mediated resistance has been reported to influence chemical drugs, radiotherapy, and targeted therapies such as TKIs (Goel et al., 2013; Seguin et al., 2014). It has been reported that the treatment of fibronectin or collagen-deficient ECMs with cisplatin increases the sensitivity of tumor cells by about 40% (Senthebane et al., 2018). The loss of integrin subunits, such as $\alpha v \beta 3$ or $\alpha v \beta 5$, can significantly restore the sensitization of glioblastoma and breast tumor cells to radiotherapy (Cao et al., 2006; Belli et al., 2018). The silencing of the αv subunit also increases the efficacy of oxaliplatin in colon tumor cells (He et al., 2009; Cruz da Silva et al., 2019).

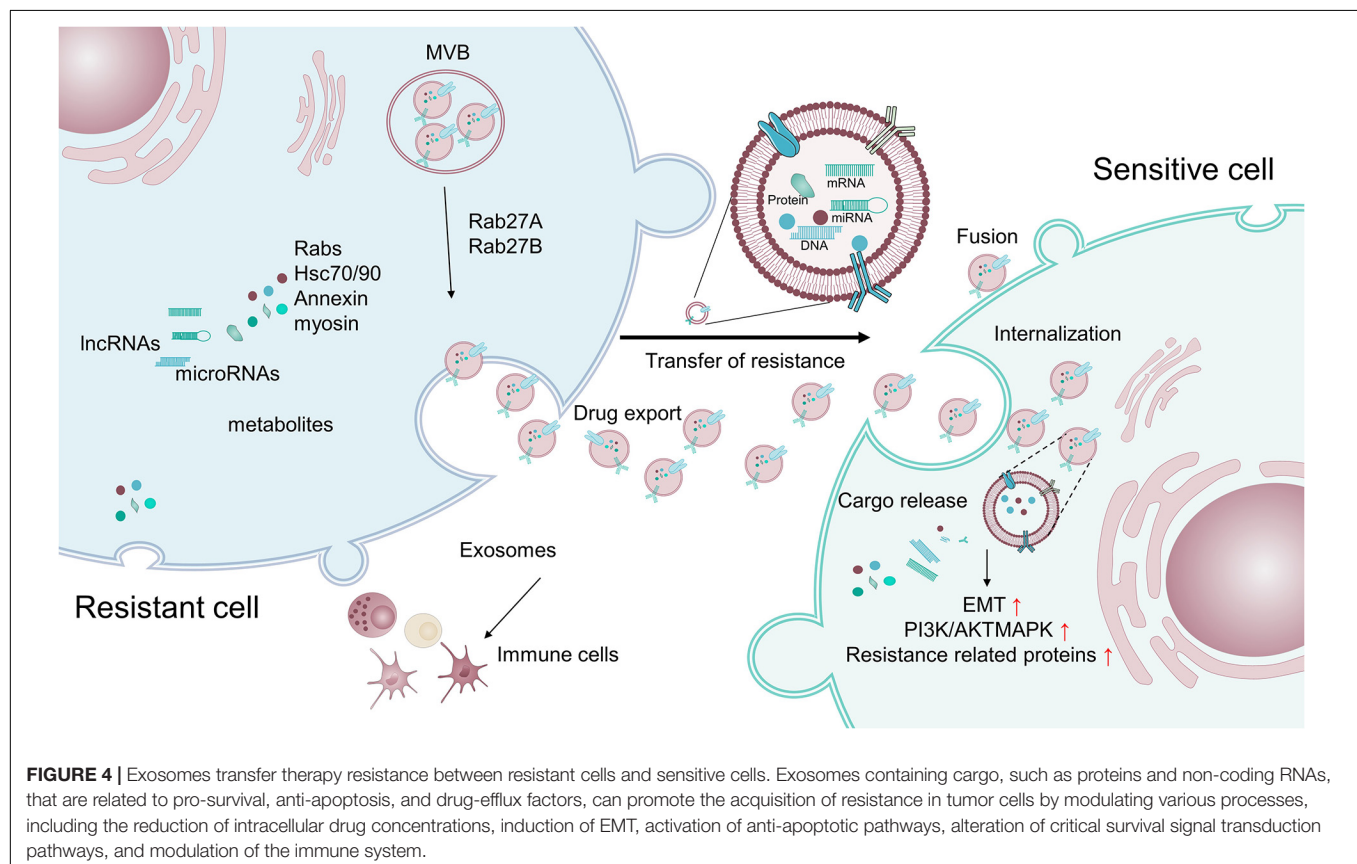
Additionally, the over-expression of $\beta 1$ integrin significantly inhibits cell death in hepatocellular carcinoma exposed to etoposide, cisplatin, or docetaxel (Zhang et al., 2002, 2019; Ogawa et al., 2008). Mechanically, integrins transmit the signals in the microenvironment into intracellular pathways through focal adhesion kinase (FAK) and integrin-linked kinase (ILK) (Eke and Cordes, 2015). The complexes of FAK, ILK, cortactin, and cysteine-histidine-rich 1 as well as parvin α have been reported to inhibit the outcome of radiotherapy (Eke and Cordes, 2015). Integrin $\beta 1$ regulates the dephosphorylation of FAK to protect tumor cells resistant to radiotherapy in a JNK-dependent manner on HNSCC and PDAC *in vitro* and *in vivo* (Goel et al., 2013; DeRita et al., 2019). Blocking the $\alpha 5 \beta 1$ subunit reduces the resistance to ellipticine and temozolomide dependent on p53 mutation status in glioblastoma cells (Martinkova et al., 2010; Fujita et al., 2020). Upregulated $\alpha 4$ integrin is responsible for the resistance in AML and esophageal cancer cells via the PI3K/Akt pathway (Layani-Bazar et al., 2014; Chen and Chang, 2019; Cruz da Silva et al., 2019). Additionally, a few findings suggest that the NF- κ B or ILK-RhoB pathways may be involved in integrin-mediated resistance (Monferran et al., 2008; Ahmed et al., 2013). The ECM proteoglycan, versican, can impact immune surveillance evasion along with hyaluronan by increasing the expression of inflammatory cytokines such as IL-6, TNF α , and NF- κ B (Kang et al., 2017; Gordon-Weeks and Yuzhalin, 2020; Wight et al., 2020; Gamradt et al., 2021). Taken together, the complexity of the ECM in composition

and structure as well as heterogeneity still needs to be further understood for therapeutic purposes.

TME-Derived Exosomes

Exosomes or extracellular vesicles (EVs) with sizes of 40 to 100 nm, originating from large multivesicular bodies (MVBs), mediate cell-to-cell communication by transferring biologically active cargo, including DNAs, RNAs, proteins, and metabolites (Schneider and Simons, 2013; Sun, 2016; Mashouri et al., 2019). Exosomes have been demonstrated to be crucial signaling mediators in the TME, participating in tumorigenesis, metastasis, TME remodeling, angiogenesis, and therapeutic resistance (Figure 4) (Luga et al., 2012; Yoshizaki et al., 2013; Jeppesen et al., 2014; Sung et al., 2015; You et al., 2015; Paolillo and Schinelli, 2017; Wang X. et al., 2018; Zeng et al., 2018; Mashouri et al., 2019; Steinbichler et al., 2019; Yang E. et al., 2020). For example, exosomes have been found to control metabolic reprogramming (Yang E. et al., 2020). Exosomes can also scavenge unfavorable molecules in normal cells. Cancer cells hijack exosomes for the efflux of anti-cancer drugs, resulting in drug resistance (Safaei et al., 2005). Thus, drug-resistant ovarian carcinoma cells exhibit an enhanced exosomal export of cisplatin together with putative transporters MRP2, ATP7A, and ATP7B (Safaei et al., 2005).

Exosomes and their cargos can also promote the drug resistance of target cells (Shedden et al., 2003; Corrado et al., 2013). Exosomes extracted from resistant breast and



prostate cancer cells have been shown to contain MDR1/P-gp transporters, conferring resistance to drug-sensitive tumor cells (Levchenko et al., 2005; Corcoran et al., 2012; Lv et al., 2014). miR-155 in exosomes has been reported to induce chemo-resistance by increasing the FOXO-3a, TGF- β , and C/EBP- β -mediated expression of EMT markers (Du and Shim, 2016; Crow et al., 2017; Lobb et al., 2017; Wang et al., 2019). Notably, exosomes isolated from triple-negative breast cancer cells can induce drug resistance on non-tumorigenic breast cells by modulating the PI3K/AKT, MAPK, and HIF1A pathways (Ozawa et al., 2018). Additionally, lymphoma exosomes carrying CD20 shield target cells from an antibody attack via the complement consumption of therapeutic anti-CD20 antibodies, leading to evasion of humoral immunotherapy (Aung et al., 2011).

Intriguingly, exosomes also promote therapeutic resistance by facilitating the intricate crosstalk between tumor cells and non-tumor cells within the TME. RNAs within exosomes derived from stromal cells activate the pattern recognition receptor RIG-I and downstream STAT1 signaling, which facilitates the growth of resistant tumor cells (Boelens et al., 2014). Exosomes secreted by TAMs transfer miR-21 to gastric cancer cells, which activates the PI3K/AKT signaling pathway and suppresses cell apoptosis to confer resistance (Zheng et al., 2017). Meanwhile, TAMs can directly deliver mRNAs to enhance the expression of CDK6, mTOR, STAT3, and β -catenin, leading to cisplatin resistance in BCa cells (Wu et al., 2020). In another example, exosomes released from CAFs strengthen the chemo-resistance of pancreatic cancer cells and colorectal cancer cells by activating β -catenin and the Snail pathway (Richards et al., 2017; Ren et al., 2018).

Collectively, exosomes can cause tumor cells to acquire resistance by various pathways, including the reduction of intracellular drug concentrations, induction of EMT, activation of anti-apoptotic pathways, alteration of critical survival signal transduction pathways, and modulation of the immune system (Mashouri et al., 2019; Steinbichler et al., 2019; Dai et al., 2020).

Hypoxia, Acidity, and Oxidative Stress

The abnormal vasculature and heavy requirement for oxygen in tumors create a chronic or diffusion-limited hypoxia and acid environment (Bussink et al., 2003; Heldin et al., 2004; Milosevic et al., 2004; Gargiulo et al., 2019; Zaidi et al., 2019). The hypoxic environment of tumors leads to a decreased supply of nutrients such as glucose and essential amino acids (Lee et al., 2014; Tan et al., 2015; Ma et al., 2020). Moreover, tumor cells prefer to undergo glycolysis rather than oxidative metabolism which often converts glucose to lactate for the production of ATP, resulting in sequential acidic microenvironments (Dang and Semenza, 1999; Singh et al., 2017; Moloney and Cotter, 2018). Furthermore, a decreased capability of removing these acidic products results in low interstitial pH, another feature of solid tumors (Tran et al., 2016; Singh et al., 2017). These hypoxic and acidic conditions will induce aberrant activation of oncogenic pathways and genetic instability, contributing to tumor development and resistance (Li and Sun, 2018). For example, hypoxia in tumors increases the expression of multiple genes associated with angiogenesis and cell survival by activating HIF-1, a basic helix-loop-helix

transcription factor (bHLH) (Pouyssegur et al., 2006; Chen and Sang, 2016; Petrova et al., 2018; Lee et al., 2020). Serving as an oxygen sensor, HIF-1 may promote the expansion of tumor cell populations and alteration of biochemical metabolites involved in a resistant phenotype in response to hypoxia. It has been shown that hypoxia reduces sensitivity to p53-mediated apoptosis and promotes chemotherapeutic resistance in tumor cells (Kinoshita et al., 2001; Holle et al., 2016; Ritter, 2017). In solid tumors, the activation of major oncogenic signaling pathways such as Ras and PI3K/AKT, and the silencing of tumor suppressors LKB1, PTEN, and TSC2/1 can activate HIF-1, contributing to resistance (Shaw et al., 2004; Shackelford et al., 2009). Stabilization of HIF-1 α through interaction with Hsp90/Hsp70 also facilitates cell survival under stress conditions (Luo et al., 2010; Taipale et al., 2010). Additionally, HIF-1 α can cooperate with CAF-secreted TGF- β 2 to induce GLI2 signaling cancer stem cells, leading to enhanced stemness and chemotherapy resistance (Tang et al., 2018).

Mechanically, HIF-1 activation induces the transcription of genes that facilitate pathophysiological alterations related to resistance, including the suppression of apoptosis and the induction of drug efflux and metabolism (Warfel and El-Deiry, 2014; Xia et al., 2018). Apoptosis may be a major factor in cell death induced by chemo- or radio-therapies (Krakstad and Chekenya, 2010; Mohammad et al., 2015; Zhao et al., 2015). Interestingly, HIF-1 α has been found to both inhibit proapoptotic proteins, including TRAIL, and activate anti-apoptotic proteins, such as survivin, c-myc, STAT3, and TCF4, to promote the survival of tumor cells under chemo- or radio-therapies (Pei et al., 2010; Rohwer et al., 2010; Nishimoto et al., 2014; Zhao et al., 2016). HIF-1 α also influences sensitivity to therapy through regulation of genes related to metabolic pathways (Lu et al., 2011; Meijer et al., 2012; Huang et al., 2013). HIF-1 α can upregulate GLUT-1 to promote glycolysis, leading to increased intracellular ATP, pyruvate, and lactate levels (Meijer et al., 2012), while the suppression of HIF-1 α results in a reduced glucose uptake, decreased lactate production, and increased oxygen species (ROS), which contribute to the enhanced efficacy of radiotherapy (Meijer et al., 2012). Hypoxia has been reported to promote temozolomide (TMZ) resistance in glioblastoma multiforme (GBM), through the activation of HIF-1 α and NF- κ B, followed by upregulated expression of Bcl-xL (Kitange et al., 2009; Chen W.L. et al., 2015). Transient hypoxia has also been found to cause an increase in dihydrofolate reductase and P-glycoprotein, which contributes to the resistance of drugs targeting topoisomerase II (Kovacic and Osuna, 2000; Gray et al., 2005). Interestingly, oxygen concentration may affect the efficacy of the anti-cancer drugs doxorubicin and mitomycin C, by delivering electrons to the oxygen (Brown and Wilson, 2004; Trédan et al., 2007; Yang G. et al., 2020).

Acidity in the TME has been demonstrated to affect the efficacy of various therapies. It can influence the transport of chemical drugs across the membrane due to the pH gradient caused by the acidic extracellular pH and near neutral or alkaline intracellular pH in tumors (Gerweck et al., 2006; Trédan et al., 2007). Hence, drugs with an acidic dissociation constant of 7.5–9.5 may show a significantly reduced rate of uptake,

such as vincristine, mitoxantrone, doxorubicin, and vinblastine (Cowan and Tannock, 2001; Gerweck et al., 2006; Trédan et al., 2007; Zhou et al., 2019). Therefore, the cytotoxicity of these drugs is suppressed, resulting in a resistant phenotype (Raghunand et al., 2003; Trédan et al., 2007; Stepka et al., 2020). However, the concentration of some weakly acidic drugs including cyclophosphamide and chlorambucil may be increased in the neutral intracellular region (Gerweck et al., 2006; Trédan et al., 2007). Moreover, an acidic TME also alters the cellular proteome, cellular metabolism, and signaling pathways, facilitating stemness and drug resistance in cancer cells. The acidosis induces SOX2 expression by inhibiting vitamin D receptor (VDR)-mediated transcription, resulting in drug resistance (Hu et al., 2020). Enhanced lactate uptake and oxidation-induced lactic acidosis foster the resistance to uprosertib, a pan-Akt inhibitor, in colon cancer cells (Barnes et al., 2020). Moreover, the acidic environment induces the activity of p-glycoprotein (pGP) by activating p38 signaling, leading to multi-drug resistance in rat prostate cancer cells (AT1) (Sauvant et al., 2008). Clearly, the acidity of the TME must be considered when designing the delivery of drugs to obtain maximal therapeutic effect.

Oxidative stress is another feature of the TME, which is caused by the overproduction of reactive oxygen species (ROS) from both tumor cells and non-malignant cells in the TME. Oxidative stress plays a pivotal role in tumor progression, particularly through immune cell suppression. ROS downregulates the anti-tumor functions of effector immune cells that are recruited to the tumor site, notably T lymphocytes and natural killer (NK) cells which mediate anti-tumor immunity. MDSCs have been found to inhibit T cell proliferation to promote colorectal cancer cell proliferation by increasing ROS levels (OuYang et al., 2015; Weinberg et al., 2019). ROS and peroxynitrite in MDSC trigger the nitration of the TCR/CD8 complex which inhibits its interaction with pMHC, contributing to T cell tolerance and tumor escape (Nagaraj et al., 2007). ROS generated from NOX2-sufficient myeloid cells inhibits the NK cell-mediated clearance of malignant cells, facilitating the metastasis of melanoma cells (Aydin et al., 2017). The NK cells residing in the tumor core or primed by IL-15 exhibit higher thiol densities that can prevent other lymphocytes from ROS within the TME (Yang Y. et al., 2020). High levels of ROS following TCR and CD28 stimulation enhance Treg cell-mediated tumor immunosuppression and attenuate anti-tumor T cell responses by stabilizing SENP3 (Yu et al., 2018). In conclusion, oxidative stress acts as an important mediator of anti-tumor immunity. Achieving targeted oxidative stress could be a potential strategy to improve the efficacies of existing immunotherapy treatment.

Heterocellular Metabolic Interactions

Growing evidence has demonstrated that disordered metabolism in the TME plays a crucial role in malignancy, metastasis, and immune resistance. The impact of metabolism on immune-resistance is mainly caused by two aspects: a reshaped immunosuppressive TME from tumor metabolic stress and immune-inhibiting metabolites generated by tumor cells.

Cancer cells usually exhibit high rates of glycolysis and aggressive depletion of amino acids such as tryptophan, arginine,

and glutamine compared with normal cells. Tumor metabolic stress modulates the metabolic properties of malignant cells, which in turn influences nutrient shortage, oxygen competition, and acidity in the TME to create an immune-resistant environment (Martinez-Outschoorn et al., 2017). It is known that the demand for nutrients is especially high in TME, and this nutrient competition can impair the anti-cancer immune response. For example, the competition of carbohydrates can inhibit the anti-tumor effect of cytotoxic T cells by inducing the expression of immunosuppressive cytokines and immune checkpoint inhibitors (Wu et al., 2021). The restriction of glucose supplies due to the high rates of glycolysis in tumor cells impairs the anti-tumor function of CD4⁺ T cells, possibly by blocking the secretion of IFN- γ (Chang et al., 2015; Ho et al., 2015). Similarly, L-arginine deprivation has been found to inhibit anti-tumor immunity by inducing MDSC infiltration or suppressing the toxicity of IFN- γ . L-arginine depletion also promotes the immune evasion of cancer cells by elevating the tumoral level of PD-L1 (Morrow et al., 2013; Fletcher et al., 2015; Hugo et al., 2016; Prima et al., 2017; Kim et al., 2018; Jiang Z. et al., 2020). Tryptophan is another crucial amino acid that contributes to the anti-tumor immune response by regulating the kynurenine metabolic pathway (Jiang Z. et al., 2020; Xie et al., 2020). Indoleamine 2,3-dioxygenase (IDO), an essential enzyme of the tryptophan metabolic pathway, controls the production of kynurenine which exerts immunosuppressive effects by inducing differentiation of T cells and reduces immunogenicity (Wang et al., 2015; Ramapriyan et al., 2019). Both inhibitory immune cells such as MDSCs, DCs, and M2 macrophages as well as tumor cells can express IDO (Ramapriyan et al., 2019). Cancer cells have also been found to reduce tryptophan levels in TME to inhibit immune response (Ramapriyan et al., 2019). Besides glucose and amino acid metabolic pathways, lipid-related metabolism also plays an essential regulatory role in immunosuppressive function (Kamphorst et al., 2013). Obesity induces a desmoplastic TME by promoting inflammation and TAN infiltration, leading to impaired response to chemotherapy in PDAC. Reversal of obesity-aggravated desmoplasia by blocking the angiotensin-II type-1 receptor (AT1) improves response to chemotherapy. Meanwhile, cholesterol depletion can also recover the cytotoxic effect of chemical agents on PDAC and HCC (Guillaumond et al., 2015; Incio et al., 2016). Fatty acids have also been demonstrated to determine the cell fate of T cells and CD8⁺ effector T cells (O'Sullivan et al., 2014).

In addition, a variety of tumor metabolites have been reported to promote immune evasion. Glutamine is the most abundant amino acid in the TME, playing an essential role in anabolic growth and metastasis (Pusch et al., 2017; Zhang et al., 2017). Recent research has demonstrated that glutamine metabolism can impair anti-cancer immune response (Zhang et al., 2017; Oh et al., 2020). Glutamine blockade causes increased glucose and glutamine levels in the TME, inducing MDSCs apoptosis, promoting their differentiation toward the M1 type, and sensitizing resistant tumor cells to immunotherapies (Zhang et al., 2017; Leone et al., 2019; Oh et al., 2020). Adenosine, the breakdown product of ATP, can activate the adenosine-AR pathway to escape from the killing effects of the immune system

by reducing the response of NK cells, M1 macrophages, and CD8⁺ effector T cells. In addition, methylglyoxal (MG), a side-product of glycolysis, is an immunosuppressive metabolite that promotes tumor cell growth and resistance (Nokin et al., 2017; Antognelli and Talesa, 2018; Antognelli et al., 2019; Oh et al., 2020). The high concentration of methylglyoxal in the TME derived from MDSCs leads to the accumulation of methylglyoxal in T cells, contributing to anti-tumor evasion (Baumann et al., 2020). DMBG (*N,N*-dimethylbiguanide) can recover the sensitivity of immunotherapy-resistant tumor cells by removing the glycation activity of methylglyoxal (Baumann et al., 2020). Another molecule that can establish an immunosuppressive TME is lactate, a product of glycolysis and glycogenolysis (Gabrilovich et al., 2012; Mantovani et al., 2017; Pucino et al., 2017; Tong et al., 2018; García-Cañaveras et al., 2019). Lactate induces the development of MDSCs, polarization of macrophages into an immunosuppressive phenotype, maturation of DCs, and inhibition of effector T cells, thereby promoting immune evasion (Husain et al., 2013; Brand et al., 2016; Laoui et al., 2016; Angelin et al., 2017; Morrot et al., 2018). Furthermore, lactate can control CAFs to produce growth factors including hyaluronan (Wu et al., 2017; Apicella et al., 2018; Feichtinger and Lang, 2019).

Collectively, tumor cells reshape their metabolism adaptively which leads to the remodeling of the TME. The heterocellular metabolic interactions create an immunosuppressive TME, which subsequently enhances tumor proliferation and immunotherapy resistance. Thus, targeting tumor cell metabolism or metabolites in the TME should have great potential for recovering immunotherapy resistance.

The Epithelial Pathway in Response to TME

It is well known that tumor initiation and progression rely on bidirectional communications between tumor cells and the associated environment. Several signaling pathways in tumor cells, including Akt, mTOR, STAT3, and Notch, may be responsible for the altered tumor environment exposed to tumor therapies (Figure 5). Surprisingly, tumor cells can adaptively inhibit oncogenic AKT, which induces the secretion of inflammatory molecules such as IL-6/8 and extracellular vesicles (EVs) to restrict the damage induced by therapy (Salony et al., 2016). Thus, suppression of AKT signaling can increase drug resistance in tumor cells (Manning and Cantley, 2007). Moreover, mTOR acts as a vital protein to regulate cell growth both in physiological and pathological conditions (Guri and Hall, 2016). It has been shown that the secretome in the TME can activate mTOR signaling after treatment. Blocking mTOR signaling can restore the sensitivity of several anti-tumor drugs including crizotinib, vemurafenib, and erlotinib (Obenauf et al., 2015). Additionally, the ATM-TRAF6-TAK1 axis related with DNA damage may be involved in these processes (Zhang B. et al., 2018). Surprisingly, some metabolites in the TME, such as the lactate, have been reported to activate the mTOR pathway through glutamine metabolic pathways, inducing the resistance to VEGF inhibitors (Allen et al., 2016).

In addition, the STAT3 pathway can rapidly respond to cytokines, including L-1 β and IL-6 released from neutrophils, TAMs, and CAFs in the TME (Samavati et al., 2009; Kim et al., 2016). Activated STAT3 induces resistance by promoting EMT, increasing anti-apoptotic signaling, and regulating miRNAs and exosomes (Yin et al., 2017; Wang L. et al., 2018). For example, STAT3 can promote the secretion of exosomes by upregulating Rab, which induces platinum resistance in ovarian tumors (Dorayappan et al., 2018). In addition, activated STAT3 can regulate the delivery of drugs by triggering vascular abnormalities (Nagathihalli et al., 2015). Notch is another crucial adaptive signaling pathway responsible for the TME-induced chemotherapy resistance of tumor cells (Meurette and Mehlen, 2018). Exosomes derived from the stroma deliver Jag1, a Notch ligand, activate the Notch pathway to trigger resistance in breast tumor cells (Boelens et al., 2014). CAFs also can release IL-6 to activate the Notch pathway in breast tumor cells (Studebaker et al., 2008). Induction of Notch3 is also relevant to CSCs transformation in liver cancer (Lin et al., 2017). Accordingly, these signaling pathways response to TME may be potential targets from a therapeutic perspective.

TARGETING THE TUMOR MICROENVIRONMENT FOR THERAPY

Multiple preclinical studies implicate the TME as a potential therapeutic target (Jin and Jin, 2020). For instance, multiple strategies of combined therapy related to the TME have shown interesting potential (Table 1). In the TME, tumor cells usually hijack CAFs, ECM, the immune system, hypoxia, and acidosis-related pathways to escape immune surveillance. For example, dysregulated immune signaling pathways have been proven to impair several processes including antigen presentation and T cell infiltration. Thus, targeting the TME might have the potential ability to reverse the resistance of tumor cells.

Targeting Cancer-Associated Fibroblasts

Given the critical role of CAFs, the most abundant cell type in the TME, in therapeutic resistance of tumor cells, emerging evidence supports targeting protumorigenic CAF functions as a promising approach for tumor therapy (Truffi et al., 2020). For example, conophylline is used to treat refractory pancreatic cancers by suppressing CAF activity and the proliferation and secretion of cytokines (Zhen et al., 2017; Umezawa et al., 2018; Ishii et al., 2019). The cell surface markers GPR77 and CD10, specifically expressed in CAFs, are involved in chemoresistance in lung and breast cancer (Vaquero et al., 2018). Treatment with inhibitors of these molecules is a breakthrough in overcoming resistance. For example, using a GPR77-neutralizing antibody to selectively inhibit CAFs is an effective way to restore the sensitivity of drugs. Another strategy is to inhibit the activation of protumorigenic pathways in CAFs. Inhibition of Hedgehog signaling in CAFs successfully enhances the effect of docetaxel chemotherapy in TNBC patients (Cazet et al., 2018). In addition, reversing activated CAFs into a dormant state is also an effective therapeutic strategy. The VDR is considered to

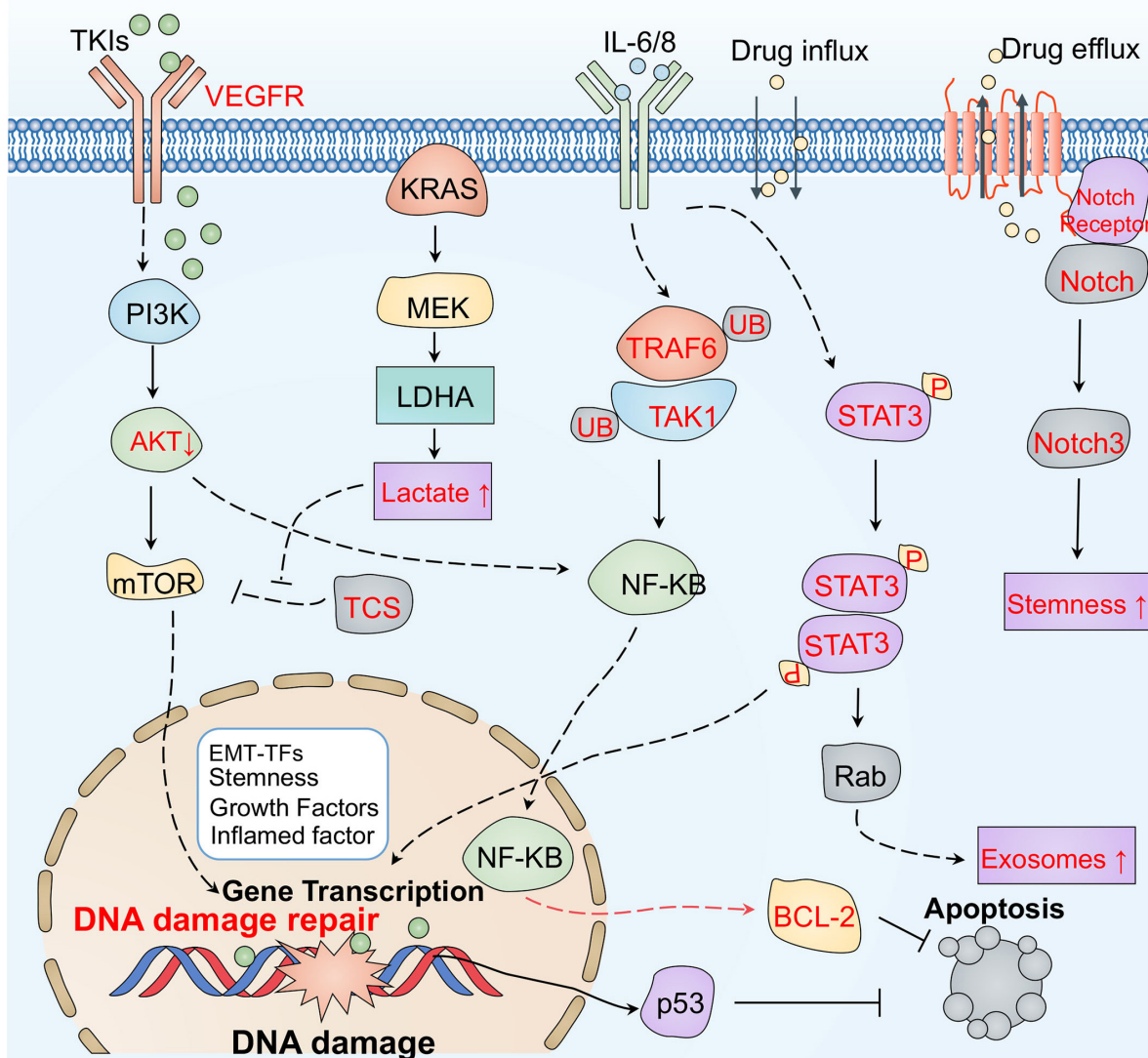


FIGURE 5 | The main signaling pathways responsible for therapeutic resistance mediated by the tumor environment. Tumor cells can adaptively inhibit oncogenic AKT, which induces the secretion of inflammatory molecules such as IL-6/8, and EVs to restrict damage during therapy. The ATM-TRAF6-TAK1 axis related with DNA damage may also be involved in resistance. Some metabolites, such as lactate, in the TME have been reported to activate the mTOR pathway through glutamine metabolic pathways, inducing resistance to VEGF inhibitors. In addition, the STAT3 pathway may also rapidly respond to cytokines, promoting the secretion of exosomes, by upregulating Rab and increasing anti-apoptotic signaling in the TME. IL-6 and exosomes derived from the stroma deliver Jag1, Notch ligand, and Notch3 activate the Notch pathway to trigger resistance.

be a targeted molecule that regulates the transcriptional process to activate CAFs in pancreatic cancer (Yamashita et al., 2012). Interestingly, compared with gemcitabine alone, the synergistic effect of gemcitabine and a VDR ligand suppresses fibrosis and inflammation, and restores the sensitivity of gemcitabine by increasing tumor uptake, thereby improving the survival rate to 57% (Yamashita et al., 2012; Yang et al., 2016). Studies have also found that nanoparticles loaded with a secreted sTRAIL can reduce the activation of CAFs in pancreatic cancers (Yang et al., 2016). Currently, some clinical trials targeting CAFs are being implemented. The agent RO6874281 is an interleukin-2 variant

targeting FAP that is being evaluated for its clinical benefit in combination with atezolizumab, gemcitabine, or vinorelbine in the treatment of advanced tumors. The synergistic treatment of RO6874281 with trastuzumab or cetuximab in patients with head and neck cancer or breast tumors is also in clinical trials.

Targeting the Extracellular Matrix

Blocking the communication between tumor cells and their environment by targeting adhesion molecules, proteolytic enzymes, and ECM components has been demonstrated as an efficient strategy for tumor therapy (Pickup et al., 2014;

TABLE 1 | Combination therapies against cancer used in recent clinical trials.

Conventional drug	Combination therapy	Cancer targeted
Statin	Targeted therapy such as erlotinib, sorafenib, fulvestrant, aromatase inhibitors, anti-HER2	NSCLC, HCC, ESCA, and breast cancer
	Radiotherapy	GBM
	Chemotherapy such as topotecan, zoledronate, bendamustine, and capecitabine	TNBC, pediatric solid and CNS tumor, rectal cancer
Metformin	Targeted therapy such as lanreotide, toremifene, trametinib, gefitinib, and lapatinib	NSCLC, CRC, TNBC, LAML, UCEC and melanoma, kidney cancer, breast cancer
	Radiotherapy	HNSCC, CESC, lung cancer
	Chemotherapy such as docetaxel, oxaliplatin, temozolomide, gemcitabine, and paclitaxel	ESCA, PDAC, GBM, and prostate cancer, breast cancer
Aspirin	Targeted therapy such as osimertinib	NSCLC
	Immunotherapy such as atezolizumab, avelumab, bevacizumab, and ipilimumab	HNSCC, TNBC, and OV
Celecoxib	Targeted therapy such as gefitinib, depsipeptide, toripalimab	ESCA, CRC, HNSCC, NSCLC, OV, and breast cancer
	Radiotherapy	NSCLC
	Chemotherapy such as docetaxel, cisplatin, paclitaxel, and methotrexate	NSCLC, GBM, TNBC, CRC, and PDAC
	Immunotherapy such as nivolumab	NSCLC

Hirata and Sahai, 2017). For example, suppression of the integrin-mediated bidirectional transmitting signals between cells and ECM has been used to prevent therapeutic resistance (Kechagia et al., 2019). Blocking the activity of $\beta 1$ integrin with monoclonal antibody AIIB2 can significantly increase the outcome of HER2-targeting agents as well as radiotherapy (Park et al., 2008; Weigelt et al., 2010; Hirata and Sahai, 2017). The antagonist of integrin $\alpha 4\beta 1$ and $\alpha 4\beta 7$, natalizumab, has been proven to recover the sensitivity of chemotherapy drugs in malignant tumors, including acute lymphoblastic leukemia (AML) and ovarian tumor (Podar et al., 2011; Hsieh et al., 2013; Scalici et al., 2014; Hirata and Sahai, 2017). Matrix metalloproteinases (MMPs), one of the major ECM components, function as proteases to detach cancer cells out of the ECM, participating in tumor development, metastasis, and resistance (Najafi et al., 2019). Several agents targeting MMPs have

been developed for treating advanced carcinomas including incyclinide, JNJ0966 for MMP-9, and the antibody Fab 3369 for MMP-14 (Ling et al., 2017; Scannevin et al., 2017).

TGF- β signaling is another pathway which mediates communication between tumor cells and their ECM. Therefore, anti-TGF β drugs, including neutralizing antibodies, ligand traps, small-molecule kinase inhibitors, and antisense oligonucleotides (AONs), are a potential strategy for improving therapeutic efficacy. Blocking TGF- β by 1D11, a TGF- β neutralizing antibody, can improve the intra-tumoral penetration of both chemotherapeutic drugs and nanotherapeutic agents by normalizing the tumor interstitial matrix, thereby resulting in a better control of tumor growth (Liu et al., 2012). Galunisertib (LY2157299), an oral small-molecule inhibitor of T β RI, sensitizes colorectal cancer cells to RTK inhibitors (Brunen et al., 2013; Colak and ten Dijke, 2017). Blockade of TGF- β has been found to promote the anti-tumor activity of CD8⁺ T cells, thereby reversing the resistance to a PD-1/PD-L1 blockade in the TME (Chen et al., 2018). Moreover, TGF- β blockade by expressing dominant-negative TGF- β receptor II enhances the efficacy of TCR gene therapy against advanced cancers (Bendle et al., 2013). Both fresolimumab, a pan-TGF- β neutralizing antibody, and LY3022859, an anti-T β RII IgG1 monoclonal antibody, exhibited anti-tumor activity in a phase 1 clinical trial for various cancers (Colak and ten Dijke, 2017). T β R inhibitors, including LY2157299 and PF06952229, have been tested in clinical trials for patients with advanced or drug-resistant cancers (NCT03685591) (Liu et al., 2021).

However, some studies suggest that targeting the ECM has limited outcomes in advanced malignancies such as GBM, melanoma, and prostate tumors, suggesting that different tumors with different extracellular matrices can exhibit different results (Eisele et al., 2014; Stupp et al., 2014; Hirata and Sahai, 2017). Therefore, further investigation and clinical trials are necessary to ensure treatment using ECM-targeting strategies are effective and safe.

Targeting the Immune System

As mentioned above, the immune system in TME dramatically affects the response of tumors to various treatment approaches. Therefore, multiple strategies based on targeting the immune system have been used to tackle cancers: (i) inhibiting the recruitment of macrophages to tumor tissues; (ii) blocking the differentiation of macrophages toward TAMs; (iii) enhancing the anti-tumor activity of the immune system (Joyce, 2005; Tsai et al., 2014; Roma-Rodrigues et al., 2019). Several studies indicate that combination treatment using conventional therapies and immunotherapy achieves satisfactory clinical outcomes. Indeed, the combination of chemotherapy drugs and immune checkpoint inhibitors (ICIs) has shown a better result compared with chemotherapy alone (Ridker et al., 2017; Tulotta and Ottewell, 2018). Consistently, targeting CTLs with pembrolizumab enhances the clinical efficacy of cisplatin in drug-resistant patients (Ridker et al., 2017). These promising results have prompted a series of clinical studies to validate this combination therapy strategy. The suppression of MDSCs by anti-CSF-1R neutralizing antibodies or small molecule inhibitors

has been shown to reduce tumor growth and metastasis (Noy and Pollard, 2014; Szebeni et al., 2016; Ridker et al., 2017). Immune checkpoint molecules in NKs were also reported to be potential targets for immunotherapy (Cao et al., 2020). To date approximately 174 clinical trials involving CTLA-4 and 750 involving PD-1 and its receptor PD-L1 have been reported (as reviewed in Boohaker et al., 2018; Darvin et al., 2018; Chen T. et al., 2019). A combination with blocking antibodies against CTLA-4 and PD-1 results in significantly higher response rates and improved survival in patients with metastatic melanoma (Wolchok et al., 2013; Horvat et al., 2015; Larkin et al., 2015; Robert et al., 2015). Moreover, Kineret, an IL-1 receptor antagonist that is often used for rheumatoid arthritis, has exhibited promising results for breast cancer patients (Tulotta and Ottewell, 2018). The anti-IL-1 antibody canakinumab, which is often used for inflammatory diseases, has shown improved clinical outcomes in lung cancer (Ridker et al., 2017). More recently, canakinumab has been proposed for the treatment of highly aggressive tumors NSCLC and triple negative breast cancer (Houriet et al., 2017; Dhorepatil et al., 2019; Paz-Ares et al., 2019; Schenk et al., 2019; Sehested et al., 2019). In addition, combining traditional therapies with immune therapies has shown potential to reverse resistance (Patel and Minn, 2018; Gomez et al., 2020). For example, the combination of HMTs with immune therapy has shown efficacy for various cancer in pre-clinical studies (Zingg et al., 2017; Patel and Minn, 2018; Gomez et al., 2020). Treatment with EZH2 inhibitor and antibodies blocking CTLA-4 was reported to reverse immunosuppressive effects and significantly improve survival in preclinical models (Zingg et al., 2017). Moreover, DNMTi or HDACi treatment was reported to sensitize resistant cancer cells in mouse models of melanoma and lung adenocarcinoma (Chiappinelli et al., 2016; Strick et al., 2016; Zheng et al., 2016; Stone et al., 2017). The combination of HDACis, DNMTis, anti-CTLA4, and anti-PD1 together showed significantly improved rates of survival, with 75% of mice with tumors being cured (Kim et al., 2014; Zheng et al., 2016). Thus, targeting the immune system, especially in combination with traditional chemotherapy to promote survival and reverse resistance, may prove to be a safe and effective strategy for multiple types of tumors, benefitting more patients.

Targeting Hypoxia and Acidosis

As mentioned above, low oxygen pressure and acidosis conditions in the TME dramatically affect a tumor's response to treatment. Therefore, it is rational to manipulate hypoxia and acidosis conditions in the TME to hinder tumor progression (Paolicchi et al., 2016; Roma-Rodrigues et al., 2019). Accordingly, topotecan, an inhibitor of HIF-1 α , has been used to cure advanced tumors including ovarian and small cell lung cancers (Roma-Rodrigues et al., 2019). Topotecan has also been used in a clinical study for the treatment of refractory advanced solid neoplasms expressing HIF-1 α . Additionally, several clinical trials based on intervention against hypoxia are underway, including the evaluation of everolimus, which downregulates HIF-1 α , in combination with lenvatinib in renal cancer (NCT01206764), as well as an evaluation of the metformin outcomes in tissue

oxygenation of head and neck cancer (NCT03510390) (Roma-Rodrigues et al., 2019). The acidified environment has been considered to protect tumor cells from chemotherapy by affecting the concentration of drugs (Kolosenko et al., 2017). Hence, recent clinical trials have focused on alteration of the acidification environment by targeting carbonic anhydrases, a family of enzymes that regulate the pH of active cells/tissues in tumors (Supuran, 2018). For example, the synergistic treatment of acetazolamide, a carbonic anhydrase inhibitor, with radiotherapy has been tested in lung cancer (NCT03467360) while the combination of acetazolamide and temozolomide has also been trialed for brain cancer (NCT03011671).

DISCUSSION

In this review, we have summarized the current insights into how the TME regulates cancer resistance to therapies. The adaptive resistance to cancer treatment driven by the TME may play a vital role in tumor recurrence and metastasis. Therefore, a variety of approaches targeting the TME have been developed to reverse resistance to radiotherapy, chemotherapy, and immunotherapy (Xu et al., 2015; Zhang et al., 2015; Hu et al., 2017; Tan et al., 2018; Bhat et al., 2021). Hijacking the TME to increase drug delivery has also been demonstrated to enhance the efficacy of chemotherapeutic drugs (Fang et al., 2018; Amini et al., 2019). Although a large number of studies have shown the successful application of manipulating the TME to overcome resistance, there are several key questions that still need to be resolved. Firstly, the mechanisms underlying adaptive and non-adaptive resistance need further investigation in a real TME. To date, most of the studies have been based on resistant cells *in vitro*, which excludes the factors in the TME that may be vital for acquired resistance *in vivo*. Co-culture of tumor cells with other types of cells within the TME and tumor-microenvironment-on-a-chip (TMOC) models can only partially mimic the real TME. More studies should be conducted using appropriate mouse models, or the use of human organoids isolated from patient biopsies, to fully understand the role of TME adaptive and non-adaptive resistance (Papapetrou, 2016; Mazzarella and Curigliano, 2018; Vlachogiannis et al., 2018). Secondly, since the TME changes dynamically during the development and treatment of tumors, understanding and monitoring the factors that influence the therapeutic effects of targeting the TME is necessary to improve patient safety and survival outcome. Lastly, some drawbacks of targeting the TME, such as immune-related side-effects, may lead to the cessation of treatment (Liu et al., 2017; García-Aranda and Redondo, 2019). Hopefully, as our understating of intrinsic biology of the TME is improved, we will be more capable of preempting or reversing cancer therapy resistance.

AUTHOR CONTRIBUTIONS

NX, JL, and PW conceptualized the manuscript. PW and WG collected the literature and wrote the manuscript. MS and WZ made the figures. EN made significant revisions to the manuscript. All authors read and approved the final manuscript.

FUNDING

This work was supported by grants from the National Natural Science Foundation of China (81821002, 81790251, 81972665, and 81960423), the National Key Research and Development Project (2020YFA0509400 and 2020YFC2002705), the Guangdong Basic and Applied Basic Research Foundation (2019B030302012), and the Potential Postdoctoral

Program of Chengdu University of Traditional Chinese Medicine (BSH2019019).

ACKNOWLEDGMENTS

We thank the collaborators for their contributions to the publications cited in this review article.

REFERENCES

- Acosta, J. C., Banito, A., Wuestefeld, T., Georgilis, A., Janich, P., Morton, J. P., et al. (2013). A complex secretory program orchestrated by the inflammasome controls paracrine senescence. *Nat. Cell Biol.* 15, 978–990. doi: 10.1038/ncb2784
- Ahmed, K. M., Zhang, H., and Park, C. C. (2013). NF- κ B regulates radioresistance mediated By β 1-Integrin in three-dimensional culture of breast cancer cells. *Cancer Res.* 73, 3737–3748. doi: 10.1158/0008-5472.Can-12-3537
- Allen, E., Miéville, P., Warren, C. M., Saghafinia, S., Li, L., Peng, M. W., et al. (2016). Metabolic symbiosis enables adaptive resistance to anti-angiogenic therapy that is dependent on mTOR signaling. *Cell Rep.* 15, 1144–1160. doi: 10.1016/j.celrep.2016.04.029
- Amini, M. A., Abbasi, A. Z., Cai, P., Lip, H., Gordijo, C. R., Li, J., et al. (2019). Combining tumor microenvironment modulating nanoparticles with doxorubicin to enhance chemotherapeutic efficacy and boost antitumor immunity. *J. Natl. Cancer Inst.* 111, 399–408. doi: 10.1093/jnci/djy131
- Angelin, A., Gil-de-Gómez, L., Dahiya, S., Jiao, J., Guo, L., Levine, M. H., et al. (2017). Foxp3 reprograms T Cell metabolism to function in low-glucose, high-lactate environments. *Cell Metab.* 25, 1282.e7–1293.e7. doi: 10.1016/j.cmet.2016.12.018
- Antognelli, C., Moretti, S., Frosini, R., Puxeddu, E., Sidoni, A., and Talesa, V. N. (2019). Methylglyoxal acts as a tumor-promoting factor in anaplastic thyroid cancer. *Cells* 8:547. doi: 10.3390/cells8060547
- Antognelli, C., and Talesa, V. N. (2018). Glyoxalases in urological malignancies. *Int. J. Mol. Sci.* 19:415. doi: 10.3390/ijms19020415
- Apicella, M., Giannoni, E., Fiore, S., Ferrari, K. J., Fernández-Pérez, D., Isella, C., et al. (2018). Increased lactate secretion by cancer cells sustains non-cell-autonomous adaptive resistance to MET and EGFR targeted therapies. *Cell Metab.* 28, 848.e6–865.e6. doi: 10.1016/j.cmet.2018.08.006
- Ariotti, C., Wagner, V. P., Salvadori, G., Carrard, V. C., Martins, M. A. T., da Cunha Filho, J. J., et al. (2015). VEGFR1 and VEGFR2 in lip carcinogenesis and its association with microvessel density. *Tumor Biol.* 36, 7285–7292.
- Arneth, B. (2019). Tumor microenvironment. *Medicina* 56:15. doi: 10.3390/medicina56010015
- Assaraf, Y. G., Brozovic, A., Gonçalves, A. C., Jurkovicova, D., Linē, A., Machuqueiro, M., et al. (2019). The multi-factorial nature of clinical multidrug resistance in cancer. *Drug Resistance Updates* 46:100645. doi: 10.1016/j.drug.2019.100645
- Aung, T., Chapuy, B., Vogel, D., Wenzel, D., Oppermann, M., Lahmann, M., et al. (2011). Exosomal evasion of humoral immunotherapy in aggressive B-cell lymphoma modulated by ATP-binding cassette transporter A3. *Proc. Natl. Acad. Sci. U.S.A.* 108, 15336–15341.
- Aydin, E., Johansson, J., Nazir, F. H., Hellstrand, K., and Martner, A. (2017). Role of NOX2-derived reactive oxygen species in NK cell-mediated control of murine melanoma metastasis. *Cancer Immunol. Res.* 5, 804–811. doi: 10.1158/2326-6066.Cir-16-0382
- Balkwill, F. R., Capasso, M., and Hagemann, T. (2012). The tumor microenvironment at a glance. *J. Cell Sci.* 125(Pt 23), 5591–5596. doi: 10.1242/jcs.116392
- Barnes, E. M. E., Xu, Y., Benito, A., Herendi, L., Siskos, A. P., Aboagye, E. O., et al. (2020). Lactic acidosis induces resistance to the pan-Akt inhibitor uprosertib in colon cancer cells. *Br. J. Cancer* 122, 1298–1308. doi: 10.1038/s41416-020-0777-y
- Baumann, T., Dunkel, A., Schmid, C., Schmitt, S., Hiltensperger, M., Lohr, K., et al. (2020). Regulatory myeloid cells paralyze T cells through cell-cell transfer of the metabolite methylglyoxal. *Nat. Immunol.* 21, 555–566. doi: 10.1038/s41590-020-0666-9
- Belli, C., Trapani, D., Viale, G., D'Amico, P., Duso, B. A., Della Vigna, P., et al. (2018). Targeting the microenvironment in solid tumors. *Cancer Treat. Rev.* 65, 22–32. doi: 10.1016/j.ctrv.2018.02.004
- Bendle, G. M., Linnemann, C., Bies, L., Song, J. Y., and Schumacher, T. N. (2013). Blockade of TGF- β signaling greatly enhances the efficacy of TCR gene therapy of cancer. *J. Immunol.* 191, 3232–3239. doi: 10.4049/jimmunol.1301270
- Benjamin, L. E., Golijanin, D., Itin, A., Podes, D., and Keshet, E. (1999). Selective ablation of immature blood vessels in established human tumors follows vascular endothelial growth factor withdrawal. *J. Clin. Invest.* 103, 159–165.
- Bhat, A. A., Yousuf, P., Wani, N. A., Rizwan, A., Chauhan, S. S., Siddiqi, M. A., et al. (2021). Tumor microenvironment: an evil nexus promoting aggressive head and neck squamous cell carcinoma and avenue for targeted therapy. *Signal Transduct. Target. Ther.* 6:12. doi: 10.1038/s41392-020-00419-w
- Billotet, C., Tuefferd, M., Gentien, D., Rapinat, A., Thiery, J. P., Bröet, P., et al. (2008). Modulation of several waves of gene expression during FGF-1 induced epithelial-mesenchymal transition of carcinoma cells. *J. Cell Biochem.* 104, 826–839. doi: 10.1002/jcb.21667
- Boelens, M. C., Wu, T. J., Nabat, B. Y., Xu, B., Qiu, Y., Yoon, T., et al. (2014). Exosome transfer from stromal to breast cancer cells regulates therapy resistance pathways. *Cell* 159, 499–513.
- Boohaker, R. J., Sambandam, V., Segura, I., Miller, J., Suto, M., and Xu, B. (2018). Rational design and development of a peptide inhibitor for the PD-1/PD-L1 interaction. *Cancer Lett.* 434, 11–21. doi: 10.1016/j.canlet.2018.04.031
- Brand, A., Singer, K., Koehl, G. E., Kolitzus, M., Schoenhammer, G., Thiel, A., et al. (2016). LDHA-associated lactic acid production blunts tumor immunosurveillance by T and NK cells. *Cell Metab.* 24, 657–671. doi: 10.1016/j.cmet.2016.08.011
- Brown, J. M., and Wilson, W. R. (2004). Exploiting tumour hypoxia in cancer treatment. *Nat. Rev. Cancer* 4, 437–447. doi: 10.1038/nrc1367
- Brunen, D., Willems, S., Kellner, U., Midgley, R., Simon, I., and Bernards, R. (2013). TGF- β : an emerging player in drug resistance. *Cell Cycle* 12, 2960–2968. doi: 10.4161/cc.26034
- Bussink, J., Kaanders, J. H., and van der Kogel, A. J. (2003). Tumor hypoxia at the micro-regional level: clinical relevance and predictive value of exogenous and endogenous hypoxic cell markers. *Radiother. Oncol.* 67, 3–15.
- Calvo, F., Ege, N., Grande-Garcia, A., Hooper, S., Jenkins, R. P., Chaudhry, S. I., et al. (2013). Mechanotransduction and YAP-dependent matrix remodelling is required for the generation and maintenance of cancer-associated fibroblasts. *Nat. Cell Biol.* 15, 637–646. doi: 10.1038/ncb2756
- Cao, Q., Cai, W., Li, T., Yang, Y., Chen, K., Xing, L., et al. (2006). Combination of integrin siRNA and irradiation for breast cancer therapy. *Biochem. Biophys. Res. Commun.* 351, 726–732. doi: 10.1016/j.bbrc.2006.10.100
- Cao, Y., Wang, X., Jin, T., Tian, Y., Dai, C., Widarma, C., et al. (2020). Immune checkpoint molecules in natural killer cells as potential targets for cancer immunotherapy. *Signal Transduct. Target. Ther.* 5:250. doi: 10.1038/s41392-020-00348-8
- Carmeliet, P., and Jain, R. K. (2000). Angiogenesis in cancer and other diseases. *Nature* 407, 249–257. doi: 10.1038/35025220
- Cassim, S., and Pouyssegur, J. (2019). Tumor microenvironment: a metabolic player that shapes the immune response. *Int. J. Mol. Sci.* 21:157. doi: 10.3390/ijms21010157
- Cazet, A. S., Hui, M. N., Elsworth, B. L., Wu, S. Z., Roden, D., Chan, C. L., et al. (2018). Targeting stromal remodeling and cancer stem cell plasticity overcomes

- chemoresistance in triple negative breast cancer. *Nat. Commun.* 9:2897. doi: 10.1038/s41467-018-05220-6
- Cervantes-Villagrana, R. D., Albores-García, D., Cervantes-Villagrana, A. R., and García-Acevez, S. J. (2020). Tumor-induced neurogenesis and immune evasion as targets of innovative anti-cancer therapies. *Signal Transduct. Target. Ther.* 5:99. doi: 10.1038/s41392-020-0205-z
- Chakravarthy, A., Khan, L., Bensler, N. P., Bose, P., and De Carvalho, D. D. (2018). TGF- β -associated extracellular matrix genes link cancer-associated fibroblasts to immune evasion and immunotherapy failure. *Nat. Commun.* 9, 1–10.
- Chan, T. S., Hsu, C. C., Pai, V. C., Liao, W. Y., Huang, S. S., Tan, K. T., et al. (2016). Metronomic chemotherapy prevents therapy-induced stromal activation and induction of tumor-initiating cells. *J. Exp. Med.* 213, 2967–2988. doi: 10.1084/jem.20151665
- Chang, C. H., Qiu, J., O'Sullivan, D., Buck, M. D., Noguchi, T., Curtis, J. D., et al. (2015). Metabolic competition in the tumor microenvironment is a driver of cancer progression. *Cell* 162, 1229–1241. doi: 10.1016/j.cell.2015.08.016
- Che, Y., Wang, J., Li, Y., Lu, Z., Huang, J., Sun, S., et al. (2018). Cisplatin-activated PAI-1 secretion in the cancer-associated fibroblasts with paracrine effects promoting esophageal squamous cell carcinoma progression and causing chemoresistance. *Cell Death Dis.* 9, 1–13.
- Chen, F., Zhuang, X., Lin, L., Yu, P., Wang, Y., Shi, Y., et al. (2015). New horizons in tumor microenvironment biology: challenges and opportunities. *BMC Med.* 13:45. doi: 10.1186/s12916-015-0278-7
- Chen, W. L., Wang, C. C., Lin, Y. J., Wu, C. P., and Hsieh, C. H. (2015). Cycling hypoxia induces chemoresistance through the activation of reactive oxygen species-mediated B-cell lymphoma extra-long pathway in glioblastoma multiforme. *J. Transl. Med.* 13:389. doi: 10.1186/s12967-015-0758-8
- Chen, S., and Sang, N. (2016). Hypoxia-inducible factor-1: a critical player in the survival strategy of stressed cells. *J. Cell Biochem.* 117, 267–278. doi: 10.1002/jcb.25283
- Chen, S.-H., and Chang, J.-Y. (2019). New insights into mechanisms of cisplatin resistance: from tumor cell to microenvironment. *Int. J. Mol. Sci.* 20:4136. doi: 10.3390/ijms20174136
- Chen, T., Li, Q., Liu, Z., Chen, Y., Feng, F., and Sun, H. (2019). Peptide-based and small synthetic molecule inhibitors on PD-1/PD-L1 pathway: a new choice for immunotherapy? *Eur. J. Med. Chem.* 161, 378–398. doi: 10.1016/j.ejmech.2018.10.044
- Chen, Y., Liu, X., Yuan, H., Yang, Z., von Roemeling, C. A., Qie, Y., et al. (2019). Therapeutic remodeling of the tumor microenvironment enhances nanoparticle delivery. *Adv. Sci.* 6:1802070.
- Chen, X., Wang, L., Li, P., Song, M., Qin, G., Gao, Q., et al. (2018). Dual TGF- β and PD-1 blockade synergistically enhances MAGE-A3-specific CD8(+) T cell response in esophageal squamous cell carcinoma. *Int. J. Cancer* 143, 2561–2574. doi: 10.1002/ijc.31730
- Cheng, P., Levesque, M. P., Dummer, R., and Mangana, J. (2020). Targeting complex, adaptive responses in melanoma therapy. *Cancer Treatm. Rev.* 86:101997. doi: 10.1016/j.ctrv.2020.101997
- Cheteh, E. H., Augsten, M., Rundqvist, H., Bianchi, J., Sarne, V., Egevad, L., et al. (2017). Human cancer-associated fibroblasts enhance glutathione levels and antagonize drug-induced prostate cancer cell death. *Cell Death Dis.* 8:e2848. doi: 10.1038/cddis.2017.225
- Chiappinelli, K. B., Zahnow, C. A., Ahuja, N., and Baylin, S. B. (2016). Combining epigenetic and immunotherapy to combat cancer. *Cancer Res.* 76, 1683–1689. doi: 10.1158/0008-5472.Can-15-2125
- Colak, S., and ten Dijke, P. (2017). Targeting TGF- β signaling in cancer. *Trends Cancer* 3, 56–71.
- Corcoran, C., Rani, S., O'Brien, K., O'Neill, A., Principe, M., Sheikh, R., et al. (2012). Docetaxel-resistance in prostate cancer: evaluating associated phenotypic changes and potential for resistance transfer via exosomes. *PLoS One* 7:e50999. doi: 10.1371/journal.pone.0050999
- Corrado, C., Raimondo, S., Chiesi, A., Ciccia, F., De Leo, G., and Alessandro, R. (2013). Exosomes as intercellular signaling organelles involved in health and disease: basic science and clinical applications. *Int. J. Mol. Sci.* 14, 5338–5366. doi: 10.3390/ijms14035338
- Correia, A. L., and Bissell, M. J. (2012). The tumor microenvironment is a dominant force in multidrug resistance. *Drug Resist. Updat* 15, 39–49. doi: 10.1016/j.drug.2012.01.006
- Cowan, D. S., and Tannock, I. F. (2001). Factors that influence the penetration of methotrexate through solid tissue. *Int. J. Cancer* 91, 120–125.
- Crow, J., Atay, S., Banskota, S., Artale, B., Schmitt, S., and Godwin, A. K. (2017). Exosomes as mediators of platinum resistance in ovarian cancer. *Oncotarget* 8:11917.
- Cruz da Silva, E., Dontenwill, M., Choulier, L., and Lehmann, M. (2019). Role of integrins in resistance to therapies targeting growth factor receptors in cancer. *Cancers* 11:692.
- Dai, J., Su, Y., Zhong, S., Cong, L., Liu, B., Yang, J., et al. (2020). Exosomes: key players in cancer and potential therapeutic strategy. *Signal Transduct. Target. Ther.* 5:145. doi: 10.1038/s41392-020-00261-0
- Dang, C. V., and Semenza, G. L. (1999). Oncogenic alterations of metabolism. *Trends Biochem. Sci.* 24, 68–72.
- Darvin, P., Toor, S. M., Sasidharan Nair, V., and Elkord, E. (2018). Immune checkpoint inhibitors: recent progress and potential biomarkers. *Exp. Mol. Med.* 50, 1–11. doi: 10.1038/s12276-018-0191-1
- Dauer, P., Zhao, X., Gupta, V. K., Sharma, N., Kesh, K., Gnamlin, P., et al. (2018). Inactivation of cancer-associated-fibroblasts disrupts oncogenic signaling in pancreatic cancer cells and promotes its regression. *Cancer Res.* 78, 1321–1333. doi: 10.1158/0008-5472.Can-17-2320
- Denkert, C., Loibl, S., Noske, A., Roller, M., Muller, B., Komor, M., et al. (2010). Tumor-associated lymphocytes as an independent predictor of response to neoadjuvant chemotherapy in breast cancer. *J. Clin. Oncol.* 28, 105–113.
- DeRita, R. M., Sayeed, A., Garcia, V., Krishn, S. R., Shields, C. D., Sarker, S., et al. (2019). Tumor-derived extracellular vesicles require $\alpha_5\beta_1$ integrins to promote anchorage-independent growth. *iScience* 14, 199–209. doi: 10.1016/j.isci.2019.03.022
- Dhorepatil, A., Ball, S., Ghosh, R. K., Kondapaneni, M., and Lavie, C. J. (2019). Canakinumab: promises and future in cardiometabolic diseases and malignancy. *Am. J. Med.* 132, 312–324.
- Díaz-Valdés, N., Basagoiti, M., Dotor, J., Aranda, F., Monreal, I., Riezu-Boj, J. I., et al. (2011). Induction of monocyte chemoattractant protein-1 and interleukin-10 by TGF β 1 in melanoma enhances tumor infiltration and immunosuppression. *Cancer Res.* 71, 812–821. doi: 10.1158/0008-5472.Can-10-2698
- Dorayappan, K. D. P., Wanner, R., Wallbillich, J. J., Saini, U., Zingarelli, R., Suarez, A. A., et al. (2018). Hypoxia-induced exosomes contribute to a more aggressive and chemoresistant ovarian cancer phenotype: a novel mechanism linking STAT3/Rab proteins. *Oncogene* 37, 3806–3821. doi: 10.1038/s41388-018-0189-0
- Du, B., and Shim, J. S. (2016). Targeting epithelial-mesenchymal transition (EMT) to overcome drug resistance in cancer. *Molecules* 21:965. doi: 10.3390/molecules21070965
- Durand, R. E. (2001). Intermittent blood flow in solid tumours—an under-appreciated source of 'drug resistance'. *Cancer Metastasis Rev.* 20, 57–61.
- Eisele, G., Wick, A., Eisele, A.-C., Clément, P. M., Tonn, J., Tabatabai, G., et al. (2014). Cilengitide treatment of newly diagnosed glioblastoma patients does not alter patterns of progression. *J. Neuro Oncol.* 117, 141–145. doi: 10.1007/s11060-014-1365-x
- Eke, I., and Cordes, N. (2015). Focal adhesion signaling and therapy resistance in cancer. *Semin. Cancer Biol.* 31, 65–75. doi: 10.1016/j.semcancer.2014.07.009
- Fang, J., Zhang, S., Xue, X., Zhu, X., Song, S., Wang, B., et al. (2018). Quercetin and doxorubicin co-delivery using mesoporous silica nanoparticles enhance the efficacy of gastric carcinoma chemotherapy. *Int. J. Nanomed.* 13, 5113–5126. doi: 10.2147/ijn.S170862
- Feichtinger, R. G., and Lang, R. (2019). Targeting L-Lactate metabolism to overcome resistance to immune therapy of melanoma and other tumor entities. *J. Oncol.* 2019:2084195. doi: 10.1155/2019/2084195
- Ferlay, J., Colombet, M., Soerjomataram, I., Mathers, C., Parkin, D. M., Piñeros, M., et al. (2019). Estimating the global cancer incidence and mortality in 2018: GLOBOCAN sources and methods. *Int. J. Cancer* 144, 1941–1953. doi: 10.1002/ijc.31937
- Fiori, M. E., Di Franco, S., Villanova, L., Bianca, P., Stassi, G., and De Maria, R. (2019). Cancer-associated fibroblasts as abettors of tumor progression at the crossroads of EMT and therapy resistance. *Mol. Cancer* 18:70. doi: 10.1186/s12943-019-0994-2

- Fiori, M. E., Villanova, L., and De Maria, R. (2017). Cancer stem cells: at the forefront of personalized medicine and immunotherapy. *Curr. Opin. Pharmacol.* 35, 1–11. doi: 10.1016/j.coph.2017.04.006
- Flaherty, K. T., Manola, J. B., Pins, M., McDermott, D. F., Atkins, M. B., Dutcher, J. J., et al. (2015). BEST: a randomized phase II study of vascular endothelial growth factor, RAF kinase, and mammalian target of rapamycin combination targeted therapy with bevacizumab, sorafenib, and temsirolimus in advanced renal cell carcinoma—A trial of the ECOG-ACRIN Cancer Research Group (E2804). *J. Clin. Oncol.* 33:2384.
- Fletcher, M., Ramirez, M. E., Sierra, R. A., Raber, P., Thevenot, P., Al-Khami, A. A., et al. (2015). L-Arginine depletion blunts antitumor T-cell responses by inducing myeloid-derived suppressor cells. *Cancer Res.* 75, 275–283. doi: 10.1158/0008-5472.Can-14-1491
- Freund, A., Orjalo, A. V., Desprez, P. Y., and Campisi, J. (2010). Inflammatory networks during cellular senescence: causes and consequences. *Trends Mol. Med.* 16, 238–246. doi: 10.1016/j.molmed.2010.03.003
- Fu, H., Yang, H., Zhang, X., and Xu, W. (2016). The emerging roles of exosomes in tumor-stroma interaction. *J. Cancer Res. Clin. Oncol.* 142, 1897–1907. doi: 10.1007/s00432-016-2145-0
- Fujita, M., Sasada, M., Iyoda, T., and Fukai, F. (2020). Involvement of integrin-activating peptides derived from tenascin-c in cancer aggression and new anticancer strategy using the fibronectin-derived integrin-inactivating peptide. *Molecules* 25:3239. doi: 10.3390/molecules25143239
- Gabrilovich, D. I., Ostrand-Rosenberg, S., and Bronte, V. (2012). Coordinated regulation of myeloid cells by tumours. *Nat. Rev. Immunol.* 12, 253–268. doi: 10.1038/nri3175
- Galmarini, F. C., Galmarini, C. M., Sarchi, M. I., Abulafia, J., and Galmarini, D. (2000). Heterogeneous distribution of tumor blood supply affects the response to chemotherapy in patients with head and neck cancer. *Microcirculation* 7, 405–410.
- Gamrad, P., De La Fouchardière, C., and Hennino, A. (2021). Stromal protein-mediated immune regulation in digestive cancers. *Cancers* 13:146. doi: 10.3390/cancers13010146
- Gandhi, L., Rodríguez-Abreu, D., Gadgeel, S., Esteban, E., Felip, E., De Angelis, F., et al. (2018). Pembrolizumab plus chemotherapy in metastatic non-small-cell lung cancer. *N. Engl. J. Med.* 378, 2078–2092.
- García-Aranda, M., and Redondo, M. (2019). Immunotherapy: a challenge of breast cancer treatment. *Cancers* 11:1822.
- García-Cañaveras, J. C., Chen, L., and Rabinowitz, J. D. (2019). The tumor metabolic microenvironment: lessons from lactate. *Cancer Res.* 79, 3155–3162. doi: 10.1158/0008-5472.Can-18-3726
- Gargiulo, E., Paggetti, J., and Moussay, E. (2019). Hematological malignancy-derived small extracellular vesicles and tumor microenvironment: the art of turning foes into friends. *Cells* 8:511.
- Gerweck, L. E., Vijayappa, S., and Kozin, S. (2006). Tumor pH controls the in vivo efficacy of weak acid and base chemotherapeutics. *Mol. Cancer Ther.* 5, 1275–1279. doi: 10.1158/1535-7163.Mct-06-0024
- Gillies, R. J., Schomack, P. A., Secomb, T. W., and Raghunand, N. (1999). Causes and effects of heterogeneous perfusion in tumors. *Neoplasia* 1, 197–207.
- Goel, H. L., Sayeed, A., Breen, M., Zarif, M. J., Garlick, D. S., Leav, I., et al. (2013). β 1 integrins mediate resistance to ionizing radiation in vivo by inhibiting c-Jun amino terminal kinase 1. *J. Cell. Physiol.* 228, 1601–1609. doi: 10.1002/jcp.24323
- Gomez, S., Tabernacki, T., Kobrya, J., Roberts, P., and Chiappinelli, K. B. (2020). Combining epigenetic and immune therapy to overcome cancer resistance. *Semin. Cancer Biol.* 65, 99–113. doi: 10.1016/j.semcancer.2019.12.019
- Gordon-Weeks, A., and Yuzhalin, A. E. (2020). Cancer extracellular matrix proteins regulate tumour immunity. *Cancers* 12:3331. doi: 10.3390/cancers12113331
- Gray, M. D., Mann, M., Nitiss, J. L., and Hendershot, L. M. (2005). Activation of the unfolded protein response is necessary and sufficient for reducing topoisomerase II α protein levels and decreasing sensitivity to topoisomerase-targeted drugs. *Mol. Pharmacol.* 68, 1699–1707. doi: 10.1124/mol.105.014753
- Grivennikov, S. I., Greten, F. R., and Karin, M. (2010). Immunity, inflammation, and cancer. *Cell* 140, 883–899. doi: 10.1016/j.cell.2010.01.025
- Guillaumond, F., Bidaut, G., Ouassii, M., Servais, S., Gouirand, V., Olivares, O., et al. (2015). Cholesterol uptake disruption, in association with chemotherapy, is a promising combined metabolic therapy for pancreatic adenocarcinoma. *Proc. Natl. Acad. Sci. U.S.A.* 112, 2473–2478. doi: 10.1073/pnas.1421601112
- Guri, Y., and Hall, M. N. (2016). mTOR signaling confers resistance to targeted cancer drugs. *Trends Cancer* 2, 688–697. doi: 10.1016/j.trecan.2016.10.006
- Halama, N., Michel, S., Kloor, M., Zoernig, I., Benner, A., Spille, A., et al. (2011). Localization and density of immune cells in the invasive margin of human colorectal cancer liver metastases are prognostic for response to chemotherapy. *Cancer Res.* 71, 5670–5677.
- Hanahan, D. (2014). Rethinking the war on cancer. *Lancet* 383, 558–563. doi: 10.1016/s0140-6736(13)62226-6
- Hanahan, D., and Coussens, L. M. (2012). Accessories to the crime: functions of cells recruited to the tumor microenvironment. *Cancer Cell* 21, 309–322. doi: 10.1016/j.ccr.2012.02.022
- Hanahan, D., and Weinberg, R. A. (2011). Hallmarks of cancer: the next generation. *Cell* 144, 646–674. doi: 10.1016/j.cell.2011.02.013
- Hashizume, H., Baluk, P., Morikawa, S., McLean, J. W., Thurston, G., Roberge, S., et al. (2000). Openings between defective endothelial cells explain tumor vessel leakiness. *Am. J. Pathol.* 156, 1363–1380.
- He, J.-M., Wang, F.-C., Qi, H.-B., Li, Y., and Liang, H.-J. (2009). Down-regulation of α v integrin by retroviral delivery of small interfering RNA reduces multicellular resistance of HT29. *Cancer Lett.* 284, 182–188. doi: 10.1016/j.canlet.2009.04.023
- Hegde, P. S., Jubb, A. M., Chen, D., Li, N. F., Meng, Y. G., Bernaards, C., et al. (2013). Predictive impact of circulating vascular endothelial growth factor in four phase III trials evaluating bevacizumab. *Clin. Cancer Res.* 19, 929–937.
- Heldin, C.-H., Rubin, K., Pietras, K., and Östman, A. (2004). High interstitial fluid pressure—an obstacle in cancer therapy. *Nat. Rev. Cancer* 4, 806–813.
- Hirata, E., and Sahai, E. (2017). Tumor microenvironment and differential responses to therapy. *Cold Spring Harbor Perspect. Med.* 7:a026781. doi: 10.1101/cshperspect.a026781
- Ho, P. C., Bihuniak, J. D., Macintyre, A. N., Staron, M., Liu, X., Amezcua, R., et al. (2015). phosphoenolpyruvate is a metabolic checkpoint of anti-tumor T Cell responses. *Cell* 162, 1217–1228. doi: 10.1016/j.cell.2015.08.012
- Holle, A. W., Young, J. L., and Spatz, J. P. (2016). In vitro cancer cell-ECM interactions inform in vivo cancer treatment. *Adv. Drug Deliv. Rev.* 97, 270–279.
- Holohan, C., Van Schaeybroeck, S., Longley, D. B., and Johnston, P. G. (2013). Cancer drug resistance: an evolving paradigm. *Nat. Rev. Cancer* 13, 714–726. doi: 10.1038/nrc3599
- Horvat, T. Z., Adel, N. G., Dang, T.-O., Momtaz, P., Postow, M. A., Callahan, M. K., et al. (2015). Immune-related adverse events, need for systemic immunosuppression, and effects on survival and time to treatment failure in patients with melanoma treated with ipilimumab at memorial sloan kettering cancer center. *J. Clin. Oncol.* 33, 3193–3198. doi: 10.1200/JCO.2015.60.8448
- Houriet, C., Jafari, S. M. S., Thomi, R., Schlapbach, C., Borradori, L., Yawalkar, N., et al. (2017). Canakinumab for severe hidradenitis suppurativa: preliminary experience in 2 cases. *JAMA Dermatol.* 153, 1195–1197.
- Housman, G., Byler, S., Heerboth, S., Lapinska, K., Longacre, M., Snyder, N., et al. (2014). Drug resistance in cancer: an overview. *Cancers* 6, 1769–1792. doi: 10.3390/cancers6031769
- Hsieh, Y.-T., Gang, E. J., Geng, H., Park, E., Huantes, S., Chudziak, D., et al. (2013). Integrin α 4 blockade sensitizes drug resistant pre-B acute lymphoblastic leukemia to chemotherapy. *Blood* 121, 1814–1818. doi: 10.1182/blood-2012-01-406272
- Hu, K., Miao, L., Goodwin, T. J., Li, J., Liu, Q., and Huang, L. (2017). Quercetin remodels the tumor microenvironment to improve the permeation, retention, and antitumor effects of nanoparticles. *ACS Nano* 11, 4916–4925. doi: 10.1021/acsnano.7b01522
- Hu, P.-S., Li, T., Lin, J.-F., Qiu, M.-Z., Wang, D.-S., Liu, Z.-X., et al. (2020). VDR-SOX2 signaling promotes colorectal cancer stemness and malignancy in an acidic microenvironment. *Signal Transduct. Target. Ther.* 5:183. doi: 10.1038/s41392-020-00230-7
- Huang, C. Y., Kuo, W. T., Huang, Y. C., Lee, T. C., and Yu, L. C. (2013). Resistance to hypoxia-induced necroptosis is conferred by glycolytic pyruvate scavenging of mitochondrial superoxide in colorectal cancer cells. *Cell Death Dis.* 4:e622. doi: 10.1038/cddis.2013.149

- Hugo, W., Zaretsky, J. M., Sun, L., Song, C., Moreno, B. H., Hu-Lieskovan, S., et al. (2016). Genomic and transcriptomic features of response to Anti-PD-1 therapy in metastatic melanoma. *Cell* 165, 35–44. doi: 10.1016/j.cell.2016.02.065
- Hui, L., and Chen, Y. (2015). Tumor microenvironment: sanctuary of the devil. *Cancer Lett.* 368, 7–13. doi: 10.1016/j.canlet.2015.07.039
- Husain, Z., Huang, Y., Seth, P., and Sukhatme, V. P. (2013). Tumor-derived lactate modifies antitumor immune response: effect on myeloid-derived suppressor cells and NK cells. *J. Immunol.* 191, 1486–1495. doi: 10.4049/jimmunol.1202702
- Incio, J., Liu, H., Suboj, P., Chin, S. M., Chen, I. X., Pinter, M., et al. (2016). Obesity-induced inflammation and desmoplasia promote pancreatic cancer progression and resistance to chemotherapy. *Cancer Discov.* 6, 852–869. doi: 10.1158/2159-8290.Cd-15-1177
- Ishii, N., Araki, K., Yokobori, T., Hagiwara, K., Gantumur, D., Yamanaka, T., et al. (2019). Conophylline suppresses pancreatic cancer desmoplasia and cancer-promoting cytokines produced by cancer-associated fibroblasts. *Cancer Sci.* 110, 334–344. doi: 10.1111/cas.13847
- Itoh, G., Chida, S., Yanagihara, K., Yashiro, M., Aiba, N., and Tanaka, M. (2017). Cancer-associated fibroblasts induce cancer cell apoptosis that regulates invasion mode of tumours. *Oncogene* 36, 4434–4444. doi: 10.1038/ncr.2017.49
- Jackaman, C., Majewski, D., Fox, S. A., Nowak, A. K., and Nelson, D. J. (2012). Chemotherapy broadens the range of tumor antigens seen by cytotoxic CD8(+) T cells in vivo. *Cancer Immunol. Immunother.* 61, 2343–2356. doi: 10.1007/s00262-012-1307-4
- Jain, R. K. (1988). Determinants of tumor blood flow: a review. *Cancer Res.* 48, 2641–2658.
- Jeppesen, D. K., Nawrocki, A., Jensen, S. G., Thorsen, K., Whitehead, B., Howard, K. A., et al. (2014). Quantitative proteomics of fractionated membrane and lumen exosome proteins from isogenic metastatic and nonmetastatic bladder cancer cells reveal differential expression of EMT factors. *Proteomics* 14, 699–712.
- Jiang, L., Wang, Y.-J., Zhao, J., Uehara, M., Hou, Q., Kasinath, V., et al. (2020). Direct tumor killing and immunotherapy through Anti-SerpB9 therapy. *Cell* 183, 1219.e18–1233.e18. doi: 10.1016/j.cell.2020.10.045
- Jiang, W., Xia, J., Xie, S., Zou, R., Pan, S., Wang, Z.-W., et al. (2020). Long non-coding RNAs as a determinant of cancer drug resistance: towards the overcoming of chemoresistance via modulation of lncRNAs. *Drug Resistance Updates* 50:100683. doi: 10.1016/j.drug.2020.100683
- Jiang, Z., Hsu, J. L., Li, Y., Hortobagyi, G. N., and Hung, M.-C. (2020). Cancer cell metabolism bolsters immunotherapy resistance by promoting an immunosuppressive tumor microenvironment. *Front. Oncol.* 10:1197. doi: 10.3389/fonc.2020.01197
- Jin, M. Z., and Jin, W. L. (2020). The updated landscape of tumor microenvironment and drug repurposing. *Signal Transduct. Target. Ther.* 5:166. doi: 10.1038/s41392-020-00280-x
- Jinushi, M., Chiba, S., Yoshiyama, H., Masutomi, K., Kinoshita, I., Dosaka-Akita, H., et al. (2011). Tumor-associated macrophages regulate tumorigenicity and anticancer drug responses of cancer stem/initiating cells. *Proc. Natl. Acad. Sci. U.S.A.* 108, 12425–12430. doi: 10.1073/pnas.1106645108
- Jo, Y., Choi, N., Kim, K., Koo, H. J., Choi, J., and Kim, H. N. (2018). Chemoresistance of cancer cells: requirements of tumor microenvironment-mimicking in vitro models in anti-cancer drug development. *Theranostics* 8, 5259–5275. doi: 10.7150/thno.29098
- Joyce, J. A. (2005). Therapeutic targeting of the tumor microenvironment. *Cancer Cell* 7, 513–520. doi: 10.1016/j.ccr.2005.05.024
- Kalluri, R., and Zeisberg, M. (2006). Fibroblasts in cancer. *Nat. Rev. Cancer* 6, 392–401. doi: 10.1038/nrc1877
- Kamphorst, J. J., Cross, J. R., Fan, J., de Stanchina, E., Mathew, R., White, E. P., et al. (2013). Hypoxic and Ras-transformed cells support growth by scavenging unsaturated fatty acids from lysophospholipids. *Proc. Natl. Acad. Sci. U.S.A.* 110, 8882–8887. doi: 10.1073/pnas.1307237110
- Kanazawa, Y., Yamada, T., Fujita, I., Kakinuma, D., Matsuno, K., Arai, H., et al. (2017). In vitro chemosensitivity test for gastric cancer specimens predicts effectiveness of oxaliplatin and 5-fluorouracil. *Anticancer Res.* 37, 6401–6405.
- Kang, I., Harten, I. A., Chang, M. Y., Braun, K. R., Sheih, A., Nivison, M. P., et al. (2017). Versican deficiency significantly reduces lung inflammatory response induced by polyinosine-polycytidylic acid stimulation. *J. Biol. Chem.* 292, 51–63. doi: 10.1074/jbc.M116.753186
- Kechagia, J. Z., Ivaska, J., and Roca-Cusachs, P. (2019). Integrins as biomechanical sensors of the microenvironment. *Nat. Rev. Mol. Cell Biol.* 20, 457–473.
- Kesh, K., Gupta, V. K., Durden, B., Garrido, V., Mateo-Victoriano, B., Lavania, S. P., et al. (2020). Therapy resistance, cancer stem cells and ECM in cancer: the matrix reloaded. *Cancers* 12:3067. doi: 10.3390/cancers12103067
- Kim, B. H., Yi, E. H., and Ye, S. K. (2016). Signal transducer and activator of transcription 3 as a therapeutic target for cancer and the tumor microenvironment. *Arch. Pharm. Res.* 39, 1085–1099. doi: 10.1007/s12272-016-0795-8
- Kim, K., Skora, A. D., Li, Z., Liu, Q., Tam, A. J., Blosser, R. L., et al. (2014). Eradication of metastatic mouse cancers resistant to immune checkpoint blockade by suppression of myeloid-derived cells. *Proc. Natl. Acad. Sci. U.S.A.* 111, 11774–11779. doi: 10.1073/pnas.1410626111
- Kim, S. H., Roszik, J., Grimm, E. A., and Ekmekcioglu, S. (2018). Impact of L-Arginine metabolism on immune response and anticancer immunotherapy. *Front. Oncol.* 8:67. doi: 10.3389/fonc.2018.00067
- Kinoshita, M., Johnson, D. L., Shatney, C. H., Lee, Y. L., and Mochizuki, H. (2001). Cancer cells surviving hypoxia obtain hypoxia resistance and maintain anti-apoptotic potential under reoxygenation. *Int. J. Cancer* 91, 322–326.
- Kitange, G. J., Carlson, B. L., Schroeder, M. A., Grogan, P. T., Lamont, J. D., Decker, P. A., et al. (2009). Induction of MGMT expression is associated with temozolomide resistance in glioblastoma xenografts. *Neuro Oncol.* 11, 281–291. doi: 10.1215/15228517-2008-090
- Klemm, F., and Joyce, J. A. (2015). Microenvironmental regulation of therapeutic response in cancer. *Trends Cell Biol.* 25, 198–213.
- Kojima, Y., Acar, A., Eaton, E. N., Melody, K. T., Scheel, C., Ben-Porath, I., et al. (2010). Autocrine TGF- β and stromal cell-derived factor-1 (SDF-1) signaling drives the evolution of tumor-promoting mammary stromal myofibroblasts. *Proc. Natl. Acad. Sci.* 107, 20009–20014.
- Kolosenko, I., Avnet, S., Baldini, N., Viklund, J., and De Milito, A. (2017). Therapeutic implications of tumor interstitial acidification. *Semin. Cancer Biol.* 43, 119–133. doi: 10.1016/j.semcancer.2017.01.008
- Korneev, K. V., Atretkhany, K.-S. N., Drutska, M. S., Grivennikov, S. I., Kuprash, D. V., and Nedospasov, S. A. (2017). TLR-signaling and proinflammatory cytokines as drivers of tumorigenesis. *Cytokine* 89, 127–135.
- Kovacic, P., and Osuna, J. A. Jr. (2000). Mechanisms of anti-cancer agents: emphasis on oxidative stress and electron transfer. *Curr. Pharm. Des.* 6, 277–309. doi: 10.2174/1381612003401046
- Koyama, S., Akbay, E. A., Li, Y. Y., Herter-Sprie, G. S., Buczkowski, K. A., Richards, W. G., et al. (2016). Adaptive resistance to therapeutic PD-1 blockade is associated with upregulation of alternative immune checkpoints. *Nat. Commun.* 7, 1–9.
- Krakstad, C., and Chekenya, M. (2010). Survival signalling and apoptosis resistance in glioblastomas: opportunities for targeted therapeutics. *Mol. Cancer* 9:135. doi: 10.1186/1476-4598-9-135
- Laoui, D., Keirsse, J., Morias, Y., Van Overmeire, E., Geeraerts, X., Elkrim, Y., et al. (2016). The tumour microenvironment harbours ontogenically distinct dendritic cell populations with opposing effects on tumour immunity. *Nat. Commun.* 7:13720. doi: 10.1038/ncomms13720
- Larkin, J., Chiarion-Sileni, V., Gonzalez, R., Grob, J. J., Cowey, C. L., Lao, C. D., et al. (2015). Combined nivolumab and ipilimumab or monotherapy in untreated melanoma. *N. Engl. J. Med.* 373, 23–34. doi: 10.1056/NEJMoa1504030
- Layani-Bazar, A., Skornick, I., Berrebi, A., Pauker, M. H., Noy, E., Silberman, A., et al. (2014). Redox modulation of adjacent thiols in VLA-4 by AS101 converts myeloid leukemia cells from a drug-resistant to drug-sensitive state. *Cancer Res.* 74, 3092–3103. doi: 10.1158/0008-5472.Can-13-2159
- Lee, C.-T., Boss, M.-K., and Dewhirst, M. W. (2014). Imaging tumor hypoxia to advance radiation oncology. *Antioxidants Redox Signal.* 21, 313–337.
- Lee, J. G., and Wu, R. (2015). Erlotinib-cisplatin combination inhibits growth and angiogenesis through c-MYC and HIF-1 α in EGFR-mutated lung cancer in vitro and in vivo. *Neoplasia* 17, 190–200.
- Lee, P., Chandel, N. S., and Simon, M. C. (2020). Cellular adaptation to hypoxia through hypoxia inducible factors and beyond. *Nat. Rev. Mol. Cell Biol.* 21, 268–283.
- Lei, X., Lei, Y., Li, J.-K., Du, W.-X., Li, R.-G., Yang, J., et al. (2020). Immune cells within the tumor microenvironment: biological functions and roles in cancer immunotherapy. *Cancer Lett.* 470, 126–133. doi: 10.1016/j.canlet.2019.11.009

- Leone, R. D., Zhao, L., Englert, J. M., Sun, I. M., Oh, M. H., Sun, I. H., et al. (2019). Glutamine blockade induces divergent metabolic programs to overcome tumor immune evasion. *Science* 366, 1013–1021. doi: 10.1126/science.aav2588
- Leu, A. J., Berk, D. A., Lymboussaki, A., Alitalo, K., and Jain, R. K. (2000). Absence of functional lymphatics within a murine sarcoma: a molecular and functional evaluation. *Cancer Res.* 60, 4324–4327.
- Levchenko, A., Mehta, B. M., Niu, X., Kang, G., Villafania, L., Way, D., et al. (2005). Inter-cellular transfer of P-glycoprotein mediates acquired multidrug resistance in tumor cells. *Proc. Natl. Acad. Sci. U.S.A.* 102, 1933–1938. doi: 10.1073/pnas.0401851102
- Li, W., and Sun, X. (2018). Recent advances in developing novel anti-cancer drugs targeting tumor hypoxic and acidic microenvironments. *Recent Pat Anticancer Drug Discov.* 13, 455–468. doi: 10.2174/1574892813666180831102519
- Lin, S., Negulescu, A., Bulusu, S., Gibert, B., Delcros, J.-G., Ducarouge, B., et al. (2017). Non-canonical NOTCH3 signalling limits tumour angiogenesis. *Nat. Commun.* 8, 1–12.
- Lin, Y., Xu, J., and Lan, H. (2019). Tumor-associated macrophages in tumor metastasis: biological roles and clinical therapeutic applications. *J. Hematol. Oncol.* 12:76. doi: 10.1186/s13045-019-0760-3
- Ling, B., Watt, K., Banerjee, S., Newsted, D., Truesdell, P., Adams, J., et al. (2017). A novel immunotherapy targeting MMP-14 limits hypoxia, immune suppression and metastasis in triple-negative breast cancer models. *Oncotarget* 8, 58372–58385. doi: 10.18632/oncotarget.17702
- Liu, J., Dang, H., and Wang, X. W. (2018). The significance of intertumor and intratumor heterogeneity in liver cancer. *Exp. Mol. Med.* 50:e416. doi: 10.1038/emmm.2017.165
- Liu, J., Liao, S., Diop-Frimpong, B., Chen, W., Goel, S., Naxerova, K., et al. (2012). TGF- β blockade improves the distribution and efficacy of therapeutics in breast carcinoma by normalizing the tumor stroma. *Proc. Natl. Acad. Sci. U.S.A.* 109, 16618–16623. doi: 10.1073/pnas.1117610109
- Liu, R., Fernandez-Peñas, P., and Sebatnam, D. F. (2017). Management of adverse events related to new cancer immunotherapy (immune checkpoint inhibitors). *Med. J. Aust.* 206:412. doi: 10.5694/mja16.01357
- Liu, S., Ren, J., and Ten Dijke, P. (2021). Targeting TGF β signal transduction for cancer therapy. *Signal. Transduct. Target. Ther.* 6:8. doi: 10.1038/s41392-020-00436-9
- Lobb, R. J., van Amerongen, R., Wiegman, A., Ham, S., Larsen, J. E., and Möller, A. (2017). Exosomes derived from mesenchymal non-small cell lung cancer cells promote chemoresistance. *Int. J. Cancer* 141, 614–620.
- Löffek, S. (2018). Transforming of the tumor microenvironment: implications for TGF- β inhibition in the context of immune-checkpoint therapy. *J. Oncol.* 2018:9732939. doi: 10.1155/2018/9732939
- Long, L., Assaraf, Y. G., Lei, Z.-N., Peng, H., Yang, L., Chen, Z.-S., et al. (2020). Genetic biomarkers of drug resistance: a compass of prognosis and targeted therapy in acute myeloid leukemia. *Drug Resistance Updates* 52:100703. doi: 10.1016/j.drug.2020.100703
- Lotti, F., Jarrar, A. M., Pai, R. K., Hitomi, M., Lathia, J., Mace, A., et al. (2013). Chemotherapy activates cancer-associated fibroblasts to maintain colorectal cancer-initiating cells by IL-17A. *J. Exp. Med.* 210, 2851–2872. doi: 10.1084/jem.20131195
- Lu, C. W., Lin, S. C., Chien, C. W., Lin, S. C., Lee, C. T., Lin, B. W., et al. (2011). Overexpression of pyruvate dehydrogenase kinase 3 increases drug resistance and early recurrence in colon cancer. *Am. J. Pathol.* 179, 1405–1414. doi: 10.1016/j.ajpath.2011.05.050
- Luga, V., Zhang, L., Vitoria-Petit, A. M., Ogunjimi, A. A., Inanlou, M. R., Chiu, E., et al. (2012). Exosomes mediate stromal mobilization of autocrine Wnt-PCP signaling in breast cancer cell migration. *Cell* 151, 1542–1556. doi: 10.1016/j.cell.2012.11.024
- Luo, W., Zhong, J., Chang, R., Hu, H., Pandey, A., and Semenza, G. L. (2010). Hsp70 and CHIP selectively mediate ubiquitination and degradation of hypoxia-inducible factor (HIF)-1 α but not HIF-2 α . *J. Biol. Chem.* 285, 3651–3663. doi: 10.1074/jbc.M109.068577
- Luraghi, P., Reato, G., Cipriano, E., Sassi, F., Orzan, F., Bigatto, V., et al. (2014). MET signaling in colon cancer stem-like cells blunts the therapeutic response to EGFR inhibitors. *Cancer Res.* 74, 1857–1869. doi: 10.1158/0008-5472.Can-13-2340-t
- Lv, M. M., Zhu, X. Y., Chen, W. X., Zhong, S. L., Hu, Q., Ma, T. F., et al. (2014). Exosomes mediate drug resistance transfer in MCF-7 breast cancer cells and a probable mechanism is delivery of P-glycoprotein. *Tumour. Biol.* 35, 10773–10779. doi: 10.1007/s13277-014-2377-z
- Ma, Z., Yuan, D., Cheng, X., Tuo, B., Liu, X., and Li, T. (2020). Function of ion transporters in maintaining acid-base homeostasis of the mammary gland and the pathophysiological role in breast cancer. *Am. J. Physiol. Regul. Integr. Comp. Physiol.* 318, R98–R111.
- Maeda, H., and Khatami, M. (2018). Analyses of repeated failures in cancer therapy for solid tumors: poor tumor-selective drug delivery, low therapeutic efficacy and unsustainable costs. *Clin. Transl. Med.* 7:11.
- Maj, T., Wang, W., Crespo, J., Zhang, H., Wang, W., Wei, S., et al. (2017). Oxidative stress controls regulatory T cell apoptosis and suppressor activity and PD-L1-blockade resistance in tumor. *Nat. Immunol.* 18, 1332–1341. doi: 10.1038/ni.3868
- Maman, S., and Witz, I. P. (2018). A history of exploring cancer in context. *Nat. Rev. Cancer* 18, 359–376. doi: 10.1038/s41568-018-0006-7
- Mangan, M. S., Vega-Ramos, J., Joeckel, L. T., Mitchell, A. J., Rizzitelli, A., Roediger, B., et al. (2017). Serpinb9 is a marker of antigen cross-presenting dendritic cells. *Mol. Immunol.* 82, 50–56. doi: 10.1016/j.molimm.2016.12.011
- Manning, B. D., and Cantley, L. C. (2007). AKT/PKB signaling: navigating downstream. *Cell* 129, 1261–1274. doi: 10.1016/j.cell.2007.06.009
- Mantoni, T. S., Lunardi, S., Al-Assar, O., Masamune, A., and Brunner, T. B. (2011). Pancreatic stellate cells radioprotect pancreatic cancer cells through β 1-integrin signaling. *Cancer Res.* 71, 3453–3458. doi: 10.1158/0008-5472.Can-10-1633
- Mantovani, A., Allavena, P., Sica, A., and Balkwill, F. (2008). Cancer-related inflammation. *Nature* 454, 436–444. doi: 10.1038/nature07205
- Mantovani, A., Marchesi, F., Malesci, A., Laghi, L., and Allavena, P. (2017). Tumour-associated macrophages as treatment targets in oncology. *Nat. Rev. Clin. Oncol.* 14, 399–416. doi: 10.1038/nrclinonc.2016.217
- Martinez-Lostao, L., Anel, A., and Pardo, J. (2015). How do cytotoxic lymphocytes kill cancer cells? *Clin. Cancer Res.* 21, 5047–5056. doi: 10.1158/1078-0432.Ccr-15-0685
- Martinez-Outschoorn, U. E., Peiris-Pagés, M., Pestell, R. G., Sotgia, F., and Lisanti, M. P. (2017). Cancer metabolism: a therapeutic perspective. *Nat. Rev. Clin. Oncol.* 14, 11–31. doi: 10.1038/nrclinonc.2016.60
- Martinkova, E., Maglott, A., Leger, D. Y., Bonnet, D., Stiborova, M., Takeda, K., et al. (2010). α 5 β 1 integrin antagonists reduce chemotherapy-induced premature senescence and facilitate apoptosis in human glioblastoma cells. *Int. J. Cancer* 127, 1240–1248. doi: 10.1002/ijc.25187
- Martino, M. M., Briquez, P. S., Güç, E., Tortelli, F., Kilarski, W. W., Metzger, S., et al. (2014). Growth factors engineered for super-affinity to the extracellular matrix enhance tissue healing. *Science* 343, 885–888.
- Mashouri, L., Yousefi, H., Aref, A. R., Ahadi, A. M., Molaei, F., and Alahari, S. K. (2019). Exosomes: composition, biogenesis, and mechanisms in cancer metastasis and drug resistance. *Mol. Cancer* 18:75. doi: 10.1186/s12943-019-0991-5
- Matsunuma, S., Handa, S., Kamei, D., Yamamoto, H., Okuyama, K., and Kato, Y. (2019). Oxaliplatin induces prostaglandin E2 release in vascular endothelial cells. *Cancer Chemother. Pharmacol.* 84, 345–350.
- Mazzarella, L., and Curigliano, G. (2018). A new approach to assess drug sensitivity in cells for novel drug discovery. *Expert Opin. Drug Discov.* 13, 339–346. doi: 10.1080/17460441.2018.1437136
- McAndrews, K. M., McGrail, D. J., Ravikumar, N., and Dawson, M. R. (2015). Mesenchymal stem cells induce directional migration of invasive breast cancer cells through TGF- β . *Sci. Rep.* 5:16941. doi: 10.1038/srep16941
- Meijer, T. W., Kaanders, J. H., Span, P. N., and Bussink, J. (2012). Targeting hypoxia, HIF-1, and tumor glucose metabolism to improve radiotherapy efficacy. *Clin. Cancer Res.* 18, 5585–5594. doi: 10.1158/1078-0432.Ccr-12-0858
- Meurette, O., and Mehlen, P. (2018). Notch signaling in the tumor microenvironment. *Cancer Cell* 34, 536–548. doi: 10.1016/j.ccell.2018.07.009
- Miller, K. D., Nogueira, L., Mariotto, A. B., Rowland, J. H., Yabroff, K. R., Alfano, C. M., et al. (2019). Cancer treatment and survivorship statistics, 2019. *CA Cancer J. Clin.* 69, 363–385. doi: 10.3322/caac.21565
- Milman, N., Ginini, L., and Gil, Z. (2019). Exosomes and their role in tumorigenesis and anticancer drug resistance. *Drug Resistance Updates* 45, 1–12. doi: 10.1016/j.drug.2019.07.003
- Milosevic, M., Fyles, A., Hedley, D., and Hill, R. (2004). The human tumor microenvironment: invasive (needle) measurement of oxygen and interstitial fluid pressure. *Semin. Radiat. Oncol.* 14, 249–258.

- Mohammad, R. M., Muqbil, I., Lowe, L., Yedjou, C., Hsu, H. Y., Lin, L. T., et al. (2015). Broad targeting of resistance to apoptosis in cancer. *Semin. Cancer Biol.* 35(Suppl.00), S78–S103. doi: 10.1016/j.semcancer.2015.03.001
- Moloney, J. N., and Cotter, T. G. (2018). ROS signalling in the biology of cancer. *Semin. Cell Dev. Biol.* 80, 50–64.
- Monferran, S., Skuli, N., Delmas, C., Favre, G., Bonnet, J., Cohen-Jonathan-Moyal, E., et al. (2008). $\alpha v\beta 3$ and $\alpha v\beta 5$ integrins control glioma cell response to ionising radiation through ILK and RhoB. *Int. J. Cancer* 123, 357–364. doi: 10.1002/ijc.23498
- Morrot, A., da Fonseca, L. M., Salustiano, E. J., Gentile, L. B., Conde, L., Filardy, A. A., et al. (2018). Metabolic symbiosis and immunomodulation: how tumor cell-derived lactate may disturb innate and adaptive immune responses. *Front. Oncol.* 8:81. doi: 10.3389/fonc.2018.00081
- Morrow, K., Hernandez, C. P., Raber, P., Del Valle, L., Wilk, A. M., Majumdar, S., et al. (2013). Anti-leukemic mechanisms of pegylated arginase I in acute lymphoblastic T-cell leukemia. *Leukemia* 27, 569–577. doi: 10.1038/leu.2012.247
- Nagaraj, S., Gupta, K., Pisarev, V., Kinarsky, L., Sherman, S., Kang, L., et al. (2007). Altered recognition of antigen is a mechanism of CD8+ T cell tolerance in cancer. *Nat. Med.* 13, 828–835. doi: 10.1038/nm1609
- Nagathihalli, N. S., Castellanos, J. A., Shi, C., Beesetty, Y., Reyzer, M. L., Caprioli, R., et al. (2015). Signal transducer and activator of transcription 3, mediated remodeling of the tumor microenvironment results in enhanced tumor drug delivery in a mouse model of pancreatic cancer. *Gastroenterology* 149, 1932.e9–1943.e9. doi: 10.1053/j.gastro.2015.07.058
- Najafi, M., Farhood, B., and Mortezaee, K. (2019). Extracellular matrix (ECM) stiffness and degradation as cancer drivers. *J. Cell Biochem.* 120, 2782–2790. doi: 10.1002/jcb.27681
- Nishimoto, A., Kugimiya, N., Hosoyama, T., Enoki, T., Li, T. S., and Hamano, K. (2014). HIF-1 α activation under glucose deprivation plays a central role in the acquisition of anti-apoptosis in human colon cancer cells. *Int. J. Oncol.* 44, 2077–2084. doi: 10.3892/ijo.2014.2367
- Nokin, M. J., Durieux, F., Bellier, J., Peulen, O., Uchida, K., Spiegel, D. A., et al. (2017). Hormetic potential of methylglyoxal, a side-product of glycolysis, in switching tumours from growth to death. *Sci. Rep.* 7:11722. doi: 10.1038/s41598-017-12119-7
- Noy, R., and Pollard, J. W. (2014). Tumor-associated macrophages: from mechanisms to therapy. *Immunity* 41, 49–61. doi: 10.1016/j.immuni.2014.06.010
- Obenauf, A. C., Zou, Y., Ji, A. L., Vanharanta, S., Shu, W., Shi, H., et al. (2015). Therapy-induced tumour secretomes promote resistance and tumour progression. *Nature* 520, 368–372. doi: 10.1038/nature14336
- O'Donnell, J. S., Long, G. V., Scolyer, R. A., Teng, M. W. L., and Smyth, M. J. (2017). Resistance to PD1/PDL1 checkpoint inhibition. *Cancer Treatm. Rev.* 52, 71–81. doi: 10.1016/j.ctrv.2016.11.007
- Ogawa, R., Ishiguro, H., Kuwabara, Y., Kimura, M., Mitsui, A., Mori, Y., et al. (2008). Identification of candidate genes involved in the radiosensitivity of esophageal cancer cells by microarray analysis. *Dis. Esophagus* 21, 288–297. doi: 10.1111/j.1442-2050.2007.00759.x
- Oh, M. H., Sun, I. H., Zhao, L., Leone, R. D., Sun, I. M., Xu, W., et al. (2020). Targeting glutamine metabolism enhances tumor-specific immunity by modulating suppressive myeloid cells. *J. Clin. Invest.* 130, 3865–3884. doi: 10.1172/jci131859
- Olive, K. P., Jacobetz, M. A., Davidson, C. J., Gopinathan, A., McIntyre, D., Honess, D., et al. (2009). Inhibition of Hedgehog signaling enhances delivery of chemotherapy in a mouse model of pancreatic cancer. *Science* 324, 1457–1461.
- Orimo, A., Gupta, P. B., Sgroi, D. C., Arenzana-Seisdedos, F., Delaunay, T., Naeem, R., et al. (2005). Stromal fibroblasts present in invasive human breast carcinomas promote tumor growth and angiogenesis through elevated SDF-1/CXCL12 secretion. *Cell* 121, 335–348. doi: 10.1016/j.cell.2005.02.034
- O'Sullivan, D., van der Windt, G. J., Huang, S. C., Curtis, J. D., Chang, C. H., Buck, M. D., et al. (2014). Memory CD8(+) T cells use cell-intrinsic lipolysis to support the metabolic programming necessary for development. *Immunity* 41, 75–88. doi: 10.1016/j.immuni.2014.06.005
- OuYang, L. Y., Wu, X. J., Ye, S. B., Zhang, R. X., Li, Z. L., Liao, W., et al. (2015). Tumor-induced myeloid-derived suppressor cells promote tumor progression through oxidative metabolism in human colorectal cancer. *J. Transl. Med.* 13:47. doi: 10.1186/s12967-015-0410-7
- Ozawa, P. M. M., Alkhilaiwi, F., Cavalli, I. J., Malheiros, D., de Souza Fonseca Ribeiro, E. M., and Cavalli, L. R. (2018). Extracellular vesicles from triple-negative breast cancer cells promote proliferation and drug resistance in non-tumorigenic breast cells. *Breast Cancer Res. Treat.* 172, 713–723. doi: 10.1007/s10549-018-4925-5
- Pauw, M., Schoonderwoerd, M. J., Helder, R. F., Harryvan, T. J., Groenewoud, A., van Pelt, G. W., et al. (2018). Endoglin expression on cancer-associated fibroblasts regulates invasion and stimulates colorectal cancer metastasis. *Clin. Cancer Res.* 24, 6331–6344.
- Padera, T. P., Stoll, B. R., Tooredman, J. B., Capen, D., di Tomaso, E., and Jain, R. K. (2004). Cancer cells compress intratumour vessels. *Nature* 427, 695–695.
- Paolicchi, E., Gemignani, F., Krstic-Demonacos, M., Dedhar, S., Mutti, L., and Landi, S. (2016). Targeting hypoxic response for cancer therapy. *Oncotarget* 7, 13464–13478. doi: 10.18632/oncotarget.7229
- Paolillo, M., and Schinelli, S. (2017). Integrins and exosomes, a dangerous liaison in cancer progression. *Cancers* 9:95. doi: 10.3390/cancers9080095
- Papapetrou, E. P. (2016). Patient-derived induced pluripotent stem cells in cancer research and precision oncology. *Nat. Med.* 22, 1392–1401. doi: 10.1038/nm.4238
- Park, C. C., Zhang, H. J., Yao, E. S., Park, C. J., and Bissell, M. J. (2008). $\beta 1$ Integrin inhibition dramatically enhances radiotherapy efficacy in human breast cancer xenografts. *Cancer Res.* 68, 4398–4405. doi: 10.1158/0008-5472.Can-07-6390
- Patel, S. A., and Minn, A. J. (2018). Combination cancer therapy with immune checkpoint blockade: mechanisms and strategies. *Immunity* 48, 417–433. doi: 10.1016/j.immuni.2018.03.007
- Paz-Ares, L., Garon, E., Ardizzoni, A., Barlesi, F., Cho, B., de Castro Junior, G., et al. (2019). CANOPY phase III program: three studies evaluating canakinumab in patients with non-small cell lung cancer (NSCLC). *Ann. Oncol.* 30, v654–v655.
- Pei, G. T., Wu, C. W., and Lin, W. W. (2010). Hypoxia-induced decoy receptor 2 gene expression is regulated via a hypoxia-inducible factor 1 α -mediated mechanism. *Biochem. Biophys. Res. Commun.* 391, 1274–1279. doi: 10.1016/j.bbrc.2009.12.058
- Petrova, V., Annicchiarico-Petruzzelli, M., Melino, G., and Amelio, I. (2018). The hypoxic tumour microenvironment. *Oncogenesis* 7, 1–13.
- Pickup, M. W., Mouw, J. K., and Weaver, V. M. (2014). The extracellular matrix modulates the hallmarks of cancer. *EMBO Rep.* 15, 1243–1253. doi: 10.15252/embr.201439246
- Podar, K., Zimmerhackl, A., Fulciniti, M., Tonon, G., Hainz, U., Tai, Y. T., et al. (2011). The selective adhesion molecule inhibitor Natalizumab decreases multiple myeloma cell growth in the bone marrow microenvironment: therapeutic implications. *Br. J. Haematol.* 155, 438–448. doi: 10.1111/j.1365-2141.2011.08864.x
- Pouyssegur, J., Dayan, F., and Mazure, N. M. (2006). Hypoxia signalling in cancer and approaches to enforce tumour regression. *Nature* 441, 437–443.
- Prima, V., Kaliberova, L. N., Kaliberov, S., Curiel, D. T., and Kusmartsev, S. (2017). COX2/mPGES1/PGE2 pathway regulates PD-L1 expression in tumor-associated macrophages and myeloid-derived suppressor cells. *Proc. Natl. Acad. Sci. U.S.A.* 114, 1117–1122. doi: 10.1073/pnas.1612920114
- Pucino, V., Bombardieri, M., Pitzalis, C., and Mauro, C. (2017). Lactate at the crossroads of metabolism, inflammation, and autoimmunity. *Eur. J. Immunol.* 47, 14–21. doi: 10.1002/eji.201646477
- Purcell, J. W., Tanlimco, S. G., Hickson, J., Fox, M., Sho, M., Durkin, L., et al. (2018). LRRCL15 is a novel mesenchymal protein and stromal target for antibody-drug conjugates. *Cancer Res.* 78, 4059–4072. doi: 10.1158/0008-5472.Can-18-0327
- Pusch, S., Krausert, S., Fischer, V., Balss, J., Ott, M., Schrimpf, D., et al. (2017). Pan-tumor IDH1 inhibitor BAY 1436032 for effective treatment of IDH1 mutant astrocytoma in vivo. *Acta Neuropathol.* 133, 629–644. doi: 10.1007/s00401-017-1677-y
- Qiao, Y., Zhang, C., Li, A., Wang, D., Luo, Z., Ping, Y., et al. (2018). IL6 derived from cancer-associated fibroblasts promotes chemoresistance via CXCR7 in esophageal squamous cell carcinoma. *Oncogene* 37, 873–883. doi: 10.1038/ncr.2017.387
- Quail, D. F., and Joyce, J. A. (2013). Microenvironmental regulation of tumor progression and metastasis. *Nat. Med.* 19, 1423–1437. doi: 10.1038/nm.3394
- Raghu, N., Mahoney, B. P., and Gillies, R. J. (2003). Tumor acidity, ion trapping and chemotherapeutics. II. pH-dependent partition coefficients predict importance of ion trapping on pharmacokinetics of weakly basic

- chemotherapeutic agents. *Biochem. Pharmacol.* 66, 1219–1229. doi: 10.1016/s0006-2952(03)00468-4
- Räihä, M. R., and Puolakkainen, P. A. (2018). Tumor-associated macrophages (TAMs) as biomarkers for gastric cancer: a review. *Chronic Dis. Transl. Med.* 4, 156–163. doi: 10.1016/j.cdtm.2018.07.001
- Ramapriyan, R., Caetano, M. S., Barsoumian, H. B., Mafra, A. C. P., Zambalde, E. P., Menon, H., et al. (2019). Altered cancer metabolism in mechanisms of immunotherapy resistance. *Pharmacol. Ther.* 195, 162–171. doi: 10.1016/j.pharmthera.2018.11.004
- Räsänen, K., and Vaheri, A. (2010). Activation of fibroblasts in cancer stroma. *Exp. Cell Res.* 316, 2713–2722. doi: 10.1016/j.yexcr.2010.04.032
- Ren, J., Ding, L., Zhang, D., Shi, G., Xu, Q., Shen, S., et al. (2018). Carcinoma-associated fibroblasts promote the stemness and chemoresistance of colorectal cancer by transferring exosomal lncRNA H19. *Theranostics* 8:3932.
- Restifo, N. P., Smyth, M. J., and Snyder, A. (2016). Acquired resistance to immunotherapy and future challenges. *Nat. Rev. Cancer* 16, 121–126. doi: 10.1038/nrc.2016.2
- Richards, K. E., Zeleniak, A. E., Fishel, M. L., Wu, J., Littlepage, L. E., and Hill, R. (2017). Cancer-associated fibroblast exosomes regulate survival and proliferation of pancreatic cancer cells. *Oncogene* 36, 1770–1778.
- Ridker, P. M., MacFadyen, J. G., Thuren, T., Everett, B. M., Libby, P., and Glynn, R. J. (2017). Effect of interleukin-1 β inhibition with canakinumab on incident lung cancer in patients with atherosclerosis: exploratory results from a randomised, double-blind, placebo-controlled trial. *Lancet* 390, 1833–1842. doi: 10.1016/s0140-6736(17)32247-x
- Ritter, V. (2017). *Role of Bcl-2 Protein Family Members and Associated Mitochondrial Factors in Hypoxia-Mediated Resistance of Tumor Cells to Apoptosis and Radiotherapy*. Duisburg: Universität Duisburg-Essen.
- Robert, C., Schachter, J., Long, G. V., Arance, A., Grob, J. J., Mortier, L., et al. (2015). Pembrolizumab versus ipilimumab in advanced melanoma. *N. Engl. J. Med.* 372, 2521–2532. doi: 10.1056/NEJMoa1503093
- Rohwer, N., Dame, C., Haugstetter, A., Wiedenmann, B., Detjen, K., Schmitt, C. A., et al. (2010). Hypoxia-inducible factor 1 α determines gastric cancer chemosensitivity via modulation of p53 and NF- κ B. *PLoS One* 5:e12038. doi: 10.1371/journal.pone.0012038
- Roma-Rodrigues, C., Mendes, R., Baptista, P. V., and Fernandes, A. R. (2019). Targeting tumor microenvironment for cancer therapy. *Int. J. Mol. Sci.* 20:840. doi: 10.3390/ijms20040840
- Roswall, P., Bocci, M., Bartoschek, M., Li, H., Kristiansen, G., Jansson, S., et al. (2018). Microenvironmental control of breast cancer subtype elicited through paracrine platelet-derived growth factor-CC signaling. *Nat. Med.* 24, 463–473. doi: 10.1038/nm.4494
- Ruffell, B., and Coussens, L. M. (2015). Macrophages and therapeutic resistance in cancer. *Cancer Cell* 27, 462–472. doi: 10.1016/j.ccell.2015.02.015
- Safaei, R., Larson, B. J., Cheng, T. C., Gibson, M. A., Otani, S., Naerdemann, W., et al. (2005). Abnormal lysosomal trafficking and enhanced exosomal export of cisplatin in drug-resistant human ovarian carcinoma cells. *Mol. Cancer Ther.* 4, 1595–1604. doi: 10.1158/1535-7163.Mct-05-0102
- Saleh, R., and Elkord, E. (2020). Acquired resistance to cancer immunotherapy: role of tumor-mediated immunosuppression. *Semin. Cancer Biol.* 65, 13–27. doi: 10.1016/j.semcancer.2019.07.017
- Salmaninejad, A., Valilou, S. F., Soltani, A., Ahmadi, S., Abarghan, Y. J., Rosengren, R. J., et al. (2019). Tumor-associated macrophages: role in cancer development and therapeutic implications. *Cell Oncol.* 42, 591–608. doi: 10.1007/s13402-019-00453-z
- Salnikov, A. V., Iversen, V. V., Koisti, M., Sundberg, C., Johansson, L., Stuhr, L. B., et al. (2003). Lowering of tumor interstitial fluid pressure specifically augments efficacy of chemotherapy. *FASEB J.* 17, 1756–1758.
- Salony, Solé, X., Alves, C. P., Dey-Guha, I., Ritsma, L., Boukhali, M., et al. (2016). AKT inhibition promotes nonautonomous cancer cell survival. *Mol. Cancer Ther.* 15, 142–153. doi: 10.1158/1535-7163.Mct-15-0414
- Salvagno, C., Ciampicotti, M., Tuit, S., Hau, C.-S., van Weverwijk, A., Coffelt, S. B., et al. (2019). Therapeutic targeting of macrophages enhances chemotherapy efficacy by unleashing type I interferon response. *Nat. Cell Biol.* 21, 511–521.
- Samavati, L., Rastogi, R., Du, W., Hüttemann, M., Fite, A., and Franchi, L. (2009). STAT3 tyrosine phosphorylation is critical for interleukin 1 β and interleukin-6 production in response to lipopolysaccharide and live bacteria. *Mol. Immunol.* 46, 1867–1877. doi: 10.1016/j.molimm.2009.02.018
- Sato, N., Kohi, S., Hirata, K., and Goggins, M. (2016). Role of hyaluronan in pancreatic cancer biology and therapy: once again in the spotlight. *Cancer Sci.* 107, 569–575. doi: 10.1111/cas.12913
- Sauvant, C., Nowak, M., Wirth, C., Schneider, B., Riemann, A., Gekle, M., et al. (2008). Acidosis induces multi-drug resistance in rat prostate cancer cells (AT1) in vitro and in vivo by increasing the activity of the p-glycoprotein via activation of p38. *Int. J. Cancer* 123, 2532–2542. doi: 10.1002/ijc.23818
- Sawa-Wejksza, K., and Kandefer-Szerszeń, M. (2018). Tumor-associated macrophages as target for antitumor therapy. *Arch. Immunol. Ther. Exp.* 66, 97–111. doi: 10.1007/s00005-017-0480-8
- Scalici, J. M., Harrer, C., Allen, A., Jazaeri, A., Atkins, K. A., McLachlan, K. R., et al. (2014). Inhibition of α 4 β 1 integrin increases ovarian cancer response to carboplatin. *Gynecol. Oncol.* 132, 455–461. doi: 10.1016/j.ygyno.2013.12.031
- Scannevin, R. H., Alexander, R., Haarlander, T. M., Burke, S. L., Singer, M., Huo, C., et al. (2017). Discovery of a highly selective chemical inhibitor of matrix metalloproteinase-9 (MMP-9) that allosterically inhibits zymogen activation. *J. Biol. Chem.* 292, 17963–17974. doi: 10.1074/jbc.M117.806075
- Schenk, K. M., Reuss, J. E., Choquette, K., and Spira, A. I. (2019). A review of canakinumab and its therapeutic potential for non-small cell lung cancer. *Anti Cancer Drugs* 30, 879–885.
- Schneider, A., and Simons, M. (2013). Exosomes: vesicular carriers for intercellular communication in neurodegenerative disorders. *Cell Tissue Res.* 352, 33–47.
- Schrader, J., Gordon-Walker, T. T., Aucott, R. L., van Deemter, M., Quaas, A., Walsh, S., et al. (2011). Matrix stiffness modulates proliferation, chemotherapeutic response, and dormancy in hepatocellular carcinoma cells. *Hepatology* 53, 1192–1205. doi: 10.1002/hep.24108
- Seguin, L., Kato, S., Franovic, A., Camargo, M. F., Lesperance, J., Elliott, K. C., et al. (2014). An integrin β 3–KRAS–Rab complex drives tumour stemness and resistance to EGFR inhibition. *Nat. Biol.* 16, 457–468.
- Sehsted, T. S., Bjerre, J., Ku, S., Chang, A., Jahansouz, A., Owens, D. K., et al. (2019). Cost-effectiveness of Canakinumab for prevention of recurrent cardiovascular events. *JAMA Cardiol.* 4, 128–135.
- Semenza, G. L. (2013). Cancer-stromal cell interactions mediated by hypoxia-inducible factors promote angiogenesis, lymphangiogenesis, and metastasis. *Oncogene* 32, 4057–4063.
- Sentebane, D. A., Jonker, T., Rowe, A., Thomford, N. E., Munro, D., Dandara, C., et al. (2018). The role of tumor microenvironment in chemoresistance: 3D extracellular matrices as accomplices. *Int. J. Mol. Sci.* 19:2861.
- Sevick, E. M., and Jain, R. K. (1989). Geometric resistance to blood flow in solid tumors perfused ex vivo: effects of tumor size and perfusion pressure. *Cancer Res.* 49, 3506–3512.
- Shackelford, D. B., Vazquez, D. S., Corbeil, J., Wu, S., Leblanc, M., Wu, C. L., et al. (2009). mTOR and HIF-1 α -mediated tumor metabolism in an LKB1 mouse model of Peutz-Jeghers syndrome. *Proc. Natl. Acad. Sci. U.S.A.* 106, 11137–11142. doi: 10.1073/pnas.0900465106
- Shalabi, H., Kraft, I. L., Wang, H. W., Yuan, C. M., Yates, B., Delbrook, C., et al. (2018). Sequential loss of tumor surface antigens following chimeric antigen receptor T-cell therapies in diffuse large B-cell lymphoma. *Haematologica* 103, e215–e218. doi: 10.3324/haematol.2017.183459
- Sharma, P., Hu-Lieskovan, S., Wargo, J. A., and Ribas, A. (2017). Primary, adaptive, and acquired resistance to cancer immunotherapy. *Cell* 168, 707–723. doi: 10.1016/j.cell.2017.01.017
- Shaw, R. J., Bardeesy, N., Manning, B. D., Lopez, L., Kosmatka, M., DePinho, R. A., et al. (2004). The LKB1 tumor suppressor negatively regulates mTOR signaling. *Cancer Cell* 6, 91–99. doi: 10.1016/j.ccr.2004.06.007
- Shayan, G., Srivastava, R., Li, J., Schmitt, N., Kane, L. P., and Ferris, R. L. (2017). Adaptive resistance to anti-PD1 therapy by Tim-3 upregulation is mediated by the PI3K-Akt pathway in head and neck cancer. *Oncol Immunology* 6:e1261779. doi: 10.1080/2162402X.2016.1261779
- Shedden, K., Xie, X. T., Chandaroy, P., Chang, Y. T., and Rosania, G. R. (2003). Expulsion of small molecules in vesicles shed by cancer cells: association with gene expression and chemosensitivity profiles. *Cancer Res.* 63, 4331–4337.
- Shiga, K., Hara, M., Nagasaki, T., Sato, T., Takahashi, H., and Takeyama, H. (2015). Cancer-associated fibroblasts: their characteristics and their roles in tumor growth. *Cancers* 7, 2443–2458. doi: 10.3390/cancers7040902
- Shree, T., Olson, O. C., Elie, B. T., Kester, J. C., Garfall, A. L., Simpson, K., et al. (2011). Macrophages and cathepsin proteases blunt chemotherapeutic response in breast cancer. *Genes Dev.* 25, 2465–2479. doi: 10.1101/gad.180331.111

- Singh, D., Arora, R., Kaur, P., Singh, B., Mannan, R., and Arora, S. (2017). Overexpression of hypoxia-inducible factor and metabolic pathways: possible targets of cancer. *Cell Biosci.* 7, 1–9.
- Socinski, M. A., Jotte, R. M., Cappuzzo, F., Orlandi, F., Stroyakovskiy, D., Nogami, N., et al. (2018). Atezolizumab for first-line treatment of metastatic nonsquamous NSCLC. *N. Engl. J. Med.* 378, 2288–2301.
- Solinas, G., Schiarea, S., Liguori, M., Fabbri, M., Pesce, S., Zammataro, L., et al. (2010). Tumor-conditioned macrophages secrete migration-stimulating factor: a new marker for M2-polarization, influencing tumor cell motility. *J. Immunol.* 185, 642–652. doi: 10.4049/jimmunol.1000413
- Steinbichler, T. B., Dudás, J., Skvortsov, S., Ganswindt, U., Riechelmann, H., and Skvortsova, I. I. (2018). Therapy resistance mediated by cancer stem cells. *Semin. Cancer Biol.* 53, 156–167. doi: 10.1016/j.semcancer.2018.11.006
- Steinbichler, T. B., Dudás, J., Skvortsov, S., Ganswindt, U., Riechelmann, H., and Skvortsova, I. I. (2019). Therapy resistance mediated by exosomes. *Mol. Cancer* 18:58. doi: 10.1186/s12943-019-0970-x
- Stepka, P., Vsiansky, V., Raudenska, M., Gumulec, J., Adam, V., and Masarik, M. (2020). Metabolic and amino acid alterations of the tumor microenvironment. *Curr. Med. Chem.* 27:1. doi: 10.2174/0929867327666200207114658
- Stohrer, M., Boucher, Y., Stangassinger, M., and Jain, R. K. (2000). Oncotic pressure in solid tumors is elevated. *Cancer Res.* 60, 4251–4255.
- Stone, M. L., Chiappinelli, K. B., Li, H., Murphy, L. M., Travers, M. E., Topper, M. J., et al. (2017). Epigenetic therapy activates type I interferon signaling in murine ovarian cancer to reduce immunosuppression and tumor burden. *Proc. Natl. Acad. Sci. U.S.A.* 114, E10981–E10990. doi: 10.1073/pnas.1712514114
- Straussman, R., Morikawa, T., Shee, K., Barzily-Rokni, M., Qian, Z. R., Du, J., et al. (2012). Tumour micro-environment elicits innate resistance to RAF inhibitors through HGF secretion. *Nature* 487, 500–504. doi: 10.1038/nature11183
- Strick, R., Strissel, P. L., Baylin, S. B., and Chiappinelli, K. B. (2016). Unraveling the molecular pathways of DNA-methylation inhibitors: human endogenous retroviruses induce the innate immune response in tumors. *Oncoimmunology* 5:e1122160. doi: 10.1080/2162402x.2015.1122160
- Studebaker, A. W., Storci, G., Werbeck, J. L., Sansone, P., Sasser, A. K., Tavori, S., et al. (2008). Fibroblasts isolated from common sites of breast cancer metastasis enhance cancer cell growth rates and invasiveness in an interleukin-6-dependent manner. *Cancer Res.* 68, 9087–9095. doi: 10.1158/0008-5472.Can-08-0400
- Stupp, R., Hegi, M. E., Gorlia, T., Erridge, S. C., Perry, J., Hong, Y.-K., et al. (2014). Cilengitide combined with standard treatment for patients with newly diagnosed glioblastoma with methylated MGMT promoter (CENTRIC EORTC 26071-22072 study): a multicentre, randomised, open-label, phase 3 trial. *Lancet Oncol.* 15, 1100–1108. doi: 10.1016/S1470-2045(14)70379-1
- Su, S., Chen, J., Yao, H., Liu, J., Yu, S., Lao, L., et al. (2018). CD10(+)GPR77(+) Cancer-associated fibroblasts promote cancer formation and chemoresistance by sustaining cancer stemness. *Cell* 172, 841.e16–856.e16. doi: 10.1016/j.cell.2018.01.009
- Sun, Y. (2016). Tumor microenvironment and cancer therapy resistance. *Cancer Lett.* 380, 205–215. doi: 10.1016/j.canlet.2015.07.044
- Sun, Y., Campisi, J., Higano, C., Beer, T. M., Porter, P., Coleman, I., et al. (2012). Treatment-induced damage to the tumor microenvironment promotes prostate cancer therapy resistance through WNT16B. *Nat. Med.* 18, 1359–1368. doi: 10.1038/nm.2890
- Sung, B. H., Ketova, T., Hoshino, D., Zijlstra, A., and Weaver, A. M. (2015). Directional cell movement through tissues is controlled by exosome secretion. *Nat. Commun.* 6:7164. doi: 10.1038/ncomms8164
- Supuran, C. T. (2018). Carbonic anhydrase inhibitors as emerging agents for the treatment and imaging of hypoxic tumors. *Expert Opin. Invest. Drugs* 27, 963–970.
- Szakács, G., Paterson, J. K., Ludwig, J. A., Booth-Genthe, C., and Gottesman, M. M. (2006). Targeting multidrug resistance in cancer. *Nat. Rev. Drug Discov.* 5, 219–234. doi: 10.1038/nrd1984
- Szebeni, G. J., Vizler, C., Nagy, L. I., Kitajka, K., and Puskas, L. G. (2016). pro-tumoral inflammatory myeloid cells as emerging therapeutic targets. *Int. J. Mol. Sci.* 17:1958. doi: 10.3390/ijms17111958
- Taipale, M., Jarosz, D. F., and Lindquist, S. (2010). HSP90 at the hub of protein homeostasis: emerging mechanistic insights. *Nat. Rev. Mol. Cell Biol.* 11, 515–528. doi: 10.1038/nrm2918
- Tan, H. Y., Wang, N., Lam, W., Guo, W., Feng, Y., and Cheng, Y. C. (2018). Targeting tumour microenvironment by tyrosine kinase inhibitor. *Mol. Cancer* 17:43. doi: 10.1186/s12943-018-0800-6
- Tan, Q., Saggari, J. K., Yu, M., Wang, M., and Tannock, I. F. (2015). Mechanisms of drug resistance related to the microenvironment of solid tumors and possible strategies to inhibit them. *Cancer J.* 21, 254–262.
- Tanaka, H., Yoshizawa, H., Yamaguchi, Y., Ito, K., Kagamu, H., Suzuki, E., et al. (1999). Successful adoptive immunotherapy of murine poorly immunogenic tumor with specific effector cells generated from gene-modified tumor-primed lymph node cells. *J. Immunol.* 162, 3574–3582.
- Tang, Y. A., Chen, Y. F., Bao, Y., Mahara, S., Yatim, S., Oguz, G., et al. (2018). Hypoxic tumor microenvironment activates GLI2 via HIF-1 α and TGF- β 2 to promote chemoresistance in colorectal cancer. *Proc. Natl. Acad. Sci. U.S.A.* 115, E5990–E5999. doi: 10.1073/pnas.1801348115
- Tatum, J. L. (2006). Hypoxia: importance in tumor biology, noninvasive measurement by imaging, and value of its measurement in the management of cancer therapy. *Int. J. Radiat. Biol.* 82, 699–757.
- Thomasset, N., Lochter, A., Sympon, C. J., Lund, L. R., Williams, D. R., Behrendtsen, O., et al. (1998). Expression of autoactivated stromelysin-1 in mammary glands of transgenic mice leads to a reactive stroma during early development. *Am. J. Pathol.* 153, 457–467. doi: 10.1016/s0002-9440(10)65589-7
- Tong, D., Liu, Q., Wang, L. A., Xie, Q., Pang, J., Huang, Y., et al. (2018). The roles of the COX2/PGE2/EP axis in therapeutic resistance. *Cancer Metastasis Rev.* 37, 355–368. doi: 10.1007/s10555-018-9752-y
- Tran, Q., Lee, H., Park, J., Kim, S.-H., and Park, J. (2016). Targeting cancer metabolism-revisiting the Warburg effects. *Toxicol. Res.* 32, 177–193.
- Trédan, O., Galmarini, C. M., Patel, K., and Tannock, I. F. (2007). Drug resistance and the solid tumor microenvironment. *J. Natl. Cancer Inst.* 99, 1441–1454.
- Truffi, M., Sorrentino, L., and Corsi, F. (2020). “Fibroblasts in the tumor microenvironment,” in *Tumor Microenvironment: Non-Hematopoietic Cells*, ed. A. Birbrair (Cham: Springer International Publishing), 15–29.
- Tsai, M. J., Chang, W. A., Huang, M. S., and Kuo, P. L. (2014). Tumor microenvironment: a new treatment target for cancer. *ISRN Biochem.* 2014:351959. doi: 10.1155/2014/351959
- Tulotta, C., and Ottewill, P. (2018). The role of IL-1B in breast cancer bone metastasis. *Endocr. Relat. Cancer* 25, R421–R434. doi: 10.1530/erc-17-0309
- Umezawa, K., Kojima, I., Simizu, S., Lin, Y., Fukatsu, H., Koide, N., et al. (2018). Therapeutic activity of plant-derived alkaloid conophylline on metabolic syndrome and neurodegenerative disease models. *Hum. Cell* 31, 95–101. doi: 10.1007/s13577-017-0196-4
- Upagupta, C., Shimbori, C., Alsilmi, R., and Kolb, M. (2018). Matrix abnormalities in pulmonary fibrosis. *Eur. Respir. Rev.* 27:180033. doi: 10.1183/16000617.0033-2018
- Valencia, A. M., and Kadoch, C. (2019). Chromatin regulatory mechanisms and therapeutic opportunities in cancer. *Nat. Cell Biol.* 21, 152–161. doi: 10.1038/s41556-018-0258-1
- Vaquero, J., Lobe, C., Tahraoui, S., Clapéron, A., Mergey, M., Merabte, F., et al. (2018). The IGF2/IR/IGF1R pathway in tumor cells and myofibroblasts mediates resistance to egfr inhibition in cholangiocarcinoma. *Clin. Cancer Res.* 24, 4282–4296. doi: 10.1158/1078-0432.Ccr-17-3725
- Vaupel, P. (2004). Tumor microenvironmental physiology and its implications for radiation oncology. *Semin. Radiat. Oncol.* 14, 198–206.
- Vlachogiannis, G., Hedayat, S., Vatsiou, A., Jamin, Y., Fernández-Mateos, J., Khan, K., et al. (2018). Patient-derived organoids model treatment response of metastatic gastrointestinal cancers. *Science* 359, 920–926. doi: 10.1126/science.aao2774
- Walker, C., Mojares, E., and del Río Hernández, A. (2018). Role of extracellular matrix in development and cancer progression. *Int. J. Mol. Sci.* 19:3028.
- Wang, L., Zhang, F., Cui, J. Y., Chen, L., Chen, Y. T., and Liu, B. W. (2018). CAFs enhance paclitaxel resistance by inducing EMT through the IL-6/JAK2/STAT3 pathway. *Oncol. Rep.* 39, 2081–2090. doi: 10.3892/or.2018.6311
- Wang, X., Luo, G., Zhang, K., Cao, J., Huang, C., Jiang, T., et al. (2018). Hypoxic tumor-derived exosomal miR-301a mediates M2 macrophage polarization via PTEN/PI3K γ to promote pancreatic cancer metastasis. *Cancer Res.* 78, 4586–4598. doi: 10.1158/0008-5472.Can-17-3841
- Wang, M., Qiu, R., Yu, S., Xu, X., Li, G., Gu, R., et al. (2019). Paclitaxel-resistant gastric cancer MGC-803 cells promote epithelial-to-mesenchymal transition

- and chemoresistance in paclitaxel-sensitive cells via exosomal delivery of miR-155-5p. *Int. J. Oncol.* 54, 326–338.
- Wang, W., Kryczek, I., Dostál, L., Lin, H., Tan, L., Zhao, L., et al. (2016). Effector T Cells abrogate stroma-mediated chemoresistance in ovarian cancer. *Cell* 165, 1092–1105. doi: 10.1016/j.cell.2016.04.009
- Wang, W. L., Chang, W. L., Yang, H. B., Chang, I. W., Lee, C. T., Chang, C. Y., et al. (2015). Quantification of tumor infiltrating Foxp3+ regulatory T cells enables the identification of high-risk patients for developing synchronous cancers over upper aerodigestive tract. *Oral. Oncol.* 51, 698–703. doi: 10.1016/j.oraloncology.2015.04.015
- Wang, Y., Fang, Z., Hong, M., Yang, D., and Xie, W. (2020). Long-noncoding RNAs (lncRNAs) in drug metabolism and disposition, implications in cancer chemoresistance. *Acta Pharmaceut. Sin. B* 10, 105–112. doi: 10.1016/j.apsb.2019.09.011
- Warfel, N. A., and El-Deiry, W. S. (2014). HIF-1 signaling in drug resistance to chemotherapy. *Curr. Med. Chem.* 21, 3021–3028. doi: 10.2174/0929867321666140414101056
- Watnick, R. S. (2012). The role of the tumor microenvironment in regulating angiogenesis. *Cold Spring Harbor Perspect. Med.* 2:a006676.
- Wei, S. C., Duffy, C. R., and Allison, J. P. (2018). Fundamental mechanisms of immune checkpoint blockade therapy. *Cancer Discov.* 8, 1069–1086. doi: 10.1158/2159-8290.Cd-18-0367
- Weigelt, B., Lo, A. T., Park, C. C., Gray, J. W., and Bissell, M. J. (2010). HER2 signaling pathway activation and response of breast cancer cells to HER2-targeting agents is dependent strongly on the 3D microenvironment. *Breast Cancer Res. Treatm.* 122, 35–43. doi: 10.1007/s10549-009-0502-2
- Weinberg, F., Ramnath, N., and Nagrath, D. (2019). Reactive oxygen species in the tumor microenvironment: an overview. *Cancers* 11:1191. doi: 10.3390/cancers11081191
- Weis, S. M., and Cheresh, D. A. (2011). Tumor angiogenesis: molecular pathways and therapeutic targets. *Nat. Med.* 17, 1359–1370.
- Wight, T. N., Kang, I., Evanko, S. P., Harten, I. A., Chang, M. Y., Pearce, O. M. T., et al. (2020). Versican-A critical extracellular matrix regulator of immunity and inflammation. *Front. Immunol.* 11:512. doi: 10.3389/fimmu.2020.00512
- Wolchok, J. D., Kluger, H., Callahan, M. K., Postow, M. A., Rizvi, N. A., Lesokhin, A. M., et al. (2013). Nivolumab plus ipilimumab in advanced melanoma. *N. Engl. J. Med.* 369, 122–133. doi: 10.1056/NEJMoa1302369
- Wu, A. T., Srivastava, P., Yadav, V. K., Tzeng, D. T., Iamsaard, S., Su, C.-Y., et al. (2020). Ovatodiolide, isolated from *Anisomeles indica*, suppresses bladder carcinogenesis through suppression of mTOR/β-catenin/CDK6 and exosomal miR-21 derived from M2 tumor-associated macrophages. *Toxicol. Appl. Pharmacol.* 401:115109.
- Wu, D., Zhuo, L., and Wang, X. (2017). Metabolic reprogramming of carcinoma-associated fibroblasts and its impact on metabolic heterogeneity of tumors. *Semin. Cell Dev. Biol.* 64, 125–131. doi: 10.1016/j.semcdb.2016.11.003
- Wu, J., Li, G., Li, L., Li, D., Dong, Z., and Jiang, P. (2021). Asparagine enhances LCK signalling to potentiate CD8+ T-cell activation and anti-tumour responses. *Nat. Cell Biol.* 23, 75–86. doi: 10.1038/s41556-020-00615-4
- Xia, Y., Jiang, L., and Zhong, T. (2018). The role of HIF-1α in chemo-/radioresistant tumors. *OncoTargets Ther.* 11, 3003–3011. doi: 10.2147/OTT.S158206
- Xie, N., Zhang, L., Gao, W., Huang, C., Huber, P. E., Zhou, X., et al. (2020). NAD(+) metabolism: pathophysiologic mechanisms and therapeutic potential. *Signal Transduct. Target. Ther.* 5:227. doi: 10.1038/s41392-020-00311-7
- Xu, M., Liu, M., Du, X., Li, S., Li, H., Li, X., et al. (2015). Intratumoral delivery of IL-21 overcomes Anti-Her2/Neu resistance through shifting tumor-associated macrophages from M2 to M1 Phenotype. *J. Immunol.* 194, 4997–5006. doi: 10.4049/jimmunol.1402603
- Yamada, K., Maishi, N., Akiyama, K., Towfik Alam, M., Ohga, N., Kawamoto, T., et al. (2015). CXCL12–CXCR7 axis is important for tumor endothelial cell angiogenic property. *Int. J. Cancer* 137, 2825–2836.
- Yamashita, M., Ogawa, T., Zhang, X., Hanamura, N., Kashikura, Y., Takamura, M., et al. (2012). Role of stromal myofibroblasts in invasive breast cancer: stromal expression of alpha-smooth muscle actin correlates with worse clinical outcome. *Breast Cancer* 19, 170–176. doi: 10.1007/s12282-010-0234-5
- Yang, E., Wang, X., Gong, Z., Yu, M., Wu, H., and Zhang, D. (2020). Exosome-mediated metabolic reprogramming: the emerging role in tumor microenvironment remodeling and its influence on cancer progression. *Signal Transduct. Target. Ther.* 5:242. doi: 10.1038/s41392-020-00359-5
- Yang, G., Shi, R., and Zhang, Q. (2020). Hypoxia and oxygen-sensing signaling in gene regulation and cancer progression. *Int. J. Mol. Sci.* 21:8162. doi: 10.3390/ijms21218162
- Yang, Y., Neo, S. Y., Chen, Z., Cui, W., Chen, Y., Guo, M., et al. (2020). Thioredoxin activity confers resistance against oxidative stress in tumor-infiltrating NK cells. *J. Clin. Invest.* 130, 5508–5522. doi: 10.1172/jci137585
- Yang, J., Lu, Y., Lin, Y. Y., Zheng, Z. Y., Fang, J. H., He, S., et al. (2016). Vascular mimicry formation is promoted by paracrine TGF-β and SDF1 of cancer-associated fibroblasts and inhibited by miR-101 in hepatocellular carcinoma. *Cancer Lett.* 383, 18–27. doi: 10.1016/j.canlet.2016.09.012
- Yarnold, J., and Brotons, M. C. (2010). Pathogenetic mechanisms in radiation fibrosis. *Radiother. Oncol.* 97, 149–161. doi: 10.1016/j.radonc.2010.09.002
- Yin, W. M., Li, Y. W., Gu, Y. Q., and Luo, M. (2020). Nanoengineered targeting strategy for cancer immunotherapy. *Acta Pharmacol. Sin.* 41, 902–910. doi: 10.1038/s41401-020-0417-3
- Yin, Y., Yao, S., Hu, Y., Feng, Y., Li, M., Bian, Z., et al. (2017). The immune-microenvironment confers chemoresistance of colorectal cancer through macrophage-derived IL6. *Clin. Cancer Res.* 23, 7375–7387. doi: 10.1158/1078-0432.Ccr-17-1283
- Yonenaga, Y., Mori, A., Onodera, H., Yasuda, S., Oe, H., Fujimoto, A., et al. (2005). Absence of smooth muscle actin-positive pericyte coverage of tumor vessels correlates with hematogenous metastasis and prognosis of colorectal cancer patients. *Oncology* 69, 159–166.
- Yoshizaki, T., Kondo, S., Wakisaka, N., Muro, S., Endo, K., Sugimoto, H., et al. (2013). Pathogenic role of Epstein-Barr virus latent membrane protein-1 in the development of nasopharyngeal carcinoma. *Cancer Lett.* 337, 1–7. doi: 10.1016/j.canlet.2013.05.018
- You, Y., Shan, Y., Chen, J., Yue, H., You, B., Shi, S., et al. (2015). Matrix metalloproteinase 13-containing exosomes promote nasopharyngeal carcinoma metastasis. *Cancer Sci.* 106, 1669–1677. doi: 10.1111/cas.12818
- Yu, X., Lao, Y., Teng, X. L., Li, S., Zhou, Y., Wang, F., et al. (2018). SENP3 maintains the stability and function of regulatory T cells via BACH2 deSUMOylation. *Nat. Commun.* 9:3157. doi: 10.1038/s41467-018-05676-6
- Yuan, M.-M., Xu, Y.-Y., Chen, L., Li, X.-Y., Qin, J., and Shen, Y. (2015). TLR3 expression correlates with apoptosis, proliferation and angiogenesis in hepatocellular carcinoma and predicts prognosis. *BMC Cancer* 15:245. doi: 10.1186/s12885-015-1262-5
- Zaidi, M., Fu, F., Cococari, D., McKee, T. D., and Wouters, B. G. (2019). Quantitative visualization of hypoxia and proliferation gradients within histological tissue sections. *Front. Bioeng. Biotechnol.* 7:397. doi: 10.3389/fbioe.2019.00397
- Zeng, Z., Li, Y., Pan, Y., Lan, X., Song, F., Sun, J., et al. (2018). Cancer-derived exosomal miR-25-3p promotes pre-metastatic niche formation by inducing vascular permeability and angiogenesis. *Nat. Commun.* 9:5395. doi: 10.1038/s41467-018-07810-w
- Zhang, B., Fu, D., Xu, Q., Cong, X., Wu, C., Zhong, X., et al. (2018). The senescence-associated secretory phenotype is potentiated by feedforward regulatory mechanisms involving Zscan4 and TAK1. *Nat. Commun.* 9:1723. doi: 10.1038/s41467-018-04010-4
- Zhang, D., Li, L., Jiang, H., Li, Q., Wang-Gillam, A., Yu, J., et al. (2018). Tumor-stroma IL1β-IRAK4 feedforward circuitry drives tumor fibrosis, chemoresistance, and poor prognosis in pancreatic cancer. *Cancer Res.* 78, 1700–1712. doi: 10.1158/0008-5472.Can-17-1366
- Zhang, H., Ozaki, I., Mizuta, T., Matsushashi, S., Yoshimura, T., Hisatomi, A., et al. (2002). β1-integrin protects hepatoma cells from chemotherapy induced apoptosis via a mitogen-activated protein kinase dependent pathway. *Cancer* 95, 896–906. doi: 10.1002/cncr.10751
- Zhang, J., Pavlova, N. N., and Thompson, C. B. (2017). Cancer cell metabolism: the essential role of the nonessential amino acid, glutamine. *Embo J.* 36, 1302–1315. doi: 10.15252/embj.201696151
- Zhang, Q., Bing, Z., Tian, J., Wang, X., Liu, R., Li, Y., et al. (2019). Integrating radiosensitive genes improves prediction of radiosensitivity or radioresistance in patients with oesophageal cancer. *Oncol. Lett.* 17, 5377–5388. doi: 10.3892/ol.2019.10240

- Zhang, Z., Yu, X., Wang, Z., Wu, P., and Huang, J. (2015). Anthracyclines potentiate anti-tumor immunity: a new opportunity for chemoimmunotherapy. *Cancer Lett.* 369, 331–335. doi: 10.1016/j.canlet.2015.10.002
- Zhao, J. (2016). Cancer stem cells and chemoresistance: the smartest survives the raid. *Pharmacol. Ther.* 160, 145–158. doi: 10.1016/j.pharmthera.2016.02.008
- Zhao, J., Du, F., Luo, Y., Shen, G., Zheng, F., and Xu, B. (2015). The emerging role of hypoxia-inducible factor-2 involved in chemo/radioresistance in solid tumors. *Cancer Treat. Rev.* 41, 623–633. doi: 10.1016/j.ctrv.2015.05.004
- Zhao, P., Wang, Y., Kang, X., Wu, A., Yin, W., Tang, Y., et al. (2018). Dual-targeting biomimetic delivery for anti-glioma activity via remodeling the tumor microenvironment and directing macrophage-mediated immunotherapy. *Chem. Sci.* 9, 2674–2689.
- Zhao, Q., Tan, B. B., Li, Y., Fan, L. Q., Yang, P. G., and Tian, Y. (2016). Enhancement of drug sensitivity by knockdown of HIF-1 α in gastric carcinoma cells. *Oncol. Res.* 23, 129–136. doi: 10.3727/096504015x14500513118029
- Zhen, Z., Tang, W., Wang, M., Zhou, S., Wang, H., Wu, Z., et al. (2017). Protein nanocage mediated fibroblast-activation protein targeted photoimmunotherapy to enhance cytotoxic t cell infiltration and tumor control. *Nano Lett.* 17, 862–869. doi: 10.1021/acs.nanolett.6b04150
- Zheng, H., Zhao, W., Yan, C., Watson, C. C., Massengill, M., Xie, M., et al. (2016). HDAC inhibitors enhance T-Cell chemokine expression and augment response to PD-1 immunotherapy in lung adenocarcinoma. *Clin. Cancer Res.* 22, 4119–4132. doi: 10.1158/1078-0432.Ccr-15-2584
- Zheng, P., Chen, L., Yuan, X., Luo, Q., Liu, Y., Xie, G., et al. (2017). Exosomal transfer of tumor-associated macrophage-derived miR-21 confers cisplatin resistance in gastric cancer cells. *J. Exp. Clin. Cancer Res.* 36:53.
- Zhong, A., Cheng, C. S., Kai, J., Lu, R., and Guo, L. (2020). Clinical significance of glucose to lymphocyte ratio (GLR) as a prognostic marker for patients with pancreatic cancer. *Front. Oncol.* 10:520330. doi: 10.3389/fonc.2020.520330
- Zhong, Z., and Virshup, D. M. (2020). Wnt signaling and drug resistance in cancer. *Mol. Pharmacol.* 97, 72–89. doi: 10.1124/mol.119.117978
- Zhou, Z., Piao, Y., Hao, L., Wang, G., Zhou, Z., and Shen, Y. (2019). Acidity-responsive shell-sheddable camptothecin-based nanofibers for carrier-free cancer drug delivery. *Nanoscale* 11, 15907–15916.
- Zingg, D., Arenas-Ramirez, N., Sahin, D., Rosalia, R. A., Antunes, A. T., Haeusel, J., et al. (2017). The histone methyltransferase Ezh2 controls mechanisms of adaptive resistance to tumor immunotherapy. *Cell Rep.* 20, 854–867. doi: 10.1016/j.celrep.2017.07.007

Conflict of Interest: The authors declare that the research was conducted in the absence of any commercial or financial relationships that could be construed as a potential conflict of interest.

Copyright © 2021 Wu, Gao, Su, Nice, Zhang, Lin and Xie. This is an open-access article distributed under the terms of the Creative Commons Attribution License (CC BY). The use, distribution or reproduction in other forums is permitted, provided the original author(s) and the copyright owner(s) are credited and that the original publication in this journal is cited, in accordance with accepted academic practice. No use, distribution or reproduction is permitted which does not comply with these terms.



Identification of an Immune-Related Risk Signature Correlates With Immunophenotype and Predicts Anti-PD-L1 Efficacy of Urothelial Cancer

OPEN ACCESS

Edited by:

Wei Zhao,
Chengdu Medical College, China

Reviewed by:

An Zhao,
University of Chinese Academy
of Sciences, China
Qing Zhang,
Nanjing Drum Tower Hospital, China

*Correspondence:

Jiazheng Cao
530694776@qq.com
Junhang Luo
luojunh@mail.sysu.edu.cn
Wei Chen
chenw3@mail.sysu.edu.cn

[†] These authors have contributed
equally to this work

Specialty section:

This article was submitted to
Molecular and Cellular Oncology,
a section of the journal
Frontiers in Cell and Developmental
Biology

Received: 28 December 2020

Accepted: 03 February 2021

Published: 18 March 2021

Citation:

Li P, Hao S, Ye Y, Wei J, Tang Y,
Tan L, Liao Z, Zhang M, Li J, Gui C,
Xiao J, Huang Y, Chen X, Cao J, Luo J
and Chen W (2021) Identification
of an Immune-Related Risk Signature
Correlates With Immunophenotype
and Predicts Anti-PD-L1 Efficacy
of Urothelial Cancer.
Front. Cell Dev. Biol. 9:646982.
doi: 10.3389/fcell.2021.646982

Pengju Li^{1,2†}, Shihui Hao^{3†}, Yongkang Ye^{4†}, Jinhuan Wei^{1†}, Yiming Tang¹, Lei Tan¹,
Zhuangyao Liao¹, Mingxiao Zhang¹, Jiaying Li¹, Chengpeng Gui¹, Jiefei Xiao⁵,
Yong Huang¹, Xu Chen¹, Jiazheng Cao^{6*}, Junhang Luo^{1,2*} and Wei Chen^{1*}

¹ Department of Urology, First Affiliated Hospital of Sun Yat-sen University, Guangzhou, China, ² Institute of Precision
Medicine, The First Affiliated Hospital, Sun Yat-sen University, Guangzhou, China, ³ State Key Laboratory of Oncology
in South China, Collaborative Innovation Center for Cancer Medicine, Sun Yat-sen University Cancer Center, Guangzhou,
China, ⁴ Department of Urology, Dongguan People's Hospital, Affiliated to Southern Medical University, Dongguan, China,
⁵ Department of Extracorporeal Circulation, First Affiliated Hospital of Sun Yat-sen University, Guangzhou, China,
⁶ Department of Urology, Jiangmen Central Hospital, Affiliated Jiangmen Hospital of Sun Yat-sen University, Jiangmen, China

Immune checkpoint inhibitor (ICI) treatment has been used to treat advanced urothelial cancer. Molecular markers might improve risk stratification and prediction of ICI benefit for urothelial cancer patients. We analyzed 406 cases of bladder urothelial cancer from The Cancer Genome Atlas (TCGA) data set and identified 161 messenger RNAs (mRNAs) as differentially expressed immunity genes (DEIGs). Using the LASSO Cox regression model, an eight-mRNA-based risk signature was built. We validated the prognostic and predictive accuracy of this immune-related risk signature in 348 metastatic urothelial cancer (mUC) samples treated with anti-PD-L1 (atezolizumab) from IMvigor210. We built an immune-related risk signature based on the eight mRNAs: ANXA1, IL22, IL9R, KLRK1, LRP1, NRG3, SEMA6D, and STAP2. The eight-mRNA-based risk signature successfully categorizes patients into high-risk and low-risk groups. Overall survival was significantly different between these groups, regardless if the initial TCGA training set, the internal TCGA testing set, all TCGA set, or the ICI treatment set. The hazard ratio (HR) of the high-risk group to the low-risk group was 3.65 ($p < 0.0001$), 2.56 ($p < 0.0001$), 3.36 ($p < 0.0001$), and 2.42 ($p = 0.0009$). The risk signature was an independent prognostic factor for prediction survival. Moreover, the risk signature was related to immunity characteristics. In different tumor mutational burden (TMB) subgroups, it successfully categorizes patients into high-risk and low-risk groups, with significant differences of clinical outcome. Our eight-mRNA-based risk signature is a stable biomarker for urothelial cancer and might be able to predict which patients benefit from ICI treatment. It might play a role in precision individualized immunotherapy.

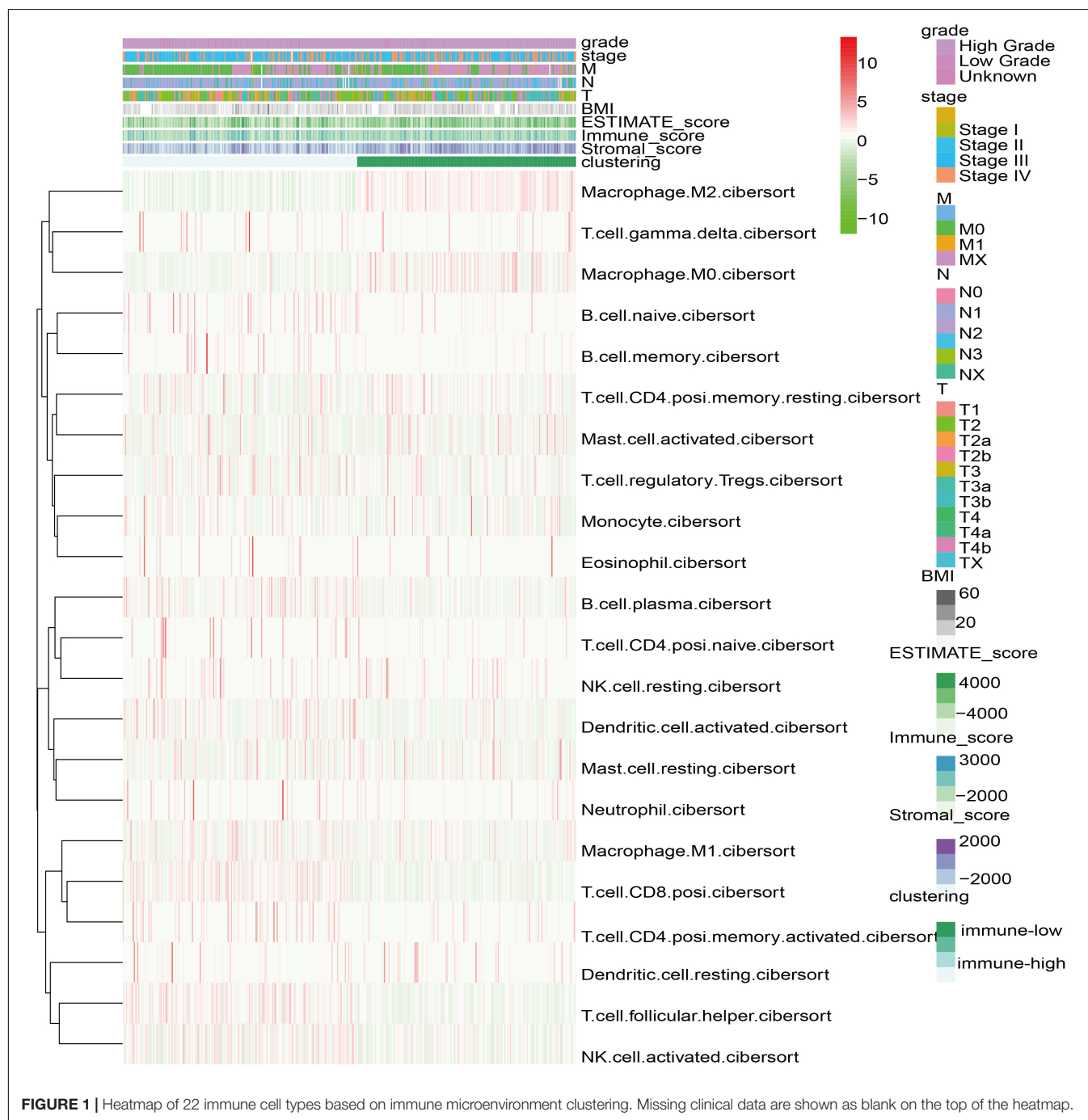
Keywords: immune-related risk signature, immunity gene, immune checkpoint inhibitor, urothelial cancer, tumor microenvironment

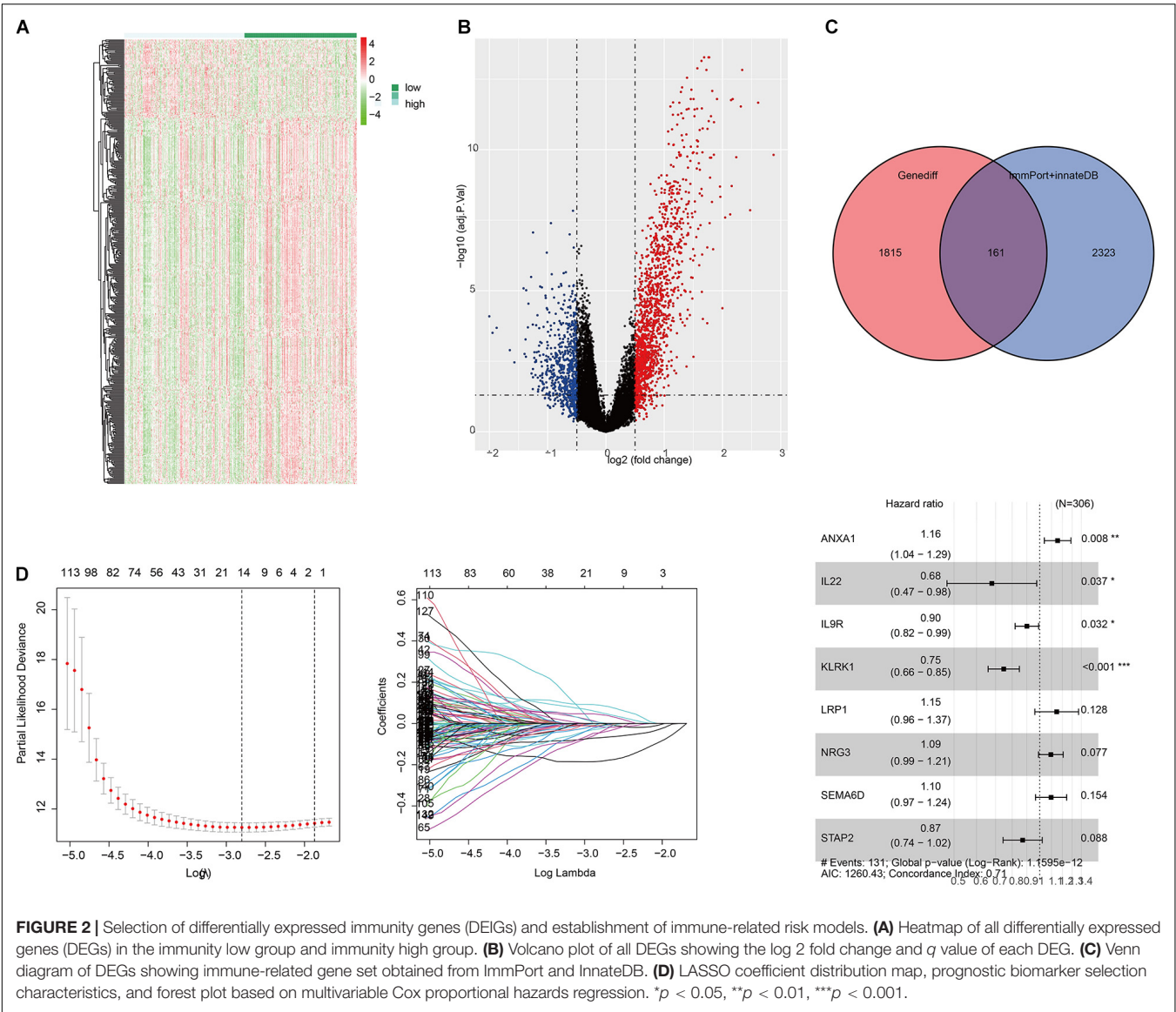
INTRODUCTION

Bladder cancer is a common tumor of the urinary system; 90% of the pathological types are urothelial cancer (UC). For bladder cancer patients with local progression or distant metastasis, cisplatin combined with gemcitabine is the first choice. However, the effect is not satisfactory. The median survival time of patients is only 15 months, and the 5 years survival rate is difficult to reach 15% (Griffiths et al., 2011). In recent years, with the rapid development of tumor immune checkpoint inhibitors (ICIs),

especially the rapid development of programmed cell death molecule 1 (PD-1)/programmed cell death molecule ligand 1 (PD-L1) inhibitors, the treatment of bladder cancer patients has brought new options. In patients with metastatic UC (mUC) who cannot receive cisplatin chemotherapy and PD-L1 positive, ICIs can already be used as a first-line treatment (Nadal and Bellmunt, 2019).

Although it is proved the efficacy of PD-1/PD-L1 inhibitors is better than that of traditional platinum-based chemotherapy (Bellmunt et al., 2017; Sidaway, 2017), studies have confirmed





that only about 20% of solid tumor patients can benefit from the treatment (Braun et al., 2016). Therefore, it is becoming more and more important to identify and verify biomarkers that can accurately predict ICI treatment efficacy. There have been some clinical studies exploring the corresponding biomarkers, such as PD-L1 expression (Powles et al., 2014), CD8⁺ T cell (Ghatalia and Plimack, 2019), tumor mutational burden (TMB) (Yarchoan et al., 2017), and microsatellite instability (MSI) (Dudley et al., 2016). However, these biomarkers have shortcomings in clinical application. In addition, multi-factor joint prediction may be able to provide better prediction results (Mazzaschi et al., 2020).

In this study, we analyzed the messenger RNA (mRNA) transcriptome data of 406 bladder cancer patients from The Cancer Genome Atlas (TCGA) data combined with immune-related genes to establish an immune-related risk signature, and we verified the 348 mUC patients receiving anti-PD-L1 therapy

from IMvigor210 study. We emphasized the strong predictive power of the risk score in selecting patients with good response to atezolizumab and verified its role in ICI treatment.

TABLE 1 | Characteristics of differentially expressed immunity genes (DEIGs) in the risk signature.

	coef	HR	HR.95L	p-value
ANXA1	0.1444935	1.16	1.04–1.29	0.0085
IL22	−0.3872357	0.68	0.47–0.98	0.0365
IL9R	−0.1038636	0.9	0.82–0.99	0.0325
KLRK1	−0.2910349	0.75	0.66–0.85	< 0.0001
LRP1	0.13726797	1.15	0.96–1.37	0.128
NRG3	0.09008937	1.09	0.99–1.21	0.0771
SEMA6D	0.0918811	1.1	0.97–1.24	0.1539
STAP2	−0.1380731	0.87	0.74–1.02	0.0878

MATERIALS AND METHODS

Clinical Cohorts and Data Sets

The gene expression sequence matrix and clinical characteristics of 406 bladder cancer patients can be downloaded from TCGA data set¹. The immune gene sets come from the ImmPort² and InnateDB³ data sets (Breuer et al., 2013; Bhattacharya et al., 2014). Clinical information and gene transcription information of 348 patients with mUC who received ICI treatment are downloaded

¹ <https://portal.gdc.cancer.gov>

² <https://www.immport.org>

³ <http://www.innatedb.com>

from⁴ (Mariathasan et al., 2018). The infiltration of 22 immune cells was downloaded from the TIMER database⁵ and Dongqiang Zeng's research (Li T. et al., 2020; Zeng et al., 2020).

Bioinformatic Analysis

R package DESeq2 was used for gene expression differential analysis, and R package clusterProfiler for Gene Ontology/Kyoto Encyclopedia of Genes and Genomes/Gene Set Enrichment Analysis (GO/KEGG/GSEA) function enrichment analysis and visualization (Subramanian et al., 2005; Love et al., 2014). The

⁴ <http://research-pub.gene.com/IMvigor210CoreBiologies>

⁵ <http://timer.cistrome.org>

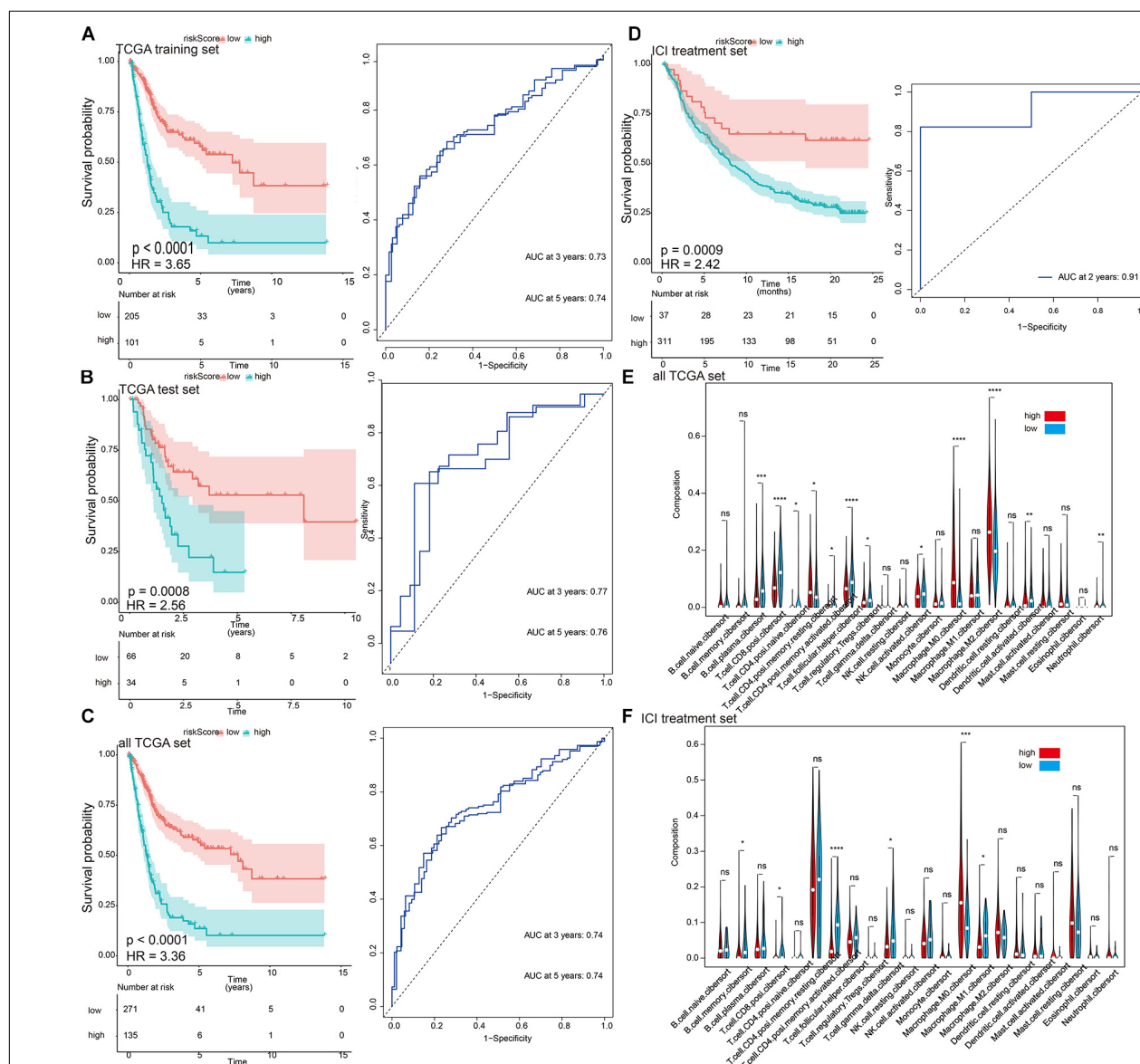


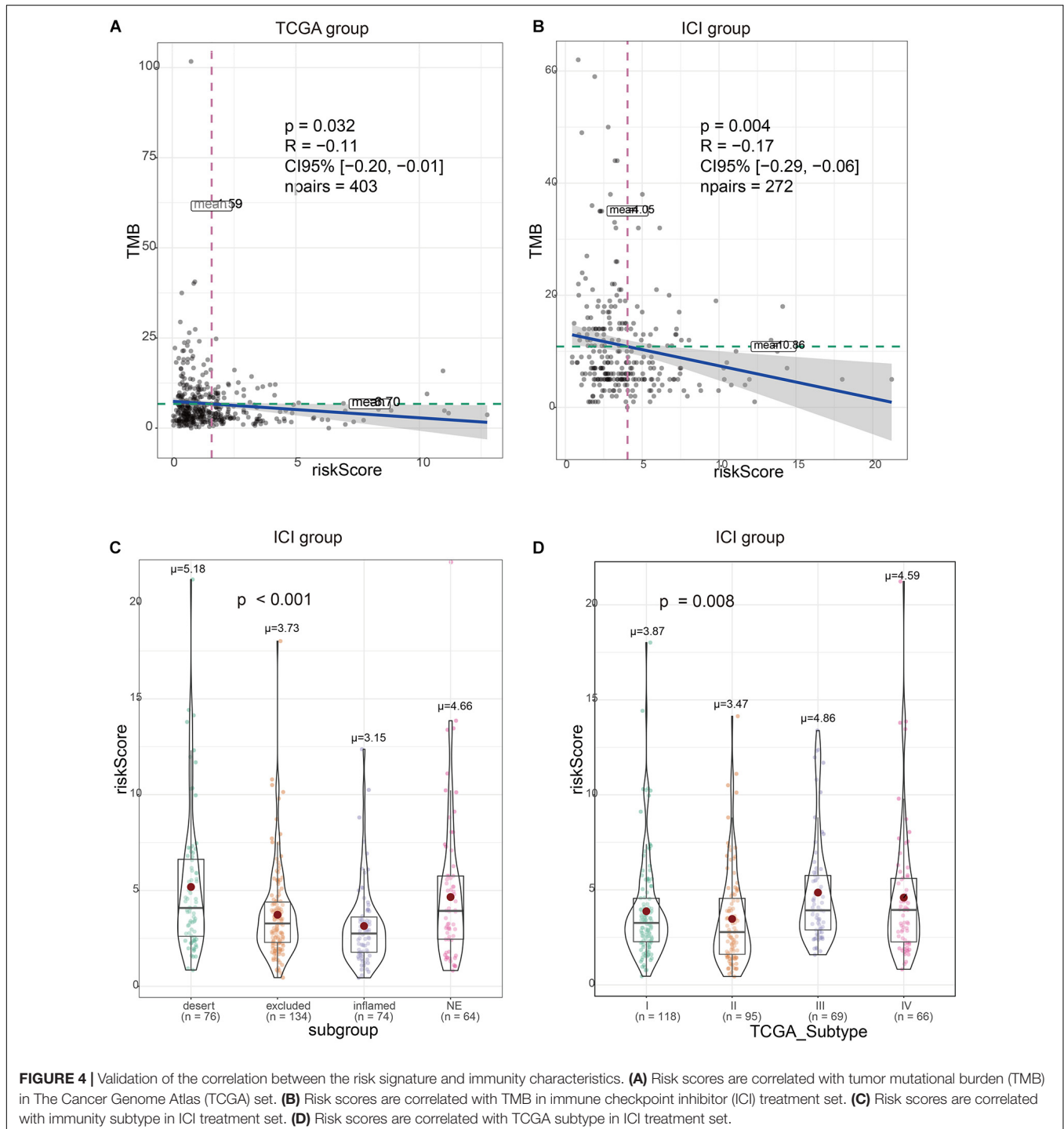
FIGURE 3 | The characterization of the training and validation cohorts highlights that risk scores are potential biomarkers. **(A–D)** Kaplan–Meier survival analysis and time-dependent receiver operating characteristic (ROC) curve of the risk signature. The risk score derived from the constructed model is significantly correlated with overall survival. **(E,F)** The infiltration trends of 22 immune cells are consistent in the two data sets. * $p < 0.05$, ** $p < 0.01$, *** $p < 0.001$, **** $p < 0.0001$.

ggstatsplot package was used to evaluate the relationship between risk score, TMB, and immunophenotype.

Establishment and Evaluation of Risk Prediction Model

We randomly divide the samples in TCGA cohort into training/validation (3:1) groups to identify and evaluate

predictors. The “glmnet” R package was used for LASSO analysis, and 14 immune-related genes were identified (Ternes et al., 2016). Then we conducted multiple Cox regression analysis to establish an eight-mRNA-based risk prediction model. Use the formula to generate the risk score for each patient: $\text{risk score} = \text{EXP}_1 * \beta_1 + \text{EXP}_2 * \beta_2 + \dots + \text{EXP}_N * \beta_N$, where “EXP” represents the expression level of key genes and β is the corresponding regression coefficient.



The “timeROC” package was used to establish the receiver operating characteristic (ROC) curve and verify the area value under it (AUC). Draw a Kaplan–Meier curve to show the association of risk scores and potential prognostic genes with patient survival.

Statistical Analysis

The Kaplan–Meier method was used to analyze the correlation between relative risk factors with patient survival. Statistical tests were performed using R software, version 3.6. 2 (R Foundation for Statistical Computing;

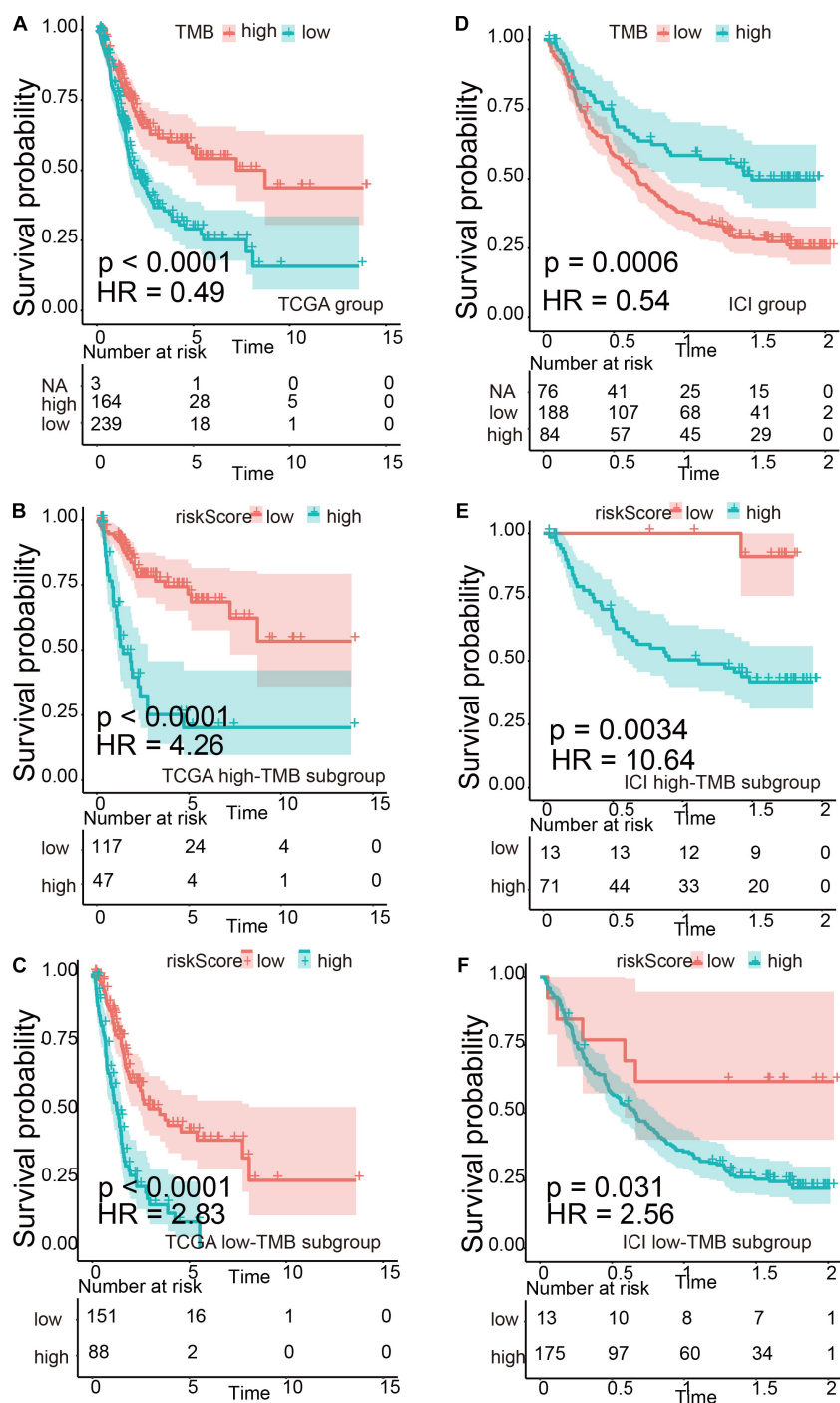


FIGURE 5 | Verification of the risk signature to be used as a stable predictor. (A–C) Kaplan–Meier survival analysis based on tumor mutational burden (TMB) levels and TMB subgroups in The Cancer Genome Atlas (TCGA) data set. (D–F) Kaplan–Meier survival analysis based on TMB levels and TMB subgroups in the immune checkpoint inhibitor (ICI) treatment set.

Vienna, Austria). Values of $p < 0.05$ were considered statistically significant.

RESULTS

Describe Immune-Related Gene Features and Construct Immune-Related Prediction Models

Based on the Cibersort algorithm, the infiltration levels of 22 immune cells in 406 bladder cancer patients in TCGA data set were evaluated. The fuzzy clustering algorithm divided the samples into two categories: 210 samples were clustered into cluster 1 and 196 samples were clustered into cluster 2 (Figure 1). Cluster 1 had high-level immune characteristics (high-immunity group), and cluster 2 had low-level immune characteristics (low-immunity group). Missing clinical data are shown as blank on the top of the heatmap.

We were trying to study immune-related genes stratified by immune phenotype and their prognostic potential and to establish a good immunological prediction model, which can make more accurate individual risk stratification and prognosis prediction for UC patients. After preliminary screening through single-factor regression analysis and difference analysis based on immunity clustering, a total of 1,976 genes were identified as differentially expressed genes (DEGs). All DEG expression levels are shown in Figure 2A, and the log2 and p -values of all DEGs are shown in Figure 2B. Subsequently, 161 genes were identified as differentially expressed immunity genes (DEIGs) based on ImmPort and InnateDB databases (Figure 2C). In order to further explore the prognostic significance of DEIGs, 161 important genes were used for multiple LASSO regression and multiple Cox regression analysis (Figure 2D), and eight key DEIGs were identified. Distribution of each DEIG in TCGA set and ICI treatment set is shown in Supplementary Figure 1. The Kaplan–Meier curve of each DEIG in TCGA set is shown in Supplementary Figure 2 [ANXA1: $p < 0.0001$, hazard ratio (HR) = 2.02; IL22: $p < 0.0001$, HR = 0.50; IL9R: $p < 0.0001$, HR = 0.71; KLRK1: $p < 0.0001$, HR = 0.54; LRP1: $p = 0.0051$, HR = 1.96; NRG3: $p = 0.00065$, HR = 1.40; SEMA6D: $p = 0.01$, HR = 1.65; STAP2: $p = 0.00029$, HR = 0.68]. Finally, according to the relative coefficient in the multiple regression analysis, the risk score was calculated according to the following formula: $(0.144493498 * ANXA1) + (-0.387235675 * IL22) + (-0.103863619 * IL9R) + (-0.291034924 * KLRK1) + (0.137267967 * LRP1) + (0.090089369 * NRG3) + (0.091881101 * SEMA6D) + (-0.138073124 * STAP2)$ (Table 1).

Survival Analysis, Prognostic Value, and Immune Infiltration Verification of the Risk Signature

The prognostic value of eight DEIG signatures was further evaluated in three verification sets (TCGA test set, all TCGA set, and independent ICI treatment set). We calculated the risk score of each patient using the same formula, and we divided them

into high-risk and low-risk groups by 1.54 as a cutoff. Consistent with the results of TCGA training set, the prognosis of high-risk patients in the three validation sets was worse than that of patients in the low-risk group (Figures 3A–D, left; TCGA training set: $p < 0.0001$, HR = 3.65; TCGA test set: $p < 0.0001$, HR = 2.56; all TCGA set: $p < 0.0001$, HR = 3.36; ICI treatment set: $p = 0.0009$, HR = 2.42). The results of the time-dependent ROC curve analysis verified the predictive value of the established risk model (Figures 3A–D, right), suggesting that the prognosis prediction for 3–5 years was more robust. The univariate and multivariate Cox analyses of TCGA set showed that the risk signature can be used as an independent prognostic factor (Supplementary Table 1). We examined the correlation between risk signature and the bladder cancer immune microenvironment. Both TCGA and ICI data sets showed a relatively consistent trend of infiltration. In terms of immune cell infiltration, such as T.cell.CD8.positive, T.cell.CD4.activated, and Macrophage.M0, the infiltration trend was the same in the two data sets. The differences were statistically significant (Figures 3E,F).

Verification and Comparison of the Correlation Between the Risk Signature and Immune Checkpoint Inhibitor Treatment Efficacy

There was a significant correlation between the risk signature and TMB, regardless if in TCGA or ICI treatment set (Figures 4A,B). At the same time, the immune subtypes classified according to CD8 cell infiltration (desert, excluded, and inflamed) were also obviously related to the risk signature (Figure 4C). TCGA type II subgroup had the lowest risk score (Figure 4D). This is consistent with the previous results (Mariathasan et al., 2018).

We divided TMB into high-risk and low-risk groups and then subdivided them into subgroups based on the risk scores level (TCGA set: $p < 0.0001$, HR = 0.49; ICI treatment set: $p = 0.0006$, HR = 0.54). The results suggested that even in the TMB subgroup, the risk signature still remained its prognostic ability, regardless if in TCGA or ICI treatment set (Figure 5, TCGA high-TMB group: $p < 0.0001$, HR = 4.26; TCGA low-TMB group: $p < 0.0001$, HR = 2.83; ICI treatment high-TMB group: $p = 0.0034$, HR = 10.64; ICI treatment low-TMB group: $p = 0.031$, HR = 2.56). Multivariate risk regression also confirmed this result (Table 2).

Gene Ontology/Kyoto Encyclopedia of Genes and Genomes/Gene Set Enrichment Analysis

In order to further explore the molecular mechanisms related to risk scores, we divided TCGA cohort patients into high-risk

TABLE 2 | Multivariate Cox regression of risk scores and tumor mutational burden (TMB) in immune checkpoint inhibitor (ICI) treatment set.

	HR	95%CI	p -value
Risk score	4.83	2.14–10.93	0.0002
TMB	0.96	0.94–0.99	0.0012

and low-risk groups. The results of GO and KEGG suggested that the risk signature was related to the extracellular matrix and energy metabolism changes in the tumor microenvironment (Figures 6A,B). GSEA results suggested that the high-risk group is positively correlated with steroid metabolism and YP450 metabolism, while pathways such as cytokine interaction and immune response are positively correlated with low-scoring risks (Figure 6C).

DISCUSSION

As a new treatment method, ICI has initially proven efficacy and safety in the treatment of UC. Unfortunately, not all

patients with cancer respond to ICI treatment. In previous studies, the use of risk signature derived from the gene transcriptome to monitor the immune status of tumors and guide individualized treatment has proven to be meaningful (Li et al., 2017; Cristescu et al., 2018; Wang et al., 2019). Therefore, the development of meaningful genetic markers to monitor the immune status of patients not only can monitor the prognosis of patients but also can screen out potential ICI responding patients, avoiding the waste of medical resources and overtreatment. In this study, we validated immune-related gene risk model based on eight DEIGs, which proved to be a reliable indicator of favorable ICI efficacy and can identify bladder cancer patients with poor prognosis. Our results showed that the prognosis is worse if the risk score is higher. At the

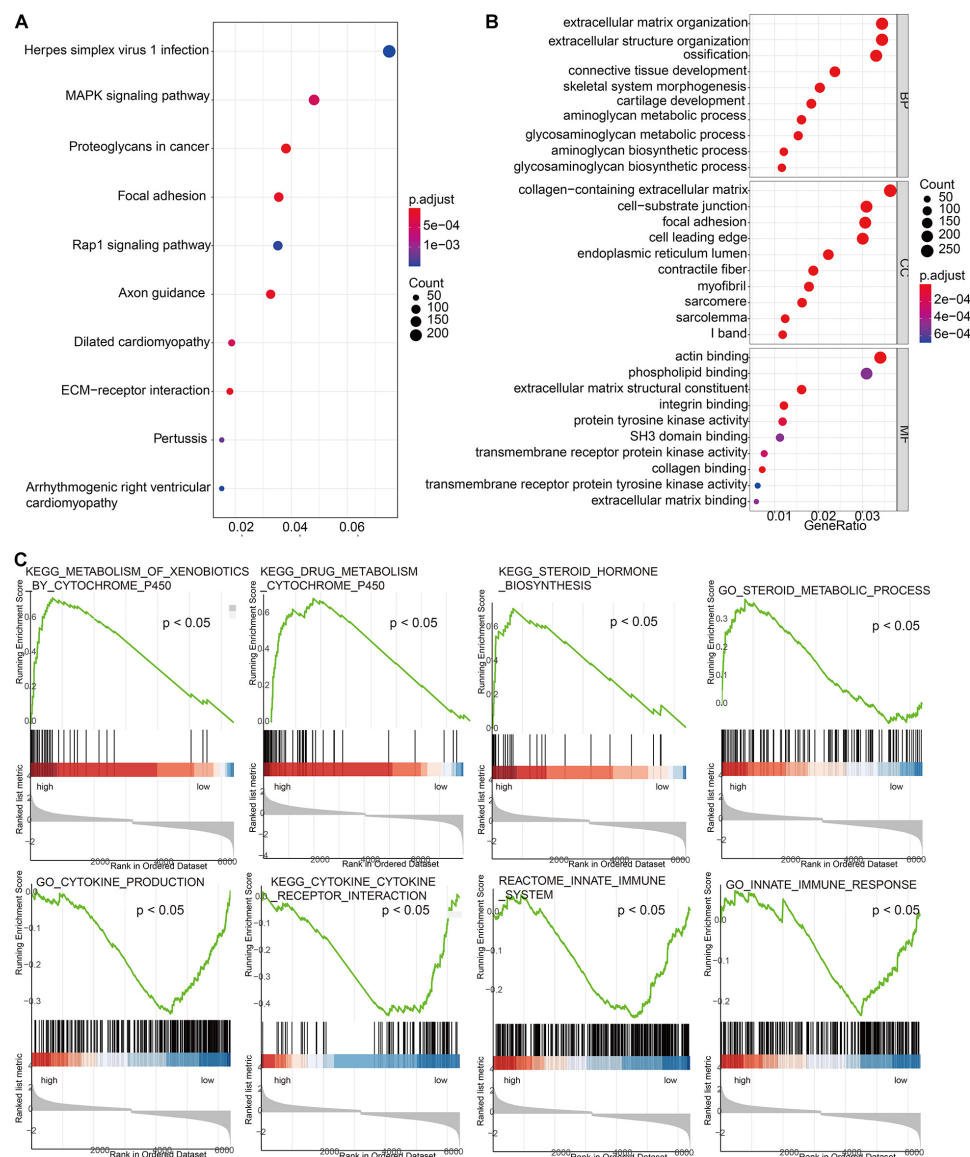


FIGURE 6 | Exploration of the molecular mechanisms related to risk scores. **(A)** Gene Ontology enrichment analysis based on risk scores. **(B)** Kyoto Encyclopedia of Genes and Genomes (KEGG) enrichment analysis based on risk scores. **(C)** Gene Set Enrichment Analysis (GSEA) based on risk scores.

same time, the time-dependent ROC curve results suggested that the 3–5 years' prognosis prediction for UC patients was more robust. In terms of tumor immune cell infiltration, whether in TCGA group or the ICI treatment group, the differences in T.cell.CD8.positive, T.cell.CD4.activated, and Macrophage.M0 were statistically significant. Patients in the high-risk group had significantly lower representation of T.cell.CD8.positive and T.cell.CD4.activated and significantly higher abundance of Macrophage.M0. This is also consistent with the results of other studies (Li W. et al., 2020; Lin et al., 2020).

PD-L1 is currently the most mature and in-depth biomarker, but the results obtained in different ICI studies are not consistent. It may be due to the different monitoring methods and positive standards between different platforms, and the evaluation is subjective. At present, due to technical requirements, it is difficult to apply TMB to routine clinical practice (Fenizia et al., 2018). In addition, TMB has not yet proven its predictive or prognostic value for overall survival (Addeo et al., 2019). According to the immune microenvironment, most solid tumors can be divided into three different immunological phenotypes: immune inflamed, immune excluded, or immune desert (Chen and Mellman, 2013; Hegde et al., 2016). Studies have shown that immune inflamed subtypes have the best response to ICI treatments (such as anti-PD-1 and anti-CTLA-4) (Mariathasan et al., 2018; Galon and Bruni, 2019). The immune-related risk signature we established was significantly correlated with TMB and immunophenotype. A lower risk score means a higher TMB, a better response, and a better prognosis. At last, the K-M curve of TMB subtype showed that the risk signature was able to be used as a stable predictor. In order to further clarify the mechanism of immune risk score, we subsequently used TCGA data set to conduct GO, KEGG, and GSEA. The results of GO and KEGG show that the risk score is related to the energy metabolism and synthesis of the tumor microenvironment, and the formation and activation of extracellular matrix. In the analysis of GSEA results, we can see that the synthesis and metabolism of steroids are positively correlated with high-scoring risks, while pathways such as cytokine interaction and immune response are positively correlated with low-scoring risks. This is consistent with the results of other studies. Zeng et al. (2020) found that the defect of M1 macrophage function is related to poor prognosis of UC immunotherapy, and it is also positively related to steroid synthesis and metabolism.

Among the eight DEIGs, there are few studies in bladder cancer, but some of their interactions with immunity have been explored and verified in other researches. ANXA1 can enhance the function of regulatory T cells (Tregs) and reduce the survival rate of patients with breast cancer (Bai et al., 2020). IL-22 producing T cells in colorectal cancer enhance T cell function by recruiting neutrophils, thereby enhancing immune response (Tosti et al., 2020). Th9 cells promote the expansion of CD8⁺ T cells in an IL-9R-dependent manner in colorectal cancer (Wang et al., 2020). CIK cells can target lung cancer cells expressing NKG2D/KLRK1 ligand, and the killing effect can be partially blocked by NKG2D/KLRK1 ligand inhibitors (Yin et al., 2017). The correlation between

LRP1 mRNA expression and patient survival was observed in bladder urothelial carcinoma. At the same time, the LRP1 protein can regulate the immune function by regulating the movement and adhesion of T cells (Gonias et al., 2017; Panezai et al., 2017). STAP2 maintains the cytotoxicity of functional memory CD8⁺ T cells by controlling cytokine signaling inhibitor 3 (Muraoka et al., 2017). SEMA6D act as a modulator in the late stage of the primary immune response (O'Connor et al., 2008).

Although the risk signature based on eight DEIGs embodies a powerful predictive function in selecting patients with good response to atezolizumab, its accuracy and effectiveness should be further verified in a prospective cohort study receiving immunotherapy. In addition, the molecular mechanism of the protein encoded by DEIGs in UC still needs to be explored *in vitro* and *in vivo*.

The risk signature is a stable biomarker that can be used to predict immunotherapy efficacy and immunophenotype determination, and it can be used as a supplement to TMB.

DATA AVAILABILITY STATEMENT

Publicly available datasets were analyzed in this study. This data can be found here: The gene expression sequence matrix and clinical characteristics of 406 bladder cancer patients was downloaded from the TCGA data set (<https://portal.gdc.cancer.gov>). The immune gene sets were downloaded from the Immport (<https://s3.immport.org/release/genelists/GeneList.txt?download=true>) and InnateDB (https://www.innatedb.com/download/innatedb_curated_genes.xls) data sets. Clinical information and gene transcription information of 348 patients with mUC who received ICI treatment was downloaded from <http://research-pub.gene.com/IMvigor210CoreBiologies>. The infiltration of 22 immune cells was downloaded from the TIMER database (http://timer.cistrome.org/infiltration_estimation_for_tcga.csv.gz) and Dongqiang Zeng's research (<https://www.thno.org/v10/p7002/thnov10p7002s2.xlsx>).

AUTHOR CONTRIBUTIONS

JLu and WC designed the study. PL, SH, YY, YT, LT, CG, and JW obtained and assembled data. PL, SH, JLi, JW, YH, ZL, and JC analyzed and interpreted the data. PL, JX, MZ, XC, and WC wrote the report. All authors approved the final version. JC, JLu, and WC are the guarantors.

FUNDING

This study was supported by grants from the National Natural Science Foundation of China (Award Nos. 81725016,

81872094, 81772718, 81602219, 81972376, and 81902576) and the Guangdong Provincial Science and Technology Foundation of China (Award Nos. 2017B020227004 and 2017A030313538).

ACKNOWLEDGMENTS

We thank TCGA, ImmPort, InnateDB, TIMER, study IMvigor210, and Dongqiang Zeng's research for their efforts and for providing the data.

REFERENCES

- Addeo, A., Banna, G. L., and Weiss, G. J. (2019). Tumor mutation burden-from hopes to doubts. *JAMA Oncol.* 5, 934–935. doi: 10.1001/jamaoncol.2019.0626
- Bai, F., Zhang, P., Fu, Y., Chen, H., Zhang, M., Huang, Q., et al. (2020). Targeting ANXA1 abrogates Treg-mediated immune suppression in triple-negative breast cancer. *J. Immunother. Cancer* 8:e000169. doi: 10.1136/jitc-2019-000169
- Bellmunt, J., de Wit, R., Vaughn, D. J., Fradet, Y., Lee, J. L., Fong, L., et al. (2017). Pembrolizumab as second-line therapy for advanced urothelial carcinoma. *N. Engl. J. Med.* 376, 1015–1026. doi: 10.1056/NEJMoa1613683
- Bhattacharya, S., Andorf, S., Gomes, L., Dunn, P., Schaefer, H., Pontius, J., et al. (2014). ImmPort: disseminating data to the public for the future of immunology. *Immunol. Res.* 58, 234–239. doi: 10.1007/s12026-014-8516-1
- Braun, D. A., Burke, K. P., and Van Allen, E. M. (2016). Genomic approaches to understanding response and resistance to immunotherapy. *Clin. Cancer Res.* 22, 5642–5650. doi: 10.1158/1078-0432.CCR-16-0066
- Breuer, K., Foroushani, A. K., Laird, M. R., Chen, C., Sribnaia, A., Lo, R., et al. (2013). InnateDB: systems biology of innate immunity and beyond—recent updates and continuing curation. *Nucleic Acids Res.* 41, D1228–D1233. doi: 10.1093/nar/gks1147
- Chen, D. S., and Mellman, I. (2013). Oncology meets immunology: the cancer-immunity cycle. *Immunity* 39, 1–10. doi: 10.1016/j.immuni.2013.07.012
- Cristescu, R., Mogg, R., Ayers, M., Albright, A., Murphy, E., Yearley, J., et al. (2018). Pan-tumor genomic biomarkers for PD-1 checkpoint blockade-based immunotherapy. *Science* 362, eaar3593. doi: 10.1126/science.aar3593
- Dudley, J. C., Lin, M. T., Le, D. T., and Eshleman, J. R. (2016). Microsatellite instability as a biomarker for PD-1 blockade. *Clin. Cancer Res.* 22, 813–820. doi: 10.1158/1078-0432.CCR-15-1678
- Fenizia, F., Pasquale, R., Roma, C., Bergantino, F., Iannaccone, A., and Normanno, N. (2018). Measuring tumor mutation burden in non-small cell lung cancer: tissue versus liquid biopsy. *Transl. Lung Cancer Res.* 7, 668–677. doi: 10.21037/tlcr.2018.09.23
- Galon, J., and Bruni, D. (2019). Approaches to treat immune hot, altered and cold tumours with combination immunotherapies. *Nat. Rev. Drug Discov.* 18, 197–218. doi: 10.1038/s41573-018-0007-y
- Ghatalia, P., and Plimack, E. (2019). Biomarkers for neoadjuvant checkpoint blockade response in urothelial cancer. *Nat. Med.* 25, 1650–1651. doi: 10.1038/s41591-019-0645-6
- Gonias, S. L., Karimi-Mostowfi, N., Murray, S. S., Mantuano, E., and Gilder, A. S. (2017). Expression of LDL receptor-related proteins (LRPs) in common solid malignancies correlates with patient survival. *PLoS One* 12:e0186649. doi: 10.1371/journal.pone.0186649
- Griffiths, G., Hall, R., Sylvester, R., Raghavan, D., and Parmar, M. K. (2011). International phase III trial assessing neoadjuvant cisplatin, methotrexate, and vinblastine chemotherapy for muscle-invasive bladder cancer: long-term results of the BA06 30894 trial. *J. Clin. Oncol.* 29, 2171–2177. doi: 10.1200/JCO.2010.32.3139
- Hegde, P. S., Karanikas, V., and Evers, S. (2016). The where, the when, and the how of immune monitoring for cancer immunotherapies in the era of checkpoint inhibition. *Clin. Cancer Res.* 22, 1865–1874. doi: 10.1158/1078-0432.CCR-15-1507

SUPPLEMENTARY MATERIAL

The Supplementary Material for this article can be found online at: <https://www.frontiersin.org/articles/10.3389/fcell.2021.646982/full#supplementary-material>

Supplementary Figure 1 | Distribution of each DEIG in TCGA set and ICI treatment set.

Supplementary Figure 2 | Kaplan–Meier curve of each DEIG in TCGA set.

Supplementary Table 1 | Univariate and multivariate Cox regression analysis of clinical pathologic features in TCGA set.

- Li, B., Cui, Y., Diehn, M., and Li, R. (2017). Development and validation of an individualized immune prognostic signature in early-stage nonsquamous non-small cell lung cancer. *JAMA Oncol.* 3, 1529–1537. doi: 10.1001/jamaoncol.2017.1609
- Li, T., Fu, J., Zeng, Z., Cohen, D., Li, J., Chen, Q., et al. (2020). TIMER2.0 for analysis of tumor-infiltrating immune cells. *Nucleic Acids Res.* 48, W509–W514. doi: 10.1093/nar/gkaa407
- Li, W., Zeng, J., Luo, B., Mao, Y., Liang, Y., Zhao, W., et al. (2020). [High expression of activated CD4(+) memory T cells and CD8(+) T cells and low expression of M0 macrophage are associated with better clinical prognosis in bladder cancer patients]. *Xi Bao Yu Fen Zi Mian Yi Xue Za Zhi* 36, 97–103.
- Lin, J., Yang, J., Xu, X., Wang, Y., Yu, M., and Zhu, Y. (2020). A robust 11-genes prognostic model can predict overall survival in bladder cancer patients based on five cohorts. *Cancer Cell Int.* 20:402. doi: 10.1186/s12935-020-01491-6
- Love, M. I., Huber, W., and Anders, S. (2014). Moderated estimation of fold change and dispersion for RNA-seq data with DESeq2. *Genome Biol.* 15:550. doi: 10.1186/s13059-014-0550-8
- Mariathasan, S., Turley, S. J., Nickles, D., Castiglioni, A., Yuen, K., Wang, Y., et al. (2018). TGFβ attenuates tumour response to PD-L1 blockade by contributing to exclusion of T cells. *Nature* 554, 544–548. doi: 10.1038/nature25501
- Mazzaschi, G., Minari, R., Zecca, A., Cavazzoni, A., Ferri, V., Mori, C., et al. (2020). Soluble PD-L1 and circulating CD8+PD-1+ and NK cells enclose a prognostic and predictive immune effector score in immunotherapy treated NSCLC patients. *Lung Cancer* 148, 1–11. doi: 10.1016/j.lungcan.2020.07.028
- Muraoka, D., Seo, N., Hayashi, T., Hyuga-Amaike, C., Okamori, K., Tawara, I., et al. (2017). Signal-transducing adaptor protein-2 promotes generation of functional long-term memory CD8+ T cells by preventing terminal effector differentiation. *Oncotarget* 8, 30766–30780. doi: 10.18632/oncotarget.15403
- Nadal, R., and Bellmunt, J. (2019). Management of metastatic bladder cancer. *Cancer Treat. Rev.* 76, 10–21. doi: 10.1016/j.ctrv.2019.04.002
- O'Connor, B. P., Eun, S. Y., Ye, Z., Zozulya, A. L., Lich, J. D., Moore, C. B., et al. (2008). Semaphorin 6D regulates the late phase of CD4+ T cell primary immune responses. *Proc. Natl. Acad. Sci. U.S.A.* 105, 13015–13020. doi: 10.1073/pnas.0803386105
- Panezai, J., Bergdahl, E., and Sundqvist, K. G. (2017). T-cell regulation through a basic suppressive mechanism targeting low-density lipoprotein receptor-related protein 1. *Immunology* 152, 308–327. doi: 10.1111/imm.12770
- Powles, T., Eder, J. P., Fine, G. D., Braiteh, F. S., Loriot, Y., Cruz, C., et al. (2014). MPDL3280A (anti-PD-L1) treatment leads to clinical activity in metastatic bladder cancer. *Nature* 515, 558–562. doi: 10.1038/nature13904
- Sidaway, P. (2017). Bladder cancer: pembrolizumab is superior to chemotherapy. *Nat. Rev. Urol.* 14:261. doi: 10.1038/nrur.2017.38
- Subramanian, A., Tamayo, P., Mootha, V. K., Mukherjee, S., Ebert, B. L., Gillette, M. A., et al. (2005). Gene set enrichment analysis: a knowledge-based approach for interpreting genome-wide expression profiles. *Proc. Natl. Acad. Sci. U.S.A.* 102, 15545–15550. doi: 10.1073/pnas.0506580102
- Ternes, N., Rotolo, F., and Michiels, S. (2016). Empirical extensions of the lasso penalty to reduce the false discovery rate in high-dimensional Cox regression models. *Stat. Med.* 35, 2561–2573. doi: 10.1002/sim.6927
- Tosti, N., Cremonesi, E., Governa, V., Basso, C., Kancherla, V., Coto-Llerena, M., et al. (2020). Infiltration by interleukin-22 producing T cells promotes neutrophil recruitment and predicts favorable clinical outcome in human

- colorectal cancer. *Cancer Immunol. Res.* 8, 1452–1462. doi: 10.1158/2326-6066.CIR-19-0934
- Wang, C., Lu, Y., Chen, L., Gao, T., Yang, Q., Zhu, C., et al. (2020). Th9 cells are subjected to PD-1/PD-L1-mediated inhibition and are capable of promoting CD8 T cell expansion through IL-9R in colorectal cancer. *Int. Immunopharmacol.* 78:106019. doi: 10.1016/j.intimp.2019.106019
- Wang, Z., Song, Q., Yang, Z., Chen, J., Shang, J., and Ju, W. (2019). Construction of immune-related risk signature for renal papillary cell carcinoma. *Cancer Med.* 8, 289–304. doi: 10.1002/cam4.1905
- Yarchoan, M., Hopkins, A., and Jaffee, E. M. (2017). Tumor mutational burden and response rate to PD-1 inhibition. *N. Engl. J. Med.* 377, 2500–2501. doi: 10.1056/NEJMc1713444
- Yin, X., Lu, X., Xiuwen, Z., Min, Z., Xiao, R., Mao, Z., et al. (2017). Role of NKG2D in cytokine-induced killer cells against lung cancer. *Oncol. Lett.* 13, 3139–3143. doi: 10.3892/ol.2017.5800
- Zeng, D., Ye, Z., Wu, J., Zhou, R., Fan, X., Wang, G., et al. (2020). Macrophage correlates with immunophenotype and predicts anti-PD-L1 response of urothelial cancer. *Theranostics* 10, 7002–7014. doi: 10.7150/thno.46176

Conflict of Interest: The authors declare that the research was conducted in the absence of any commercial or financial relationships that could be construed as a potential conflict of interest.

Copyright © 2021 Li, Hao, Ye, Wei, Tang, Tan, Liao, Zhang, Li, Gui, Xiao, Huang, Chen, Cao, Luo and Chen. This is an open-access article distributed under the terms of the Creative Commons Attribution License (CC BY). The use, distribution or reproduction in other forums is permitted, provided the original author(s) and the copyright owner(s) are credited and that the original publication in this journal is cited, in accordance with accepted academic practice. No use, distribution or reproduction is permitted which does not comply with these terms.



Advances in Drug Resistance of Esophageal Cancer: From the Perspective of Tumor Microenvironment

Siyuan Luan^{1†}, Xiaoxi Zeng^{2†}, Chao Zhang², Jiajun Qiu², Yushang Yang¹, Chengyi Mao¹, Xin Xiao¹, Jianfeng Zhou¹, Yonggang Zhang^{3,4*} and Yong Yuan^{1*}

¹ Department of Thoracic Surgery, National Clinical Research Center for Geriatrics, West China Hospital, Sichuan University, Chengdu, China, ² West China Biomedical Big Data Center, West China Hospital, Sichuan University, Chengdu, China,

³ Department of Periodical Press, National Clinical Research Center for Geriatrics, West China Hospital, Sichuan University, Chengdu, China, ⁴ Nursing Key Laboratory of Sichuan Province, Chengdu, China

OPEN ACCESS

Edited by:

Wei Zhao,
City University of Hong Kong,
Hong Kong

Reviewed by:

Yan Zheng,
Henan Provincial Cancer Hospital,
China
Dong Tian,
Affiliated Hospital of North Sichuan
Medical College, China

*Correspondence:

Yonggang Zhang
jebm_zhang@yahoo.com
Yong Yuan
yongyuan@scu.edu.cn

[†] These authors have contributed
equally to this work

Specialty section:

This article was submitted to
Molecular and Cellular Oncology,
a section of the journal
Frontiers in Cell and Developmental
Biology

Received: 06 February 2021

Accepted: 28 February 2021

Published: 19 March 2021

Citation:

Luan S, Zeng X, Zhang C, Qiu J,
Yang Y, Mao C, Xiao X, Zhou J,
Zhang Y and Yuan Y (2021) Advances
in Drug Resistance of Esophageal
Cancer: From the Perspective
of Tumor Microenvironment.
Front. Cell Dev. Biol. 9:664816.
doi: 10.3389/fcell.2021.664816

Drug resistance represents the major obstacle to get the maximum therapeutic benefit for patients with esophageal cancer since numerous patients are inherently or adaptively resistant to therapeutic agents. Notably, increasing evidence has demonstrated that drug resistance is closely related to the crosstalk between tumor cells and the tumor microenvironment (TME). TME is a dynamic and ever-changing complex biological network whose diverse cellular and non-cellular components influence hallmarks and fates of tumor cells from the outside, and this is responsible for the development of resistance to conventional therapeutic agents to some extent. Indeed, the formation of drug resistance in esophageal cancer should be considered as a multifactorial process involving not only cancer cells themselves but cancer stem cells, tumor-associated stromal cells, hypoxia, soluble factors, extracellular vesicles, etc. Accordingly, combination therapy targeting tumor cells and tumor-favorable microenvironment represents a promising strategy to address drug resistance and get better therapeutic responses for patients with esophageal cancer. In this review, we mainly focus our discussion on molecular mechanisms that underlie the role of TME in drug resistance in esophageal cancer. We also discuss the opportunities and challenges for therapeutically targeting tumor-favorable microenvironment, such as membrane proteins, pivotal signaling pathways, and cytokines, to attenuate drug resistance in esophageal cancer.

Keywords: esophageal cancer, drug resistance, tumor microenvironment, chemotherapy, targeted therapy, immunotherapy, chemoresistance, therapeutic response

INTRODUCTION

Esophageal cancer (EC) is the sixth leading cause of cancer-related death globally, with a dismal overall 5-year survival of 20% (Lagergren et al., 2017; Bray et al., 2018). EC can be histologically classified as esophageal squamous cell carcinoma (ESCC) or esophageal adenocarcinoma (EAC), which has distinct pathogenesis, molecular characteristics, and geographical distribution (Cancer Genome et al., 2017; Lagergren et al., 2017). Clinically, chemotherapy has been one of the major therapeutic approaches in the trimodality therapy of EC; molecular targeted therapy and immune

checkpoint inhibitors have been evaluating in preclinical and clinical trials (van Hagen et al., 2012; Smyth et al., 2017, 2021; Yang et al., 2020). However, despite recent advances in multidisciplinary management, the treatment of EC is still a relentless challenge partly owing to the fact that numerous patients are intrinsically insensitive or adaptively resistant to therapeutic agents. Indeed, over 70% of patients with locally advanced EC did not reach a pathological complete response (pCR) after the neoadjuvant chemoradiotherapy, ultimately leading to a risk of tumor relapse and poor prognosis (van Hagen et al., 2012). These patients suffered from unacceptable adverse events and were delayed to surgery with virtually no therapeutic benefits. Definitive chemoradiotherapy, as an alternative to neoadjuvant chemoradiotherapy plus surgery, may offer a chance of cure. Unfortunately, a subset of these patients still require reintervention because of local relapse or distant metastasis (Swisher et al., 2002; Ilson and Lordick, 2018). To overcome these major challenges, the development of chemosensitizers and combined therapy is urgently needed, which requires further elucidation of the mechanism of drug resistance in EC.

The mechanism of cancer drug resistance is a complex multifactor process, including blockage of drug distribution, increased drug efflux, mutations of the drug target, DNA damage repair, activation of alternative pro-tumorigenic signaling pathways, evasion of programmed cell death, etc. (Holohan et al., 2013). This not only depends on malignant hallmarks of tumor cells, but also closely related to the aberrant state of the tumor microenvironment (TME) and the crosstalk between tumor cells and TME (Dalton, 1999). The solid tumor consists not only of cancer cells and cancer stem cells but also tumor-associated stromal cells (tumor-associated fibroblasts, immune and inflammatory cells, endothelial cells, etc.) and non-cellular elements (hypoxia, acidity, cytokines, extracellular matrix, exosomes, etc.), collectively defined as the TME (Hanahan and Weinberg, 2011; Hanahan and Coussens, 2012). Over the past few decades, increasing evidence has demonstrated that TME plays an important role in the initiation, progression, and therapeutic response of human cancer (Dalton, 1999; Trédan et al., 2007; Quail and Joyce, 2013). In this review, we mainly focus our discussion on molecular mechanisms that underlie the role of TME in drug resistance in EC. We also discuss the opportunities and challenges for therapeutically targeting tumor-favorable microenvironment, such as membrane proteins, pivotal signaling pathways, and cytokines, to attenuate drug resistance in EC.

CELLULAR COMPONENTS

Cancer Stem Cells

It is increasingly evident that carcinogenesis initiates from a particular subset of cells termed cancer stem cells (CSCs) which express particular surface markers and have stem-cell-like traits, including plasticity, quiescence, renewal, and drug resistance (Batlle and Clevers, 2017). Although the theory of CSCs has not yet been well-established, a plethora of studies have demonstrated that CSCs, or cancer cells with stem-cell-like properties, were more resistant to chemotherapy (Zhao, 2016). In EC, CSCs

protect themselves against cytotoxic agents partly by facilitating the process of drug efflux. This self-protective mechanism is frequently found among side population (SP) cells, a subset of cells identified by flow cytometry that express specific surface markers (Hadnagy et al., 2006; Huang D. et al., 2009; Zhao et al., 2014). Although they are rare in TME, SP cells enrich in CSCs and express high levels of ATP-binding cassette (ABC) transporters, such as ABCG2 and ABCG5, which are responsible for drug efflux and multidrug resistance (Gottesman et al., 2002; Li et al., 2011). Studies demonstrated that expression of ABCG2 was significantly upregulated in esophageal CSCs, leading to the resistance to cisplatin and 5-fluorouracil, as well as offering a potential therapeutic target to avert chemoresistance (Cheng et al., 2012; Yue et al., 2015). Beyond this, esophageal CSCs may also have the ability to hinder the process of drug influx. A study demonstrated that p75 neurotrophin receptor (p75NTR) + cells have stem-cell-like properties, including cisplatin resistance, and this was possibly due to the downregulation of copper uptake protein 1 (CTR1), a major copper influx transporter in mammalian cells (Huang S. D. et al., 2009). Taken together, esophageal CSCs take advantage of the specific distribution of membrane transporters to maintain the intracellular drug concentration at a harmless level and avoid the cytotoxic effect of chemotherapy (Figure 1A).

The resistance mechanism of esophageal CSCs is driven by multiple crucial signaling pathways (Figure 1A). Notch signaling is a cell-fate-determination pathway participating in various aspects of cell biology and interactions between cancer cells and TME (Meurette and Mehlen, 2018). Notch signaling also plays a vital role in the initiation and progression of EC (Song et al., 2014; Kunze et al., 2020). Notably, Notch signaling was demonstrated to enhance chemoresistance in both ESCC and EAC (Wang et al., 2014; Kunze et al., 2020). The aberrant activation of Notch signaling is partly owing to overexpression of Protein arginine methyltransferase 1 (PRMT1) which mediates mono and asymmetric dimethylation of the guanidino nitrogens of arginyl residues (Tang et al., 2000). Histone H4R3me2a mediated by PRMT1 promotes proliferation of CSCs and activates Notch and Wnt/ β -catenin signaling, leading to enhanced drug resistance (Zhao et al., 2019a). Moreover, somatic mutations on the Notch1 gene were commonly found in patients with partial responses or stable diseases after neoadjuvant chemotherapy (Liu et al., 2020). Yes-associated protein (YAP), a Hippo pathway coactivator, confers stem-cell-like properties on EC cells by upregulating SOX9 (Wang L. et al., 2019). Notably, YAP induces the expression of EGFR, which is associated with the resistance to 5-fluorouracil and docetaxel (Song et al., 2015). Inhibition of YAP can reduce stem-cell-like properties and is a potential therapeutic strategy to attenuate drug resistance in EC. In addition, the maintenance of drug resistance in esophageal CSCs also depends on the activation of various critical signaling pathways, such as Wnt/catenin, TGF β , and hedgehog pathway (Liu et al., 2017; Wang D. et al., 2019; Zhao et al., 2019b).

Like other cancers, the identification of esophageal CSCs is based on the specific expression of stemness-related surface markers, including CD24, CD44, CD90, CD133, CLDN4, EpCAM, OV6, and p75NTR, some of which are associated with

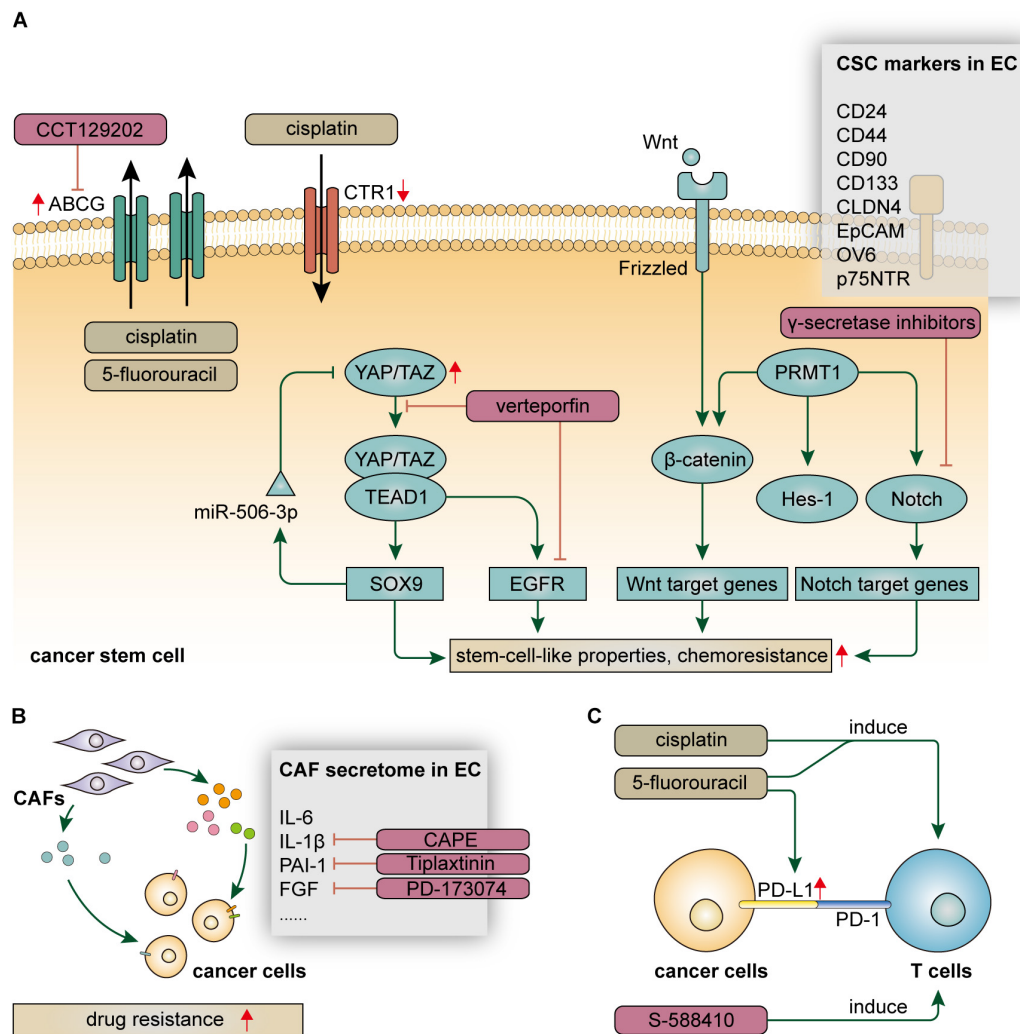


FIGURE 1 | Resistance mechanisms of cellular components, including **(A)** cancer stem cells, **(B)** cancer-associated fibroblasts, and **(C)** immune inflammatory cells, in the tumor microenvironment in EC.

drug resistance and have the potential to predict the therapeutic response (Yamaguchi et al., 2016; Jiménez et al., 2017; Liu et al., 2017; Wang et al., 2017; Wang D. et al., 2019; Sun et al., 2018; Xu et al., 2018; Lin et al., 2019; **Figure 1A**). p75NTR, also referred to as CD271, is a receptor of the neurotrophic growth factor family that mediates various cell outcomes, such as cell apoptosis during neurodevelopmental processes (Barker, 2004). In EC, p75NTR is a specific marker for CSCs at mitotic quiescent periods; p75NTR + cells exhibit enhanced drug resistance and have the potential to serve as therapeutic targets (Huang S. D. et al., 2009; Yamaguchi et al., 2016). OV6 + is a potential marker for esophageal CSCs, which has been demonstrated to be associated with drug resistance (Wang et al., 2017). In OV6 + cells, autophagy is significantly activated to maintain stem-cell-like properties, including drug resistance, by stabilizing ATG7-dependent B-catenin. Beyond these, CLDN4 is a CSC marker that has the potential to predict therapeutic response after chemotherapy, which is of great clinical importance to

select proper candidates for chemotherapy (Lin et al., 2019). Nevertheless, most of the studies to date only focused on demonstrating the guilt-by-association between drug resistance and specific expression of surface markers. In-depth analyses regarding the causal association and clinical applicability of CSC markers in the chemotherapeutic setting are urgently needed.

Cancer-Associated Fibroblasts

Cancer-associated fibroblasts (CAFs), characterized by high expression of α -smooth muscle actin and fibroblast activation protein- α , represent a dominant component of tumor stroma in the TME and play prominent functional roles in cancer progression and drug resistance (Kalluri, 2016). Normal fibroblasts (NFs) are usually quiescent and can be activated in response to specific circumstances, such as wound healing, leading to increased production of TGF- β and a highly contractile phenotype (Rockey et al., 2013). Like many other cancers, the tumorigenesis of EC is associated with chronic inflammatory

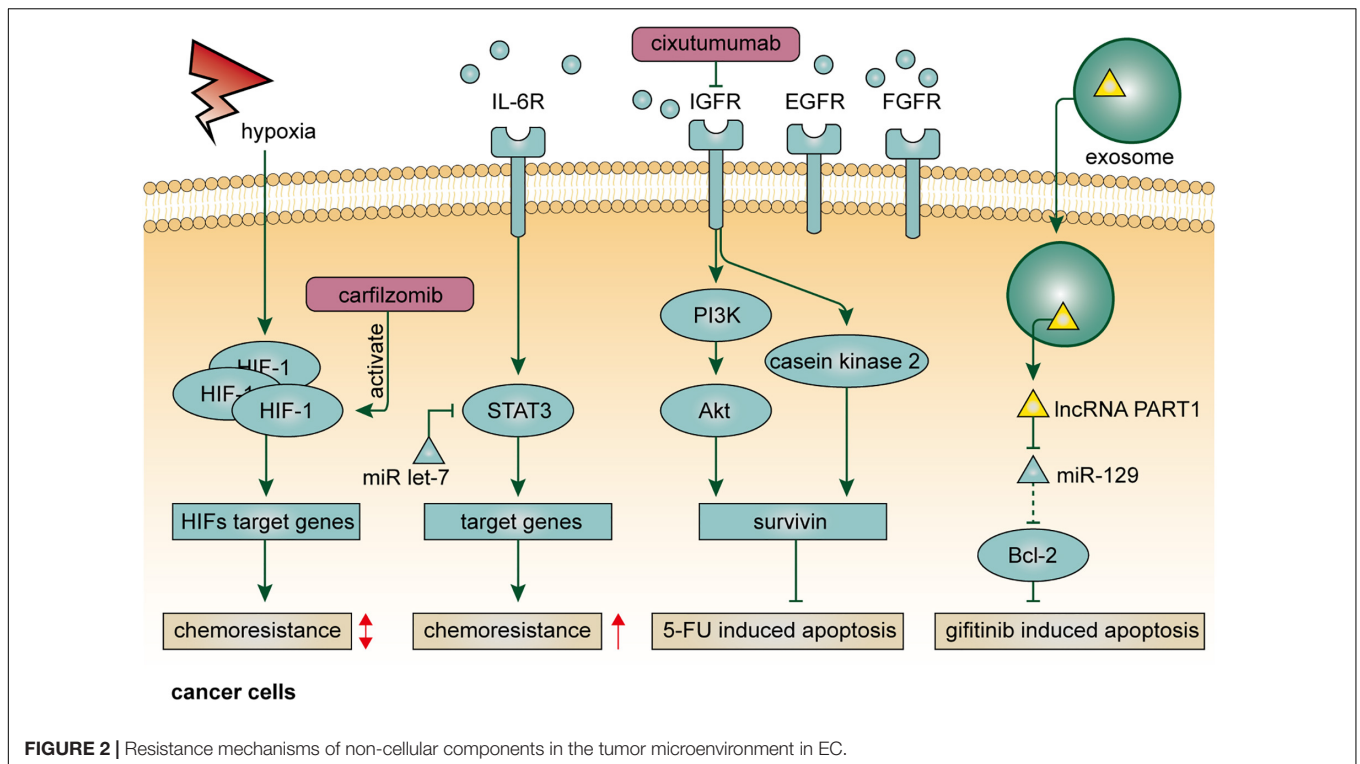
and mucosal injury. Mediated by functional molecules, such as microRNAs and lncRNAs, NFs are transformed into CAFs and confer drug resistance on surrounding EC cells by secreting soluble factors and stimulating pro-tumorigenic signals (Tanaka et al., 2015; Tong et al., 2020). Interleukin 6 (IL-6), a multifunctional cytokine, not only mediate immune and inflammatory response but also participate in various hallmarks of cancer, including drug resistance. CAFs are major sources of IL-6 in the TME, which enhance the chemoresistance of ESCC cells by upregulating C-X-C motif chemokine receptor 7 (CXCR7) through STAT3/NF- κ B pathway (Qiao et al., 2018). CAFs-derived IL-6 also confers resistance to chemoradiotherapy on EAC patients. Interestingly, although serum IL-6 cannot stratify patients with different response to neoadjuvant chemoradiotherapy, circulating ADAM12 is significantly associated with poor response to chemoradiation, indicating its potential to predict therapeutic response in patients with EAC (Ebbing et al., 2019). Plasminogen activator inhibitor-1 (PAI-1) is a well-known cytokine that functions as a principal inhibitor of vascular fibrinolysis (Ghosh and Vaughan, 2012). Cisplatin-induced DNA damage in CAFs promotes the paracrine of PAI-1 and activate AKT and ERK1/2 pathway in EC cells, eventually leading to enhanced cancer cell proliferation and reduced cytotoxic effect of cisplatin (Che et al., 2018). Furthermore, TGF- β signaling is involved in crosstalk between cancer cells and CAFs that protect ESCC cells from several conventional chemotherapeutic agents, likely due to the transcriptional activation induced by FOXO1 which can stimulate TGF- β 1 promoter activity (Zhang et al., 2017). In the context of molecular targeted therapy, FGF in fibroblast supernatant may play a role in attenuating the effect of lapatinib on ESCC cells, which can be abrogated by additionally treating it with FGFR inhibitor (Saito et al., 2015). Taken together, the CAF secretome, as well as corresponding receptors on cancer cells, represents attractive therapeutic targets that hold the promise to address drug resistance in a combined manner (**Figure 1B**).

Immune Inflammatory Cells

The programmed death 1 (PD-1) pathway serves as a critical immune checkpoint to limit immune responses mediated by T cells in the TME. Tumor cells can evade the immune responses by two ligands, programmed death ligand 1 (PD-L1) and programmed death ligand 2 (PD-L2), both of which engage the PD-1 receptor and inhibit T-cell activation, known as tumor immune evasion (Freeman et al., 2000; Latchman et al., 2001; Juneja et al., 2017; Dong et al., 2018; Zhao and Huang, 2020). The discovery of tumor immune evasion paves the way to treat cancer in an immune-checkpoint-based manner, which is now one of the most promising therapeutic strategies for various types of cancer (Hamid et al., 2013; Borghaei et al., 2015; Nanda et al., 2016). Currently, immune checkpoint inhibitors, represented by nivolumab and pembrolizumab, have achieved initial success in the treatment of advanced or refractory EC (Hong and Ding, 2019; Kato et al., 2019; Shah et al., 2019). Due to low response rates among EC patients, however, further efforts are needed to

elucidate the resistance mechanism of immunotherapy. Among all the patients with EC, less than 20% of them express PD-L1 (Okadome et al., 2020), which means a certain number of patients with EC are hard to get any therapeutic benefit from immune checkpoint inhibitors. Moreover, the expression of PD-L1 on the cell surface was found to be highly heterogeneous in EC (Yan et al., 2019). These facts are responsible for the low response rates of immunotherapy. On the other hand, although immune inflammatory cells infiltrating in the TME are considered as a double-edged sword for tumor progression (Hanahan and Weinberg, 2011), the lower status of tumor-infiltrating lymphocytes (TILs) has been demonstrated to be associated with unfavorable clinical outcomes of patients with EC (Yagi et al., 2019a; Däster et al., 2020). To overcome these challenges, identifying reliable biomarkers to select proper populations who can get the maximum therapeutic benefit is of great clinical importance. Notably, the combination of PD-L1 expression and TILs status has the potential to serve as predictive biomarkers for patients with EC (Yagi et al., 2019a). PD-L2 has also been demonstrated to be associated with a worse prognosis in EC (Ohigashi et al., 2005; Okadome et al., 2020). The identification of these biomarkers contributes not only to prognosis prediction but also to patient classification and selection (Baba et al., 2020). Based on PD-L1 expression and T-cell infiltration, a cancer stratification model including four types of TME status has been proposed to tailor ideal immune-based therapeutic strategy (Teng et al., 2015).

Furthermore, combining immunotherapy with conventional therapy has the potential to overcome drug resistance and provide better therapeutic benefits (Gotwals et al., 2017; Kelly et al., 2018). EC cell lines treated with 5-fluorouracil exhibits a high level of PD-L1, which provides factual bases for the combination of chemotherapy and immunotherapy to some extent (Van Der Kraak et al., 2016). It is also evident that neoadjuvant chemotherapy could induce CD4 and CD8 T cells in the TME of EC (Tsuchikawa et al., 2012). Moreover, a recent study found that paclitaxel-nedaplatin could induce the reconstruction of TILs, which was partly due to the migration of T cells from peripheral blood to the TME (Zhang et al., 2018). These findings further unraveled the modulatory role of chemotherapy in T cell immune response and provided theoretical bases for the rational combination of chemotherapy and immunotherapy. That is, in addition to their cytotoxicity, some chemotherapeutic agents also have the potential to be used as sensitizers for immunotherapy. Importantly, adverse events (AEs) must be taken into account, especially in the context of combined therapy. Beyond these, inducing anti-tumor immune responses by cancer vaccines is another therapeutic strategy. A recent clinical trial reported that vaccination with the CPV S-588410 induced functional CD8 + and CD4 + TILs, as well as PD-L1 expression, in EC, indicating that S-588410 vaccine combined with PD-L1 inhibitors might be an effective therapeutic option (Daiko et al., 2020; **Figure 1C**). Moreover, a recent study found that high density of tumor-associated macrophages (TAMs) was associated with increased PD-L1 expression and a worse outcome in EC, indicating a rational combination therapy targeting TAMs and PD-L1 (Yagi et al., 2019b).



NON-CELLULAR COMPONENTS

Hypoxia

Within the TME, the formation of the hypoxic region is usually associated with the imbalance between the rapid expansion of solid tumors and abnormal structure and function of tumor vasculature (Jain, 2005). Insufficient blood supply, on the one hand, influences the effective delivery of antitumor drugs, and on the other hand, alters the local concentration of oxygen and other nutrients, resulting in compromised metabolism and reduced drug sensitivity in cancer cells (Tang et al., 2020). Hypoxia confers drug resistance through various signaling pathways involved in apoptosis, autophagy, DNA damage repair, mitochondrial activity, p53, and drug efflux (Graeber et al., 1996; Jing et al., 2019). Hypoxia-inducible factors (HIFs) are transcription factors that represent the pivotal mediator of the hypoxic response in the cellular microenvironment and play key roles in resistance to conventional anticancer therapy (Rohwer and Cramer, 2011). In EC, expression of HIF-1 is correlated with venous invasion, VEGF expression, and microvessel density (Kimura et al., 2004). Alleviation of the hypoxic condition in EC is usually accompanied by downregulation of HIF-1 expression and complete response to chemotherapy (Lee et al., 2015). Clinically, combined with p53 and p21, overexpression of HIF-1 is a sensitive indicator to predict treatment response after chemoradiotherapy (Sohda et al., 2004). However, the effect of HIF-1 on drug resistance in EC is likely bidirectional (Figure 2). By single-cell RNA-seq, a recent study found that paclitaxel-resistant EC cells were characterized with lower expression of HIF-1 signaling genes, and that the chemoresistance could

be attenuated through activating HIF-1 signaling by using carfilzomib, indicating a rational therapeutic combination of carfilzomib and paclitaxel (Wu et al., 2018).

Cytokines

Cytokines serve important roles in intra- or intercellular signal transduction by autocrine, paracrine, and endocrine fashions. IL-6 is a principal mediator involved in the acute-phase response to injury and infection (Xing et al., 1998). Besides its pro-inflammatory functions, IL-6 also plays a crucial role in drug resistance in human cancer. As mentioned above, IL-6 derives from stromal cells in the TME, such as CAFs, and confer chemoresistance on EC cells via multiple pathways (Qiao et al., 2018; Ebbing et al., 2019). Indeed, the upregulation of IL-6 can be found in Barrett's esophagus, a widely accepted precancerous lesion of EAC, and enables esophageal epithelia resistant to cell apoptosis, leading to a higher risk of carcinogenesis (Dvorakova et al., 2004). EC cells treated with cisplatin exhibit higher expression of IL-6, which promotes phosphorylation of STAT3 and thereby confers cancer hallmarks, including evasion of apoptosis and chemoresistance, on themselves or surrounding EC cells in autocrine or paracrine manners (Sugimura et al., 2012). Notably, microRNA let-7 can restore the efficacy of chemotherapy by targeting IL-6/STAT3 prosurvival pathway activated by cisplatin (Figure 2). Therefore, treating with let-7 may have the potential to prolong the duration of cytotoxic effect in the TME, and the functional role of let-7 in tumor-associated stromal cells requires further investigations. In addition to IL-6, the serum level of IL-6R is also associated with chemoresistance (Makuuchi et al., 2013). EC patients with an

elevated level of serum IL-6R are more resistant to neoadjuvant chemoradiotherapy, indicating the clinical value of IL-6R to serve as a biomarker for patient selection. IL-1 β , another member of the interleukin family, promotes tumor development by driving chronic inflammation, tumor angiogenesis, and induction of immunosuppressive cells (Bent et al., 2018). In EC, IL-1 β expression was found to be correlated with chemoradiotherapy response (Chen et al., 2012). The same study also demonstrated that caffeic acid phenethyl ester (CAPE), a pro-inflammatory natural chemical compound that can specifically block NF- κ B and attenuate IL-1 β expression, increased the sensitivity of EC cells to cisplatin. However, to date, the resistance mechanism of IL-1 β in EC still lacks in-depth investigation.

Growth Factors

Growth factors typically function as signaling molecules that mediate intercellular communication and trigger various critical cellular processes, such as cell proliferation and differentiation (Werner and Grose, 2003; Hicklin and Ellis, 2005; Normanno et al., 2006; Pollak, 2008; Turner and Grose, 2010). Unfortunately, in the context of TME, the blocking effect of growth factors on cell apoptotic pathways leads to stronger resistance to anticancer drugs, since the cell apoptotic program is considered a natural barrier preventing normal cells transform into malignancy (Adams and Cory, 2007). In EC, IGF-1 inhibits cell apoptosis induced by a variety of common chemical agents, including cisplatin, 5-fluorouracil, and camptothecin (Liu et al., 2002). Mechanistically, IGF-1, partly induced by Id1, can upregulate the expression of survivin via PI3K/Akt and casein kinase 2 signaling pathways, leading to inhibition of Smac/DIABLO release and activation of caspases, which are responsible for 5-fluorouracil-induced cell apoptosis (Juan et al., 2011; Li et al., 2014, 2016; **Figure 2**). The secretion of IGF-1 depends on both autocrine and paracrine manners. Blocking IGF-1R may be a useful method to not only retard tumor growth, but also make EC cells more sensitive to chemotherapy. Indeed, cixutumumab, a monoclonal antibody against IGF-1R, was demonstrated to significantly inhibited EC progression and metastasis, as well as chemoresistance to cisplatin and 5-fluorouracil (Li et al., 2014). Targeting IGF-2 or PI3K/Akt pathway is also a promising way to enhance chemosensitivity in EC. A study demonstrated that IGF-2-neutralizing antibody and PI3K/Akt pathway inhibitors could inhibit capacities of self-renew and chemoresistance to 5-fluorouracil in CD133-positive esophageal CSCs (Xu et al., 2018). Apart from the IGF family, EGFR and FGFR also contribute to drug resistance in EC. As mentioned above, YAP1 can transcriptionally upregulate EGFR, which is of importance to chemoresistance in EC (Song et al., 2015). Targeting YAP1 by verteporfin reduces the expression of YAP and EGFR and makes EC cells more sensitive to cytotoxic agents. Moreover, FGFR inhibitors can reduce FGF-mediated lapatinib resistance, although the mechanism is as yet unknown (Saito et al., 2015).

Exosomes

Exosomes are a category of extracellular vesicles comprising various bioactive molecules, such as proteins, lipids, and nucleic acids. Recent advances in exosome-based biology processes have

opened up a whole new range of intercellular communications within the TME (Valadi et al., 2007). Typically, functional molecules derived from host cells can invade nearby recipient cells through exosome-based transfer, resulting in the diffusion of malignant hallmarks (Melo et al., 2014). In EC, microRNAs and lncRNAs usually take advantage of this mode of action to facilitate drug resistance. For example, miRNA-193, one of the upregulated microRNAs in exosomes, was demonstrated to attenuate cisplatin-induced cell cycle inhibition to enhance chemoresistance in EC (Shi et al., 2020). Moreover, as mentioned above, EC-cell-derived lncRNA POU3F3 could enter into NFs via exosome-based transfer to induce their activation, which enhanced cisplatin resistance in EC in an IL-6-dependent manner (Tong et al., 2020). In terms of molecular targeted therapy, exosome-mediated transfer of lncRNA PART1 could competitively bind to miRNA-129 in recipient EC cells to upregulate Bcl-2 and inhibit cell apoptosis mediated by Bax, caspase-3, and c-PARP, leading to gefitinib resistance (Kang et al., 2018; **Figure 2**). Due to intratumoral heterogeneity, the sensitivity of cancer cells to therapeutic regimens is diverse. The spread of drug resistance in the TME is, at least in part, ascribed to exosome-mediated intercellular communication.

CONCLUSION AND FUTURE DIRECTION

It is paramount to understand the underlying mechanism of drug resistance in EC, of which the TME is an indispensable participant. TME is a dynamic and ever-changing complex biological network, whose diverse cellular and non-cellular components influence specific traits and fates of tumor cells from the outside, and this is responsible for the development of resistance to conventional therapeutic agents to some extent. It is now evident that the formation of drug resistance in EC is a multifactorial complex process involving not only cancer cells but CSCs, tumor-associated stromal cells, hypoxia, soluble factors, extracellular vesicles, etc. CSCs, with multiple upregulated stemness markers and activated pro-survival signaling pathways, are a major component of resistant subpopulations in the TME. Given that chemotherapy or molecular targeted therapy are difficult to fully eradicate CSCs, poor pathological response and tumor relapse can be considered as inevitable posttreatment events. Autocrine and paracrine activities of CAFs and exosome-mediated intercellular communication can exacerbate the spread of drug resistance from resistant cells to sensitive cells. This multipath-dependent resistance makes treatment even trickier.

Looking forward, although adverse events are inevitable, combination therapy still represents a promising strategy to overcome the obstacle. By targeting crucial molecules in the TME, different combinations among chemotherapy, molecular targeted therapy, and immunotherapy hold the promise to thoroughly eradicate EC cells, which require a more comprehensive elucidation of the TME in EC. The heterogeneity within the TME, as well as individual differences, limit the general implementation of antitumor drugs to clinical scenarios. Therefore, it is critical to identify reliable microenvironmental biomarkers that can predict therapeutic response before initial treatment. Although

conventional therapy, including surgery, radiotherapy, and chemotherapy are still predominant in the clinical management of EC, an increasing number of preclinical and clinical research will hopefully translate to novel, safe, and effective clinical treatment options in the foreseeable future.

AUTHOR CONTRIBUTIONS

YZ and YY conceptualized the study, revised the manuscript, and supervised the study. SL and XZ conceptualized the study, drafted the manuscript, and made the figures. CZ, JQ, YSY, CM, XX, and JZ collected the literature and revised the manuscript. All authors read and approved the final manuscript.

REFERENCES

- Adams, J. M., and Cory, S. (2007). The Bcl-2 apoptotic switch in cancer development and therapy. *Oncogene* 26, 1324–1337. doi: 10.1038/sj.onc.1210220
- Baba, Y., Nomoto, D., Okadome, K., Ishimoto, T., Iwatsuki, M., Miyamoto, Y., et al. (2020). Tumor immune microenvironment and immune checkpoint inhibitors in esophageal squamous cell carcinoma. *Cancer Sci.* 111, 3132–3141. doi: 10.1111/cas.14541
- Barker, P. A. (2004). p75NTR is positively promiscuous: novel partners and new insights. *Neuron* 42, 529–533. doi: 10.1016/j.neuron.2004.04.001
- Battle, E., and Clevers, H. (2017). Cancer stem cells revisited. *Nat. Med.* 23, 1124–1134.
- Bent, R., Moll, L., Grabbe, S., and Bros, M. (2018). Interleukin-1 Beta-A friend or foe in malignancies? *Int. J. Mol. Sci.* 19:2155. doi: 10.3390/ijms19082155
- Borghaei, H., Paz-Ares, L., Horn, L., Spigel, D. R., Steins, M., Ready, N. E., et al. (2015). Nivolumab versus docetaxel in advanced nonsquamous non-small-cell lung cancer. *N. Engl. J. Med.* 373, 1627–1639.
- Bray, F., Ferlay, J., Soerjomataram, I., Siegel, R. L., Torre, L. A., and Jemal, A. (2018). Global cancer statistics 2018: GLOBOCAN estimates of incidence and mortality worldwide for 36 cancers in 185 countries. *CA Cancer J. Clin.* 68, 394–424. doi: 10.3322/caac.21492
- Cancer Genome Atlas Research, Network, Analysis Working, Group, Asan University, B. C., et al. (2017). Integrated genomic characterization of oesophageal carcinoma. *Nature* 541, 169–175. doi: 10.1038/nature20805
- Che, Y., Wang, J., Li, Y., Lu, Z., Huang, J., Sun, S., et al. (2018). Cisplatin-activated PAI-1 secretion in the cancer-associated fibroblasts with paracrine effects promoting esophageal squamous cell carcinoma progression and causing chemoresistance. *Cell Death Dis.* 9:759.
- Chen, M. F., Lu, M. S., Chen, P. T., Chen, W. C., Lin, P. Y., and Lee, K. D. (2012). Role of interleukin 1 beta in esophageal squamous cell carcinoma. *J. Mol. Med.* 90, 89–100.
- Cheng, C., Liu, Z. G., Zhang, H., Xie, J. D., Chen, X. G., Zhao, X. Q., et al. (2012). Enhancing chemosensitivity in ABCB1- and ABCG2-overexpressing cells and cancer stem-like cells by an Aurora kinase inhibitor CCT129202. *Mol. Pharm.* 9, 1971–1982. doi: 10.1021/mp2006714
- Daiko, H., Marafioti, T., Fujiwara, T., Shirakawa, Y., Nakatsura, T., Kato, K., et al. (2020). Exploratory open-label clinical study to determine the S-588410 cancer peptide vaccine-induced tumor-infiltrating lymphocytes and changes in the tumor microenvironment in esophageal cancer patients. *Cancer Immunol. Immunother.* 69, 2247–2257. doi: 10.1007/s00262-020-02619-3
- Dalton, W. S. (1999). The tumor microenvironment as a determinant of drug response and resistance. *Drug Resist. Updat.* 2, 285–288. doi: 10.1054/drup.1999.0097
- Däster, S., Eppenberger-Castori, S., Mele, V., Schäfer, H. M., Schmid, L., Weixler, B., et al. (2020). Low expression of programmed death 1 (PD-1), PD-1 Ligand 1 (PD-L1), and Low CD8+ T Lymphocyte infiltration identify a subgroup of patients with gastric and esophageal adenocarcinoma with severe prognosis. *Front. Med.* 7:144.

FUNDING

This study was supported by the National Natural Science Foundation of China (Grant Nos. 81970481 and 81602627) and 1.3.5 project for disciplines of excellence, West China Hospital, Sichuan University (Grant Nos. 2020HXFH047 and 20HXJS005).

SUPPLEMENTARY MATERIAL

The Supplementary Material for this article can be found online at: <https://www.frontiersin.org/articles/10.3389/fcell.2021.664816/full#supplementary-material>

- Dong, J., Li, B., Zhou, Q., and Huang, D. (2018). Advances in evidence-based medicine for immunotherapy of non-small cell lung cancer. *J. Evid. Based Med.* 11, 278–287. doi: 10.1111/jebm.12322
- Dvorakova, K., Payne, C. M., Ramsey, L., Holubec, H., Sampliner, R., Dominguez, J., et al. (2004). Increased expression and secretion of interleukin-6 in patients with Barrett's esophagus. *Clin. Cancer Res.* 10, 2020–2028. doi: 10.1158/1078-0432.ccr-0437-03
- Ebbing, E. A., van der Zalm, A. P., Steins, A., Creemers, A., Hermsen, S., Rentenaar, R., et al. (2019). Stromal-derived interleukin 6 drives epithelial-to-mesenchymal transition and therapy resistance in esophageal adenocarcinoma. *Proc. Natl. Acad. Sci. U.S.A.* 116, 2237–2242. doi: 10.1073/pnas.1820459116
- Freeman, G. J., Long, A. J., Iwai, Y., Bourque, K., Chernova, T., Nishimura, H., et al. (2000). Engagement of the PD-1 immunoinhibitory receptor by a novel B7 family member leads to negative regulation of lymphocyte activation. *J. Exp. Med.* 192, 1027–1034. doi: 10.1084/jem.192.7.1027
- Ghosh, A. K., and Vaughan, D. E. (2012). PAI-1 in tissue fibrosis. *J. Cell Physiol.* 227, 493–507. doi: 10.1002/jcp.22783
- Gottesman, M. M., Fojo, T., and Bates, S. E. (2002). Multidrug resistance in cancer: role of ATP-dependent transporters. *Nat. Rev. Cancer* 2, 48–58. doi: 10.1038/nrc706
- Gotwals, P., Cameron, S., Cipolletta, D., Cremasco, V., Crystal, A., Hewes, B., et al. (2017). Prospects for combining targeted and conventional cancer therapy with immunotherapy. *Nat. Rev. Cancer* 17, 286–301. doi: 10.1038/nrc.2017.17
- Graeber, T. G., Osmanian, C., Jacks, T., Housman, D. E., Koch, C. J., Lowe, S. W., et al. (1996). Hypoxia-mediated selection of cells with diminished apoptotic potential in solid tumours. *Nature* 379, 88–91. doi: 10.1038/379088a0
- Hadnagy, A., Gaboury, L., Beaulieu, R., and Balicki, D. (2006). SP analysis may be used to identify cancer stem cell populations. *Exp. Cell Res.* 312, 3701–3710. doi: 10.1016/j.yexcr.2006.08.030
- Hamid, O., Robert, C., Daud, A., Hodi, F. S., Hwu, W. J., Keeford, R., et al. (2013). Safety and Tumor responses with Pembrolizumab (Anti-PD-1) in melanoma. *N. Engl. J. Med.* 369, 134–144. doi: 10.1056/nejmoa1305133
- Hanahan, D., and Coussens, L. M. (2012). Accessories to the crime: functions of cells recruited to the tumor microenvironment. *Cancer Cell* 21, 309–322. doi: 10.1016/j.ccr.2012.02.022
- Hanahan, D., and Weinberg, R. A. (2011). Hallmarks of cancer: the next generation. *Cell* 144, 646–674. doi: 10.1016/j.cell.2011.02.013
- Hicklin, D. J., and Ellis, L. M. (2005). Role of the vascular endothelial growth factor pathway in tumor growth and angiogenesis. *J. Clin. Oncol.* 23, 1011–1027. doi: 10.1200/jco.2005.06.081
- Holohan, C., Van Schaeybroeck, S., Longley, D. B., and Johnston, P. G. (2013). Cancer drug resistance: an evolving paradigm. *Nat. Rev. Cancer* 13, 714–726. doi: 10.1038/nrc3599
- Hong, Y., and Ding, Z. Y. (2019). PD-1 Inhibitors in the advanced esophageal cancer. *Front. Pharmacol.* 10:1418.
- Huang, D., Gao, Q., Guo, L., Zhang, C., Jiang, W., Li, H., et al. (2009). Isolation and identification of cancer stem-like cells in esophageal carcinoma cell lines. *Stem Cells Dev.* 18, 465–473. doi: 10.1089/scd.2008.0033

- Huang, S. D., Yuan, Y., Liu, X. H., Gong, D. J., Bai, C. G., Wang, F., et al. (2009). Self-renewal and chemotherapy resistance of p75NTR positive cells in esophageal squamous cell carcinomas. *BMC Cancer* 9:9.
- Ilsos, D., and Lordick, F. (2018). Definitive or neoadjuvant chemoradiotherapy for squamous cell oesophageal cancer? *Lancet Oncol.* 19, 1285–1286. doi: 10.1016/s1470-2045(18)30662-4
- Jain, R. K. (2005). Normalization of tumor vasculature: an emerging concept in antiangiogenic therapy. *Science* 307, 58–62. doi: 10.1126/science.1104819
- Jiménez, P., Chueca, E., Arruebo, M., Strunk, M., Solanas, E., Serrano, T., et al. (2017). CD24 expression is increased in 5-fluorouracil-treated esophageal adenocarcinoma cells. *Front. Pharmacol.* 8:321.
- Jing, X., Yang, F., Shao, C., Wei, K., Xie, M., Shen, H., et al. (2019). Role of hypoxia in cancer therapy by regulating the tumor microenvironment. *Mol. Cancer* 18:157.
- Juan, H. C., Tsai, H. T., Chang, P. H., Huang, C. Y., Hu, C. P., and Wong, F. H. (2011). Insulin-like growth factor 1 mediates 5-fluorouracil chemoresistance in esophageal carcinoma cells through increasing survivin stability. *Apoptosis* 16, 174–183. doi: 10.1007/s10495-010-0555-z
- Juneja, V. R., McGuire, K. A., Manguso, R. T., LaFleur, M. W., Collins, N., Haining, W. N., et al. (2017). PD-L1 on tumor cells is sufficient for immune evasion in immunogenic tumors and inhibits CD8 T cell cytotoxicity. *J. Exp. Med.* 214, 895–904. doi: 10.1084/jem.20160801
- Kalluri, R. (2016). The biology and function of fibroblasts in cancer. *Nat. Rev. Cancer* 16, 582–598. doi: 10.1038/nrc.2016.73
- Kang, M., Ren, M., Li, Y., Fu, Y., Deng, M., and Li, C. (2018). Exosome-mediated transfer of lncRNA PART1 induces gefitinib resistance in esophageal squamous cell carcinoma via functioning as a competing endogenous RNA. *J. Exp. Clin. Cancer Res.* 37:171.
- Kato, K., Cho, B. C., Takahashi, M., Okada, M., Lin, C. Y., Chin, K., et al. (2019). Nivolumab versus chemotherapy in patients with advanced oesophageal squamous cell carcinoma refractory or intolerant to previous chemotherapy (ATTRACTION-3): a multicentre, randomised, open-label, phase 3 trial. *Lancet Oncol.* 20, 1506–1517. doi: 10.1016/s1470-2045(19)30626-6
- Kelly, R. J., Zaidi, A. H., Smith, M. A., Omstead, A. N., Kosovec, J. E., Matsui, D., et al. (2018). The dynamic and transient immune microenvironment in locally advanced esophageal adenocarcinoma post chemoradiation. *Ann. Surg.* 268, 992–999. doi: 10.1097/sla.0000000000002410
- Kimura, S., Kitada, Y., Tanaka, S., Kuwai, T., Hihara, J., Yoshida, K., et al. (2004). Expression of hypoxia-inducible factor (HIF)-1 α is associated with vascular endothelial growth factor expression and tumour angiogenesis in human oesophageal squamous cell carcinoma. *Eur. J. Cancer* 40, 1904–1912. doi: 10.1016/j.ejca.2004.04.035
- Kunze, B., Wein, F., Fang, H. Y., Anand, A., Baumeister, T., Strangmann, J., et al. (2020). Notch signaling mediates differentiation in barrett's esophagus and promotes progression to adenocarcinoma. *Gastroenterology* 159, 575–590. doi: 10.1053/j.gastro.2020.04.033
- Lagergren, J., Smyth, E., Cunningham, D., and Lagergren, P. (2017). Oesophageal cancer. *Lancet* 390, 2383–2396.
- Latchman, Y., Wood, C. R., Chernova, T., Chaudhary, D., Borde, M., Chernova, I., et al. (2001). PD-L2 is a second ligand for PD-1 and inhibits T cell activation. *Nat. Immunol.* 2, 261–268. doi: 10.1038/85330
- Lee, N. P., Chan, K. T., Choi, M. Y., Lam, H. Y., Tung, L. N., Tzang, F. C., et al. (2015). Oxygen carrier YQ23 can enhance the chemotherapeutic drug responses of chemoresistant esophageal tumor xenografts. *Cancer Chemother. Pharmacol.* 76, 1199–1207. doi: 10.1007/s00280-015-2897-2
- Li, B., Tsao, S. W., Chan, K. W., Ludwig, D. L., Novosyadlyy, R., Li, Y. Y., et al. (2014). Id1-induced IGF-II and its autocrine/endocrine promotion of esophageal cancer progression and chemoresistance—implications for IGF-II and IGF-IR-targeted therapy. *Clin. Cancer Res.* 20, 2651–2662. doi: 10.1158/1078-0432.ccr-13-2735
- Li, B., Xu, W. W., Guan, X. Y., Qin, Y. R., Law, S., Lee, N. P., et al. (2016). Competitive binding between Id1 and E2F1 to Cdc20 regulates E2F1 degradation and thymidylate synthase expression to promote esophageal cancer chemoresistance. *Clin. Cancer Res.* 22, 1243–1255. doi: 10.1158/1078-0432.ccr-15-1196
- Li, H., Gao, Q., Guo, L., and Lu, S. H. (2011). The PTEN/PI3K/Akt pathway regulates stem-like cells in primary esophageal carcinoma cells. *Cancer Biol. Ther.* 11, 950–958. doi: 10.4161/cbt.11.11.15531
- Lin, C. H., Li, H. Y., Liu, Y. P., Kuo, P. F., Wang, W. C., Lin, F. C., et al. (2019). High-CLDN4 ESCC cells harbor stem-like properties and indicate for poor concurrent chemoradiation therapy response in esophageal squamous cell carcinoma. *Ther. Adv. Med. Oncol.* 11:1758835919875324.
- Liu, A., Zhu, J., Wu, G., Cao, L., Tan, Z., Zhang, S., et al. (2017). Antagonizing miR-455-3p inhibits chemoresistance and aggressiveness in esophageal squamous cell carcinoma. *Mol. Cancer* 16:106.
- Liu, J., Xing, W., Tian, Q., Li, Y., Liu, X., Sun, H., et al. (2020). Application of next-generation sequencing in resistance genes of neoadjuvant chemotherapy for esophageal cancer. *Trans. Cancer Res.* 9, 4847–4856. doi: 10.21037/tcr-20-322
- Liu, Y. C., Leu, C. M., Wong, F. H., Fong, W. S., Chen, S. C., Chang, C., et al. (2002). Autocrine stimulation by insulin-like growth factor I is involved in the growth, tumorigenicity and chemoresistance of human esophageal carcinoma cells. *J. Biomed. Sci.* 9(6 Pt 2), 665–674. doi: 10.1007/bf02254995
- Makuuchi, Y., Honda, K., Osaka, Y., Kato, K., Kojima, T., Daiko, H., et al. (2013). Soluble interleukin-6 receptor is a serum biomarker for the response of esophageal carcinoma to neoadjuvant chemoradiotherapy. *Cancer Sci.* 104, 1045–1051. doi: 10.1111/cas.12187
- Melo, S. A., Sugimoto, H., O'Connell, J. T., Kato, N., Villanueva, A., Vidal, A., et al. (2014). Cancer exosomes perform cell-independent MicroRNA biogenesis and promote tumorigenesis. *Cancer Cell* 26, 707–721. doi: 10.1016/j.ccell.2014.09.005
- Meurette, O., and Mehlen, P. (2018). Notch signaling in the tumor microenvironment. *Cancer Cell* 34, 536–548. doi: 10.1016/j.ccell.2018.07.009
- Nanda, R., Chow, L. Q. M., Dees, E. C., Berger, R., Gupta, S., Geva, R., et al. (2016). Pembrolizumab in patients with advanced triple-negative breast cancer: phase Ib KEYNOTE-012 Study. *J. Clin. Oncol.* 34, 2460–2467. doi: 10.1200/jco.2015.64.8931
- Normanno, N., De Luca, A., Bianco, C., Strizzi, L., Mancino, M., Maiello, M. R., et al. (2006). Epidermal growth factor receptor (EGFR) signaling in cancer. *Gene* 366, 2–16. doi: 10.1016/0169-5002(94)93777-x
- Ohigashi, Y., Sho, M., Yamada, Y., Tsurui, Y., Hamada, K., Ikeda, N., et al. (2005). Clinical significance of programmed death-1 ligand-1 and programmed death-1 ligand-2 expression in human esophageal cancer. *Clin. Cancer Res.* 11, 2947–2953. doi: 10.1158/1078-0432.ccr-04-1469
- Okadome, K., Baba, Y., Nomoto, D., Yagi, T., Kalikawe, R., Harada, K., et al. (2020). Prognostic and clinical impact of PD-L2 and PD-L1 expression in a cohort of 437 oesophageal cancers. *Br. J. Cancer* 122, 1535–1543. doi: 10.1038/s41416-020-0811-0
- Pollak, M. (2008). Insulin and insulin-like growth factor signalling in neoplasia. *Nat. Rev. Cancer* 8, 915–928. doi: 10.1038/nrc2536
- Qiao, Y., Zhang, C., Li, A., Wang, D., Luo, Z., Ping, Y., et al. (2018). IL6 derived from cancer-associated fibroblasts promotes chemoresistance via CXCR7 in esophageal squamous cell carcinoma. *Oncogene* 37, 873–883. doi: 10.1038/ncr.2017.387
- Quail, D. F., and Joyce, J. A. (2013). Microenvironmental regulation of tumor progression and metastasis. *Nat. Med.* 19, 1423–1437. doi: 10.1038/nm.3394
- Rockey, D. C., Weymouth, N., and Shi, Z. (2013). Smooth muscle α actin (Acta2) and myofibroblast function during hepatic wound healing. *PLoS One* 8:e77166. doi: 10.1371/journal.pone.0077166
- Rohwer, N., and Cramer, T. (2011). Hypoxia-mediated drug resistance: novel insights on the functional interaction of HIFs and cell death pathways. *Drug Resist. Updat.* 14, 191–201. doi: 10.1016/j.drug.2011.03.001
- Saito, S., Morishima, K., Ui, T., Hoshino, H., Matsubara, D., Ishikawa, S., et al. (2015). The role of HGF/MET and FGF/FGFR in fibroblast-derived growth stimulation and lapatinib-resistance of esophageal squamous cell carcinoma. *BMC Cancer* 15:82.
- Shah, M. A., Kojima, T., Hochhauser, D., Enzinger, P., Raimbourg, J., Hollebecque, A., et al. (2019). Efficacy and safety of pembrolizumab for heavily pretreated patients with advanced, metastatic adenocarcinoma or squamous cell carcinoma of the esophagus: the Phase 2 KEYNOTE-180 study. *JAMA Oncol.* 5, 546–550. doi: 10.1001/jamaoncol.2018.5441
- Shi, S., Huang, X., Ma, X., Zhu, X., and Zhang, Q. (2020). Research of the mechanism on miRNA193 in exosomes promotes cisplatin resistance in esophageal cancer cells. *PLoS One* 15:e0225290. doi: 10.1371/journal.pone.0225290

- Smyth, E. C., Gambardella, V., Cervantes, A., and Fleitas, T. (2021). Checkpoint inhibitors for gastroesophageal cancers: dissecting heterogeneity to better understand their role in first line and adjuvant therapy. *Ann. Oncol.* doi: 10.1016/j.annonc.2021.02.004. [Epub ahead of print].
- Smyth, E. C., Lagergren, J., Fitzgerald, R. C., Lordick, F., Shah, M. A., Lagergren, P., et al. (2017). Oesophageal cancer. *Nat. Rev. Dis. Primers* 3:21.
- Sohda, M., Ishikawa, H., Masuda, N., Kato, H., Miyazaki, T., Nakajima, M., et al. (2004). Pretreatment evaluation of combined HIF-1 α , p53 and p21 expression is a useful and sensitive indicator of response to radiation and chemotherapy in esophageal cancer. *Int. J. Cancer* 110, 838–844. doi: 10.1002/ijc.20215
- Song, S., Honjo, S., Jin, J., Chang, S. S., Scott, A. W., Chen, Q., et al. (2015). The hippo coactivator YAP1 Mediates EGFR overexpression and confers chemoresistance in esophageal cancer. *Clin. Cancer Res.* 21, 2580–2590. doi: 10.1158/1078-0432.ccr-14-2191
- Song, Y., Li, L., Ou, Y., Gao, Z., Li, E., Li, X., et al. (2014). Identification of genomic alterations in oesophageal squamous cell cancer. *Nature* 509, 91–95.
- Sugimura, K., Miyata, H., Tanaka, K., Hamano, R., Takahashi, T., Kurokawa, Y., et al. (2012). Let-7 expression is a significant determinant of response to chemotherapy through the regulation of IL-6/STAT3 pathway in esophageal squamous cell carcinoma. *Clin. Cancer Res.* 18, 5144–5153. doi: 10.1158/1078-0432.ccr-12-0701
- Sun, X., Martin, R. C. G., Zheng, Q., Farmer, R., Pandit, H., Li, X., et al. (2018). Drug-induced expression of EpCAM contributes to therapy resistance in esophageal adenocarcinoma. *Cell Oncol.* 41, 651–662. doi: 10.1007/s13402-018-0399-z
- Swisher, S. G., Wynn, P., Putnam, J. B., Mosheim, M. B., Correa, A. M., Komaki, R. R., et al. (2002). Salvage esophagectomy for recurrent tumors after definitive chemotherapy and radiotherapy. *J. Thorac. Cardiovasc. Surg.* 123, 175–183. doi: 10.1067/mtc.2002.119070
- Tanaka, K., Miyata, H., Sugimura, K., Fukuda, S., Kanemura, T., Yamashita, K., et al. (2015). miR-27 is associated with chemoresistance in esophageal cancer through transformation of normal fibroblasts to cancer-associated fibroblasts. *Carcinogenesis* 36, 894–903. doi: 10.1093/carcin/bgv067
- Tang, H. W., Feng, H. L., Wang, M., Zhu, Q. L., Liu, Y. Q., and Jiang, Y. X. (2020). In vivo longitudinal and multimodal imaging of hypoxia-inducible factor 1 α and angiogenesis in breast cancer. *Chin. Med. J.* 133, 205–211. doi: 10.1097/cm9.0000000000000616
- Tang, J., Kao, P. N., and Herschman, H. R. (2000). Protein-arginine methyltransferase I, the predominant protein-arginine methyltransferase in cells, interacts with and is regulated by interleukin enhancer-binding factor 3. *J. Biol. Chem.* 275, 19866–19876. doi: 10.1074/jbc.m000023200
- Teng, M. W. L., Ngiew, S. F., Ribas, A., and Smyth, M. J. (2015). Classifying Cancers Based on T-cell Infiltration and PD-L1. *Cancer Res.* 75, 2139–2145. doi: 10.1158/0008-5472.can-15-0255
- Tong, Y., Yang, L., Yu, C., Zhu, W., Zhou, X., Xiong, Y., et al. (2020). Tumor-secreted exosomal lncRNA POU3F3 promotes cisplatin resistance in ESCC by inducing fibroblast differentiation into CAFs. *Mol. Ther. Oncolytics* 18, 1–13. doi: 10.1016/j.omto.2020.05.014
- Trédan, O., Galmarini, C. M., Patel, K., and Tannock, I. F. (2007). Drug resistance and the solid tumor microenvironment. *J. Natl. Cancer Inst.* 99, 1441–1454.
- Tsuchikawa, T., Miyamoto, M., Yamamura, Y., Shichinohe, T., Hirano, S., and Kondo, S. (2012). The immunological impact of neoadjuvant chemotherapy on the tumor microenvironment of esophageal squamous cell carcinoma. *Ann. Surg. Oncol.* 19, 1713–1719. doi: 10.1245/s10434-011-1906-x
- Turner, N., and Grose, R. (2010). Fibroblast growth factor signalling: from development to cancer. *Nat. Rev. Cancer* 10, 116–129. doi: 10.1038/nrc2780
- Valadi, H., Ekstrom, K., Bossios, A., Sjostrand, M., Lee, J. J., and Lotvall, J. O. (2007). Exosome-mediated transfer of mRNAs and microRNAs is a novel mechanism of genetic exchange between cells. *Nat. Cell Biol.* 9, 654–U672.
- Van Der Kraak, L., Goel, G., Ramanan, K., Kaltenmeier, C., Zhang, L., Normolle, D. P., et al. (2016). 5-Fluorouracil upregulates cell surface B7-H1 (PD-L1) expression in gastrointestinal cancers. *J. Immunother. Cancer* 4:65.
- van Hagen, P., Hulshof, M., van Lanschot, J. J. B., Steyerberg, E. W., Henegouwen, M. I. V., Wijnhoven, B. P. L., et al. (2012). Preoperative chemoradiotherapy for esophageal or junctional cancer. *N. Engl. J. Med.* 366, 2074–2084.
- Wang, C., Yan, F. H., Zhang, J. J., Huang, H., Cui, Q. S., Dong, W., et al. (2017). OV6(+) cancer stem cells drive esophageal squamous cell carcinoma progression through ATG7-dependent β -catenin stabilization. *Cancer Lett.* 391, 100–113. doi: 10.1016/j.canlet.2017.01.026
- Wang, D., Nagle, P. W., Wang, H. H., Smit, J. K., Faber, H., Baanstra, M., et al. (2019). Hedgehog pathway as a potential intervention target in esophageal cancer. *Cancers* 11:821. doi: 10.3390/cancers11060821
- Wang, L., Zhang, Z., Yu, X., Huang, X., Liu, Z., Chai, Y., et al. (2019). Unbalanced YAP-SOX9 circuit drives stemness and malignant progression in esophageal squamous cell carcinoma. *Oncogene* 38, 2042–2055. doi: 10.1038/s41388-018-0476-9
- Wang, Z., Da Silva, T. G., Jin, K., Han, X., Ranganathan, P., Zhu, X., et al. (2014). Notch signaling drives stemness and tumorigenicity of esophageal adenocarcinoma. *Cancer Res.* 74, 6364–6374. doi: 10.1158/0008-5472.can-14-2051
- Werner, S., and Grose, R. (2003). Regulation of wound healing by growth factors and cytokines. *Physiol. Rev.* 83, 835–870. doi: 10.1152/physrev.2003.83.3.835
- Wu, H., Chen, S., Yu, J., Li, Y., Zhang, X. Y., Yang, L., et al. (2018). Single-cell transcriptome analyses reveal molecular signals to intrinsic and acquired paclitaxel resistance in esophageal squamous cancer cells. *Cancer Lett.* 420, 156–167. doi: 10.1016/j.canlet.2018.01.059
- Xing, Z., Gauldie, J., Cox, G., Baumann, H., Jordana, M., Lei, X. F., et al. (1998). IL-6 is an antiinflammatory cytokine required for controlling local or systemic acute inflammatory responses. *J. Clin. Invest.* 101, 311–320. doi: 10.1172/jci1368
- Xu, W. W., Li, B., Zhao, J. F., Yang, J. G., Li, J. Q., Tsao, S. W., et al. (2018). IGF2 induces CD133 expression in esophageal cancer cells to promote cancer stemness. *Cancer Lett.* 425, 88–100. doi: 10.1016/j.canlet.2018.03.039
- Yagi, T., Baba, Y., Ishimoto, T., Iwatsuki, M., Miyamoto, Y., Yoshida, N., et al. (2019a). PD-L1 expression, tumor-infiltrating lymphocytes, and clinical outcome in patients with surgically resected esophageal cancer. *Ann. Surg.* 269, 471–478. doi: 10.1097/sla.00000000000002616
- Yagi, T., Baba, Y., Okadome, K., Kiyozumi, Y., Hiyoshi, Y., Ishimoto, T., et al. (2019b). Tumour-associated macrophages are associated with poor prognosis and programmed death ligand 1 expression in oesophageal cancer. *Eur. J. Cancer* 111, 38–49. doi: 10.1016/j.ejca.2019.01.018
- Yamaguchi, T., Okumura, T., Hirano, K., Watanabe, T., Nagata, T., Shimada, Y., et al. (2016). p75 neurotrophin receptor expression is a characteristic of the mitotically quiescent cancer stem cell population present in esophageal squamous cell carcinoma. *Int. J. Oncol.* 48, 1943–1954. doi: 10.3892/ijo.2016.3432
- Yan, T., Cui, H., Zhou, Y., Yang, B., Kong, P., Zhang, Y., et al. (2019). Multi-region sequencing unveils novel actionable targets and spatial heterogeneity in esophageal squamous cell carcinoma. *Nat. Commun.* 10:1670.
- Yang, Y. M., Hong, P., Xu, W. W., He, Q. Y., and Li, B. (2020). Advances in targeted therapy for esophageal cancer. *Signal Transduct. Target. Ther.* 5:229.
- Yue, D., Zhang, Z., Li, J., Chen, X., Ping, Y., Liu, S., et al. (2015). Transforming growth factor-beta1 promotes the migration and invasion of sphere-forming stem-like cell subpopulations in esophageal cancer. *Exp. Cell Res.* 336, 141–149. doi: 10.1016/j.yexcr.2015.06.007
- Zhang, C., Palashati, H., Tan, Q., Ku, W., Miao, Y., Xiong, H., et al. (2018). Immediate and substantial evolution of T-cell repertoire in peripheral blood and tumor microenvironment of patients with esophageal squamous cell carcinoma treated with preoperative chemotherapy. *Carcinogenesis* 39, 1389–1398. doi: 10.1093/carcin/bgy116
- Zhang, H., Xie, C., Yue, J., Jiang, Z., Zhou, R., Xie, R., et al. (2017). Cancer-associated fibroblasts mediated chemoresistance by a FOXO1/TGF β 1 signaling loop in esophageal squamous cell carcinoma. *Mol. Carcinog.* 56, 1150–1163. doi: 10.1002/mc.22581
- Zhao, J. (2016). Cancer stem cells and chemoresistance: the smartest survives the raid. *Pharmacol. Ther.* 160, 145–158. doi: 10.1016/j.pharmthera.2016.02.008
- Zhao, J., and Huang, J. (2020). Breast cancer immunology and immunotherapy: targeting the programmed cell death protein-1/programmed cell death protein ligand-1. *Chin. Med. J.* 133, 853–862. doi: 10.1097/cm9.0000000000000710
- Zhao, Y., Bao, Q., Schwarz, B., Zhao, L., Mysliwicz, J., Ellwart, J., et al. (2014). Stem cell-like side populations in esophageal cancer: a source of chemotherapy

- resistance and metastases. *Stem Cells Dev.* 23, 180–192. doi: 10.1089/scd.2013.0103
- Zhao, Y., Lu, Q., Li, C., Wang, X., Jiang, L., Huang, L., et al. (2019a). PRMT1 regulates the tumour-initiating properties of esophageal squamous cell carcinoma through histone H4 arginine methylation coupled with transcriptional activation. *Cell Death Dis.* 10:359.
- Zhao, Y., Zhu, J., Shi, B., Wang, X., Lu, Q., Li, C., et al. (2019b). The transcription factor LEF1 promotes tumorigenicity and activates the TGF- β signaling pathway in esophageal squamous cell carcinoma. *J. Exp. Clin. Cancer Res.* 38:304.

Conflict of Interest: The authors declare that the research was conducted in the absence of any commercial or financial relationships that could be construed as a potential conflict of interest.

Copyright © 2021 Luan, Zeng, Zhang, Qiu, Yang, Mao, Xiao, Zhou, Zhang and Yuan. This is an open-access article distributed under the terms of the Creative Commons Attribution License (CC BY). The use, distribution or reproduction in other forums is permitted, provided the original author(s) and the copyright owner(s) are credited and that the original publication in this journal is cited, in accordance with accepted academic practice. No use, distribution or reproduction is permitted which does not comply with these terms.



CARD-Associated Risk Score Features the Immune Landscape and Predicts the Responsiveness to Anti-PD-1 Therapy in IDH Wild-Type Gliomas

OPEN ACCESS

Edited by:

Zhe-Sheng Chen,
St. John's University, United States

Reviewed by:

Jun Dong,
Second Affiliated Hospital
of Soochow University, China
Jinquan Cai,
Harbin Medical University, China

*Correspondence:

Ke Sai
saik@sysucc.org.cn
Zhongping Chen
chenzhp@sysucc.org.cn
Yonggao Mou
mouyg@sysucc.org.cn

† These authors have contributed
equally to this work

Specialty section:

This article was submitted to
Molecular and Cellular Oncology,
a section of the journal
Frontiers in Cell and Developmental
Biology

Received: 14 January 2021

Accepted: 19 February 2021

Published: 19 March 2021

Citation:

Li D, Hu W, Lin X, Zhang J, He Z,
Zhong S, Wen X, Zhang P, Jiang X,
Duan H, Guo C, Wang J, Zeng J,
Chen Z, Mou Y and Sai K (2021)
CARD-Associated Risk Score
Features the Immune Landscape
and Predicts the Responsiveness
to Anti-PD-1 Therapy in IDH
Wild-Type Gliomas.
Front. Cell Dev. Biol. 9:653240.
doi: 10.3389/fcell.2021.653240

Depei Li^{1,2†}, Wanming Hu^{2,3†}, Xiaoping Lin^{2,4†}, Ji Zhang^{1,2}, Zhenqiang He^{1,2},
Sheng Zhong^{1,2}, Xia Wen^{1,2}, Peiyu Zhang^{1,2}, Xiaobing Jiang^{1,2}, Hao Duan^{1,2},
Chengcheng Guo^{1,2}, Jian Wang^{1,2}, Jing Zeng^{2,3}, Zhongping Chen^{1,2*}, Yonggao Mou^{1,2*}
and Ke Sai^{1,2*}

¹ Department of Neurosurgery/Neuro-oncology, Sun Yat-sen University Cancer Center, Guangzhou, China, ² State Key Laboratory of Oncology in South China, Collaborative Innovation Center for Cancer Medicine, Sun Yat-sen University Cancer Center, Guangzhou, China, ³ Department of Pathology, Sun Yat-sen University Cancer Center, Guangzhou, China, ⁴ Department of Nuclear Medicine, Sun Yat-sen University Cancer Center, Guangzhou, China

Background: Proteins containing the caspase recruitment domain (CARD) play critical roles in cell apoptosis and immunity. However, the impact of CARD genes in tumor immune cell infiltration, responsiveness to checkpoint immunotherapy, and clinical outcomes of gliomas remains unclear. Here, we explore using CARD genes to depict the immune microenvironment and predict the responsiveness of gliomas to anti-PD-1 therapy.

Methods: The genome and transcriptome data of 231 patients with isocitrate dehydrogenase wild-type (IDH-wt) gliomas were retrieved from The Cancer Genome Atlas (TCGA) database to screen CARD genes associated with T lymphocyte infiltration in gliomas. Weighted co-expression network and LASSO penalized regression were employed to generate a CARD-associated risk score (CARS). Two independent and publicly available datasets were used to validate the effectiveness of CARS.

Results: The CARS divided the 231 glioma patients into high- and low-risk subgroups with distinct immune microenvironment and molecular features. The high-risk group had high CARS and was characterized by enrichment of dysfunctional T lymphocytes in a profound immunosuppressive microenvironment, whereas the low-risk group had low CARS and exhibited an immune exclusion genotype. Moreover, signaling aberrations including upregulation of PI3K/Akt/mTOR, NF- κ B, and TGF- β were found in the high-risk group. In contrast, the activated WNT pathway was more evident in the low-risk group. Furthermore, we found that an elevated CARS indicated a decreased overall survival for IDH-wt gliomas under standard care but a clinical benefit from checkpoint immunotherapy.

Conclusion: This study developed an immune- and prognosis-relevant risk score, which could be used to enhance our understanding of the heterogeneity of immune microenvironment of gliomas and facilitate to identify patients who will benefit from checkpoint immunotherapy.

Keywords: IDH, gliomas, CARD, tumor immune microenvironment, checkpoint immunotherapy

BACKGROUND

Glioma represents one of the most prevalent primary brain tumors in adults (Alexander and Cloughesy, 2017). Mutation in isocitrate dehydrogenase (IDH) is a critical genetic alteration and a key biomarker for pathological classification and prognosis in gliomas (Chen et al., 2012). IDH mutation is identified in the majority of low-grade gliomas (LGG) and generally predicts an indolent clinical course. In contrast, primary glioblastoma multiforme (GBM) as well as a subset of LGGs are IDH-wt manifest with an aggressive behavior and therapeutic resistance. The prognosis of IDH-wt gliomas remains disappointing. The median overall survival (OS) of GBMs is only 20.5 months regardless of intensive treatment (Stupp et al., 2015). Meanwhile, IDH-wt LGGs exhibit molecular and clinical traits similar to GBMs and have much worse prognosis compared to the IDH-mutated counterparts (Reuss et al., 2015). The management of IDH-wt gliomas is challenging and novel therapies are needed.

Checkpoint blockade immunotherapy revolutionized the treatment landscape across various types of solid cancers, and therefore generated interests in glioma (Waldman et al., 2020). Unfortunately, the success of immune checkpoint inhibition (ICI) in other malignancies has not been reproduced in gliomas. Despite the promising preclinical results, some phase III clinical trials of ICI with Nivolumab failed to yield significant survival benefit in unselected recurrent or newly diagnosed GBM (Dunn et al., 2020; Reardon et al., 2020). The heterogeneity of tumor immune microenvironment in gliomas may account for these clinical outcomes. Dissecting the intrinsic properties that confer the immunosuppression and identifying predictive biomarkers for the responsiveness to anti-PD-1 therapy is of paramount necessity.

The caspase recruitment domain (CARD), a member of the death domain family, is a critical protein interaction module (Park, 2019). More than 30 CARD-containing proteins have been identified in human. Functioning as a homotypic protein interaction motif, CARD orchestrates the networks of proteins through CARD–CARD interaction (Damiano and Reed, 2004). CARD was originally found in a subset of apoptotic proteins such as caspase-2, -9, Apaf-1, and cIAP-1. The CARD-containing caspases interact with their adaptor molecules to trigger the apoptotic cascade through facilitating the assembly of the apoptosome (Bouchier-Hayes and Martin, 2002). In addition to the activation of apoptosis, accumulating evidence suggests that CARD-containing proteins also function as scaffold components in a variety of signaling pathways crucial for immune response (Matusiak et al., 2015). Caspase-1, a CARD-containing protease, is essential for the maturation of secreted IL-1 β and plays a crucial role in inflammatory and immunogenic cell death

(Miao et al., 2011). PYCARD, also known as apoptosis-associated speck-like protein containing a CARD (ASC), functions as an adaptor to bridge sensor proteins and effector molecules such as procaspase-1 within the inflammasome complex. The activation of inflammasome may be crucial for vaccine-induced humoral and cell-mediated immune responses. It has been reported that CD4⁺ T cells deficient for PYCARD exhibit impaired proliferative responses and a suppressive cytokine profile (Narayan et al., 2011). To date, the immune and clinical relevance of CARD genes and associated signaling in gliomas remains unclear.

Here, we leveraged the transcriptome expression data from the TCGA database to identify CARD genes that are associated with T lymphocyte infiltration in glioma. A CARD-associated risk score (CARS) was developed by using co-expression network and penalized regression. CARS stratified IDH-wt gliomas into two groups with distinct distribution of immune cell infiltration and molecular features. The effectiveness of CARS was validated by two other independent cohorts. Importantly, we found that an elevated CARS was associated with an unfavorable outcome of glioma patients under standard care but a survival benefit from anti-PD-1 immunotherapy. Our findings may facilitate to identify glioma patients who are potentially benefited from checkpoint immunotherapy.

MATERIALS AND METHODS

Data Extraction and Grouping

Gene expression data [read counts and transcripts per million (TPM) values] and corresponding clinical information of glioma patients were downloaded from UCSC Xena browser: Toil RNA-seq recomputed project and TCGA Pan-Cancer cohort¹ (Vivian et al., 2017). Among these, 231 IDH-wt glioma samples with survival data were retrieved for further analyses. Two independent datasets (CGGA and GSE16011) were used for validation (Gravendeel et al., 2009; Bao et al., 2014). RNA sequencing data (FPKM value) of gene expression was downloaded from the Chinese Glioma Genome Atlas (CGGA) database². Then FPKM value was transformed into TPM values. Affymetrix microarray-based gene expression matrix with RMA normalization was downloaded from the Gene Expression Omnibus (GEO) database (accession: GSE16011³) (Gravendeel et al., 2009). The clinical information of these three cohorts is summarized in **Supplementary Table 1**.

¹<https://xenabrowser.net>

²<http://www.cgga.org.cn>

³<https://www.ncbi.nlm.nih.gov/geo>

Transcriptomic and Genomic Data Processing

Genes were first filtered to include only protein-coding genes, and gene expressions were omitted when TPM values were less than 0.01. Genes with null expression in more than 75% of samples were removed, followed by removal of genes with median TPM expression <0.1. The filtered TPM values were then log₂ transformed and normalized to the mean and standard deviation among the samples (*z* score transformation). *z* score transformation was also performed in microarray-based expression data across samples. Subsequent gene-expression analyses were implemented with the normalized TPM values. Somatic mutation and copy-number variation were estimated and visualized by using the TCGA OncoGrid algorithm. Tumor mutation burden (TMB) was represented by the sum of the number of non-synonymous mutations. Mutation rate, aneuploidy score, and neoantigen count of glioma samples were obtained from Thorsson's study (Thorsson et al., 2019).

Protein–Protein Interaction (PPI), Unsupervised Clustering, and Principal Component Analyses (PCAs)

Principal component analyses was implemented by using software R package *ade4* with the normalized TPM values. Unsupervised clustering analysis was performed by using *ConsensusClusterPlus* package and *k*-means method with 80% item resampling and 1,000 times repetition (Wilkerson and Hayes, 2010). The cumulative distribution function and consensus heatmap were used to determine the optimal *K*-value. PPI network was constructed by using the STRING online tool⁴.

Differential Gene-Expression and Gene Set Enrichment Analyses

RNA-seq read counts were employed for DGE analysis by using *edgeR* package (Robinson et al., 2010). Immport database⁵ was used for immune function annotation of differentially expressed genes. A ranked list of genes created using $-\log_{10}(P) \times \text{sign}(\log_2(\text{fold change}))$ (Reimand et al., 2019) from *edgeR* DGE output was conducted to generate enrichment scores by using the Preranked module of GSEA software (version 4.1) (Subramanian et al., 2005) and C2: Canonical Pathway gene sets from the MSigDB database (version 7.1) (Liberzon et al., 2011) with 1,000 permutations. The resulting enriched gene sets, with normalized enrichment score (NES) >2 and FDR < 0.01, were visualized in an enrichment map using Cytoscape (version 3.7.2) software as described previously (Reimand et al., 2019). Fold change to median TPM value of each gene was calculated, then log₂ transformed, and used for single-sample GSEA (ssGSEA), implemented in the GSVA package (Hänzelmann et al., 2013). ssGSEA enrichment score was calculated using gene sets composed of transcripts characteristic of an established T cell signature (Spranger et al., 2015), overall lymphocyte infiltration (Calabrò et al., 2009), immune cell populations

(Charoentong et al., 2017), and signaling pathways (Liberzon et al., 2011). The enrichment scores generated by ssGSEA analysis were used to represent the relative abundance of immune cell or activity of signaling in each sample. CIBERSORT algorithm and signature matrix “LM22” were also used to deconvolve immune cell fractions (Newman et al., 2019). Cytotoxic activity (Davoli et al., 2017), MHC class-I (Lauss et al., 2017), and Batf3-dendritic cell (Batf3-DC) (Spranger et al., 2017) were calculated by taking mean expressions of genes in the gene sets. All gene sets we utilized are presented in **Supplementary Table 2**.

Development of a CARS

Weighted gene co-expression network analysis (WGCNA) was done by using WGCNA package to find modules of highly correlated genes (Langfelder and Horvath, 2008). Gene modules associated with both the CARD cluster and lymphocyte infiltrations were selected. Hub genes in the selected modules were employed to conducting LASSO penalized Cox proportional hazards regression by using *glmnet* package for identifying genes with best prognostic significance. The linear combination of gene expressions weighted by the estimated regression coefficients in the multivariate model was used to calculate the risk scores of each patient.

Tissue Microarray and Immunohistochemistry

Tissue microarrays (TMAs) were constructed by using paraffin-embedded specimens from 103 IDH-wt glioma patients who were treated at the Sun Yat-sen University Cancer Center (SYSUCC) from 2010 to 2016. Patient informed consent was obtained, and the study was approved by the Ethics Committee of the Sun Yat-sen University Cancer Center. TMAs were stained with PTX3 (Abcam, Cambridge, United Kingdom) by immunohistochemistry (IHC) method as previously described (Hu et al., 2017). IHC scoring criteria were established by combining the positive proportion (1 for 0–25%, 2 for 26–50%, 3 for 51–75%, 4 for >75%) and staining intensity (0 for no staining, 1 for light yellow, 2 for yellowish brown, 3 for brown) of the stained tumor cells. The final PTX3 expression score (0–12) was achieved by positive ratio \times staining intensity. The best cutoff value of PTX3 staining was determined by using ROC curves with respect to OS, and applied for developing a two-level grade system of PTX3 expression. All the samples were scored separately by two independent neuropathologists, who were blinded to the patient data. The discrepancies were resolved by consensus under a microscope for multi-viewing.

Prediction of Survival Benefit From ICI Therapy

Genomic, transcriptomic, and clinical data of GBM patients underwent ICI treatment was obtained from a recently published study by Zhao et al. (2019) IDH-wt gliomas with resected tissues obtained after recurrence were included for analysis. Median risk score, PD-L1 expression, and TMB were investigated for prognostic prediction.

⁴<https://string-preview.org>

⁵<https://www.immport.org>

Statistical Analysis

Normalized gene expressions and ssGSEA scores between two groups were compared by Wilcoxon tests. Categorical variables were compared by chi-squared or Fisher Exact test. Kaplan–Meier analyses with log-rank tests were performed to assess survival differences. Univariate and multivariate Cox regression were conducted to calculate hazard ratio (HR). Time-dependent ROC curve was depicted for OS prediction with *survivalROC* package. R (version 3.6.2) and GraphPad Prism (version 8.0.1) software were applied for the statistical analyses. $P < 0.05$ was considered statistically significant.

RESULTS

The CARD Genes Are Associated With T Lymphocyte Infiltration in IDH-wt Gliomas

Previous studies from other cancer types suggested that the tumor-infiltrating lymphocytes, particularly activated T lymphocytes (T cell inflamed genotype), are linked to prognosis and response to checkpoint immunotherapy (Olson and Luke, 2019). To determine the association between CARD-containing genes and T lymphocyte infiltration in glioma, we analyzed the expression profiles of 31 known CARD genes and correlated them with an established T cell-inflamed score (Spranger et al., 2015) using the ssGSEA method in these 231 IDH-wt glioma patients from the TCGA dataset. Six CARD genes, namely, *PYCARD*, *NLRC4*, *CASP1*, *CASP4*, *NOD2*, and *CARD16*, were found to be associated with the T cell inflamed metrics (Figure 1A, Spearman $R > 0.4$, $P < 0.001$). K-means clustering based on the expressions of the six CARD genes identified two main clusters (CL1 and CL2) in the IDH-wt gliomas (Figures 1B,C). PCA revealed pronounced difference in the expression portraits between the two clusters (Figure 1D). ESTIMATE algorithm (Yoshihara et al., 2013) showed elevated immune cell infiltration in CL1 (Figure 1E). We then evaluated the infiltration of lymphocytes and T cells using five scoring systems, including ESTIMATE immune score, Lymphocyte infiltration score, T cell inflamed score, CYT score, and MHC score. We demonstrated that the CL1 cluster had an enrichment of lymphocytes and T cells with increased immunological activities including cytotoxicity and antigen presentation (Figure 1E).

The CARD Genes Are Associated With the Activation of Immune-Modulating Pathways

To explore the difference of gene expression pattern and activation of signaling pathways between the two clusters, we compared the transcriptional profiles by using differential gene-expression (DGE) analysis. A total of 814 and 987 transcripts were identified to be up- and downregulated in CL1, respectively ($|\log_2 \text{Fold change}| > 1$ and $\text{FDR} < 0.01$, Supplementary Table 3). We found that many of the top upregulated genes in CL1 had well-known immune-related functions in the ImmPort database annotation (Figure 2A and Supplementary Table 3),

indicating differences in immune modulation between the two clusters. Meanwhile, Gene set enrichment analysis (GSEA) was performed, and it revealed a prominent enrichment of genes in key immune-related processes such as T cell receptor and signaling, innate immunity, and cytotoxic activity in CL1. Activation of immune-stimulating pathways (e.g., IFN- γ and NOD-like receptor signalings) and those related with immune escape (e.g., PD-1 and IL-10 signalings) were observed in CL1 (Figures 2B,C and Supplementary Table 4).

A CARS Predicts the Prognosis of IDH-wt Gliomas

To identify hub genes that are functionally linked to CARD clusters, WGCNA was performed to determine the co-expression modules. As shown in Figure 3A, transcripts in the green module displayed strong positive correlation with CARD clusters, as well as immune cell infiltration and cytotoxic T cell function (Figure 3A). Approximately half of the transcripts in the green module were differentially expressed between the two CARD clusters (Figure 3B). The 444 overlapped genes were thus used for least absolute shrinkage and selection operator (LASSO) penalized Cox proportional hazards regression to identify genes with best prognostic contribution in IDH-wt glioma (Figure 3C). A CARD-associated gene signature containing four genes (*SPP1*, *PTX3*, *ABCC3*, and *BST1*) with prognostic relevance was obtained (Figure 3D). Their expression was highly correlated with CARD-containing genes (Supplementary Figure 1A), and PPI network revealed underlying interactions (Figure 3E). To the survival significance of the CARD-associated genes, we investigated the protein level of one of the four genes, *PTX3*, in 103 IDH-wt glioma samples from the SYSUCC cohort by using TMA and IHC methods (Figure 3F). We found that the high expression of *PTX3* was associated with a decreased OS (Figure 3G), which is consistent with the results of the transcriptional analysis from the TCGA dataset.

Then, a CARS was calculated for each patient using a formula based on the expression levels of these four CARD-associated genes weighted by their regression coefficients in multivariate analysis:

$$\begin{aligned} \text{Risk score} = & (0.279 * \text{expression of SPP1}) + (0.193 * \\ & \text{expression of PTX3}) + (0.114 * \text{expression of BST1}) + \\ & (0.118 * \text{expression of ABCC3}) \end{aligned}$$

The distribution of risk score and the corresponding expression levels of these genes are shown in Supplementary Figures 1B–D. Higher CARS was observed in CL1 as compared with CL2 (Figure 3H). We segregated IDH-wt gliomas into high- and low-risk groups with the median CARS value. We found that GBM and mesenchymal subtypes were enriched in the high-risk group. According to the immune subtype classification proposed by Thorsson et al. (2019), we found that gliomas in high-risk group were dominantly attributed to the C4 subtype whereas the low-risk group had more tumors in the C5 subtype (Supplementary Figure 2). An alluvial diagram was used to visualize the attribute changes of individual

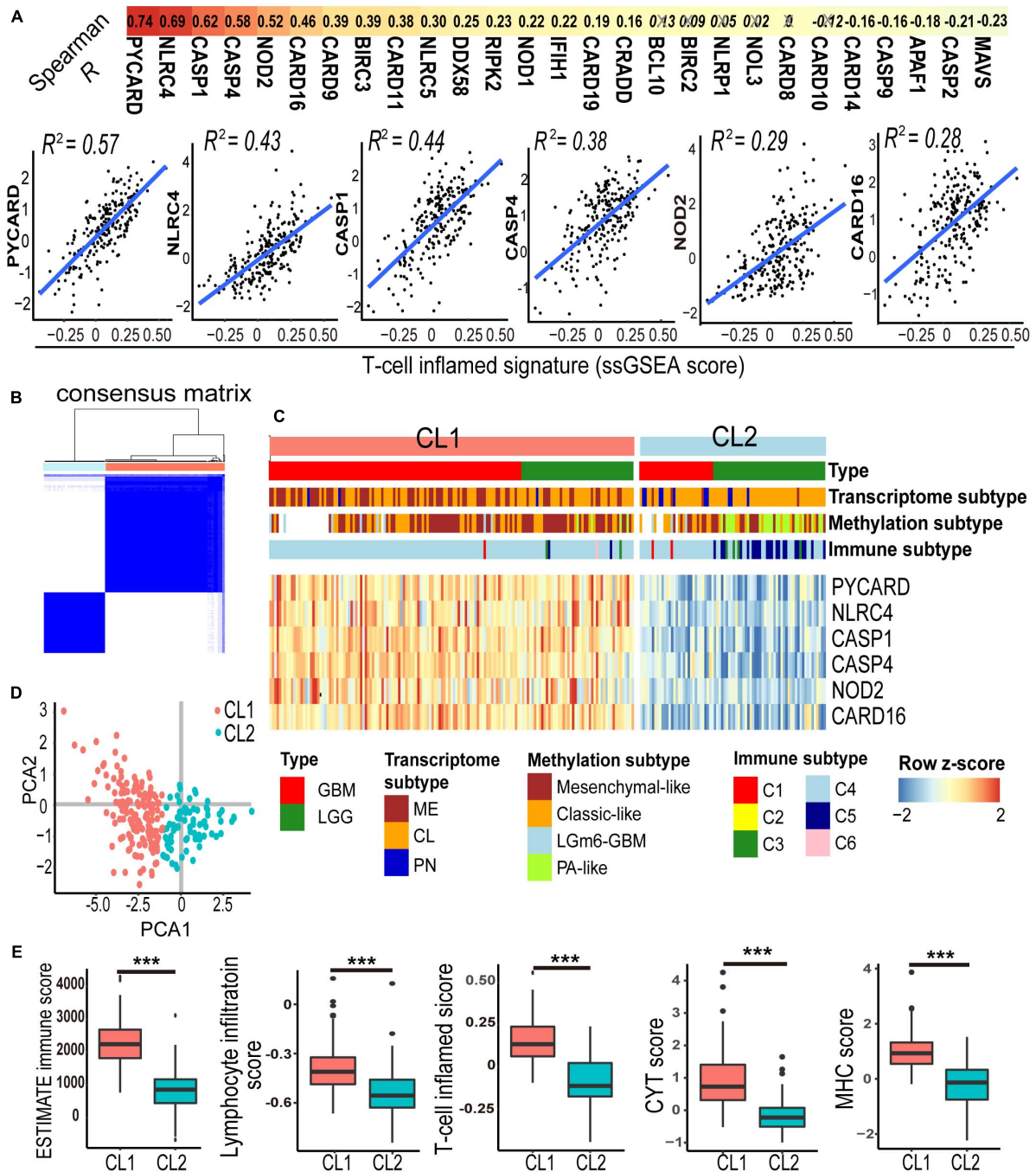


FIGURE 1 | A panel of six-CARD genes associates with T lymphocyte infiltration in TCGA IDH wild-type gliomas. **(A)** Correlation between CARD gene expression and T-cell inflamed ssGSEA score. Top depicts Spearman R values. Non-significant correlations are crossed out. Scatter plots show fitted coefficient R^2 values. **(B,C)** Consensus clustering matrix and heatmap with the six-CARD genes identified two clusters (CL1 and CL2). Histological and molecular subtypes were annotated for each patient. **(D)** PCA of two clusters. **(E)** Comparisons of immune score (from ESTIMATE), lymphocyte infiltration and T cell inflamed scores (from ssGSEA), and CYT and MHC scores (from mean gene expressions) between two clusters. P values: ***, <0.001 .

samples (Figure 3I). More importantly, patients in the high-risk group exhibited significantly worse outcomes compared with those in the low-risk group (Figure 3J). The prognostic significance of CARS was validated in two additional independent datasets from the CGGA and GSE16011 cohorts (Figure 3H).

Multivariate analyses also confirmed the independent prognostic value of the CARS (Table 1). Furthermore, CARS had a higher area under the curve (AUC) in receiver operating characteristic (ROC) analysis as compared with T cell inflamed score and clinical factors such as age, histological grade, and

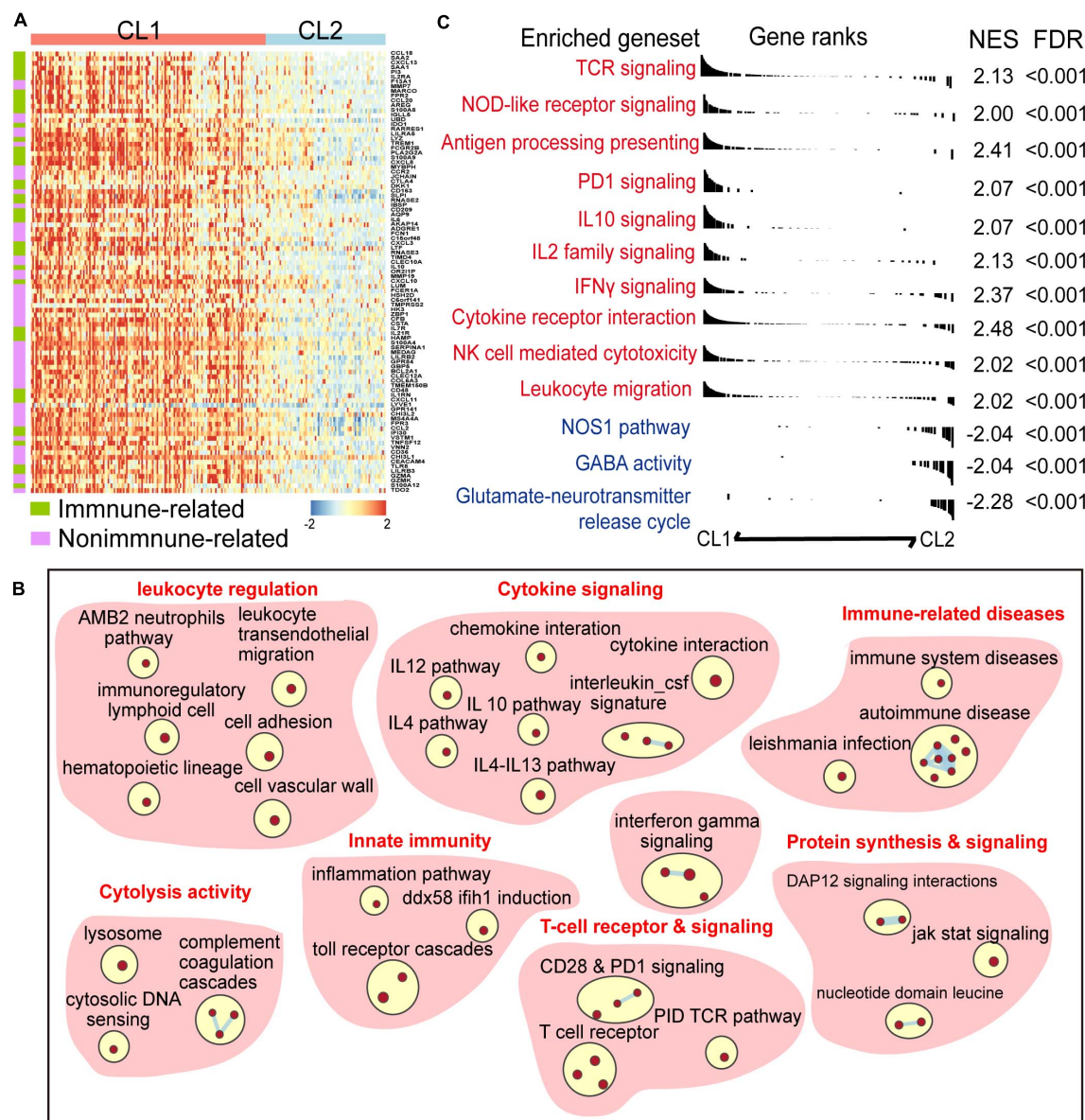


FIGURE 2 | A panel of six-CARD genes associates with activation of immune pathway. **(A)** Top upregulated genes in CL1 versus CL2 (\log_2 fold change >2 and $FDR < 0.01$). Genes were sorted by the fold change and annotated using Immport database. **(B)** Overview of gene sets enriched in CL1 versus CL2 [normalized enrichment score (NES) >2 and $FDR < 0.01$]. **(C)** Differences in canonical gene sets between CL1 and CL2.

MGMT promoter status, indicating its superiority for prognosis-prediction (Figure 3K).

High CARS Indicates the Activation of Adaptive Immunity

To further unveil the difference of tumor microenvironment (TME) in the high- and low-risk glioma groups, ssGSEA was employed to profile the level of immune cell infiltration and immune cell function in each group. We found a significant difference in major cell components associated with anti-tumor immunity in the two groups (Figure 4A and

Supplementary Figure 3). Of note, TME of the high-risk group displayed a prominent T cell infiltration at baseline. We found that biomarkers for activated and memory T cells (Figure 4C, left and middle panels), as well as elevated cytolytic activity (Figure 4D), were dominantly enriched in the high-risk group, indicating the pre-existing adaptive immune response. It has been suggested that the recruitment and priming of effector T cells rely on chemotaxis and the presence of licensed professional antigen-presenting cell populations (Sanchez-Paulete et al., 2017). We showed that significant upregulation of chemokines, including CCL5, CXCL9, and CXCL10, that are pivotal for the intratumoral trafficking of effector T cells was observed in the high-risk group

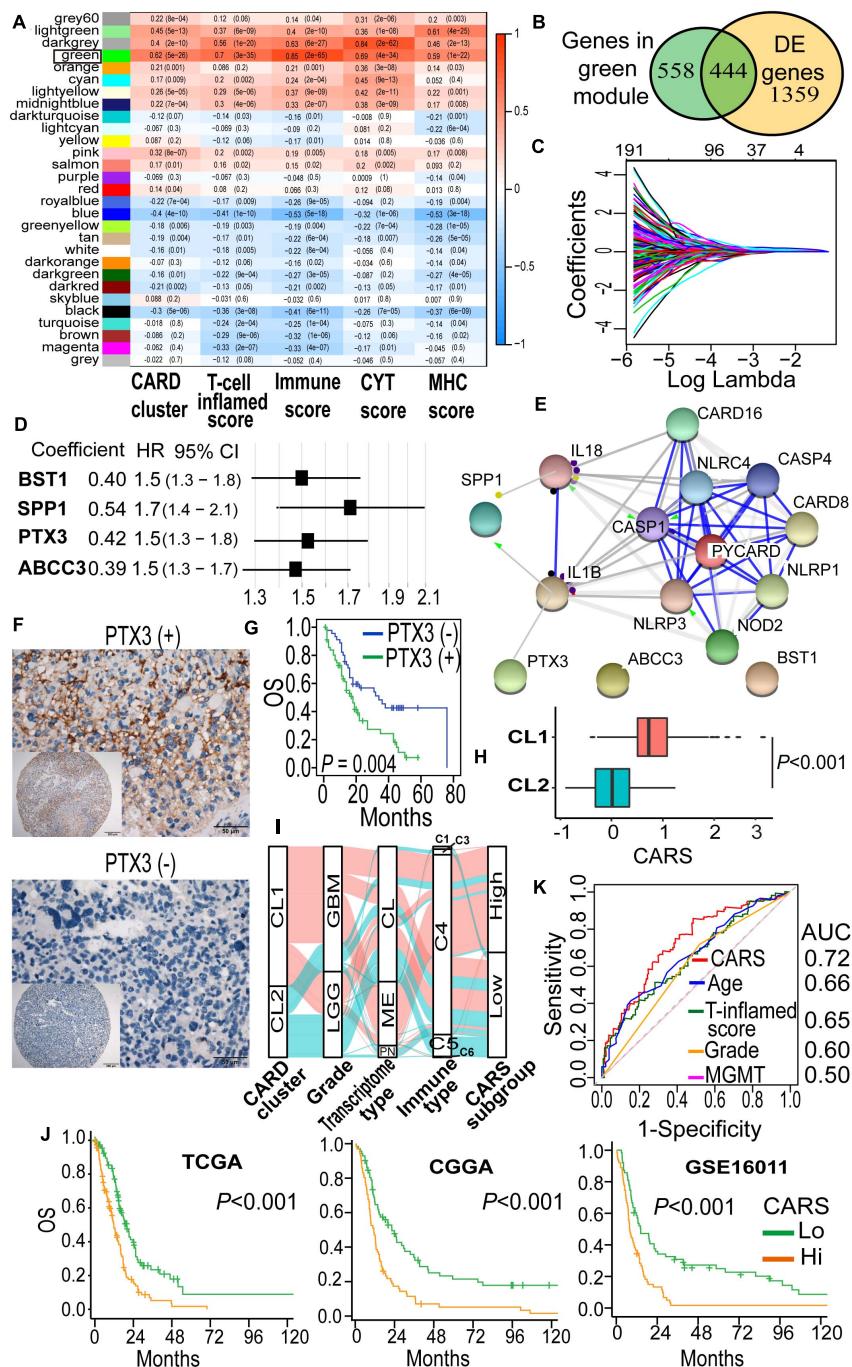


FIGURE 3 | Development of a CARD-associated risk score (CARS) with prognostic significance. **(A)** WGCNA revealed the correlations of gene modules with CARD clusters and immune phenotypes. Coefficient and *P* value of correlations were depicted in heatmap. **(B)** Venn plot shows the overlap of module genes and differentially expressed genes. **(C)** LASSO penalized regression identified four genes with optimal prognostic contributions. **(D)** Coefficient and hazard ratio of the four identified genes in the Cox regression model. **(E)** PPI network indicated interactions among the identified genes. **(F)** Representative images of IHC staining for PTX3 expression in IDH-wt glioma samples from SYSUCC cohort. **(G)** Kaplan–Meier analysis of overall survival according to the levels of PTX3 expression. **(H)** Comparison of CARS between CL1 and CL2. **(I)** Alluvial diagram showed the changes of CARD clusters, glioma molecular subtype, and CARS subgroup. **(J)** Kaplan–Meier curves between high- and low-risk groups in TCGA, CGGA, and GSE16011 cohorts. **(K)** ROC curve analyses of CARS, T cell inflamed score and clinical factors.

(Figure 4B). In addition, gliomas in the high-risk group had an elevated expression of genes involved in APC activation and function, including activated DC (Figure 4A), MHC-I class,

and Batf3-DC signature, which represent cross-presentation of antigen (Figure 4D). Infiltrating cells that enhance innate immune response such as CD56^{bright} natural killer (NK) cells

TABLE 1 | Univariate and multivariate Cox regression analyses for overall survival of IDH-wt glioma patients in public datasets.

Variables	Univariate analysis			Multivariate analysis		
	HR	95% CI	P value	HR	95% CI	P value
TCGA cohort (n = 231)						
Risk score	2.84	2.05–3.93	<0.001	2.98	2.04–4.35	<0.001
Age	1.03	1.02–1.05	<0.001	1.03	1.01–1.04	0.001
Gender (Male/Female)	1.30	0.94–1.80	0.115	–	–	–
Grade (GBM/LGG)	2.34	1.67–3.28	<0.001	1.23	0.80–1.88	0.342
RT (yes/no)	0.57	0.38–0.87	0.009	0.27	0.17–0.42	<0.001
MGMT						
Unmethylated	ref			–	–	–
Methylated	1.02	0.71–1.45	0.918	–	–	–
Unknown	1.47	0.96–2.25	0.078	–	–	–
CGGA cohort (n = 147)						
Risk score	2.17	1.57–3.93	<0.001	1.85	1.32–2.60	<0.001
Age	1.02	1.00–1.03	0.029	1.01	1.00–1.03	0.102
Gender (Male/Female)	1.30	0.89–1.90	0.176	–	–	–
Grade (GBM/LGG)	2.17	1.57–3.00	<0.001	1.77	1.14–2.73	0.011
RT (yes/no)						
No	ref			–	–	–
Yes	0.77	0.48–1.23	0.277	–	–	–
Unknown	1.79	0.76–4.21	0.183	–	–	–
MGMT						
Unmethylated	ref			–	–	–
Methylated	0.88	0.61–1.30	0.540	–	–	–
Unknown	0.43	0.14–1.38	0.158	–	–	–
GSE16011 cohort (n = 126)						
Risk score	2.76	1.87–4.07	<0.001	1.58	1.04–2.39	0.033
Age	1.04	1.03–1.06	<0.001	1.03	1.02–1.05	<0.001
Gender (Male/Female)	0.96	0.63–1.45	0.839	–	–	–
Grade (GBM/LGG)	3.91	2.41–6.34	<0.001	2.50	1.46–4.29	0.001
RT (yes/no)	1.10	0.71–1.69	0.672	–	–	–

Risk score and age were evaluated as continuous variables.

HR, hazard ratio; CI, confidence interval.

were also enriched (**Figure 4A**). Collectively, these results indicated that the high-risk glioma group had high CARS and exhibited T cell inflamed features with an increased pre-existing immunological activity.

High CARS Is Associated With T Cell Exhaustion and a Profound Immunosuppressive Microenvironment

As demonstrated above, patients in the high-risk group had a decreased survival despite the presence of cytotoxic T cells. The impaired function of inflamed T cells might partly account for this paradox. We found that multiple checkpoint receptors and their ligands such as PD-1, PD-L1, CTLA-4, LAG-3, TIM-3, IDO1, and CD39, as well as other immune inhibitory molecules including STAT1, were significantly upregulated in the high-risk group (**Figure 4C**, right panel) and thus might lead to inhibited function of T cells. The hyporesponsive T cells failed to incite effective anti-tumor immunity to maintain a durable tumor control. Moreover, the immunosuppressive

microenvironment has been linked to the oncogenesis and tumor progression. Here, CIBERSORT deconvolution method revealed that macrophages dominantly infiltrated in gliomas of both groups (**Supplementary Figure 4A** and **Figure 4E**), whereas the proportion of overall and immunosuppressive M2-type macrophage (**Figure 4E** and **Supplementary Figure 4B**) as well as the macrophage/T cell ratio (**Figure 4F**) was higher in the high-risk group. Similarly, enrichment of regulatory T cells (Treg; **Figure 4A**) and an elevated Treg/T cell ratio (**Figure 4G**) were also observed in the high-risk group. In addition, we found an accumulation of other immune inhibitory cellular components (e.g., immature DC, CD56^{dim} NK cell, MDSC; **Figure 4A**) and cytokines (e.g., IL10, IL11, and TGFβ1; **Figure 4B**) in the high-risk group. Consistent findings were also observed in the CGGA cohort (**Supplementary Figure 3**). In addition, we evaluated the immune homeostasis in these two groups by looking at the interaction between cells with anti-tumor or pro-tumor activities. Pearson's correlation analysis revealed that the abundance of immune cells of these two populations was positively associated with each group

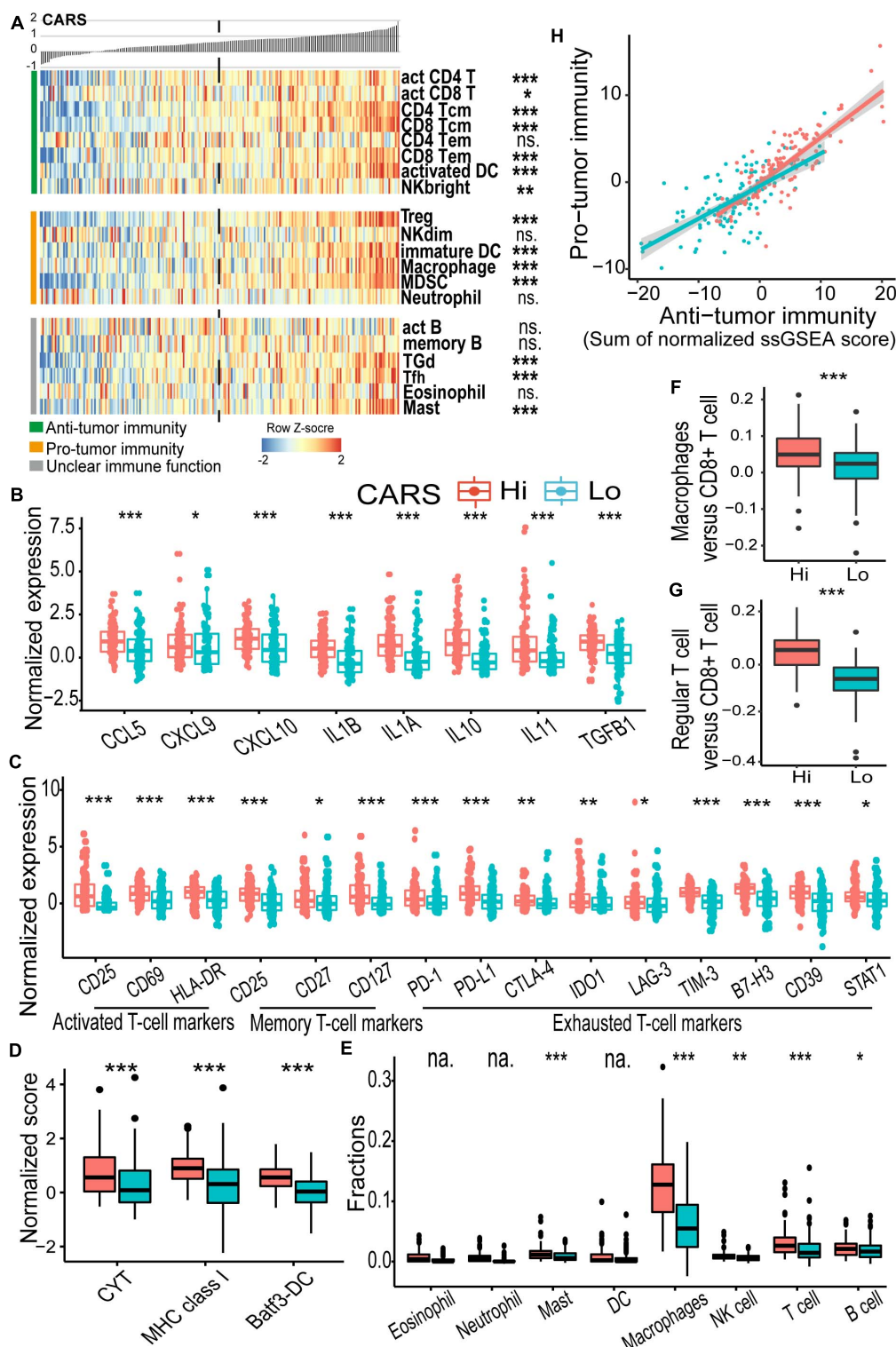


FIGURE 4 | CARS indicates distinct immune landscape in TCGA IDH wild-type gliomas. **(A)** Heatmap showed the ssGSEA score of each immune cell populations between high- and low-risk groups. Immune cells were categorized into anti-tumor immunity, pro-tumor immunity, and unclear immune function. **(B)** Comparisons of expressions of cytokines; **(C)** genes of T cell biomarkers; **(D)** normalized score of CYT, MHC, and Batf3-DC gene sets; **(E)** fractions of infiltrating leukocyte estimated by using CIBERSORT algorithm. **(F,G)** Ratio of macrophages versus CD8+ T cell and regular T cell versus CD8+ T cell between high- and low-risk groups. **(H)** Correlation between infiltrated immune cells for anti- and pro-tumor immunity. Comparison was not implemented when median of cell fraction is less than 0.001. P values: *, <0.05; **, <0.01; ***, <0.001; ns., not significant; na., not applicable.

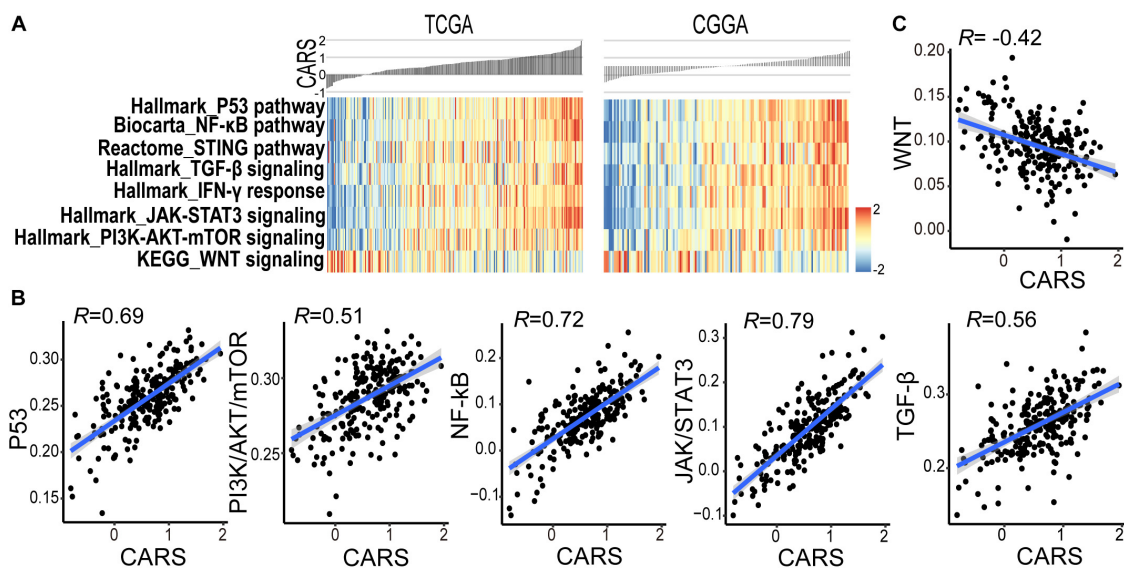


FIGURE 5 | CARS associates with disturbed oncogenic pathways. **(A)** Heatmap showed the ssGSEA score of the signaling pathway from the MSigDB database between high- and low-risk groups in TCGA (left) and CGGA (right) cohorts. **(B,C)** Spearman correlations between CARS and ssGSEA score of oncogenic pathways.

(Figure 4H), indicating the activation of immunosuppressive components in the TME.

CARS Is Associated With the Disturbance of Oncogenic Pathways in Gliomas

Accumulating evidence suggests that cancer-cell-intrinsic properties play a critical role in shaping the tumor immune microenvironment (Wellenstein and de Visser, 2018). In our study, we found that the major oncogenic pathways, such as PI3K/Akt/mTOR, JAK/STAT3, NF-κB, and TGF-β, were upregulated in the high-risk group (Figures 5A,B and Supplementary Figure 5), and activation of the WNT/β-catenin pathway was evident in the low-risk group (Figure 5C and Supplementary Figure 5). We also analyzed the genomic alterations in both groups. Significant enrichments of mutations of PTEN, PIK3R1, RB1, and MUC16 were observed in the high-risk group (Figure 6A and Supplementary Figure 6). There was no statistical difference in overall tumor mutation, aneuploidy, and neoantigen loads between the two groups (Figure 6B).

A High CARS Implicates an Improved Outcome of Anti-PD-1 Immunotherapy for IDH-wt Gliomas

Although several multi-gene expression signatures were developed to delineate tumor immune microenvironment and implied to be candidate biomarkers for predicting ICI treatment response in gliomas, none of them have been validated (Zhu et al., 2019; Wu et al., 2020). Here, we investigated the predictive performance of CARS by using recently published data on transcriptome as well as clinical data of patients with recurrent

IDH-wt gliomas under anti-PD-1 therapy (Zhao et al., 2019). In that study, responders, who were defined as radiologically stable for at least 6 months and/or having very few to no tumor cells in surgical tissues after anti-PD-1 therapy, had a favorable prognosis compared to non-responders (Figure 7A). We showed that recurrent gliomas with a high CARS were enriched in responders of anti-PD-1 therapy (Figure 7B). Moreover, we also found that an increased CARS was associated with a prolonged OS after anti-PD-1 therapy (Figure 7C). The median OS was not reached in patients with a high CARS and 8.1 months for those with a low CARS (HR: 0.12; 95% CI: 0.02–0.88; $P = 0.036$). In contrast, PD-L1 expression (Figure 7D) and tumor mutation burden (Figure 7E) failed to predict the prognosis of ICI in IDH-wt gliomas. Our data suggested that CARS had the capability to identify glioma patients who are more likely to benefit from anti-PD-1 therapy.

DISCUSSION

Large randomized trials have failed to recapitulate the efficacy of immune checkpoint blockade in unselected patients with gliomas. The heterogeneity of glioma immune microenvironment and the lack of predictive biomarkers for responsiveness to ICI may account for these clinical outcomes. Although several signaling pathways and cellular mechanisms have been explored in immune modulations in gliomas (Quail and Joyce, 2017; Cai et al., 2018; Zha et al., 2020), none of them have been successfully translated to the clinic to identify patients who will benefit from immunotherapy. Here, by integrating the TCGA dataset, publicly available transcriptional profiles and clinical outcome data, we developed a CARD-associated risk scoring system, which integrated with the heterogeneity of immune microenvironment and molecular landscape, as

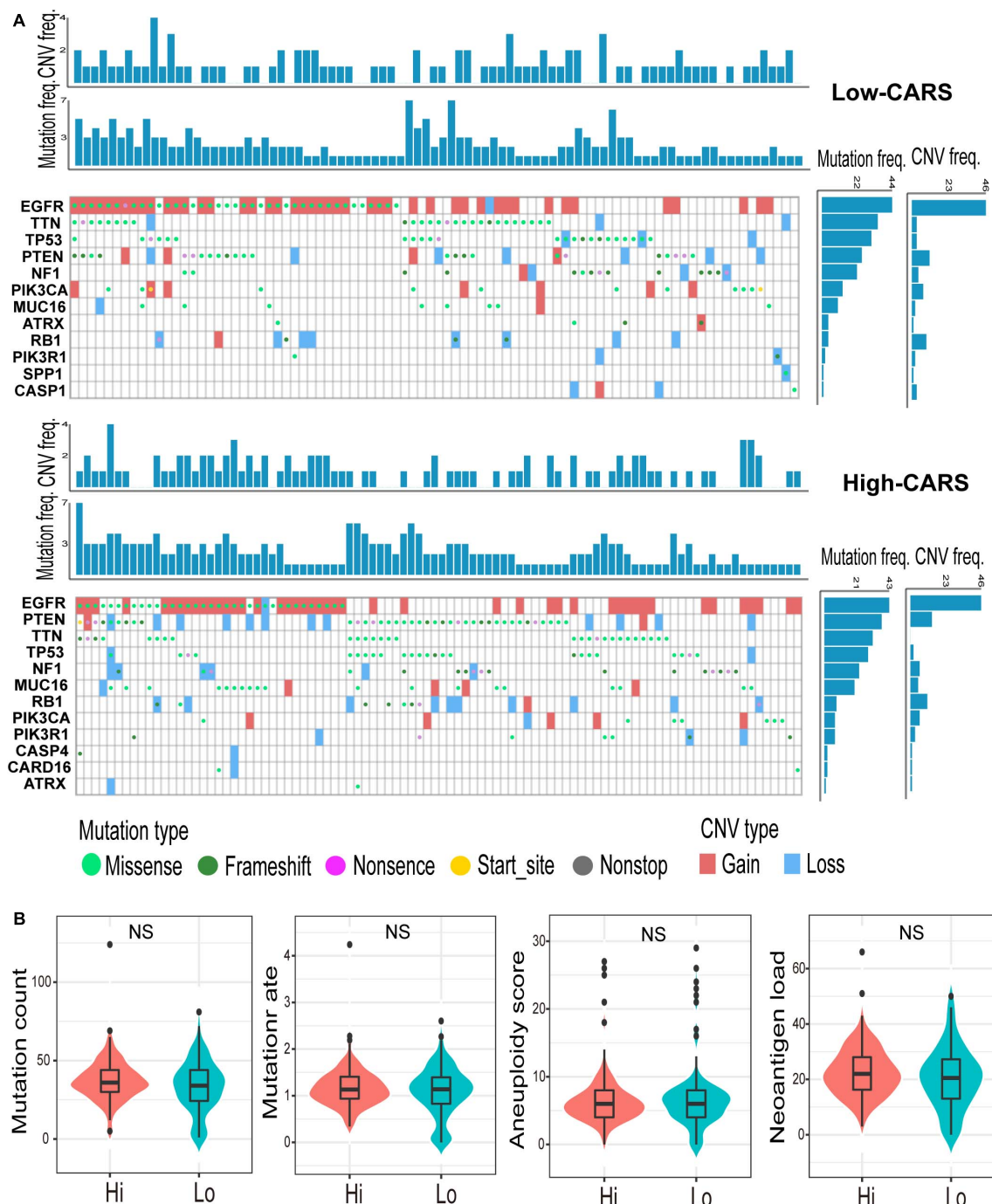
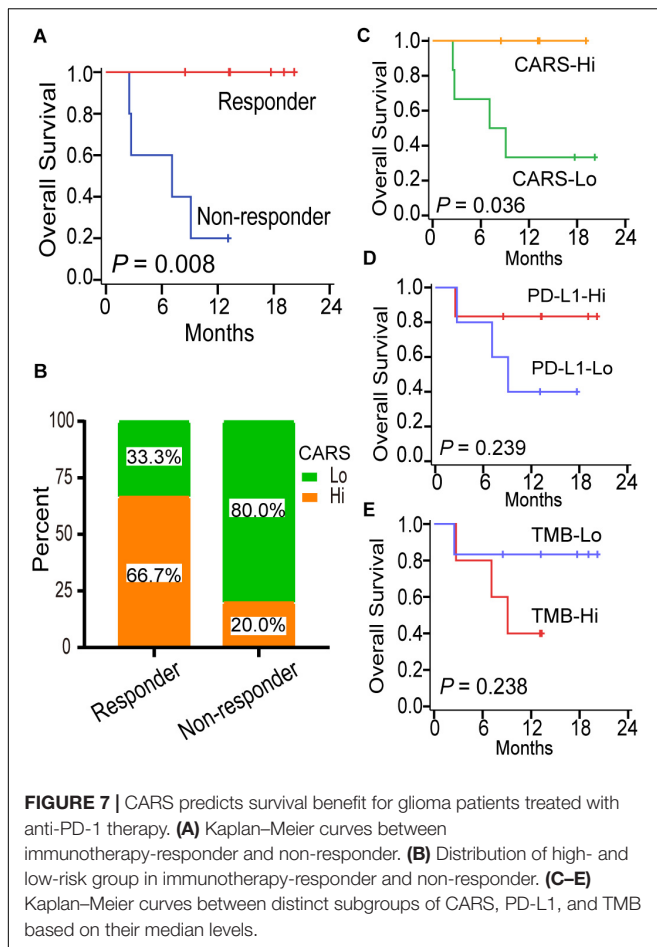


FIGURE 6 | Genomic alterations in the high- and low-risk group. **(A)** Waterfall plot of glioma somatic mutation and copy-number variation (CNV) in the high- (up) and low-risk group (down). Each column represented individual samples. The upper barplot showed mutation and CNV loads in each sample, and the right barplot indicated mutation and CNV frequencies in each gene. **(B)** Comparisons of non-silence mutation count, mutation rate, aneuploidy score, and neoantigen load between high- and low-risk groups. ns., not significant.

well as the difference in prognosis and responsiveness to ICI in IDH-wt gliomas.

Glioma is generally considered as a “cold” tumor with less lymphocyte infiltration. A pan-cancer immunogenomic classifier attributed gliomas to C4 (lymphocyte depleted) or C5

(immunologically quiet) subtypes, and both are characterized by the paucity of tumor-infiltrating lymphocytes (TILs) (Thorsson et al., 2019). In fact, TILs can be frequently identified in gliomas, but the extent varies greatly among tumors. We demonstrated that TILs were more evident in high-risk gliomas.



The mechanisms that underpin the accumulation or exclusion of lymphocytes within TME have not been fully understood. Results from previous studies suggested that tumor neoantigens are crucial to the recruitment of lymphocytes (Becht et al., 2014). However, no difference was found in neoantigen load between the high- and low-risk group in the present study. Spranger et al. revealed that upregulation of the oncogenic β -catenin pathway suppressed the production of crucial chemokine CCL4 and subsequently prevented recruitment of intratumoral CD103⁺ DCs, followed by diminishing T lymphocytes in melanomas (Spranger et al., 2015). In our study, activation of β -catenin signaling pathway as well as reduction in DCs and cross-presentation process was observed in low-risk gliomas, which may contribute to the exclusion of T cells.

The infiltration of lymphocytes has been reported to imply an adaptive immunity against tumor progression and positively impact clinical survival in a variety of tumor types including gliomas (Lohr et al., 2011; Sanchez-Canteli et al., 2020). However, conflicting evidences exist. Rutledge et al. (2013) quantified TILs in 171 GBMs from the TCGA database and found that the number of TILs is correlated with specific histopathological features but not with survival. Zhai and colleagues (Zhai et al., 2017) showed that infiltrating T lymphocytes in GBMs contributed to the worse prognosis by directly inducing IDO1

expression. In this study, we found that high-risk IDH-wt glioma was enriched with TILs but had a decreased overall survival. There are several reasons that may account for the inconsistency. Firstly, various approaches were employed to characterize lymphocyte infiltration. Here, we inferred TILs by using the transcription-based algorithms. In some other studies, TILs were determined through visual evaluation of stained slides. The accuracy of histopathological estimation was affected by factors such as the inter-observer bias and heterogeneous distribution of T cells in tissue sections and slides (Khoury et al., 2018). Secondly, the difference in the sample size among studies may also result in the discrepancy. Moreover, we found that the prominent lymphocytes infiltration was accompanied by the dominance of M2-type macrophage as well as abundant negative regulators (e.g., CTLA-4 and IDO1), which constituted a microenvironment preferentially toward pro-tumor activities and fostered tumor progression.

T cell exhaustion was initially described in a mouse model of chronic viral infection, where the presence of persistent antigen diminished the pathogen-specific T cell response. Cancer also exploits this mechanism to induce immune escape. Our findings demonstrated that T cells in high-risk glioma shared key features of T cell exhaustion such as the expression of co-inhibitory receptors including PD-1, LAG-3, and TIM-3, as observed in chronic infections. Traditionally, T cell exhaustion was defined as a terminal differentiation state with the characteristics of anergy, which suppresses the immunosurveillance against tumorigenesis. However, accumulating evidence suggested that exhausted T cells are not fully inert but retain the expansion capacity and the capability to produce chemokines (Li et al., 2019). Furthermore, intratumoral exhausted T cells exhibit cytotoxic and effector potential. Davidson et al. (2019) demonstrated that PD1⁺CD8⁺ T cells in gliomas had elevated TCR clonality and decreased diversity, reflecting the activation of specific anti-tumor machinery within this cell population. In line with those findings, we revealed that T cells in high-risk glioma also displayed activated features by increased expression of effector T cell genes (e.g., CD25, CD69, and HLA-DR), as well as cytolytic biomarkers. The pre-existing exhausted T cells in high-risk glioma partially sustain immunocompetence and are the targets of checkpoint-based immunotherapy.

Multi-gene signatures have been developed to predict treatment benefits of ICI in a variety of cancers. An 11-immune-related gene signature was found to be prognostic for patients with cervical cancer when treated with ICI (Yang et al., 2019). Ayers et al. (2017) confirmed the predictive usefulness of an IFN- γ -related mRNA profile for the response to pembrolizumab in melanomas. However, no predictive transcriptional biomarker has been established with validation in gliomas due to the scarcity of both pre-treatment tumor samples with sequencing data and associated clinical outcomes. In our study, we evaluated the predictive value of CARS in a recently published cohort of glioma patients treated with PD-1 inhibitors (Zhao et al., 2019). We showed that an increased CARS was dominantly identified in ICI responders and predicted a prolonged survival, whereas PD-L1 transcription and TMB were not associated with clinical outcomes. Our data suggested that CARS can be employed to

identify glioma patients who will obtain the most benefit from PD-1 checkpoint blockade, but validation in clinical trials with large sample size is warranted.

Our study also suggests different mechanisms underlying the primary resistance to ICI among IDH-wt gliomas. High-risk glioma showed evidence of pre-existing T cells that can be potentially reinvigorated by the blockade of PD-1. However, a broad set of immunosuppressive mechanisms are active in the TME. Overexpression of immune inhibitory molecules such as IDO1 and TIM-3, together with higher proportions of M2-type macrophage, Treg, and MDSCs, impeded the antitumor immune response triggered by ICI. Accordingly, antagonism of immunosuppressive signaling other than the PD-1/PD-L1 axis is feasible to increase the activity of checkpoint-based therapies in the high-risk group. On the other hand, the lack of priming signals and T cell infiltration at baseline in low-risk glioma appears to correlate with ICI insensitivity. Detonating the immunogenicity with tumor- and dendritic cell-based vaccination or oncolytic viruses will enhance the anti-PD-1 efficacy in this subset of tumors.

CONCLUSION

Our study developed a CARS, which categorized IDH-wt gliomas into two groups with distinct immune and molecular characteristics. An increased CARS is associated with a profound immunosuppressive microenvironment with pre-existing adaptive immunity. Patients in the high-risk group had a reduced OS under standard care but tended to benefit from checkpoint immunotherapy. We believe that our findings will enhance the understanding of heterogeneity in the tumor immune microenvironment and contribute to tailoring immunotherapy for IDH-wt gliomas.

DATA AVAILABILITY STATEMENT

The datasets presented in this study can be found in online repositories. The names of the repository is the Research Data

Deposit public platform (www.researchdata.org.cn), with the approval number as RDDB2021001075.

ETHICS STATEMENT

The studies involving human participants were reviewed and approved by the Ethics Committee of Sun Yat-sen University Cancer Center. Written informed consent to participate in this study was provided by the participants' legal guardian/next of kin.

AUTHOR CONTRIBUTIONS

KS, YM, and ZC designed this study. WH, ZH, and HD performed the experiments. DL, PZ, XW, SZ, XJ, and JZh analyzed the data. DL, XL, and CG drafted this manuscript. KS, JW, and JZe revised the manuscript. All authors approved the publication of the manuscript.

FUNDING

This work was supported by the National Natural Science Foundation of China (81772675 and 81872324).

ACKNOWLEDGMENTS

We thank Dr. Junfei Zhao from the Department of Biomedical Informatics at Columbia University for providing processed transcriptome data and the associated clinical information.

SUPPLEMENTARY MATERIAL

The Supplementary Material for this article can be found online at: <https://www.frontiersin.org/articles/10.3389/fcell.2021.653240/full#supplementary-material>

REFERENCES

- Alexander, B. M., and Cloughesy, T. F. (2017). Adult glioblastoma. *J. Clin. Oncol.* 35, 2402–2409.
- Ayers, M., Lunceford, J., Nebozhyn, M., Murphy, E., Loboda, A., Kaufman, D. R., et al. (2017). IFN-gamma-related mRNA profile predicts clinical response to PD-1 blockade. *J. Clin. Invest.* 127, 2930–2940. doi: 10.1172/jci91190
- Bao, Z. S., Chen, H. M., Yang, M. Y., Zhang, C. B., Yu, K., Ye, W. L., et al. (2014). RNA-seq of 272 gliomas revealed a novel, recurrent PTPRZ1-MET fusion transcript in secondary glioblastomas. *Genome Res.* 24, 1765–1773. doi: 10.1101/gr.165126.113
- Becht, E., Goc, J., Germain, C., Giraldo, N. A., Dieu-Nosjean, M. C., Sautes-Fridman, C., et al. (2014). Shaping of an effective immune microenvironment to and by cancer cells. *Cancer Immunol. Immunother.* 63, 991–997. doi: 10.1007/s00262-014-1590-3
- Bouchier-Hayes, L., and Martin, S. J. (2002). CARD games in apoptosis and immunity. *EMBO Rep.* 3, 616–621. doi: 10.1093/embo-reports/kvf139
- Cai, J., Chen, Q., Cui, Y., Dong, J., Chen, M., Wu, P., et al. (2018). Immune heterogeneity and clinicopathologic characterization of IGFBP2 in 2447 glioma samples. *Oncoimmunology* 7:e1426516. doi: 10.1080/2162402x.2018.1426516
- Calabrò, A., Beissbarth, T., Kuner, R., Stojanov, M., Benner, A., Asslaber, M., et al. (2009). Effects of infiltrating lymphocytes and estrogen receptor on gene expression and prognosis in breast cancer. *Breast Cancer Res. Treat.* 116, 69–77. doi: 10.1007/s10549-008-0105-3
- Charoentong, P., Finotello, F., Angelova, M., Mayer, C., Efremova, M., Rieder, D., et al. (2017). Pan-cancer immunogenomic analyses reveal genotype-immunophenotype relationships and predictors of response to checkpoint blockade. *Cell Rep.* 18, 248–262. doi: 10.1016/j.celrep.2016.12.019
- Chen, J., McKay, R. M., and Parada, L. F. (2012). Malignant glioma: lessons from genomics, mouse models, and stem cells. *Cell* 149, 36–47. doi: 10.1016/j.cell.2012.03.009
- Damiano, J. S., and Reed, J. C. (2004). CARD proteins as therapeutic targets in cancer. *Curr. Drug Targets* 5, 367–374. doi: 10.2174/1389450043345470

- Davidson, T. B., Lee, A., Hsu, M., Sedighim, S., Orpilla, J., Treger, J., et al. (2019). Expression of PD-1 by T Cells in malignant glioma patients reflects exhaustion and activation. *Clin. Cancer Res.* 25, 1913–1922. doi: 10.1158/1078-0432.ccr-18-1176
- Davoli, T., Uno, H., Wooten, E. C., and Elledge, S. J. (2017). Tumor aneuploidy correlates with markers of immune evasion and with reduced response to immunotherapy. *Science* 355:eaaf8399. doi: 10.1126/science.aaf8399
- Dunn, G. P., Cloughesy, T. F., Maus, M. V., Prins, R. M., Reardon, D. A., and Sonabend, A. M. (2020). Emerging immunotherapies for malignant glioma: from immunogenomics to cell therapy. *Neuro Oncol.* 22, 1425–1438. doi: 10.1093/neuonc/noaa154
- Gravendeel, L. A., Kouwenhoven, M. C., Gevaert, O., de Rooij, J. J., Stubbs, A. P., Duijm, J. E., et al. (2009). Intrinsic gene expression profiles of gliomas are a better predictor of survival than histology. *Cancer Res.* 69, 9065–9072. doi: 10.1158/0008-5472.can-09-2307
- Hänzelmann, S., Castelo, R., and Guinney, J. (2013). GSEA: gene set variation analysis for microarray and RNA-seq data. *BMC Bioinform.* 14:7. doi: 10.1186/1471-2105-14-7
- Hu, W. M., Zhang, J., Sun, S. X., Xi, S. Y., Chen, Z. J., Jiang, X. B., et al. (2017). Identification of P4HA1 as a prognostic biomarker for high-grade gliomas. *Pathol. Res. Pract.* 213, 1365–1369. doi: 10.1016/j.prp.2017.09.017
- Khoury, T., Peng, X., Yan, L., Wang, D., and Nagrle, V. (2018). Tumor-infiltrating lymphocytes in breast cancer: evaluating interobserver variability, heterogeneity, and fidelity of scoring core biopsies. *Am. J. Clin. Pathol.* 150, 441–450.
- Langfelder, P., and Horvath, S. (2008). WGCNA: an R package for weighted correlation network analysis. *BMC Bioinform.* 9:559. doi: 10.1186/1471-2105-9-559
- Lauss, M., Donia, M., Harbst, K., Andersen, R., Mitra, S., Rosengren, F., et al. (2017). Mutational and putative neoantigen load predict clinical benefit of adoptive T cell therapy in melanoma. *Nat. Commun.* 8:1738.
- Li, H., van der Leun, A. M., Yofe, I., Lubling, Y., Gelbard-Solodkin, D., van Akkooi, A. C. J., et al. (2019). Dysfunctional CD8 T cells form a proliferative, dynamically regulated compartment within human melanoma. *Cell* 176, 775.e18–89.e18.
- Liberzon, A., Subramanian, A., Pinchback, R., Thorvaldsdóttir, H., Tamayo, P., and Mesirov, J. P. (2011). Molecular signatures database (MSigDB) 3.0. *Bioinformatics* 27, 1739–1740. doi: 10.1093/bioinformatics/btr260
- Lohr, J., Ratliff, T., Huppertz, A., Ge, Y., Dictus, C., Ahmadi, R., et al. (2011). Effector T-cell infiltration positively impacts survival of glioblastoma patients and is impaired by tumor-derived TGF- β . *Clin. Cancer Res.* 17, 4296–4308. doi: 10.1158/1078-0432.ccr-10-2557
- Matusiak, M., Van Opdenbosch, N., and Lamkanfi, M. (2015). CARD- and pyrin-only proteins regulating inflammasome activation and immunity. *Immunol. Rev.* 265, 217–230. doi: 10.1111/immr.12282
- Miao, E. A., Rajan, J. V., and Aderem, A. (2011). Caspase-1-induced pyroptotic cell death. *Immunol. Rev.* 243, 206–214. doi: 10.1111/j.1600-065x.2011.01044.x
- Narayan, S., Kolly, L., So, A., and Busso, N. (2011). Increased interleukin-10 production by ASC-deficient CD4⁺ T cells impairs bystander T-cell proliferation. *Immunology* 134, 33–40. doi: 10.1111/j.1365-2567.2011.03462.x
- Newman, A. M., Steen, C. B., Liu, C. L., Gentles, A. J., Chaudhuri, A. A., Scherer, F., et al. (2019). Determining cell type abundance and expression from bulk tissues with digital cytometry. *Nat. Biotechnol.* 37, 773–782. doi: 10.1038/s41587-019-0114-2
- Olson, D. J., and Luke, J. J. (2019). The T-cell-inflamed tumor microenvironment as a paradigm for immunotherapy drug development. *Immunotherapy* 11, 155–159. doi: 10.2217/imt-2018-0171
- Park, H. H. (2019). Caspase recruitment domains for protein interactions in cellular signaling (Review). *Int. J. Mol. Med.* 43, 1119–1127.
- Quail, D. F., and Joyce, J. A. (2017). The microenvironmental landscape of brain tumors. *Cancer Cell* 31, 326–341. doi: 10.1016/j.ccell.2017.02.009
- Reardon, D. A., Brandes, A. A., Omuro, A., Mulholland, P., Lim, M., Wick, A., et al. (2020). Effect of nivolumab vs bevacizumab in patients with recurrent glioblastoma: the checkmate 143 phase 3 randomized clinical trial. *JAMA Oncol.* 6, 1003–1010. doi: 10.1001/jamaoncol.2020.1024
- Reimand, J., Isserlin, R., Voisin, V., Kucera, M., Tannus-Lopes, C., Rostamianfar, A., et al. (2019). Pathway enrichment analysis and visualization of omics data using g:Profiler, GSEA, Cytoscape and EnrichmentMap. *Nat. Protocol.* 14, 482–517. doi: 10.1038/s41596-018-0103-9
- Reuss, D. E., Kratz, A., Sahm, F., Capper, D., Schrimpf, D., Koelsche, C., et al. (2015). Adult IDH wild type astrocytomas biologically and clinically resolve into other tumor entities. *Acta Neuropathol.* 130, 407–417. doi: 10.1007/s00401-015-1454-8
- Robinson, M. D., McCarthy, D. J., and Smyth, G. K. (2010). edgeR: a bioconductor package for differential expression analysis of digital gene expression data. *Bioinformatics* 26, 139–140. doi: 10.1093/bioinformatics/btp616
- Rutledge, W. C., Kong, J., Gao, J., Gutman, D. A., Cooper, L. A., Appin, C., et al. (2013). Tumor-infiltrating lymphocytes in glioblastoma are associated with specific genomic alterations and related to transcriptional class. *Clin. Cancer Res.* 19, 4951–4960. doi: 10.1158/1078-0432.ccr-13-0551
- Sanchez-Canteli, M., Granda-Diaz, R., Del Rio-Ibáñez, N., Allonca, E., Lopez-Alvarez, F., Agorreta, J., et al. (2020). PD-L1 expression correlates with tumor-infiltrating lymphocytes and better prognosis in patients with HPV-negative head and neck squamous cell carcinomas. *Cancer Immunol. Immunother.* 69, 2089–2100. doi: 10.1007/s00262-020-02604-w
- Sanchez-Paulete, A. R., Teixeira, A., Cueto, F. J., Garasa, S., Perez-Gracia, J. L., Sanchez-Arrea, A., et al. (2017). Antigen cross-presentation and T-cell cross-priming in cancer immunology and immunotherapy. *Ann. Oncol.* 28:xii74. doi: 10.1093/annonc/mdx727
- Spranger, S., Bao, R., and Gajewski, T. F. (2015). Melanoma-intrinsic β -catenin signalling prevents anti-tumour immunity. *Nature* 523, 231–235. doi: 10.1038/nature14404
- Spranger, S., Dai, D., Horton, B., and Gajewski, T. F. (2017). Tumor-residing Batf3 dendritic cells are required for effector T cell trafficking and adoptive T cell therapy. *Cancer Cell* 31, 711.e4–723.e4.
- Stupp, R., Taillibert, S., Kanner, A. A., Kesari, S., Steinberg, D. M., Toms, S. A., et al. (2015). Maintenance therapy with tumor-treating fields plus temozolomide vs temozolomide alone for glioblastoma: a randomized clinical trial. *JAMA* 314, 2535–2543. doi: 10.1001/jama.2015.16669
- Subramanian, A., Tamayo, P., Mootha, V. K., Mukherjee, S., Ebert, B. L., Gillette, M. A., et al. (2005). Gene set enrichment analysis: a knowledge-based approach for interpreting genome-wide expression profiles. *Proc. Natl. Acad. Sci. U.S.A.* 102, 15545–15550. doi: 10.1073/pnas.0506580102
- Thorsson, V., Gibbs, D. L., Brown, S. D., Wolf, D., Bortone, D. S., Ou Yang, T. H., et al. (2019). The immune landscape of cancer. *Immunity* 51, 411–412.
- Vivian, J., Rao, A. A., Nothhaft, F. A., Ketchum, C., Armstrong, J., Novak, A., et al. (2017). Toil enables reproducible, open source, big biomedical data analyses. *Nat. Biotechnol.* 35, 314–316. doi: 10.1038/nbt.3772
- Waldman, A. D., Fritz, J. M., and Lenardo, M. J. (2020). A guide to cancer immunotherapy: from T cell basic science to clinical practice. *Nat. Rev. Immunol.* 20, 651–668. doi: 10.1038/s41577-020-0306-5
- Wellenstein, M. D., and de Visser, K. E. (2018). Cancer-cell-intrinsic mechanisms shaping the tumor immune landscape. *Immunity* 48, 399–416. doi: 10.1016/j.immuni.2018.03.004
- Wilkerson, M. D., and Hayes, D. N. (2010). ConsensusClusterPlus: a class discovery tool with confidence assessments and item tracking. *Bioinformatics* 26, 1572–1573. doi: 10.1093/bioinformatics/btq170
- Wu, F., Wang, Z. L., Wang, K. Y., Li, G. Z., Chai, R. C., Liu, Y. Q., et al. (2020). Classification of diffuse lower-grade glioma based on immunological profiling. *Mol. Oncol.* 14, 2081–2095. doi: 10.1002/1878-0261.12707
- Yang, S., Wu, Y., Deng, Y., Zhou, L., Yang, P., Zheng, Y., et al. (2019). Identification of a prognostic immune signature for cervical cancer to predict survival and response to immune checkpoint inhibitors. *Oncoimmunology* 8:e1659094. doi: 10.1080/2162402x.2019.1659094
- Yoshihara, K., Shahmoradgol, M., Martínez, E., Vegesna, R., Kim, H., Torres-García, W., et al. (2013). Inferring tumour purity and stromal and immune cell admixture from expression data. *Nat. Commun.* 4:2612.
- Zha, C., Meng, X., Li, L., Mi, S., Qian, D., Li, Z., et al. (2020). Neutrophil extracellular traps mediate the crosstalk between glioma progression and the tumor microenvironment via the HMGB1/RAGE/IL-8 axis. *Cancer Biol. Med.* 17, 154–168.

- Zhai, L., Ladomersky, E., Lauing, K. L., Wu, M., Genet, M., Gritsina, G., et al. (2017). Infiltrating T cells increase IDO1 expression in glioblastoma and contribute to decreased patient survival. *Clin. Cancer Res.* 23, 6650–6660. doi: 10.1158/1078-0432.ccr-17-0120
- Zhao, J., Chen, A. X., Gartrell, R. D., Silverman, A. M., Aparicio, L., Chu, T., et al. (2019). Immune and genomic correlates of response to anti-PD-1 immunotherapy in glioblastoma. *Nat. Med.* 25, 462–469.
- Zhu, C., Zou, C., Guan, G., Guo, Q., Yan, Z., Liu, T., et al. (2019). Development and validation of an interferon signature predicting prognosis and treatment response for glioblastoma. *Oncoimmunology* 8:e1621677. doi: 10.1080/2162402x.2019.1621677

Conflict of Interest: The authors declare that the research was conducted in the absence of any commercial or financial relationships that could be construed as a potential conflict of interest.

Copyright © 2021 Li, Hu, Lin, Zhang, He, Zhong, Wen, Zhang, Jiang, Duan, Guo, Wang, Zeng, Chen, Mou and Sai. This is an open-access article distributed under the terms of the Creative Commons Attribution License (CC BY). The use, distribution or reproduction in other forums is permitted, provided the original author(s) and the copyright owner(s) are credited and that the original publication in this journal is cited, in accordance with accepted academic practice. No use, distribution or reproduction is permitted which does not comply with these terms.



OPEN ACCESS

Edited by:

Giovanni Gaudino,
University of Hawaii Cancer Center,
United States

Reviewed by:

Suneet Shukla,
United States Food and Drug
Administration, United States
Junjiang Chen,
The Chinese University of Hong Kong,
China
Milica Pešić,
University of Belgrade, Serbia

*Correspondence:

Zhe-Sheng Chen
chenz@stjohns.edu

†These authors have contributed
equally to this work

†Present address:

Pranav Gupta,
Departments of Medicine
and Pathology,
Massachusetts General Hospital
and Harvard Medical School,
Boston, MA, United States

Specialty section:

This article was submitted to
Molecular and Cellular Oncology,
a section of the journal
Frontiers in Cell and Developmental
Biology

Received: 12 December 2020

Accepted: 02 March 2021

Published: 22 March 2021

Citation:

Lei Z-N, Teng Q-X, Gupta P,
Zhang W, Narayanan S, Yang D-H,
Wurpel JND, Fan Y-F and Chen Z-S
(2021) Cabozantinib Reverses
Topotecan Resistance in Human
Non-Small Cell Lung Cancer
NCI-H460/TPT10 Cell Line and Tumor
Xenograft Model.
Front. Cell Dev. Biol. 9:640957.
doi: 10.3389/fcell.2021.640957

Cabozantinib Reverses Topotecan Resistance in Human Non-Small Cell Lung Cancer NCI-H460/TPT10 Cell Line and Tumor Xenograft Model

Zi-Ning Lei^{††}, Qiu-Xu Teng^{††}, Pranav Gupta^{1†}, Wei Zhang^{1,2}, Silpa Narayanan¹, Dong-Hua Yang¹, John N. D. Wurpel¹, Ying-Fang Fan^{1,3} and Zhe-Sheng Chen^{1*}

¹ Department of Pharmaceutical Sciences, College of Pharmacy and Health Sciences, St. John's University, Queens, NY, United States, ² Institute of Plastic Surgery, Weifang Medical University, Weifang, China, ³ Department of Hepatobiliary Surgery, Zhujiang Hospital of Southern Medical University, Guangzhou, China

Cabozantinib (CBZ) is a small molecule tyrosine kinase receptor inhibitor, which could also inhibit the ABCG2 transporter function. Therefore, CBZ could re-sensitize cancer cells that are resistant to ABCG2 substrate drugs including topotecan (TPT). However, its reversal effect against TPT resistance has not been tested in a TPT-induced resistant cancer model. In this study, a new TPT selected human non-small cell lung cancer (NSCLC)-resistant cell model NCI-H460/TPT10 with ABCG2 overexpression and its parental NCI-H460 cells were utilized to investigate the role of CBZ in drug resistance. The *in vitro* study showed that CBZ, at a non-toxic concentration, could re-sensitize NCI-H460/TPT10 cells to TPT by restoring intracellular TPT accumulation via inhibiting ABCG2 function. In addition, the increased cytotoxicity by co-administration of CBZ and TPT may be contributed by the synergistic effect on downregulating ABCG2 expression in NCI-H460/TPT10 cells. To further verify the applicability of the NCI-H460/TPT10 cell line to test multidrug resistance (MDR) reversal agents *in vivo* and to evaluate the *in vivo* efficacy of CBZ on reversing TPT resistance, a tumor xenograft mouse model was established by implanting NCI-H460 and NCI-H460/TPT10 into nude mice. The NCI-H460/TPT10 xenograft tumors treated with the combination of TPT and CBZ dramatically reduced in size compared to tumors treated with TPT or CBZ alone. The TPT-resistant phenotype of NCI-H460/TPT10 cell line and the reversal capability of CBZ in NCI-H460/TPT10 cells could be extended from *in vitro* cell model to *in vivo* xenograft model. Collectively, CBZ is considered to be a potential approach in overcoming ABCG2-mediated MDR in NSCLC. The established NCI-H460/TPT10 xenograft model could be a sound clinically relevant resource for future drug screening to eradicate ABCG2-mediated MDR in NSCLC.

Keywords: cabozantinib, non-small cell lung cancer, topotecan resistance, NCI-H460/TPT10, ABCG2, tumor xenograft model, micro-environment

INTRODUCTION

Lung cancer remains a leading cause of cancer-related death worldwide (Bray et al., 2018; Siegel et al., 2020). Non-small cell lung cancer (NSCLC) accounts for most of the lung cancer cases with a 5-year survival rate as low as 20% (Osmani et al., 2018). Topotecan (TPT), an FDA-approved anti-cancer drug for small cell lung cancer (SCLC), has exhibited efficacy for advanced NSCLC patients as a first- or second-line treatment (Powell et al., 2013; Vennepureddy et al., 2015). However, resistance to TPT has been shown in NSCLC with multidrug resistance (MDR) phenotype (d'Amato et al., 2007; Li et al., 2017). Cancer MDR refers to the resistance against multiple mechanistically and structurally unrelated antitumor drugs in cancer cells, which has become a major contributor to clinical failure in cancer chemotherapy (Ejendal and Hrycyna, 2002; Zhang et al., 2015). The overexpression of ATP-binding cassette (ABC) transporters on the plasma membrane of cancer cells, which efflux an extensive spectrum of chemotherapeutic agents out of the cancer cells, is one of the primary mechanisms contributing to cancer MDR (Sharom, 2008; Zhang et al., 2015). In particular, ABCG2, also known as breast cancer resistance protein (BCRP; Mao and Unadkat, 2015), has been suggested to be closely associated with the resistance against topoisomerase I inhibitors in NSCLC, including TPT, irinotecan, and SN-38 (d'Amato et al., 2007; Fan et al., 2019). To investigate the mechanisms of TPT resistance in NSCLC, we established a TPT-resistant human NSCLC cell line NCI-H460/TPT10. Consistent with the aforementioned hypothesis, overexpression of ABCG2 was observed in the NCI-H460/TPT10 cells compared to their parental NCI-H460 cells, and mechanistic studies indicated that ABCG2 was the major factor conferring TPT resistance in NCI-H460/TPT10 cells (Lei et al., 2020). The established NCI-H460/TPT10 cell line could be a useful model for studying TPT resistance and discovering novel reversal agents to overcome MDR in NSCLC, yet applicability of NCI-H460/TPT10 cell line as a TPT-resistant model *in vivo* has not been verified.

Cabozantinib (CBZ) is a small molecule tyrosine kinase receptor inhibitor (TKI), which targets c-Met and vascular endothelial growth factor receptor 2 (VEGFR2), that has been approved by the FDA to treat advanced renal cell carcinoma and medullary thyroid cancer (Kurzrock et al., 2011; Yakes et al., 2011). In a previous study, the capability of CBZ to inhibit the function of ABCG2 and re-sensitize ABCG2 overexpressing cells to ABCG2 substrate drugs, including TPT, has been demonstrated in *in vitro* settings (Zhang G.N. et al., 2017). Nevertheless, the tests on monolayer-cultured cell models could not mimic the complicated natural tumor micro-environment, which is an important factor affecting tumor growth, metastasis, as well as resistance to therapies *in vivo* (Gillet et al., 2011; Quail and Joyce, 2013). The present study aims to validate the NCI-H460/TPT10 cell line as a clinically relevant model *in vivo* by establishing an NCI-H460/TPT10 tumor xenograft mouse model and to verify the *in vivo* efficacy of CBZ on reversing TPT resistance using the established animal model.

MATERIALS AND METHODS

Chemicals and Reagents

Dulbecco's modified Eagle's medium (DMEM), fetal bovine serum (FBS), bovine calf serum (BS), penicillin/streptomycin, and trypsin 0.25% were purchased from Hyclone (GE Healthcare Life Science, Pittsburgh, PA, United States). The radio-labeled [³H]-mitoxantrone (4 Ci/mmol) was purchased from Moravex Biochemicals, Inc. (Brea, CA, United States). Phosphate buffered saline (PBS) and dimethyl sulfoxide (DMSO) were obtained from Thermo Fisher Scientific Inc. (Rockford, IL, United States). Mitoxantrone (MX), SN-38, cisplatin, geneticin (G418), and Ko143 were obtained from Enzo Life Sciences (Farmingdale, NY, United States). CBZ was purchased from Chemietek Company (Indianapolis, IL, United States). The mouse monoclonal antibodies for ABCG2 and glyceraldehyde phosphate dehydrogenase (GAPDH) were obtained from Thermo Fisher Scientific Inc. (Rockford, IL, United States). The rabbit monoclonal antibodies against human DNA topoisomerase I, the HRP-labeled anti-mouse secondary antibody, and the HRP-linked anti-rabbit secondary antibody were purchased from Cell Signaling Technology (Danvers, MA, United States). TPT, 3-(4, 5-dimethylthiazol-2-yl)-5-diphenyltetrazolium bromide (MTT), and all other chemicals were purchased from Sigma Chemical Co. (St. Louis, MO, United States).

Cell Lines and Cell Culture

The human NSCLC NCI-H460 cell line was cultured in DMEM containing 10% FBS and 1% penicillin/streptomycin. Its TPT-resistant cell line NCI-H460/TPT10 was maintained in the same culture media supplemented with 10 μ M TPT (Lei et al., 2020) and switched into a drug-free medium for more than 2 weeks prior to their use. The ABCG2 gene knockout subline of NCI-H460/TPT10 and the corresponding vector control, which were constructed using clustered regularly interspaced short palindromic repeats (CRISPR)/CRISPR-associated (Cas) 9 system (Lei et al., 2020), were maintained in growth medium supplemented with 1.5 mg/mL G418. The HEK293/ABCG2 and HEK293/pcDNA3.1 cell lines, which were established by transfecting HEK293 cells with the pcDNA3.1 vector containing full-length ABCG2 and the empty vector, respectively, were cultured in growth medium containing 2 mg/mL G418. All cell lines were cultured in a humidified atmosphere at 37°C with 5% CO₂.

Cytotoxicity Assay

The MTT colorimetric assay was performed to measure the sensitivity of cells to TPT in the presence or absence of CBZ or positive ABCG2 inhibitor Ko143. Briefly, 5×10^3 cells/well were evenly seeded into 96-well plates and cultured overnight. Different concentrations of TPT were added into assigned wells in the presence or absence of CBZ or Ko143 at a fixed concentration. CBZ and Ko143 were added 2 h before TPT. After incubating the plates for 68 h, 4 mg/mL MTT solution

was added to each well, and the plates were incubated for an additional 4 h. The medium in each well was subsequently replaced by 100 μ L of DMSO. The absorbance at 570 nm was determined by the accuSkan GO UV/Vis Microplate Spectrophotometer. The concentration of CBZ used in the reversal experiment was selected at its IC₂₀ (80% of cells remain viable at this concentration) for both cell lines from MTT assay.

Intracellular Topotecan Accumulation Assay

The intracellular accumulation of TPT in NCI-H460/TPT10 and the parental NCI-H460 cells with or without pre-treatment with CBZ was determined by flow cytometric analysis. Cells (1×10^6 /mL) were incubated at 37°C in the culture medium with or without 5 μ M CBZ for 2 h followed by an additional 2 h incubation with the culture medium containing 100 μ M TPT with or without 5 μ M CBZ. At the end of the incubation, cells were washed and resuspended with ice-cold 0.5% bovine serum albumin (BSA) prepared in PBS. The fluorescence from intracellular TPT was analyzed on BD Accuri C6 flow cytometer (BD Biosciences, San Jose, CA, United States) as previously described (Lei et al., 2020).

[³H]-Mitoxantrone Accumulation and Efflux Assay

The effect of CBZ on the intracellular accumulation and efflux of [³H]-mitoxantrone was determined in NCI-H460, NCI-H460/TPT10, HEK293, and HEK293/ABCG2 cells. The drug accumulation and efflux assay was performed as previously described (Wang et al., 2020). Briefly, 1×10^5 cells/well were evenly seeded into 24-well plates and cultured overnight. Then, cells were incubated at 37°C in a medium with or without CBZ (5 μ M) or Ko143 (5 μ M) for 2 h followed by additional 2 h incubation in a medium containing 10 nM [³H]-mitoxantrone with or without CBZ or Ko143. After incubation, cells were washed with ice-cold PBS and then incubated in [³H]-mitoxantrone-free medium with or without CBZ or Ko143. At various time points (0, 30, 60, and 120 min), cells were harvested and transferred into scintillation fluid. The radioactivity was determined using the liquid scintillation counter (Packard Instrument, IL, United States).

Western Blotting Analysis

The NCI-H460 and NCI-H460/TPT10 cells were incubated at 37°C for 72 h with vehicle control, 30 nM TPT, 5 μ M CBZ, and the combination of 30 nM TPT and 5 μ M CBZ, respectively. At the end of incubation, the cell lysates were collected for protein extraction, and the protein expression levels of ABCG2, DNA topoisomerase I (TOP I), and GAPDH were determined using Western blotting analysis. The protein extraction and quantification, gel electrophoresis, and Western blotting analysis were carried

out as previously described (Zhang G.N. et al., 2017). A 1:1000 dilution using the blocking agent was applied to all antibodies before use.

Experimental Animals

Male athymic NCR nude mice (14–16 g, age 4–5 weeks) were used for the tumor xenograft model. The project was conducted following the Animal Welfare Act and other federal statutes. The maintenance of the mice and all the *in vivo* studies were conducted in the Animal Care Center of St. John's University. The animal study was reviewed and approved by the Institutional Animal Care and Use Committee of St. John's University (Protocol #1925).

In vivo Tumor Model

The TPT-resistant NCI-H460/TPT10 model was modified from the NCI-H460 tumor xenograft model previously established by Chen's Laboratory (Sodani et al., 2014). A 40 mg/kg oral dose of CBZ was selected based on previous preclinical studies that gave 30 or 40 mg/kg of cabozantinib daily for at least 14 days and showed no remarkable toxicity in mice (Zhou et al., 2016; Koinis et al., 2020). Briefly, 4×10^6 of NCI-H460 cells and 6×10^6 of NCI-H460/TPT10 cells were injected subcutaneously in the same male nude mice, with NCI-H460 and NCI-H460/TPT10 in the left and right flank near the armpit, respectively. The mice were randomized into four groups (6 in each group) after the subcutaneous tumors reached a mean diameter of 0.5 cm. Different groups then received various treatments every 3rd day with a total of 6 times: (1) vehicle solution (10% N-methyl-pyrrolidinone + 90% polyethylene glycol 300) as a negative control by mouth (p.o.); (2) TPT (3.0 mg/kg, i.p.); (3) CBZ (40 mg/kg, p.o.); and (4) combination of TPT (3.0 mg/kg, i.p.) and CBZ (40 mg/kg, p.o.). CBZ was given 1 h before TPT administration. Throughout the study, all mice were weighed, and tumors were measured with a caliper every 3rd day before the treatment. Tumor volumes (V) were calculated as previously described (Tiwari et al., 2013). After the treatment cycle, the mice were euthanized by carbon dioxide, and the tumors were excised and weighed. The ratio of growth inhibition (IR) was calculated according to the formula: $IR = 1 - (\text{Mean tumor weight of experimental group} / \text{Mean tumor weight of vehicle control group}) \times 100\%$ (Tiwari et al., 2013).

Statistical Analysis

One-way ANOVA followed by Tukey's *post hoc* test was performed for the *in vitro* studies. Two-way ANOVA followed by Tukey's *post hoc* test was performed for comparing multiple groups with repeated tumor volume measurements in the animal study. Statistical significance was set at $p < 0.05$, and statistical analysis was carried out using GraphPad Prism 8 for macOS (GraphPad Software, La Jolla, CA, United States).

RESULTS

The Effect of Cabozantinib on Reversing Topotecan Resistance and Restoring Intracellular Topotecan in NCI-H460/TPT10 Cells

Cell-based MTT assay showed that CBZ did not have significant cytotoxicity in NCI-H460 and NCI-H460/TPT10 cells, with an IC_{50} value higher than 10 μ M (Figure 1A). Based on this result, CBZ at a concentration of 5 μ M, from which 80% of the cells could survive, was selected for reversal studies. As shown in Figure 1B, CBZ, at a non-toxic concentration (5 μ M), could significantly decrease the IC_{50} value of TPT in NCI-H460/TPT10 cells. The cross-resistance to other ABCG2 substrates in NCI-H460/TPT10 cells, including mitoxantrone and SN-38, could also be reversed by CBZ with comparable potency to the ABCG2

inhibitor Ko143 (Table 1). On the other hand, the IC_{50} value of cisplatin, which is not a substrate of ABCG2, was not affected by co-administration of 5 μ M CBZ (Figure 1C). Furthermore, CBZ could restore TPT accumulation in ABCG2 overexpressing NCI-H460/TPT10 cells (Figures 1D,E). These observations indicated that the CBZ can alleviate TPT resistance most likely by increasing intracellular TPT level, which could be a result from the ABCG2 inhibitory effect of CBZ. A slight reduction of TPT IC_{50} and elevation of TPT accumulation in parental NCI-H460 cells treated with CBZ were observed (Figures 1B,D,E), possibly due to the endogenous ABCG2 expression in NCI-H460 cells.

Involvement of ABCG2 in the Reversal Activity of Cabozantinib

The reversal activity of CBZ was further tested in ABCG2 gene knockout cells derived from NCI-H460/TPT10 cells to further

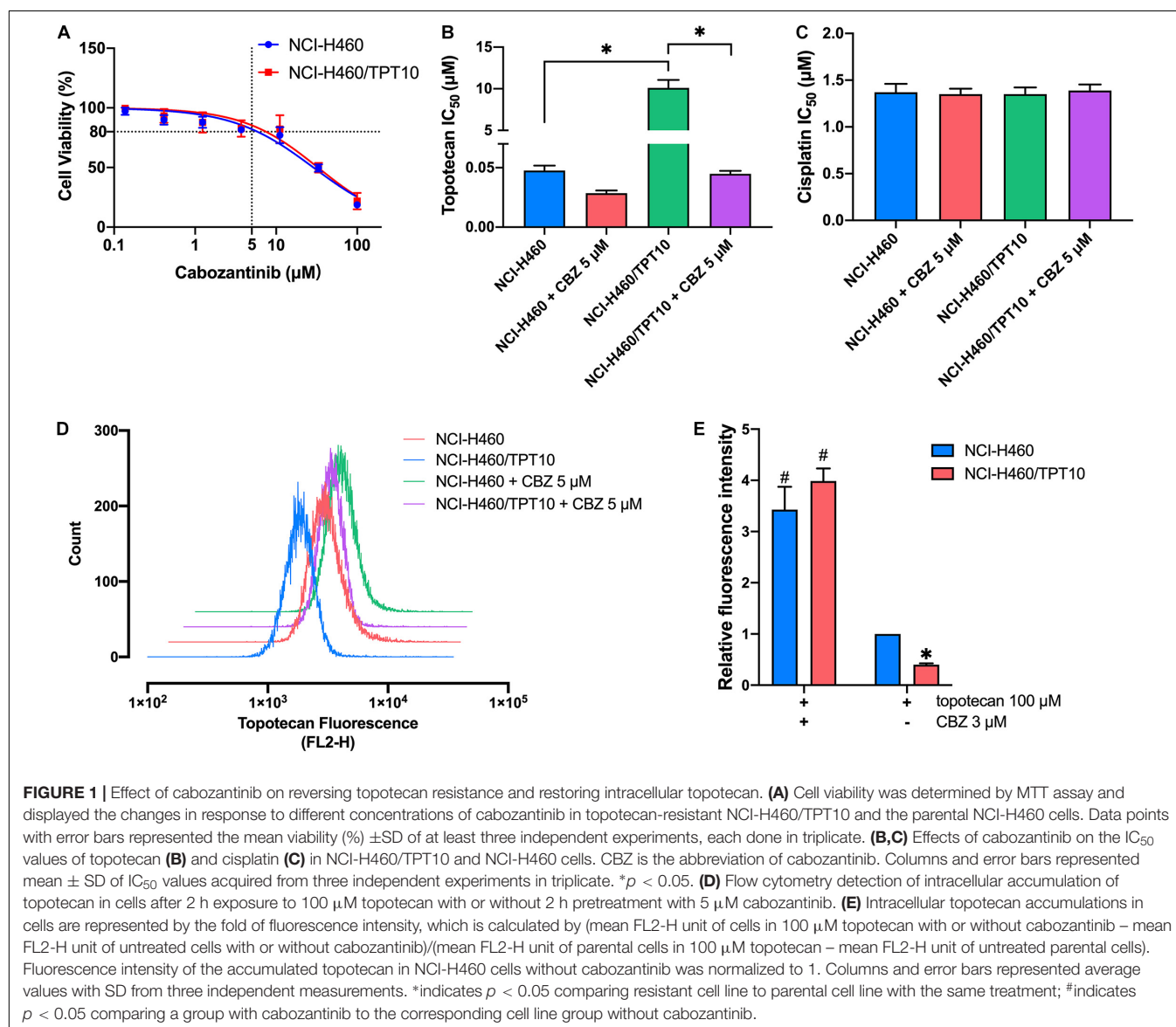


TABLE 1 | The drug-resistance of NCI-H460/TPT10 and the reversal effect with cabozantinib.

Treatment	IC ₅₀ ± SD ^a (μM; Resistance fold ^b)	
	NCI-H460	NCI-H460/TPT10
Topotecan	0.0476 ± 0.0042 (1.00)	10.1044 ± 0.9571 (212.39)*
+CBZ 3 μM	0.0468 ± 0.0041 (0.98)	0.0883 ± 0.0072 (1.86)
+CBZ 5 μM	0.0287 ± 0.0022 (0.60)	0.0449 ± 0.0024 (0.94)
+Ko143 5 μM	0.0292 ± 0.0027 (0.61)	0.0401 ± 0.0042 (0.84)
Mitoxantrone	0.0363 ± 0.0043 (1.00)	4.2621 ± 0.5715 (117.36)*
+CBZ 3 μM	0.0391 ± 0.0022 (1.08)	0.0554 ± 0.0188 (1.53)
+CBZ 5 μM	0.0376 ± 0.0012 (1.04)	0.0373 ± 0.0031 (1.03)
+Ko143 5 μM	0.0325 ± 0.0028 (0.90)	0.0302 ± 0.0042 (0.83)
SN-38	0.0112 ± 0.0020 (1.00)	1.3125 ± 0.1991 (116.96)*
+CBZ 3 μM	0.0131 ± 0.0015 (1.17)	0.0385 ± 0.0052 (3.44)
+CBZ 5 μM	0.0139 ± 0.0022 (1.24)	0.0129 ± 0.0044 (0.98)
+Ko143 5 μM	0.0130 ± 0.0007 (1.16)	0.0188 ± 0.0022 (1.68)
Cisplatin	1.3750 ± 0.0908 (1.00)	1.3575 ± 0.0409 (0.99)
+CBZ 3 μM	1.3883 ± 0.0744 (1.01)	1.3582 ± 0.0722 (0.99)
+CBZ 5 μM	1.3514 ± 0.0591 (0.98)	1.3952 ± 0.0642 (1.01)
+Ko143 5 μM	1.3868 ± 0.0668 (1.01)	1.3765 ± 0.0837 (1.00)

^aIC₅₀: concentration that inhibited cell survival by 50% (mean ± SD).

^bResistance fold represents IC₅₀ value for topotecan, mitoxantrone, SN-38, or cisplatin with or without CBZ or Ko143 divided by IC₅₀ value for topotecan, mitoxantrone, SN-38, or cisplatin of NCI-H460 cells without CBZ or Ko143. Values in table are determined from at least three independent experiments performed in triplicate. *indicates significant difference from IC₅₀ of NCI-H460/TPT10 (*P < 0.05).

confirm the involvement of ABCG2. The NCI-H460/TPT10-ABCG2 knockout cells restored sensitivity to TPT and was slightly more sensitive compared to NCI-H460 cells that express low level of ABCG2. While CBZ effectively reduced the IC₅₀ value of TPT in NCI-H460/TPT10 cells transfected with the vector control plasmid, it failed in further sensitizing NCI-H460/TPT10-ABCG2 knockout cells to TPT (Figure 2A), suggesting that ABCG2 is the key target of CBZ in reversing TPT resistance. As cisplatin was a non-substrate control, the IC₅₀ values remained consistent among the cell lines tested regardless of ABCG2 expression level (Figure 2B), which confirmed that the reversal effect of CBZ was specific against ABCG2 substrates.

The results from [³H]-mitoxantrone accumulation and efflux assay further verified the aforementioned inference. In consistent to the result from TPT accumulation assay, the intracellular accumulation of [³H]-mitoxantrone was significantly higher and the ABCG2 efflux activity was reduced in the NCI-H460 control group, compared to that of the ABCG2 overexpressing NCI-H460/TPT10 cells (Figures 2C,D). CBZ at 5 μM significantly increased the accumulation of [³H]-mitoxantrone and mitigated [³H]-mitoxantrone efflux, which was comparable to the inhibitory effect on ABCG2 function of 5 μM Ko143. Besides, the intracellular [³H]-mitoxantrone level in NCI-H460 cells got a slight rise and the efflux activity was relatively lessened with the presence of CBZ or Ko143, indicating that a low extent of ABCG2 inhibitory effect was exerted to NCI-H460 cells by CBZ or Ko143. Similar reversal effects by CBZ and Ko143 were observed from HEK293/ABCG2

cells (Figures 2E,F). No obvious difference in the intracellular [³H]-mitoxantrone accumulation level and efflux activity was shown among HEK293/pcDNA3.1 control, CBZ, and Ko143 group, confirming that the effect of CBZ in increasing drug accumulation and decreasing efflux relied on the expression of functional ABCG2.

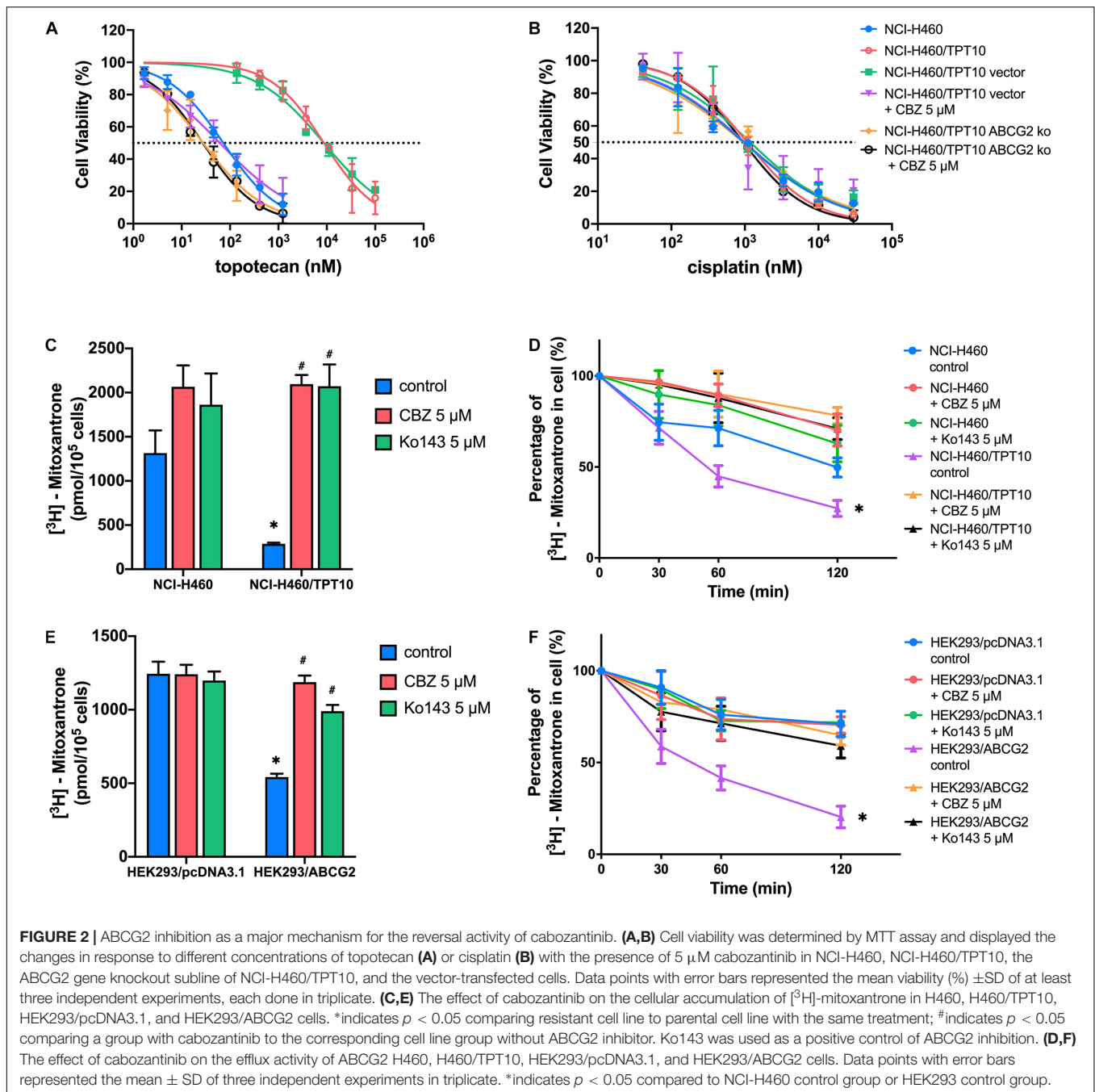
The Effect of Cabozantinib Combined With Topotecan on Protein Expression of ABCG2 and Topoisomerase I

The protein expression levels of ABCG2 and topoisomerase I were investigated to further evaluate the interaction of CBZ with TPT. The low level of endogenous ABCG2 expression in NCI-H460 cells and the overexpression of ABCG2 in NCI-H460/TPT10 cells were verified. As illustrated in Figure 3A, neither CBZ nor TPT alters the ABCG2 protein expression when administrated alone. However, co-administration of 5 μM CBZ and 30 nM TPT downregulated the ABCG2 expression in NCI-H460/TPT10 cells but not in NCI-H460 cells, indicating that the synergistic effect of CBZ and TPT on reducing ABCG2 protein level may be ABCG2-dependent.

As the target of TPT, the topoisomerase I expression in NCI-H460 cells was downregulated by 30 nM TPT monotherapy or combination treatment with 5 μM CBZ. In TPT-resistant NCI-H460/TPT10 cells, the expression of topoisomerase I was not reduced by 30 nM TPT but was significantly reduced by co-administration of 30 nM TPT and 5 μM CBZ (Figure 3B). This is consistent with the cytotoxicity results that resistance to TPT in NCI-H460/TPT10 cells was reversed by CBZ and with the TPT accumulation results that the low intracellular TPT level in NCI-H460/TPT10 cells was restored by CBZ. Specially, although the TPT-resistant NCI-H460/TPT10 cell line did not have differential expression of topoisomerase I with the parental NCI-H460 cell line, CBZ specifically downregulates the topoisomerase I expression in the parental NCI-H460 cells.

The Efficacy of Cabozantinib Combined With Topotecan in NCI-H460/TPT10 Tumor Xenograft Mouse Model

To verify whether the *in vitro* findings could extend to an *in vivo* model, NCI-H460 cells and NCI-H460/TPT10 cells were implanted subcutaneously into athymic nude mice to establish tumor xenograft models. As demonstrated in Figures 4, 5, TPT at 3.0 mg/kg with or without CBZ showed different degrees of anti-cancer activity in tumor xenograft mice without apparent adverse effects or weight loss. TPT alone at 3.0 mg/kg i.p. dose demonstrated significant growth retardation in the drug-sensitive NCI-H460 tumors (Figures 4A,B) but not in the drug-resistance NCI-H460/TPT10 tumors (Figures 4C,D). Similarly, the inhibitory effect of TPT on tumor weight was significantly lower in the NCI-H460/TPT tumors than in the NCI-H460 tumors (Figures 5A–C), suggesting a TPT resistant phenotype in NCI-H460/TPT10 xenograft model. The average tumor volume and tumor weight of implanted NCI-H460 cells and NCI-H460/TPT10 cells were significantly diminished in the CBZ–TPT combination treatment group as compared to the



vehicle and TPT alone groups (**Figures 4, 5**). Besides, the CBZ–TPT combination treatment showed a higher inhibition rate in NCI-H460 xenograft tumors compared to NCI-H460/TPT10 xenograft tumors, indicating possible MDR mechanisms that were not modulated by CBZ in NCI-H460/TPT10 cells *in vivo*. The CBZ alone group also exhibited significant reductions in tumor weight in both cell lines, though the tumor growth inhibitory effect was not as much as that in the CBZ–TPT combination group. These results suggested that the combination of CBZ and TPT could have synergistic effects on both NCI-H460 and NCI-H460/TPT10 xenograft tumors. Overall, the

NCI-H460/TPT xenograft model presented the same phenotype of drug-resistance to TPT, and this resistance could be reversed by the ABCG2 inhibitor CBZ in the xenograft mouse model.

DISCUSSION

It has been suggested that TPT has a good prospect as a first- or second-line treatment for progressed or relapsed NSCLC because of its high efficacy and favorable side effect profile (Vennepureddy et al., 2015). However, as TPT is

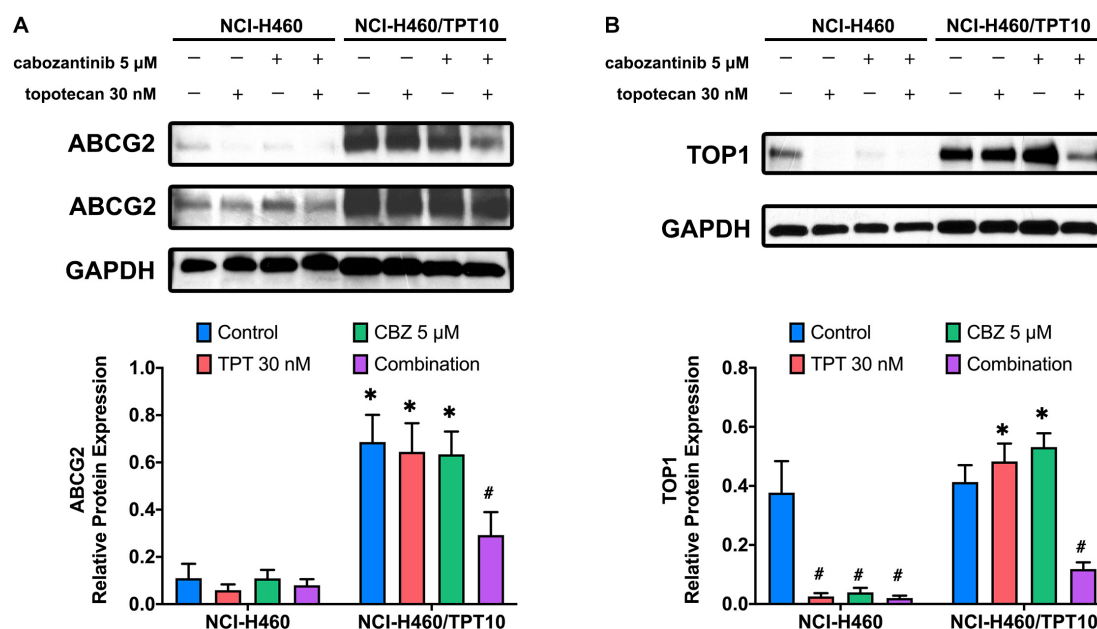


FIGURE 3 | Effect of cabozantinib combined with topotecan on the expression of ABCG2 and topoisomerase I (TOP1). Expression of ABCG2 protein (**A**) and TOP1 protein (**B**) in H460 and H460/TPT10 cell lines treated for 72 h with vehicle control, topotecan (TPT) 30 nM, cabozantinib (CBZ) 5 μ M, and combination of topotecan and cabozantinib, respectively, followed by the quantitative analysis. For ABCG2 expression, an imaged obtained with extended exposure time was shown as evidence for the endogenous ABCG2 expression in NCI-H460 cells and was not for quantitative use. The relative protein expression was calculated based on the ratio of target protein versus the loading control protein GAPDH. Columns and error bars represented average values with SD from three independent measurements. *indicates $p < 0.05$ comparing resistant cell line to parental cell line with the same treatment; #indicates $p < 0.05$ comparing treatment group to control group of the corresponding cell line.

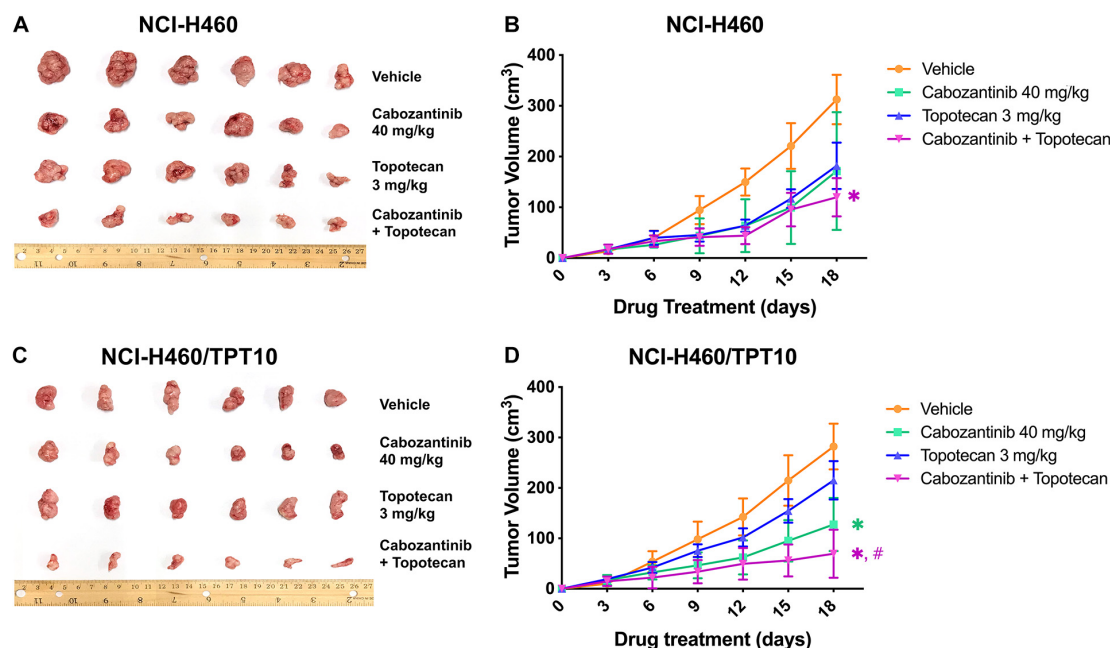
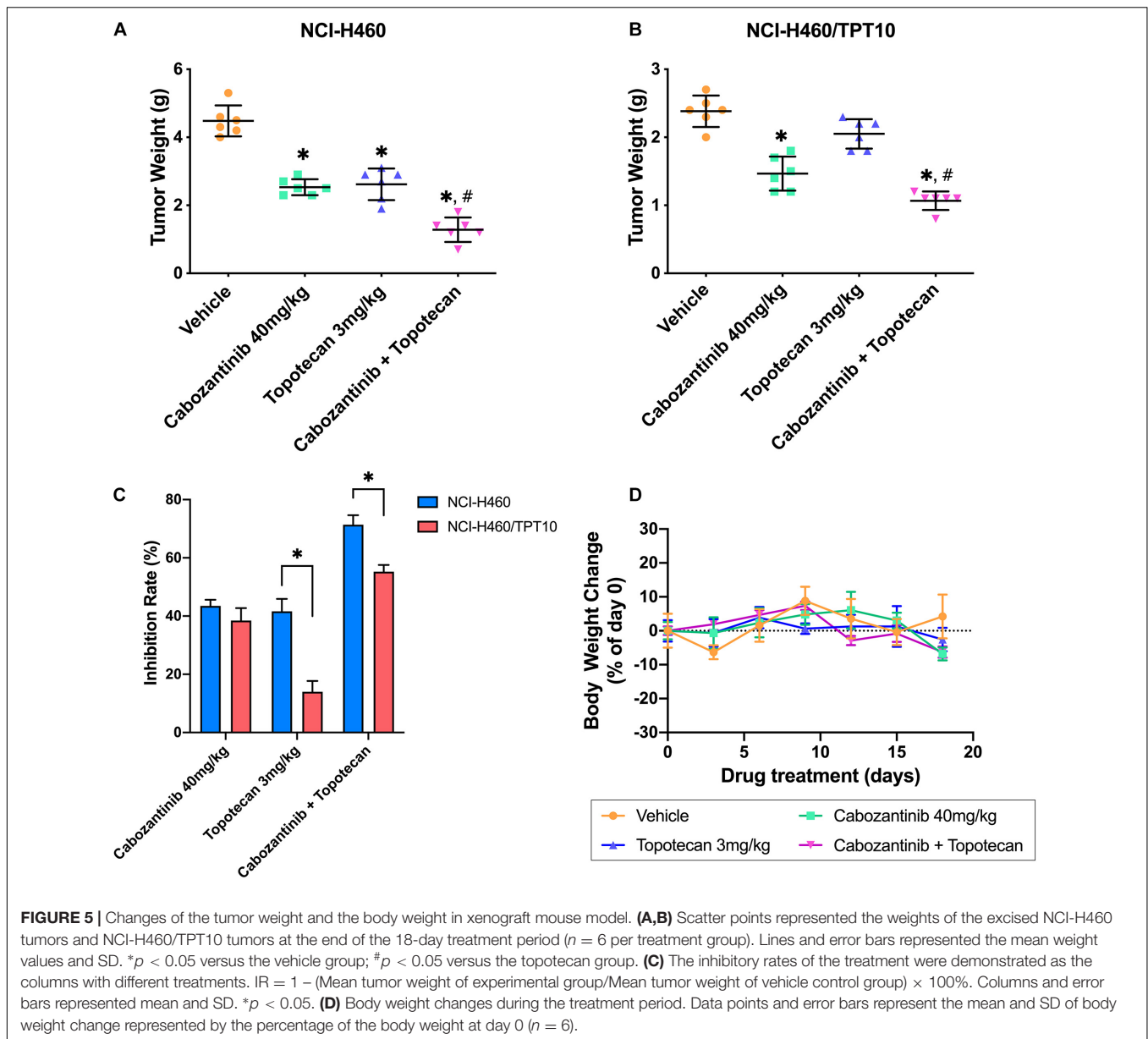


FIGURE 4 | Effect of topotecan and cabozantinib on the growth of NCI-H460 and NCI-H460/TPT10 tumors in male nude mice. (**A,C**) The images of resected tumors at the end of the treatment period from nude mice ($n = 6$ per treatment group) implanted with NCI-H460 and NCI-H460/TPT10 tumors. (**B,D**) The changes in NCI-H460 tumor volume and NCI-H460/TPT10 tumor volume throughout the study after the implantation. Data points and error bars represent the mean and SD of tumor volume ($n = 6$). * and # signs were shown in the same color scheme as the figure legends. * $p < 0.05$ versus the vehicle group; # $p < 0.05$ versus the topotecan only group.



a substrate of ABCG2, ABCG2-mediated drug exportation could induce TPT resistance in cancer cells, leading to failure in chemotherapy (Mao and Unadkat, 2015). ABCG2 is overexpressed on the plasma membrane of various types of cancer cells functioning as an efflux pump to excrete a broad spectrum of chemotherapeutic drugs (Khunweeraphong et al., 2019). A potential approach to ameliorate Cancer MDR mediated by ABCG2 is co-administration of ABCG2 inhibitors with ABCG2 substrate antineoplastic drugs (Hasanabady and Kalalinia, 2016). Previously, we identified CBZ, a c-Met and VEGFR2 inhibitor, as a novel modulator of ABCG2 with the capability of reversing resistance to mitoxantrone, SN-38, and TPT without affecting ABCG2 protein expression in NSCLC cells (Zhang G.N. et al., 2017). In Zhang et al.'s study, a mitoxantrone-selected MDR cell model that is cross-resistant

to TPT due to ABCG2 overexpression was used; however, the effect of CBZ in reversing TPT resistance has not been verified from a TPT-selected resistant NSCLC model. Considering that different biological characters in a TPT-induced resistant model may alter the reversal efficacy of CBZ, in the present study, we utilized our newly-established TPT-resistant human NSCLC cell line NCI-H460/TPT10.

The TPT-resistant NCI-H460/TPT10 cell line was developed from the parental human NSCLC NCI-H460 cell line by stepwise selection with increasing concentration of TPT up to 10 μM (Lei et al., 2020). Analysis of MTT assays in this study showed that the NCI-H460/TPT10 cells retained strong resistance to TPT and cross-resistance to other ABCG2 substrates like mitoxantrone and SN-38 compared to the parental NCI-H460 cells, with resistance folds of 212.39-, 117.36-, and 116.96-fold, respectively.

And the intracellular TPT accumulation was remarkably lower in NCI-H460/TPT10 cells than in the parental cells. CBZ, acting as a potent ABCG2 inhibitor at its non-toxic concentration (5 μ M), could restore the TPT level within NCI-H460/TPT10 cells and significantly re-sensitize NCI-H460/TPT10 to TPT and other ABCG2 substrates, with IC₅₀ values comparable to those in the drug-sensitive NCI-H460 cells. Meanwhile, the IC₅₀ values of a non-ABCG2 substrate, cisplatin, remained relatively constant between parental and resistant cells with or without CBZ, indicating that CBZ may reduce TPT resistance in NCI-H460/TPT10 cells by the ABCG2 inhibitory mechanism showed in other ABCG2 overexpressing MDR models (Zhang G.N. et al., 2017). Furthermore, CBZ could not sensitize NCI-H460/TPT10-ABCG2 knockout cells to TPT as it did on ABCG2 overexpressing NCI-H460/TPT10 cells, which confirms the involvement of ABCG2 in the reversal activity of CBZ. The inhibitory effect of CBZ on ABCG2 transporting function was further verified by the increased [³H]-mitoxantrone accumulation and reduced drug efflux by CBZ in ABCG2 overexpressing NCI-H460/TPT10 cells as well as HEK293/ABCG2 cells. The ABCG2 gene transfected HEK293/ABCG2 cell line and the vector control HEK293/pcDNA3.1 cell line were used to exclude other factors that may be involved in the effect of CBZ on [³H]-mitoxantrone accumulation and efflux. As similar results were observed from both pairs of cell lines (NCI-H460 and NCI-H460/TPT10, HEK293/pcDNA3.1 and HEK293/ABCG2, respectively), it was confirmed that CBZ reversed drug resistance by inhibiting ABCG2 efflux function, and ABCG2 may be a major factor responsible for TPT resistance in NCI-H460/TPT10 cells, which are consistent with the previous findings (Lei et al., 2020).

The change in the protein expression level of ABCG2 further revealed the interaction of CBZ with TPT. Consistent to the report from Zhang G.N. et al.'s study (2017), CBZ at 5 μ M did not alter the ABCG2 expression in NCI-H460 and NCI-H460/TPT10 cells. However, 5 μ M CBZ and 30 nM TPT exhibited synergistic effect in downregulating ABCG2 expression in NCI-H460/TPT10 cells but not in parental NCI-H460 cells, which suggested that the synergistic effect may be dependent on ABCG2 expression. This may be one of the mechanisms accounting for the high toxicity of CBZ and TPT co-administration to NCI-H460/TPT10 cells. The underlying mechanism for CBZ and TPT synergistically downregulating ABCG2 expression and their possible effects on ABCG2-related regulatory factors in ABCG2 overexpressing cells required further study to ascertain. The change of topoisomerase I, which is the target of TPT, was also investigated upon combination treatment of CBZ and TPT. Reduction of topoisomerase I protein expression was observed in NCI-H460 cells treated with 30 nM TPT and the combination of TPT and 5 μ M CBZ, as well as in NCI-H460/TPT10 cells treated with the drug combination. It has been reported that TPT could decrease the protein expression of topoisomerase I in ovarian cancer cells and breast cancer cells (D'Onofrio et al., 2011; Parmakhtiar et al., 2019). The downregulation of topoisomerase I expression in NCI-H460 cells upon TPT or combination treatment and in NCI-H460/TPT10 cells upon combination treatment may be explained by the accumulated TPT in NCI-H460 cells and the restored TPT level by CBZ

in NCI-H460/TPT10 cells. Interestingly, CBZ downregulated the topoisomerase I expression in the parental NCI-H460 cells but not in NCI-H460/TPT10 cells. It has been found that c-Met expression was positively correlated with topoisomerase I expression in SCLC cells, and inhibition of c-Met could reduce topoisomerase I activity (Rolle et al., 2014). However, considering the topoisomerase I expression levels are similar in NCI-H460 and NCI-H460/TPT10 cell lines, it is less likely that CBZ exerted differential effects on topoisomerase I expression via c-Met inhibition in NCI-H460 cells. In addition, as the concentration of CBZ was non-toxic, the change of topoisomerase I in NCI-H460 cells may not be cell death-related. Nevertheless, it could not be excluded that long-term TPT selection induced topoisomerase I-related gene profile alteration, resulting in irresponsiveness to the regulatory effect of CBZ on topoisomerase I, which needs to be further elucidated.

Although *in vitro* models have been useful tools in studying cancer MDR and developing novel anti-cancer drugs, their direct relevance to clinical cancer cases has been uncertain. Cultured cancer cells that have adapted to the *in vitro* micro-environment that often differs from the actual tumor found in patients, because they do not capture the regulations from the extracellular matrix, cell-matrix interactions, cell-cell interactions in a three-dimensional tumor structure, and the multi-cellular heterogeneous components of the tumor micro-environment such as stromal cells and blood vessels (Asghar et al., 2015). The xenograft animal models based on conventional cancer cell lines have been developed and used for decades to improve the shortage. In order to assess the applicability of the NCI-H460/TPT10 cell line to test MDR reversal agents *in vivo* and to verify the *in vivo* efficacy of CBZ on reversing TPT resistance, a tumor xenograft nude mouse model implanted with NCI-H460 and NCI-H460/TPT10 tumors in the left and right flank near the armpit, respectively, was further established and investigated. In consideration of the clinical relevance of the *in vivo* study, the designed dose of CBZ was evaluated by converting to the corresponding human dose using the method provided by Nair et al. (Nair and Jacob, 2016; Nair et al., 2018). The calculated corresponding human dose for 40 mg/kg mouse dose is 0.813 mg/kg, which is closed to the FDA approved 60 mg/day orally for patients with hepatocellular carcinoma (FDA, 2019), suggesting the potential of the results of this preclinical study to be achieved in the further clinical studies.

The *in vivo* study showed lower TPT efficacy in NCI-H460/TPT10 tumors than NCI-H460 tumors and synergistic anti-cancer effects from CBZ-TPT combination treatment were observed, which verified that the findings of TPT resistant phenotype of NCI-H460/TPT10 cell line and the reversal capability of CBZ in both NCI-H460 and NCI-H460/TPT10 cells could be extended to *in vivo* xenograft models. Similar results were reported by Zhang W. et al. (2017) that a mitoxantrone-selected resistant cell line derived from the NCI-H460 cell line could retain its MDR phenotype and original cytological features after xenografting in athymic nude mice. The NCI-H460 cell line and its drug-resistant sublines may serve as sound models for cancer pharmacology research as they are likely to possess

clinically relevant characters such as drug resistance both *in vitro* and *in vivo*. Our results also supported that the NCI-H460/TPT10 cell line could be a favorable model for studying TPT resistance, ABCG2-mediated MDR, and pharmacological evaluations on potential MDR reversal agents.

Interestingly, although our *in vivo* study suggested that the TPT resistance of NCI-H460/TPT10 cells was largely mediated by overexpression of ABCG2, it was observed that the combination of CBZ and TPT had relatively lower efficacy in treating NCI-H460/TPT10 xenograft tumors compared to NCI-H460/TPT10 xenograft tumors, indicating novel MDR mechanisms not being modulated by CBZ in NCI-H460/TPT10 cells *in vivo*, which might be independent to ABCG2 function or expression. In an *in vivo* setting, it is more likely that multiple factors are involved in cancer MDR compared to in a setting of monolayer cell culture with general growth media. Tumor cells can influence the surrounding micro-environment by releasing extracellular signals, promote tumor vascular proliferation and inhibit peripheral immune cells, all these factors can affect the growth and resistance phenotype of tumor cells (Wu and Dai, 2017; Hinshaw and Shevde, 2019). Intra-tumor heterogeneity in the implanted tumors and tumor-host interactions, such as the interplay between the tumors and their micro-environment (Assaraf et al., 2019), may be a factor contributing to the ABCG2-independent MDR observed in NCI-H460/TPT10 xenograft models.

In summary, the reversal effect of CBZ against ABCG2-mediated TPT resistance has been confirmed in the TPT-resistant human NSCLC NCI-H460/TPT10 tumor xenograft model. The established H460/TPT10 cell line and its xenograft model could serve as an invaluable, clinical-relevant resource for future drug screening and the development of novel ABCG2-targeted approaches to eradicate MDR in NSCLC.

REFERENCES

- Asghar, W., El Assal, R., Shafiee, H., Pitteri, S., Paulmurugan, R., and Demirci, U. (2015). Engineering cancer microenvironments for in vitro 3-D tumor models. *Mater Today (Kidlington)* 18, 539–553. doi: 10.1016/j.mattod.2015.05.002
- Assaraf, Y. G., Brozovic, A., Goncalves, A. C., Jurkovicova, D., Line, A., Machuqueiro, M., et al. (2019). The multi-factorial nature of clinical multidrug resistance in cancer. *Drug Resist. Updat.* 46:100645. doi: 10.1016/j.drug.2019.100645
- Bray, F., Ferlay, J., Soerjomataram, I., Siegel, R. L., Torre, L. A., and Jemal, A. (2018). Global cancer statistics 2018: GLOBOCAN estimates of incidence and mortality worldwide for 36 cancers in 185 countries. *CA Cancer J. Clin.* 68, 394–424. doi: 10.3322/caac.21492
- d'Amato, T. A., Landreneau, R. J., Ricketts, W., Huang, W., Parker, R., Mechetner, E., et al. (2007). Chemotherapy resistance and oncogene expression in non-small cell lung cancer. *J. Thorac. Cardiovasc. Surg.* 133, 352–363. doi: 10.1016/j.jtcvs.2006.10.019
- D'Onofrio, G., Tramontano, F., Dorio, A. S., Muzi, A., Maselli, V., Fulgione, D., et al. (2011). Poly (ADP-ribose) polymerase signaling of topoisomerase 1-dependent DNA damage in carcinoma cells. *Biochem. Pharmacol.* 81, 194–202.
- Ejendal, K. F., and Hrycyna, C. A. (2002). Multidrug resistance and cancer: the role of the human ABC transporter ABCG2. *Curr. Protein Pept. Sci.* 3, 503–511. doi: 10.2174/1389203023380521
- Fan, Y., Mansoor, N., Ahmad, T., Wu, Z. X., Khan, R. A., Czejka, M., et al. (2019). Enzyme and transporter kinetics for CPT-11 (Irinotecan) and SN-38: an insight on tumor tissue compartment pharmacokinetics using

DATA AVAILABILITY STATEMENT

The raw data supporting the conclusions of this article will be made available by the authors, without undue reservation.

ETHICS STATEMENT

The animal study was reviewed and approved by the Institutional Animal Care and Use Committee of St. John's University.

AUTHOR CONTRIBUTIONS

Z-NL, Q-XT, and Z-SC designed the experiments. Q-XT, PG, SN, and WZ performed the experiments. Y-FF, D-HY, and JW provided the technical and material support. Z-SC, Y-FF, and D-HY reviewed and revised the manuscript. All authors discussed the results and implications and commented on the manuscript at all stages.

FUNDING

This study was supported by the Department of Pharmaceutical Sciences, St. John's University.

ACKNOWLEDGMENTS

We are thankful to Chemietek Company (Indianapolis, IL, United States) for sending us a free sample of cabozantinib and giving us a discount for ordering.

- BPBK. *Recent Pat. Anticancer Drug Discov.* 14, 177–186. doi: 10.2174/1574892814666190212164356
- FDA (2019). *FDA Approved Drug Products: Labels for CABOMETYX (Cabozantinib) Tablets*. Available online at: https://www.accessdata.fda.gov/drugsatfda_docs/label/2019/208692s003lbl.pdf (accessed February 22nd, 2021)
- Gillet, J. P., Calcagno, A. M., Varma, S., Marino, M., Green, L. J., Vora, M. I., et al. (2011). Redefining the relevance of established cancer cell lines to the study of mechanisms of clinical anti-cancer drug resistance. *Proc. Natl. Acad. Sci. U. S. A.* 108, 18708–18713. doi: 10.1073/pnas.1111840108
- Hasanabady, M. H., and Kalalinia, F. (2016). ABCG2 inhibition as a therapeutic approach for overcoming multidrug resistance in cancer. *J. Biosci.* 41, 313–324.
- Hinshaw, D. C., and Shevde, L. A. (2019). The tumor microenvironment innately modulates cancer progression. *Cancer Res.* 79, 4557–4566. doi: 10.1158/0008-5472.can-18-3962
- Khunweeraphong, N., Szöllösi, D., Stockner, T., and Kuchler, K. (2019). The ABCG2 multidrug transporter is a pump gated by a valve and an extracellular lid. *Nat. Commun.* 10, 5433–5433. doi: 10.1038/s41467-019-13302-2
- Koinis, F., Corn, P., Parikh, N., Song, J., Vardaki, I., Mourkioti, I., et al. (2020). Resistance to MET/VEGFR2 inhibition by cabozantinib is mediated by YAP/TBX5-dependent induction of FGFR1 in castration-resistant prostate cancer. *Cancers (Basel)* 12:244. doi: 10.3390/cancers12010244
- Kurzrock, R., Sherman, S. I., Ball, D. W., Forastiere, A. A., Cohen, R. B., Mehra, R., et al. (2011). Activity of XL184 (Cabozantinib), an oral tyrosine kinase inhibitor, in patients with medullary thyroid cancer. *J. Clin. Oncol.* 29, 2660–2666. doi: 10.1200/JCO.2010.32.4145

- Lei, Z.-N., Teng, Q.-X., Zhang, W., Fan, Y.-F., Wang, J.-Q., Cai, C.-Y., et al. (2020). Establishment and characterization of a topotecan resistant non-small cell lung cancer NCI-H460/TPT10 cell line. *Front. Cell Dev. Biol.* 8:607275. doi: 10.3389/fcell.2020.607275
- Li, J., Kumar, P., Anreddy, N., Zhang, Y. K., Wang, Y. J., Chen, Y., et al. (2017). Quizartinib (AC220) reverses ABCG2-mediated multidrug resistance: in vitro and in vivo studies. *Oncotarget* 8, 93785–93799. doi: 10.18632/oncotarget.21078
- Mao, Q., and Unadkat, J. D. (2015). Role of the breast cancer resistance protein (BCRP/ABCG2) in drug transport—an update. *AAPS J.* 17, 65–82.
- Nair, A., Morsy, M. A., and Jacob, S. (2018). Dose translation between laboratory animals and human in preclinical and clinical phases of drug development. *Drug Dev. Res.* 79, 373–382. doi: 10.1002/ddr.21461
- Nair, A. B., and Jacob, S. (2016). A simple practice guide for dose conversion between animals and human. *J. Basic Clin. Pharm.* 7, 27–31. doi: 10.4103/0976-0105.177703
- Osmani, L., Askin, F., Gabrielson, E., and Li, Q. K. (2018). Current WHO guidelines and the critical role of immunohistochemical markers in the subclassification of non-small cell lung carcinoma (NSCLC): moving from targeted therapy to immunotherapy. *Semin. Cancer Biol.* 52(Pt 1), 103–109. doi: 10.1016/j.semcancer.2017.11.019
- Parmakhtiar, B., Burger, R. A., Kim, J.-H., and Fruehauf, J. P. (2019). HIF inactivation of p53 in ovarian cancer can be reversed by topotecan, restoring cisplatin and paclitaxel sensitivity. *Mol. Cancer Res.* 17, 1675–1686.
- Powell, S. F., Beitinjaneh, A., Tessema, M., Bliss, R. L., Kratzke, R. A., Leach, J., et al. (2013). Phase II study of topotecan and bevacizumab in advanced, refractory non-small-cell lung cancer. *Clin. Lung Cancer* 14, 495–501. doi: 10.1016/j.clcc.2013.04.009
- Quail, D. F., and Joyce, J. A. (2013). Microenvironmental regulation of tumor progression and metastasis. *Nat. Med.* 19, 1423–1437. doi: 10.1038/nm.3394
- Rolle, C. E., Kanteti, R., Surati, M., Nandi, S., Dhanasingh, I., Yala, S., et al. (2014). Combined MET inhibition and topoisomerase I inhibition block cell growth of small cell lung cancer. *Mol. Cancer Ther.* 13, 576–584. doi: 10.1158/1535-7163.Mct-13-0109
- Sharom, F. J. (2008). ABC multidrug transporters: structure, function and role in chemoresistance. *Pharmacogenomics* 9, 105–127. doi: 10.2217/14622416.9.1.105
- Siegel, R. L., Miller, K. D., and Jemal, A. (2020). Cancer statistics, 2020. *CA Cancer J. Clin.* 70, 7–30. doi: 10.3322/caac.21590
- Sodani, K., Patel, A., Anreddy, N., Singh, S., Yang, D. H., Kathawala, R. J., et al. (2014). Telatinib reverses chemotherapeutic multidrug resistance mediated by ABCG2 efflux transporter in vitro and in vivo. *Biochem. Pharmacol.* 89, 52–61. doi: 10.1016/j.bcp.2014.02.012
- Tiwari, A. K., Sodani, K., Dai, C. L., Abuznait, A. H., Singh, S., Xiao, Z. J., et al. (2013). Nilotinib potentiates anticancer drug sensitivity in murine ABCB1-, ABCG2-, and ABCC10-multidrug resistance xenograft models. *Cancer Lett.* 328, 307–317. doi: 10.1016/j.canlet.2012.10.001
- Vennepureddy, A., Atallah, J. P., and Terjanian, T. (2015). Role of topotecan in non-small cell lung cancer: a review of literature. *World J. Oncol.* 6, 429–436. doi: 10.14740/wjon950e
- Wang, J.-Q., Li, J. Y., Teng, Q.-X., Lei, Z.-N., Ji, N., Cui, Q., et al. (2020). Venetoclax, a BCL-2 inhibitor, enhances the efficacy of chemotherapeutic agents in wild-type ABCG2-overexpression-mediated MDR cancer cells. *Cancers* 12:466.
- Wu, T., and Dai, Y. (2017). Tumor microenvironment and therapeutic response. *Cancer Lett.* 387, 61–68. doi: 10.1016/j.canlet.2016.01.043
- Yakes, F. M., Chen, J., Tan, J., Yamaguchi, K., Shi, Y., Yu, P., et al. (2011). Cabozantinib (XL184), a novel MET and VEGFR2 inhibitor, simultaneously suppresses metastasis, angiogenesis, and tumor growth. *Mol. Cancer Ther.* 10, 2298–2308. doi: 10.1158/1535-7163.MCT-11-0264
- Zhang, G. N., Zhang, Y. K., Wang, Y. J., Barbuti, A. M., Zhu, X. J., Yu, X. Y., et al. (2017). Modulating the function of ATP-binding cassette subfamily G member 2 (ABCG2) with inhibitor cabozantinib. *Pharmacol. Res.* 119, 89–98. doi: 10.1016/j.phrs.2017.01.024
- Zhang, W., Chen, Z., Chen, L., Wang, F., Li, F., Wang, X., et al. (2017). ABCG2-overexpressing H460/MX20 cell xenografts in athymic nude mice maintained original biochemical and cytological characteristics. *Sci. Rep.* 7:40064.
- Zhang, Y. K., Wang, Y. J., Gupta, P., and Chen, Z. S. (2015). Multidrug resistance proteins (MRPs) and cancer therapy. *AAPS J.* 17, 802–812. doi: 10.1208/s12248-015-9757-1
- Zhou, L., Liu, X. D., Sun, M., Zhang, X., German, P., Bai, S., et al. (2016). Targeting MET and AXL overcomes resistance to sunitinib therapy in renal cell carcinoma. *Oncogene* 35, 2687–2697. doi: 10.1038/onc.2015.343

Conflict of Interest: The authors declare that the research was conducted in the absence of any commercial or financial relationships that could be construed as a potential conflict of interest.

Copyright © 2021 Lei, Teng, Gupta, Zhang, Narayanan, Yang, Wurpel, Fan and Chen. This is an open-access article distributed under the terms of the Creative Commons Attribution License (CC BY). The use, distribution or reproduction in other forums is permitted, provided the original author(s) and the copyright owner(s) are credited and that the original publication in this journal is cited, in accordance with accepted academic practice. No use, distribution or reproduction is permitted which does not comply with these terms.



Extracellular Matrix Proteins Confer Cell Adhesion-Mediated Drug Resistance Through Integrin α_v in Glioblastoma Cells

Qi Yu^{1,2}, Weikun Xiao¹, Songping Sun¹, Alireza Sohrabi¹, Jesse Liang¹ and Stephanie K. Seidlits^{1,3,4,5*}

¹ Department of Bioengineering, University of California, Los Angeles, Los Angeles, CA, United States, ² Department of Neurosurgery, Shengjing Hospital of China Medical University, Shenyang, China, ³ Jonsson Comprehensive Cancer Center, University of California, Los Angeles, Los Angeles, CA, United States, ⁴ Brain Research Institute, University of California, Los Angeles, Los Angeles, CA, United States, ⁵ Broad Stem Cell Research Center, University of California, Los Angeles, Los Angeles, CA, United States

OPEN ACCESS

Edited by:

Liwu Fu,
Sun Yat-sen University, China

Reviewed by:

Vanessa Morais Freitas,
University of São Paulo, Brazil
Jian-ye Zhang,
Guangzhou Medical University, China

*Correspondence:

Stephanie K. Seidlits
seidlits@ucla.edu

Specialty section:

This article was submitted to
Molecular and Cellular Oncology,
a section of the journal
Frontiers in Cell and Developmental
Biology

Received: 12 October 2020

Accepted: 26 January 2021

Published: 23 March 2021

Citation:

Yu Q, Xiao W, Sun S, Sohrabi A,
Liang J and Seidlits SK (2021)
Extracellular Matrix Proteins Confer
Cell Adhesion-Mediated Drug
Resistance Through Integrin α_v
in Glioblastoma Cells.
Front. Cell Dev. Biol. 9:616580.
doi: 10.3389/fcell.2021.616580

Chemotherapy resistance to glioblastoma (GBM) remains an obstacle that is difficult to overcome, leading to poor prognosis of GBM patients. Many previous studies have focused on resistance mechanisms intrinsic to cancer cells; the microenvironment surrounding tumor cells has been found more recently to have significant impacts on the response to chemotherapeutic agents. Extracellular matrix (ECM) proteins may confer cell adhesion-mediated drug resistance (CAMDR). Here, expression of the ECM proteins laminin, vitronectin, and fibronectin was assessed in clinical GBM tumors using immunohistochemistry. Then, patient-derived GBM cells grown in monolayers on precoated laminin, vitronectin, or fibronectin substrates were treated with cilengitide, an integrin inhibitor, and/or carmustine, an alkylating chemotherapy. Cell adhesion and viability were quantified. Transcription factor (TF) activities were assessed over time using a bioluminescent assay in which GBM cells were transduced with lentiviruses containing consensus binding sites for specific TFs linked to expression a firefly luciferase reporter. Apoptosis, mediated by p53, was analyzed by Western blotting and immunocytofluorescence. Integrin α_v activation of the FAK/paxillin/AKT signaling pathway and effects on expression of the proliferative marker Ki67 were investigated. To assess effects of integrin α_v activation of AKT and ERK pathways, which are typically deregulated in GBM, and expression of epidermal growth factor receptor (EGFR), which is amplified and/or mutated in many GBM tumors, shRNA knockdown was used. Laminin, vitronectin, and fibronectin were abundant in clinical GBM tumors and promoted CAMDR in GBM cells cultured on precoated substrates. Cilengitide treatment induced cell detachment, which was most pronounced for cells cultured on vitronectin. Cilengitide treatment increased cytotoxicity of carmustine, reversing CAMDR. ECM adhesion increased activity of NF κ B and decreased that of p53, leading to suppression of p53-mediated apoptosis and upregulation of multidrug resistance gene 1 (MDR1; also known as ABCB1 or P-glycoprotein). Expression of Ki67 was correlative with activation

of the integrin α_v -mediated FAK/paxillin/AKT signaling pathway. EGFR expression increased with integrin α_v knockdown GBM cells and may represent a compensatory survival mechanism. These results indicate that ECM proteins confer CAMDR through integrin α_v in GBM cells.

Keywords: cell adhesion-mediated drug resistance, integrin α_v , glioblastoma, extracellular matrix, laminin, vitronectin, fibronectin

INTRODUCTION

Glioblastoma (GBM) is the most common primary brain tumor and the most aggressive in nature. For many decades, the standard therapy for GBM remains the same, including maximum feasible surgical resection, followed by radiation (XRT) plus concomitant chemotherapy with temozolomide (TMZ), and then followed by adjuvant TMZ (Ellor et al., 2014; Patel et al., 2014). The combined therapy resulted in an improved median overall survival from 12.1 to 14.6 months and an increase in the 2 years survival rate from 10 to 27% (Miranda et al., 2017). The Gliadel wafer (Arbor Pharmaceuticals, Atlanta, GA) is a carmustine-impregnated wafer that is placed in the surgical cavity after maximal tumor resection. Prospective data regarding use of carmustine wafers included all high-grade gliomas, and some of the survival benefits were largely a result of grade 3 patients with long-term survival (Chowdhary et al., 2015). Some retrospective studies also suggest a modest gain of 2–3 months for patients with GBM (Dixit et al., 2011). Nevertheless, the rising chemotherapeutic agent resistance leading to the treatment failure is still a challenge and has been one of the priorities in neuroscience. Additional concomitant chemotherapeutics for newly diagnosed GBM have not shown an incremental survival benefit. Concomitant bevacizumab with TMZ against newly diagnosed GBM in two large phase III trials showed prolonged progression-free survival but failed to show survival benefit (Chinot et al., 2014; Gilbert et al., 2014). Similarly, cilengitide, as an selective $\alpha_v\beta_3$ and $\alpha_v\beta_5$ integrin inhibitor, although cilengitide exhibited antitumor activity in phase II trials, it failed to show overall survival improvement in patients with methylated MGMT promoter in phase III trials (Stupp et al., 2014; Nabors et al., 2015). Rindopepimut is a peptide vaccine against the most common epidermal growth factor receptor (EGFR) deletion mutation (EGFR variant III) in GBM. Although single-arm phase II studies showed promising results, a randomized phase III trial (ACT IV) failed to show benefit over the control group (Weller et al., 2017).

Advanced knowledge has been established with regard to the mechanism of chemoresistance in GBM. One reason why GBM has a very poor prognosis is related with the lack of successful drug delivery across the physiologic barriers, especially the blood–brain barrier (BBB), which protects the central nervous system (CNS) from the passage of foreign and harmful substances through the bloodstream (Pourgholi et al., 2016). The relevant mechanisms underlying the barrier function include enzymatic barrier, transport barrier (para-cellular and transcellular), immunologic barrier, and efflux transport

systems (Hendricks et al., 2015). Mutation of DNA repair systems is another cause responsible for the chemoresistance such as enhanced MGMT activity, impaired DNA mismatch repair system, and enhanced base excision repair system (Thon et al., 2013; Messaoudi et al., 2015; Motegi et al., 2019). In addition, other factors have been shown to interfere with TMZ activity, contributing to the poor prognosis of GBM. Such factors include EGFR, PI3K/AKT/mTOR pathway (the mechanistic target of rapamycin), galectin-1, p53, murine double minute 2 (Mdm2), ATP-binding cassette transports, phosphatase and tensin homolog (PTEN), isocitrate dehydrogenase (IDH-1), and cell cycle checkpoint pathways (Messaoudi et al., 2015; Tivnan et al., 2015; Pourgholi et al., 2016; Yan et al., 2016; Kim and Kim, 2020; Pine et al., 2020). More recently, a series of publications identified cell adhesion to the extracellular matrix (ECM) as a key determinant among the myriad of microenvironmental factors impacting cancer cell resistance (Xiao et al., 2017). It has been reported that adhesion to laminin, vitronectin, or fibronectin confers cell adhesion-mediated drug resistance (CAMDR) in various cancer models (Fei et al., 2014; Nakagawa et al., 2014; Sun et al., 2014; Sanchez et al., 2019). Data have revealed that $\alpha_v\beta_3$ and $\alpha_v\beta_5$ integrins mediate the interaction between endothelial cells and components of the ECM (Varner et al., 1995). Integrin $\alpha_v\beta_3$ binds to Arg-Gly-Asp (RGD) in vitronectin, fibronectin, and fibrinogen, among other substrates. Cilengitide, one of the cyclic RGD peptides, was found to disrupt VE-cadherin localization at cell junctions, increase endothelial monolayer permeability, and restrain angiogenesis *in vitro* and *in vivo* (Chowdhary et al., 2015).

The p53 transcription factor (TF) was initially known as the guardian of the genome due to the fact that it prevents the proliferation of cells with damaged nuclear DNA (Olotu and Soliman, 2019; Horikawa, 2020). However, p53 acts as a TF to regulate the expression of a variety of genes that coordinate the DNA damage responses. On the one hand, it can initiate apoptosis through death receptor and mitochondrial pathway. On the other hand, it can arrest growth by holding the cell cycle at the G1/S regulation point through p53-dependent p21^{WAF1/CIP1}, which binds to the G1-S/CDK complex and inhibits their activity.

Carmustine [1,3-bis(2-chloroethyl)-1-nitrosourea (BCNU)] was first introduced for chemotherapy against malignant gliomas in the 1980's (Walker et al., 1978; Walker et al., 1980). During the past 30 years, the evaluation of the role of chemotherapy has not produced impressive results to date. Beyond TMZ, the US Food and Drug Administration (FDA) has approved two other agents for treatment of newly diagnosed malignant glioma till now: carmustine wafers and bevacizumab

(Affronti et al., 2009). Gliadel wafers (Arbor Pharmaceuticals, Atlanta, GA) are commercial products of biodegradable copolymers (proliferospan 20) impregnated with carmustine. Wafer efficacy has been well documented (Stewart, 2002). Subsequent trials revealed increased benefit from combining Gliadel wafers with XRT/TMZ. Median overall survival tended to be improved by 3–4 months beyond that observed for Gliadel wafers or TMZ when used alone in the respective III trials (Ashby et al., 2016).

In this study, we found that laminin, vitronectin, and fibronectin, three main components of ECM proteins, could affect CAMDR in GBM cells. Enrichment of these proteins in the microenvironment promotes tumor cell proliferation through integrin α_v -mediated FAK/paxillin/AKT signaling pathway and suppresses p53-mediated apoptosis. In addition, we found that the efflux transporter ABCB1 was elevated with ECM adhesion. Compensatory activation of EGFR occurred when integrin α_v was knocked down. These findings will provide promising insights to overcome chemotherapeutic resistance for GBM.

MATERIALS AND METHODS

Cell Lines, Cell Culture, and Treatment Setup

The GBM cell line U87MG was obtained from American Type Culture Collection (ATCC) and cultured in Dulbecco's modified Eagle's medium (DMEM) supplemented with 10% fetal bovine serum (FBS) and 1% penicillin/streptomycin. Primary GBM cell line HK308 (patient background: a 50-year-old female with recurrent GBM with wild-type IDH 1/2 received XRT, TMZ, and Avastin treatment) was established from patient tumors in accordance with UCLA Institutional Review Board protocol 10-000655 and generously gifted by Dr. Harley Kornblum at UCLA. Authentication was conducted by immunoblot studies (Laks et al., 2016). Primary GBM6 (patient background: a 65 years old male with newly diagnosed GBM with mutant p53 and amplification of EGFR vIII mutant received XRT and TMZ treatment) was obtained from Dr. David Nathanson and authenticated by DNA fingerprinting (Sarkaria et al., 2006; Akhavan et al., 2013). DMEM/F12 with G21 (Gemini Bio, Sacramento, CA, United States, 1:50), 50 ng/ml of EGF (PeproTech, Rocky Hill, NJ, United States), 20 ng/ml of FGF-2 (PeproTech), 25 μ g/ml of heparin (Sigma-Aldrich, St. Louis, MO, United States), and 1% penicillin/streptomycin was used for primary GBM cell line culture. All cell lines were used fewer than 30 passages and incubated in a 5% CO₂-humidified incubator at 37°C.

ECM proteins including laminin (Thermo Fisher Scientific, Waltham, MA, United States), vitronectin and fibronectin (Sigma-Aldrich, St. Louis, MO, United States) were used, respectively, as coating protein in a 12-well plate at a dilution of 10 μ g/ml. The plate was then incubated at 37°C for over 4 h before the cells were seeded. Carmustine was purchased from Sigma-Aldrich and dissolved at 100 mmol/L in 100% ethanol for stocking. It was then added in culture medium at a final concentration of 100 μ mol/L. Ethanol alone was used as the

negative control. Cilengitide (Sigma-Aldrich, St. Louis, MO, United States) was dissolved in phosphate-buffered saline (PBS) as 10 mmol/L of stock and then added in culture medium at a final concentration of 50 μ mol/L.

Tissue Microarray

Tissue microarray (TMA) containing 34 GBM samples and 19 other low-grade CNS tumors were employed to analyze laminin, vitronectin, and fibronectin expressions. All the patients had given informed consent, and collection of these tissue samples had been studied for other researches before (Choe et al., 2003; Guo et al., 2009; Lu et al., 2009). TMA was a high-throughput screening platform that enables a bunch of patient tumor samples to be analyzed on the same slide. It was constructed using a 0.6 mm needle to exact 54 representative tumor tissue cores from the paraffin-embedded tissue blocks (Akhavan et al., 2013). These cores were placed in a grid pattern into two recipient paraffin blocks, from which tissue sections were cut for immunohistochemistry (IHC) analysis, as previously described (Zhou et al., 2015). Briefly, the slides were first deparaffinized, followed by blocking with 30% normal donkey serum for 10 min. Then the sections were incubated with the primary laminin, vitronectin, and fibronectin antibodies (Thermo Fisher, PA1-16730/PA5-27909/PA1-26205, respectively; Waltham, MA, United States, dilution 1:500) overnight at 4°C. Appropriate secondary antibodies were applied for 30 min. Negative controls were carried out by replacement of the primary antibody with substituting PBS. Images were scored and calculated by Fisher's exact test.

Cell Adhesion Assay

A 96-well plate was coated with PBS (as negative control) and 10 μ g/ml of laminin, vitronectin, and fibronectin, over 4 h at 37°C. To block any remaining protein binding sites on the plate, coating solutions were removed, and then 1% bovine serum albumin (BSA) was added for another hour. Appropriate density of GBM cell suspension (10,000 cells/well for GBM6; 5,000 cells/well for U87MG and HK308) was seeded, followed by another 2 h incubation. Non-adherent GBM cells were removed by careful washing two times with PBS. Then, 100% ethanol was used to fix the adherent cells for 15 min followed by 0.1% crystal violet (Thermo Fisher Scientific, Pittsburgh, PA, United States, dissolved in 100% ethanol) staining for another 30 min. After excessive stain was removed and 0.3% Triton-X was applied to lyse cells, the absorbance was measured at 570 nm using a microplate reader (BioTek, Winooski, VT, United States). The percentage of adhesion was determined by dividing the corrected (background subtracted) optical density of adherent cells by the total corrected optical of cells added to each microplate well and multiplying by 100%. Experiments were repeated three times with five replications per experiment.

Cell Viability Assay

Cell viability and drug-response curves were assessed using a CellTiter 96 AQueous One Solution (MTS) kit (Promega, Madison, WI, United States) as described before (Kong et al., 2015). Briefly, GBM cells (5,000 cells/well for GBM6; 3,000 cells/well for

U87MG and HK308) were cultured on a 96-well plate precoated with PBS, laminin, vitronectin, or fibronectin for 24 h. Cells were then treated with 100 μ M of carmustine or ethanol (as control). At the end of the treatment, 20 μ l/well of MTS solution was added and incubated at 37°C for 2 h. Absorbance was measured at 490 nm. All data points were set up with five replicates for each experiment. The IC₅₀ was determined by GraphPad Prism Software Version 7 (San Diego, CA, United States).

Immunofluorescent Staining

GBM cells were fixed with 4% paraformaldehyde for 20 min at room temperature and permeabilized with a blocking solution containing 5% BSA and 0.01% Triton X-100 diluted in PBS. Then, cells were incubated overnight at 4°C with anti-Ki67 primary antibody (1:200, Thermo Fisher Scientific, Waltham, MA, United States). Goat anti-rabbit secondary antibody was then added at a dilution 1:500 for 2 h. Secondary antibody alone without primary antibody was used as negative control. All the GBM cells were later counterstained with Hoechst 33242 (Thermo Fisher Scientific, Waltham, MA, United States). Glass coverslips were mounted with fluorescence Mounting Medium (SouthernBiotech, Birmingham, AL, United States). Images were captured with an AXIO-Observer inverted microscope equipped for wide-field fluorescence and phase contrast (Zeiss, Oberkochen, Germany).

Lentiviral Construction and Transfection

Plasmids pTA-/p53-/NF κ B-/c-myc-FLuc were kindly obtained from Dr. Lonnie D. Shea at Northwestern University. The plasmids were designed so that each contained a consensus binding sequence for a particular TF in the enhancer region upstream of a minimal TATA-box promoter driving expression of the reporter gene firefly luciferase (**Supplementary Table 1**; Penalver Bernabe et al., 2016). TP53bp1 was a gift from Nicola Burgess-Brown (Addgene plasmid #73252). ITGAV shRNA was obtained from Dharmacon (V2LHS_133468, Lafayette, CO, United States). Lentivirus was produced by co-transfecting HEK-293T cells with a third-generation packaging system (Dull et al., 1998). As quantified by lentix-rtPCR kit (Takara), transduction was performed with a virus concentration of 2,000 physical particles/cell. Fresh media were replaced 24 h after transfection. TA-/p53-/NF κ B-/c-myc-FLuc, integrin α_v knockdown, and TP53bp1⁺ stable cell lines were created and continuously cultured for 3 days before use in the subsequent assay. All experiments with regard to the virus were performed on BSL2 laboratory under relevant management regulations.

Bioluminescence Assay

TF activity was assessed by bioluminescence imaging of firefly luciferase using an IVIS imaging system (Caliper Life Sciences, Hopkinton, MA, United States) as described previously (Bellis et al., 2011). D-Luciferin (Sigma-Aldrich, St. Louis, MO, United States) was added as the substrate for FLuc at 1 μ M/well, followed by incubation for 1 h. Exposure time was 5 min, and images were taken every 24 h for 3 days. After each time point of any dynamic imaging experiment, the medium was refreshed. Normalized TF activity was determined by dividing

the normalized light emission for target TFs by the average normalized light emission for TA. Each condition was performed in triplicate.

Western Blotting Antibody Information Table

Proteins were extracted by lysing GBM cell lines in radioimmunoprecipitation assay (RIPA) buffer with a protease/phosphatase inhibitor cocktail. Then the sodium dodecyl sulfate–polyacrylamide gel electrophoresis and transfer were performed, followed by blocking in 5% BSA as described previously (Xiao et al., 2018; Yu et al., 2018). Relevant primary antibodies were used for detecting target bands overnight at 4°C (integrin $\alpha_v/\beta_1/\beta_3/\beta_5$, t-/p-FAK, p-paxillin, t-/p-AKT, t-/p-EGFR, p53, cleaved PARP, ABCB1, p-ERK1/2, and cyclin D1, obtained from Cell Signaling Technology, Danvers, MA, United States, dilution 1:1,000). Horseradish peroxidase (HRP) goat anti-mouse IgG or anti-rabbit IgG were used as secondary antibodies (dilution 1:2,000). Immunoreactive bands were visualized using Clarity ECL substrate (Bio-Rad, Hercules, CA, United States) and imaged (MyECL imager) without overexposing the target bands. Equal loading was assessed after probing the same membrane with anti-GAPDH antibody (Thermo Fisher Scientific, Waltham, MA, United States). Images of blots were analyzed using ImageJ (NIH).

Statistical Analysis

Statistical analysis was performed using GraphPad Prism Software Version 7 (San Diego, CA, United States). Two-way ANOVA test was applied to examine the statistical significance followed by Dunnett's test as a *post hoc* test for within- or between-group comparisons. Probability values less than 0.05 were regarded as statistically significant.

RESULTS

Extracellular Matrix Proteins Confer Cell Adhesion-Mediated Drug Resistance in Glioblastoma Cell Lines

To investigate the impact of ECM on GBM tumor cells, IHC of patient TMAs was used to analyze expression of laminin, vitronectin, and fibronectin in GBM and low-grade CNS tumors (**Figure 1A**). Compared with tumors in the low-grade CNS group, GBM tumors showed higher expression of laminin ($p = 0.0178$) and vitronectin ($p < 0.0001$). Fibronectin was widely expressed in both GBM and low-grade CNS tumor groups. An *in vitro* assay showed that fibronectin induced the highest degree of attachment for the U87 GBM cell line and two patient-derived GBM cell lines (GBM6 and HK308), followed by vitronectin and laminin, respectively (**Figure 1B**). All ECM proteins investigated significantly increased attachment over non-coated substrates (laminin, $p < 0.05$ for all; vitronectin, $p < 0.05$ for all; fibronectin, $p < 0.05$ for GBM6; $p < 0.01$ for U87MG and HK308).

Adhered cells were treated with carmustine, an alkylating agent that forms interstrand cross-links in DNA to prevent

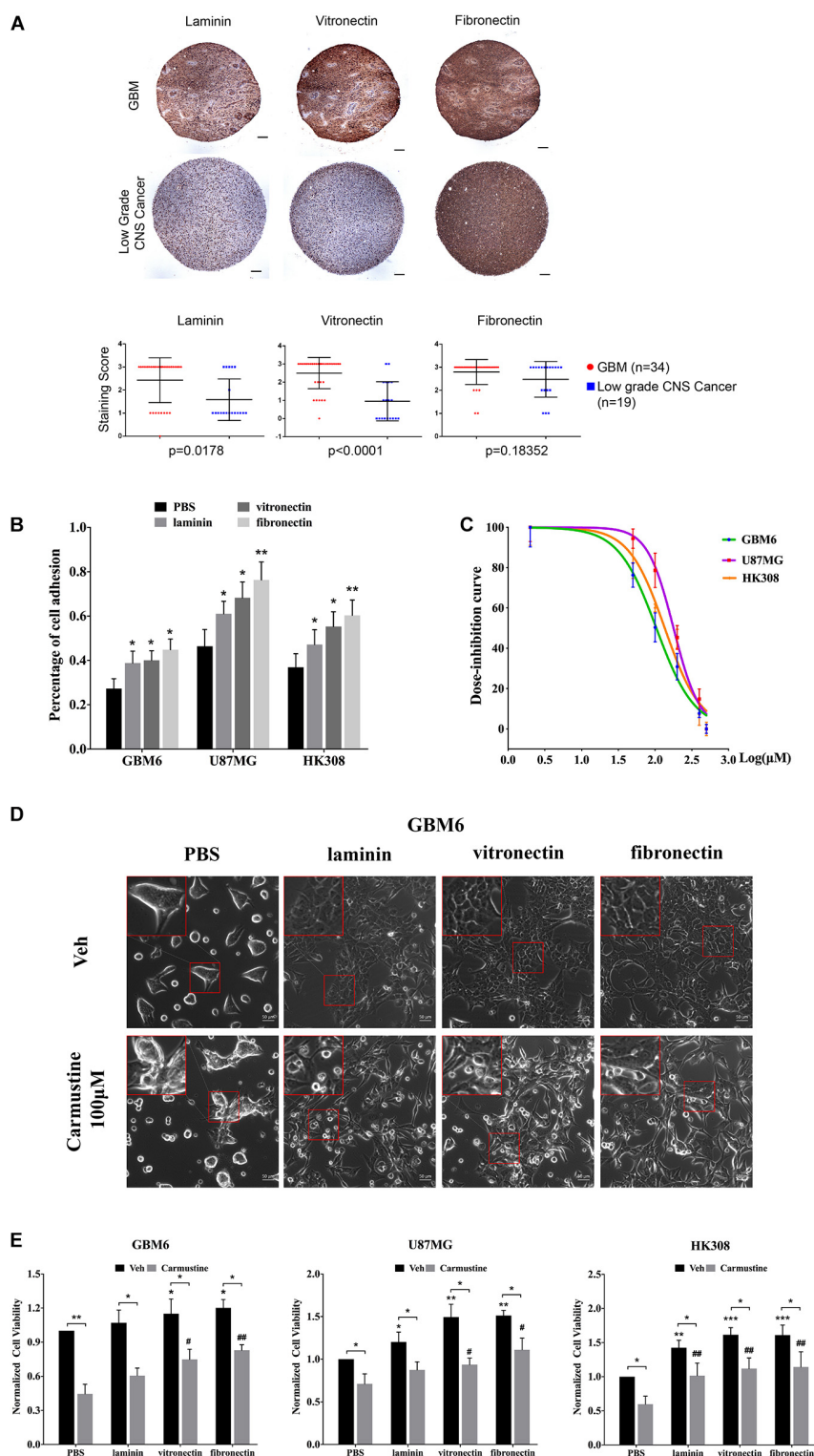


FIGURE 1 | Extracellular matrix (ECM) proteins confer cell adhesion-mediated drug resistance (CAMDR) in glioblastoma (GBM) cell lines. **(A)** Tissue microarray (TMA) of expressions of laminin, vitronectin, and fibronectin in patient-derived GBM and low-grade central nervous system (CNS) tumors. Scale bars, 100 μ m. GBM group, $n = 34$; low-grade CNS cancer, $n = 19$. **(B)** Attachment assay of GBM cell lines GBM6, U87MG, and HK308 on fibronectin, laminin, and vitronectin. Error bars, SD ($n = 3$). **(C)** Dose inhibition curve of carmustine on GBM6, U87MG, and HK308. Error bars, SD ($n = 3$). **(D)** Representative light images of GBM6 with or without carmustine [100 μ M, phosphate-buffered saline (PBS) as control] treatment on precoated fibronectin, laminin, and vitronectin. Scale bars, 50 μ m. **(E)** Cell viability assay of carmustine on GBM6, U87MG, and HK308. Error bars, SD ($n = 3$). * $p < 0.05$, ** $p < 0.01$, *** $p < 0.001$, # $p < 0.05$, ## $p < 0.01$.

its replication and transcription. GBM cells were inhibited by carmustine in a dose-dependent manner, with a half maximal inhibitory concentration (IC_{50}) of $106 \pm 13 \mu\text{M}$ for GBM6, $179 \pm 29 \mu\text{M}$ for U87MG, and $137 \pm 27 \mu\text{M}$ for HK308 (**Figure 1C**). To assess whether ECM proteins conferred CAMDR, GBM cells were cultured on substrates precoated with PBS (as a negative control), laminin, vitronectin, or fibronectin for 24 h prior to treatment with carmustine (or vehicle control) for 48 h. In the absence of precoated ECM, carmustine treatment significantly reduced numbers of adhered cells (**Figure 1D** and **Supplementary Figure S1**). While some rounded cells were observed on ECM-coated substrates, more rounded cells were apparent on non-coated substrates after treatment. Quantitative assays showed a significant increase in cell viability when cultured on either vitronectin- or fibronectin-coated (compared with uncoated) substrates (vitronectin, $p < 0.05$ for GBM6, $p < 0.01$ for U87MG, $p < 0.001$ for HK308; fibronectin, $p < 0.05$ for GBM6, $p < 0.01$ for U87MG, $p < 0.001$ for HK308), while adhesion to laminin significantly increased viability of U87MG and HK308 ($p < 0.05$ for U87MG; $p < 0.01$ for HK308), but not GBM6, cells (**Figure 1E**). Treatment with carmustine for 48 h significantly decreased cell viability in all cases; however, ECM adhesion provided significant protection over non-coated substrates (**Figure 1E**, PBS, $p < 0.05$ for all cell lines; laminin, $p < 0.05$ for GBM6 and U87MG, $p < 0.01$ for HK308; vitronectin, $p < 0.05$ for U87MG, $p < 0.01$ for GBM6 and HK308; fibronectin, $p < 0.01$ for all).

Cilengitide Reverses Cell Adhesion-Mediated Drug Resistance Through Integrin α_v in a Matrix-Specific Manner

Cilengitide, a selective inhibitor of the integrin α_v receptor, decreases adhesion of GBM6, U87MG, and HK308 cells on precoated laminin and vitronectin, but not fibronectin (**Figure 2A**).

Compared with cells grown on substrates without precoated ECM protein, only coating with fibronectin results in higher levels of GBM6 cell viability (**Figure 2B**, $p < 0.01$). However, treatment with cilengitide only reduced viability of cells when cultured on vitronectin-coated substrates (**Figure 2B**, $p < 0.05$). Similarly, coating with fibronectin, but not laminin or vitronectin, leads to restoration of U87MG cell viability when treated with cilengitide plus carmustine (**Supplementary Figure S2A**, $p < 0.05$). U87MG shows less viability, with cilengitide on precoated laminin and vitronectin substrates (**Supplementary Figure S2A**, $p < 0.05$). On the contrary, cilengitide does not reverse cell viability of HK308 on any precoated substrates (**Supplementary Figure S2A**). In general, a loss of cell adhesion and spreading after cilengitide treatment (**Figure 2C** and **Supplementary Figure S2B**) was associated with increased efficacy carmustine treatment (**Figure 2B** and **Supplementary Figure S2A**). Cell responses after detachment by cilengitide are also different between cell types. For GBM6, detachment was only observed on precoated vitronectin, which

resulted in higher chemotherapeutic toxicity. For U87MG, detachment occurred in all substrates except fibronectin, which leads to lower cell viability on relative substrates. Cilengitide did not affect cell adhesion and carmustine efficacy in HK308. Next, we investigated candidate integrins, which were required as the receptor for GBM6 cells responding to cilengitide administration on varying ECMs (**Figures 2D,E**). All integrin subunits evaluated were upregulated by cells cultured on fibronectin, when compared with those cultured on laminin or vitronectin (**Figures 2D,E**). Moreover, culture fibronectin-coated substrates also induced upregulation of EGFR expression.

Compared with GBM6, cells grown on uncoated substrates, cilengitide treatment induced upregulation of integrin subunits in an ECM-dependent way. Specifically, integrin α_v expression was higher in cells grown on fibronectin, integrin β_1 in cells grown on vitronectin, and integrins β_3 and β_5 with cells grown on fibronectin or vitronectin (**Figure 2E**, $p < 0.05$). When treated with a combination of cilengitide and carmustine, shifts in integrin expression were again dependent on the type of ECM coating. Cells grown on uncoated substrates increased expression of integrins β_3 and β_5 , while those on fibronectin downregulated integrins α_v and β_5 . When cultured on vitronectin, dual treatment with cilengitide and carmustine increased integrin α_v and total EGFR expression.

Extracellular Matrix Induces Activation of NF κ B and Deactivation of p53

Binding events to consensus sequences for the TFs NF κ B, p53, and c-myc in response to treatments were assessed using GBM6 cells transduced with bioluminescent reporters of TF activity when cultured on ECM-coated substrates (**Figure 3A**) as previously reported (Penalver Bernabe et al., 2016). In all cases, there was a trend towards increased NF κ B reporter during the 48 h after seeding (**Figure 3B**). This trend was more pronounced with carmustine treatment. Activity of the p53 reporter was only affected in cells seeded on uncoated substrates and treated with both carmustine and cilengitide. There were no obvious effects of any condition on c-myc activity.

After 48 h of treatment with carmustine or carmustine and cilengitide, GBM6 cells on uncoated substrates exhibited significantly higher NF κ B reporter activity (**Figure 3C**, $p < 0.05$). Activity of the p53 reporter increased in cells on uncoated substrates with carmustine treatment, but this effect was lost with combined treatment with carmustine and cilengitide. When seeded on vitronectin or fibronectin, NF κ B activity increased significantly with carmustine treatment alone, but this effect was lost when treated with both carmustine and cilengitide (**Figure 3C**, $p < 0.05$). Activity of the p53 reporter significantly decreased with affected by dual treatment with carmustine and cilengitide in cells seeded on vitronectin (**Figure 3C**, $p < 0.05$). No other differences in p53 reporter activity were observed. Likewise, no significant changes in activities of NF κ B, p53,

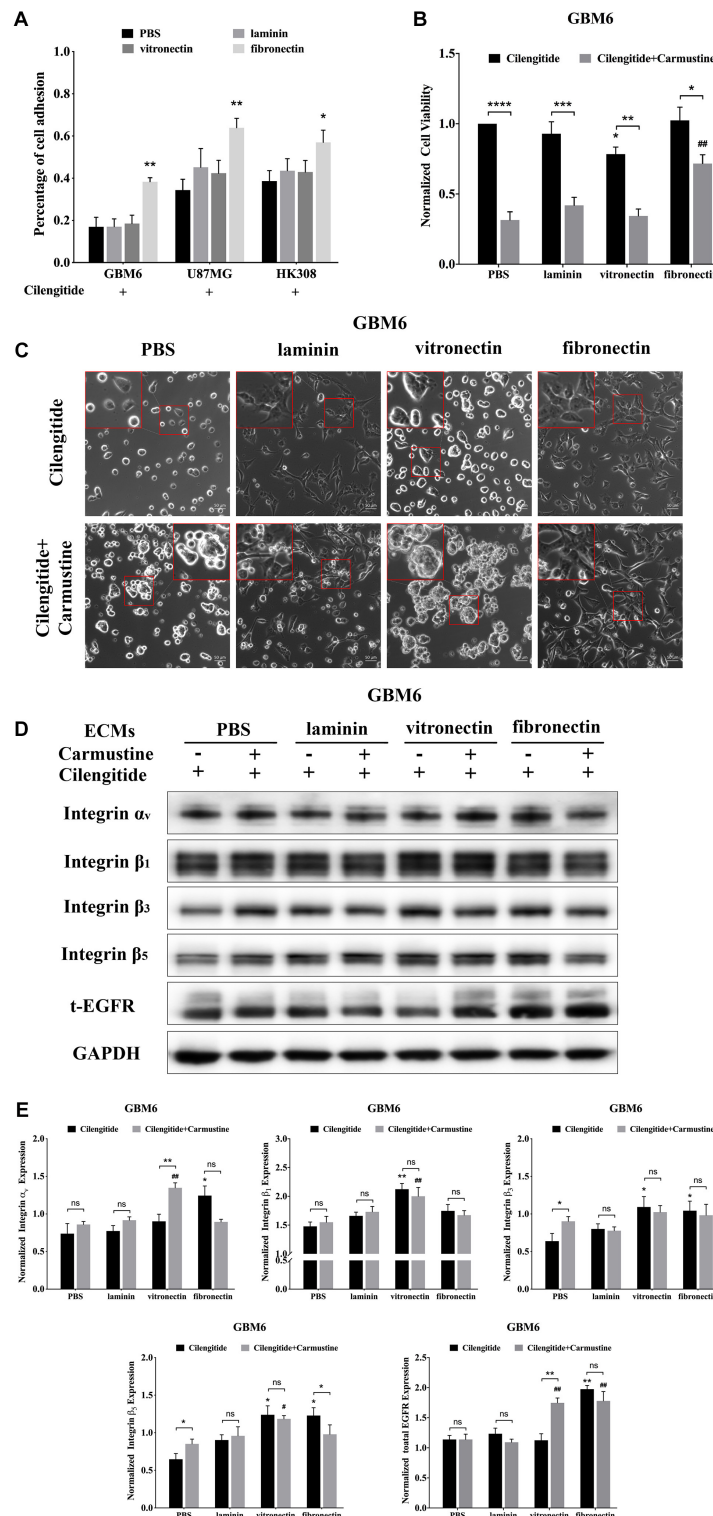


FIGURE 2 | Cilengitide reverses cell adhesion-mediated drug resistance (CAMDR) through of integrin α_v in a matrix-specific manner. **(A)** Attachment assay of cilengitide treated glioblastoma (GBM) cell lines GBM6, U87MG, and HK308 on fibronectin, laminin, and vitronectin. Error bars, SD ($n = 3$). **(B)** Cell viability assay of carmustine and cilengitide on GBM6 cells. Error bars, SD ($n = 3$, $^*p < 0.05$, $^{**}p < 0.01$, $^{***}p < 0.001$, $^{****}p < 0.0001$, $^{\#}p < 0.05$, $^{\#\#}p < 0.01$). **(C)** Representative light images of GBM6 cells with or without carmustine and cilengitide [100 μ M, phosphate-buffered saline (PBS) as control] treatment on precoated fibronectin, laminin, and vitronectin. Scale bars, 50 μ m. **(D,E)** Representative western blot of GBM6 with or without carmustine and cilengitide (100 μ M, PBS as control) treatment on integrin subunits (α_v , β_1 , β_3 , and β_5) and epidermal growth factor receptor (EGFR) expression ($n = 3$).

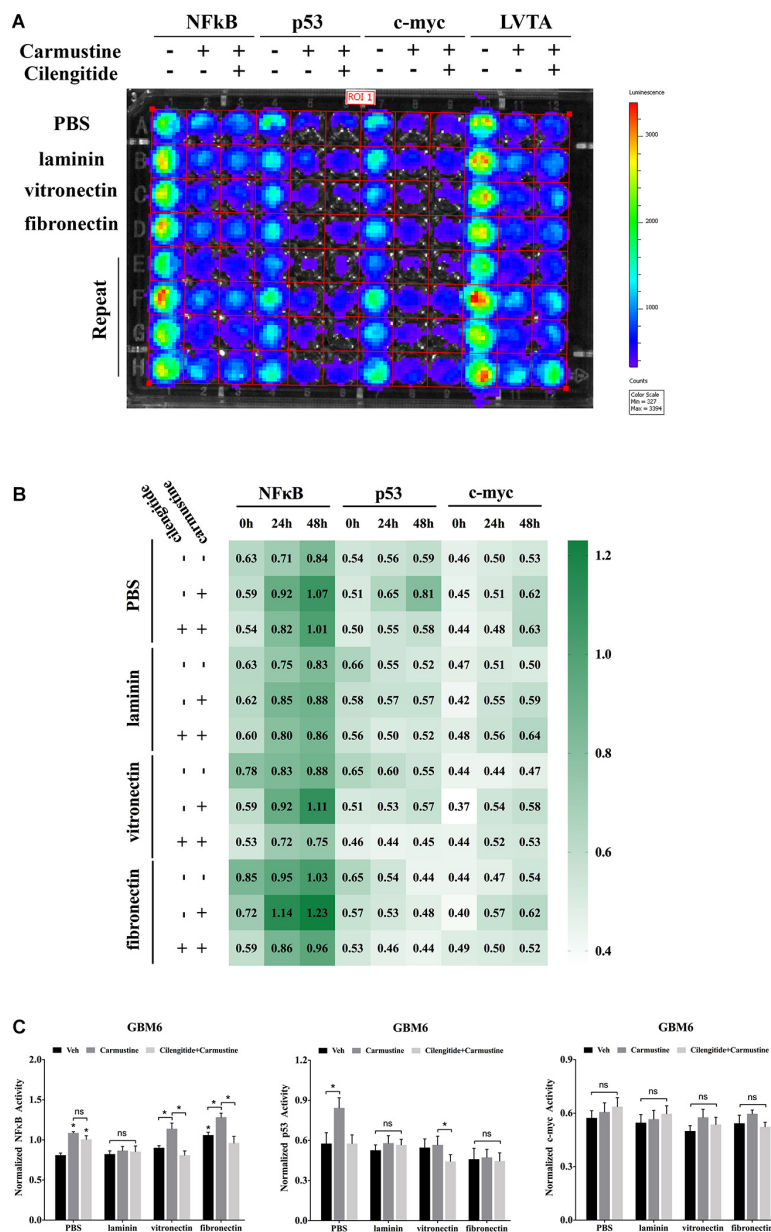


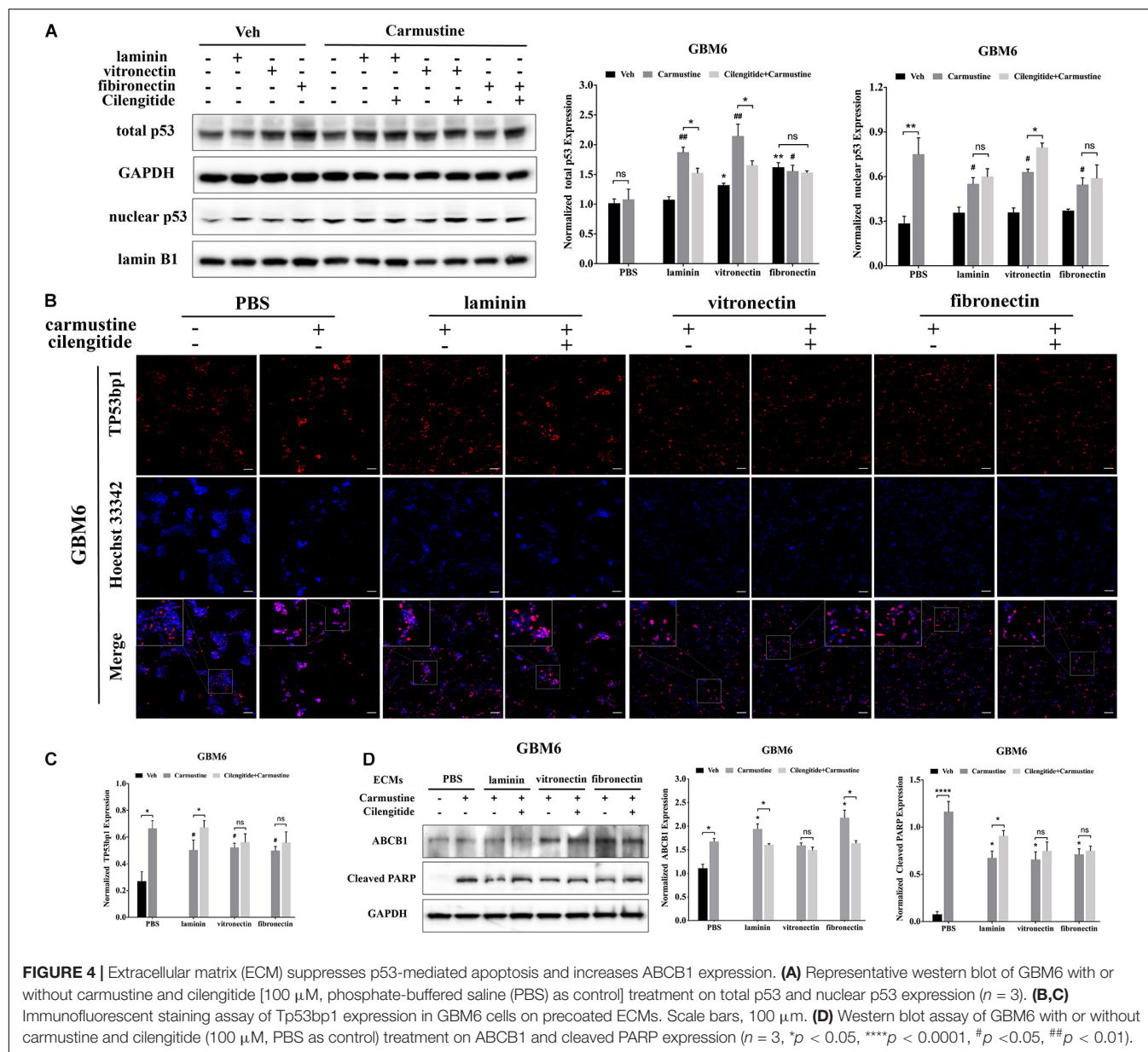
FIGURE 3 | Extracellular matrix induces activation of NFκB and deactivation of p53. **(A)** Bioluminescence assay of GBM6 cells with or without carmustine and cilengitide on precoated extracellular matrix (ECM) proteins ($n = 3$). **(B)** Heatmap of sequential expression of transcription factors (TFs) in GBM6 cells over time with or without carmustine and cilengitide ($n = 3$). **(C)** Normalized TFs activity in GBM6 cells after 48 h treatment with or without carmustine and cilengitide on precoated ECM proteins ($n = 3$). * $p < 0.05$.

and c-myc reporters were observed with laminin coating. No significant differences in c-myc reporter activities were observed in any conditions.

Extracellular Matrix Suppresses p53-Mediated Apoptosis and Increases ABCB1 Expression

Translocation of p53 to the nucleus, where it acts as a TF to regulate gene expression, is associated with apoptosis

in response to DNA damage (Castrogiovanni et al., 2018). Western blots were performed to characterize levels of p53 in the nucleus. In untreated GBM6 cells, total p53 expression was elevated for cells when grown on vitronectin or fibronectin (Figure 4A). However, nuclear expression of p53 was unaffected by the ECM substrate in cells grown on any ECM protein. Expression of nuclear p53 was significantly higher with carmustine treatment in cells all conditions ($p < 0.05$). However, carmustine treatment induced higher expression of total p53 only in cells cultured on laminin and



vitronectin. Dual treatment with carmustine and cilengitide significantly reduced total p53 levels, compared with carmustine alone, in GBM6 cells cultured on precoated laminin or vitronectin, but not fibronectin. Nuclear expression of p53 increased in cells on vitronectin substrates with dual treatment, compared with carmustine alone. Dual treatment had no effects on nuclear p53 levels on laminin- or fibronectin-coated substrates. Consistent with TF reporter and Western blot results, quantification of numbers of cells with nuclear TP53bp1 from immunofluorescence images showed elevated nuclear p53 with carmustine treatment and decreased by precoated laminin, vitronectin, and fibronectin, consistent with the nuclear p53 results (Figures 4B,C).

Western blots for c-PARP expression, indicative of apoptotic cells, showed an increased in c-PARP with carmustine

treatment in all conditions for GBM6 (Figure 4D), and U87 and HK308 cells (Supplementary Figure S3). However, culture on ECM-coated substrates significantly reduced c-PARP, which was significantly compared with cells on uncoated substrates. In GBM6 cells cultured on laminin, dual treatment with carmustine and cilengitide significantly increased c-PARP levels.

Expression of efflux transporter ABCB1, a product of the MDR1 gene, increased with carmustine treatment in all cases (Figure 4D and Supplementary Figure S3). For carmustine-treated GBM6 cells cultured on precoated laminin or fibronectin, but not vitronectin, substrates, ABCB1 expression was significantly higher than cells on uncoated substrates. Addition of cilengitide to carmustine reduced this increase in ABCB1 expression. Similar patterns of expression for cleaved

PARP and ABCB1 were detected in U87MG and HK308 (Supplementary Figure S3).

Integrin α_v -Mediated FAK/Paxillin/AKT Signaling Pathway Is Essential for Glioblastoma Cell Proliferation

The FAK/paxillin signaling pathway, downstream of integrin α_v , is involved in tumor progression, angiogenesis, and metastasis (Eke and Cordes, 2015; Noh et al., 2020). In the current study, Western blots showed decreased expression of integrin α_v by GBM6 cells cultured on all substrates after 48 h of treatment with carmustine, when compared with non-treated cells (Figures 5A,B). Integrin α_v expression was significantly elevated by carmustine-treated GBM6 cells cultured on vitronectin or fibronectin, compared with uncoated or laminin-coated substrates. On all substrates, combined treatment with carmustine and cilengitide significantly reduced expression of integrin α_v compared with carmustine treatment alone (Figure 5 and Supplementary Figure S6). While integrin α_v expression was significantly elevated by carmustine treatment in HK308 cells cultured on uncoated or laminin-coated substrates,

expression decreased on fibronectin and was unchanged on vitronectin (Supplementary Figure S5). For HK308 cells that adhered to laminin, but not fibronectin or vitronectin, dual treatment with carmustine and cilengitide significantly reduced expression of integrin α_v compared with carmustine treatment alone. Similarly, expression of integrin α_v decreased with carmustine treatment in U87 cells on uncoated substrates; however, no significant effects were observed in cells on ECM-coated substrates (Supplementary Figure S4). In contrast to patient-derived GBM6 and HK308 cells, combined treatment with carmustine and cilengitide significantly upregulated expression of integrin α_v in immortalized U87 cells cultured on vitronectin or fibronectin, when compared with carmustine treatment alone.

While integrin α_v levels in GBM6 cells decreased when cilengitide was added to carmustine treatment, total levels of FAK increased in cultures on vitronectin and fibronectin (Figure 5). Levels of phosphorylated FAK increased significantly in GBM6 cells cultured on vitronectin, but not laminin, fibronectin, or PBS control (Supplementary Figure S6). Similarly, t-/p-FAK was decreased after carmustine treatment in cells growing on precoated PBS and was not found restored in cells growing on

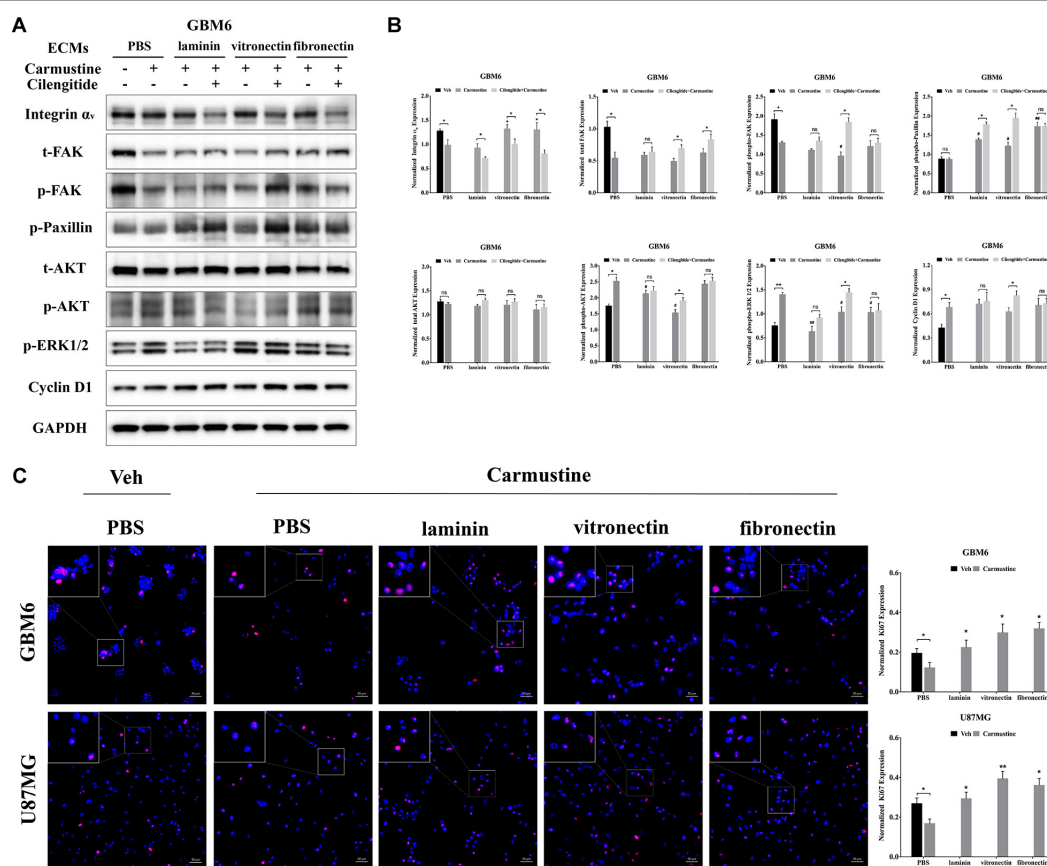


FIGURE 5 | Integrin α_v -mediated FAK/paxillin/AKT signaling pathway is essential for glioblastoma (GBM) cell proliferation. **(A,B)** Western blot assay of GBM6 cells with or without carmustine and cilengitide [100 μ M, phosphate-buffered saline (PBS) as control] treatment on integrin α_v , total/p-FAK, paxillin, total/p-AKT, p-ERK 1/2, and cyclin D1 ($n = 3$, $^*p < 0.05$, $^{**}p < 0.01$, $^{\#}p < 0.05$, $^{##}p < 0.01$). **(C)** Immunofluorescent staining assay of Ki67 expression in GBM6 and U87MG cells on precoated extracellular matrices (ECMs) Ki67 positive cells were normalized to total cell numbers. Scale bars, 50 μ m ($n = 3$, $^*p < 0.05$, $^{**}p < 0.01$).

precoated laminin, vitronectin, or fibronectin. Phosphorylation of paxillin, a focal adhesion protein recruited to the intracellular domain of ECM-engaged integrins, was upregulated significantly when GBM6 cells on all ECM-coated, but not uncoated, substrates were treated with carmustine (Figure 5). With dual carmustine and cilengitide treatment, p-paxillin was further increased in cells on laminin and vitronectin.

In addition, p-AKT, p-ERK 1/2, and cyclin D1 were increased in a large degree by carmustine without ECM protein presence. Cilengitide induced a significant elevation of p-AKT, p-ERK 1/2, and cyclin D1 in cells growing on vitronectin. U87MG and HK308 showed variant changes but the same activation trend in FAK/paxillin/AKT signaling pathway (Supplementary Figures S4, S5). In GBM6 and U87MG cells, numbers of proliferating Ki67 positive cells were significantly decreased with carmustine treatment on precoated PBS, but this effect was lost when cells were cultured on precoated laminin, vitronectin, and fibronectin (Figure 5C).

Increased Activity of Epidermal Growth Factor Receptor-Mediated Pathways Correlates With Increased Cell Survival in Integrin α_v Knockdowns

To investigate the relationship between integrin α_v and EGFR-mediated oncogenic pathways, integrin α_v was knocked down in GBM6 cells using a lentiviral vector encoding shRNA against integrin α_v . Green fluorescent protein (GFP) was used to identify transfected cells expressing the shRNA (Figure 6A). Compared with uncoated or laminin-coated substrates, culture on vitronectin- or fibronectin-coated substrates significantly reduced efficacy of the shRNA knockdown of integrin α_v , indicating its importance for cell survival (Figures 6B,C). When treated with carmustine, levels of integrin α_v in knockdown cultures on uncoated and laminin substrates were elevated to those found in wild-type cultures on uncoated substrates. In contrast, knockdown cultures treated with carmustine on fibronectin further decreased integrin α_v expression. Strikingly, when integrin α_v expression was knocked down in GBM6 cells on all substrates, carmustine treatment induced robust apoptosis, with levels of nuclear c-PARP significantly increased over treated, wild-type cells on uncoated substrates.

When integrin α_v was knocked down, expression of total EGFR increased in GBM6 cells that adhered to laminin, vitronectin, or fibronectin, compared with cells on uncoated substrates (Figures 6B,C). Although total AKT was decreased in integrin α_v knockdown cells, vitronectin and fibronectin promoted total AKT expression. There was also a significant elevation of phospho-AKT in integrin α_v knockdown cells growing on precoated vitronectin and fibronectin (Figures 6B,C). Cyclin D1 was decreased remarkably in integrin α_v knockdown cells treated with carmustine (Figures 6B,C). As shown in Figure 6D, schematic diagram depicted the involvement of integrin α_v and EGFR for the survival pathway in the CAMDR. Although knockdown of integrin α_v might

prevent the survival of GBM cells, compensatory activation of EGFR and driving its downstream signal molecule AKT and ERK acted as a survival pathway, preventing GBM cells from being killed by carmustine.

DISCUSSION

Cancer cells may exhibit intrinsic resistance, where they are resistant at the time of initial treatment, and acquired resistance, where resistance develops during the treatment, leading to therapeutic failure. Although a series of publications have revealed the possible mechanisms by which cancer cells become resistant to chemotherapeutic agents, such as decreased loss of receptor or transporter, specific metabolism, enhanced efflux pumps, and limited drug uptake (Zaal and Berkers, 2018), it remains unclear how the tumor microenvironment confers drug resistance to cancer cells. In the current study, our data show three major components of ECM, laminin, vitronectin, and fibronectin, induce GBM cells to become drug resistant by activation of integrin α_v and EGFR. First, upregulated integrin α_v activates FAK/paxillin/AKT pathway, leading to a suppression of p53-mediated apoptosis and promoting proliferation by altered cell cycle checkpoints. At the same time, increased expression of ABCB1 indicates that more drug was pumped out by the cells. Second, a compensatory survival pathway was required through activation of EGFR, especially when the integrin α_v was missing or inhibited by the integrin receptor antagonist cilengitide.

The composition of the ECM in tumors is vastly different from that found in the normal part tissue, but little was known on their exact role in the tumor progression. As the main soluble particles in the ECM, laminin, vitronectin, and fibronectin were found present in the GBM biopsy samples (Schiffer et al., 1984; Shinoda et al., 1989; Gladson and Cheresch, 1991). Similar findings were observed in the current study; by using the TMA, laminin, vitronectin, and fibronectin were expressed in the GBM at a high level. On the contrary, only fibronectin was abundant in the low-grade CNS tumors, indicating that ECM evolved with tumor progression. It was clear from our data that cell attachment was increased when growing on laminin, vitronectin, and fibronectin, enabling GBM cells to acquire the chemotherapeutic resistance, which was also called CAMDR. Our data revealed a variant cell adhesion between cell lines on the same ECM protein, probably as a result of the distribution of certain integrin receptors on the cell surface. Furthermore, integrin receptors have also been shown to bind ECM proteins on sites other than RGD sequences (Albelda and Buck, 1990). Integrins are not the only cell surface receptors for ECM molecules (Venstrom and Reichardt, 1993). CD44 can also mediate glioma cell adhesion to hyaluroonic acid in the ECM and invasion *in vitro* (Xiao et al., 2018). As shown in Figure 1E, fibronectin increased the cell viability in all three cell lines, revealing its strong CAMDR effect, which was also in accordance with the TMA results. It has been reported that fibronectin induced CAMDR in multiple myeloma and bladder cancer (Gao et al., 2017; Wu et al., 2019). Laminins

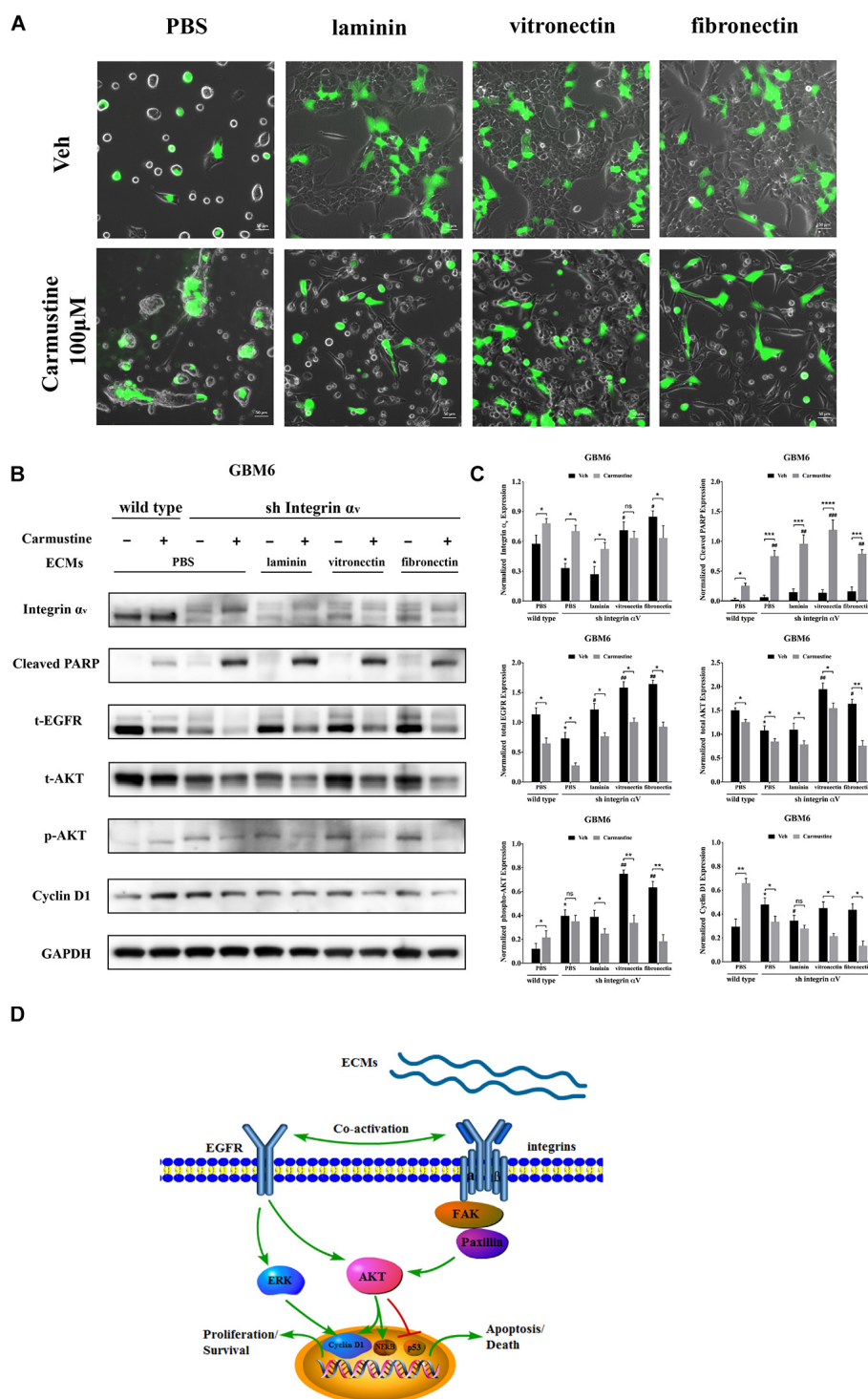


FIGURE 6 | Increased activity of epidermal growth factor receptor (EGFR)-mediated pathways correlates with increased cell survival in integrin α_v knockdowns. **(A)** Representative light images of GBM6 cells transfected with integrin α_v shRNA [identified by green carmustine [100 μ M, phosphate-buffered saline (PBS) as control] treatment on precoated fibronectin, laminin and vitronectin. Scale bars, 50 μ m. **(B,C)** Western blot assay of wild-type and sh integrin α_v transfected GBM6 cells with or without carmustine and cilengitide (100 μ M, PBS as control) treatment on integrin α_v , c-PARP, total-EGFR, total/p-AKT, and cyclin D1 ($n = 3$, $^*p < 0.05$, $^{**}p < 0.01$, $^{***}p < 0.001$, $^{****}p < 0.0001$, $^{\#}p < 0.05$, $^{\#\#}p < 0.01$, $^{\#\#\#}p < 0.001$). **(D)** Hypothetic schematic diagram illustrated the mechanism of extracellular matrices (ECMs) induced cell adhesion-mediated drug resistance (CAMDR) by activation of integrin α_v -mediated FAK/paxillin/AKT signaling pathway and co-activation of EGFR-mediated pathways when integrin α_v was knocked down.

are high-molecular-weight proteins of ECM and are thought as an important and biologically active part of basal lamina, influencing cell differentiation, migration, and adhesion (Yap et al., 2019; Barros et al., 2020). It is also documented that laminin was involved in the acquired chemotherapeutic resistance in gastric cancer (Sun et al., 2014). Only HK308 attached to laminin developed drug resistance in our study.

Cilengitide is based on the cyclin peptide cyclo (-RGDfV-), which is a selective for integrin α_v and is reported beneficial for GBM patients only in phase II trials (Reardon et al., 2008; Khasraw et al., 2016). Here, cilengitide had different antagonistic effects on GBM6, U87MG, and HK308. As shown in **Supplementary Figure S2** and **Figure 2**, cilengitide detached U87MG completely when cells were not grown on ECM, and more cells detached after vitronectin treatment. A similar result was found in GBM6 in that cells grown on vitronectin more easily detached after carmustine treatment. On the contrary, only attachment to fibronectin was not influenced by cilengitide. Hence, we assume that predominance of integrin receptors of vitronectin is more enriched over other types of receptors on these GBM cells. Expression of vitronectin and its integrin receptor $\alpha_v\beta_3$ have been described in human GBM *in vivo* (Franovic et al., 2015). Other integrin receptors such as integrins β_1 and β_8 are also reported in literature (Tchaicha et al., 2011; Cosset et al., 2012). Although integrins β_1 , β_3 and β_5 were upregulated in cells grown on vitronectin, there were no changes after the cells were detached by cilengitide. Meanwhile, integrin α_v was boosted, likely due to the negative feedback response when the cells lost attachment. Since the trend of integrins α and β is not exactly the same, we cannot accurately determine which β subunit plays a major role. Previous literature and research show that fibronectin laminin and vitronectin have different specific integrin receptors. Integrin $\alpha_v\beta_3$, is the main binding receptor of vitronectin (Hermann et al., 1999). Therefore, cilengitide has the most obvious antagonistic effect on cell adhesion to vitronectin compared to on laminin or fibronectin, which is consistent with our current results. In addition to $\alpha_v\beta_3$, $\alpha_v\beta_1$ is also found as a receptor of vitronectin (Ding et al., 2002), whereas the main binding receptors of fibronectin are $\alpha_v\beta_1$ (Ye et al., 2020), $\alpha_v\beta_6$ (Mould et al., 2014), and $\alpha_5\beta_1$ (Mould et al., 2014) and the main binding receptor of laminin is $\alpha_6\beta_1$ (Corsini and Martin-Villalba, 2010). Previous research also confirmed that M21 human melanoma cells not only lost the ability to attach to vitronectin but showed a dramatic reduction in tumorigenicity when lacking integrin α_v gene expression (Lacaria et al., 2020). In addition, accompanied with the elevation of integrin α_v , in our study EGFR was also found upregulated in carmustine- and cilengitide-treated cells growing on vitronectin. Other researchers have proposed that integrin α_v associates with the EGFR on the cell membrane in a macromolecular complex including the adaptor protein p130Cas and the c-Src kinase that could lead to phosphorylation of specific EGFR tyrosine residues (Kosibaty et al., 2020).

Many studies have addressed the association between NF κ B and cell adhesion events. NF κ B activity is required for the expression of several cell adhesion molecules such

as vascular cell adhesion molecule-1 (VCAM-1), intracellular adhesion molecule-1 (ICAM-1), and endothelial leukocyte adhesion molecule-1 (ELAM-1) (Ampofo et al., 2019). Previous publication also reported that over-expression of NF κ B subunits in GBM cells elevated the levels of fibronectin gene expression, indicating a positive loop in the regulatory role for NF κ B in ECM protein-cell communication. Activation of NF κ B also led to an increase in the levels of mRNA for the α_v and β_3 integrin subunits, which was in accordance with our present results (Ritchie et al., 2000). Bioluminescent analysis of genetic reporters has been previously used in live cells to assess dynamic changes in TF activity (Pannier et al., 2007; Penalver Bernabe et al., 2016). Our data indicated that activity of NF κ B was promoted by either drug treatment as a feedback response or increased attachment to vitronectin and fibronectin, but detachment induced by cilengitide dramatically suppressed activity of NF κ B. The result was in accordance with the prior studies showing that NF κ B was involved in the proliferation progress in many tumors (Zeligs et al., 2016). Another interesting thing was that the activity of p53 was only elevated by carmustine in cells growing on precoated PBS but decreased in cells growing on laminin, vitronectin, and fibronectin. Along with the downregulation, p53-mediated apoptosis was reduced accordingly. It has been reported that high expression of fibronectin is associated with the cell proliferation and malignancy via NF κ B/p53-apoptosis signaling pathway in colorectal cancer (Yi et al., 2016).

A number of studies have demonstrated that chemotherapeutic resistance against alkylating agents is often associated with the overexpression of ABCB1 (Munoz et al., 2014; Stavrovskaya et al., 2016). Generally, ABCB1 serves as a drug efflux pump actively reducing intracellular drug concentrations in resistant tumor cells, but its biological regulation remains unclear. We found that ABCB1 was elevated by the treatment of carmustine without precoated ECM proteins, which is probably due to negative feedback to the alkylating agent. ABCB1 went to an even higher-level expression with precoated fibronectin, which was correlated with the upregulation of EGFR, as was also reported in the prior work (Munoz et al., 2014). Among microenvironment-cell interaction-mediated regulation of ABCB1, a family of ECM proteins called CCN (CYR61/CTGF/NOV) was demonstrated to regulate ABCB1 and to confer vinblastine resistance in renal cell carcinoma cells targeting $\alpha_v\beta_3$ (Long et al., 2013). HA-CD44 interactions have been shown to be involved in multidrug resistance in breast tumor cells and are linked to a positive feedback circuit involving HA, phosphoinositide 3-kinase (PI3K), and ErbB2 (Ma et al., 2018).

As shown in the present study, activation of integrin α_v -mediated FAK/paxillin/AKT signaling pathway was required for the proliferation, which was consistent with studies in other tumor cells that integrin α_v facilitates a proliferative role (Hayashido et al., 2014; Hung et al., 2014). Some research also indicated the integrin α_v was involved in the GBM neurosphere formation. Integrin α_v -mediated cell-cell adhesion limited cell dispersion from spheroids in a fibronectin-poor microenvironment. However, in a fibronectin-rich

microenvironment, α_v promoted cell dispersion (Blandin et al., 2016). EGFR has been well identified as a predictor for the chemoresistance of GBM in the last decade (Taylor et al., 2012). Here, we show that with integrin α_v knock down, compensatory activation of EGFR may enable the cells to escape apoptotic effects of alkylating agents. Overall, this study emphasizes that importance of interactions of the ECM and a corresponding profile of cell surface receptors to regulation of cancer cell survival.

DATA AVAILABILITY STATEMENT

The original contributions presented in the study are included in the article/**Supplementary Material**, further inquiries can be directed to the corresponding author/s.

ETHICS STATEMENT

The patient-derived GBM cell lines were in accordance with UCLA Institutional Review Board protocol 10-000655.

AUTHOR CONTRIBUTIONS

SS and QY conceived the studies and wrote the manuscript. QY and WX designed the methodology. QY, WX, SS, AS, and JL conducted the experiments and acquired and analyzed the data. All authors contributed to the article and approved the submitted version.

FUNDING

This work was supported with funding from the National Institutes of Health (NIH) (R21NS093199) and the UCLA ARC 3R's Award.

ACKNOWLEDGMENTS

We thank Dr. Harley Kornblum for the provision of the HK308 cell lines; Dr. David Nathanson for the provision of the GBM6 cell line; and Dr. William Yong, Director

of the Brain Tumor Tissue Resource at UCLA, for the provision of the patient tumor specimens for TMA. We also thank UCLA Crump Institute for Molecular Imaging using the IVIS imaging system. TP53bp1 was a gift from Nicola Burgess-Brown (Addgene plasmid #73252). ITGAV shRNA was obtained from Dharmacon (V2LHS_133468, Lafayette, CO, United States).

SUPPLEMENTARY MATERIAL

The Supplementary Material for this article can be found online at: <https://www.frontiersin.org/articles/10.3389/fcell.2021.616580/full#supplementary-material>

Supplementary Figure 1 | (A) Representative light images of U87MG cells with or without carmustine (100 μ M, PBS as control) treatment on precoated fibronectin, laminin, and vitronectin. Scale bars, 50 μ m. **(B)** Representative light images of HK308 cells with or without carmustine (100 μ M, PBS as control) treatment on precoated fibronectin, laminin, and vitronectin. Scale bars, 50 μ m.

Supplementary Figure 2 | (A) Cell viability assay of carmustine and cilengitide on U87MG and HK308 cells. Error bars, SD ($n = 3$, * $p < 0.05$, ** $p < 0.01$, *** $p < 0.001$, # $p < 0.05$, ## $p < 0.01$). **(B)** Representative light images of U87MG cells with or without carmustine and cilengitide (100 μ M, PBS as control) treatment on precoated fibronectin, laminin, and vitronectin. Scale bars, 50 μ m. **(C)** Representative light images of HK308 cells with or without carmustine and cilengitide (100 μ M, PBS as control) treatment on precoated fibronectin, laminin, and vitronectin. Scale bars, 50 μ m.

Supplementary Figure 3 | (A) Western blot assay of U87MG cells with or without carmustine and cilengitide (100 μ M, PBS as control) treatment on ABCB1 and Cleaved PARP expression ($n = 3$, * $p < 0.05$, ** $p < 0.01$, *** $p < 0.001$, # $p < 0.05$, ### $p < 0.001$). **(B)** Western blot assay of HK308 cells with or without carmustine and cilengitide (100 μ M, PBS as control) treatment on ABCB1 and Cleaved PARP expression ($n = 3$, * $p < 0.05$, *** $p < 0.001$, # $p < 0.05$, ### $p < 0.001$).

Supplementary Figure 4 | (A,B) Western blot assay of U87MG cells with or without carmustine and cilengitide (100 μ M, PBS as control) treatment on integrin α_v , total/p-FAK, paxillin, total/p-AKT, p-ERK 1/2, and cyclin D1 ($n = 3$, * $p < 0.05$, ** $p < 0.01$, *** $p < 0.001$, # $p < 0.05$).

Supplementary Figure 5 | (A,B) Western blot assay of HK308 cells with or without carmustine and cilengitide (100 μ M, PBS as control) treatment on integrin α_v , total/p-FAK, paxillin, total/p-AKT, p-ERK 1/2, and cyclin D1 ($n = 3$, * $p < 0.05$, ** $p < 0.01$, # $p < 0.05$).

Supplementary Figure 6 | (A,B) Western blot assay of GBM6 cells with dual treatment of carmustine and cilengitide on uncoated ECMs (100 μ M, PBS as control) ($n = 3$, * $p < 0.05$, ** $p < 0.01$, *** $p < 0.001$, # $p < 0.05$, ## $p < 0.01$, ### $p < 0.001$).

REFERENCES

- Affronti, M. L., Heery, C. R., Herndon, J. E. II, Rich, J. N., Reardon, D. A., Desjardins, A., et al. (2009). Overall survival of newly diagnosed glioblastoma patients receiving carmustine wafers followed by radiation and concurrent temozolomide plus rotational multiagent chemotherapy. *Cancer* 115, 3501–3511. doi: 10.1002/cncr.24398
- Akhavan, D., Pourzia, A. L., Nourian, A. A., Williams, K. J., Nathanson, D., Babic, I., et al. (2013). De-repression of PDGFRbeta transcription promotes acquired resistance to EGFR tyrosine kinase inhibitors in glioblastoma patients. *Cancer Discov.* 3, 534–547. doi: 10.1158/2159-8290.cd-12-0502
- Albelda, S. M., and Buck, C. A. (1990). Integrins and other cell adhesion molecules. *FASEB J.* 4, 2868–2880. doi: 10.1096/fasebj.4.11.2199285
- Ampofo, E., Berg, J. J., Menger, M. D., and Laschke, M. W. (2019). Maslinic acid alleviates ischemia/reperfusion-induced inflammation by downregulation of NFkappaB-mediated adhesion molecule expression. *Sci. Rep.* 9:6119.
- Ashby, L. S., Smith, K. A., and Stea, B. (2016). Gliadel wafer implantation combined with standard radiotherapy and concurrent followed by adjuvant temozolomide for treatment of newly diagnosed high-grade glioma: a systematic literature review. *World J. Surg. Oncol.* 14:225.

- Barros, D., Amaral, I. F., and Pego, A. P. (2020). Laminin-inspired cell-instructive microenvironments for neural stem cells. *Biomacromolecules* 21, 276–293. doi: 10.1021/acs.biomac.9b01319
- Bellis, A. D., Penalver-Bernabe, B., Weiss, M. S., Yarrington, M. E., Barbolina, M. V., Pannier, A. K., et al. (2011). Cellular arrays for large-scale analysis of transcription factor activity. *Biotechnol. Bioeng.* 108, 395–403. doi: 10.1002/bit.22916
- Blandin, A. F., Noulet, F., Renner, G., Mercier, M. C., Choulier, L., Vauchelles, R., et al. (2016). Glioma cell dispersion is driven by alpha5 integrin-mediated cell-matrix and cell-cell interactions. *Cancer Lett.* 376, 328–338. doi: 10.1016/j.canlet.2016.04.007
- Castrogiovanni, C., Waterschoot, B., De Backer, O., and Dumont, P. (2018). Serine 392 phosphorylation modulates p53 mitochondrial translocation and transcription-independent apoptosis. *Cell Death Differ.* 25, 190–203. doi: 10.1038/cdd.2017.143
- Chinot, O. L., Wick, W., and Cloughesy, T. (2014). Bevacizumab for newly diagnosed glioblastoma. *N. Engl. J. Med.* 370:2049.
- Choe, G., Horvath, S., Cloughesy, T. F., Crosby, K., Seligson, D., Palotie, A., et al. (2003). Analysis of the phosphatidylinositol 3'-kinase signaling pathway in glioblastoma patients in vivo. *Cancer Res.* 63, 2742–2746.
- Chowdhary, S. A., Ryken, T., and Newton, H. B. (2015). Survival outcomes and safety of carmustine wafers in the treatment of high-grade gliomas: a meta-analysis. *J. Neurooncol.* 122, 367–382. doi: 10.1007/s11060-015-1724-2
- Corsini, N. S., and Martin-Villalba, A. (2010). Integrin alpha 6: anchors away for glioma stem cells. *Cell Stem Cell* 6, 403–404. doi: 10.1016/j.stem.2010.04.003
- Cosset, E. C., Godet, J., Entz-Werle, N., Guerin, E., Guenot, D., Froelich, S., et al. (2012). Involvement of the TGFbeta pathway in the regulation of alpha5 beta1 integrins by caveolin-1 in human glioblastoma. *Int. J. Cancer* 131, 601–611. doi: 10.1002/ijc.26415
- Ding, Q., Stewart, J. Jr., Prince, C. W., Chang, P. L., Trikha, M., Han, X., et al. (2002). Promotion of malignant astrocytoma cell migration by osteopontin expressed in the normal brain: differences in integrin signaling during cell adhesion to osteopontin versus vitronectin. *Cancer Res.* 62, 5336–5343.
- Dixit, S., Hingorani, M., Achawal, S., and Scott, I. (2011). The sequential use of carmustine wafers (Gliadel(R)) and post-operative radiotherapy with concomitant temozolomide followed by adjuvant temozolomide: a clinical review. *Br. J. Neurosurg.* 25, 459–469. doi: 10.3109/02688697.2010.550342
- Dull, T., Zufferey, R., Kelly, M., Mandel, R. J., Nguyen, M., Trono, D., et al. (1998). A third-generation lentivirus vector with a conditional packaging system. *J. Virol.* 72, 8463–8471. doi: 10.1128/jvi.72.11.8463-8471.1998
- Eke, I., and Cordes, N. (2015). Focal adhesion signaling and therapy resistance in cancer. *Semin. Cancer Biol.* 31, 65–75. doi: 10.1016/j.semcancer.2014.07.009
- Ellor, S. V., Pagano-Young, T. A., and Avgeropoulos, N. G. (2014). Glioblastoma: background, standard treatment paradigms, and supportive care considerations. *J. Law Med. Ethics* 42, 171–182. doi: 10.1111/jlme.12133
- Fei, M., Hang, Q., Hou, S., He, S., and Ruan, C. (2014). Adhesion to fibronectin induces p27(Kip1) nuclear accumulation through down-regulation of Jab1 and contributes to cell adhesion-mediated drug resistance (CAM-DR) in RPMI 8,226 cells. *Mol. Cell Biochem.* 386, 177–187. doi: 10.1007/s11010-013-1856-7
- Franovic, A., Elliott, C., Seguin, L., Camargo, M. F., Weis, S. M., and Cheresch, D. A. (2015). Glioblastomas require integrin alphavbeta3/PAK4 signaling to escape senescence. *Cancer Res.* 75, 4466–4473. doi: 10.1158/0008-5472.can-15-0988
- Gao, F., Xu, T., Wang, X., Zhong, S., Chen, S., Zhang, M., et al. (2017). CIP2A mediates fibronectin-induced bladder cancer cell proliferation by stabilizing beta-catenin. *J. Exp. Clin. Cancer Res.* 36:70.
- Gilbert, M. R., Dignam, J. J., Armstrong, T. S., Wefel, J. S., Blumenthal, D. T., Vogelbaum, M. A., et al. (2014). A randomized trial of bevacizumab for newly diagnosed glioblastoma. *N. Engl. J. Med.* 370, 699–708.
- Gladson, C. L., and Cheresch, D. A. (1991). Glioblastoma expression of vitronectin and the alpha v beta 3 integrin. Adhesion mechanism for transformed glial cells. *J. Clin. Invest.* 88, 1924–1932. doi: 10.1172/jci115516
- Guo, D., Prins, R. M., Dang, J., Kuga, D., Iwanami, A., Soto, H., et al. (2009). EGFR signaling through an Akt-SREBP-1-dependent, rapamycin-resistant pathway sensitizes glioblastomas to antiproliferative therapy. *Sci. Signal.* 2:ra82. doi: 10.1126/scisignal.2000446
- Hayashido, Y., Kitano, H., Sakaue, T., Fujii, T., Suematsu, M., Sakurai, S., et al. (2014). Overexpression of integrin alphav facilitates proliferation and invasion of oral squamous cell carcinoma cells via MEK/ERK signaling pathway that is activated by interaction of integrin alphavbeta8 with type collagen. *Int. J. Oncol.* 45, 1875–1882. doi: 10.3892/ijo.2014.2642
- Hendricks, B. K., Cohen-Gadol, A. A., and Miller, J. C. (2015). Novel delivery methods bypassing the blood-brain and blood-tumor barriers. *Neurosurg. Focus* 38:E10.
- Hermann, P., Armant, M., Brown, E., Rubio, M., Ishihara, H., Ulrich, D., et al. (1999). The vitronectin receptor and its associated CD47 molecule mediates proinflammatory cytokine synthesis in human monocytes by interaction with soluble CD23. *J. Cell Biol.* 144, 767–775. doi: 10.1083/jcb.144.4.767
- Horikawa, I. (2020). Balancing and differentiating p53 activities toward longevity and no cancer? *Cancer Res.* 80, 5164–5165. doi: 10.1158/0008-5472.can-20-3080
- Hung, C. J., Hsu, H. I., Lin, C. C., Huang, T. H., Wu, B. C., Kao, C. T., et al. (2014). The role of integrin alphav in proliferation and differentiation of human dental pulp cell response to calcium silicate cement. *J. Endod.* 40, 1802–1809. doi: 10.1016/j.joen.2014.07.016
- Khasraw, M., Lee, A., Mccowatt, S., Kerestes, Z., Buyse, M. E., Back, M., et al. (2016). Cilengitide with metronomic temozolomide, procarbazine, and standard radiotherapy in patients with glioblastoma and unmethylated MGMT gene promoter in ExCentric, an open-label phase II trial. *J. Neurooncol.* 128, 163–171. doi: 10.1007/s11060-016-2094-0
- Kim, H. J., and Kim, D. Y. (2020). Present and future of anti-glioblastoma therapies: a deep look into molecular dependencies/features. *Molecules* 25:4641. doi: 10.3390/molecules25204641
- Kong, L. R., Chua, K. N., Sim, W. J., Ng, H. C., Bi, C., Ho, J., et al. (2015). MEK inhibition overcomes cisplatin resistance conferred by SOS/MAPK pathway activation in squamous cell carcinoma. *Mol. Cancer Ther.* 14, 1750–1760. doi: 10.1158/1535-7163.mct-15-0062
- Kosibaty, Z., Murata, Y., Minami, Y., Noguchi, M., and Sakamoto, N. (2020). ECT2 promotes lung adenocarcinoma progression through extracellular matrix dynamics and focal adhesion signaling. *Cancer Sci.* 00, 1–12.
- Lacaria, L., Lange, J. R., Goldmann, W. H., Rico, F., and Alonso, J. L. (2020). alphavbeta3 integrin expression increases elasticity in human melanoma cells. *Biochem. Biophys. Res. Commun.* 525, 836–840. doi: 10.1016/j.bbrc.2020.02.156
- Laks, D. R., Crisman, T. J., Shih, M. Y., Mottahedeh, J., Gao, F., Sperry, J., et al. (2016). Large-scale assessment of the gliomasphere model system. *Neuro Oncol.* 18, 1367–1378. doi: 10.1093/neuonc/now045
- Long, Q. Z., Zhou, M., Liu, X. G., Du, Y. F., Fan, J. H., Li, X., et al. (2013). Interaction of CCN1 with alphavbeta3 integrin induces P-glycoprotein and confers vinblastine resistance in renal cell carcinoma cells. *Anticancer Drugs* 24, 810–817. doi: 10.1097/cad.0b013e328363046d
- Lu, K. V., Zhu, S., Cvrljevic, A., Huang, T. T., Sarkaria, S., Ahkavan, D., et al. (2009). Fyn and SRC are effectors of oncogenic epidermal growth factor receptor signaling in glioblastoma patients. *Cancer Res.* 69, 6889–6898. doi: 10.1158/0008-5472.can-09-0347
- Ma, J. W., Wang, X., Chang, L., Zhong, X. Y., Jing, H., Zhu, X., et al. (2018). CD44 collaborates with ERBB2 mediate radiation resistance via p38 phosphorylation and DNA homologous recombination pathway in prostate cancer. *Exp. Cell Res.* 370, 58–67. doi: 10.1016/j.yexcr.2018.06.006
- Messaoudi, K., Clavreul, A., and Lagarde, F. (2015). Toward an effective strategy in glioblastoma treatment. Part I: resistance mechanisms and strategies to overcome resistance of glioblastoma to temozolomide. *Drug Discov. Today* 20, 899–905. doi: 10.1016/j.drudis.2015.02.011
- Miranda, A., Blanco-Prieto, M., Sousa, J., Pais, A., and Vitorino, C. (2017). Breaching barriers in glioblastoma. Part I: molecular pathways and novel treatment approaches. *Int. J. Pharm.* 531, 372–388. doi: 10.1016/j.ijpharm.2017.07.056
- Motegi, A., Masutani, M., Yoshioka, K. I., and Bessho, T. (2019). Aberrations in DNA repair pathways in cancer and therapeutic significances. *Semin. Cancer Biol.* 58, 29–46. doi: 10.1016/j.semcancer.2019.02.005
- Mould, A. P., Craig, S. E., Byron, S. K., Humphries, M. J., and Jowitt, T. A. (2014). Disruption of integrin-fibronectin complexes by allosteric but not ligand-mimetic inhibitors. *Biochem. J.* 464, 301–313. doi: 10.1042/bj20141047
- Munoz, J. L., Rodriguez-Cruz, V., Greco, S. J., Nagula, V., Scotto, K. W., and Rameshwar, P. (2014). Temozolomide induces the production of epidermal

- growth factor to regulate MDR1 expression in glioblastoma cells. *Mol. Cancer Ther.* 13, 2399–2411. doi: 10.1158/1535-7163.mct-14-0011
- Nabors, L. B., Fink, K. L., Mikkelsen, T., Grujicic, D., Tarnawski, R., Nam, D. H., et al. (2015). Two cilengitide regimens in combination with standard treatment for patients with newly diagnosed glioblastoma and unmethylated MGMT gene promoter: results of the open-label, controlled, randomized phase II CORE study. *Neuro Oncol.* 17, 708–717. doi: 10.1093/neuonc/nou356
- Nakagawa, Y., Nakayama, H., Nagata, M., Yoshida, R., Kawahara, K., Hirose, A., et al. (2014). Overexpression of fibronectin confers cell adhesion-mediated drug resistance (CAM-DR) against 5-FU in oral squamous cell carcinoma cells. *Int. J. Oncol.* 44, 1376–1384. doi: 10.3892/ijo.2014.2265
- Noh, K., Bach, D. H., Choi, H. J., Kim, M. S., Wu, S. Y., Pradeep, S., et al. (2020). The hidden role of paxillin: localization to nucleus promotes tumor angiogenesis. *Oncogene* 40, 384–395. doi: 10.1038/s41388-020-01517-3
- Olotu, F. A., and Soliman, M. E. S. (2019). Dynamic perspectives into the mechanisms of mutation-induced p53-DNA binding loss and inactivation using active perturbation theory: structural and molecular insights toward the design of potent reactivators in cancer therapy. *J. Cell Biochem.* 120, 951–966. doi: 10.1002/jcb.27458
- Pannier, A. K., Ariazi, E. A., Bellis, A. D., Bengali, Z., Jordan, V. C., and Shea, L. D. (2007). Bioluminescence imaging for assessment and normalization in transfected cell arrays. *Biotechnol. Bioeng.* 98, 486–497. doi: 10.1002/bit.21477
- Patel, M. A., Kim, J. E., Ruzevick, J., Li, G., and Lim, M. (2014). The future of glioblastoma therapy: synergism of standard of care and immunotherapy. *Cancers (Basel)* 6, 1953–1985. doi: 10.3390/cancers6041953
- Penalver Bernabe, B., Shin, S., Rios, P. D., Broadbelt, L. J., Shea, L. D., and Seidlits, S. K. (2016). Dynamic transcription factor activity networks in response to independently altered mechanical and adhesive microenvironmental cues. *Integr. Biol. (Camb)* 8, 844–860. doi: 10.1039/c6ib00093b
- Pine, A. R., Cirigliano, S. M., Nicholson, J. G., Hu, Y., Linkous, A., Miyaguchi, K., et al. (2020). Tumor microenvironment is critical for the maintenance of cellular states found in primary glioblastomas. *Cancer Discov.* 10, 964–979. doi: 10.1158/2159-8290.cd-20-0057
- Pourgholi, F., Hajivalili, M., Farhad, J. N., Kafil, H. S., and Yousefi, M. (2016). Nanoparticles: novel vehicles in treatment of Glioblastoma. *Biomed. Pharmacother.* 77, 98–107. doi: 10.1016/j.biopha.2015.12.014
- Reardon, D. A., Fink, K. L., Mikkelsen, T., Cloughesy, T. F., O'Neill, A., Plotkin, S., et al. (2008). Randomized phase II study of cilengitide, an integrin-targeting arginine-glycine-aspartic acid peptide, in recurrent glioblastoma multiforme. *J. Clin. Oncol.* 26, 5610–5617. doi: 10.1200/jco.2008.16.7510
- Ritchie, C. K., Giordano, A., and Khalili, K. (2000). Integrin involvement in glioblastoma multiforme: possible regulation by NF-kappaB. *J. Cell Physiol.* 184, 214–221. doi: 10.1002/1097-4652(200008)184:2<214::aid-jcp9>3.0.co;2-z
- Sanchez, V. E., Nichols, C., Kim, H. N., Gang, E. J., and Kim, Y. M. (2019). Targeting PI3K signaling in acute lymphoblastic leukemia. *Int. J. Mol. Sci.* 20:412. doi: 10.3390/ijms20020412
- Sarkaria, J. N., Carlson, B. L., Schroeder, M. A., Grogan, P., Brown, P. D., Giannini, C., et al. (2006). Use of an orthotopic xenograft model for assessing the effect of epidermal growth factor receptor amplification on glioblastoma radiation response. *Clin. Cancer Res.* 12, 2264–2271. doi: 10.1158/1078-0432.ccr-05-2510
- Schiffer, D., Giordano, M. T., Mauro, A., and Migheli, A. (1984). GFAP, FVIII/RAG, laminin, and fibronectin in gliosarcomas: an immunohistochemical study. *Acta Neuropathol.* 63, 108–116. doi: 10.1007/bf00697192
- Shinoda, J., Hirayama, H., Araki, Y., Andoh, T., Sakai, N., and Yamada, H. (1989). [Morphological changes in basement membrane associated with endothelial proliferation in astrocytic tumors—an immunohistochemical study of laminin]. *No To Shinkei* 41, 263–271.
- Stavrovskaya, A. A., Shushanov, S. S., and Rybalkina, E. Y. (2016). Problems of glioblastoma multiforme drug resistance. *Biochemistry (Mosc)* 81, 91–100. doi: 10.1134/s0006297916020036
- Stewart, L. A. (2002). Chemotherapy in adult high-grade glioma: a systematic review and meta-analysis of individual patient data from 12 randomised trials. *Lancet* 359, 1011–1018. doi: 10.1016/s0140-6736(02)08091-1
- Stupp, R., Hegi, M. E., Gorlia, T., Erridge, S. C., Perry, J., Hong, Y. K., et al. (2014). Cilengitide combined with standard treatment for patients with newly diagnosed glioblastoma with methylated MGMT promoter (CENTRIC EORTC 26071-22072 study): a multicentre, randomised, open-label, phase 3 trial. *Lancet Oncol.* 15, 1100–1108. doi: 10.1016/s1470-2045(14)70379-1
- Sun, L., Liu, L., Liu, X., Wang, Y., Li, M., Yao, L., et al. (2014). Gastric cancer cell adhesion to laminin enhances acquired chemotherapeutic drug resistance mediated by MGr1-Ag/37LRP. *Oncol. Rep.* 32, 105–114. doi: 10.3892/or.2014.3184
- Taylor, T. E., Furnari, F. B., and Cavenee, W. K. (2012). Targeting EGFR for treatment of glioblastoma: molecular basis to overcome resistance. *Curr. Cancer Drug Targets* 12, 197–209. doi: 10.2174/156800912799277557
- Tchaicha, J. H., Reyes, S. B., Shin, J., Hossain, M. G., Lang, F. F., and McCarty, J. H. (2011). Glioblastoma angiogenesis and tumor cell invasiveness are differentially regulated by beta8 integrin. *Cancer Res.* 71, 6371–6381. doi: 10.1158/0008-5472.can-11-0991
- Thon, N., Kreth, S., and Kreth, F. W. (2013). Personalized treatment strategies in glioblastoma: MGMT promoter methylation status. *Onco Targets Ther.* 6, 1363–1372. doi: 10.2147/ott.s50208
- Tivnan, A., Zakaria, Z., O'leary, C., Kogel, D., Pokorný, J. L., Sarkaria, J. N., et al. (2015). Inhibition of multidrug resistance protein 1 (MRP1) improves chemotherapy drug response in primary and recurrent glioblastoma multiforme. *Front. Neurosci.* 9:218. doi: 10.3389/fnins.2015.00218
- Varner, J. A., Brooks, P. C., and Chereseth, D. A. (1995). REVIEW: the integrin alpha V beta 3: angiogenesis and apoptosis. *Cell Adhes. Commun.* 3, 367–374.
- Venstrom, K. A., and Reichardt, L. F. (1993). Extracellular matrix. 2: role of extracellular matrix molecules and their receptors in the nervous system. *FASEB J.* 7, 996–1003. doi: 10.1096/fasebj.7.11.8370483
- Walker, M. D., Alexander, E. Jr., Hunt, W. E., McCarty, C. S., Mahaley, M. S. Jr., Mealey, J. Jr., et al. (1978). Evaluation of BCNU and/or radiotherapy in the treatment of anaplastic gliomas. A cooperative clinical trial. *J. Neurosurg.* 49, 333–343. doi: 10.3171/jns.1978.49.3.0333
- Walker, M. D., Green, S. B., Byar, D. P., Alexander, E. Jr., Batzdorf, U., Brooks, W. H., et al. (1980). Randomized comparisons of radiotherapy and nitrosoureas for the treatment of malignant glioma after surgery. *N. Engl. J. Med.* 303, 1323–1329. doi: 10.1056/nejm198012043032303
- Weller, M., Butowski, N., Tran, D. D., Recht, L. D., Lim, M., Hirte, H., et al. (2017). Rindopepimut with temozolomide for patients with newly diagnosed, EGFRvIII-expressing glioblastoma (ACT IV): a randomised, double-blind, international phase 3 trial. *Lancet Oncol.* 18, 1373–1385.
- Wu, Y., Zhu, X., Shen, R., Huang, J., Xu, X., and He, S. (2019). miR-182 contributes to cell adhesion-mediated drug resistance in multiple myeloma via targeting PDCD4. *Pathol. Res. Pract.* 215:152603.
- Xiao, W., Sohrabi, A., and Seidlits, S. K. (2017). Integrating the glioblastoma microenvironment into engineered experimental models. *Future Sci. OA* 3:FSO189.
- Xiao, W., Zhang, R., Sohrabi, A., Ehsanipour, A., Sun, S., Liang, J., et al. (2018). Brain-mimetic 3D culture platforms allow investigation of cooperative effects of extracellular matrix features on therapeutic resistance in glioblastoma. *Cancer Res.* 78, 1358–1370.
- Yan, Y., Xu, Z., Dai, S., Qian, L., Sun, L., and Gong, Z. (2016). Targeting autophagy to sensitive glioma to temozolomide treatment. *J. Exp. Clin. Cancer Res.* 35:23.
- Yap, L., Tay, H. G., Nguyen, M. T. X., Tjin, M. S., and Tryggvason, K. (2019). Laminins in cellular differentiation. *Trends Cell Biol.* 29, 987–1000.
- Ye, Y., Zhang, R., and Feng, H. (2020). Fibronectin promotes tumor cells growth and drugs resistance through a CDC42-YAP-dependent signaling pathway in colorectal cancer. *Cell Biol. Int.* 44, 1840–1849.
- Yi, W., Xiao, E., Ding, R., Luo, P., and Yang, Y. (2016). High expression of fibronectin is associated with poor prognosis, cell proliferation and malignancy via the NF-kappaB/p53-apoptosis signaling pathway in colorectal cancer. *Oncol. Rep.* 36, 3145–3153.
- Yu, Q., Xue, Y., Liu, J., Xi, Z., Li, Z., and Liu, Y. (2018). Fibronectin promotes the malignancy of glioma stem-like cells via modulation of cell adhesion, differentiation, proliferation and chemoresistance. *Front. Mol. Sci.* 11:130. doi: 10.3389/fnmol.2018.00130

- Zaal, E. A., and Berkers, C. R. (2018). The influence of metabolism on drug response in cancer. *Front. Oncol.* 8:500.
- Zeligs, K. P., Neuman, M. K., and Annunziata, C. M. (2016). Molecular pathways: the balance between cancer and the immune system challenges the therapeutic specificity of targeting nuclear factor-kappaB signaling for cancer treatment. *Clin. Cancer Res.* 22, 4302–4308.
- Zhou, S. M., Cheng, L., Guo, S. J., Wang, Y., Czajkowsky, D. M., Gao, H., et al. (2015). Lectin RCA-I specifically binds to metastasis-associated cell surface glycans in triple-negative breast cancer. *Breast Cancer Res.* 17:36.

Conflict of Interest: The authors declare that the research was conducted in the absence of any commercial or financial relationships that could be construed as a potential conflict of interest.

Copyright © 2021 Yu, Xiao, Sun, Sohrabi, Liang and Seidlits. This is an open-access article distributed under the terms of the Creative Commons Attribution License (CC BY). The use, distribution or reproduction in other forums is permitted, provided the original author(s) and the copyright owner(s) are credited and that the original publication in this journal is cited, in accordance with accepted academic practice. No use, distribution or reproduction is permitted which does not comply with these terms.



Girdin Knockdown Increases Gemcitabine Chemosensitivity to Pancreatic Cancer by Modulating Autophagy

Sheng Wang^{1†}, Wei Feng^{1†}, Wulin Wang², Xiaoman Ye³, Hao Chen² and Chunzhao Yu^{2*}

¹ Department of General Surgery, The Affiliated Suqian Hospital of Xuzhou Medical University, Suqian, China, ² Department of General Surgery, The Second Affiliated Hospital of Nanjing Medical University, Nanjing, China, ³ Department of Critical Care Medicine, The Fourth Affiliated Hospital of Nanjing Medical University, Nanjing, China

OPEN ACCESS

Edited by:

Wei Zhao,
City University of Hong Kong,
Hong Kong

Reviewed by:

Eugenia Morselli,
Pontificia Universidad Católica
de Chile, Chile
Marco Tafani,
Sapienza University of Rome, Italy

*Correspondence:

Sheng Wang
shengwang2020@sina.com
Chunzhao Yu
chunzhaoyu@hotmail.com

[†]These authors have contributed
equally to this work

Specialty section:

This article was submitted to
Molecular and
Cellular Oncology,
a section of the journal
Frontiers in Oncology

Received: 18 October 2020

Accepted: 26 February 2021

Published: 29 March 2021

Citation:

Wang S, Feng W, Wang W, Ye X,
Chen H and Yu C (2021) Girdin
Knockdown Increases Gemcitabine
Chemosensitivity to Pancreatic Cancer
by Modulating Autophagy.
Front. Oncol. 11:618764.
doi: 10.3389/fonc.2021.618764

Chemotherapy is crucial for the treatment of pancreatic cancer (PC). Gemcitabine (GEM) as the first-line chemotherapy drug has a high resistance rate. Increasing the sensitivity of gemcitabine is currently the objectives and challenges of this study. Our previous study showed Girdin was closely related to the progression and prognosis of PC, indicating that Girdin may be associated with chemosensitivity. In the current study, we use recombinant adenovirus to specifically knockdown Girdin in PC cell lines to determine the effect of Girdin in the process of gemcitabine chemosensitivity. Autophagy is one of the pathways affecting the gemcitabine chemosensitivity in PC. Further research validated that Girdin may activate autophagy by interacting with autophagy protein p62/SQSTM1, which could enhance chemotherapy resistance to gemcitabine in PC. Down-regulation of Girdin may therefore increase gemcitabine chemosensitivity in PC. Our results reveal that Girdin acted as a negative regulator of gemcitabine chemosensitivity in PC. Increased autophagy activity caused by abnormally high Girdin expression may be one of the main factors for the reduction in chemosensitivity, which may provide new perspectives on understanding chemosensitization in PC.

Keywords: girdin, gemcitabine, chemosensitivity, autophagy, p62/SQSTM1

INTRODUCTION

Pancreatic cancer (PC) is one of the most malignant tumors in the digestive system, and its incidence has been increasing annually worldwide (1, 2). Early diagnosis of PC is highly difficult due to the concealed pathogenesis and rapid disease progression. Most patients show locally advanced diseases or have distant metastases at the time of diagnosis, making the treatment for PC difficult and the mortality rate especially high. At present, the median survival time of the disease is only 6 months, with a 5-year survival rate of less than 5% (3). Patients with PC still rely on comprehensive treatment, including chemotherapy to improve the prognosis. Chemotherapy is one of the important methods for the treatment of PC. Gemcitabine, a deoxycytidine analogue, is known as the first-line chemotherapy drug for PC, which prevents cell cycle progression from G1 into S phase by inhibiting DNA polymerase. Gemcitabine can help prolong the median survival time and

provide benefits for the patients (4). However, the rate of resistance to gemcitabine is almost above 80%, limiting the effect of the chemotherapy against PC. Chemotherapy resistance is the main reason for treatment failure in PC. The development of chemotherapy resistance is a complex process that involves multifactors, multiple genes, and multiple mechanisms. Increasing the sensitivity of chemotherapy has been one of the hotspots in PC research (5–7). At present, existing studies have shown that changes in the related genes, tumor microenvironment, cellular signaling pathways, and regulation of autophagy are the main causes for the development of chemotherapy resistance. Still, the specific mechanism remains to be improved. Therefore, further elucidating the mechanism of chemotherapy resistance, searching for anti-resistance strategies, and enhancing the sensitivity of chemotherapy drugs are still problematic in PC.

Girdin (girders of actin filament), an actin-binding protein, has received increasing attention in recent years. It is an encoded protein first named by a Japanese scientist consisting of 1,870 amino acids (8). With an extensive study, Miyake et al. (9), found that Girdin is involved in the formation of neointima after vascular injury. Feng et al. (10), have also shown that Girdin is closely associated with the migration and invasion of gliomas, and high expression of Girdin shows lower progression-free survival. Furthermore, Mikel (11) found that Girdin is involved in the regulation of autophagy through its guanine nucleotide exchange factor. Ghosh et al. (12) followed hundreds of patients and found that high expression of Girdin is positively correlated with the risk of recurrence in colon cancer patients. Interestingly, it is found that down-regulation of Girdin can enhance the sensitivity of colon cancer to chemotherapy (13). Results in the literature indicate that Girdin may play an important role in the occurrence and development of malignant tumors. However, the role of Girdin in the development of PC remains to be studied.

Previous studies from our group showed that Girdin is overexpressed in PC, which promotes cell proliferation and inhibits the apoptosis of PC cells (14). In current study, we aimed to determine the effect of Girdin in the process of gemcitabine chemosensitivity in PC and to explore its underlying molecular mechanism, especially the correlation with autophagy. Our results could help prove Girdin is a potential therapeutic target for PC by enhancing the effects of current therapy through increased chemosensitivity in PC.

MATERIALS AND METHODS

Cell Culture and Adenoviral Infection

Human pancreatic ductal epithelial cells (hTERT-HPNE) and human PC cell lines (AsPC-1, BxPC-3, PANC-1) were acquired from American Type Culture Collection (Manassas, VA, USA). AsPC-1 cells were cultured in RPMI-1640 (Gibco; Thermo Fisher Scientific, Waltham, MA, USA) while others were cultured in DMEM (Gibco). Both growth media were supplemented with 10% fetal bovine serum (FBS) (Wisent, St. Bruno, QC, Canada), and all cells were maintained in 37°C and 5% CO₂.

Recombinant adenoviruses containing the Girdin shRNA (rAd-shGirdin) or an empty vector (rAd-GFP) were synthesized using the vector pAd-U6-CMV-GFP (Shanghai Lici Biotechnology, Shanghai, China). Empty vector was used as a negative control. 293A cells (ATCC) were used for packaging the recombinant adenovirus. All the cell lines and viruses have been described in the previous study (14). The P62 siRNA sequences used for expression silencing were:

siRNA-1 (forward), 5'-GUGACGAGGAAUUGACAAU dTdT-3' and siRNA-1 (reverse), 5'-AUUGUCAAUUCCUC GUCACdTdT-3';

siRNA-2 (forward), 5'-GGAGUCGGAUAACUG UUCAdTdT-3' and siRNA-2 (reverse), 5'-UGAACAGUUAUC CGACUCCdTdT-3'.

Western Blot Analysis

Proteins were extracted by RIPA buffer supplemented with Phenylmethanesulfonyl fluoride (PMSF). Cell lysates with the same amount of total protein (30 µg) were subjected to sodium dodecyl sulphate-polyacrylamide gel electrophoresis (SDS-PAGE) and transferred to polyvinylidene fluoride (PVDF) membranes (Millipore, Billerica, MA, USA). Membranes were blocked in Tris-buffered saline containing 0.05% Tween-20 (TBST) and 5% bovine serum albumin (BSA; Sigma-Aldrich; Merck KGaA, Darmstadt, Germany) for 2 h at room temperature. After blocking, the membranes were then incubated with primary antibodies at 4°C overnight, followed by the incubation with specific secondary antibodies for 2 h at room temperature. Antibodies against caspase-3, cleaved caspase-3, LC-3, beclin-1, and P62 were purchased from Cell Signaling Technology (Beverly, MA, USA). Antibodies against Girdin, Bcl-2, and BAX were purchased from Abcam (Cambridge, UK). GAPDH, β-actin, and goat anti-rabbit IgG antibodies were acquired from Santa Cruz Biotechnology (Santa Cruz, CA, USA). Relative protein expression level was evaluated using ImageJ software.

Cell Apoptosis Analysis by Flow Cytometry

Cells were incubated with different treatment conditions. Following the treatment, cells were then collected and washed twice with ice-cold PBS, and resuspended in 1×binding buffer (BD Pharmingen; BD Biosciences, Franklin Lakes, NJ, USA). Subsequently, 5 µl of 7-AAD (BD Pharmingen; BD Biosciences) and 5 µl of APC (BD Pharmingen; BD Biosciences) were added. The samples were then analyzed *via* a flow cytometer (BD FACS Calibur equipped with Cell Quest Pro software).

Co-Immunoprecipitation Analysis

Protein lysates (1000 µg) were prepared from cultured cells using NP40. Immunocomplex pull-down was achieved *via* overnight incubation of protein lysates with relevant antibodies bound to Glutathione Sepharose beads (GE Healthcare, USA) at 4°C. After careful washing, 2×SDS loading buffer was added and the samples boiled at 95°C for 10 min to allow for protein degeneration. Co-immunoprecipitated proteins were then subjected to western blotting as described above.

Immunofluorescence Staining

Paraformaldehyde (4%) was used to fix pre-treated cells overnight at 4°C. Fixed cells were then incubated in PBS containing 0.1% Triton and 5 mg/mL BSA. Cells were then blocked with 5% BSA for 30 min at 37°C. Afterwards, cells were stained with antibodies against P62 (1:100; CST, Beverly, MA, USA) and Girdin (1:100; Abcam Cambridge, UK) overnight at 4°C, and subsequently incubated with a fluorescent dye-conjugated goat anti-rabbit IgG (Thermo Fisher Scientific) for 30 min at 37°C. Nuclei were stained with DAPI (Sigma-Aldrich; Merck KGaA, Darmstadt, Germany). Images were captured using a confocal laser scanning microscope (Olympus Corp.). Anti-LC3 purchased from CST (1:100) was used in another immunofluorescence staining.

Mass Spectrometry

Cell lysates were immunoprecipitated with anti-Girdin antibody. Protein digestion, labeling, mass spectrometry data acquisition, and identification were completed in the analysis center of Nanjing Medical University. The labeled peptides were analyzed on a LTQ-Orbitrap instrument (Thermo Fisher Scientific) connected to a Nano ACQUITY UPLC system *via* a nanospray source. The LC-MS/MS was operated in the positive ion model as described previously. The MS/MS spectra acquired from precursor ions were submitted to Maxquant (version 1.2.2.5).

Tumor Xenograft Model

Fifteen female nu/nu mice at the age of 6 weeks (Beijing Vital River Laboratory Animal Technology Co. Ltd., Beijing, China) were housed in sterile cages by conventional feeding. The left flank of each mouse was subcutaneously injected with BxPC-3 cells (5×10^6 cells/100 μ L PBS) to establish the PC xenograft model. Cells were infected with rAd-shGirdin prior to subcutaneous inoculation. After five days, the mice were randomly divided into different groups for different sets of experiments. Gemcitabine was intraperitoneally injected at a dose of 100mg/kg three times per week for three weeks. Tumor volumes were observed every three days and were calculated

using the formula $(A \times B^2)/2$, where A and B are the long and short dimensions, respectively. Mice were sacrificed by cervical dislocation on day 21 and the weights and volumes of the tumors were measured. Half of the tumor specimens were fixed with 4% paraformaldehyde and the other half was cryopreserved at -80°C. All animals received humane care, and all experiments were performed according to the guidelines outlined in the Guide for the Care and Use of Laboratory Animals. All of our experiments were reviewed and approved by the Animal Ethics and Welfare Committee with approval no. IACUC-1601161.

Statistical Analysis of Data

All of the experiments were carried out at least three independent times. All statistical analyses were performed using GraphPad Prism 5.0 software (GraphPad Software, Inc., La Jolla, CA, USA). All data are expressed as mean \pm SEM. Data from each group were statistically analyzed using a two-tailed Student's *t*-test. Differences with $P < 0.05$ were considered statistically significant. P-values shown in the figures are labeled as * $P < 0.05$, ** $P < 0.01$, and *** $P < 0.001$.

RESULTS

Girdin Expression Is Positively Correlated With Gemcitabine Chemosensitivity in PCs

According to our previous results from tissue microarray analysis, Girdin was abnormally highly expressed in PC, and may be related to the pathological classification of PC (14). However, the microarray study did not include the prognostic relationship analysis. We therefore queried the public databases to determine whether Girdin is associated with patient prognosis. We first analyzed the gene expression data from the GEO database, accession number GES62452. We found that the expression of Girdin in tumor tissues was significantly higher than in normal tissues ($P < 0.05$) (Figure 1A). Analysis of the data from The Cancer Genome Atlas (TCGA) database showed that among the 177 patients with PC, patients with Girdin

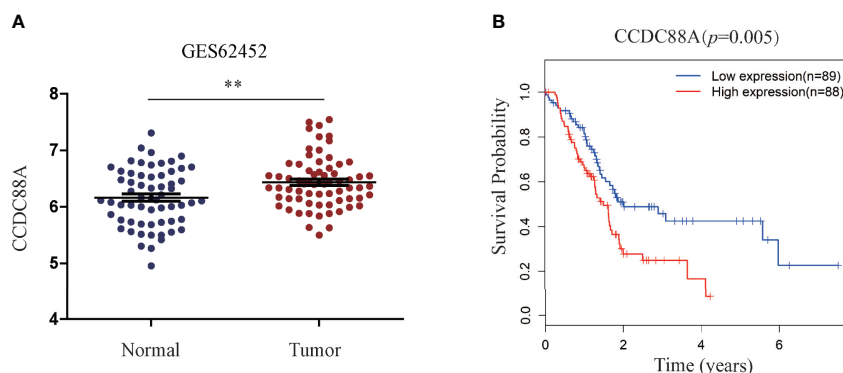


FIGURE 1 | Statistical analysis of the correlation between Girdin expression and pancreatic cancer through databases. **(A)** Girdin expression level in PC tissue was significantly higher than that seen in the Normal tissue, data from GEO database, numbered GES62452. **(B)** Overall survival (OS) was compared between patients with low and high expression Girdin, data from TCGA database. ** $P < 0.01$.

overexpression had significantly lower overall survival than the patients with relatively low levels of Girdin expression (Figure 1B).

One of the reasons for the poor prognosis of PC is the decreased chemotherapy sensitivity, which led us to suspect that abnormal overexpression of Girdin may affect the sensitivity to chemotherapy in PC. To further verify this conjecture, the levels of mRNA and protein expression of Girdin were analyzed in the PC cell lines AsPC-1, PANC1, and BxPC3 by qRT-PCR and western blotting, respectively (Figures 2A, B). The pancreatic ductal epithelial cell line HPNE was used as a contrasting non-cancer control. Both Girdin gene and protein expressions were significantly increased in PC cell lines when compared to HPNE. The highest level of Girdin protein expression was observed in AsPC-1 cells, which also display the greatest gemcitabine tolerance, with an IC₅₀ of 15 μ M. The lowest expression of Girdin protein was found in BxPC3 cells, which were the least tolerance to gemcitabine, with an IC₅₀ of 7.5 μ M (Figure 2C). Next, we treated PANC1 and BxPC3 cells with the corresponding IC₅₀ concentration of gemcitabine and analyzed the expression of Girdin with western blotting and qRT-PCR. As shown in Figures 2D and 2E, Girdin expression was significantly increased at protein and mRNA levels following exposure to gemcitabine. Moreover, The BxPC-3 and PANC-1 cells were successfully infected with the recombinant adenoviruses, and Girdin expression was silenced. Hence, we

speculated that the level of Girdin may be correlated with the sensitivity to gemcitabine in human PC cells.

Down-Regulation of Girdin Increased Chemosensitivity to Gemcitabine in PC

In order to further explore the relationship between Girdin and the chemosensitivity to gemcitabine chemotherapy, recombinant adenovirus of Girdin knockdown was constructed (rAd-shGirdin), while the empty rAd-GFP vector was used as an experimental control. Previous experiments have verified the effectiveness of this recombinant adenovirus. In the next experiment, we measured the expression levels of apoptosis-related proteins XIAP, Bcl-2, BAX, cleaved caspase-3, and cleaved caspase-9 by western blotting (Figure 3A). It was found that the levels of XIAP and Bcl-2/BAX were reduced while cleaved caspase-3 and -9 were up-regulated after a single transfection with rAd-shGirdin or gemcitabine treatment. When rAd-shGirdin infection and gemcitabine treatment were combined, we found the changes of apoptosis related proteins were more pronounced compared to the single-treatment and control groups ($P < 0.05$), indicating there was increased apoptosis during the combined treatment. Thus, we hypothesized that Girdin knockdown may increase cellular sensitivity to gemcitabine. To further confirm our idea, the flow cytometric apoptosis experiments were performed. As shown in Figure 3, after treatment with an optimal concentration of

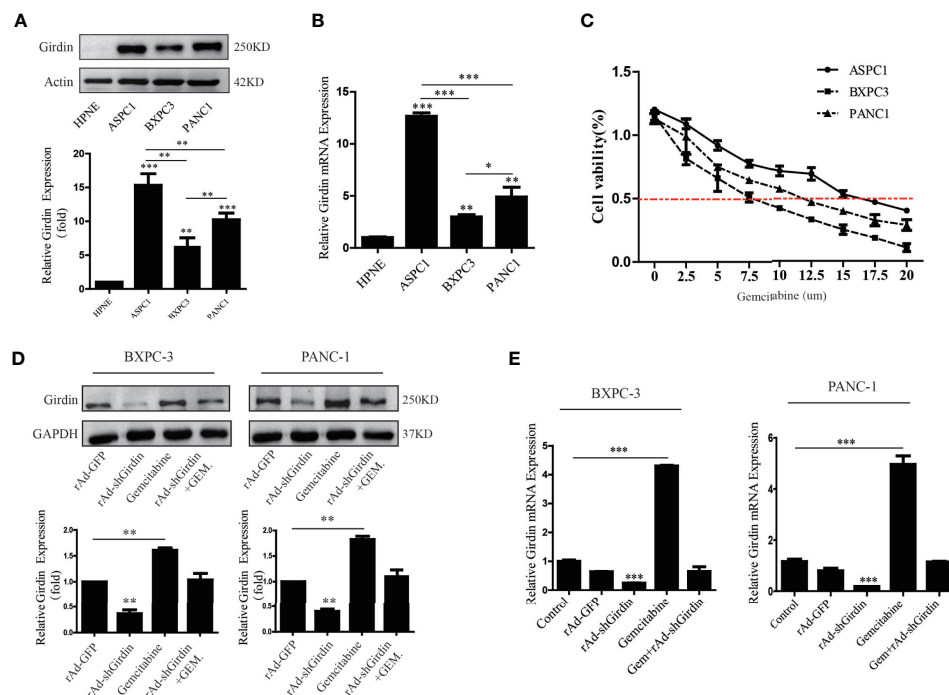


FIGURE 2 | Girdin expression is positively correlated with gemcitabine chemosensitivity in pancreatic cancers. (A, B) Western blots and qRT-PCR were performed to analysis of Girdin protein levels in PC cell lines (Aspc-1, Bxpc-3 and Panc-1) infected with rAd-shGirdin. Bars represent the SEM. (C) The optimal concentration of gemcitabine in different pancreatic cancer cell lines was clarified by MTT assay. (D, E) Western blots and qRT-PCR were performed to evaluate the variation of Girdin level after stimulate with gemcitabine. The empty rAd-GFP vector was constructed as an experimental control. The data are representative of three independent experiments and are expressed as means \pm SEM; * $P < 0.05$, ** $P < 0.01$, *** $P < 0.001$.

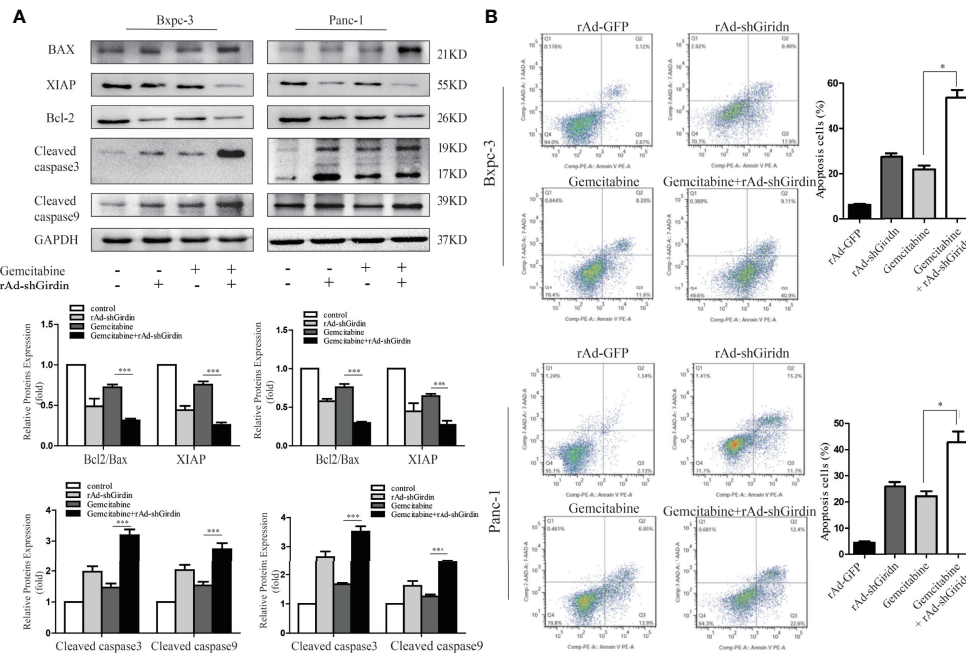


FIGURE 3 | Down-regulation of Girdin increase chemosensitivity of gemcitabine in pancreatic cancers. **(A)** Apoptosis related proteins were detected by western blotting after cells were treated with single rAd-shGirdin or gemcitabine treatment, and combination of the two. The combination treatment could induce apoptosis through down-regulating the Bcl-2/Bax ratio, XIAP and activating caspase-3 and caspase-9. **(B)** Cell apoptosis was determined by flow cytometry. The combination of rAd-shGirdin and gemcitabine could induce significant apoptosis compared with the cells treated with gemcitabine alone in pancreatic cancer. Each experiment was performed three times and all data were expressed as mean \pm SEM; * $P < 0.05$, ** $P < 0.01$, and *** $P < 0.001$.

gemcitabine in the rAd-shGirdin transfected PANC1 and BxPC3 cells, the combination of rAd-shGirdin and gemcitabine had a dramatically increased rate of cell death. Through the above experiments, we confirmed that down-regulation of Girdin can induce cellular apoptosis and increase the chemosensitivity to gemcitabine.

Girdin Interacts With Autophagy Protein P62/SQSTM1 in PC Cells

Girdin knockdown can increase the gemcitabine chemosensitivity in PC cells. However, its molecular mechanism remains to be further explored. In order to investigate this question, we conducted mass spectrometric analysis experiments (Table 1). Many of the proteins were detected that may be related to Girdin. We noticed that among the identified proteins, P62/SQSTM1 is closely related to the cellular autophagy pathway. Subsequently, we verified that Girdin and P62 could interact as shown by co-immunoprecipitation (Figure 4A). Further immunofluorescence experiments confirmed that Girdin physically interacted with P62 in the PC cells (Figure 4B), which further proves the correlation between Girdin and P62/SQSTM1.

Down-regulation of Girdin reduces the autophagy activity of PC cells

Due to the interaction between Girdin and P62, we next explored the effect of Girdin on cellular autophagy activity. First, we verified the effects of Girdin on autophagy-related proteins LC3 and Beclin1

by western blotting. It was found that comparing to the control group, the levels of LC3B and Beclin1 clearly decreased after down-regulating Girdin (Figure 5A), suggesting that knockdown of Girdin can reduce the autophagy activity in PC cells. Next, we studied the effects on the PC cells following starvation in serum-free growth conditions with or without rAd-shGirdin infection by projection electron microscopy. It was discovered that when Girdin was down-regulated, fewer autophagosomes were observed (Figure 5B). Immunofluorescence analysis was then performed to detect the level of LC3. Cells were starved to induce autophagy in serum-free conditions for 24 h. It can be seen that when Girdin was down-regulated, the fluorescence level of LC3 decreased, suggesting that the autophagy activity was inhibited (Figure 5C). The above experiments have shown that down-regulation of Girdin can reduce the autophagy activity of PC cells.

Decreased Autophagy Activity Can Increase Gemcitabine Chemosensitivity in PC Cells

We attempted to probe whether the level of autophagy correlates with gemcitabine chemosensitivity in the PC cells. As shown in Figure 6A, we treated PANC1 and BxPC3 cells with gemcitabine and detected the expression of autophagy-related proteins with western blotting. It was found that in comparison with the control group, the level of LC3B increased while the level of P62 was decreased. These results suggest that the sensitivity to gemcitabine may be related to autophagy levels. Interestingly,

TABLE 1 | Analysis of protein interaction about Girdin in MS.

Function	Gene	Protein	ScrambleTSC ^a	Girdin ^{OE} TSC ^b	Value
protein folding	FKBP4	Peptidyl-prolyl cis-trans isomerase FKBP4	+	–	13
	CCT8	T-complex protein 1 subunit theta	–	+	18
	CANX	Calnexin	+	+	10
	TCP1	T-complex protein 1 subunit alpha	+	+	10
	P4HB	prolyl 4-hydroxylase subunit beta	+	+	19
glycolytic process	ALDOA	Fructose-bisphosphate aldolase	+	+	12
	ENO1	Alpha-enolase	+	–	13
	PKM	Pyruvate kinase PKM	+	+	14
	PGK1	Phosphoglycerate kinase 1	–	+	14
	GPI	Glucose-6-phosphate isomerase (Fragment)	+	–	11
	TPI1	Isoform 2 of Triosephosphate isomerase	+	+	13
	LDHA	L-lactate dehydrogenase A chain	+	+	14
	LDHB	L-lactate dehydrogenase B chain	+	–	12
actin cytoskeleton organization	EZR	Ezrin	+	+	10
	MYH9	Myosin-9	–	+	99
	FLNB	Isoform 8 of Filamin-B	–	+	61
	LIMA1	Isoform 4 of LIM domain and actin-binding protein 1	–	+	27
	PLEC	Isoform 4 of Plectin	–	+	142
	CALD1	Caldesmon	–	–	14
	DBN1	Drebrin	–	+	12
	CAPZB	Isoform 2 of F-actin-capping protein subunit beta	+	+	10
	VIM	Vimentin	–	+	32
	ACTN4	Alpha-actinin-4	+	+	17
regulation of cell death	SQSTM1	Sequestosome-1	+	+	13
	RPS3	40S ribosomal protein S3	+	–	10
	FHL2	Four and a half LIM domains protein 2	+	+	13
	HSP90AB1	Heat shock protein HSP 90-beta	+	+	19
	HSP90B1	Endoplasmic	+	+	14
	HSPA5	78 kDa glucose-regulated protein	+	–	23
	YWHAE	14-3-3 protein epsilon	+	+	11
	HNRNP K	Isoform 3 of Heterogeneous nuclear ribonucleoprotein K	+	–	13
translational elongation	TUFM	Elongation factor Tu, mitochondrial	+	+	10
	RPL7	60S ribosomal protein L7	+	+	10
	EEF2	Elongation factor 2	+	+	24
nucleotide biosynthetic process	MTHFD1	C-1-tetrahydrofolate synthase, cytoplasmic	–	+	16
protein complex biogenesis	ATP1A1	Isoform 4 of Sodium/potassium-transporting ATPase subunit alpha-1	+	–	13
	JUP	Junction plakoglobin	+	–	10
	RRM1	Ribonucleoside-diphosphate reductase large subunit	–	–	11
intracellular transport	FLNA	Filamin-A	+	+	68
	HSPD1	60 kDa heat shock protein, mitochondrial	+	+	18
	MYO1E	Unconventional myosin-Ie	–	–	27
	HSP90AA1	Heat shock protein HSP 90-alpha	+	+	15
	CLTC	Clathrin heavy chain	+	+	19
blood vessel development	MYH10	Myosin-10	–	–	20
	NCL	Nucleolin	+	+	15
	ANXA2	Annexin A2	–	+	13
protein targeting	HSPA9	Stress-70 protein, mitochondrial	–	+	22
	SPTBN1	Spectrin beta chain, non-erythrocytic 1	–	+	44
	AKAP12	Isoform 3 of A-kinase anchor protein 12	+	–	16

Scramble Bxpc3 cells transfected with Scramble Lentivirus.

Girdin^{OE}Bxpc3 cells transfected with Girdin Lentivirus.

TSC, total spectral counts.

after Girdin was down-regulated, the autophagy activity caused by GEM was decreased (**Figure 7D**). Chloroquine (CQ) is currently an effective and commonly used autophagy inhibitor and has been widely used in many research studies (15, 16). Our study found that combined treatment with CQ and GEM significantly increased the levels of cleaved caspase-3 ($P < 0.05$) while the XIAP and Bcl2/Bax expression levels were significantly lower ($P < 0.05$) when compared with the CQ or GEM treatment alone (**Figure 6B**). Flow cytometric analysis found that when

cells were simultaneously treated with CQ and GEM, the number of apoptotic cells was increased compared to single-agent exposure (**Figure 6C**). These results show that when the autophagy activity of PC was inhibited, treatment with GEM can induce higher levels of cellular apoptosis, which also means the chemosensitivity to GEM by PC cells was enhanced.

To further demonstrate its relevance, we conducted the following experiments. Rapamycin has been used as a stable autophagy activator in many studies (17). We used rapamycin to

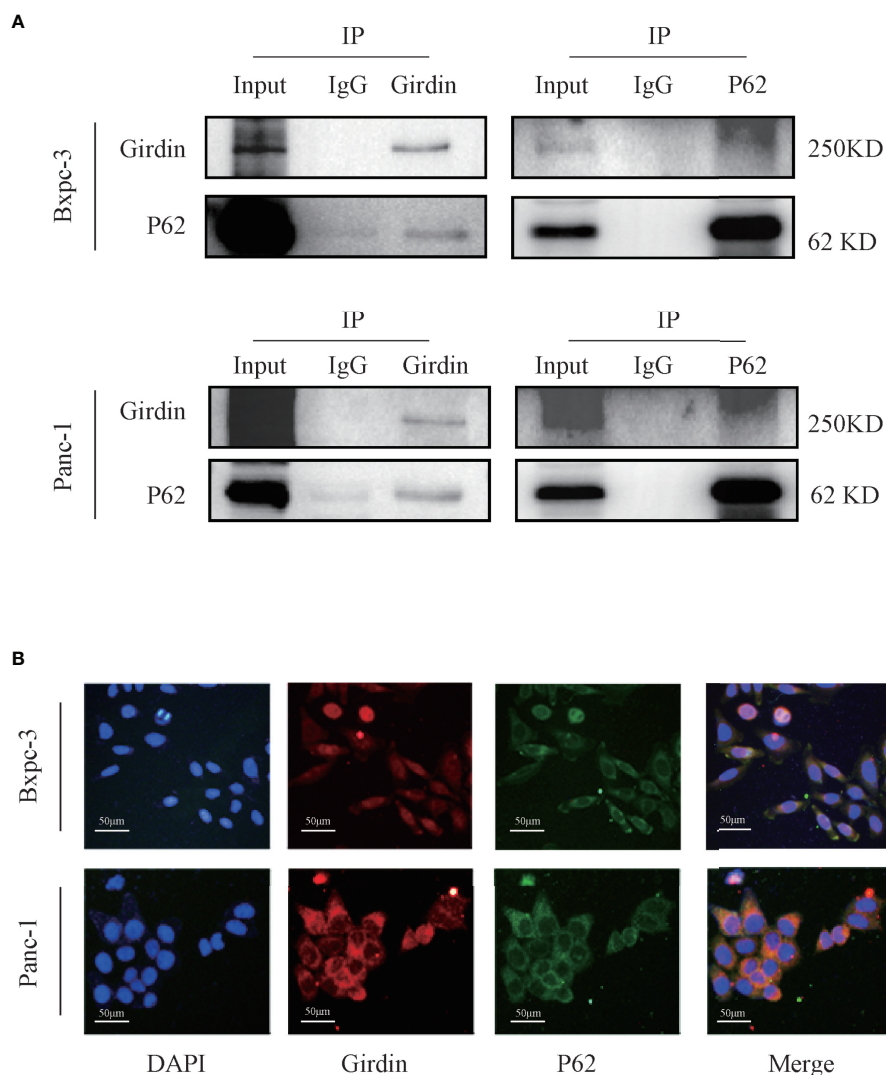


FIGURE 4 | Girdin interacts with autophagy protein P62/SQSTM1 in pancreatic cancer cells. **(A)** The interaction between Girdin and P62 was detected in the co-IP analysis Bxpc-3 and Panc-1 cells. The binding signals of P62 with Girdin were also confirmed using anti-Girdin antibodies in IPs, and subsequent blotting with P62 antibodies. **(B)** The expressions of Girdin and P62 were endogenous and immunofluorescence staining images showed a significant physically interacted with each other in the cytoplasm. Red represents Girdin, green represents P62, and the nuclei were labelled with DAPI.

induce autophagy in the PC cell lines. Compared to the 0 h of treatment, rapamycin significantly increased the level of LC3B at 48 h along with an increase in the expression of Girdin. These results indicate that autophagy is activated after 48 hours of induction by rapamycin (**Figure 7A**). In the following experiments, we used rapamycin to induced autophagy after the cells were treated with both rAd-shGirdin and GEM combined. It was found that cleaved caspase-9 levels were lower while the XIAP and Bcl2 expression levels were higher when compared to the group without rapamycin treatment, and the differences was statistically significant ($P < 0.05$) (**Figure 7B**). Furthermore, a flow cytometry was carried out and to verify that the number of apoptotic cells induced by rapamycin during the

combined treatment with rAd-shGirdin and GEM was reduced, indicating that rapamycin-activated autophagy reversed the GEM chemosensitivity during the downregulation of Girdin (**Figure 7C**). These results suggest that Girdin may affect the chemotherapy sensitivity in PC by regulating autophagy.

Through the above experiments, we confirmed that Girdin is closely related to the gemcitabine chemosensitivity, and it can also affect the autophagy activity of PC cells. Suppression of cellular autophagy can increase the sensitivity to gemcitabine chemotherapy in PC. Rapamycin-activated autophagy reversed the GEM chemosensitivity caused by the knockdown of Girdin. It is plausible to assume that Girdin influences the autophagy activity and regulates the GEM chemosensitivity in PC cells.

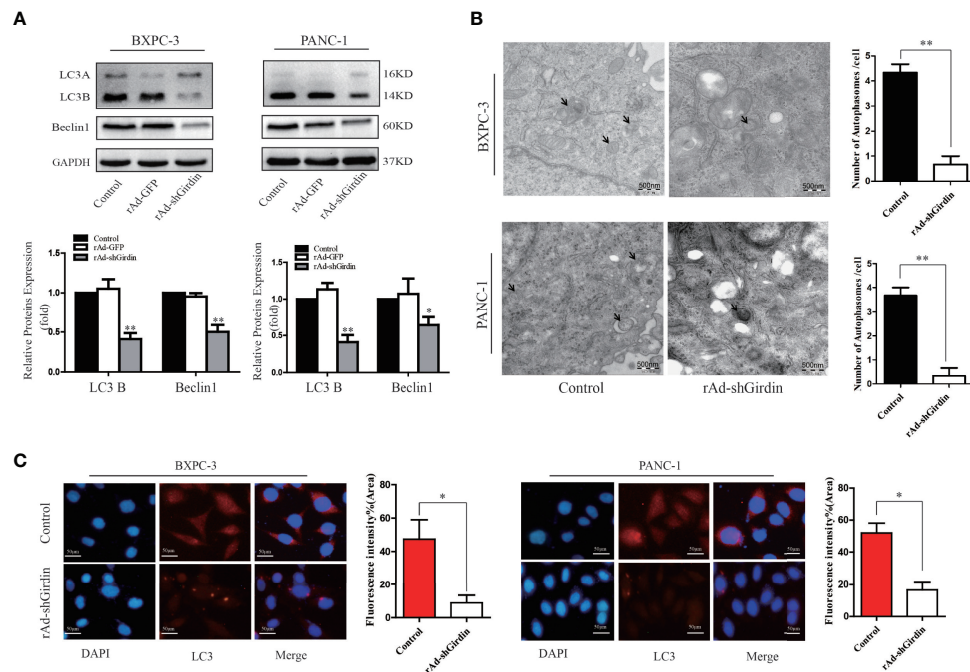


FIGURE 5 | Down-regulation of Girdin reduce the autophagy activity of pancreatic cancer cells. **(A)** Autophagy related proteins LC3 and Beclin-1 were detected by western blotting after cells were transfected with rAd-shGirdin. Bars represent the SEM. * $P < 0.05$, ** $P < 0.01$. **(B)** Autophagosomes were observed by transmission electron microscopy in Bxpc-3 cells and Panc-1 cells after knockdown of Girdin. Cells were cultured with serum-free DMEM. **(C)** Immunofluorescence staining images showed that the LC3 protein level was decreased after infected with rAd-shGirdin.

Girdin Down-Regulation Suppresses PC Growth and Enhances Gemcitabine Chemosensitivity in a Xenograft Model

We subcutaneously injected nude mice with rAd-Girdin-infected BxPC-3 cells to further confirm the effects of Girdin on PC *in vivo*. It was shown that while the expression of Girdin was knocked down the tumor growth was inhibited in the xenograft mouse model as expected. GEM was intraperitoneally injected into the mice and shown to suppress tumor growth irrespective of body weight or tumor volume. Moreover, the tumor-inhibiting capacity of GEM was further increased when rAd-shGirdin and GEM were administered concurrently (**Figures 8A–C**). Subsequent immunohistochemical staining using antibodies against cleaved caspase-3 revealed that combined treatment with GEM and rAd-shGirdin further enhanced the induction of apoptosis in tissues from xenograft tumors (**Figure 8D**), further suggesting that the down-regulation of Girdin increases the chemosensitivity to gemcitabine in PC.

DISCUSSION

PC is one of the most common causes of cancer-related deaths in humans, with a very high mortality rate worldwide. It was reported that adjuvant chemotherapy for postoperative patients can significantly reduce the recurrence rate of PC (18, 19).

Gemcitabine is commonly used as the first-line chemotherapy drug for PC. Unfortunately, most PC patients acquire resistance to gemcitabine treatment. Ineffective chemotherapy cannot completely eradicate the cancer cells and often lead to a poor patient prognosis. Clarifying the molecular mechanism that occurs during the development of gemcitabine chemoresistance will improve the PC treatments.

Cancer chemoresistance results from a complex interplay between gene regulations. A great deal of studies have reported the main causes of chemotherapy resistance, such as changes in related genes, tumor microenvironment, novel activation of cellular pathways, autophagy, and many other factors. Our previous study has confirmed that Girdin promotes the proliferation, migration, and invasion of PC cells. Most importantly, down-regulation of Girdin could induce the apoptosis in PC cells. We also found that Girdin arrests cell cycle at G1 phase, which has similar function as gemcitabine. We therefore proposed that a combination of gemcitabine and down-regulation Girdin may have a synergistic effect that could improve the sensitivity to gemcitabine.

Here, we first sought to examine the expression of Girdin in PC and its impact on the prognosis. GEO and TCGA databases were interrogated, from which we found that Girdin is expressed at high levels in PC tissues and cells, and the expression correlates with the OS of PC. Next, *in vitro* experiments found that the higher expression level of Girdin in each PC cell line, the lower sensitivity of the cell line to gemcitabine, which suggested that Girdin may be associated with chemosensitivity in PC. Further

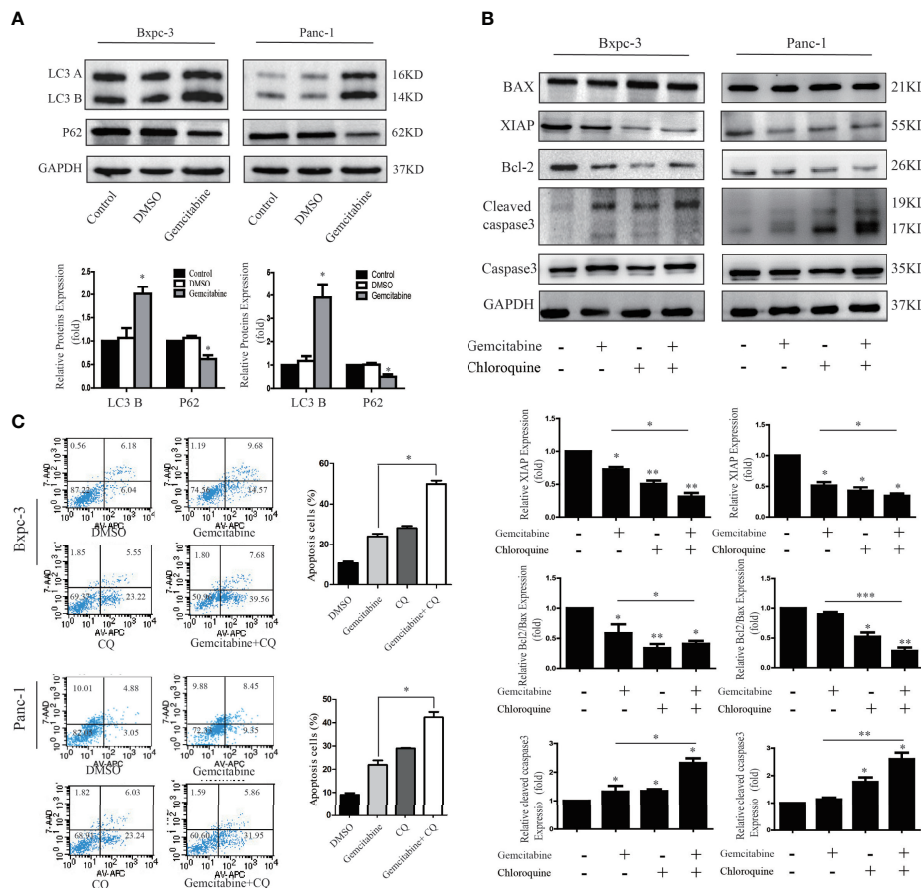


FIGURE 6 | Decreased autophagy activity can increase gemcitabine chemosensitivity to pancreatic cancer cells. **(A)** Autophagy related proteins LC3 and P62 were detected by western blotting after cells were treated with gemcitabine. **(B)** Apoptosis related proteins were detected by western blotting after cells were treated with single Chloroquine (CQ) or gemcitabine, and combination of the two. The combination treatment could down-regulate the Bcl-2/Bax ratio, XIAP and activate caspase-3. **(C)** Flow cytometry was performed using Bxpc-3 and Panc-1 cells treated with gemcitabine+CQ, which significantly induced apoptosis compared with single usage in pancreatic cancer cells.

analysis found that after down-regulating Girdin, the chemotherapy sensitivity to gemcitabine was increased in PC cell lines, resulting in a higher rate of apoptosis. Mass spectrometry analysis experiments were then performed, from which an autophagy-related protein P62/SQSTM1 was identified. P62/SQSTM1 is an important selective autophagy adaptor protein, and its relationship with autophagy is bidirectional (20, 21). In one hand, the intracellular p62 level is strictly regulated by autophagy activity. On the other hand, p62 can also negatively regulate the autophagy activity of cells by activating the mammalian target of rapamycin complex 1 (mTORC1) signaling pathway. The expression level of p62/SQSTM1 has also been used as a marker for autophagy activity in other studies (22). At the same time, we found that when Girdin was down-regulated, PC cell autophagy activity, which is often known as one of the possible causes of chemotherapy resistance, was significantly decreased. Autophagy is an evolutionarily conserved self-defense mechanism, which sequesters and degrades proteins and organelles. Usually, autophagy can dispose damaged mitochondria and reduce the incidence of cancer (23). Once

tumor has occurred, autophagy may maintain cell survival in response to hypoxia and nutrient limitation (24). Tumor cells can take advantage of autophagy, resist the damage and the apoptosis process induced by chemotherapeutic drugs (25, 26). Many studies have described the relationship between autophagy and chemoresistance in cancers, which found that the suppression of autophagy activity can often enhance the chemosensitivity. The development of many different cancers is accompanied by a high level of autophagy, including PC (27–29). Perera et al. (30) discovered that cellular stress caused by autophagy can alter the cell metabolism, which in turn promotes the development of PC. Therefore, we hypothesized that Girdin may activate the protective autophagy in PC cells by directly binding to p62/SQSTM1, increasing the gemcitabine chemoresistance in PC. Down-regulation of Girdin can increase the sensitivity to gemcitabine chemotherapy in PC (**Figure 9**). Next, we further confirmed that the autophagy activity of PC cells is directly related to its chemosensitivity. Chloroquine was employed as an inhibitor that can reduce autophagy activity, and simultaneously increases

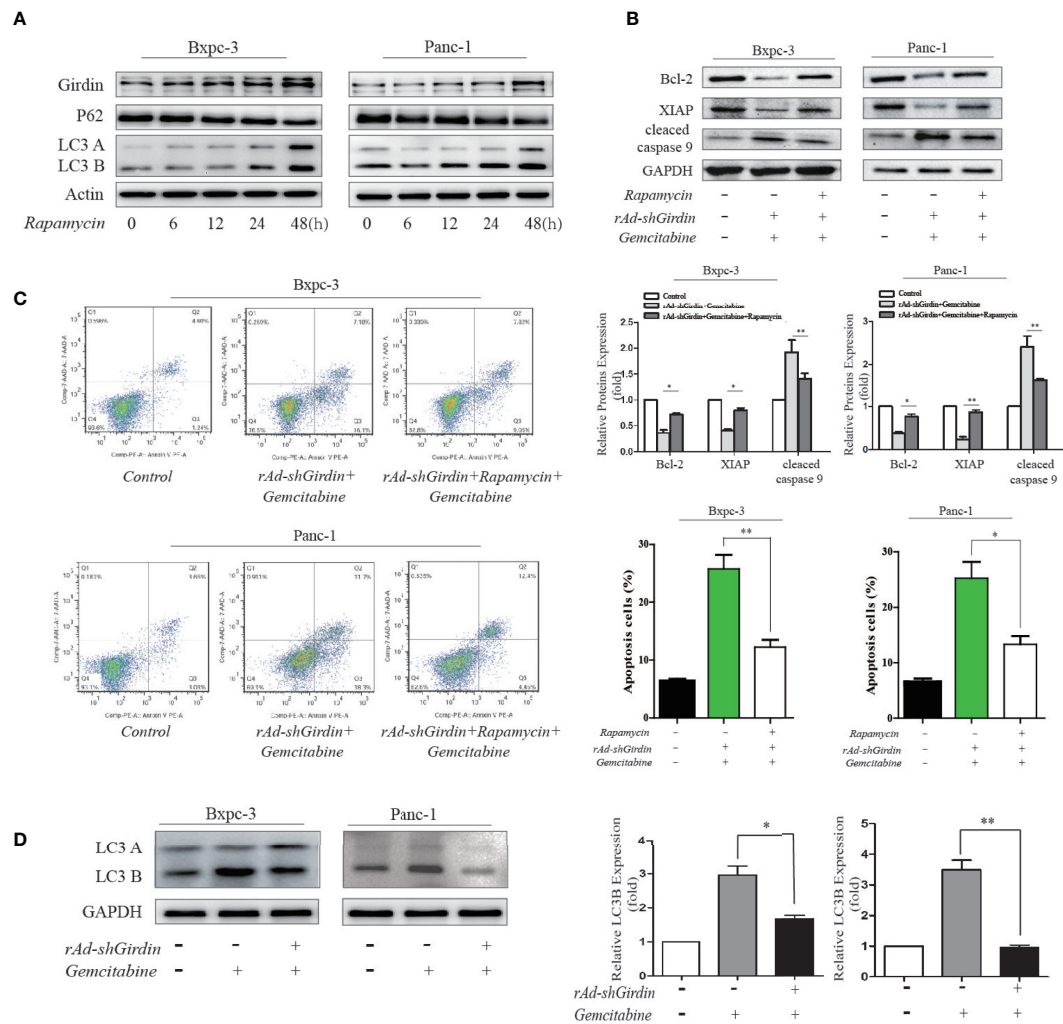


FIGURE 7 | Rapamycin-activated autophagy reversed the GEM chemosensitivity caused by the downregulation of Girdin. **(A)** Girdin, P62 and LC3 were detected by western blotting after cells were induced with rapamycin. Time for 0, 6, 12, 24, 48 hours after rapamycin was administered. **(B)** Apoptosis related proteins were detected by western blotting after cells were treated with rAd-shGirdin and GEM, and with or without rapamycin applied. The combination treatment could up-regulate the Bcl-2, XIAP and down-regulate caspase-9, while compared with the group without rapamycin. **(C)** Apoptosis of BxPC-3 and PANC-1 cells was detected by flow cytometer. Cells were infected with rAd-shGirdin+GEM, and subsequently treated with rapamycin, which significantly reduced apoptosis compared with the group without rapamycin in pancreatic cancer cells. **(D)** Western blots of BxPC-3 and PANC-1 cells were performed. Levels of the LC3B proteins were decreased in the rAd-shGirdin group. Gemcitabine was used at half the previous dose to reduce cell necrosis caused by the combination of the two drugs. Each experiment was performed 3 independent times, and all data are expressed as means \pm SEM; * $P < 0.05$, ** $P < 0.01$.

chemosensitivity. Therefore, Girdin may affect the chemosensitivity of PC cells through the autophagy pathway. The author further conducted western blotting to verify the regulatory correlation between Girdin and P62. Interestingly, it was found that P62 did not significantly changed after Girdin was down-regulated. Similarly, after P62 was down-regulated, Girdin was not significantly changed (**Supplemental Figures S1A, B**) Therefore, we suspected that Girdin and P62 may form a complex that results in the promotion of protein function to affect autophagy activity in PC cells. Next, it was further verified in mouse tumor-bearing experiments that down-regulating Girdin could increase gemcitabine sensitivity in PC, which was consistent with the results from *in vitro* experiments.

Admittedly, Girdin has multiple functional domains, including AKT phosphorylation sites which involved in the PI3K/AKT signaling pathway. The functional domain GEF of Girdin is related to G α -interacting vesicle-associated domains associated with the hook-related proteins. Girdin protein function is diverse. Some scholars (11) have shown that in HeLa cells, Girdin can inhibit autophagy by activating the G protein. However, there are many major activators for the regulation of autophagy, and many different factors and conditions maintain the balance between promotion and inhibition of autophagy. The underlying molecular mechanism describing the relationship between Girdin and autophagy needs to be further studied. In addition, some researchers have

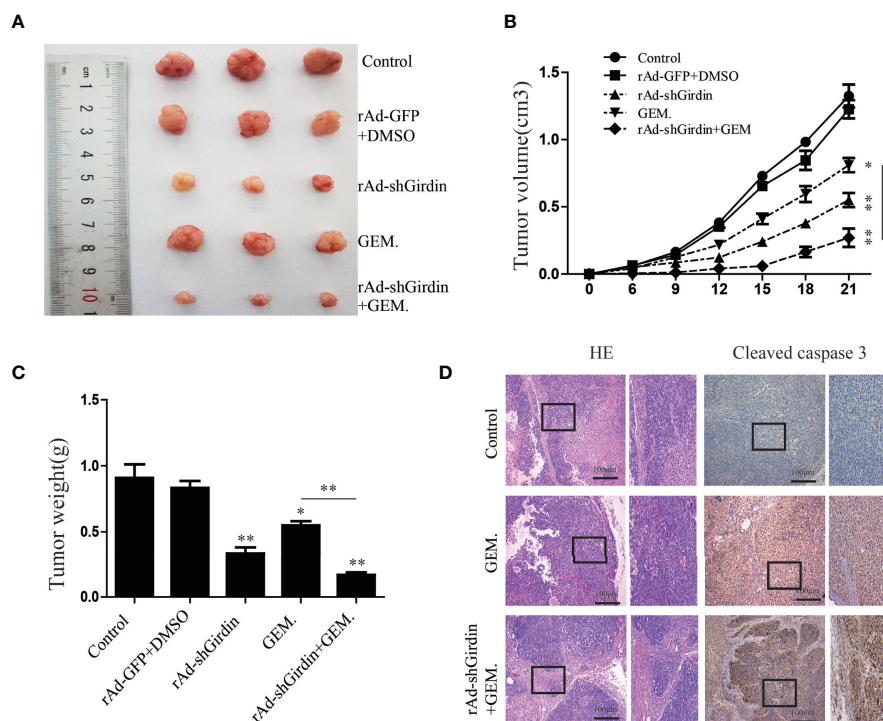


FIGURE 8 | Girdin down-regulating suppresses pancreatic cancer growth and enhances gemcitabine chemosensitivity in a xenograft model. **(A)** Representative data from xenograft tumors in mice in the different groups. **(B, C)** Statistical analysis of tumour volumes and weights in the different groups ($n = 4$). **(D)** Images of immunohistochemical staining using antibodies against cleaved caspase-3.

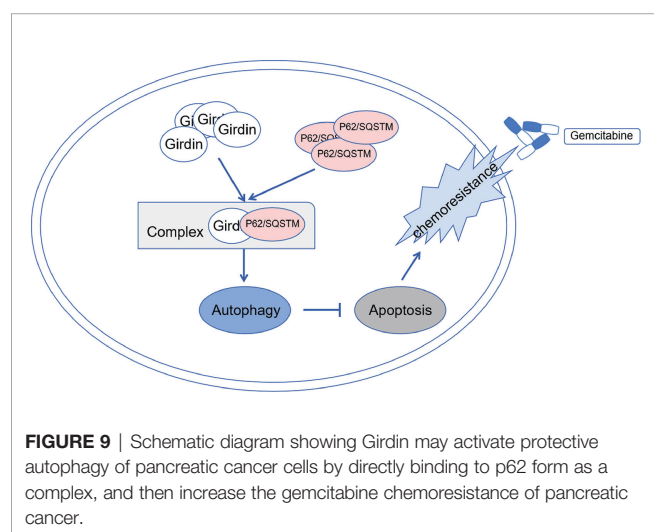


FIGURE 9 | Schematic diagram showing Girdin may activate protective autophagy of pancreatic cancer cells by directly binding to p62 form as a complex, and then increase the gemcitabine chemoresistance of pancreatic cancer.

confirmed that Girdin is also closely linked to the activation of the PI3K/AKT signaling pathway (31). The PI3K/AKT signaling pathway controls cell growth and death, and to some extent, also changes the sensitivity to chemotherapy (32). While it may not be the only mechanism that Girdin influences gemcitabine chemosensitivity in PC by modulating autophagy, this protein truly plays a vital role in the regulation of chemosensitivity.

In conclusion, we found that the abnormally high expression of Girdin affects the prognosis of PC and the chemosensitivity to gemcitabine. Down regulation of Girdin can increase the chemosensitivity in PC cells. In addition, Girdin maintains the delicate equilibrium of autophagy in PC cells *via* P62. Increased autophagy activity caused by abnormally high Girdin expression may be one of the main reasons for the decreased sensitivity of PC cells to gemcitabine chemotherapy. Our results suggest that a combination of Girdin-targeted therapy and gemcitabine chemotherapy is potentially useful as a novel therapeutic approach for the treatment of resistant PC in the clinical setting. Its effectiveness and detailed molecular mechanisms remain to be further explored.

DATA AVAILABILITY STATEMENT

The original contributions presented in the study are included in the article/Supplementary Material. Further inquiries can be directed to the corresponding authors.

ETHICS STATEMENT

The animal study was reviewed and approved by Animal Ethics and Welfare Committee with approval no. IACUC-1601161.

AUTHOR CONTRIBUTIONS

All authors contributed to the article and approved the submitted version. SW and WF contributed equally to this paper as the main completer of the experiments and article. WW designed and carried out some experiments. XY helped with animal experiment and cell culture. HC was responsible for the statistical analysis of their results. CY provided funds and designed ideas.

FUNDING

This work was funded by grants from the National Natural Science Foundation of China (nos. 30972910 and 81172269) and the key research and development Foundation of Suqian, China (S201809).

REFERENCES

- Chen W, Zheng R, Baade PD, Zhang S, Zeng H, Bray F, et al. Cancer statistics in China, 2015. *CA Cancer J Clin* (2016) 66(2):115–32. doi: 10.3322/caac.21338
- Siegel RL, Miller KD, Jemal A. Cancer statistics, 2020. *CA: A Cancer J Clin* (2020) 70(1):7–30. doi: 10.3322/caac.21590
- Kamisawa T, Wood LD, Itoi T, Takaori K. Pancreatic cancer. *Lancet* (2016) 388(10039):73–85. doi: 10.1016/S0140-6736(16)00141-0
- Rd BH, Moore MJ, Andersen J, Green MR, Rothenberg ML, Modiano MR, et al. Improvements in survival and clinical benefit with gemcitabine as first-line therapy for patients with advanced pancreas cancer: a randomized trial. *J Clin Oncol* (1997) 15(6):2403–13. doi: 10.1200/JCO.1997.15.6.2403
- Deplanque G, Demartines N. Pancreatic cancer: are more chemotherapy and surgery needed? *Lancet* (2017) 389(10073):985–6. doi: 10.1016/S0140-6736(17)30126-5
- Oettle H, Neuhaus P, Hochhaus A, Hartmann JT, Gellert K, Ridwelski K, et al. Adjuvant Chemotherapy With Gemcitabine and Long-term Outcomes Among Patients With Resected Pancreatic Cancer: The CONKO-001 Randomized Trial. *JAMA J Am Med Assoc* (2013) 310(14):1473–81. doi: 10.1001/jama.2013.279201
- Oettle H, Lehmann T. Gemcitabine-resistant pancreatic cancer: A second-line option. *Lancet* (2015) 387(10018):507–8. doi: 10.1016/S0140-6736(15)01035-1
- Enomoto A, Murakami H, Asai N, Morone N, Watanabe T, Kawai K, et al. Akt/PKB regulates actin organization and cell motility via Girdin/APE. *Dev Cell* (2005) 9(3):389–402. doi: 10.1016/j.devcel.2005.08.001
- Miyake H, Maeda K, Asai N, Shibata R, Ichimiya H, Isotani-Sakakibara M, et al. The actin-binding protein Girdin and its Akt-mediated phosphorylation regulate neointima formation after vascular injury. *Circ Res* (2011) 108(10):1170–9. doi: 10.1161/CIRCRESAHA.110.236174
- Gu F, Wang L, He J, Liu X, Zhang H, Li W, et al. Girdin, an actin-binding protein, is critical for migration, adhesion, and invasion of human glioblastoma cells. *J Neurochem* (2014) 131(4):457–69. doi: 10.1111/jnc.12831
- Garcia-Marcos M, Ear J, Farquhar MG, Ghosh P. A GDI (AGS3) and a GEF (GIV) regulate autophagy by balancing G protein activity and growth factor signals. *Mol Biol Cell* (2011) 22(5):673–86. doi: 10.1091/mbc.E10-08-0738
- Ghosh P, Tie J, Muranyi A, Singh S, Gibbs P. Girdin (GIV) Expression as a Prognostic Marker of Recurrence in Mismatch Repair Proficient Stage II Colon Cancer. *Clin Cancer Res* (2016) 22(14):3488–98. doi: 10.1158/1078-0432.CCR-15-2290
- Zhang YJ, Li AJ, Han Y, Yin L, Lin MB. Inhibition of Girdin enhances chemosensitivity of colorectal cancer cells to oxaliplatin. *World J Gastroenterol* (2014) 20(25):8229–36. doi: 10.3748/wjg.v20.i25.8229
- Sheng W, Yiqun L, Zeling C, Xiaoman Y, Lianhong L, Xiagang L, et al. Girdin regulates the proliferation and apoptosis of pancreatic cancer cells

ACKNOWLEDGMENTS

The authors thank Miss Min Li for the technical support. We thank LetPub (www.letpub.com) for its linguistic assistance during the preparation of this manuscript.

SUPPLEMENTARY MATERIAL

The Supplementary Material for this article can be found online at: <https://www.frontiersin.org/articles/10.3389/fonc.2021.618764/full#supplementary-material>

Supplementary Figure 1 | Regulatory correlation between Girdin and P62.

(A) Western blots were performed to analysis of Girdin protein levels after transfected with P62-siRNA. Bars represent the SEM. **(B)** Western blots were performed to analysis of P62 protein levels after infected with rAd-shGirdin. The data are representative of three independent experiments. Bars represent the SEM. ***P < 0.001.

- via the PI3K/Akt signalling pathway. *Oncol Rep* (2018) 40(2):599–608. doi: 10.3892/or.2018.6469
- Liang X, Vera MED, Buchser WJ, Chavez ARDV, Lotze MT. Inhibiting Systemic Autophagy during Interleukin 2 Immunotherapy Promotes Long-term Tumor Regression. *Cancer Res* (2012) 72(11):2791–801. doi: 10.1158/0008-5472.CAN-12-0320
- Kung CP, Budina A, Balaburski G, Bergenstock MK, Murphy ME. Autophagy in tumor suppression and cancer therapy. *Crit Rev Eukaryot Gene Expr. Crit Rev Eukaryot Gene Expr* (2011) 21(1):71–100. doi: 10.1615/CritRevEukaryotGeneExpr.v21.i1.50
- Qiao J, Zhang D, Wang Y, Li X, Liu Q. Identification of AaAtg8 as a marker of autophagy and a functional autophagy-related protein in *Aedes albopictus*. *PeerJ* (2018) 6(11):e5988. doi: 10.7717/peerj.5988
- Neoptolemos JP, Kleeff J, Michl P, Costello E, Greenhalf W, Palmer DH. Therapeutic developments in pancreatic cancer: current and future perspectives. *Nat Rev Gastroenterol Hepatol* (2018) 15(6):333–48. doi: 10.1038/s41575-018-0005-x
- Tempero MA, Malafa MP, Alhawary M, Asbun H, Bain A, Behrman SW, et al. Pancreatic Adenocarcinoma, Version 2.2017, NCCN Clinical Practice Guidelines in Oncology. *J Natl Compr Cancer Netw Jncn* (2017) 15(8):1028–61. doi: 10.6004/jnccn.2017.0131
- Katsuragi Y, Ichimura Y, Komatsu M. p62/SQSTM1 functions as a signaling hub and an autophagy adaptor. *FEBS J* (2015) 282(24):4672–78. doi: 10.1111/febs.13540
- Moscat J, Diaz-Meco MT. p62 at the Crossroads of Autophagy, Apoptosis, and Cancer. *Cell* (2009) 137(6):9–1004. doi: 10.1016/j.cell.2009.05.023
- Moscat J, Karin M, Diaz-Meco MT. p62 in Cancer: Signaling Adaptor Beyond Autophagy. *Cell* (2016) 167(3):606–9. doi: 10.1016/j.cell.2016.09.030
- Belaid A, Ndiaye PD, Cerezo M, Caillateau L, Brest P, Klionsky DJ, et al. Autophagy and SQSTM1 on the RHOA(d) again Emerging roles of autophagy in the degradation of signaling proteins. *Autophagy* (2013) 73(10):4311–22. doi: 10.4161/auto.27198
- Mathew R, Karantzis-Wadsworth V, White E. Role of autophagy in cancer. *Med Recapitulate* (2008) 7(12):961–7. doi: 10.1038/nrc2254
- Yu TC, Guo F, Yu Y, Sun T, Ma D, Han J, et al. Fusobacterium nucleatum Promotes Chemoresistance to Colorectal Cancer by Modulating Autophagy. *Cell* (2017) 170(3):548–63. doi: 10.1016/j.cell.2017.07.008
- Maes H, Rubio N, Garg AD, Agostinis P. Autophagy: shaping the tumor microenvironment and therapeutic response. *Trends Mol Med* (2013) 19(7):428–46. doi: 10.1016/j.molmed.2013.04.005
- Wang Q, Zeng F, Sun Y, Qiu Q, Zhang J, Guo L. P21-010 Etk Interacting with PFKFB4 Modulates Chemoresistance of Small Cell Lung Cancer by Regulating Autophagy. *Clin Cancer Res* (2018) 12(11):S2186–7. doi: 10.1016/j.jtho.2017.09.1402

28. Kim M, Jung J-Y, Choi S, Lee H, Morales LD, Koh J-T, et al. GFRA1 Promotes Cisplatin-induced Chemoresistance in Osteosarcoma by Inducing Autophagy. *Autophagy* (2017) 13(1):149–68. doi: 10.1080/15548627.2016.1239676
29. Hombach-Klonisch S, Mehrpour M, Shojaei S, Harlos C, Ghavami S. Glioblastoma and Chemoresistance to Alkylating Agents: Involvement of Apoptosis, Autophagy, and Unfolded Protein Response. *Pharmacol Ther* (2018) 184:13–41. doi: 10.1016/j.pharmthera.2017.10.017
30. Perera RM, Stoykova S, Nicolay BN, Ross KN, Fitamant J, Boukhali M, et al. Transcriptional control of autophagy-lysosome function drives pancreatic cancer metabolism. *Nature* (2015) 524(7565):361–5. doi: 10.1038/nature14587
31. Hayano S, Takefuji M, Maeda K, Noda T, Ichimiya H, Kobayashi K, et al. Akt-dependent Girdin phosphorylation regulates repair processes after acute myocardial infarction. *J Mol Cell Cardiol* (2015) 88:55–63. doi: 10.1016/j.yjmcc.2015.09.012
32. Osaki M, Oshimura M, Ito H. PI3K-Akt pathway: its functions and alterations in human cancer. *Apoptosis* (2004) 9(6):667–76. doi: 10.1023/B:APPT.0000045801.15585.dd

Conflict of Interest: The authors declare that the research was conducted in the absence of any commercial or financial relationships that could be construed as a potential conflict of interest.

Copyright © 2021 Wang, Feng, Wang, Ye, Chen and Yu. This is an open-access article distributed under the terms of the Creative Commons Attribution License (CC BY). The use, distribution or reproduction in other forums is permitted, provided the original author(s) and the copyright owner(s) are credited and that the original publication in this journal is cited, in accordance with accepted academic practice. No use, distribution or reproduction is permitted which does not comply with these terms.



Targeting c-Jun in A549 Cancer Cells Exhibits Antiangiogenic Activity *In Vitro* and *In Vivo* Through Exosome/miRNA-494-3p/PTEN Signal Pathway

Chen Shao¹, Yingying Huang¹, Bingjie Fu¹, Shunli Pan¹, Xiaoxia Zhao¹, Ning Zhang¹, Wei Wang², Zhe Zhang¹, Yuling Qiu¹, Ran Wang¹, Meihua Jin^{1*} and Dexin Kong^{1,3*}

OPEN ACCESS

Edited by:

Liwu Fu,
Sun Yat-Sen University, China

Reviewed by:

Xavier Bofill-De Ros,
National Cancer Institute (NCI),
United States
Keith R. Laderoute,
Consultant, Redwood City, CA,
United States
Ling-Zhi Liu,
Thomas Jefferson University,
United States

*Correspondence:

Meihua Jin
jinmeihua@tmu.edu.cn
Dexin Kong
kongdexin@tmu.edu.cn

Specialty section:

This article was submitted to
Molecular and Cellular Oncology,
a section of the journal
Frontiers in Oncology

Received: 02 February 2021

Accepted: 18 March 2021

Published: 09 April 2021

Citation:

Shao C, Huang Y, Fu B, Pan S, Zhao X, Zhang N, Wang W, Zhang Z, Qiu Y, Wang R, Jin M and Kong D (2021) Targeting c-Jun in A549 Cancer Cells Exhibits Antiangiogenic Activity *In Vitro* and *In Vivo* Through Exosome/miRNA-494-3p/PTEN Signal Pathway. *Front. Oncol.* 11:663183. doi: 10.3389/fonc.2021.663183

¹ Tianjin Key Laboratory on Technologies Enabling Development of Clinical Therapeutics and Diagnostics, School of Pharmacy, Tianjin Medical University, Tianjin, China, ² Department of Otorhinolaryngology Head and Neck, Institute of Otorhinolaryngology, Tianjin First Central Hospital, Tianjin, China, ³ School of Medicine, Tianjin Tianshi College, Tianyuan University, Tianjin, China

The oncogene c-Jun is activated by Jun N-terminal kinase (JNK). Exosomes are nanometer-sized membrane vesicles released from a variety of cell types, and are essential for cell-to-cell communication. By using specific JNK inhibitor SP600125 or CRISPR/Cas9 to delete c-Jun, we found that exosomes from SP600125-treated A549 cancer cells (Exo-SP) or from c-Jun-KO-A549 cells (Exo-c-Jun-KO) dramatically inhibited tube formation of HUVECs. And the miR-494 levels in SP600125 treated or c-Jun-KO A549 cells, Exo-SP or Exo-c-Jun-KO, and HUVECs treated with Exo-SP or Exo-c-Jun-KO were significantly decreased. Meanwhile, Exo-SP and Exo-c-Jun-KO enhanced expression of phosphatase and tensin homolog deleted on chromosome ten (PTEN). Addition of miR-494 agomir in Exo-c-Jun-KO treated HUVECs inhibited PTEN expression and promoted tube formation, suggesting the target of miR-494 might be PTEN in HUVECs. Moreover, A549 tumor xenograft model and Matrigel plug assay demonstrated that Exo-c-Jun-KO attenuated tumor growth and angiogenesis through reducing miR-494. Taken together, inhibition of c-Jun in A549 cancer cells exhibited antiangiogenic activity *in vitro* and *in vivo* through exosome/miRNA-494-3p/PTEN signal pathway.

Keywords: c-Jun, exosomes, CRISPR/Cas9, lung cancer, miR-494, angiogenesis

INTRODUCTION

c-Jun, encoded by the *c-jun* proto-oncogene, appears to play a central role in cellular signal transduction and positively regulate cell proliferation through inhibiting tumor suppressor gene expression and function (1, 2). The Jun is positively autoregulated by its product Jun/AP-1 (2). AP-1 (activating protein-1) dimers include the Jun, Fos and activating transcription factor (ATF) subgroups of transcription factors that bind to a common DNA site (3). c-Jun activation requires an upstream molecule Jun N-terminal kinase (JNK), which binds to the c-Jun transactivation domain and phosphorylates at Ser63 and Ser73 (4).

Angiogenesis is the formation of new blood vessels from pre-existing ones. To support the growth or local metastasis of cancer cells, tumor tissue needs oxygen and nutrients provided by blood vessels (5). So suppression of tumor angiogenesis has become an essential strategy for cancer therapy.

Different cell types such as hematopoietic cells, primary and normal cells, and tumor cells release exosomes to epigenetically reprogram their neighboring cells (6). Exosomes are a class of extracellular vesicles defined as 40–100 nm diameter membrane, present with a characteristic cup-shaped morphology as observed by electron microscopy (7, 8). Exosomes contain proteins, nucleic acids, lipids and other bioactive molecules, which are shuttled from donor cells to the recipient cells (9). Tumor-derived exosomes could alter local and systemic microenvironment and therefore facilitate cancer cell proliferation, chemoresistance, and tumor angiogenesis (10).

Micro RNAs (miRNAs) are single stranded non-coding RNA with 19–25 nucleotides in length, which regulate gene expression at the post-transcriptional level with predominant mechanism of epigenetic regulation by binding sites in the 3'-untranslated region (UTR) of target messenger RNA (mRNA) (11). Numerous miRNAs are enriched in tumor-derived exosomes, and are transferred to endothelial cells to regulate angiogenesis (12).

However, the role of c-Jun in cancer cells in angiogenic effect of exosomes remained unreported. Recently, we found that Exosomes from SP600125 (JNK specific inhibitor)-treated non-small cell lung carcinoma (NSCLC) A549 cells (Exo-SP) inhibited human umbilical vein endothelial cells (HUVECs) tube formation. In the present study, we investigated the detailed mechanism of c-Jun in cancer cells to regulate angiogenesis through mediating exosome/miRNA/tensin homolog deleted on chromosome ten (PTEN) signal pathway.

METHODS

Cell Culture

A549 cells were obtained from the Cell Resource Center, Peking Union Medical College (Beijing, China). A549 cells have been authenticated using STR profiling within the last three years and all experiments were performed with mycoplasma-free cells. A549 cells and c-Jun-KO A549 cells were cultured in RPMI 1640 medium containing 10% fetal bovine serum (FBS), 100 U/ml penicillin, and 100 µg/ml streptomycin. HUVECs were obtained from Lifeline Cell Technology (Frederick, MD, USA). Cell cultures were maintained in a humidified atmosphere with 5% CO₂ at 37°C.

Reagents

RPMI1640, DMEM, FBS, the enhanced chemiluminescence (ECL) reagent, and Total Exosome Isolation Reagents (from cells) were purchased from Thermo Fisher Scientific (Waltham, MA, USA). The antibodies specific for phosphatidylinositol 3-kinase (PI3K) 110β, phospho-Akt (Ser 473, #9271), phospho-Akt (Thr 308, #2965), Akt (#9272), β-actin (#4967) and the

horseradish peroxidase-conjugated goat anti-rabbit secondary antibody (#7074) were purchased from Cell Signaling Technology, Inc. (Danvers, MA, USA). Ki-67 (27309-1-AP) was purchased from Proteintech (Rosemont, IL, USA). The antibody specific for c-Jun (sc-44) was obtained from Santa Cruz Biotechnology, Inc. (Dallas, TX, USA). The α-SMA specific antibody, SP600125, and PKH26 Red fluorescent cell linker kit were purchased from Sigma Chemicals (St. Louis, MO, USA). The antibody specific for phosphatase and PTEN (abs131550) was purchased from Absin Bioscience Inc. (Shanghai, China). The exosome specific primary antibodies including CD81, CD9 and CD63 were purchased from SBI System Biosciences (EXOAB-KIT-1, Palo Alto, CA, USA). The Matrigel was purchased from BD Biosciences (San José, CA, USA). Anti-CD31 (ab28364) antibody was purchased from Abcam (Cambridge, MA, USA).

Cell Viability

Cell viability was assessed using MTT assay as we previously reported (13), with a small modification. Briefly, A549 cells were seeded onto a 96-well culture plate and incubated with various concentrations of SP600125 (10, 25, 50, 100 µM) for 24 h or 48 h. In the case of HUVECs, the cells were seeded onto a 96-well culture plate and incubated with various concentrations of Exo, Exo-SP600125, or Exo-c-Jun-KO for 24 h or 48 h, and then 20 µl of MTT (5 mg/ml) was added to each well. After 4 h of incubation, the formazan was dissolved in DMSO, and optical density (OD) at 490 nm was measured using microplate reader iMark (BIO-RAD, Hercules, CA, USA).

Isolation of Exosomes

After cell cultures reached 80% confluent, A549 cells or c-Jun-KO A549 cells were washed with PBS and incubated with FBS free RPMI 1640 medium for 48 h, or were treated with SP600125 for 48 h in FBS free medium. Exosomes were isolated from the medium by Total Exosome Isolation Reagent as described in the manufacture's manual. Briefly, the harvested supernatants were filtered through 0.22 µm membrane to remove cells and debris, then concentrated using Amicon Ultra-15 100K centrifuge tube (MERCK Millipore). After transferring the cell-free culture media to a new tube, 0.5 volumes of the Total Exosome Isolation Reagent were added. After incubation at 4°C overnight, the suspension was centrifuged at 10,000×g for 1 h to remove the supernatant. The resulting exosomes were re-suspended in PBS and stored at 4°C to be available for use.

Cell Migration Assay and Tube Formation Assay

The cell migration assay was performed as we reported previously (14), with a small modification. Confluent HUVEC monolayers were mechanically wounded with a pipette tip and washed with PBS to remove the debris. Then the monolayers were cultured in the RPMI 1640 medium containing 1% FBS. The wound healing was observed and the images were taken under inverted microscopy after 18 h.

The tube formation assay was carried out as reported by us (15), with a small modification. HUVECs were treated with Exo,

Exo-SP, or Exo-c-Jun-KO for 24 h. Fifty microliters of growth factor-reduced Matrigel were added in the wells of 96-well plates and incubated at 37°C for 1 h. Then the pretreated HUVECs were re-suspended and added to the Matrigel. Images of tube formation were captured by inverted microscope after 3 h. For quantification, total tubular length and nodes of tubes per well were measured by computer-assisted image analysis using ImageJ software.

Protein Extraction and Western Blot

Western blot analysis was carried out as we previously reported (16). Cells and exosomes were collected with lysis buffer, and the protein concentration of each sample was determined by the BCA protein assay kit. Equal amounts of proteins were run on sodium dodecyl sulfate-polyacrylamide gel electrophoresis (SDS-PAGE) and transferred to the PVDF membrane. After being blocked with 5% skim milk, the membranes were incubated with each primary antibody overnight at 4°C, and then incubated with the respective HRP-conjugated secondary antibody for 1 h at room temperature. The signals were detected with ChemiDoc™ XRS+ System (BIO-RAD, Hercules, CA, USA) after exposure to ECL reagent.

Fluorescent Imaging of Exosome Uptake

The cellular uptake of exosomes was measured by fluorescence microscopy. Exosomes were labeled with PKH26 red fluorescent cell linker kit according to the manufacturer's instructions, and then cultured with HUVEC for 3 h. After washing, HUVECs nuclei were stained with Hoechst for 15 min. Exosome uptake was measured using a fluorescence microscope.

miRNA Isolation and Real-Time Quantitative Reverse Transcription-PCR (qRT-PCR) Assay

Total RNA from the cells and exosomes was isolated using the TRIzol reagent (Life Technologies, Carlsbad, CA, USA) or

E.Z.N.A.™ miRNA Kit (Omega Bio-tek, Norcross, GA, USA) in accordance with the manufacturer's instructions. First-strand cDNA was synthesized from RNA primed by oligo (dT) using M-MLV reverse transcriptase. The RT-qPCR assay for multiple genes was performed with the miScript SYBR Green PCR Kit by an CFX96™ Real-Time PCR Detection System (BIO-RAD, Hercules, CA, USA). The primer of miRNA sequences is listed in **Table 1**. The expression levels of U6 snRNA were used to normalize the relative amount of miRNA (RT-Primer 5'-TTCACGAATTTGCGTGTTCATC-3', Forward 5'-CGCTTCGGCAGCACATATAC-3', Reverse 5'-TTCACGAATTTGCGTGTTCATC-3'). The fold-change of miRNA was calculated using the $2^{-\Delta\Delta CT}$ method.

The Gene of c-Jun Knockout (KO) With CRISPR/Cas9 Gene Editing

We used the CRISPR/Cas9 to disrupt the c-Jun gene. The c-Jun is reported to contain one exon and to be located at chromosome 1 (The National Center for Biotechnology Information, NCBI). The gRNA sequences targets c-Jun on exon1, with target-sequence as TGCTCTGTTTCAGGATCTTG. A549 cells were transfected with pX330A-1x2 plasmid of the c-Jun-targeted gRNA encoding SpCas9 by Lipofectamine 3000. Following 72 h of puromycin selection, the cell culture was extended for another 96 h without puromycin, and the surviving clonal cells were sub-cultured into 96 well with a density of one cell/well. Afterward, cells were cultured for 7-10 days. Individual clones constructed with knockout of c-Jun were expanded and screened for c-Jun depletion by genomic DNA sequencing and Western blot.

miRNA Agomir Transfection

HUVECs were transfected with miR-494 agomir (sense: 5'-UGAAACAUAACACGGGAAACCUC-3'; anti-sense: 5'-GGUUUCCCCGUGUAUGUUUCAUU-3') using Lipofectamine 6000 transfection reagent for 24 h, according to the

TABLE 1 | List of miRNA primers.

miRNA	RT-Primer (5'-3')	Forward (5'-3')
hsa-miR-21	GTCGTATCCAGTGCAGGGTCCGAGGTATTGCACTGGATACGACTCAACA	GCGCGTAGCTTATCAGACTGA
hsa-miR-23a	GTCGTATCCAGTGCAGGGTCCGAGGTATTGCACTGGATACGACGGAAAT	GCGATCACATTGCCAGGG
hsa-miR-221	GTCGTATCCAGTGCAGGGTCCGAGGTATTGCACTGGATACGACGAAACC	CGCGAGCTACATTGTCTGCTG
hsa-miR-222	GTCGTATCCAGTGCAGGGTCCGAGGTATTGCACTGGATACGACACCCAG	CGCGAGCTACATCTGGCTA
hsa-miR-449a	GTCGTATCCAGTGCAGGGTCCGAGGTATTGCACTGGATACGACACCAGC	CGCGTGGCAGTGATTGTTA
hsa-miR-494	GTCGTATCCAGTGCAGGGTCCGAGGTATTGCACTGGATACGACGAGGTT	CGCGTGAACATACACGGGA
hsa-miR-9	GTCGTATCCAGTGCAGGGTCCGAGGTATTGCACTGGATACGACTCATAC	GCGCGTCTTTGGTTATCTAGCT
hsa-miR-34a	GTCGTATCCAGTGCAGGGTCCGAGGTATTGCACTGGATACGACACAACC	CGCGTGGCAGTGCTTAGCT
hsa-miR-125-3p	GTCGTATCCAGTGCAGGGTCCGAGGTATTGCACTGGATACGACAGCTCC	GCGACGGGTAGGCTCTTG
hsa-miR-125-5p	GTCGTATCCAGTGCAGGGTCCGAGGTATTGCACTGGATACGACTCACAA	CGCGTCCCTGAGACCCCTAAC
hsa-miR-126	GTCGTATCCAGTGCAGGGTCCGAGGTATTGCACTGGATACGACCGCATT	CGCGTCGTACCGTGAGTAAT
hsa-miR-145	GTCGTATCCAGTGCAGGGTCCGAGGTATTGCACTGGATACGACAGGGAT	CGGTCCAGTTTTCCAGGA
hsa-miR-146a	GTCGTATCCAGTGCAGGGTCCGAGGTATTGCACTGGATACGACAACCCA	CGCGTGAGAACTGAATCCA
hsa-miR-148a	GTCGTATCCAGTGCAGGGTCCGAGGTATTGCACTGGATACGACACAAAG	GCGCGTCAGTGCACTACAGAA
hsa-miR-152	GTCGTATCCAGTGCAGGGTCCGAGGTATTGCACTGGATACGACCCAAGT	CGCGTCAGTGCACTGACAGA
hsa-miR-497	GTCGTATCCAGTGCAGGGTCCGAGGTATTGCACTGGATACGACACAAAC	GCGCAGCAGCAGCTGTG
hsa-miR-519c	GTCGTATCCAGTGCAGGGTCCGAGGTATTGCACTGGATACGACATCCTC	GCGCGAAAGTGATCTTTTA
hsa-miR-155	GTCGTATCCAGTGCAGGGTCCGAGGTATTGCACTGGATACGACAACCCC	GCGGTTAATGCTAATCGTGATA
Reverse (5'-3')	AGTGCAGGGTCCGAGGTATT	

manufacturer's instructions. All experimental control samples were treated with equal concentrations of a non-targeting control (NC) agomir (sense: 5'-UUCUCCGAACGUGUCACGUTT-3'; anti-sense: 5'-ACGUGACACGUUCGGAGAATT-3'). Chemically modified miR-494 agomir and NC agomir were purchased from Shanghai GenePharma Co., Ltd. Simultaneously, Exo or Exo-c-Jun-KO were added. After 24 h, cells were washed by PBS and collected to be available for use.

Nude Mice Xenograft Tumor Experiments

BALB/c athymic nude mice (6 weeks old male) were kept in a specific pathogen-free environment. All animal experiments were conducted at Laboratory Animal Center of Institute of Radiation Medicine, the Chinese Academy of Medical Sciences in accordance with the Institutional Animal Care and Use Committee guidelines. Mice were injected subcutaneously (s.c.) in the flank with 1×10^7 A549 cells. When subcutaneous tumors grew to 30 to 50 mm³, the mice were randomly divided into four groups, with six mice each. For exosome treatment, 2 µg of exosomes such as Exo, Exo-c-Jun-KO, and those treated with miR-494 agomir or agomir NC was injected intratumorally every other day for 14 days. Tumor volume was measured every other day. Mice were sacrificed by cervical dislocation 16 days after treatment, and tumor specimens were fixed with 4% formaldehyde, embedded in paraffin, and subjected to routine histological experiment. Immunohistochemistry (IHC) was carried out on 5-µm sections to visualize cells by using Ki-67, CD31, α -smooth muscle actin (α -SMA) antibodies. Six field images were collected using a Leica photomicroscope from three biopsies per specimen. Staining intensity was analyzed by Image-pro plus software.

In Vivo Matrigel Plug Assay

HUVECs mixed with or without exosome, miR-494 agomir and Lipofectamine 6000, were added in 200 µl of High Concentration MatrigelTM Matrix and then subcutaneously injected into BALB/c nude mice (6 weeks old, male). After 14 days, mice were sacrificed and the Matrigel plugs were harvested for analysis. The degree of vascularization was evaluated by measuring hemoglobin content using the Hemoglobin test kit.

Statistical Analysis

All data are expressed as means \pm SD of triplicate values. One-way ANOVA followed by Tukey's Multiple Comparison Test was utilized to determine the statistical significance with GraphPad Prism 5 (GraphPad, San Diego, CA, USA). A p value less than 0.05 was considered statistically significant.

RESULTS

A549 Cells Showed High Sensitivity to JNK Inhibitor SP600125 With High Expression of c-Jun

The transcription factor c-Jun is implicated with several cellular processes such as proliferation and cell transformation, and is

up-regulated in numerous carcinomas. To identify the tumor cells with high level of c-Jun, we examined c-Jun protein expression in 11 human tumor cell lines including CaCO₂ (colon cancer), HCT116 (colon cancer), A375 (melanoma cancer), A549 (non-small cell lung carcinoma), MKN-1 (gastric cancer), DU145 (prostate cancer), SKOV-3 (ovarian cancer), MDA-MB-231 (breast cancer), PC3 (prostate cancer), SF295 (glioblastoma cancer), and U251 (glioblastoma cancer). Among them, A375, A549, MKN-1, DU145, SKOV-3, MDA-MB-231 and PC3 showed relatively higher expression of c-Jun (**Figure 1A**). Since the c-Jun activation domain is phosphorylated only by the JNKs, and the c-Jun promoter activity is autoregulated by c-Jun/AP-1, we treated the above 7 kinds of cancer cell lines with specific JNK inhibitor SP600125 to find out the most sensitive cancer cells to c-Jun. As a result, SP600125 showed most potent cytotoxic activity on A549 lung cancer cells (**Figure 1B** and **Figure S1**). SP600125 inhibits JNK activity and, thus, c-Jun phosphorylation (Ser-63, -73). In A549 cells, the expression of c-Jun was dose-dependently inhibited by SP600125 (**Figure 1C**).

Exo-SP Inhibits Tube Formation and PTEN-Akt Pathway in the Recipient HUVECs

Tumor-derived exosomes induce alterations in their recipient cells, thereby play crucial roles in tumor growth, metastasis and angiogenesis (17, 18). Firstly, A549 cells were incubated in FBS-free RPMI 1640 medium for 24 h, and treated with or without 50 µM of SP600125 for 48 h. Then we isolated exosomes from A549 cells and prepared Exo and Exo-SP lysates for immunoblot with antibodies of CD81, CD63 and CD9, which are known as exosome markers (**Figure 2A**). We further examined whether Exo and Exo-SP from tumor cells affect endothelial cells, by performing endothelial cell exosome uptake, proliferation assay, and tube formation assay. The confocal imaging in **Figure 2B** suggested that Exo and Exo-SP were successfully uptaken by HUVECs.

Angiogenesis process involves the proliferation, migration, and tube formation of endothelial cells, allowing subsequent new vessel growth toward tumor (19). To investigate the influence of Exo or Exo-SP on proliferation of endothelial cells, HUVECs were treated with Exo or Exo-SP at concentration of 5, 10 and 20 µg/ml for 24 h or 48 h. Then the percentage of viable cells was measured using MTT assay. As a result, the percentage of viable cells was elevated by Exo, and reduced by Exo-SP (**Figure 2C**). The treatment of Exo-SP for 24 h was more effective than that for 48 h, and the effect of 5 µg/ml was too weak while that of 20 µg/ml too strong. Therefore, in order to eliminate the influence of exosome-induced cell cytotoxicity, we used the 10 µg/ml of exosome to evaluate the effect on HUVECs in the following study.

In tube formation assay, HUVECs were pre-incubated with Exo or Exo-SP for 24 h, and then seeded into matrigel. Three hours later, tube formation was photographed. Treatment with Exo promoted the tube formation, which was reduced by Exo-SP (**Figures 2D, E**).

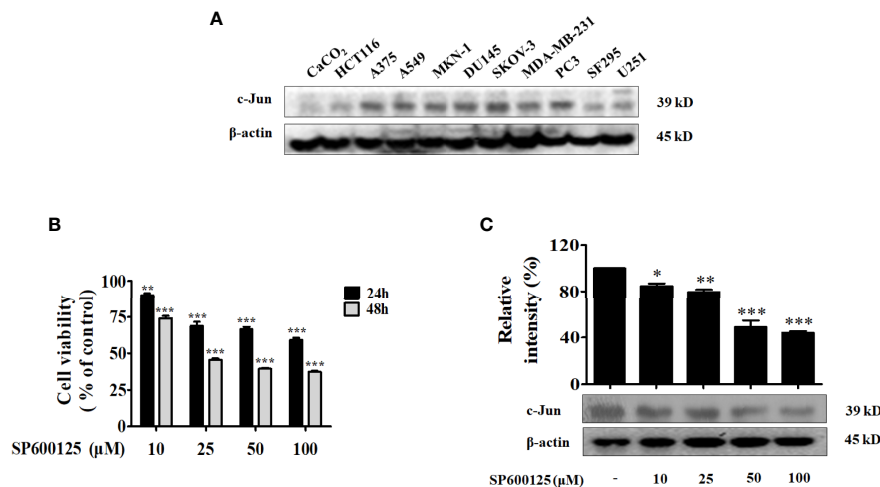


FIGURE 1 | A549 was most sensitive to JNK inhibitor SP600125. **(A)** The expression of c-Jun in various tumor cells (CaCO₂, HCT116, A375, A549, MKN-1, DU145, SKOV-3, MDA-MB-231, PC3, SF295, and U251) was determined by Western blot. **(B)** A549 cells were incubated with various concentrations (10, 25, 50, and 100 μM) of JNK inhibitor SP600125 for 24 h or 48 h. Cell viability was determined by MTT assay. **(C)** The cell lysates were collected and immunoblotted with antibody for c-Jun after treatment with 10, 25, 50, and 100 μM of SP600125 for 48 h, the relative ratios of c-Jun was calculated by analyzing immunoblot band intensities. Data show the mean ± SD of three independent experiments. **p* < 0.05, ***p* < 0.01, and ****p* < 0.001, compared to the non-treated HUVECs.

In order to investigate angiogenic or anti-angiogenic effects of Exo or Exo-SP, we detected the angiogenesis-related proteins such as PI3K/Akt pathway proteins by Western blot, since PI3K/Akt pathway could activate endothelial cell proliferation and migration (20). After treatment for 24 h, Exo decreased the level of PTEN and increased the phosphorylation of Akt, without effect on PI3K 110β. In contrast, Exo-SP increased the level of PTEN and decreased the phosphorylation of Akt (Figures 2F, G).

The Level of miR-494 Was Reduced in SP-Treated A549 Cells, Exo-SP and Exo-SP-Treated HUVECs

Exosomes isolated from human islets were found to carry a subset of miRNAs. The miRNAs have become attractive because they were reported to post-transcriptionally down-regulate target mRNAs that initiate or facilitate the development of several diseases. Particularly, miRNAs play crucial roles in vascular remodeling (21). In this study we examined the levels of 18 human miRNAs such as miR-9, miR-21, miR-23a, miR-34a, miR-125-3p, miR-125-5p, miR-126, miR-145, miR-146a, miR-148a, miR-152, miR-155, miR-221, miR-222, miR-449a, miR-494, miR-497, miR-519c, which were reported to target genes that are involved in vascular remodeling processes (22–30). In order to determine whether treatment of SP600125 leads to miRNA variation, we evaluated the levels of miRNAs in SP600125 treated A549 cells, Exo-SP, and Exo-SP treated HUVECs. A549 cells were treated with or without SP600125 for 48 h, and then the miRNAs were isolated. qRT-PCR results showed that the expressions of miR-494 and miR-155 were significantly lower in SP600125 treated A549 cells relative to non-treated group, and there were no obvious changes of other miRNAs (Figure 2H). Between them, miR-494 was the more

significantly decreased, therefore, we investigated the effect of miR-494 in the following study. A549 cells were treated with or without SP600125 for 48 h, and then miRNAs were isolated from Exo or Exo-SP. As shown in Figure 2I, the level of miRNA-494 was significantly reduced in Exo-SP compared with Exo. Furthermore, miR-494 level was also decreased in HUVECs treated with Exo-SP compared to the Exo treated group (Figure 2J).

Exo-c-Jun-KO Inhibits Angiogenesis Through Down-Regulation of Angiogenesis Related Signal Proteins in HUVEC Cells

In order to verify whether c-Jun affects the expression of miR-494 in A549 cell derived exosomes, thereby the angiogenesis of HUVECs, we used CRISPR/Cas9 to knockout the c-Jun in A549 cells (c-Jun-KO A549). Diagram of c-Jun gene exon 1 of gRNA targeting site is shown in Figure 3A. The sequence character of exon 1 in c-Jun was confirmed in A549 cells with Sanger sequencing carrying a 1-bp addition at the gRNA-targeting region (Figure S2). In addition, Western blot further confirmed no expression of c-Jun in gene-edited A549 cells (Figure 3B).

The isolated particles from c-Jun-KO A549 cells were confirmed to be exosomes, by examining the expression of the exosome markers including CD81, CD63 and CD9 (Figure 3C). Confocal images in Figure 3D showed that Exo-c-Jun-KO was uptaken by HUVECs. To confirm whether Exo-c-Jun-KO could exhibit anti-angiogenic effect on HUVECs as Exo-SP, we used MTT assay to determine the cell viability of HUVECs firstly. As shown in Figure 3E, the results were consistent with results of Exo-SP. Exo promoted, but Exo-c-Jun-KO suppressed, HUVEC proliferation, relative to untreated control for 24 h. However,

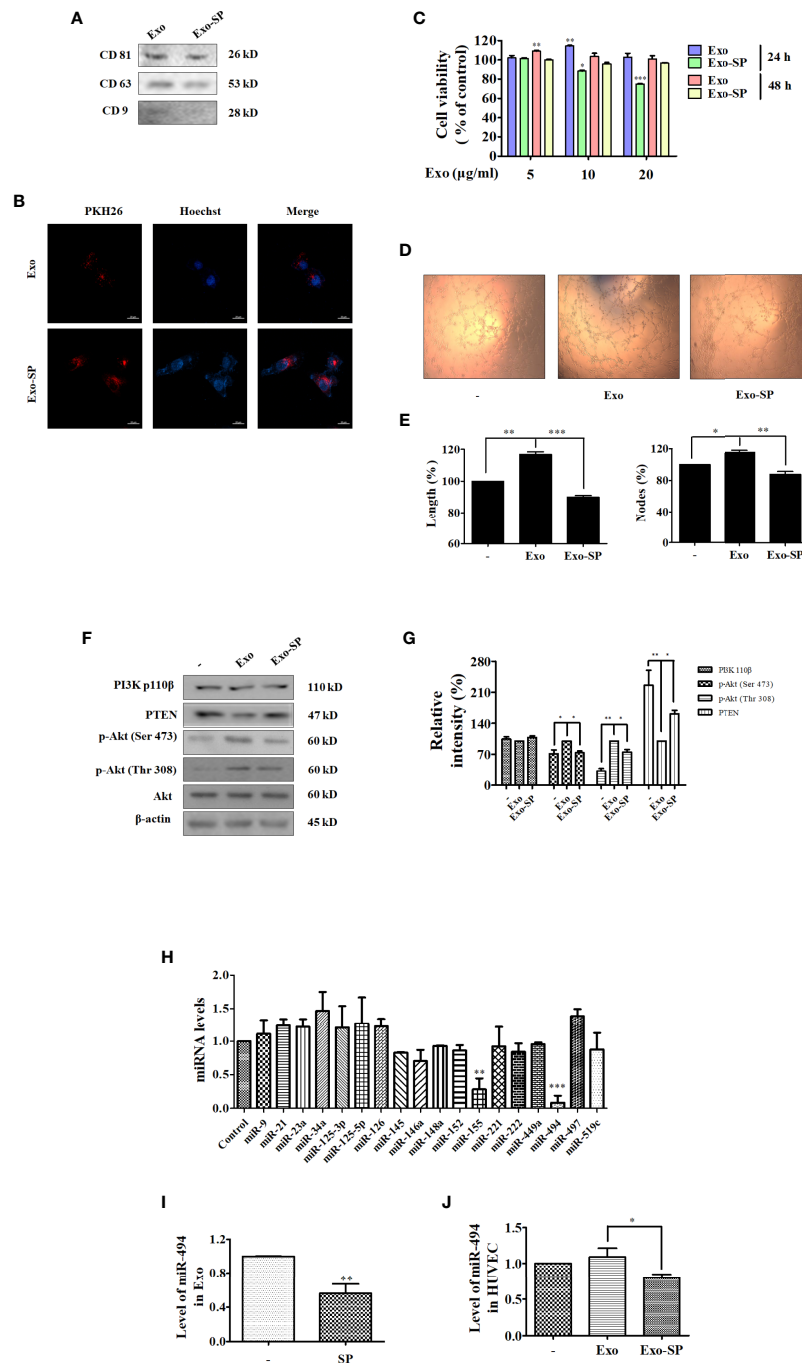


FIGURE 2 | Exo-SP inhibits tube formation and suppresses PTEN/Akt pathway in the recipient HUVECs, and the levels of miRNAs in A549 or SP600125 treated A549 cells, Exo or Exo-SP, and HUVECs treated with Exo or Exo-SP. **(A)** A549 cells were treated with or without 50 µM of SP600125 for 48 h in FBS free RPMI 1640 medium, and Exo and Exo-SP were isolated. Expression of exosomes markers CD81, CD63 and CD9 in the Exo and Exo-SP was detected by Western blot. **(B)** The isolated Exo and Exo-SP were labeled with PKH26 and Hoechst, and incubated with HUVECs for 3 h. The cellular uptake of Exo or Exo-SP was observed under fluorescent microscope. **(C)** HUVECs were treated with different concentrations (5, 10, 20 µg/ml) of Exo or Exo-SP for 24 h or 48 h, respectively. Cell viability was determined by MTT assay. **(D)** HUVECs were treated with Exo or Exo-SP for 24 h, and then seeded on Matrigel. Formation of tube-like structures was examined 3 h later. **(E)** Quantitative data for the tube-like structures were obtained by analyzing Length (%) and Nodes (%) density with Image J software. **(F)** HUVECs were treated with Exo or Exo-SP for 24 h, and then collected and lysed for immunoblot with specific antibodies. **(G)** Quantification of the results in **(F)**. **(H)** The levels of various miRNAs in A549 cells treated with or without SP600125 for 48 h. **(I)** The level of miR-494 in Exo and Exo-SP. Exosomes isolated from A549 cells were treated with or without SP600125 for 48 h, to be available for miR-494 analysis. **(J)** The level of miR-494 in HUVECs treated with Exo or Exo-SP for 24 h. Data show the mean ± SD of three independent experiments. **p* < 0.05, ***p* < 0.01, and ****p* < 0.001.

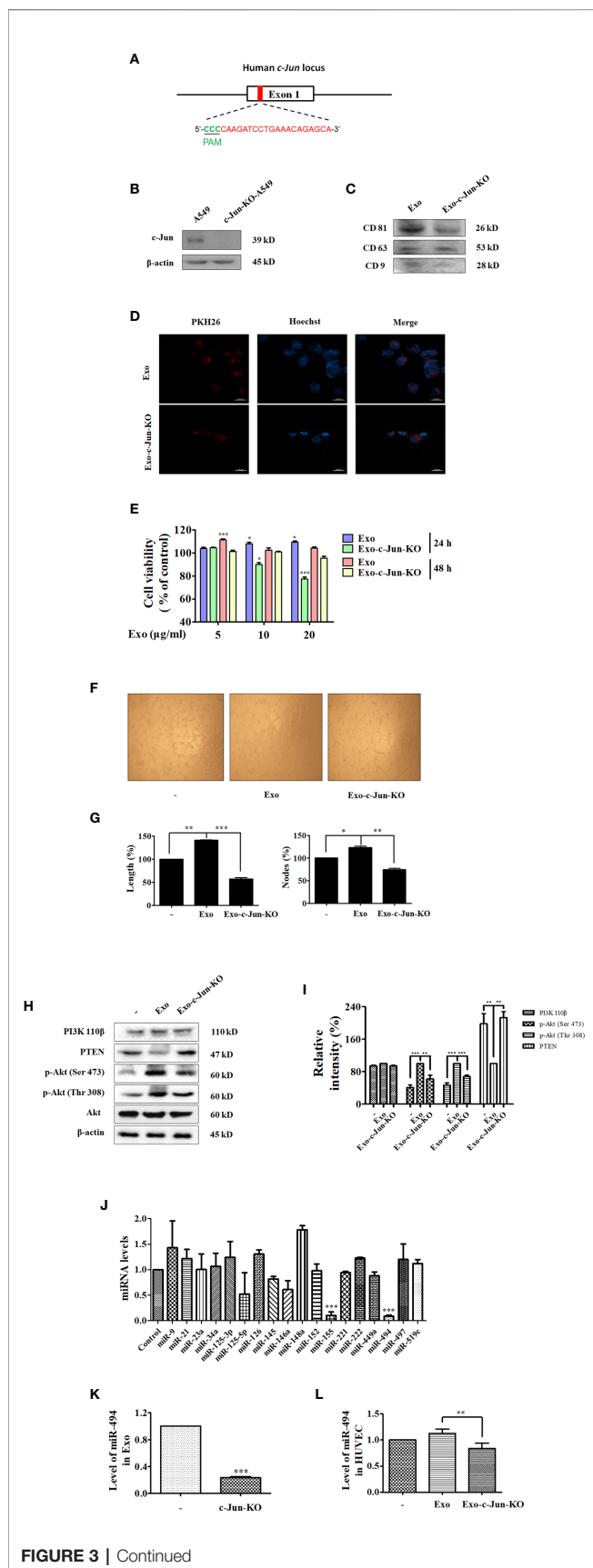


FIGURE 3 | Exo-c-Jun-KO inhibits angiogenesis in HUVECs, and the levels of miRNAs in A549 and c-Jun-KO A549 cells, Exo and Exo-c-Jun-KO, and HUVECs treated with Exo and Exo-c-Jun-KO. **(A)** Diagram of target site of c-Jun. gRNA targeting site is at exon 1 (red), protospacer adjacent motif (PAM) sequence (green). **(B)** Gene edited c-Jun-KO-A549 cells does not express the c-Jun. **(C)** The expression of CD81, CD63 and CD9 in Exo and Exo-c-Jun-KO. **(D)** Exosomes uptake determined by fluorescence staining assay. Exo and Exo-c-Jun-KO were labeled with PKH26, and then cultured with HUVECs for 3 h. HUVEC nuclei were labeled with Hoechst. **(E)** Cell viability of HUVECs after treated with Exo or Exo-c-Jun-KO for 24 h or 48 h. **(F)** Tube formation of HUVECs after treated with Exo or Exo-c-Jun-KO for 24 h. **(G)** Length (%) and Nodes (%) of tube formation were determined by Image J software. **(H)** The expression of PI3K p110 β , PTEN, and phosphorylation of Akt in Exo or Exo-c-Jun-KO treated HUVECs. **(I)** Quantification of the results in **(H)**. **(J)** The levels of various miRNAs in A549 or c-Jun-KO A549 cells. **(K)** The level of miR-494 in Exo and Exo-c-Jun-KO. Exosomes isolated from A549 or c-Jun-KO A549 cells were cultured with FBS free RPMI 1640 medium for 48 h, to be available for miR-494 analysis. **(L)** The level of miR-494 in HUVECs treated with Exo or Exo-c-Jun-KO for 24 h. Data show the mean \pm SD of three independent experiments. * $p < 0.05$, ** $p < 0.01$, and *** $p < 0.001$.

treatment with Exo-c-Jun-KO for 48 h did not alter cell viability obviously. Furthermore, we investigated the effect of Exo-c-Jun-KO on tube formation in HUVECs. After incubation for 24 h, the length and nodes of tube were reduced by Exo-c-Jun-KO compared with the Exo-treated group (**Figures 3F, G**). Meanwhile, Exo-c-Jun-KO decreased the Exo elevated phosphorylation of Akt, but enhanced the expression of PTEN, without obvious change of PI3K 110 β (**Figures 3H, I**). These results are consistent with Exo-SP treatment, indicating that Exo-c-Jun-KO might suppress angiogenesis through PTEN-Akt pathway.

The Level of miR-494 Was Reduced in c-Jun-KO-A549 Cells, Exo-c-Jun-KO and HUVECs Treated With Exo-c-Jun-KO

Exosomal miRNAs could stimulate angiogenesis and facilitate metastasis in cancer (31). To verify whether c-Jun acts on the exosomal miRNAs to influence endothelial angiogenesis, we measured the miRNA levels in c-Jun-KO-A549 cells, Exo-c-Jun-KO, and Exo-c-Jun-KO treated HUVECs. The qRT-PCR analysis showed only miR-494 and miR-155 changed significantly in c-Jun knockout A549 cells (**Figure 3J**). Consistent with Exo-SP, miR-494 was more reduced than miR-155. In addition, we also found c-Jun-KO-related reduction of miR-494 level in Exo-c-Jun-KO and Exo-c-Jun-KO treated HUVECs, respectively (**Figures 3K, L**).

Exosomal miR-494 Derived From c-Jun-KO-A549 Cells Inhibits Angiogenesis Through Targeting PTEN in Recipient HUVECs

To investigate the effect of miR-494 on tumor-angiogenesis, we established HUVECs with over expression of miR-494 by miR-494 agomir transfection, and then performed the tube formation assay and wound healing experiments. Firstly, HUVECs were transfected with miR-494 agomir or their scramble control agomir NC. qRT-PCR revealed that the transfection increased

level of miR-494 to be 5 times over the agomir NC group (**Figure 4A**), indicating that the miR-494 agomir was successfully transfected in HUVECs. Tube formation results showed that Exo-c-Jun-KO plus miR-494 agomir in HUVECs significantly elevated tubular length and nodes compared with the cells treated with Exo-c-Jun-KO plus agomir NC (**Figures 4B, C**). In addition, Exo-c-Jun-KO inhibited endothelial cell migration compared with the Exo treated group, and Exo-c-Jun-KO plus miR-494 agomir increased endothelial cell migration compared with the Exo-c-Jun-KO treated group (**Figures 4D, E**).

The binding site between miR-494 sequence and PTEN sequence is shown in **Figure 4F**, indicating that PTEN coding sequence might be a potential target of miR-494. And several previous reports have shown that miR-494 directly targets PTEN (32–34). To demonstrate the target protein of miR-494 from Exo-c-Jun-KO, we investigated the effect of miR-494 on Akt pathway. HUVECs were cultured with Exo, Exo-c-Jun-KO, or Exo-c-Jun-KO plus miR-494 agomir for 24 h, and the expression and phosphorylation of the PI3K/Akt pathway proteins were detected using Western blot. PTEN is the negative regulator of the PI3K/Akt oncogenic signaling pathway, thereby inhibiting uncontrolled cell survival, growth and migration (35). PTEN has been reported as a target gene of miR-494, therefore, we verified that PTEN was down-regulated by miR-494 agomir in HUVECs. Exo-c-Jun-KO plus miR-494 agomir led to lower levels of PTEN expression compared with Exo-c-Jun-KO group. However, the phosphorylation of Akt was increased in Exo-c-Jun-KO plus miR-494 agomir treated group compared with Exo-c-Jun-KO (**Figures 4G, H**). These findings demonstrated that the PTEN was the target gene of miR-494 in HUVECs.

Exo-c-Jun-KO Suppressed A549 Lung Cancer Growth and Angiogenesis *In Vivo*

We used mouse xenograft model to investigate whether miR-494 from Exo-c-Jun-KO could affect tumor growth *in vivo*. A549 cells were subcutaneously inoculated into the flanks of nude mice. And Exo, Exo-c-Jun-KO, or Exo-c-Jun-KO plus miR-494 agomir was intratumoral administered every other day for 14 days. Mice were sacrificed and the representative tumor images were shown in **Figure 5A**. The tumors from the Exo group were significantly larger than non-treated control group, and those from the Exo-c-Jun-KO group were smaller than Exo group. Tumors from Exo-c-Jun-KO plus miR-494 group were larger than Exo-c-Jun-KO group. The tumor growth pattern showed similar results (**Figure 5B**). Accordingly, the immunohistochemical analysis showed that Exo treated tumors had a higher number of cells positive for the proliferative marker Ki-67 than control group, and Exo-c-Jun-KO had shown less number of cancer cells than Exo group, and Exo-c-Jun-KO plus miR-494 had higher number of cells than Exo-c-Jun-KO group (**Figures 5C, D**). In addition, tumors from Exo group also had more cells positive for endothelial cell marker CD31, with stronger staining than control group, and Exo-c-Jun-KO treatment had lower level of CD31 in the xenograft tumor than Exo treatment. Fibroblasts are important component of the tumor stroma, which are thought to be critical driver of

tumor progression in a number of organs (36). We found that the higher levels of α -SMA, a cancer (carcinoma)-associated fibroblasts (CAF) marker, positive stromal cells were detected in Exo treatment group, and Exo-c-Jun-KO treatment showed lower levels of α -SMA (**Figures 5C, D**).

Exo-c-Jun-KO Suppressed A549 Lung Cancer Angiogenesis *In Vivo*

To further investigate the anti-angiogenic effect of Exo-c-Jun-KO, we examined the effect of Exo-c-Jun-KO by use of Matrigel plug assay *in vivo*. HUVECs mixed with exosomes, agomir and Matrigel were subcutaneously injected into nude mice, and the vasculature was examined. Consistent with the *in vitro* and above *in vivo* results, the photo of Matrigel plugs showed that Exo-stimulated vascularization was markedly suppressed by Exo-c-Jun-KO (**Figure 5E**). ELISA result showed that Exo accumulated hemoglobin, while Exo-c-Jun-KO treatment led to decrease of hemoglobin content (**Figure 5F**). And treatment of Exo-c-Jun-KO plus miR-494 agomir reversed the reduction by Exo-c-Jun-KO.

DISCUSSION

c-Jun was reported as an oncoprotein, of which the overexpression greatly enhanced the tumorigenic properties of the MCF7 human breast cancer cell line (37). c-Jun is highly expressed in tumor cells of patients with classical Hodgkin's disease (38), and the number and size of hepatic tumors were significantly attenuated when *c-jun* was inactivated (39). In the present study, we found that tumor cell lines including A375, A549, MKN-1, DU145, SKOV-3, MDA-MB-231 and PC3 expressed the c-Jun protein. JNK phosphorylates and regulates the activity and expression of the Jun proteins (2, 4). Therefore, we used JNK specific inhibitor SP600125 to find out JNK sensitive cell line. Among the above 7 tumor cell lines, NSCLC A549 was most sensitive, and therefore was selected to investigate the c-Jun related mechanism.

Exosomes are a class of extracellular vesicles released by various cell types, act as a mediator of cell-to-cell communication (31). In this study, exosomes derived from A549, SP600125 treated A549, or c-Jun-KO-A549 cells were successfully isolated and characterized. Tumor-derived exosomes reprogram endothelial cells by ligand/receptor signaling, miRNA and RNA transfer after fusion with the plasma membrane, internalization through phagocytosis, endocytosis, micropinocytosis or lipid raft-mediated internalization (12). In this study we found that PKH26-labeled Exo, Exo-SP, Exo-c-Jun-KO were localized in the cytoplasm of HUVECs, implying that exosomes could be internalized by HUVECs.

Most cancer cells release exosomes, which dictate the behavior of the recipient cells for the ultimate benefit of the cancer cells (18, 40). Blood vessels deliver oxygen and essential nutrients to nourish cancers. Neovascularization promotes tumor extension and invasion into nearby normal tissue, as

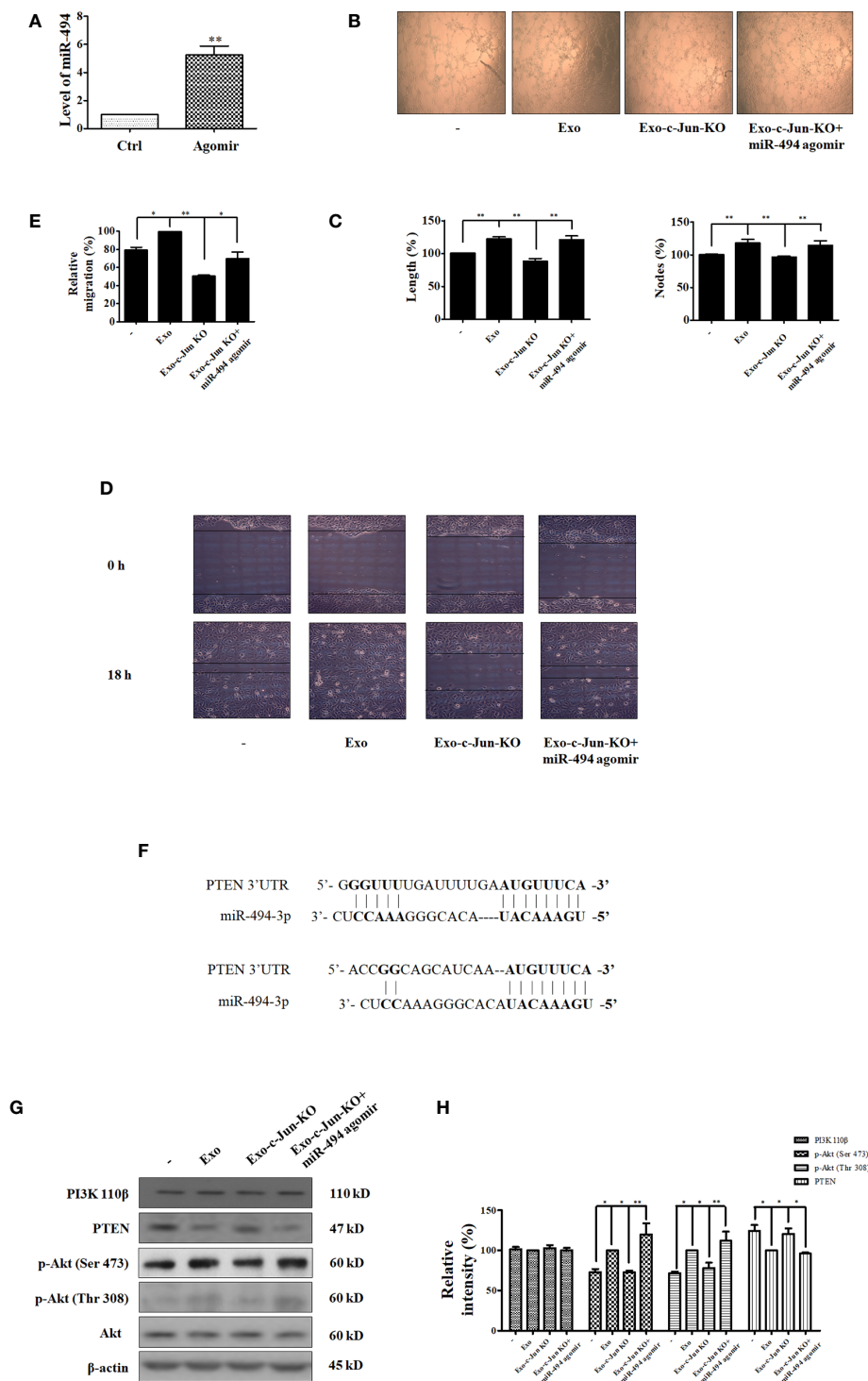


FIGURE 4 | miR-494/PTEN is involved in angiogenesis inhibited by Exo-c-Jun-KO. **(A)** The level of miR-494 in HUVECs transfected with the miR-494 agomir or agomir NC. **(B)** Tube formation of HUVECs treated with Exo, Exo-c-Jun-KO, and those simultaneously transfected with miR-494 agomir or agomir NC. **(C)** Length (%) and Nodes (%) were determined by Image J software. **(D)** Migration of HUVECs treated with Exo, Exo-c-Jun-KO, and those simultaneously transfected with miR-494 agomir or agomir NC. **(E)** Quantification of the results in (D). **(F)** PTEN as the target gene of miR-494. **(G)** Changes of PTEN/Akt related proteins in HUVECs treated with or without Exo or Exo-c-Jun-KO, and those simultaneously transfected with miR-494 agomir or agomir NC. **(H)** Quantification of the results in (G). Data show the mean \pm SD of three independent experiments. * $p < 0.05$ and ** $p < 0.01$.

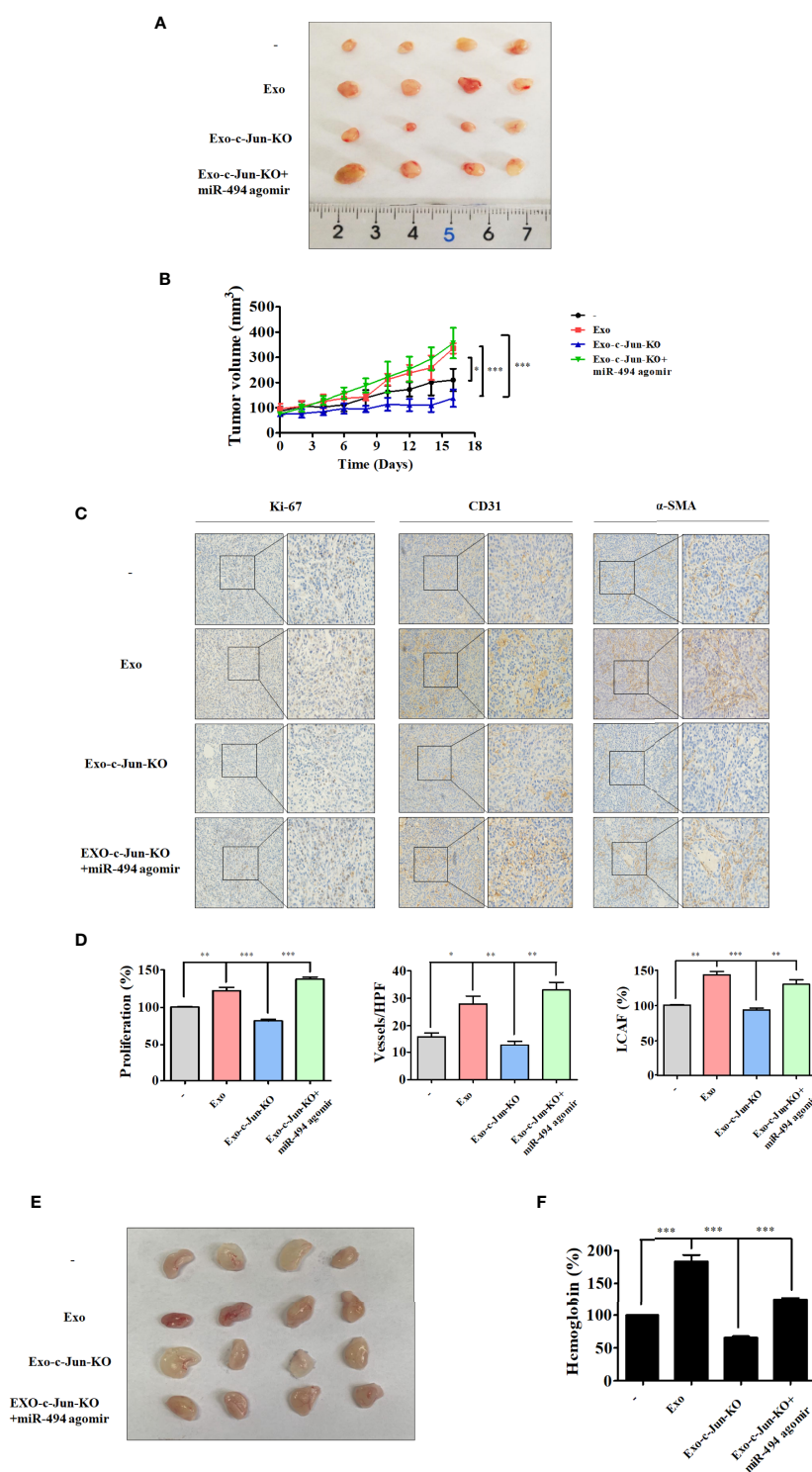


FIGURE 5 | Exo-c-Jun-KO suppresses lung cancer growth and angiogenesis *in vivo*. A549 cells were inoculated subcutaneously in the flank site of nude mice. Exo, Exo-c-Jun-KO, miR-494 agomir were intratumorally injected every other day for 14 days. After 16 days, the tumors were excised from mice. **(A)** Representative images of the tumors removed from nude mice. **(B)** Quantification of tumor volume. Tumor volumes were measured every other day starting from the day before the first treatment. **(C, D)** Immunohistochemical staining of Ki-67, CD31 and α-SMA in tumor tissues of different groups and their quantification. **(E)** Photos of the matrigel plugs from nude mice after various treatments. **(F)** Hemoglobin level in the matrigel plugs. Data show the mean ± SD (n=4). *p < 0.05, **p < 0.01, and ***p < 0.001.

well as distant metastasis to form new colonies of cancer cells (5, 19). Therefore, angiogenesis plays an important role in tumor growth and metastasis. It was reported that exosomes from Chronic Myelogenous Leukemia (CML) cells modulate the process of neovascularization by directly affecting endothelial cells (41); exosomes from glioblastoma multiforme (GBM) cells growing in hypoxic induce angiogenesis by phenotypic modulation of endothelial cells (42). However, the role of c-Jun in exosome-mediated angiogenesis has not been reported. In the present study, we found that angiogenesis of HUVECs was enhanced after stimulated by Exo. However, Exo-SP and Exo-c-Jun-KO inhibited HUVEC tube formation and proliferation. These results suggest that down-regulation of c-Jun in tumor cells reduced the vascular development caused by Exo in the neighborhood of the tumor.

Cancer exosomes carry malignant information in the form of miRNA, mRNA, DNA fragment and proteins that can reprogram recipient cells (43). miRNAs are small, endogenous, conserved, single-stranded, non-coding RNAs, which degrade target mRNAs or inhibit translation post-transcriptionally (21). Recently, exosomal miRNAs and their relation with cancer have been frequently reported. Among which, exosomal miR-135b from hypoxic multiple myeloma cells enhances angiogenesis by targeting factor-inhibiting hypoxia-inducible factor 1 (44); miR-23a from nasopharyngeal carcinoma derived exosomes mediated angiogenesis by targeting testis-specific gene antigen (45). In this

regard, we investigated variation of miRNA levels in A549 cells, exosomes and exosomes treated HUVECs, and found that level of miR-494 was reduced in A549 cells with SP treatment or c-Jun-KO compared with non-treated group. And the level of miR-494 was down-regulated in Exo-SP and Exo-c-Jun-KO. In addition, incubation with Exo-SP and Exo-c-Jun-KO showed lower level of miR-494 compared with Exo in recipient HUVECs. These results revealed that miR-494 level might be involved in the Exo-SP and Exo-c-Jun-KO mediated angiogenesis behaviors of HUVECs.

Angiogenesis is a multistep process controlled by the balance of pro- and anti-angiogenesis factors. PI3K/Akt pathway is considered to play an important role in tumorigenesis (46). PI3K regulates cell-cycle progression, protein synthesis, cell growth, and angiogenesis mainly through Akt (46). In the present study we found that Exo-SP and Exo-c-Jun-KO decreased the phosphorylation of Akt elevated by Exo. However, the level of PI3K 110 was unchanged. The second messenger phosphatidylinositol 3,4,5-triphosphate (PIP3) is produced through phosphorylation of phosphatidylinositol 4,5-bisphosphate (PIP2) catalyzed by PI3K. The PTEN dephosphorylates PIP3 to PIP2, acting thereby as a direct antagonist of PI3K (47). PTEN is known as a tumor suppressor and appears to be mutated at considerable frequency in human cancers (48). PTEN has been reported to be lowly expressed in lung cancer (49). In this study we found

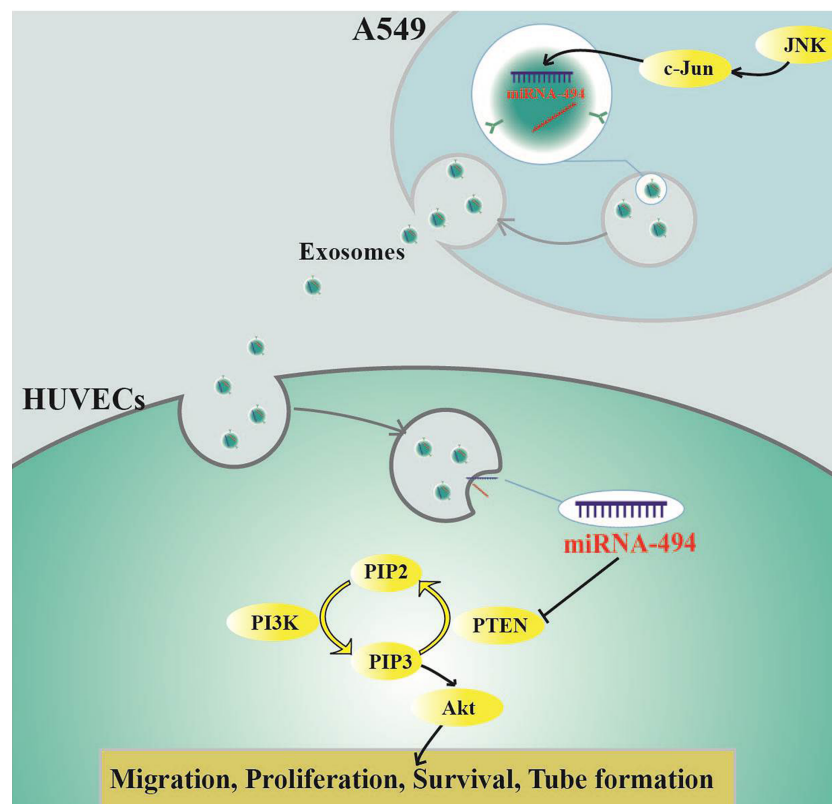


FIGURE 6 | Schematic diagram indicating how c-Jun affects angiogenesis in HUVECs through exosome/miR-494/PTEN signal pathway.

that the anti-angiogenesis efficacy of Exo-SP and Exo-c-Jun-KO might be mediated *via* elevation of PTEN expression in HUVECs. We also found that increase of miR-494 by the miR-494 agomir resulted in the reversal of the anti-angiogenesis effect of Exo-c-Jun-KO including tube formation and migration. Exo-c-Jun-KO plus miR-494 agomir further flipped the effect of Exo-c-Jun-KO on phosphorylation of Akt. miR-494 activates the PI3K/Akt pathway by targeting of PTEN and hence not only enhances the ability of myeloid-derived suppressor cells (MDSCs) to infiltrate into tumor tissue but also facilitates tumor invasion and metastasis (50). Low PTEN expression and high miR-494 expression are associated with high proliferation, low differentiation of tumor tissues and high possibility of early invasion and metastasis in NSCLC (51). In this study we verified that PTEN was downregulated by miR-494 agomir compared with the non-treated control group (Data not shown), and the expression of PTEN was decreased in HUVECs by Exo-c-Jun-KO plus miR-494 agomir compared with Exo-c-Jun-KO treated group. These results suggest that the reduced exosomal miR-494 from c-Jun-KO-A549 cells regulate the angiogenesis through up-regulation of expression of PTEN, which inactivated Akt and the downstream pathway in HUVECs.

Exo-c-Jun-KO blocked tumor growth and reduced tumor volume by approximately 57.8% compared with Exo treated mice, and Exo-c-Jun-KO plus miR-494 agomir converted the tumor growth. CD31 was used as a marker to indicate vascularization or blood vessel formation within tumor. CAFs, recognized by expression of α -SMA, are known to promote malignant growth, angiogenesis, invasion and metastasis (52). Immunohistochemical analysis showed that Exo-c-Jun-KO suppressed Ki-67, CD31 and α -SMA expression in the tumor section, and Exo-c-Jun-KO plus miR-494 agomir could neutralize such effect. These data indicated that low miR-494 expression in Exo-c-Jun-KO is correlated with lung cancer progression. Matrigel plug is a classic model to assess angiogenesis *in vivo*. In this work, Exo-c-Jun-KO decreased blood vessel formation in the Matrigel plug model compared with the Exo treated mice. And the blood vessels were increased after addition of miR-494 agomir. These results further revealed that Exo-c-Jun-KO possessed the vascular recruitment and organization through miR-494.

CONCLUSIONS

In conclusion, we first elucidated that miR-494 was reduced in Exo-c-Jun-KO and Exo-SP, resulting in elevation of PTEN

expression and down-regulation of Akt pathway in Exo-c-Jun-KO and Exo-SP treated HUVECs, which might contribute to the suppression of tumor angiogenesis. Our data demonstrated that Exo-c-Jun-KO attenuates the lung cancer angiogenesis by transferring exosomal miR-494 to recipient endothelial cells (Figure 6), suggesting targeting oncogene c-Jun might be a promising therapeutic approach for lung cancer.

DATA AVAILABILITY STATEMENT

The original contributions presented in the study are included in the article/Supplementary Material. Further inquiries can be directed to the corresponding authors.

ETHICS STATEMENT

The animal study was reviewed and approved by Laboratory Animal Center of Institute of Radiation Medicine, the Chinese Academy of Medical Sciences.

AUTHOR CONTRIBUTIONS

MJ and DK designed the experiments and acquired funding for the study. CS, YH, BF, SP, XZ, and NZ performed the experiments. WW, ZZ, RW, and YQ provided technical assistances. CS and MJ wrote the manuscript. DK edited the manuscript. All authors contributed to the article and approved the submitted version.

FUNDING

This study was supported by grants from the National Natural Science Foundation of China (81672809, 81673464, 81373441), grant for Major Project of Tianjin for New Drug Development (17ZXXYSY00050).

SUPPLEMENTARY MATERIAL

The Supplementary Material for this article can be found online at: <https://www.frontiersin.org/articles/10.3389/fonc.2021.663183/full#supplementary-material>

REFERENCES

- Shaulian E, Karin M. AP-1 in cell proliferation and survival. *Oncogene* (2001) 20(19):2390–400. doi: 10.1038/sj.onc.1204383
- Angel P, Hattori K, Smeal T, Karin M. The jun proto-oncogene is positively autoregulated by its product, Jun/AP-1. *Cell* (1988) 55(5):875–85. doi: 10.1016/0092-8674(88)90143-2
- Karin M, Liu Z, Zandi E. AP-1 function and regulation. *Curr Opin Cell Biol* (1997) 9(2):240–6. doi: 10.1016/s0955-0674(97)80068-3
- Derijard B, Hibi M, Wu IH, Barrett T, Su B, Deng T, et al. JNK1: a protein kinase stimulated by UV light and Ha-Ras that binds and phosphorylates the c-Jun activation domain. *Cell* (1994) 76(6):1025–37. doi: 10.1016/0092-8674(94)90380-8
- Rajabi M, Mousa SA. The Role of Angiogenesis in Cancer Treatment. *Biomedicine* (2017) 5(2):34. doi: 10.3390/biomedicine5020034
- Simpson RJ, Jensen SS, Lim JW. Proteomic profiling of exosomes: current perspectives. *Proteomics* (2008) 8(19):4083–99. doi: 10.1002/pmic.200800109

7. Simons M, Raposo G. Exosomes-vesicular carriers for intercellular communication. *Curr Opin Cell Biol* (2009) 21(4):575–81. doi: 10.1016/j.ceb.2009.03.007
8. Mathivanan S, Ji H, Simpson RJ. Exosomes: extracellular organelles important in intercellular communication. *J Proteomics* (2010) 73(10):1907–20. doi: 10.1016/j.jprot.2010.06.006
9. Wan Z, Gao X, Dong Y, Zhao Y, Chen X, Yang G, et al. Exosome-mediated cell-cell communication in tumor progression. *Am J Cancer Res* (2018) 8(9):1661–73.
10. Kahlert C, Kalluri R. Exosomes in tumor microenvironment influence cancer progression and metastasis. *J Mol Med (Berl)* (2013) 91(4):431–7. doi: 10.1007/s00109-013-1020-6
11. Kai K, Dittmar RL, Sen S. Secretory microRNAs as biomarkers of cancer. *Semin Cell Dev Biol* (2018) 78:22–36. doi: 10.1016/j.semcdb.2017.12.011
12. Ludwig N, Whiteside TL. Potential roles of tumor-derived exosomes in angiogenesis. *Expert Opin Ther Targets* (2018) 22(5):409–17. doi: 10.1080/14728222.2018.1464141
13. Peng X, Wang Z, Liu Y, Peng X, Liu Y, Zhu S, et al. Oxyfadiachalcone C inhibits melanoma A375 cell proliferation and metastasis via suppressing PI3K/Akt and MAPK/ERK pathways. *Life Sci* (2018) 206:35–44. doi: 10.1016/j.lfs.2018.05.032
14. Wang Z, Wang Y, Zhu S, Liu Y, Peng X, Zhang S, et al. DT-13 Inhibits Proliferation and Metastasis of Human Prostate Cancer Cells Through Blocking PI3K/Akt Pathway. *Front Pharmacol* (2018) 9:1450:1450. doi: 10.3389/fphar.2018.01450
15. Kong D, Okamura M, Yoshimi H, Yamori T. Antiangiogenic effect of ZSTK474, a novel phosphatidylinositol 3-kinase inhibitor. *Eur J Cancer* (2009) 45(5):857–65. doi: 10.1016/j.ejca.2008.12.007
16. Zhang Z, Liu J, Wang Y, Tan X, Zhao W, Xing X, et al. Phosphatidylinositol 3-kinase β and δ isoforms play key roles in metastasis of prostate cancer DU145 cells. *FASEB J* (2018) 32(11):5967–75. doi: 10.1096/fj.201800183R
17. Kosaka N, Yoshioka Y, Fujita Y, Ochiya T. Versatile roles of extracellular vesicles in cancer. *J Clin Invest* (2016) 126(4):1163–72. doi: 10.1172/jci81130
18. Guo W, Gao Y, Li N, Shao F, Wang C, Wang P, et al. Exosomes: New players in cancer (Review). *Oncol Rep* (2017) 38(2):665–75. doi: 10.3892/or.2017.5714
19. Mousa SA, Mousa AS. Angiogenesis inhibitors: current & future directions. *Curr Pharm Des* (2004) 10(1):1–9. doi: 10.2174/1381612043453531
20. Patel-Hett S, D'Amore PA. Signal transduction in vasculogenesis and developmental angiogenesis. *Int J Dev Biol* (2011) 55(4–5):353–63. doi: 10.1387/ijdb.103213sp
21. Fang YC, Yeh CH. Role of microRNAs in Vascular Remodeling. *Curr Mol Med* (2015) 15(8):684–96. doi: 10.2174/1566524015666150921105031
22. Welten SM, Goossens EA, Quax PH, Nossent AY. The multifactorial nature of microRNAs in vascular remodelling. *Cardiovasc Res* (2016) 110(1):6–22. doi: 10.1093/cvr/cvw039
23. Tiwari A, Mukherjee B, Dixit M. MicroRNA Key to Angiogenesis Regulation: MiRNA Biology and Therapy. *Curr Cancer Drug Targets* (2018) 18(3):266–77. doi: 10.2174/1568009617666170630142725
24. Qin B, Yang H, Xiao B. Role of microRNAs in endothelial inflammation and senescence. *Mol Biol Rep* (2012) 39(4):4509–18. doi: 10.1007/s11033-011-1241-0
25. Cha ST, Chen PS, Johansson G, Chu CY, Wang MY, Jeng YM, et al. MicroRNA-519c suppresses hypoxia-inducible factor-1 α expression and tumor angiogenesis. *Cancer Res* (2010) 70(7):2675–85. doi: 10.1158/0008-5472.can-09-2448
26. Lu J, Liu QH, Wang F, Tan JJ, Deng YQ, Peng XH, et al. Exosomal miR-9 inhibits angiogenesis by targeting MDK and regulating PDK/AKT pathway in nasopharyngeal carcinoma. *J Exp Clin Cancer Res* (2018) 37(1):147. doi: 10.1186/s13046-018-0814-3
27. Petrek H, Yu AM. MicroRNAs in non-small cell lung cancer: Gene regulation, impact on cancer cellular processes, and therapeutic potential. *Pharmacol Res Perspect* (2019) 7: (6):e00528. doi: 10.1002/prp2.528
28. Seo HH, Lee SY, Lee CY, Kim R, Kim P, Oh S, et al. Exogenous miRNA-146a Enhances the Therapeutic Efficacy of Human Mesenchymal Stem Cells by Increasing Vascular Endothelial Growth Factor Secretion in the Ischemia/Reperfusion-Injured Heart. *J Vasc Res* (2017) 54(2):100–8. doi: 10.1159/000461596
29. Xu Q, Liu LZ, Yin Y, He J, Li Q, Qian X, et al. Regulatory circuit of PKM2/NF-kappaB/miR-148a/152-modulated tumor angiogenesis and cancer progression. *Oncogene* (2015) 34(43):5482–93. doi: 10.1038/onc.2015.6
30. Zhou TB, Jiang ZP, Liu ZS, Zhao ZZ. Roles of miR-497 and its potential signaling pathway in diseases and with vascular endothelial growth factor. *J Recept Signal Transduct Res* (2015) 35(4):303–6. doi: 10.3109/10799893.2014.977452
31. Zhang J, Li S, Li L, Li M, Guo C, Yao J, et al. Exosome and exosomal microRNA: trafficking, sorting, and function. *Genomics Proteomics Bioinf* (2015) 13(1):17–24. doi: 10.1016/j.gpb.2015.02.001
32. Sun HB, Chen X, Ji H, Wu T, Lu HW, Zhang Y, et al. miR-494 is an independent prognostic factor and promotes cell migration and invasion in colorectal cancer by directly targeting PTEN. *Int J Oncol* (2014) 45(6):2486–94. doi: 10.3892/ijo.2014.2665
33. Zhao Q, Xiong Y, Xu J, Chen S, Li P, Huang Y, et al. Host MicroRNA hsa-miR-494-3p Promotes EV71 Replication by Directly Targeting PTEN. *Front Cell Infect Microbiol* (2018) 8:278. doi: 10.3389/fcimb.2018.00278
34. Wang X, Zhang X, Ren XP, Chen J, Liu H, Yang J, et al. MicroRNA-494 targeting both proapoptotic and antiapoptotic proteins protects against ischemia/reperfusion-induced cardiac injury. *Circulation* (2010) 122(13):1308–18. doi: 10.1161/circulationaha.110.964684
35. Gkoutakos A, Sartori G, Falcone I, Piro G, Ciuffreda L, Carbone C, et al. PTEN in Lung Cancer: Dealing with the Problem, Building on New Knowledge and Turning the Game Around. *Cancers (Basel)* (2019) 11(8):1141. doi: 10.3390/cancers11081141
36. Franco OE, Shaw AK, Strand DW, Hayward SW. Cancer associated fibroblasts in cancer pathogenesis. *Semin Cell Dev Biol* (2010) 21(1):33–9. doi: 10.1016/j.semcdb.2009.10.010
37. Smith LM, Wise SC, Hendricks DT, Sabichi AL, Bos T, Reddy P, et al. cJun overexpression in MCF-7 breast cancer cells produces a tumorigenic, invasive and hormone resistant phenotype. *Oncogene* (1999) 18(44):6063–70. doi: 10.1038/sj.onc.1202989
38. Mathas S, Hinz M, Anagnostopoulos I, Krappmann D, Lietz A, Jundt F, et al. Aberrantly expressed c-Jun and JunB are a hallmark of Hodgkin lymphoma cells, stimulate proliferation and synergize with NF-kappa B. *EMBO J* (2002) 21(15):4104–13. doi: 10.1093/emboj/cdf389
39. Eferl R, Ricci R, Kenner L, Zenz R, David JP, Rath M, et al. Liver tumor development. c-Jun antagonizes the proapoptotic activity of p53. *Cell* (2003) 112(2):181–92. doi: 10.1016/s0092-8674(03)00042-4
40. Brinton LT, Sloane HS, Kester M, Kelly KA. Formation and role of exosomes in cancer. *Cell Mol Life Sci* (2015) 72(4):659–71. doi: 10.1007/s00018-014-1764-3
41. Taverna S, Flugy A, Saieva L, Kohn EC, Santoro A, Meraviglia S, et al. Role of exosomes released by chronic myelogenous leukemia cells in angiogenesis. *Int J Cancer* (2012) 130(9):2033–43. doi: 10.1002/ijc.26217
42. Kucharzewska P, Christianson HC, Welch JE, Svensson KJ, Fredlund E, Ringnér M, et al. Exosomes reflect the hypoxic status of glioma cells and mediate hypoxia-dependent activation of vascular cells during tumor development. *Proc Natl Acad Sci USA* (2013) 110(18):7312–7. doi: 10.1073/pnas.1220998110
43. Ruivo CF, Adem B, Silva M, Melo SA. The Biology of Cancer Exosomes: Insights and New Perspectives. *Cancer Res* (2017) 77(23):6480–8. doi: 10.1158/0008-5472.can-17-0994
44. Umez T, Tadokoro H, Azuma K, Yoshizawa S, Ohyashiki K, Ohyashiki JH. Exosomal miR-135b shed from hypoxic multiple myeloma cells enhances angiogenesis by targeting factor-inhibiting HIF-1. *Blood* (2014) 124(25):3748–57. doi: 10.1182/blood-2014-05-576116
45. Bao L, You B, Shi S, Shan Y, Zhang Q, Yue H, et al. Metastasis-associated miR-23a from nasopharyngeal carcinoma-derived exosomes mediates angiogenesis by repressing a novel target gene TSGA10. *Oncogene* (2018) 37: (21):2873–89. doi: 10.1038/s41388-018-0183-6
46. Kong D, Yamori T. Phosphatidylinositol 3-kinase inhibitors: promising drug candidates for cancer therapy. *Cancer Sci* (2008) 99(9):1734–40. doi: 10.1111/j.1349-7006.2008.00891.x
47. Sarris EG, Saif MW, Syrigos KN. The Biological Role of PI3K Pathway in Lung Cancer. *Pharm (Basel)* (2012) 5(11):1236–64. doi: 10.3390/ph511236
48. Li J, Yen C, Liaw D, Podsypanina K, Bose S, Wang SI, et al. PTEN, a putative protein tyrosine phosphatase gene mutated in human brain, breast, and

- prostate cancer. *Science* (1997) 275(5308):1943–7. doi: 10.1126/science.275.5308.1943
49. Ji Y, Zheng M, Ye S, Chen J, Chen Y. PTEN and Ki67 expression is associated with clinicopathologic features of non-small cell lung cancer. *J BioMed Res* (2014) 28(6):462–7. doi: 10.7555/jbr.27.20130084
 50. Liu Y, Lai L, Chen Q, Song Y, Xu S, Ma F, et al. MicroRNA-494 is required for the accumulation and functions of tumor-expanded myeloid-derived suppressor cells via targeting of PTEN. *J Immunol* (2012) 188(11):5500–10. doi: 10.4049/jimmunol.1103505
 51. Wang J, Chen H, Liao Y, Chen N, Liu T, Zhang H, et al. Expression and clinical evidence of miR-494 and PTEN in non-small cell lung cancer. *Tumour Biol* (2015) 36(9):6965–72. doi: 10.1007/s13277-015-3416-0
 52. Bremnes RM, Donnem T, Al-Saad S, Al-Shibli K, Andersen S, Sirera R, et al. The role of tumor stroma in cancer progression and prognosis: emphasis on carcinoma-associated fibroblasts and non-small cell lung cancer. *J Thorac Oncol* (2011) 6(1):209–17. doi: 10.1097/JTO.0b013e3181f8a1bd
- Conflict of Interest:** The authors declare that the research was conducted in the absence of any commercial or financial relationships that could be construed as a potential conflict of interest.

Copyright © 2021 Shao, Huang, Fu, Pan, Zhao, Zhang, Wang, Zhang, Qiu, Wang, Jin and Kong. This is an open-access article distributed under the terms of the Creative Commons Attribution License (CC BY). The use, distribution or reproduction in other forums is permitted, provided the original author(s) and the copyright owner(s) are credited and that the original publication in this journal is cited, in accordance with accepted academic practice. No use, distribution or reproduction is permitted which does not comply with these terms.



Lansoprazole Alone or in Combination With Gefitinib Shows Antitumor Activity Against Non-small Cell Lung Cancer A549 Cells *in vitro* and *in vivo*

Xiaoxia Zhao¹, Ning Zhang¹, Yingying Huang¹, Xiaojing Dou¹, Xiaolin Peng², Wei Wang², Zhe Zhang¹, Ran Wang¹, Yuling Qiu¹, Meihua Jin^{1*} and Dexin Kong^{1,3*}

OPEN ACCESS

Edited by:

Liwu Fu,
Sun Yat-sen University, China

Reviewed by:

Yan-yan Yan,
Shanxi Datong University, China
Giuseppe Palma,
Istituto Nazionale Tumori Scientific
Institute for Research, Hospitalization
and Healthcare (IRCCS) "Fondazione
G. Pascale", Italy

*Correspondence:

Meihua Jin
jinmeihua@tmu.edu.cn
Dexin Kong
kongdexin@tmu.edu.cn

Specialty section:

This article was submitted to
Molecular and Cellular Oncology,
a section of the journal
Frontiers in Cell and Developmental
Biology

Received: 19 January 2021

Accepted: 29 March 2021

Published: 20 April 2021

Citation:

Zhao X, Zhang N, Huang Y,
Dou X, Peng X, Wang W, Zhang Z,
Wang R, Qiu Y, Jin M and Kong D
(2021) Lansoprazole Alone or
in Combination With Gefitinib Shows
Antitumor Activity Against Non-small
Cell Lung Cancer A549 Cells *in vitro*
and *in vivo*.
Front. Cell Dev. Biol. 9:655559.
doi: 10.3389/fcell.2021.655559

¹ Tianjin Key Laboratory on Technologies Enabling Development of Clinical Therapeutics and Diagnostics, School of Pharmacy, Tianjin Medical University, Tianjin, China, ² Department of Otorhinolaryngology Head and Neck, Institute of Otorhinolaryngology, Tianjin First Central Hospital, Tianjin, China, ³ School of Medicine, Tianjin Tianshi College, Tianyuan University, Tianjin, China

Lansoprazole (Lpz) is an FDA-approved proton pump inhibitor (PPI) drug for the therapy of acid-related diseases. Aiming to explore the new application of old drugs, we recently investigated the antitumor effect of Lpz. We demonstrated that the PPI Lpz played a tumor suppressive role in non-small cell lung cancer (NSCLC) A549 cells. Mechanistically, Lpz induced apoptosis and G0/G1 cell cycle arrest by inhibiting the activation of signal transducer and activator of transcription (Stat) 3 and the phosphoinositide 3-kinase (PI3K)/Akt and Raf/ERK pathways. In addition, Lpz inhibited autophagy by blocking the fusion of autophagosomes with lysosomes. Furthermore, Lpz in combination with gefitinib (Gef) showed a synergistic antitumor effect on A549 cells, with enhanced G0/G1 cell cycle arrest and apoptosis. The combination inhibited Stat3 phosphorylation, PI3K/Akt and Raf/ERK signaling, affecting cell cycle-related proteins such as p-Rb, cyclin D1 and p27, as well as apoptotic proteins such as Bax, Bcl-2, caspase-3, and poly (ADP-ribose) polymerase (PARP). *In vivo*, coadministration with Lpz and Gef significantly attenuated the growth of A549 nude mouse xenograft models. These findings suggest that Lpz might be applied in combination with Gef for NSCLC therapy, but further evidence is required.

Keywords: lansoprazole, gefitinib, lung cancer, combination, autophagy

INTRODUCTION

The tumor microenvironment plays a pivotal role in tumor malignancy. The acidic microenvironment strongly contributes to tumor progression by stimulating invasion and metastasis, inhibiting the immune surveillance of cancers, and conferring chemoresistance (Taylor et al., 2015; Ibrahim-Hashim and Estrella, 2019). As an ATP-dependent proton pump, the vacuolar-H⁺ ATPase (V-ATPase) seems to be involved in the acidification of the tumor microenvironment (Spugnini et al., 2015). The V-ATPase proton pump is a multisubunit membrane protein complex

that is present in intracellular membranes, such as lysosomes, endosomes, and secretory vesicles, and in the plasma membranes of specialized cells (Stransky et al., 2016).

Proton pump inhibitors (PPIs) are prodrugs that are activated by acid and are currently used as anti-acid drugs for the treatment of acid-related diseases (Shi and Klotz, 2008; Shin and Kim, 2013); these disorders include peptic ulcer disease, gastroesophageal reflux disease, and idiopathic hypersecretion (Der, 2003). PPIs include omeprazole, esomeprazole, lansoprazole (Lpz), pantoprazole, and rabeprazole (Shi and Klotz, 2008). They act as potent inhibitors of gastric acid pumps and have been used for short- or long-term treatments with very high doses without major side effects (Der, 2003; Martín de Argila, 2005). Several studies have shown that PPIs have antitumor effects against different tumor types; for example, esomeprazole inhibits the proliferation of melanoma cells *in vitro* and reduces tumor growth in human melanoma engrafted mice (De Milito et al., 2010), and Lpz induces cell apoptosis in human breast cancer cells and attenuates tumorigenesis in MDA-MB-231 breast cancer cell xenografted mice (Zhang et al., 2014). In addition, Lpz showed most potent anti-tumor effect when compared to the other PPIs (omeprazole, esomeprazole, Lpz, pantoprazole, and rabeprazole) in human melanoma cells (Lugini et al., 2016); Among several PPIs (omeprazole, esomeprazole, Lpz, and pantoprazole), Lpz was the most effective to induce cell death in breast cancer cells (Zhang et al., 2014). However, the antitumor effects of Lpz in non-small cell lung cancer (NSCLC) have not yet been reported. Therefore, in the present study, we focused on the development of Lpz targeting acidic microenvironments in lung cancer.

Lung cancer is the most common cancer and the leading cause of cancer death in men and is the third most common cancer and the second leading cause of cancer death worldwide (Mao et al., 2016). Lung cancers are divided into two main groups: small-cell lung cancer (13% of the cases) and NSCLC (83% of the cases). Surgery is the major treatment modality for early stage NSCLC; cytotoxic chemotherapy remains a substantial part of therapy for most patients in locally advanced and metastatic stages, and targeted therapies have become standard therapies for patients with NSCLC (Rodríguez-Canales et al., 2016). Epidermal growth factor receptor (EGFR) is overexpressed in 40–80% of NSCLC cases (Rodríguez-Canales et al., 2016). Gefitinib (Gef, Iressa), a small molecule EGFR tyrosine kinase inhibitor, is one of the classical first-line treatment drugs that can benefit certain patients with EGFR-mutant NSCLC. Consistently, Gef inhibits cell growth in PC-9 NSCLC cells with EGFR mutation, with a much higher potency than that in A549 and H226 NSCLC cells with wild type EGFR (Sugita et al., 2015). However, Gef also has adverse effects, such as hypersensitivity myocarditis related to Gef being the probable cause of death (Truell et al., 2005); adding pemetrexed and carboplatin chemotherapy to Gef significantly prolonged both progression-free and overall survival but also increased toxicity (Noronha et al., 2020). The drug combination could reduce the drug use concentration. Based on these theories, we extensively investigated the anticancer activity of Lpz and the antitumor synergistic effect of Lpz in combination with Gef in NSCLC A549 cells.

MATERIALS AND METHODS

Cell Culture

A549 cells were obtained from the Cell Resource Center, Peking Union Medical College (Beijing, China). A549 cells have been authenticated using STR profiling within the last 3 years and A549 cells were confirmed by PCR to be free of mycoplasma contamination. A549 cells were cultured in RPMI 1640 medium containing 10% fetal bovine serum (FBS), 100 U/ml penicillin, and 100 µg/ml streptomycin. Cell cultures were maintained in a humidified atmosphere with 5% CO₂ at 37°C.

Reagents

Lansoprazole and gefitinib were purchased from Selleck Chemicals (Houston, TX, United States) and Target Molecule Corp. (Boston, MA, United States), respectively. Monodansylcadaverine (MDC) and propidium iodide (PI) were obtained from Sigma-Aldrich (St. Louis, MO, United States). A FITC-Annexin V apoptosis detection kit was obtained from BD Bioscience (San José, CA, United States). RPMI 1640 and FBS were purchased from the Biological Industries (Beit Haemek, Israel). Enhanced chemiluminescence (ECL) reagent was purchased from Thermo Fisher Scientific (Waltham, MA, United States). Antibodies specific for p27, p-Rb, cyclin D1, LC3B, p-signal transducer and activator of transcription (Stat) 3, phosphatidylinositol 3-kinase (PI3K)-p110α, PI3K-p110β, p-mammalian target of rapamycin complex 1 (mTORC1) (Ser2448), Akt, p-Akt (Ser473), p-p70 S6 kinase (S6K) (Thr389), p-glycogen synthase kinase 3 (GSK-3)β, poly (ADP-ribose) polymerase (PARP), caspase-3, K-Ras, p-extracellular signal-regulated kinase (ERK)1/2, p-c-Raf, Ki67, β-actin, and horseradish peroxidase-conjugated goat anti-rabbit and horse anti-mouse secondary antibodies were purchased from Cell Signaling Technology, Inc. (Danvers, MA, United States). Antibodies specific for Bcl-2 and Bax were obtained from Santa Cruz Biotechnology, Inc. (Dallas, TX, United States).

Determination of Cell Viability

Cell viability was assessed using the MTT assay as we previously reported, with a small modification (Zhou et al., 2016). Briefly, A549 cells were plated in 96-well culture plates and incubated with various concentrations of Lpz for 48 h, and then 20 µl of MTT (5 mg/ml) was added to each well. After 4 h of incubation, the formazan was dissolved in DMSO, and the optical density (OD) at 490 nm was measured using an iMark microplate reader (Bio-Rad, Hercules, CA, United States).

Flow Cytometric Analysis

The effects of Lpz and Gef on cell cycle distribution and apoptosis in A549 cells were analyzed by flow cytometry. Briefly, A549 cells were seeded in six-well plates and treated with Lpz for 48 h. For cycle analysis, cells were collected and fixed with 75% ethanol at 4°C overnight and stained with PI solution (25 µg/ml). The treated cells were analyzed with a BD Accuri C6 flow cytometer (BD Biosciences, San Jose, CA, United States).

For cell apoptosis analysis, Annexin V-FITC/PI double staining was used as reported by us previously with small modifications (Zhang et al., 2019). After harvesting, the cells were resuspended in binding buffer and incubated with Annexin V-FITC/PI solution in the dark for 15 min. Finally, samples were analyzed using a BD Accuri C6 flow cytometer.

Data were quantified with Flow Jo Software (Tristar, Long Beach, CA, United States).

Measurement of Intracellular Reactive Oxygen Species (ROS) Levels

Intracellular reactive oxygen species (ROS) levels were determined as we reported previously with a small modification (Zhang et al., 2019). The ROS assay kit (Beyotime Biotechnology, China) was used. Briefly, A549 cells were plated in six-well culture plates and treated with various concentrations of Lpz for 24 h. Following the treatment, the cells were harvested and then incubated with 10 μ M of 2',7'-dichlorofluorescein diacetate (DCFH-DA) for 30 min at 37°C. The resulting fluorescent intensity was measured using a BD Accuri C6 flow cytometer.

Wound Healing Assay

The wound healing assay was performed as we reported previously with a small modification (Wang et al., 2018). A549 cells were plated in 24-well plates and incubated overnight to a density of 70–80% in RPMI 1640 medium. Cell monolayers were mechanically wounded with a pipette tip and washed with PBS to remove debris. Then, different concentrations of Lpz were added to cells cultivated with fresh culture containing 2% FBS for 48 h. The wound areas were imaged with a microscope.

Protein Extraction and Western Blotting

Western blot analysis was carried out as we previously reported with small modifications (Shao et al., 2018). Cells were collected with lysis buffer, and the protein concentration of each sample was determined using a BCA protein assay kit. Equal amounts of proteins were separated by sodium dodecyl sulfate-polyacrylamide gel electrophoresis (SDS-PAGE) and were subsequently transferred to PVDF membranes. After being blocked with 5% non-fat milk, the membranes were exposed to specified primary antibodies overnight at 4°C and then incubated with the respective HRP-conjugated secondary antibody for 1 h at room temperature. The binding was visualized by ECL reagents on a Bio-Rad ChemiDoc™ XRS + System (Bio-Rad, Hercules, CA, United States).

Monodansylcadaverine (MDC) Staining

Monodansylcadaverine, a specific marker for autophagic vacuoles, was used to measure whether Lpz induces autophagy. A549 cells were seeded in six-well plates on coverslips overnight, and Lpz was administered for 48 h. The cells were washed with ice-cold PBS and incubated with MDC (50 μ M) for 30 min in the dark at 37°C. Then, the cells were washed twice with PBS, fixed in 4% paraformaldehyde for 10 min, and washed again with PBS. The slides were observed by fluorescence microscopy (BX51, Olympus, Japan).

Analysis of Autophagic Flux

To analyze autophagic influx, A549 cells were transfected with a tandem fluorescent mRFP-GFP-LC3 plasmid using Lipofectamine 2000 according to the manufacturer's instructions. The transfected cells were treated with Lpz for 24 h. The expression of GFP and mRFP was visualized with an Olympus FV1000 laser scanning confocal microscope (Olympus, Tokyo, Japan). Images were acquired using FV10-ASW3.0 software. Autophagic flux was evaluated by the color change of GFP/mRFP.

Nude Mouse Xenograft Tumor Experiments

To establish xenograft tumors *in vivo*, individual mice were injected subcutaneously with A549 cells. When subcutaneous tumors grew to 30 to 50 mm³, the mice were randomized into four groups and treated with Lpz (25 mg/kg) or Gef (80 mg/kg) alone or in combination (Lpz was administered orally 2 h before Gef) every other day for 19 days. The growth of implanted tumors was monitored every other day, and the tumor volumes were calculated. Their body weights were also measured every other day. Mice were sacrificed after 19 days of treatment, and the tumors were excised.

Tumors were fixed in paraformaldehyde for immunohistochemistry (IHC) analysis. For IHC analysis, 5- μ m paraffin sections underwent dewaxing, and endogenous peroxidase was blocked. The sections were heated in an antigen retrieval solution and were then incubated with Ki67 antibody overnight at 4°C, and the bound antibodies were detected with Bond Polymer (anti-rabbit poly-HRP-IgG) and visualized using a diaminobenzidine (DAB) peroxidase substrate. The images were collected using O8 microscope and slide scanner (Precipoint, Germany).

Statistical Analysis

All data are expressed as the means \pm SD of triplicate values. One-way ANOVA followed by Tukey's multiple comparison test was utilized to determine the statistical significance with GraphPad Prism 5 (GraphPad, San Diego, CA, United States). Differences were considered statistically significant when $p < 0.05$.

RESULTS

Antitumor Activity of Lpz in A549 Cells

First, we determined the dose responses to Lpz in different kinds of cancer cell lines, including MDA-MB-231 (human breast cancer), A549 (human NSCLC), U251 (human glioma), SK-Hep1 (human hepatocellular carcinoma), and MCF-7 (breast cancer), by MTT. As shown in **Figure 1A**, cancer cells were treated with Lpz for 48 h, and Lpz inhibited the proliferation of all tested cancer cells and showed the most potent antiproliferative activity in A549 cells. Therefore, we used A549 cancer cells to perform a subsequent antitumor mechanism study of Lpz. Next, A549 cells were treated with Lpz for 24, 48, and 72 h. The proliferation of A549 cells was significantly inhibited by Lpz in a dose- and time-dependent manner, with IC₅₀ values of 110.4 and 69.5 μ M at 48

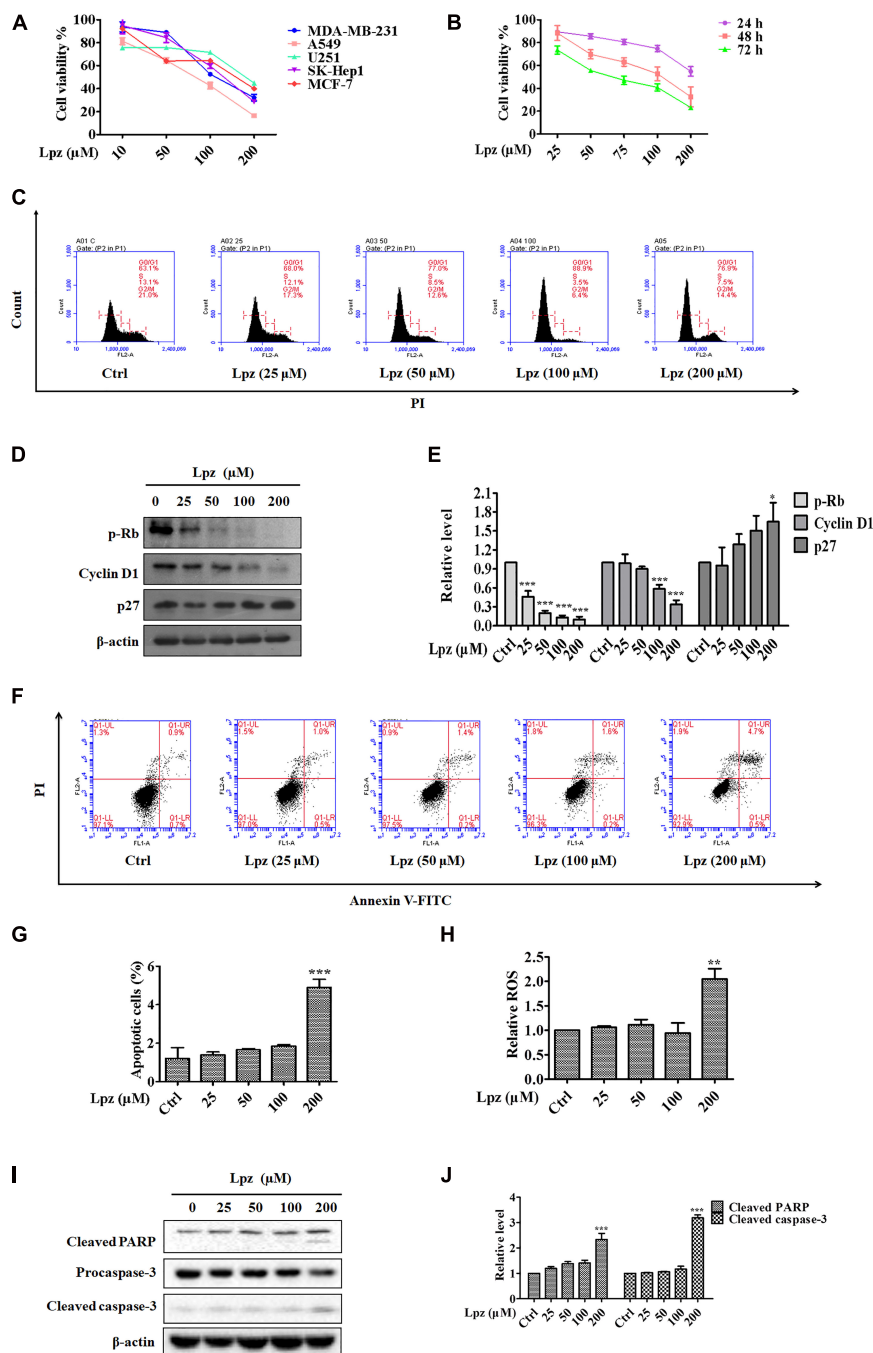


FIGURE 1 | The antitumor effect of Lpz in A549 cells. **(A)** The antiproliferative effect of Lpz on a variety of cancer cells after 48 h. **(B)** Lpz inhibited A549 cell proliferation in a time- and concentration-dependent manner. **(C)** Lpz induced cell cycle arrest at G0/G1 phase. **(D)** Effect of Lpz on G0/G1 cell cycle-related proteins. **(E)** Quantification of the results in panel **(D)**. **(F)** Lpz induced apoptosis in A549 cells. **(G)** The population analysis of the apoptotic cells. **(H)** Lpz enhanced intracellular ROS generation. **(I)** Lpz increased the levels of cleaved PARP and caspase-3. **(J)** Quantification of the results in panel **(I)**. Data shown are the mean \pm SD of three independent experiments. *: $p < 0.05$, **: $p < 0.01$, and ***: $p < 0.001$.

and 72 h, respectively (**Figure 1B**). However, treatment with Lpz did not inhibit 50% of cell viability until 200 μ M at 24 h.

Dysregulation of the cell cycle is a hallmark of cancer that leads to aberrant cellular proliferation. The cell cycle consists of sequential phases that go from quiescence (G0 phase) to

proliferation (G1, S, G2, and M phases) and back to quiescence (Diaz-Moralli et al., 2013). To determine whether Lpz-induced growth inhibition was influenced by cell cycle arrest, A549 cells were incubated with or without Lpz for 48 h, and the cell cycle was examined through flow cytometry. Cell cycle arrest at G0/G1

phase was observed more frequently in the Lpz-treated A549 cells compared with the non-treated cells (**Figure 1C**). The relative percentages of G0/G1 phase cells progressively increased Lpz-treated A549 cells, respectively. p-Rb and a target of CDKs were involved in G1 and the restriction checkpoint. Cyclin D1 affects the function of p-Rb by binding with CDK4 and CDK6 (Wenzel and Singh, 2018). CDK activity is negatively regulated by p27. Therefore, the CDK4/6-cyclin D complex facilitates G1 progression. Western blot analysis also showed that Lpz treatment decreased p-Rb and cyclin D1 but increased p27 expression compared with non-treated cells (**Figures 1D,E**).

Next, the cell apoptosis-inducing effects were analyzed by flow cytometry with Annexin V/PI staining. Apoptosis is a form of programmed cell death, and its molecular signaling pathway is well known. **Figures 1F,G** show increase in the proportions of apoptotic cells of 1.6, 1.5, 1.6, 1.8, and 5.2% after 0, 25, 50, 100, and 200 μ M Lpz treatment, respectively. ROS are potent stimulators of apoptosis (Hayes et al., 2020), therefore, we investigated if Lpz increased ROS or not. A549 cells were treated with Lpz and the intracellular ROS levels were determined by flow cytometer. As indicated in **Figure 1H**, the level of ROS was dramatically enhanced after treatment with Lpz at 200 μ M. The apoptosis pathway involves the activation of a series of caspases (Sankari et al., 2012). Apoptosomes (made up of cytochrome-C, apoptotic protease activating factor-1, and caspase-9) activate the downstream caspase-9/-3 signaling cascade and consequently result in apoptosis (Ou et al., 2017). Caspase-3 cleavage of PARP is a hallmark of apoptotic cell death (Cohen, 1997). Moreover, Western blot analysis showed that the expression levels of cleaved PARP and caspase-3 were distinctly higher in response to Lpz treatment than in the non-treated group (**Figures 1I–J**).

Effect of Lpz on Migration in A549 Cells

Next, a wound healing assay was performed to evaluate the role of Lpz in A549 cell migration. The cell mobility was reflected by wounded areas. After the scratches were formed, the cells were cultivated with different concentrations of Lpz (10, 25, 50, and 75 μ M), pictures were taken at different time points at the same position (0 and 48 h), and the width of the scratch was calculated in A549 cells. To eliminate the possibility that cytotoxicity could influence migration, we chose concentrations lower than the IC₅₀. It is important to highlight that cell migration was assessed at lower concentrations to avoid cytotoxic effects. Thus, we chose concentrations of 10, 25, 50, and 75 μ M Lpz incubated with A549 cells. As illustrated in **Figure 2A**, the wound closure incidence was lower in the Lpz exposure group than in the control group ($p < 0.001$) (**Figure 2B**).

Lpz Inhibits Autophagic Flux in A549 Cells

Autophagy describes the intracellular lysosomal degradation and recycling of proteins and organelles. To confirm whether Lpz affects autophagy in A549 cells, we determined the effect of Lpz on autophagy with various assays over 48 h. First, the number of autophagic vacuoles was detected in an MDC incorporation assay. Under MDC staining, the number of bright

green fluorescent dots increased significantly after treatment with Lpz compared with non-treated cells (**Figure 2C**).

Next, we used Western blotting to investigate the conversion of LC3B I to LC3B II in control and Lpz-treated A549 cells. A549 cells were treated with different concentrations of Lpz for 48 h, and cell lysates were collected for immunoblot analysis with LC3B antibody. The increased level of LC3B II has been used to represent the extent of autophagy. As shown in **Figure 2D**, the conversion of LC3B I to LC3B II protein expression was increased by Lpz treatment in a concentration-dependent manner.

The dynamic process of autophagy consists of three parts: autophagosome formation, fusion of autophagosomes with lysosomes, and degradation (Zhang et al., 2013). To evaluate the dynamic influence of Lpz on the autophagic flux process, A549 cells were infected with mRFP (monomeric red fluorescent protein)-GFP (green fluorescent protein)-tagged LC3. The acidic pH inside the autolysosome quenches the fluorescent signal of GFP; in contrast, mRFP is not quenched in autolysosomes. Therefore, autophagosomes and autolysosomes are labeled with yellow (mRFP and GFP) and red (mRFP only) signals ("puncta"), respectively (Maulucci et al., 2015). Therefore, if most puncta exhibit both red and green signals, autophagy is impaired. Non-treated cells revealed few yellow dots. However, Lpz treatment led to an obvious increase in the number of yellow dots, and most of the green puncta were colocalized with red puncta (**Figure 2E**), indicating that Lpz inhibited autophagic flux in A549 cells in a concentration-dependent manner.

To further confirm that Lpz indeed attenuates autophagy, we further examined p62, a marker of autophagolysosomal levels, and the expression and conversion of LC3B I into LC3B II in control and Lpz-treated cells in the presence or absence of the specific V-ATPase inhibitor bafilomycin A1 (Baf-A1) by Western blot analysis. p62 is a selective autophagy substrate and is continuously degraded by autophagy (Johansen and Lamark, 2011). A549 cells were pre-treated with or without 0.1 μ M Baf-A1 for 4 h and were then further treated with 100 μ M Lpz for 4 h. Lpz treatment resulted in a significant increase in the p62 expression level compared with the control; Baf-A1 also increased the expression of p62. However, Lpz in combination with Baf-A1 treatment did not reverse the Baf-A1-induced conversion of LC3B I to LC3B II, and the level of p62 was non-significant (**Figures 2F,G**). These findings demonstrated that Lpz suppressed the fusion of autophagosomes with lysosomes.

Effect of Lpz on the Phosphorylation of Stat3, PI3K/Akt, and the Raf/ERK Pathway in A549 Cells

To verify the antitumor mechanism of Lpz, we detected the effect of Lpz on the phosphorylation of Stat3, PI3K/Akt, and the Raf/ERK pathway. Stat3 is an important class of transcription factors that have been implicated in a wide variety of essential biological processes, including cell cycle progression, survival and angiogenesis (Chai et al., 2016; Srivastava and DiGiovanni, 2016). Therefore, we examined the activation of Stat3 using Western blotting. The results showed that Stat3 was potentially phosphorylated in non-treated A549 cells, while

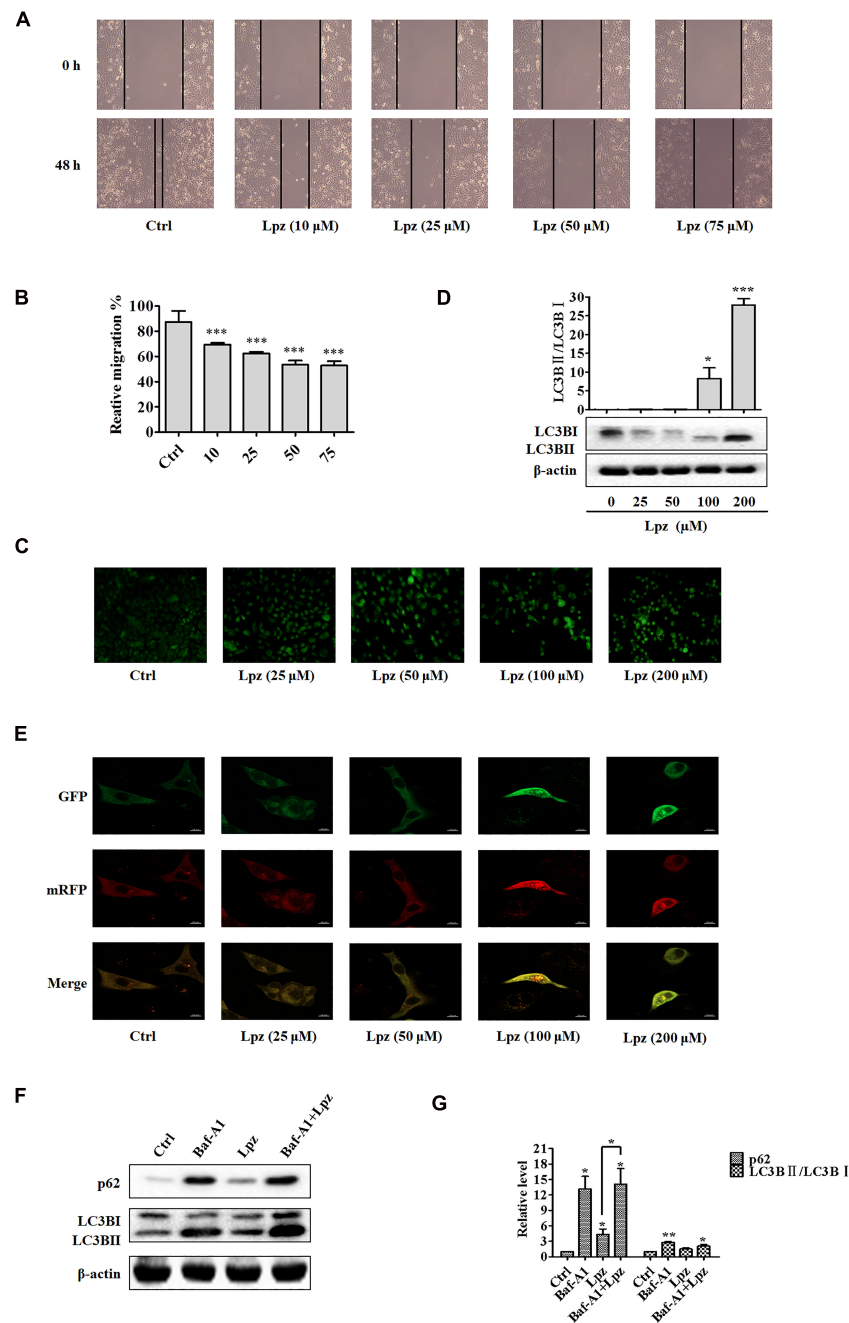


FIGURE 2 | Lansoprazole inhibits migration and autophagy in A549 cells. **(A)** Representative images depicting the wound healing ability of A549 cells with or without Lpz treatment. **(B)** Quantification of the results in panel **(A)**. **(C)** Observation of autophagic vesicle formation by MDC staining. **(D)** Western blot analysis of the levels of LC3B in the absence or presence of Lpz. **(E)** Lpz suppresses autophagic flux in A549 cells. **(F)** Western blot analysis of the levels of p62 and LC3B in the presence of Lpz or Baf-A1 alone or in combination. **(G)** Quantification of the results in panel **(F)**. Data shown are the mean \pm SD of three independent experiments. *: $p < 0.05$, **: $p < 0.01$, and ***: $p < 0.001$.

this phosphorylation of Stat3 was inhibited by Lpz treatment (**Figures 3A,B**).

The PI3K/Akt pathway is one of the major intracellular signaling pathways responsible for promoting cell survival. Therefore, we investigated the effect of Lpz on the PI3K/Akt pathway in A549 cells. The results showed that Lpz significantly

reduced the levels of PI3K 110 α and 110 β , which are PI3K isoforms (**Figures 3A,B**). Furthermore, we examined the phosphorylation levels of PI3K downstream effectors, including Akt, mTORC1, p70 S6K, and GSK-3 β . As shown in **Figures 3A,C**, the phosphorylation of Akt was markedly decreased by Lpz compared with the vehicle control. However, the total Akt

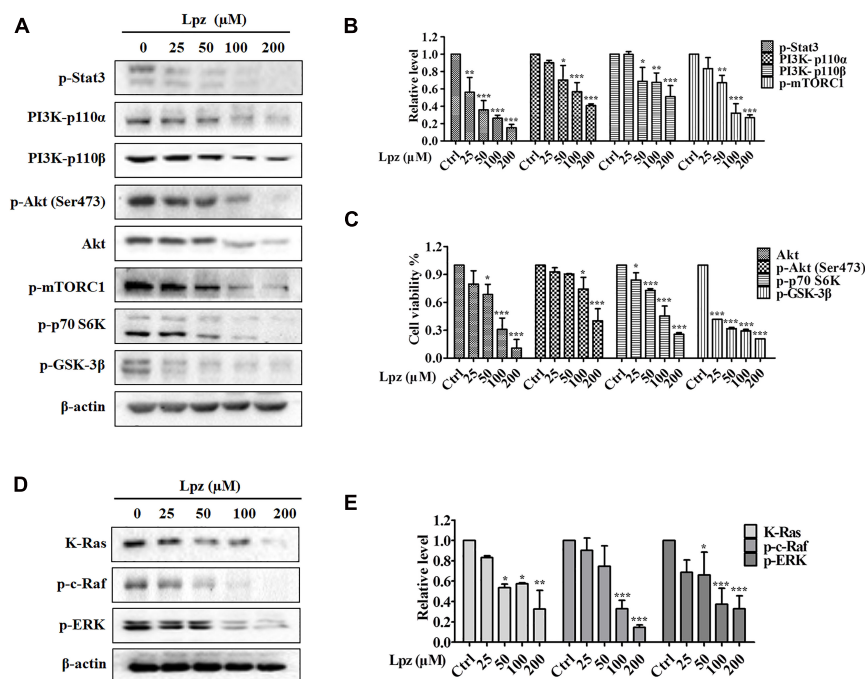


FIGURE 3 | Lansoprazole inhibits phosphorylation of the Stat3, PI3K/Akt/mTOR, and Ras/Raf/ERK pathways. **(A)** Lpz downregulated the phosphorylation of Stat3, Akt, mTOR, p70 S6K, and GSK-3 β and the expression of PI3K. **(B,C)** Quantification of the results in panel **(A)**. **(D)** Lpz suppressed the expression of K-Ras and the phosphorylation of c-Raf and ERK. **(E)** Quantification of the results in panel **(D)**. Data shown are the mean \pm SD of three independent experiments. *: $p < 0.05$, **: $p < 0.01$, and ***: $p < 0.001$.

level was also suppressed by Lpz treatment. In addition, the phosphorylation levels of mTORC1, p70 S6K, and GSK-3 β were also downregulated in cells treated with Lpz.

The Ras/Raf/MEK/ERK pathway also plays a pivotal role in cell survival during various stages of cancer. We further validated the effect of Lpz on the Ras/Raf/ERK pathway in A549 cells. K-Ras level was depressed by Lpz treatment in a concentration-dependent manner. Concomitantly, the phosphorylation levels of Raf and ERK were also upregulated in non-treated A549 cells, and these levels were reduced by the addition of Lpz compared with non-treated cells (**Figures 3D,E**).

Synergistic Effect of Lpz and Gef in A549 Cells *in vitro*

Lansoprazole has shown potent antitumor activity in A549 cells; thus, we asked whether the combination of Lpz and the current anticancer drug would produce synergistic antitumor activity in lung cancer. Currently, Gef is still the classical drug used in the clinic against NSCLC. Therefore, we next investigated whether Lpz could synergize with Gef in A549 cells. To analyze the synergistic effect, Chou and Talalay's method (Chou, 2010) was used. As a first approach to test this hypothesis, we analyzed the antiproliferative effect of Gef in A549 cells. Cells were treated with Gef for 48 h, and Gef suppressed cell proliferation with an IC_{50} value of 15.83 μ M (data not shown). Then, drug combinations were carried out by altering the ratio of Lpz to Gef ($1 \times IC_{50Lpz}$: $1 \times IC_{50Gef}$; $1/2 \times IC_{50Lpz}$: $1 \times IC_{50Gef}$) and using a series of drug

combinations (20, 40, 60, 80, and 100% of the IC_{50} value of each drug). In Lpz and Gef combinations, cells were pre-treated with Lpz for 2 h and were then treated with Gef for further 48 h. As shown in **Figure 4A**, the combination of Lpz and Gef when the ratio was $1 \times IC_{50Lpz}$: $1 \times IC_{50Gef}$ or $1/2 \times IC_{50Lpz}$: $1 \times IC_{50Gef}$ led to greater inhibitory effects of proliferation compared with drug alone. The combination index (CI), which describes the interaction between drugs, was analyzed, and the ED50, ED75, and ED90 values were calculated with CalcuSyn software. When $CI < 1$ at the indicated fraction affected (Fa) points, their combination exhibited synergism. To reduce the concentration of Lpz, we chose an 80% ratio of $1/2 \times IC_{50Lpz}$: $1 \times IC_{50Gef}$. Therefore, the concentrations of Lpz and Gef used were 44 and 12.66 μ M, respectively (**Figure 4A**).

To understand the action of these therapeutic strategies, we investigated the combined effect of Lpz and Gef on the cell cycle progression of A549 cells. As shown in **Figures 4B,C**, treatment with the combination of Lpz and Gef caused a significant increase in the proportion of cells in the G0/G1 phase compared with the Lpz or Gef alone group. Consistent with these results, the combination treatment significantly reduced the levels of phosphorylated Rb and cyclin D1, while the p27 level was increased compared with that of Lpz or Gef alone (**Figures 4D,E**).

Furthermore, Lpz or Gef alone did not potently increase the percentages of apoptotic cells, while treatment with a combination of Lpz and Gef significantly increased the percentages of apoptotic A549 cells (**Figures 4F,G**). There are two groups of Bcl-2 family proteins, pro- and antiapoptotic proteins,

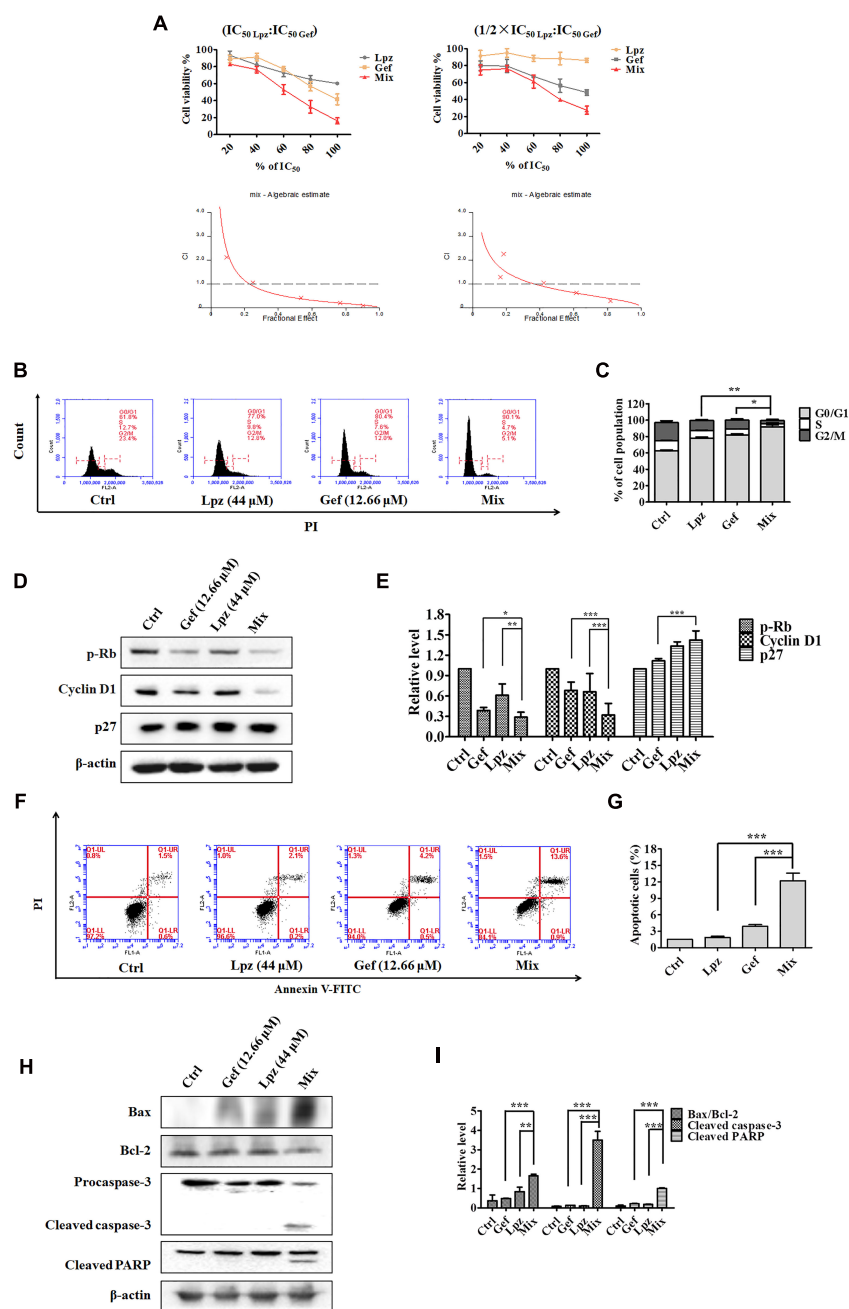


FIGURE 4 | Antitumor effect of Lpz in combination with Gef on A549 cells. **(A)** A549 cells were treated with Lpz and Gef (20, 40, 60, 80, or 100% IC₅₀ values of each drug), either alone or in combination for 48 h. In particular, in the combination groups, cells were pre-treated with Lpz for 2 h and were then treated with Gef for 48 h. Two fixed ratios of IC₅₀ lansoprazole:IC₅₀ gefitinib and 1/2 × IC₅₀ lansoprazole:IC₅₀ gefitinib were used. The combined effect was analyzed using CalcuSyn software, and the resulting CI-Fa plots are shown for A549 cells. **(B)** Lpz combined with Gef obviously arrested the A549 cell cycle in G0/G1 phase compared with either Lpz or Gef alone. **(C)** Quantification of the results in panel **(B)**. **(D)** Identification of the G0/G1-related proteins by Western blot. **(E)** Quantification of the results in panel **(D)**. **(F)** Lpz in combination with Gef facilitates A549 cell apoptosis. **(G)** Quantification of the results in panel **(F)**. **(H)** Identification of the apoptosis-related proteins by Western blot. **(I)** Quantification of the results in panel **(H)**. Data shown are the mean ± SD of three independent experiments. *: $p < 0.05$, **: $p < 0.01$, and ***: $p < 0.001$.

and cell health relies on the balance among these proapoptotic and antiapoptotic Bcl-2 proteins (Sankari et al., 2012; Goldar et al., 2015). As shown in **Figures 4H,I**, the combination of Lpz and Gef substantially enhanced the ratio of Bax (proapoptotic

protein)/Bcl-2 and the levels of cleaved caspase-3 and cleaved PARP compared with treatment with Lpz or Gef alone.

We next examined the effect of the Lpz and Gef combination on the Stat3, PI3K, and Raf/ERK pathways. Western blot analysis

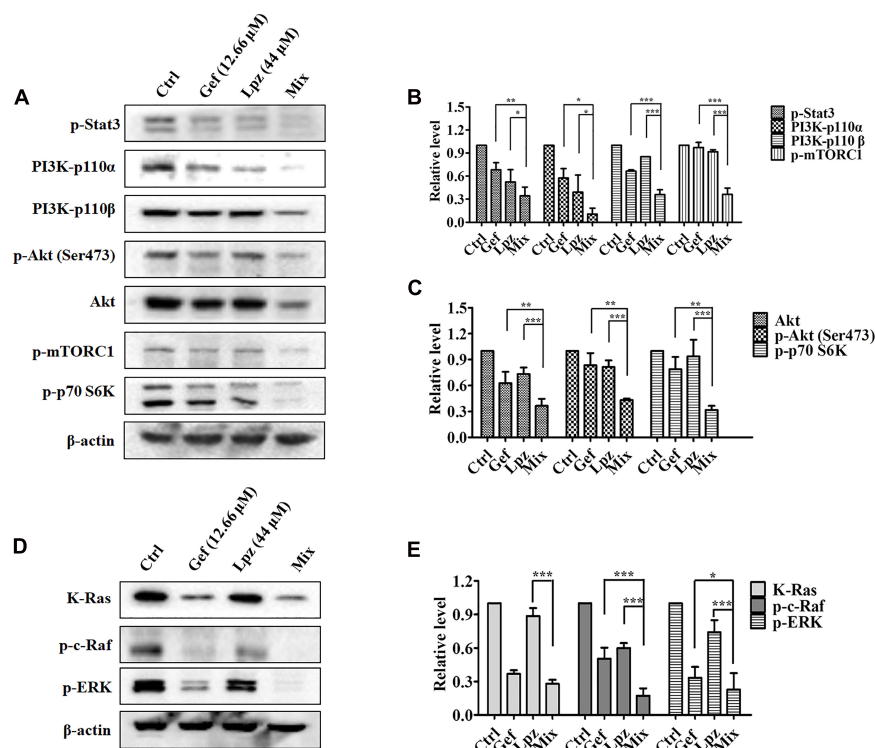


FIGURE 5 | The combination of Lpz and Gef synergistically inhibits phosphorylation of the Stat3, PI3K/Akt/mTOR, and Ras/Raf/ERK pathways. **(A)** Lpz and Gef suppressed the phosphorylation of Stat3, Akt, mTOR, and p70 S6K and the expression of PI3K. **(B,C)** Quantification of the results in panel **(A)**. **(D)** Lpz and Gef suppressed the expression of K-Ras and phosphorylation of c-Raf and ERK. **(E)** Quantification of the results in panel **(D)**. Data shown are the mean \pm SD of three independent experiments. *: $p < 0.05$, **: $p < 0.01$, and ***: $p < 0.001$.

revealed that Lpz in combination with Gef decreased Stat3 phosphorylation (Figures 5A,B). PI3K 110α and 110β were positively expressed in non-treated cells, whereas they were downregulated by Lpz in combination with Gef treatment. Furthermore, Lpz in combination with Gef suppressed Akt phosphorylation. However, the combination treatment had an evident influence on the total Akt. mTORC1 and p70 S6K, important molecules downstream of Akt, were found to be obviously decreased by Lpz in combination with Gef treatment (Figures 5A,C).

Furthermore, we also performed Western blotting to analyze the effect of Lpz in combination with Gef on the Raf/ERK pathway. As shown in Figures 5D,E, a markedly high expression of K-Ras in A549 cells was observed, but this expression significantly decreased to 27.5% after Lpz and Gef combination treatment. In addition, the combination treatment led to the downregulation of Raf and ERK phosphorylation compared with the Lpz or Gef alone group.

Effect of Lpz Alone or in Combination With Gef on Tumor Growth *in vivo*

To further investigate the antitumor efficacy of Lpz in combination with Gef *in vivo*, we studied the effect of oral administration of Lpz and Gef in A549 cell-injected tumor xenografts. A549 cells were subcutaneously injected

into six-week-old BALB/c nude mice. When tumors were approximately 30–50 mm³, mice were divided randomly into four groups of four animals, and drug intervention was initiated. Mice were orally administered 25 mg/kg Lpz, 80 mg/kg Gef, or the two in combination every other day. After 19 days of oral administration, mice were sacrificed, and representative tumor images are shown in Figure 6A. As shown in Figure 6B, treatment with Lpz inhibited the growth of lung tumors compared with untreated control xenografts, and combining Lpz and Gef decreased tumor growth compared with Lpz or Gef alone. Oral administration of Lpz or Gef did not change the mouse body weight (Figure 6C).

Hematoxylin and eosin (H&E) staining was performed to determine tissue morphology. Immunostaining of Ki67 was used to determine tumor cell proliferation. Lpz positively reduced tumor cell proliferation compared with the non-treated control group (Figure 6D). Furthermore, the antiproliferative effect was potentiated when mice were treated concomitantly with Lpz and Gef compared with the Lpz or Gef alone group.

DISCUSSION

Vacuolar-H⁺ ATPase mediates various functions in tumors. V-ATPase contributes to lower extracellular pH and activates extracellular metalloproteinases that promote

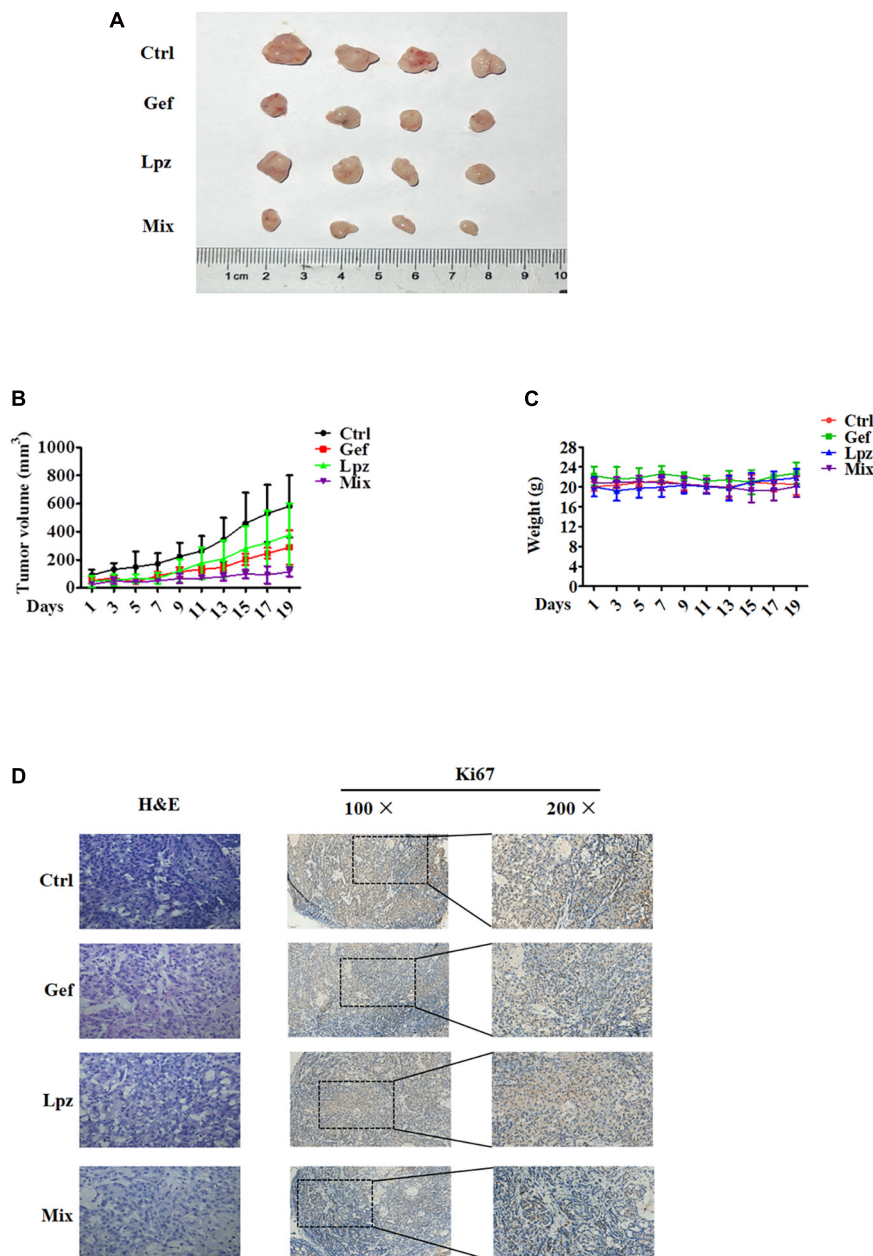


FIGURE 6 | Lansoprazole in combination with Gef reduces the growth of A549 subcutaneous xenografts. Equal amounts of A549 cells were injected subcutaneously into nude mice. Once the tumor volume grew to 30–50 mm³, mice were randomized into four groups and treated with Lpz (25 mg/kg) or Gef (80 mg/kg) either alone or in combination (Lpz was administered orally 2 h before Gef) every other day for 19 days. **(A)** Representative images of the tumors removed from nude mice. **(B)** Quantification of tumor volume. **(C)** No significant differences in weight were found between the Lpz-, Gef-, or combination-treated groups. **(D)** Immunohistochemical staining of Ki67 in tumor tissues of different groups.

tumor proliferation, motility and invasion, resulting in enhanced malignancy ability. Also, the abnormal pH gradient characterizing tumor cells is tuned by different ion/proton pumps such as vacuolar V-ATPase (Nishi and Forgac, 2002; De Milito et al., 2010). Pre-treatment of PPIs could inhibit V-ATPase and increase both extracellular pH and pH of lysosomal organelles (De Milito and Fais, 2005). The antitumor efficacy and mechanistic action of V-ATPase inhibitors have

been reported in both human and murine models encompassing many tumor types; for example, omeprazole induces cell death of human B-cell tumors through severe alteration of pH gradient regulation, and the growth of human B-cell lymphomas in xenograft mice treated with omeprazole is significantly reduced compared with that in control animals (De Milito et al., 2007). Oral administration of V-ATPase inhibitors is efficacious in ameliorating osteolysis induced by metastatic breast cancer

(Niikura, 2007), and inhibiting V-ATPase function through RNA interference can effectively retard cancer growth and prevent cancer metastasis by decreasing proton extrusion and downregulating gelatinase activity (Lu et al., 2005).

In this study, we investigated the antitumor activity of Lpz alone or in combination with Gef in A549 lung cancer cells. Lpz showed an excellent antitumor effect on A549 cells in our present work. The cell cycle is a complex sequence of events responsible for proper cell division into genetically identical daughter cells; therefore, the cell cycle is essential for cell growth and reproduction (Diaz-Moralli et al., 2013; Wenzel and Singh, 2018). Cells can enter the first gap phase G1 from the quiescent state G0. Our present results showed that Lpz treatment induced significant G0/G1 phase arrest in A549 cells. During G1 phase, D-type cyclins (D1, D2, and D3) promote CDK4 and CDK6 activation (Bonelli et al., 2019). D-type cyclins bind to CDK4/6, forming complexes that are stabilized by p27 (Goel et al., 2018). CDK4/6-cyclin D complexes enter the nucleus and phosphorylate Rb (Goel et al., 2018; Bonelli et al., 2019). We found that p-Rb and cyclin D1 were decreased after Lpz treatment, while p27 expression was elevated with Lpz treatment compared with the non-treated control group in the present study. Another interesting finding is the occurrence of apoptosis after Lpz treatment, and this efficacy was extreme when the concentration was 200 μ M. In addition, Lpz potently increased level of intracellular ROS, particularly at 200 μ M. Misbalancing of the fine-tuning between the levels of ROS and endogenous antioxidants could induce oxidative stress and, in worse conditions, apoptosis (Sinha et al., 2013). Apoptosis is recognized as the most important form of cell death and involves multiple factors. Induction of apoptosis is conducted by two main apoptotic pathways, including intrinsic and extrinsic pathways (Sankari et al., 2012). The intrinsic pathway is mitochondrial-mediated apoptosis, which is mediated by cytochrome C release and the activation of caspase-9 and caspase-3 (Goldar et al., 2015). PARP1 plays an important role in DNA repair (Morales et al., 2014); therefore, inhibition of PARP1 prevents DNA repair and leads to cell death. Western blot analysis also revealed that the cleavage of caspase-3 and PARP was upregulated after Lpz treatment. Connecting all these phenomena suggested that Lpz-mediated cell death involves cell cycle arrest and apoptosis.

After establishing the primary tumor and organized nutrition as well as protection against immune cell attacks, tumor cells have to acquire changes to migrate to distant sites and to establish metastasis (Popper, 2016). In our *in vitro* experiments, we found that treatment with Lpz decreased the migration of A549 cell monolayers. Therefore, these data indicate that Lpz plays an essential role in suppressing the migration of A549 cells.

Emerging evidence suggests that the dysregulation of autophagy has implications in a broad spectrum of human diseases, such as cancer (Zhang et al., 2013). Autophagy is a tightly orchestrated process that sequesters misfolded proteins, damaged or aged organelles, and mutated proteins in double-membrane vacuoles called autophagosomes that ultimately fuse with lysosomes, resulting in the degradation of sequestered content, known as autophagic cargo (Mowers et al., 2018; Onorati et al., 2018). MDCs can accumulate in mature autophagic

vacuoles and are usually used to detect autophagic vacuoles. Lpz treatment resulted in an increase in MDC fluorescence in a concentration-dependent manner. In addition, the conversion of LC3B I to LC3B II was also elevated with Lpz treatment. LC3 II accumulation is a marker of autophagy. These results suggested that Lpz can increase the number of autophagic vacuoles in A549 cells. However, it was unclear whether this was due to enhanced autophagosome accumulation from increased autophagic flux or from decreased autophagic flux due to suppressed autophagosome clearance in the lysosome. It has been reported that pantoprazole, a PPI, appears to inhibit autophagy through a mechanism similar to Baf-A1 in PC3 cells (Tan et al., 2015). Baf-A1, as a potent and specific inhibitor of V-ATPase, prevents the maturation of autophagosomes into autolysosomes by suppressing fusion between autophagosomes and lysosomes (Yamamoto et al., 1998). To confirm the effect of Lpz on autophagy, we also monitored the autophagic flux morphologically traced with mRFP-GFP-LC3. If autophagic flux increases, both yellow and red puncta are increased; if autophagosome maturation into autolysosomes is blocked, only yellow puncta are increased (Maulucci et al., 2015). In the present study, we found that Lpz exposure led to potent blockade of autophagic flux in A549 cells. These results suggest that Lpz lead to the accumulation of autophagosomes by blocking the fusion of autophagosomes with lysosomes, possibly by impairing acidification of the luminal space of lysosomes by inhibiting V-ATPase, thereby suppressing autophagy. Degradation of p62 and LC3II could indicate autophagic flux. Our results revealed that p62 degradation was blocked by Lpz. Furthermore, we found that Baf-A1 in combination with Lpz did not change the Baf-A1-enhanced levels of p62 and LC3B II. The concurrent increases in LC3B II and p62 suggested a blockage of autophagic flux; therefore, it was concluded that Lpz could inhibit autophagy. These findings further suggested that Lpz has potent antitumor effects not only by inducing apoptosis and cell cycle arrest but also by diminishing cell migration and autophagy.

Persistently activated or tyrosine-phosphorylated Stat3 (p-Stat3) is found in 54% of NSCLC primary tumors, suggesting that Stat3 is a promising molecular target for lung cancer. Stat3 is considered to play a tumor-promoting role in NSCLC; for example, a Stat3 inhibitor significantly suppresses the growth of NSCLC tumors by promoting apoptosis and reducing angiogenesis and cell proliferation (Weerasinghe et al., 2007), and miR-98-5p promotes apoptosis and inhibits the migration of A549 cells by downregulating Stat3 expression (Liu et al., 2018). The Stat3 signaling pathway is a multicomponent cascade. It has been reported that Stat3, as a transcription factor, can promote the expression of cyclin D1. Herein, we present evidence showing that Stat3 phosphorylation was markedly reduced with Lpz treatment.

The PI3K/Akt/mTOR pathway is frequently activated in human cancers (Zhao et al., 2017). PI3K phosphorylates phosphatidylinositol 4,5-bisphosphate (PIP2) to phosphatidylinositol 3,4,5-triphosphate (PIP3), a second messenger that in turn activates Akt, a serine/threonine kinase (Thorpe et al., 2015). Class I PI3Ks are heterodimeric proteins that consist of a catalytic subunit and a regulatory subunit. There

are four isoforms of the catalytic subunit: 110 α , 110 β , 110 δ , and 110 γ (Zhao and Vogt, 2008). Therefore, we first investigated the protein expression of upstream members of the PI3K pathway that affect downstream activity, including PI3K isoforms. In the present study, we found that Lpz significantly decreased the levels of PI3K 110 α and 110 β . Additionally, Lpz reduced both the phosphorylation and expression of Akt. Why Lpz attenuates the level of total Akt might be studied in further studies. Activated Akt promotes cell growth by phosphorylation of downstream mTORC1, which phosphorylates p70 S6K and eukaryotic initiation factor 4E binding protein 1 (4EBP1), leading to increased protein synthesis (Sarris et al., 2012; Zhao et al., 2017). We found that Lpz markedly suppressed the phosphorylation of mTORC1 and p70 S6K. Akt signals also regulate inactivation of GSK-3 β (Zhao and Vogt, 2008). In addition, we found that Lpz reduced the phosphorylation of GSK-3 β .

The Ras-regulated Raf-MEK-ERK signaling pathway is deregulated in a variety of cancers, and activation of the terminal kinases in the ERK1/2 cascade results in their accumulation in the nucleus, where they phosphorylate various transcription factors to stimulate or repress gene expression (Kidger et al., 2018). We found that the phosphorylation of c-Raf and ERK was reduced by treatment with Lpz. A549 is a K-RASmut cell line, and we found that the expression of K-Ras was effectively decreased with Lpz. These results demonstrated that Lpz inhibits the proliferation of A549 cells by inhibiting the phosphorylation of Stat3, PI3K/Akt and the Ras/Raf/ERK pathway.

Several studies have indicated that PPIs have promising activity to enhance sensitivity to anticancer drugs, such as Lpz (Lpz pre-treatment), which enhances the therapeutic effects of doxorubicin both by improving its distribution and increasing its activity in solid tumors (Yu et al., 2015); paclitaxel and the Lpz combination (Lpz pre-treatment), which was extremely efficient against metastatic melanoma cells (Azzarito et al., 2015); and the PPI drug esomeprazole, which sensitizes both human osteosarcoma cell lines and xenografts to cisplatin (Ferrari et al., 2013). Gef, approved for therapy of patients with advanced NSCLC, causes G1 arrest and induces apoptosis in A549 cells (Chang et al., 2004). Based on this theory, we investigated Lpz and Gef combination chemotherapy. Our study showed that combining Lpz and Gef represents a therapeutic strategy in A549 lung cancer both *in vitro* and *in vivo*. Treatment with Lpz is usually delivered as pre-treatment in most research papers, including the abovementioned reports. Therefore, we also pre-treated with Lpz in the present study. A549 cells were pre-treated for 2 h with Lpz and were then treated for an additional 48 h with Gef. We found that combined treatment with Lpz and Gef had a significantly greater efficacy against A549 cells than either drug alone. Furthermore, to obtain further insight into the mechanism of operation in solid lung cancers, we used Western blotting to determine the influence of Lpz and Gef in combination. We found that the combination of Lpz and Gef had a synergistic effect against the proliferation of A549 cells by triggering apoptosis and cell cycle arrest.

Consistent with the *in vitro* results, we also found therapeutic activity of Lpz in combination with Gef in human lung cancer xenograft models. Treatment with Lpz or Gef alone led to a reduction in the size of the tumors, and the effect was further enhanced when the two treatments were combined. In addition, immunohistochemical analysis of Ki67 showed that cancer cell proliferation was strikingly reduced upon combined administration of Lpz and Gef. Taken together, these results show that the anticancer efficacy of Lpz combined with Gef is greater than that of either drug used alone. In addition, all of the results further confirm that Lpz alone or in combination with Gef had positive inhibitory effects on the development and progression of NSCLC.

CONCLUSION

In conclusion, the results of this study indicated that Lpz has an antitumor effect in A549 lung cancer by inducing apoptosis and cell cycle arrest, inhibiting migration, and suppressing autophagy by inhibiting the phosphorylation of Stat3 and reducing the activation of the PI3K/Akt and Raf/ERK pathways. Furthermore, Lpz in combination with Gef has shown more potent anticancer activity than either Lpz or Gef alone. Our results provide an experimental foundation for Lpz as a potential treatment for lung cancer.

DATA AVAILABILITY STATEMENT

The raw data supporting the conclusions of this article will be made available by the authors, without undue reservation.

ETHICS STATEMENT

The animal study was reviewed and approved by Laboratory Animal Center of the Institute of Radiation Medicine, Chinese Academy of Medical Sciences.

AUTHOR CONTRIBUTIONS

MJ and DK designed the experiments and acquired funding for the study. XZ, NZ, YH, and XD performed the experiments. XP, WW, ZZ, RW, and YQ provided the technical assistances. XZ and MJ wrote the manuscript. DK edited the manuscript. All authors contributed to the article and approved the submitted version.

FUNDING

This project was supported by grants from National Natural Science Foundation of China (81672809 to MJ, 82061148017, 82073890, and 81673464 to DK), and Tianjin Science and Technology Commission (20JCYBJC00670).

REFERENCES

- Azzarito, T., Venturi, G., Cesolini, A., and Fais, S. (2015). Lansoprazole induces sensitivity to suboptimal doses of paclitaxel in human melanoma. *Cancer Lett.* 356, 697–703. doi: 10.1016/j.canlet.2014.10.017
- Bonelli, M., La Monica, S., Fumarola, C., and Alfieri, R. (2019). Multiple effects of CDK4/6 inhibition in cancer: from cell cycle arrest to immunomodulation. *Biochem. Pharmacol.* 170:113676. doi: 10.1016/j.bcp.2019.113676
- Chai, E. Z., Shanmugam, M. K., Arfuso, F., Dharmarajan, A., Wang, C., Kumar, A. P., et al. (2016). Targeting transcription factor STAT3 for cancer prevention and therapy. *Pharmacol. Ther.* 162, 86–97. doi: 10.1016/j.pharmthera.2015.10.004
- Chang, G. C., Hsu, S. L., Tsai, J. R., Liang, F. P., Lin, S. Y., Sheu, G. T., et al. (2004). Molecular mechanisms of ZD1839-induced G1-cell cycle arrest and apoptosis in human lung adenocarcinoma A549 cells. *Biochem. Pharmacol.* 68, 1453–1464. doi: 10.1016/j.bcp.2004.06.006
- Chou, T. C. (2010). Drug combination studies and their synergy quantification using the Chou-Talalay method. *Cancer Res.* 70, 440–446. doi: 10.1158/0008-5472.can-09-1947
- Cohen, G. M. (1997). Caspases: the executioners of apoptosis. *Biochem. J.* 326(Pt 1), 1–16. doi: 10.1042/bj3260001
- De Milito, A., Canese, R., Marino, M. L., Borghi, M., Iero, M., Villa, A., et al. (2010). pH-dependent antitumor activity of proton pump inhibitors against human melanoma is mediated by inhibition of tumor acidity. *Int. J. Cancer* 127, 207–219. doi: 10.1002/ijc.25009
- De Milito, A., and Fais, S. (2005). Tumor acidity, chemoresistance and proton pump inhibitors. *Future Oncol.* 1, 779–786. doi: 10.2217/14796694.1.6.779
- De Milito, A., Iessi, E., Logozzi, M., Lozupone, F., Spada, M., Marino, M. L., et al. (2007). Proton pump inhibitors induce apoptosis of human B-cell tumors through a caspase-independent mechanism involving reactive oxygen species. *Cancer Res.* 67, 5408–5417. doi: 10.1158/0008-5472.can-06-4095
- Der, G. (2003). An overview of proton pump inhibitors. *Gastroenterol. Nurs.* 26, 182–190. doi: 10.1097/00001610-200309000-00003
- Diaz-Moralli, S., Tarrado-Castellarnau, M., Miranda, A., and Cascante, M. (2013). Targeting cell cycle regulation in cancer therapy. *Pharmacol. Ther.* 138, 255–271. doi: 10.1016/j.pharmthera.2013.01.011
- Ferrari, S., Perut, F., Fagioli, F., Brach Del Prever, A., Meazza, C., Parafioriti, A., et al. (2013). Proton pump inhibitor chemosensitization in human osteosarcoma: from the bench to the patients' bed. *J. Transl. Med.* 11:268. doi: 10.1186/1479-5876-11-268
- Goel, S., Decristo, M. J., McAllister, S. S., and Zhao, J. J. (2018). CDK4/6 inhibition in cancer: beyond cell cycle arrest. *Trends Cell Biol.* 28, 911–925. doi: 10.1016/j.tcb.2018.07.002
- Goldar, S., Khaniani, M. S., Derakhshan, S. M., and Baradaran, B. (2015). Molecular mechanisms of apoptosis and roles in cancer development and treatment. *Asian Pac. J. Cancer Prev.* 16, 2129–2144. doi: 10.7314/apjcp.2015.16.6.2129
- Hayes, J. D., Dinkova-Kostova, A. T., and Tew, K. D. (2020). Oxidative stress in cancer. *Cancer Cell* 38, 167–197. doi: 10.1016/j.ccell.2020.06.001
- Ibrahim-Hashim, A., and Estrella, V. (2019). Acidosis and cancer: from mechanism to neutralization. *Cancer Metastasis Rev.* 38, 149–155. doi: 10.1007/s10555-019-09787-4
- Johansen, T., and Lamark, T. (2011). Selective autophagy mediated by autophagic adapter proteins. *Autophagy* 7, 279–296. doi: 10.4161/auto.7.3.14487
- Kidger, A. M., Sipthorp, J., and Cook, S. J. (2018). ERK1/2 inhibitors: new weapons to inhibit the RAS-regulated RAF-MEK1/2-ERK1/2 pathway. *Pharmacol. Ther.* 187, 45–60. doi: 10.1016/j.pharmthera.2018.02.007
- Liu, H., Wei, M., and Wang, G. (2018). [miR-98-5p promotes apoptosis and inhibits migration by reducing the level of STAT3 in A549 cells]. *Xi Bao Yu Fen Zi Mian Yi Xue Za Zhi* 34, 522–527.
- Lu, X., Qin, W., Li, J., Tan, N., Pan, D., Zhang, H., et al. (2005). The growth and metastasis of human hepatocellular carcinoma xenografts are inhibited by small interfering RNA targeting to the subunit ATP6L of proton pump. *Cancer Res.* 65, 6843–6849. doi: 10.1158/0008-5472.can-04-3822
- Lugini, L., Federici, C., Borghi, M., Azzarito, T., Marino, M. L., Cesolini, A., et al. (2016). Proton pump inhibitors while belonging to the same family of generic drugs show different anti-tumor effect. *J. Enzyme Inhib. Med. Chem.* 31, 538–545. doi: 10.3109/14756366.2015.1046062
- Mao, Y., Yang, D., He, J., and Krasna, M. J. (2016). Epidemiology of lung cancer. *Surg. Oncol. Clin. N. Am.* 25, 439–445. doi: 10.1016/j.soc.2016.02.001
- Martin de Argila, C. (2005). Safety of potent gastric acid inhibition. *Drugs* 65(Suppl. 1), 97–104. doi: 10.2165/00003495-200565001-00013
- Maulucci, G., Chiarpotto, M., Papi, M., Samengo, D., Pani, G., and De Spirito, M. (2015). Quantitative analysis of autophagic flux by confocal pH-imaging of autophagic intermediates. *Autophagy* 11, 1905–1916. doi: 10.1080/15548627.2015.1084455
- Morales, J., Li, L., Fattah, F. J., Dong, Y., Bey, E. A., Patel, M., et al. (2014). Review of poly (ADP-ribose) polymerase (PARP) mechanisms of action and rationale for targeting in cancer and other diseases. *Crit. Rev. Eukaryot. Gene Expr.* 24, 15–28. doi: 10.1615/critrevukaryotgeneexpr.2013006875
- Mowers, E. E., Sharifi, M. N., and Macleod, K. F. (2018). Functions of autophagy in the tumor microenvironment and cancer metastasis. *FEBS J.* 285, 1751–1766. doi: 10.1111/febs.14388
- Niikura, K. (2007). Effect of a V-ATPase inhibitor, FR202126, in syngeneic mouse model of experimental bone metastasis. *Cancer Chemother. Pharmacol.* 60, 555–562. doi: 10.1007/s00280-006-0401-8
- Nishi, T., and Forgac, M. (2002). The vacuolar (H⁺)-ATPases—nature's most versatile proton pumps. *Nat. Rev. Mol. Cell Biol.* 3, 94–103. doi: 10.1038/nrm729
- Noronha, V., Patil, V. M., Joshi, A., Menon, N., Chougule, A., Mahajan, A., et al. (2020). Gefitinib versus gefitinib plus pemetrexed and carboplatin chemotherapy in EGFR-Mutated lung cancer. *J. Clin. Oncol.* 38, 124–136. doi: 10.1200/jco.19.01154
- Onorati, A. V., Dyczynski, M., Ojha, R., and Amaravadi, R. K. (2018). Targeting autophagy in cancer. *Cancer* 124, 3307–3318. doi: 10.1002/cncr.31335
- Ou, L., Lin, S., Song, B., Liu, J., Lai, R., and Shao, L. (2017). The mechanisms of graphene-based materials-induced programmed cell death: a review of apoptosis, autophagy, and programmed necrosis. *Int. J. Nanomedicine* 12, 6633–6646. doi: 10.2147/ijn.s140526
- Popper, H. H. (2016). Progression and metastasis of lung cancer. *Cancer Metastasis Rev.* 35, 75–91. doi: 10.1007/s10555-016-9618-0
- Rodriguez-Canales, J., Parra-Cuentas, E., and Wistuba, I. I. (2016). Diagnosis and molecular classification of lung cancer. *Cancer Treat. Res.* 170, 25–46. doi: 10.1007/978-3-319-40389-2_2
- Sankari, S. L., Masthan, K. M., Babu, N. A., Bhattacharjee, T., and Elumalai, M. (2012). Apoptosis in cancer—an update. *Asian Pac. J. Cancer Prev.* 13, 4873–4878. doi: 10.7314/apjcp.2012.13.10.4873
- Sarris, E. G., Saif, M. W., and Syrigos, K. N. (2012). The biological role of PI3K pathway in lung cancer. *Pharmaceuticals (Basel)* 5, 1236–1264. doi: 10.3390/ph5111236
- Shao, C., Fu, B., Ji, N., Pan, S., Zhao, X., Zhang, Z., et al. (2018). Alisol B 23-acetate inhibits IgE/Ag-Mediated mast cell activation and allergic reaction. *Int. J. Mol. Sci.* 19:4092. doi: 10.3390/ijms19124092
- Shi, S., and Klotz, U. (2008). Proton pump inhibitors: an update of their clinical use and pharmacokinetics. *Eur. J. Clin. Pharmacol.* 64, 935–951. doi: 10.1007/s00228-008-0538-y
- Shin, J. M., and Kim, N. (2013). Pharmacokinetics and pharmacodynamics of the proton pump inhibitors. *J. Neurogastroenterol. Motil.* 19, 25–35. doi: 10.5056/jnm.2013.19.1.25
- Sinha, K., Das, J., Pal, P. B., and Sil, P. C. (2013). Oxidative stress: the mitochondria-dependent and mitochondria-independent pathways of apoptosis. *Arch. Toxicol.* 87, 1157–1180. doi: 10.1007/s00204-013-1034-4
- Spugnini, E. P., Sonveaux, P., Stock, C., Perez-Sayans, M., De Milito, A., Avnet, S., et al. (2015). Proton channels and exchangers in cancer. *Biochim. Biophys. Acta* 1848, 2715–2726. doi: 10.1016/j.bbame.2014.10.015
- Srivastava, J., and DiGiovanni, J. (2016). Non-canonical Stat3 signaling in cancer. *Mol. Carcinog.* 55, 1889–1898. doi: 10.1002/mc.22438
- Stransky, L., Cotter, K., and Forgac, M. (2016). The function of V-ATPases in cancer. *Physiol. Rev.* 96, 1071–1091. doi: 10.1152/physrev.00035.2015
- Sugita, S., Ito, K., Yamashiro, Y., Moriya, S., Che, X. F., Yokoyama, T., et al. (2015). EGFR-independent autophagy induction with gefitinib and enhancement of its cytotoxic effect by targeting autophagy with clarithromycin in non-small cell lung cancer cells. *Biochem. Biophys. Res. Commun.* 461, 28–34. doi: 10.1016/j.bbrc.2015.03.162
- Tan, Q., Joshua, A. M., Saggari, J. K., Yu, M., Wang, M., Kanga, N., et al. (2015). Effect of pantoprazole to enhance activity of docetaxel against human tumour

- xenografts by inhibiting autophagy. *Br. J. Cancer* 112, 832–840. doi: 10.1038/bjc.2015.17
- Taylor, S., Spugnini, E. P., Assaraf, Y. G., Azzarito, T., Rauch, C., and Fais, S. (2015). Microenvironment acidity as a major determinant of tumor chemoresistance: proton pump inhibitors (PPIs) as a novel therapeutic approach. *Drug Resist. Updat.* 23, 69–78. doi: 10.1016/j.drug.2015.08.004
- Thorpe, L. M., Yuzugullu, H., and Zhao, J. J. (2015). PI3K in cancer: divergent roles of isoforms, modes of activation and therapeutic targeting. *Nat. Rev. Cancer* 15, 7–24. doi: 10.1038/nrc3860
- Truell, J. S., Fishbein, M. C., and Figlin, R. (2005). Myocarditis temporally related to the use of gefitinib (Iressa). *Arch. Pathol. Lab. Med.* 129, 1044–1046.
- Wang, Z., Wang, Y., Zhu, S., Liu, Y., Peng, X., Zhang, S., et al. (2018). DT-13 inhibits proliferation and metastasis of human prostate cancer cells through blocking PI3K/Akt pathway. *Front. Pharmacol.* 9:1450. doi: 10.3389/fphar.2018.01450
- Weerasinghe, P., Garcia, G. E., Zhu, Q., Yuan, P., Feng, L., Mao, L., et al. (2007). Inhibition of Stat3 activation and tumor growth suppression of non-small cell lung cancer by G-quartet oligonucleotides. *Int. J. Oncol.* 31, 129–136.
- Wenzel, E. S., and Singh, A. T. K. (2018). Cell-cycle checkpoints and aneuploidy on the path to cancer. *In Vivo* 32, 1–5. doi: 10.21873/invivo.11197
- Yamamoto, A., Tagawa, Y., Yoshimori, T., Moriyama, Y., Masaki, R., and Tashiro, Y. (1998). Bafilomycin A1 prevents maturation of autophagic vacuoles by inhibiting fusion between autophagosomes and lysosomes in rat hepatoma cell line, H-4-II-E cells. *Cell Struct. Funct.* 23, 33–42. doi: 10.1247/csf.23.33
- Yu, M., Lee, C., Wang, M., and Tannock, I. F. (2015). Influence of the proton pump inhibitor lansoprazole on distribution and activity of doxorubicin in solid tumors. *Cancer Sci.* 106, 1438–1447. doi: 10.1111/cas.12756
- Zhang, L., Chen, T., Dou, Y., Zhang, S., Liu, H., Khishignyam, T., et al. (2019). Atorvastatin exerts antileukemia activity via inhibiting mevalonate-YAP axis in K562 and HL60 cells. *Front. Oncol.* 9:1032. doi: 10.3389/fonc.2019.01032
- Zhang, S., Wang, Y., and Li, S. J. (2014). Lansoprazole induces apoptosis of breast cancer cells through inhibition of intracellular proton extrusion. *Biochem. Biophys. Res. Commun.* 448, 424–429. doi: 10.1016/j.bbrc.2014.04.127
- Zhang, X. J., Chen, S., Huang, K. X., and Le, W. D. (2013). Why should autophagic flux be assessed? *Acta Pharmacol. Sin.* 34, 595–599. doi: 10.1038/aps.2012.184
- Zhao, L., and Vogt, P. K. (2008). Class I PI3K in oncogenic cellular transformation. *Oncogene* 27, 5486–5496. doi: 10.1038/onc.2008.244
- Zhao, W., Qiu, Y., and Kong, D. (2017). Class I phosphatidylinositol 3-kinase inhibitors for cancer therapy. *Acta Pharm. Sin. B* 7, 27–37. doi: 10.1016/j.apsb.2016.07.006
- Zhou, Q., Chen, Y., Chen, X., Zhao, W., Zhong, Y., Wang, R., et al. (2016). In vitro antileukemia activity of ZSTK474 on K562 and multidrug resistant K562/A02 cells. *Int. J. Biol. Sci.* 12, 631–638. doi: 10.7150/ijbs.14878

Conflict of Interest: The authors declare that the research was conducted in the absence of any commercial or financial relationships that could be construed as a potential conflict of interest.

Copyright © 2021 Zhao, Zhang, Huang, Dou, Peng, Wang, Zhang, Wang, Qiu, Jin and Kong. This is an open-access article distributed under the terms of the Creative Commons Attribution License (CC BY). The use, distribution or reproduction in other forums is permitted, provided the original author(s) and the copyright owner(s) are credited and that the original publication in this journal is cited, in accordance with accepted academic practice. No use, distribution or reproduction is permitted which does not comply with these terms.



The Role of Tumor-Stroma Interactions in Drug Resistance Within Tumor Microenvironment

Yanghong Ni^{1,2†}, Xiaoting Zhou^{1,2†}, Jia Yang^{1,2}, Houhui Shi^{1,2}, Hongyi Li^{1,2}, Xia Zhao^{2*} and Xuelel Ma^{1*}

¹ Department of Biotherapy, State Key Laboratory of Biotherapy and Cancer Center, West China Hospital, Collaborative Innovation Center of Biotherapy, Sichuan University, Chengdu, China, ² Department of Gynecology and Obstetrics, Development and Related Disease of Women and Children Key Laboratory of Sichuan Province, Key Laboratory of Birth Defects and Related Diseases of Women and Children, Ministry of Education, West China Second Hospital, Sichuan University, Chengdu, China

OPEN ACCESS

Edited by:

Yong Song,
Nanjing University, China

Reviewed by:

Hongzhi Du,
Hubei University of Chinese Medicine,
China
Yinlong Zhang,
National Center for Nanoscience
and Technology (CAS), China

*Correspondence:

Xia Zhao
xia-zhao@126.com
Xuelel Ma
drmaxuelel@gmail.com

[†] These authors have contributed
equally to this work and share first
authorship

Specialty section:

This article was submitted to
Molecular and Cellular Oncology,
a section of the journal
Frontiers in Cell and Developmental
Biology

Received: 04 December 2020

Accepted: 19 April 2021

Published: 20 May 2021

Citation:

Ni Y, Zhou X, Yang J, Shi H, Li H,
Zhao X and Ma X (2021) The Role
of Tumor-Stroma Interactions in Drug
Resistance Within Tumor
Microenvironment.
Front. Cell Dev. Biol. 9:637675.
doi: 10.3389/fcell.2021.637675

Cancer cells resistance to various therapies remains to be a key challenge nowadays. For a long time, scientists focused on tumor cells themselves for the mechanisms of acquired drug resistance. However, recent evidence showed that tumor microenvironment (TME) is essential for regulating immune escape, drug resistance, progression and metastasis of malignant cells. Reciprocal interactions between cancer cells and non-malignant cells within this milieu often reshape the TME and promote drug resistance. Therefore, advanced knowledge about these sophisticated interactions is significant for the design of effective therapeutic approaches. In this review, we highlight cancer-associated fibroblasts (CAFs), tumor-associated macrophages (TAMs), tumor-associated neutrophils (TANs), myeloid-derived suppressor cells (MDSCs), T-regulatory lymphocytes (Tregs), mesenchymal stem cells (MSCs), cancer-associated adipocytes (CAAs), and tumor endothelial cells (TECs) existing in TME, as well as their multiple cross-talk with tumor cells, which eventually endows tumor cells with therapeutic resistance.

Keywords: tumor microenvironment, antineoplastic drug resistance, cell-cell interplays, CAFs, TAMs, MSCs

INTRODUCTION

Over decades, cancer has always been a major public health problem worldwide. According to the statistics reported by the American Cancer Society in 2020, there are nearly 1.8 million new cancer cases and 600 thousand cancer deaths in the United States (Siegel et al., 2020). In general, antitumor treatments mainly include surgery, chemotherapy, radiotherapy, immunotherapy, hormone therapy and targeted therapy. Patients can obtain more obvious effects in the initial stage of treatment, while the emergence of drug resistance often becomes an inevitable obstacle to clinical recovery in the late stage. For a long time, scientists focused on tumor cells themselves for the mechanisms of acquired drug resistance, such as the up-regulation of drug efflux pump protein (Amawi et al., 2019), epigenetic abnormalities (Shah and Rawal, 2019), oncogenic mutations and tumor heterogeneity etc. (Hientz et al., 2017; Zhang H. et al., 2017; Vaidya et al., 2020). The concept of tumor microenvironment (TME) was first proposed by Stephen Paget who indicated that the relationship between breast cancer and its microenvironment is like “seed and soil” (Paget, 1989).

TME refers to the local biological environment where tumor cells exist and the number of cancer cells varies from 5 to 100% (Ambrose et al., 2015). It is currently considered to be an acidic and hypoxic milieu infiltrated by cancer cells and accessory cells, including stromal cells, endothelial cells, immune cells, mesenchymal cells, adipocytes and pericytes, as well as extracellular matrix and cytokines (Hui and Chen, 2015; Yamaguchi and Perkins, 2018).

Tumor microenvironment serves as safeguard to tumor cells by providing mechanical support or secreting different cytokines to evade treatment (Figure 1; Kodet et al., 2018). Diverse heterogeneous cells along with their secretory cytokines constitute a complex network, which allows tumor cells to proliferate rapidly, maintain stemness, insensitive to medication and escape from immune surveillance. In fact, non-inherent-adaptive resistance, also called non-cell-autonomous resistance, is therapeutically dependent (Calcinotto et al., 2018). TME is involved in the initiation and maintenance of non-cell autonomous resistance by a variety of mechanisms, including hypoxia, low PH, shifts and polarizations in the immune cell population, vascular abnormalities and diverse stroma cells-derived secretomes, exosomes, soluble factors. In order to deeply understand progression and drug resistance of tumor cells, a thorough knowledge of the interactions between tumor cells and their microenvironment is needed. Therefore, we reviewed a series of non-malignant cells constituting the tumor microenvironment and how they interplay with tumor cells to promote therapeutic resistance with an expectance to spark new ideas of designing more specific approaches for cancer.

CANCER ASSOCIATED FIBROBLASTS (CAFs) AND DRUG RESISTANCE

Cancer associated fibroblasts (CAFs) are one of the most important components of TME. Numerous researches have suggested its role in forming the communication networks with tumor cells and other elements in TME, which is responsible for therapeutic resistance in pancreatic cancer, colorectal neoplasm, breast cancer, ovarian neoplasm, lung cancer, gastric cancer and so on (Mao et al., 2015; Zhou B. et al., 2016; Wen et al., 2017; Cazet et al., 2018; Tang et al., 2018; Wei et al., 2018; Yi et al., 2018; Hu et al., 2019; Wang L. et al., 2019). The origins of CAFs are diverse. In addition to the normal activated fibroblasts, marked by the expression of α -smooth muscle actin (α -SMA), CAFs can also evolve from other cell types, such as bone marrow-derived cells (BMDCs) (Mishra et al., 2008), epithelial cells undergone epithelial-mesenchymal transition (EMT) (Kalluri and Neilson, 2003), endothelial cells following endothelial-to-mesenchymal transition (EndMT) (Zeisberg et al., 2007), adipocytes and stellate cells (Yin et al., 2013). As a result, the subgroups of CAFs are highly heterogeneous which makes it difficult to identify a specific population of CAFs in TME (Fiori et al., 2019). Currently recognized biological hallmarks of CAFs include α -SMA, fibroblast-specific protein 1 (FSP1/S100A4), platelet-derived growth factor receptor (PDGFR) and type-I collagen etc. (Sugimoto et al., 2006).

Briefly, the intricate mechanisms of antineoplastic drug resistance mediated by CAFs can be summarized into the following aspects: (1) secreting soluble factors; (2) remodeling extracellular matrix (ECM); (3) reprogramming the metabolic process of tumor cells; (4) inducing epigenetic modifications of tumor cells; (5) delivering exosomes.

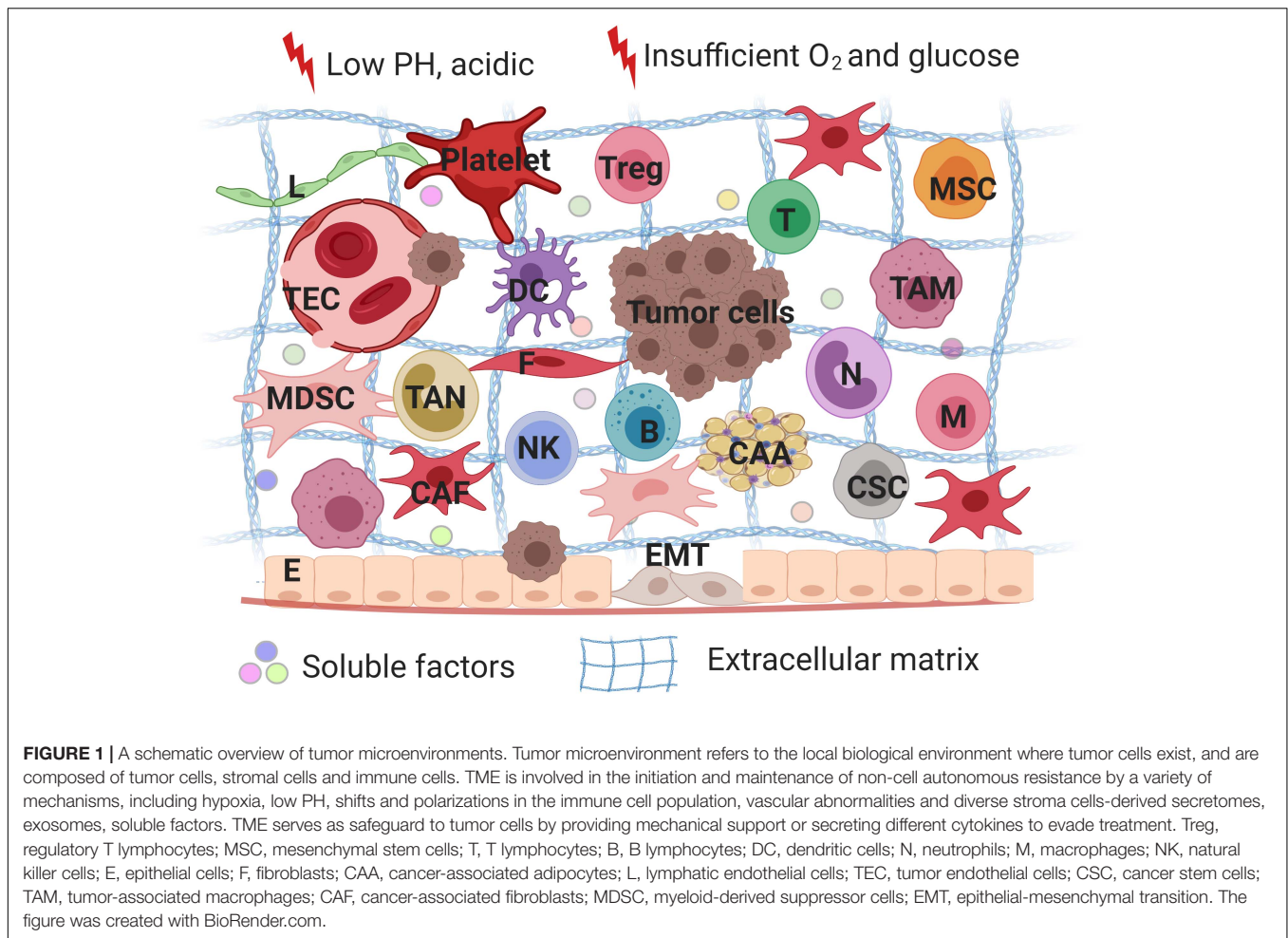
Secreting Soluble Factors

It has been proven that CAFs can secrete various cytokines or factors which enable to activate a series of signaling cascades, leading to drug resistance and tumor cells relapse eventually. CAFs secrete diverse growth factors (including fibroblast growth factor, hepatocyte growth factor, transforming growth factor, and stromal cell derived factor), cytokines (such as IL-6, IL-8, IL-10 etc.), chemokines and protease (Figure 2; Mathot et al., 2017).

IL-6 was described to induce drug resistance. Multiple pathways such as nuclear factor- κ B (NF- κ B), JAK/STAT3, PI3K/AKT have been activated under therapeutic pressure in breast cancer and non-small cell lung cancer (Mao et al., 2015; Shien et al., 2017). Secretion of IL-6 causes the upregulation of C-X-C motif chemokine receptor 7 (CXCR7) through STAT3/NF- κ B pathway. The expression of CXCR7 in esophageal squamous cell carcinoma tissues from chemotherapy resistant patients was significantly higher than that of chemotherapy sensitive patients (Qiao et al., 2018). In addition, the potential of IL-6 to drive epithelial-mesenchymal transition (EMT) has been identified in esophageal adenocarcinoma (Ebbing et al., 2019). IL-8 is another cytokine relating to CAFs. High levels of IL-8 were detected in gastric cancer patients who were insensitive to platinum-based therapy, which was associated with NF- κ B activation and increased expression of ATP-binding cassette subfamily B member 1 (ABCB1) (Zhai et al., 2019). Moreover, in gastric cancer and lung adenocarcinoma, CAFs drive chemoresistance through IL-11 secretion via IL-11/STAT3/Bcl2 signaling pathway (Tao et al., 2016; Ma et al., 2019).

Stromal cell derived factor-1 (SDF-1) was found to be overexpressed in CAFs and played an essential role in tumor cell metastasis and chemoresistance by activating its receptor chemokine receptor 4 (CXCR4) (Orimo and Weinberg, 2006; Teng et al., 2016; Zou et al., 2017). The expression level of SDF-1 in CAFs was regulated by microRNA mir-1 negatively, with NF- κ B and Bcl-xL signaling pathways involved in lung cancer chemoresistance (Li et al., 2016). Wei et al. found that SDF-1 secreted by CAFs promoted chemoresistance through paracrine induction of special AT-rich sequence-binding protein 1 (SATB-1) in pancreatic tumor cells. In turn, SDF-1/CXCR4/SATB-1 axis helped to maintain CAFs characteristics. Therefore, a reciprocal feedback loop was formed (Wei et al., 2018).

Transforming growth factor- β (TGF- β) expression in cancers is generally regarded as an important therapeutic target because it plays a key role in regulating the proliferation, differentiation and survival of cancer cells (Ciardiello et al., 2020; Li et al., 2020). CAFs conferred esophageal squamous cell carcinoma cells significant chemoresistance by activating FOXO 1, a member of the forkhead transcription factors in the O-box sub-family, inducing the secretion of TGF- β 1 (Zhang H. et al., 2017).



Hypoxia-inducible factor (HIF-1 α) has been shown to synergize with CAFs paracrine signals, namely TGF- β 2, to activate hedgehog transcription factor GLI2 in cancer stem cells (CSCs), leading to enhanced stemness/dedifferentiation and intrinsic resistance to chemotherapy of colorectal cancer (Tang et al., 2018). Apart from their assembly effect, CAFs also play a part in HIF-1 pathway modulation which mediates the photodynamic treatment resistance of colorectal cancer (Lamberti et al., 2019).

Hepatocyte growth factor (HGF) is one of the growth factors derived from CAFs. Recent evidence has revealed the role of HGF in transmitting resistance to epidermal growth factor receptor (EGFR) targeted therapy in lung cancer (Kasahara et al., 2010; Yi et al., 2018). HGF was identified to be a major mediator of CAFs induced resistance to EGFR tyrosine kinase inhibitor (EGFR-TKI) (Apicella et al., 2018; Suzuki et al., 2019). HGF derived from CAFs activated the c-Met/PI3K/Akt and glucose-regulated protein 78 (GRP78) pathways of SKOV3 and HO-8910 cells to attenuate the inhibition of cell proliferation and apoptosis caused by paclitaxel (PAC). Furthermore, HGF induced drug resistance has been validated in nude mice (Deying et al., 2017).

Cancer-associated fibroblasts have been found to constrict cisplatin-induced ovarian cancer cell apoptosis through activating STAT3 signaling (Yan et al., 2016). Consistently,

another study demonstrated that cisplatin resistance in ovarian cells was attributed to the secretion of chemokine C-C motif ligand-5 (CCL5) by CAFs. Its molecular mechanism related to enhanced STAT3 and PI3K/Akt phosphorylation levels in ovarian cells (Zhou B. et al., 2016). Chemokine C-C motif ligand-1 (CCL1), combining exclusively with chemokine (C-C motif) receptor 8 (CCR8), is an inflammatory factor. However, its role has already gone beyond inflammation (Korbecki et al., 2020). Li et al. (2018) suggested that CCL1 participated in CAFs mediated chemoresistance by activation of TGF- β /NF- κ B signaling pathway in colorectal cancer.

Besides the factors mentioned above, CAFs are capable of secreting many other humoral elements to induce therapeutic resistance. Evidence of increased expression of insulin-like growth factor 2 (IGF2) and insulin-like growth factor receptor-1 (IGF-1R) in CAF accumulating-lung cancer tissues proved that CAFs promote chemoresistance through IGF2/IGF-1R signal. It led to the activation of AKT/SoX2 pathway, elevating the expression of P-glycoprotein, decreasing drug retention and increasing drug efflux ultimately (Zhang Q. et al., 2018). Midkine (MK) is a kind of heparin-binding growth factor, promoting carcinogenesis and chemoresistance. CAFs in TME lead to high levels of MK in tumors. As a result, CAF-derived MK

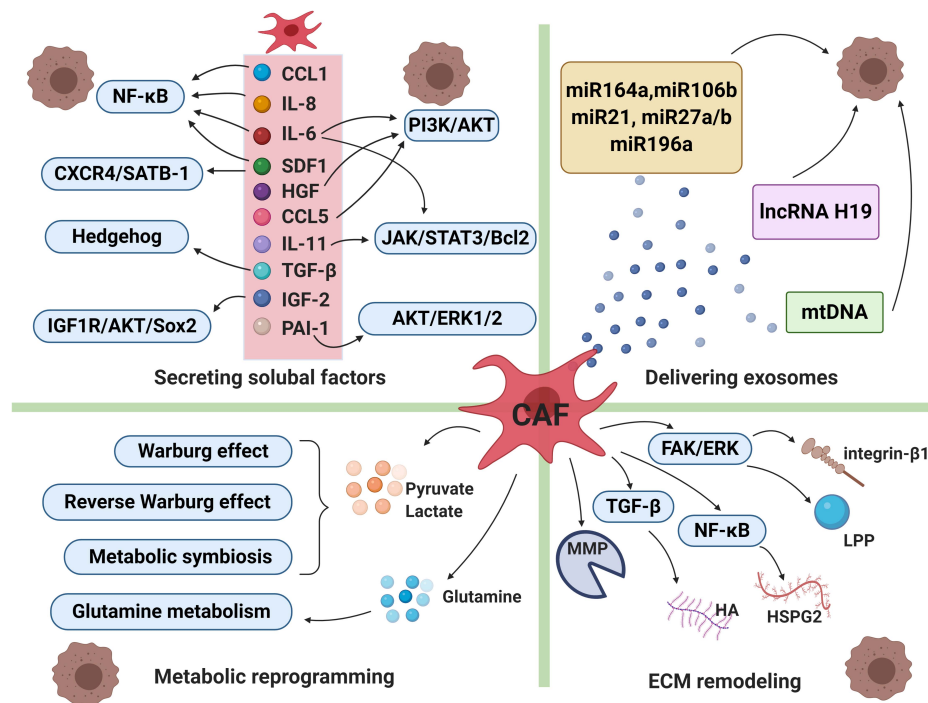


FIGURE 2 | Cancer-associated fibroblasts and drug resistance. The intricate mechanisms of drug resistance mediated by CAFs include secreting soluble factors, delivering exosomes, metabolic reprogramming and extracellular matrix (ECM) remodeling. CAFs can secrete a broad range of cytokines or factors which enable to activate a series of signaling cascades, leading to therapeutic resistance. CAFs-derived exosomes deliver miRNAs, lncRNAs and mtDNA to cancer cells, which participate in transmitting paracrine signals of therapeutic resistance. Moreover, in order to adapt to a glucose-deficient microenvironment, CAFs coordinate with tumor cells to modulate metabolic mode. Lastly, activated signals within CAFs increased production of extracellular matrix components, resulting in changes of its physical and biochemical characteristics under therapeutic pressure. CCL1, chemokine C-C motif ligand-1; CCL5, chemokine C-C motif ligand-5; IL-6, interleukin-6; IL-8, interleukin-8; IL-11, interleukin-11; SDF1, stromal cell derived factor-1; HGF, hepatocyte growth factor; TGF-β, transforming growth factor-β; IGF-2, insulin-like growth factor 2; PAI-1, plasminogen activator inhibitor-1, MMP, matrix metalloproteinase; HA, hyaluronan; HSPG2, heparin sulphate proteoglycan 2; LPP, lipoma-preferred partner. The figure was created with BioRender.com.

can induce cisplatin resistance through increased expression of lncRNA (Zhang D. et al., 2017). It has also shown that cisplatin treatment triggered the AKT and ERK1/2 signal cascades in esophageal squamous cell carcinoma cells mediated by releasing of plasminogen activator inhibitor-1 (PAI-1) from CAFs. The study confirmed that there is relevance between elevated PAI-1 level in CAFs and poor progression-free survival after therapy (Che et al., 2018). When cultured head and neck squamous cell carcinoma (HNSCC) cell lines with CAFs, cetuximab resistance was induced and elevated level of matrix metalloproteinase-1 (MMP-1) was detected, and the resistance can be reversed by using MMP inhibitor. The result suggested that drug resistance was achieved by CAFs derived MMP family (Johansson et al., 2012).

Remodeling Extracellular Matrix

Extracellular matrix is a dynamic system which changes its physical and biochemical characteristics under pathological conditions, for example, its molecular composition and elasticity (Gilbert et al., 2010). ECM can also sufficiently impede drug delivery by increasing microvascular endothelial cell remodeling (Figure 2). A study on ovarian cancer chemoresistance showed that CAFs increased the expression of lipoma-preferred

partner (LPP) in endothelial cells through microfibrillar associated protein 5 (MFAP5)/FAK/ERK/LPP signaling pathway. Mechanically, LPP enhanced the formation of focal adhesion and stress fibers, promoting the mobility and permeability of endothelial cells. As a result, paclitaxel delivery to malignant cells has been decreased via increased intra-tumoral microvascular leakiness (Leung et al., 2018). In addition, hyaluronan (HA) has also been found to participate in remodeling extracellular matrix by producing high interstitial fluid pressure (IFP) to reduce the amount of drug exchange through capillaries (Paunescu et al., 2011; Jacobetz et al., 2013). CAFs are involved in producing HA in a TGF-β dependent manner (Sapudom et al., 2020). Meanwhile, CAFs are found to delay cancer cell response to chemotherapy through another critical component in matrix, heparin sulfate proteoglycan 2 (HSPG2). Stromal deposition of HSPG2 was partly mediated by NF-κB signaling, which enhanced the invasion, metastasis of pancreatic cells and induced gemcitabine resistance (Vennin et al., 2019). CAFs in BRAF mutant melanoma may participate in resistance to BRAF inhibitor PLX4720 by generating fibronectin-rich matrix. Melanoma-associated fibroblasts conferred PLX4720 tolerance dependent on the upregulation of integrin-β1 and the activation

of focal adhesion kinase (FAK)/Src/ERK signaling pathway (Hirata et al., 2015).

Reprogramming the Metabolic Process of Tumor Cells

The abnormal proliferation of tumor cells relies on the enhanced adaptation to the nutritional microenvironment mediated through reprogrammed metabolic process. As a result, alterations in energy metabolism are considered to be one of the characteristics of tumor cells (Hanahan and Weinberg, 2011). In order to adapt to a glucose-deficient microenvironment, cancer cells undergo a metabolic switch to aerobic glycolysis, also known as the Warburg effect (Siska et al., 2020). Lactate is the end product of aerobic glycolysis and increased lactate production in MET/EGFR TKI-resistant breast cancer cells has been observed. Interestingly, lactate served as a critical media between breast cells and CAFs. Specifically, lactate uptake by CAFs activates NF- κ B signals of CAFs, resulting in the upregulation of HGF. In turn, increased HGF turns on MET signals in cancers and confers resistance to TKIs (Apicella et al., 2018).

Although Warburg effect is a distinctive character of tumor cells, recent studies showed that other metabolic features, notably the reverse Warburg effect, metabolic symbiosis, and glutamine metabolism, pose challenges to antitumor therapy due to adaptive or acquired drug resistance (Figure 2; Yoshida, 2015). Migneco proposed a new model for understanding the reverse Warburg effect, in which glycolytic CAFs secreted pyruvate/lactate used by adjacent epithelial cancer cells as a source of mitochondrial tricarboxylic acid cycle (TCA) cycle, oxidative phosphorylation and ATP production. The result suggested that metabolic products produced by glycolytic CAFs promote tumor cells to escape from antiangiogenic drugs via decreasing the reliance of cancer cells on a vascular blood supply (Migneco et al., 2010). Metabolic symbiosis of CAFs with epithelial cancer cells has been identified in (monocarboxylate transporter 1) MCT1-positive prostate tumor cells and MCT4-positive CAFs (Pértega-Gomes et al., 2014). MCT4-positive hypoxic cells create a low PH acidic microenvironment through aerobic glycolysis and secreting lactate, while MCT1-positive oxidative cells take up lactate as a substrate for TCA cycle, which is termed as metabolic symbiosis (Montenegro and Indraccolo, 2020). Besides, it has been proved that angiogenesis inhibitors resistance mediated by metabolic symbiosis was dependent on mTOR signaling (Allen et al., 2016; Jiménez-Valerio et al., 2016). Tumor cells also achieve metabolic process via glutamine metabolic reprogramming. For example, in prostate cancer, the increase in glutamine synthesis after macropinocytosis of extracellular fluid was detected in CAFs, which was related to the cascade activation of RAS signaling. In turn, CAFs-secreting glutamine promoted mitochondrial metabolism in prostate cancer cells, inducing neuroendocrine differentiation, facilitating the development of resistance to androgen deprivation therapy (ADT). In consistence, prostate cancer patients with ADT resistance displayed increased blood glutamine level than those with satisfactory treatment outcomes (Mishra et al., 2018).

Inducing Epigenetic Modifications of Tumor Cells

Accumulating evidence underscores the epigenetic modification of tumor cells induced by CAFs plays a part in drug resistance. Dysregulated DNA methylation in CAFs has been reported to be concerned with breast cancer, stomach cancer and pancreatic cancer (Liu M. et al., 2017). It is proved that DNA methylation level in stromal cells is related to that of adjacent cancer cells (Hanson et al., 2006; Rodriguez-Canales et al., 2007). Soluble factors secreted by CAFs obviously upregulated the level of methylated CpGs on their regulated gene region (372 genes) in breast cancer cells, which shed light on the importance of epigenetic modifications of tumor cells induced by CAFs (Mathot et al., 2017). In addition, factors derived from CAFs were capable to induce reversible DNA hyper- and hypomethylation during (epithelial-to-mesenchymal transition) EMT and (mesenchymal-to-epithelial transition) MET, leading to castration resistance and cancer stem cells expansion, predicting poor prognosis in prostate cancer (Pistore et al., 2017). Much evidence has already proven that EMT and stemness are also major contributors to drug resistance (Shibue and Weinberg, 2017; Nilsson et al., 2020). Moreover, EMT process was mediated by TGF- β derived from CAFs. Extensive methylation changes following TGF- β releasing were detected in ovarian cancer cells. Treatment with DNA methyltransferases inhibitor blockades DNA methylation in the EMT process (Cardenas et al., 2014). To develop a better therapeutic approach, a deeper knowledge of the impact of epigenetic regulation on the tumor microenvironment is necessary for combining epigenetic and checkpoint blockage therapies.

Delivering Exosomes

Cancer-associated fibroblasts derived exosomes have also emerged as active mediators of cancer progression and drug resistance by transmitting paracrine signals. Exosomes are membrane vesicles with a diameter of approximately 30-100 nm, containing protein, DNA, mRNA and miRNA (Fu et al., 2016; Kalluri, 2016; Li and Nabet, 2019). Exosomes are taken up by adjacent cells through endocytosis and act on the recipient cells. Recent studies have proven that exosomes are involved in the dynamic interplays between CAFs and cancer cells to promote tumor progression and chemoresistance (Figure 2; Ren et al., 2018).

Dysregulation of miRNAs in CAFs and the transfer of exosomal miRNAs between cancer cells and the microenvironment are associated with chemoresistance in multiple cancer types (Tanaka et al., 2015; Zhang L. et al., 2018; Qin et al., 2019; Guo et al., 2020). In pancreatic cancer, gemcitabine (GEM) treatment induced resistant CAFs that released exosomes containing SNAIL and miRNA 164a. SNAIL expression in exosomes was significant in inducing EMT. Moreover, the resistance can be reversed by treatment with GW4869, an inhibitor of exosome release (Richards et al., 2017; You et al., 2019). miRNA 106b was delivered directly from CAFs to pancreatic tumor cells via exosomes, leading to GEM insensitivity of tumor cells by targeting

TP53INP1 (Fang et al., 2019). Except for miRNA 164a and miRNA 106b, miRNA 21 was also reported in GEM-induced chemoresistance of pancreatic cancer (Zhang L. et al., 2018). In ovarian neoplasm, miRNA 21 derived from CAFs and cancer associated adipocytes was transferred to cancer cells, which conferred paclitaxel resistance by directly targeting apoptotic protease activating factor-1 (APAF1) (Yeung et al., 2016). Further, it has been demonstrated that cisplatin and paclitaxel treatment of gastric cancer promoted the secretion of miRNA 522 from CAFs, with the activation of ubiquitin-specific protease 7 (USP7)/heterogeneous nuclear ribonucleoprotein A1 (hnRNP A1) axis, resulting in arachidonate lipoxygenase 15 (ALOX15) inhibition and ultimately decreased chemo-sensitivity (Zhang H. et al., 2020). Additionally, miRNA 27a/b over-expressed CAFs in esophageal cancer microenvironment were correlated with cisplatin resistance by upregulation of TGF- β (Tanaka et al., 2015). In head and neck cancer, cisplatin resistance was found to be linked exosomal miRNA 196a and its targets, CDKN1B and ING5 (Qin et al., 2019).

Long non-coding RNA signatures of tumor-derived exosomes have been identified to be responsible for drug resistance. Exosome-enriched lncRNA H19 and colorectal-associated lncRNA can be transferred from CAFs to adjacent colorectal cells, inducing stemness of CSC and chemoresistance by

activating Wnt/ β -catenin signaling pathway (Ren et al., 2018; Deng et al., 2020). Besides, mitochondrial DNA (mtDNA) transfer from CAFs to hormonal therapy-resistant breast cancer cells occurred via exosomes. Specifically, cancer cells with impaired metabolism received the exosomes loaded with full mitochondrial genome, causing restoration of oxidative phosphorylation. The delivery of mtDNA promoted resistance to hormone therapy and induced self-renewal potential of breast cancer cells (Sansone et al., 2017).

In short, exosomes transfer and secretion of soluble molecules constitute a major communication channel between CAFs and tumor cells as well as other stromal components in TME, which promotes cancer progression and therapeutic resistance.

Based on these multiple effects of CAFs on drug resistance (Table 1), CAF have become an interesting therapeutic target for cancer intervention. Here, we will briefly discuss the main advances in CAF-targeted therapeutic strategies. Firstly, direct elimination of CAFs can significantly enhance the efficacy of chemotherapy. Co-delivery of cyclopamine (CPA), a kind of sonic hedgehog inhibitor, and paclitaxel (PTX) by construction of polymeric micelle (M-CPA/PTX) shows promising therapeutic outcomes for Pancreatic ductal adenocarcinoma (PDAC). M-CPA can deplete CAFs and modulate stroma thus to enhance the cytotoxic activity of PTX. *In vivo*, the compounds remarkably

TABLE 1 | Mechanisms of antitumor drug resistance mediated by CAFs.

Tumor type	Drug resistance	Mechanisms	References
Breast cancer	Trastuzumab	CAFs secreting IL-6, thus activating NF- κ B, JAK/STAT3 and PI3K/AKT pathways.	Mao et al., 2015
	Hormonal therapy	mtDNA transfer from CAFs to cancer cells via exosomes.	Sansone et al., 2017
CRC	Photodynamic therapy	CAFs reducing the sensitivity of cancer cells to photodynamic activity.	Lamberti et al., 2019
	Oxaliplatin	CAFs expressing lncRNA, activating Wnt/ β -catenin pathway.	Deng et al., 2020
ESCC	Cisplatin	CAFs secreting IL-6, upregulating CXCR7 through STAT3/NF- κ B pathway.	Qiao et al., 2018
	Cisplatin	CAFs secreting PAI-1 activating AKT and ERK1/2 signal.	Che et al., 2018
Gastric cancer	Cisplatin	CAFs secreting IL-8, activating NF- κ B signal and increasing the expression of ABCB1.	Zhai et al., 2019
	Chemoresistance	CAFs expressing IL-11 and activating IL-11/IL-11R/gp130/ JAK/STAT3 signal.	Ma et al., 2019
	Cisplatin, paclitaxel	CAFs-derived miRNA 522 leading to ALOX15 suppression and decreased lipid-ROS accumulation.	Zhang H. et al., 2020
Lung adenocarcinoma	EGFR-TKI	CAFs expressing HGF.	Suzuki et al., 2019
	Cisplatin	CAFs expressing IL-11 and activating IL-11/IL-11R α /STAT3 signal.	Tao et al., 2016
Melanoma	PLX4720	CAFs upregulating integrin- β 1, activating FAK/Src/ERK pathway.	Hirata et al., 2015
NSCLC	Selumetinib, erlotinib	CAFs secreting IL-6 inducing EMT switch via JAK1/STAT3 activation.	Shien et al., 2017
	Crizotinib, erlotinib	CAFs utilizing lactate to increase HGF expression.	Apicella et al., 2018
Ovarian cancer	Paclitaxel	miRNA 21 derived from CAFs binding directly to its novel target APAF1.	Au Yeung et al., 2016
	Paclitaxel	CAF-derived HGF activating c-Met/PI3K/Akt and GRP78 signal.	Deying et al., 2017
PDAC	Gemcitabine	CAFs-derived exosomes containing Snail and microRNA-146a, inducing EMT.	Richards et al., 2017
	Gemcitabine	CAFs increasing the expression of HSPG2 via NF- κ B signal.	Vennin et al., 2019
	Gemcitabine	CAFs-derived SDF-1 promoting cancer cells SATB-1 expression.	Wei et al., 2018
Prostate cancer	Castration resistance	CAFs inducing DNA hyper- and hypo-methylation during EMT and MET.	Pistore et al., 2017

CRC, colorectal cancer; ESCC, esophageal squamous cell carcinoma; PAI-1, plasminogen activator inhibitor-1; CXCR7, C-X-C motif chemokine receptor 7; ABCB1, ATP-binding cassette subfamily B member 1; ALOX15, arachidonate lipoxygenase 15; EGFR-TKI, epidermal growth factor receptor tyrosine kinase inhibitor; NSCLC, non-small cell lung cancer; EMT, epithelial-to-mesenchymal transition; HGF, hepatocyte growth factor; APAF1, apoptotic protease activating factor-1; GRP78, glucose-regulated protein 78; PDAC, pancreatic ductal adenocarcinomas; HSPG2, heparin sulfate proteoglycan 2; SDF-1, stromal cell derived factor-1; SATB-1, special AT-rich sequence-binding protein 1.

prolonged the survival time and inhibited tumor growth (Zhao et al., 2018). However, in a hybrid mouse model of spontaneous PDAC mice with α -SMA thymidine kinase (TK) transgenic mice, depletion of myofibroblasts reduced the production of type I collagen and altered ECM, with enhanced tumor hypoxia, immunosuppression and reduced survival (Özdemir et al., 2015). From this point of view, it seems that we need to be more cautious about the strategy of exhausting CAFs. Secondly, given the potential risks of depleting CAFs, normalization or inactivation of activated CAFs is another choice for regulating the functions of CAFs. By loading fibroblast activation protein- α (FAP- α) antibody and CXCL12 siRNA onto the peptide nanoparticles (PNP), the nanosystem (PNP/siCXCL12/mAb) can selectively downregulate the expression of CXCL12 in CAFs via FAP- α recognition, causing inactivation of CAFs and blockade of CAFs-related tumor metastasis. As such, attempts to inactivate or normalize CAFs rather than diminish them, may be more preferable approaches and can promote the development of novel anticancer therapy. Thirdly, it is feasible to restore chemotherapy sensitivity of tumor cells by blocking the cross-talk between CAFs and tumor cells. IL-1 β and TGF- β 1 pathways are involved in CAFs recruitment and polarization. Simultaneous inhibition of IL-1 β and TGF- β 1 pathways with TAK1 inhibitor plus TGFBR1 inhibitor could restrain the activation of NF- κ B, reduce the secretion of IL-6 and IL-11, and sensitize colorectal cancer tumor cell line (DLD1) to oxaliplatin. *In vivo*, the combined therapy diminished colorectal tumor cells metastasis and CAFs aggregation (Guillén Díaz-Maroto et al., 2019).

IMMUNE INFLAMMATORY CELLS AND DRUG RESISTANCE

Tumor Associated Macrophages (TAMs)

Tumor associated macrophages are the most abundant immune cells found in TME (Perrotta et al., 2018; Najafi et al., 2019). Increased TAMs infiltration within TME is declared to be concerned with poor prognosis and unsatisfactory response to chemotherapies for cancer patients (Sugimura et al., 2015; Li et al., 2019). TAMs derive from the circulating Ly6C⁺CCR2⁺ monocytes. TAMs are characterized with great heterogeneity in TME and they can be separated into two subgroups conventionally: M1 and M2 (Liu and Cao, 2015). M1-type macrophages are activated via classical pathway while M2-type macrophages are alternatively activated. In general, the role of M2 phenotype is defined to promote tumor progression and drug resistance, to produce anti-inflammatory cytokines, and to induce Th2 response. Macrophage polarization from M1 to M2 state is common in cancer condition educated by microenvironment (Moradi-Chaleshtori et al., 2020).

The interaction between tumor cells and TAMs which associated with therapeutic resistance lies on that tumor cells promote TAMs to differentiate into immunosuppressive M2-polarized macrophages under treatment pressure. In turn, M2 TAMs endow cancer cells with acquired chemoresistance through diverse mechanisms. IL-34 secreted by chemo-resistant tumor cells in a paracrine manner enhanced the polarization of

M2 TAMs by activating colony stimulating factor 1 receptor (CSF1R)/AKT signaling pathway (Baghdadi et al., 2016). Besides, elevated expression of macrophage inhibitory factor (MIF) was detected in cisplatin resistant lung cancer cells, which mediated M2 polarization of TAMs through Src/CD155/MIF signaling (Huang et al., 2019). In aromatase inhibitors resistant breast cancer cells, Jagged1-Notch pathway was activated, leading to macrophage differentiation toward M2 TAMs and upregulated expression of IL-10. M2 TAMs, in turn, contributed to the acquisition of drug resistance and metastasis (Liu H. et al., 2017). In gastric cancer treated with 5-fluorouracil (5-FU), transformation of M2-type TAMs was ascribed to accumulation of reactive oxygen species (ROS), activating hypoxia-inducible factor 1 α (HIF-1 α) signaling, driving the expression of high-mobility group box 1 (HMGB1). As a result, tumor-protected M2-type TAMs produced growth differentiation factor 15 (GDF15) to enhance the fatty acid β -oxidation in tumor cells, which induced chemoresistance (Yu et al., 2020).

Like CAFs, TAMs secrete numerous soluble factors into TME to protect tumor cells from drug attack, including enzymes, exosomes, interleukins, chemokines etc. It was found that cathepsin B and S expressing macrophages protected against paclitaxel-induced tumor cells death. The combined application of paclitaxel and cathepsin inhibitor can effectively enhance the therapeutic effect (Shree et al., 2011). Halbrook et al. (2019) pointed that alternatively activated TAMs secreting a series of pyrimidine nucleosides conferred pancreatic tumor cells resistance to gemcitabine, through molecular competition at the level of drug uptake and metabolism. TAMs also induced upregulation of cytidine deaminase, mediating inactivation of gemcitabine (Weizman et al., 2014). In colorectal cancer cells, 5-fluorouracil (5-FU) promotes the production of putrescine by TAMs. As a result, putrescine endows resistance to 5-FU by inhibiting the activation of p-JNK/caspase-3 apoptosis pathway (Zhang et al., 2016). M2-polarized TAMs are found to produce NO to protect tumor cells from apoptosis induced by cisplatin. The mechanism lies on NO/cGMP/PKG signaling pathway, leading to the inhibition of acid sphingomyelinase (Perrotta et al., 2018). Exosomal transfer of miRNA from macrophages to tumor cells has been noted as well. TAMs-derived exosomes transfer miR-365 to pancreatic adenocarcinoma cells to elicit gemcitabine resistance, which is performed by enhanced expression of triphosphate nucleotide and cytidine deaminase (Binenbaum et al., 2018). In addition, exosomes containing miR-223 and miR-21 are demonstrated to be associated with PTEN-PI3K/AKT signaling pathway in cisplatin chemoresistance of epithelial ovarian cancer and gastric cancer cell, respectively (Zheng et al., 2017; Zhu et al., 2019). Macrophages are usually recruited into TME and secrete various chronic inflammatory cytokines, both pro-inflammatory and anti-inflammatory factors. Angst et al. (2008) highlighted that TAMs protect pancreatic cancer cells from apoptosis by secreting IL-1 β , a pro-inflammatory cytokine, increasing the expression of cyclooxygenase-2 (COX-2) and prostaglandin E2 (PGE2) through activating MAPK and ERK1/2 pathway. It has been observed that the dysregulation of miR155-5p/C/EBP β /IL-6 signaling in TAMs was responsible for chemoresistance in colorectal cancer. As a result, TAMs secreted

IL-6 to activate IL-6R/STAT3/miR-204-5p signaling pathway in tumor cells (Yin et al., 2017). Hedgehog pathway inhibitor cyclopamine treatment increased the infiltration of M2-type TAMs in breast cancer, attenuating the efficacy of chemotherapy due to the accumulation of IL-6 (Xu X. et al., 2019). Besides, IL-10/STAT3/bcl-2 signaling pathway has been proven to be linked with breast cancer cell resistance to paclitaxel. Inhibition of TAMs derived-IL-10 using neutralizing antibody significantly enhanced sensitivity of breast cancer cells (Yang et al., 2015). The cross-talk between TAMs and HNSCC cells was mediated by IL-6 and C-C motif chemokine ligand 15 (CCL15). HNSCC cells secrete (vascular endothelial growth factors) VEGF to recruit macrophages and induce their polarization by secreting IL-6. Polarized TAMs produce CCL15 to weaken the sensitivity of tumor cells to gefitinib via CCL15/CCR1/NF- κ B signaling pathway (Yin et al., 2019).

Targeting of immune-regulatory receptors, for example, programmed cell death protein-1 (PD-1) and its ligand PD-L1, as well as cytotoxic T-lymphocyte-associated antigen-4 (CTLA-4), reduces T cell suppression, and relieves T cell function, thereby restoring antitumor immunity. However, accumulating reports have displayed that TAMs may account for drug resistance to immune checkpoint blockades (ICBs). Wu *et al.* demonstrated HIF-1 α enhanced the level of triggering receptor expressed on myeloid cells-1 (TREM-1) of TAMs. On the one hand, TREM-1⁺ TAMs damaged the cytotoxic functions of CD8⁺ T cells and caused CD8⁺ T cell apoptosis, in a PD-1/PD-L1 dependent manner. On the other hand, TREM-1⁺ TAMs recruited abundant CCR6⁺Foxp3⁺ Tregs into TME via CCL20/ERK/NF- κ B pathway. Application of TREM-1 signaling inhibitor GF9 statistically decreased CCR6⁺Foxp3⁺ Tregs infiltration, increasing the therapeutic efficacy of ICBs, as a result postponed tumor progression (Wu et al., 2019). Aside from negatively regulating CD8⁺ T cells, TAMs also interfere the function of CD4⁺ T cells. It was reported that the mechanisms of glioma cells resistance to anti-PD-1 and anti-CTLA-4 were mediated by TAMs through PD-1/PD-L1/CD80 axis, accompanied by Treg accumulation. Co-culture of naïve CD4⁺ T cells with PD-L1-positive TAMs induced the expression of CD80 on CD4⁺ T cells. PD-L1/CD80 interaction blockades antitumor immune responses to anti-PD-1 and anti-CTLA-4 therapies (Aslan et al., 2020).

Evidence from prostate cancer treated by ADT demonstrates that the interconnection between TAMs and CSCs can also lead to drug resistance. CSCs are capable of remodeling macrophages toward TAMs. Reciprocally, TAMs enhanced the stem-like characteristics of CSCs and drug resistance via IL-6/STAT3 signaling pathway (Huang et al., 2018). Consistent with this finding, in C57BL/6 mice model inoculated with MC38-CSCs (colon tumor) and 3LL-CSCs (lung cancer), TAMs generated milk-fat globule epidermal growth factor-VIII (MFG-E8) to regulate CSCs. MFG-E8 cooperated with IL-6 to stimulate STAT3 and hedgehog signaling pathways in CSCs, driving anticancer drug resistance (Jinushi et al., 2011). Moreover, the EMT induced by TAMs could be a potential mechanism amplifying peritoneal dissemination and causing chemoresistance in pancreatic cancer (Kuwada et al., 2018).

In conclusion, the mechanisms involved in antitumor drug resistance mediated by TAMs include release of multiple cytokines, transformation toward suppressive-M2 phenotype, suppressive effects on immune cells, modulation of CSC properties and promotion of EMT, which have been summarized in **Table 2**.

Furthermore, tumor-associated neutrophils (TANs) high infiltration within TME was related to tumor progression and drug resistance (Incio et al., 2016). Neutrophil polarization may affect their role in the tumor microenvironment. Similar to the classification of M1/M2 macrophages, TANs are sorted into antitumorigenic N1 phenotype and pro-tumorigenic N2 phenotype on the basis of their functional differences (Zhang Y. et al., 2020). TGF- β and type I IFN- γ were suggested to play essential roles in the polarization of TANs switching from N1 to N2 (Fridlender et al., 2009; Pylaeva et al., 2016). CXCL5 serves as a key factor in recruiting TANs (Nywening et al., 2018). Sorafenib administration led to increased secretion of CXCL5 derived from HCC cells, inhibiting TANs apoptosis by inducing HIF1 α /NF- κ B/CXCL5 pathways, enhancing TAN infiltration in both animal models and HCC patients. Besides, HCC cells were able to polarize TANs and promote secretion of CCL2 and CCL17 by TANs through activating PI3K/Akt and p38/MAPK signals. As a response to HCC cells, TANs facilitate intra-tumoral infiltration of CCR2⁺ macrophages and CCR4⁺ Treg cells via CCL2-CCR2 and CCL17-CCR4 connections (Zhou S.L. et al., 2016). Therefore, combined blockade of TANs and TAMs present advantages in improving therapeutic outcomes (Nywening et al., 2018).

Generally, there are three approaches to target TAMs: reduced recruitment, direct depletion, and repolarization. CCL2 is a potent chemokine for monocytes recruitment and CCL2-CCR2 axis is the primary mediator for the expansion of macrophages in TME. In a PDAC mouse model, tumor cells-derived CCL2 inhibited the efficacy of ablative radiotherapy by recruiting inflammatory monocytes/macrophages into the TME to accelerate tumor proliferation and angiogenesis. While selective blockade of CCL2 using neutralizing antibodies interrupted the recruitment of monocytes/macrophages and produced synergistic antitumor effects with radiotherapy and prolonged survival time (Kalbasi et al., 2017). Next, colony-stimulating factor 1 receptor (CSF1R), receptor of CSF-1 and IL-34, is necessary for the proliferation, differentiation and survival of macrophages (Muñoz-García et al., 2021). Therefore, avenues of targeting CSF-1R alone or combined with standard therapies seem to be feasible. Enhanced infiltration of TAMs was observed after radiotherapy in gliomas mouse model, which was responsible for tumor recurrence. While combined therapies of CSF-1R inhibitor, BLZ945, with radiotherapy significantly delayed glioma relapse. Particularly, CSF-1R could inhibit both resident-microglia and recruited monocyte-derived macrophage. Neutralizing antibody of CD49d could only inhibit the recruitment of monocyte-derived macrophage without effect on resident microglia. Compared to the CD49d neutralizing antibody, CSF-1R displays stronger efficacy in delaying relapse (Akkari et al., 2020). Nevertheless, existence of antigen presenting cells (APCs) including macrophages and dendritic cells (DCs) are essential for T cells activation. Elimination of macrophages

TABLE 2 | Mechanisms of antitumor drug resistance mediated by TAMs.

Tumor type	Drug resistance	Mechanisms	References
Breast cancer	Paclitaxel	TAMs secreting cathepsins B and S.	Shree et al., 2011
	Cyclophosphamide	TAMs increasing the production of IL-6.	Xu X. et al., 2019
	Paclitaxel	TAMs secreting IL-10, activating STAT3 and elevating the expression of Bcl-2.	Yang et al., 2015
CRC	5-FU	TAMs secreting putrescine that inhibits the activation of JNK/caspase-3 pathway.	Zhang et al., 2016
	Oxaliplatin	TAMs secreting IL-6, activating IL-6R/STAT3/miR-204-5p pathway of tumor cells.	Yin et al., 2017
	Cisplatin	TAMs secreting MFG-E8 to regulate CSCs via activating STAT3 and hedgehog signal.	Jinushi et al., 2011
Gastric cancer	Cisplatin	TAMs producing exosomes containing miR-21, downregulating PTEN and enhancing PI3K/AKT.	Zheng et al., 2017
Glioma	Cisplatin	TAMs producing NO, inhibiting acid sphingomyelinase via NO/cGMP/PKA pathway.	Perrotta et al., 2018
	Anti-PD-L1/CTLA-4	PD-L1 of TAMs binding with CD80 of CD4 ⁺ T cells, inhibiting antitumor T cell responses.	Aslan et al., 2020
HCC	Anti-PD-L1	TREM-1 ⁺ TAMs damaging the cytotoxic functions of CD8 ⁺ T cells and causing CD8 ⁺ T cell apoptosis.	Wu et al., 2019
HNSCC	Gefitinib	TAMs secreting CCL15, activating CCL15/CCR1/NF- κ B pathway.	Yin et al., 2019
Ovarian cancer	Cisplatin	TAMs secreting exosomes delivering miR-223, inactivating PI3K/AKT signal by targeting PTEN.	Zhu et al., 2019
Pancreatic cancer	Gemcitabine	TAM secreting pyrimidines competitively inhibits gemcitabine uptake and metabolism.	Halbrook et al., 2019
	Gemcitabine	TAMs upregulating cytidine deaminase, promoting drug degradation.	Weizman et al., 2014
	Gemcitabine	TAMs derived-exosomes transfer miR-365, upregulating cytidine deaminase.	Binenbaum et al., 2018
	Camptothecin	TAMs secreting IL-1 β , promoting the production of COX-2 and PGE2 via ERK1/2.	Angst et al., 2008
	5-FU	TAMs inducing EMT.	Kuwada et al., 2018
Prostate cancer	ADT	TAMs enhancing the stem-like properties of CSCs via IL-6/STAT3 pathway.	Huang et al., 2018

CRC, colorectal cancer; HCC, hepatocellular carcinoma; HNSCC, head and neck squamous cell carcinoma; 5-FU, 5-fluorouracil; ADT, androgen deprivation therapy; EMT, epithelial-mesenchymal transition.

could reduce the efficacy of immunotherapy (Diggs et al., 2020). Repolarization of TAMs by phenotype switch from M2 to M1 provides an opportunity to balance immune microenvironment, and compensates for the disadvantages of depletion of all macrophages. In 4T1 breast cancer mouse model, selectively targeting M2 TAMs, by simultaneously delivery of CSF-1R and CD47/SIRP α inhibitors via dual-inhibitor-loaded nanotherapeutic technique, results in increased M2 repolarizations into M1, enhanced phagocytosis activity, and satisfactory anticancer outcome (Ramesh et al., 2019). This preclinical trial suggests a promising and preferable strategy of targeting TAM.

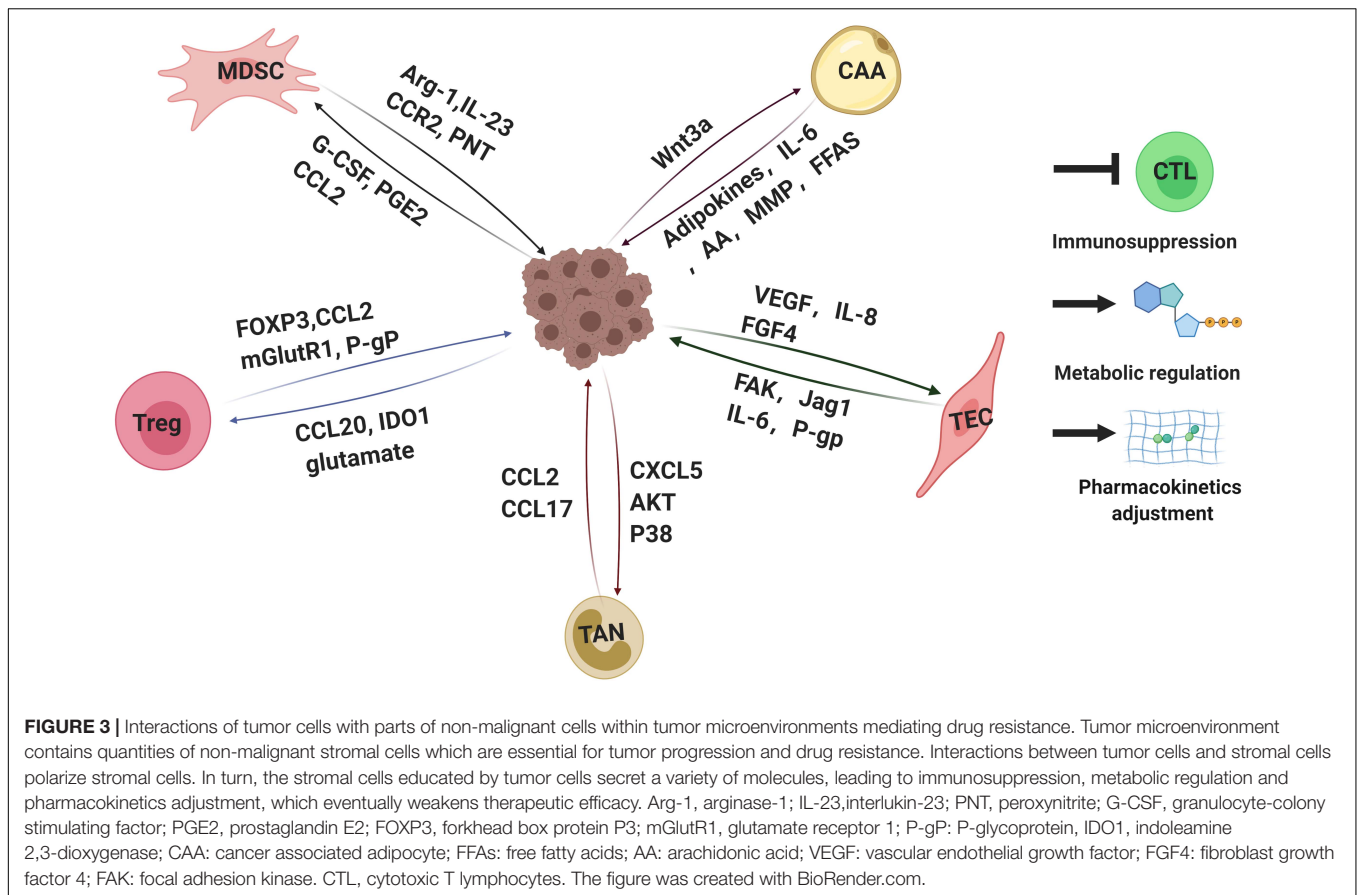
Myeloid-Derived Suppressor Cells (MDSCs)

Myeloid-derived suppressor cells are an immature heterogeneous population of the myeloid family, which contain two subsets of cells. One group is defined as granulocytic-MDSCs (G-MDSCs), with the CD11b⁺Ly-6G⁺Ly-6C^{low} phenotype, expressing high levels of arginase-1 (Arg-1). This population are also termed as PMN-MDSC due to their polymorphonuclear (PMN) morphology. The other group is identified as monocytic-MDSCs (Mo-MDSCs) because of their monocytic-like morphology, with the CD11b⁺Ly-6G^{low}Ly-6C^{hi} marker (Youn et al., 2008; Talmadge and Gabrilovich, 2013).

One of the main features of MDSCs is immunosuppression (Figure 3). MDSCs lead to the inhibition of different types of

immune cells, but the primary targets of MDSCs are T cells. The factors participated in MDSCs-mediated immunosuppression including Arg-1, IL-23, IL-10, TGF- β , PGE2, and many others (Gabrilovich, 2017; Xu et al., 2017). Recent studies elucidated that the reciprocal action between malignant cells and MDSCs plays a critical role in immunosuppressive chemoresistance. The level of PMN-MDSC and Arg-1 in serum of multiple melanoma (MM) patients was higher than that of healthy individuals. Furthermore, PMN-MDSC extracted from MM patients could suppress the activation of T cells effectively and protect MM cells from bortezomib treatment. However, this protection was offset by Arg-1 inhibitor (Romano et al., 2018). Mechanically, MM cells survival induced by MDSCs is dependent on AMPK activation, MCL-1 and BCL-2 expression in myeloma cells (De Veirman et al., 2019). In addition, it has been elucidated that the acquired ADT resistance of prostate cancer could be blamed on IL-23 secreted by MDSCs. IL-23-IL-23R-ROR γ axis activated the androgen receptor pathway in prostate cancer cells, regulating resistance to ADT (Calcinotto et al., 2018).

Besides the mechanisms mentioned above, tumor cells are found to recruit and activate MDSCs in TME under therapeutic pressure. *In vitro* and *in vivo* results as well as clinical samples demonstrated that the expression of granulocyte-colony stimulating factor (G-CSF) in cervical cancer cells was significantly linked with MDSC infiltration and chemoresistance (Kawano et al., 2015). Blockade of colony stimulating factor-1 receptor (CSF-1R) can prevent immune resistance to immunotherapy (Holmgaard et al., 2016). Doxorubicin resistant



breast cancer cells escape immune surveillance by secreting PGE2. PGE2 then binds with its receptor on MDSCs, EP2/EP4, leading to accumulation of MDSCs. PGE2/miR-10/AMPK signaling pathway of MDSCs was activated, with inhibition of CD4⁺CD25⁻ T cells and decreased production of IFN- γ (Rong et al., 2016). BRAF inhibitor-resistant melanomas induced expansion of CCR2-expressing monocytic-MDSCs in the TME by producing CCL2, activating MDSCs through MAPK signaling. Combination of checkpoint blockade with MDSC depletion significantly reversed BRAF inhibitor resistance (Steinberg et al., 2017). Of note, MDSCs not only play a part in functional suppression of T cells, but also participate in (cytotoxic T lymphocytes) CTL-mediated cytotoxicity. Lu et al. (2011) demonstrated that MDSCs are a predominant origin of the free radical peroxynitrite (PNT) in lung, pancreatic, and breast cancer samples. PNT induces post-translational modifications of cell surface molecules while not affecting cell viability, inhibiting processed peptides presentation to tumor-associated MHC molecules. Thus, tumor cells escape from antigen-specific CTLs and acquire immunological resistance (Lu et al., 2011).

These findings suggest the important role of MDSCs (Table 3), which motivate us to consider them as a target to overcome tumor resistance. MDSCs can be diminished by using chemotherapeutic drugs. CD33 is identified as a pathological marker for recognizing MDSCs across cancer subtypes and is responsible for immunosuppressive microenvironment. Conjugating anti-CD33

antibody with toxin calicheamicin, so called as gemtuzumab ozogamicin, can deplete CD33⁺ MDSCs thus to restore T cell activity and reactive CAR-T cell response (Fultang et al., 2019). Meanwhile, this strategy shows good results in clinical trials (Lancet et al., 2020; Schlenk et al., 2020). Another approach to inhibit MDSCs is to block their signaling cascades. IL-1 β is an upstream mediator of myeloid resistance. Anti-IL-1 β significantly decreases the infiltration of PMN-MDSCs and TAMs in TME. The combined use of anti-IL-1 β and anti-PD-1 or cabozantinib increased anti-tumor activity (Aggen et al., 2021). One of the most promising techniques for targeting MDSCs is to promote their reprogramming. Increased activation of PKR-like endoplasmic reticulum kinase (PERK) in MDSC contributes to MDSC-mediated T cell dysfunction by stimulating transcriptional factor NRF2. Inhibition of PERK interrupts cytosolic mitochondrial DNA-STING-type I IFN axis and converts MDSCs into normal myeloid cells with activated CTL immunity. PERK inhibitor combined with anti-PD-L1 therapy shows synergetic effects in B16 bearing mice (Mohamed et al., 2020).

T-Regulatory Lymphocytes (T-Reg)

Tregs are a subpopulation of immunosuppressive T cells identified as CD4⁺CD25⁺, and are characterized by expression of the Foxp3, which is essential for Tregs development and differentiation. In the TME, increased infiltration of Tregs has

TABLE 3 | Mechanisms of antitumor drug resistance mediated by MDSCs.

Tumor type	Drug resistance	Mechanisms	References
Breast cancer	Doxorubicin	Cancer cells secreting PGE2 and activating PGE2/miR-10/AMPK signals within MDSCs.	Rong et al., 2016
Cervical cancer	Platinum-based chemotherapy	Cancer cells expressing G-CSF, causing MDSCs accumulation and T cell suppression.	Kawano et al., 2015
HCC	5-FU, ADM	Cancer cells-derived IL-6 enhancing the activity and expansion of MDSCs.	Xu et al., 2017
Melanoma	PLX4720	Melanomas inducing expansion of CCR2-expressing monocytic-MDSCs in the TME by producing CCL2, activating MDSCs through MAPK signaling.	Steinberg et al., 2017
MM	5-FU, bortezomib	MDSCs inducing AMPK activation and MCL-1 and BCL-2 expression in myeloma cells.	De Veirman et al., 2019
Prostate cancer	Castration-resistance	IL-23 secreted by MDSCs activating IL-23-IL-23R-ROR γ axis of androgen receptor pathway in prostate cancer cells.	Calcinotto et al., 2018

PGE2, prostaglandin E2; G-CSF, granulocyte-colony stimulating factor; HCC, hepatocellular cancer; 5-FU, 5-fluorouracil; ADM, adriamycin; MM, multiple myeloma.

TABLE 4 | Mechanisms of antitumor drug resistance mediated by Tregs.

Tumor type	Drug resistance	Mechanisms	References
CRC	Immunotherapy resistance	PI3K δ -driven Foxp3 $^{+}$ Treg cells compensating CSF1R $^{+}$ TAMs to limit the function of CD8 $^{+}$ T cells.	Gyori et al., 2018
	5-FU	CCL20 secreted by colorectal cancer cells activating FOXO1/CEBPB/NF- κ B signaling, promoting the recruitment of Tregs.	Wang D. et al., 2019
Glioblastoma	VEGF mAb	Expression of glutamate/cystine antiporter SLC7A11/xCT causing elevated extracellular glutamate in glioblastoma cells, promoting Tregs proliferation.	Long et al., 2020
LLC cells	ADM, MMC	Foxp3 upregulating the expression of mdr1 mRNA and P-gp, reducing the sensitivity of LLC cells to ADM and MMC.	Li et al., 2012
Medulloblastoma	Rapamycin	IDO1 expression in medulloblastoma cells causing Treg expansion by CCL2 mediator.	Folgiero et al., 2016

CRC, colorectal cancer; TAM, tumor associated macrophage; 5-FU, 5-fluorouracil; VEGF, vascular endothelial growth factors; mAb, monoclonal antibody; LLC, Lewis lung cancer; ADM, adriamycin; MMC, mitomycin C; mdr1, multidrug resistance protein 1; P-gp, P-glycoprotein; IDO1, indoleamine 2,3-dioxygenase 1.

been defined to positively associate with poor prognosis and chemoresistance in melanoma, glioblastoma, HNSCC, ovarian, colorectal, renal and lung cancer (Bamias et al., 2008; Li et al., 2012; Schuler et al., 2013; Liu X.D. et al., 2015; Wang D. et al., 2019; Imbert et al., 2020; Long et al., 2020). Acquired resistance to ICBs remains a challenge in cancer therapy as a compensatory pathway emerges in TME to evade the antitumor effects induced by ICBs. Apart from the induction of MDSCs we summarized above, increased ratio of Tregs within TME suggests another cellular mechanism (Figure 3).

In vivo, 5-FU treatment elevated the expression of CCL20 in colorectal cancer cells (CRC) by activating FOXO1/CEBPB/NF- κ B signaling, which promoted the recruitment of Tregs within TME. The proportion of CD4 $^{+}$ Foxp3 $^{+}$ Tregs in tumor infiltrating lymphocytes (TIL) of CRC was dramatically higher than that of paired controls. Expression of Foxp3 $^{+}$ was obviously associated with resistance-related genes, including BCL2, WNT1, ATP8A2 and VIM. CCL20 blockers inhibit tumor progression and restore sensitivity to 5-FU of CRC (Wang D. et al., 2019). *In vitro*, mouse Lewis lung cancer (LLC) cells, overexpression of Foxp3 $^{+}$ was also identified to increase the IC50 values of Adriamycin (ADM) and mitomycin C (MMC) (Li et al., 2012). Moreover, recent evidences have proven that amino acid metabolism could affect immune cell response to tumor cells by regulating Tregs. Folgiero et al. (2016) disclosed that mTOR inhibitor, rapamycin, induces indoleamine 2,3-dioxygenase (IDO1) expression in medulloblastoma cells. IDO1, one of three enzymes catalyzing the degradation of TRP along the kynurenine pathway, led to Treg expansion by inducing CCL2

expression, creating an immune-tolerance microenvironment. VEGF inhibition is a critical method for inhibiting angiogenesis. While results showed that resistance to VEGF inhibitors is elicited by upregulation of Tregs. Specifically, the increased expression of glutamate/cystine antiporter SLC7A11/xCT causes elevated extracellular glutamate in the VEGF inhibitors treated glioblastoma cells, promoting Tregs proliferation, activation and suppressive function (Long et al., 2020). Indeed, high levels of ATP metabolism within TME have been determined to be linked with Tregs as well as immunosuppression (Deaglio et al., 2007). Experiments conducted by Gourdin et al. (2018) showed that CD73 $^{+}$ CD4 $^{+}$ effector T cells (Teffs) act synergistically with CD39 $^{+}$ Tregs to metabolize ATP to immunosuppressive adenosine, restraining the function of Teffs on IL-17A production. What is more, the compensatory mechanisms between CSF1R $^{+}$ TAMs and Foxp3 $^{+}$ Treg cells promote resistance to tumor immunotherapeutic agents. Either reduction of CSF1R $^{+}$ TAMs or Foxp3 $^{+}$ Tregs will limit the function of CD8 $^{+}$ T cells on tumor growth. Only co-blockade of CSF1R $^{+}$ TAMs and Foxp3 $^{+}$ Tregs can obtain a synergistic effect on augmentation of CD8 $^{+}$ T cells and tumor suppression (Gyori et al., 2018).

Collectively, over time and as a result of stress selection, some tumors augment Tregs function by producing more self-antigens and acquire compensatory pathways to evade the antitumor therapy, as well as resistance to ICBs (Table 4). Therefore, a deeper comprehension of the mechanisms and molecular pathways by which ICBs regulate T cells and Tregs, is necessary to design better immunotherapeutic strategies. Therapeutic

approaches depleting Tregs mainly focused on their molecular markers, such as CD25, CCR8. Treg depletion using anti-25 antibody combined with dual immunotherapy and radiotherapy restored antitumor immunity durably and induced immunologic memory (Oweida et al., 2018). Fc-optimized anti-human CCR8 antibody results in restrict Treg exhaustion without influence on Teffs (Campbell et al., 2021). CCR8-directed Treg elimination shows synergistic effect with PD-1 blockade in mouse model (Van Damme et al., 2021). In addition, CCR4 is a robust chemokine receptor for Treg recruitment in TME. Anti-CCR4 mAb (mogamulizumab) is under clinical investigation either as a monotherapy or combinational choice of anti-PD-1 mAb (Kurose et al., 2015; Doi et al., 2019).

In summary, due to the presence of TAMs, MDSCs, Tregs and their related factors, immunosuppressive microenvironments are now considered a major obstacle to ICBs. A range of investigations on turning non-immunogenic tumors into immunogenic tumors have been developed, for example, combinations of ICBs with anti-angiogenic agents (Makker et al., 2019), targeted therapies (De Henau et al., 2016), and other checkpoint inhibitors (Bedke et al., 2021). These therapeutic strategies should maximize the effectiveness of immunotherapy and induce sustained anti-tumor immune responses, to reach better clinical outcomes and response rates in cancer patients.

MESENCHYMAL STEM CELLS (MSCs)

Mesenchymal stem cells (MSCs), commonly called mesenchymal stromal cells, are one of another pivotal components of the TME (Shi et al., 2017). MSCs have been reported to be involved in many distinct steps of tumorigenesis, such as angiogenesis, metastasis, epithelial-mesenchymal transition, anti-apoptosis, pro-survival, immunosuppression and therapy resistance. A growing body of researches suggest the important role of MSCs in drug resistance. MSCs inherently possess the ability to be chemoresistance and can confer this resistance to many types of cancer cells, including osteosarcoma, acute lymphoblastic leukemia, breast cancer, ovarian cancer, oral squamous cell carcinoma, hepatocellular carcinoma and so on (Roodhart et al., 2011; Han et al., 2014; Ji et al., 2015; Xu et al., 2018; Lu et al., 2020; Raghavan et al., 2020; Wang S. et al., 2020). Apart from bone marrow, where MSCs were originally discovered, adipose tissue, peripheral blood, umbilical cord are also important sources of MSCs. As a heterogeneous group of progenitor cells, MSCs are known for the capacity to transdifferentiate into multicellular lineages including chondrocytes, osteocytes, adipocytes, myocytes, astrocytes, fibroblasts, and pericytes (Shan, 2004). Featured for their ability to adhere to the plastic, MSCs are also typically positive for certain patterns of surface markers (CD73, CD105, CD44, CD29, and CD90), concomitantly they lack expression of endothelial markers (CD34, CD31, and vWF) and hematopoietic markers (CD34, CD45, and CD14) (Reagan and Kaplan, 2011).

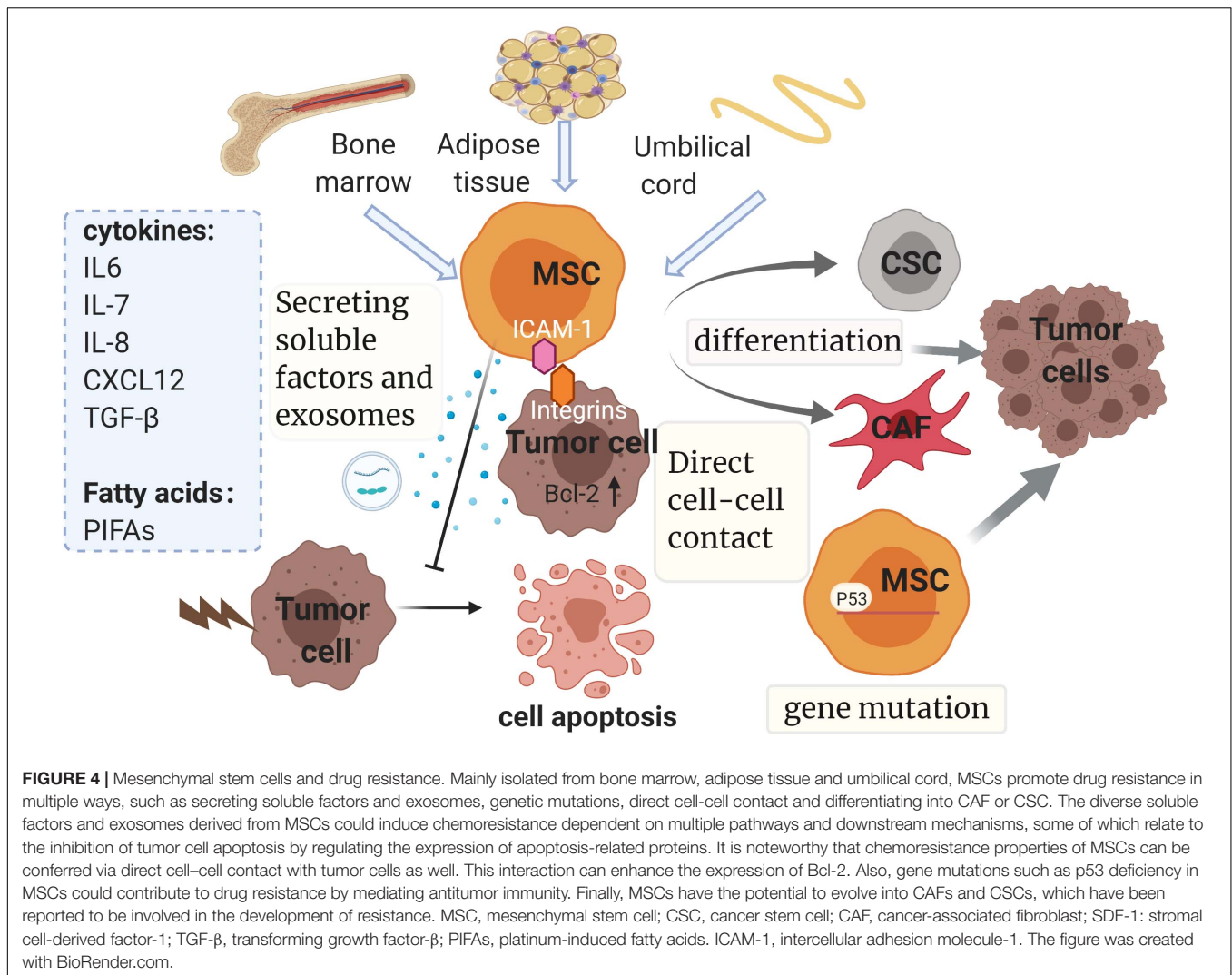
According to recent studies, MSCs can promote drug resistance in different ways as follows (**Figure 4**): (1) secreting

soluble factors; (2) delivering MSC-exosomes; (3) genetic mutations in MSCs; (4) direct cell-cell contact; (5) differentiating into CAF or CSC.

Secreting Soluble Factors

Mesenchymal stem cells can release diverse growth factors, cytokines and fatty acids which are involved in multiple pathways and downstream mechanisms, leading to the acquisition of drug resistance (Scherzed et al., 2011; Luo et al., 2014; Senthebane et al., 2017). As discussed earlier, increased IL-6 secretion by CAFs was described to induce chemoresistance. Similarly, MSCs derived IL-6 plays an important role in the resistance via the activation of downstream STAT3 cascades in different tumors. For example, in breast cancer, MSCs secreting IL-6 causes protection of MCF-7 cells from cisplatin-induced apoptosis, which is mediated by activating STAT3 signaling pathway with the markedly decreasing expression of Bax (Xu et al., 2018). In osteosarcoma cells, IL-6 produced by MSCs activates the JAK2/STAT3 signaling, with the subsequent up-regulation of multidrug resistance protein (MRP) and P-gP expression, which is relevant to poor response rates of clinical osteosarcoma chemotherapy (Tu et al., 2016). And in NPC, MSC-derived IL-6 was found to significantly upregulate STAT3 signal pathway, which could bind to the promoter region of NET5 gene, thus contributing to the increased expression of CD73. Subsequently, the elevated expression of CD73 promotes NPC tumor growth and inhibition of cisplatin-induced apoptosis, mediating resistance of NPC cells to cisplatin (Zeng et al., 2020). In head and neck carcinoma, other paracrine cytokines secreted by MSCs, including IL-6, IL-7, IL-8, and growth factors such as VEGF, have also been reported to be involved in the development of tumor drug resistance (Scherzed et al., 2011). IL-7 was demonstrated to be highly expressed by MSCs in chronic myeloid leukemia (CML). It is known that imatinib (IM) and nilotinib (NI) are remarkably effective therapeutic agent of BCR/ABL-positive CML and have improved the clinical outcomes. The IL-7-mediated JAK1/STAT5 pathway bypasses BCR/ABL signals, protecting tumor cells from imatinib (IM) and nilotinib (NI) in a BCR/ABL-independent way. Interestingly this could explain the early resistance before the BCR/ABL genetic mutation (Zhang et al., 2019). IL-8, a neutrophil chemoattractant, is one of the CXC chemokine receptors 1 and 2 (CXCR1/2) ligands. It has been reported that through highly releasing chemokine (C-X-C motif) ligand 1 (CXCL1), CXCL2, and IL-8, MSCs manipulate metabolic programs to promote M2 macrophages differentiation, leading to abolition of their tumoricidal functions, thus facilitating the acquisition of chemoresistance in ovarian tumor cells. As expected, CXCR1/2 inhibitor reparixin could revert MSC-mediated drug resistance in ovarian cancer by restoring the anti-tumoral function of macrophages both *in vitro* and *in vivo*. Hence, reparixin has the potential to improve the efficacy of carboplatin in cancer cells (Le Naour et al., 2020).

Another chemokine CXCL12, also named SDF-1, is constitutively secreted by MSCs. SDF-1a/CXCR4 interactions between CML cells and MSCs protect CML cells from imatinib-induced cell death by reducing activation of caspase-3 and



promoting the expression of Bcl-XL, an important anti-apoptotic protein inhibited by imatinib (Vianello et al., 2010). SDF-1a/CXCR4 axis was also reported to mediated drug resistance in acute lymphoblastic leukemia (ALL). MSCs increase the secretion of CXCL12, accompanied with the elevated expression of surface CXCR4 on chemo-resistant leukemic cells in the presence of vincristine. Furthermore, vincristine induced ALL apoptosis can be attenuated by upregulating Bcl-2 and downregulating Bax. Interestingly, all of these could be effectively reversed by the CXCR4 antagonist, AMD3100, which blocks the SDF-1a/CXCR4 axis and then restores sensitivity of ALL to chemotherapy (Wang S. et al., 2020). In addition, MSCs derived SDF-1a was also noted to mediate the cross-talk with the ovarian cancer cells, thus inducing their thermotolerance from hyperthermia intraperitoneal chemotherapy, a selective therapeutic approach for ovarian carcinoma (Lis et al., 2011).

Fatty acids are another important factor released by MSCs. Researches have demonstrated that the MSCs induced chemoresistance could be mediated by secreting two unique platinum-induced fatty acids (PIFAs). These two distinct

PIFAs, namely 12-oxo-5,8,10-heptadecatrienoic acid (KHT) and hexadeca-4,7,10,13-tetraenoic acid [16:4(n-3)] are reported to confer resistance to a broad spectrum of anticancer drugs in minor quantities. Interestingly, inhibition of the central enzymes (cyclooxygenase-1 and thromboxane synthase), associated with the production of PIFAs, significantly enhances the chemotherapy efficacy (Roodhart et al., 2011). While the exact mechanism by which MSCs derived PIFAs induce chemoresistance remains to be elucidated.

Apart from cytokines, chemokines and fatty acids, the expression of growth factors like TGF-β was also reported to be upregulated in MSCs. In hepatocellular carcinoma (HCC), the tumor inflammatory microenvironment stimulates the overexpression of TGF-β in MSCs, inducing chemoresistance of HCC cells by promoting autophagy. Knockdown the expression of TGF-β by transfecting siRNA attenuates the ability of MSCs to induced autophagy and restore the sensitivity to chemotherapy in HCC cell (Han et al., 2014). In gastric cancer (GC), evidence presents that MSCs secreted TGF-β1 promotes fatty acid oxidation (FAO) to support stemness features and drug

resistance, which is mediated by activating SMAD2 and SMAD3 and promoting lncRNA MACC1AS1 expression (He et al., 2019).

Delivering MSC-Exosomes

Exosomes transferring a variety of bioactive molecules including mRNAs, miRNAs and proteins, play important roles in inter- and intra-cellular interplay through pathways that influence TME regulation and drug resistance (Zhang X. et al., 2017; Adamo et al., 2019). Accumulating evidence suggests that MSC-derived exosomes contribute to chemoresistance through different ways, including drug sequestration, delivering specific mRNA molecules and proteins, mediating communication between MSCs and cancer cells (Adamo et al., 2019).

Mesenchymal stem cell-derived exosomes are reported as important mediators of drug resistance in gastric cancer. MSC-exosomes incorporate into the gastric cancer cells, stimulating the activation of CaM-Ks (predominantly CaM-KII and CaM-KIV), triggering downstream Raf/MEK/ERK signaling cascade activation, which consequently upregulates the expression of multi-drug resistance associated proteins including MDR, MRP, and LRP, eventually conferring chemoresistance in gastric cancer (Ji et al., 2015). MSC-derived exosomes could deliver the contents to cancer cells, and this interaction is responsible for drug resistance. For instance, in breast cancer, MSCs released exosomes contain miR-222/223, entering breast cancer cells (BCCs) to promote the transition into cycling quiescence, which plays a key role in drug evasion. Further study observed that delivering anti-miR-222/223 by antagomiR-loaded MSCs to the dormant BCCs improves the efficiency of carboplatin and then increased host survival (Bliss et al., 2016). Moreover, MSC-exosomes mediated drug resistance has been documented in hematological tumors as well. For example, bone marrow stromal cells (BMSCs) derived exosomes function as a communicator mediating cell-to-cell communication through transference of their contents in multiple myeloma (MM) cells. BMSC-derived exosomes activate several pathways including p38, p53, c-Jun N-terminal kinase, and AKT pathways related to survival, promoting MM cell survival and chemoresistance *in vivo* by increasing antiapoptotic protein Bcl-2 and reducing the cleavage of caspase-9, caspase-3 (Wang et al., 2014).

Direct Cell-Cell Contact

In addition to releasing paracrine factors and exosomes, MSCs could confer resistance through direct cellular interactions. This cross-talk between cancer cells and MSCs enables to promote the activation of a series of signaling cascades in different tumors (Wang J. et al., 2018). Mudry et al. (2000) has demonstrated that MSCs protect leukemia cells from cytarabine and etoposide cytotoxicity by directly contacting with leukemic cells, thus promoting the expression of vascular cell adhesion molecule-1 (VCAM-1). Further investigations have been done to figure out the detailed protective mechanisms of MSCs adhesion. In T cell acute lymphoblastic leukemia (T-ALL), MSCs adherence to cancer cells, mediated by intercellular adhesion molecule-1 (ICAM-1), is proved to induce mitochondria transfer between MSCs and T-ALL cells, leading to the decrease of mitochondrial intracellular ROS levels in T-ALL cells. It is well accepted

that excess ROS is responsible for cell apoptosis, which is one of major mechanisms for chemotherapy (Wang J. et al., 2018). Noteworthy, treating with blocking antibody against ICAM-1 could effectively reduce adhesion between T-ALL cells and MSCs, reducing mitochondrial transfer, thereby restoring chemotherapy sensitivity. Additionally, MSCs protect CML stem/progenitor cells from TKI induced apoptosis by increasing N-Cadherin-mediated adhesion and enhancing transcription of β -catenin target genes in primary CML CD34⁺ cells. Not surprisingly, the β -catenin inhibitor, ICG001, targeting Wnt signaling enhanced the sensitivity of CML to TKI cocultured with MSC (Zhang et al., 2013).

Aside from hematological malignancies, MSCs are also elucidated to be involved in the drug resistance in solid tumors by direct contact. In oral squamous cell carcinomas (OSCCs), co-cultured with MSCs, the human derived OSCC cell lines are shown activation of PDGF-AA/PDGFR- α autocrine loop, accompanied with the upregulation of AKT, which reduced apoptotic response by increasing expression of Bcl-2 and eventually contributed to cisplatin resistance in OSCC (Wang J. et al., 2020). MSCs co-culture also improves stemness and confers chemo-resistance in gastric cancer (GC) cells by inducing the expression of metabolic pathways related lncRNA histocompatibility leukocyte antigen complex P5 (HCP5) in GC cells. Mechanistically, HCP5 is confirmed to target miR-3619-5p, facilitating FAO by activating AMPK/PGC1 α /CEBPB axis to promote stemness and concomitantly mediate chemoresistance in GC cells (Wu et al., 2020).

Genetic Mutations in MSCs

It has long been acknowledged that somatic mutations in tumor cells is a major cause of drug resistance. Some recent studies found genomic alterations also occur in non-malignant cells, which contribute to latent tumor recurrence in patients receiving chemotherapy and radiotherapy (Shi et al., 2017). Patocs et al. (2007) observed genetic mutations in breast cancer stromal cells partly contribute to the poor clinical outcome. In B16F0 melanoma cells, p53-deficient MSCs increase the expression of inducible nitric oxide synthase (iNOS), which is known to be responsible for regulating antitumor immunity and cell survival, leading to vigorous immunosuppression, promoting the facilitation of tumor growth, thus conferring therapy resistance. The inhibition of iNOS could reverse the enhanced tumor-promoting effects of p53-deficient MSCs, suggesting a window of opportunity to target iNOS to restore the sensitivity of MSCs (Huang et al., 2014).

Differentiating Into CAF or CSC

As mentioned before MSCs have the potential to differentiate into multicellular lineages and their conversion to CSCs or CAFs could be another mechanism to confer therapeutic resistance. CSCs have the ability to induce tumor progression and metastasis, and are considered to be inherently resistant to chemotherapy. It has been shown that targeting the methylation of two tumor suppressor gene HIC1 and RassF1A in MSCs induces their differentiating into CSCs and obtaining CSCs characteristics, including the acquisition of drug resistance along

with loss of anchorage dependence, increasing colony-forming capacity and pluripotency (Teng et al., 2011). CAFs, as discussed above, play critical role in drug resistance. Some studies have suggested human BM-MSC from healthy donors can transform toward α SMA- and FSP-1-expressing CAFs when exposed to the conditioned medium of tumor cells (Mishra et al., 2008). Dzobo et al. (2016) observed that longer incubation of breast cancer MDAMB 231 cells with human MSCs promotes hMSCs differentiate into CAF, along with the increasing levels of α -SMA and type I collagen, which is mediated by TGF- β /Smad signaling pathway (Senthebane et al., 2017). Further investigation reveals the relation between CAF and MSC in human cancer and their common contribution to drug resistance. Through analyzing human neuroblastoma (NB) tumor, Borriello et al. demonstrated a group of α FAP- and FSP-1-positive CAF cells that harbor similar phenotype and functionality to BM-MSC in the tumor stroma. These cells (designated CAF-MSC) contribute to various steps of tumor development, ranging from enhancing cell proliferation, decreasing cell apoptosis to endowing resistance to chemotherapy. Further study demonstrated that pro-tumorigenic effects mediated by CAF-MSC are associated with the activation of STAT3 and ERK1/2 in NB cells, consistent with IL-6 induced drug resistance mentioned above (Borriello et al., 2017). Hence the inhibition of STAT3 and ERK1/2 may open a new window to enhance the chemotherapy sensitivity.

Based on these multiple mechanisms of MSCs mediated drug resistance (Table 5), targeting the secreting of paracrine factors such as CXCR1/2, CXCL12 and PIFAs is proved to be a novel therapeutic approach (Le Naour et al., 2020; Wang S. et al., 2020). Moreover, due to the multifaceted role of MSCs in tumor progression, MSC-based anti-cancer therapies guide new strategies to overcome therapy resistance. For example, MSCs are being exploited as selective carriers for drug delivery in cancers because of their strong tropism and recruitment to tumors (Li et al., 2021). Several preclinical studies have been conducted to exploit the tumor-targeting ability of MSCs, using MSCs as an excellent *in vivo* vehicle to deliver tumor-killing drugs (Kim et al., 2015; Yin et al., 2018). Further therapeutic strategy is genetic modification of MSC to overexpress specific immunomodulatory cytokines, suicide genes and other molecules that can effectively inhibit tumor progression, including IFN α , IFN β and (TNF)-related apoptosis-inducing ligand (TRAIL) (Kidd et al., 2010; Kim et al., 2012). Phase I and Phase II clinical trials of MSC-based anti-cancer therapies are currently in progress (von Einem et al., 2019). In conclusion, an in-depth exploration of the cellular and molecular mechanisms of drug resistance in MSCs is essential to improve existing anticancer therapies.

CANCER ASSOCIATED ADIPOCYTES

Clinical data have shown epidemiological evidence linking obesity and poor prognosis in cancers at multiple specific sites (Calle et al., 2003). Growing researches highlight the independent effect of obesity to induce resistance to chemotherapies especially in breast cancer, ovarian cancer, prostate cancer, and leukemia (Ewertz et al., 2011), all of which implicate the underlying

role of adipocytes in tumor drug resistance. Adipocytes are key components as one of stromal cells in TME (Nieman et al., 2013). It is noteworthy that the bidirectional cross-talk between adipocytes and cancer cells may partly explain cancer progression. Co-cultured with cancer cells, adipocytes are observed to exhibit remarkable phenotypic changes, designated as cancer associated adipocytes (CAAs) (Muller, 2013). And these phenotypic and functional alterations including the delipidation, reduced expression of adipose markers such as Ap2(FABP4), adiponectin and the overexpression of inflammatory cytokines are found to be related to drug resistance (Dirat et al., 2011). Bochet et al. (2013) demonstrated Wnt3a secreted by tumor cells could contribute to the alteration of adipocyte. Emerging evidence indicates that CAAs in TME play dynamic and sophisticated roles in determining resistance to treatments through distinct mechanisms involving regulating metabolism, secreting various factors, altering chemotherapy pharmacokinetics, and remodeling extracellular matrix (Muller, 2013; Choi et al., 2018; Zhang M.M. et al., 2018; Lehuédé et al., 2019).

Regulating Metabolism

Adipocytes were initially identified as a tremendous energy storage providing high-energy metabolites. It is natural to expect a metabolic cross-talk between adipocytes and tumor cells contributing to the progression of tumor cells (Figure 3). The “Warburg effect” and “reverse Warburg effect” have been shown to be responsible for the drug resistance mediated by CAFs, and this concept could be applied to adipocytes as well (Duong et al., 2017). Under hypoxic conditions, lactate released from adipocytes increases dramatically (Pérez de Heredia et al., 2010). Alternatively, accumulating evidence indicates that lipids is the major energy source provided by adipocytes to tumor cells. CAAs release exogenous free fatty acids (FFAs), which are taken up by cancer cells via surface molecule CD36. FFAs could yield large quantity of ATP by increasing the rate of fatty acid β -oxydation (FAO) (Yang et al., 2020), thus contributing to the tumor progression and therapy resistance. In ovarian cancer cells, adipocytes adjust tumor metabolism by upregulating the expression of CD36, which was observed to regulate cellular metabolism including extracellular acidification, intracellular cholesterol accumulation and oxygen consumption, leading to substantial lipid droplets (LDs) accumulation and intracellular reactive oxygen species (ROS) increase (Ladanyi et al., 2018). Growing evidence has indicated that LDs function as organelles influencing chemotherapy response by storing excessive cholesterol and lipids (Guillaumond et al., 2015). Apart from CD36, FATPs (fatty acid transport protein family) and FABPpm (plasma membrane fatty acid binding protein) are reported to facilitate the FA transport process (Zhang M.M. et al., 2018). Likewise, adipocytes induce FABP4 expression, promoting metastasis and mediates carboplatin resistance in ovarian cancer cells. Meanwhile, knockdown of FABP4 leads to increased levels of DNA demethylation, downregulating genetic markers associated with OvCa metastasis and reducing the survival of clonal cancer cell, which provides theoretical

TABLE 5 | Mechanisms of antitumor drug resistance mediated by MSCs.

Tumor type	Drug resistance	Mechanisms	References
ALL	Cytarabine, etoposide	T-ALL cell/MSC adhesion mediating mitochondria transferring.	Wang J. et al., 2018
	Vincristine	MSCs secreting CXCL12, binding to surface CXCR4 on ALL cells, mediating apoptosis rate, and apoptosis-related protein expression.	Wang S. et al., 2020
Breast cancer	Platinum	MSCs secreting two unique PIFAs.	Roodhart et al., 2011
	Carboplatin	MSCs releasing exosomes containing miR-222/223.	Bliss et al., 2016
	Cisplatin	MSCs-derived IL-6 activating STAT3 pathway with the markedly decreasing expression of Bax.	Xu et al., 2018
CML	Imatinib	MSCs secreting CXCL12, reducing activation of caspase-3 and promoting the expression of Bcl-XL.	Vianello et al., 2010
	TKI	MSCs increasing N-Cadherin-mediated adhesion and enhancing transcription of β -catenin target genes in primary CML CD34 ⁺ cells.	Zhang et al., 2013
	TKI	MSCs releasing IL-7, mediating JAK1/STAT5 pathway, activating bypassed BCR/ABL signals.	Zhang et al., 2019
Gastric cancer	5-FU	MSC-exosomes activating CaM-Ks, triggering downstream Raf/MEK/ERK signaling cascade activation.	Ji et al., 2015
	5-FU, oxaliplatin	MSCs secreting TGF- β 1, promoting FAO to support stemness features and drug resistance.	He et al., 2019
	5-FU, oxaliplatin	MSC-induced lncRNA HCP5 driving FAO through miR-3619-5p/AMPK/PGC1 α /CEBPB axis.	Wu et al., 2020
HCC	Cisplatin	The overexpression of TGF- β in MSCs promoting autophagy.	Han et al., 2014
Multiple myeloma	Bortezomib	MSC-exosomes activating several pathways including p38, p53, c-Jun N-terminal kinase, and AKT pathways related to survival.	Wang et al., 2014
NPC	Cisplatin	MSC-derived IL-6 upregulating STAT3 signal pathway, increasing expression of CD73.	Zeng et al., 2020
Osteosarcoma	Doxorubicin	MSC-derived IL-6 activating the JAK2/STAT3 signaling, with the subsequent up-regulation of MRP and P-gP expression.	Tu et al., 2016
Ovarian cancer	Carboplatin	MSCs highly releasing CXCL1/2 and IL-8, promoting M2 macrophages differentiation.	Le Naour et al., 2020
HNSCC	Paclitaxel	MSCs secreting various cytokines in a paracrine manner.	Scherzed et al., 2011

MSCs, mesenchymal stem cells; ALL, acute lymphoblastic leukemia; PIFAs, platinum-induced fatty acids; CML, chronic myeloid leukemia; TKI, tyrosine kinase inhibitors; 5-FU, 5-fluorouracil; FAO, fatty acid oxidation; lncRNA, long non-coding RNA; HCC, hepatocellular carcinoma; NPC, nasopharyngeal carcinoma; MRP, multidrug resistance protein; P-gp, p-glycoprotein; HNSCC, head and neck squamous cell carcinoma.

support for targeting FABP combined with platinum treatment (Mukherjee et al., 2020).

Secreting Various Factors

It is well acknowledged that aside from the energy storing function, adipose tissue is also a major endocrine organ producing a range of growth factors, adipokines, and adipocytokines, several of which have been demonstrated to confer therapy resistance (Duong et al., 2017).

The generation and secretion of leptin are found to be elevated in CAAs, compared to mature adipocytes. Previous studies have shown the up-regulated leptin could reduce toxicity of chemotherapy agents *in vitro* through the suppression of intracellular ROS. Further study revealed that adipocytes-derived leptin promotes myeloma cells proliferation and reduces the chemotherapy induced-apoptosis by mediating proliferation and apoptosis related proteins, which is related to the activation of JAK/STAT-PI3K/AKT pathway (Yu et al., 2016). Leptin could bind to the leptin receptor (OB-R), and then contributes to the drug resistance in melanoma cells via activating the PI3K/AKT and MEK/ERK signaling. Interestingly, siRNA knockdown of OB-Rb reverses the activation of AKT and ERK and enhances the chemosensitivity melanoma cells (Chi et al., 2014). Similar

finding was reported in colon cancer cells, the combination of leptin and OB-R activates the PI3K/AKT signaling pathway, enhances tumor growth and promotes sphere formation through the overexpression of E-cadherin. Meanwhile, leptin could interfere with the efficacy of the chemotherapeutic agent 5-FU through promoting cell proliferation and suppressing 5-FU-induced apoptosis (Bartucci et al., 2010). In breast cancer cells, leptin participates in resistance to hormonal therapy. Leptin activates the estrogen receptor-alpha (ER- α) through the MAPK pathway regardless of the presence of estradiol, leading to nuclear localization of ER via promoting the expression of pS2, a classic estrogen-dependent gene. Consequently, the estrogen withdrawal status induced by aromatase inhibitors is alleviated, thus contributing to the progression of estrogen-dependent breast cancer (Catalano et al., 2004).

Adipocyte-secreted cytokines have been found to induce resistance via the modulation of cell death. IL-6, IL-8, MCP-1 are the most abundantly adipocyte-secreted cytokines (Duong et al., 2017). Recent studies suggested that increased expression and secretion of IL-6 in CAAs plays a key role in mediating breast cancer progression (Kim et al., 2018). In HER2-positive breast cancers, IL-6 expression can induce CSC-positive phenotype through activating NF- κ B and STAT3 pathways, thus driving

tumorigenesis and promoting chemotherapy resistance (Liu S. et al., 2018). SDF-1 α , another adipocyte-derived chemoattractant, was reported to promote the migration of ALL toward adipose tissue, where leukemia cells could be protected from chemotherapy by remaining in a dormant state, thereby gaining survival advantage (Pramanik et al., 2013).

L-asparaginase (ASNase) is a major treatment regimen for ALL by depleting plasma asparagine and glutamine, while glutamine synthetase was found to be remarkably elevated in CAAs in ALL. That means adipocytes prevent leukemic cell from ASNase induced cytotoxicity through directly increasing secretion of glutamine (Ehsanipour et al., 2013). Arachidonic acid (AA) is another chemo-protective lipid mediator secreted by adipocytes. It has been shown that AA significantly promotes the resistance of ovarian cancer cells to chemotherapeutic agents, partly dependent on AKT pathway. In addition, AA may participate in the modulation of drug resistance-related cell surface proteins including MRP1 and P-gp, influencing their organization, distribution and activity (Yang et al., 2019). Moreover, adipose-derived factors were demonstrated to confer the inhibition of trastuzumab-mediated ADCC in HER2⁺ breast tumor cells through decreasing the secretion of INF- γ in natural killer cells without altering their cytotoxicity. Further investigation remains to be done to determine the exact factor (Duong et al., 2015). Additional evidence suggests that adipocyte-derived adipokines activate JAK/STAT3 signaling and induce the upregulation of autophagic proteins, such as Atg5, Atg3, and LC3-I/II, activating autophagy thereby decreasing chemotherapy-induced apoptosis in myeloma cells, which highlights a novel therapeutic target for enhancing chemotherapy sensitivity in myeloma patients (Liu Z.Q. et al., 2015).

In addition to these factors, exosomes derived from CAAs also contribute to drug resistance in tumor cells, as a novel method of transmitting information among cells. Yeung *et al.* confirmed that CAAs-derived exosomes transfer higher levels of microRNA-21 (miR21) to ovarian cancer cells, which binds to a direct downstream target APAF1, known as a chemoresistance-associated gene, downregulating its expression, leading to paclitaxel resistance. Briefly, adipocytes derived exosomes could promote drug resistance and a malignant phenotype by decreasing the expression of APAF1 in ovarian cancer cells (Yeung et al., 2016).

Altering Chemotherapy Pharmacokinetics

The concentration of active drugs is of particular importance in tumor treatment. However, it was found to be reduced in adipocyte-rich microenvironments, including adipose tissue, omentum, and bone marrow, leading to a localized decrease in the cytotoxic activity of chemotherapy, which partly accounts for chemoresistance (Sheng et al., 2017). Adipocytes alter chemotherapeutic pharmacokinetics mainly through two pathways, including increasing drug clearance and altering drug distribution. Anthracyclines are widely used in a variety of cancers as classical DNA-damaging agents, while adipocytes were demonstrated to highly expressed

daunorubicin-metabolizing enzymes, aldo-keto reductases (AKR) and carbonyl reductases (CBR) isoenzymes to deactivate anthracyclines. Specifically, adipocytes reduce the antileukemia effect of daunorubicin by converting it to a less toxic metabolite, thereby reducing active drug concentration in the local microenvironment. Furthermore, Lehuédé et al. (2019) shown the doxorubicin subcellular distribution modified by adipocytes is associated with upregulating major vault protein (MVP). MVP is known as a major component of vault particles, involving in intracellular molecules transportation, including anti-cancer drugs. Therefore, increased expression of MVP in tumor cells induced by adipocytes increases drug efflux and decreases drug intracellular accumulation. Also, it has been demonstrated that overexpression of MVP clinically relates to drug resistance in human breast tumors, indicating a poor prognosis for chemotherapy (Lehuédé et al., 2019).

Extracellular Matrix Remodeling

As previously mentioned, the dynamic adaptation of ECM is essential for cancer progression and invasion as well as drug resistance. Interestingly, adipocytes are vital source of ECM components. In breast tumors, adipocytes increased expression of matrix metalloproteinase-11 (MMP11), along with MMP1, MMP7, MMP10, and MMP14, involving in cisplatin resistance (Sato et al., 1994; Choi et al., 2018). Collagen VI, another adipocyte-secreted ECM protein was reported to trigger tumor progression *in vivo* via activation of the NG2 receptor in cancer cells and sequentially inducing Akt, β -catenin, and cyclin D1 (Iyengar et al., 2005). Remarkably, the presence of collagen VI protein was found to promote resistance in cisplatin-sensitive ovarian cells, suggesting that reorganization of the EMC near the tumor is of great importance in drug resistance (Sherman-Baust et al., 2003). Furthermore, a cleavage product of collagen VI, endotrophin highly secreted from adipocytes upon chemotherapy was demonstrated to act as a signaling molecule enhancing EMT process, causing cisplatin resistance. Thiazolidinediones and the neutralization of endotrophin were found to increase chemo-sensitivity by suppressing EMT (Park et al., 2013).

Taken together, the aforementioned studies suggest the complicated role of adipocytes and lipid metabolism in the regulation of anticancer drug sensitivity (Table 6), which makes CAAs targeted therapy a potentially effective treatment. CAAs secrete metabolic substrates, adipokines, and cytokines and promote drug resistance, which may become a potential target for new treatments. For instance, targeting serum IL-6 by tocilizumab, an anti-IL-6 receptor antibody was demonstrated to improve prognosis and alleviate cachexia in chemotherapy-resistant patients with metastatic lung cancer (Ando et al., 2014). In addition, inhibition of CAAs lipolysis provides an opportunity of anticancer therapy. Mechanistically, inhibit the release of FFA and other metabolites from CAAs, thereby constrain the supply of lipid fuel to cancer cells. Alternatively, interference with FFA uptake provide another way to limit FFA supply to tumor cells. Usage of the CD36-neutralizing antibodies to inhibit fatty acid receptor CD36 leads to therapeutically suppression of tumor growth and metastasis in oral squamous cell carcinomas

TABLE 6 | Mechanisms of antitumor drug resistance mediated by CAAs.

Tumor type	Drug resistance	Mechanisms	References
ALL	ASNase	CAAs producing both ASN and GLN, counteracting the effects of ASNase.	Ehsanipour et al., 2013
	Vincristine	CAAs secreting SDF-1 α , promoting the migration of ALL toward adipose tissue.	Pramanik et al., 2013
	Daunorubicin	CAAs decreasing daunorubicin concentration in ALL cells by expressing daunorubicin-metabolizing enzymes.	Sheng et al., 2017
Breast cancer	Trastuzumab	Adipose-derived factors decreasing the secretion of INF- γ in natural killer cells.	Duong et al., 2015
	Doxorubicin	CAAs inducing the overexpression of MVP in tumor cells, increasing drug efflux and decreasing drug intracellular accumulation.	Lehuédé et al., 2019
CRC	5-FU	CAAs secreting leptin activating the PI3K/AKT signaling pathway.	Bartucci et al., 2010
Myeloma	Bortezomib	CAAs derived leptin promoting the activation of JAK/STAT-PI3K/AKT pathway.	Yu et al., 2016
	Melphalan, bortezomib	CAAs derived adipokines activating JAK/STAT3 signaling and inducing the upregulation of autophagic proteins, promoting autophagy.	Liu Z. et al., 2015
Ovarian cancer	Paclitaxel	CAAs-derived exosomes transferring higher levels of miR21 to the cancer cells.	Yeung et al., 2016
	Cisplatin	CAAs releasing AA, activating the Akt pathway in ovarian cancer cells.	Yang et al., 2019
	Carboplatin	Adipocytes inducing FABP4 expression.	Mukherjee et al., 2020

CAAs, cancer associated adipocytes; ALL, acute lymphoblastic leukemia; ASNase, L-asparaginase; ASN, amino acids asparagine; GLN, glutamine; ADCC, antibody-dependent cellular cytotoxicity; CRC, Colorectal cancer; 5-FU, 5-fluorouracil; miR21, microRNA-21; LDs, lipid droplets; ROS, reactive oxygen species; AA, Arachidonic acid; PDAC, pancreatic ductal adenocarcinoma.

(Pascual et al., 2017). In ovarian cancer, small molecule inhibition of FABP4 diminishes fatty acids transfer and lipid accumulation in cancer cells, impeding intraabdominal metastasis and growth (Nieman et al., 2011). Recent study also demonstrated that BMS309403, a small molecule inhibitor of FABP4, markedly blocks cell proliferation as well as efficiently restores sensitivity of tumor cells to platinum both *in vitro* and *in vivo* (Mukherjee et al., 2020). However, it is still challenging to selectively target CAAs without affecting other cells. Therefore, identifying the specific molecular mechanisms of adipocyte-mediated drug resistance can help explore additional targets and develop new ways to combat drug resistance in combination with chemotherapy.

ENDOTHELIAL CELLS

In addition to the cells mentioned above, endothelial cells (ECs), covering the inner surfaces of tumor blood vessels, are yet another vital stroma cells in tumor microenvironment that contribute to drug resistance (Hida et al., 2016). As a key mediator in blood vessel growth, ECs are now regarded as the main target cells for anti-vascular therapy. Cumulative evidence indicates that there is considerable heterogeneity in ECs. Tumor endothelial cells (TECs), a special subpopulation of ECs, are phenotypically and functionally different from normal endothelial cells (NECs), which exhibit the property of being quiescent and proliferate only once every 150 days (Hida et al., 2018). And it is the phenotypic and genotypic heterogeneities of TECs that offer novel mechanisms of resistance (Annan et al., 2020).

Cytogenetic abnormalities, including chromosomal aberration like aneuploidy and abnormal centrosomes, have been observed in TECs isolated from human and murine renal cell carcinoma (Akino et al., 2009; Maishi et al., 2019), suggesting that genetic instability is likely to account for the high frequency of resistance to chemotherapeutic drugs in TECs. TECs isolated from HCC were observed to possess enhanced angiogenic activity and acquire resistance to doxorubicin and

5-fluorouracil (Xiong et al., 2009). *In vivo*, several studies have elucidated that the expression of multidrug resistance protein 1 gene (MDR1) and its product, p-glycoprotein were increased in TECs compared to NECs, resulting in tumor growth and drug resistance (Huang et al., 2013; Kikuchi et al., 2020). MDR1 (ABCB1), MRP1 (ABCC1), and ABCG2 are all important ABC (ATP-binding cassette) transporters, which are known for conferring multidrug resistance by pumping drugs out of cells, decreasing intracellular drug concentrations (Gottesman et al., 2002). The up-regulation of MDR1 in TECs may be related to AKT activation caused by high level of VEGF secreted from tumor cells, which could be sufficiently impeded by the VEGFR kinase inhibitor, Ki8751 (Akiyama et al., 2012). Chemotherapy induced high IL-8 expression in tumor cells contributes to the upregulation of MDR1 expression in TECs, which in turn causes drug resistance in human bladder cancer cells (Kikuchi et al., 2020). Moreover, some studies showed that TECs express p-glycoprotein and confer resistance to anti-angiogenic drugs (Naito et al., 2016). Accordingly, drugs of P-glycoprotein inhibitor, such as verapamil, suppressed tumor angiogenesis and abrogated TEC resistance, and increased the sensitivity of tumor endothelium to chemotherapeutics (Akiyama et al., 2015; Bani et al., 2017). In a word, the high expression of P-glycoprotein and other ABC transporters in TECs plays a vital role in mediating multidrug resistance (**Figure 3**).

Hyperglycolytic metabolism has been noted as another major character of TECs versus NECs. The RNA sequencing of TECs and NECs revealed that the expression of most glycolytic genes are up-regulated in TECs, such as PFKFB3, encoding glucose transporter GLUT1 (Slc2a1). And this altered glycolytic metabolism is involved in the formation of abnormal tumor vessels, thus rendering chemoresistance by impairing the delivery and efficacy of chemotherapy. Targeting PFKFB3 in ECs, rather than angiogenic signals, to modulate ECs' metabolism is an effective way to promote tumor vessel normalization (TVN), with increased chemotherapy sensitivity (Cantelmo et al., 2016).

The stemness properties of TECs was claimed to be responsible for resistance to anticancer drugs as well. It has been elucidated that TECs express stem cell markers including the ABC transporter, MDR1, as demonstrated above (Annan et al., 2020). Besides, aldehyde metabolism associated enzyme, namely aldehyde dehydrogenase (ALDH), is considered to be a stem cell marker in TECs. Hida et al. (2017) demonstrated that the increased ALDH^{high} TECs population induced by tumor-secreting factors in TME were accompanied by upregulation of stem-related genes such as MDR1, CD90, ALP, and Oct-4. That may be the cause of resistance to drug therapy.

Tavora et al. (2014) described that TEC-derived focal adhesion kinase (FAK) contributes to the acquisition of chemoresistance, via regulating DNA-damaging related NF- κ B pathway and enhancing the subsequent production of cytokines from endothelial cells *in vivo* and *in vitro*. Additionally, endothelial-cell FAK deficiency is sufficient to restore the sensitivity of tumor cells to DNA-damaging therapies through decreasing the activation of NF- κ B and the following cytokine production. In consistence, the work is supported by clinical relevance as well. In lymphoma patients, disease progression is found to be correlated with altered endothelial cell FAK expression (Tavora et al., 2014).

Endothelial cells-derived paracrine factors, angiocrine factors, are highlighted in conferring drug resistance by the network of endothelial-carcinoma signaling interactions. Tumor-necrosis factor- α (TNF- α), an essential upstream activator of the NF- κ B signaling cascade, was found to be strikingly upregulated in adjacent endothelial cells in breast cancer after doxorubicin chemotherapy treatment (Acharyya et al., 2012), which was induced by the overexpression of CXCL1/2 in breast cancer cells and S100A8/9 in CD11b⁺Gr1⁺ myeloid cells. Moreover, NF- κ B activation amplified the CXCL1/2-S100A8/9 loop in turn. As a result, the highly activation of TNF- α -CXCL1/2-S100A8/9 paracrine network drives chemoresistance by activating ERK1/2, p38 MAPK, and p70S6K, mediating the pro-survival effect in tumor cells. Fibroblast growth factor (FGF) 4, originated from B cell lymphoma cells (LCs), was reported to activate FGFR1, which upregulated the expression of Notch ligand Jagged1 (Jag1) on neighboring ECs. Reciprocally, the elevated EC-derived angiocrine Jag1 promotes LC chemoresistance by activating Notch2-Hey1 signals in LCs. In brief, these results suggested the importance of FGF4-FGFR1/Jag1-Notch2 loop between LCs and ECs in fostering chemoresistance. Obviously angiocrine Jag1 is central to this loop and inhibiting the FGF4/Jag1 feed-forward signaling loop between LCs and ECs could sensitize LCs to chemotherapeutics such as doxorubicin (Cao et al., 2014). Furthermore, the importance of Notch signaling in drug resistance has been proven in other tumors. Hoarau-Vechot et al. (2019) demonstrated that AKT-activated ECs increase the expression of Jagged 1, activating notch signaling and inducing chemoresistance in ovarian cancer. Clinically, high Notch3 expression is notably associated with poorer overall survival and enhanced drug resistance. Thus, targeting of aberrant NOTCH signaling plays a critical role in suppressing ECs-mediated pro-tumoral niche in combination with other therapeutic strategies. IL-6, a proinflammatory cytokine increasingly secreted by other stroma cells, is an important angiocrine factor secreted

by TECs as well. Bent et al. (2016) showed that strong expression of IL-6 from ECs was mediated by ROS-induced p38 activation *in vitro* under doxorubicin treatment. In consequence, IL-6 represses senescence-associated inflammation, promoting chemoresistance via the suppression of PI3K/AKT/mTOR pathway in B-cell lymphoma. Additionally, insulin growth factor (IGF) binding protein-7 (IGFBP7/angiomodulin), an important tumor-suppressive checkpoint expressed by TEC, was reported to participate in the TEC angiocrine mediated chemoresistance as well. Tumor derived FGF4 activates FGFR1 in endothelial cells and stimulates EST-2-dependent upregulation of IGF1 and suppression of IGFBP7, leading to chemotherapy tolerance and promoting tumor recurrence and lethality (Cao et al., 2017).

Moreover, it has been shown that ECs play an important part in mediating resistance to anti-vascular drugs and immunotherapy (Nagl et al., 2020). In glioblastoma, tumor derived PDGF activates ECs, inducing NF- κ B-dependent Snail expression, resulting in endothelial-mesenchymal transformation (Endo-MT). Further, Endo-MT abrogates the expression of VEGFR-2, the major regulator of angiogenesis, causing endothelial resistance to anti-VEGF treatment (Liu T. et al., 2018). Remarkably, PDGFR- β knockout in ECs robustly sensitizes GBM tumors to anti-VEGF therapy, suggesting targeting PDGF/NF- κ B/Snail axis and preventing Endo-MT in ECs may offer exciting opportunities in antiangiogenic therapy resistance. In addition to encasing blood vessels, endothelial cells also form the inner layer of lymphatic vessels, which implicates ECs also involve in treatment response to checkpoint antibody therapy as key mediators of immune regulation (Nagl et al., 2020). By detecting 1,592 endothelial cells in lung cancer, Lambrechts et al. (2018) revealed that TECs downregulate immune attraction pathways by reducing the expression of chemotaxis (CCL2, CCL18, and IL6), adhesion molecules (ICAM1) and antigen presentation associated molecular (major histocompatibility complex class I and II), which contributes to tumor immunotolerance in TME. Besides, TECs promote the formation of abnormal tumor vessels, which facilitates the presence of immunosuppressive immune cells, attenuating the efficacy of immunotherapy based on immune checkpoint inhibitors (ICIs) (Schaaf et al., 2018).

As discussed above, ECs induce resistance to chemotherapy, anti-vascular therapy, and immunotherapy through multiple mechanisms, including cytogenetic abnormalities, hyperglycolytic metabolism, secreting paracrine factors and inducing abnormal tumor vasculature (Table 7). Hence, targeting these crosstalks and signaling axis as stated before can help overcome tolerogenic events. In particular, reprogramming the ECs glycolytic phenotype and promoting tumor vasculature-normalizing, combined with immunotherapy are promising strategy (Stapor et al., 2014; Cantelmo et al., 2016).

PLATELETS

Derived from common hematopoietic progenitor cells, platelet is a key regulator in hemostasis and thrombosis (Contursi et al., 2017). However, emerging studies have focused on

TABLE 7 | Mechanisms of antitumor drug resistance mediated by ECs.

Tumor type	Drug resistance	Mechanisms	References
B cell lymphoma	Doxorubicin	ECs producing Jag1, inducing Notch2-Hey1 in LCs.	Cao et al., 2014
	Doxorubicin	TECs releasing IL-6, promoting suppression of PI3K/AKT/mTOR pathway in B-cell lymphoma.	Bent et al., 2016
Breast cancer	Doxorubicin, cyclophosphamide	ECs secreting TNF- α , activating NF- κ B pathway.	Acharyya et al., 2012
Glioblastoma	Anti-angiogenic drug	Hypoxia inducing the differentiation of tumor cells to ECs.	Soda et al., 2011
	Anti-angiogenic drug	Activated by PDGF, ECs inducing NF- κ B-dependent Snail expression, resulting in VEGFR-2 down-expression and Endo-MT.	Liu T. et al., 2018
HCC	Doxorubicin	Abnormal activation of FGFR1-ETS2 pathway in TECs	Cao et al., 2017
	Anti-angiogenic drug	CD105 ⁺ TECs showing increased apoptosis resistance and motility and proangiogenic properties.	Xiong et al., 2009
Lung cancer	Anti-angiogenic drug	ECs contributing to new blood vessel formation.	Naito et al., 2016
Melanoma	Doxorubicin	TEC-derived FAK regulating DNA-damaging related NF- κ B pathway.	Tavora et al., 2014
Ovarian cancer	Paclitaxel, doxorubicin, vincristine	Highly expression of P-gp and other ABC transporters in TECs.	Bani et al., 2017
RCC	Fluorouracil	TEC containing stem cell-like populations with high ALDH activity ALDH ^{high} TEC	Hida et al., 2017
Urothelial carcinoma	Paclitaxel	Increased tumor IL-8 secretion promoting TECs express high levels of a drug efflux transporter, ABCB1.	Kikuchi et al., 2020

ECs, endothelial cells; TECs, tumor endothelial cells; LCs, lymphoma cells; TNF- α , tumor-necrosis factor- α ; PDGF, platelet-derived growth factor; Endo-MT, endothelial-mesenchymal transformation; HCC, hepatocellular carcinoma; FAK, focal adhesion kinase; P-gp, P-glycoprotein; ABC transporters, ATP-binding cassette transporters; RCC, renal cell carcinoma; 5-FU, 5-fluorouracil; ALDH, aldehyde dehydrogenase.

TABLE 8 | Mechanisms of antitumor drug resistance mediated by platelets.

Tumor type	Drug resistance	Mechanisms	References
Adenocarcinoma	Paclitaxel	Platelets secreting thrombospondin-1, and RANTES, modulating cancer cell cycle, DNA damage repair pathways and MAPK levels.	Radziwon-Balicka et al., 2012
HCC	Multikinase inhibitor	Platelets derived growth factors such as PDGF, TGF- α and - β , EGF and serotonin, regulating the sensitivity and resistance to multikinase inhibitors.	D'Alessandro et al., 2015
NSCLC	Cisplatin	Platelets rescuing cisplatin-induced apoptosis via the Akt/Bad/Bcl-2 signaling pathway.	Wang Z. et al., 2018
Pancreatic cancer	Cisplatin	Platelets releasing TGF- β , activating PI3K/Akt and MEK/Erk signaling.	Chen et al., 2013

HCC, hepatocellular carcinoma; PDGF, platelet-derived growth factor; EGF, epidermal growth factor; NSCLC, non-small cell lung cancer.

its contributions to various aspects of cancer progression, including angiogenesis, tumor growth, metastasis and drug resistance (D'Alessandro et al., 2015; Tesfamariam, 2016; Contursi et al., 2017). Multiple reports have shown a strong link between platelets and the efficiency of tumor chemotherapy. For instance, platelet-sparing phenomenon was reported in patients treated with carboplatin and paclitaxel chemotherapy (Pertusini et al., 2001). Moreover, differential platelet levels or the platelet/lymphocyte ratios have been suggested to be a potential predictive factor of chemotherapy response or survival prognosis in various tumors, including breast cancer, gastric cancer, NSCLC, pancreatic neuroendocrine tumor, ovarian cancer and so on (Bottsford-Miller et al., 2015; Cuello-López et al., 2018; Fang et al., 2018; Gong et al., 2018; Xu S.S. et al., 2019). Tumor-educated platelets (TEPs) are even considered to be potential non-invasive biomarker in achieving effective cancer management (In 't Veld and Wurdinger, 2019). Clinically, high platelet count has been correlated with chemotherapy resistance. Therefore, it is necessary to understand the association between platelets and drug-resistance in TME.

Platelets contribute to drug resistance through secreting various factors, altering chemotherapy pharmacokinetics, and eliciting multiple signaling pathways (Table 8).

Many reports have indicated platelets to be an important source of diverse growth factors and cytokines, leading to drug resistance in TME (Assoian et al., 1983). As mentioned earlier, TGF- β /NF- κ B signaling is a vital pathway involved in tumor drug resistance. Recent experiment demonstrated that platelets not only function as the major source of TGF- β but also express the cell surface-docking receptor glycoprotein A repetitions predominant (GARP), increasing the active TGF- β levels. The GARP-TGF- β axis promoted by platelets constrain T cell immunity against cancer, thus rendering resistance to therapy (Rachidi et al., 2017). Besides, platelet-derived TGF- β could activate the TGF- β /Smad and NF- κ B pathways, subsequently leading to the EMT in tumor cells (Labelle et al., 2011), which was suggested to significantly contribute to the development of chemoresistance (Fischer et al., 2015). In pancreatic cancer, TGF- β released by platelets diminished cisplatin sensitivity through activating PI3K/Akt and MEK/Erk signaling (Chen et al., 2013). Apart from TGF- β , other platelet factors were reported to mediate drug resistance *in vitro* as well. Clusterin, thrombospondin-1, and RANTES secreted by platelet are demonstrated to protect adenocarcinoma cells from anticancer drugs via modulating cancer cell cycle, DNA damage repair pathways and MAPK levels (Radziwon-Balicka et al., 2012).

Another important mechanism lies in modulating drug metabolism. Clinical studies have shown the association of multidrug resistance-associated protein 1 (MRP1) expression and platelet count with clinical outcome in 427 operable NSCLC patients (Wang Z. et al., 2018). In fact, the expression of two ABC transporter in platelets, MRP4 and MRP1, was suggested to be relatively high (Köck et al., 2007), which confers drug resistance by promoting drug efflux, reducing intracellular drug concentrations (Oevermann et al., 2009).

In addition to chemotherapy drugs, platelets can also lead to tolerance to anti-angiogenic therapy. In HCC, platelets derived growth factors such as PDGF, TGF- α , and - β , EGF and serotonin, are ascribed to modulate the sensitivity and resistance to multikinase inhibitors (D'Alessandro et al., 2015). In glioblastoma multiforme (GBM) patients, platelet-derived VEGF shows potent pro-angiogenic effects on GBM-derived endothelial cells. Patients with GBM have significantly higher intraplatelet VEGF concentrations compared to healthy controls (Di Vito et al., 2017). Consistently, it has been accepted that redundancy of vascular stimulation signals may be the basis for resistance to anti-angiogenic therapy (van Beijnum et al., 2015).

Accordingly, in terms of platelet-induced drug resistance, apart from targeting relevant platelet-originated factors (e.g., PDGF, TGF β 1, and EGF) and pathways including TGF- β /NF- κ B signaling, targeting the activity of platelets in TME is an important approach to improve the sensitivity of tumor therapy. Aspirin, a potent inhibitor of platelet function, has been suggested to potentially enhance the sensitivity to 5-Fu-based chemotherapy in colorectal cancer (CRC) via abrogating the activation of NF- κ B both *in vivo* and *in vitro* (Fu et al., 2019). Ticagrelor, an inhibitor of the ADP-P2Y₁₂ axis, was demonstrated to boost chemotherapeutic efficacy synergized with chemotherapeutic agents in pancreatic cancer cells, which was mediated by reducing EGF-dependent AKT activation (Elaskalani et al., 2020). Noteworthy, potential challenges remain in antiplatelet strategies during cancer therapy, including the risk of bleeding and comorbidity. Further experimental and clinical confirmation validation are warranted to validate the benefits and risks of combined antiplatelet therapy in cancer patients.

CONCLUSION

Taken together, the evidence we summarized here clearly demonstrate that TME has a considerable impact on tumorigenesis and resistance in the context of therapeutic intervention. Therefore, TME is an attractive target for

both sensitizing tumors to traditional therapies and as an alternative choice for resistant disease. Targeting these stroma cells is a potentially helpful adjunct to immunotherapy and targeted therapy. Repolarization and normalization rather than elimination of these cells seems a preferable choice. Despite of the heat of immunotherapy, we cannot ignore the fact that chemotherapies and molecular targeted therapies are still basic and effective in many cancers, especially for early-stage patients. The primary challenges lie in that we need to determine the best combinations or sequences and manage patients based on whether they are likely to benefit from a specific drug or drug combination.

In any case, our current insight into the cancer therapy suggests that rapid tumor cell elimination is crucial to prevent acquired therapeutic resistance. In order to achieve this goal, treatment combinations need to be optimized to delay the progression of drug resistance. Meanwhile, novel strategies targeting and reshaping the microenvironment to block pro-tumor cross-talk and restore immune surveillance are urgently required. Lastly, because current preclinical models of TME cannot completely represent variations exhibited by patients of different histological types, detailed molecular and cellular profiles are needed for clinical trials, which is necessary for identifying predictive biomarkers and promoting the development of personalized treatment.

AUTHOR CONTRIBUTIONS

YN and XTZ contributed to the first draft of the article, the tables, and the figures. JY provided assistance in making figures. HS and HL revised the manuscript. XZ and XM conceived the presented idea, revised the manuscript again, and approved the final version. All authors approved the manuscript for publication.

FUNDING

This work was supported by the Funding of Sichuan Provincial Science and Technology Department (No. 2018JY0165), the National Major Scientific and Technological Special Project for the "Significant New Drugs Development" (No. 2018ZX09201018-013), the National Natural Science Foundation of China (No. 81821002), the National Science and Technology Major Projects for Major New Drugs Innovation and Development (No. 2018ZX09733001-004), and the National Natural Science Foundation of China (No. 81902662).

REFERENCES

- Acharyya, S., Oskarsson, T., Vanharanta, S., Malladi, S., Kim, J., Morris, P. G., et al. (2012). A CXCL1 paracrine network links cancer chemoresistance and metastasis. *Cell* 150, 165–178. doi: 10.1016/j.cell.2012.04.042
- Adamo, A., Dal Collo, G., Bazzoni, R., and Krampfer, M. (2019). Role of mesenchymal stromal cell-derived extracellular vesicles in tumour microenvironment. *Biochim. Biophys. Acta Rev. Cancer* 1871, 192–198. doi: 10.1016/j.bbcan.2018.12.001
- Aggen, D. H., Ager, C. R., Obradovic, A. Z., Chowdhury, N., Ghasemzadeh, A., Mao, W., et al. (2021). Blocking IL1 beta promotes tumor regression and remodeling of the myeloid compartment in a renal cell carcinoma model: multidimensional analyses. *Clin. Cancer Res.* 27, 608–621. doi: 10.1158/1078-0432.CCR-20-1610
- Akino, T., Hida, K., Hida, Y., Tsuchiya, K., Freedman, D., Muraki, C., et al. (2009). Cytogenetic abnormalities of tumor-associated endothelial cells in human malignant tumors. *Am. J. Pathol.* 175, 2657–2667. doi: 10.2353/ajpath.2009.090202

- Akiyama, K., Maishi, N., Ohga, N., Hida, Y., Ohba, Y., Alam, M. T., et al. (2015). Inhibition of multidrug transporter in tumor endothelial cells enhances antiangiogenic effects of low-dose metronomic paclitaxel. *Am. J. Pathol.* 185, 572–580. doi: 10.1016/j.ajpath.2014.10.017
- Akiyama, K., Ohga, N., Hida, Y., Kawamoto, T., Sadamoto, Y., Ishikawa, S., et al. (2012). Tumor endothelial cells acquire drug resistance by MDR1 up-regulation via VEGF signaling in tumor microenvironment. *Am. J. Pathol.* 180, 1283–1293. doi: 10.1016/j.ajpath.2011.11.029
- Akkari, L., Bowman, R. L., Tessier, J., Klemm, F., Handgraaf, S. M., de Groot, M., et al. (2020). Dynamic changes in glioma macrophage populations after radiotherapy reveal CSF-1R inhibition as a strategy to overcome resistance. *Sci. Transl. Med.* 12:eaaw7843. doi: 10.1126/scitranslmed.aaw7843
- Allen, E., Miéville, P., Warren, C. M., Saghaflinia, S., Li, L., Peng, M. W., et al. (2016). Metabolic symbiosis enables adaptive resistance to anti-angiogenic therapy that is dependent on mtor signaling. *Cell Rep.* 15, 1144–1160. doi: 10.1016/j.celrep.2016.04.029
- Amawi, H., Sim, H. M., Tiwari, A. K., Ambudkar, S. V., and Shukla, S. (2019). ABC transporter-mediated multidrug-resistant cancer. *Adv. Exp. Med. Biol.* 1141, 549–580. doi: 10.1007/978-981-13-7647-4_12
- Ambrose, J., Livitz, M., Wessels, D., Kuhl, S., Lusche, D. F., Scherer, A., et al. (2015). Mediated coalescence: a possible mechanism for tumor cellular heterogeneity. *Am. J. Cancer Res.* 5, 3485–3504.
- Ando, K., Takahashi, F., Kato, M., Kaneko, N., Doi, T., Ohe, Y., et al. (2014). Tocilizumab, a proposed therapy for the cachexia of Interleukin6-expressing lung cancer. *PLoS One* 9:e102436. doi: 10.1371/journal.pone.0102436
- Angst, E., Reber, H. A., Hines, O. J., and Eibl, G. (2008). Mononuclear cell-derived interleukin-1 beta confers chemoresistance in pancreatic cancer cells by upregulation of cyclooxygenase-2. *Surgery* 144, 57–65. doi: 10.1016/j.surg.2008.03.024
- Annan, D. A., Kikuchi, H., Maishi, N., Hida, Y., and Hida, K. (2020). Tumor endothelial cell-a biological tool for translational cancer research. *Int. J. Mol. Sci.* 21:3238. doi: 10.3390/ijms21093238
- Apicella, M., Giannoni, E., Fiore, S., Ferrari, K. J., Fernández-Pérez, D., Isella, C., et al. (2018). Increased lactate secretion by cancer cells sustains non-cell-autonomous adaptive resistance to MET and EGFR targeted therapies. *Cell Metab.* 28, 848.e6–865.e6. doi: 10.1016/j.cmet.2018.08.006
- Aslan, K., Turco, V., Blobner, J., Sonner, J. K., Liuzzi, A. R., Núñez, N. G., et al. (2020). Heterogeneity of response to immune checkpoint blockade in hypermutated experimental gliomas. *Nat. Commun.* 11:931. doi: 10.1038/s41467-020-14642-0
- Assoian, R. K., Komoriya, A., Meyers, C. A., Miller, D. M., and Sporn, M. B. (1983). Transforming growth factor-beta in human platelets. Identification of a major storage site, purification, and characterization. *J. Biol. Chem.* 258, 7155–7160.
- Baghdadi, M., Wada, H., Nakanishi, S., Abe, H., Han, N., Putra, W. E., et al. (2016). Chemotherapy-Induced IL34 enhances immunosuppression by tumor-associated macrophages and mediates survival of chemoresistant lung cancer cells. *Cancer Res.* 76, 6030–6042. doi: 10.1158/0008-5472.Can-16-1170
- Bamias, A., Koutsoukou, V., Terpos, E., Tsiatas, M. L., Liakos, C., Tsitsilonis, O., et al. (2008). Correlation of NK T-like CD3+CD56+ cells and CD4+CD25+(hi) regulatory T cells with VEGF and TNFalpha in ascites from advanced ovarian cancer: association with platinum resistance and prognosis in patients receiving first-line, platinum-based chemotherapy. *Gynecol. Oncol.* 108, 421–427. doi: 10.1016/j.ygyno.2007.10.018
- Bani, M., Decio, A., Giavazzi, R., and Ghilardi, C. (2017). Contribution of tumor endothelial cells to drug resistance: anti-angiogenic tyrosine kinase inhibitors act as p-glycoprotein antagonists. *Angiogenesis* 20, 233–241. doi: 10.1007/s10456-017-9549-6
- Bartucci, M., Svensson, S., Ricci-Vitiani, L., Dattilo, R., Biffoni, M., Signore, M., et al. (2010). Obesity hormone leptin induces growth and interferes with the cytotoxic effects of 5-fluorouracil in colorectal tumor stem cells. *Endocr. Relat. Cancer* 17, 823–833. doi: 10.1677/ERC-10-0083
- Bedke, J., Albiges, L., Capitano, U., Giles, R. H., Hora, M., Lam, T. B., et al. (2021). Updated European Association of urology guidelines on renal cell carcinoma: nivolumab plus cabozantinib joins immune checkpoint inhibition combination therapies for treatment-naïve metastatic clear-cell renal cell carcinoma. *Eur. Urol.* 79, 339–342. doi: 10.1016/j.eururo.2020.12.005
- Bent, E. H., Gilbert, L. A., and Hemann, M. T. (2016). A senescence secretory switch mediated by PI3K/AKT/mTOR activation controls chemoprotective endothelial secretory responses. *Genes Dev.* 30, 1811–1821. doi: 10.1101/gad.284851.116
- Binenbaum, Y., Fridman, E., Yaari, Z., Milman, N., Schroeder, A., Ben David, G., et al. (2018). Transfer of miRNA in macrophage-derived exosomes induces drug resistance in pancreatic adenocarcinoma. *Cancer Res.* 78, 5287–5299. doi: 10.1158/0008-5472.Can-18-0124
- Bliss, S. A., Sinha, G., Sandiford, O. A., Williams, L. M., Engelberth, D. J., Guiro, K., et al. (2016). Mesenchymal stem cell-derived exosomes stimulate cycling quiescence and early breast cancer dormancy in bone marrow. *Cancer Res.* 76, 5832–5844. doi: 10.1158/0008-5472.Can-16-1092
- Bochet, L., Lehuédé, C., Dauvillier, S., Wang, Y. Y., Dirat, B., Laurent, V., et al. (2013). Adipocyte-derived fibroblasts promote tumor progression and contribute to the desmoplastic reaction in breast cancer. *Cancer Res.* 73, 5657–5668. doi: 10.1158/0008-5472.Can-13-0530
- Borriello, L., Nakata, R., Sheard, M. A., Fernandez, G. E., Sposto, R., Malvar, J., et al. (2017). Cancer-associated fibroblasts share characteristics and protumorigenic activity with mesenchymal stromal cells. *Cancer Res.* 77, 5142–5157. doi: 10.1158/0008-5472.CAN-16-2586
- Bottsford-Miller, J., Choi, H. J., Dalton, H. J., Stone, R. L., Cho, M. S., Haemmerle, M., et al. (2015). Differential platelet levels affect response to taxane-based therapy in ovarian cancer. *Clin. Cancer Res.* 21, 602–610. doi: 10.1158/1078-0432.Ccr-14-0870
- Calcinotto, A., Spataro, C., Zagato, E., Di Mitri, D., Gil, V., Crespo, M., et al. (2018). IL-23 secreted by myeloid cells drives castration-resistant prostate cancer. *Nature* 559, 363–369. doi: 10.1038/s41586-018-0266-0
- Calle, E. E., Rodriguez, C., Walker-Thurmond, K., and Thun, M. J. (2003). Overweight, obesity, and mortality from cancer in a prospectively studied cohort of US adults. *N. Engl. J. Med.* 348, 1625–1638. doi: 10.1056/NEJMoa021423
- Campbell, J. R., McDonald, B. R., Mesko, P. B., Siemers, N. O., Singh, P. B., Selby, M., et al. (2021). Fc-optimized Anti-CCR8 antibody depletes regulatory T cells in human tumor models. *Cancer Res.* doi: 10.1158/0008-5472.Can-20-3585 [Epub ahead of print].
- Cantelmo, A. R., Conradi, L. C., Brajic, A., Goveia, J., Kalucka, J., Pircher, A., et al. (2016). Inhibition of the glycolytic activator PFKFB3 in endothelium induces tumor vessel normalization, impairs metastasis, and improves chemotherapy. *Cancer Cell* 30, 968–985. doi: 10.1016/j.ccell.2016.10.006
- Cao, Z., Ding, B. S., Guo, P., Lee, S. B., Butler, J. M., Casey, S. C., et al. (2014). Angiocrine factors deployed by tumor vascular niche induce B cell lymphoma invasiveness and chemoresistance. *Cancer Cell* 25, 350–365. doi: 10.1016/j.ccr.2014.02.005
- Cao, Z., Scandura, J. M., Inghirami, G. G., Shido, K., Ding, B. S., and Rafii, S. (2017). Molecular checkpoint decisions made by subverted vascular niche transform indolent tumor cells into chemoresistant cancer stem cells. *Cancer Cell* 31, 110–126. doi: 10.1016/j.ccell.2016.11.010
- Cardenas, H., Vieth, E., Lee, J., Segar, M., Liu, Y., Nephew, K. P., et al. (2014). TGF-β induces global changes in DNA methylation during the epithelial-to-mesenchymal transition in ovarian cancer cells. *Epigenetics* 9, 1461–1472. doi: 10.4161/15592294.2014.971608
- Catalano, S., Mauro, L., Marsico, S., Giordano, C., Rizza, P., Rago, V., et al. (2004). Leptin induces, via ERK1/ERK2 signal, functional activation of estrogen receptor alpha in MCF-7 cells. *J. Biol. Chem.* 279, 19908–19915. doi: 10.1074/jbc.M313191200
- Cazet, A. S., Hui, M. N., Elsworth, B. L., Wu, S. Z., Roden, D., Chan, C. L., et al. (2018). Targeting stromal remodeling and cancer stem cell plasticity overcomes chemoresistance in triple negative breast cancer. *Nat. Commun.* 9:2897. doi: 10.1038/s41467-018-05220-6
- Che, Y., Wang, J., Li, Y., Lu, Z., Huang, J., Sun, S., et al. (2018). Cisplatin-activated PAI-1 secretion in the cancer-associated fibroblasts with paracrine effects promoting esophageal squamous cell carcinoma progression and causing chemoresistance. *Cell Death Dis.* 9:759. doi: 10.1038/s41419-018-0808-2
- Chen, H., Lan, X., Liu, M., Zhou, B., Wang, B., and Chen, P. (2013). Direct TGF-β1 signaling between activated platelets and pancreatic cancer cells primes cisplatin insensitivity. *Cell Biol. Int.* 37, 478–484. doi: 10.1002/cbin.10067
- Chi, M., Chen, J., Ye, Y., Tseng, H. Y., Lai, F., Tay, K. H., et al. (2014). Adipocytes contribute to resistance of human melanoma cells to chemotherapy and targeted therapy. *Curr. Med. Chem.* 21, 1255–1267. doi: 10.2174/0929867321666131129114742
- Choi, J., Cha, Y. J., and Koo, J. S. (2018). Adipocyte biology in breast cancer: from silent bystander to active facilitator. *Prog. Lipid Res.* 69, 11–20. doi: 10.1016/j.plipres.2017.11.002

- Ciardiello, D., Elez, E., Tabernero, J., and Seoane, J. (2020). Clinical development of therapies targeting TGF β : current knowledge and future perspectives. *Ann. Oncol.* 31, 1336–1349. doi: 10.1016/j.annonc.2020.07.009
- Contursi, A., Sacco, A., Grande, R., Dovizio, M., and Patrignani, P. (2017). Platelets as crucial partners for tumor metastasis: from mechanistic aspects to pharmacological targeting. *Cell Mol. Life Sci.* 74, 3491–3507. doi: 10.1007/s00118-017-2536-7
- Cuello-López, J., Fidalgo-Zapata, A., López-Agudelo, L., and Vásquez-Trespalcacios, E. (2018). Platelet-to-lymphocyte ratio as a predictive factor of complete pathologic response to neoadjuvant chemotherapy in breast cancer. *PLoS One* 13:e0207224. doi: 10.1371/journal.pone.0207224
- D'Alessandro, R., Messa, C., Refolo, M. G., and Carr, B. I. (2015). Modulation of sensitivity and resistance to multikinase inhibitors by microenvironmental platelet factors in HCC. *Expert Opin. Pharmacother.* 16, 2773–2780. doi: 10.1517/14656566.2015.1101065
- De Henau, O., Rausch, M., Winkler, D., Campesato, L. F., Liu, C., Cymerman, D. H., et al. (2016). Overcoming resistance to checkpoint blockade therapy by targeting PI3K γ in myeloid cells. *Nature* 539, 443–447. doi: 10.1038/nature20554
- De Veirman, K., Menu, E., Maes, K., De Beule, N., De Smedt, E., Maes, A., et al. (2019). Myeloid-derived suppressor cells induce multiple myeloma cell survival by activating the AMPK pathway. *Cancer Lett.* 442, 233–241. doi: 10.1016/j.canlet.2018.11.002
- Deaglio, S., Dwyer, K. M., Gao, W., Friedman, D., Usheva, A., Erat, A., et al. (2007). Adenosine generation catalyzed by CD39 and CD73 expressed on regulatory T cells mediates immune suppression. *J. Exp. Med.* 204, 1257–1265. doi: 10.1084/jem.20062512
- Deng, X., Ruan, H., Zhang, X., Xu, X., Zhu, Y., Peng, H., et al. (2020). Long noncoding RNA CCAL transferred from fibroblasts by exosomes promotes chemoresistance of colorectal cancer cells. *Int. J. Cancer* 146, 1700–1716. doi: 10.1002/ijc.32608
- Deying, W., Feng, G., Shumei, L., Hui, Z., Ming, L., and Hongqing, W. (2017). CAF-derived HGF promotes cell proliferation and drug resistance by up-regulating the c-Met/PI3K/Akt and GRP78 signalling in ovarian cancer cells. *Biosci. Rep.* 37:BSR20160470. doi: 10.1042/bsr20160470
- Di Vito, C., Navone, S. E., Marfia, G., Abdel Hadi, L., Mancuso, M. E., Pecci, A., et al. (2017). Platelets from glioblastoma patients promote angiogenesis of tumor endothelial cells and exhibit increased VEGF content and release. *Platelets* 28, 585–594. doi: 10.1080/09537104.2016.1247208
- Diggs, L. P., Ruf, B., Ma, C., Heinrich, B., Cui, L., Zhang, Q., et al. (2020). CD40-mediated immune cell activation enhances response to anti-PD-1 in murine intrahepatic cholangiocarcinoma. *J. Hepatol.* 74, 1145–1154. doi: 10.1016/j.jhep.2020.11.037
- Dirat, B., Bochet, L., Dabek, M., Daviaud, D., Dauvillier, S., Majed, B., et al. (2011). Cancer-associated adipocytes exhibit an activated phenotype and contribute to breast cancer invasion. *Cancer Res.* 71, 2455–2465. doi: 10.1158/0008-5472.Can-10-3323
- Doi, T., Muro, K., Ishii, H., Kato, T., Tsushima, T., Takenoyama, M., et al. (2019). A Phase I study of the Anti-CC Chemokine Receptor 4 antibody, mogamulizumab, in combination with nivolumab in patients with advanced or metastatic solid tumors. *Clin. Cancer Res.* 25, 6614–6622. doi: 10.1158/1078-0432.Ccr-19-1090
- Duong, M. N., Cleret, A., Matera, E. L., Chettab, K., Mathe, D., Valsesia-Wittmann, S., et al. (2015). Adipose cells promote resistance of breast cancer cells to trastuzumab-mediated antibody-dependent cellular cytotoxicity. *Breast Cancer Res.* 17:57. doi: 10.1186/s13058-015-0569-0
- Duong, M. N., Geneste, A., Fallone, F., Li, X., Dumontet, C., and Muller, C. (2017). The fat and the bad: mature adipocytes, key actors in tumor progression and resistance. *Oncotarget* 8, 57622–57641. doi: 10.18632/oncotarget.18038
- Dzobo, K., Vogelsang, M., Thomford, N. E., Dandara, C., Kallmeyer, K., Pepper, M. S., et al. (2016). Wharton's jelly-derived mesenchymal stromal cells and fibroblast-derived extracellular matrix synergistically activate apoptosis in a p21-dependent mechanism in WHCO1 and MDA MB 231 cancer cells in vitro. *Stem Cells Int.* 2016:4842134. doi: 10.1155/2016/4842134
- Ebbing, E. A., van der Zalm, A. P., Steins, A., Creemers, A., Hermesen, S., Rentenaar, R., et al. (2019). Stromal-derived interleukin 6 drives epithelial-to-mesenchymal transition and therapy resistance in esophageal adenocarcinoma. *Proc. Natl. Acad. Sci. U.S.A.* 116, 2237–2242. doi: 10.1073/pnas.1820459116
- Ehsanipour, E. A., Sheng, X., Behan, J. W., Wang, X. C., Butturini, A., Avramis, V. I., et al. (2013). Adipocytes cause leukemia cell resistance to L-Asparaginase via release of glutamine. *Cancer Res.* 73, 2998–3006. doi: 10.1158/0008-5472.Can-12-4402
- Elaskalani, O., Domenichini, A., Abdol Razak, N. B., Dye D. E., Falasca, M., and Metharom, P. (2020). Antiplatelet drug ticagrelor enhances chemotherapeutic efficacy by targeting the novel P2Y12-AKT pathway in pancreatic cancer cells. *Cancers* 12:250. doi: 10.3390/cancers12010250
- Ewertz, M., Jensen, M. B., Gunnarsdottir, K. A., Hojris, I., Jakobsen, E. H., Nielsen, D., et al. (2011). Effect of obesity on prognosis after early-stage breast cancer. *J. Clin. Oncol.* 29, 25–31. doi: 10.1200/JCO.2010.29.7614
- Fang, L., Sheng, H., Wan, D., Zhu, C., Jiang, R., Sun, X., et al. (2018). Prognostic role of multidrug resistance-associated protein 1 expression and platelet count in operable non-small cell lung cancer. *Oncol. Lett.* 16, 1123–1132. doi: 10.3892/ol.2018.8763
- Fang, Y., Zhou, W., Rong, Y., Kuang, T., Xu, X., Wu, W., et al. (2019). Exosomal miRNA-106b from cancer-associated fibroblast promotes gemcitabine resistance in pancreatic cancer. *Exp. Cell Res.* 383:111543. doi: 10.1016/j.yexcr.2019.111543
- Fiori, M. E., Di Franco, S., Villanova, L., Bianca, P., Stassi, G., and De Maria, R. (2019). Cancer-associated fibroblasts as abettors of tumor progression at the crossroads of EMT and therapy resistance. *Mol. Cancer* 18:70. doi: 10.1186/s12943-019-0994-2
- Fischer, K. R., Durrans, A., Lee, S., Sheng, J., Li, F., Wong, S. T., et al. (2015). Epithelial-to-mesenchymal transition is not required for lung metastasis but contributes to chemoresistance. *Nature* 527, 472–476. doi: 10.1038/nature15748
- Folgiero, V., Miele, E., Carai, A., Ferretti, E., Alfano, V., Po, A., et al. (2016). IDO1 involvement in mTOR pathway: a molecular mechanism of resistance to mTOR targeting in medulloblastoma. *Oncotarget* 7, 52900–52911. doi: 10.18632/oncotarget.9284
- Fridlender, Z. G., Sun, J., Kim, S., Kapoor, V., Cheng, G., Ling, L., et al. (2009). Polarization of tumor-associated neutrophil phenotype by TGF- β : “N1” versus “N2”. *TAN. Cancer Cell* 16, 183–194. doi: 10.1016/j.ccr.2009.06.017
- Fu, H., Yang, H., Zhang, X., and Xu, W. (2016). The emerging roles of exosomes in tumor-stroma interaction. *J. Cancer Res. Clin. Oncol.* 142, 1897–1907. doi: 10.1007/s00432-016-2145-0
- Fu, J., Xu, Y., Yang, Y., Liu, Y., Ma, L., and Zhang, Y. (2019). Aspirin suppresses chemoresistance and enhances antitumor activity of 5-Fu in 5-Fu-resistant colorectal cancer by abolishing 5-Fu-induced NF- κ B activation. *Scie. Rep.* 9:16937. doi: 10.1038/s41598-019-53276-1
- Fultang, L., Panetti, S., Ng, M., Collins, P., Graef, S., Rizkalla, N., et al. (2019). MDSC targeting with Gemtuzumab ozogamicin restores T cell immunity and immunotherapy against cancers. *EBioMedicine* 47, 235–246. doi: 10.1016/j.ebiom.2019.08.025
- Gabrilovich, D. I. (2017). Myeloid-derived suppressor cells. *Cancer Immunol. Res.* 5, 3–8. doi: 10.1158/2326-6066.Cir-16-0297
- Gilbert, P. M., Havenstrite, K. L., Magnusson, K. E., Sacco, A., Leonardi, N. A., Kraft, P., et al. (2010). Substrate elasticity regulates skeletal muscle stem cell self-renewal in culture. *Science* 329, 1078–1081. doi: 10.1126/science.1191035
- Gong, W., Zhao, L., Dong, Z., Dou, Y., Liu, Y., Ma, C., et al. (2018). After neoadjuvant chemotherapy platelet/lymphocyte ratios negatively correlate with prognosis in gastric cancer patients. *J. Clin. Lab. Anal.* 32:e22364. doi: 10.1002/jcla.22364
- Gottesman, M. M., Fojo, T., and Bates, S. E. (2002). Multidrug resistance in cancer: role of ATP-dependent transporters. *Nat. Rev. Cancer* 2, 48–58. doi: 10.1038/nrc706
- Gourdin, N., Bossennec, M., Rodriguez, C., Vigano, S., Machon, C., Jandus, C., et al. (2018). Autocrine adenosine regulates tumor polyfunctional CD73(+)CD4(+) effector T Cells devoid of immune checkpoints. *Cancer Res.* 78, 3604–3618. doi: 10.1158/0008-5472.Can-17-2405
- Guillaumond, F., Bidaut, G., Ouassiss, M., Servais, S., Gouirand, V., Olivares, O., et al. (2015). Cholesterol uptake disruption, in association with chemotherapy, is a promising combined metabolic therapy for pancreatic adenocarcinoma. *Proc. Natl. Acad. Sci. U.S.A.* 112, 2473–2478. doi: 10.1073/pnas.1421601112
- Guillén Díaz-Maroto, N., Sanz-Pamplona, R., Berdiel-Acer, M., Cimas, F. J., García, E., Gonçalves-Ribeiro, S., et al. (2019). Noncanonical TGF β pathway relieves the blockade of IL1 β /TGF β -Mediated crosstalk between tumor and stroma:

- TGFBRI and TAK1 inhibition in colorectal cancer. *Clin. Cancer Res.* 25, 4466–4479. doi: 10.1158/1078-0432.CCR-18-3957
- Guo, Q. R., Wang, H., Yan, Y. D., Liu, Y., Su, C. Y., Chen, H. B., et al. (2020). The role of exosomal microRNA in cancer drug resistance. *Front. Oncol.* 10:472. doi: 10.3389/fonc.2020.00472
- Gyori, D., Lim, E. L., Grant, F. M., Spensberger, D., Roychoudhuri, R., Shuttleworth, S. J., et al. (2018). Compensation between CSF1R+ macrophages and Foxp3+ Treg cells drives resistance to tumor immunotherapy. *JCI Insight* 3:e120631. doi: 10.1172/jci.insight.120631
- Halbrook, C. J., Pontious, C., Kovalenko, I., Lapienyte, L., Dreyer, S., Lee, H. J., et al. (2019). Macrophage-released pyrimidines inhibit gemcitabine therapy in pancreatic Cancer. *Cell Metab.* 29, 1390.e6–1399.e6. doi: 10.1016/j.cmet.2019.02.001
- Han, Z. P., Jing, Y. Y., Xia, Y., Zhang, S. S., Hou, J., Meng, Y., et al. (2014). Mesenchymal stem cells contribute to the chemoresistance of hepatocellular carcinoma cells in inflammatory environment by inducing autophagy. *Cell Biosci.* 4:22. doi: 10.1186/2045-3701-4-22
- Hanahan, D., and Weinberg, R. A. (2011). Hallmarks of cancer: the next generation. *Cell* 144, 646–674. doi: 10.1016/j.cell.2011.02.013
- Hanson, J. A., Gillespie, J. W., Grover, A., Tangrea, M. A., Chuaqui, R. F., Emmert-Buck, M. R., et al. (2006). Gene promoter methylation in prostate tumor-associated stromal cells. *J. Natl. Cancer Inst.* 98, 255–261. doi: 10.1093/jnci/djj051
- He, W., Liang, B., Wang, C., Li, S., Zhao, Y., Huang, Q., et al. (2019). MSC-regulated lncRNA MACC1-AS1 promotes stemness and chemoresistance through fatty acid oxidation in gastric cancer. *Oncogene* 38, 4637–4654. doi: 10.1038/s41388-019-0747-0
- Hida, K., Maishi, N., Akiyama, K., Ohmura-Kakutani, H., Torii, C., Ohga, N., et al. (2017). Tumor endothelial cells with high aldehyde dehydrogenase activity show drug resistance. *Cancer Sci.* 108, 2195–2203. doi: 10.1111/cas.13388
- Hida, K., Maishi, N., Annan, D. A., and Hida, Y. (2018). Contribution of tumor endothelial cells in cancer progression. *Int. J. Mol. Sci.* 19:1272. doi: 10.3390/ijms19051272
- Hida, K., Maishi, N., Sakurai, Y., Hida, Y., and Harashima, H. (2016). Heterogeneity of tumor endothelial cells and drug delivery. *Adv. Drug Deliv. Rev.* 99(Pt B), 140–147. doi: 10.1016/j.addr.2015.11.008
- Hientz, K., Mohr, A., Bhakta-Guha, D., and Efferth, T. (2017). The role of p53 in cancer drug resistance and targeted chemotherapy. *Oncotarget* 8, 8921–8946. doi: 10.18632/oncotarget.13475
- Hirata, E., Girotti, M. R., Viros, A., Hooper, S., Spencer-Dene, B., Matsuda, M., et al. (2015). Intravital imaging reveals how BRAF inhibition generates drug-tolerant microenvironments with high integrin β 1/FAK signaling. *Cancer Cell* 27, 574–588. doi: 10.1016/j.ccell.2015.03.008
- Hoarau-Vechot, J., Touboul, C., Halabi, N., Blot-Dupin, M., Lis, R., Abi Khalil, C., et al. (2019). Akt-activated endothelium promotes ovarian cancer proliferation through notch activation. *J. Transl. Med.* 17:194. doi: 10.1186/s12967-019-1942-z
- Holmgard, R. B., Zamarin, D., Lesokhin, A., Merghoub, T., and Wolchok, J. D. (2016). Targeting myeloid-derived suppressor cells with colony stimulating factor-1 receptor blockade can reverse immune resistance to immunotherapy in indoleamine 2,3-dioxygenase-expressing tumors. *EBioMedicine* 6, 50–58. doi: 10.1016/j.ebiom.2016.02.024
- Hu, J. L., Wang, W., Lan, X. L., Zeng, Z. C., Liang, Y. S., Yan, Y. R., et al. (2019). CAFs secreted exosomes promote metastasis and chemotherapy resistance by enhancing cell stemness and epithelial-mesenchymal transition in colorectal cancer. *Mol. Cancer* 18:91. doi: 10.1186/s12943-019-1019-x
- Huang, H., Wang, C., Liu, F., Li, H. Z., Peng, G., Gao, X., et al. (2018). Reciprocal network between cancer stem-like cells and macrophages facilitates the progression rogen deprivation therapy resistance of prostate Cancer. *Clin. Cancer Res.* 24, 4612–4626. doi: 10.1158/1078-0432.Ccr-18-0461
- Huang, L., Perrault, C., Coelho-Martins, J., Hu, C., Dulong, C., Varna, M., et al. (2013). Induction of acquired drug resistance in endothelial cells and its involvement in anticancer therapy. *J. Hematol. Oncol.* 6:49. doi: 10.1186/1756-8722-6-49
- Huang, W. C., Kuo, K. T., Wang, C. H., Yeh, C. T., and Wang, Y. (2019). Cisplatin resistant lung cancer cells promoted M2 polarization of tumor-associated macrophages via the Src/CD155/MIF functional pathway. *J. Exp. Clin. Cancer Res.* 38:180. doi: 10.1186/s13046-019-1166-3
- Huang, Y., Yu, P., Li, W., Ren, G., Roberts, A. I., Cao, W., et al. (2014). p53 regulates mesenchymal stem cell-mediated tumor suppression in a tumor microenvironment through immune modulation. *Oncogene* 33, 3830–3838. doi: 10.1038/ncr.2013.355
- Hui, L., and Chen, Y. (2015). Tumor microenvironment: sanctuary of the devil. *Cancer Lett.* 368, 7–13. doi: 10.1016/j.canlet.2015.07.039
- Imbert, C., Montfort, A., Fraisse, M., Marcheteau, E., Gilhodes, J., Martin, E., et al. (2020). Resistance of melanoma to immune checkpoint inhibitors is overcome by targeting the sphingosine kinase-1. *Nat. Commun.* 11:437. doi: 10.1038/s41467-019-14218-7
- In 't Veld, S., and Wurdinger, T. (2019). Tumor-educated platelets. *Blood* 133, 2359–2364. doi: 10.1182/blood-2018-12-852830
- Incio, J., Liu, H., Suboj, P., Chin, S. M., Chen, I. X., Pinter, M., et al. (2016). Obesity-induced inflammation and desmoplasia promote pancreatic cancer progression and resistance to chemotherapy. *Cancer Discov.* 6, 852–869. doi: 10.1158/2159-8290.Cd-15-1177
- Iyengar, P., Espina, V., Williams, T. W., Lin, Y., Berry, D., Jelicks, L. A., et al. (2005). Adipocyte-derived collagen VI affects early mammary tumor progression in vivo, demonstrating a critical interaction in the tumor/stroma microenvironment. *J. Clin. Invest.* 115, 1163–1176. doi: 10.1172/jci23424
- Jacobetz, M. A., Chan, D. S., Neesse, A., Bapiro, T. E., Cook, N., Frese, K. K., et al. (2013). Hyaluronan impairs vascular function and drug delivery in a mouse model of pancreatic cancer. *Gut* 62, 112–120. doi: 10.1136/gutjnl-2012-302529
- Ji, R. B., Zhang, B., Zhang, X., Xue, J. G., Yuan, X., Yan, Y. M., et al. (2015). Exosomes derived from human mesenchymal stem cells confer drug resistance in gastric cancer. *Cell Cycle* 14, 2473–2483. doi: 10.1080/15384101.2015.1005530
- Jiménez-Valerio, G., Martínez-Lozano, M., Bassani, N., Vidal, A., Ochoa-de-Olza, M., Suárez, C., et al. (2016). Resistance to antiangiogenic therapies by metabolic symbiosis in renal cell carcinoma PDX models and patients. *Cell Rep.* 15, 1134–1143. doi: 10.1016/j.celrep.2016.04.015
- Jinushi, M., Chiba, S., Yoshiyama, H., Masutomi, K., Kinoshita, I., Dosaka-Akita, H., et al. (2011). Tumor-associated macrophages regulate tumorigenicity and anticancer drug responses of cancer stem/initiating cells. *Proc. Natl. Acad. Sci. U.S.A.* 108, 12425–12430. doi: 10.1073/pnas.1106645108
- Johansson, A. C., Ansell, A., Jerhammar, F., Lindh, M. B., Grénman, R., Munck-Wikland, E., et al. (2012). Cancer-associated fibroblasts induce matrix metalloproteinase-mediated cetuximab resistance in head and neck squamous cell carcinoma cells. *Mol. Cancer Res.* 10, 1158–1168. doi: 10.1158/1541-7786.Mcr-12-0030
- Kalbasi, A., Komar, C., Tooker, G. M., Liu, M., Lee, J. W., Gladney, W. L., et al. (2017). Tumor-Derived CCL2 mediates resistance to radiotherapy in pancreatic ductal adenocarcinoma. *Clin. Cancer Res.* 23, 137–148. doi: 10.1158/1078-0432.Ccr-16-0870
- Kalluri, R. (2016). The biology and function of fibroblasts in cancer. *Nat. Rev. Cancer* 16, 582–598. doi: 10.1038/nrc.2016.73
- Kalluri, R., and Neilson, E. G. (2003). Epithelial-mesenchymal transition and its implications for fibrosis. *J. Clin. Invest.* 112, 1776–1784. doi: 10.1172/jci20530
- Kasahara, K., Arao, T., Sakai, K., Matsumoto, K., Sakai, A., Kimura, H., et al. (2010). Impact of serum hepatocyte growth factor on treatment response to epidermal growth factor receptor tyrosine kinase inhibitors in patients with non-small cell lung adenocarcinoma. *Clin. Cancer Res.* 16, 4616–4624. doi: 10.1158/1078-0432.Ccr-10-0383
- Kawano, M., Mabuchi, S., Matsumoto, Y., Sasano, T., Takahashi, R., Kuroda, H., et al. (2015). The significance of G-CSF expression and myeloid-derived suppressor cells in the chemoresistance of uterine cervical cancer. *Sci. Rep.* 5:18217. doi: 10.1038/srep18217
- Kidd, S., Caldwell, L., Dietrich, M., Samudio, I., Spaeth, E. L., Watson, K., et al. (2010). Mesenchymal stromal cells alone or expressing interferon-beta suppress pancreatic tumors in vivo, an effect countered by anti-inflammatory treatment. *Cytotherapy* 12, 615–625. doi: 10.3109/14653241003631815
- Kikuchi, H., Maishi, N., Annan, D. A., Alam, M. T., Dawood, R. I. H., Sato, M., et al. (2020). Chemotherapy-Induced IL8 Upregulates MDR1/ABCB1 in tumor blood vessels and results in unfavorable outcome. *Cancer Res.* 80, 2996–3008. doi: 10.1158/0008-5472.CAN-19-3791
- Kim, H. S., Jung, M., Choi, S. K., Woo, J., Piao, Y. J., Hwang, E. H., et al. (2018). IL-6-mediated cross-talk between human preadipocytes and ductal carcinoma

- in situ in breast cancer progression. *J. Exp. Clin. Cancer Res.* 37:200. doi: 10.1186/s13046-018-0867-3
- Kim, J., Hall, R. R., Lesniak, M. S., and Ahmed, A. U. (2015). Stem cell-based cell carrier for targeted oncolytic virotherapy: translational opportunity and open questions. *Viruses* 7, 6200–6217. doi: 10.3390/v7122921
- Kim, S. M., Woo, J. S., Jeong, C. H., Ryu, C. H., Lim, J. Y., and Jeun, S. S. (2012). Effective combination therapy for malignant glioma with TRAIL-secreting mesenchymal stem cells and lipoxygenase inhibitor MK886. *Cancer Res.* 72, 4807–4817. doi: 10.1158/0008-5472.Can-12-0123
- Köck, K., Grube, M., Jedlitschky, G., Oevermann, L., Siegmund, W., Ritter, C. A., et al. (2007). Expression of adenosine triphosphate-binding cassette (ABC) drug transporters in peripheral blood cells: relevance for physiology and pharmacotherapy. *Clin. Pharmacokinet.* 46, 449–470. doi: 10.2165/00003088-200746060-00001
- Kodet, O., Dvořáková, B., Bendlová, B., Sýkorová, V., Krajsová, I., Štork, J., et al. (2018). Microenvironment-driven resistance to B-Raf inhibition in a melanoma patient is accompanied by broad changes of gene methylation and expression in distal fibroblasts. *Int. J. Mol. Med.* 41, 2687–2703. doi: 10.3892/ijmm.2018.3448
- Korbecki, J., Grochans, S., Gutowska, I., Barczak, K., and Baranowska-Bosiacka, I. (2020). CC Chemokines in a tumor: a review of pro-cancer and anti-cancer properties of receptors CCR5, CCR6, CCR7, CCR8, CCR9, and CCR10 Ligands. *Int. J. Mol. Sci.* 21:7619. doi: 10.3390/ijms21207619
- Kurose, K., Ohue, Y., Wada, H., Iida, S., Ishida, T., Kojima, T., et al. (2015). Phase Ia study of Foxp3+ CD4 Treg depletion by infusion of a humanized Anti-CCR4 Antibody, KW-0761, in Cancer Patients. *Clin. Cancer Res.* 21, 4327–4336. doi: 10.1158/1078-0432.Ccr-15-0357
- Kuwada, K., Kagawa, S., Yoshida, R., Sakamoto, S., Ito, A., Watanabe, M., et al. (2018). The epithelial-to-mesenchymal transition induced by tumor-associated macrophages confers chemoresistance in peritoneally disseminated pancreatic cancer. *J. Exp. Clin. Cancer Res.* 37:307. doi: 10.1186/s13046-018-0981-2
- Labelle, M., Begum, S., and Hynes, R. O. (2011). Direct signaling between platelets and cancer cells induces an epithelial-mesenchymal-like transition and promotes metastasis. *Cancer Cell* 20, 576–590. doi: 10.1016/j.ccr.2011.09.009
- Ladanyi, A., Mukherjee, A., Kenny, H. A., Johnson, A., Mitra, A. K., Sundaresan, S., et al. (2018). Adipocyte-induced CD36 expression drives ovarian cancer progression and metastasis. *Oncogene* 37, 2285–2301. doi: 10.1038/s41388-017-0093-z
- Lamberti, M. J., Rettel, M., Krijgsveld, J., Rivaola, V. A., and Rumie Vittar, N. B. (2019). Secretome profiling of heterotypic spheroids suggests a role of fibroblasts in HIF-1 pathway modulation and colorectal cancer photodynamic resistance. *Cell Oncol.* 42, 173–196. doi: 10.1007/s13402-018-00418-8
- Lambrechts, D., Wauters, E., Boeckx, B., Aibar, S., Nittner, D., Burton, O., et al. (2018). Phenotype molding of stromal cells in the lung tumor microenvironment. *Nat. Med.* 24, 1277–1289. doi: 10.1038/s41591-018-0096-5
- Lancet, J. E., Moseley, A. B., Coutre, S. E., DeAngelo, D. J., Othus, M., Tallman, M. S., et al. (2020). A phase 2 study of ATRA, arsenic trioxide, and gemtuzumab ozogamicin in patients with high-risk APL (SWOG 0535). *Blood Adv.* 4, 1683–1689. doi: 10.1182/bloodadvances.2019001278
- Le Naour, A., Prat, M., Thibault, B., Mevel, R., Lemaître, L., Leray, H., et al. (2020). Tumor cells educate mesenchymal stromal cells to release chemoprotective and immunomodulatory factors. *J. Mol. Cell Biol.* 12, 202–215. doi: 10.1093/jmcb/mjz090
- Lehuédé, C., Li, X., Dauvillier, S., Vaysse, C., Franchet, C., Clement, E., et al. (2019). Adipocytes promote breast cancer resistance to chemotherapy, a process amplified by obesity: role of the major vault protein (MVP). *Breast Cancer Res.* 21:7. doi: 10.1186/s13058-018-1088-6
- Leung, C. S., Yeung, T. L., Yip, K. P., Wong, K. K., Ho, S. Y., Mangala, L. S., et al. (2018). Cancer-associated fibroblasts regulate endothelial adhesion protein LPP to promote ovarian cancer chemoresistance. *J. Clin. Invest.* 128, 589–606. doi: 10.1172/jci95200
- Li, C., Yang, W., Gai, X., Zhang, Y., Li, Y., and Fu, H. (2012). Foxp3 overexpression decreases sensitivity to chemotherapy in mouse Lewis lung cancer cells. *Mol. Med. Rep.* 6, 977–982. doi: 10.3892/mmr.2012.1066
- Li, C., Zhao, H., and Wang, B. (2021). Mesenchymal stem/stromal cells: developmental origin, tumorigenesis and translational cancer therapeutics. *Transl. Oncol.* 14:100948. doi: 10.1016/j.tranon.2020.100948
- Li, I., and Nabet, B. Y. (2019). Exosomes in the tumor microenvironment as mediators of cancer therapy resistance. *Mol. Cancer* 18, 32. doi: 10.1186/s12943-019-0975-5
- Li, J., Guan, J., Long, X., Wang, Y., and Xiang, X. (2016). mir-1-mediated paracrine effect of cancer-associated fibroblasts on lung cancer cell proliferation and chemoresistance. *Oncol. Rep.* 35, 3523–3531. doi: 10.3892/or.2016.4714
- Li, S., Liu, M., Do, M. H., Chou, C., Stamatiades, E. G., Nixon, B. G., et al. (2020). Cancer immunotherapy via targeted TGF- β signalling blockade in T(H) cells. *Nature* 587, 121–125. doi: 10.1038/s41586-020-2850-3
- Li, X., Liu, R., Su, X., Pan, Y., Han, X., Shao, C., et al. (2019). Harnessing tumor-associated macrophages as aids for cancer immunotherapy. *Mol. Cancer* 18:177. doi: 10.1186/s12943-019-1102-3
- Li, Z., Chan, K., Qi, Y., Lu, L., Ning, F., Wu, M., et al. (2018). Participation of CCL1 in snail-positive fibroblasts in colorectal cancer contribute to 5-Fluorouracil/Paclitaxel chemoresistance. *Cancer Res. Treat.* 50, 894–907. doi: 10.4143/crt.2017.356
- Lis, R., Touboul, C., Mirshahi, P., Ali, F., Mathew, S., Nolan, D. J., et al. (2011). Tumor associated mesenchymal stem cells protects ovarian cancer cells from hyperthermia through CXCL12. *Int. J. Cancer* 128, 715–725. doi: 10.1002/ijc.25619
- Liu, H., Wang, J., Zhang, M., Xuan, Q., Wang, Z., Lian, X., et al. (2017). Jagged1 promotes aromatase inhibitor resistance by modulating tumor-associated macrophage differentiation in breast cancer patients. *Breast Cancer Res. Treat.* 166, 95–107. doi: 10.1007/s10549-017-4394-2
- Liu, M., Zhou, J., Chen, Z., and Cheng, A. S. (2017). Understanding the epigenetic regulation of tumours and their microenvironments: opportunities and problems for epigenetic therapy. *J. Pathol.* 241, 10–24. doi: 10.1002/path.4832
- Liu, S., Lee, J. S., Jie, C., Park, M. H., Iwakura, Y., Patel, Y., et al. (2018). HER2 overexpression triggers an IL1 α proinflammatory circuit to drive tumorigenesis and promote chemotherapy resistance. *Cancer Res.* 78, 2040–2051. doi: 10.1158/0008-5472.Can-17-2761
- Liu, T., Ma, W., Xu, H., Huang, M., Zhang, D., He, Z., et al. (2018). PDGF-mediated mesenchymal transformation renders endothelial resistance to anti-VEGF treatment in glioblastoma. *Nat. Commun.* 9:3439. doi: 10.1038/s41467-018-05982-z
- Liu, X. D., Hoang, A., Zhou, L., Kalra, S., Yetil, A., Sun, M., et al. (2015). Resistance to antiangiogenic therapy is associated with an immunosuppressive tumor microenvironment in metastatic renal cell carcinoma. *Cancer Immunol. Res.* 3, 1017–1029. doi: 10.1158/2326-6066.Cir-14-0244
- Liu, Y., and Cao, X. (2015). The origin and function of tumor-associated macrophages. *Cell Mol. Immunol.* 12, 1–4. doi: 10.1038/cmi.2014.83
- Liu, Z., Xu, J., He, J., Liu, H., Lin, P., Wan, X., et al. (2015). Mature adipocytes in bone marrow protect myeloma cells against chemotherapy through autophagy activation. *Oncotarget* 6, 34329–34341.
- Liu, Z. Q., Xu, J. D., He, J., Liu, H., Lin, P., Wan, X. H., et al. (2015). Mature adipocytes in bone marrow protect myeloma cells against chemotherapy through autophagy activation. *Oncotarget* 6, 34329–34341. doi: 10.18632/oncotarget.6020
- Long, Y., Tao, H., Karachi, A., Grippin, A. J., Jin, L., Chang, Y. E., et al. (2020). Dysregulation of glutamate transport enhances Treg function that promotes VEGF blockade resistance in glioblastoma. *Cancer Res.* 80, 499–509. doi: 10.1158/0008-5472.Can-19-1577
- Lu, M., Xie, K., Lu, X., Lu, L., Shi, Y., and Tang, Y. (2020). Notoginsenoside R1 counteracts mesenchymal stem cell-evoked oncogenesis and doxorubicin resistance in osteosarcoma cells by blocking IL-6 secretion-induced JAK2/STAT3 signaling. *Invest. New Drugs* 39, 416–425. doi: 10.1007/s10637-020-01027-9
- Luo, J., Lee, S. O., Liang, L., Huang, C. K., Li, L., Wen, S., et al. (2014). Infiltrating bone marrow mesenchymal stem cells increase prostate cancer stem cell population and metastatic ability via secreting cytokines to suppress androgen receptor signaling. *Oncogene* 33, 2768–2778. doi: 10.1038/ncr.2013.233
- Ma, J., Song, X., Xu, X., and Mou, Y. (2019). Cancer-associated fibroblasts promote the chemo-resistance in gastric cancer through secreting IL-11 Targeting JAK/STAT3/Bcl2 pathway. *Cancer Res. Treat.* 51, 194–210. doi: 10.4143/crt.2018.031

- Maishi, N., Annan, D. A., Kikuchi, H., Hida, Y., and Hida, K. (2019). Tumor endothelial heterogeneity in cancer progression. *Cancers* 11:1511. doi: 10.3390/cancers11101511
- Makker, V., Rasco, D., Vogelzang, N. J., Brose, M. S., Cohn, A. L., Mier, J., et al. (2019). Lenvatinib plus pembrolizumab in patients with advanced endometrial cancer: an interim analysis of a multicentre, open-label, single-arm, phase 2 trial. *Lancet Oncol.* 20, 711–718. doi: 10.1016/S1470-2045(19)30020-8
- Mao, Y., Zhang, Y., Qu, Q., Zhao, M., Lou, Y., Liu, J., et al. (2015). Cancer-associated fibroblasts induce trastuzumab resistance in HER2 positive breast cancer cells. *Mol. Biosyst.* 11, 1029–1040. doi: 10.1039/c4mb00710g
- Mathot, P., Grandin, M., Devailly, G., Souaze, F., Cahais, V., Moran, S., et al. (2017). DNA methylation signal has a major role in the response of human breast cancer cells to the microenvironment. *Oncogenesis* 6:e390. doi: 10.1038/oncsis.2017.88
- Migneco, G., Whitaker-Menezes, D., Chiavarina, B., Castello-Cros, R., Pavlides, S., Pestell, R. G., et al. (2010). Glycolytic cancer associated fibroblasts promote breast cancer tumor growth, without a measurable increase in angiogenesis: evidence for stromal-epithelial metabolic coupling. *Cell Cycle* 9, 2412–2422. doi: 10.4161/cc.9.12.11989
- Mishra, P. J., Mishra, P. J., Humeniuk, R., Medina, D. J., Alexe, G., Mesirov, J. P., et al. (2008). Carcinoma-associated fibroblast-like differentiation of human mesenchymal stem cells. *Cancer Res.* 68, 4331–4339. doi: 10.1158/0008-5472.CAN-08-0943
- Mishra, R., Haldar, S., Placencio, V., Madhav, A., Rohena-Rivera, K., Agarwal, P., et al. (2018). Stromal epigenetic alterations drive metabolic and neuroendocrine prostate cancer reprogramming. *J. Clin. Invest.* 128, 4472–4484. doi: 10.1172/jci99397
- Mohamed, E., Sierra, R. A., Trillo-Tinoco, J., Cao, Y., Innamarato, P., Payne, K. K., et al. (2020). The Unfolded protein response mediator PERK governs myeloid cell-driven immunosuppression in tumors through inhibition of STING signaling. *Immunity* 52, 668.e7–682.e7. doi: 10.1016/j.immuni.2020.03.004
- Montenegro, F., and Indraccolo, S. (2020). Metabolism in the tumor microenvironment. *Adv. Exp. Med. Biol.* 1263, 1–11. doi: 10.1007/978-3-030-44518-8_1
- Moradi-Chaleshtori, M., Bandehpour, M., Soudi, S., Mohammadi-Yeganeh, S., and Hashemi, S. M. (2020). In vitro and in vivo evaluation of anti-tumoral effect of M1 phenotype induction in macrophages by miR-130 and miR-33 containing exosomes. *Cancer Immunol. Immunother.* 70, 1323–1339. doi: 10.1007/s00262-020-02762-x
- Mudry, R. E., Fortney, J. E., York, T., Hall, B. M., and Gibson, L. F. (2000). Stromal cells regulate survival of B-lineage leukemic cells during chemotherapy. *Blood* 96, 1926–1932.
- Mukherjee, A., Chiang, C. Y., Daifotis, H. A., Nieman, K. M., Fahrman, J. F., Lastra, R. R., et al. (2020). Adipocyte-induced FABP4 expression in ovarian cancer cells promotes metastasis and mediates carboplatin resistance. *Cancer Res.* 80, 1748–1761. doi: 10.1158/0008-5472.CAN-19-1999
- Muller, C. (2013). Tumour-surrounding adipocytes are active players in breast cancer progression. *Ann. Endocrinol.* 74, 108–110. doi: 10.1016/j.ando.2013.02.007
- Muñoz-García, J., Cochonneau, D., Télétchéa, S., Moranton, E., Lanoe, D., Brion, R., et al. (2021). The twin cytokines interleukin-34 and CSF-1: masterful conductors of macrophage homeostasis. *Theranostics* 11, 1568–1593. doi: 10.7150/thno.50683
- Nagl, L., Horvath, L., Pircher, A., and Wolf, D. (2020). Tumor endothelial cells (TECs) as potential immune directors of the tumor microenvironment – new findings and future perspectives. *Front. Cell Dev. Biol.* 8:766. doi: 10.3389/fcell.2020.00766
- Naito, H., Wakabayashi, T., Kidoya, H., Muramatsu, F., Takara, K., Eino, D., et al. (2016). Endothelial side population cells contribute to tumor angiogenesis and antiangiogenic drug resistance. *Cancer Res.* 76, 3200–3210. doi: 10.1158/0008-5472.CAN-15-2998
- Najafi, M., Goradel, N. H., Farhood, B., Salehi, E., Solhjoo, S., Toole, H., et al. (2019). Tumor microenvironment: Interactions and therapy. *J. Cell Physiol.* 234, 5700–5721. doi: 10.1002/jcp.27425
- Nieman, K. M., Kenny, H. A., Penicka, C. V., Ladanyi, A., Buell-Gutbrod, R., Zillhardt, M. R., et al. (2011). Adipocytes promote ovarian cancer metastasis and provide energy for rapid tumor growth. *Nat. Med.* 17, 1498–1503. doi: 10.1038/nm.2492
- Nieman, K. M., Romero, I. L., Van Houten, B., and Lengyel, E. (2013). Adipose tissue and adipocytes support tumorigenesis and metastasis. *Biochim. Biophys. Acta Mol. Cell Biol. Lipids* 1831, 1533–1541. doi: 10.1016/j.bbalip.2013.02.010
- Nilsson, M. B., Sun, H., Robichaux, J., Pfeifer, M., McDermott, U., Travers, J., et al. (2020). A YAP/FOXM1 axis mediates EMT-associated EGFR inhibitor resistance and increased expression of spindle assembly checkpoint components. *Sci. Transl. Med.* 12:eaa4589. doi: 10.1126/scitranslmed.aaa4589
- Nywenning, T. M., Belt, B. A., Cullinan, D. R., Panni, R. Z., Han, B. J., Sanford, D. E., et al. (2018). Targeting both tumour-associated CXCR2(+) neutrophils and CCR2(+) macrophages disrupts myeloid recruitment and improves chemotherapeutic responses in pancreatic ductal adenocarcinoma. *Gut* 67, 1112–1123. doi: 10.1136/gutjnl-2017-313738
- Oevermann, L., Scheitz, J., Starke, K., Köck, K., Kiefer, T., Dölken, G., et al. (2009). Hematopoietic stem cell differentiation affects expression and function of MRP4 (ABCC4), a transport protein for signaling molecules and drugs. *Int. J. Cancer* 124, 2303–2311. doi: 10.1002/ijc.24207
- Orimo, A., and Weinberg, R. A. (2006). Stromal fibroblasts in cancer: a novel tumor-promoting cell type. *Cell Cycle* 5, 1597–1601. doi: 10.4161/cc.5.15.3112
- Oweida, A., Hararah, M. K., Phan, A., Binder, D., Bhatia, S., Lennon, S., et al. (2018). Resistance to radiotherapy and PD-L1 blockade is mediated by TIM-3 upregulation and regulatory t-cell infiltration. *Clin. Cancer Res.* 24, 5368–5380. doi: 10.1158/1078-0432.CCR-18-1038
- Özdemir, B. C., Pentcheva-Hoang, T., Carstens, J. L., Zheng, X., Wu, C.-C., Simpson, T. R., et al. (2015). Depletion of carcinoma-associated fibroblasts and fibrosis induces immunosuppression and accelerates pancreas cancer with reduced survival. *Cancer Cell* 28, 831–833. doi: 10.1016/j.ccell.2015.11.002
- Paget, S. (1989). The distribution of secondary growths in cancer of the breast. 1889. *Cancer Metastasis Rev.* 8, 98–101.
- Park, J., Morley, T. S., and Scherer, P. E. (2013). Inhibition of endotrophin, a cleavage product of collagen VI, confers cisplatin sensitivity to tumours. *EMBO Mol. Med.* 5, 935–948. doi: 10.1002/emmm.201202006
- Pascual, G., Avgustinova, A., Mejetta, S., Martín, M., Castellanos, A., Attolini, C. S., et al. (2017). Targeting metastasis-initiating cells through the fatty acid receptor CD36. *Nature* 541, 41–45. doi: 10.1038/nature20791
- Patocs, A., Zhang, L., Xu, Y., Weber, F., Caldes, T., Mutter, G. L., et al. (2007). Breast-cancer stromal cells with TP53 mutations and nodal metastases. *N. Engl. J. Med.* 357, 2543–2551. doi: 10.1056/NEJMoa071825
- Paunescu, V., Bojin, F. M., Tatu, C. A., Gavriluc, O. I., Rosca, A., Gruia, A. T., et al. (2011). Tumour-associated fibroblasts and mesenchymal stem cells: more similarities than differences. *J. Cell Mol. Med.* 15, 635–646. doi: 10.1111/j.1582-4934.2010.01044.x
- Pérez de Heredia, F., Wood, I. S., and Trayhurn, P. (2010). Hypoxia stimulates lactate release and modulates monocarboxylate transporter (MCT1, MCT2, and MCT4) expression in human adipocytes. *Pflugers Arch.* 459, 509–518. doi: 10.1007/s00424-009-0750-3
- Perrotta, C., Cervia, D., Di Renzo, I., Moscheni, C., Bassi, M. T., Campana, L., et al. (2018). Nitric Oxide generated by tumor-associated macrophages is responsible for cancer resistance to cisplatin and correlated with syntaxin 4 and acid sphingomyelinase inhibition. *Front. Immunol.* 9:1186. doi: 10.3389/fimmu.2018.01186
- Pértiga-Gomes, N., Vizcaino, J. R., Attig, J., Jurmeister, S., Lopes, C., and Baltazar, F. (2014). A lactate shuttle system between tumour and stromal cells is associated with poor prognosis in prostate cancer. *BMC Cancer* 14:352. doi: 10.1186/1471-2407-14-352
- Pertusini, E., Ratajczak, J., Majka, M., Vaughn, D., Ratajczak, M. Z., and Gewirtz, A. M. (2001). Investigating the platelet-sparing mechanism of paclitaxel/carboplatin combination chemotherapy. *Blood* 97, 638–644. doi: 10.1182/blood.v97.3.638
- Pistore, C., Giannoni, E., Colangelo, T., Rizzo, F., Magnani, E., Muccillo, L., et al. (2017). DNA methylation variations are required for epithelial-to-mesenchymal transition induced by cancer-associated fibroblasts in prostate cancer cells. *Oncogene* 36, 5551–5566. doi: 10.1038/onc.2017.159
- Pramanik, R., Sheng, X., Ichihara, B., Heisterkamp, N., and Mittelman, S. D. (2013). Adipose tissue attracts and protects acute lymphoblastic leukemia cells from chemotherapy. *Leuk. Res.* 37, 503–509. doi: 10.1016/j.leukres.2012.12.013
- Pylaeva, E., Lang, S., and Jablonska, J. (2016). The essential role of Type I interferons in differentiation and activation of tumor-associated neutrophils. *Front. Immunol.* 7:629. doi: 10.3389/fimmu.2016.00629

- Qiao, Y., Zhang, C., Li, A., Wang, D., Luo, Z., Ping, Y., et al. (2018). IL6 derived from cancer-associated fibroblasts promotes chemoresistance via CXCR7 in esophageal squamous cell carcinoma. *Oncogene* 37, 873–883. doi: 10.1038/onc.2017.387
- Qin, X., Guo, H., Wang, X., Zhu, X., Yan, M., Wang, X., et al. (2019). Exosomal miR-196a derived from cancer-associated fibroblasts confers cisplatin resistance in head and neck cancer through targeting CDKN1B and ING5. *Genome Biol.* 20:12. doi: 10.1186/s13059-018-1604-0
- Rachidi, S., Metelli, A., Riesenberger, B., Wu, B. X., Nelson, M. H., Wallace, C., et al. (2017). Platelets subvert T cell immunity against cancer via GARP-TGF β axis. *Sci. Immunol.* 2:eai7911. doi: 10.1126/sciimmunol.aai7911
- Radziwon-Balicka, A., Medina, C., O'Driscoll, L., Treumann, A., Bazou, D., Inkielewicz-Stepniak, I., et al. (2012). Platelets increase survival of adenocarcinoma cells challenged with anticancer drugs: mechanisms and implications for chemoresistance. *Br. J. Pharmacol.* 167, 787–804. doi: 10.1111/j.1476-5381.2012.01991.x
- Raghavan, S., Snyder, C. S., Wang, A., McLean, K., Zamarin, D., Buckanovich, R. J., et al. (2020). Carcinoma-associated mesenchymal stem cells promote chemoresistance in ovarian cancer stem cells via PDGF signaling. *Cancers* 12:2063. doi: 10.3390/cancers12082063
- Ramesh, A., Kumar, S., Nandi, D., and Kulkarni, A. (2019). CSF1R- and SHP2-inhibitor-loaded nanoparticles enhance cytotoxic activity and phagocytosis in tumor-associated macrophages. *Adv. Mater.* 31:e1904364. doi: 10.1002/adma.201904364
- Reagan, M. R., and Kaplan, D. L. (2011). Concise review: mesenchymal stem cell tumor-homing: detection methods in disease model systems. *Stem Cells* 29, 920–927. doi: 10.1002/stem.645
- Ren, J., Ding, L., Zhang, D., Shi, G., Xu, Q., Shen, S., et al. (2018). Carcinoma-associated fibroblasts promote the stemness and chemoresistance of colorectal cancer by transferring exosomal lncRNA H19. *Theranostics* 8, 3932–3948. doi: 10.7150/thno.25541
- Richards, K. E., Zeleniak, A. E., Fishel, M. L., Wu, J., Littlepage, L. E., and Hill, R. (2017). Cancer-associated fibroblast exosomes regulate survival and proliferation of pancreatic cancer cells. *Oncogene* 36, 1770–1778. doi: 10.1038/onc.2016.353
- Rodriguez-Canales, J., Hanson, J. C., Tangrea, M. A., Erickson, H. S., Albert, P. S., Wallis, B. S., et al. (2007). Identification of a unique epigenetic sub-microenvironment in prostate cancer. *J. Pathol.* 211, 410–419. doi: 10.1002/path.2133
- Romano, A., Parrinello, N. L., La Cava, P., Tibullo, D., Giallongo, C., Camiolo, G., et al. (2018). PMN-MDSC and arginase are increased in myeloma and may contribute to resistance to therapy. *Expert Rev. Mol. Diagn.* 18, 675–683. doi: 10.1080/14737159.2018.1470929
- Rong, Y., Yuan, C. H., Qu, Z., Zhou, H., Guan, Q., Yang, N., et al. (2016). Doxorubicin resistant cancer cells activate myeloid-derived suppressor cells by releasing PGE2. *Sci. Rep.* 6:23824. doi: 10.1038/srep23824
- Roodhart, J. M., Daenen, L. G., Stigter, E. C., Prins, H. J., Gerrits, J., Houthuijzen, J. M., et al. (2011). Mesenchymal stem cells induce resistance to chemotherapy through the release of platinum-induced fatty acids. *Cancer Cell* 20, 370–383. doi: 10.1016/j.ccr.2011.08.010
- Sansone, P., Savini, C., Kurelac, I., Chang, Q., Amato, L. B., Strillacci, A., et al. (2017). Packaging and transfer of mitochondrial DNA via exosomes regulate escape from dormancy in hormonal therapy-resistant breast cancer. *Proc. Natl. Acad. Sci. U.S.A.* 114, E9066–E9075. doi: 10.1073/pnas.1704862114
- Sapudom, J., Müller, C. D., Nguyen, K. T., Martin, S., Anderegg, U., and Pompe, T. (2020). Matrix remodeling and hyaluronan production by myofibroblasts and cancer-associated fibroblasts in 3D collagen matrices. *Gels* 6:33. doi: 10.3390/gels6040033
- Satoh, M., Cherian, M. G., Imura, N., and Shimizu, H. (1994). Modulation of resistance to anticancer drugs by inhibition of metallothionein synthesis. *Cancer Res.* 54, 5255–5257.
- Schaaf, M. B., Garg, A. D., and Agostinis, P. (2018). Defining the role of the tumor vasculature in antitumor immunity and immunotherapy. *Cell Death Dis.* 9:115. doi: 10.1038/s41419-017-0061-0
- Scherzed, A., Hackenberg, S., Froelich, K., Kessler, M., Koehler, C., Hagen, R., et al. (2011). BMSC enhance the survival of paclitaxel treated squamous cell carcinoma cells in vitro. *Cancer Biol. Ther.* 11, 349–357. doi: 10.4161/cbt.11.3.14179
- Schlenk, R. F., Paschka, P., Krzykalla, J., Weber, D., Kapp-Schworer, S., Gaidzik, V. I., et al. (2020). Gemtuzumab ozogamicin in – mutated acute myeloid leukemia: early results from the prospective randomized AMLSG 09-09 Phase III study. *J. Clin. Oncol.* 38, 623–632. doi: 10.1200/JCO.19.01406
- Schuler, P. J., Harasymczuk, M., Schilling, B., Saze, Z., Strauss, L., Lang, S., et al. (2013). Effects of adjuvant chemoradiotherapy on the frequency and function of regulatory T cells in patients with head and neck cancer. *Clin. Cancer Res.* 19, 6585–6596. doi: 10.1158/1078-0432.Ccr-13-0900
- Senthebane, D. A., Rowe, A., Thomford, N. E., Shipanga, H., Munro, D., Mazeedi, M., et al. (2017). The role of tumor microenvironment in chemoresistance: to survive, keep your enemies closer. *Int. J. Mol. Sci.* 18:1586. doi: 10.3390/ijms18071586
- Shah, K., and Rawal, R. M. (2019). Genetic and epigenetic modulation of drug resistance in cancer: challenges and opportunities. *Curr. Drug Metab.* 20, 1114–1131. doi: 10.2174/1389200221666200103111539
- Shan, L. (2004). “FluidMAG iron nanoparticle-labeled mesenchymal stem cells for tracking cell homing to tumors,” in *Molecular Imaging and Contrast Agent Database (MICAD)*, (Bethesda, MD: National Center for Biotechnology Information (US)).
- Sheng, X., Parmentier, J. H., Tucci, J., Pei, H., Cortez-Toledo, O., Dieli-Conwright, C. M., et al. (2017). Adipocytes sequester and metabolize the chemotherapeutic daunorubicin. *Mol. Cancer Res.* 15, 1704–1713. doi: 10.1158/1541-7786.MCR-17-0338
- Sherman-Baust, C. A., Weeraratna, A. T., Rangel, L. B., Pizer, E. S., Cho, K. R., Schwartz, D. R., et al. (2003). Remodeling of the extracellular matrix through overexpression of collagen VI contributes to cisplatin resistance in ovarian cancer cells. *Cancer Cell* 3, 377–386. doi: 10.1016/s1535-6108(03)00058-8
- Shi, Y., Du, L., Lin, L., and Wang, Y. (2017). Tumour-associated mesenchymal stem/stromal cells: emerging therapeutic targets. *Nat. Rev. Drug Discov.* 16, 35–52. doi: 10.1038/nrd.2016.193
- Shibue, T., and Weinberg, R. A. (2017). EMT, CSCs, and drug resistance: the mechanistic link and clinical implications. *Nat. Rev. Clin. Oncol.* 14, 611–629. doi: 10.1038/nrclinonc.2017.44
- Shien, K., Papadimitrakopoulou, V. A., Ruder, D., Behrens, C., Shen, L., Kalhor, N., et al. (2017). JAK1/STAT3 activation through a proinflammatory cytokine pathway leads to resistance to molecularly targeted therapy in non-small cell lung cancer. *Mol. Cancer Ther.* 16, 2234–2245. doi: 10.1158/1535-7163.Mct-17-0148
- Shree, T., Olson, O. C., Elie, B. T., Kester, J. C., Garfall, A. L., Simpson, K., et al. (2011). Macrophages and cathepsin proteases blunt chemotherapeutic response in breast cancer. *Genes Dev.* 25, 2465–2479. doi: 10.1101/gad.180331.111
- Siegel, R. L., Miller, K. D., and Jemal, A. (2020). Cancer statistics, 2020. *CA Cancer J. Clin.* 70, 7–30. doi: 10.3322/caac.21590
- Siska, P. J., Singer, K., Evert, K., Renner, K., and Kreutz, M. (2020). The immunological Warburg effect: can a metabolic-tumor-stroma score (MeTS) guide cancer immunotherapy? *Immunol. Rev.* 295, 187–202. doi: 10.1111/imr.12846
- Soda, Y., Marumoto, T., Friedmann-Morvinski, D., Soda, M., Liu, F., Michiue, H., et al. (2011). Transdifferentiation of glioblastoma cells into vascular endothelial cells. *Proc. Natl. Acad. Sci. U.S.A.* 108, 4274–4280. doi: 10.1073/pnas.1016030108
- Stapor, P., Wang, X., Goveia, J., Moens, S., and Carmeliet, P. (2014). Angiogenesis revisited – role and therapeutic potential of targeting endothelial metabolism. *J. Cell Sci.* 127(Pt 20), 4331–4341. doi: 10.1242/jcs.153908
- Steinberg, S. M., Shabaneh, T. B., Zhang, P., Martynov, V., Li, Z., Malik, B. T., et al. (2017). Myeloid cells that impair immunotherapy are restored in melanomas with acquired resistance to BRAF Inhibitors. *Cancer Res.* 77, 1599–1610. doi: 10.1158/0008-5472.Can-16-1755
- Sugimoto, H., Mundel, T. M., Kieran, M. W., and Kalluri, R. (2006). Identification of fibroblast heterogeneity in the tumor microenvironment. *Cancer Biol. Ther.* 5, 1640–1646. doi: 10.4161/cbt.5.12.3354
- Sugimura, K., Miyata, H., Tanaka, K., Takahashi, T., Kurokawa, Y., Yamasaki, M., et al. (2015). High infiltration of tumor-associated macrophages is associated with a poor response to chemotherapy and poor prognosis of patients undergoing neoadjuvant chemotherapy for esophageal cancer. *J. Surg. Oncol.* 111, 752–759. doi: 10.1002/jso.23881
- Suzuki, E., Yamazaki, S., Naito, T., Hashimoto, H., Okubo, S., Udagawa, H., et al. (2019). Secretion of high amounts of hepatocyte growth factor is a characteristic

- feature of cancer-associated fibroblasts with EGFR-TKI resistance-promoting phenotype: a study of 18 cases of cancer-associated fibroblasts. *Pathol. Int.* 69, 472–480. doi: 10.1111/pin.12838
- Talmadge, J. E., and Gabrilovich, D. I. (2013). History of myeloid-derived suppressor cells. *Nat. Rev. Cancer* 13, 739–752. doi: 10.1038/nrc3581
- Tanaka, K., Miyata, H., Sugimura, K., Fukuda, S., Kanemura, T., Yamashita, K., et al. (2015). miR-27 is associated with chemoresistance in esophageal cancer through transformation of normal fibroblasts to cancer-associated fibroblasts. *Carcinogenesis* 36, 894–903. doi: 10.1093/carcin/bgv067
- Tang, Y. A., Chen, Y. F., Bao, Y., Mahara, S., Yatim, S., Oguz, G., et al. (2018). Hypoxic tumor microenvironment activates GLI2 via HIF-1 α and TGF- β 2 to promote chemoresistance in colorectal cancer. *Proc. Natl. Acad. Sci. U.S.A.* 115, E5990–E5999. doi: 10.1073/pnas.1801348115
- Tao, L., Huang, G., Wang, R., Pan, Y., He, Z., Chu, X., et al. (2016). Cancer-associated fibroblasts treated with cisplatin facilitates chemoresistance of lung adenocarcinoma through IL-11/IL-11R/STAT3 signaling pathway. *Sci. Rep.* 6:38408. doi: 10.1038/srep38408
- Tavora, B., Reynolds, L. E., Batista, S., Demircioglu, F., Fernandez, I., Lechertier, T., et al. (2014). Endothelial-cell FAK targeting sensitizes tumours to DNA-damaging therapy. *Nature* 514, 112–116. doi: 10.1038/nature13541
- Teng, F., Tian, W. Y., Wang, Y. M., Zhang, Y. F., Guo, F., Zhao, J., et al. (2016). Cancer-associated fibroblasts promote the progression of endometrial cancer via the SDF-1/CXCR4 axis. *J. Hematol. Oncol.* 9:8. doi: 10.1186/s13045-015-0231-4
- Teng, I. W., Hou, P. C., Lee, K. D., Chu, P. Y., Yeh, K. T., Jin, V. X., et al. (2011). Targeted methylation of two tumor suppressor genes is sufficient to transform mesenchymal stem cells into cancer stem/initiating cells. *Cancer Res.* 71, 4653–4663. doi: 10.1158/0008-5472.CAN-10-3418
- Tesfamariam, B. (2016). Involvement of platelets in tumor cell metastasis. *Pharmacol. Ther.* 157, 112–119. doi: 10.1016/j.pharmthera.2015.11.005
- Tu, B., Zhu, J., Liu, S., Wang, L., Fan, Q., Hao, Y., et al. (2016). Mesenchymal stem cells promote osteosarcoma cell survival and drug resistance through activation of STAT3. *Oncotarget* 7, 48296–48308. doi: 10.18632/oncotarget.10219
- Vaidya, F. U., Sufiyan Chhipa, A., Mishra, V., Gupta, V. K., Rawat, S. G., Kumar, A., et al. (2020). Molecular and cellular paradigms of multidrug resistance in cancer. *Cancer Rep.* e1291. doi: 10.1002/cnr.21291 [Epub ahead of print].
- van Beijnum, J. R., Nowak-Sliwinska, P., Huijbers, E. J., Thijssen, V. L., and Griffioen, A. W. (2015). The great escape; the hallmarks of resistance to antiangiogenic therapy. *Pharmacol. Rev.* 67, 441–461. doi: 10.1124/pr.114.010215
- Van Damme, H., Dombrecht, B., Kiss, M., Roose, H., Allen, E., Van Overmeire, E., et al. (2021). Therapeutic depletion of CCR8 tumor-infiltrating regulatory T cells elicits antitumor immunity and synergizes with anti-PD-1 therapy. *J. Immunother. Cancer* 9:e001749. doi: 10.1136/jitc-2020-001749
- Vennin, C., Méléne, P., Rouet, R., Nobis, M., Cazet, A. S., Murphy, K. J., et al. (2019). CAF hierarchy driven by pancreatic cancer cell p53-status creates a pro-metastatic and chemoresistant environment via perlecan. *Nat. Commun.* 10:3637. doi: 10.1038/s41467-019-10968-6
- Vianello, F., Villanova, F., Tisato, V., Lymperi, S., Ho, K. K., Gomes, A. R., et al. (2010). Bone marrow mesenchymal stromal cells non-selectively protect chronic myeloid leukemia cells from imatinib-induced apoptosis via the CXCR4/CXCL12 axis. *Haematologica* 95, 1081–1089. doi: 10.3324/haematol.2009.017178
- von Einem, J. C., Guenther, C., Volk, H. D., Grütz, G., Hirsch, D., Salat, C., et al. (2019). Treatment of advanced gastrointestinal cancer with genetically modified autologous mesenchymal stem cells: results from the phase 1/2 TREAT-ME-1 trial. *Int. J. Cancer* 145, 1538–1546. doi: 10.1002/ijc.32230
- Wang, D., Yang, L., Yu, W., Wu, Q., Lian, J., Li, F., et al. (2019). Colorectal cancer cell-derived CCL20 recruits regulatory T cells to promote chemoresistance via FOXO1/CEBPB/NF- κ B signaling. *J. Immunother. Cancer* 7:215. doi: 10.1186/s40425-019-0701-2
- Wang, J., Cui, R., Clement, C. G., Nawgiri, R., Powell, D. W., Pinchuk, I. V., et al. (2020). Activation PDGFR- α /AKT mediated signaling pathways in oral squamous cell carcinoma by mesenchymal stem/stromal cells promotes anti-apoptosis and decreased sensitivity to cisplatin. *Front. Oncol.* 10:552. doi: 10.3389/fonc.2020.00552
- Wang, J., Hendrix, A., Hernot, S., Lemaire, M., De Bruyne, E., Van Valckenborgh, E., et al. (2014). Bone marrow stromal cell-derived exosomes as communicators in drug resistance in multiple myeloma cells. *Blood* 124, 555–566. doi: 10.1182/blood-2014-03-562439
- Wang, J., Liu, X., Qiu, Y., Shi, Y., Cai, J., Wang, B., et al. (2018). Cell adhesion-mediated mitochondria transfer contributes to mesenchymal stem cell-induced chemoresistance on T cell acute lymphoblastic leukemia cells. *J. Hematol. Oncol.* 11:11. doi: 10.1186/s13045-018-0554-z
- Wang, L., Li, X., Ren, Y., Geng, H., Zhang, Q., Cao, L., et al. (2019). Cancer-associated fibroblasts contribute to cisplatin resistance by modulating ANXA3 in lung cancer cells. *Cancer Sci.* 110, 1609–1620. doi: 10.1111/cas.13998
- Wang, S., Wang, X., Liu, S., Zhang, S., Wei, X., Song, Y., et al. (2020). The CXCR4 antagonist, AMD3100, reverses mesenchymal stem cell-mediated drug resistance in relapsed/refractory acute lymphoblastic leukemia. *Oncotargets Ther.* 13, 6583–6591. doi: 10.2147/ott.S249425
- Wang, Z., Fang, M., Li, J., Yang, R., Du, J., and Luo, Y. (2018). High platelet levels attenuate the efficacy of platinum-based treatment in non-small cell lung cancer. *Cell. Physiol. Biochem.* 48, 2456–2469. doi: 10.1159/000492683
- Wei, L., Ye, H., Li, G., Lu, Y., Zhou, Q., Zheng, S., et al. (2018). Cancer-associated fibroblasts promote progression and gemcitabine resistance via the SDF-1/SATB-1 pathway in pancreatic cancer. *Cell Death Dis.* 9:1065. doi: 10.1038/s41419-018-1104-x
- Weizman, N., Krelin, Y., Shabtay-Orbach, A., Amit, M., Binenbaum, Y., Wong, R. J., et al. (2014). Macrophages mediate gemcitabine resistance of pancreatic adenocarcinoma by upregulating cytidine deaminase. *Oncogene* 33, 3812–3819. doi: 10.1038/onc.2013.357
- Wen, X., He, X., Jiao, F., Wang, C., Sun, Y., Ren, X., et al. (2017). Fibroblast activation protein- α -positive fibroblasts promote gastric cancer progression and resistance to immune checkpoint blockade. *Oncol. Res.* 25, 629–640. doi: 10.3727/096504016x14768383625385
- Wu, H., Liu, B., Chen, Z., Li, G., and Zhang, Z. (2020). MSC-induced lncRNA HCP5 drove fatty acid oxidation through miR-3619-5p/AMPK/PGC1 α /CEBPB axis to promote stemness and chemo-resistance of gastric cancer. *Cell Death Dis.* 11:233. doi: 10.1038/s41419-020-2426-z
- Wu, Q., Zhou, W., Yin, S., Zhou, Y., Chen, T., Qian, J., et al. (2019). Blocking triggering receptor expressed on myeloid cells-1-positive tumor-associated macrophages induced by hypoxia reverses immunosuppression and anti-programmed cell death ligand 1 resistance in liver cancer. *Hepatology* 70, 198–214. doi: 10.1002/hep.30593
- Xiong, Y. Q., Sun, H. C., Zhang, W., Zhu, X. D., Zhuang, P. Y., Zhang, J. B., et al. (2009). Human hepatocellular carcinoma tumor-derived endothelial cells manifest increased angiogenesis capability and drug resistance compared with normal endothelial cells. *Clin. Cancer Res.* 15, 4838–4846. doi: 10.1158/1078-0432.CCR-08-2780
- Xu, H., Zhou, Y., Li, W., Zhang, B., Zhang, H., Zhao, S., et al. (2018). Tumor-derived mesenchymal-stem-cell-secreted IL-6 enhances resistance to cisplatin via the STAT3 pathway in breast cancer. *Oncol. Lett.* 15, 9142–9150. doi: 10.3892/ol.2018.8463
- Xu, M., Zhao, Z., Song, J., Lan, X., Lu, S., Chen, M., et al. (2017). Interactions between interleukin-6 and myeloid-derived suppressor cells drive the chemoresistant phenotype of hepatocellular cancer. *Exp. Cell Res.* 351, 142–149. doi: 10.1016/j.yexcr.2017.01.008
- Xu, S. S., Xu, H. X., Wang, W. Q., Li, S., Li, H., Li, T. J., et al. (2019). Tumor-infiltrating platelets predict postoperative recurrence and survival in resectable pancreatic neuroendocrine tumor. *World J. Gastroenterol.* 25, 6248–6257. doi: 10.3748/wjg.v25.i41.6248
- Xu, X., Ye, J., Huang, C., Yan, Y., and Li, J. (2019). M2 macrophage-derived IL6 mediates resistance of breast cancer cells to hedgehog inhibition. *Toxicol. Appl. Pharmacol.* 364, 77–82. doi: 10.1016/j.taap.2018.12.013
- Yamaguchi, R., and Perkins, G. (2018). Animal models for studying tumor microenvironment (TME) and resistance to lymphocytic infiltration. *Cancer Biol. Ther.* 19, 745–754. doi: 10.1080/15384047.2018.1470722
- Yan, H., Guo, B. Y., and Zhang, S. (2016). Cancer-associated fibroblasts attenuate Cisplatin-induced apoptosis in ovarian cancer cells by promoting STAT3 signaling. *Biochem. Biophys. Res. Commun.* 470, 947–954. doi: 10.1016/j.bbrc.2016.01.131
- Yang, C., He, L., He, P., Liu, Y., Wang, W., He, Y., et al. (2015). Increased drug resistance in breast cancer by tumor-associated macrophages through IL-10/STAT3/bcl-2 signaling pathway. *Med. Oncol.* 32:352. doi: 10.1007/s12032-014-0352-6

- Yang, E., Wang, X., Gong, Z., Yu, M., Wu, H., and Zhang, D. (2020). Exosome-mediated metabolic reprogramming: the emerging role in tumor microenvironment remodeling and its influence on cancer progression. *Signal. Transduct. Target Ther.* 5:242. doi: 10.1038/s41392-020-00359-5
- Yang, J., Zaman, M. M., Vlasakov, I., Roy, R., Huang, L., Martin, C. R., et al. (2019). Adipocytes promote ovarian cancer chemoresistance. *Sci. Rep.* 9:13316. doi: 10.1038/s41598-019-49649-1
- Yeung, C. L. A., Co, N.-N., Tsuruga, T., Yeung, T.-L., Kwan, S.-Y., Leung, C. S., et al. (2016). Exosomal transfer of stroma-derived miR21 confers paclitaxel resistance in ovarian cancer cells through targeting APAF1. *Nat. Commun.* 7:11150. doi: 10.1038/ncomms11150
- Yi, Y., Zeng, S., Wang, Z., Wu, M., Ma, Y., Ye, X., et al. (2018). Cancer-associated fibroblasts promote epithelial-mesenchymal transition and EGFR-TKI resistance of non-small cell lung cancers via HGF/IGF-1/ANXA2 signaling. *Biochim. Acta Mol. Basis Dis.* 1864, 793–803. doi: 10.1016/j.bbdis.2017.12.021
- Yin, C., Evason, K. J., Asahina, K., and Stainier, D. Y. (2013). Hepatic stellate cells in liver development, regeneration, and cancer. *J. Clin. Invest.* 123, 1902–1910. doi: 10.1172/jci66369
- Yin, X., Han, S., Song, C., Zou, H., Wei, Z., Xu, W., et al. (2019). Metformin enhances gefitinib efficacy by interfering with interactions between tumor-associated macrophages and head and neck squamous cell carcinoma cells. *Cell Oncol.* 42, 459–475. doi: 10.1007/s13402-019-00446-y
- Yin, Y., Yao, S., Hu, Y., Feng, Y., Li, M., Bian, Z., et al. (2017). The immune-microenvironment confers chemoresistance of colorectal cancer through macrophage-derived IL6. *Clin. Cancer Res.* 23, 7375–7387. doi: 10.1158/1078-0432.Ccr-17-1283
- Yin, Z., Jiang, K., Li, R., Dong, C., and Wang, L. (2018). Multipotent mesenchymal stromal cells play critical roles in hepatocellular carcinoma initiation, progression and therapy. *Mol. Cancer* 17, 178. doi: 10.1186/s12943-018-0926-6
- Yoshida, G. J. (2015). Metabolic reprogramming: the emerging concept and associated therapeutic strategies. *J. Exp. Clin. Cancer Res.* 34:111. doi: 10.1186/s13046-015-0221-y
- You, J., Li, M., Cao, L. M., Gu, Q. H., Deng, P. B., Tan, Y., et al. (2019). Snail1-dependent cancer-associated fibroblasts induce epithelial-mesenchymal transition in lung cancer cells via exosomes. *Qjm* 112, 581–590. doi: 10.1093/qjmed/hcz093
- Youn, J. I., Nagaraj, S., Collazo, M., and Gabrilovich, D. I. (2008). Subsets of myeloid-derived suppressor cells in tumor-bearing mice. *J. Immunol.* 181, 5791–5802. doi: 10.4049/jimmunol.181.8.5791
- Yu, S., Li, Q., Yu, Y., Cui, Y., Li, W., Liu, T., et al. (2020). Activated HIF1 α of tumor cells promotes chemoresistance development via recruiting GDF15-producing tumor-associated macrophages in gastric cancer. *Cancer Immunol. Immunother.* 69, 1973–1987. doi: 10.1007/s00262-020-02598-5
- Yu, W., Cao, D.-D., Li, Q.-B., Mei, H.-L., Hu, Y., and Guo, T. (2016). Adipocytes secreted leptin is a pro-tumor factor for survival of multiple myeloma under chemotherapy. *Oncotarget* 7, 86075–86086. doi: 10.18632/oncotarget.13342
- Zeisberg, E. M., Potenta, S., Xie, L., Zeisberg, M., and Kalluri, R. (2007). Discovery of endothelial to mesenchymal transition as a source for carcinoma-associated fibroblasts. *Cancer Res.* 67, 10123–10128. doi: 10.1158/0008-5472.Can-07-3127
- Zeng, J., Chen, S., Li, C., Ye, Z., Lin, B., Liang, Y., et al. (2020). Mesenchymal stem/stromal cells-derived IL-6 promotes nasopharyngeal carcinoma growth and resistance to cisplatin via upregulating CD73 expression. *J. Cancer* 11, 2068–2079. doi: 10.7150/jca.37932
- Zhai, J., Shen, J., Xie, G., Wu, J., He, M., Gao, L., et al. (2019). Cancer-associated fibroblasts-derived IL-8 mediates resistance to cisplatin in human gastric cancer. *Cancer Lett.* 454, 37–43. doi: 10.1016/j.canlet.2019.04.002
- Zhang, B., Li, M., McDonald, T., Holyoake, T. L., Moon, R. T., Campana, D., et al. (2013). Microenvironmental protection of CML stem and progenitor cells from tyrosine kinase inhibitors through N-cadherin and Wnt- β -catenin signaling. *Blood* 121, 1824–1838. doi: 10.1182/blood-2012-02-412890
- Zhang, D., Ding, L., Li, Y., Ren, J., Shi, G., Wang, Y., et al. (2017). Midkine derived from cancer-associated fibroblasts promotes cisplatin-resistance via up-regulation of the expression of lncRNA ANRIL in tumour cells. *Sci. Rep.* 7:16231. doi: 10.1038/s41598-017-13431-y
- Zhang, H., Deng, T., Liu, R., Ning, T., Yang, H., Liu, D., et al. (2020). CAF secreted miR-522 suppresses ferroptosis and promotes acquired chemo-resistance in gastric cancer. *Mol. Cancer* 19:43. doi: 10.1186/s12943-020-01168-8
- Zhang, H., Xie, C., Yue, J., Jiang, Z., Zhou, R., Xie, R., et al. (2017). Cancer-associated fibroblasts mediated chemoresistance by a FOXO1/TGF β 1 signaling loop in esophageal squamous cell carcinoma. *Mol. Carcinog.* 56, 1150–1163. doi: 10.1002/mc.22581
- Zhang, L., Yao, J., Li, W., and Zhang, C. (2018). Micro-RNA-21 regulates cancer-associated fibroblast-mediated drug resistance in pancreatic Cancer. *Oncol. Res.* 26, 827–835. doi: 10.3727/096504017x14934840662335
- Zhang, M. M., Di Martino, J. S., Bowman, R. L., Campbell, N. R., Baksh, S. C., Simon-Vermot, T., et al. (2018). Adipocyte-derived lipids mediate melanoma progression via FATP proteins. *Cancer Discov.* 8, 1006–1025. doi: 10.1158/2159-8290.Cd-17-1371
- Zhang, Q., Yang, J., Bai, J., and Ren, J. (2018). Reverse of non-small cell lung cancer drug resistance induced by cancer-associated fibroblasts via a paracrine pathway. *Cancer Sci.* 109, 944–955. doi: 10.1111/cas.13520
- Zhang, X., Chen, Y., Hao, L., Hou, A., Chen, X., Li, Y., et al. (2016). Macrophages induce resistance to 5-fluorouracil chemotherapy in colorectal cancer through the release of putrescine. *Cancer Lett.* 381, 305–313. doi: 10.1016/j.canlet.2016.08.004
- Zhang, X., Tu, H., Yang, Y., Fang, L., Wu, Q., and Li, J. (2017). Mesenchymal stem cell-derived extracellular vesicles: roles in tumor growth, progression, and drug resistance. *Stem Cells Int.* 2017:1758139. doi: 10.1155/2017/1758139
- Zhang, X., Tu, H., Yang, Y., Jiang, X., Hu, X., Luo, Q., et al. (2019). Bone marrow-derived mesenchymal stromal cells promote resistance to tyrosine kinase inhibitors in chronic myeloid leukemia via the IL-7/JAK1/STAT5 pathway. *J. Biol. Chem.* 294, 12167–12179. doi: 10.1074/jbc.RA119.008037
- Zhang, Y., Guoqiang, L., Sun, M., and Lu, X. (2020). Targeting and exploitation of tumor-associated neutrophils to enhance immunotherapy and drug delivery for cancer treatment. *Cancer Biol. Med.* 17, 32–43. doi: 10.20892/j.issn.2095-3941.2019.0372
- Zhao, J., Wang, H., Hsiao, C.-H., Chow, D. S. L., Koay, E. J., Kang, Y., et al. (2018). Simultaneous inhibition of hedgehog signaling and tumor proliferation remodels stroma and enhances pancreatic cancer therapy. *Biomaterials* 159, 215–228. doi: 10.1016/j.biomaterials.2018.01.014
- Zheng, P., Chen, L., Yuan, X., Luo, Q., Liu, Y., Xie, G., et al. (2017). Exosomal transfer of tumor-associated macrophage-derived miR-21 confers cisplatin resistance in gastric cancer cells. *J. Exp. Clin. Cancer Res.* 36:53. doi: 10.1186/s13046-017-0528-y
- Zhou, B., Sun, C., Li, N., Shan, W., Lu, H., Guo, L., et al. (2016). Cisplatin-induced CCL5 secretion from CAFs promotes cisplatin-resistance in ovarian cancer via regulation of the STAT3 and PI3K/Akt signaling pathways. *Int. J. Oncol.* 48, 2087–2097. doi: 10.3892/ijo.2016.3442
- Zhou, S. L., Zhou, Z. J., Hu, Z. Q., Huang, X. W., Wang, Z., Chen, E. B., et al. (2016). Tumor-associated neutrophils recruit macrophages and T-Regulatory cells to promote progression of hepatocellular carcinoma and resistance to sorafenib. *Gastroenterology* 150, 1646.e17–1658.e17. doi: 10.1053/j.gastro.2016.02.040
- Zhu, X., Shen, H., Yin, X., Yang, M., Wei, H., Chen, Q., et al. (2019). Macrophages derived exosomes deliver miR-223 to epithelial ovarian cancer cells to elicit a chemoresistant phenotype. *J. Exp. Clin. Cancer Res.* 38:81. doi: 10.1186/s13046-019-1095-1
- Zou, F., Zhang, Z. H., Zhang, Y. T., Zhao, J. Q., Zhang, X. L., Wen, C. L., et al. (2017). Cancer-associated-fibroblasts regulate the chemoresistance of lung cancer cell line A549 via SDF-1 secretion. *Zhonghua Zhong Liu Za Zhi* 39, 339–343. doi: 10.3760/cma.j.issn.0253-3766.2017.05.004

Conflict of Interest: The authors declare that the research was conducted in the absence of any commercial or financial relationships that could be construed as a potential conflict of interest.

Copyright © 2021 Ni, Zhou, Yang, Shi, Li, Zhao and Ma. This is an open-access article distributed under the terms of the Creative Commons Attribution License (CC BY). The use, distribution or reproduction in other forums is permitted, provided the original author(s) and the copyright owner(s) are credited and that the original publication in this journal is cited, in accordance with accepted academic practice. No use, distribution or reproduction is permitted which does not comply with these terms.



Salubrinol Exposes Anticancer Properties in Inflammatory Breast Cancer Cells by Manipulating the Endoplasmic Reticulum Stress Pathway

Andrew Alsterda^{1†}, Kumari Asha^{1†}, Olivia Powrozek¹, Miroslava Repak¹, Sudeshna Goswami¹, Alexandra M. Dunn², Heidi C. Memmel³ and Neelam Sharma-Walia^{1*†}

OPEN ACCESS

Edited by:

Wei Zhao,
City University of Hong Kong,
Hong Kong

Reviewed by:

Lei Yang,
Shenzhen University, China
Zhi-hang Zhou,
Chongqing Medical University, China

*Correspondence:

Neelam Sharma-Walia
neelam.sharma-walia@
rosalindfranklin.edu

[†]These authors have contributed
equally to this work

Specialty section:

This article was submitted to
Molecular and Cellular Oncology,
a section of the journal
Frontiers in Oncology

Received: 18 January 2021

Accepted: 14 April 2021

Published: 20 May 2021

Citation:

Alsterda A, Asha K, Powrozek O,
Repak M, Goswami S, Dunn AM,
Mammel HC and Sharma-Walia N
(2021) Salubrinol Exposes Anticancer
Properties in Inflammatory Breast
Cancer Cells by Manipulating
the Endoplasmic Reticulum
Stress Pathway.
Front. Oncol. 11:654940.
doi: 10.3389/fonc.2021.654940

¹ H. M. Bligh Cancer Research Laboratories, Department of Microbiology and Immunology, Chicago Medical School, Rosalind Franklin University of Medicine and Science, North Chicago, IL, United States, ² Lake Forest College, Lake Forest, IL, United States, ³ Advocate Health Care, Park Ridge, IL, United States

The endoplasmic reticulum (ER) regulates protein folding, post-translational modifications, lipid synthesis, and calcium signaling to attenuate the accumulation of misfolded proteins causing ER stress and maintains cellular homeostasis. The tumor microenvironment is rich in soluble cytokines, chemokines, growth, and angiogenic factors and can drive the ER's abnormal functioning in healthy cells. Cancer cells adapt well to the tumor microenvironment induced ER stress. We identified that the inflammatory breast cancer (IBC) cells abundantly express osteoprotegerin (OPG) and their tumor microenvironment is rich in OPG protein. OPG also called osteoclast differentiation factor/osteoclastogenesis inhibitory factor (OCIF) is a soluble decoy receptor for receptor activator of nuclear factor-kappa B ligand (RANKL). Employing mass spectrometry analysis, we identified a set of ER chaperones associated with OPG in IBC cell lysates (SUM149PT, SUM1315MO2) compared to healthy human mammary epithelial cells (HMEC). Proximity ligation assay (PLA) and immunoprecipitation assay validated the interaction between OPG and ER chaperone and master regulator of unfolded protein response (UPR) GRP78/BiP (glucose-regulated protein/Binding immunoglobulin protein). We detected remarkably high gene expression of CCAAT enhancer-binding protein homologous protein (CHOP), inositol-requiring enzyme 1 (IRE1 α), protein disulfide-isomerase (PDI), PKR-like ER kinase (PERK), activating transcription factor 4 (ATF4), X-box binding protein 1 (XBP-1) and growth arrest and DNA damage-inducible protein (GADD34) in SUM149PT and SUM190PT cells when compared to HMEC. Similarly, tissue sections of human IBC expressed high levels of ER stress proteins. We evaluated cell death and apoptosis upon Salubrinol and phenylbutyrate treatment in healthy and IBC cells by caspase-3 activity and cleaved poly (ADP-ribose) polymerase (PARP) protein assay. IBC (SUM149PT and SUM190PT) cells were chemosensitive to Salubrinol treatment, possibly via inhibition in OPG secretion, upregulating ATF4, and CHOP, thus ultimately driving caspase-3

mediated IBC cell death. Salubrinal treatment upregulated PDI, which connects ER stress to oxidative stress. We observed increased ROS production and reduced cell proliferation of Salubrinal treated IBC cells. Treatment with antioxidants could rescue IBC cells from ROS and aborted cell proliferation. Our findings implicate that manipulating ER stress with Salubrinal may provide a safer and tailored strategy to target the growth of inflammatory and aggressive forms of breast cancer.

Keywords: endoplasmic reticulum stress, inflammatory breast cancer, Salubrinal, phenylbutyrate, osteoprotegerin

INTRODUCTION

Inflammatory breast cancer (IBC), a rare but extremely invasive and aggressive disease, is characterized clinically by inflammation symptoms. Invasion of dermal lymphatics leads to tissue swelling, warmth, and tenderness, and a distinctive peau d'orange appearance of the skin. Histologically, IBC identifies as an invasive ductal carcinoma (IDC) with high-grade features, including pleomorphic cells and atypical mitotic figures (1, 2). IBC is commonly estrogen, progesterone, and HER-2 receptor-negative (triple-negative breast cancer) or TN-IBC (3). It is not vulnerable to current trimodal (chemotherapy, radiation, and surgery) (4) and there is a strong need for novel targeted therapies (5). These characteristics collectively amount to a particularly poor prognosis and the likely chemotherapy resistance development (2, 4, 6). Even though advances in treatment modalities, including neoadjuvant chemotherapy, have increased survival rates, the forecast for IBC remains significantly worse than non-inflammatory locally advanced breast cancer (7, 8). Thus, there is a critical need to advance our understanding of IBC biology and develop novel treatments (9, 10). Resistance to apoptosis is a significant problem associated with the poor prognosis of IBC. Tumor necrosis factor-related apoptosis-inducing ligand (TRAIL), a potent endogenous activator of cell death, preferentially kills transformed cells over healthy cells. Ionizing radiation can sensitize breast carcinoma cells to TRAIL-induced apoptosis in a p53-dependent manner (11). We demonstrated that IBC cell lines heavily express osteoprotegerin (OPG) and secrete it in their tumor microenvironment (12, 13). OPG induced survival, proliferation, and aneuploidy when added to the growth medium of healthy human mammary epithelial cells (HMEC) (14). OPG also plays an essential role in multiple myeloma and cancers of the prostate, bladder, and stomach (15). Expression of OPG, TRAIL, and receptor activator of nuclear factor κ B ligand

(RANKL) in human breast tumors has also been reported by other research groups (16–18). Interestingly, OPG binds to TRAIL and suppresses TRAIL's function in inducing apoptosis in ameloblastomas (19, 20). OPG protects ovarian cancer cells from TRAIL-mediated apoptosis, and recombinant OPG could abrogate the antitumor effect of TRAIL and correlates with poor prognosis (20).

ER stress pathway plays an essential role in cancers of the breast, prostate, pancreas, liver, CNS, colon, and ovary (21–24). Tumor microenvironment-induced cellular stress has emerged as one of the critical factors involved in the evolution of cancers towards aggressiveness and metastatic dissemination. The ability of tumors to adapt to a hostile environment is an essential hallmark of the disease. As cancer expands, it outgrows its primary blood supply, leading to hypoxia, nutrient deprivation, oxidative stress, an acidic pH, and cell-based cancer-associated fibroblasts (CAFs), cancer-associated macrophages (CAMs), endothelial precursors induced stress mechanisms. These stressors are especially burdensome on the ER of rapidly dividing cells, which must synthesize proteins needed for growth (25–27). The ER provides a unique environment that facilitates the folding and transport of various secretory proteins. This tightly regulated environment involves coordinating many protein folding enzymes, including calcium-dependent chaperones that help proteins attain their native conformation. The ER also regulates calcium homeostasis through Ca^{2+} ATPases that actively transport calcium into the ER. Besides, the oxidative environment facilitated by ER chaperones protein disulfide-isomerase (PDI) and ER oxidoreductase-1 (ERO1) promotes the formation of disulfide bonds needed for proper protein folding. Significant changes to this environment disrupt protein folding and lead to an accumulation of unfolded proteins within the ER lumen; such a state is known as ER stress.

A buildup of unfolded or misfolded proteins within the ER induces unfolded protein response (UPR), which is the first step to stop protein synthesis and allow selective ER chaperones such as binding immunoglobulin protein GRP78/BiP to restore balance. UPR can be both cytoprotective and cytotoxic. At first, the UPR works to regain protein folding, but prolonged stress may induce apoptosis. The UPR is activated when ER chaperones bind to exposed hydrophobic groups of unfolded proteins. GRP78/BiP is critical for protein quality control in the ER. GRP78/BiP is primarily responsible for activating the UPR and ER-transmembrane signaling molecules such as inositol-

Abbreviations: ATF4, activating transcription factor 4; CHOP, C/EBP homologous protein; GADD153, growth arrest and DNA damage-inducible gene 153; eIF2 α , eukaryotic initiation factor 2 (alpha-subunit); ER, endoplasmic reticulum; ERO1, ER oxidoreductase 1; GRP78, glucose-regulated protein (78 kDa); GADD34, growth arrest and DNA damage-inducible protein 34; HER-2, human epidermal growth factor receptor 2; HMEC, human mammary epithelial cells; IBC, inflammatory breast cancer; IRE1 α , Inositol-requiring enzyme 1; PARP, poly-ADP-ribose polymerase; PERK, PKR-like endoplasmic reticulum kinase; EIF2AK3, eukaryotic initiation factor 2 alpha kinase 3; PDI, protein disulfide-isomerase; XBP-1, X-box binding protein 1; TME, tumor microenvironment.

requiring enzyme 1 (IRE1 α), PKR-like ER kinase (PERK), activating transcription factor 6 (ATF6) (28). These proteins are stress sensors that activate three corresponding signaling pathways responsible for restoring homeostasis and upregulate chaperones' production, arresting proteins' translation, and stimulating protein degradation (28). PERK activation also leads to ATF4 and CHOP production, a well-characterized marker for activation of the proapoptotic module of the ER stress pathway (29, 30). We identified the proteins by mass spectrometric analysis of the immunoprecipitate of anti-OPG with lysates prepared from healthy mammary epithelial cells (HMEC), IBC cell lines (SUM149PT, SUM1315MO2). We observed a strong association between OPG and cellular chaperone GRP78/BiP in IBC cells and IBC tumor sections from patients (12). OPG's interaction with the master regulator of UPR suggested that OPG overexpression and substantial secretion from IBC cells may have a potential link in regulating ER stress or UPR in IBC (12). To understand this link, we first assessed ER stress proteins' levels in human IBC tissues and cell lines. Having observed the abundant expression of ER stress/UPR proteins in IBC cell lines and tissue sections compared to their healthy counterparts, we chose to study the effect of Salubrinal treatment on IBC cells. Salubrinal is a synthetic cell-permeable chemical agent (phosphatase inhibitor) that can be taken as an oral pill and is known to elevate the levels of phosphorylated eukaryotic translation initiation factor 2 α (eIF2 α) (31–33). Salubrinal was chosen because a) its therapeutic potential has been tested in other cancers (31–33), b) its ability to target ER stress pathways (31–33), and c) Salubrinal's enhanced activity in cells harvested from the osteoporotic bone samples in context with RANKL (34, 35). Recent studies using Salubrinal demonstrated its potential for the treatment of osteoporosis, the role of stimulation of bone formation, attenuation of bone resorption also encouraged us to study its effect in the context of highly metastatic IBC, which is strongly associated with bone loss. Salubrinal has demonstrated antitumor potential as a combination therapy with doxorubicin (36) and rapamycin (37). The specific role of ER stress in IBC biology remains unclear, and a greater understanding will promote the development of new therapeutic strategies and more favorable prognoses.

MATERIALS AND METHODS

Agents, Cell Lines and Cell Culture

Primary human mammary epithelial cells (HMEC) (#830-05a, Cell Applications, San Diego, CA) were cultured in HMEC medium (#815-500, Cell Applications). Inflammatory breast cancer cells (SUM149PT and SUM190PT) were obtained from Asterand, Detroit, MI. All cells were tested for mycoplasma contamination by the standard Limulus assay (Limulus amoebocyte lysate endochrome; Charles River Endosafe, Charleston, SC) method as per the manufacturer's instructions. All cells were cultured in lipopolysaccharides (LPS) free medium. Antibodies against GRP78/BiP (#3183), PERK (#5683S), IRE1 α

(#3294S), Calnexin (#2433S), Cleaved PARP (#5625), ERO1 α (#3264S), and PDI (#2446S) were obtained from Cell Signaling Technology, Danvers, MA. Antibody against β -actin (#A2228) was obtained from Sigma Aldrich, St. Louis, MO. Antibody against Caspase 3 (66470-2-Ig) was obtained from Proteintech., Rosemont, IL.

Anti-Caspase 3 Antibody, active (cleaved) form (AP1027) was obtained from Calbiochem. Salubrinal; C₂₁H₁₇Cl₃N₄OS (#CML0951), N-Acetyl-L-cysteine (#A7250) and phenylbutyrate (#SML0309) were purchased from Sigma Aldrich.

Tissue Sections

We received 12 samples of inflammatory carcinoma, healthy breast tissue from Advocate Lutheran General Hospital under the approved IRB (IRB00001341). The Inclusion criteria were Pre- and post-menopausal women who have been diagnosed with inflammatory breast cancer *via* biopsy but have not received therapy for this disease yet. The Inclusion criteria also included the women of age 18 years or older. Exclusion criteria were 1) Patients with a psychiatric history that would prevent informed consent, 2) Patients with prior history of invasive malignancy within the last ten years, 3) Pregnant or lactating patients. Healthy breast tissue was obtained from non-cancer/healthy individuals undergoing reduction mammoplasty.

Immunohistochemistry (IHC)

Paraffin-embedded sections (patients with IBC tumors and sections from healthy individuals) were obtained through our collaboration with Lutheran General Hospital. Sections were deparaffinized with HistoChoice clearing reagent and hydrated with water before microwave treatment in 1 mmol/liter EDTA (pH 8.0) for 15 min for antigen retrieval and then blocked with blocking solution (2% donkey serum, 0.3% Triton X-100 in phosphate-buffered saline). Cells were incubated with the primary antibody for GRP78/BiP overnight at room temperature. Slides were then washed with phosphate-buffered saline (PBS) and incubated with HRP-labeled secondary antibodies for 30 min and developed using DAB reagent (DAKO) as per methods described previously (38). IHC was also performed using IgG control antibody as described previously (38). Counterstaining was done by hematoxylin (38). Conjugates of anti-mouse/rabbit-alkaline phosphatase and anti-mouse/rabbit-horseradish peroxidase were from Kirkegaard and Perry Laboratories, Inc., Gaithersburg, MD.

Gene Expression Analysis by Real-Time qRT-PCR

Total RNA was isolated using TRIzol Reagent (#15596026, Life Technologies Corporation, Grand Island, NY) from IBC tissue samples (Biochain, breast tumor tissue array # T22350862-2) and treated with DNase I (#18068015, Life Technologies Corporation) at 37°C for 30 min for DNA removal. RNA quantification was done using NanoDrop (Thermo Fisher Scientific). Reverse transcription was performed using the high-capacity cDNA reverse transcription kit (#4368814, Life Technologies Corporation), converting RNA to cDNA. Transcripts of the genes of interest were detected by real-time

quantitative PCR using gene-specific primers. The relative abundance of target gene mRNA was calculated using the delta-delta method (ratio, $2^{-[\Delta C_t \text{ sample} - \Delta C_t \text{ control}]}$) as described previously (38). Normalization was done with respect to 18S ribosomal RNA levels.

Proximity Ligation Assay (PLA)

SUM149PT and SUM190PT cells were fixed, permeabilized, and incubated with primary antibodies from different species against OPG and BiP/GRP78. They were then labeled with corresponding DuoLink PLA plus and minus probes as per the manufacturer's protocol (# DUO92101Sigma Aldrich). Following ligation and amplification, amplified DNA was detected *via* the hybridization of a red fluorescent probe. Nuclei were visualized using 4', 6-diamidino-2-phenylindole (DAPI), a blue-fluorescent DNA stain (Ex358/Em461; # P36962, Molecular Probes, Eugene, OR).

Western Blot Analysis

Total cell lysates were prepared from respective cells in RIPA buffer containing 15 mM NaCl, 1 mM MgCl₂, 1 mM MnCl₂, 2 mM CaCl₂, 2 mM phenyl-methylsulfonyl fluoride, and protease inhibitor mixture (Sigma). The cell lysates were centrifuged at 13,000g for 20 min at 4°C and protein concentration was quantified using Pierce BCA protein assay. Equal amounts of protein (20 µg/lane) were separated on SDS-PAGE, electrotransferred to 0.45-µm nitrocellulose membranes, blocked with 5% BSA, probed with specific primary antibodies (overnight at 4°C) of interest, and visualized using an enhanced chemiluminescence detection system as described previously (38). Species-specific horseradish peroxidase secondary antibodies were used for detection. Immunoreactive bands were developed by Pierce Super Signal West Pico or Femto reagents (Pierce, Rockford, IL). The bands were scanned and quantitated with ImageJ software following standard protocols (38). β-Actin was used as a loading control.

Immunofluorescence Assay (IFA)

HMEC, SUM149PT, and SUM190PT cells were seeded in eight-well chamber slides (Nalge Nunc International, Naperville, IL.) fixed with 4% paraformaldehyde, permeabilized with 0.4% Triton X-100, and stained with primary antibody overnight at 4°C. Cells were washed and developed with Alexa 594 or Alexa 488-coupled secondary antibody (Molecular Probes), and nuclei were visualized using DAPI counterstain. Stained cells were washed and viewed with the appropriate filters on an Olympus confocal laser-scanning microscope (Fluoview FV10i) with the Metamorph digital imaging system (38–40).

Cytotoxicity Assay

The viability of the cells after treatment with Salubrinal or phenylbutyrate was determined by lactate dehydrogenase (LDH) measuring cytotoxicity assay (#G1780) (Promega, Madison, WI), as described previously (40). LDH is released into cell culture media when the plasma membrane is damaged. The assay measures this extracellular LDH using an enzymatic reaction that results in a red formazan product, which absorbs

strongly at 490 nm and can be measured spectrophotometrically. The amount of color formed is proportional to the number of lysed cells.

Caspase-3 Activity Assay

Caspase-3 activity was measured in cell lysates prepared from untreated, or Salubrinal treated HMEC, SUM149PT, and SUM190PT cells by a Caspase-Glo-3 test from Promega (#G8091) as per the manufacturer's instructions (40). Cells are seeded in a 96-well plate, the reagent is added, including a luminogenic caspase-3 substrate, and the luminescent signal is measured to determine the amount of caspase activity that is present.

Cleaved Poly (ADP-Ribose) Polymerase (PARP) Protein Assay

The activity of PARP, a nuclear DNA-repair enzyme, is increased in response to DNA damage. However, PARP can activate a unique cell death program during excessive DNA damage by generating large branched ADP-ribose polymers. During apoptosis, PARP is cleaved by activated caspase-3. Following Salubrinal treatment in HMEC, SUM149PT, and SUM190PT cells, the cleaved PARP level was measured using the human cleaved PARP1 in-cell ELISA kit (Abcam Cambridge, MA) per the manufacturer's instructions.

Cell Viability Assay

IBC cell lines, SUM149PT and SUM190PT, were seeded in 96-well plates and treated with and without Salubrinal in the absence or presence of specific, irreversible caspase inhibitors (caspase-2, -3, -6, -8, -9, and -10) from R&D systems. Enhanced cell survival was determined using the CellTiter-fluor cell viability assay from Promega (#G6080) per the manufacturer's instructions. This assay measures a conserved and constitutive protease activity within live cells using a fluorogenic substrate. Loss of cell membrane integrity inactivates this protease.

BrdU ELISA

The effect of Salubrinal treatment on SUM149PT cell proliferation was determined by using a BrdU Cell Proliferation ELISA (#6813) kit (Cell Signaling Technology). This technique is based on the incorporation of the pyrimidine analog BrdU into the DNA of proliferating cells. After its incorporation into DNA, BrdU is detected by immunoassay. Briefly, untreated Salubrinal treated, and NAC and Salubrinal treated cells were cultured 48h. After Salubrinal treatment, cells were pulsed with BrdU for 4 h. The ELISA was performed in triplicate and the absorbance was read at 450 nm.

OPG ELISA

The conditioned media of untreated or Salubrinal treated SUM149PT and SUM190PT cells were collected, centrifuged, and OPG levels were measured in the supernatants were measured by ELISA (Raybiotech, Peachtree Corners, GA) according to the manufacturer's instructions. Results are expressed as the amount of OPG secreted (pg/ml) per 10⁶ cells (14).

DCFDA/H2DCFDA Cellular ROS Assay

DCFDA/H2DCFDA (2',7'-dichlorofluorescein diacetate, also known as H2DCFDA) is a fluorogenic dye that measures hydroxyl, peroxy, and other reactive oxygen species (ROS) activity within the cell. DCFDA/H2DCFDA is a cell-permeant reagent and cellular ROS assay from Abcam (#ab113851) quantitatively assess reactive oxygen species in live cell samples. Briefly, untreated Salubrinal treated, and NAC (5 mM), and Salubrinal treated cells were cultured 48h. Cells were collected and stained (30 min at 37°C) with oxidative-sensitive dye DCFDA/H2DCFDA and analyzed immediately with a flowcytometer as per the manufacturer's instructions. Exogenous H₂O₂ is frequently used as a representative ROS in modeling and inducing oxidative stress.

Statistical Analysis

Differences between samples were analyzed with the Student's t-test. The statistical significance (t-test) was conducted with respect to untreated cells. Significant differences at $P < 0.05$, 0.01, 0.005, and 0.001 between conditions are indicated by *, **, ***, and **** respectively. All calculations were performed using the GraphPad PRISM version 4.00 for Windows (GraphPad Software, La Jolla, CA, USA).

RESULTS

OPG interacts With Major ER Chaperone Protein GRP78/BiP in IBC Cells

Previous studies from our lab discovered OPG's role as an essential paracrine factor involved in reprogramming healthy

cells into tumor cells and provided novel mechanisms *via* which OPG activates the downstream signaling pathways driving cell proliferation, cell cycle, and aneuploidy (14). We identified the OPG binding proteins in HMEC and IBC cell lines (SUM149PT and SUM1315MO2). Cell lysates prepared from different cell types were immunoprecipitated using an anti-OPG antibody, followed by LC-ESI-MS mass spectrometry analysis (12). Seventeen bands were selected for the study, and proteins were identified with a confidence range of 99.1% to 68.2% (12). OPG bound to several cellular chaperones such as heat shock 70kDa protein (mortalin), GRP78/BiP, heat shock 60kDa protein (chaperonin), and heat shock gp96 precursor, HSP90AB1 protein, and stress-70 protein (12). To understand whether IBC cells are addicted to OPG (12) and use OPG as a critical survival factor by interacting with master ER stress regulator GRP78/BiP (41), we performed IHC, real-time qPCR, Western blotting, and immunofluorescence assay (IFA) to compare the expression of ER stress proteins in healthy human breast tissue as compared to IBC tumor tissue obtained from patients (**Figures 1–3**).

Breast tissue sections were analyzed by comparing chaperone GRP78/BiP expression in healthy tissue and IBC tumor from patients (**Figure 1A**). IBC tissue sections (**Figure 1A**; Ab, Ae, Af) showed upregulation of the target cellular chaperone in addition to increased proliferation and pleomorphism compared to the healthy tissue (**Figure 1A**; Aa, Ac, Ad). BiP/GRP78 protein staining was further validated by immunofluorescence assay using BiP/GRP78 antibody in healthy and IBC tissue (**Figure 1B**). We observed heavy staining for BiP/GRP78 around vessels in the IBC tissue section compared to healthy tissue (**Figure 1B**).

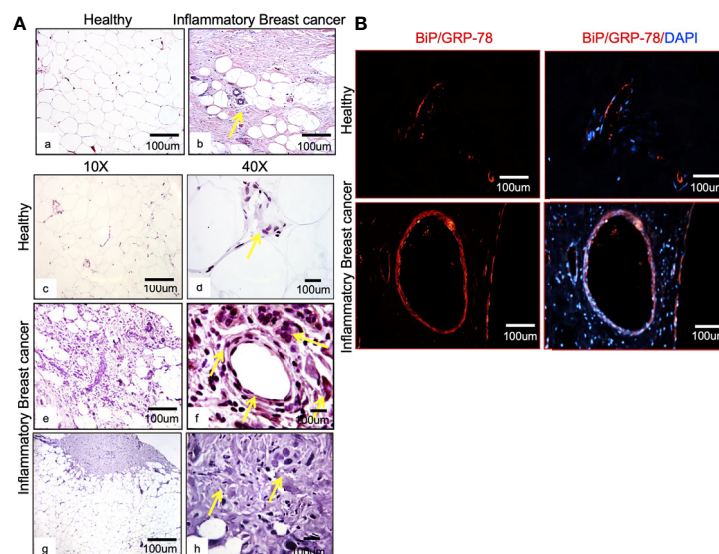


FIGURE 1 | BiP/GRP78 is expressed abundantly in human IBC tissue sections. **(A)** Hematoxylin and Eosin (H & E) staining of healthy (left) **(Aa)** and IBC tissue (right) **(Ab)** is shown at 10X and 40X magnification. Healthy **(Ac, Ad)** and IBC tissue sections **(Ae, Af)** were stained using an antibody against BiP/GRP78. Human IBC tissue sections **(Ag, Ah)** were stained using an anti-IgG antibody. **(Aa–Ac, Ae, Ag)** are 10X, whereas **(Ad, Af, Ah)** represent 40X magnification. **(B)** BiP/GRP78 immunostaining (red) and healthy and IBC tissue are shown at 10X magnification. Tissue sections were developed with Alexa-594 coupled secondary antibody (red). Nuclei were visualized using DAPI as the counterstain (blue).

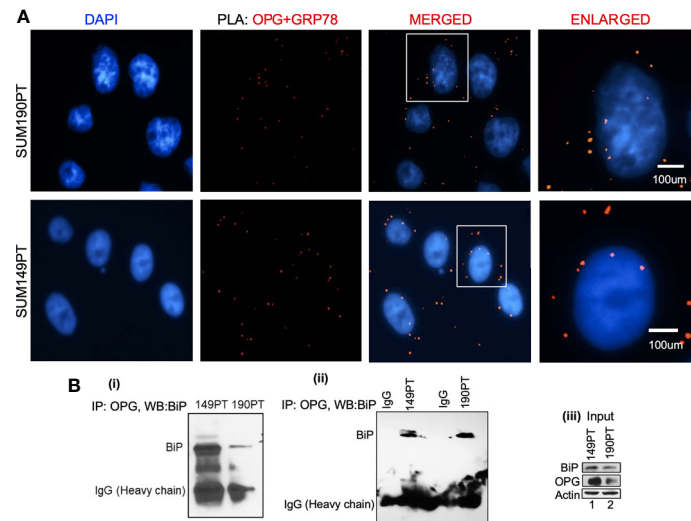


FIGURE 2 | OPG interacts with BiP/GRP78 in IBC cell lines. **(A)** Proximity ligation assay (PLA) was performed using IBC cell lines, SUM149PT, and SUM190PT. Cells were fixed, permeabilized, and incubated with primary antibodies against OPG and BiP/GRP78, and then labeled with DuoLink PLA plus and minus probes. A red fluorescent probe was used to detect amplified DNA. Nuclei were visualized using DAPI as the counterstain (blue). **(B)** Association of OPG and GRP78 in IBC cell lines. Co-immunoprecipitation of OPG-BiP/GRP78 complex using anti-OPG antibody or anti-IgG antibody and visualization of the complex *via* Western blotting using anti-BiP/GRP78 antibody.

A Proximity ligation assay (PLA) and co-immunoprecipitation were used to evaluate OPG and GRP78/BiP interaction. PLA with primary antibodies against OPG and GRP78/BiP was used to detect OPG and GRP78/BiP interaction (**Figure 2A**). PLA is a highly sensitive and specific technique capable of identifying protein-protein interactions within close-proximity (<40 nm). OPG and GRP78/BiP interaction were visualized as red dots in both IBC cell lines, SUM149PT and SUM190PT (**Figure 2A**). The lack of detection of any PLA signals when either primary antibody was used alone validated the antibody specificity and observed interaction (data not shown).

OPG and GRP78/BiP association were confirmed by co-immunoprecipitation analysis (**Figure 2B**; i and ii). The OPG-GRP78/BiP complex was isolated using an anti-OPG antibody, and then the complex was visualized *via* Western blot analysis using an anti-GRP78 antibody. The OPG-GRP78 complex was seen in IBC cell lines (SUM149PT and SUM190PT) (**Figure 2B**; i and ii). This observed interaction's specificity was confirmed by an immunoprecipitation reaction using an anti-IgG antibody (**Figure 2B**; ii). Input for the total lysate is shown for OPG and BiP (**Figure 2B**; iii).

Tissue sections obtained from IBC patients also showed upregulation of ER stress markers, including ATF4, CHOP, GADD34, GRP78/BiP, IRE1 α , and XBP-1 as compared to the healthy tissue obtained from healthy controls (**Figure 3A**). Compared to the healthy control, HMEC cells, increased expression of ER stress markers was observed in inflammatory breast cancer cell lines SUM149PT and SUM190PT. Real-time PCR results demonstrated 10- to 1000- fold upregulation of ER stress-associated genes in IBC cell lines compared to HMEC

controls (**Figure 3B**). These results were corroborated by Western blot analysis (**Figure 3C**) and immunofluorescence (**Figure 3D**). Western blot analysis demonstrated the upregulation of ER stress-associated proteins in IBC cells, albeit not always consistent between the cell lines (**Figure 3C**). Overall, these results support the premise that ER stress is an inherent IBC biology attribute. Immunofluorescence staining showed abundant expression of calnexin, ERO1 α , and IRE1 α in IBC cell lines SUM149PT and SUM190PT compared to healthy control, HMEC cells (**Figure 3D**).

Salubrinal Exhibits Cytotoxicity Against IBC Cancer Cells

Salubrinal and phenylbutyrate have been shown to modulate ER stress pathways (42, 43), and we tested their effect on healthy control cells (HMEC) and IBC cancer cell lines (SUM149PT and SUM190PT) (**Figure 4**). The IBC cell lines and HMEC cells were treated with varying Phenylbutyrate concentrations (**Figure 4A**) or Salubrinal (**Figure 4B**) for different time intervals to select a suitable drug concentration and time interval for subsequent experiments. Cellular cytotoxicity was evaluated using a lactate dehydrogenase (LDH) cytotoxicity assay, which uses spectrophotometry to measure the amount of LDH released from damaged cells. Phenylbutyrate was extremely cytotoxic to healthy control cells (HMEC) than IBC cell lines (SUM149PT and SUM190PT), which designated Phenylbutyrate as a poor candidate for further study (**Figure 4A**). In contrast, Salubrinal was highly cytotoxic to IBC cell lines (SUM149PT and SUM190PT) with minimal effect on the HMEC control cells' viability at 10µM (**Figure 4B**). We also tested the effect of

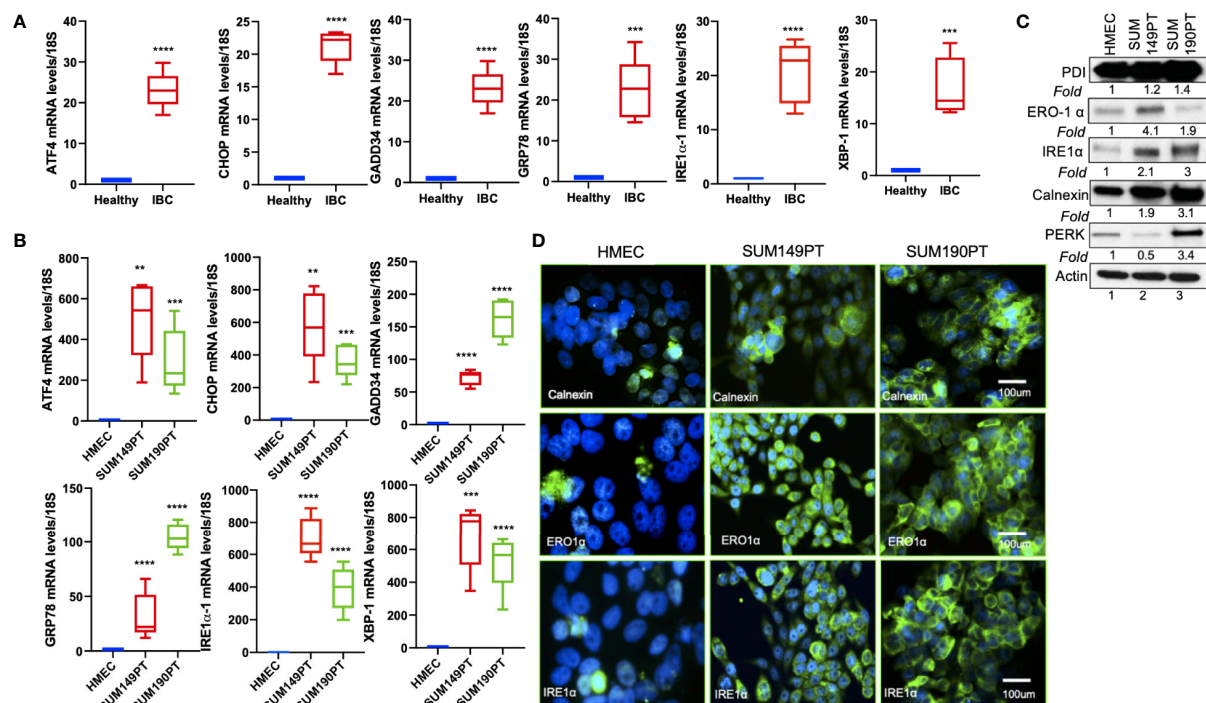


FIGURE 3 | ER stress genes are abundantly expressed in IBC tissue sections and IBC cell lines. **(A)** RNA isolated from healthy and IBC tumor tissue was prepared, converted to cDNA, and gene expression was quantified by real-time RT-PCR using specific primers for ER stress markers as indicated. Each data point represents the average gene expression from six IBC and six healthy control samples. Each point represents the average \pm the standard deviation of three experiments. (***) $p < 0.005$, (****) $p < 0.001$ indicates a statistically significant difference compared with healthy tissue. Each reaction was done in triplicate. **(B)** RNA isolated from HMEC, SUM149PT, and SUM190PT cells was converted to cDNA, and gene expression was quantified by real-time RT-PCR using specific primers for ATF4, CHOP, GADD34, GRP78, IRE1 α , and XBP-1. Each point represents the average \pm the standard deviation of three experiments. (**) $p < 0.01$, (***) $p < 0.005$, (****) $p < 0.001$ indicate a statistically significant difference compared with HMEC cells. Each reaction was done in triplicate. **(C)** ER stress genes proteins are abundantly expressed in IBC cell lines. Lysates prepared from HMEC, SUM149PT, and SUM190PT cells, were tested for protein levels of PERK, IRE1 α , calnexin, ERO1 α , and PDI. Blots were reprobed with anti- β -actin antibody as a loading control for normalization. Fold expression of each protein was calculated by considering the expression of the protein in HMEC as 1. **(D)** Immunostaining of HMEC and SUM149PT cells seeded in eight-well chamber slides. Cells were fixed, permeabilized, and then stained with primary monoclonal antibodies against ER stress markers, including calnexin, ERO1 α , and IRE1 α . Cells were developed with Alexa-488 coupled secondary antibody (green). Nuclei were visualized using DAPI as the counterstain (blue).

Salubrinal and Phenylbutyrate on HMEC, SUM149PT and SUM190PT cells and identified the cytotoxic concentration by assessing cell membrane integrity using trypan blue staining and counting live/dead cells (data not shown). Consequently, 10 μ M Salubrinal was selected for future experiments.

Salubrinal Regulates ER Stress Pathway Players at Their Gene Expression and Protein Level

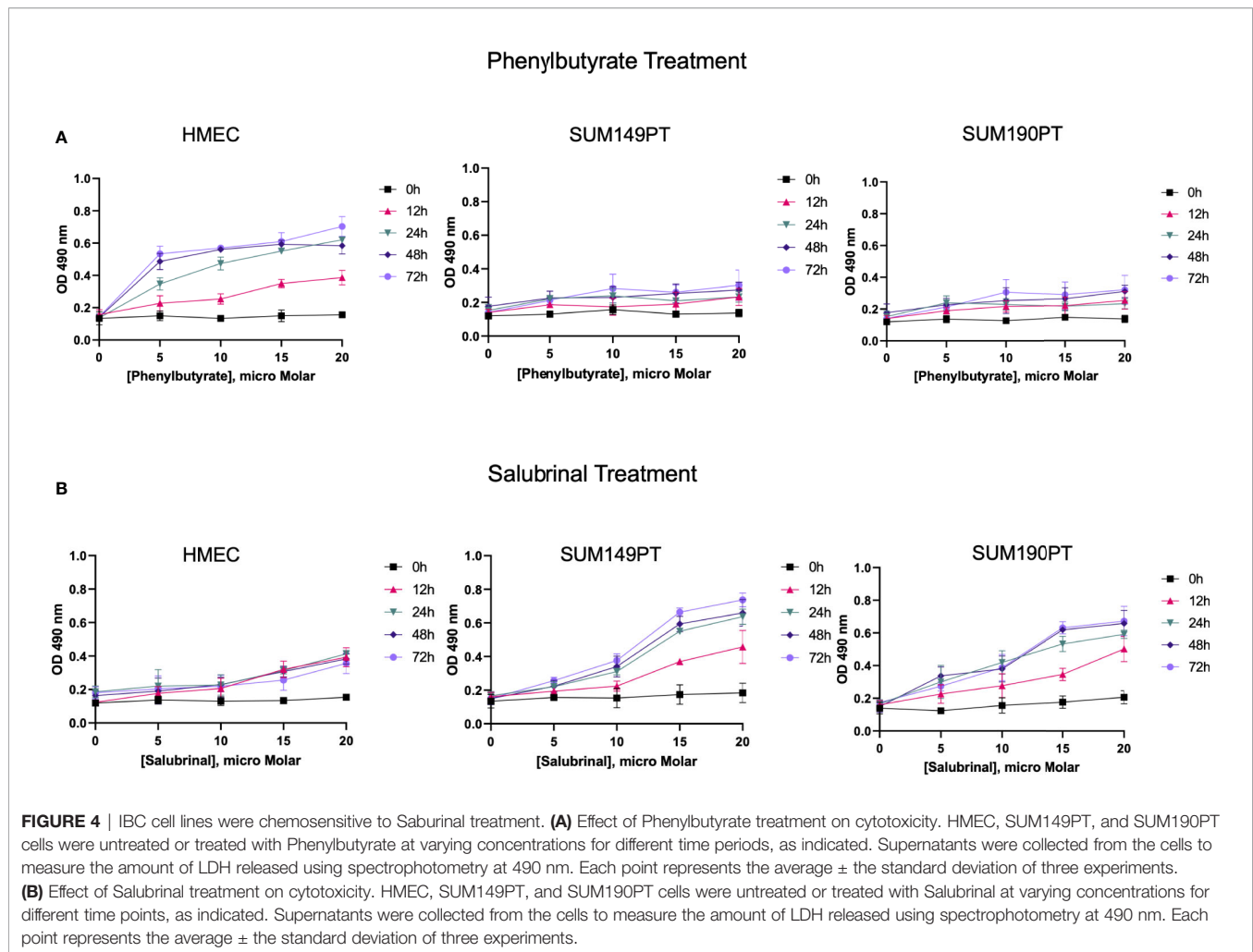
To determine Salubrinal treatment's effect on the ER stress pathway, IBC (SUM149PT and SUM190PT) cell lines were grown with 10 μ M Salubrinal for 24h and 48h (Figure 5). Quantitative RT-PCR and Western blot analysis were used to evaluate ATF4, ATF6, CHOP, and GRP78 gene expression (Figures 5A, B) and protein levels (Figure 5C).

Salubrinal treatment for 24h or 48h significantly induced ATF4 and CHOP gene expression in SUM149PT and SUM190PT cells (Figures 5A, B). Western blot results showed

upregulation of CHOP, ERO1, and PDI and downregulation of calnexin in SUM149PT and SUM190PT (Figure 5C). However, changes in ER stress markers were variable between cell lines. Salubrinal treatment-induced ERO1 levels in SUM149PT more than SUM190PT cells (Figure 5C). IRE1 α levels were reduced in SUM190PT more than SUM149PT cells (Figure 5C). Salubrinal treatment reduced PERK levels in SUM190PT more than in SUM149PT cells (Figure 5C). Overall, treatment of SUM149PT with Salubrinal induced a more substantial increase in ER stress-related proteins compared to SUM190PT (Figure 5C).

Salubrinal Induces Caspase-3-Mediated Apoptosis in IBC Cells

Further characterization of the Salubrinal induced cell death mechanism was sought by analyzing caspases' activity, a proteases family that plays an essential role in apoptosis. To determine which caspase family member is activated with Salubrinal treatment, we observed the enhanced survival of



cells incubated with or without Salubrinol in the absence or presence of specific caspase inhibitors, which included inhibitors of initiator caspases (caspase -2, -8, -9, and -10) and executioner caspases (caspase 3 and 6) (**Supplement Figure 1**). Enhanced survival of SUM149PT and SUM190PT cells was noted with the application of the caspase-3 inhibitor, which indicates a critical role that caspase-3 likely plays in mediating Salubrinol induced cell death in IBC cell lines (**Supplement Figure 1**).

Caspase 3 is processed into cleaved caspase 3 in the early steps of apoptosis and its level positively correlates with the rate of cell death. In cells grown with and without Salubrinol, we analyzed the activation of caspase-3 and the proteolytic cleavage of PARP, a DNA repair enzyme the proteolytic target of caspase-3. Treatment of IBC cell lines SUM149PT and SUM190PT with Salubrinol induced caspase-3 activity with time (**Figures 6B, C**) as well as cleavage of PARP (**Figures 6E, F**), clear indications of apoptosis. Treatment of HMEC cells with Salubrinol did not increase caspase-3 activity with time (**Figure 6A**), as well as cleavage of PARP (**Figure 6D**), clear indications of apoptosis. Salubrinol treatment-induced cleaved caspase-3 and cleaved PARP protein levels in IBC cell lines SUM149PT and

SUM190PT cell lysates by Western blotting (**Figure 6G**), which further validated the ELISA results (**Figures 6A–F**).

Salubrinol treatment significantly reduced OPG secretion from SUM149PT and SUM190PT cells as tested by OPG ELISA (data not shown). PARP cleavage was blocked by co-treatment with the broad-range irreversible pan-caspase inhibitor Z-VAD-FMK (inhibits caspase processing and apoptosis induction), suggesting that a caspase cascade mediates Salubrinol-induced apoptosis in IBC cells.

We next examined the effect of Salubrinol treatment on major cell survival protein p-Akt and inflammatory protein p-NF κ B (**Figure 7A**). Compared to untreated cells, 48 h Salubrinol treatment down-regulated p-NF κ B by about 50% and p-Akt by about 80% (**Figure 7A**). At 48h Salubrinol post-treatment, we observed dramatic upregulation of pro-apoptotic Bax, and downregulation of anti-apoptotic Bcl-2, and Bcl-xL (**Figure 7A**). Next, we detected the effect of Salubrinol treatment on eIF2 α phosphorylation and ER stress pro-apoptotic protein CHOP (**Figure 7A**). Compared to untreated cells, 48 h Salubrinol treatment up-regulated eIF2 α phosphorylation by about 2-fold and CHOP by about 3-fold (**Figure 7A**).

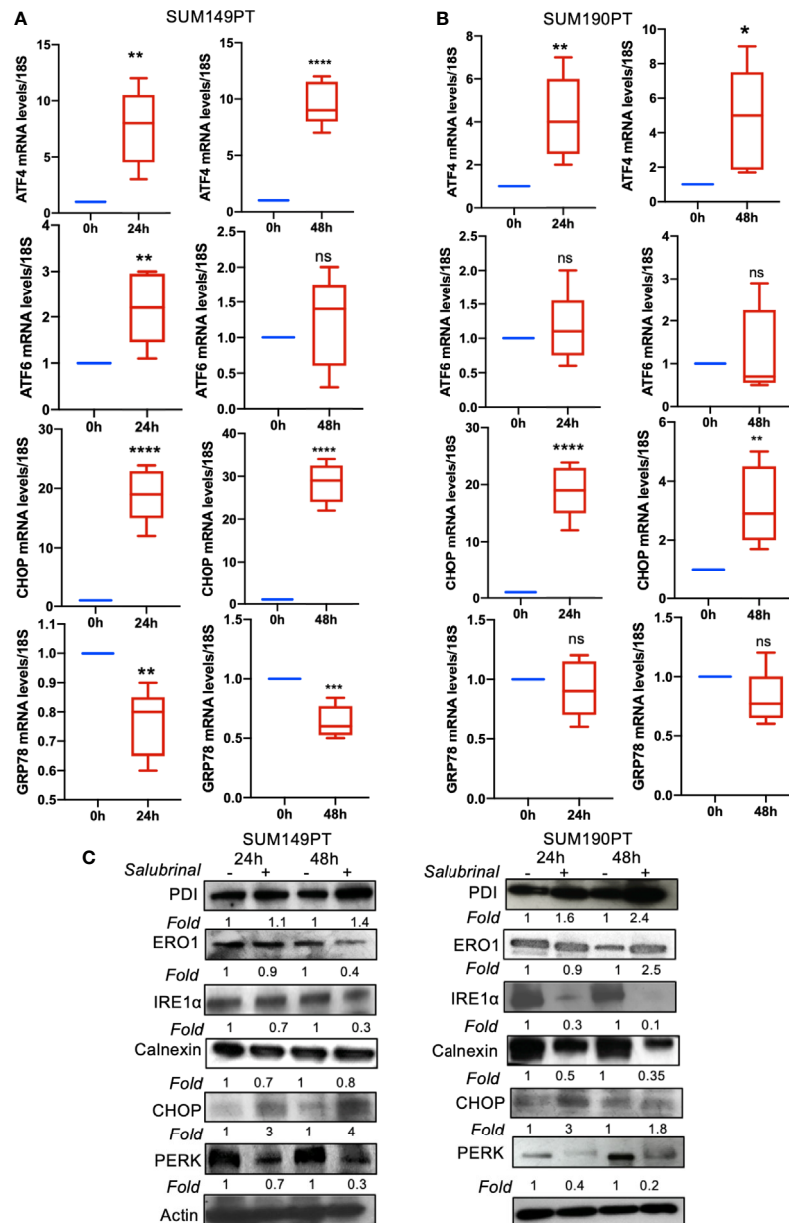


FIGURE 5 | Effect of Salubrinal treatment on ER stress gene expression levels in IBC cell lines. IBC cell lines **(A)** SUM149PT and **(B)** SUM190PT were cultured with or without 10 μ M Salubrinal for 24 and 48 hours. RNA was prepared from SUM149PT and SUM190PT cells. RNA was converted to cDNA, and ER stress markers ATF4, ATF6, CHOP, and GRP78 were quantitated using real-time PCR, as mentioned in the methods section. Each point represents the average \pm the standard deviation of three experiments. (*), $p < 0.05$, (**) $p < 0.01$, (***) $p < 0.005$, (****) $p < 0.001$ indicate a statistically significant difference compared with cells treated for 0h. ns, not significant. **(C)** Effect of Salubrinal treatment on ER protein levels in IBC cell lines. IBC cell lines SUM149PT and SUM190PT were cultured with or without 10 μ M Salubrinal for 24 and 48 hours. Lysates prepared from SUM149PT and SUM190PT cells were tested for protein levels of ER stress markers ERO1 α , PERK, PDI, CHOP, IRE1 α calnexin using Western blot analysis. Blots were reprobated with anti- β -actin antibody as a loading control.

Salubrinal Induces ROS-Mediated Downregulation of Cell Proliferation in IBC Cells

To determine whether Salubrinal treatment had any effect on ROS level in IBC cells, we performed a cellular ROS assay using oxidative stress-sensitive probe DCFDA (**Figures 7B, D**).

Compared to untreated cells, 48 h Salubrinal treatment significantly up-regulated cellular ROS level (**Figures 7B, D**). Cotreatment with antioxidant NAC and Salubrinal exhibited downregulated ROS levels (**Figures 7B, D**). Similar results (**Figures 7C, E**) were obtained in the experiments where exogenous H_2O_2 was used as a representative ROS inducer.

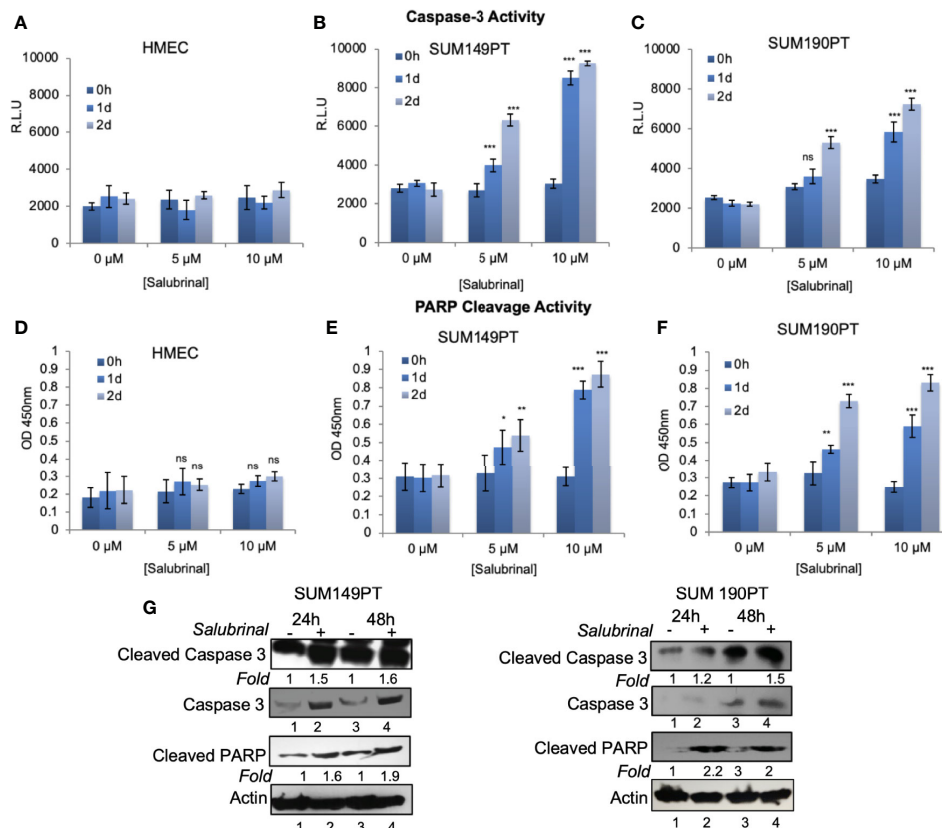


FIGURE 6 | Salubrinal treatment induces caspase-3 activation and PARP cleavage in IBC cells. **(A–C)** HMEC and IBC cell lines, SUM149PT and SUM190PT, were treated with various concentrations of Salubrinal for different time intervals. A luminogenic caspase-3 substrate is added, and the luminescence is measured in relative light units (RLU) as an index for caspase-3 activity. Each reaction was done in triplicate, and each bar represents the mean \pm SD for three experiments. **(D–F)** HMEC and IBC cell lines, SUM149PT and SUM190PT, were treated with various concentrations of Salubrinal for different time intervals. Cells were fixed, permeabilized, and incubated with a particular anti-cleaved PARP primary antibody followed by an HRP-labeled secondary antibody. Absorbance (OD) was measured at 450 nm as an index of PARP cleavage. Each reaction was done in triplicate, and each bar represents the mean \pm SD for three experiments. (*), $p < 0.05$, (**) $p < 0.01$, (***) $p < 0.005$ indicate a statistically significant difference compared with cells treated for 0h. ns, not significant. **(G)** SUM149PT and SUM190PT cells were cultured with or without 10M Salubrinal for 24 and 48 hours. Lysates prepared and tested for caspase-3, cleaved caspase-3 and cleaved PARP as indicated by Western blot analysis. Blots were reprobbed with anti-actin antibody as a loading control. The level of proteins in untreated samples was considered one for fold activation or down-regulation using the quantification method as described in the *Methods* section.

Interestingly, ROS is associated with multiple cell signaling pathways, cell proliferation, and cell death, and we observed downregulation of p-AKT, anti-apoptotic proteins Bcl-2, and Bcl-xL upon Salubrinal in IBC cells. Therefore, we determined whether Salubrinal treatment mediated down-regulation of IBC cell proliferation is mediated *via* ROS using BrdU cell proliferation assay (**Figures 7F, G**). Compared to untreated cells, Salubrinal treatment significantly down-regulated BrdU incorporation during DNA synthesis measured quantitatively as absorbance (**Figures 7F, G**). Cotreatment with antioxidant NAC and Salubrinal exhibited up-regulated BrdU incorporation, an indicator of cell proliferation (**Figures 7F, G**).

DISCUSSION

IBC presents at a locally advanced or metastatic stage with a poor prognosis. The current standard of care and improved survival

rates require advancement in screening and state-of-the-art treatment modalities. Activation of the ER stress response or UPR is associated with numerous fatalities such as the progression of B cell chronic lymphocytic leukemia (CLL) (44, 45), multiple myeloma, and cancers of the breast, prostate, pancreas, and liver (44–46). This hallmark has been exploited with bortezomib development, a proteasome inhibitor used in patients with multiple myeloma. Since the ER stress pathway is a recognized target for therapeutic intervention in cancer, we aimed to understand ER stress and UPR in IBC in context with its unique OPG rich microenvironment (14). OPG is a soluble decoy receptor for tumor necrosis factor receptor (TNF)-related apoptosis-inducing ligand (TRAIL). The rationale for selecting to study UPR has based on 1) our findings in the previous study, where we identified that OPG binds to cellular chaperones including mortalin, chaperonin, BiP protein, HSP90AB1 protein, and heat shock protein gp96 in IBC cells

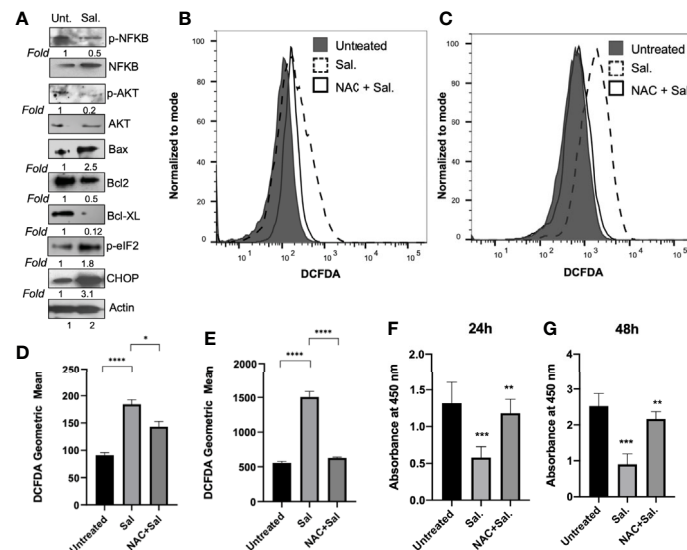


FIGURE 7 | Salubrinal treatment induces cell death potentially by induction of ROS in IBC cells. **(A)** SUM149PT cells were cultured with or without 10 μ M Salubrinal for 48 hours. Lysates prepared and tested for various inflammation, proliferation, and apoptosis-specific proteins as indicated by Western blot analysis. Blots were reprobated with anti- β -actin antibody as a loading control. p-NF κ B and p-AKT were normalized with respect to total NF κ B and AKT, respectively. The level of proteins in untreated samples was considered one for fold activation or down-regulation using the quantitation method as described in the Methods section. **(B)** ROS analysis in SUM149PT cells (untreated, Salubrinal treated or NAC and Salubrinal treated) for 48h was done. Raw data of DCFDA fluorescence peaks of a representative experiment. **(C)** ROS analysis in SUM149PT cells (untreated, Salubrinal treated or NAC and Salubrinal treated) for 48h was done. Cells were pulsed with H₂O₂ right before analyses in the flowcytometer. Raw data of DCFDA fluorescence peaks of a representative experiment. **(D, E)** Quantification of ROS levels from **(B, C)**, respectively. Each reaction was done in triplicate, and each bar represents the geometric mean \pm SD for three experiments. (*), $p < 0.05$ and (****) $p < 0.001$ indicate a statistically significant difference between either untreated and Salubrinal treated or Salubrinal treated and NAC and Salubrinal cotreatment. **(F, G)** Cell proliferation assay in SUM149PT cells (untreated, Salubrinal treated or NAC and Salubrinal treated) for 48h was measured by BrdU assay as described in the methods section. Each reaction was done in triplicate, and each bar represents the absorbance mean \pm SD for three experiments. (**), $p < 0.01$ and (***) $p < 0.005$ indicate a statistically significant difference between either untreated and Salubrinal treated or Salubrinal treated and NAC and Salubrinal cotreatment.

(12) and 2) significantly high expression of ER stress proteins and UPR sensors in IBC cell lines and IBC tumors as compared to their healthy counterparts (**Figures 1–3**). Here, we validated the interaction between OPG and an ER chaperone protein critical for protein quality control of the ER called GRP78/BiP (**Figure 2**). These results demonstrate that an OPG rich IBC tumor microenvironment is involved in tweaking the cellular protein homeostasis and driving ER stress in IBC cells. GRP78/BiP has been reported as a prosurvival factor for cells undergoing ER stress. GRP78/BiP directly interacts with apoptotic pathway intermediates, blocks caspase activation, and eventually leads to apoptosis inhibition (47, 48) and increased cell survival (41). GRP78 is also implicated in promoting drug resistance in cancers and regulating angiogenesis (41), an essential hallmark of IBC. We speculate that the OPG-GRP78 interaction in IBC cells cooperatively works to enhance the growth, survival, and spread of IBC.

To determine the effect of the ER stress modulators in IBC cells, we chose Salubrinal and Phenylbutyrate. Salubrinal is a cell-permeable selective inhibitor of eIF2 α dephosphorylation that has been associated with up-regulation of ER stress-related cell apoptosis and oxidative stress (49). Salubrinal was preferentially cytotoxic to IBC cell lines, while Phenylbutyrate was cytotoxic to the healthy control cells (**Figure 4**). Importantly, Salubrinal

demonstrated minimal toxicity to control HMEC cells (**Figure 4**). Choice of Salubrinal does not undermine the therapeutic potential of Phenylbutyrate, a histone deacetylase inhibitor, approved for the treatment of urea cycle disorders, cancer, hemoglobinopathies, motor neuron diseases, and cystic fibrosis clinical trials (50). It possesses a broad spectrum of molecular functions such as antiviral (51), chromatin regulator and modulator of multiple cell cycle, and apoptosis-related genes (50). Phenylbutyrate has been well studied for its potential in prostate cancer alone (52) or in a combination of Phenylbutyrate and 13-cis retinoic acid (53). Phenylbutyrate along with curcumin could attenuate PA-induced increase in CHOP and GRP78 expression and protect H9C2 cardiomyocytes from lipotoxicity-induced cell death (54). The choice of Salubrinal in the current study was completely based on its minimal toxicity to control HMEC cells and selective toxicity to IBC cells at a low dose (**Figure 4**).

Salubrinal treatment of IBC cell lines upregulated ATF4 and CHOP gene expression (**Figure 5**). ERO1 α , PDI, and CHOP consistently increased upon Salubrinal treatment of SUM149PT and SUM190PT cell lines (**Figure 5**). However, the trends in the decrease of PERK and IRE1 α levels upon Salubrinal treatment were more pronounced in SUM190PT cells when compared to SUM149PT (**Figure 5**). These differences may be due to cell type

variations. Upregulation of CHOP, a proapoptotic transcription factor downstream of PERK and ATF4, demonstrates a potential antitumor strategy of Salubrinal in IBC cells (55) (**Figure 5**).

The ER is also a reservoir for intracellular calcium. It requires IRE1 α , and little is known about the molecular mechanisms by which excessive ER stress triggers cell death and Ca(2+) dysregulation *via* the IRE1 α -dependent signaling pathway (56). The increased cytosolic concentration of Ca(2+) induces mitochondrial production of reactive oxygen species (ROS), resulting in severe mitochondrial fragmentation, depolarization of membrane potential, and subsequent cell death in IRE1 α -deficient cells (56). Cross-talk between oxidative and ER stress has also been observed in palmitic acid (PA)-induced H9c2 cardiomyocytes apoptosis leading to lipotoxic cardiomyopathy (57).

Recently, IRE1 α 's potential has been implicated in Ca(2+) homeostasis and cell survival during ER stress and revealed the IRE1 α -InsP3R pathway in the ER and the redox-dependent apoptotic pathway in the mitochondrion (56). Salubrinal treatment significantly reduced IRE1 α levels in SUM190PT cells, especially at 48h of treatment, suggesting that it might be causing Ca(2+) dysregulation induced mitochondrial abnormalities and eventually cell death in these cells. ERO1 α has been shown to mediate ER luminal hyper oxidation, leading to calcium leakage and autophagy and mitochondria-mediated apoptosis (58). Salubrinal cytotoxicity in IBC cell lines is associated with activation caspase-3, which appears to be a

critical mediator of apoptosis in this pathway (**Figure 6** and **Supplement Figure 1**).

Inhibition of ER stress inhibited the inflammatory response by LPS in mouse granulosa cells, thus highlighting the cross-talk between ER stress and inflammation (59). Consistent with the survival (AKT) protein kinase phosphorylation, we observed the downregulation of inflammatory NF κ B (p65) signaling upon Salubrinal treatment (**Figure 7A**).

Oxidative protein folding is catalyzed by several multifunctional ER oxidoreductases, including protein disulfide isomerases (PDI) in eukaryotic cells (60). Oxidative protein folding is a vital resource of ROS production in the cell. After accepting electrons from PDI, ERO1 transfers the electrons to molecular oxygen (O₂) and produces H₂O₂, the major ROS created in the ER (61). Although the activation cascade of caspase pathways during the ER stress is still elusive, our results indicate that Salubrinal induced PDI levels in both IBC cells (**Figure 5C**) and induced ROS (**Figure 7**). N-acetyl-cysteine (NAC), an antioxidant, the ROS scavenger, could rescue ROS induction and cell proliferation (**Figure 7**), suggesting ROS's role in Salubrinal mediated cell death in IBC cells. CHOP also induces oxidative stress and contributes to cell death during ER stress. CHOP leads to protein misfolding and mitochondrion-dependent induction of oxidative stress (62–64). Since we quantitated total cellular ROS, therefore we can only speculate about the mitochondrial ROS induction upon Salubrinal treatment in IBC cells.

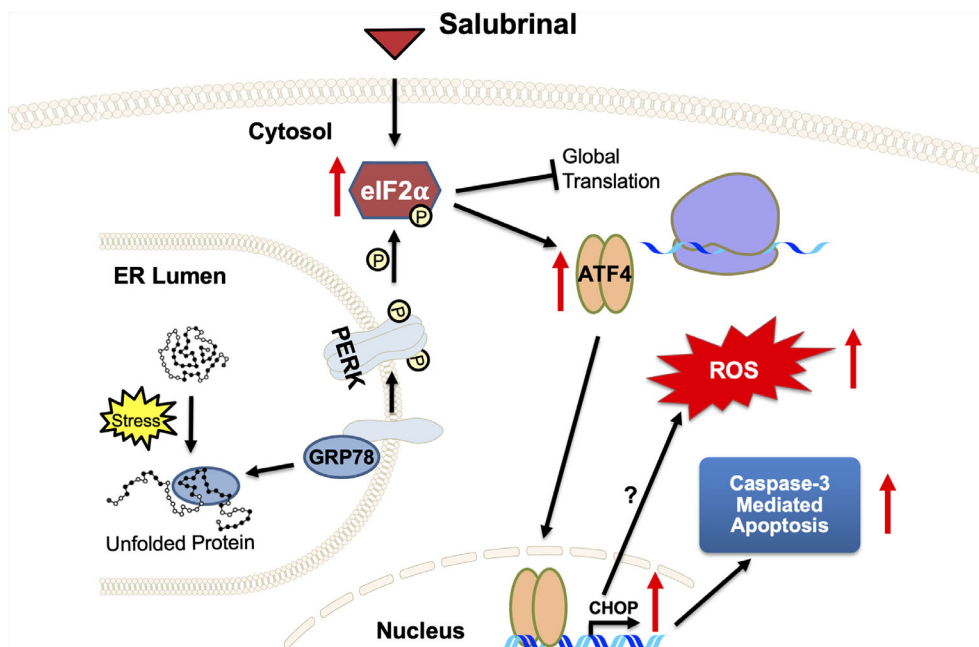


FIGURE 8 | A proposed mechanism of action of ER stress-prolonging agent Salubrinal on IBC cells. Cellular stress causes unfolded proteins to accumulate in the ER lumen. Chaperone dissociation leads to the activation of the PERK arm of the UPR. PERK is a transmembrane protein that serves as an ER stress sensor and activator of the UPR. PERK phosphorylates eIF2 α , thereby inhibiting global translation and selectively promoting ATF4 and CHOP translation, stress-inducible transcription factors. Salubrinal, an eIF2 α phosphatase inhibitor, activates the PERK arm of the UPR. Upregulation of CHOP, a proapoptotic transcription factor downstream of PERK and ATF4, demonstrates a potential antitumor strategy of Salubrinal in IBC cells. Salubrinal-treated IBC cells are driven to caspase-3 mediated cell death. Salubrinal treatment-induced cellular ROS and downregulated IBC cell proliferation, which could be rescued upon treatment with antioxidant along with Salubrinal. There may be CHOP-mediated induction of ROS or ROS is the outcome of upregulated oxidoreductases and protein oxidation in the IBC cells.

Salubrinal has been shown to cause TRAIL-induced PARP cleavage through eIF2 α phosphorylation in hepatoma cells (65). Our results support Salubrinal as a potential targeted therapy for the ER stress pathway in IBC cells (**Figure 8**), which may be beneficial as an adjuvant to standard chemotherapy for breast cancer or maintenance therapy after induction chemotherapy. As described in the introduction, the ultimate effect of Salubrinal on cell survival is multifactorial and depends on the state of the targeted cells. Salubrinal has been shown to have both cytoprotective and cytotoxic impacts when applied to different cells (31, 36, 66, 67). Salubrinal treatment significantly inhibited OPG secretion from IBC cell lines, opening up new avenues for follow-up. It would be interesting to decipher if Salubrinal treatment disrupts the association of OPG-BiP/GRP78 and secretion of RANKL levels in IBC cells. At this point, we do not know whether OPG drives the expression of anti-apoptotic GRP78/BiP. Many studies have supported Paclitaxel as an effective chemotherapeutic modality for IBC (68–70). Paclitaxel appears to be one of the most promising antineoplastic agents of the last decade, with demonstrated activity in advanced and refractory ovarian, breast, lung, and head and neck cancers. Given this proposed anti-proliferative mechanism and safety profile, Salubrinal may be ideal to be tested in combination treatment with Paclitaxel *in vitro* in IBC cell lines. Salubrinal mediated upregulation of eIF2 α phosphorylation could increase doxorubicin sensitivity in MCF-7-driven cells that have acquired resistance to doxorubicin (MCF-7/ADR) (36). Salubrinal and rapamycin combination demonstrated antitumor effects in a highly aggressive tumor called cholangiocarcinoma (37). An exquisite study extensively studied the adaptive redox mechanisms of SUM149 cells, and it was demonstrated these cells become resistant to chemo- and radio- therapeutics (71). This resistance is because they lose their ability to accumulate ROS, which results in apoptosis inhibition and enhances cancer cell survival (71). Given the fact that Salubrinal treatment induces ROS in SUM149PT (**Figure 8**) makes it a good drug of choice for combination therapy to regulate their redox status (71). Our study has some limitations as it is focused on few cell lines, utilizes a limited set of human tissue sections, and lacks *in vivo* testing. Still, it opens up new avenues for Salubrinal to be tested in IBC. It is a proof-of-concept study for Salubrinal's potential as a novel therapeutic intervention in IBC cells that demands further investigation.

DATA AVAILABILITY STATEMENT

The raw data supporting the conclusions of this article will be made available by the authors, without undue reservation.

REFERENCES

1. Makki J. Diversity of Breast Carcinoma: Histological Subtypes and Clinical Relevance. *Clin Med Insights Pathol* (2015) 8:23–31. doi: 10.4137/CPath.S31563
2. Yamauchi H, Woodward WA, Valero V, Alvarez RH, Lucci A, Buchholz TA, et al. Inflammatory Breast Cancer: What We Know and What We Need to Learn. *Oncol* (2012) 17(7):891–9. doi: 10.1634/theoncologist.2012-0039

ETHICS STATEMENT

The studies involving human participants were reviewed and approved by Advocate Lutheran General Hospital under the approved IRB (IRB00001341). The patients/participants provided their written informed consent to participate in this study.

AUTHOR CONTRIBUTIONS

NS-W: Conception and design, AA, KA, OP, MR, SG, and AD: acquisition of data, analysis, and interpretation. NS-W, AA and KA: interpretation of data and writing of the manuscript. HM provided human samples. All authors contributed to the article and approved the submitted version.

FUNDING

We are grateful for funding support from the Center for Cancer Cell Biology, Immunology and Infection, RFUMS-Advocate Lutheran General Hospital grant and RFUMS start-up fund to NS-W. The funders had no role in the design, decision to publish, or preparation of the manuscript.

ACKNOWLEDGMENTS

We gratefully acknowledge the team of HM, including YY, GS, MA, and SV, for their help with IRB (IRB00001341: Role of tumor microenvironment in inflammatory breast cancer) and for providing the breast tissue sections from healthy individuals and inflammatory breast cancer patients. We appreciate help from Ms. Megan Manion for gene expression analysis for a few ER stress genes as her learning during the summer research.

SUPPLEMENTARY MATERIAL

The Supplementary Material for this article can be found online at: <https://www.frontiersin.org/articles/10.3389/fonc.2021.654940/full#supplementary-material>

Supplementary Figure 1 | Salubrinal treatment induces caspase-3 mediated cell death in IBC cells. IBC cell lines SUM149PT and SUM190PT were treated with and without Salubrinal in the absence or presence of specific, irreversible caspase inhibitors (caspase -2, -3, -6, -8, -9, and -10). The fluorogenic substrate GF-AFC was added, and fluorescence was measured in relative fluorescence units (RFU) as an index of viability. Each reaction was done in triplicate, and each bar represents the mean \pm SD for three experiments. * $p < 0.05$, ** $p < 0.01$, *** $p < 0.005$, **** $p < 0.001$ indicate a statistically significant difference compared with respective untreated cells. ns, not significant.

3. Funakoshi Y, Wang Y, Semba T, Masuda H, Hout D, Ueno NT, et al. Comparison of Molecular Profile in Triple-Negative Inflammatory and Non-Inflammatory Breast Cancer not of Mesenchymal Stem-Like Subtype. *PLoS One* (2019) 14(9):e0222336. doi: 10.1371/journal.pone.0222336
4. Ueno NT, Espinosa Fernandez JR, Cristofanilli M, Overmoyer B, Rea D, Berdichevski F, et al. International Consensus on the Clinical Management of Inflammatory Breast Cancer from the Morgan Welch Inflammatory Breast

- Cancer Research Program 10th Anniversary Conference. *J Cancer* (2018) 9 (8):1437–47. doi: 10.7150/jca.23969
5. Wang X, Semba T, Phi LTH, Chaintitkun S, Iwase T, Lim B, et al. Targeting Signaling Pathways in Inflammatory Breast Cancer. *Cancers (Basel)* (2020) 12 (9):1–19. doi: 10.3390/cancers12092479
 6. Rueth NM, Lin HY, Bedrosian I, Shaitelman SF, Ueno NT, Shen Y, et al. Underuse of Trimodality Treatment Affects Survival For Patients With Inflammatory Breast Cancer: An Analysis of Treatment and Survival Trends From The National Cancer Database. *J Clin Oncol Off J Am Soc Clin Oncol* (2014) 32(19):2018–24. doi: 10.1200/JCO.2014.55.1978
 7. Anderson WF, Schairer C, Chen BE, Hance KW, Levine PH. Epidemiology of Inflammatory Breast Cancer (IBC). *Breast Dis* (2005) 22:9–23. doi: 10.3233/BD-2006-22103
 8. Hance KW, Anderson WF, Devesa SS, Young HA, Levine PH. Trends in Inflammatory Breast Carcinoma Incidence and Survival: The Surveillance, Epidemiology, and End Results Program at the National Cancer Institute. *J Natl Cancer Inst* (2005) 97(13):966–75. doi: 10.1093/jnci/dji172
 9. Schairer C, Brown LM, Mai PL. Inflammatory Breast Cancer: High Risk of Contralateral Breast Cancer Compared to Comparably Staged Non-Inflammatory Breast Cancer. *Breast Cancer Res Treat* (2011) 129(1):117–24. doi: 10.1007/s10549-010-1324-y
 10. Robertson JF, Ellis IO, Pearson D, Elston CW, Nicholson RI, Blamey RW. Biological Factors of Prognostic Significance in Locally Advanced Breast Cancer. *Breast Cancer Res Treat* (1994) 29(3):259–64. doi: 10.1007/BF00666479
 11. Chinnaiyan AM, Prasad U, Shankar S, Hamstra DA, Shanaiah M, Chenevert TL, et al. Combined Effect of Tumor Necrosis Factor-Related Apoptosis-Inducing Ligand and Ionizing Radiation in Breast Cancer Therapy. *Proc Natl Acad Sci USA* (2000) 97(4):1754–9. doi: 10.1073/pnas.030545097
 12. Goswami S, Sharma-Walia N. Crosstalk Between Osteoprotegerin (OPG), Fatty Acid Synthase (FASN) and Cyclooxygenase-2 (COX-2) in Breast Cancer: Implications in Carcinogenesis. *Oncotarget* (2016) 7(37):58953–74. doi: 10.18632/oncotarget.9835
 13. Goswami S, Sharma-Walia N. Osteoprotegerin Rich Tumor Microenvironment: Implications in Breast Cancer. *Oncotarget* (2016) 7(27):42777–91. doi: 10.18632/oncotarget.8658
 14. Goswami S, Sharma-Walia N. Osteoprotegerin Secreted by Inflammatory and Invasive Breast Cancer Cells Induces Aneuploidy, Cell Proliferation and Angiogenesis. *BMC Cancer* (2015) 15(1):935. doi: 10.1186/s12885-015-1837-1
 15. Holen I, Shipman CM. Role of Osteoprotegerin (OPG) in cancer. *Clin Sci* (2006) 110(3):279–91. doi: 10.1042/CS20050175
 16. Holen I, Cross SS, Neville-Webbe HL, Cross NA, Balasubramanian SP, Croucher PI, et al. Osteoprotegerin (OPG) Expression by Breast Cancer Cells In Vitro and Breast Tumours In Vivo—a Role in Tumour Cell Survival? *Breast Cancer Res Treat* (2005) 92(3):207–15. doi: 10.1007/s10549-005-2419-8
 17. Infante M, Fabi A, Cognetti F, Gorini S, Caprio M, Fabbri A. RANKL/RANK/OPG System Beyond Bone Remodeling: Involvement in Breast Cancer And Clinical Perspectives. *J Exp Clin Cancer Res CR* (2019) 38(1):12. doi: 10.1186/s13046-018-1001-2
 18. Clezardin P. The role of RANK/RANKL/Osteoprotegerin (OPG) triad in Cancer-Induced Bone Diseases: Physiopathology and Clinical Implications. *Bull Du Cancer* (2011) 98(7):837–46. doi: 10.1684/bdc.2011.1398
 19. Cheng K, Agarwal R, Mitra S, Mills G. Rab25 Small GTPase Mediates Secretion of Tumor Necrosis Factor Receptor Superfamily Member 11b (Osteoprotegerin) Protecting Cancer Cells from Effects of TRAIL. *J Genet Syndromes Gene Ther* (2013) 4:1–22. doi: 10.4172/2157-7412.1000153
 20. Lane D, Matte I, Rancourt C, Piche A. Osteoprotegerin (OPG) protects Ovarian Cancer Cells From TRAIL-Induced Apoptosis But Does Not Contribute to Malignant Ascites-Mediated Attenuation of TRAIL-Induced Apoptosis. *J Ovarian Res* (2012) 5(1):34. doi: 10.1186/1757-2215-5-34
 21. Jin HR, Zhao J, Zhang Z, Liao Y, Wang CZ, Huang WH, et al. The Antitumor Natural Compound Falcariindiol Promotes Cancer Cell Death by Inducing Endoplasmic Reticulum Stress. *Cell Death Dis* (2012) 3:e376. doi: 10.1038/cddis.2012.122
 22. Bruning A, Burger P, Vogel M, Rahmeh M, Friese K, Lenhard M, et al. Bortezomib Treatment of Ovarian Cancer Cells Mediates Endoplasmic Reticulum Stress, Cell Cycle Arrest, and Apoptosis. *Investigational New Drugs* (2009) 27(6):543–51. doi: 10.1007/s10637-008-9206-4
 23. Wielenga MCB, Colak S, Heijmans J, van Lidde de Jeude JF, Rodermond HM, Paton JC, et al. ER-Stress-Induced Differentiation Sensitizes Colon Cancer Stem Cells to Chemotherapy. *Cell Rep* (2015) 13(3):489–94. doi: 10.1016/j.celrep.2015.09.016
 24. Hetz C, Chevet E, Harding HP. Targeting the Unfolded Protein Response in Disease. *Nat Rev Drug Discov* (2013) 12(9):703–19. doi: 10.1038/nrd3976
 25. Kutomi G, Tamura Y, Tanaka T, Kajiwara T, Kukita K, Ohmura T, et al. Human Endoplasmic Reticulum Oxidoreductin 1-Alpha is a Novel Predictor For Poor Prognosis of Breast Cancer. *Cancer Sci* (2013) 104(8):1091–6. doi: 10.1111/cas.12177
 26. Davies MP, Barraclough DL, Stewart C, Joyce KA, Eccles RM, Barraclough R, et al. Expression and Splicing of the Unfolded Protein Response Gene XBP-1 are Significantly Associated With Clinical Outcome of Endocrine-Treated Breast Cancer. *Int J Cancer* (2008) 123(1):85–8. doi: 10.1002/ijc.23479
 27. Bobrovnikova-Marjon E, Grigoriadou C, Pytel D, Zhang F, Ye J, Koumenis C, et al. PERK Promotes Cancer Cell Proliferation and Tumor Growth by Limiting Oxidative DNA Damage. *Oncogene* (2010) 29(27):3881–95. doi: 10.1038/onc.2010.153
 28. Walter P, Ron D. The Unfolded Protein Response: From Stress Pathway to Homeostatic Regulation. *Science* (2011) 334(6059):1081–6. doi: 10.1126/science.1209038
 29. Hu H, Tian M, Ding C, Yu S. The C/EBP Homologous Protein (CHOP) Transcription Factor Functions in Endoplasmic Reticulum Stress-Induced Apoptosis and Microbial Infection. *Front Immunol* (2018) 9:3083. doi: 10.3389/fimmu.2018.03083
 30. Fusakio ME, Willy JA, Wang Y, Mirek ET, Al Baghdadi RJ, Adams CM, et al. Transcription Factor ATF4 Directs Basal and Stress-Induced Gene Expression in the Unfolded Protein Response and Cholesterol Metabolism in the Liver. *Mol Biol Cell* (2016) 27(9):1536–51. doi: 10.1091/mbc.E16-01-0039
 31. Drexler HC. Synergistic Apoptosis Induction in Leukemic Cells by the Phosphatase Inhibitor Salubrinal and Proteasome Inhibitors. *PLoS One* (2009) 4(1):e4161. doi: 10.1371/journal.pone.0004161
 32. Iwata Y, Koizumi N. Plant Transducers of the Endoplasmic Reticulum Unfolded Protein Response. *Trends Plant Sci* (2012) 17(12):720–7. doi: 10.1016/j.tplants.2012.06.014
 33. Liu JF, Chang CS, Fong YC, Kuo SC, Tang CH. FPipTB, a Benzimidazole Derivative, Induces Chondrosarcoma Cell Apoptosis via Endoplasmic Reticulum Stress and apoptosis Signal-Regulating Kinase 1. *Mol Carcinogen* (2012) 51(4):315–26. doi: 10.1002/mc.20787
 34. Takigawa S, Frondorf B, Liu S, Liu Y, Li B, Sudo A, et al. Salubrinal Improves Mechanical Properties of the Femur in Osteogenesis Imperfecta Mice. *J Pharmacol Sci* (2016) 132(2):154–61. doi: 10.1016/j.jphs.2016.09.006
 35. Yokota H, Hamamura K, Chen A, Dodge TR, Tanjung N, Abedinpoor A, et al. Effects of Salubrinal on Development of Osteoclasts and Osteoblasts From Bone Marrow-Derived Cells. *BMC Musculoskeletal Disord* (2013) 14:197. doi: 10.1186/1471-2474-14-197
 36. Jeon YJ, Kim JH, Shin JJ, Jeong M, Cho J, Lee K. Salubrinal-Mediated Upregulation of eIF2alpha Phosphorylation Increases Doxorubicin Sensitivity in MCF-7/ADR Cells. *Mol Cells* (2016) 39(2):129–35. doi: 10.14348/molcells.2016.2243
 37. Zhao X, Zhang C, Zhou H, Xiao B, Cheng Y, Wang J, et al. Synergistic Antitumor Activity of the Combination of Salubrinal and Rapamycin Against Human Cholangiocarcinoma Cells. *Oncotarget* (2016) 7(51):85492–501. doi: 10.18632/oncotarget.13408
 38. Sharma-Walia N, Paul AG, Bottero V, Sadagopan S, Veetil MV, Kerur N, et al. Kaposi's Sarcoma Associated Herpes Virus (KSHV) Induced COX-2: A Key Factor in Latency, Inflammation, Angiogenesis, Cell Survival and Invasion. *PLoS Pathog* (2010) 6(2):e1000777. doi: 10.1371/journal.ppat.1000777
 39. Sharma-Walia N, George Paul A, Patel K, Chandran K, Ahmad W, Chandran B. NFAT and CREB regulate Kaposi's Sarcoma-Associated Herpesvirus-Induced Cyclooxygenase 2 (COX-2). *J Virol* (2010) 84(24):12733–53. doi: 10.1128/JVI.01065-10
 40. Sharma-Walia N, Patel K, Chandran K, Marginean A, Bottero V, Kerur N, et al. COX-2/PGE2: Molecular Ambassadors of Kaposi's Sarcoma-Associated Herpes Virus Oncoprotein-v-FLIP. *Oncogenesis* (2012) 1:e5. doi: 10.1038/oncsis.2012.5

41. Wang M, Wey S, Zhang Y, Ye R, Lee AS. Role of The Unfolded Protein Response Regulator GRP78/BiP in Development, Cancer, and Neurological Disorders. *Antioxid Redox Signaling* (2009) 11(9):2307–16. doi: 10.1089/ars.2009.2485
42. Xiao C, Giacca A, Lewis GF. Sodium Phenylbutyrate, a Drug With Known Capacity to Reduce Endoplasmic Reticulum Stress, Partially Alleviates Lipid-Induced Insulin Resistance and Beta-Cell Dysfunction in Humans. *Diabetes* (2011) 60(3):918–24. doi: 10.2337/db10-1433
43. Logsdon AF, Lucke-Wold BP, Nguyen L, Matsumoto RR, Turner RC, Rosen CL, et al. Salubrinal Reduces Oxidative Stress, Neuroinflammation and Impulsive-Like Behavior in a Rodent Model of Traumatic Brain Injury. *Brain Res* (2016) 1643:140–51. doi: 10.1016/j.brainres.2016.04.063
44. Khateb A, Ronai ZA. Unfolded Protein Response in Leukemia: From Basic Understanding to Therapeutic Opportunities. *Trends Cancer* (2020) 6(11):960–73. doi: 10.1016/j.trecan.2020.05.012
45. Doron B, Abdelhamed S, Butler JT, Hashmi SK, Horton TM, Kurre P. Transmissible ER Stress Reconfigures the AML Bone Marrow Compartment. *Leukemia* (2019) 33(4):918–30. doi: 10.1038/s41375-018-0254-2
46. Lin Y, Jiang M, Chen W, Zhao T, Wei Y. Cancer and ER Stress: Mutual Crosstalk Between Autophagy, Oxidative Stress and Inflammatory Response. *BioMed Pharmacother* (2019) 118:109249. doi: 10.1016/j.biopha.2019.109249
47. Pootrakul L, Datar RH, Shi SR, Cai J, Hawes D, Groshen SG, et al. Expression of Stress Response Protein Grp78 is Associated With The Development of Castration-Resistant Prostate Cancer. *Clin Cancer Res An Off J Am Assoc Cancer Res* (2006) 12(20 Pt 1):5987–93. doi: 10.1158/1078-0432.CCR-06-0133
48. Daneshmand S, Quek ML, Lin E, Lee C, Cote RJ, Hawes D, et al. Glucose-Regulated Protein GRP78 is Up-Regulated in Prostate Cancer and Correlates With Recurrence and Survival. *Hum Pathol* (2007) 38(10):1547–52. doi: 10.1016/j.humpath.2007.03.014
49. Wu CT, Sheu ML, Tsai KS, Chiang CK, Liu SH. Salubrinal, an eIF2alpha Dephosphorylation Inhibitor, Enhances Cisplatin-Induced Oxidative Stress and Nephrotoxicity in a Mouse Model. *Free Radical Biol Med* (2011) 51(3):671–80. doi: 10.1016/j.freeradbiomed.2011.04.038
50. Iannitti T, Palmieri B. Clinical and Experimental Applications of Sodium Phenylbutyrate. *Drugs R D* (2011) 11(3):227–49. doi: 10.2165/11591280-000000000-00000
51. Yadavalli T, Suryawanshi R, Koganti R, Hopkins J, Ames J, Koujah L, et al. Standalone or Combinatorial Phenylbutyrate Therapy Shows Excellent Antiviral Activity and Mimics CREB3 Silencing. *Sci Adv* (2020) 6(49):1–11. doi: 10.1126/sciadv.abd9443
52. Xu Y, Zheng S, Chen B, Wen Y, Zhu S. Sodium Phenylbutyrate Antagonizes Prostate Cancer Through The Induction of Apoptosis and Attenuation of Cell Viability and Migration. *Onco Targets Ther* (2016) 9:2825–33. doi: 10.2147/OTT.S101794
53. Pili R, Kruszewski MP, Hager BW, Lantz J, Carducci MA. Combination of Phenylbutyrate and 13-Cis Retinoic Acid Inhibits Prostate Tumor Growth and Angiogenesis. *Cancer Res* (2001) 61(4):1477–85.
54. Guan G, Lei L, Lv Q, Gong Y, Yang L. Curcumin Attenuates Palmitic Acid-Induced Cell Apoptosis by Inhibiting Endoplasmic Reticulum Stress in H9C2 Cardiomyocytes. *Hum Exp Toxicol* (2019) 38(6):655–64. doi: 10.1177/0960327119836222
55. Yadav RK, Chae SW, Kim HR, Chae HJ. Endoplasmic Reticulum Stress and Cancer. *J Cancer Prev* (2014) 19(2):75–88. doi: 10.15430/JCP.2014.19.2.75
56. Son SM, Byun J, Roh SE, Kim SJ, Mook-Jung I. Reduced IRE1alpha Mediates Apoptotic Cell Death by Disrupting Calcium Homeostasis via the InsP3 Receptor. *Cell Death Dis* (2014) 5:e1188. doi: 10.1038/cddis.2014.129
57. Yang L, Guan G, Lei L, Liu J, Cao L, Wang X. Oxidative and Endoplasmic Reticulum Stresses are Involved in Palmitic Acid-Induced H9c2 Cell Apoptosis. *Biosci Rep* (2019) 39(5):1–9. doi: 10.1042/BSR20190225
58. Seervi M, Sobhan PK, Joseph J, Ann Mathew K, Santhoshkumar TR. ERO1alpha-Dependent Endoplasmic Reticulum-Mitochondrial Calcium Flux Contributes to ER Stress and Mitochondrial Permeabilization by Procaspase-Activating Compound-1 (PAC-1). *Cell Death Dis* (2013) 4:e968. doi: 10.1038/cddis.2013.502
59. Lei L, Ge J, Zhao H, Wang X, Yang L. Role of Endoplasmic Reticulum Stress in Lipopolysaccharide-Inhibited Mouse Granulosa Cell Estradiol Production. *J Reprod Dev* (2019) 65(5):459–65. doi: 10.1262/jrd.2019-052
60. Tu BP, Weissman JS. Oxidative Protein Folding in Eukaryotes: Mechanisms and Consequences. *J Cell Biol* (2004) 164(3):341–6. doi: 10.1083/jcb.200311055
61. Santos CX, Tanaka LY, Wosniak J, Laurindo FR. Mechanisms and Implications of Reactive Oxygen Species Generation During The Unfolded Protein Response: Roles of Endoplasmic Reticulum Oxidoreductases, Mitochondrial Electron Transport, and NADPH oxidase. *Antioxid Redox Signal* (2009) 11(10):2409–27. doi: 10.1089/ars.2009.2625
62. Back SH, Scheuner D, Han J, Song B, Ribick M, Wang J, et al. Translation Attenuation Through eIF2alpha Phosphorylation Prevents Oxidative Stress and Maintains The Differentiated State in Beta Cells. *Cell Metab* (2009) 10(1):13–26. doi: 10.1016/j.cmet.2009.06.002
63. Han J, Back SH, Hur J, Lin YH, Gildersleeve R, Shan J, et al. ER-Stress-Induced Transcriptional Regulation Increases Protein Synthesis Leading to Cell Death. *Nat Cell Biol* (2013) 15(5):481–90. doi: 10.1038/ncb2738
64. Marciniak SJ, Yun CY, Oyadomari S, Novoa I, Zhang Y, Jungreis R, et al. CHOP Induces Death by Promoting Protein Synthesis and Oxidation in the Stressed Endoplasmic Reticulum. *Genes Dev* (2004) 18(24):3066–77. doi: 10.1101/gad.1250704
65. Teng Y, Gao M, Wang J, Kong Q, Hua H, Luo T, et al. Inhibition of eIF2alpha Dephosphorylation Enhances TRAIL-Induced Apoptosis in Hepatoma Cells. *Cell Death Dis* (2014) 5:e1060. doi: 10.1038/cddis.2014.24
66. Boyce M, Bryant KF, Jousse C, Long K, Harding HP, Scheuner D, et al. A Selective Inhibitor of eIF2alpha Dephosphorylation Protects Cells From ER Stress. *Science* (2005) 307(5711):935–9. doi: 10.1126/science.1101902
67. Matsuoka M, Komoike Y. Experimental Evidence Shows Salubrinal, an eIF2alpha Dephosphorylation Inhibitor, Reduces Xenotoxicant-Induced Cellular Damage. *Int J Mol Sci* (2015) 16(7):16275–87. doi: 10.3390/ijms160716275
68. Lehmann BD, Bauer JA, Chen X, Sanders ME, Chakravarthy AB, Shyr Y, et al. Identification of Human Triple-Negative Breast Cancer Subtypes and Preclinical Models for Selection of Targeted Therapies. *J Clin Invest* (2011) 121(7):2750–67. doi: 10.1172/JCI45014
69. Gogas H, Pectasides D, Kostopoulos I, Lianos E, Skarlos D, Papaxoinis G, et al. Paclitaxel and Carboplatin As Neoadjuvant Chemotherapy in Patients With Locally Advanced Breast Cancer: A Phase II Trial of the Hellenic Cooperative Oncology Group. *Clin Breast Cancer* (2010) 10(3):230–7. doi: 10.3816/CBC.2010.n.031
70. Cristofanilli M, Gonzalez-Angulo AM, Buzdar AU, Kau SW, Frye DK, Hortobagyi GN. Paclitaxel Improves the Prognosis in Estrogen Receptor Negative Inflammatory Breast Cancer: The M. D. Anderson Cancer Center Experience. *Clin Breast Cancer* (2004) 4(6):415–9. doi: 10.3816/CBC.2004.n.004
71. Williams KP, Allensworth JL, Ingram SM, Smith GR, Aldrich AJ, Sexton JZ, et al. Quantitative High-Throughput Efficacy Profiling of Approved Oncology Drugs in Inflammatory Breast Cancer Models of Acquired Drug Resistance and Re-Sensitization. *Cancer Lett* (2013) 337(1):77–89. doi: 10.1016/j.canlet.2013.05.017

Conflict of Interest: The authors declare that the research was conducted in the absence of any commercial or financial relationships that could be construed as a potential conflict of interest.

Copyright © 2021 Alsterda, Asha, Powrozek, Repak, Goswami, Dunn, Memmel and Sharma-Walia. This is an open-access article distributed under the terms of the Creative Commons Attribution License (CC BY). The use, distribution or reproduction in other forums is permitted, provided the original author(s) and the copyright owner(s) are credited and that the original publication in this journal is cited, in accordance with accepted academic practice. No use, distribution or reproduction is permitted which does not comply with these terms.



Markers and Reporters to Reveal the Hierarchy in Heterogeneous Cancer Stem Cells

Amrutha Mohan^{1,2}, Reshma Raj Rajan¹, Gayathri Mohan¹,
Padmaja Kollenchery Puthenveetil¹ and Tessy Thomas Maliekal^{1*}

¹Cancer Research, Rajiv Gandhi Centre for Biotechnology, Thiruvananthapuram, India, ²Manipal Academy of Higher Education, Manipal, India

OPEN ACCESS

Edited by:

Zhe-Sheng Chen,
St. John's University, United States

Reviewed by:

Pei-Shan Hou,
National Yang Ming Chiao Tung
University, Taiwan
Duohui Jing,
Shanghai Jiao Tong University, China

*Correspondence:

Tessy Thomas Maliekal
tessy@rgcb.res.in
orcid.org/0000-0002-7311-7950

Specialty section:

This article was submitted to
Molecular and Cellular Oncology,
a section of the journal
Frontiers in Cell and Developmental
Biology

Received: 17 February 2021

Accepted: 30 April 2021

Published: 03 June 2021

Citation:

Mohan A, Raj Rajan R, Mohan G,
Kollenchery Puthenveetil P and
Maliekal TT (2021) Markers and
Reporters to Reveal the Hierarchy in
Heterogeneous Cancer Stem Cells.
Front. Cell Dev. Biol. 9:668851.
doi: 10.3389/fcell.2021.668851

A subpopulation within cancer, known as cancer stem cells (CSCs), regulates tumor initiation, chemoresistance, and metastasis. At a closer look, CSCs show functional heterogeneity and hierarchical organization. The present review is an attempt to assign marker profiles to define the functional heterogeneity and hierarchical organization of CSCs, based on a series of single-cell analyses. The evidences show that analogous to stem cell hierarchy, self-renewing Quiescent CSCs give rise to the Progenitor CSCs with limited proliferative capacity, and later to a Progenitor-like CSCs, which differentiates to Proliferating non-CSCs. Functionally, the CSCs can be tumor-initiating cells (TICs), drug-resistant CSCs, or metastasis initiating cells (MICs). Although there are certain marker profiles used to identify CSCs of different cancers, molecules like CD44, CD133, ALDH1A1, ABCG2, and pluripotency markers [Octamer binding transcriptional factor 4 (OCT4), SOX2, and NANOG] are used to mark CSCs of a wide range of cancers, ranging from hematological malignancies to solid tumors. Our analysis of the recent reports showed that a combination of these markers can demarcate the heterogeneous CSCs in solid tumors. Reporter constructs are widely used for easy identification and quantification of marker molecules. In this review, we discuss the suitability of reporters for the widely used CSC markers that can define the heterogeneous CSCs. Since the CSC-specific functions of CD44 and CD133 are regulated at the post-translational level, we do not recommend the reporters for these molecules for the detection of CSCs. A promoter-based reporter for ABCG2 may also be not relevant in CSCs, as the expression of the molecule in cancer is mainly regulated by promoter demethylation. In this context, a dual reporter consisting of one of the pluripotency markers and ALDH1A1 will be useful in marking the heterogeneous CSCs. This system can be easily adapted to high-throughput platforms to screen drugs for eliminating CSCs.

Keywords: cancer stem cells, pHCT4-EGFP, SORE6-GFP, NANOG-GFP, ALDH1A1-DsRed2, cancer stem cell heterogeneity

INTRODUCTION

Tumor heterogeneity had been considered as a hallmark of tumors from the very beginning, since the origin of the clonal evolution of cancer. With the tremendous technological advancement over these years, when cells at a single-cell level can be analyzed, it is evident that malignant cells exhibit heterogeneity at the genetic level as well as phenotypic level. Another important feature is the plasticity of these heterogeneous populations, which can be defined as the ability to dynamically switch between these phenotypes. Among these heterogeneous cancer cells, a highly plastic subpopulation with tumor initiation capacity, drug resistance, and metastatic ability, known as cancer stem cells (CSCs), have gained attention as they are responsible for the bad prognosis of the disease (Visvader and Lindeman, 2012). Recent advancement in the field shows that even the CSCs are heterogeneous in nature (Visvader and Lindeman, 2012; Zeng et al., 2014; Turdo et al., 2019; Vander Linden and Corbet, 2019; Velasco-Velazquez et al., 2019; Yang et al., 2020). There are several markers and their combinations used to identify CSCs in a variety of cancers (Table 1). As shown in Table 1, many of the molecules are specific to cancer types, though a few other molecules like CD133, CD44, ABCG2, Aldehyde dehydrogenase (ALDH), and pluripotency markers like octamer binding transcriptional factor 4 (OCT4), SOX2, and NANOG are expressed by a wide variety of cancers, including hematological malignancies and solid tumors. Hence the present review focuses on these molecules and discusses how these molecules and their combinations can be used to demarcate the functionally heterogeneous CSCs in light of the recent advancement in the field. Based on the existing literature, we have gathered a great deal of information for the heterogeneous CSCs in solid tumors. So in the present review, we will focus on solid tumors, with more emphasis on breast cancer.

The tumor microenvironment surrounding CSCs or a “CSC niche” plays a critical role in regulating the high plasticity exhibited by CSCs subpopulations (Thankamony et al., 2020). Several factors existing in the CSC niche, including hypoxia, acidic pH, cancer-associated fibroblasts (CAFs), and altered cytokine levels, contribute to the characteristics acquired by CSCs (Saygin et al., 2019). Thus even in a single tumor, there could be heterogeneity in the CSCs, depending on the niche they reside (Visvader and Lindeman, 2012). The existence of a dormant CSC population as well as proliferative CSCs is known in many cancers, and they show different levels of differentiation (Bliss et al., 2016; Shanmugam et al., 2019). Although CSCs might have properties like tumor initiation capacity, drug resistance, and/or metastatic ability, a single CSC at a given time point may not show all the three properties. But all the widely-used markers identify CSCs enriched for tumor initiation potential, drug resistance, and metastasis initiating efficiency (Table 1). In other words, these markers identify a group of CSCs exhibiting different characteristics and levels of differentiation. Though the functional characterization assign CSCs to different hierarchical groups akin to stem cell hierarchy, it was difficult to physically separate

them because of the inadequacy of markers (Boesch et al., 2016) until recent developments in the CSC field using single-cell analyses. A detailed analysis revealing the phenotype of each CSC-subpopulation can reveal a marker profile that can demarcate the subpopulations of CSCs.

HETEROGENEITY AND HIERARCHY IN CSCS

A hallmark of CSCs is their potential to generate phenotypically and functionally heterogeneous populations, as a result of metabolic reprogramming and a series of symmetric and asymmetric cell divisions. These subpopulations show the ability to interconvert, or they exhibit plasticity, which is the outcome of a reprogramming initiated by stemness signals present in the “CSC niche” (Thankamony et al., 2020). The CSCs which are dormant can acquire characteristics including drug resistance and metastatic initiation potential. Additionally, this dormant population can acquire proliferative capacity to facilitate differentiation. Recent advances in the single-cell-based technologies, such as single-cell DNA/RNA-Sequencing, mass cytometry (CyTOF), next-generation fluorescence flow cytometry, and “imaging mass cytometry” platform, help us to understand how functional heterogeneity is reflected by phenotypic heterogeneity (Akrap et al., 2016; Puram et al., 2017; Colacino et al., 2018; Sharma et al., 2018; Prieto-Vila et al., 2019; Taverna et al., 2020; Frank et al., 2021; Gonzalez Castro et al., 2021).

Hypothetically, distinct states of long-term CSCs and committed Progenitor cells exist in CSC pool. According to this, a Quiescent CSC is equivalent to an adult stem cell, which gets converted to a Progenitor CSC, probably by an asymmetrical cell division. This cell further undergoes proliferation to generate a subpopulation of Progenitor-like population, still possessing CSC characteristics. Further divisions of these cells generate proliferating cells, devoid of CSC characteristics (Proliferating non-CSCs; Figure 1). Later, these non-CSCs might lose the proliferative capacity, and can attain dormancy. The single-cell analyses have provided some evidences to show the hierarchy in CSCs (Akrap et al., 2016; Colacino et al., 2018; Sharma et al., 2018). Yet, a direct proof for this differentiation in a biological assay is still lacking. We need a clear understanding of the marker profiles for each of the different stages of differentiation to trace the hierarchy in the stem-like CSCs. If we can generate reporter constructs to mark each of the stages, we can trace the fate of CSCs. In the following sections, we describe the hierarchical organization of the heterogeneous CSCs and their marker profiles.

Functional Heterogeneity in CSCs

Hypoxia is one of the critical cues that initiate reprogramming in cancer cells to escape unfavorable conditions like nutrient deprivation or therapy by inducing dormancy/quiescence or epithelial-mesenchymal transition (EMT), which in turn help them to acquire invasive capacity, metastatic ability, and chemoresistance (Xiong et al., 2020). Thus a hypoxia-mediated reprogramming can generate heterogeneous CSCs. The functional

TABLE 1 | CSC markers identified in different cancers.

Markers	Tumor initiating capacity	Drug resistance	Metastasis initiating capacity
CD133	Pancreatic cancer (Banerjee et al., 2014; Nomura et al., 2015)	Colorectal cancer (Yuan et al., 2020) Breast cancer (Nadal et al., 2013) Ovarian carcinoma (Liu et al., 2020) T-cell acute lymphoblastic leukemia (Anbarlou et al., 2015)	Pancreatic cancer (Nomura et al., 2015) Colorectal cancers (Huang et al., 2012a; Fang et al., 2016; Kishikawa et al., 2016) Ovarian cancer (Long et al., 2015)
CD44	Cervical cancer (Feng et al., 2009) Prostate cancer (Ni et al., 2014)	Prostate cancer (Ni et al., 2014) Ovarian cancer (Zhang et al., 2019) Breast cancer (Liu et al., 2017) T-cell acute lymphoblastic leukemia (Hoofd et al., 2016)	Prostate cancer (Ni et al., 2014) Ovarian cancer (Zhang et al., 2019) Oral squamous cell carcinoma (Ortiz et al., 2018) Colorectal cancers (Huang et al., 2012b)
CD123	Acute myeloid leukemia (Abdollahpour-Alitappeh et al., 2018)	Acute myeloid leukemia (Yabushita et al., 2018; Yan et al., 2019)	—
CD26	—	—	Chronic myeloid leukemia (Herrmann et al., 2014)
CD117/c-KIT	Hepatocellular carcinoma (Xu et al., 2018)	Ovarian cancer (Fang et al., 2020)	Hepatocellular carcinoma (Xu et al., 2018)
CD93	—	Chronic myeloid leukemia (Kinstrie et al., 2020)	—
CD9	Acute myeloid leukemia (Liu et al., 2021)	Acute myeloid leukemia (Liu et al., 2021)	—
CD25	—	Acute myeloid leukemia (Allan et al., 2018; Yabushita et al., 2018)	—
ABCG2	Breast cancer (Sicchieri et al., 2015) Colon cancer (Xie et al., 2014)	Colon cancer (Xie et al., 2014) Bladder cancer cells (Roh et al., 2018) Esophageal squamous cancer cells (Huang et al., 2012a) Chronic myeloid leukemia (Jing et al., 2021) Triple negative breast cancer (Gomez-Miragaya and Gonzalez-Suarez, 2017) Ovarian carcinoma (Sedlak et al., 1996)	Esophageal squamous cancer cells (Huang et al., 2012a) Hepatocellular carcinoma (Hu et al., 2020) Breast invasive ductal carcinoma (Xiang et al., 2011) Breast cancer (Vassilopoulos et al., 2014) Human cervical cancer (Ammothumkandy et al., 2016)
CD49f (ITGA6)	Osteosarcoma (Penfornis et al., 2014) Triple negative breast cancer (Gomez-Miragaya and Gonzalez-Suarez, 2017) Colon cancer (Haraguchi et al., 2013)	—	Human cervical cancer (Bajaj et al., 2011; Ammothumkandy et al., 2016)
CD66	Human cervical Cancer (Bajaj et al., 2011; Ammothumkandy et al., 2016)	—	Human colorectal cancer (Chen et al., 2020)
EpCAM/ESA	Hepatocellular carcinoma (Chen et al., 2012)	Hepatocellular carcinoma (Chen et al., 2012)	Human colorectal cancer (Chen et al., 2020)
CD90	Nasopharyngeal carcinoma (Hoe et al., 2017) Lung cancer (Yan et al., 2013) Esophageal squamous cell carcinoma (Tang et al., 2013)	Esophageal squamous cell carcinoma (Tang et al., 2013)	Esophageal squamous cell carcinoma (Tang et al., 2013)
CD166	—	—	Human nasopharyngeal carcinoma (Sun et al., 2019)
LGR5	Breast cancer (Yang et al., 2015)	Colorectal cancer (Hsu et al., 2013)	Colorectal cancer (Valladares-Ayerbes et al., 2012)
OCT4	Hepatocellular carcinoma (Machida, 2018) Gastric cancer (Chen et al., 2019) Breast cancer (Huang et al., 2015)	Gastric cancer (Chen et al., 2019) Breast cancer (Huang et al., 2015) Cholangiocarcinoma (Choodetwattana et al., 2019) Chronic myeloid leukemia (Lettnin et al., 2019) Chronic myeloid leukemia (Xin et al., 2013) Gastric cancer (Chen et al., 2019) Breast cancer (Guan and Guan, 2020) Melanoma (Si et al., 2020) Chronic myeloid leukemia (Xin et al., 2013) Breast cancer (Huang et al., 2015)	Gastric cancer (Chen et al., 2019) Breast cancer (Litviakov et al., 2020) Colorectal cancer (Roudi et al., 2020)
SOX2	Hepatocellular carcinoma (Machida, 2018) Gastric cancer (Chen et al., 2019)	Gastric cancer (Chen et al., 2019) Breast cancer (Guan and Guan, 2020) Melanoma (Si et al., 2020) Chronic myeloid leukemia (Xin et al., 2013) Breast cancer (Huang et al., 2015)	Gastric cancer (Chen et al., 2019) Breast cancer (Guan and Guan, 2020; Xiao et al., 2020)
NANOG	Hepatocellular carcinoma (Machida, 2018) Breast cancer (Huang et al., 2015)	Esophageal squamous cancer (Deng et al., 2017) Chronic myeloid leukemia (Xin et al., 2013) Ovarian cancer (Januchowski et al., 2016) Multiple myeloma (Yang et al., 2014) Acute lymphoblastic leukemia (Ahlers et al., 2014)	Urinary bladder cancer (Gawlik-Rzemieniewska et al., 2016)
ALDH1A1	Human pancreatic adenocarcinoma (Kim et al., 2011) Prostate cancer (Nishida et al., 2012)	—	Breast cancer (Wang et al., 2018) Papillary thyroid carcinoma (Yue et al., 2015)

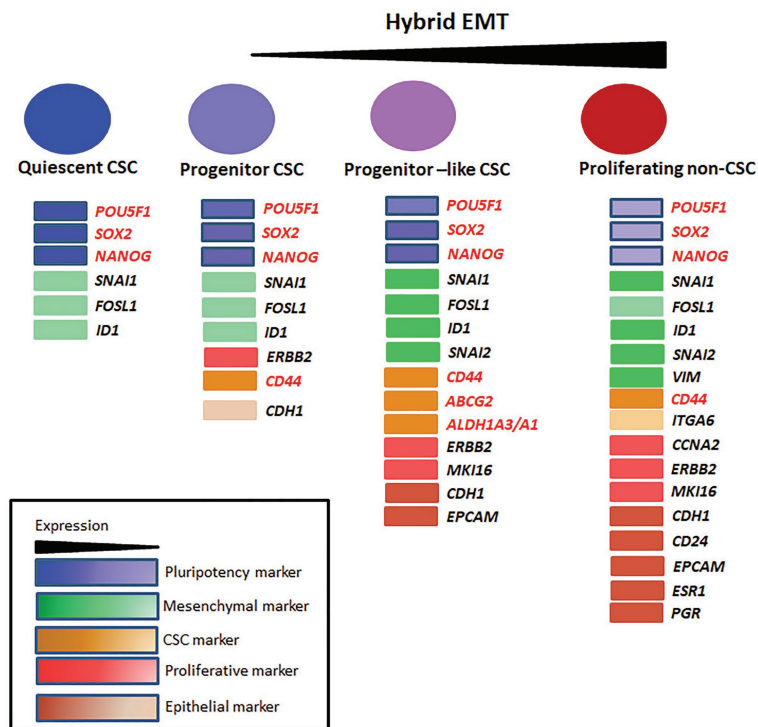


FIGURE 1 | The heterogeneity in cancer stem cells (CSCs). The different populations identified in breast CSCs and their markers are represented. The non-dividing Quiescent population, Progenitor population, Progenitor-like population, and the differentiated non-CSC population express a gradient of pluripotent, mesenchymal/epithelial and proliferative markers. The Quiescent population expresses a high level of pluripotent transcriptional factors and a moderate level of mesenchymal markers. With differentiation, the level of pluripotent markers comes down. The Progenitor population starts to express proliferative markers, CD44 and epithelial markers in very low levels. The Progenitor-like population co-expresses mesenchymal and epithelial markers manifesting a gradual increase in hybrid-epithelial-mesenchymal transition (EMT) phenotype. This population also expresses CSC markers ALDH1A1/A3 and ABCG2 contributing to drug-resistance. Non-CSCs lose the expression of pluripotent and other CSC markers except for CD44. The proliferative markers, epithelial markers, and mesenchymal markers are at maximum expression level in this population. This population can metastasize, but cannot initiate tumor until they dedifferentiate into CSCs.

heterogeneity of CSCs is exhibited as Quiescent CSCs, tumor-initiating cells (TICs), metastasis-initiating cells (MICs), and drug-resistant CSCs (Figure 2). The Quiescent CSCs are marked with low metabolic rate, slow cell division, and a shift of oxidative respiration to glycolysis, manifesting the Warburg effect (Yuen et al., 2016). These slow cycling cells can survive in extreme conditions and can overcome chemotherapy because a majority of the chemotherapeutic drugs are targeting dividing cells. Once they survive the adverse condition, they try to escape from that site by inducing EMT. During EMT, cells lose their polarity, cell-cell adhesion and undergo cell cycle arrest to gain mesenchymal properties like increased motility. EMT programs bring about changes in the cell shape, cytoskeleton, and secretome profiles, which is brought about by the tight regulation of a set of EMT genes and transcription factors (Celia-Terrassa and Jolly, 2020). This process might have three progressive stages, where cells can have EMT with more epithelial nature or a hybrid EMT with equal epithelial and mesenchymal nature or EMT with more mesenchymal characteristics (Celia-Terrassa and Jolly, 2020). Though EMT was shown to induce stemness in cancer cells (Mani et al., 2008), the stemness property is limited to the population showing hybrid EMT (Celia-Terrassa and Jolly, 2020).

Hence in the CSC context, the cells with the hybrid EMT will have increased invasiveness, motility, and CSC characteristics like tumor-initiating property. These cells are the MICs. The other two populations are not able to establish metastasis as the more epithelial EMT cells lack motility and the extreme mesenchymal cells are devoid of tumor-initiating properties (Celia-Terrassa and Jolly, 2020). The metastatic cells with extreme mesenchymal characteristics can remain dormant at distant sites and can undergo mesenchymal-epithelial transition to acquire hybrid phenotype and tumor initiation potential (Weidenfeld and Barkan, 2018). Apart from the metastatic ability, EMT can regulate chemoresistance also to generate drug-resistant CSCs. The EMT transcription factors like TWIST and SNAI1 are reported to regulate chemoresistance through the upregulation of drug metabolizing enzymes and drug efflux molecules (Rodriguez-Aznar et al., 2019). Additionally, the EMT factors like ZEB1, ZNF281, and SNAI2 modulate DNA damage and DNA repair to impart chemoresistance (Rodriguez-Aznar et al., 2019).

When the heterogeneity of populations in the context of drug resistance was analyzed at a single-cell resolution in breast cancer cells, expansion of a pre-existing subpopulation was identified (Prieto-Vila et al., 2019). The parental population

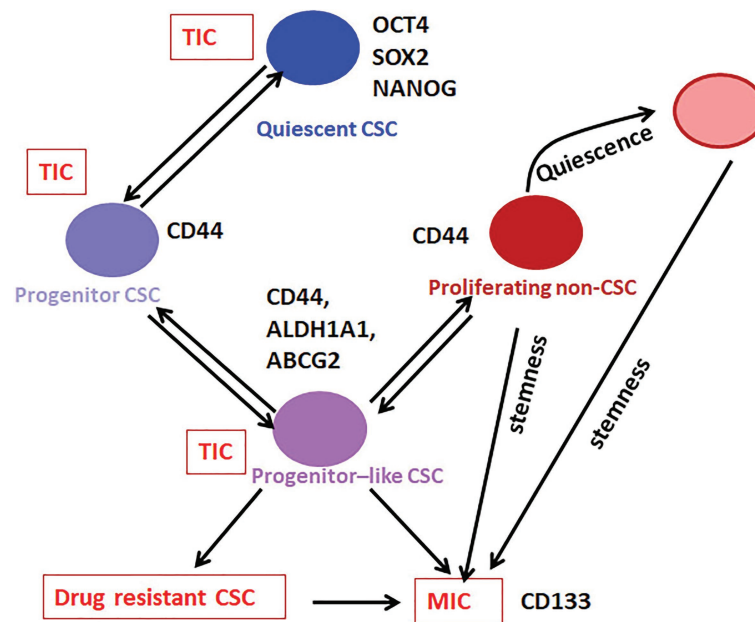


FIGURE 2 | The hierarchy in CSCs. Our analysis on the available literature on single-cell analyses conducted in breast cancer has revealed that the expression of pluripotency markers without CD44 marks the Quiescent CSC, while CD44 along with moderate expression of pluripotency markers define the Progenitor CSC population. These cells gradually lose the expression of pluripotency markers and gain the expression of ABCG2 and ALDH1A1 to get converted to Progenitor-like CSC population. According to the niche factors, these cells can be converted to the drug-resistant-CSCs or metastasis initiating cells (MICs). When this Progenitor-like CSC population loses all the CSC markers except CD44, they are converted to the Proliferating non-CSCs. The Quiescent cells, Progenitor cells, and Progenitor-like cells are considered as CSCs or tumor-initiating cells (TICs), which exhibit tumor initiation potential. The Progenitor like population having hybrid EMT phenotype might be the drug-resistant CSCs and MICs. The proliferating population with hybrid EMT might be highly metastatic, and they can remain dormant at distant sites. These cells are the seeds of recurrence at a different site. They might initiate tumor if they acquire stemness depending on the metastatic niche.

had a high expression of epithelial markers like *CDH1* and *PGR* as well as a moderate expression of mesenchymal markers *VIM* and *SNAIL1* denoting the hybrid EMT phenotype (Prieto-Vila et al., 2019). The stemness markers like *ABCG2*, *SOX2*, *ITGA6*, and *CAV1/2* were also high in this subpopulation. Notably, there was some amount of proliferative markers also present in this population, so that they could proliferate. When these cells were exposed to docetaxel, the resistant population emerged retained a majority of the markers except *ITGA6*, *SNAIL1*, and the proliferative markers that showed a diminishing pattern (Prieto-Vila et al., 2019). So, probably these cells represent the slow cycling CSCs that acquired *ABCG2* and hybrid EMT. When the mechanism of drug resistance induced by cisplatin was analyzed in oral cancer cell lines, it was noted that drug resistance could be achieved by pre-existing pools of resistant cells or by reprogramming as an adaptive mechanism. They showed that cisplatin resistance could be achieved by either the selection of *SOX2*⁺/*CDH1*⁺ population or by reprogramming to mesenchymal *SOX9*⁺/*VIM*⁺ population (Sharma et al., 2018).

Epithelial-mesenchymal transition, more specifically the hybrid EMT, is the prerequisite for metastasis. In this state, the cells express both epithelial and mesenchymal markers. Induction of hybrid EMT in CSCs might convert them to MICs. A single-cell RNA-Seq analysis conducted in head and neck squamous cell carcinoma cells showed that the classical

signature genes for hybrid EMT are *EPCAM*, *VIM*, *TGFBI*, and *SNAIL2* (Puram et al., 2017). Single-cell RNA-Seq analysis conducted with breast cancer CSCs showed a population with hybrid EMT and CSC markers *CD44*, *ABCG2*, and *ALDH1A1/3*, which might mark the MICs (Akrap et al., 2016). At the same time, there was another hybrid EMT population lacking *ABCG2* and *ALDH1A1/3*, but with *ITGA6*, probably representing metastatic cells without tumor-initiating efficiency (Figure 1; Akrap et al., 2016). In majority of the studies, they are treated as proliferating non-CSC cells, but they need to be considered separately, because they exhibit high hybrid EMT. Here, we have to recall that majority of the non-CSC population do not exhibit high hybrid EMT. We have reported a fraction of *ITGA6*⁺ cells exhibiting epithelial characteristics involved in metastasis (Ammothumkandy et al., 2016). The recent evidences suggest that the proliferative non-CSCs can acquire resistance and aid in metastasis after stemness induction depending on the CSC niche, probably explaining why the *ITGA6*⁺ cells showed metastatic ability. In a proteomic analysis, *CD133* was observed in hybrid EMT phenotype, which is shown to be important for metastatic cells (Taverna et al., 2020). Whether the *CD133* expression is exclusive to the Progenitor-like population is not yet evident. At least in colon cancer, *ITGA6* expressing cells fall into *CD44*⁺/*CD133*⁺ cell fraction, probably representing the metastatic non-CSCs (Haraguchi et al., 2013).

When we analyze the level of differentiation, these functionally different CSCs fall into distinct stages. The Quiescent population resembles the G₀-arrested stem cells, while the drug-resistant CSCs and MICs have limited proliferative capacity and self-renewal ability, similar to the Progenitor-like population. At the same time, the majority of the cancer cells, which do not have self-renewal ability but possess proliferative capacity, mimics the differentiated population. Recent evidences show that these subsets can be differentially identified using the marker profiles, and they show a hierarchical organization.

Hierarchical Organization in CSCs

Cancer stem cells are enriched by different methods, like spheroid culture (showing anoikis resistance), sorting using markers of CSCs, sorting based on label retention (indicating slow cycling population) or by inducing hypoxia. An elegant study in which breast cancer CSCs were enriched by these three methods and subjected to single-cell RNA-Seq has shed light on the phenotypic heterogeneity exhibited by CSCs (Akrap et al., 2016). They identified a Quiescent stem-like population, a Progenitor population, a more proliferative Progenitor-like population and a proliferating population (Figure 1). Among these, the subpopulations except the proliferating cells are generally considered as CSCs (Akrap et al., 2016).

When cells are exposed to hypoxia, very few cells are Quiescent, and Progenitor-like population predominates. But anoikis resistance enriches the Quiescent cells, Progenitor cells, and Progenitor-like cells in equal proportions. When slow cycling cells were picked up by label-retention, the majority of the population was the Progenitor population, followed by the Progenitor-like population and Quiescent population (Akrap et al., 2016). In this case, when cells were analyzed, the Quiescent population had low expression of all the genes including pluripotency genes compared to the Progenitor population (Akrap et al., 2016). So it suggests that the Quiescent population itself might have two populations, one with pluripotent markers denoting the stem-like CSCs and the other without pluripotent markers, which might be the non-CSCs.

Except for the pluripotency markers, all the other markers were low in the Quiescent stem-like population compared to other populations, although mesenchymal markers *SNAI1* and *FOSL1* were expressed in these cells (Akrap et al., 2016; Figure 1). These cells started expressing more epithelial markers like *CDH1* along with proliferative marker *ERBB2* to get converted to the Progenitor population expressing *CD44*. At this stage, the expressions of pluripotency markers were progressively lost (Akrap et al., 2016). Since the later differentiation process requires a series of cell divisions, they started expressing more proliferative markers like *MKI67* and acquire a hybrid EMT phenotype with the expression of *EPCAM*, *SNAI2*, and *ID1*. At this stage, they expressed stemness markers like *ALDH1A3* and *ABCG2*. This population is the proliferative Progenitor-like population. These cells proliferated further and expressed more proliferative markers and increased the expression of epithelial markers along with mesenchymal marker *VIM*. At this stage, these proliferating cells expressed a modest amount of

POU5F1, *NANOG*, and *ITGA6* but started losing *CD44*, *ABCG2*, and *ALDH1A3* (Akrap et al., 2016).

At present, CSCs can be considered as a heterogeneous population that has tumor initiation potential comprising of stem-like Quiescent cells, Progenitor cells, and Progenitor-like cells, which progressively lose self-renewal capacity and acquire proliferative capacity (Figure 2). From the Progenitor cell stage, cells start acquiring hybrid EMT and there is a population with the highest hybrid EMT, but lacks tumor initiation potential. All these populations are important with respect to cancer progression, metastasis, and chemoresistance. At the marker profile, the Quiescent stem-like population expresses the pluripotency markers, while the Progenitor population in breast cancer cells can be marked by *CD44* with diminished pluripotency markers and without other CSC markers like *ALDH1A1/3* or *ABCG2* (Figure 1). When the cells attain the Progenitor-like phenotype, they express all these markers. The proliferating cells do not express CSC markers except *CD44* and *ITGA6*. Thus, the stem-like Quiescent cells express only pluripotency markers at high levels. A moderate amount of pluripotency markers and *CD44* marks the Progenitor population, while high expression of *ALDH1A1/3*, *ABCG2*, *CD44*, and low amount of pluripotency marker denote Progenitor-like population. At the same time, *CD44* and *ITGA6* mark the proliferative non-CSC population.

Taken together, there are certain marker profiles that can demarcate the heterogeneous CSCs. It is evident that many of these molecules were used as CSC markers for different cancers, as shown in Table 1. The currently used markers for CSCs are the molecules regulating CSC characteristics, which are expressed specifically in this population. They include several cell surface molecules, pluripotency markers, and other molecules like *ALDH* (Table 1). In the following sections, we give a short account of some of the consistently used markers for CSCs, and discuss how they regulate different properties of CSCs. Special emphasis is given to the molecules used for making reporters of CSCs.

MARKERS OF CSCS

Cell Surface Molecules as CSC Markers

Cell surface markers are an important class comprising receptors or ligands, which mediate signaling cascades regulating tumorigenic properties, cell adhesion molecules, and transporter molecules like ATP binding cassette (ABC) transporters. Some of the most important receptors include *CD133* and *CD44*, while *ABCG2* is a vital drug transporter that marks CSCs.

CD133

CD133 (Prominin 1) is a penta-transmembrane surface glycoprotein coded by the gene *PROM1*. Following two papers reporting *CD133* as a marker for CSCs in colorectal cancer (O'Brien et al., 2007; Ricci-Vitiani et al., 2007), there was a surge of reports showing *CD133* as a marker for CSCs of different origin. Consistent with that, there are reports showing

CD133⁺ subset's association with chemo-resistance, metastasis, and poor prognosis (Irollo and Pirozzi, 2013). Hence, initially it appeared that this molecule will be a universal marker for CSCs. But as the field evolved it was evident that discrepancies exist even in the same cancer. There are accumulating evidences that question the CSC nature of CD133⁺ population in several cancers, including colon cancer, glioma, and lung cancer, as CD133⁻ population initiated long term tumors *in vivo* in these studies (Shmelkov et al., 2008; Irollo and Pirozzi, 2013).

There are several factors that determine the suitability of a molecule as a marker. The method of detection is critical in the case of CD133. It is generally detected using an antibody raised against AC133 epitope, which is exposed only after glycosylation of the region. So the antibody recognizes only the glycosylated form of the molecule. A comparative study of this antibody and another antibody that recognizes the non-glycosylated form showed that only the glycosylation is negatively regulated with differentiation (Florek et al., 2005). In colon cancer, the reduction in population expressing the AC133 epitope and loss of clonogenicity upon differentiation of CSCs did not correspond to a reduction of CD133 promoter activity or its expression at mRNA or protein level (Kemper et al., 2010). Thus it is evident that only the glycosylated CD133 is the

actual marker for stemness. Since reporter constructs cannot reflect the post-transcriptional and post-translational modifications, a reporter construct for this molecule may not be useful in identifying CSCs, which was actually observed. A knock-in lacZ reporter mouse (CD133lacZ/+) was generated in which the expression of lacZ is driven by the endogenous CD133 promoter. Using this reporter, they showed that CD133 is ubiquitously expressed in colonic epithelium. A modified form of this murine model showed that in murine colon adenocarcinoma, all the cells except stromal cells and infiltrating cells are CD133⁺ (Shmelkov et al., 2008).

Even though CD133 is not a suitable marker to make reporters for CSCs, the glycosylated functional CD133 imparts several CSC characteristics to CSCs (**Figure 3**). The significance of CD133 signaling was not unraveled for a long time. A report that showed CD133's interaction with cholesterol to act as an organizer for membrane topology was the first report that suggested its role in signaling (Florek et al., 2005). However, its relevance in stem cell biology was not unraveled until a physical interaction of CD133 to p85 subunit of PI3K was shown to activate its catalytic subunit p110 (Wei et al., 2013). Further, the CD133/PI3K/AKT pathway is shown to activate WNT signaling to drive glioblastoma tumor-initiating cells

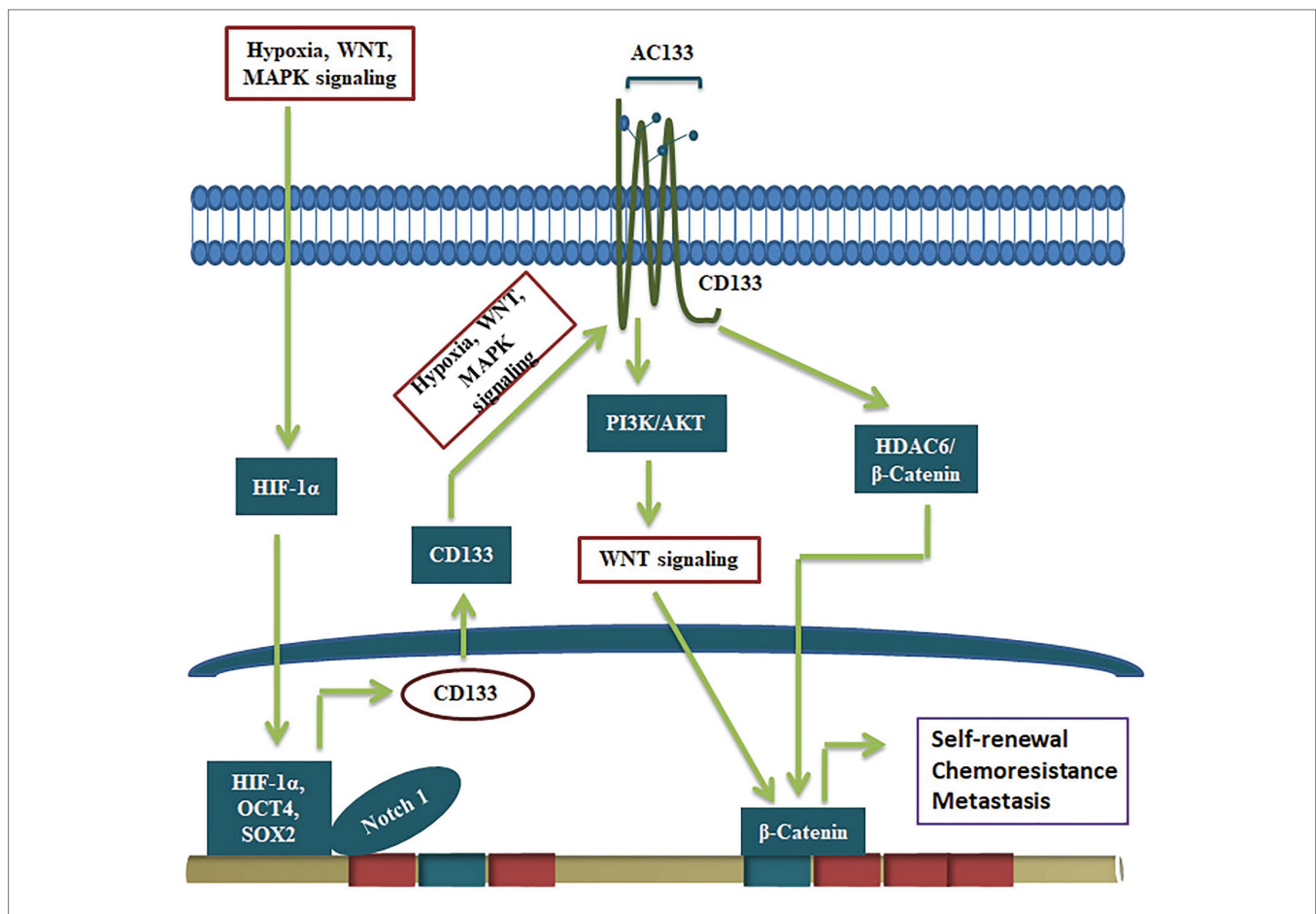


FIGURE 3 | CD133 in the regulation of CSCs. The expression of CD133 and its conversion to active form containing AC133 epitope by glycosylation is regulated by upstream signals like hypoxia and pathways like MAPK and WNT. The active CD133 primarily regulate WNT/β-catenin pathway to drive self-renewal.

(Manoranjan et al., 2020). CD133 can regulate WNT signaling by another mode, where it forms a ternary complex with HDAC6 and β -catenin, stabilizing β -catenin, resulting in the activation of WNT/ β -catenin signaling (Figure 3). Further, the CD133 expression, the resultant WNT activation and the increase in the CSC properties are shown to be regulated by several other self-renewal pathways. Hypoxia, a known stemness-inducing factor, is shown to increase CD133 expression at the RNA level and enhances the glycosylation and the AC133 epitope (Wu and Chu, 2019). The expression and surface localization of CD133 is activated by MAPK/ERK, HIF-1 α , Wnt/ β -catenin, and JAK/STAT3 (Gzil et al., 2019). Consistent with that, the depletion of CD133 leads to loss of CSC properties and conversely, its over-expression leads to a gain of stemness characteristics (Chen et al., 2011; Simbulan-Rosenthal et al., 2019).

Single-cell sequencing of CD133⁺ cells from colorectal cancer cells from a patient has revealed the heterogeneity among the population with respect to copy number and mutational profile (Min et al., 2020). When CD133⁺ cells were compared with CD133⁻ cells, bulk tumor cells, and tumor cells from metastatic sites, the heterogeneity among CD133⁺ cells was revealed. However, mutations of at least three genes among the seven genes (*RNF144A*, *PAK2*, *PARP4*, *ADAM21*, *HYDIN*, *KRT38*, and *CELSR1*) was consistently observed in CD133⁺ cells, while all the seven mutations were observed in metastatic tumor cells, suggesting that a subset of CD133⁺ cells are primarily responsible for establishing metastatic lesions (Min et al., 2020). There was another study conducted in parallel using single-cell proteomic profiling with lung cancer samples, where a CyTOF panel of 21 antibodies was designed to probe lung cancer cells. They observed a higher level of CD133 in comparison to other stemness markers (OCT3/4, NANOG, CD44, and ALDH1A1) in a subpopulation that exhibited a hybrid nature of epithelial/mesenchymal plasticity (Taverna et al., 2020). Recently it is postulated that epithelial-mesenchymal plasticity is the driving force of CSCs during metastasis (Celia-Terrassa and Jolly, 2020). So, the molecular evaluation to the resolution of single cells reveal that co-expression of CD133, OCT3/4, NANOG, CD44, and ALDH1A1 might mark cells with CSC characteristics, while increased expression of CD133 is observed in hybrid EMT phenotype, which is a pre-requisite for metastasis.

CD44

CD44 is a cell surface adhesion receptor that sense, integrate, and transduce extracellular matrix signals to cells, and regulate several genes resulting in changes in cell behavior. The expression of CD44 is reported in a wide variety of epithelia of both squamous and glandular origin along with their neoplastic counterparts. In this context, we need to examine the relevance of this molecule as a CSC marker. Apart from the standard CD44 isoform (CD44s ~85 kDa), at least nine variants formed by alternative splicing (CD44v) are identified in humans. Using specific antibodies, it was shown that CD44s and CD44-9v are ubiquitously expressed in all epithelial tissues but their expression in glandular tissue was restricted to the basal layer (Mackay et al., 1994). Their observations suggest that CD44v is

expressed by stem/progenitor cells of both squamous and glandular epithelia. When they differentiate, the expression of CD44v is retained in squamous epithelium till terminal differentiation, while its expression is lost during differentiation of glandular epithelium. Later, several other reports reinforced this notion in different epithelia (Ylagan et al., 2000). So when a primitive marker is re-expressed in cancer cells of glandular origin, it marks the CSCs as observed in many adenocarcinoma cells (Table 1). Consistent with that, intestinal stem cells isolated using Lrg5 marker from mouse and familial adenomatous polyposis samples express CD44v, but lack the standard CD44s isoform (Zeilstra et al., 2014). Also, in experiments using knock-in mice expressing either CD44v4-10 or CD44s, it was demonstrated that the CD44v isoform, but not CD44s, promotes adenoma initiation in Apc (Min/+) mice (Zeilstra et al., 2014). At the same time, in cancers of squamous cell origin, CSCs are a subpopulation within CD44s/CD44v expressing cells (Table 1). Further, the expression of CD44, both CD44s and CD44v, is associated with poor prognosis in a majority of cancers (Thapa and Wilson, 2016), since CD44 signaling leads to EMT, metastasis, and resistance to therapy.

CD44 is a non-kinase glycoprotein membrane receptor for hyaluronic acid (HA), osteopontin (OPN), chondroitin, collagen, fibronectin, and sulphated proteoglycans. Even though it is not clearly understood the specificity of variants to different ligands, it is well established that when CD44 binds to HA, it leads to a conformational change in the CD44 molecule allowing it to act as a co-receptor or adaptor for other signaling molecules (Bourguignon, 2019). There are many reports showing that the expressions of stemness markers like SOX2, NANOG, and OCT4 are high in CD44⁺ population (Gzil et al., 2019). Though the signaling cascades downstream of CD44 is not well-characterized, it is known that CD44 activates different signaling pathways like Rho GTPases, Ras-MAPK, and PI3K/AKT pathways to regulate different tumor properties (Al-Othman et al., 2020). In the CSC context, it is reported that the interaction of HA with CD44 leads to NANOG-STAT3 activation in ovarian cancer cells, making it a potential molecule for marking self-renewing population (Fang and Kitamura, 2018).

The relevance of the variants and the choice of the ligand might be critical in defining the downstream signaling of CD44. Among the variants, it is almost clear that CD44v is more critical for maintaining the CSC population than CD44s (Figure 4). Even though several ligands are reported for CD44, the well-characterized ones in context to cancer are HA and OPN. HA can bind to all forms of CD44, while OPN does not bind to CD44s but binds to the CD44v, specifically CD44v6 (Katagiri et al., 1999). Both HA and OPN are reported to regulate CSCs in different contexts. HA, directly and indirectly, affects CSC self-renewal by influencing the behavior of both cancer and stromal cells by regulating EMT (Chanmee et al., 2015). When HA mediates the signaling through CD44v, a set of miRNAs including, miR-21, miR-302, and miR-10b are upregulated that regulate different CSC properties (Bourguignon, 2019). So, HA can mediate signaling through all CD44 forms and regulate EMT, which is a determinant of stemness, invasion, and metastasis, explaining how overexpression of CD44 correlates

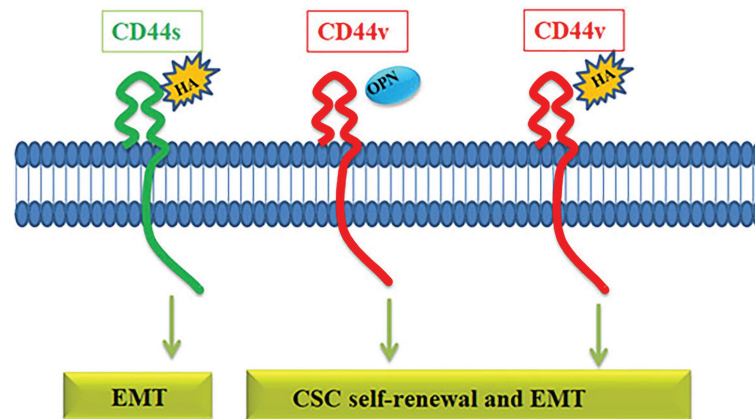


FIGURE 4 | The role of CD44 in the regulation of CSC properties. The CD44 gene gives rise to CD44s variant or CD44v variant. CD44s interacts with hyaluronic acid (HA) activating pathways that induce EMT. HA can also bind to CD44v receptor and activate EMT and self-renewal through various pathways. Another ligand osteopontin (OPN) binds specifically to CD44v, which induces EMT and self-renewal.

with poor prognosis. OPN, a possible ligand for CD44v variants, is reported to be enriched in glial tumors and the OPN-CD44 axis promotes CSCs in glioma (Lamour et al., 2015). Further analysis has shown that OPN-silenced glioma-initiating cells are unable to grow as spheres, and lose the expression of SOX2, OCT3/4, and NANOG. Further, AKT/mTOR/p70S6K pathway was identified as the main signaling pathway triggered by OPN in glioma-initiating cells (Lamour et al., 2015). Collectively, a preference of the ligand present in the microenvironment might be a critical regulator in determining the cell fate of CD44 expressing cells. If HA is expressed, all the CD44 expressing cells respond to it by acquiring EMT, and if the ligand switches to OPN, only the CD44v subsets respond to it by showing CSC properties. Consistently, hypoxia, a known regulator of stemness, regulates the expression of OPN without affecting the expression of CD44 variants in colorectal cancer cells (Wohlleben et al., 2018). All these facts point out that CD44 expression *per se* is not a marker of CSCs, but the expression of specific variants and the choice of ligands might define the CSCs. Thus reporter for this molecule may not be relevant in CSC detection.

Single-cell RNA profiling of CSCs from breast cancer cells, where CD44 is considered as a CSC marker, has revealed some significant information regarding CD44 expression in the context of hypoxia and the hierarchy of CSCs. When CSCs were enriched by either anoikis resistance, label retention or induction of hypoxia, there were subpopulations within CSCs, a Quiescent population, a Progenitor population and a more proliferative Progenitor-like population, which eventually differentiated to bulk tumor cells. This Quiescent population had less CD44, which was increased in the Progenitor-like, more proliferative CSCs (Akrap et al., 2016). In the differentiated bulk cells, the expression of CD44 was less compared to the Progenitor population, but high compared to the Quiescent population. Yet this conclusion is not final because the expression of variants had not been taken into account in this analysis.

ABCG2

ABCG2 is a member of the ABC transporters, which function as membrane transporters, ion channels, or receptors to pump a wide variety of endogenous and exogenous compounds out of cells (Polgar et al., 2008). It confers side population phenotype and is considered as a universal marker of stem cells. The high expression of ABCG2 is observed in various malignancies, and is usually associated with poor prognosis (Ding et al., 2010; Table 1). One of the possible roles suggested for ABCG2 is pumping the differentiation factors out of the cells, so that the cell retains the self-renewal capacity (Sabnis et al., 2017). The high expression of ABCG2 in CSCs is regulated by promoter demethylation, histone modification, and transcriptional upregulation by different self-renewal pathways (Ding et al., 2010; Stacy et al., 2013). Another factor important in clinical relevance is the single nucleotide polymorphism of ABCG2, which critically regulates the pharmacokinetics of different drugs (Heyes et al., 2018).

Even though ABCG2 is reported to be active in embryonic stem cells and other Quiescent stem cells, it is enriched more in the Progenitor-like population than in the Quiescent population, when analyzed by single-cell RNA-Seq in CSCs of breast cancer (Akrap et al., 2016). Anoikis-resistance and hypoxic conditions, which induce Quiescent cells, increase the expression of ABCG2, as reported before (Ni et al., 2010; Prabavathy et al., 2018), but the expression is restricted to the Progenitor-like subpopulation in these conditions (Akrap et al., 2016). Among the stem cell markers used, CD44 and ABCG2 were regulated in a similar pattern, and were enriched in the Progenitor-like population.

Pluripotency Transcription Factors That Mark CSCs

Octamer binding transcriptional factor 4 (OCT4, OCT3, and OCT3/4), encoded by *POU5F1* gene, is the master regulator of pluripotency in embryonic stem cells. The functional *POU5F1*

gene is located on chromosome 6 in humans, while six different pseudogenes of it are located at different chromosomes- *POU5F1P1*, *P2*, *P3*, *P4*, *P5*, and *P6* (Villodre et al., 2016). *POU5F1* gene is transcribed into three mRNA forms, *OCT4A*, *OCT4B*, and *OCT4B1*. The different isoforms of OCT4 and the pseudogene products at the mRNA level and protein level are represented in **Figures 5A,B**. The critical residues of OCT4A important for self-renewal property are marked in **Figure 5C**. As shown in the figure, detection of OCT4 by RT-PCR or

antibody will give results of different pseudogenes and isoforms together. Different isoforms of OCT4 (*OCT4A*, *B* and *B1*) are coming under the regulation of the same promoter, and are regulated by alternative splicing of exons. While *OCT4A* regulates self-renewal property, *OCT4B* and *OCT4B1* control stress response (Guo et al., 2012). These isoforms expressed in the stem cell population respond to stress conditions, and their expression is not limited to stem cells (Guo et al., 2012). High *OCT4* expression is a marker for poor prognosis; aggressiveness,

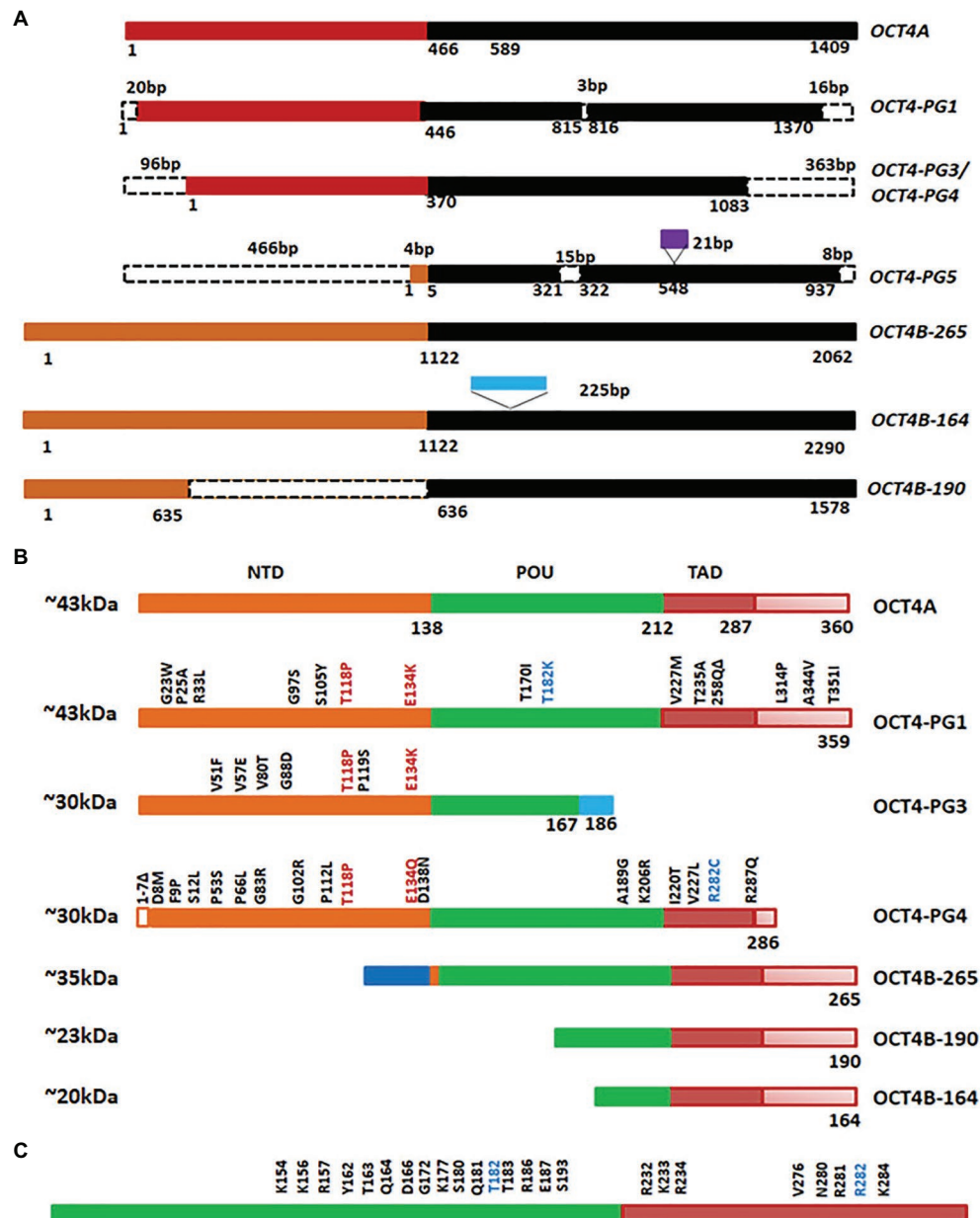


FIGURE 5 | Octamer binding transcriptional factor 4 (OCT4) variants in cancer. **(A)** The different isoforms and pseudogenes of OCT4 expressed in cancer at the RNA level. The conserved regions are shown in the same color. The dotted lines indicate absence of the region. The sequences inserted are shown in purple or blue boxes. **(B)** Protein expression of the variants. Conserved amino acid stretches are shown by the same color. The point mutations in the pseudogenes are shown in the figure. **(C)** The important residues of human OCT4A (POU and TAD domain) that are critical for self-renewal.

short over-all survival and chemo-resistance, in several malignancies, and thus it is considered as a CSC marker (Table 1; Mohiuddin et al., 2020). Although the expression of OCT4A is shown in some cancers, its relevance is doubtful, since the products of pseudogenes were not considered in the experimental design (De Resende et al., 2013; Asadi et al., 2016; Soheili et al., 2017). OCT4B and B1 forms are over-expressed in various malignancies and consistent with their anti-proliferative effect and anti-apoptotic function, its expression is correlated to aggressiveness of the tumor (Asadi et al., 2011, 2016; Gazouli et al., 2012; De Resende et al., 2013; Soheili et al., 2017). Pseudogenes, like OCT4-PG1, are also implicated in cancer as the over-expression of this gene promotes tumorigenicity *in vitro* and *in vivo*, consistent with the association of OCT4-PG1 over-expression and poor prognosis in gastric cancer (Hayashi et al., 2015). In spite of the confusion regarding the isoforms and pseudogenes of OCT4 expressed in CSCs, many studies show the importance of the molecule in CSC characteristics (Zhang et al., 2020). The signaling event leading to the regulation of OCT4 expression and its downstream targets, regulating CSC characteristics, are summarized in Figure 6.

SOX2 is a transcriptional factor involved in embryonic development and generation of iPSCs, which controls the expression of genes required for maintenance of pluripotency and self-renewal (Chan et al., 2011). NANOG is a homeo-box binding transcriptional factor essential for the maintenance of pluripotency and self-renewal of embryonic stem cells, being one of the downstream targets of OCT4 and SOX2. The downstream signaling of pluripotency genes regulating CSC characteristics are summarized in Figure 6. NANOG has two transcript variants coding for two isoforms performing the same function with comparable efficiency. Even though NANOG is silenced in normal somatic cells, an aberrant expression is reported in a wide variety of cancers, correlating to poor survival (Yang et al., 2020). During the early stages of embryogenesis, NANOG prevents the activation of the BMP pathway to block differentiation. Even though NANOG undergoes auto-repression with differentiation, its aberrant overexpression leads to increased proliferation by entering into S-phase (Yu and Cirillo, 2020).

Hypoxia, one of the factors that induce the expression of pluripotency markers, is shown to enrich a Quiescent population, characterized by the high expressions of *POU5F1*, *SOX2*, and

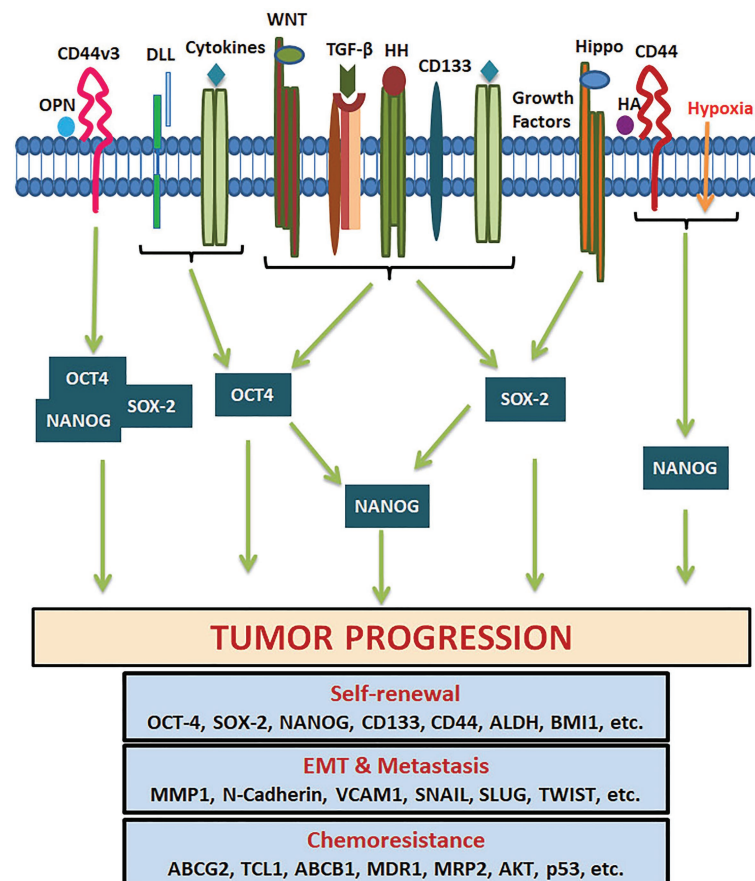


FIGURE 6 | Pluripotency genes in the regulation of tumor properties. Several tumor microenvironment factors and extracellular matrix components activate different signaling pathways that regulate the expression of OCT4, SOX-2, and NANOG. They either act alone or together for the transcriptional activation of genes responsible for CSC self-renewal, EMT, metastasis, cell survival, and chemoresistance.

NANOG; low expression of proliferative markers (*CCNA2* and *MKI67*) and EMT marker like *ID1*, when analyzed by single-cell RNA-Seq using breast cancer cells (Akrup et al., 2016). When there is a transition of this Quiescent population to a Progenitor-like population, the proliferative markers and *ID1* increase with a concomitant down-regulation of *POU5F1*, *SOX2*, and *NANOG* (Akrup et al., 2016).

OTHER MOLECULES AS CSC MARKERS

ALDH1A1

Aldehyde dehydrogenase comprises a family of enzymes including 19 subtypes that converts aldehydes to their corresponding carboxylic acids to prevent oxidative stress in cells. They are located at different chromosomal loci controlled by unique promoters, and they may localize to different cellular compartments like cytoplasm, mitochondria, nucleus, and endoplasmic reticulum. Among the different isoforms, the cytoplasmic variants are responsible for the retinoic acid (RA) biosynthesis, which is a critical molecule involved in retinoic acid receptor (RAR) signaling, regulating stemness. Though retinol can be oxidized by any of the cytosolic ALDH to retinaldehyde, its irreversible conversion to RA requires specific ALDH isozymes *ALDH1A1*, *ALDH1A2*, *ALDH1A3*, or *ALDH8A1* (Zhao et al., 1996; Elizondo et al., 2000; Marchitti et al., 2008). These isoforms that can convert retinaldehyde to RA are associated with stem cells of normal and cancer origin. *ALDH1A1* was first identified as a stemness marker in hematopoietic stem cells and neural stem cells (Storms et al., 1999; Corti et al., 2006). Later, when the hypothesis of CSCs emerged, it was recognized as a CSC marker in a wide variety of cancers (Vassalli, 2019). Different oncogenic signaling including TGF- β , Notch, and WNT pathways and feedback activation by RA signaling is shown to regulate the expression of *ALDH1A1* (Tomita et al., 2016). Apart from the RAR signaling, *ALDH1A1* promotes a self-renewing population through tumor growth, self-protection by anti-oxidant activity and the development of drug resistance by its catalytic potential (Tomita et al., 2016). All these factors point out that *ALDH1A1* is also a universal marker for the self-renewing population.

ALDH^{Hi} cells are considered as stem cells capable of forming mammospheres in normal and malignant breast tissue. The heterogeneity within normal mammary *ALDH^{Hi}* cells were evaluated by single-cell RNA-Seq from normal human breast samples (Colacino et al., 2018). The study revealed that *ALDH^{Hi}* cells that co-express *CD44* have a different gene signature from cells that do not express *CD44*. The dual positive cells have high expression of *SOX2*, and EMT markers *ID1*, *TWIST*, and *VIM* (Colacino et al., 2018). *ALDH^{Hi}* cells segregate to four clusters, where cluster 1 had gene expression in low amount in general with a modest amount of stemness markers *ALDH1A3*, *CD44*, and *SOX2*, epithelial marker *PGR*, and EMT markers *ID1* and *VIM*, probably denoting a Quiescent population. Cluster 2 showed CSC features with high expression of stemness markers *ALDH1A3*, *CD44*, *CD133*, *ITGA6*, and *SOX2*, epithelial

marker *CDH1* and *EPCAM*, and EMT markers *ID1* and *VIM*, denoting a hybrid EMT phenotype. Cluster 3 and Cluster 4 were representing epithelial and mesenchymal phenotype, respectively. In Cluster 3, the subtype of ALDH was *ALDH1A1* instead of *ALDH1A3*. In breast tissue, the expression of subtypes of ALDH is dependent on localization. *ALDH1A1* cells localize in small lobules, while *ALDH1A3* cells localize to extralobular ducts (Colacino et al., 2018). The significance of *ALDH^{Hi}* population expressing *ALDH1A1* at the single-cell level was investigated in the cancer context also. In lung cancer, there is a subpopulation of *ALDH1A1* cells, the population size of which increases progressively with the stage of the disease (Taverna et al., 2020). But this increase was not associated with acquisition of drug resistance (Taverna et al., 2020).

REPORTERS FOR CSCS

Conventionally, CSCs are identified and isolated by fluorescent activated cell sorting (FACS) or magnetic activated cell sorting (MACS) using antibodies for cell surface markers. But most of the cell surface markers alone are not reliable markers for CSCs. The intracellular molecules like pluripotency markers, which are more reliable CSCs markers, cannot be used for isolating live CSCs using their antibodies, because the permeabilization for detection will kill the cells. An alternative way of detection of CSCs in cultured cells is by making reporters for the CSCs markers. In the majority of the cases, the reporters are made to read the promoter activity of the particular gene. In some cases, where the CSC marker itself is a transcription factor, the reporter can be made using the promoter of the target gene. So, it is evident that a reporter construct for a CSC marker is not possible if the function of the molecule is regulated post-translationally or the function is limited to certain splice variants. Thus reporters for *CD133* and *CD44* are not useful for marking CSCs. So far, there are reports for preclinical studies using reporters for *OCT4*, *SOX2*, *NANOG*, *ALDH1A1*, and *ABCG2*, which will be discussed in detail.

Since the expression of *OCT4* is associated with stemness, chemoresistance, and metastatic property of cancer cells, several attempts were made to construct reporters for *OCT4* to track the CSCs. One of the widely used reporters is *phOCT4-EGFP*, where the expression of EGFP is under the control of the human *OCT4* promoter. In breast cancer, the cells that express high EGFP (*OCT4^{hi}*) mark highly immature cell population possessing self-renewal ability, quiescence, asymmetric division, long doubling time, and high metastatic and invasive capacity (Patel et al., 2012). It is also shown to mark dormant breast cancer cells residing in bone marrow, which are responsible for metastasis and tumor recurrence (Bliss et al., 2016). The relevance of this reporter in tracking MICs was shown in osteosarcoma and colorectal cancer also (Levings et al., 2009; Fujino and Miyoshi, 2019). It might also be useful to identify drug-resistant CSCs, as *OCT4^{hi}* cells were shown to be enriched in the sorafenib-resistant population in liver cancer (Wu et al., 2015). Taken together, the activation of *POU5F1* promoter, irrespective of the isoforms

expressed, is an indication of dormancy in CSCs, which might lead to drug resistance or metastasis.

Although SOX2 can be considered as a robust marker for CSCs, a promoter-based reporter for SOX2 is not advisable in several malignancies. The gene amplification of SOX2 is leading to the over-expression of the molecule. It is not resulted by the hyperactivity of a single promoter, but a cumulative activation of multiple promoters (Zhang et al., 2012). So, for analyzing SOX2 hyperactivation, another kind of reporter is widely used. SOX2 SRR2 pGreenFire Response Reporter is made by taking SOX2 regulatory region 2 (SRR2), a consensus DNA sequence seen on SOX2 target genes, to drive GFP. Using this reporter, CSCs were identified in different cancers (Wu et al., 2012, 2018; Iglesias et al., 2014), and it is shown to mark CSCs with cisplatin resistance in breast cancer (Soleymani Abyaneh et al., 2018). SORE6-GFP is another reporter made to evaluate the transcriptional activity of SOX2 in complex with OCT4. Six tandem repeats of composite OCT4/SOX2 response element, derived from NANOG promoter was cloned upstream to EGFP fluorescent protein to generate this reporter (Tang et al., 2015). This reporter identifies CSCs with metastatic potential and chemoresistance in breast cancer (Tang et al., 2015), gastric cancer (Padua et al., 2020), and prostate cancer (Vaddi et al., 2019).

Since NANOG is considered as a *bona fide* CSC marker, NANOG promoter-driven GFP is used to mark CSCs of different origins. NANOG-GFP was useful in characterizing CSCs of triple-negative breast cancer (Thiagarajan et al., 2015) and ovarian cancer (Wiechert et al., 2016). Similar NANOG reporters were constructed later by other groups (Buczek et al., 2018; Wei et al., 2018). A lentiviral NANOG-GFP reporter expressing luciferase was shown to mark drug-resistant CSCs in colorectal cancer, both *in vitro* and in mouse xenograft models (Wei et al., 2018).

As ALDH1A1 is a CSC marker for a wide variety of cancers, reporter constructs for CSCs based on ALDH1A1 promoter have been generated (Gener et al., 2015; Shanmugam et al., 2019). An ALDH1A1 promoter-driven tdTomato is reported for evaluating the drug sensitivity in breast cancer and colon cancer cell lines (Gener et al., 2015). Recently, we reported a similar construct, ALDH1A1-DsRed2, for marking CSCs of oral cancer (Shanmugam et al., 2019).

The expression of ABCG2, at the transcriptional level, is regulated by an epigenetic mechanism. It has been shown that the acquisition of multidrug-resistant phenotype by the upregulation of ABCG2 is achieved by the reversal of promoter methylation (Bram et al., 2009). Since transcriptional regulation, at least in part, is driven by epigenetic mechanisms, the stable expression of a reporter driven by the ABCG2 promoter will not be useful for identification of the drug-resistant CSCs. So, a reporter cell line is recently made using CRISPR-Cas9 gene editing coupled with the homology-directed repair. They targeted the EGFP coding sequence to the translational start site of ABCG2, generating ABCG2 knock-out and *in situ* tagged ABCG2 reporter cells (Kovacsics et al., 2020). This fluorescent reporter system allowed the detection of endogenous regulation of ABCG2 expression by different stress responses and offers a method to screen molecules that can inhibit drug-resistant CSCs.

THE CLINICAL RELEVANCE OF MARKERS AND REPORTERS

Considering the importance of CSCs in prognosis, there were many attempts to target CSCs at the preclinical and clinical level (Saygin et al., 2019). The different approaches to target CSCs were using drugs that (a) inhibit self-renewal pathways like Notch, hedgehog (HH), and WNT (b) target CSC niche, and (c) block drug transporters (Saygin et al., 2019). Another important strategy is immunotherapy (Saygin et al., 2019). Though some drugs were successful in both preclinical and clinical trials, there were many other drugs that proved successful in preclinical studies *in vitro*, but did not prove efficient in clinical studies (Saygin et al., 2019). Vismodegib is an antagonist for HH signaling that efficiently decreased CSCs of pancreatic cancer and lung cancer *in vitro* (Singh et al., 2011; Ahmad et al., 2013). When this molecule was tested in colorectal cancer patients, there was no significant benefit observed for the drug (Berlin et al., 2013).

One of the reasons for the unsuccessful translation of CSC targeting drugs is the inefficient detection of CSCs in preclinical screening. At present, CSCs are characterized by functional properties, like sphere formation efficiency and tumor initiation potential in serial dilutions and by using different phenotypic markers. Conventionally, we evaluate a drug for its efficacy in reducing CSCs based on the expression profile of markers, which do not identify all the CSCs. As we have discussed earlier (Figure 2), a combination of pluripotency marker and ALDH1A1/3 or ABCG2 will identify all the CSC sub-populations. Since an ideal CSC targeting drug should deplete all the heterogeneous CSCs, a screening strategy should include these marker profiles. Additionally, all these CSC subpopulations are maintained by different signaling pathways and hence they show differences in their responses to chemotherapeutic drugs. If we identify the critical molecules or pathways that are ideal for targeting each population, we might achieve good therapeutic outcome. Further, if we can use reporter constructs, it will be extremely useful not only for the isolation of these population, but also for designing drug screening strategies and real-time monitoring of these population *in vitro* and *in vivo*.

CONCLUSION AND PERSPECTIVES

All the CSC populations can initiate a tumor but the drug resistance and metastasis initiating capacity might be exhibited by cells in the Progenitor-like stage. The proliferating cells exhibiting high hybrid EMT might also be important in metastasis, even though they lack the tumor-initiation potential. These cells can migrate to new sites and reside as dormant cells, which might have been the dormant population observed in label-retaining cells with low expression of all the genes, including the pluripotency markers. These cells may later acquire tumor-initiation potential, since all these populations exhibit plasticity (Figure 2). Among the different populations described, this high hybrid EMT dormant population is the least

characterized, and warrants more studies to understand their biology to come up with a reliable marker for this population.

If we use a single pluripotency marker to screen drugs targeting CSCs, we identify the Quiescent and Progenitor population, but do not take the Progenitor-like population into account, which are really important with respect to drug response and metastasis. Even though they are proliferating cells, they show chemoresistance attributed to the expression of drug resistance proteins like ABCG2 and ALDH. On the other hand, if we use ALDH1A1 or ABCG2, we miss the Quiescent and Progenitor population, which remain dormant and cause recurrence. So, an ideal marker profile to use for drug screening will be a combination of pluripotency markers, CD44, CD133, ALDH1A1, and ABCG2, where we can pick up all the heterogeneous CSCs including Quiescent CSC, Progenitor CSC, Progenitor-like CSC, and MIC (Figure 2). Among these markers, CD44 and CD133 reporters are not relevant as their function is not regulated at the transcriptional level. Though ABCG2 reporters are available, they are not useful in CSCs because the expression is regulated by the promoter demethylation in cancer. Hence, we propose that a dual reporter including one of the pluripotency markers (phOCT4-EGFP/NANOG-GFP/SORE6-GFP/SOX2 SRR2-pGreen fire) and ALDH1A1-DsRed2 can efficiently mark all the heterogeneous CSCs, at least in breast cancer. Though this system does not distinguish between drug-resistant CSCs and MICs, a low pluripotency marker/high ALDH1A1 population will include both the subsets. Another shortcoming of the system is that it will not mark the proliferative non-CSCs possessing hybrid EMT. This system can be easily adapted for high-throughput screening of CSC-targeting drugs. A successful CSC-targeting drug should eradicate all the different pools of CSCs.

REFERENCES

- Abdollahpour-Alitappeh, M., Razavi-Vakhshourpour, S., and Abolhassani, M. (2018). Development of a new anti-CD123 monoclonal antibody to target the human CD123 antigen as an acute myeloid leukemia cancer stem cell biomarker. *Biotechnol. Appl. Biochem.* 65, 841–847. doi: 10.1002/bab.1681
- Ahlers, J., Witte, K. E., Schwarze, C. P., Lang, P., Handgretinger, R., and Ebinger, M. (2014). Therapy response correlates with ALDH activity in ALDH low-positive childhood acute lymphoblastic leukemias. *Pediatr. Hematol. Oncol.* 31, 303–310. doi: 10.3109/08880018.2013.859189
- Ahmad, A., Maitah, M. Y., Ginnebaugh, K. R., Li, Y., Bao, B., Gadgil, S. M., et al. (2013). Inhibition of hedgehog signaling sensitizes NSCLC cells to standard therapies through modulation of EMT-regulating miRNAs. *J. Hematol. Oncol.* 6:77. doi: 10.1186/1756-8722-6-77
- Akrup, N., Andersson, D., Bom, E., Gregersson, P., Stahlberg, A., and Landberg, G. (2016). Identification of distinct breast cancer stem cell populations based on single-cell analyses of functionally enriched stem and progenitor pools. *Stem Cell Rep.* 6, 121–136. doi: 10.1016/j.stemcr.2015.12.006
- Allan, J. N., Roboz, G. J., Askin, G., Ritchie, E., Scandura, J., Christos, P., et al. (2018). CD25 expression and outcomes in older patients with acute myelogenous leukemia treated with plerixafor and decitabine. *Leuk. Lymphoma* 59, 821–828. doi: 10.1080/10428194.2017.1352089
- Al-Othman, N., Alhendi, A., Ihabaisha, M., Barahmeh, M., Alqaraleh, M., and Al-Momany, B. Z. (2020). Role of CD44 in breast cancer. *Breast Dis.* 39, 1–13. doi: 10.3233/BD-190409
- Ammothumkandy, A., Maliekal, T. T., Bose, M. V., Rajkumar, T., Shirley, S., Thejaswini, B., et al. (2016). CD66 and CD49f expressing cells are associated with distinct neoplastic phenotypes and progression in human cervical cancer. *Eur. J. Cancer* 60, 166–178. doi: 10.1016/j.ejca.2016.03.072
- Anbarlou, A., Atashi, A., Soleimani, M., Akhavanrahnama, M., Bohloli, M., and Mossahebi-Mohammadi, M. (2015). Differential characteristics of CD133⁺ and CD133⁻ Jurkat cells. *In Vitro Cell. Dev. Biol. Animal* 51, 556–561. doi: 10.1007/s11626-015-9869-z
- Asadi, M. H., Khalifeh, K., and Mowla, S. J. (2016). OCT4 spliced variants are highly expressed in brain cancer tissues and inhibition of OCT4B1 causes G2/M arrest in brain cancer cells. *J. Neuro-Oncol.* 130, 455–463. doi: 10.1007/s11060-016-2255-1
- Asadi, M. H., Mowla, S. J., Fathi, F., Aleyasin, A., Asadzadeh, J., and Atlasi, Y. (2011). OCT4B1, a novel spliced variant of OCT4, is highly expressed in gastric cancer and acts as an antiapoptotic factor. *Int. J. Cancer* 128, 2645–2652. doi: 10.1002/ijc.25643
- Bajaj, J., Maliekal, T. T., Vivien, E., Pattabiraman, C., Srivastava, S., Krishnamurthy, H., et al. (2011). Notch signaling in CD66⁺ cells drives the progression of human cervical cancers. *Cancer Res.* 71, 4888–4897. doi: 10.1158/0008-5472.CAN-11-0543
- Banerjee, S., Nomura, A., Sangwan, V., Chugh, R., Dudeja, V., Vickers, S. M., et al. (2014). CD133⁺ tumor initiating cells in a syngenic murine model of pancreatic cancer respond to minnelide. *Clin. Cancer Res.* 20, 2388–2399. doi: 10.1158/1078-0432.CCR-13-2947
- Berlin, J., Bendell, J. C., Hart, L. L., Firdaus, I., Gore, I., Hermann, R. C., et al. (2013). A randomized phase II trial of vismodegib versus placebo with FOLFIRI or FOLFIRI and bevacizumab in patients with previously untreated metastatic colorectal cancer. *Clin. Cancer Res.* 19, 258–267. doi: 10.1158/1078-0432.CCR-12-1800

The proliferative population with high hybrid EMT probably will be eliminated by standard chemotherapeutic drugs targeting proliferating cells. Still, a population that gets converted to dormant stage poses a threat to the treatment outcome. Since we know that functional diversity exists in these heterogeneous populations, the response of these populations to drugs will be different. More studies are required to identify specific molecular targets that can be used for drug development to abolish all the relevant populations that lead to recurrence. All these observations and conclusions of the marker profiles to identify different subpopulations are based on studies on breast cancer. Whether these marker profiles will be applicable to other forms of cancer is yet to be explored.

AUTHOR CONTRIBUTIONS

AM performed the analysis, interpreted the data, and drafted the manuscript. RR, PK, and GM contributed critically for important intellectual content of the manuscript. TM conceptualized and designed the study and revised the manuscript critically. All authors contributed to the article and approved the submitted version.

FUNDING

AM received financial support from University Grant Commission, India (19/06/2016 (1) EU-V/318501) and RR received funding from Council of Scientific & Industrial Research, India (09/716(0188)/2019-EMR-I). This work was supported by Department of Science and Technology, India (EMR/2015/001170).

- Bliss, S. A., Sinha, G., Sandiford, O. A., Williams, L. M., Engelberth, D. J., Guiro, K., et al. (2016). Mesenchymal stem cell-derived exosomes stimulate cycling quiescence and early breast cancer dormancy in bone marrow. *Cancer Res.* 76, 5832–5844. doi: 10.1158/0008-5472.CAN-16-1092
- Boesch, M., Sopfer, S., Zeimet, A. G., Reimer, D., Gastl, G., Ludwig, B., et al. (2016). Heterogeneity of cancer stem cells: rationale for targeting the stem cell niche. *Biochim. Biophys. Acta* 1866, 276–289. doi: 10.1016/j.bbcan.2016.10.003
- Bourguignon, L. Y. W. (2019). Matrix hyaluronan-CD44 interaction activates microRNA and lncRNA signaling associated with chemoresistance, invasion, and tumor progression. *Front. Oncol.* 9:492. doi: 10.3389/fonc.2019.00492
- Bram, E. E., Stark, M., Raz, S., and Assaraf, Y. G. (2009). Chemotherapeutic drug-induced ABCG2 promoter demethylation as a novel mechanism of acquired multidrug resistance. *Neoplasia* 11, 1359–1370. doi: 10.1593/neo.91314
- Buczek, M. E., Reeder, S. P., and Regad, T. (2018). Identification and isolation of cancer stem cells using NANOG-EGFP reporter system. *Methods Mol. Biol.* 1692, 139–148. doi: 10.1007/978-1-4939-7401-6_13
- Celia-Terrassa, T., and Jolly, M. K. (2020). Cancer stem cells and epithelial-to-mesenchymal transition in cancer metastasis. *Cold Spring Harb. Perspect. Med.* 10:a036905. doi: 10.1101/cshperspect.a036905
- Chan, Y. S., Yang, L., and Ng, H. H. (2011). Transcriptional regulatory networks in embryonic stem cells. *Prog. Drug Res.* 67, 239–252. doi: 10.1007/978-3-7643-8989-5_12
- Chanmee, T., Ontong, P., Kimata, K., and Itano, N. (2015). Key roles of hyaluronan and its CD44 receptor in the stemness and survival of cancer stem cells. *Front. Oncol.* 5:180. doi: 10.3389/fonc.2015.00180
- Chen, H. N., Liang, K. H., Lai, J. K., Lan, C. H., Liao, M. Y., Hung, S. H., et al. (2020). EpCAM signaling promotes tumor progression and protein stability of PD-L1 through the EGFR pathway. *Cancer Res.* 80, 5035–5050. doi: 10.1158/0008-5472.CAN-20-1264
- Chen, Y. S., Wu, M. J., Huang, C. Y., Lin, S. C., Chuang, T. H., Yu, C. C., et al. (2011). CD133/Src axis mediates tumor initiating property and epithelial-mesenchymal transition of head and neck cancer. *PLoS One* 6:e28053. doi: 10.1371/journal.pone.0028053
- Chen, Y., Yu, D., Zhang, H., He, H., Zhang, C., Zhao, W., et al. (2012). CD133⁺ EpCAM⁺ phenotype possesses more characteristics of tumor initiating cells in hepatocellular carcinoma Huh7 cells. *Int. J. Biol. Sci.* 8, 992–1004. doi: 10.7150/ijbs.4454
- Chen, B., Zhu, Z., Li, L., Ye, W., Zeng, J., Gao, J., et al. (2019). Effect of overexpression of Oct4 and Sox2 genes on the biological and oncological characteristics of gastric cancer cells. *Oncotargets Ther.* 12, 4667–4682. doi: 10.2147/OTT.S209734
- Choodetwattana, P., Proungvitaya, S., Jearanaikoon, P., and Limpaboon, T. (2019). The upregulation of OCT4 in acidic extracellular pH is associated with gemcitabine resistance in cholangiocarcinoma cell lines. *Asian Pac. J. Cancer Prev.* 20, 2745–2748. doi: 10.31557/APJCP.2019.20.9.2745
- Colacino, J. A., Azizi, E., Brooks, M. D., Harouaka, R., Fouladdel, S., McDermott, S. P., et al. (2018). Heterogeneity of human breast stem and progenitor cells as revealed by transcriptional profiling. *Stem Cell Rep.* 10, 1596–1609. doi: 10.1016/j.stemcr.2018.03.001
- Corti, S., Locatelli, F., Papadimitriou, D., Donadoni, C., Salani, S., Del Bo, R., et al. (2006). Identification of a primitive brain-derived neural stem cell population based on aldehyde dehydrogenase activity. *Stem Cells* 24, 975–985. doi: 10.1634/stemcells.2005-0217
- Deng, L., Xiang, X., Yang, F., Xiao, D., Liu, K., Chen, Z., et al. (2017). Functional evidence that the self-renewal gene NANOG regulates esophageal squamous cancer development. *Biochem. Biophys. Res. Commun.* 490, 161–168. doi: 10.1016/j.bbrc.2017.06.016
- De Resende, M. F., Chinen, L. T., Vieira, S., Jampietro, J., Da Fonseca, F. P., Vassallo, J., et al. (2013). Prognostication of OCT4 isoform expression in prostate cancer. *Tumour Biol.* 34, 2665–2673. doi: 10.1007/s13277-013-0817-9
- Ding, X. W., Wu, J. H., and Jiang, C. P. (2010). ABCG2: a potential marker of stem cells and novel target in stem cell and cancer therapy. *Life Sci.* 86, 631–637. doi: 10.1016/j.lfs.2010.02.012
- Elizondo, G., Corchero, J., Sterneck, E., and Gonzalez, F. J. (2000). Feedback inhibition of the retinaldehyde dehydrogenase gene ALDH1 by retinoic acid through retinoic acid receptor alpha and CCAAT/enhancer-binding protein beta. *J. Biol. Chem.* 275, 39747–39753. doi: 10.1074/jbc.M004987200
- Fang, C., Fan, C., Wang, C., Huang, Q., Meng, W., Yu, Y., et al. (2016). CD133⁺CD54⁺CD44⁺ circulating tumor cells as a biomarker of treatment selection and liver metastasis in patients with colorectal cancer. *Oncotarget* 7, 77389–77403. doi: 10.18632/oncotarget.12675
- Fang, D., and Kitamura, H. (2018). Cancer stem cells and epithelial-mesenchymal transition in urothelial carcinoma: possible pathways and potential therapeutic approaches. *Int. J. Urol.* 25, 7–17. doi: 10.1111/iju.13404
- Fang, C. H., Lin, Y. T., Liang, C. M., and Liang, S. M. (2020). A novel c-kit/phospho-prohibitin axis enhances ovarian cancer stemness and chemoresistance via Notch3-PBX1 and beta-catenin-ABCG2 signaling. *J. Biomed. Sci.* 27:42. doi: 10.1186/s12929-020-00638-x
- Feng, D., Peng, C., Li, C., Zhou, Y., Li, M., Ling, B., et al. (2009). Identification and characterization of cancer stem-like cells from primary carcinoma of the cervix uteri. *Oncol. Rep.* 22, 1129–1134. doi: 10.3892/or.00000545
- Florek, M., Haase, M., Marzesco, A. M., Freund, D., Ehninger, G., Huttner, W. B., et al. (2005). Proliferin-1/CD133, a neural and hematopoietic stem cell marker, is expressed in adult human differentiated cells and certain types of kidney cancer. *Cell Tissue Res.* 319, 15–26. doi: 10.1007/s00441-004-1018-z
- Frank, M. H., Wilson, B. J., Gold, J. S., and Frank, N. Y. (2021). Clinical implications of colorectal cancer stem cells in the age of single-cell OMICs and targeted therapies. *Gastroenterology* 160, 1947–1960. doi: 10.1053/j.gastro.2020.12.080
- Fujino, S., and Miyoshi, N. (2019). Oct4 gene expression in primary colorectal cancer promotes liver metastasis. *Stem Cells Int.* 2019:7896524. doi: 10.1155/2019/7896524
- Gawlik-Rzemieniewska, N., Galilejczyk, A., Krawczyk, M., and Bednarek, I. (2016). Silencing expression of the NANOG gene and changes in migration and metastasis of urinary bladder cancer cells. *Arch. Med. Sci.* 12, 889–897. doi: 10.5114/aoms.2015.55368
- Gazouli, M., Roubelakis, M. G., Theodoropoulos, G. E., Papailiou, J., Vaiopoulou, A., Pappa, K. I., et al. (2012). OCT4 spliced variant OCT4B1 is expressed in human colorectal cancer. *Mol. Carcinog.* 51, 165–173. doi: 10.1002/mc.20773
- Gener, P., Gouveia, L. P., Sabat, G. R., De Sousa Rafael, D. E., Fort, N. B., Arranja, A., et al. (2015). Fluorescent CSC models evidence that targeted nanomedicines improve treatment sensitivity of breast and colon cancer stem cells. *Nanomedicine* 11, 1883–1892. doi: 10.1016/j.nano.2015.07.009
- Gomez-Miragaya, J., and Gonzalez-Suarez, E. (2017). Tumor-initiating CD49f cells are a hallmark of chemoresistant triple negative breast cancer. *Mol. Cell. Oncol.* 4:e1338208. doi: 10.1080/23723556.2017.1338208
- Gonzalez Castro, L. N., Tirosh, I., and Suva, M. L. (2021). Decoding cancer biology one cell at a time. *Cancer Discov.* 11, 960–970. doi: 10.1158/2159-8290.CD-20-1376
- Guan, X., and Guan, Y. (2020). miR-145-5p attenuates paclitaxel resistance and suppresses the progression in drug-resistant breast cancer cell lines. *Neoplasma* 67, 972–981. doi: 10.4149/neo_2020_190622N536
- Guo, C. L., Liu, L., Jia, Y. D., Zhao, X. Y., Zhou, Q., and Wang, L. (2012). A novel variant of Oct3/4 gene in mouse embryonic stem cells. *Stem Cell Res.* 9, 69–76. doi: 10.1016/j.scr.2012.04.004
- Gzil, A., Zarebska, I., Bursiewicz, W., Antosik, P., Grzanka, D., and Szyberg, L. (2019). Markers of pancreatic cancer stem cells and their clinical and therapeutic implications. *Mol. Biol. Rep.* 46, 6629–6645. doi: 10.1007/s11033-019-05058-1
- Haraguchi, N., Ishii, H., Mimori, K., Ohta, K., Uemura, M., Nishimura, J., et al. (2013). CD49f-positive cell population efficiently enriches colon cancer-initiating cells. *Int. J. Oncol.* 43, 425–430. doi: 10.3892/ijo.2013.1955
- Hayashi, H., Arai, T., Togashi, Y., Kato, H., Fujita, Y., De Velasco, M. A., et al. (2015). The OCT4 pseudogene POU5F1B is amplified and promotes an aggressive phenotype in gastric cancer. *Oncogene* 34, 199–208. doi: 10.1038/onc.2013.547
- Herrmann, H., Sadovnik, I., Cerny-Reiterer, S., Rulicke, T., Stefanl, G., Willmann, M., et al. (2014). Dipeptidylpeptidase IV (CD26) defines leukemic stem cells (LSC) in chronic myeloid leukemia. *Blood* 123, 3951–3962. doi: 10.1182/blood-2013-10-536078
- Heyes, N., Kapoor, P., and Kerr, I. D. (2018). Polymorphisms of the multidrug pump ABCG2: a systematic review of their effect on protein expression, function, and drug pharmacokinetics. *Drug Metab. Dispos.* 46, 1886–1899. doi: 10.1124/dmd.118.083030
- Hoe, S. L. L., Tan, L. P., Abdul Aziz, N., Liew, K., Teow, S. Y., Abdul Razak, F. R., et al. (2017). CD24, CD44 and EpCAM enrich for tumour-initiating cells

- in a newly established patient-derived xenograft of nasopharyngeal carcinoma. *Sci. Rep.* 7:12372. doi: 10.1038/s41598-017-12045-8
- Hoofd, C., Wang, X., Lam, S., Jenkins, C., Wood, B., Giambra, V., et al. (2016). CD44 promotes chemoresistance in T-ALL by increased drug efflux. *Exp. Hematol.* 44:e117. doi: 10.1016/j.exphem.2015.12.001
- Hsu, H. C., Liu, Y. S., Tseng, K. C., Hsu, C. L., Liang, Y., Yang, T. S., et al. (2013). Overexpression of Lgr5 correlates with resistance to 5-FU-based chemotherapy in colorectal cancer. *Int. J. Color. Dis.* 28, 1535–1546. doi: 10.1007/s00384-013-1721-x
- Hu, H., Luo, S. J., Cao, Z. R., Wu, Y., Mo, Z., Wang, Y., et al. (2020). Depressive disorder promotes hepatocellular carcinoma metastasis via upregulation of ABCG2 gene expression and maintenance of self-renewal. *J. Cancer* 11, 5309–5317. doi: 10.7150/jca.45712
- Huang, L., Lu, Q., Han, Y., Li, Z., Zhang, Z., and Li, X. (2012a). ABCG2/V-ATPase was associated with the drug resistance and tumor metastasis of esophageal squamous cancer cells. *Diagn. Pathol.* 7:180. doi: 10.1186/1746-1596-7-180
- Huang, X., Sheng, Y., and Guan, M. (2012b). Co-expression of stem cell genes CD133 and CD44 in colorectal cancers with early liver metastasis. *Surg. Oncol.* 21, 103–107. doi: 10.1016/j.suronc.2011.06.001
- Huang, Z. J., You, J., Luo, W. Y., Chen, B. S., Feng, Q. Z., Wu, B. L., et al. (2015). Reduced tumorigenicity and drug resistance through the downregulation of octamer-binding protein 4 and Nanog transcriptional factor expression in human breast stem cells. *Mol. Med. Rep.* 11, 1647–1654. doi: 10.3892/mmr.2014.2972
- Iglesias, J. M., Leis, O., Perez Ruiz, E., Gumuzio Barrie, J., Garcia-Garcia, F., Aduriz, A., et al. (2014). The activation of the Sox2 RR2 pluripotency transcriptional reporter in human breast cancer cell lines is dynamic and labels cells with higher tumorigenic potential. *Front. Oncol.* 4:308. doi: 10.3389/fonc.2014.00308
- Irollo, E., and Pirozzi, G. (2013). CD133: to be or not to be, is this the real question? *Am. J. Transl. Res.* 5, 563–581.
- Januchowski, R., Wojtowicz, K., Sterzyska, K., Sosiska, P., Andrzejewska, M., Zawierucha, P., et al. (2016). Inhibition of ALDH1A1 activity decreases expression of drug transporters and reduces chemotherapy resistance in ovarian cancer cell lines. *Int. J. Biochem. Cell Biol.* 78, 248–259. doi: 10.1016/j.biocel.2016.07.017
- Jing, W., Zhou, M., Chen, R., Ye, X., Li, W., Su, X., et al. (2021). In vitro and ex vivo antitumor effect and mechanism of Tucatinib in leukemia stem cells and ABCG2overexpressing leukemia cells. *Oncol. Rep.* 45, 1142–1152. doi: 10.3892/or.2020.7915
- Katagiri, Y. U., Sleeman, J., Fujii, H., Herrlich, P., Hotta, H., Tanaka, K., et al. (1999). CD44 variants but not CD44s cooperate with beta1-containing integrins to permit cells to bind to osteopontin independently of arginine-glycine-aspartic acid, thereby stimulating cell motility and chemotaxis. *Cancer Res.* 59, 219–226.
- Kemper, K., Sprick, M. R., De Bree, M., Scopelliti, A., Vermeulen, L., Hoek, M., et al. (2010). The AC133 epitope, but not the CD133 protein, is lost upon cancer stem cell differentiation. *Cancer Res.* 70, 719–729. doi: 10.1158/0008-5472.CAN-09-1820
- Kim, M. P., Fleming, J. B., Wang, H., Abbruzzese, J. L., Choi, W., Kopetz, S., et al. (2011). ALDH activity selectively defines an enhanced tumor-initiating cell population relative to CD133 expression in human pancreatic adenocarcinoma. *PLoS One* 6:e20636. doi: 10.1371/journal.pone.0020636
- Kinstrie, R., Horne, G. A., Morrison, H., Irvine, D., Munje, C., Castaneda, E. G., et al. (2020). CD93 is expressed on chronic myeloid leukemia stem cells and identifies a quiescent population which persists after tyrosine kinase inhibitor therapy. *Leukemia* 34, 1613–1625. doi: 10.1038/s41375-019-0684-5
- Kishikawa, J., Kazama, S., Oba, K., Hasegawa, K., Anzai, H., Harada, Y., et al. (2016). CD133 expression at the metastatic site predicts patients' outcome in colorectal cancer with synchronous liver metastasis. *Ann. Surg. Oncol.* 23, 1916–1923. doi: 10.1245/s10434-016-5099-1
- Kovacsics, D., Brozik, A., Tihanyi, B., Matula, Z., Borsy, A., Meszaros, N., et al. (2020). Precision-engineered reporter cell lines reveal ABCG2 regulation in live lung cancer cells. *Biochem. Pharmacol.* 175:113865. doi: 10.1016/j.bcp.2020.113865
- Lamour, V., Henry, A., Kroonen, J., Nokin, M. J., Von Marschall, Z., Fisher, L. W., et al. (2015). Targeting osteopontin suppresses glioblastoma stem-like cell character and tumorigenicity in vivo. *Int. J. Cancer* 137, 1047–1057. doi: 10.1002/ijc.29454
- Lettnin, A. P., Wagner, E. F., Carrett-Dias, M., Dos Santos Machado, K., Werhli, A., Canedo, A. D., et al. (2019). Silencing the OCT4-PG1 pseudogene reduces OCT-4 protein levels and changes characteristics of the multidrug resistance phenotype in chronic myeloid leukemia. *Mol. Biol. Rep.* 46, 1873–1884. doi: 10.1007/s11033-019-04639-4
- Levings, P. P., McGarry, S. V., Currie, T. P., Nickerson, D. M., McClellan, S., Ghivizzani, S. C., et al. (2009). Expression of an exogenous human Oct-4 promoter identifies tumor-initiating cells in osteosarcoma. *Cancer Res.* 69, 5648–5655. doi: 10.1158/0008-5472.CAN-08-3580
- Litviakov, N. V., Bychkov, V. A., Stakheeva, M. N., Ibragimova, M. K., Tsyganov, M. M., Gaptulbarova, K. A., et al. (2020). Breast tumour cell subpopulations with expression of the MYC and OCT4 proteins. *J. Mol. Histol.* 51, 717–728. doi: 10.1007/s10735-020-09917-1
- Liu, C. L., Chen, Y. J., Fan, M. H., Liao, Y. J., and Mao, T. L. (2020). Characteristics of CD133-sustained chemoresistant cancer stem-like cells in human ovarian carcinoma. *Int. J. Mol. Sci.* 21:6467. doi: 10.3390/ijms21186467
- Liu, Y., Wang, G., Zhang, J., Chen, X., Xu, H., Heng, G., et al. (2021). CD9, a potential leukemia stem cell marker, regulates drug resistance and leukemia development in acute myeloid leukemia. *Stem Cell Res Ther* 12:86. doi: 10.1186/s13287-021-02155-6
- Liu, Y., Yu, C., Wu, Y., Sun, X., Su, Q., You, C., et al. (2017). CD44⁺ fibroblasts increases breast cancer cell survival and drug resistance via IGF2BP3-CD44-IGF2 signalling. *J. Cell. Mol. Med.* 21, 1979–1988. doi: 10.1111/jcmm.13118
- Long, H., Xiang, T., Qi, W., Huang, J., Chen, J., He, L., et al. (2015). CD133⁺ ovarian cancer stem-like cells promote non-stem cancer cell metastasis via CCL5 induced epithelial-mesenchymal transition. *Oncotarget* 6, 5846–5859. doi: 10.18632/oncotarget.3462
- Machida, K. (2018). Pluripotency transcription factors and metabolic reprogramming of mitochondria in tumor-initiating stem-like cells. *Antioxid. Redox Signal.* 28, 1080–1089. doi: 10.1089/ars.2017.7241
- Mackay, C. R., Terpe, H. J., Stauder, R., Marston, W. L., Stark, H., and Gunthert, U. (1994). Expression and modulation of CD44 variant isoforms in humans. *J. Cell Biol.* 124, 71–82. doi: 10.1083/jcb.124.1.71
- Mani, S. A., Guo, W., Liao, M. J., Eaton, E. N., Ayyanan, A., Zhou, A. Y., et al. (2008). The epithelial-mesenchymal transition generates cells with properties of stem cells. *Cell* 133, 704–715. doi: 10.1016/j.cell.2008.03.027
- Manoranjani, B., Chokshi, C., Venugopal, C., Subapanditha, M., Savage, N., Tatar, N., et al. (2020). A CD133-AKT-Wnt signaling axis drives glioblastoma brain tumor-initiating cells. *Oncogene* 39, 1590–1599. doi: 10.1038/s41388-019-1086-x
- Marchitti, S. A., Brocker, C., Stagos, D., and Vasilou, V. (2008). Non-P450 aldehyde oxidizing enzymes: the aldehyde dehydrogenase superfamily. *Expert Opin. Drug Metab. Toxicol.* 4, 697–720. doi: 10.1517/17425255.4.6.697
- Min, D. W., Kim, H. P., Kim, J., Wen, X., Kim, S., Cho, Y. W., et al. (2020). Phenotype-based single cell sequencing identifies diverse genetic subclones in CD133 positive cancer stem cells. *Biochem. Biophys. Res. Commun.* 558, 209–215. doi: 10.1016/j.bbrc.2020.09.005
- Mohiuddin, I. S., Wei, S. J., and Kang, M. H. (2020). Role of OCT4 in cancer stem-like cells and chemotherapy resistance. *Biochim. Biophys. Acta Mol. Basis Dis.* 1866:165432. doi: 10.1016/j.bbdis.2019.03.005
- Nadal, R., Ortega, F. G., Salido, M., Lorente, J. A., Rodriguez-Rivera, M., Delgado-Rodriguez, M., et al. (2013). CD133 expression in circulating tumor cells from breast cancer patients: potential role in resistance to chemotherapy. *Int. J. Cancer* 133, 2398–2407. doi: 10.1002/ijc.28263
- Ni, Z., Bikadi, Z., Rosenberg, M. F., and Mao, Q. (2010). Structure and function of the human breast cancer resistance protein (BCRP/ABCG2). *Curr. Drug Metab.* 11, 603–617. doi: 10.2174/138920010792927325
- Ni, J., Cozzi, P. J., Hao, J. L., Beretov, J., Chang, L., Duan, W., et al. (2014). CD44 variant 6 is associated with prostate cancer metastasis and chemo-/radioresistance. *Prostate* 74, 602–617. doi: 10.1002/pros.22775
- Nishida, S., Hirohashi, Y., Torigoe, T., Kitamura, H., Takahashi, A., Masumori, N., et al. (2012). Gene expression profiles of prostate cancer stem cells isolated by aldehyde dehydrogenase activity assay. *J. Urol.* 188, 294–299. doi: 10.1016/j.juro.2012.02.2555
- Nomura, A., Banerjee, S., Chugh, R., Dudeja, V., Yamamoto, M., Vickers, S. M., et al. (2015). CD133 initiates tumors, induces epithelial-mesenchymal transition

- and increases metastasis in pancreatic cancer. *Oncotarget* 6, 8313–8322. doi: 10.18632/oncotarget.3228
- O'Brien, C. A., Pollett, A., Gallinger, S., and Dick, J. E. (2007). A human colon cancer cell capable of initiating tumour growth in immunodeficient mice. *Nature* 445, 106–110. doi: 10.1038/nature05372
- Ortiz, R. C., Lopes, N. M., Amor, N. G., Ponce, J. B., Schmerling, C. K., Lara, V. S., et al. (2018). CD44 and ALDH1 immunoreexpression as prognostic indicators of invasion and metastasis in oral squamous cell carcinoma. *J. Oral Pathol. Med.* 47, 740–747. doi: 10.1111/jop.12734
- Padua, D., Barros, R., Amaral, A. L., Mesquita, P., Freire, A. F., Sousa, M., et al. (2020). A SOX2 reporter system identifies gastric cancer stem-like cells sensitive to monensin. *Cancer* 12:495. doi: 10.3390/cancers12020495
- Patel, S. A., Ramkissoon, S. H., Bryan, M., Pliner, L. F., Dontu, G., Patel, P. S., et al. (2012). Delineation of breast cancer cell hierarchy identifies the subset responsible for dormancy. *Sci. Rep.* 2:906. doi: 10.1038/srep00906
- Penforis, P., Cai, D. Z., Harris, M. R., Walker, R., Licini, D., Fernandes, J. D., et al. (2014). High CD49f expression is associated with osteosarcoma tumor progression: a study using patient-derived primary cell cultures. *Cancer Med.* 3, 796–811. doi: 10.1002/cam4.249
- Polgar, O., Robey, R. W., and Bates, S. E. (2008). ABCG2: structure, function and role in drug response. *Expert Opin. Drug Metab. Toxicol.* 4, 1–15. doi: 10.1517/17425255.4.1.1
- Prabavathy, D., Swarnalatha, Y., and Ramadoss, N. (2018). Lung cancer stem cells-origin, characteristics and therapy. *Stem Cell Investig.* 5:6. doi: 10.21037/sci.2018.02.01
- Prieto-Vila, M., Usuba, W., Takahashi, R. U., Shimomura, I., Sasaki, H., Ochiya, T., et al. (2019). Single-cell analysis reveals a preexisting drug-resistant subpopulation in the luminal breast cancer subtype. *Cancer Res.* 79, 4412–4425. doi: 10.1158/0008-5472.CAN-19-0122
- Puram, S. V., Tirosh, I., Park, A. S., Patel, A. P., Yizhak, K., Gillespie, S., et al. (2017). Single-cell transcriptomic analysis of primary and metastatic tumor ecosystems in head and neck cancer. *Cell* 171:e1624. doi: 10.1016/j.cell.2017.10.044
- Ricci-Vitiani, L., Lombardi, D. G., Pilozzi, E., Biffoni, M., Todaro, M., Peschle, C., et al. (2007). Identification and expansion of human colon-cancer-initiating cells. *Nature* 445, 111–115. doi: 10.1038/nature05384
- Rodriguez-Aznar, E., Wiesmuller, L., Sainz, B. Jr., and Hermann, P. C. (2019). EMT and stemness-key players in pancreatic cancer stem cells. *Cancer* 11:1136. doi: 10.3390/cancers11081136
- Roh, Y. G., Mun, M. H., Jeong, M. S., Kim, W. T., Lee, S. R., Chung, J. W., et al. (2018). Drug resistance of bladder cancer cells through activation of ABCG2 by FOXM1. *BMB Rep.* 51, 98–103. doi: 10.5483/BMBRep.2018.51.2.222
- Roudi, R., Barodabi, M., Madjd, Z., Roviello, G., Corona, S. P., and Panahei, M. (2020). Expression patterns and clinical significance of the potential cancer stem cell markers OCT4 and NANOG in colorectal cancer patients. *Mol. Cell. Oncol.* 7:1788366. doi: 10.1080/23723556.2020.1788366
- Sabnis, N. G., Miller, A., Titus, M. A., and Huss, W. J. (2017). The efflux transporter ABCG2 maintains prostate stem cells. *Mol. Cancer Res.* 15, 128–140. doi: 10.1158/1541-7786.MCR-16-0270-T
- Saygin, C., Matei, D., Majeti, R., Reizes, O., and Lathia, J. D. (2019). Targeting cancer stemness in the clinic: from hype to hope. *Cell Stem Cell* 24, 25–40. doi: 10.1016/j.stem.2018.11.017
- Sedlak, J., Sedlakova, O., Hlavcak, P., Hunakova, L., Bizik, J., Grofova, M., et al. (1996). Cell surface phenotype and increased penetration of human multidrug-resistant ovarian carcinoma cells into in vitro collagen-fibroblasts matrix. *Neoplasma* 43, 389–395.
- Shanmugam, G., Mohan, A., Kumari, K., Louis, J. M., Soumya Krishnan, U., Balagopal, P. G., et al. (2019). A novel reporter construct for screening small molecule inhibitors that specifically target self-renewing cancer cells. *Exp. Cell Res.* 383:111551. doi: 10.1016/j.yexcr.2019.111551
- Sharma, A., Cao, E. Y., Kumar, V., Zhang, X., Leong, H. S., Wong, A. M. L., et al. (2018). Longitudinal single-cell RNA sequencing of patient-derived primary cells reveals drug-induced infidelity in stem cell hierarchy. *Nat. Commun.* 9:4931. doi: 10.1038/s41467-018-07261-3
- Shmelkov, S. V., Butler, J. M., Hooper, A. T., Hormigo, A., Kushner, J., Milde, T., et al. (2008). CD133 expression is not restricted to stem cells, and both CD133⁺ and CD133[−] metastatic colon cancer cells initiate tumors. *J. Clin. Invest.* 118, 2111–2120. doi: 10.1172/JCI34401
- Si, X., Gao, Z., Xu, F., and Zheng, Y. (2020). SOX2 upregulates side population cells and enhances their chemoresistant ability by transactivating ABCG1 expression contributing to intrinsic resistance to paclitaxel in melanoma. *Mol. Carcinog.* 59, 257–264. doi: 10.1002/mc.23148
- Sicchieri, R. D., Da Silveira, W. A., Mandarano, L. R., De Oliveira, T. M., Carrara, H. H., Muglia, V. F., et al. (2015). ABCG2 is a potential marker of tumor-initiating cells in breast cancer. *Tumour Biol.* 36, 9233–9243. doi: 10.1007/s13277-015-3647-0
- Simbulan-Rosenthal, C. M., Dougherty, R., Vakili, S., Ferraro, A. M., Kuo, L. W., Alobaidi, R., et al. (2019). CRISPR-Cas9 knockdown and induced expression of CD133 reveal essential roles in melanoma invasion and metastasis. *Cancer* 11:1490. doi: 10.3390/cancers11101490
- Singh, B. N., Fu, J., Srivastava, R. K., and Shankar, S. (2011). Hedgehog signaling antagonist GDC-0449 (Vismodegib) inhibits pancreatic cancer stem cell characteristics: molecular mechanisms. *PLoS One* 6:e27306. doi: 10.1371/journal.pone.0027306
- Soheili, S., Asadi, M. H., and Farsinejad, A. (2017). Distinctive expression pattern of OCT4 variants in different types of breast cancer. *Cancer Biomark.* 18, 69–76. doi: 10.3233/CBM-160675
- Soleymani Abyaneh, H., Gupta, N., Alshareef, A., Gopal, K., Lavasanifar, A., and Lai, R. (2018). Hypoxia induces the acquisition of cancer stem-like phenotype via upregulation and activation of signal transducer and activator of transcription-3 (STAT3) in MDA-MB-231, a triple negative breast cancer cell line. *Cancer Microenviron.* 11, 141–152. doi: 10.1007/s12307-018-0218-0
- Stacy, A. E., Jansson, P. J., and Richardson, D. R. (2013). Molecular pharmacology of ABCG2 and its role in chemoresistance. *Mol. Pharmacol.* 84, 655–669. doi: 10.1124/mol.113.088609
- Storms, R. W., Trujillo, A. P., Springer, J. B., Shah, L., Colvin, O. M., Ludeman, S. M., et al. (1999). Isolation of primitive human hematopoietic progenitors on the basis of aldehyde dehydrogenase activity. *Proc. Natl. Acad. Sci. U. S. A.* 96, 9118–9123. doi: 10.1073/pnas.96.16.9118
- Sun, Y., Lin, H., Qu, S., Li, L., Chen, K., Yu, B., et al. (2019). Downregulation of CD166 inhibits invasion, migration, and EMT in the radio-resistant human nasopharyngeal carcinoma cell line CNE-2R. *Cancer Manag. Res.* 11, 3593–3602. doi: 10.2147/CMAR.S194685
- Tang, K. H., Dai, Y. D., Tong, M., Chan, Y. P., Kwan, P. S., Fu, L., et al. (2013). A CD90⁺ tumor-initiating cell population with an aggressive signature and metastatic capacity in esophageal cancer. *Cancer Res.* 73, 2322–2332. doi: 10.1158/0008-5472.CAN-12-2991
- Tang, B., Raviv, A., Esposito, D., Flanders, K. C., Daniel, C., Nghiem, B. T., et al. (2015). A flexible reporter system for direct observation and isolation of cancer stem cells. *Stem Cell Rep.* 4, 155–169. doi: 10.1016/j.stemcr.2014.11.002
- Taverna, J. A., Hung, C. N., Dearmond, D. T., Chen, M., Lin, C. L., Osmulski, P. A., et al. (2020). Single-cell proteomic profiling identifies combined AXL and JAK1 inhibition as a novel therapeutic strategy for lung cancer. *Cancer Res.* 80, 1551–1563. doi: 10.1158/0008-5472.CAN-19-3183
- Thankamony, A. P., Saxena, K., Murali, R., Jolly, M. K., and Nair, R. (2020). Cancer stem cell plasticity—a deadly deal. *Front. Mol. Biosci.* 7:79. doi: 10.3389/fmolb.2020.00079
- Thapa, R., and Wilson, G. D. (2016). The importance of CD44 as a stem cell biomarker and therapeutic target in cancer. *Stem Cells Int.* 2016:2087204. doi: 10.1155/2016/2087204
- Thiagarajan, P. S., Hitomi, M., Hale, J. S., Alvarado, A. G., Otvos, B., Sinyuk, M., et al. (2015). Development of a fluorescent reporter system to delineate cancer stem cells in triple-negative breast cancer. *Stem Cells* 33, 2114–2125. doi: 10.1002/stem.2021
- Tomita, H., Tanaka, K., Tanaka, T., and Hara, A. (2016). Aldehyde dehydrogenase 1A1 in stem cells and cancer. *Oncotarget* 7, 11018–11032. doi: 10.18632/oncotarget.6920
- Turdo, A., Veschi, V., Gaggiani, M., Chinnici, A., Bianca, P., Todaro, M., et al. (2019). Meeting the challenge of targeting cancer stem cells. *Front. Cell Dev. Biol.* 7:16. doi: 10.3389/fcell.2019.00016
- Vaddi, P. K., Stamnes, M. A., Cao, H., and Chen, S. (2019). Elimination of SOX2/OCT4-associated prostate cancer stem cells blocks tumor development and enhances therapeutic response. *Cancer* 11:1331. doi: 10.3390/cancers11091331
- Valladares-Ayerbes, M., Blanco-Calvo, M., Reboredo, M., Lorenzo-Patino, M. J., Iglesias-Diaz, P., Haz, M., et al. (2012). Evaluation of the adenocarcinoma-associated gene AGR2 and the intestinal stem cell marker LGR5 as biomarkers in colorectal cancer. *Int. J. Mol. Sci.* 13, 4367–4387. doi: 10.3390/ijms13044367

- Vander Linden, C., and Corbet, C. (2019). Therapeutic targeting of cancer stem cells: integrating and exploiting the acidic niche. *Front. Oncol.* 9:159. doi: 10.3389/fonc.2019.00159
- Vassalli, G. (2019). Aldehyde dehydrogenases: not just markers, but functional regulators of stem cells. *Stem Cells Int.* 2019:3904645. doi: 10.1155/2019/3904645
- Vassilopoulos, A., Chisholm, C., Lahusen, T., Zheng, H., and Deng, C. X. (2014). A critical role of CD29 and CD49f in mediating metastasis for cancer-initiating cells isolated from a Brca1-associated mouse model of breast cancer. *Oncogene* 33, 5477–5482. doi: 10.1038/ncr.2013.516
- Velasco-Velazquez, M. A., Velazquez-Quesada, I., Vasquez-Bochm, L. X., and Perez-Tapia, S. M. (2019). Targeting breast cancer stem cells: a methodological perspective. *Curr. Stem Cell Res. Ther.* 14, 389–397. doi: 10.2174/1574888X13666180821155701
- Villodre, E. S., Kipper, F. C., Pereira, M. B., and Lenz, G. (2016). Roles of OCT4 in tumorigenesis, cancer therapy resistance and prognosis. *Cancer Treat. Rev.* 51, 1–9. doi: 10.1016/j.ctrv.2016.10.003
- Visvader, J. E., and Lindeman, G. J. (2012). Cancer stem cells: current status and evolving complexities. *Cell Stem Cell* 10, 717–728. doi: 10.1016/j.stem.2012.05.007
- Wang, Q., Jiang, J., Ying, G., Xie, X. Q., Zhang, X., Xu, W., et al. (2018). Tamoxifen enhances stemness and promotes metastasis of ERα36⁺ breast cancer by upregulating ALDH1A1 in cancer cells. *Cell Res.* 28, 336–358. doi: 10.1038/cr.2018.15
- Wei, Y., Jiang, Y., Zou, F., Liu, Y., Wang, S., Xu, N., et al. (2013). Activation of PI3K/Akt pathway by CD133-p85 interaction promotes tumorigenic capacity of glioma stem cells. *Proc. Natl. Acad. Sci. U. S. A.* 110, 6829–6834. doi: 10.1073/pnas.1217002110
- Wei, F., Zhang, T., Yang, Z., Wei, J. C., Shen, H. F., Xiao, D., et al. (2018). Gambogic acid efficiently kills stem-like colorectal cancer cells by upregulating ZFP36 expression. *Cell. Physiol. Biochem.* 46, 829–846. doi: 10.1159/000488740
- Weidenfeld, K., and Barkan, D. (2018). EMT and stemness in tumor dormancy and outgrowth: are they intertwined processes? *Front. Oncol.* 8:381. doi: 10.3389/fonc.2018.00381
- Wiechert, A., Saygin, C., Thiagarajan, P. S., Rao, V. S., Hale, J. S., Gupta, N., et al. (2016). Cisplatin induces stemness in ovarian cancer. *Oncotarget* 7, 30511–30522. doi: 10.18632/oncotarget.8852
- Wohlleben, G., Hauff, K., Gasser, M., Waaga-Gasser, A. M., Grimmig, T., Flentje, M., et al. (2018). Hypoxia induces differential expression patterns of osteopontin and CD44 in colorectal carcinoma. *Oncol. Rep.* 39, 442–448. doi: 10.3892/or.2017.6068
- Wu, H. J., and Chu, P. Y. (2019). Role of cancer stem cells in cholangiocarcinoma and therapeutic implications. *Int. J. Mol. Sci.* 20:4154. doi: 10.3390/ijms20174154
- Wu, C., Gupta, N., Huang, Y. H., Zhang, H. F., Alshareef, A., Chow, A., et al. (2018). Oxidative stress enhances tumorigenicity and stem-like features via the activation of the Wnt/beta-catenin/MYC/Sox2 axis in ALK-positive anaplastic large-cell lymphoma. *BMC Cancer* 18:361. doi: 10.1186/s12885-018-4300-2
- Wu, G., Wilson, G., Zhou, G., Hebbard, L., George, J., and Qiao, L. (2015). Oct4 is a reliable marker of liver tumor propagating cells in hepatocellular carcinoma. *Discov. Med.* 20, 219–229.
- Wu, F., Zhang, J., Wang, P., Ye, X., Jung, K., Bone, K. M., et al. (2012). Identification of two novel phenotypically distinct breast cancer cell subsets based on Sox2 transcription activity. *Cell. Signal.* 24, 1989–1998. doi: 10.1016/j.cellsig.2012.07.008
- Xiang, L., Su, P., Xia, S., Liu, Z., Wang, Y., Gao, P., et al. (2011). ABCG2 is associated with HER-2 expression, lymph node metastasis and clinical stage in breast invasive ductal carcinoma. *Diagn. Pathol.* 6:90. doi: 10.1186/1746-1596-6-90
- Xiao, W., Zheng, S., Xie, X., Li, X., Zhang, L., Yang, A., et al. (2020). SOX2 promotes brain metastasis of breast cancer by upregulating the expression of FSCN1 and HBEGF. *Mol. Ther. Oncolytics* 17, 118–129. doi: 10.1016/j.omto.2020.03.001
- Xie, Z. Y., Lv, K., Xiong, Y., and Guo, W. H. (2014). ABCG2-mediated multidrug resistance and tumor-initiating capacity of side population cells from colon cancer. *Oncol. Res. Treat.* 37, 670–662. doi: 10.1159/000368842
- Xin, H., Kong, Y., Jiang, X., Wang, K., Qin, X., Miao, Z. H., et al. (2013). Multi-drug-resistant cells enriched from chronic myeloid leukemia cells by doxorubicin possess tumor-initiating-cell properties. *J. Pharmacol. Sci.* 122, 299–304. doi: 10.1254/jphs.13025FP
- Xiong, Q., Liu, B., Ding, M., Zhou, J., Yang, C., and Chen, Y. (2020). Hypoxia and cancer related pathology. *Cancer Lett.* 486, 1–7. doi: 10.1016/j.canlet.2020.05.002
- Xu, J., Tan, Y., Shao, X., Zhang, C., He, Y., Wang, J., et al. (2018). Evaluation of NCAM and c-kit as hepatic progenitor cell markers for intrahepatic cholangiocarcinomas. *Pathol. Res. Pract.* 214, 2011–2017. doi: 10.1016/j.prp.2018.09.005
- Yabushita, T., Satake, H., Maruoka, H., Morita, M., Katoh, D., Shimomura, Y., et al. (2018). Expression of multiple leukemic stem cell markers is associated with poor prognosis in de novo acute myeloid leukemia. *Leuk. Lymphoma* 59, 2144–2151. doi: 10.1080/10428194.2017.1410888
- Yan, B., Chen, Q., Shimada, K., Tang, M., Li, H., Gurumurthy, A., et al. (2019). Histone deacetylase inhibitor targets CD123/CD47-positive cells and reverse chemoresistance phenotype in acute myeloid leukemia. *Leukemia* 33, 931–944. doi: 10.1038/s41375-018-0279-6
- Yan, X., Luo, H., Zhou, X., Zhu, B., Wang, Y., and Bian, X. (2013). Identification of CD90 as a marker for lung cancer stem cells in A549 and H460 cell lines. *Oncol. Rep.* 30, 2733–2740. doi: 10.3892/or.2013.2784
- Yang, L., Shi, P., Zhao, G., Xu, J., Peng, W., Zhang, J., et al. (2020). Targeting cancer stem cell pathways for cancer therapy. *Signal Transduct. Target. Ther.* 5:8. doi: 10.1038/s41392-020-0110-5
- Yang, L., Tang, H., Kong, Y., Xie, X., Chen, J., Song, C., et al. (2015). LGR5 promotes breast cancer progression and maintains stem-like cells through activation of Wnt/beta-catenin signaling. *Stem Cells* 33, 2913–2924. doi: 10.1002/stem.2083
- Yang, Y., Zhou, W., Xia, J., Gu, Z., Wendlandt, E., Zhan, X., et al. (2014). NEK2 mediates ALDH1A1-dependent drug resistance in multiple myeloma. *Oncotarget* 5, 11986–11997. doi: 10.18632/oncotarget.2388
- Ylagan, L. R., Scholes, J., and Demopoulos, R. (2000). Cd44: a marker of squamous differentiation in adenosquamous neoplasms. *Arch. Pathol. Lab. Med.* 124, 212–215. doi: 10.5858/2000-124-0212-C
- Yu, S. S., and Cirillo, N. (2020). The molecular markers of cancer stem cells in head and neck tumors. *J. Cell. Physiol.* 235, 65–73. doi: 10.1002/jcp.28963
- Yuan, Z., Liang, X., Zhan, Y., Wang, Z., Xu, J., Qiu, Y., et al. (2020). Targeting CD133 reverses drug-resistance via the AKT/NF-kappaB/MDR1 pathway in colorectal cancer. *Br. J. Cancer* 122, 1342–1353. doi: 10.1038/s41416-020-0783-0
- Yue, C., Zhao, X., Tian, C., Jin, Y., and Liu, H. (2015). High aldehyde dehydrogenase 1A1 (ALDH1A1) expression correlated with risk of lymph node metastasis in papillary thyroid carcinoma. *Zhonghua Bing Li Xue Za Zhi* 44, 490–494.
- Yuen, C. A., Asuthkar, S., Guda, M. R., Tsung, A. J., and Velpula, K. K. (2016). Cancer stem cell molecular reprogramming of the Warburg effect in glioblastomas: a new target gleaned from an old concept. *CNS Oncol.* 5, 101–108. doi: 10.2217/cns-2015-0006
- Zeilstra, J., Joosten, S. P., Van Andel, H., Tolg, C., Berns, A., Snoek, M., et al. (2014). Stem cell CD44v isoforms promote intestinal cancer formation in Apc(min) mice downstream of Wnt signaling. *Oncogene* 33, 665–670. doi: 10.1038/ncr.2012.611
- Zeng, J., Ruan, J., Luo, L., Shi, J., Cui, Q., Yang, J., et al. (2014). Molecular portraits of heterogeneity related to cancer stem cells in human ovarian cancer. *Int. J. Gynecol. Cancer* 24, 29–35. doi: 10.1097/IGC.000000000000024
- Zhang, J., Chang, D. Y., Mercado-Urbe, I., and Liu, J. (2012). Sex-determining region Y-box 2 expression predicts poor prognosis in human ovarian carcinoma. *Hum. Pathol.* 43, 1405–1412. doi: 10.1016/j.humpath.2011.10.016
- Zhang, Q., Han, Z., Zhu, Y., Chen, J., and Li, W. (2020). The role and specific mechanism of OCT4 in cancer stem cells: a review. *Int. J. Stem Cells* 13, 312–325. doi: 10.15283/ijsc20097
- Zhang, J., Yuan, B., Zhang, H., and Li, H. (2019). Human epithelial ovarian cancer cells expressing CD105, CD44 and CD106 surface markers exhibit increased invasive capacity and drug resistance. *Oncol. Lett.* 17, 5351–5360. doi: 10.3892/ol.2019.10221
- Zhao, D., McCaffery, P., Ivins, K. J., Neve, R. L., Hogan, P., Chin, W. W., et al. (1996). Molecular identification of a major retinoic-acid-synthesizing enzyme, a retinaldehyde-specific dehydrogenase. *Eur. J. Biochem.* 240, 15–22. doi: 10.1111/j.1432-1033.1996.0015h.x

Conflict of Interest: The authors declare that the research was conducted in the absence of any commercial or financial relationships that could be construed as a potential conflict of interest.

Copyright © 2021 Mohan, Raj Rajan, Mohan, Kollenchery Puthenveetil and Maliekal. This is an open-access article distributed under the terms of the Creative Commons Attribution License (CC BY). The use, distribution or reproduction in other forums is permitted, provided the original author(s)

and the copyright owner(s) are credited and that the original publication in this journal is cited, in accordance with accepted academic practice. No use, distribution or reproduction is permitted which does not comply with these terms.



Tumor Immune Microenvironment Components and Checkpoint Molecules in Anaplastic Variant of Diffuse Large B-Cell Lymphoma

OPEN ACCESS

Edited by:

Yong Song,
Nanjing University, China

Reviewed by:

Zhuqing Liu,
Tongji University, China
Shouyin Di,
PLA General Hospital, China
Peifeng Li,
960th Hospital of the PLA, China

*Correspondence:

Rong Liang
rongliang1017@fmmu.edu.cn
Mingyang Li
limingyang1108@sina.com
Zhe Wang
zhwang@fmmu.edu.cn

[†]These authors have contributed
equally to this work

Specialty section:

This article was submitted to
Molecular and Cellular Oncology,
a section of the journal
Frontiers in Oncology

Received: 05 December 2020

Accepted: 12 May 2021

Published: 16 June 2021

Citation:

Xu T, Chai J, Wang K, Jia Q, Liu Y,
Wang Y, Xu J, Yu K, Zhao D, Ma J,
Fan L, Yan Q, Guo S, Chen G, Chen Q,
Xiao H, Liu F, Qi C, Liang R, Li M and
Wang Z (2021) Tumor Immune
Microenvironment Components
and Checkpoint Molecules
in Anaplastic Variant of Diffuse
Large B-Cell Lymphoma.
Front. Oncol. 11:638154.
doi: 10.3389/fonc.2021.638154

Tianqi Xu^{1†}, Jia Chai^{1†}, Kaijing Wang^{1†}, Qingge Jia^{2†}, Yixiong Liu^{1†}, Yingmei Wang¹, Junpeng Xu¹, Kangjie Yu¹, Danhui Zhao¹, Jing Ma¹, Linni Fan¹, Qingguo Yan¹, Shuangping Guo¹, Gang Chen³, Qiongrong Chen⁴, Hualiang Xiao⁵, Fang Liu⁶, Chubo Qi⁴, Rong Liang^{7*}, Mingyang Li^{1*} and Zhe Wang^{1*}

¹ State Key Laboratory of Cancer Biology, Department of Pathology, Xijing Hospital and School of Basic Medicine, Air Force Medical University, Xi'an, China, ² Xi'an International Medical Center, Northwest University, Xi'an, China, ³ Department of Pathology, Fujian Cancer Hospital, Fuzhou, China, ⁴ Department of Pathology, Hubei Cancer Hospital, Wuhan, China, ⁵ Department of Pathology, Daping Hospital, Third Military Medical University, Chongqing, China, ⁶ Department of Pathology, The First People's Hospital of Foshan, Foshan, China, ⁷ Department of Hematology, People's Liberation Army Centre for Hematologic Disorders, Xijing Hospital, Air Force Medical University, Xi'an, China

Background: Anaplastic diffuse large B-cell lymphoma(A-DLBCL) is a rare morphological subtype characterized by the presence of polygonal, bizarre-shaped tumor cells. Our previous research found that A-DLBCL displays many genetic alterations and biological features that differ greatly from those of ordinary DLBCL. However, the status of tumor immune microenvironment components and checkpoint molecules in A-DLBCL remains unclear.

Methods: Thirty A-DLBCL patients were enrolled to study tumor immune microenvironment components and checkpoint molecules and their associations with clinicopathological features and prognosis.

Results: Patients with A-DLBCL presented higher expression of PD-L1 (40% vs 10%, $P=0.004$) than patients with ordinary DLBCL. FISH analysis showed that extra copies of PD-L1 were more frequent in A-DLBCL cases than in ordinary DLBCL cases (23.3% vs 4.0%, $P=0.001$). The numbers of PD-1⁺ TILs (tumor infiltrating lymphocytes) and CD8⁺T cells were significantly lower in A-DLBCL versus ordinary DLBCL. In contrast, the numbers of GATA3⁺ Th2 cells, FOXP3⁺ Tregs and CD33⁺ myeloid-derived suppressor cells (MDSCs) were significantly higher in A-DLBCL than in ordinary DLBCL. The associations between clinicopathological features and tumor immune microenvironment cell frequency were analyzed in A-DLBCL patients. Briefly, the number of PD-1⁺ TILs was lower and the number of CD33⁺ MDSCs was higher in patients with mutated *TP53* compared to those with wild-type *TP53*. The number of FOXP3⁺ Tregs was much lower in patients with a noncomplete response (CR) to chemotherapy than in those with a complete response. The number of CD8⁺ T cells showed a decreasing trend in patients with high International Prognostic Index (IPI) scores and in those with concurrent MYC and

BCL2 and/or BCL6 abnormalities. Univariate survival analysis showed that patients with PD-L1⁺, mPD-L1⁺(PD-L1⁺ nonmalignant stromal cells) or mPD-L1⁺ status had a significantly poorer overall survival (OS) than those with PD-L1⁻ status. An increase in the number of CD3⁺ T cells, FOXP3⁺ Treg cells and T-bet⁺ Th1 cells was significantly associated with prolonged OS in patients with A-DLBCL.

Conclusion: Our study suggests that A-DLBCL displays a distinct pattern of tumor immune microenvironment components and checkpoint molecules that distinguish it from ordinary DLBCL. The analysis of tumor immune microenvironment components and checkpoint molecules could help in predicting the prognosis of A-DLBCL patients and determining therapeutic strategies targeting the tumor immune microenvironment.

Keywords: tumor immune microenvironment (TIME), checkpoint molecules, anaplastic variant of diffuse large B-cell lymphoma, PD-L1, prognosis

INTRODUCTION

Diffuse large B-cell lymphoma (DLBCL) is the most common type of lymphoma; it is more prevalent in elderly patients, with a median age in the 70s. However, it also occurs in young adults but rarely occurs in children. Clinically, most patients present with a rapidly growing tumor mass involving one or more lymph nodes and extranodal sites (1, 2). DLBCL displays tremendous heterogeneity in terms of its clinicopathologic and molecular genetic features. DLBCL cases can be subdivided into morphologic variants, molecular and immunophenotypical subgroups, and distinct disease entities.

Anaplastic variant of diffuse large B-cell lymphoma (A-DLBCL) is a rare morphological type, representing approximately 3–4% of all DLBCL cases (1, 2), that is characterized by large or very large, pleomorphic or bizarre-shaped lymphoma cells. Our previous research found that A-DLBCL showed a high frequency of the *TP53* mutation, as well as concurrent abnormalities of *MYC* and *BCL2* and/or *BCL6*, and most cases had a non-GCB immunophenotype. Patients with A-DLBCL follow an aggressive disease course and have poor prognosis (3). In our study on 3 cases of primary CNS A-DLBCL, patients also had *MYC/BCL2* co-expression, and concurrent *MYC* and *BCL2* and/or *BCL6* genetic abnormalities, and constitutive NF- κ B pathway activation (4). Our results suggest that A-DLBCL displays many genetic alterations and biological features that differ greatly from ordinary DLBCL.

The PD-1/PD-L1 pathway is an inhibitory immune checkpoint that has the ability to suppress T cell immune activity. However, this pathway inhibits the immune activity of tumor-specific CD8⁺ T cells, allowing tumor cells to escape T-cell-mediated tumor-specific immunity, thereby promoting tumor development. Various studies have reported an association between increased expression of PD-L1 and poor prognosis in several cancers, including melanoma, lung cancer, ovarian cancer, and DLBCL (5–8). PD-L1 is also expressed on DLBCL tumor cells and tumor infiltrating nonmalignant cells, primarily macrophages (9, 10). Furthermore, the presence of high levels of PD-L1 is associated with poor OS and acts as a

potent novel biomarker in DLBCL (7). Extensively pretreated patients with relapsed or refractory DLBCL achieve beneficial therapeutic effects with blockade of the PD-1/PD-L1 pathway (11–13). These results suggest that the PD-1/PD-L1 pathway contributes to tumor cell survival and that manipulation of this pathway may be an applicable therapeutic modality to treat DLBCL.

The tumor microenvironment (TME) of B-cell lymphoma significantly contributes to tumor progression and immune evasion (14). Recently, some researchers separate tumor immune microenvironment (TIME) from the TME, focusing on the immune cells around tumor cells (15, 16). The TIME in B cell malignancies includes multiple different cell types, including NLCs/tumor-associated macrophages (TAMs), tumor-infiltrating lymphocytes (TILs), regulatory T cells, dendritic cells (DCs), myeloid suppressor cells (MSCs) and endothelial stromal cells, which interact with and are enlisted by malignant cells (17, 18). Research has revealed that in DLBCL, the microenvironment is crucial for the provision of survival and proliferation signals and makes critical contributions to both disease progression and drug resistance/disease relapse (14). However, the status of the TIME and checkpoint molecules in A-DLBCL remains unclear. The aim of this study was to evaluate the checkpoint molecules and TIME of A-DLBCL and their associations with clinicopathological features and prognosis.

MATERIALS AND METHODS

Patients and Samples

We analyzed 30 patients with A-DLBCL and 50 patients with ordinary DLBCL, both originally diagnosed, from June 2004 to April 2016. Four pathologists (M.L., Q.Y., S.G. and Z.W.) reviewed all cases according to the 2016 World Health Organization classification of tumors of hematopoietic and lymphoid tissues (2). All cases were tested by EBER hybridization, and EBV-positive cases were excluded. The diagnosis was based on lymph node biopsy specimens of 20 patients or from the resection samples of extranodal involvement

in the other 10 patients. The corresponding medical records were reviewed to obtain clinical information. A total of 30 well-documented patients were treated with different chemotherapy regimens, including cyclophosphamide, doxorubicin, vincristine, and prednisone (CHOP) or rituximab plus cyclophosphamide, doxorubicin, vincristine, and prednisone (R-CHOP), or etoposide, prednisone, vincristine, cyclophosphamide and doxorubicin (EPOCH). All 30 cases were exactly came from our previous 35 A-DLBCL study (3), while in this study we deleted 5 cases with incomplete data vital to analyze. **Table 1** summarizes the major clinical characteristics, treatment, and follow-up for all 30 patients. These patients and their tumors were compared with 50 cases of DLBCL-NOS without anaplastic features (common DLBCL). The 50 consecutive control cases were derived from one institution (Xijing Hospital) spanning the time interval of April 2009 through September 2014, and only DLBCL-NOS cases were enrolled in the study. Institutional ethical approval was obtained in compliance with the Helsinki Declaration.

Immunohistochemistry and Fluorescence *In Situ* Hybridization (FISH) Analysis

All immunohistochemical staining was performed using fully automated protocols on a Bond-III Autostainer (Leica Biosystems, Melbourne, Australia). Sections were subjected to staining protocols (detailed information on the antibodies is listed in **Table S1**).

The tumor immune microenvironment was characterized by immunostaining for CD3 (tumor-infiltrating lymphocytes, TILs), CD8 (cytotoxic T lymphocytes), T-bet (Th1 cells), GATA3 (Th2 cells), FOXP3 (regulatory T cells), CD68 (tumor-associated macrophages, TAMs), CD163 (M2-TAMs), and CD33 (myeloid-derived suppressor cells, MDSCs). Germinal center B cell (GCB) and non-GCB subtypes of DLBCL were classified using the Hans (19) and Choi (20) algorithms. Each marker was investigated in a single stain with 5 high-power fields (HPFs) of the representative areas evaluated (21). PD-L1/PAX5 IHC double staining was used to evaluate PD-L1 expression in tumor cells (PD-L1⁺) or in nonmalignant stromal cells (defined as microenvironmental PD-L1, mPD-L1⁺). PD-L1 staining on tumor cells was considered positive in cases with moderate (2+) or strong (3+) cytoplasm reaction, and the percentage of the positive tumor cells was set as above 30%. Once reaching the 30% threshold, the PD-L1 positivity of nonmalignant stromal cells was ignored. Among PD-L1-negative DLBCL cases, in which PD-L1⁺ nonmalignant microenvironment cells represented 20% or more of the total tissue, cellularity was defined as microenvironmental PD-L1 (mPD-L1⁺) DLBCL (22). PD-1⁺ TILs were similarly evaluated. The number of tumor cells and cells in the TME were quantified in whole-tissue sections of all samples using an automated scanning microscope image analysis system (Ariol 2.1, SL-50; Applied Imaging, Melville, NY). Quantification of cells was performed with the nuclear Kisight assay provided by the manufacturer (Applied Imaging) (23).

FISH analysis was performed using LSI probes for PD-L1 (Vysis, Abbott Laboratories, USA) on a Thermobrite System (Abbott Laboratories S500-24, USA) according to the

manufacturer's instructions. Images were collected using a workstation equipped with software (Imstar Pathfinder CellscaFluoSpot, France). Areas with a minimum of 70% tumor cells were counted, and signals from 100 non-overlapping nuclei were analyzed. Positivity was determined above and a 30% threshold for extra copies (defined as copy number $\geq 3/\text{cell}$). The 9p24.1 gene (PD-L1 gene) was labeled with Spectrum Red, and centromeres were labeled with Spectrum Green as a control probe on 9p. After calculation of red and green in areas with a minimum of 70% tumor cells were counted, and signals from 100 non-overlapping nuclei, the numbers of red and green was calculated. 4 or more was considered as amplification. 3 was considered as copy gains (24).

Statistical Analysis

Statistical analysis including data description was performed using the Statistical Package of Social Sciences 14.0 software (Chicago, IL, USA). Pearson's χ^2 statistic, Fisher's exact test or Spearman's correlation test was used to analyze relationships between the markers and the clinical variables. The Kaplan-Meier method was used for survival analyses. Two-sided P-values of <0.05 were considered to be statistically significant for all analyses.

RESULTS

Patient Characteristics and Histologic Findings

Thirty patients with A-DLBCL were enrolled, of whom 20 were male (66.7%) and 10 were female (33.3%), with a median age of 61.5 years. Only 1 (3.3%) patient was classified as Ann Arbor stage I, 3 (10%) as Ann Arbor stage II and 8 (26.7%) as Ann Arbor stage III. The remaining 13 (43.3%) patients were at Ann Arbor stage IV. Sixteen (53.3%) patients had elevated serum LDH, while 9 (30%) had normal LDH levels. Clinical data are summarized in **Table 1**.

Immunohistochemical and FISH Analysis of PD-L1 in Tumor Cells

All A-DLBCL cases contained large bizarre-shaped tumor cells with abundant cytoplasm containing irregularly shaped nuclei. Membrane expression of PD-L1 by the tumor cells was observed in the investigated sections. PD-L1⁺ A-DLBCL was identified based on double immunostaining for PD-L1 and PAX-5. Representative IHC images for PD-L1 are shown in **Figures 1A–C**. The prevalence of PD-L1⁺ A-DLBCL was 40% (12 of 30), which was higher than that of ordinary DLBCL (10%, $P=0.001$) according to our results.

Amplifications targeting the PD-L1 locus were observed in 7 out of 30 A-DLBCL cases. Seven cases (23.3%) were amplifications, and 2 (6.6%) were copy gains, and the other 21 cases (70%) were normal. Representative examples of cytogenetic alterations identified by FISH are presented in **Figures 1D–F**. Detailed features of 7 A-DLBCL cases with PD-L1 locus gain were listed in **Supplementary Table 2**. In 50 ordinary DLBCL

TABLE 1 | Clinical Features of the 30 Patients With ADLBCL.

Characteristics	Values (n[%])
Age (y)	
Median	61.5
Range	26-89
Sex	
Male	20(66.7)
Female	10(33.3)
Stage at diagnosis (Ann Arbor stage)	
I	1(3.3)
II	3(10)
III	8(26.7)
IV	13(43.3)
B symptoms	11(36.7)
Extranodal sites ≥ 2	12(40)
Serum LDH	
Normal	9(30)
High	16(53.3)
Chemotherapy CR rate	6(15)
IPI score	
1	2(6.7)
2	7(23.3)
3	8(26.7)
4	4(13.3)
5	4(13.3)
Immunophenotype	
Non-GCB subtype	25(83.3)
BCL-2	21(70)
c-MYC	17(56.7)
MYC/BCL2 DEL	13(21.7)
Ki-67 ($\geq 80\%$)	20(66.7)
p53	24(80)
Fluorescence in situ hybridization	
MYC abnormalities	10(33.3)
BCL2 abnormalities	10(33.3)
BCL6 abnormalities	11(36.6)
Concurrent abnormalities of MYC and BCL2 and/or BCL6	9(30)
Mutation statuses	
TP53 MUT	17(56.7)
DEL, double-expressor lymphoma	

cases, only 2 cases(4%) harbored amplifications and 2 cases (4%) were copy gains. In comparison with ordinary DLBCL cases, extra copies of PD-L1 were more frequent in A-DLBCL (23.3% vs 4.0%, $P=0.001$).

Composition and Distribution of the TIME

To evaluate the cellular composition of the TIME in A-DLBCL, we used markers targeting various cells of the TIME in IHC analysis. Representative immunostaining of A-DLBCL cases is shown in **Figure 2**. The immunohistochemical and FISH results of 30 Patients with A-DLBCL are listed in **Table 2**. Afterwards, the differences in TIME in A-DLBCL and ordinary DLBCL cases were analyzed and are listed in **Table 3**.

mPD-L1 Expression

In addition to cases containing PD-L1⁺ large bizarre-shaped tumor cells, there were also cases with PD-L1⁺ nonmalignant stromal cells, and we defined them as mPD-L1⁺ (PD-L1⁺/PAX5⁻) (**Figure 1B**). PD-L1/PAX5 double staining showed that the proportion of mPD-L1⁺ cells was higher (72.2% vs 33.3%, $P=0.005$) in A-DLBCL patients than patients with ordinary DLBCL.

MDSCs and Tumor-associated Macrophages

We found that MDSCs were more abundant in A-DLBCL than in ordinary DLBCL ($P=0.039$), with $33.8 \pm 4.2/\text{HPF}$ vs $20.6 \pm 4.1/\text{HPF}$, represented by CD33, while M2 TAMs (CD163) and M1/M2 TAMs (CD68) showed no significant difference between A-DLBCL and ordinary DLBCL.

TILs

The distribution of TILs was diffuse in all cases. The difference between the numbers of cells expressing GATA3 and FOXP3 in A-DLBCL and DLBCL was significant ($P=0.039$; $P=0.048$) after

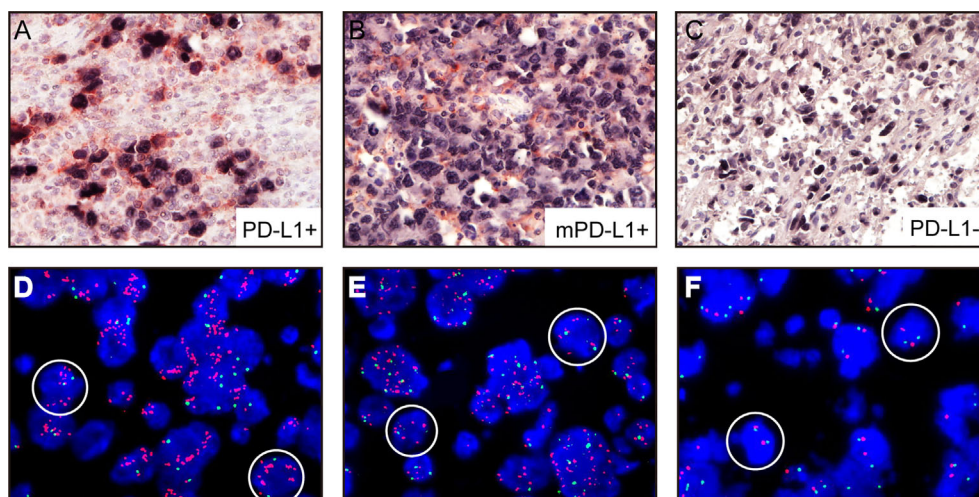


FIGURE 1 | Representative immunohistochemical analysis of PD-L1 and PD-L1 FISH in A-DLBCL (400x magnification). **(A)** PD-L1⁺ A-DLBCL, tumor cells were double positive for PD-L1 (red) and PAX5 (black); **(B)** mPD-L1⁺ DLBCL, tumor cells were positive for PAX5 and negative for PD-L1; **(C)** PD-L1⁻ A-DLBCL, tumor cells were negative for PD-L1 (red) and positive for PAX5 (black); **(D)** Copy number gains in PD-L1 locus; **(E)** Amplification in PD-L1 locus; **(F)** Normal PD-L1 FISH signal.

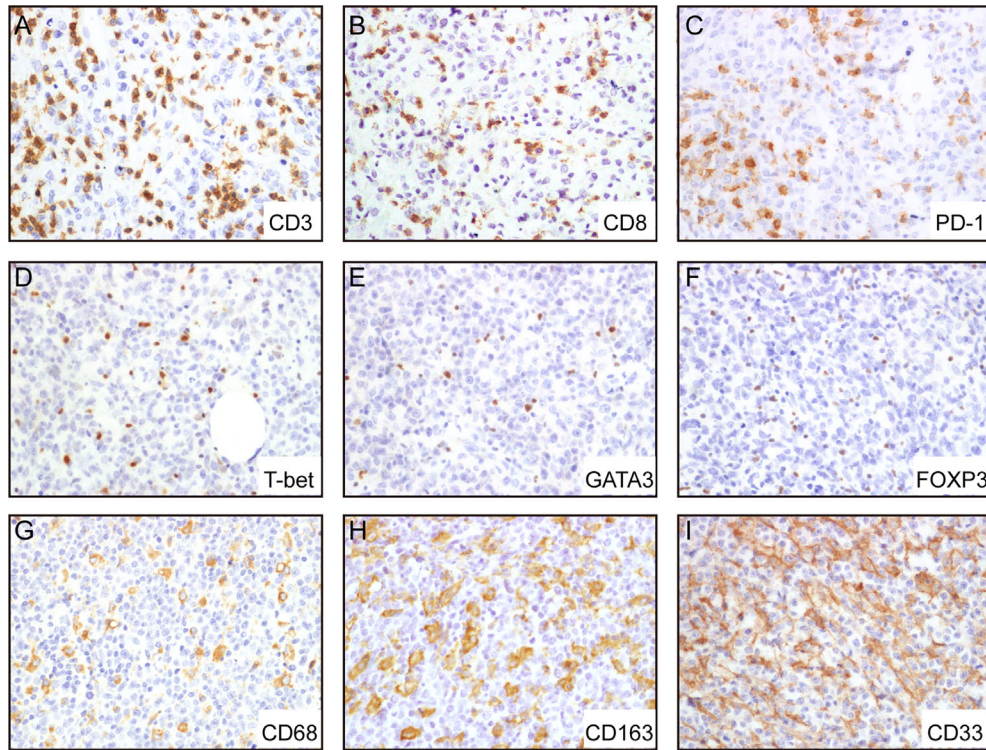


FIGURE 2 | Representative immunohistochemical analysis of A-DLBCL. Representative IHC staining expressions of CD3 (A), CD8 (B), PD-1 (C), CD68 (G), CD163 (H), CD33 (I), and negative expressions of T-bet (D), GATA3 (E), FOXP3 (F).

statistical analysis, indicating that there were more Th2 cells and Treg cells in the TME of A-DLBCL than in ordinary DLBCL. In contrast, staining of CD8 showed decreased numbers of CD8⁺ T cells ($34.7 \pm 5.7/\text{HPF}$ vs $58.6 \pm 7.5/\text{HPF}$, $P=0.026$) and PD-1⁺ TILs ($23.3 \pm 6.0/\text{HPF}$ vs $50.6 \pm 7.2/\text{HPF}$, $P=0.010$) in A-DLBCL compared to ordinary DLBCL. Moreover, there seemed to be no significant difference in CD3⁺ T cells and Th1 cells between A-DLBCL and ordinary DLBCL cases.

Clinicopathological Association and Prognostic Factors

Same as in our previous study (3), the mutation states of ADLBCL cases were already performed and all were available in cases. In this study, TP53 mutation status was associated with the numbers of PD-L1⁺ TILs (CD3) and MDSCs (CD33) in A-DLBCL cases. There seemed to be fewer PD-L1⁺ TILs in TP53 mutant cases than in TP53 wild type cases ($14.7 \pm 5.2/\text{HPF}$ vs $42.5 \pm 16.3/\text{HPF}$, $P=0.049$). For MDSCs, the result was the opposite ($37.4 \pm 5.0/\text{HPF}$ vs $19.3 \pm 6.2/\text{HPF}$, $P=0.044$). The comparison also showed that patients with fewer Treg cells ($10.3 \pm 4.5/\text{HPF}$ vs $35 \pm 13.4/\text{HPF}$, $P=0.032$) in the TME (FOXP3) had a non-complete response (Non-CR) to chemotherapy, since high FOXP3 expression had a significant correlation with complete response. The number of CD8⁺ cells showed a decreasing trend in patients with high International

Prognostic Index (IPI) scores ($23.8 \pm 5.7/\text{HPF}$ vs $47.4 \pm 8.2/\text{HPF}$, $P=0.075$). All results are shown in **Figure 3**.

Figure 4 shows the univariate overall survival analysis of A-DLBCL patients according to the expression of different markers, showing that patients with PD-L1⁺/mPD-L1⁺ or mPD-L1⁺ had significantly poorer overall survival (OS) than those with PD-L1⁻ status ($P=0.034$ and $P=0.046$, respectively). In consistent with DLCL, A-DLBCL patients with PD-L1⁺ has a poorer prognosis than PD-L1⁻. An increase in CD3⁺, FOXP3⁺ and T-bet⁺ cell numbers was significantly associated with prolonged OS in patients with A-DLBCL ($P=0.040$, $P=0.000$ and $P=0.046$, respectively).

DISCUSSION

In this study, we demonstrated the molecular pathogenesis of primary A-DLBCL and its association with clinical characteristics. In brief, our findings showed high expression of PD-L1⁺ and mPD-L1⁺ in A-DLBCL compared with ordinary DLBCL. In the TME, the numbers of PD-1⁺ TILs and CD8⁺ cells were significantly lower in A-DLBCL. In contrast, the numbers of GATA3⁺ cells, FOXP3⁺ cells and CD33⁺ cells were significantly higher in A-DLBCL patients. These differences between A-DLBCL and ordinary DLBCL were associated with poor prognosis in A-DLBCL.

TABLE 2 | Immunohistochemical and FISH Analysis of 30 Patients with A-DLBCL.

Patient Number	PD-L1			TIME								
	Tum PD-L1*	mPD-L1**	PD-L1 FISH***	PD-1 TIL (/HPF****)	CD3 (/HPF)	CD8 (/HPF)	T-bet (/HPF)	GATA3 (/HPF)	FOXP3 (/HPF)	CD68 (/HPF)	CD163 (/HPF)	CD33 (/HPF)
1	+		+	10	70	20	55	0	0	80	70	20
2	–	–	–	50	130	55	60	15	0	100	80	15
3	+		+	0	160	140	120	110	120	90	50	50
4	–	+	–	100	150	30	60	30	0	80	60	20
5	+		+	0	110	60	75	15	0	60	50	40
6	+		–	0	50	35	45	5	0	70	50	50
7	–	+	–	0	130	70	110	120	100	60	60	40
8	–	–	–	60	150	40	120	5	10	85	80	0
9	+		+	0	150	30	130	0	0	110	90	0
10	–	+	–	0	80	10	60	20	0	70	60	25
11	–	+	–	0	50	2	10	60	0	50	50	20
12	–	–	–	0	50	5	0	30	15	25	0	0
13	–	–	–	20	50	50	0	0	0	60	50	30
14	+		–	30	160	30	100	80	25	70	60	5
15	+		+	120	150	35	80	30	15	80	70	80
16	+		–	0	5	5	0	0	0	50	80	10
17	–	+	–	70	150	40	50	100	50	50	40	30
18	–	+	–	70	140	120	30	10	10	80	80	60
19	–	–	–	10	120	35	90	95	90	90	80	60
20	–	+	–	0	90	10	0	0	0	65	20	30
21	+		–	25	100	20	60	40	60	50	40	25
22	+		–	0	80	40	0	0	0	40	80	60
23	–	+	–	20	40	35	3	0	0	60	45	50
24	+		+	0	60	40	20	30	0	30	5	80
25	–	+	–	5	120	3	50	20	10	50	50	25
26	–	+	–	10	50	25	15	0	0	65	40	30
27	–	+	–	0	40	20	10	5	0	85	80	70
28	–	+	–	0	70	5	55	0	0	60	60	50
29	–	+	–	40	30	10	0	0	0	60	60	10
30	+		+	60	120	20	30	80	20	40	40	30

*Tum PD-L1, tumor PD-L1.

**mPD-L1, microenvironment PD-L1. Once tumor PD-L1 was defined positive, the mPD-L1 positivity was ignored.

***+ stands for amplification of PD-L1 in tumor cells.

****/HPF, per high power field.

TABLE 3 | Comparison of TME markers and checkpoint molecules between A-DLBCL and ordinary DLBCL.

Features	A-DLBCL (n = 30)	Ordinary DLBCL (n = 50)	P value
PD-L1+	12/30 (40%)	5/50 (10%)	0.001
mPD-L1+	13/18 (72.2%)	15/45 (33.3%)	0.005
CD3+	78.2 ± 7.2/HPF	92.5 ± 8.6/HPF	0.214
CD8+	34.7 ± 5.7/HPF	58.6 ± 7.5/HPF	0.026
PD-1+ TILs	23.3 ± 6.0/HPF	50.6 ± 7.2/HPF	0.01
T-bet+	49.8 ± 7.6/HPF	41.1 ± 6.3/HPF	0.394
GATA3+	30.5 ± 7.1/HPF	15.1 ± 3.8/HPF	0.039
FOXP3+	17.5 ± 6.0/HPF	6.6 ± 2.1/HPF	0.048
CD68+	65.5 ± 3.6/HPF	59.9 ± 5.5/HPF	0.461
CD163+	56 ± 4.0/HPF	50.3 ± 6.3/HPF	0.514
CD33+	33.8 ± 4.2/HPF	20.6 ± 4.1/HPF	0.039

Traverse-Glehen et al. (25) divided GZL into 3 distinct subgroups (namely, cHL-like GZL, large B-cell lymphoma-like GZL, and composite/sequential cases) according to the evaluation and integration of tumor cell morphology, architecture and growth pattern, microenvironmental composition, and immunophenotype. CHL-like GZL and

LBCL-like GZL were then divided into 2 subgroups (namely, groups 0 and 1 for cHL-like cases and groups 2 and 3 for LBCL-like cases). A-DLBCL differs from these four subtypes as we stained for CD15 with immunohistochemistry. In CD15 IHC found that it was negative in all of our cases, and A-DLBCL cases showed a large B-cell-like morphology with an

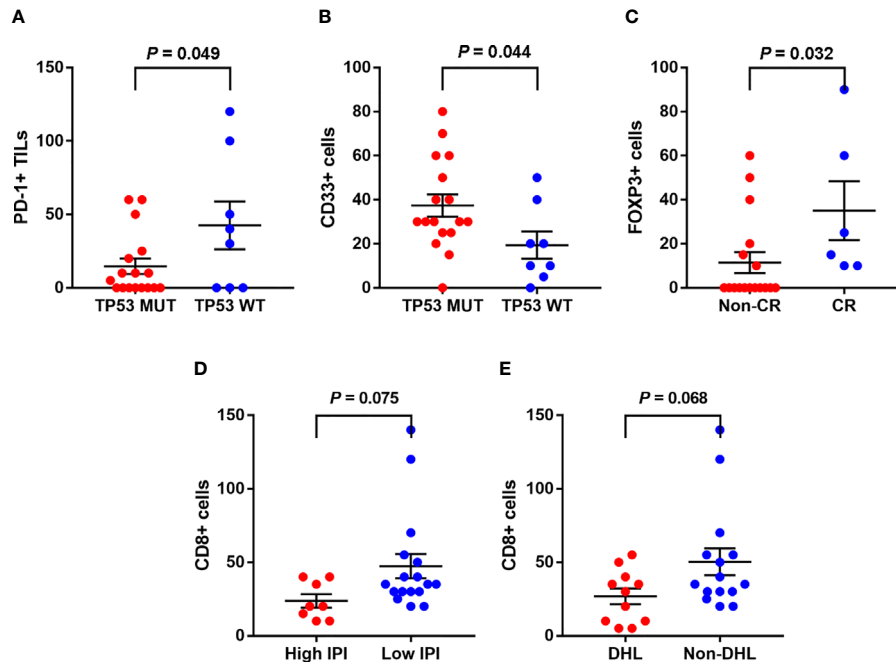


FIGURE 3 | Associations between clinicopathological features and the tumor immune microenvironment markers in A-DLBCL. There were less PD-L1⁺ TILs in TP53 mutant cases than in TP53 wild type cases (A), the result was opposite as to CD33⁺ cells (MDSCs) (B). Patients with less Treg cells ($10.3 \pm 4.5/\text{HPF}$ vs $35 \pm 13.4/\text{HPF}$, $P=0.032$) in TME (FOXP3) ended in non-complete response (CR) to chemotherapy (C). CD8⁺ cells showed a trend of decreasing in number in patients with high International Prognostic Index (IPI) score (D). CD8⁺ cells showed a trend of decreasing in patients with double-hit lymphoma (DHL) (E).

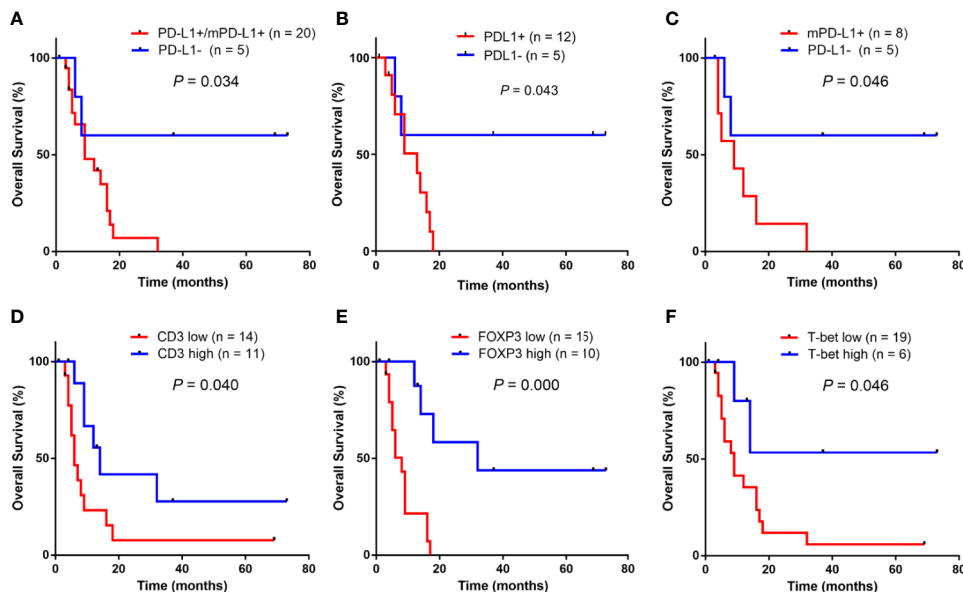


FIGURE 4 | Univariate survival analysis for anaplastic variant of diffuse large B-cell lymphoma in ADLBCL, patients with PD-L1⁺ and/or mPD-L1⁺ (A–C) had a significantly poorer overall survival (OS) than those with PD-L1[−]. An increase in CD3⁺ cell numbers, FOXP3⁺ cells numbers and T-bet⁺ cell numbers were significantly associated with prolonged OS in patients with A-DLBCL was significantly worse than those who tested negative ($P < 0.05$) (C–F).

obvious sinusoidal growth pattern and was not on an inflammatory background.

PD-1 belongs to the B7/CD28 family and is expressed on the surface of activated T and B cells, follicular helper T cells, dendritic cells (DCs), and monocytes. The interaction between PD-1 and its ligand PD-L1 reduces T cell proliferation and cytokine release and inhibits survival proteins (e.g. bcl-xl), which results in apoptosis (21, 26, 27). Non-Hodgkin lymphomas harbor decreased PD-L1 expression with the notable exceptions of nodal diffuse large B-cell lymphoma (DLBCL) and virus-associated lymphoma (28). Retrospective analyses have shown that PD-L1 positivity in tumor cells, as detected by immunohistochemistry, may predict an improved response to anti-PD-1/PD-L1 therapy in melanoma (29), non-small-cell lung carcinoma (30), breast cancer (31), esophageal adenocarcinoma (32), glioblastoma (33), renal cell carcinoma (34), pancreatic carcinoma (35) and urothelial carcinoma (36). Consistent with Kiyasu et al. in DLBCL patients, our findings on A-DLBCL patients also revealed that PD-L1 expression was associated with poor overall survival. In the meantime, we confirmed the consistency of the cases of PD-L1 amplification and PD-L1 overexpression, which suggested that such cytogenetic alteration correlated with increased expression of PD-L1. Overall, these findings indicated that anti-PD-1/PD-L1 therapy could be a novel therapeutic approach for A-DLBCL. mPD-L1⁺ DLBCL is defined as 20% or more PD-L1⁺ nonmalignant cells among the total tissue cellularity in PD-L1⁻ DLBCL. Studies have shown that the prevalence of mPD-L1⁺ DLBCL is approximately 15% in DLBCL (22, 37). Our results told the same story as those DLBCL studies. In addition, patients with PD-L1⁺ and/or mPD-L1⁺ had significantly poorer overall survival (OS) than those with PD-L1⁻ in DLBCL. These results may help explain both tumor escape from host immune surveillance and inhibition of activated T-cells in A-DLBCL.

TIME cells include tumor-infiltrating lymphocytes (TILs), regulatory T cells, and myeloid-derived suppressor cells (MDSCs). Some studies have demonstrated that PD-L1-expressing tumor cells can induce apoptosis in PD-1⁺ tumor-infiltrating lymphocytes (TILs). Others have reported that the quantity of PD-1⁺ TILs is significantly positively correlated not only with PD-L1 expression in tumor cells but also with PD-L1 expression in tumor cells/macrophages. Moreover, the therapeutic response can be affected by several parameters, such as the mutational load of GATA3⁺ cells, FOXP3⁺ cells and CD33⁺ cells and the abundance of TILs in lung cancer or melanoma (38–40). The TP53 gene is mutated in approximately 20% of cases of DLBCL; TP53 mutation predicts poor prognosis (41) and is widely used in clinical evaluation. Patients with more CD3⁺ cells have lower risks of relapse after antitumor treatment. In speaking of FOXP3, the prognostic influence is controversial, reported as being correlated with a good prognosis in some studies or with an adverse outcome in others (42–44). To be detailed, in follicular lymphoma, germinal center-like diffuse large B-cell lymphoma and classical Hodgkin's lymphoma, the increased FOXP3⁺ Treg cells being associated with better OS, while in non-germinal center diffuse large B-cell lymphomas the conclusion is opposite. As we observed a

significantly reduced quantity of PD-1⁺ TILs, an increased quantity of CD33⁺ cells, and a high possibility of non-CR to treatment related to a low quantity of FOXP3⁺ cells in our study, we propose that the prognosis of A-DLBCL is poorer than that of ordinary DLBCL. Accumulating evidence suggests that myeloid-derived suppressor cells (MDSCs) (45, 46) can enhance their inhibitory function to further dampen the T cell mediated antitumor response. In accordance with the observations of Y. Liu et al., our findings may suggest that the antitumor response is inhibited within the malignant node. Although some studies point towards a negative prognostic impact of regulatory T cells in lymphoma (47, 48), it is possible that regulatory T cells directly suppress malignant B cells or counteract tumor-supporting T cells. Moreover, the abundance of Tregs has been proven by research on predictors of progression-free survival (49). In our study, CD3 and FOXP3 were related to opposite outcomes, which deserves further study.

Several studies have used CD163 as an M2 tumor-associated macrophage (TAM) marker and CD68 as a pan macrophage marker (M1+M2) (50–52). Emerging research has shown that M2-like TAMs expressing PD-L1 correspond to the majority of immune cells in DLBCL and may play a role in tumor immune escape, angiogenesis, or matrix remodeling; in addition, a high M2-TAM level at diagnosis may be an unfavorable prognostic factor in DLBCL patients (53). Unfortunately, our data did not show results consistent with those of previous DLBCL studies, and there was no significant difference in M1 and M2 cell quantity between A-DLBCL and ordinary DLBCL ($P=0.461$ and 0.514), which may suggest a less important role for TAMs in A-DLBCL.

T-bet and GATA3 are two transcription factors that determine Th cell differentiation into Th1 or Th2 cells, respectively, and both are expressed in the nuclei of tumor-infiltrating lymphoid cells. Immune balance controlled by Th1 and Th2 cells is critical for protecting the host against pathogenic invasion, while imbalance can cause various immune disorders. We found that the expression of Th1 markers did not show a significant difference in A-DLBCL and ordinary DLBCL ($P=0.394$), while the expression of Th2 markers in A-DLBCL was increased. According to existing reports, increased Th2 marker levels accelerate the secretion of interleukin (IL)-10 and IL-4 and inhibit cellular immune function, and the GATA3/T-bet (G/T) ratio of tumor-infiltrating lymphoid cells is an independent negative predictive marker for survival (54, 55). Overall, our findings verify the elevated G/T ratio in A-DLBCL, in line with studies of gene-expressing profiles in nodal DLBCL, revealing a high number of M2 macrophages in the TIME (56). All of the above findings suggest that there may be an immunosuppressive state in/around the focus in A-DLBCL patients. Moreover, this could be one of the potential mechanisms that explains why the prognosis of A-DLBCL is worse than that of ordinary DLBCL. CD8⁺ T cells are generally thought to play a central role in the antitumor immune response, and the presence of CD8⁺ has been reported as a prognostic factor in cancer (57, 58). Our results showed that a significantly lower level ($P=0.026$) of CD8⁺ T cells existed in A-DLBCL, suggesting an immunosuppressive state within the focus.

The standard therapy for patients with DLBCL contains rituximab, cyclophosphamide, doxorubicin, vincristine, and prednisone(R-CHOP). By such regimen, approximately 60–70% of patients with DLBCL are cured of the disease. However, 30–40% of patients experience disease relapses or, in a small patient subset, are refractory to R-CHOP therapy. The great potential of our recent advances is based on the understanding of the molecular characteristics of DLBCL, and we hope this will be translated into the development of novel, highly effective therapies for patients with A-DLBCL. With the advent of novel targeting agents/regimens, one that specifically targets A-DLBCL will eventually be developed. In addition, our final cohort contains only 30 A-DLBCL cases, which make the results relatively preliminary. Our study requires more cases to make the conclusion closer to the real world.

CONCLUSION

In conclusion, an immunosuppressive state in A-DLBCL may be described by both high levels of PD-L1⁺, mPD-L1⁺, CD33⁺, CD163⁺ and GATA3⁺ cells and low levels of CD8⁺ and PD-1⁺ cells in the TIME; these TIME features could highlight key molecular markers of the prognosis of A-DLBCL, which is poorer than that of ordinary DLBCL. A-DLBCL displays a distinct pattern of tumor immune microenvironment components and checkpoint molecules that distinguish it from ordinary DLBCL. These results could help in understanding the prognosis of A-DLBCL patients and determining therapeutic strategies that target the tumor immune microenvironment.

DATA AVAILABILITY STATEMENT

The original contributions presented in the study are included in the article/**Supplementary Material**. Further inquiries can be directed to the corresponding authors.

REFERENCES

1. Martelli M, Ferreri AJ, Agostinelli C, Di Rocco A, Pfreundschuh M, Pileri SA. Diffuse Large B-Cell Lymphoma. *Crit Rev Oncology/Hematol* (2013) 87:146–71. doi: 10.1016/j.critrevonc.2012.12.009
2. Swerdlow SH, Campo E, Pileri SA, Harris NL, Stein H, Siebert R, et al. The 2016 Revision of the World Health Organization Classification of Lymphoid Neoplasms. *Blood* (2016) 127:2375–90. doi: 10.1182/blood-2016-01-643569
3. Li M, Liu Y, Wang Y, Chen G, Chen Q, Xiao H, et al. Anaplastic Variant of Diffuse Large B-Cell Lymphoma Displays Intricate Genetic Alterations and Distinct Biological Features. *Am J Surg Pathol* (2017) 41:1322–32. doi: 10.1097/PAS.0000000000000836
4. Xu T, Jia Q, Wang Y, Liu Y, Han D, Li P, et al. Rare Cases of Primary Central Nervous System Anaplastic Variant of Diffuse Large B-Cell Lymphoma. *Diagn Pathol* (2019) 14:45. doi: 10.1186/s13000-019-0826-0
5. Hino R, Kabashima K, Kato Y, Yagi H, Nakamura M, Honjo T, et al. Tumor Cell Expression of Programmed Cell Death-1 Ligand 1 Is a Prognostic Factor for Malignant Melanoma. *Cancer* (2010) 116:1757–66. doi: 10.1002/cncr.24899
6. Mu CY, Huang JA, Chen Y, Chen C, Zhang XG. High Expression of PD-L1 in Lung Cancer May Contribute to Poor Prognosis and Tumor Cells Immune

ETHICS STATEMENT

The studies involving human participants were reviewed and approved by Medical Ethics Committee of the First Affiliated Hospital of the Air Force Medical University (Forth Military Medical University). The patients/participants provided their written informed consent to participate in this study.

AUTHOR CONTRIBUTIONS

RL, ML and ZW contributed to the conception of the study; JX and KY performed the experiment; DZ, JM, JC, KW and YL contributed significantly to analysis and manuscript preparation; TX, JC and KW performed the data analyses and wrote the manuscript; QJ contributed greatly to the revised manuscript. YW, LF, QY, SG, GC, QC, HX, FL and CQ helped perform the analysis with constructive discussions. All authors contributed to the article and approved the submitted version.

FUNDING

National Natural Science Foundation of China (81570180).

SUPPLEMENTARY MATERIAL

The Supplementary Material for this article can be found online at: <https://www.frontiersin.org/articles/10.3389/fonc.2021.638154/full#supplementary-material>

Supplementary Table 1 | Detailed Information of Primary Antibodies.

Supplementary Table 2 | Detailed Features of A-DLBCL Cases with PD-L1 Gain.

- Escape Through Suppressing Tumor Infiltrating Dendritic Cells Maturation. *Med Oncol* (2011) 28:682–8. doi: 10.1007/s12032-010-9515-2
7. Rossille D, Gressier M, Damotte D, Maucourt-Boulch D, Pangault C, Semana G, et al. High Level of Soluble Programmed Cell Death Ligand 1 in Blood Impacts Overall Survival in Aggressive Diffuse Large B-Cell Lymphoma: Results From a French Multicenter Clinical Trial. *Leukemia* (2014) 28:2367–75. doi: 10.1038/leu.2014.137
8. Kim JR, Moon YJ, Kwon KS, Bae JS, Wagle S, Kim KM, et al. Tumor Infiltrating PD1-Positive Lymphocytes and the Expression of PD-L1 Predict Poor Prognosis of Soft Tissue Sarcomas. *PloS One* (2013) 8:e82870. doi: 10.1371/journal.pone.0082870
9. Andorsky DJ, Yamada RE, Said J, Pinkus GS, Betting DJ, Timmerman JM. Programmed Death Ligand 1 Is Expressed by Non-Hodgkin Lymphomas and Inhibits the Activity of Tumor-Associated T Cells. *Clin Cancer Res* (2011) 17:4232–44. doi: 10.1158/1078-0432.CCR-10-2660
10. Chen BJ, Chapuy B, Ouyang J, Sun HH, Roemer MG, Xu ML, et al. Pd-L1 Expression Is Characteristic of a Subset of Aggressive B-Cell Lymphomas and Virus-Associated Malignancies. *Clin Cancer Res* (2013) 19:3462–73. doi: 10.1158/1078-0432.CCR-13-0855
11. Lesokhin AM, Ansell SM, Armand P, Scott EC, Halwani A, Gutierrez M, et al. Nivolumab in Patients With Relapsed or Refractory Hematologic Malignancy:

- Preliminary Results of a Phase Ib Study. *J Clin Oncol* (2016) 34:2698–704. doi: 10.1200/JCO.2015.65.9789
12. Armand P, Nagler A, Weller EA, Devine SM, Avigan DE, Chen YB, et al. Disabling Immune Tolerance by Programmed Death-1 Blockade With Pidilizumab After Autologous Hematopoietic Stem-Cell Transplantation for Diffuse Large B-Cell Lymphoma: Results of an International Phase II Trial. *J Clin Oncol* (2013) 31:4199–206. doi: 10.1200/JCO.2012.48.3685
 13. Brahmer JR, Tykodi SS, Chow LQ, Hwu WJ, Topalian SL, Hwu P, et al. Safety and Activity of Anti-PD-L1 Antibody in Patients With Advanced Cancer. *N Engl J Med* (2012) 366:2455–65. doi: 10.1056/NEJMoa1200694
 14. Shain KH, Dalton WS, Tao J. The Tumor Microenvironment Shapes Hallmarks of Mature B-cell Malignancies. *Oncogene* (2015) 34:4673–82. doi: 10.1038/onc.2014.403
 15. Carreras J, Yukie Kikuti Y, Miyaoka M, Hiraiwa S, Tomita S, Ikoma H, et al. Genomic Profile and Pathologic Features of Diffuse Large B-Cell Lymphoma Subtype of Methotrexate-Associated Lymphoproliferative Disorder in Rheumatoid Arthritis Patients. *Am J Surg Pathol* (2018) 42:936–50. doi: 10.1097/PAS.0000000000001071
 16. Kim TS, da Silva E, Coit DG, Tang LH. Intratumoral Immune Response to Gastric Cancer Varies by Molecular and Histologic Subtype. *Am J Surg Pathol* (2019) 43:851–60. doi: 10.1097/PAS.0000000000001253
 17. Burger JA, Gribben JG. The Microenvironment in Chronic Lymphocytic Leukemia (CLL) and Other B Cell Malignancies: Insight Into Disease Biology and New Targeted Therapies. *Semin Cancer Biol* (2014) 24:71–81. doi: 10.1016/j.semcancer.2013.08.011
 18. Scott DW, Steidl C. The Classical Hodgkin Lymphoma Tumor Microenvironment: Macrophages and Gene Expression-Based Modeling. *Hematol Am Soc Hematol Educ Program* (2014) 2014:144–50. doi: 10.1182/asheducation-2014.1.144
 19. Hans CP, Weisenburger DD, Greiner TC, Gascoyne RD, Delabie J, Ott G, et al. Confirmation of the Molecular Classification of Diffuse Large B-Cell Lymphoma by Immunohistochemistry Using a Tissue Microarray. *Blood* (2004) 103:275–82. doi: 10.1182/blood-2003-05-1545
 20. Choi WW, Weisenburger DD, Greiner TC, Piris MA, Banham AH, Delabie J, et al. A New Immunostain Algorithm Classifies Diffuse Large B-Cell Lymphoma Into Molecular Subtypes With High Accuracy. *Clin Cancer Res* (2009) 15:5494–502. doi: 10.1158/1078-0432.CCR-09-0113
 21. Llosa NJ, Cruise M, Tam A, Wicks EC, Hechenbleikner EM, Taube JM, et al. The Vigorous Immune Microenvironment of Microsatellite Instable Colon Cancer Is Balanced by Multiple Counter-Inhibitory Checkpoints. *Cancer Discov* (2015) 5:43–51. doi: 10.1158/2159-8290.CD-14-0863
 22. Kiyasu J, Miyoshi H, Hirata A, Arakawa F, Ichikawa A, Niino D, et al. Expression of Programmed Cell Death Ligand 1 is Associated With Poor Overall Survival in Patients With Diffuse Large B-cell Lymphoma. *Blood* (2015) 126:2193–201. doi: 10.1182/blood-2015-02-629600
 23. Carreras J, Lopez-Guillermo A, Fox BC, Colomo L, Martinez A, Roncador G, et al. High Numbers of Tumor-Infiltrating FOXP3-Positive Regulatory T Cells Are Associated With Improved Overall Survival in Follicular Lymphoma. *Blood* (2006) 108:2957–64. doi: 10.1182/blood-2006-04-018218
 24. Georgiou K, Chen L, Berglund M, Ren W, de Miranda NF, Lisboa S, et al. Genetic Basis of PD-L1 Overexpression in Diffuse Large B-Cell Lymphomas. *Blood* (2016) 127:3026–34. doi: 10.1182/blood-2015-12-686550
 25. Sarkozy C, Copie-Bergman C, Damotte D, Ben-Neriah S, Burroni B, Cornillon J, et al. Gray-Zone Lymphoma Between cHL and Large B-Cell Lymphoma: A Histopathologic Series From the LYSA. *Am J Surg Pathol* (2019) 43:341–51. doi: 10.1097/PAS.0000000000001198
 26. Xiao Y, Freeman GJ. The Microsatellite Instable Subset of Colorectal Cancer Is a Particularly Good Candidate for Checkpoint Blockade Immunotherapy. *Cancer Discov* (2015) 5:16–8. doi: 10.1158/2159-8290.CD-14-1397
 27. Leng C, Li Y, Qin J, Ma J, Liu X, Cui Y, et al. Relationship Between Expression of PD-L1 and PD-L2 on Esophageal Squamous Cell Carcinoma and the Antitumor Effects of CD8(+) T Cells. *Oncol Rep* (2016) 35:699–708. doi: 10.3892/or.2015.4435
 28. Xu-Monette ZY, Zhou J, Young KH. PD-1 Expression and Clinical PD-1 Blockade in B-Cell Lymphomas. *Blood* (2018) 131:68–83. doi: 10.1182/blood-2017-07-740993
 29. Oba J, Nakahara T, Abe T, Hagihara A, Moroi Y, Furue M. Expression of Programmed Death Receptor Ligand 1 in Melanoma May Indicate Tumor Progression and Poor Patient Survival. *J Am Acad Dermatol* (2014) 70:954–6. doi: 10.1016/j.jaad.2014.01.880
 30. Chen YB, Mu CY, Huang JA. Clinical Significance of Programmed Death-1 Ligand-1 Expression in Patients With Non-Small Cell Lung Cancer: A 5-Year-Follow-Up Study. *Tumori* (2012) 98:751–5. doi: 10.1177/030089161209800612
 31. Ghebeh H, Mohammed S, Al-Omair A, Qattan A, Lehe C, Al-Qudaihi G, et al. The B7-H1 (Pd-L1) T Lymphocyte-Inhibitory Molecule is Expressed in Breast Cancer Patients With Infiltrating Ductal Carcinoma: Correlation With Important High-Risk Prognostic Factors. *Neoplasia* (2006) 8:190–8. doi: 10.1593/neo.05733
 32. Ohigashi Y, Sho M, Yamada Y, Tsurui Y, Hamada K, Ikeda N, et al. Clinical Significance of Programmed Death-1 Ligand-1 and Programmed Death-1 Ligand-2 Expression in Human Esophageal Cancer. *Clin Cancer Res* (2005) 11:2947–53. doi: 10.1158/1078-0432.CCR-04-1469
 33. Nduom EK, Wei J, Yaghi NK, Huang N, Kong LY, Gabrusiewicz K, et al. Pd-L1 Expression and Prognostic Impact in Glioblastoma. *Neuro Oncol* (2016) 18:195–205. doi: 10.1093/neuonc/nov172
 34. Thompson RH, Dong H, Kwon ED. Implications of B7-H1 Expression in Clear Cell Carcinoma of the Kidney for Prognostication and Therapy. *Clin Cancer Res* (2007) 13:709s–15s. doi: 10.1158/1078-0432.CCR-06-1868
 35. Nomi T, Sho M, Akahori T, Hamada K, Kubo A, Kanehiro H, et al. Clinical Significance and Therapeutic Potential of the Programmed Death-1 Ligand/Programmed Death-1 Pathway in Human Pancreatic Cancer. *Clin Cancer Res* (2007) 13:2151–7. doi: 10.1158/1078-0432.CCR-06-2746
 36. Nakanishi J, Wada Y, Matsumoto K, Azuma M, Kikuchi K, Ueda S. Overexpression of B7-H1 (Pd-L1) Significantly Associates With Tumor Grade and Postoperative Prognosis in Human Urothelial Cancers. *Cancer Immunol Immunother CII* (2007) 56:1173–82. doi: 10.1007/s00262-006-0266-z
 37. Kwon D, Kim S, Kim PJ, Go H, Nam SJ, Paik JH, et al. Clinicopathological Analysis of Programmed Cell Death 1 and Programmed Cell Death Ligand 1 Expression in the Tumour Microenvironments of Diffuse Large B Cell Lymphomas. *Histopathology* (2016) 68:1079–89. doi: 10.1111/his.12882
 38. Taube JM, Anders RA, Young GD, Xu H, Sharma R, McMiller TL, et al. Colocalization of Inflammatory Response With B7-h1 Expression in Human Melanocytic Lesions Supports an Adaptive Resistance Mechanism of Immune Escape. *Sci Trans Med* (2012) 4:127ra37. doi: 10.1126/scitranslmed.3003689
 39. Teng MW, Ngiew SF, Ribas A, Smyth MJ. Classifying Cancers Based on T-Cell Infiltration and PD-L1. *Cancer Res* (2015) 75:2139–45. doi: 10.1158/0008-5472.CAN-15-0255
 40. Topalian SL, Taube JM, Anders RA, Pardoll DM. Mechanism-Driven Biomarkers to Guide Immune Checkpoint Blockade in Cancer Therapy. *Nat Rev Cancer* (2016) 16:275–87. doi: 10.1038/nrc.2016.36
 41. Young KH, Weisenburger DD, Dave BJ, Smith L, Sanger W, Iqbal J, et al. Mutations in the DNA-binding Codons of TP53, Which Are Associated With Decreased Expression of TRAILreceptor-2, Predict for Poor Survival in Diffuse Large B-Cell Lymphoma. *Blood* (2007) 110:4396–405. doi: 10.1182/blood-2007-02-072082
 42. Tzankov A, Meier C, Hirschmann P, Went P, Pileri SA, Dirnhofer S. Correlation of High Numbers of Intratumoral FOXP3+ Regulatory T Cells With Improved Survival in Germinal Center-Like Diffuse Large B-Cell Lymphoma, Follicular Lymphoma and Classical Hodgkin's Lymphoma. *Haematologica* (2008) 93:193–200. doi: 10.3324/haematol.11702
 43. Lee NR, Song EK, Jang KY, Choi HN, Moon WS, Kwon K, et al. Prognostic Impact of Tumor Infiltrating FOXP3 Positive Regulatory T Cells in Diffuse Large B-Cell Lymphoma at Diagnosis. *Leukemia Lymphoma* (2008) 49:247–56. doi: 10.1080/10428190701824536
 44. Hasselblom S, Sigurdadottir M, Hansson U, Nilsson-Ehle H, Ridell B, Andersson PO. The Number of Tumour-Infiltrating TIA-1+ Cytotoxic T Cells But Not FOXP3+ Regulatory T Cells Predicts Outcome in Diffuse Large B-Cell Lymphoma. *Br J Haematol* (2007) 137:364–73. doi: 10.1111/j.1365-2141.2007.06593.x
 45. Liu Y, Yu Y, Yang S, Zeng B, Zhang Z, Jiao G, et al. Regulation of Arginase I Activity and Expression by Both PD-1 and CTLA-4 on the Myeloid-Derived Suppressor Cells. *Cancer Immunol Immunother CII* (2009) 58:687–97. doi: 10.1007/s00262-008-0591-5
 46. Liu Y, Zeng B, Zhang Z, Zhang Y, Yang R. B7-H1 on Myeloid-Derived Suppressor Cells in Immune Suppression by a Mouse Model of Ovarian Cancer. *Clin Immunol* (2008) 129:471–81. doi: 10.1016/j.clim.2008.07.030
 47. Yang ZZ, Novak AJ, Stenson MJ, Witzig TE, Ansell SM. Intratumoral CD4 +CD25+ Regulatory T-Cell-Mediated Suppression of Infiltrating CD4+ T

- Cells in B-cell non-Hodgkin Lymphoma. *Blood* (2006) 107:3639–46. doi: 10.1182/blood-2005-08-3376
48. Galani IE, Wendel M, Stojanovic A, Jesiak M, Muller MM, Schellack C, et al. Regulatory T Cells Control Macrophage Accumulation and Activation in Lymphoma. *Int J Cancer* (2010) 127:1131–40. doi: 10.1002/ijc.25132
 49. Coutinho R, Clear AJ, Mazzola E, Owen A, Greaves P, Wilson A, et al. Revisiting the Immune Microenvironment of Diffuse Large B-cell Lymphoma Using a Tissue Microarray and Immunohistochemistry: Robust Semi-Automated Analysis Reveals CD3 and FoxP3 as Potential Predictors of Response to R-CHOP. *Haematologica* (2015) 100:363–9. doi: 10.3324/haematol.2014.110189
 50. Nam SJ, Go H, Paik JH, Kim TM, Heo DS, Kim CW, et al. An Increase of M2 Macrophages Predicts Poor Prognosis in Patients With Diffuse Large B-Cell Lymphoma Treated With Rituximab, Cyclophosphamide, Doxorubicin, Vincristine and Prednisone. *Leukemia Lymphoma* (2014) 55:2466–76. doi: 10.3109/10428194.2013.879713
 51. Hu H, Hang JJ, Han T, Zhuo M, Jiao F, Wang LW. The M2 Phenotype of Tumor-Associated Macrophages in the Stroma Confers a Poor Prognosis in Pancreatic Cancer. *Tumour Biol* (2016) 37:8657–64. doi: 10.1007/s13277-015-4741-z
 52. Elliott LA, Doherty GA, Sheahan K, Ryan EJ. Human Tumor-Infiltrating Myeloid Cells: Phenotypic and Functional Diversity. *Front Immunol* (2017) 8:86. doi: 10.3389/fimmu.2017.00086
 53. Menguy S, Prochazkova-Carlotti M, Beylot-Barry M, Saltel F, Vergier B, Merlio JP, et al. PD-L1 and PD-L2 Are Differentially Expressed by Macrophages or Tumor Cells in Primary Cutaneous Diffuse Large B-Cell Lymphoma, Leg Type. *Am J Surg Pathol* (2018) 42:326–34. doi: 10.1097/PAS.0000000000000983
 54. Michel G, Mirmohammadsadeh A, Olasz E, Jarzebska-Deussen B, Muschen A, Kemeny L, et al. Demonstration and Functional Analysis of IL-10 Receptors in Human Epidermal Cells: Decreased Expression in Psoriatic Skin, Down-Modulation by IL-8, and Up-Regulation by an Antipsoriatic Glucocorticosteroid in Normal Cultured Keratinocytes. *J Immunol* (1997) 159:6291–7.
 55. De Monte L, Reni M, Tassi E, Clavenna D, Papa I, Recalde H, et al. Intratumor T Helper Type 2 Cell Infiltrate Correlates With Cancer-Associated Fibroblast Thymic Stromal Lymphopoietin Production and Reduced Survival in Pancreatic Cancer. *J Exp Med* (2011) 208:469–78. doi: 10.1084/jem.20101876
 56. Liu C, Sun C, Huang H, Janda K, Edgington T. Overexpression of Legumain in Tumors Is Significant for Invasion/Metastasis and a Candidate Enzymatic Target for Prodrug Therapy. *Cancer Res* (2003) 63:2957–64.
 57. Cho Y, Miyamoto M, Kato K, Fukunaga A, Shichinohe T, Kawarada Y, et al. CD4+ and CD8+ T Cells Cooperate to Improve Prognosis of Patients With Esophageal Squamous Cell Carcinoma. *Cancer Res* (2003) 63:1555–9.
 58. Schumacher K, Haensch W, Roefzaad C, Schlag PM. Prognostic Significance of Activated CD8(+) T Cell Infiltrations Within Esophageal Carcinomas. *Cancer Res* (2001) 61:3932–6.

Conflict of Interest: The authors declare that the research was conducted in the absence of any commercial or financial relationships that could be construed as a potential conflict of interest.

Copyright © 2021 Xu, Chai, Wang, Jia, Liu, Wang, Xu, Yu, Zhao, Ma, Fan, Yan, Guo, Chen, Chen, Xiao, Liu, Qi, Liang, Li and Wang. This is an open-access article distributed under the terms of the Creative Commons Attribution License (CC BY). The use, distribution or reproduction in other forums is permitted, provided the original author(s) and the copyright owner(s) are credited and that the original publication in this journal is cited, in accordance with accepted academic practice. No use, distribution or reproduction is permitted which does not comply with these terms.



Hypoxia-Related Gene FUT11 Promotes Pancreatic Cancer Progression by Maintaining the Stability of PDK1

Wenpeng Cao^{1*}, Zhirui Zeng^{2†}, Runsang Pan^{3†}, Hao Wu⁴, Xiangyan Zhang⁵, Hui Chen⁵, Yingjie Nie⁶, Zijiang Yu^{1*} and Shan Lei^{2*}

¹ Department of Anatomy, School of Basic Medicine, Guizhou Medical University, Guiyang, China, ² Department of Physiology, School of Basic Medicine, Guizhou Medical University, Guiyang, China, ³ Department of Orthopedics, Guiyang Maternal and Child Health Care Hospital, Guiyang, China, ⁴ Department of Pediatric Surgery, The Affiliated Hospital of Guizhou Medical University, Guiyang, China, ⁵ NHC Key Laboratory of Pulmonary, Guizhou Provincial People's Hospital, Guiyang, China, ⁶ The Clinical Lab Center, Guizhou Provincial People's Hospital, Guiyang, China

OPEN ACCESS

Edited by:

Wei Zhao,
City University of Hong Kong,
Hong Kong

Reviewed by:

Tongzheng LIU,
Jinan University, China
Chenxi Zhang,
Nanjing Chest Hospital, China

*Correspondence:

Wenpeng Cao
1006074061@qq.com
Zijiang Yu
893767473@qq.com
Shan Lei
1109974497@qq.com

[†]These authors have contributed
equally to this work

Specialty section:

This article was submitted to
Molecular and Cellular Oncology,
a section of the journal
Frontiers in Oncology

Received: 04 March 2021

Accepted: 27 May 2021

Published: 17 June 2021

Citation:

Cao W, Zeng Z, Pan R,
Wu H, Zhang X, Chen H, Nie Y,
Yu Z and Lei S (2021) Hypoxia-
Related Gene FUT11 Promotes
Pancreatic Cancer Progression by
Maintaining the Stability of PDK1.
Front. Oncol. 11:675991.
doi: 10.3389/fonc.2021.675991

Background: Hypoxia is associated with the development of pancreatic cancer (PC). However, genes associated with hypoxia response and their regulatory mechanism in PC cells were unclear. The current study aims to investigate the role of the hypoxia associated gene fucosyltransferase 11 (FUT11) in the progression of PC.

Methods: In the preliminary study, bioinformatics analysis predicted FUT11 as a key hypoxia associated gene in PC. The expression of FUT11 in PC was evaluated using quantitative real-time PCR (qRT-PCR), Western blot and immunohistochemistry. The effects of FUT11 on PC cells proliferation and migration under normoxia and hypoxia were evaluated using Cell Counting Kit 8, 5-ethynyl-2'-deoxyuridine (EDU) assay, colony formation assay and transwell assay. The effects of FUT11 *in vivo* was examined in mouse tumor models of liver metastasis and subcutaneous xenograft. Furthermore, Western blot, luciferase assay and immunoprecipitation were performed to explore the regulatory relationship among FUT11, hypoxia-inducible factor 1 α (HIF1 α) and pyruvate dehydrogenase kinase 1 (PDK1) in PC.

Results: FUT11 was markedly increased of PC cells with hypoxia, upregulated in the PC clinical tissues, and predicted a poor outcome of PC patients. Inhibition of FUT11 reduced PC cell growth and migratory ability of PC cells under normoxia and hypoxia conditions *in vitro*, and growth and tumor cell metastasis *in vivo*. FUT11 bound to PDK1 and regulated the expression PDK1 under normoxia and hypoxia. FUT11 interacted with PDK1 and decreased the ubiquitination of PDK1, lead to the activation of AKT/mTOR signaling pathway. FUT11 knockdown significantly increased the degradation of PDK1 under hypoxia, while treatment with MG132 can relieve the degradation of PDK1 induced by FUT11 knockdown. Overexpression of PDK1 in PC cells under hypoxia conditions reversed the suppressive impacts of FUT11 knockdown on PC cell growth and migration. In addition, HIF1 α bound to the promoter of FUT11 and increased its

expression, as well as co-expressed with FUT11 in PC tissues. Furthermore, overexpression of FUT11 partially rescued the suppressive effects of HIF1 α knockdown on PC cell growth and migration in hypoxia condition.

Conclusion: Our data implicate that hypoxia-induced FUT11 contributes to proliferation and metastasis of PC by maintaining the stability of PDK1, thus mediating activation of AKT/mTOR signaling pathway, and suggest that FUT11 could be a novel and effective target for the treatment of pancreatic cancer.

Keywords: pancreatic cancer, hypoxia, fucosyltransferase 11, hypoxia-inducible factor 1 α , pyruvate dehydrogenase kinase 1

BACKGROUND

Pancreatic cancer (PC) has high morbidity and mortality worldwide (1). Although the treatment for PC such as surgery, targeted therapy and chemotherapy had been improved, the number of PC related mortality is still increasing every year (2). Therefore, it is a pressing need to uncover the molecular mechanism involved in PC and explore the potential biomarkers for diagnosis and as novel targets for treatment of PC.

The tumor microenvironment plays a vital role in the development of tumors and is closely related to the efficacy of tumor treatment. Targeting the tumor environment is a therapeutic strategy for cancer treatment (3). Generally, hypoxic microenvironment of tumors up-regulates a series of hypoxic-responsive genes, and induces the proliferation, migration, drug resistance and other biological events of cancer cells (4). Hypoxia inducible factor 1- α (HIF1 α) is a main regulator of transcriptional response to hypoxia in cancer cells. HIF1 α up-regulates a number of genes that support tumor cells to adopt to the hypoxic microenvironment (5). HIF1 α overexpression has been detected in solid tumors and is associated with the progression of a variety of cancers, including ovarian cancer (6), breast cancer (7), non-small cell lung cancer (8) and pancreatic cancer (9). Studies have shown that HIF1 α affects the regulation of tumor cell proliferation, angiogenesis, apoptosis and chemotherapy resistance during tumor development (10). However, the target genes of HIF1 α in PC remain to be elucidated.

Fucosyltransferases (FUTs) are a family of enzymes which catalyzed the transfer process of fucose from GDP-fucose to glycoconjugates (11). Previous studies have demonstrated that the FUT family is closely related to the occurrence and development of tumors. Liang et al. demonstrated that miR-125a-3p/FUT5-FUT6 axis mediates the proliferation, mobility and pathological angiogenesis of colorectal cancer through the PI3K-Akt pathway (12). Kumar et al. showed that NCOA3 stabilized mucins post translationally through FUT8, which promoted the proliferation and metastasis of pancreatic cancer (13). Lin et al. reported that FUT11 and FUT1 genes were down-regulated in cisplatin-resistant cells (14). However, the functions and regulatory mechanisms of FUT11 in PC remain largely unclear.

In this study, we found that the FUT11 was a direct target gene of HIF1 α by bioinformatics analysis and it was up-regulated in PC cells under hypoxia. FUT11 promoted the proliferation and metastasis of PC cells *via* maintaining the stability of pyruvate dehydrogenase kinase 1 (PDK1) under hypoxia. Our study indicates FUT11 could be a therapeutic target for the treatment of PC.

METHODS

Bioinformatics Analysis

We downloaded the Gene expression profile GSE67549 and GSE9350 from the Gene Expression Omnibus database (GEO, <https://www.ncbi.nlm.nih.gov/gds>). GSE67549 contained 9 normoxic PC cell samples and 9 hypoxic PC cell samples, while GSE9350 contained 2 normoxic PC cell samples and 2 hypoxic PC cell samples. Differential expression genes were identified using the cut-off as Log2 fold change (FC) >1 and P value <0.05. Common differential expression genes were analyzed using intersection analysis. The expression of these genes in the PC samples of The Cancer Genome Atlas (TCGA) and The Genotype-Tissue Expression (GTEx) database was determined using GEPIA (<http://gepia.cancer-pku.cn/>). $P < 0.05$ was a threshold to be considered as statistically significant.

Clinical Samples

A total of 90 paired PC tissues and adjacent pancreatic tissues were obtained from PC patients who had surgery in the Affiliated Hospital of Guizhou Medical University. None of them received radiotherapy or chemotherapy prior to the surgery. The current study was approved by the Ethics Committee of Guizhou Medical University in accordance with the Declaration of Helsinki, and all patients who participated in the current study signed their informed consents.

Cell Culture and Transfection

Two human PC cell lines (PANC-1 and AsPC-1) used in the current study were obtained from ATCC. PANC-1 and AsPC-1 cells were cultured in DMEM with 10% FBS at 37°C with 5% CO₂. The condition of normoxia was set to 21% O₂, 74% N₂ and

5% CO₂, while the condition of hypoxia was set to 1%O₂, 94%N₂ and 5%CO₂. Oligonucleotides targeting FUT11 (GUUAGAGA CCACUGUAUCUGC) were cloned into the pLKO.1 vector (GenePharma, Shanghai, China). Full-length PDK1 coding sequence was subcloned into the lentiviral vector pCD315B-1 (System Biosciences, Beijing, China). The small interfering RNA (siRNA) targeting HIF1 α were obtained from JIMA (Shanghai, China). To construct the stable cell lines with target gene overexpression or knockdown, 1 μ g/mL puromycin (Sigma, USA) was added to culture medium after transfection with lentivirus for 48h to continuously screen the stable cells for 10 days.

Quantitative Real-Time PCR (qRT-PCR)

Total RNA in PC tissues and cells was separated using TRIZOL reagents (Beyotime Biotechnology, Hangzhou, China) and diluted into DNase/RNase-free water. After quantification, total RNA (2 μ g per sample) was reversely transcribed into cDNA using RevertAid First Strand cDNA Synthesis Kit (Fermentas, USA). Finally, quantitative real-time PCR (qRT-PCR) was conducted to determine the expression level of target genes using SYBRTM Green PCR Master Mix (Solarbio, Wuhan, China). β -actin was used as the internal control. The primer sequences in our study were purchased from Tianyi Huiyuan (Wuhan, China) and shown in **Supplementary Table 1**.

Cell Counting Kit-8 (CCK-8) Assay

PANC-1 and AsPC-1 cells were plated in a 96-well plate in sextuplicate with 3×10^3 cells/well. Briefly, 100 μ l DMEM medium containing 10 μ l CCK-8 reagent (Boster, Wuhan, China) was added to each well in 24h, 48h, 72h and 96h. The light absorbance of each well was detected at 450nm.

5-ethynyl-2'-deoxyuridine (EDU) Assay

The EDU assay was carried out using a BeyoClickTM EdU-488 Proliferation Detection Kit (Beyotime, Suzhou, China). In brief, PC cells were cultured in 6-well plates and were allowed to adhere. The primary culture medium was removed and fresh medium was added. Then, 10 μ M EDU was added into each well and cells were cultured in 37°C for 2.5h. After that, cells were fixed in 4% paraformaldehyde (Beyotime, Suzhou, China) for 15 min and permeabilization using 0.3% Triton X-100 (Boster, Wuhan, China) for 8 min. Then, 500 μ l Apollo dyeing reaction buffer was added for 40 min in the dark. After staining, the nuclei were stained using DAPI for 10 min. The EDU staining was observed under a fluorescence microscope (Zeiss, Oberkochen, Germany).

Colony Formation Assay

Cells with a density of 2000 cells/well were seeded into 6-well plates and cultured in DMEM media containing 10% FBS. After 24h, intervention factor was added and cultured for 2 weeks. After fixation in 4% paraformaldehyde for 15 min, 1% crystal violet was used to stain cell colonies. Cell colonies was counted and photographed.

Western Blotting

The proteins in PC cells and tissues were extracted using RIPA reagent contain 5% PMSF protease inhibitor. The BCA method was performed to examine the protein concentration of each sample. Proteins (30 μ g/per line) were added and separated by 10% SDS-PAGE for 120 min. Then, the proteins were transferred into the PVDF membranes (Millipore, USA) with 0.45 μ m pore diameter, which was then blocked in 5% BSA for 30min and incubated with primary antibodies including FUT11 (Abcam, cat. no. ab121411, dilution, 1:500), N-cadherin (CST, cat. no. 14215, dilution, 1:1000), E-cadherin (CST, cat. no. 3195, dilution, 1:1000), PDK1 (Santa, cat. no. 4A11F5, dilution, 1:1000), AKT (CST, cat. no. 9272, dilution, 1:1000), p-AKT (CST, cat. no. 9271, dilution, 1:1000), mTOR (CST, cat. no. 2972, dilution, 1:1000), p-mTOR (CST, cat. no. 2971, dilution, 1:1000), HIF1 α (CST, cat. no. 36169, dilution, 1:1000) and β -actin (CST, cat. no. 3700, dilution, 1:1000) for 12h in 4°C. High sensitivity ECL reagent was used to visualize the blots in MultiImager and the relative expression of protein was calculated using Image J. β -actin was set as reference for FUT11, N-cadherin, E-cadherin, PDK1 and HIF1 α .

Transwell Assay

For transwell migration assay, a total of 1×10^5 cells were suspended using 200 μ l DMEM medium without FBS and seeded into the upper transwell chambers (Becton, Dickinson and Company, USA). Total 600 μ l DMEM medium contained 10% FBS was placed in the lower transwell chambers. After 24h, migratory cells were fixed with paraformaldehyde and stained using 0.5% crystal violet. Finally, the migratory cells were counted and photos were taken.

In Vivo Assay

For subcutaneous tumor xenograft model, 10 female BALB/c nude mice were obtained from the animal central of Guizhou Medical University (Guizhou, China). After adaptive feeding, a total of 1×10^6 PANC-1 cells with FUT11 knockdown and negative control cells were subcutaneously injected into the upper-right flank of BALB/c mice ($n = 5$ in each group). The health status of mice was monitored every day. The tumor volume was monitored once a week and determined as followed: (mm³) = (Long \times Width²)/2. After 5 weeks, the mice were sacrificed and tumor tissues collected. The protein level of KI67 and PCNA in tumor tissues was determined using immunohistochemical staining. The liver metastatic tumor model was established by injecting the FUT11 knockdown and negative control PANC-1 cells into the spleen capsule. FUT11 knockdown and negative control group PANC-1 cells (1×10^7 cells) were injected into the spleen of BALB/c mice ($n=5$ in each group). Animal health and behavior after injecting were monitored each day. While the mouse had the features of hard breath and limitation of motion, mice were sacrificed in order to reduce animal suffering, and the liver tissues were dissected and used to count the metastatic foci. While mice in one group were all sacrificed, the animal experiment was terminated and the rest

of mice were all euthanasia. Finally, unpaired *t*-test was used to determine the significant between this group according to the number of metastasis foci. HE staining was also used to detect the condition of metastatic foci in the liver. All procedures of animal studies were approved by the Ethics Committee of Guizhou Medical University and followed the legal mandates and national guidelines for the care and maintenance of laboratory animals.

Immunofluorescence Staining

Cells were fixed with 4% paraformaldehyde (Solarbio, Wuhan, China) for 15 min. Then, the samples were incubated with anti-FUT11 (dilution, 1:100), anti-N-cadherin (dilution, 1:100), anti-E-cadherin (dilution, 1:100), anti-HIF1 α (dilution, 1:100) and anti-PDK1 (dilution, 1:100) primary antibodies. After washing with PBS, the samples were incubated with FITC conjugated anti-mouse secondary antibodies (Proteintech, Wuhan, China) and Cy3 conjugated anti-rabbit secondary antibodies (Proteintech, Wuhan, China). Nuclei were stained with DAPI (Boster, Wuhan, China). Finally, confocal microscopy or fluorescent microscope was used to collect the images.

Immunoprecipitation

Cells were lysed in weak RIPA buffer (Proteintech, Wuhan, China) that included a 1% PMSF (Boster, Wuhan, China). The supernatant was centrifuged and the protein was collected. Then, the anti-FUT11 (dilution, 1:50) antibody and IgG (dilution, 1:50; Beyotime Biotechnology, Hangzhou, China) was added for 6 h. The A/G agarose beads (Boster, Wuhan, China) was added for 3 h. After washing by PBS three times, isolated immunoprecipitates in beads were collected and analyzed using Western blot.

Mass Spectrometry

Immunoprecipitation strips were cut into different strips and digested with trypsin. After reductive alkylation, trypsin with mass ratio of 1:50 was added and hydrolyzed at 37°C for 20 h. After desalination, the enzymatic hydrolysate was lyophilized and re-dissolved in 0.1% formic acid solution. Mascot algorithm was used to process MS/MS signals. Parameters included variable modification, oxidation (MET), N-acetylation, and hot glutamine (Gln). Maximum leak, peptide quality tolerance, MS/MS tolerance was 0.5 Da. Proteins were identified on the basis of MS/MS data signals with at least one mascot score exceeding the threshold.

Chromatin Immunoprecipitation

Chromatin immunoprecipitation (ChIP) assays were performed using a ChIP kit (CST, USA) as per the protocol provided by the manufacturer. Briefly, formaldehyde was used to crosslink cells, and the DNA was sonicated to produce sequences of 200–500 bp in length. Immunoprecipitation was conducted using an anti-HIF1 α antibody or IgG control. The precipitated DNA was amplified by qRT-PCR.

Luciferase Assay

After predicting the binding site of HIF1 α (also named hypoxia response element, HRE) in the promoter of FUT11 using online database JASPAR (<http://jaspar.binf.ku.dk/>), dual luciferase reporter assay was performed to verify the bind. Full-length FUT11 promoter sequence and corresponding truncated fragment without HRE were carried into the psi-basic luciferase reporter vector (Promega, USA). Finally, a total of 1×10^4 PANC-1 and AsPC-1 cells were plated into 24-well plate and cultured overnight at 37°C. Then, both of luciferase reporter vectors contained full-length FUT11 promoter sequence and corresponding truncated fragment without HRE, and the si-HIF1 α /si-NC were co-transfected into PC cells using liposome 2000 (Solarbio, Wuhan, China). The luciferase activity of cells was determined after transfection at 24 h in PC cells cultured in normoxia or hypoxia.

Statistical Analysis

SPSS software (version 21.0) was employed to perform statistical analysis. The difference between two groups was analyzed using paired *t*-test, while the difference among multiple groups were determined based on one-way analysis of variance. $P < 0.05$ was used as a cut-off to consider statistical significance.

RESULTS

FUT11 Is a Crucial Hypoxia-Related Gene and Up-Regulated in PC Tissues

To identify the key hypoxia-related genes, two gene data profile of PC cells (GSE67549 and GSE9350) under normoxia and hypoxia was analyzed. The results showed that there were 18 common genes differentially expressed in PC cells in hypoxia compared with that in normoxia (**Figure 1A**). Among them, the mRNA levels of ADM, C4orf3, ERO1L, FUT11, BNIP3L, NDRG1, KCTD11, SLC2A1, and P4HA1 were increased in pancreatic cancer tissues compared to adjacent pancreatic tissues from TCGA and GTEx database (**Figure 1B**). These 9 genes were considered as key hypoxia-related genes that involved in the progression of PC. We confirmed this result in the AsPC-1 and PANC-1 cells under normoxia and hypoxia. It was found that all the mRNA levels of these 9 genes were increased under hypoxia compared with normoxia. Among them, a gene named FUT11 increased the most (>3 fold) in AsPC-1 and PANC-1 cells under hypoxia (**Figure 2A**).

We then evaluated the mRNA and protein levels of FUT11 in human PC tissues and adjacent pancreatic tissues. The results showed that the mRNA and protein levels of FUT11 was higher in pancreatic cancer tissues than that in adjacent pancreatic tissues (**Figures 2B–D**). We analyzed the correlation between FUT11 expression and the PC clinical pathology features, and found that FUT11 expression was positively correlated with tumor size (cm), lymph node metastasis, TNM stage, perineural invasion, blood vessel invasion and distant

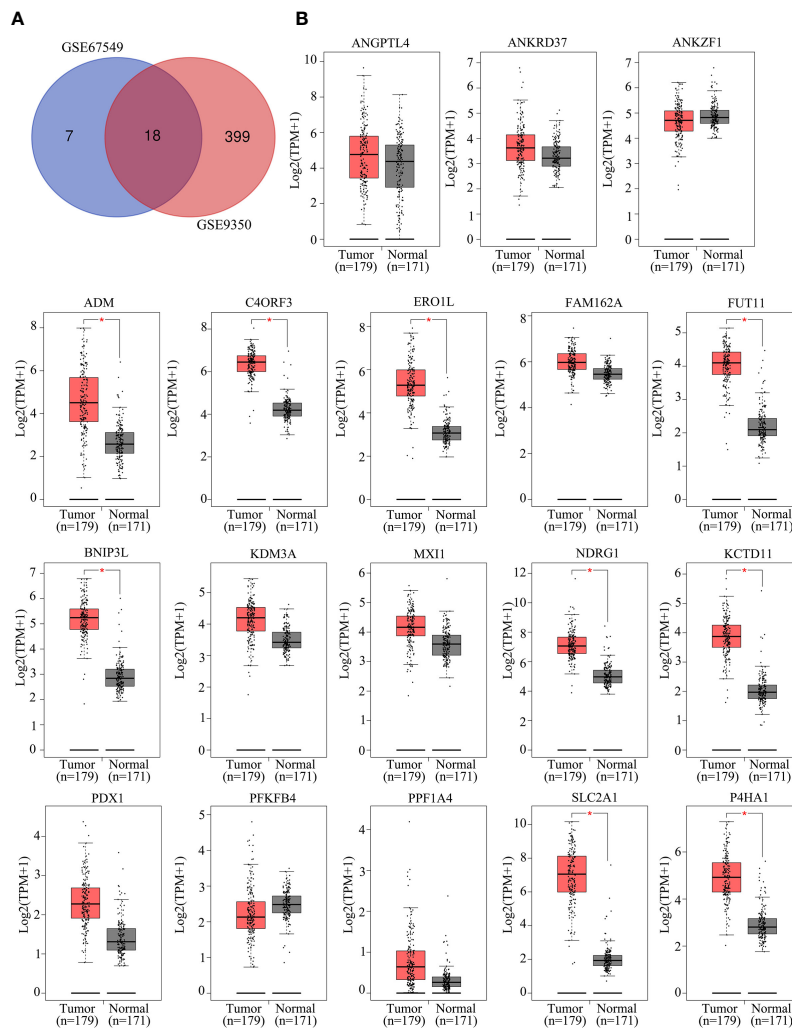


FIGURE 1 | Identification of key hypoxia-related genes in PC. **(A)** Intersection analysis of differentially expressed genes in PC samples under hypoxia based on the gene expression profiles of GSE67549 and GSE9350. **(B)** The mRNA expression of ANGPTL4, ANKRD37, ANKZF1, ADM, C4ORF3, ERO1L, FAM162A, FUT11, BNIP3L, KDM3A, MXI1, NDRG1, KCTD11, PDX1, PFKFB4, PPF1A4, SLC2A1 and P4HA1 in PC tissues compared with non-tumor tissues analyzed by GEPIA online tool.

metastasis as shown in **Supplementary Table 2**. We split the patients into high and low FUT11 expression groups based on the expression of FUT11 with the median value of 5.6. The expression of $FUT11 > 5.6$ was defined as high expression, while the expression < 5.6 was defined as low expression. Kaplan–Meier analysis show that the patients with higher FUT11 expression had a worse prognosis than those with lower FUT11 expression ($P = 0.014$, $HR = 1.884$) (**Figure 2E**).

Suppression of FUT11 Decreased PC Cell Proliferation and Migration in Normoxia and Hypoxia *In Vitro*

In order to uncover the effects of FUT11 on PC cells in normoxia and hypoxia, targeted FUT11 lentivirus was used to construct FUT11 knockdown cells. CCK-8 assay and EDU assay results showed that FUT11 knockdown reduced the growth of AsPC-1

and PANC-1 cells under normoxia, as well as decreasing the stimulative impact of hypoxia (**Figures 3A, B**). Simultaneously, suppression of FUT11 reduced the colony formation of AsPC-1 and PANC-1 cells in normoxia, as well as reducing the stimulative effects of hypoxia on colony formation (**Figure 3C**). Transwell assay indicated that decreased the expression of FUT11 in AsPC-1 and PANC-1 cells reduced the migratory ability of the cells under normoxia and hypoxia (**Figure 3D**). Western blot assay and immunofluorescence staining demonstrated that FUT11 knockdown decreased N-cadherin protein expression and increased E-cadherin protein expression levels in PC cells under normoxia and hypoxia (**Figures 3E, F**). Taken together, these results suggested that as a key hypoxia-related gene, FUT11 had the potential to regulate the proliferation and migratory ability of PC cells in normoxia and hypoxia condition.

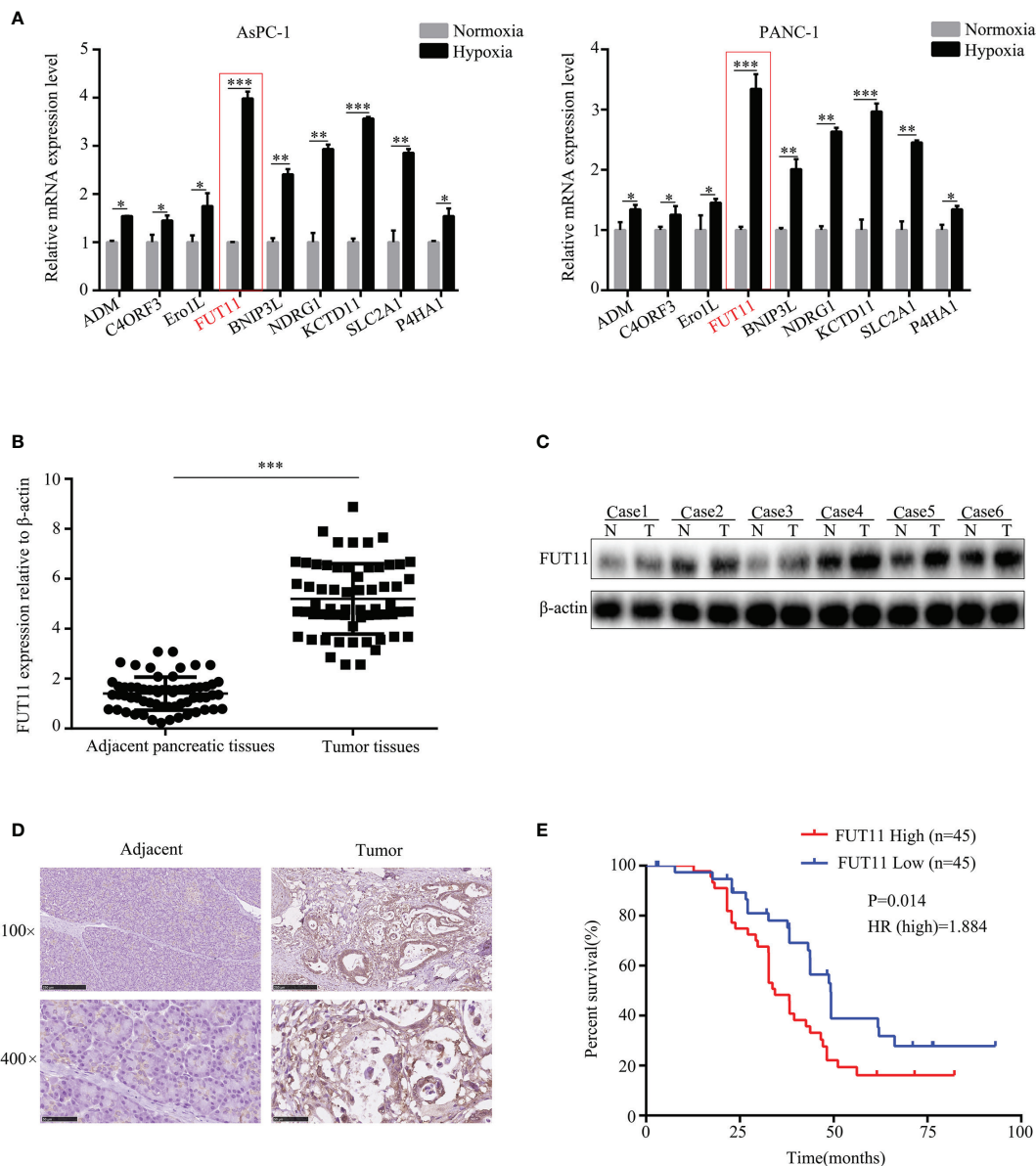


FIGURE 2 | FUT11 was up-regulated in PC and predicted poor outcome. **(A)** qRT-PCR analysis on the mRNA expression of ADM, C4ORF3, ERO1L, FUT11, BNIP3L, KDM3A, MX11, NDRG1 and KCTD11 in AsPC-1 and PANC-1 cells under normoxia and hypoxia. **(B)** qRT-PCR analysis of mRNA level of FUT11 in 62 pairs of matched PC tissue and adjacent normal tissues. **(C)** Western blot analysis of protein level of FUT11 in PC tissue and adjacent normal tissues. **(D)** IHC analysis of the protein level of FUT11 in pancreatic cancer and normal pancreatic tissue. **(E)** 90 patients with PC were divided into high- and low-expression groups based on the expression of FUT11. Kaplan survival curve showed the overall survival of high FUT11 (red) and low FUT11 (blue) expression group. * $P < 0.05$; ** $P < 0.01$; *** $P < 0.001$.

Knockdown of FUT11 Inhibits the PC Cells Proliferation and Metastasis *In Vivo*

The effects of FUT11 knockdown *in vivo* was also determined. We found that tumor tissues derived from FUT11 knockdown cells showed slower growth rate and lower tumor weight than that derived negative control cells (all $P < 0.05$, **Figures 4A–C**). We further assessed the protein expression of proliferation biomarkers KI67 and PCNA in tumor tissues. Results indicated

that KI67 and PCNA was decreased in the tumor tissues with low FUT11 expression (**Figure 4D**). The effects of FUT11 on the hepatic metastasis of PANC-1 cells was evaluated in by injecting the FUT11 knockdown and negative control PANC-1 cells into the spleen capsule. Results showed that FUT11 knockdown significantly reduced the metastatic foci in the liver (**Figures 4E–G**). Furthermore, the FUT11 knockdown group had a markedly longer survival time than the negative control group according to the survival analyses (**Figure 4H**).

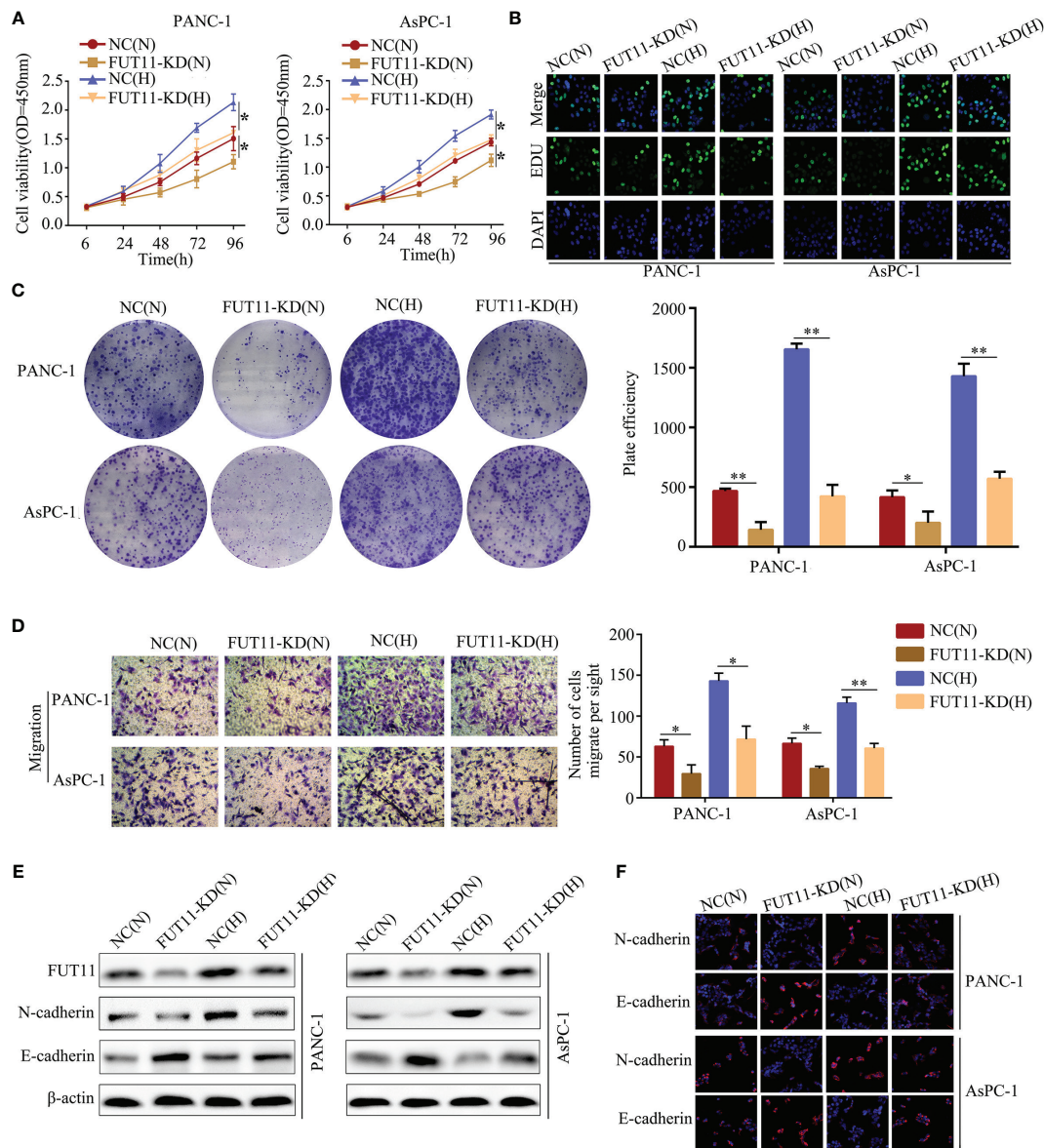


FIGURE 3 | FUT11 regulated the proliferation and migration of PC cells under normoxia and hypoxia *in vitro*. Targeted FUT11 lentivirus and negative control lentivirus were used to construct FUT11 knockdown cells and negative control cells, that were cultured either in normoxia or hypoxia. Cells were divided into four groups: NC(N), cells transfected with negative lentiviral and cultured in normoxia; FUT11-KD(N), cells with FUT11 knockdown and cultured in normoxia; NC(H), cells transfected with negative lentiviral and cultured in hypoxia; FUT11-KD(H), cells with FUT11 knockdown and cultured in hypoxia. **(A)** The effect of FUT11 on PC cell proliferation detected by CCK-8 assay. **(B)** The effect of FUT11 on PC cell proliferation detected by EDU assay. **(C)** The effect of FUT11 on PC cell colony forming ability detected by colony formation assay. **(D)** The effect of FUT11 on PC cell migratory ability detected by Transwell assays. **(E)** Western blotting used to detect the protein level of N-cadherin and E-cadherin of each group. **(F)** Immunofluorescent staining on the expression of N-cadherin and E-cadherin of each group. * $P < 0.05$; ** $P < 0.01$.

FUT11 Co-Localized With PDK1 in PC Cells and Regulated the Expression of PDK1 *via* Maintaining Its Stability Under Hypoxia

In order to explore the molecular mechanism of FUT11 in PC development, we used immunoprecipitation with mass

spectrometry analysis to determine proteins interacting with FUT11. A total of 700 proteins were found to interact with FUT11 as shown in **Supplementary Table 3**. Among the 700 interacted proteins with FUT11, PDK1 has been revealed as an oncogene in pancreatic cancer, indicating that the effect of FUT11 on PC cells might be associated with PDK1. Immunoprecipitation (IP) and immunofluorescence (IF) analysis demonstrated that

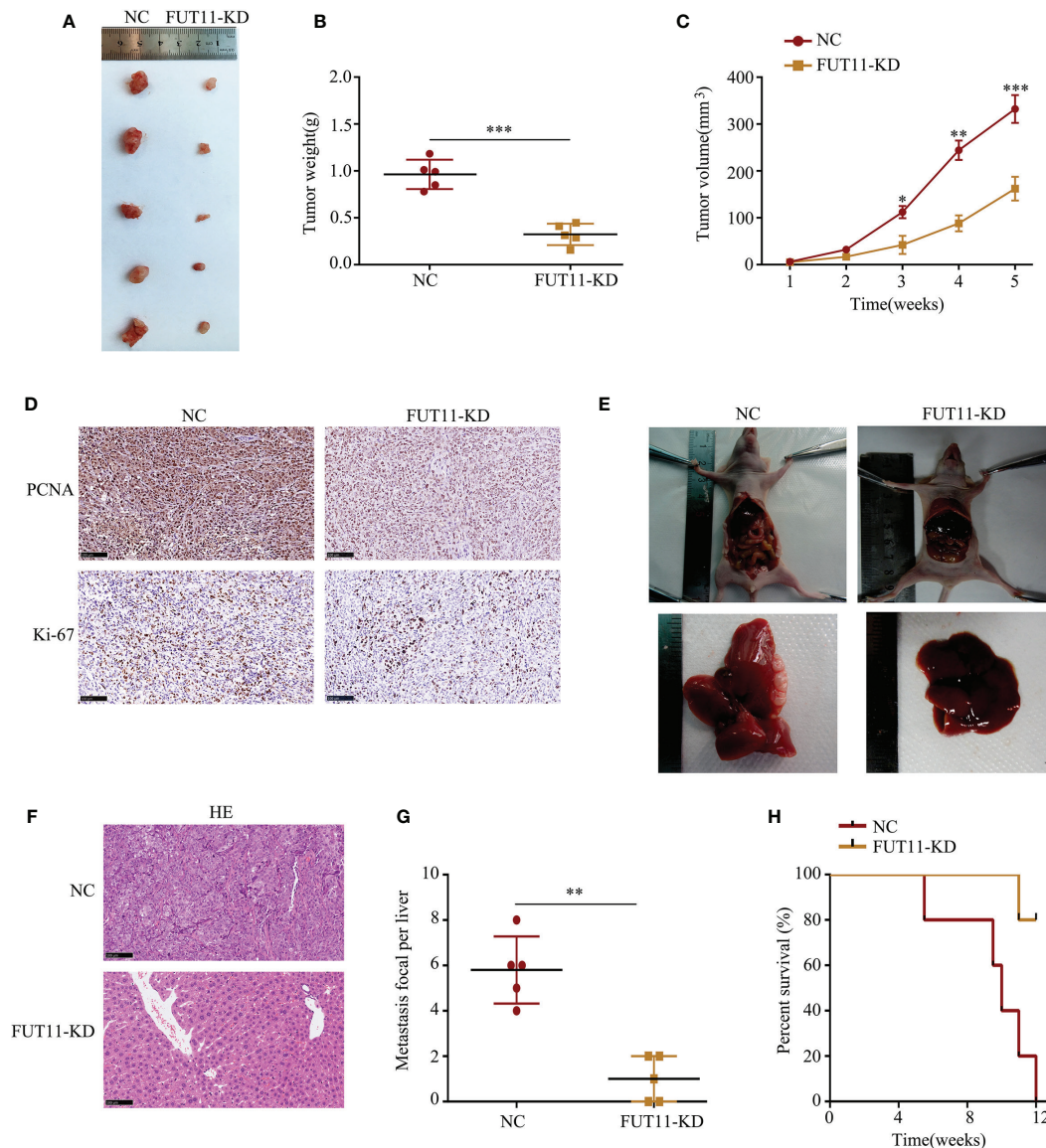


FIGURE 4 | Inhibition of FUT11 suppressed the proliferation and metastasis of PANC-1 cells *in vivo*. **(A)** Representative image of tumor tissues in negative control group and FUT11 knockdown group. **(B)** The mean tumor weight of FUT11 knockdown and negative control groups. **(C)** The proliferative rate of tumor tissues with FUT11 knockdown and negative control. **(D)** IHC staining of Ki-67 and PCNA protein expression in transplanted tumors under different experimental conditions. **(E)** Live metastatic tumor model (n=5). **(F)** IHC staining and HE images showing the metastatic foci in liver in indicated groups. **(G)** Statistical analysis of the average numbers of visible liver metastatic foci. **(H)** Kaplan–Meier survival curves for each experimental group, (n=5). **P* < 0.05; ***P* < 0.01; ****P* < 0.001.

FUT11 directly bound to and co-localized with PDK1 (**Figures 5A, B**). The suppression of FUT11 prominently decreased the protein level of FUT11 under normoxia and hypoxia in AsPC-1 and PANC-1 cell (**Figure 5C**). A previous study showed that the members of FUT family can regulate the expression of related proteins by stabilizing their binding proteins and decreasing their ubiquitination (13). Therefore, we considered that FUT11 may bind to PDK1 and protect it from degradation. We used cycloheximide (CHX) to inhibit the synthesis of protein and detect the degradation

of PDK1. The results showed that the degradation of PDK1 was increased in FUT11 knockdown cells (**Figure 5D**). To investigate whether FUT11 protect PDK1 *via* inhibiting ubiquitination, we performed the ubiquitination assay. The results showed that the suppression of FUT11 increased PDK1 ubiquitination under normoxia and hypoxia in AsPC-1 and PANC-1 cell (**Figure 5E**). Moreover, it is interesting that treatment with MG132 (10μM) restored the reduction of PDK1 induced by FUT11 suppression under hypoxia (**Figure 5F**). Furthermore, the expression of FUT11

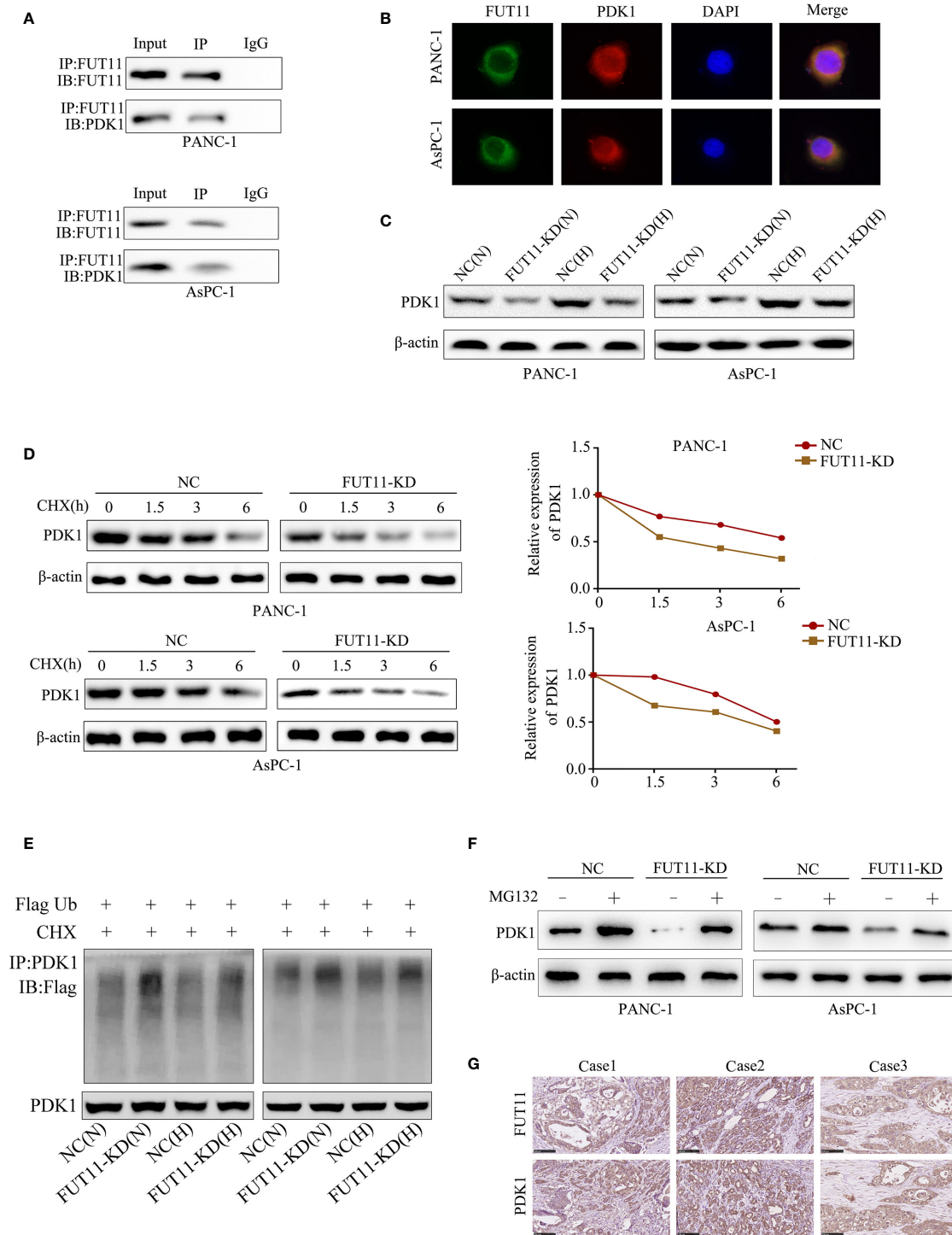


FIGURE 5 | FUT11 bound to PDK1 and regulated its expression. **(A)** Immunoprecipitation on the binding between FUT11 and PDK1. **(B)** Immunofluorescence showed FUT11 co-localized with PDK1 in PC cells. **(C)** Western blot on the expression of FUT11 in sh-scramble and FUT11 knockdown PC cells under normoxia and hypoxia. **(D)** The ubiquitination assay showed the ubiquitination level of PDK1 in sh-scramble and FUT11 knockdown PC cells under normoxia and hypoxia. **(E)** CHX was used to inhibit the protein synthesis, and the degradation of PDK1 in sh-scramble and FUT11 knockdown cells under hypoxia detected using Western blot. **(F)** Western blot on the expression of PDK1 in sh-scramble and FUT11 cells treated with MG132 under hypoxia. **(G)** IHC images showed the co-expression of FUT11 and PDK1.

and PDK1 was investigated in our PC clinical samples, results indicated that both FUT11 and PDK1 co-expressed in the PC tissues (**Figure 5G**).

PDK1 Overexpression Under Hypoxia Decreased the Inhibitory Effect of FUT11 Knockdown

To verify whether FUT11 promoted the proliferation of pancreatic cancer *via* increasing the expression of PDK1, we overexpressed PDK1 in FUT11 knockdown PC cells. Then, we used CCK-8 and EDU assays to monitor the cell viability. The results indicated that increased the expression of PDK1 significantly increased the proliferation of FUT11 low-expressed PC cells (**Figures 6A, B**). In addition, the colony formation ability of the cells co-transfected with targeting FUT11 lentivirus and PDK1 overexpression lentivirus under hypoxia was higher than cells transfected with targeting FUT11 lentivirus alone (**Figure 6C**). Similarly, PDK1 overexpressed in FUT11 knockdown PC cells remarkably increased the migratory ability of PC cells (**Figure 6D**). Results of Western blot showed that overexpressed PDK1 in FUT11 knockdown cells significantly increased the protein level of N-cadherin and decreased the protein level E-cadherin (**Figure 6E**). Furthermore, western blot demonstrated the PDK1 significantly activated the AKT/mTOR pathway, while overexpressed PDK1 in FUT11 knockdown cells significantly reversed the inhibitory effects of FUT11 knockdown on the activation of AKT/mTOR pathway (**Figure 6F**).

FUT11 Was a Target Gene of HIF1 α

Hypoxia-inducible factors including HIF1 α were the most direct hypoxia response elements. To explore the regulatory network of FUT11, we further determined whether FUT11 was directly regulated by HIF1 α . After obtaining the motif of HIF1 α in JASPAR database (**Figure 7A**), we found that there is a hypoxia-responsive element (HRE) in the promoter of FUT11 (**Figure 7B**). The results indicated that compared with the control group, hypoxia significantly increased the luciferase activity in the cells transfected with the vector contained full-length FUT11 promoter, while the lack of HRE reduced the luciferase activity. Furthermore, inhibition of HIF1 α reversed hypoxia-induced luciferase activity (**Figure 7C**). Anti-HIF1 α antibody was enrolled to perform ChIP assays in PANC-1 cells. Results indicated that the HRE in the FUT11 promoter was the major region mediating HIF1 α -induced transcription (**Figure 7D**). In addition, it is interesting that FUT11 was co-expressed with HIF1 α in TCGA PC samples (**Figure 7E**) and our clinical PC samples (**Figure 7F**).

Restoration of FUT11 Reversed the Inhibitory Effects of HIF1 α Knockdown on PC Cells

To determine whether FUT11 was involved in the biological function of PC cells induced by HIF1 α under hypoxia, we constructed negative control cells, FUT11 overexpressed cells, HIF1 α knockdown cells and FUT11 overexpressed plus HIF1 α knockdown cells, and cultured them under hypoxia (**Figure 8A**). CCK-8 and EDU assays results showed that suppression of

HIF1 α inhibited the proliferation of PC cells under hypoxia, while overexpression of FUT11 in HIF1 α knockdown cells relieved the suppressive effects of HIF1 α knockdown on cell growth (**Figures 8B, C**). Similarly, the colony number of cells with HIF1 α inhibition was obviously decreased. Overexpression of FUT11 in HIF1 α knockdown cells relieved the inhibitory effects of HIF1 α knockdown on colony forming ability under hypoxia (**Figure 8D**). Furthermore, transwell assays demonstrated that HIF1 α suppression remarkable decreased the migratory ability of PC cells in hypoxia, while overexpression of FUT11 in HIF1 α knockdown cells reversed the inhibitory effects of HIF1 α knockdown on cell migration (**Figure 8E**).

DISCUSSION

Although the therapy for PC had been improved significantly, the prognosis of patients with PC was still poor (15). Moreover, due to early metastasis, most PC patients lost the best time for treatment. Recently, increasing evidences showed that the distant metastasis in early stage of PC cells were driven by signals from tumor environment, including hypoxia (16). Therefore, uncovering the mechanism of hypoxia-regulated response in PC cells is critical for the treatment of PC.

Previous studies had revealed that bioinformatics is a powerful tool to identify genes associated with the development of tumors, including PC (17). Furthermore, online database GEO and TCGA storing thousands of gene database of tumor tissues that provide enough analytical data. In the current study, we used the bioinformatics tool to identify novel hypoxia-related genes. Through analyzing the gene expression profile, we found 18 genes were differentially expressed between hypoxic and normoxic PC samples. Among these 18 genes, 9 of them including ADM, C4orf3, ERO1L, FUT11, BNIP3L, NDRG1, KCTD11, SLC2A1 and P4HA1 were highly expressed in PC tissues. Furthermore, FUT11 was increased the most significant in PC cells under hypoxia condition, up-regulated in PC tissues and predicted poor prognosis of PC patients. These findings suggested that FUT11 may be a novel hypoxia-related gene.

The fucosyltransferase (FUT) family are the key enzymes in cell-surface antigen synthesis during various biological processes such as tumor proliferation, metastasis and drug resistance (18, 19). At present, a total of 13 members consisted FUT1 to FUT11, protein O-fucosyltransferase 1 (POFUT1) and POFUT2 were identified. A number of studies had demonstrated that some members of the FUTs play roles as oncogenes in various types of cancers. FUT8 was up-regulated in non-small cell lung cancer and promoted the process of epithelial-mesenchymal transition (20). POFUT1 increased the activity of Notch1 signaling pathway and promoted the progression of colorectal cancer (21). As shown in the previous studies, inhibition of FUTs including FUT11 significantly decreased the expression and activity of ERK1/2 and p38 MAPK pathways, as well as the progression of human invasive ductal carcinoma (22). FUT11 was highly expressed in gynecological cancers, and

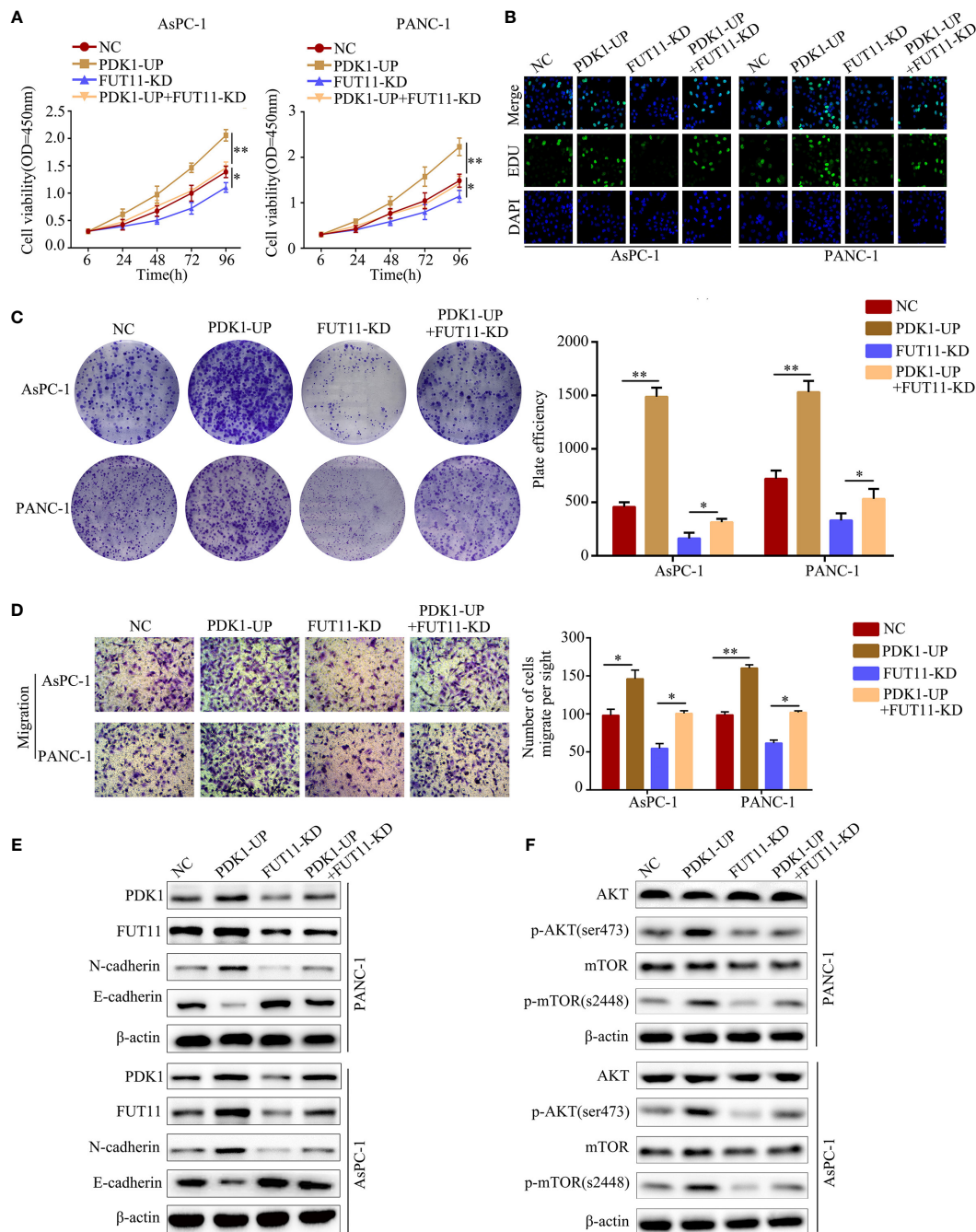


FIGURE 6 | Overexpression of PDK1 reversed the inhibitory effect of FUT11 inhibition on PC cell proliferation and migration. Cells were divided into four groups: negative control group (NC), PDK1 overexpressed group (PDK1-UP), FUT11 knockdown group (FUT11-KD) and PDK1 overexpressed plus FUT11 knockdown group (PDK1-UP + FUT11-KD). All cells were cultured in hypoxia. **(A)** CCK-8 assay on cell viability of each group. **(B)** EDU assay on cell proliferation of each group. **(C)** Colony formation on the colony forming ability of cells in each group. **(D)** Transwell assay on the cell migratory ability of each group. **(E)** Western blot on the protein level of FUT11, PDK1, N-cadherin and E-cadherin in each group. **(F)** Western blot on the protein level of phosphorylated AKT, AKT, phosphorylated mTOR and mTOR in each group. * $P < 0.05$; ** $P < 0.01$.

overexpression of FUT11 in patients predicted poor outcome (23). However, the effect of FUT11 on proliferation and metastasis of human PC cells have not yet been defined. Using CCK-8 assay, colony formation assay and transwell assay, we

found that FUT11 inhibition significantly decreased proliferation and migration of PC cells in both hypoxic and normoxic environment. These results were in consistent with previous studies. Via performing xenograft tumor model and *in vivo*

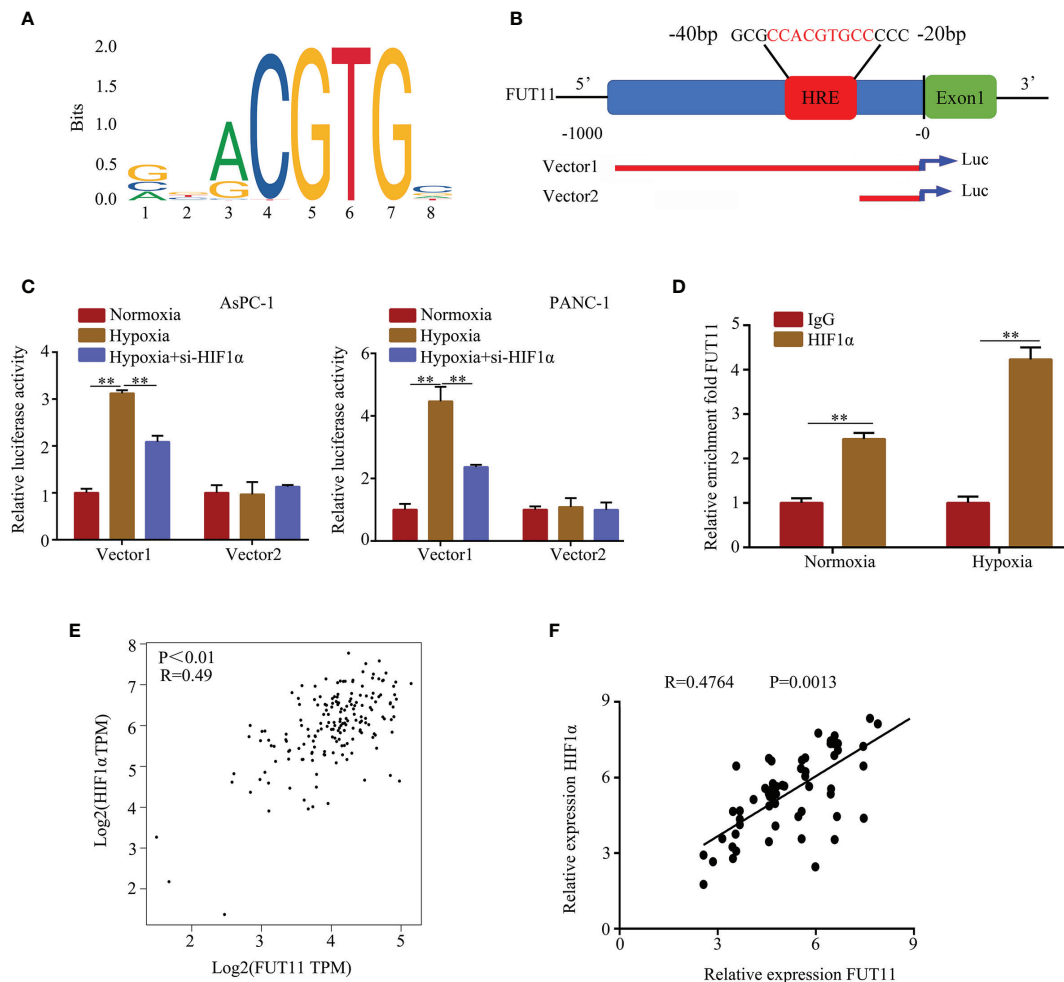


FIGURE 7 | HIF1 α regulates the expression of FUT11 by binding to the HRE of the FUT11 promoter. **(A)** The motif of HIF1 α . **(B)** The hypoxia response element (HRE) in the promoter of FUT11 (Vector 1: vector with full-length FUT11 promoter; Vector 2: vector with truncated FUT11 promoter which lack of HRE). **(C)** PANC-1 and AsPC-1 cells transfected with either a full-length or truncated FUT11 promoter-pGL3 reporter vector and cultured under hypoxia, with or without si-HIF1 α . After 48 hours, luciferase activity was measured using the dual-luciferase reporter assay system. **(D)** ChIP assays with anti-HIF1 α antibody verifying the binding between HIF1 α and hypoxia response element of the FUT11 promoter under normoxia and hypoxia. **(E)** Co-expression of FUT11 and HIF1 α based on the data from PC tissues *via* online database GEPIA. **(F)** Co-expression of FUT11 and HIF1 α based on the data from our clinical PC tissues (n=62). ***P* < 0.01.

metastatic tumor model, we found that FUT11 inhibition decreased the PC cells proliferation and metastasis *in vivo*. These results suggested that FUT11 was linked to hypoxia, because it had the potential to regulate PC cells proliferation and migration under normoxia and hypoxia.

PDK1 has emerged as an important oncogene in many types of cancers including PC (24). Lucero-Acuna A et al. has been reported that the expression of PDK1 is up-regulated in human PC and promotes cancer cell growth and mobility (25). Xia S et al. showed that knockdown of PDK1 forces cells containing activated p21(Ras) to undergo apoptosis in PC cells (26). Previous studies have shown that, one of the targets of PDK-1 was AKT, which can be activated by phosphorylation on two residues (T308 and S473) for full oncogenic activity (27). However, the mechanisms of PDK1 in regulating tumor progression is not clear. In the current study, through

immunoprecipitation with mass spectrometry analysis, PDK1 was identified as one of the potential downstream genes of FUT11, which co-expressed with FUT11. Furthermore, using immunoprecipitation and Western blot, we found that FUT11 directly bound to PDK1 and regulated its expression in normoxia and hypoxia. Based on previous studies, FUTs can bind to a series of proteins and maintain their stability *via* blocking the binding site of protease (13). Therefore, we determined whether FUT11 regulated PDK1 *via* maintaining its stability. Consistent with our speculation, knockdown of FUT11 under hypoxia increased the degradation of PDK1. Furthermore, overexpression of PDK1 in PC under hypoxia relieved the inhibitory impacts of FUT11 knockdown on cell proliferation and migration.

The relationship among hypoxia-inducible factors, hypoxia microenvironment, hypoxia related genes and the development

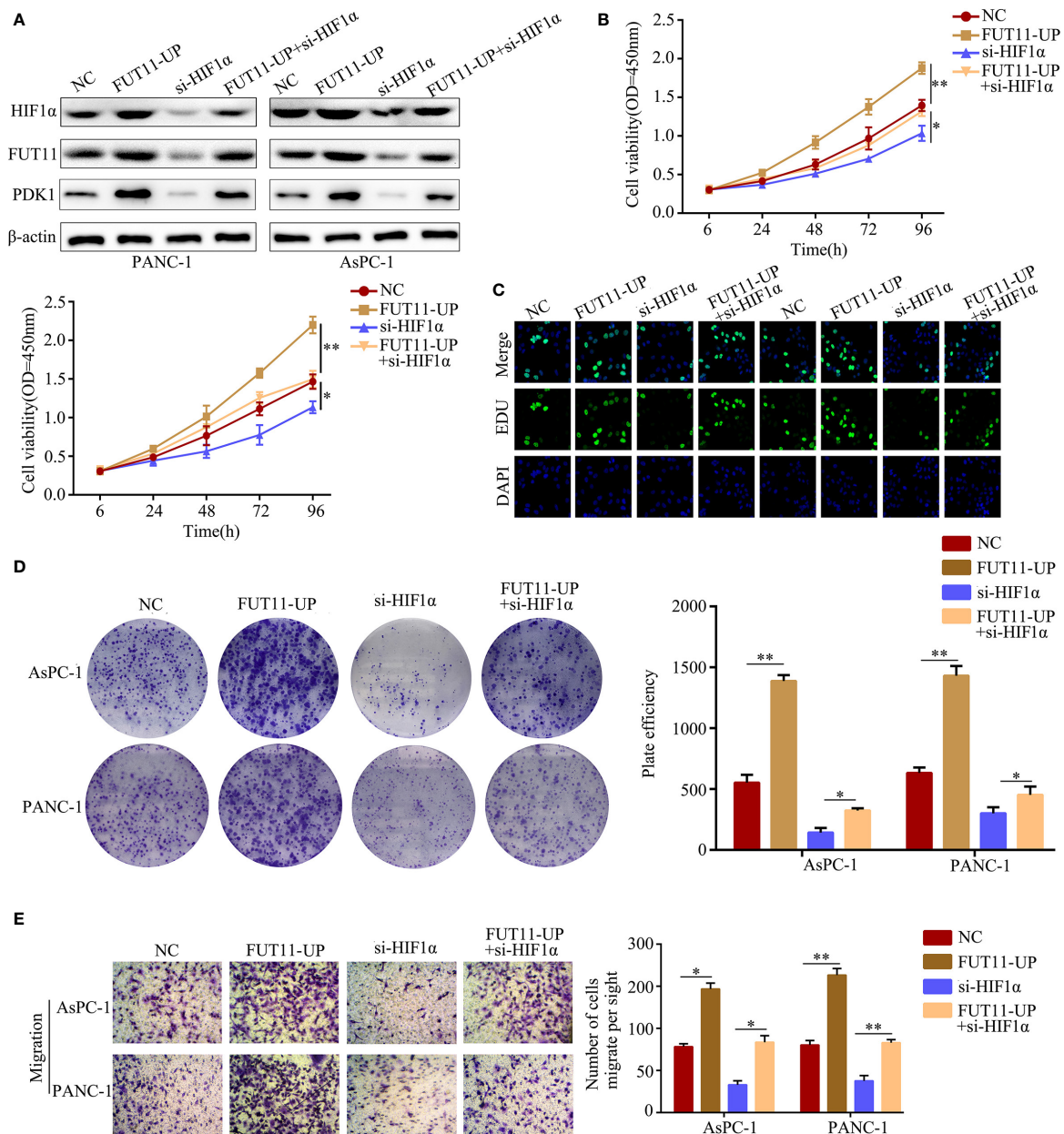


FIGURE 8 | Overexpression of FUT11 reversed the inhibitory effects of HIF1α knockdown on PC cell proliferation and migration under hypoxia. PANC-1 and AsPC-1 cells were divided into four groups: negative control (NC); FUT11 overexpression (FUT11-UP); HIF1α inhibition (si-HIF1α); HIF1α inhibition plus FUT11 overexpression (si-HIF1α+FUT11-UP). All groups of cells were cultured in hypoxia. **(A)** Western blot on the expression of HIF1α and FUT11 in each group of cells. **(B)** CCK-8 assay on the cell viability in each group of cells. **(C)** EDU assay on the proliferation in each group of cells. **(D)** Colony formation assay on the colony forming ability in each group of cells. **(E)** Transwell assays on the migratory ability in each group of cells. The data were shown as means ± S.D. of three independent assays. * $P < 0.05$, ** $P < 0.01$.

of PC were widely reported in previous studies. For example, PAFAH1B2 regulated by HIF1α under hypoxia promoted the growth and mobility of PC cells (28). MTA1 was regulated by HIF-α/VEGF axis and promoted the development of PC (29). Similarly, overexpression of hydroxyproline via EGLN/HIF1A is associated with distant metastasis in PC (30). Similarly, our previous study also demonstrated that YEATS2 directly targets

HIF1α which promotes PC cell proliferation and mobility (31). In the present study, we provided the first evidence that FUT11 was a novel target gene of HIF1α, which involved in the biological function mediating by HIF1α under hypoxia.

In conclusion, our present study demonstrated that FUT11 is a new hypoxia related gene, and is overexpressed in pancreatic cancer tissues and related to poor prognosis of pancreatic cancer

patients. FUT11 is regulated by HIF1 α and promotes PC cells proliferation and migration *via* maintaining the stability of PDK1 mediates AKT/mTOR signaling pathway. FUT11 could be an effective target for overcoming the hypoxia response of PC.

DATA AVAILABILITY STATEMENT

The original contributions presented in the study are included in the article/**Supplementary Material**. Further inquiries can be directed to the corresponding authors.

ETHICS STATEMENT

The studies involving human participants were reviewed and approved by The Ethics Committee of GuiZhou Medical University Ethics. The patients/participants provided their written informed consent to participate in this study. The animal study was reviewed and approved by Animal Experimental Ethical Inspection Form of Guizhou Medical University.

REFERENCES

- Lee KG, Roy V, Laszlo M, Atkins KM, Lin KJ, Tomassian S, et al. Symptom Management in Pancreatic Cancer. *Curr Treat Options Oncol* (2021) 22(1):8. doi: 10.1007/s11864-020-00801-4
- Chin V, Nagrial A, Sjoquist K, O'Connor CA, Chantrill L, Biankin AV, et al. Chemotherapy and Radiotherapy for Advanced Pancreatic Cancer. *Cochrane Database Syst Rev* (2018) 3:CD011044. doi: 10.1002/14651858.CD011044.pub2
- Hirata E, Sahai E. Tumor Microenvironment and Differential Responses to Therapy. *Cold Spring Harb Perspect Med* (2017) 7(7):a026781. doi: 10.1101/cshperspect.a026781
- Wozniak M, Pastuch Gawolek G, Makuch S, Wisniewski J, Ziolkowski P, Szeja W, et al. Overcoming Hypoxia-Induced Chemoresistance in Cancer Using a Novel Glycoconjugate of Methotrexate. *Pharm (Basel)* (2020) 14(1):13. doi: 10.3390/ph14010013
- Zhang Q, Han Z, Zhu Y, Chen J, Li W. Role of Hypoxia Inducible Factor-1 in Cancer Stem Cells (Review). *Mol Med Rep* (2021) 24(1):17. doi: 10.3892/mmr.2020.11655
- Guo FJ, Shao YP, Wang YP, Jin YM, Liu SS, Wang QY. Mir-92 Stimulates VEGF by Inhibiting Von Hippel-Lindau Gene Product in Epithelial Ovarian Cancer. *J Biol Regul Homeost Agents* (2017) 31(3):615–24.
- Ebright RY, Zachariah MA, Micalizzi DS, Wittner BS, Niederhoffer KL, Nieman LT, et al. HIF1A Signaling Selectively Supports Proliferation of Breast Cancer in the Brain. *Nat Commun* (2020) 11(1):6311. doi: 10.1038/s41467-020-20144-w
- Kutkowska J, Strzadala L, Rapak A. Hypoxia Increases the Apoptotic Response to Betulinic Acid and Betulin in Human Non-Small Cell Lung Cancer Cells. *Chem Biol Interact* (2021) 333:109320. doi: 10.1016/j.cbi.2020.109320
- Cui XG, Han ZT, He SH, Wu XD, Chen TR, Shao CH, et al. HIF1/2 α Mediates Hypoxia-Induced LDHA Expression in Human Pancreatic Cancer Cells. *Oncotarget* (2017) 8(15):24840–52. doi: 10.18632/oncotarget.15266
- Fan LF, Diao LM, Chen DJ, Liu MQ, Zhu LQ, Li HG, et al. Expression of HIF-1 α and its Relationship to Apoptosis and Proliferation in Lung Cancer. *Ai Zheng* (2002) 21(3):254–8.
- Hwang H, Jeong HK, Lee HK, Park GW, Lee JY, Lee SY, et al. Machine Learning Classifies Core and Outer Fucosylation of N-Glycoproteins Using Mass Spectrometry. *Sci Rep* (2020) 10(1):318. doi: 10.1038/s41598-019-57274-1

AUTHOR CONTRIBUTIONS

WC, ZZ, ZY, and SL contributed to the experiment design, and data analysis. RP, HW, WC, and SL contributed to the experiment implementation, YN, XZ, HC, and SL contributed to manuscript draft and data analysis. All authors contributed to the article and approved the submitted version.

SUPPLEMENTARY MATERIAL

The Supplementary Material for this article can be found online at: <https://www.frontiersin.org/articles/10.3389/fonc.2021.675991/full#supplementary-material>

Supplementary Table 1 | The primers used for quantitative real-time PCR (qRT-PCR) and plasmid sequence.

Supplementary Table 2 | The Association between FUT11 expression and clinicopathological features of PC patients.

Supplementary Table 3 | Mass spectrometry of immunoprecipitation proteins interacting with FUT11.

- Liang L, Gao C, Li Y, Sun M, Xu J, Li H, et al. miR-125a-3p/FUT5-FUT6 Axis Mediates Colorectal Cancer Cell Proliferation, Migration, Invasion and Pathological Angiogenesis Via PI3K-Akt Pathway. *Cell Death Dis* (2017) 8(8):e2968. doi: 10.1038/cddis.2017.352
- Kumar S, Das S, Rachagani S, Kaur S, Joshi S, Johansson SL, et al. NCOA3-Mediated Upregulation of Mucin Expression Via Transcriptional and Post-Translational Changes During the Development of Pancreatic Cancer. *Oncogene* (2015) 34(37):4879–89. doi: 10.1038/onc.2014.409
- Lin G, Zhao R, Wang Y, Han J, Gu Y, Pan Y, et al. Dynamic Analysis of N-glycosomic and Transcriptomic Changes in the Development of Ovarian Cancer Cell Line A2780 to its Three Cisplatin-Resistant Variants. *Ann Transl Med* (2015) 8(6):289. doi: 10.21037/atm.2020.03.12
- Kurihara K, Hanada K, Shimizu A. Endoscopic Ultrasonography Diagnosis of Early Pancreatic Cancer. *Diagn (Basel)* (2020) 10(12):1086. doi: 10.3390/diagnostics10121086
- Bhandari V, Hoey C, Liu LY, Lalonde E, Ray J, Livingstone J, et al. Molecular Landmarks of Tumor Hypoxia Across Cancer Types. *Nat Genet* (2019) 51(2):308–18. doi: 10.1038/s41588-018-0318-2
- Lv K, Yang J, Sun J, Guan J. Identification of Key Candidate Genes for Pancreatic Cancer by Bioinformatics Analysis. *Exp Ther Med* (2019) 18(1):451–8. doi: 10.3892/etm.2019.7619
- Gan CZ, Li G, Luo QS, Li HM. miR-339-5p Downregulation Contributes to Taxol Resistance in Small-Cell Lung Cancer by Targeting Alpha1,2-fucosyltransferase 1. *IUBMB Life* (2017) 69(11):841–9. doi: 10.1002/iub.1679
- Wang S, Zhang X, Yang C, Xu S. MicroRNA-198-5p Inhibits the Migration and Invasion of Non-Small Lung Cancer Cells by Targeting Fucosyltransferase 8. *Clin Exp Pharmacol Physiol* (2019) 46(10):955–67. doi: 10.1111/1440-1681
- Li F, Zhao S, Cui Y, Guo T, Qiang J, Xie Q, et al. Alpha1,6-Fucosyltransferase (FUT8) Regulates the Cancer-Promoting Capacity of Cancer-Associated Fibroblasts (Caf) by Modifying EGFR Core Fucosylation (CF) in Non-Small Cell Lung Cancer (NSCLC). *Am J Cancer Res* (2020) 10(3):816–37. doi: 10.21203/rs.2.18620/v1
- Du Y, Li D, Li N, Su C, Yang C, Lin C, et al. POFUT1 Promotes Colorectal Cancer Development Through the Activation of Notch1 Signaling. *Cell Death Dis* (2018) 9(10):995. doi: 10.1038/s41419-018-1055-2
- Carrascal MA, Silva M, Ramalho JS, Pen C, Martins M, Pascoal C, et al. Inhibition of Fucosylation in Human Invasive Ductal Carcinoma Reduces E-selectin Ligand Expression, Cell Proliferation, and ERK1/2 and P38 MAPK Activation. *Mol Oncol* (2018) 12(5):579–93. doi: 10.1002/1878-0261

23. Zhang X, Wang Y. Identification of Hub Genes and Key Pathways Associated With the Progression of Gynecological Cancer. *Oncol Lett* (2019) 18(6):6516–24. doi: 10.3892/ol.2019.11004
24. Wang C, Liu H, Qiu Q, Zhang Z, Gu Y, He Z. TCRP1 Promotes NIH/3T3 Cell Transformation by Over-Activating PDK1 and AKT1. *Oncogenesis* (2017) 6(4):e323. doi: 10.1038/oncsis.2017.18
25. Lucero-Acuna A, Jeffery JJ, Abril ER, Nagle RB, Guzman R, Pagel MD, et al. Nanoparticle Delivery of an AKT/PDK1 Inhibitor Improves the Therapeutic Effect in Pancreatic Cancer. *Int J Nanomed* (2014) 9:5653–65. doi: 10.2147/IJN.S68511
26. Xia S, Chen Z, Forman LW, Faller DV. Pkcdelta Survival Signaling in Cells Containing an Activated p21Ras Protein Requires PDK1. *Cell Signal* (2009) 21(4):502–8. doi: 10.1016/j.cellsig.2008
27. Lin HJ, Hsieh FC, Song H, Lin J. Elevated Phosphorylation and Activation of PDK-1/AKT Pathway in Human Breast Cancer. *Br J Cancer* (2005) 93(12):1372–81. doi: 10.1038/sj.bjc.6602862
28. Ma C, Guo Y, Zhang Y, Duo A, Jia Y, Liu C, et al. PFAH1B2 is a HIF1a Target Gene and promotes Metastasis in Pancreatic Cancer. *Biochem Biophys Res Commun* (2018) 501(3):654–60. doi: 10.1016/j.bbrc.2018.05.039
29. Sun X, Zhang Y, Li B, Yang H. MTA1 Promotes the Invasion and Migration of Pancreatic Cancer Cells Potentially Through the HIF- α /VEGF Pathway. *J Recept Signal Transduct Res* (2018) 38(4):352–8. doi: 10.1080/10799893.2018.1531887
30. Chiba N, Sunamura M, Nakagawa M, Koganezawa I, Yokozuka K, Kobayashi T, et al. Overexpression of Hydroxyproline Via EGLN/HIF1A Is Associated With Distant Metastasis in Pancreatic Cancer. *Am J Cancer Res* (2020) 10(8):2570–81.
31. Zeng Z, Lei S, He Z, Chen T, Jiang J. YEATS2 Is a Target of HIF1 α and Promotes Pancreatic Cancer Cell Proliferation and Migration. *J Cell Physiol* (2021) 236(3):2087–98. doi: 10.1002/jcp.29995

Conflict of Interest: The authors declare that the research was conducted in the absence of any commercial or financial relationships that could be construed as a potential conflict of interest.

Copyright © 2021 Cao, Zeng, Pan, Wu, Zhang, Chen, Nie, Yu and Lei. This is an open-access article distributed under the terms of the Creative Commons Attribution License (CC BY). The use, distribution or reproduction in other forums is permitted, provided the original author(s) and the copyright owner(s) are credited and that the original publication in this journal is cited, in accordance with accepted academic practice. No use, distribution or reproduction is permitted which does not comply with these terms.



Linking Tumor Microenvironment to Plasticity of Cancer Stem Cells: Mechanisms and Application in Cancer Therapy

Xiaobo Zheng^{1,2}, Chune Yu^{2*} and Mingqing Xu^{1,3*}

OPEN ACCESS

Edited by:

Liwu Fu,
Sun Yat-Sen University, China

Reviewed by:

Stefano Fais,
National Institute of Health (ISS), Italy
Sabarish Ramachandran,
Texas Tech University Health Sciences
Center, United States

*Correspondence:

Chune Yu
yuchune0125@163.com
Mingqing Xu
xumingqing0018@163.com

Specialty section:

This article was submitted to
Molecular and Cellular Oncology,
a section of the journal
Frontiers in Oncology

Received: 09 March 2021

Accepted: 16 June 2021

Published: 28 June 2021

Citation:

Zheng X, Yu C and Xu M (2021) Linking
Tumor Microenvironment to Plasticity
of Cancer Stem Cells: Mechanisms
and Application in Cancer Therapy.
Front. Oncol. 11:678333.
doi: 10.3389/fonc.2021.678333

¹ Department of Liver Surgery, West China Hospital, Sichuan University, Chengdu, China, ² Laboratory of Tumor Targeted and Immune Therapy, Clinical Research Center for Breast, State Key Laboratory of Biotherapy, West China Hospital, Sichuan University, Chengdu, China, ³ Department of Hepatopancreatobiliary Surgery, Meishan City People's Hospital, Meishan Hospital of West China Hospital, Sichuan University, Meishan, China

Cancer stem cells (CSCs) are a minority subset of cancer cells that can drive tumor initiation, promote tumor progression, and induce drug resistance. CSCs are difficult to eliminate by conventional therapies and eventually mediate tumor relapse and metastasis. Moreover, recent studies have shown that CSCs display plasticity that renders them to alter their phenotype and function. Consequently, the varied phenotypes result in varied tumorigenesis, dissemination, and drug-resistance potential, thereby adding to the complexity of tumor heterogeneity and further challenging clinical management of cancers. In recent years, tumor microenvironment (TME) has become a hotspot in cancer research owing to its successful application in clinical tumor immunotherapy. Notably, emerging evidence shows that the TME is involved in regulating CSC plasticity. TME can activate stemness pathways and promote immune escape through cytokines and exosomes secreted by immune cells or stromal cells, thereby inducing non-CSCs to acquire CSC properties and increasing CSC plasticity. However, the relationship between TME and plasticity of CSCs remains poorly understood. In this review, we discuss the emerging investigations on TME and CSC plasticity to illustrate the underlying mechanisms and potential implications in suppressing cancer progression and drug resistance. We consider that this review can help develop novel therapeutic strategies by taking into account the interlink between TME and CSC plasticity.

Keywords: cancer stem cell, plasticity, tumor microenvironment, cancer progression, resistance

INTRODUCTION

Cancer stem cells (CSCs) are a unique subpopulation of cancer cells that possess self-renewal and differentiation abilities. CSC differentiation enhances the aggressiveness of tumors, thereby aggravating cancer progression (1). CSCs are essential for intratumoral heterogeneity and are responsible for tumor relapse, metastasis, and therapeutic resistance. Moreover, these cells are difficult to eliminate by conventional therapies, rendering additional challenges in cancer management (2). Recently, emerging evidence shows that CSCs can present different phenotypes that render diverse functions with varying degrees of mediating tumorigenesis and progression (3), which is attributed to plasticity of CSCs. Notably, CSC plasticity hinders successful cancer therapies, and it is indeed a pivotal area of research to better understand CSC dynamics and thereby the subsequent development of efficient targeting therapies (4). Although CSCs display a high level of plasticity, how they dynamically transit between non-CSC and CSC states or among varied phenotypes of CSC subsets, and what are the molecular mechanisms underlying these dynamic processes remain poorly understood (5–7). Recently, tumor microenvironment (TME) has been identified as a promising target for cancer therapy, owing to its successful application in clinical tumor immunotherapy. Interestingly, an emerging role of the TME in remodeling CSC plasticity has been observed; the CSC niche is critical in regulating CSC plasticity (8). Within this niche, various cell types, including immune cells, mesenchymal stem cells (MSCs), cancer-associated fibroblasts (CAFs), and exosomes derived from live cells, in addition to the physical and chemical composition of the microenvironment, play roles in maintaining and promoting phenotypic transition of CSCs by secreting factors or providing an immunosuppressive environment (9). In this review, we comprehensively discuss the recent advances with respect to the interaction between TME and CSC plasticity and illustrate the underlying molecular mechanisms. Further, this overview can help provide new insights into the existing therapeutic approaches and designing potential strategies for cancer therapy.

EMERGENCE OF PLASTICITY OF CSCs

Cellular plasticity is the ability of cells to differentiate into multiple lineages, which occurs not only during embryonic development but throughout life (10–12). Although plasticity is a highly regulated process under physiological conditions, cancer cells can utilize this adaptive ability for their survival and progression (13). Recently, several studies have demonstrated that CSCs exhibit varied states and can transition between states dynamically during cancer progression, corroborating CSC plasticity (14–16). Chaffer et al. observed that non-CSCs could

spontaneously transit to CSC-like phenotype *in vitro* and *in vivo* in breast cancer cells; this transition was regulated by ZEB1, a key regulator of the epithelial–mesenchymal transition (EMT) (17). Further, Dirkse et al. reported that the well-accepted CSC markers, such as CD133, A2B5, SSEA, and CD15, are not uniformly expressed among glioblastoma cells. Most of the cancer cells adapt a plastic state in response to stimuli in the TME (18). Conclusively, they proposed that CSC plasticity is an adaptation of the cancer cells to the extracellular pressure in the TME, which includes chemical signals, hypoxia-induced physical pressure, or inflammatory environment. In melanoma, JARID1B, a marker of melanoma stem-like cells, was dynamically regulated, indicating the dynamic nature of CSCs (19). Colorectal cancer (CRC), a classical disease model to study CSCs, showed compelling evidence of CSC plasticity during tumor evolution. LGR5, a characteristic marker of CRC stem cells, was expressed in human colon cancer cell lines developed by Kobayashi et al., confirming CSC properties in the established cell lines (20). On treating one of these cell lines with an anticancer drug, they observed transition from LGR5⁺ to LGR5[−] state, while withdrawal of the drug resulted in the cells reverting to the LGR5⁺ state, indicating the inherent plasticity of CSCs. Interestingly, there are two contradictory opinions on the effect of CSC plasticity on inducing liver metastases: one is that CSC plasticity is primarily associated with tumorigenesis and not cancer metastasis (21), whereas the other considers that a majority of CRC metastases are seeded by CSCs (22). The controversy indicates that the non-CSC-to-CSC transition and plasticity of CSCs are crucial for both primary tumor and metastatic growth. Reportedly, vasculogenic mimicry (VM), a hallmark process of cancer cell switch by which cancer cells transdifferentiate and acquire endothelial cell-like properties, accompanies CSC plasticity (23). Zhang et al. revealed that in renal cell carcinoma, high expression of the CSC markers CD133 and CD44 and VM correlated with poor survival (24). Taken together, CSC plasticity mediates interconversion of CSC subsets, as well as gives rise to non-CSC (differentiated) cells.

PLASTICITY OF CSCs CONTRIBUTES TO TUMOR HETEROGENEITY

Tumor heterogeneity in cancer biology is widely investigated for efficient clinical management of cancers (25–27). Intrinsic intratumoral heterogeneity and acquired diversification under therapy endow some tumor cells to gain aggressiveness, rendering their survival and emergence of resistance to therapy. These properties are the driving forces for the development of therapy-resistant populations that ultimately result in relapse and metastasis (28, 29). The origin of intratumoral heterogeneity in tumor cells has been widely considered to be resulting from two controversial explanations: clonal evolution and the CSC model (30, 31). In 1976, Peter Nowell first proposed the theory of clonal evolution for tumor heterogeneity, suggesting that step-wise clonal selection is essential for introducing mutations in tumor genes. In this

Abbreviations: CAFs, cancer associated fibroblasts; CRC, colorectal cancer; CSCs, cancer stem cells; EMT, epithelial–mesenchymal transition; MSCs, mesenchymal stem cells; TME, tumor microenvironment; TNBC, triple negative breast cancer; VM, vasculogenic mimicry.

process, a new tumor is derived from a single cell, and poorer tumor outcomes result from multistep mutations, allowing the selection of more aggressive subclones in the derived clonal population. He hypothesized that in the main effective subclone, cells may acquire identical tumorigenic abilities (32). On the contrary, the CSC hypothesis proposes that only a small portion of the tumor subclone have tumorigenic potential and self-renewal ability (31, 33–36). CSCs can differentiate into non-CSCs that develop into a bulk of tumor mass, in a fashion similar to that of stem cell development (37). In 2001, Reya et al. proposed that there exists a minority of subclones with stem cell traits in the tumor tissue, with self-renewal and pluripotent differentiation potential (38). Currently, CSCs have been isolated from more than 10 tumor types, including breast and lung cancers, CRC, melanoma, and glioma (39–42). The origin of tumor cells remains vaguely understood, and tumor heterogeneity augments the difficulties encountered in tumor therapy. Tumor heterogeneity exists objectively, as supported by the fact that some cells are tumorigenic, while others are not (43–46). Therefore, questions over the origin of tumorigenic cells and whether they are CSCs or normal cells still prevail. One opinion is that tumorigenic cells emerge either from stem/progenitor cells or normal somatic cells that acquire mitotic ability (26). Clonal evolution and the CSC model are not necessarily mutually exclusive. Notably, CSC plasticity enhances complexity of intratumoral heterogeneity. However, the question whether CSCs are tumor-initiating cells or primary tumor cells remains to be clarified. The fact that CSCs can change phenotypes *via* different programs, such as dynamic epithelial/mesenchymal status, has led to the speculation that non-CSCs can transform back to CSCs (47–49). Therefore, CSC plasticity can be presumed as the cell state capable of being shaped by EMT, wherein this process can allow interconversion of CSCs and non-CSCs (50–53).

INFLUENCE OF TME ON CSC PLASTICITY

For many years, the emphasis of tumor therapy has been on the tumor cells themselves, with a focus on inhibiting their innate ability to adhere and migrate. However, in recent years many studies have shown that tumor cells and peritumor cells (the tumor niche) closely communicate through signaling pathways (54–56). Cells in the tumor niche (such as fibroblasts and immune cells) or cytokines secreted by these cells are accomplices in tumor metastasis and chemoresistance (57). Tumorigenesis and metastasis are closely related to the TME (54), where the niche is not only involved in tissue function, structure, and metabolism but also related to the intracellular milieu of tumor cells (58). The TME can alter the conduction such that they are conducive for tumor growth, survival, and development through autocrine or paracrine secretion (58). Local tissues or distant sites can in turn limit and influence tumorigenesis as well as tumor growth and development through metabolism, secretion, immunity, and structural and functional changes. Both the tumor and the surrounding environment are

interdependent and mutually promoting as well as not antagonizing each other. Further, characteristics of the TME, such as immunocyte and mesenchymal cell populations, exosomes, hypoxia, low pH, nutritional deficiencies, and angiogenesis, are key to tumor formation and progression (59, 60).

Emerging evidence suggests that the immunocytes, a critical component in the TME, can regulate phenotypic plasticity of CSCs (61–63). Macrophages, an important cell type involved in complex regulating networks in the TME, are crucial in regulating CSC plasticity. Rao et al. emphasized the mutual influence and interactions between macrophages and CSCs. They reported that CD44 overexpressed by CSCs could induce the macrophages in the TME to secrete the cytokine osteopontin that can in turn bind to CD44 on the surface of tumor cells, thereby promoting tumor cell subclone formation (64). Moreover, analysis of clinical samples showed that osteopontin and CD44 correlated with the survival rate of patients with colon cancer. Additionally, macrophages can secrete oncostatin-M, a pleiotropic cytokine belonging to the IL-6 family, during chemotherapy. Oncostatin-M in turn can activate the dedifferentiation of non-CSCs into aggressive CSCs in triple negative breast cancer (TNBC) (65). Similarly, interplay between macrophage polarization and CSC plasticity can alter the status of cancer cells in terms of EMT, thereby modulating plasticity of stemness in the TME (66). Reportedly, the stem cell factor LIN28, identified in ovarian CSCs, correlates with tumor growth and prognosis of ovarian cancer (67). Using advanced gene sequencing technology, LIN28 and the signaling molecule bone morphogenic protein-4, secreted by macrophages, were observed to be mutually regulated.

CAFs are a predominant component in the TME and play an important role in regulating CSC plasticity (68, 69). CAFs can modulate CSC plasticity through the IGF-II/IGF1R signaling pathway in lung cancer (70); FAK signaling in pancreatic adenocarcinoma (71); and c-Met/FRA1/HEY1 signaling in hepatocellular carcinoma (72). Normal non-cancerous fibroblasts embedded in the TME, upon exposure to chemotherapeutic drugs, undergo DNA damage and secrete a series of cytokines that stimulate cancer growth. Reportedly, the proteoglycan decorin, secreted by fibroblasts, inhibits tumor growth and can induce the expression of tumor-suppressor genes in the microenvironment surrounding TNBC, thereby restraining tumor metastasis (73). GATA3 can also inhibit cancer metastasis and is aberrantly expressed or deleted in most patients with breast cancer (74). Moreover, GATA3 can activate the downstream molecule miR-29b that can further inhibit the synthesis of proteins required for tumor metastasis. In the absence of GATA3, the metastasis of cancer cells cannot be stopped, and metastatic tumor cells can induce inflammatory responses, stimulate angiogenesis, and acquire nutrients for metastasis. Nakasone et al. observed increased sensitivity of breast cancer cells to drugs in mice after the selective deletion of two distinct types of TME factors, MMP9 and CCR2 (75). Moreover, treatment with HGF or combinatorial inhibition of RAF and MET can be used as potential therapeutic

strategies in *BRAF*-mutant melanoma. MSCs, which are mature progenitor cells, are essential components of the TME and considered to assist in metastasis (76). Following contact with MSCs, breast cancer cells activate lysyl oxidase expression that can enhance their metastatic ability and promote primary tumor dissemination to the lungs and bones. In a recent study, NOTCH1 signaling activated by MSC-derived dermal fibroblasts was observed to regulate plasticity and stemness of melanoma stem/initiating cells (77). This finding suggests that CAF-targeted strategies may aid in efficiently eradicating CSCs.

Recent studies have shown that exosomes derived from tumor cells or non-tumor cells are prominent messengers in regulating CSC plasticity (78, 79). For instance, exosomes secreted from CAF contribute to CSC proliferation and induce chemoresistance in colorectal cancer (80). Exosomes also play an important role in tumor metastasis through the premetastatic niche formation (81, 82). Exosomes secreted by stromal cells within the TME facilitate the transformation of non-CSCs into CSCs (83). Hu et al. demonstrated that CAF-derived exosomes significantly promote clonogenicity and increase the percentage of colorectal CSCs by activating the WNT pathway (80). Furthermore, exosomes can regenerate stem cell phenotypes by regulating the stem cell-related signaling pathways, including the Notch pathway, Wnt pathway, and Hedgehog pathway (84). In addition, exosomes derived from CSCs promote the proliferation and metastasis of clear cell renal cell carcinoma by transporting miR-19b-3p (85). Colorectal CSC-derived exosomes also facilitate tumorigenesis through mediating neutrophils (86).

The physical and chemical composition of the CSC niche, such as hypoxia and acidity, can also contribute to the regulation of CSC plasticity (87, 88). It is known that hypoxia modulates various aspects of cancer development and progression, including CSC plasticity. Reportedly, hypoxia could increase the plasticity of CSCs in glioblastoma by upregulating important molecules related to stem cell pathways, such as OCT4, NANOG, and c-MYC (89). The hypoxic niche can also determine the fate of CSCs *in vivo*. Tumor cells in the hypoxic niche show enhanced CSC properties compared to those in the non-hypoxic niche, which is attributed to activation of the ROS/HIF-1 α /c-Met pathway (90). Similarly, tumor-derived acidosis can also promote the invasion and metastasis of tumor cells *via* metabolic reprogramming (91). Furthermore, the acidic TME can facilitate immune invasion by inhibiting the activation of effector T cells and inducing M2 macrophage polarization (91, 92). Estrella et al. found that survival of CSCs depends on low pH environments that promote autophagy (93). Furthermore, Spugnini et al. demonstrated that a highly acidic TME can lead to chemoresistance, and targeted proton pumps with inhibitors can improve anti-tumor responses (94). Additionally, accumulating evidence demonstrated that the release of exosomes is significantly improved in an acidic TME, thereby leading to malignant tumor phenotypes (95–97). Collectively, CSCs are the key players in tumor recurrence and metastasis, wherein the TME provides conditions favorable for the growth of CSCs.

THERAPEUTIC STRATEGIES ENCOMPASSING PLASTICITY AND NICHE OF CSCs

Intratumoral heterogeneity and complexity of the TME are the major challenges in effective cancer treatment. CSC plasticity augments tumor heterogeneity, further enhancing and rendering difficulty in regulating drug resistance, relapse, and metastasis (98). Although chemotherapeutics can eliminate most tumor cells, a minority of CSCs and resistant cancer cells tend to escape the lethal effect of these drugs, eventually rendering tumor recurrence (1). It is even more difficult to completely eradicate CSCs with plasticity. Anticancer drugs normally only target tumor cells within their cell cycle; as plasticity of CSCs varies between the stationary and dynamic states, they are not affected, which is the primary reason for treatment failure (99). Consequently, CSC plasticity is now recognized as a major “target cell population” in oncology (4). Recent studies have shown that therapies targeting both plasticity and niche of CSCs may be promising strategies in suppressing tumor progression. For example, CAFs could activate stem cell pathways and are highly abundant in the TME. Targeting the relevant CAF–CSC signaling axis should therefore eliminate CSCs *via* induced differentiation and/or promoted apoptosis, contributing to tumor regression. Recently, a neutralizing monoclonal antibody against GPR77 was observed to effectively control tumor formation and reverse chemoresistance by eliminating CD10⁺ GPR77⁺ subpopulation of CAFs, proposing a CAF-targeted therapeutic strategy (100). Another research reported that CCL2 mediates a crosstalk between cancer cells and stromal fibroblasts that regulates breast CSCs. CCL2 secreted by CAFs activates the NOTCH1 pathway that further induces CSC phenotype in the breast cancer cells, granting them self-renewal potential, indicating CCL2 as a potential target to block non-CSC-to-CSC switch (101). Luo et al. observed that co-inhibition of glycolysis and thioredoxin and glutathione antioxidant pathways suppresses tumor-initiating potential, tumor growth, and metastasis of breast cancer cells under metabolic stress or hypoxia. The probable reason is that the combination strategy eliminates both quiescent mesenchymal-like and proliferative epithelial-like states of breast CSCs (102). Further, programmed cell death protein 1 blockade, combined with a granulocyte-macrophage colony-stimulating factor-modified CSC vaccine, was observed to enhance a specific antitumor immunotherapy response against bladder cancer (103). Exosomes, hypoxia, and acidity are indeed pivotal for CSC-niche development, and molecules capable of targeting exosomes or acidity or inducing hypoxia are potential therapeutic regimens for eliminating CSCs by reprogramming the TME.

CSCs can gain or lose stemness and switch their status by adapting to the physical conditions (hypoxia and acidity), and communicate with stroma and immune cells, corroborating the crosstalk between intrinsic CSC plasticity and niche complexity. Therefore, combination strategies that target CSC plasticity together with immunotherapy or TME-modulating agents

could be promising in inhibiting tumor progression and metastasis. However, whether CSC plasticity arises as a consequence of the microenvironment-exerted selection pressure or whether it is an intrinsic, default feature of cancer cells that enables them to adapt to varying conditions of the TME remains poorly unknown. Although most cancer cell subpopulations are capable of phenotypic transition, they vary in their speed and ability of adaptation. Recent studies on glioblastoma suggest that the intrinsic plasticity of tumor cells renders them to randomly switch between different phenotypes (defined by varied expression of CSC markers) and adapt to the TME (18, 104). In summary, these studies underscore that alterations in the CSC niche play important roles in restraining plasticity of CSCs and highlight the need to better understand the crosstalk between TME and CSC plasticity. Collectively, targeting CSCs and their niches is a promising strategy for efficient cancer therapy.

CONCLUSIONS

In this review, we present the recent advances in oncology that relate TME and CSC plasticity. All the observations pinpoint to the fact that developing novel CSC plasticity-suppressing strategies by targeting TME can improve cancer prognosis and patient survival. Therefore, we propose that exploiting the intrinsic dependence of CSCs to interact with non-tumor cell types in the CSC niche is a potential strategy for cancer therapy. The need-of-the-hour is, therefore, to understand the fundamental mechanisms underlying CSC plasticity and to illustrate the effect of the dynamic properties of CSCs; these

aspects can subsequently help improve clinical management of cancers. Further investigation on the interactions of CSC plasticity, tumor, and TME, particularly clarifying the associated signaling pathways, will greatly facilitate our understanding of the invasive and metastatic features of malignant tumors. Regarding application in clinical treatment, combination TME-targeted therapy with the molecular drugs that reverse or block CSC plasticity should be envisaged to provide new insights into effectively inhibiting tumor metastases and efficiently managing cancer. Finally, this combination therapy can be applied in neoadjuvant chemotherapy and postsurgical resection, to help eradicate residual, dormant, and distantly located CSCs, potentially preventing distant metastases.

AUTHOR CONTRIBUTIONS

MX proposed and supervised the research. XZ and CY collected the references. XZ, and CY drafted the paper. All authors contributed to the article and approved the submitted version.

FUNDING

This study was supported by grants from the National Natural Science Foundation of China (No. 81803574), China Postdoctoral Science Foundation (2019M653430), Post-Doctor Research Project, West China Hospital, Sichuan University (2018HXBH003), and Key Technology Research and Development Program of the Sichuan Province (2019YFS0208, 2021YFSY0009).

REFERENCES

- Nassar D, Blanpain C. Cancer Stem Cells: Basic Concepts and Therapeutic Implications. *Annu Rev Pathol* (2016) 11:47–76. doi: 10.1146/annurev-pathol-012615-044438
- Vlasi E, Pajonk F. Cancer Stem Cells, Cancer Cell Plasticity and Radiation Therapy. *Semin Cancer Biol* (2015) 31:28–35. doi: 10.1016/j.semcancer.2014.07.001
- Shimokawa M, Ohta Y, Nishikori S, Matano M, Takano A, Fujii M, et al. Visualization and Targeting of LGR5(+) Human Colon Cancer Stem Cells. *Nature* (2017) 545(7653):187–92. doi: 10.1038/nature22081
- Cazet AS, Hui MN, Elsworth BL, Wu SZ, Roden D, Chan C-L, et al. Targeting Stromal Remodeling and Cancer Stem Cell Plasticity Overcomes Chemoresistance in Triple Negative Breast Cancer. *Nat Commun* (2018) 9 (1):2897. doi: 10.1038/s41467-018-05220-6
- Ahmed N, Escalona R, Leung D, Chan E, Kannourakis G. Tumour Microenvironment and Metabolic Plasticity in Cancer and Cancer Stem Cells: Perspectives on Metabolic and Immune Regulatory Signatures in Chemoresistant Ovarian Cancer Stem Cells. *Semin Cancer Biol* (2018) 53:265–81. doi: 10.1016/j.semcancer.2018.10.002
- Takebe N, Miele L, Harris PJ, Jeong W, Bando H, Kahn M, et al. Targeting Notch, Hedgehog, and Wnt Pathways in Cancer Stem Cells: Clinical Update. *Nat Rev Clin Oncol* (2015) 12(8):445–64. doi: 10.1038/nrclinonc.2015.61
- Sancho P, Burgos-Ramos E, Tavera A, Bou Kheir T, Jagust P, Schoenhals M, et al. MYC/PGC-1 α Balance Determines the Metabolic Phenotype and Plasticity of Pancreatic Cancer Stem Cells. *Cell Metab* (2015) 22(4):590–605. doi: 10.1016/j.cmet.2015.08.015
- Plaks V, Kong N, Werb Z. The Cancer Stem Cell Niche: How Essential Is the Niche in Regulating Stemness of Tumor Cells? *Cell Stem Cell* (2015) 16 (3):225–38. doi: 10.1016/j.stem.2015.02.015
- Sung P-J, Rama N, Imbach J, Fiore S, Ducarouge B, Neves D, et al. Cancer-Associated Fibroblasts Produce Netrin-1 to Control Cancer Cell Plasticity. *Cancer Res* (2019) 79(14):3651–61. doi: 10.1158/0008-5472.CAN-18-2952
- Marjanovic ND, Hofree M, Chan JE, Canner D, Wu K, Trakala M, et al. Emergence of a High-Plasticity Cell State During Lung Cancer Evolution. *Cancer Cell* (2020) 38(2):229–46.e13. doi: 10.1016/j.ccell.2020.06.012
- Shenoy S. Cell Plasticity in Cancer: A Complex Interplay of Genetic, Epigenetic Mechanisms and Tumor Micro-Environment. *Surg Oncol* (2020) 34:154–62. doi: 10.1016/j.suronc.2020.04.017
- Basova L, Parfitt GJ, Richardson A, Delcroix V, Umazume T, Pelaez D, et al. Origin and Lineage Plasticity of Endogenous Lacrimal Gland Epithelial Stem/Progenitor Cells. *iScience* (2020) 23(6):101230. doi: 10.1016/j.isci.2020.101230
- Kong D, Hughes CJ, Ford HL. Cellular Plasticity in Breast Cancer Progression and Therapy. *Front Mol Biosci* (2020) 7:72. doi: 10.3389/fmolb.2020.00072
- Thankamony AP, Saxena K, Murali R, Jolly MK, Nair R. Cancer Stem Cell Plasticity - a Deadly Deal. *Front Mol Biosci* (2020) 7:79. doi: 10.3389/fmolb.2020.00079
- Christin JR, Wang C, Chung CY, Liu Y, Dravis C, Tang W, et al. Stem Cell Determinant SOX9 Promotes Lineage Plasticity and Progression in Basal-Like Breast Cancer. *Cell Rep* (2020) 31(10):107742. doi: 10.1016/j.celrep.2020.107742

16. Das PK, Pillai S, Rakib MA, Khanam JA, Gopalan V, Lam AKY, et al. Plasticity of Cancer Stem Cell: Origin and Role in Disease Progression and Therapy Resistance. *Stem Cell Rev Rep* (2020) 16(2):397–412. doi: 10.1007/s12015-019-09942-y
17. Chaffer CL, Marjanovic ND, Lee T, Bell G, Kleer CG, Reinhardt F, et al. Poised Chromatin at the ZEB1 Promoter Enables Breast Cancer Cell Plasticity and Enhances Tumorigenicity. *Cell* (2013) 154(1):61–74. doi: 10.1016/j.cell.2013.06.005
18. Dirkse A, Golebiewska A, Buder T, Nazarov PV, Muller A, Poovathingal S, et al. Stem Cell-Associated Heterogeneity in Glioblastoma Results From Intrinsic Tumor Plasticity Shaped by the Microenvironment. *Nat Commun* (2019) 10(1):1787. doi: 10.1038/s41467-019-09853-z
19. Roesch A, Fukunaga-Kalabis M, Schmidt EC, Zabierowski SE, Brafford PA, Vultur A, et al. A Temporarily Distinct Subpopulation of Slow-Cycling Melanoma Cells is Required for Continuous Tumor Growth. *Cell* (2010) 141(4):583–94. doi: 10.1016/j.cell.2010.04.020
20. Kobayashi S, Yamada-Okabe H, Suzuki M, Natori O, Kato A, Matsubara K, et al. LGR5-Positive Colon Cancer Stem Cells Interconvert With Drug-Resistant LGR5-Negative Cells and Are Capable of Tumor Reconstitution. *Stem Cells* (2012) 30(12):2631–44. doi: 10.1002/stem.1257
21. de Sousa e Melo F, Kurtova AV, Harnoss JM, Kljavin N, Hoeck JD, Hung J, et al. A Distinct Role for Lgr5 Stem Cells in Primary and Metastatic Colon Cancer. *Nature* (2017) 543(7647):676–80. doi: 10.1038/nature21713
22. Fumagalli A, Oost KC, Kester L, Morgner J, Bornes L, Bruens L, et al. Plasticity of Lgr5-Negative Cancer Cells Drives Metastasis in Colorectal Cancer. *Cell Stem Cell* (2020) 26(4):569–78. doi: 10.1016/j.stem.2020.02.008
23. Fernández-Cortés M, Delgado-Bellido D, Oliver FJ. Vasculogenic Mimicry: Become an Endothelial Cell “But Not So Much”. *Front Oncol* (2019) 9:803. doi: 10.3389/fonc.2019.00803
24. Zhang Y, Sun B, Zhao X, Liu Z, Wang X, Yao X, et al. Clinical Significances and Prognostic Value of Cancer Stem-Like Cells Markers and Vasculogenic Mimicry in Renal Cell Carcinoma. *J Surg Oncol* (2013) 108(6):414–9. doi: 10.1002/jso.23402
25. Marusyk A, Janiszewska M, Polyak K. Intratumor Heterogeneity: The Rosetta Stone of Therapy Resistance. *Cancer Cell* (2020) 37(4):471–84. doi: 10.1016/j.ccell.2020.03.007
26. Haussler J, Alon U. Tumour Heterogeneity and the Evolutionary Trade-Offs of Cancer. *Nat Rev Cancer* (2020) 20(4):247–57. doi: 10.1038/s41568-020-0241-6
27. Kinker GS, Greenwald AC, Tal R, Orlova Z, Cuoco MS, McFarland JM, et al. Pan-Cancer Single-Cell RNA-Seq Identifies Recurring Programs of Cellular Heterogeneity. *Nat Genet* (2020) 52(11):1208–18. doi: 10.1038/s41588-020-00726-6
28. Lawson ARJ, Abascal F, Coorens THH, Hooks Y, O’Neill L, Latimer C, et al. Extensive Heterogeneity in Somatic Mutation and Selection in the Human Bladder. *Sci (New York NY)* (2020) 370(6512):75–82. doi: 10.1126/science.aba8347
29. Persi E, Wolf YI, Horn D, Ruppén E, Demichelis F, Gatenby RA, et al. Mutation-Selection Balance and Compensatory Mechanisms in Tumour Evolution. *Nat Rev Genet* (2020) 22(4):251–62. doi: 10.1038/s41576-020-00299-4
30. Shackleton M, Quintana E, Fearon ER, Morrison SJ. Heterogeneity in Cancer: Cancer Stem Cells Versus Clonal Evolution. *Cell* (2009) 138(5):822–9. doi: 10.1016/j.cell.2009.08.017
31. Prasetyanti PR, Medema JP. Intra-Tumor Heterogeneity From a Cancer Stem Cell Perspective. *Mol Cancer* (2017) 16(1):41. doi: 10.1186/s12943-017-0600-4
32. Nowell PC. The Clonal Evolution of Tumor Cell Populations. *Science* (1976) 194(4260):23–8. doi: 10.1126/science.959840
33. Magee JA, Piskounova E, Morrison SJ. Cancer Stem Cells: Impact, Heterogeneity, and Uncertainty. *Cancer Cell* (2012) 21(3):283–96. doi: 10.1016/j.ccr.2012.03.003
34. Rich JN. Cancer Stem Cells: Understanding Tumor Hierarchy and Heterogeneity. *Medicine* (2016) 95(1 Suppl 1):S2–7. doi: 10.1097/md.00000000000004764
35. Clara JA, Monge C, Yang Y, Takebe N. Targeting Signalling Pathways and the Immune Microenvironment of Cancer Stem Cells - a Clinical Update. *Nat Rev Clin Oncol* (2020) 17(4):204–32. doi: 10.1038/s41571-019-0293-2
36. Butti R, Gunasekaran VP, Kumar TVS, Banerjee P, Kundu GC. Breast Cancer Stem Cells: Biology and Therapeutic Implications. *Int J Biochem Cell Biol* (2019) 107:38–52. doi: 10.1016/j.biocel.2018.12.001
37. Walcher L, Kistenmacher AK, Suo H, Kitte R, Dluczek S, Strauß A, et al. Cancer Stem Cells-Origins and Biomarkers: Perspectives for Targeted Personalized Therapies. *Front Immunol* (2020) 11:1280. doi: 10.3389/fimmu.2020.01280
38. Reya T, Morrison SJ, Clarke MF, Weissman IL. Stem Cells, Cancer, and Cancer Stem Cells. *Nature* (2001) 414(6859):105–11. doi: 10.1038/35102167
39. Meyer MJ, Fleming JM, Lin AF, Hussnain SA, Ginsburg E, Vonderhaar BK. CD44posCD49fhiCD133/2hi Defines Xenograft-Initiating Cells in Estrogen Receptor-Negative Breast Cancer. *Cancer Res* (2010) 70(11):4624–33. doi: 10.1158/0008-5472.can-09-3619
40. Boiko AD, Razorenova OV, van de Rijn M, Swetter SM, Johnson DL, Ly DP, et al. Human Melanoma-Initiating Cells Express Neural Crest Nerve Growth Factor Receptor CD271. *Nature* (2010) 466(7302):133–7. doi: 10.1038/nature09161
41. Wu Y, Zhang J, Zhang X, Zhou H, Liu G, Li Q. Cancer Stem Cells: A Potential Breakthrough in HCC-Targeted Therapy. *Front Pharmacol* (2020) 11:198. doi: 10.3389/fphar.2020.00198
42. Osman A, Afify SM, Hassan G, Fu X, Seno A, Seno M. Revisiting Cancer Stem Cells as the Origin of Cancer-Associated Cells in the Tumor Microenvironment: A Hypothetical View From the Potential of Ipscs. *Cancers* (2020) 12(4):879. doi: 10.3390/cancers12040879
43. McGranahan N, Swanton C. Clonal Heterogeneity and Tumor Evolution: Past, Present, and the Future. *Cell* (2017) 168(4):613–28. doi: 10.1016/j.cell.2017.01.018
44. Dagogo-Jack I, Shaw AT. Tumour Heterogeneity and Resistance to Cancer Therapies. *Nat Rev Clin Oncol* (2018) 15(2):81–94. doi: 10.1038/nrclinonc.2017.166
45. Cros J, Raffenne J, Couvelard A, Poté N. Tumor Heterogeneity in Pancreatic Adenocarcinoma. *Pathobiol: J Immunopathol Mol Cell Biol* (2018) 85(1-2):64–71. doi: 10.1159/000477773
46. Lawson DA, Kessenbrock K, Davis RT, Pervolarakis N, Werb Z. Tumour Heterogeneity and Metastasis at Single-Cell Resolution. *Nat Cell Biol* (2018) 20(12):1349–60. doi: 10.1038/s41556-018-0236-7
47. Celià-Terrassa T, Jolly MK. Cancer Stem Cells and Epithelial-to-Mesenchymal Transition in Cancer Metastasis. *Cold Spring Harbor Perspect Med* (2020) 10(7):a036905. doi: 10.1101/cshperspect.a036905
48. Lu W, Kang Y. Epithelial-Mesenchymal Plasticity in Cancer Progression and Metastasis. *Dev Cell* (2019) 49(3):361–74. doi: 10.1016/j.devcel.2019.04.010
49. Yang J, Antin P, Bex G, Blanpain C, Brabletz T, Bronner M, et al. Guidelines and Definitions for Research on Epithelial-Mesenchymal Transition. *Nat Rev Mol Cell Biol* (2020) 21(6):341–52. doi: 10.1038/s41580-020-0237-9
50. Beerling E, Seinstra D, de Wit E, Kester L, van der Velden D, Maynard C, et al. Plasticity Between Epithelial and Mesenchymal States Unlinks EMT From Metastasis-Enhancing Stem Cell Capacity. *Cell Rep* (2016) 14(10):2281–8. doi: 10.1016/j.celrep.2016.02.034
51. da Silva-Diz V, Lorenzo-Sanz L, Bernat-Peguera A, Lopez-Cerda M, Muñoz P. Cancer Cell Plasticity: Impact on Tumor Progression and Therapy Response. *Semin Cancer Biol* (2018) 53:48–58. doi: 10.1016/j.semcancer.2018.08.009
52. Gupta PB, Pastushenko I, Skibinski A, Blanpain C, Kuperwasser C. Phenotypic Plasticity: Driver of Cancer Initiation, Progression, and Therapy Resistance. *Cell Stem Cell* (2019) 24(1):65–78. doi: 10.1016/j.stem.2018.11.011
53. Zheng X, Dai F, Feng L, Zou H, Feng L, Xu M. Communication Between Epithelial-Mesenchymal Plasticity and Cancer Stem Cells: New Insights Into Cancer Progression. *Front Oncol* (2021) 11:617597. doi: 10.3389/fonc.2021.617597
54. Wu T, Dai Y. Tumor Microenvironment and Therapeutic Response. *Cancer Lett* (2017) 387:61–8. doi: 10.1016/j.canlet.2016.01.043
55. Locy H, de Mey S, de Mey W, De Ridder M, Thielemans K, Maenhout SK. Immunomodulation of the Tumor Microenvironment: Turn the Enemy Into Friend. *Front Immunol* (2018) 9:2909. doi: 10.3389/fimmu.2018.02909
56. Vitale I, Manic G, Coussens LM, Kroemer G, Galluzzi L. Macrophages and Metabolism in the Tumor Microenvironment. *Cell Metab* (2019) 30(1):36–50. doi: 10.1016/j.cmet.2019.06.001

57. Dougan M, Dougan SK. Targeting Immunotherapy to the Tumor Microenvironment. *J Cell Biochem* (2017) 118(10):3049–54. doi: 10.1002/jcb.26005
58. Hinshaw DC, Shevde LA. The Tumor Microenvironment Innately Modulates Cancer Progression. *Cancer Res* (2019) 79(18):4557–66. doi: 10.1158/0008-5472.can-18-3962
59. Noman MZ, Hasmin M, Lequeux A, Xiao M, Duhem C, Chouaib S, et al. Improving Cancer Immunotherapy by Targeting the Hypoxic Tumor Microenvironment: New Opportunities and Challenges. *Cells* (2019) 8(9):1083. doi: 10.3390/cells8091083
60. Zhou F, Feng B, Yu H, Wang D, Wang T, Ma Y, et al. Tumor Microenvironment-Activatable Prodrug Vesicles for Nanoenabled Cancer Chemoimmunotherapy Combining Immunogenic Cell Death Induction and CD47 Blockade. *Advanced materials (Deerfield Beach Fla)* (2019) 31(14):e1805888. doi: 10.1002/adma.201805888
61. Prager BC, Xie Q, Bao S, Rich JN. Cancer Stem Cells: The Architects of the Tumor Ecosystem. *Cell Stem Cell* (2019) 24(1):41–53. doi: 10.1016/j.stem.2018.12.009
62. Bocci F, Gearhart-Serna L, Boaretto M, Ribeiro M, Ben-Jacob E, Devi GR, et al. Toward Understanding Cancer Stem Cell Heterogeneity in the Tumor Microenvironment. *Proc Natl Acad Sci U S A* (2019) 116(1):148–57. doi: 10.1073/pnas.1815345116
63. Nazio F, Bordini M, Cianfanelli V, Locatelli F, Cecconi F. Autophagy and Cancer Stem Cells: Molecular Mechanisms and Therapeutic Applications. *Cell Death Differ* (2019) 26(4):690–702. doi: 10.1038/s41418-019-0292-y
64. Rao G, Wang H, Li B, Huang L, Xue D, Wang X, et al. Reciprocal Interactions Between Tumor-Associated Macrophages and CD44-Positive Cancer Cells via Osteopontin/CD44 Promote Tumorigenicity in Colorectal Cancer. *Clin Cancer Res* (2013) 19(4):785–97. doi: 10.1158/1078-0432.ccr-12-2788
65. Doherty MR, Parvani JG, Tamagno I, Junk DJ, Bryson BL, Cheon HJ, et al. The Opposing Effects of Interferon-Beta and Oncostatin-M as Regulators of Cancer Stem Cell Plasticity in Triple-Negative Breast Cancer. *Breast Cancer research: BCR* (2019) 21(1):54. doi: 10.1186/s13058-019-1136-x
66. Li X, Jolly MK, George JT, Pienta KJ, Levine H. Computational Modeling of the Crosstalk Between Macrophage Polarization and Tumor Cell Plasticity in the Tumor Microenvironment. *Front Oncol* (2019) 9:10. doi: 10.3389/fonc.2019.00010
67. Ma W, Ma J, Xu J, Qiao C, Branscum A, Cardenas A, et al. Lin28 Regulates BMP4 and Functions With Oct4 to Affect Ovarian Tumor Microenvironment. *Cell Cycle* (2013) 12(1):88–97. doi: 10.4161/cc.23028
68. Su S, Chen J, Yao H, Liu J, Yu S, Lao L, et al. CD10(+)GPR77(+) Cancer-Associated Fibroblasts Promote Cancer Formation and Chemoresistance by Sustaining Cancer Stemness. *Cell* (2018) 172(4):841–56.e16. doi: 10.1016/j.cell.2018.01.009
69. Huang TX, Guan XY, Fu L. Therapeutic Targeting of the Crosstalk Between Cancer-Associated Fibroblasts and Cancer Stem Cells. *Am J Cancer Res* (2019) 9(9):1889–904.
70. Chen W-J, Ho C-C, Chang Y-L, Chen H-Y, Lin C-A, Ling T-Y, et al. Cancer-Associated Fibroblasts Regulate the Plasticity of Lung Cancer Stemness via Paracrine Signalling. *Nat Commun* (2014) 5:3472. doi: 10.1038/ncomms4472
71. Begum A, McMillan RH, Chang Y-T, Penchev VR, Rajeshkumar NV, Maitra A, et al. Direct Interactions With Cancer-Associated Fibroblasts Lead to Enhanced Pancreatic Cancer Stem Cell Function. *Pancreas* (2019) 48(3):329–34. doi: 10.1097/MPA.0000000000001249
72. Lau EYT, Lo J, Cheng BYL, Ma MKF, Lee JMF, Ng JKY, et al. Cancer-Associated Fibroblasts Regulate Tumor-Initiating Cell Plasticity in Hepatocellular Carcinoma Through C-Met/FRA1/HEY1 Signaling. *Cell Rep* (2016) 15(6):1175–89. doi: 10.1016/j.celrep.2016.04.019
73. Buraschi S, Neill T, Owens RT, Iniguez LA, Purkins G, Vadigepalli R, et al. Decorin Protein Core Affects the Global Gene Expression Profile of the Tumor Microenvironment in a Triple-Negative Orthotopic Breast Carcinoma Xenograft Model. *PLoS One* (2012) 7(9):e45559. doi: 10.1371/journal.pone.0045559
74. Chou J, Lin JH, Brenot A, Kim JW, Provot S, Werb Z. GATA3 Suppresses Metastasis and Modulates the Tumour Microenvironment by Regulating microRNA-29b Expression. *Nat Cell Biol* (2013) 15(2):201–13. doi: 10.1038/ncb2672
75. Nakasone ES, Askautrud HA, Kees T, Park J-H, Plaks V, Ewald AJ, et al. Imaging Tumor-Stroma Interactions During Chemotherapy Reveals Contributions of the Microenvironment to Resistance. *Cancer Cell* (2012) 21(4):488–503. doi: 10.1016/j.ccr.2012.02.017
76. El-Haibi CP, Bell GW, Zhang J, Collmann AY, Wood D, Scherber CM, et al. Critical Role for Lysyl Oxidase in Mesenchymal Stem Cell-Driven Breast Cancer Malignancy. *Proc Natl Acad Sci U S A* (2012) 109(43):17460–5. doi: 10.1073/pnas.1206653109
77. Du Y, Shao H, Moller M, Prokupets R, Tse YT, Liu Z-J. Intracellular Notch1 Signaling in Cancer-Associated Fibroblasts Dictates the Plasticity and Stemness of Melanoma Stem/Initiating Cells. *Stem Cells* (2019) 37(7):865–75. doi: 10.1002/stem.3013
78. Spugnini EP, Logozzi M, Di Raimo R, Mizzoni D, Fais S. A Role of Tumor-Released Exosomes in Paracrine Dissemination and Metastasis. *Int J Mol Sci* (2018) 19(12):3968. doi: 10.3390/ijms19123968
79. Sun Z, Wang L, Dong L, Wang X. Emerging Role of Exosome Signalling in Maintaining Cancer Stem Cell Dynamic Equilibrium. *J Cell Mol Med* (2018) 22(8):3719–28. doi: 10.1111/jcmm.13676
80. Hu Y, Yan C, Mu L, Huang K, Li X, Tao D, et al. Fibroblast-Derived Exosomes Contribute to Chemoresistance Through Priming Cancer Stem Cells in Colorectal Cancer. *PLoS One* (2015) 10(5):e0125625. doi: 10.1371/journal.pone.0125625
81. Logozzi M, Spugnini E, Mizzoni D, Di Raimo R, Fais S. Extracellular Acidity and Increased Exosome Release as Key Phenotypes of Malignant Tumors. *Cancer Metastasis Rev* (2019) 38(1-2):93–101. doi: 10.1007/s10555-019-09783-8
82. Zhao H, Achreja A, Iessi E, Logozzi M, Mizzoni D, Di Raimo R, et al. The Key Role of Extracellular Vesicles in the Metastatic Process. *Biochim Biophys Acta Rev Cancer* (2018) 1869(1):64–77. doi: 10.1016/j.bbcan.2017.11.005
83. Lugini L, Valtieri M, Federici C, Cecchetti S, Meschini S, Condello M, et al. Exosomes From Human Colorectal Cancer Induce a Tumor-Like Behavior in Colonic Mesenchymal Stromal Cells. *Oncotarget* (2016) 7(31):50086–98. doi: 10.18632/oncotarget.10574
84. Xu J, Liao K, Zhou W. Exosomes Regulate the Transformation of Cancer Cells in Cancer Stem Cell Homeostasis. *Stem Cells Int* (2018) 2018:4837370. doi: 10.1155/2018/4837370
85. Wang L, Yang G, Zhao D, Wang J, Bai Y, Peng Q, et al. CD103-Positive CSC Exosome Promotes EMT of Clear Cell Renal Cell Carcinoma: Role of Remote Mir-19b-3p. *Mol Cancer* (2019) 18(1):86. doi: 10.1186/s12943-019-0997-z
86. Hwang WL, Lan HY, Cheng WC, Huang SC, Yang MH. Tumor Stem-Like Cell-Derived Exosomal RNAs Prime Neutrophils for Facilitating Tumorigenesis of Colon Cancer. *J Hematol Oncol* (2019) 12(1):10. doi: 10.1186/s13045-019-0699-4
87. Debele TA, Yu L-Y, Yang C-S, Shen Y-A, Lo C-L. pH- and GSH-Sensitive Hyaluronic Acid-MP Conjugate Micelles for Intracellular Delivery of Doxorubicin to Colon Cancer Cells and Cancer Stem Cells. *Biomacromolecules* (2018) 19(9):3725–37. doi: 10.1021/acs.biomac.8b00856
88. Peng F, Wang JH, Fan WJ, Meng YT, Li MM, Li TT, et al. Glycolysis Gatekeeper PDK1 Reprograms Breast Cancer Stem Cells Under Hypoxia. *Oncogene* (2018) 37(8):1062–74. doi: 10.1038/onc.2017.368
89. Srivastava C, Irshad K, Dikshit B, Chattopadhyay P, Sarkar C, Gupta DK, et al. FAT1 Modulates EMT and Stemness Genes Expression in Hypoxic Glioblastoma. *Int J Cancer* (2018) 142(4):805–12. doi: 10.1002/ijc.31092
90. Jung N, Kwon HJ, Jung HJ. Downregulation of Mitochondrial UQCRCB Inhibits Cancer Stem Cell-Like Properties in Glioblastoma. *Int J Oncol* (2018) 52(1):241–51. doi: 10.3892/ijo.2017.4191
91. Pillai SR, Damaghi M, Marunaka Y, Spugnini EP, Fais S, Gillies RJ. Causes, Consequences, and Therapy of Tumors Acidosis. *Cancer metastasis Rev* (2019) 38(1-2):205–22. doi: 10.1007/s10555-019-09792-7
92. Calcinotto A, Filipazzi P, Grioni M, Iero M, De Milito A, Ricupito A, et al. Modulation of Microenvironment Acidity Reverses Anergy in Human and Murine Tumor-Infiltrating T Lymphocytes. *Cancer Res* (2012) 72(11):2746–56. doi: 10.1158/0008-5472.Can-11-1272
93. Estrella V, Chen T, Lloyd M, Wojtkowiak J, Cornnell HH, Ibrahim-Hashim A, et al. Acidity Generated by the Tumor Microenvironment Drives Local

- Invasion. *Cancer Res* (2013) 73(5):1524–35. doi: 10.1158/0008-5472.can-12-2796
94. Spugnini EP, Fais S. Drug Repurposing for Anticancer Therapies. A Lesson From Proton Pump Inhibitors. *Expert Opin Ther patents* (2020) 30(1):15–25. doi: 10.1080/13543776.2020.1704733
 95. Logozzi M, Mizzoni D, Angelini DF, Di Raimo R, Falchi M, Battistini L, et al. Microenvironmental Ph and Exosome Levels Interplay in Human Cancer Cell Lines of Different Histotypes. *Cancers* (2018) 10(10):370. doi: 10.3390/cancers10100370
 96. Parolini I, Federici C, Raggi C, Lugini L, Palleschi S, De Milito A, et al. Microenvironmental pH Is a Key Factor for Exosome Traffic in Tumor Cells. *J Biol Chem* (2009) 284(49):34211–22. doi: 10.1074/jbc.M109.041152
 97. Logozzi M, Angelini DF, Iessi E, Mizzoni D, Di Raimo R, Federici C, et al. Increased PSA Expression on Prostate Cancer Exosomes in *In Vitro* Condition and in Cancer Patients. *Cancer Lett* (2017) 403:318–29. doi: 10.1016/j.canlet.2017.06.036
 98. Batlle E, Clevers H. Cancer Stem Cells Revisited. *Nat Med* (2017) 23(10):1124–34. doi: 10.1038/nm.4409
 99. Zhan T, Ambrosi G, Wandmacher AM, Rauscher B, Betge J, Rindtorff N, et al. MEK Inhibitors Activate Wnt Signalling and Induce Stem Cell Plasticity in Colorectal Cancer. *Nat Commun* (2019) 10(1):2197. doi: 10.1038/s41467-019-09898-0
 100. Su S, Chen J, Yao H, Liu J, Yu S, Lao L, et al. CD10GPR77 Cancer-Associated Fibroblasts Promote Cancer Formation and Chemoresistance by Sustaining Cancer Stemness. *Cell* (2018) 172(4):841–56. doi: 10.1016/j.cell.2018.01.009
 101. Tsuyada A, Chow A, Wu J, Somlo G, Chu P, Loera S, et al. CCL2 Mediates Cross-Talk Between Cancer Cells and Stromal Fibroblasts That Regulates Breast Cancer Stem Cells. *Cancer Res* (2012) 72(11):2768–79. doi: 10.1158/0008-5472.CAN-11-3567
 102. Luo M, Shang L, Brooks MD, Jiagge E, Zhu Y, Buschhaus JM, et al. Targeting Breast Cancer Stem Cell State Equilibrium Through Modulation of Redox Signaling. *Cell Metab* (2018) 28(1):69–86. doi: 10.1016/j.cmet.2018.06.006
 103. Shi X, Zhang X, Li J, Mo L, Zhao H, Zhu Y, et al. PD-1 Blockade Enhances the Antitumor Efficacy of GM-CSF Surface-Modified Bladder Cancer Stem Cells Vaccine. *Int J Cancer* (2018) 142(10):2106–17. doi: 10.1002/ijc.31219
 104. Liau BB, Sievers C, Donohue LK, Gillespie SM, Flavahan WA, Miller TE, et al. Adaptive Chromatin Remodeling Drives Glioblastoma Stem Cell Plasticity and Drug Tolerance. *Cell Stem Cell* (2017) 20(2):233–46.e7. doi: 10.1016/j.stem.2016.11.003

Conflict of Interest: The authors declare that the research was conducted in the absence of any commercial or financial relationships that could be construed as a potential conflict of interest.

Copyright © 2021 Zheng, Yu and Xu. This is an open-access article distributed under the terms of the Creative Commons Attribution License (CC BY). The use, distribution or reproduction in other forums is permitted, provided the original author(s) and the copyright owner(s) are credited and that the original publication in this journal is cited, in accordance with accepted academic practice. No use, distribution or reproduction is permitted which does not comply with these terms.



The Tumor Microenvironment Factors That Promote Resistance to Immune Checkpoint Blockade Therapy

Bonnie L. Russell^{1,2†}, Selisha A. Sooklal^{1†}, Sibusiso T. Malindisa^{1†},
Lembelani Jonathan Daka² and Monde Ntwasa^{1*}

¹ Department of Life & Consumer Sciences, University of South Africa, Johannesburg, South Africa, ² Innovation Hub, Buboo (Pty) Ltd, Pretoria, South Africa

OPEN ACCESS

Edited by:

Wei Zhao,
City University of Hong Kong,
China

Reviewed by:

Chunming Cheng,
The Ohio State University,
United States
Pier Giorgio Petroni,
University of Parma, Italy

*Correspondence:

Monde Ntwasa
ntwasmm@unisa.ac.za

[†]These authors have contributed
equally to this work

Specialty section:

This article was submitted to
Molecular and Cellular Oncology,
a section of the journal
Frontiers in Oncology

Received: 14 December 2020

Accepted: 16 June 2021

Published: 29 June 2021

Citation:

Russell BL, Sooklal SA, Malindisa ST,
Daka LJ and Ntwasa M (2021) The
Tumor Microenvironment Factors That
Promote Resistance to Immune
Checkpoint Blockade Therapy.
Front. Oncol. 11:641428.
doi: 10.3389/fonc.2021.641428

Through genetic and epigenetic alterations, cancer cells present the immune system with a diversity of antigens or neoantigens, which the organism must distinguish from self. The immune system responds to neoantigens by activating naïve T cells, which mount an anticancer cytotoxic response. T cell activation begins when the T cell receptor (TCR) interacts with the antigen, which is displayed by the major histocompatibility complex (MHC) on antigen-presenting cells (APCs). Subsequently, accessory stimulatory or inhibitory molecules transduce a secondary signal in concert with the TCR/antigen mediated stimulus. These molecules serve to modulate the activation signal's strength at the immune synapse. Therefore, the activation signal's optimum amplitude is maintained by a balance between the costimulatory and inhibitory signals. This system comprises the so-called immune checkpoints such as the programmed cell death (PD-1) and Cytotoxic T lymphocyte-associated antigen-4 (CTLA-4) and is crucial for the maintenance of self-tolerance. Cancers often evade the intrinsic anti-tumor activity present in normal physiology primarily by the downregulation of T cell activation. The blockade of the immune checkpoint inhibitors using specific monoclonal antibodies has emerged as a potentially powerful anticancer therapy strategy. Several drugs have been approved mainly for solid tumors. However, it has emerged that there are innate and acquired mechanisms by which resistance is developed against these therapies. Some of these are tumor-intrinsic mechanisms, while others are tumor-extrinsic whereby the microenvironment may have innate or acquired resistance to checkpoint inhibitors. This review article will examine mechanisms by which resistance is mounted against immune checkpoint inhibitors focussing on anti-CTLA-4 and anti-PD-1/PD-L1 since drugs targeting these checkpoints are the most developed.

Keywords: PD-1, CTLA-4, Immune checkpoint inhibitor, resistance, tumor microenvironment

INTRODUCTION

Cancers often evade the intrinsic anti-tumor activity present in normal physiology through various mechanisms one of which is the downregulation of T cell activation. Through genetic and epigenetic alterations, cancer cells present the immune system with a diversity of antigens, which are distinguishable from self. Antigen-specific T cell activation is initiated by a signal mediated by the interaction of the T cell receptor (TCR) with an antigen that is bound to the major histocompatibility complex (MHC) on antigen presenting cells and another signal transduced through co-stimulatory molecules belonging to the B7 family. The optimum amplitude of activation signal is maintained by a balance between this costimulatory signal and an inhibitory one also mediated by the B7 family (1). This system comprises the so-called immune checkpoints mediated by the inhibitory molecules and is crucial for the maintenance of self-tolerance. The blockade of the immune checkpoint inhibitors has emerged as a potentially powerful strategy for anti-cancer therapy and

several drugs, mainly for solid tumors, have been approved (**Table 1**) (35, 36).

Cancers develop within a diverse and dynamic microenvironment and possess mechanisms to survive unfavourable physiological machinery designed to suppress carcinogenesis. Thus, they are equipped with strategies to reprogram the microenvironment metabolically and immunologically. For example, cancers develop mechanisms to switch off the physiological immune response by blocking activated T cells to protect themselves from cytotoxic killing. Thus, during cancer progression, the immune checkpoint pathways mediated by the structurally similar co-inhibitory receptors; Programmed cell Death 1 (PD-1) and the Cytotoxic T lymphocyte-associated antigen-4 (CTLA-4) or CD152 receptors are often usurped by cancer cells to evade immune surveillance. These two receptors, which form part of a growing list of checkpoint inhibitors, are the foremost targets for immune checkpoint inhibition-based drug development in recent years (**Table 1**).

TABLE 1 | List of FDA-approved Immune Checkpoint Inhibitors (ICIs) targeting CTLA-4, PD-1 and PD-L1.

Drug (Trade name)	Company	Date of approval	Indication	References			
CTLA-4 inhibitors							
Ipilimumab (Yervoy®)	Bristol-Myers Squibb	2011	Melanoma	(2)			
			colorectal cancer	(3)			
			Renal cell carcinoma	(4)			
PD-1 inhibitors							
Nivolumab (Opdivo®)	Bristol-Myers Squibb	2014	Melanoma	(5)			
			Hodgkin's lymphoma	(6)			
			Diffuse large B-cell lymphoma	(7)			
			Urothelial cancer	(8)			
			Colorectal cancer	(3)			
			Hepatocellular carcinoma	(9)			
			Non-small cell lung cancer	(10)			
			Small cell lung cancer	(11)			
			Renal cell carcinoma	(12)			
			Squamous cell carcinoma	(13)			
			Pembrolizumab (Keytruda®)	Merck	2014	Melanoma	(14)
						Cervical cancer	(15)
						Hodgkin's lymphoma	(16)
Diffuse large B-cell lymphoma	(17)						
Gastric cancer	(18)						
Urothelial cancer	(19)						
Colorectal cancer	(20)						
Hepatocellular carcinoma	(21)						
Cemiplimab (Libtayo®)	Sanofi	2018	Non-small cell lung cancer	(22)			
			Small cell lung cancer	(23)			
			Renal cell carcinoma	(24)			
			Squamous cell carcinoma	(25)			
			Esophageal cancer	(26)			
			Merkel cell carcinoma	(27)			
			Cutaneous squamous cell carcinoma	(28)			
			PD-L1 inhibitors				
Atezolizumab (Tecentriq®)	Roche, Genentech	2016	Non-small cell lung cancer	(29)			
Avelumab (Bavencio®)	Merck, Pfizer	2017	Triple negative breast cancer				
			Merkel cell carcinoma	(30)			
			Renal cell carcinoma	(31)			
Durvalumab (Imfinzi®)	AstraZeneca	2017	Urothelial cancer	(32)			
			Bladder cancer	(33)			
			Non-small cell lung cancer	(34)			

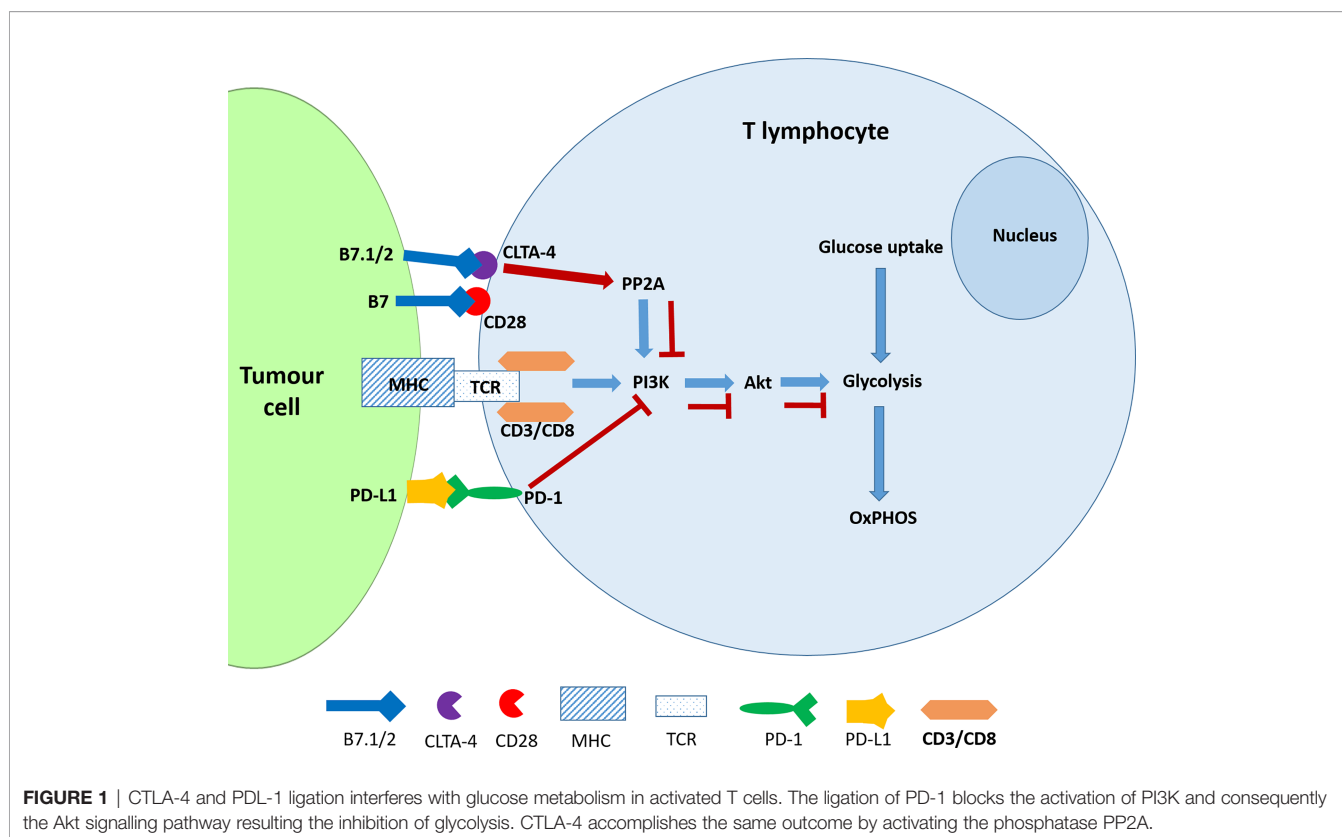
In this review we examine the mechanisms of inhibitors targeting the immune checkpoint pathways PD-1/PD-L1 and CTLA-4, as well as the types of resistance that can develop against them.

CTLA-4 AND PD-1 IMMUNE CHECKPOINT SIGNALLING PATHWAYS

The CTLA-4, which is the first co-inhibitory immune checkpoint receptor to be identified, is constitutively expressed on both CD4+ and CD8+ T lymphocytes (37). CD28 and CTLA-4 are both capable of binding two important ligands, namely B7.1 (also known as CD80) and B7.2 (also known as CD86) (38). CTLA-4 expression is up regulated in T cells after activation. This is particularly significant in cancer cells as CTLA-4 has a higher binding affinity to both ligands, compared to CD28. Consequently, it is plausible that the role of the CTLA-4 expressed on the surface of T cells is to decrease T cell activation by competing with CD28 for ligand binding as well as active removal of B7.1 and B7.2 from the cell surface of antigen-presenting cells (APCs) (39). It counteracts the activity of the co-stimulatory CD28 upon TCR engagement by the antigen-MHC complex on APCs (40). Upon T cell activation CTLA-4 is translocated *via* a genetically programmed pathway to the cell surface where it competes for binding with CD28. At the cell surface CTLA-4 is stabilized by src kinase-mediated phosphorylation and binds with higher affinity to B7 ligands

when compared with CD28. Intracellularly CTLA-4 transduces signals *via* PP2A and PI3K (41).

PD-1 is an inhibitor of both adaptive and innate immune responses and is more broadly expressed than CTLA-4 on activated T cells, B cells and myeloid cells and its depletion in experimental mice results in the disruption of immune tolerance and in multiple autoimmune features (42, 43). The TCR transduces the signal *via* the PI3K/Akt pathway and positively regulates glucose metabolism, which is reprogrammed during T cell activation (**Figure 1**). A negative signal during TCR activation may occur *via* a ligated PD-1 receptor, which mediates the recruitment of phosphatases, SHP2 (and/or SHP1) to dephosphorylate TCR-proximal molecules and displace the co-stimulatory molecule, CD28, thereby blocking lymphocyte activation. PD-1 ligation also directly inhibits phosphatidylinositol 4,5-bisphosphate-3 kinase (PI3K) (44). In the absence of PD-1, TCR signalling leads to Akt activation thereby promoting key cellular activities including glucose metabolism, cytokine production and phosphorylated glycogen synthase kinase-3 (GSK-3 β _P) associated events which include glycogen synthesis in the liver and in the muscles (45). Hence the inhibition of GSK-3 leads to the development of cancer and other developmental diseases (46). The ligands of PD-1 and CTLA-4 receptors belong to the B7 family and function by mediating “co-stimulatory” or “co-inhibitory” signals through the CD28 family of receptors on lymphocytes (47). Engagement of PD-1 by its ligands, PDL-1 and PDL-2, which are expressed on antigen presenting cells downregulates lymphocyte activation (48).



The evidence has shown that the CTLA-4 and PD-1 receptors may inhibit T-cell activation but use different signalling and synergistic pathways. Furthermore, the ligation of these receptors by their physiological ligands leads to the downregulation of glycolysis (45). It is noteworthy that, like cancer cells, activated T cells also exhibit the Warburg Effect or aerobic glycolysis which is characterised by elevated glycolysis and downregulated oxidative phosphorylation and is driven by mechanistic target of rapamycin (mTOR) signalling (49). The antagonistic effect of checkpoint inhibitors should therefore affect the metabolic reprogramming that would have occurred in activated T cells. However, this has not been specifically investigated according to our knowledge.

It has been shown that T cell activation requires upregulation of glucose metabolism and that while glucose deprivation does not affect proliferation, it diminishes the effector activities of T cells thereby driving cancer progression. Alternatively, when glycolysis was inhibited in CD8⁺ T cell using 2-deoxy-D-glucose (2-DG) in the mouse sarcoma model, interferon gamma (IFN γ) but not Interleukin-2 (IL-2) production was inhibited. Furthermore, a large-scale transcriptional analysis also showed that only 10% of genes induced by T cell activation were inhibited by 2-DG. This small subset of genes comprised those involved in effector functions (50). These observations suggest that the metabolic reprogramming associated with T cell activation specifies their functional properties. However, the impact of glucose metabolic profiles of the tumor microenvironment components on immune checkpoint blockade therapy is still not well understood.

In the solid tumor microenvironment, competition for glucose between cancer cells and tumor infiltrating CD8+

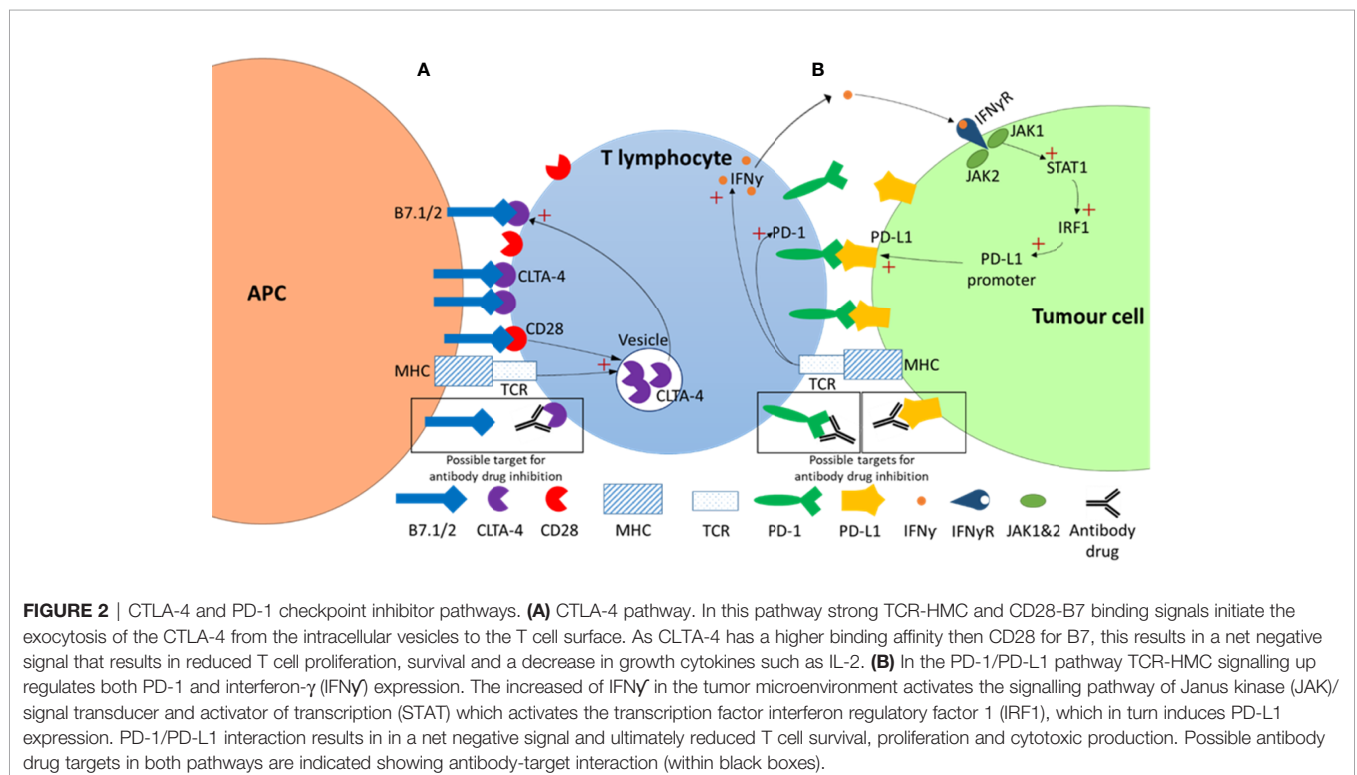
lymphocytes has been shown to result in the suppression of the T cell metabolic phenotype and effector capacity. Furthermore, it was shown that the glycolytic phenotype of cancer cells suppresses the metabolic programme and effector activities of T cells (51). Importantly, this study showed that anti-CTLA-4 and anti-PD-1 antibodies could reverse the antagonistic impact exerted by cancer cells on the TME.

Another question that requires attention is the comparative attractiveness of these receptors as therapeutic targets. Phenotypic differences in *PD-1* and *CTLA-4* knock-out mice show distinct outcomes that reveal critical features that suggests different responses to therapies that target these receptors. *PD-1*^{-/-} mice spontaneously develop lupus-like glomerulonephritis and arthritis. This phenotype is accelerated and characterized with extensive lymphadenopathy when the Fas or lymphoproliferation (*lpr*^{-/-}) mutation is added. On the other hand, transgenic mice with *CTLA-4* deficiency rapidly develop lymphoproliferative disease, multi-organ lymphocytic infiltration severe myocarditis and pancreatitis. Moreover, this mutation is lethal within four weeks (52, 53). These observations indicate that the blockade of PD-1 might be less toxic when compared to CTLA-4.

IMMUNE CHECKPOINT INHIBITORS

Mechanism of Inhibitors Targeting CTLA-4

CTLA-4 functions as a negative regulator of T-cell effector function and therefore presented as an attractive target for cancer therapy. Inhibitors targeting CTLA-4 act by preventing



the binding between CTLA-4 (on T-cells) and B7 ligands (on APCs) (**Figure 2**). As a result, Treg-associated immune suppression is inhibited and T-cell effector function is promoted, allowing the immune system to mount a response (54–56). An influential clinical trial whereby improved survival rates were seen when patients with unresectable melanomas (stage III/IV) were treated with an anti-CTLA-4 monoclonal antibody ultimately led to the FDA approval of the first immune checkpoint inhibitor, ipilimumab, for cancer therapy (2).

Ipilimumab, marketed as Yervoy® by Bristol-Myers Squibb, is a human IgG1κ anti-CTLA-4 monoclonal antibody. Ipilimumab was originally granted FDA approval for late stage, unresectable melanomas in 2011. It has subsequently been approved for patients with cutaneous melanoma, renal cell carcinoma and metastatic colorectal cancer as shown in **Table 1** (3, 4, 12, 57). Currently, ipilimumab remains as the only checkpoint inhibitor targeting CTLA-4.

Mechanism of Inhibitors Targeting PD-1

The interaction between PD-1 (on T-cells) and its ligand, PD-L1 (on APCs) (**Figure 2**), has an inhibitory effect on T-cell effector activity. The PD-1/PD-L1 pathway therefore represents an additional negative regulator of immune responses and a key mechanism in tumor evasion (58). Inhibitors that target PD-1 act by preventing its binding to PD-L1 (**Figure 2**). This interferes with the feedback mechanism between T-cells and tumor cells in the tumor microenvironment and consequently restores T-cell effector function enhancing anti-tumor activity (36).

Following the outcome of the CheckMate-037 trial, nivolumab received FDA approval in 2014 for the treatment of unresectable or metastatic melanoma in patients whose cancers had progressed following ipilimumab treatment ± BRAF inhibitors (2). Nivolumab is a human IgG4κ anti-PD-1 monoclonal antibody marketed as Opdivo® by Bristol-Myers Squibb. Nivolumab represented the first immune checkpoint inhibitor targeting PD-1 to be granted FDA approval. Its approval was subsequently expanded for the treatment of various cancers including cervical cancer (59), gastric cancer (60), urothelial cancer (8), Hodgkin's lymphoma (6), hepatocellular carcinoma (9), squamous cell carcinoma (13, 61), colorectal cancer (3), non-small cell lung cancer (10), diffuse large B-cell lymphoma (62), renal cell carcinoma (12) and small cell lung cancer (5, 6, 8–13, 61, 63) (**Table 1**).

In 2014 an additional PD-1 inhibitor, pembrolizumab, was granted accelerated approval as an alternative for nivolumab in patients with unresectable or metastatic melanoma based on the results from the NCT01295827 clinical trial (14, 64). Pembrolizumab, a humanized IgG4κ anti-PD-1 monoclonal antibody marketed as Keytruda® by Merck, later received expanded approval for the treatment of various cancers including cervical cancer (15), endometrial carcinoma (65), esophageal cancer (26), gastric cancer (18), urothelial cancer (19), Hodgkin's lymphoma (16), hepatocellular carcinoma (21), Merkel cell carcinoma (27), squamous cell carcinoma (25), colorectal cancer (20, 66), non-small cell lung cancer (22), diffuse large B-cell lymphoma (17), renal cell carcinoma (24) and small cell lung cancer (15–22, 24–27, 66, 67).

Cemiplimab, a human IgG4κ anti-PD-1 monoclonal antibody marketed as Libtayo® by Sanofi, is the most recent immune checkpoint inhibitor to be given FDA approval. In 2018, cemiplimab was approved for the treatment of metastatic cutaneous squamous cell carcinoma (28).

Mechanism of Inhibitors Targeting PD-L1

Similar to inhibitors targeting PD-1, PD-L1 inhibitors aim to disrupt the interaction between PD-1 and PD-L1 in the tumor microenvironment. Inhibiting PD-1/PD-L1 results in the stimulation of T-cell anti-tumor activity as described previously (36, 68).

The first PD-L1 inhibitor granted FDA approval was Atezolizumab in 2016. Atezolizumab is a human IgG1κ anti-PD-L1 monoclonal antibody marketed as Tecentriq®, by Genentech and Roche. The mAb was found to be effective for the treatment of metastatic urothelial carcinoma following platinum chemotherapy (69). The therapy was subsequently approved for treatment of metastatic non-small-cell lung carcinoma (NSCLC) (29) and advanced urothelial carcinoma in patients that are ineligible for chemotherapy (19). In 2018, Atezolizumab was further approved for the treatment of metastatic NSCLC in combination with chemotherapy and bevacizumab, a mAb targeting VEGF (70). Following the first combinational therapy, Atezolizumab was subsequently approved in combination with paclitaxel (71) and chemotherapy (72) for the treatment of metastatic triple negative breast cancer (TNBC) and small cell lung cancer (SCLC), respectively.

Avelumab, marketed as Bavencio® by Merck/Pfizer, is a human IgG1λ monoclonal antibody that targets PD-L1. Avelumab was first approved by the FDA for the treatment of Merkel cell carcinoma in 2017 (30). Following its first approval, avelumab was granted further approval for the treatment of locally advanced and metastatic urothelial carcinoma (32). In 2019, avelumab was approved for the treatment of advanced renal cell carcinoma (RCC) in combination with axitinib, a tyrosine kinase inhibitor (31).

Another PD-L1 inhibitor, durvalumab, was granted FDA approval in 2017 for the treatment of advanced bladder cancer in patients that previously did not respond to chemotherapy or ineligible for the treatment (33). Durvalumab is a humanized IgG1κ anti-PD-L1 monoclonal antibody marketed as Imfinzi® by AstraZeneca. In 2019, the immune checkpoint inhibitor was approved for the treatment of unresectable stage III NSCLC (34).

The Mechanism of Next Generation Inhibitors Targeting LAG-3, TIM-3, TIGIT, VISTA and B7-H3

CTLA-4, PD-1 and PD-L1 are the most broadly studied checkpoints. However, given the success seen with previous checkpoint inhibitors, new inhibitory pathways and next generation inhibitors targeting LAG-3, TIM-3, TIGIT, VISTA and B7-H3 are being investigated. The mechanisms of these checkpoints as well as inhibitors that are currently in clinical trials will be described briefly.

Lymphocyte activation gene-3 (LAG-3 or CD223) is a membrane receptor constitutively expressed by T cells and natural killer cells. LAG-3 interacts with MHC class II resulting in

a negative regulatory effect over T cell function (73). This interaction normally prevents tissue damage and autoimmunity, however, tumor-infiltrating lymphocytes (TILs) found in the TME upregulates LAG-3 thereby promoting cell dysfunction, immune exhaustion and favorable conditions for tumor growth (74). Thus, disrupting the LAG-3/MCH II interaction with blockade therapy should encourage immune activation and anti-tumor responses.

T cell immunoglobulin-3 (TIM-3) is an immune checkpoint expressed on numerous cells including effector T cells, B cells, Tregs, macrophages and natural killer cells (75). Its main ligand is galactine-9, but it is also known to interact with phosphatidyl serine and carcinoembryonic antigen-related cell adhesion molecule (CEACAM) (76, 77). TIM-3 functions as a direct negative regulator of T cells. Interaction with its various ligands results in T cell exhaustion as well as expansion of myeloid-derived suppressor cells (MDSCs) in the TME creating favorable conditions for tumor growth. Not surprisingly, TIM-3 levels have been found elevated in several malignancies. Blockade of TIM-3 decreases MDSCs while increasing T cell proliferation and cytokine production leading to anti-tumor activity (78). However, there has been some concern over TIM-3 blockade. Considering its role in immune responses against listeria and mycobacteria, inhibiting TIM-3 may result in an increased risk of these infections (79). Nevertheless, antibodies targeting this receptor have proceeded to clinical trials.

T cell immunoglobulin and ITIM domain (TIGIT) is a receptor part of the CD28 family and is expressed by T cells and natural killer cells (80). CD155 and CD112 are ligands that interact with TIGIT to bring about immunosuppressive effects (81). Studies have shown that tumor-infiltrating lymphocytes

have elevated levels of TIGIT co-expressed with PD-1, LAG-3 and TIM-3 suggesting a role in tumor progression. Dual blockade of TIGIT and either TIM-3 or PD-1 has revealed an anti-tumor mechanism through immune cell proliferation, cytokine release and reversal of T cell exhaustion (82).

V-domain Ig suppressor of T cell activation (VISTA) is an unusual immune checkpoint with dual function as an inhibitory and stimulatory molecule (83). VISTA, expressed as a receptor on T cells, interacts with VSIG-3 on tumor cells to suppress T cell activation, proliferation and production of cytokines promoting tumor progression. This co-inhibitory pathway therefore presented as an alternative strategy for blockade therapy (84). Although most studies have described the inhibitory effects of VISTA on immune responses, other studies have demonstrated that VISTA can act as a ligand expressed on APCs allowing for immune activation. Regardless, blockade of VISTA seemed to enhance T cell infiltration and reduce myeloid suppressive cells proving to be an effective anti-tumor strategy (85, 86).

B7 homolog 3 (B7-H3) is a transmembrane protein found on various solid organs as well as immune cells such as APCs, T cells, B cells and natural killer cells. Although the exact ligand remains unknown, B7-H3 is believed to interact with the CD28 receptor family (87). This interaction prevents T cell activation, proliferation, cytokine production and appears to enhance cancer aggressiveness. B7-H3 blockade promotes T cell activation, cytokine release and cytotoxic activity. Moreover, it has been associated with fewer immune-related adverse events (irAEs) due to the lower expression of B7-H3 in normal tissues as opposed to the TME allowing for localised effects (88).

TABLE 2 | Next generation immune checkpoint inhibitors.

Target	Binding partner	Drugs	Trial stage	References
LAG-3	MHC-II	Eftilagimod alpha (Immutep)	I/II	(89)
		Relatimab (Bristol Myers Squibb)	II/III	
		Ieramilimab (Novartis)	II	
		Favezelimab (Merck)	I/II	
		Fianlimab (Regeneron)	I	
		Encelimumab (AnaptysBio/GlaxoSmithKline)	I	
		Miptenlimab (Boehringer Ingelheim)	I	
		Sym 022 (Symphogen)	I	
		FS118 (F-star)	I	
		Tebotelimab (MacroGenics)	I	
TIM-3	Galactine-9, phosphatidyl serine, CEACAM	TSR-022 (GlaxoSmithKline)	I	(75)
		Sabatolimab (Novartis)	I/II	
		Sym 023 (Symphogen)	I	
		INCAGN 2390 (Incyte Corporation)	I	
		LY3321367 (Eli Lilly and Company)	I/II	
		BMS-986258 (Bristol Myers Squibb)	I/II	
		SHR-1702 (Jiangsu HengRui)	I	
TIGIT	CD155, CD112	Vibostolimab (Merck)	III	(80)
		Etigilimab (OncoMed Pharmaceuticals)	I	
		Tiragolumab (Genentech)	II	
		BMS-986207 (Bristol Myers Squibb)	I/II	
		Domvanlimab (Arcus Biosciences)	I	
VISTA	VSIG-3	JNJ-61610588 (Johnson & Johnson)	I	(90)
		CI-8993 (Curis Inc)	I	
B7-H3	Unknown	Enoblituzumab (MacroGenics)	II	(91)
		¹³¹ I-omburtamab (Y-mAbs Therapeutics)	II/III	
		¹²⁴ I-omburtamab (Y-mAbs Therapeutics)	I	

Drugs targeting LAG-3, TIM-3, TIGIT, VISTA and B7-H3 that are currently in clinical trials are listed in **Table 2**. Apart from these immune checkpoints, drugs associated with inhibitory targets beyond traditional immune checkpoints which lead to indirect repercussions on T-cell effect are also being investigated as next generation inhibitors. This has been reviewed in detail elsewhere (92).

Challenges Associated With Immune Checkpoint Inhibitors

Immune checkpoint blockade (ICB) therapy has become one of the most successful cancer treatment strategies developed to date. A pooled meta-analysis study evaluating the long-term survival of 1861 advanced melanoma patients, receiving ipilimumab therapy, estimated a 3-year survival rate of 22% (93). The significance of these results is highlighted when compared to melanoma patients treated with dacarbazine, a chemotherapeutic agent, and 3-year survival rates were only 12.2% (14). In comparison to chemotherapeutics, ICB has allowed better disease control and outcomes for some patients. Accordingly, immunotherapy is now at the forefront for management of various malignancies. But despite the remarkable progress, ICB is challenged by low response rates, immune-related adverse events (irAEs) and resistance to treatment.

Response rates are known to vary depending on the type of malignancy. While excellent response rates are seen in Hodgkin's lymphoma and melanomas which range from 40-70%, response rates in most other diseases is limited to only 10-25% (94). The unfortunate reality is that majority of patients do not experience any benefit from treatment with immune checkpoint inhibitors, and those that do, are likely to experience irAEs. Immune-related adverse events are caused from non-specific activation of the immune system resulting in immune responses that target self-antigens. ICB therapy most frequently results in dermatological irAEs such as pruritis and mucositis (68% of patients on ipilimumab therapy). Gastrointestinal distress and immune mediated colitis have also been reported in 40% of patients on ipilimumab therapy. Less common irAEs include endocrinopathies, hepatotoxicity, pneumonitis, renal toxicity, pancreatitis, neurotoxicity, cardiovascular toxicity and hematological abnormalities (95, 96). Inhibition of CTLA-4 has been associated with a higher frequency and severity of irAEs than checkpoint inhibitors targeting the PD-1/PD-L1 axis (97). Although irAEs can be managed, they often lead to the discontinuation of treatment in some patients. Lastly, a crucial limitation of ICB therapy is related to resistance. Patients that fail to respond to treatment (innate resistance) and patients that respond initially but eventually develop disease progression (acquired resistance) will be discussed further.

Mechanisms of Resistance to Immune Checkpoint Inhibitors

Immune checkpoint inhibitors targeting the CTLA-4, PD-1, and its ligand PD-L1 have been successful at inducing an anti-tumor immune response in several cancers (98). Ipilimumab was the first agent in the class of immune checkpoint inhibitors (ICIs) to

be granted FDA approval for the treatment of metastatic melanoma in 2011 albeit with significant immune-related adverse events (irAEs) which needed to be addressed (99). Since then, diverse ICIs targeting the PD-1 (cemiplimab, nivolumab and pembrolizumab), and PD-L1 (atezolizumab, avelumab and durvalumab) have been granted FDA approval for the treatment of various cancers. To date there are several other ICIs currently in clinical trials. Although these agents have been successful at maintaining a sustained response in some cancer patients, the overall response is usually low, and some patients develop resistance over time (100). Resistance to ICIs may be innate (primary) or acquired (secondary). Resistance can also be classified as intrinsic or extrinsic to tumors. In intrinsic resistance, tumor cells modify processes associated with DNA damage response, cell signalling pathways and immune recognition. Extrinsic resistance occurs external to tumor cells and is facilitated by interactions of immune cells and non-immunological mechanisms in the tumor microenvironment (101-105).

Successful blockade of CTLA-4 and PD-1/PD-L1 in tumors results in reactivation and proliferation of T-cells. Activation of T-cells is dependent on the successful presentation of tumor antigens by APCs and the recognition of these antigens by MHC I and/or II. T-cells recognise the MHC-bound antigens and stimulate T-cell proliferation through co-stimulatory factors described previously (106). Both CTLA-4 and PD-1/PD-L1 pathways play a significant role in tumor evasion through down regulation of the immune response. Tumors evolve mechanisms to evade immune checkpoint blockade, thereby reducing the effectiveness of ICI therapy. In the following sections, we describe the various mechanisms that govern the evasion of T cell cytotoxicity by tumor cells following treatment with ICIs.

INNATE AND ACQUIRED RESISTANCE

Tumor Neoantigens

Innate or primary resistance is observed in tumors that have never responded to the initial treatment with ICIs (104). The most notable trigger of intrinsic resistance relates to genetic and epigenetic alterations that influence tumor neoantigen presentation, structure, and processing (106, 107). Neoantigens are peptides produced in the tumor because of somatic mutations that occur in cancer cells (108). The tumor neoantigen repertoire is crucial for the activation of an immune response and recruitment of effector T-cells to the tumor. Tumors with high mutational rates are typically responsive to ICI therapy compared to tumors with low tumor mutational burden (TMB) apart from renal cell carcinomas (66, 109-111).

Emerging evidence indicates that some tumors lose or down regulate generation of neoantigens required to illicit an immune response and therefore the tumor escapes T-cell cytotoxicity (63). Anagnostou and colleagues (63, 82) assessed biopsies of relapsed NSLC patients and observed a downregulation of key

tumor antigens indicative of an anti-PD-1 and anti-CTLA-4 resistance. Efficacy of anti-PD-1 inhibitors is dependent on the availability of tumor antigen specific T-cells in the tumor microenvironment and the upregulation of PD-1 in effector T-cells and PD-L1 in tumor cells. This requires tumors to present specific antigens that are different from the original tumor cells. Without these antigens, the immune checkpoint blockade is attenuated.

In addition to tumor neoantigen downregulation, tumors escape immunosuppression through alteration of the antigen presentation machinery. Dendritic cells (DCs) initiate an immune response through uptake and presentation of tumor antigens to activate naïve CD4 and CD8 T cells (112, 113). DCs activate the CD8 T cells in a process called cross priming where antigens are presented to CD8 T cells *via* MCH I to generate an anti-tumor CD8 T cell response (114). Cross priming of tumor specific CD8 T cells is very important in initiation and stabilisation of the anti tumor immune response. Deficiencies in T cell priming mechanism have been shown to contribute unresponsiveness to immune checkpoint inhibition therapy (115). The TME plays a major role in the transportation of effector CD8 T cells to tumors and alterations in the TME therefore affect the anti-tumor response. In particular, the presence of tumor derived inhibitory molecules such as interleukin (IL-6, 10), transforming growth factor beta (TGF β) and VEGF produced by the tumor negatively impact the growth, maturation and differentiation of DCs (116, 117). These molecules are usually secreted by myeloid derived suppressor cells (MDSCs), tumor-associated macrophages (TAMs) and regulator T cells (Tregs) which are discussed in subsequent sections.

Dysfunctional Major Histocompatibility Complex Molecules

Alterations in the structure of MHC-I/II and the antigen presenting machinery, beta 2 microglobulin (B2M), prevents the identification and presentation of tumor antigens (118). The MHC class I pathway is responsible for antigen presentation and any defects in the genes associated with MHC-1 pathways such as the HLA class I and the *B2M* gene affect antigen presentation and ultimately immune response (119). This phenomenon has been observed in several tumors with *B2M* mutations and more specifically the loss of heterozygosity (LOH) of the *B2M* gene. Indeed, these modifications have been observed in various tumor tissues and have been associated with resistance to anti-PD-1/PD-L1 and anti-CTLA-4 immune checkpoint inhibitors (120–122).

Inadequate Anti-Tumor T-Cell Effector Function

Interestingly, mutations in the JAK1 and JAK2 pathways have also been associated with resistance to ICI treatment (123, 124). JAK1/2 are key intermediates in the interferon signaling pathways. Since the interferon pathway (INF) is particularly involved in the upregulation of PD-L1 expression, blockade of the PD-1/PD-L1 is likely ineffective in tumors with alterations in the interferon pathway. This is suggestive of an alternate

mechanism of immune evasion in tumor cells other than PD-1/PD-L1 upregulation (125). Moreover, Gao and colleagues reported anti-CTLA-4 resistance in tumors with LOH in many genes associated with the INF γ pathway (126). It has been shown in melanoma that the interferon-gamma-JAK1/JAK2-STAT1/STAT2/STAT3-IRF1 signaling cassettes primarily regulates PD-L1 expression on the cancer cell, through IRF1 binding to its promoter. This establishes PD-L1 as an interferon- γ immediate response gene. Upon tumor antigen recognition in the context of the MHC, the T cell releases interferon gamma that binds to its receptors on the cancer cell. This is followed by the transduction of a signal *via* the JAK/STAT pathway, culminating in the activation of the paralogous the PD-L1 and PD-L2 genes of the tumor cell (**Figure 2**). In this way interferon gamma can play a critical role in negative regulation of T cell activation through the expression of PD-1 receptors on the tumor cell. Immune checkpoint blockade therapy acts by blocking PD-1/PD-L1/2 interaction thereby restoring T cell activation and anti-tumor activity. The evidence shows that dysregulation of this pathway in the tumor cell produces resistance to PD-1 based ICB therapy. It was shown that loss of function mutations in *Ak1/2* and subsequent lack of PD-L1 expression led to primary resistance to anti-PD-1 antibody therapy (123, 127). Similar interferon signalling dependent resistance has been demonstrated with the anti-CTLA-4 therapy, ipilimumab (126). Though studies on delayed relapses after anti-PD-1 therapy, the interferon- γ signalling pathway has been shown to be associated with acquired immunity to anti-PD-1 immune blockade therapy (124). The inhibitory CTLA-4 is essentially an intracellular molecule whose trafficking from intracellular vesicles to the cell surface is tightly regulated to maintain an optimal balance with stimulatory molecules (41).

T-Cell Exhaustion

T cell exhaustion is a phenomenon that was first described in mice with chronic viral infections, and thereafter observed in humans with chronic viral infections and cancer (42, 128–131). More recently, however, it has been linked to resistance in ICB therapy. Exhausted T cells in the tumor microenvironment have been shown to progressively lose their functional capacity to proliferate, produce effector cytokines and lyse upon chronic antigen exposure (130, 131). While numerous pathways may individually influence T cell exhaustion, the PD-1/PD-L1 checkpoint pathway partly contributes to T cell exhaustion. In exhausted T cells, PD-1 expression is driven by demethylation of its promoter. The stability of this epigenetic mechanism blocks long-term effector function or memory development by T cells following ICB therapy, potentially explaining disease relapse in patients treated with PD-1/PD-L1 checkpoint inhibitors (132–134). Moreover, studies have reported that T cell exhaustion in acquired resistance is a consequence of the up-regulation of other checkpoint inhibitors such as TIM3, LAG3 and VISTA following checkpoint blockade (120, 135, 136). The exact mechanisms leading to T cell exhaustion following ICB therapy is largely unclear and further studies are required to validate the dysfunctional T cell states and their contribution to resistance.

The Tumor Microenvironment (TME)

The TME contains various types of cells that play a significant role in the promotion or inhibition of the tumor. The cell types include regulatory T-cells (Treg cells), myeloid derived suppressor cells (MDSCs), cancer-associated adipocytes, fibroblasts and endothelial cells; and tumor-associated macrophages (TAMs) (137). Through producing various molecules, Tregs, MDSCs, TAMs and tumor-associated stromal cells inhibit the anti-tumor T-cell response and maintain an immune tolerant tumor that attenuates the effectiveness of ICIs (138, 139). Foxp3 Treg cells, are mainly produced by the thymus as a functionally mature and distinct T-cell subpopulation, whose function is to maintain self-tolerance after an immunological response or activation (140).

Treg cells produce immunosuppressive molecules including transforming growth factor- β (TGF- β) and interleukin-10 (IL-10) which typically interfere with the activation, proliferation and survival of effector T-cells (141). Additionally, Tregs also upregulate the expression of immune checkpoints such as CTLA-4, PD-1 and others (142). The effectiveness of anti-CTLA-4 mAb is dependent on decreasing Treg cells in tumors *via* antibody-dependent cytotoxicity but this mechanism does not affect the activation of CTLA-4 (143). For this reason, anti-CTLA-4 alone selectively depletes Treg cells permitting immunosuppression stimulated by remaining Treg cells (138, 144). Several animal studies have shown a connection between amount of Treg cells in the TME and enhanced antitumor immunity (145, 146). Studies in cancer patients treated with anti-CTLA-4 therapy revealed better response to treatment in patients with a low ratio of Treg cells compared to Teff cells in the TME (140, 147). Recruitment of Tregs in the TME relies upon metabolic processes associated with lipid metabolism. A study by Pacella and colleagues (2018) showed that both increased glycolysis and oxidative metabolism influenced Tregs expansion by fueling fatty acid (FA) synthesis (148).

Tumor-associated macrophages (TAMs) support tumor growth through the expression of PD-L1 ligand and Na/H exchanger isoform 1 (NHE1) (149, 150). NHE1 maintains the alkaline intracellular pH of glioma cells, a driving force of glycolytic metabolism exploited by cancer cells in a process called Warburg Effect (151, 152). Moreover, TAMs are involved in the production of cytokines such as transforming growth factor (TGF- β) and vascular growth factor (VEGF-A) implicated in tumor evasion (153, 154). Since TAMs can regulate the production of pro-inflammatory and immune response inhibitory molecules, anti-PD-L1 inhibition alone is not sufficient for prolonged suppression of the tumor.

Myeloid-derived suppressor cells (MDSCs) alter the function of CD8+ T cells through numerous mechanisms including a (i) decrease in arginine and cysteine production in the TME, (ii) reduced transport of T cells into the lymph node and tumor, (iii) production of free radicals that ultimately block TCR and IL-2 signaling, inducing T cell death and expansion of Tregs (155). Like TAMs, MDSCs may be induced by tumor-derived factors such as TGF- β , ILs 1, 6, 10 and VEGF-A. MDSCs cells have been shown to also express immune checkpoint PD-L1, further

contributing to immunosuppression in mice models (156). The manifestation of MDSCs was associated with poor prognosis in metastatic melanoma patients treated with anti-CTLA-4 (ipilimumab) (157, 158).

Metabolic Reprogramming in the TME

Cancer cells tend to accumulate metabolic alterations that allow them to utilize eccentric sources of nutrients to support cancer cell proliferation and deprive antitumor immune cells of nutrients within the tumor microenvironment. Because tumors are heterogeneous in nature, they often have complex metabolic patterns. The first evidence of variations in nutrient metabolism observed in cancer and normal cells was reported in the 1920s by Warburg and colleagues (159). They observed a marked increase in glucose metabolism in cancer cells compared to non-proliferating normal cells; and the preference of glycolysis over oxidative phosphorylation (OXPHOS) even in the presence of oxygen and functional mitochondria. The observed phenomenon was later termed the “Warburg Effect” (159). This observation was further corroborated in a variety of tumors associated with poor prognosis (160). Even though there are other metabolic processes and molecules governing tumor resistance, we will focus on the metabolism of glucose in the TME and its impact on tumor progression and antitumor immune escape.

The high demand for glucose in cancer cells within the TME starves immune cells resulting in poor antitumor immune response (51). When T cells are inactive, they largely rely on OXPHOS and fatty acid oxidation (FAO) to support their needs. Once T cells are activated through binding of costimulatory receptors such as CD28, T cells alter their metabolism to support T-cell proliferation and T cell effector (T_{eff}) functions (161). The CD28 co-stimulation drives the activation of the PI3K/AKT pathways and glycolytic flux (162, 163). The dramatic increase in glycolysis in T cells is essential for T-cell growth, division, and differentiation into cytotoxic T cells (164). Since glucose is required by tumors and is essential to support immune cell growth, differentiation and function, its metabolism within the TME affects the function of immune cells infiltrating the TME (165). The competition for glucose metabolism within the TME deprives tumor infiltrating lymphocytes (TIL) of glucose resulting in their exhaustion and tumor immune escape (166).

In addition, the preference for aerobic glycolysis in tumors increases the levels of lactic acid in the TME resulting in an acidic environment that further supports the growth of tumors whilst inhibiting immune cell function within the TME. Indeed Muller and colleagues (2000) showed that the activation and function of tumor infiltrating immune cells (IL-2) was significantly perturbed in acidic conditions. Both the stimulated and unstimulated human PMBCs were unable to kill tumor cells after three days of culture in an acidic culture environment of pH 6.5 (167). This finding was further supported by Calcinotto and colleagues (168) using mice models and human tumor cell lines. Using *in vitro* and *in vivo* models, Calcinotto and colleagues revealed that the acidic microenvironment not only affected the function of effector cells but also induction of T-cell anergy (168).

In addition to interfering with immune cell activation and function, acidic pH in the microenvironment also upregulates the expression of CTLA-4 on T lymphocytes, therefore intensifying antitumor resistance (169).

Besides the increased uptake of glucose by tumor cells; competitive uptake of other metabolites, amino acids (glutamine, arginine, tryptophan) and growth factors by tumor cells also affects the function of immune cells (51, 165).

Amino acids are protein building blocks, the high availability of amino acids in the TME is essential for tumor growth. At the same time, amino acids are essential for immune cells differentiation and development of their antitumor effector cells (170). For example, glutamine powers the tricarboxylic acid (TCA) cycle *via* glutaminolysis, to provide metabolic intermediates that serve as building blocks for lipids, proteins, and nucleic acids, which are necessary for cancer cell proliferation. Interestingly, the metabolic pathway used by the tumors has been shown to be essential for T cell activation and proliferation (171, 172).

There are several studies that have investigated the impact of targeting different metabolic pathways to assist the immune checkpoint inhibition or circumvent resistance. The metabolic dependencies between tumor and immune cells in the TME make it challenging to obtain antitumor effects with drugs targeting metabolic processes (170). Targeting enhanced glycolytic activity of tumors through inhibition of glycolysis regulatory enzymes or *via* application of competitive glucose analogs has been shown to promote T-cell proliferation and function (166, 173). Various studies have shown that the blockade of immune checkpoints (PD/PD-L1 and CTLA-4) rescues TILs from tumor-induced glucose restrictions and restores glycolysis in T-cells.

STRATEGIES TO OVERCOME RESISTANCE TO IMMUNE CHECKPOINT BLOCKADE THERAPY

When looking at patients that experience resistance, it is helpful to define them into two broad categories, firstly are the ones with innate resistance, who never respond to the immune checkpoint therapy (ICT) and secondly are the ones who have acquired resistance, who respond positively to treatment at first, but then build up a resistance resulting in the treatment becoming ineffective over time (102). Studies have found that tumors that are infiltrated by T cells and therefore that have initiated an inflammatory response as well as have a higher mutational burden have a better response to ICT than tumors that do not, this is especially important when looking at potential strategies to combat resistance to ICI (174).

An essential aspect to combating ICT resistance requires a deeper understanding of the exact mechanisms involved, down to an individual level, so that therapies can be adapted to the tumor microenvironment. To overcome resistance against a single checkpoint inhibitor target, combinational therapies

have been conducted. Multiple combinations of different therapies have been successfully tried with the most promising combination therapies including ICT paired with (i) other checkpoint inhibitors, with a combination of anti-PD-1 and anti-CTLA-4 already having been approved for multiple cancers as they have been shown to improve T-cell activation and decrease T-cell exhaustion (175) and combinations with next generation ICT such as anti-LAG and anti-TIGIT showing similar positive results (176). (ii) Immunotherapeutic agents such as cancer vaccines and oncolytic virus therapy which can improve antigen presentation and recognition and T cell infiltration (177, 178). (iii) Removal of co-inhibitory signals and activation of co-stimulatory signals which can amplify T cell activation and T cell cytotoxicity (179). (iv) DNA damaging therapies such as chemotherapy or radiation which has been seen to increase antigen presentation, pro-inflammatory cytokines and activation of dendritic cells, to stimulate the presentation of neoantigens in non-inflamed, non T cell infiltrated tumor cells (180) and (v) more targeted therapies including monoclonal antibodies and tyrosine kinase inhibitors which have been seen to enhance antitumor immunity, increase T cell infiltration and decrease T cell exhaustion (181).

In addition to these, epigenetic modifications within cancer cell DNA can impact the presentation and processing of antigens, which can promote immune evasion, therefore, demethylating agents may also increase the response to combination ICT treatment as they have been seen to elicit an immunostimulatory response, upregulation of cytokine production as well antigen presentation and inhibition of T regulation cells (182). Interestingly a link has been reported between the gut microbiome and response to ICT, where mice suffering from sarcomas that were fed with a germ-free diet, had a very poor response to CTLA-4 blockade therapy. This was further supported when their response was restored upon being fed with *Bacteroides fragilis* (183). This has since been concluded in a number of studies that demonstrate that gut microbiome can affect a person's response to ICT treatment (184).

Lastly biomarkers have also become a topic of interest in helping overcome resistance as they can be investigated to estimate the predicted response of an individual to treatment. Biomarkers of particular interest include PD-L1 expression, tumor mutation burden (TMB), microsatellite instability-high (MSI-H) or mismatch repair (MMR) deficiency, IFN- γ signalling and T-cell infiltration (185). The only predictive biomarker that has been approved to date is PD-L1 expression using immunohistochemistry (IHC), in which higher expression correlates to a positive response to ICT and fewer side effects observed (186). However, because the detection of PD-L1 relies on antibody staining techniques, this creates inconsistencies in the accuracy of results and therefore its predictive value (187). TMB as a potential biomarker looks for somatic mutations *via* DNA sequencing, with an increased number of mutations resulting in higher neoantigen production and therefore a positive response to ICT, however not all mutations and neoantigens correlate equally towards a positive response (188). Defective DNA mismatch repair (MMR) can lead to

high microsatellite instability (MSI-H), and MSI-H is associated with higher neoantigen production by tumors and therefore a stronger immune response and better response to ICT. MSI has been argued to be the most accurate biomarker predictor (189).

Activation of IFN- γ signalling can be used as a predictive biomarker as studies have found loss of function mutations or gene knockdowns in this pathway result in resistance to ICT treatment (7, 23, 182). IFN- γ signalling up regulates the major histocompatibility complex II as well as antigen presenting cells (APCs) and increases PD-L1 expression, however on the other hand studies have found that chronic IFN- γ signalling can lead to acquired resistance, therefore it seems early IFN- γ signalling may predict positive response to ICT but once resistance is acquired, continued IFN- γ signalling can predict further resistance (190). Lastly decreased T cell infiltration and a lack of an inflammatory response has been reported to be linked to poorer prognosis and is therefore predictive of a low response to ICT (191).

FUTURE DIRECTIONS

This review examined the successes and failures of immune checkpoint inhibitors (ICIs) and focused on resistance mechanisms. Although ICIs have produced unmatched and durable clinical responses in some cases, this revolutionary strategy has not succeeded in most patients. The limited application of this revolutionary cancer treatment strategy is the most critical matter and is a subject of intense investigation. Critically, it is not possible to predict who is likely or unlikely to benefit from ICI therapy. Towards this end, the discovery of biomarkers is ongoing and is expected to allow personalized treatment approaches. Also, the immune-related adverse effects present a difficult challenge because they are unique and unlike adverse effects often seen with traditional treatments. Although irAEs are usually low-grade and reversible, they can also cause permanent disorders and affect any organ. Another challenge to ICI treatment is that poorly understood primary or secondary resistance limits treatment outcomes. The enormous impact of the tumor microenvironment on carcinogens adds a chaotic dimension to the study of cancer as the TME is a dynamic system and pliable. Presumably, there are deterministic laws or logical patterns that govern the apparent random environment. With the advances in artificial intelligence and high-throughput data,

it is possible to produce knowledge to understand the complex emergence of irAEs better. The ongoing transcriptomic and epigenetic analyses are likely to make invaluable knowledge in this regard.

CONCLUSION

Immune checkpoint therapy (ICT) is a very promising, recently developed cancer treatment. Here, we described PD-1/PD-L1 and CTLA-4 immune checkpoints and the monoclonal antibody drug inhibitors that have been approved by the FDA. Although there are positive results in some patients treated with immune checkpoint inhibitors, others never respond to treatment, while the responders often develop resistance. We have described various mechanisms by which resistance can develop and some efforts to overcome this problem. The diverse components of the tumor microenvironment play a critical role in creating ICT resistance. Strategies currently used to help combat resistance include combination therapy with multiple checkpoint inhibitors or checkpoint inhibitors with chemotherapy or radiation.

Given the increasing incidence of cancer, there is an urgent need to improve the currently available therapies and develop new alternatives. Although glucose competition exerts pressure on normal cells in the tumor microenvironment, the fine details about how this affects ICI therapy is still unclear.

AUTHOR CONTRIBUTIONS

BLR, SAS and STM contributed equally in the, composition of the main text. LD contributed in the conception of article, in intellectual input and in fundraising. MN is the corresponding author who researched and wrote the final document. All authors contributed to the article and approved the submitted version.

FUNDING

BLR and LD are funded by The Technology and Human Resources for Industry programme (THRIP). SAS and STM are funded by the National Research Foundation (NRF) GUN: 116681 and GUN: 121878 respectively.

REFERENCES

- Nurieva R, Thomas S, Nguyen T, Martin-Orozco N, Wang Y, Kaja M-K, et al. T-Cell Tolerance or Function Is Determined by Combinatorial Costimulatory Signals. *EMBO J* (2006) 25(11):2623–33. doi: 10.1038/sj.emboj.7601146
- Hodi FS, O'Day SJ, McDermott DF, Weber RW, Sosman JA, Haanen JB, et al. Improved Survival With Ipilimumab in Patients With Metastatic Melanoma. *New Engl J Med* (2010) 363(8):711–23. doi: 10.1056/NEJMoa1003466
- Overman MJ, McDermott R, Leach JL, Lonardi S, Lenz H-J, Morse MA, et al. Nivolumab in Patients With Metastatic DNA Mismatch Repair-Deficient or Microsatellite Instability-High Colorectal Cancer (Checkmate 142): An Open-Label, Multicentre, Phase 2 Study. *Lancet Oncol* (2017) 18(9):1182–91. doi: 10.1016/S1470-2045(17)30422-9
- Hammers HJ, Plimack ER, Infante JR, Rini BI, McDermott DF, Lewis LD, et al. Safety and Efficacy of Nivolumab in Combination With Ipilimumab in Metastatic Renal Cell Carcinoma: The Checkmate 016 Study. *J Clin Oncol: Off J Am Soc Clin Oncol* (2017) 35(34):3851–8. doi: 10.1200/JCO.2016.72.1985
- Weber JS, D'Angelo SP, Minor D, Hodi FS, Gutzmer R, Neyns B, et al. Nivolumab Versus Chemotherapy in Patients With Advanced Melanoma Who Progressed After Anti-CTLA-4 Treatment (Checkmate 037): A Randomised, Controlled, Open-Label, Phase 3 Trial. *Lancet Oncol* (2015) 16(4):375–84. doi: 10.1016/S1470-2045(15)70076-8
- Ansell SM, Lesokhin AM, Borrello I, Halwani A, Scott EC, Gutierrez M, et al. PD-1 Blockade With Nivolumab in Relapsed or Refractory Hodgkin's Lymphoma. *New Engl J Med* (2014) 372(4):311–9. doi: 10.1056/NEJMoa1411087

7. Ansell SM, Hurvitz SA, Koenig PA, LaPlant BR, Kabat BF, Fernando D, et al. Phase I Study of Ipilimumab, an Anti-CTLA-4 Monoclonal Antibody, in Patients With Relapsed and Refractory B-Cell Non-Hodgkin Lymphoma. *Clin Cancer Res* (2009) 15(20):6446. doi: 10.1158/1078-0432.CCR-09-1339
8. Sharma P, Retz M, Siefker-Radtke A, Baron A, Necchi A, Bedke J, et al. Nivolumab in Metastatic Urothelial Carcinoma After Platinum Therapy (Checkmate 275): A Multicentre, Single-Arm, Phase 2 Trial. *Lancet Oncol* (2017) 18(3):312–22. doi: 10.1016/S1470-2045(17)30065-7
9. El-Khoueiry AB, Sangro B, Yau T, Crocenzi TS, Kudo M, Hsu C, et al. Nivolumab in Patients With Advanced Hepatocellular Carcinoma (Checkmate 040): An Open-Label, Non-Comparative, Phase 1/2 Dose Escalation and Expansion Trial. *Lancet* (2017) 389(10088):2492–502. doi: 10.1016/S0140-6736(17)31046-2
10. Borghaei H, Paz-Ares L, Horn L, Spigel DR, Steins M, Ready NE, et al. Nivolumab Versus Docetaxel in Advanced Nonsquamous Non-Small-Cell Lung Cancer. *New Engl J Med* (2015) 373(17):1627–39. doi: 10.1056/NEJMoa1507643
11. Antonia SJ, López-Martin JA, Bendell J, Ott PA, Taylor M, Eder JP, et al. Nivolumab Alone and Nivolumab Plus Ipilimumab in Recurrent Small-Cell Lung Cancer (Checkmate 032): A Multicentre, Open-Label, Phase 1/2 Trial. *Lancet Oncol* (2016) 17(7):883–95. doi: 10.1016/S1470-2045(16)30098-5
12. Motzer RJ, Tannir NM, McDermott DF, Arén Frontera O, Melichar B, Choueiri TK, et al. Nivolumab Plus Ipilimumab Versus Sunitinib in Advanced Renal-Cell Carcinoma. *New Engl J Med* (2018) 378(14):1277–90. doi: 10.1056/NEJMoa1712126
13. Brahmer J, Reckamp KL, Baas P, Crinò L, Eberhardt WEE, Poddubskaya E, et al. Nivolumab Versus Docetaxel in Advanced Squamous-Cell Non-Small-Cell Lung Cancer. *New Engl J Med* (2015) 373(2):123–35. doi: 10.1056/NEJMoa1504627
14. Robert C, Thomas L, Bondarenko I, O'Day S, Weber J, Garbe C, et al. Ipilimumab Plus Dacarbazine for Previously Untreated Metastatic Melanoma. *New Engl J Med* (2011) 364(26):2517–26. doi: 10.1056/NEJMoa1104621
15. Chung HC, Ros W, Delord J-P, Perets R, Italiano A, Shapira-Frommer R, et al. Efficacy and Safety of Pembrolizumab in Previously Treated Advanced Cervical Cancer: Results From the Phase II KEYNOTE-158 Study. *J Clin Oncol* (2019) 37(17):1470–8. doi: 10.1200/JCO.2018.01265
16. Chen R, Zinzani PL, Fanale MA, Armand P, Johnson NA, Brice P, et al. Phase II Study of the Efficacy and Safety of Pembrolizumab for Relapsed/Refractory Classic Hodgkin Lymphoma. *J Clin Oncol: Off J Am Soc Clin Oncol* (2017) 35(19):2125–32. doi: 10.1200/JCO.2016.72.1316
17. Zinzani PL, Thieblemont C, Melnichenko V, Bouabdallah K, Walewski J, Majlis A, et al. Efficacy and Safety of Pembrolizumab in Relapsed/Refractory Primary Mediastinal Large B-Cell Lymphoma (Rrpbml): Updated Analysis of the Keynote-170 Phase 2 Trial. *Blood* (2017) 130(Supplement 1):2833. doi: 10.1002/hon.2437_49
18. Fuchs CS, Doi T, Jang RW, Muro K, Satoh T, Machado M, et al. Safety and Efficacy of Pembrolizumab Monotherapy in Patients With Previously Treated Advanced Gastric and Gastroesophageal Junction Cancer: Phase 2 Clinical KEYNOTE-059 Trial. *JAMA Oncol* (2018) 4(5):e180013–e. doi: 10.1001/jamaoncol.2018.0013
19. Balar AV, Castellano D, O'Donnell PH, Grivas P, Vuky J, Powles T, et al. First-Line Pembrolizumab in Cisplatin-Ineligible Patients With Locally Advanced and Unresectable or Metastatic Urothelial Cancer (KEYNOTE-052): A Multicentre, Single-Arm, Phase 2 Study. *Lancet Oncol* (2017) 18(11):1483–92. doi: 10.1016/S1470-2045(17)30616-2
20. Le DT, Uram JN, Wang H, Bartlett BR, Kemberling H, Eyring AD, et al. PD-1 Blockade in Tumors With Mismatch-Repair Deficiency. *New Engl J Med* (2015) 372(26):2509–20. doi: 10.1056/NEJMoa1500596
21. Zhu AX, Finn RS, Edeline J, Cattani S, Ogasawara S, Palmer D, et al. Pembrolizumab in Patients With Advanced Hepatocellular Carcinoma Previously Treated With Sorafenib (KEYNOTE-224): A Non-Randomised, Open-Label Phase 2 Trial. *Lancet Oncol* (2018) 19(7):940–52. doi: 10.1016/S1470-2045(18)30351-6
22. Herbst RS, Baas P, Kim D-W, Felip E, Pérez-Gracia JL, Han J-Y, et al. Pembrolizumab Versus Docetaxel for Previously Treated, PD-L1-Positive, Advanced Non-Small-Cell Lung Cancer (KEYNOTE-010): A Randomised Controlled Trial. *Lancet* (2016) 387(10027):1540–50. doi: 10.1016/S0140-6736(15)01281-7
23. Garon EB, Christofk HR, Hosmer W, Britten CD, Bahng A, Crabtree MJ, et al. Dichloroacetate Should be Considered With Platinum-Based Chemotherapy in Hypoxic Tumors Rather Than as a Single Agent in Advanced non-Small Cell Lung Cancer. *J Cancer Res Clin Oncol* (2014) 140(3):443–52. doi: 10.1007/s00432-014-1583-9
24. Rini BI, Plimack ER, Stus V, Gafanov R, Hawkins R, Nosov D, et al. Pembrolizumab Plus Axitinib Versus Sunitinib for Advanced Renal-Cell Carcinoma. *New Engl J Med* (2019) 380(12):1116–27. doi: 10.1056/NEJMoa1816714
25. Rischin D, Harrington KJ, Greil R, Soulieres D, Tahara M, de Castro G, et al. Protocol-Specified Final Analysis of the Phase 3 KEYNOTE-048 Trial of Pembrolizumab (Pembro) as First-Line Therapy for Recurrent/Metastatic Head and Neck Squamous Cell Carcinoma (R/M HNSCC). *J Clin Oncol* (2019) 37(15_suppl):6000. doi: 10.1200/JCO.2019.37.15_suppl.6000
26. Kojima T, Muro K, Francois E, Hsu C-H, Moriaki T, Kim S-B, et al. Pembrolizumab Versus Chemotherapy as Second-Line Therapy for Advanced Esophageal Cancer: Phase III KEYNOTE-181 Study. *J Clin Oncol* (2019) 37(4_suppl):2. doi: 10.1200/JCO.2019.37.4_suppl.2
27. Nghiem P, Bhatia S, Lipson EJ, Sharfman WH, Kudchadkar RR, Friedlander PA, et al. Durable Tumor Regression and Overall Survival (OS) in Patients With Advanced Merkel Cell Carcinoma (aMCC) Receiving Pembrolizumab as First-Line Therapy. *J Clin Oncol* (2018) 36(15_suppl):9506. doi: 10.1200/JCO.2018.36.15_suppl.9506
28. Migden MR, Rischin D, Schmults CD, Guminski A, Hauschild A, Lewis KD, et al. PD-1 Blockade With Cemiplimab in Advanced Cutaneous Squamous-Cell Carcinoma. *New Engl J Med* (2018) 379(4):341–51. doi: 10.1056/NEJMoa1805131
29. Fehrenbacher L, Spira A, Ballinger M, Kowanzet M, Vansteenkiste J, Mazieres J, et al. Atezolizumab Versus Docetaxel for Patients With Previously Treated Non-Small-Cell Lung Cancer (POPLAR): A Multicentre, Open-Label, Phase 2 Randomised Controlled Trial. *Lancet* (2016) 387(10030):1837–46. doi: 10.1016/S0140-6736(16)00587-0
30. Kaufman HL, Russell J, Hamid O, Bhatia S, Terheyden P, D'Angelo SP, et al. Avelumab in Patients With Chemotherapy-Refractory Metastatic Merkel Cell Carcinoma: A Multicentre, Single-Group, Open-Label, Phase 2 Trial. *Lancet Oncol* (2016) 17(10):1374–85. doi: 10.1016/S1470-2045(16)30364-3
31. Motzer RJ, Penkov K, Haanen J, Rini B, Albige L, Campbell MT, et al. Avelumab Plus Axitinib Versus Sunitinib for Advanced Renal-Cell Carcinoma. *New Engl J Med* (2019) 380(12):1103–15. doi: 10.1056/NEJMoa1816047
32. Apolo AB, Infante JR, Balmanoukian A, Patel MR, Wang D, Kelly K, et al. Avelumab, an Anti-Programmed Death-Ligand 1 Antibody, in Patients With Refractory Metastatic Urothelial Carcinoma: Results From a Multicentre, Phase Ib Study. *J Clin Oncol: Off J Am Soc Clin Oncol* (2017) 35(19):2117–24. doi: 10.1200/JCO.2016.71.6795
33. Powles T, O'Donnell PH, Massard C, Arkenau H-T, Friedlander TW, Hoimes CJ, et al. Efficacy and Safety of Durvalumab in Locally Advanced or Metastatic Urothelial Carcinoma: Updated Results From a Phase 1/2 Open-Label Study. *JAMA Oncol* (2017) 3(9):e172411–e. doi: 10.1001/jamaoncol.2017.2411
34. Antonia SJ, Villegas A, Daniel D, Vicente D, Murakami S, Hui R, et al. Durvalumab After Chemoradiotherapy in Stage III Non-Small-Cell Lung Cancer. *New Engl J Med* (2017) 377(20):1919–29. doi: 10.1056/NEJMoa1709937
35. Ramsay AG. Immune Checkpoint Blockade Immunotherapy to Activate Anti-Tumour T-Cell Immunity. *Br J Haematol* (2013) 162(3):313–25. doi: 10.1111/bjh.12380
36. Pardoll DM. The Blockade of Immune Checkpoints in Cancer Immunotherapy. *Nat Rev Cancer* (2012) 12(4):252–64. doi: 10.1038/nrc3239
37. Walunas TL, Lenschow DJ, Bakker CY, Linsley PS, Freeman GJ, Green JM, et al. CTLA-4 Can Function as a Negative Regulator of T Cell Activation. *Immunity* (1994) 1(5):405–13. doi: 10.1016/1074-7613(94)90071-X
38. Azuma M, Ito D, Yagita H, Okumura K, Phillips JH, Lanier LL, et al. B70 Antigen Is a Second Ligand for CTLA-4 and CD28. *Nature* (1993) 366(6450):76–9. doi: 10.1038/366076a0

39. Fallarino F, Fields PE, Gajewski TF. B7-1 Engagement of Cytotoxic T Lymphocyte Antigen 4 Inhibits T Cell Activation in the Absence of CD28. *J Exp Med* (1998) 188(1):205–10. doi: 10.1084/jem.188.1.205
40. Rudd CE, Taylor A, Schneider H. CD28 and CTLA-4 Coreceptor Expression and Signal Transduction. *Immunol Rev* (2009) 229(1):12–26. doi: 10.1111/j.1600-065X.2009.00770.x
41. Valk E, Rudd CE, Schneider H. CTLA-4 Trafficking and Surface Expression. *Trends Immunol* (2008) 29(6):272–9. doi: 10.1016/j.it.2008.02.011
42. Ahmadzadeh M, Johnson LA, Heemskerk B, Wunderlich JR, Dudley ME, White DE, et al. Tumor Antigen-Specific CD8 T Cells Infiltrating the Tumor Express High Levels of PD-1 and Are Functionally Impaired. *Blood* (2009) 114(8):1537–44. doi: 10.1182/blood-2008-12-195792
43. Fanoni D, Tavecchio S, Recalcati S, Balice Y, Venegoni L, Fiorani R, et al. New Monoclonal Antibodies Against B-Cell Antigens: Possible New Strategies for Diagnosis of Primary Cutaneous B-Cell Lymphomas. *Immunol Lett* (2011) 134(2):157–60. doi: 10.1016/j.imlet.2010.09.022
44. Xia Y, Jeffrey Medeiros L, Young KH. Signaling Pathway and Dysregulation of PD1 and its Ligands in Lymphoid Malignancies. *Biochim Biophys Acta (BBA) - Rev Cancer* (2016) 1865(1):58–71. doi: 10.1016/j.bbcan.2015.09.002
45. Parry RV, Chemnitz JM, Frauwirth KA, Lanfranco AR, Braunstein I, Kobayashi SV, et al. CTLA-4 and PD-1 Receptors Inhibit T-Cell Activation by Distinct Mechanisms. *Mol Cell Biol* (2005) 25(21):9543. doi: 10.1128/MCB.25.21.9543-9553.2005
46. Eldar-Finkelman H. Glycogen Synthase Kinase 3: An Emerging Therapeutic Target. *Trends Mol Med* (2002) 8(3):126–32. doi: 10.1016/S1471-4914(01)02266-3
47. Collins M, Ling V, Carreno BM. The B7 Family of Immune-Regulatory Ligands. *Genome Biol* (2005) 6(6):223. doi: 10.1186/gb-2005-6-6-223
48. Freeman GJ, Long AJ, Iwai Y, Bourque K, Chernova T, Nishimura H, et al. Engagement of the PD-1 Immunoinhibitory Receptor by a Novel B7 Family Member Leads to Negative Regulation of Lymphocyte Activation. *J Exp Med* (2000) 192(7):1027–34. doi: 10.1084/jem.192.7.1027
49. Salmond RJ. mTOR Regulation of Glycolytic Metabolism in T Cells. *Front Cell Dev Biol* (2018) 6(122):1–9. doi: 10.3389/fcell.2018.00122
50. Cham CM, Driessens G, O'Keefe JP, Gajewski TF. Glucose Deprivation Inhibits Multiple Key Gene Expression Events and Effector Functions in CD8+ T Cells. *Eur J Immunol* (2008) 38(9):2438–50. doi: 10.1002/eji.200838289
51. Chang C-H, Qiu J, O'Sullivan D, Buck MD, Noguchi T, Curtis JD, et al. Metabolic Competition in the Tumor Microenvironment Is a Driver of Cancer Progression. *Cell* (2015) 162(6):1229–41. doi: 10.1016/j.cell.2015.08.016
52. Nishimura H, Nose M, Hiai H, Minato N, Honjo T. Development of Lupus-Like Autoimmune Diseases by Disruption of the PD-1 Gene Encoding an ITIM Motif-Carrying Immunoreceptor. *Immunity* (1999) 11(2):141–51. doi: 10.1016/S1074-7613(00)80089-8
53. Tivol EA, Borriello F, Schweitzer AN, Lynch WP, Bluestone JA, Sharpe AH. Loss of CTLA-4 Leads to Massive Lymphoproliferation and Fatal Multiorgan Tissue. *Immunity* (1995) 3(5):541–7. doi: 10.1016/1074-7613(95)90125-6
54. Peggs KS, Quezada SA, Chambers CA, Korman AJ, Allison JP. Blockade of CTLA-4 on Both Effector and Regulatory T Cell Compartments Contributes to the Antitumor Activity of Anti-CTLA-4 Antibodies. *J Exp Med* (2009) 206(8):1717–25. doi: 10.1084/jem.20082492
55. Ramagopal UA, Liu W, Garrett-Thomson SC, Bonanno JB, Yan Q, Srinivasan M, et al. Structural Basis for Cancer Immunotherapy by the First-in-Class Checkpoint Inhibitor Ipilimumab. *Proc Natl Acad Sci* (2017) 114(21):E4223. doi: 10.1073/pnas.1617941114
56. Wei SC, Levine JH, Cogdill AP, Zhao Y, Anang N-AAS, Andrews MC, et al. Distinct Cellular Mechanisms Underlie Anti-CTLA-4 and Anti-PD-1 Checkpoint Blockade. *Cell* (2017) 170(6):1120–33.e17. doi: 10.1016/j.cell.2017.07.024
57. Eggermont AMM, Chiarion-Sileni V, Grob J-J, Dummer R, Wolchok JD, Schmidt H, et al. Prolonged Survival in Stage III Melanoma With Ipilimumab Adjuvant Therapy. *New Engl J Med* (2016) 375(19):1845–55. doi: 10.1056/NEJMoa1611299
58. Blank C, Gajewski TF, Mackensen A. Interaction of PD-L1 on Tumor Cells With PD-1 on Tumor-Specific T Cells as a Mechanism of Immune Evasion: Implications for Tumor Immunotherapy. *Cancer Immunol Immunother* (2005) 54(4):307–14. doi: 10.1007/s00262-004-0593-x
59. Naumann RW, Hollebecque A, Meyer T, Devlin MJ, Oaknin A, Kerger J, et al. Safety and Efficacy of Nivolumab Monotherapy in Recurrent or Metastatic Cervical, Vaginal, or Vulvar Carcinoma: Results From the Phase I/II Checkmate 358 Trial. *J Clin Oncol* (2019) 37(31):2825–34. doi: 10.1200/JCO.19.00739
60. Janjigian YY, Bendell JC, Calvo E, Kim JW, Ascierto PA, Sharma P, et al. Checkmate-032: Phase I/II, Open-Label Study of Safety and Activity of Nivolumab (Nivo) Alone or With Ipilimumab (Ipi) in Advanced and Metastatic (A/M) Gastric Cancer (GC). *J Clin Oncol* (2016) 34(15_suppl):4010. doi: 10.1200/JCO.2016.34.15_suppl.4010
61. Ferris RL, Blumenschein G, Fayette J, Guigay J, Colevas AD, Licitra L, et al. Nivolumab for Recurrent Squamous-Cell Carcinoma of the Head and Neck. *New Engl J Med* (2016) 375(19):1856–67. doi: 10.1056/NEJMoa1602252
62. Ansell SM, Minnema MC, Johnson P, Timmerman JM, Armand P, Shipp MA, et al. Nivolumab for Relapsed/Refractory Diffuse Large B-Cell Lymphoma in Patients Ineligible for or Having Failed Autologous Transplantation: A Single-Arm, Phase II Study. *J Clin Oncol* (2019) 37(6):481–9. doi: 10.1200/JCO.18.00766
63. Anagnostou V, Smith KN, Forde PM, Niknafs N, Bhattacharya R, White J, et al. Evolution of Neoantigen Landscape During Immune Checkpoint Blockade in Non-Small Cell Lung Cancer. *Cancer Discovery* (2017) 7(3):264. doi: 10.1158/1538-7445.AM2017-NG01
64. Robert C, Ribas A, Hamid O, Daud A, Wolchok JD, Joshua AM, et al. Three-Year Overall Survival for Patients With Advanced Melanoma Treated With Pembrolizumab in KEYNOTE-001. *J Clin Oncol* (2016) 34(15_suppl):9503. doi: 10.1200/JCO.2016.34.15_suppl.9503
65. Makker V, Rasco D, Vogelzang NJ, Brose MS, Cohn AL, Mier J, et al. Lenvatinib Plus Pembrolizumab in Patients With Advanced Endometrial Cancer: An Interim Analysis of a Multicentre, Open-Label, Single-Arm, Phase 2 Trial. *Lancet Oncol* (2019) 20(5):711–8. doi: 10.1016/S1470-2045(19)30020-8
66. Le DT, Durham JN, Smith KN, Wang H, Bartlett BR, Aulakh LK, et al. Mismatch Repair Deficiency Predicts Response of Solid Tumors to PD-1 Blockade. *Science* (2017) 357(6349):409. doi: 10.1126/science.aan6733
67. Garon EB, Rizvi NA, Hui R, Leigh N, Balmanoukian AS, Eder JP, et al. Pembrolizumab for the Treatment of Non-Small-Cell Lung Cancer. *N Engl J Med* (2015) 372(21):2018–28. doi: 10.1056/NEJMoa1501824
68. Webb ES, Liu P, Baleeiro R, Lemoine NR, Yuan M, Wang Y-H. Immune Checkpoint Inhibitors in Cancer Therapy. *J BioMed Res* (2018) 32(5):317–26. doi: 10.7555/JBR.31.20160168
69. Rosenberg JE, Hoffman-Censits J, Powles T, van der Heijden MS, Balar AV, Necchi A, et al. Atezolizumab in Patients With Locally Advanced and Metastatic Urothelial Carcinoma Who Have Progressed Following Treatment With Platinum-Based Chemotherapy: A Single-Arm, Multicentre, Phase 2 Trial. *Lancet* (2016) 387(10031):1909–20. doi: 10.1016/S0140-6736(16)00561-4
70. Socinski MA, Jotte RM, Cappuzzo F, Orlandi F, Stroyakovskiy D, Nogami N, et al. Atezolizumab for First-Line Treatment of Metastatic Nonsquamous NSCLC. *New Engl J Med* (2018) 378(24):2288–301. doi: 10.1056/NEJMoa1716948
71. Schmid P, Adams S, Rugo HS, Schneeweiss A, Barrios CH, Iwata H, et al. Atezolizumab and Nab-Paclitaxel in Advanced Triple-Negative Breast Cancer. *New Engl J Med* (2018) 379(22):2108–21. doi: 10.1056/NEJMoa1809615
72. Horn L, Mansfield AS, Szczesna A, Havel L, Krzakowski M, Hochmair MJ, et al. First-Line Atezolizumab Plus Chemotherapy in Extensive-Stage Small-Cell Lung Cancer First-Line Atezolizumab Plus Chemotherapy in Extensive-Stage Small-Cell Lung Cancer. *N Engl J Med* (2018) 379(23):2220–9. doi: 10.1056/NEJMoa1809064
73. Woo SR, Turnis ME, Goldberg MV, Bankoti J, Selby M, Nirschl CJ, et al. Immune Inhibitory Molecules LAG-3 and PD-1 Synergistically Regulate T-Cell Function to Promote Tumoral Immune Escape. *Cancer Res* (2012) 72(4):917–27. doi: 10.1158/0008-5472.CAN-11-1620
74. Wang-Gillam A, Plambeck-Suess S, Goedegebuure P, Simon PO, Mitchem JB, Hornick JR, et al. A Phase I Study of IMP321 and Gemcitabine as the Front-Line Therapy in Patients With Advanced Pancreatic

- Adenocarcinoma. *Invest New Drugs* (2013) 31(3):707–13. doi: 10.1007/s10637-012-9866-y
75. He Y, Cao J, Zhao C, Li X, Zhou C, Hirsch FR. TIM-3, A Promising Target for Cancer Immunotherapy. *Onco Targets Ther* (2018) 11:7005–9. doi: 10.2147/OTT.S170385
 76. Wada J, Kanwar YS. Identification and Characterization of Galectin-9, a Novel Beta-Galactoside-Binding Mammalian Lectin. *J Biol Chem* (1997) 272(9):6078–86. doi: 10.1074/jbc.272.9.6078
 77. Anderson AC, Joller N, Kuchroo VK. Lag-3, Tim-3, and TIGIT: Co-Inhibitory Receptors With Specialized Functions in Immune Regulation. *Immunity* (2016) 44(5):989–1004. doi: 10.1016/j.immuni.2016.05.001
 78. Du W, Yang M, Turner A, Xu C, Ferris RL, Huang J, et al. TIM-3 as a Target for Cancer Immunotherapy and Mechanisms of Action. *Int J Mol Sci* (2017) 18(3):1–12. doi: 10.3390/ijms18030645
 79. Gorman JV, Starbeck-Miller G, Pham NL, Traver GL, Rothman PB, Hartly JT, et al. Tim-3 Directly Enhances CD8 T Cell Responses to Acute Listeria Monocytogenes Infection. *J Immunol* (2014) 192(7):3133–42. doi: 10.4049/jimmunol.1302290
 80. Yu X, Harden K C, Gonzalez L, Francesco M, Chiang E, Irving B, et al. The Surface Protein TIGIT Suppresses T Cell Activation by Promoting the Generation of Mature Immunoregulatory Dendritic Cells. *Nat Immunol* (2009) 10(1):48–57. doi: 10.1038/ni.1674
 81. Deuss FA, Gully BS, Rossjohn J, Berry R. Recognition of Nectin-2 by the Natural Killer Cell Receptor T Cell Immunoglobulin and ITIM Domain (TIGIT). *J Biol Chem* (2017) 292(27):11413–22. doi: 10.1074/jbc.M117.786483
 82. Chauvin JM, Pagliano O, Fourcade J, Sun Z, Wang H, Sander C, et al. TIGIT and PD-1 Impair Tumor Antigen-Specific CD8⁺ T Cells in Melanoma Patients. *J Clin Invest* (2015) 125(5):2046–58. doi: 10.1172/JCI80445
 83. Huang X, Zhang X, Li E, Zhang G, Wang X, Tang T, et al. VISTA: An Immune Regulatory Protein Checking Tumor and Immune Cells in Cancer Immunotherapy. *J Hematol Oncol* (2020) 13(1):83. doi: 10.1186/s13045-020-00917-y
 84. Wang J, Wu G, Manick B, Hernandez V, Renelt M, Erickson C, et al. VSIG-3 as a Ligand of VISTA Inhibits Human T-Cell Function. *Immunology* (2019) 156(1):74–85. doi: 10.1111/imm.13001
 85. Loeser H, Kraemer M, Gebauer F, Bruns C, Schröder W, Zander T, et al. The Expression of the Immune Checkpoint Regulator VISTA Correlates With Improved Overall Survival in Pt1/2 Tumor Stages in Esophageal Adenocarcinoma. *Oncoimmunology* (2019) 8(5):e1581546. doi: 10.1080/2162402X.2019.1581546
 86. Böger C, Behrens HM, Krüger S, Röcken C. The Novel Negative Checkpoint Regulator VISTA is Expressed in Gastric Carcinoma and Associated With PD-L1/PD-1: A Future Perspective for a Combined Gastric Cancer Therapy? *Oncoimmunology* (2017) 6(4):e1293215. doi: 10.1080/2162402X.2017.1293215
 87. Yang S, Wei W, Zhao Q. B7-H3, A Checkpoint Molecule, as a Target for Cancer Immunotherapy. *Int J Biol Sci* (2020) 16(11):1767–73. doi: 10.7150/ijbs.41105
 88. Picarda E, Ohaegbulam KC, Zang X. Molecular Pathways: Targeting B7-H3 (CD276) for Human Cancer Immunotherapy. *Clin Cancer Res* (2016) 22(14):3425–31. doi: 10.1158/1078-0432.CCR-15-2428
 89. Huang R-Y, Eppolito C, Lele S, Shrikant P, Matsuzaki J, Odunsi K. LAG3 and PD1 Co-Inhibitory Molecules Collaborate to Limit CD8⁺ T Cell Signaling and Dampen Antitumor Immunity in a Murine Ovarian Cancer Model. *Oncotarget* (2015) 6(29):27359–77. doi: 10.18632/oncotarget.4751
 90. Lines JL, Pantazi E, Mak J, Sempere LF, Wang L, Connell S, et al. VISTA Is an Immune Checkpoint Molecule for Human T Cells. *Cancer Res* (2014) 74(7):1924. doi: 10.1158/0008-5472.CAN-13-1504
 91. Prasad DVR, Nguyen T, Li Z, Yang Y, Duong J, Wang Y, et al. Murine B7-H3 Is a Negative Regulator of T Cells. *J Immunol* (2004) 173(4):2500. doi: 10.4049/jimmunol.173.4.2500
 92. Marin-Acevedo JA, Kimbrough EO, Lou Y. Next Generation of Immune Checkpoint Inhibitors and Beyond. *J Hematol Oncol* (2021) 14(1):45. doi: 10.1186/s13045-021-01056-8
 93. Schadendorf D, Hodi FS, Robert C, Weber JS, Margolin K, Hamid O, et al. Pooled Analysis of Long-Term Survival Data From Phase II and Phase III Trials of Ipilimumab in Unresectable or Metastatic Melanoma. *J Clin Oncol* (2015) 33(17):1889–94. doi: 10.1200/JCO.2014.56.2736
 94. Schoenfeld AJ, Hellmann MD. Acquired Resistance to Immune Checkpoint Inhibitors. *Cancer Cell* (2020) 37(4):443–55. doi: 10.1016/j.ccell.2020.03.017
 95. Kumar V, Chaudhary N, Garg M, Floudas CS, Soni P, Chandra AB. Current Diagnosis and Management of Immune Related Adverse Events (irAEs) Induced by Immune Checkpoint Inhibitor Therapy. *Front Pharmacol* (2017) 8(49):1–14. doi: 10.3389/fphar.2017.00049
 96. Puzanov I, Diab A, Abdallah K, Bingham CO, Brogdon C, Dadu R, et al. Managing Toxicities Associated With Immune Checkpoint Inhibitors: Consensus Recommendations From the Society for Immunotherapy of Cancer (SITC) Toxicity Management Working Group. *J Immunother Cancer* (2017) 5(1):95. doi: 10.1186/s40425-017-0300-z
 97. El Osta B, Hu F, Sadek R, Chintalapally R, Tang SC. Not All Immune-Checkpoint Inhibitors are Created Equal: Meta-Analysis and Systematic Review of Immune-Related Adverse Events in Cancer Trials. *Crit Rev Oncol Hematol* (2017) 119:1–12. doi: 10.1016/j.critrevonc.2017.09.002
 98. Hirano F, Kaneko K, Tamura H, Dong H, Wang S, Ichikawa M, et al. Blockade of B7-H1 and PD-1 by Monoclonal Antibodies Potentiates Cancer Therapeutic Immunity. *Cancer Res* (2005) 65(3):1089.
 99. Lipson EJ, Drake CG. Ipilimumab: An Anti-CTLA-4 Antibody for Metastatic Melanoma. *Clin Cancer Res* (2011) 17(22):6958. doi: 10.1158/1078-0432.CCR-11-1595
 100. Sami M, Bagheri L, Szewczuk MR. Current Challenges in Cancer Immunotherapy: Multimodal Approaches to Improve Efficacy and Patient Response Rates. *J Oncol* (2019) 2019:4508794. doi: 10.1155/2019/4508794
 101. Gide TN, Wilmott JS, Scolyer RA, Long GV. Primary and Acquired Resistance to Immune Checkpoint Inhibitors in Metastatic Melanoma. *Clin Cancer Res* (2018) 24(6):1260. doi: 10.1158/1078-0432.CCR-17-2267
 102. Jenkins RW, Barbie DA, Flaherty KT. Mechanisms of Resistance to Immune Checkpoint Inhibitors. *Br J Cancer* (2018) 118(1):9–16. doi: 10.1038/bjc.2017.434
 103. Fares CM, Van Allen EM, Drake CG, Allison JP, Hu-Lieskova S. Mechanisms of Resistance to Immune Checkpoint Blockade: Why Does Checkpoint Inhibitor Immunotherapy Not Work for All Patients? *Am Soc Clin Oncol Educ Book* (2019) 39:147–64. doi: 10.1200/EDBK_240837
 104. Fujiwara Y, Mittra A, Naqash AR, Takebe N. A Review of Mechanisms of Resistance to Immune Checkpoint Inhibitors and Potential Strategies for Therapy. *Cancer Drug Resistance* (2020) 3(3):252–75. doi: 10.20517/cdr.2020.11
 105. Syn NL, Teng MWL, Mok TSK, Soo RA. De-Novo and Acquired Resistance to Immune Checkpoint Targeting. *Lancet Oncol* (2017) 18(12):e731–e41. doi: 10.1016/S1470-2045(17)30607-1
 106. Schumacher TN, Schreiber RD. Neoantigens in Cancer Immunotherapy. *Science* (2015) 348(6230):69. doi: 10.1126/science.aaa4971
 107. Gubin MM, Zhang X, Schuster H, Caron E, Ward JP, Noguchi T, et al. Checkpoint Blockade Cancer Immunotherapy Targets Tumour-Specific Mutant Antigens. *Nature* (2014) 515(7528):577–81. doi: 10.1038/nature13988
 108. Tran L, Theodorescu D. Determinants of Resistance to Checkpoint Inhibitors. *Int J Mol Sci* (2020) 21(5):1–21. doi: 10.3390/ijms21051594
 109. de Velasco G, Miao D, Voss MH, Hakimi AA, Hsieh JJ, Tannir NM, et al. Tumor Mutational Load and Immune Parameters Across Metastatic Renal Cell Carcinoma Risk Groups. *Cancer Immunol Res* (2016) 4(10):820. doi: 10.1158/2326-6066.CIR-16-0110
 110. Rizvi NA, Hellmann MD, Snyder A, Kvistborg P, Makarov V, Havel JJ, et al. Mutational Landscape Determines Sensitivity to PD-1 Blockade in Non-Small Cell Lung Cancer. *Science* (2015) 348(6230):124. doi: 10.1126/science.aaa1348
 111. van Rooij N, van Buuren MM, Philips D, Velds A, Toebes M, Heemskerk B, et al. Tumor Exome Analysis Reveals Neoantigen-Specific T-Cell Reactivity in an Ipilimumab-Responsive Melanoma. *J Clin Oncol* (2013) 31(32):e439–e42. doi: 10.1200/JCO.2012.47.7521
 112. Fu C, Jiang A. Dendritic Cells and CD8 T Cell Immunity in Tumor Microenvironment. *Front Immunol* (2018) 9:3059. doi: 10.3389/fimmu.2018.03059
 113. Ma Y, Shurin GV, Peiyuan Z, Shurin MR. Dendritic Cells in the Cancer Microenvironment. *J Cancer* (2013) 4(1):36–44. doi: 10.7150/jca.5046

114. Wylie B, Macri C, Mintern JD, Waithman J. Dendritic Cells and Cancer: From Biology to Therapeutic Intervention. *Cancers (Basel)* (2019) 11(4):1–21. doi: 10.3390/cancers11040521
115. Vonderheide RH. The Immune Revolution: A Case for Priming, Not Checkpoint. *Cancer Cell* (2018) 33(4):563–9. doi: 10.1016/j.ccell.2018.03.008
116. Alshamsan A. Induction of Tolerogenic Dendritic Cells by IL-6-Secreting CT26 Colon Carcinoma. *Immunopharmacol Immunotoxicol* (2012) 34(3):465–9. doi: 10.3109/08923973.2011.625034
117. Pahne-Zeppenfeld J, Schröer N, Walch-Rückheim B, Oldak M, Gorter A, Hegde S, et al. Cervical Cancer Cell-Derived Interleukin-6 Impairs CCR7-Dependent Migration of MMP-9-Expressing Dendritic Cells. *Int J Cancer* (2014) 134(9):2061–73. doi: 10.1002/ijc.28549
118. Sucker A, Zhao F, Real B, Hecke C, Bielefeld N, Maßen S, et al. Genetic Evolution of T-Cell Resistance in the Course of Melanoma Progression. *Clin Cancer Res* (2014) 20(24):6593. doi: 10.1158/1078-0432.CCR-14-0567
119. Hulpke S, Tampé R. The MHC I Loading Complex: A Multitasking Machinery in Adaptive Immunity. *Trends Biochem Sci* (2013) 38(8):412–20. doi: 10.1016/j.tibs.2013.06.003
120. Gettinger S, Choi J, Hastings K, Truini A, Datar I, Sowell R, et al. Impaired HLA Class I Antigen Processing and Presentation as a Mechanism of Acquired Resistance to Immune Checkpoint Inhibitors in Lung Cancer. *Cancer Discov* (2017) 7(12):1420. doi: 10.1158/2159-8290.CD-17-0593
121. Sade-Feldman M, Jiao YJ, Chen JH, Rooney MS, Barzily-Rokni M, Eliane J-P, et al. Resistance to Checkpoint Blockade Therapy Through Inactivation of Antigen Presentation. *Nat Commun* (2017) 8(1):1136. doi: 10.1038/s41467-017-01062-w
122. Rooney MS, Shukla SA, Wu CJ, Getz G, Hacohen N. Molecular and Genetic Properties of Tumors Associated With Local Immune Cytolytic Activity. *Cell* (2015) 160(1–2):48–61. doi: 10.1016/j.cell.2014.12.033
123. Shin DS, Zaretsky JM, Escuin-Ordinas H, Garcia-Diaz A, Hu-Lieskovan S, Kalbasi A, et al. Primary Resistance to PD-1 Blockade Mediated by JAK1/2 Mutations. *Cancer Discovery* (2017) 7(2):188. doi: 10.1158/2159-8290.CD-16-1223
124. Zaretsky JM, Garcia-Diaz A, Shin DS, Escuin-Ordinas H, Hugo W, Hu-Lieskovan S, et al. Mutations Associated With Acquired Resistance to PD-1 Blockade in Melanoma. *N Engl J Med* (2016) 375(9):819–29. doi: 10.1056/NEJMoal604958
125. Liu D, Jenkins RW, Sullivan RJ. Mechanisms of Resistance to Immune Checkpoint Blockade. *Am J Clin Dermatol* (2019) 20(1):41–54. doi: 10.1007/s40257-018-0389-y
126. Gao J, Shi LZ, Zhao H, Chen J, Xiong L, He Q, et al. Loss of IFN- γ Pathway Genes in Tumor Cells as a Mechanism of Resistance to Anti-CTLA-4 Therapy. *Cell* (2016) 167(2):397–404.e9. doi: 10.1016/j.cell.2016.08.069
127. Garcia-Diaz A, Shin DS, Moreno BH, Saco J, Escuin-Ordinas H, Rodriguez GA, et al. Interferon Receptor Signaling Pathways Regulating PD-L1 and PD-L2 Expression. *Cell Rep* (2017) 19(6):1189–201. doi: 10.1016/j.celrep.2017.04.031
128. Zajac AJ, Blattman JN, Murali-Krishna K, Sourdive DJD, Suresh M, Altman JD, et al. Viral Immune Evasion Due to Persistence of Activated T Cells Without Effector Function. *J Exp Med* (1998) 188(12):2205–13. doi: 10.1084/jem.188.12.2205
129. Blackburn SD, Shin H, Haining WN, Zou T, Workman CJ, Polley A, et al. Coregulation of CD8+ T Cell Exhaustion by Multiple Inhibitory Receptors During Chronic Viral Infection. *Nat Immunol* (2009) 10(1):29–37. doi: 10.1038/ni.1679
130. Zarour HM. Reversing T-Cell Dysfunction and Exhaustion in Cancer. *Clin Cancer Res* (2016) 22(8):1856. doi: 10.1158/1078-0432.CCR-15-1849
131. Wherry EJ, Blattman JN, Murali-Krishna K, van der Most R, Ahmed R. Viral Persistence Alters CD8 T-Cell Immunodominance and Tissue Distribution and Results in Distinct Stages of Functional Impairment. *J Virol* (2003) 77(8):4911. doi: 10.1128/JVI.77.8.4911-4927.2003
132. Ahn E, Youngblood B, Lee J, Sarkar S, Ahmed R. Demethylation of the PD-1 Promoter Is Imprinted During the Effector Phase of CD8 T Cell Exhaustion. *J Virol* (2016) 90(19):8934. doi: 10.1128/JVI.00798-16
133. Pauken KE, Sammons MA, Odorizzi PM, Manne S, Godec J, Khan O, et al. Epigenetic Stability of Exhausted T Cells Limits Durability of Reinvigoration by PD-1 Blockade. *Science* (2016) 354(6316):1160. doi: 10.1126/science.aaf2807
134. Hargadon KM, Johnson CE, Williams CJ. Immune Checkpoint Blockade Therapy for Cancer: An Overview of FDA-Approved Immune Checkpoint Inhibitors. *Int Immunopharmacol* (2018) 62:29–39. doi: 10.1016/j.intimp.2018.06.001
135. Koyama S, Akbay EA, Li YY, Herter-Sprie GS, Buczkowski KA, Richards WG, et al. Adaptive Resistance to Therapeutic PD-1 Blockade Is Associated With Upregulation of Alternative Immune Checkpoints. *Nat Commun* (2016) 7(1):10501. doi: 10.1038/ncomms10501
136. Kakavand H, Jackett LA, Menzies AM, Gide TN, Carlino MS, Saw RPM, et al. Negative Immune Checkpoint Regulation by VISTA: A Mechanism of Acquired Resistance to Anti-PD-1 Therapy in Metastatic Melanoma Patients. *Modern Pathol* (2017) 30(12):1666–76. doi: 10.1038/modpathol.2017.89
137. Xia A, Zhang Y, Xu J, Yin T, Lu X-J. T Cell Dysfunction in Cancer Immunity and Immunotherapy. *Front Immunol* (2019) 10(1719):1–15. doi: 10.3389/fimmu.2019.01719
138. Li X, Liu R, Su X, Pan Y, Han X, Shao C, et al. Harnessing Tumor-Associated Macrophages as Aids for Cancer Immunotherapy. *Mol Cancer* (2019) 18(1):177. doi: 10.1186/s12943-019-1102-3
139. Jiang P, Gu S, Pan D, Fu J, Sahu A, Hu X, et al. Signatures of T Cell Dysfunction and Exclusion Predict Cancer Immunotherapy Response. *Nat Med* (2018) 24(10):1550–8. doi: 10.1038/s41591-018-0136-1
140. Tanaka A, Sakaguchi S. Targeting Treg Cells in Cancer Immunotherapy. *Eur J Immunol* (2019) 49(8):1140–6. doi: 10.1002/eji.201847659
141. Wherry EJ, Kurachi M. Molecular and Cellular Insights Into T Cell Exhaustion. *Nat Rev Immunol* (2015) 15(8):486–99. doi: 10.1038/nri3862
142. Saleh R, Elkord E. Treg-Mediated Acquired Resistance to Immune Checkpoint Inhibitors. *Cancer Lett* (2019) 457:168–79. doi: 10.1016/j.canlet.2019.05.003
143. Simpson TR, Li F, Montalvo-Ortiz W, Sepulveda MA, Bergerhoff K, Arce F, et al. Fc-Dependent Depletion of Tumor-Infiltrating Regulatory T Cells Co-Defines the Efficacy of Anti-CTLA-4 Therapy Against Melanoma. *J Exp Med* (2013) 210(9):1695–710. doi: 10.1084/jem.20130579
144. Magnuson AM, Kiner E, Ergun A, Park JS, Asinovsky N, Ortiz-Lopez A, et al. Identification and Validation of a Tumor-Infiltrating Treg Transcriptional Signature Conserved Across Species and Tumor Types. *Proc Natl Acad Sci* (2018) 115(45):E10672. doi: 10.1073/pnas.1810580115
145. Linehan DC, Goedegebuure PS. CD25+ CD4+ Regulatory T-Cells in Cancer. *Immunol Res* (2005) 32(1–3):155–68. doi: 10.1385/IR:32:1-3:155
146. Viehl CT, Moore TT, Liyanage UK, Frey DM, Ehlers JP, Eberlein TJ, et al. Depletion of CD4+CD25+ Regulatory T Cells Promotes a Tumor-Specific Immune Response in Pancreas Cancer-Bearing Mice. *Ann Surg Oncol* (2006) 13(9):1252–8. doi: 10.1245/s10434-006-9015-y
147. Hamid O, Schmidt H, Nissan A, Ridolfi L, Aamdal S, Hansson J, et al. A Prospective Phase II Trial Exploring the Association Between Tumor Microenvironment Biomarkers and Clinical Activity of Ipilimumab in Advanced Melanoma. *J Transl Med* (2011) 9:204. doi: 10.1186/1479-5876-9-204
148. Pacella I, Procaccini C, Focaccetti C, Miaci S, Timperi E, Faicchia D, et al. Fatty Acid Metabolism Complements Glycolysis in the Selective Regulatory T Cell Expansion During Tumor Growth. *Proc Natl Acad Sci USA* (2018) 115(28):E6546–e55. doi: 10.1073/pnas.1720113115
149. Kourepini E, Paschalidis N, Simoes DCM, Aggelakopoulou M, Grogan JL, Panoutsakopoulou V. TIGIT Enhances Antigen-Specific Th2 Recall Responses and Allergic Disease. *J Immunol* (2016) 196(9):3570. doi: 10.4049/jimmunol.1501591
150. Guan X, Hasan MN, Begum G, Kohanbash G, Carney KE, Pigott VM, et al. Blockade of Na/H Exchanger Stimulates Glioma Tumor Immunogenicity and Enhances Combinatorial TMZ and Anti-PD-1 Therapy. *Cell Death Dis* (2018) 9(10):1010. doi: 10.1038/s41419-018-1062-3
151. Liberti MV, Locasale JW. The Warburg Effect: How Does it Benefit Cancer Cells? *Trends Biochem Sci* (2016) 41(3):211–8. doi: 10.1016/j.tibs.2015.12.001
152. McLean LA, Roscoe J, Jørgensen NK, Gorin FA, Cala PM. Malignant Gliomas Display Altered Ph Regulation by NHE1 Compared With Nontransformed Astrocytes. *Am J Physiol-Cell Physiol* (2000) 278(4):C676–C88. doi: 10.1152/ajpcell.2000.278.4.C676
153. Huang Y, Snuderl M, Jain RK. Polarization of Tumor-Associated Macrophages: A Novel Strategy for Vascular Normalization and

- Antitumor Immunity. *Cancer Cell* (2011) 19(1):1–2. doi: 10.1016/j.ccr.2011.01.005
154. Farooque A, Afrin F, Adhikari JS, Dwarakanath BSR. Polarization of Macrophages Towards M1 Phenotype by a Combination of 2-Deoxy-D-Glucose and Radiation: Implications for Tumor Therapy. *Immunobiology* (2016) 221(2):269–81. doi: 10.1016/j.imbio.2015.10.009
 155. Groth C, Hu X, Weber R, Fleming V, Altevoigt P, Utikal J, et al. Immunosuppression Mediated by Myeloid-Derived Suppressor Cells (MDSCs) During Tumour Progression. *Br J Cancer* (2019) 120(1):16–25. doi: 10.1038/s41416-018-0333-1
 156. Lu C, Redd PS, Lee JR, Savage N, Liu K. The Expression Profiles and Regulation of PD-L1 in Tumor-Induced Myeloid-Derived Suppressor Cells. *Oncoimmunology* (2016) 5(12):e1247135. doi: 10.1080/2162402X.2016.1247135
 157. Meyer C, Cagnon L, Costa-Nunes CM, Baumgaertner P, Montandon N, Leyvraz L, et al. Frequencies of Circulating MDSC Correlate With Clinical Outcome of Melanoma Patients Treated With Ipilimumab. *Cancer Immunol Immunother* (2014) 63(3):247–57. doi: 10.1007/s00262-013-1508-5
 158. Weber R, Fleming V, Hu X, Nagibin V, Groth C, Altevoigt P, et al. Myeloid-Derived Suppressor Cells Hinder the Anti-Cancer Activity of Immune Checkpoint Inhibitors. *Front Immunol* (2018) 9:1310. doi: 10.3389/fimmu.2018.01310
 159. Warburg O, Wind F, Negelein E. The Metabolism of Tumors in the Body. *J Gen Physiol* (1927) 8(6):519–30. doi: 10.1085/jgp.8.6.519
 160. Som P, Atkins HL, Bandyopadhyay D, Fowler JS, MacGregor RR, Matsui K, et al. A Fluorinated Glucose Analog, 2-Fluoro-2-Deoxy-D-Glucose (F-18): Nontoxic Tracer for Rapid Tumor Detection. *J Nucl Med* (1980) 21(7):670–5. doi: 10.1097/00004728-198012000-00045
 161. O'Neill LA, Kishton RJ, Rathmell J. A Guide to Immunometabolism for Immunologists. *Nat Rev Immunol* (2016) 16(9):553–65. doi: 10.1038/nri.2016.70
 162. Frauwirth KA, Riley JL, Harris MH, Parry RV, Rathmell JC, Plas DR, et al. The CD28 Signaling Pathway Regulates Glucose Metabolism. *Immunity* (2002) 16(6):769–77. doi: 10.1016/S1074-7613(02)00323-0
 163. Michalek RD, Gerriets VA, Jacobs SR, Macintyre AN, MacIver NJ, Mason EF, et al. Cutting Edge: Distinct Glycolytic and Lipid Oxidative Metabolic Programs Are Essential for Effector and Regulatory CD4+ T Cell Subsets. *J Immunol* (2011) 186(6):3299–303. doi: 10.4049/jimmunol.1003613
 164. Fox CJ, Hammerman PS, Thompson CB. Fuel Feeds Function: Energy Metabolism and the T-Cell Response. *Nat Rev Immunol* (2005) 5(11):844–52. doi: 10.1038/nri1710
 165. Xia L, Oyang L, Lin J, Tan S, Han Y, Wu N, et al. The Cancer Metabolic Reprogramming and Immune Response. *Mol Cancer* (2021) 20(1):28. doi: 10.1186/s12943-021-01316-8
 166. Sukumar M, Roychoudhuri R, Restifo NP. Nutrient Competition: A New Axis of Tumor Immunosuppression. *Cell* (2015) 162(6):1206–8. doi: 10.1016/j.cell.2015.08.064
 167. Müller B, Fischer B, Kreutz W. An Acidic Microenvironment Impairs the Generation of non-Major Histocompatibility Complex-Restricted Killer Cells. *Immunology* (2000) 99(3):375–84. doi: 10.1046/j.1365-2567.2000.00975.x
 168. Calcinotto A, Filipazzi P, Groni M, Iero M, De Milito A, Ricupito A, et al. Modulation of Microenvironment Acidity Reverses Anergy in Human and Murine Tumor-Infiltrating T Lymphocytes. *Cancer Res* (2012) 72(11):2746–56. doi: 10.1158/0008-5472.CAN-11-1272
 169. Bosticardo M, Ariotti S, Losana G, Bernabei P, Forni G, Novelli F. Biased Activation of Human T Lymphocytes Due to Low Extracellular Ph is Antagonized by B7/CD28 Costimulation. *Eur J Immunol* (2001) 31(9):2829–38. doi: 10.1002/1521-4141(200109)31:9<2829::AID-IMMU2829>3.0.CO;2-U
 170. Cerezo M, Rocchi S. Cancer Cell Metabolic Reprogramming: A Keystone for the Response to Immunotherapy. *Cell Death Dis* (2020) 11(11):964. doi: 10.1038/s41419-020-03175-5
 171. Carr EL, Kelman A, Wu GS, Gopaul R, Senkevitch E, Aghvanyan A, et al. Glutamine Uptake and Metabolism Are Coordinately Regulated by ERK/MAPK During T Lymphocyte Activation. *J Immunol* (2010) 185(2):1037–44. doi: 10.4049/jimmunol.0903586
 172. Zhang J, Pavlova NN, Thompson CB. Cancer Cell Metabolism: The Essential Role of the Nonessential Amino Acid, Glutamine. *EMBO J* (2017) 36(10):1302–15. doi: 10.15252/embj.201696151
 173. Bonuccelli G, Whitaker-Menezes D, Castello-Cros R, Pavlides S, Pestell RG, Fatatis A, et al. The Reverse Warburg Effect: Glycolysis Inhibitors Prevent the Tumor Promoting Effects of Caveolin-1 Deficient Cancer Associated Fibroblasts. *Cell Cycle* (2010) 9(10):1960–71. doi: 10.4161/cc.9.10.11601
 174. Yarchoan M, Hopkins A, Jaffee EM. Tumor Mutational Burden and Response Rate to PD-1 Inhibition. *New Engl J Med* (2017) 377(25):2500–1. doi: 10.1056/NEJMc1713444
 175. Ott PA, Hu Z, Keskin DB, Shukla SA, Sun J, Bozym DJ, et al. An Immunogenic Personal Neoantigen Vaccine for Patients With Melanoma. *Nature* (2017) 547(7662):217–21. doi: 10.1038/nature22991
 176. Hung AL, Maxwell R, Theodros D, Belcaid Z, Mathios D, Luksik AS, et al. TIGIT and PD-1 Dual Checkpoint Blockade Enhances Antitumor Immunity and Survival in GBM. *Oncoimmunology* (2018) 7(8):e1466769. doi: 10.1080/2162402X.2018.1466769
 177. Guo ZS, Liu Z, Bartlett DL. Oncolytic Immunotherapy: Dying the Right Way Is a Key to Eliciting Potent Antitumor Immunity. *Front Oncol* (2014) 4:74. doi: 10.3389/fonc.2014.00074
 178. Peng M, Mo Y, Wang Y, Wu P, Zhang Y, Xiong F, et al. Neoantigen Vaccine: An Emerging Tumor Immunotherapy. *Mol Cancer* (2019) 18(1):128. doi: 10.1186/s12943-019-1055-6
 179. Whiteside TL, Demaria S, Rodriguez-Ruiz ME, Zarour HM, Melero I. Emerging Opportunities and Challenges in Cancer Immunotherapy. *Clin Cancer Res* (2016) 22(8):1845. doi: 10.1158/1078-0432.CCR-16-0049
 180. Buqué A, Bloy N, Aranda F, Castoldi F, Eggermont A, Cremer I, et al. Trial Watch: Immunomodulatory Monoclonal Antibodies for Oncological Indications. *OncoImmunology* (2015) 4(4):e1008814. doi: 10.1080/2162402X.2015.1008814
 181. Chen DS, Hurwitz H. Combinations of Bevacizumab With Cancer Immunotherapy. *Cancer J* (2018) 24(4):193–204. doi: 10.1097/PPO.0000000000000327
 182. Loo Yau H, Ettayebi I, De Carvalho DD. The Cancer Epigenome: Exploiting its Vulnerabilities for Immunotherapy. *Trends Cell Biol* (2019) 29(1):31–43. doi: 10.1016/j.tcb.2018.07.006
 183. Vétizou M, Pitt JM, Daillère R, Lepage P, Waldschmitt N, Flament C, et al. Anticancer Immunotherapy by CTLA-4 Blockade Relies on the Gut Microbiota. *Science* (2015) 350(6264):1079–84. doi: 10.1126/science.aad1329
 184. Jain T, Sharma P, Are AC, Vickers SM, Dudeja V. New Insights Into the Cancer-Microbiome-Immune Axis: Decrypting a Decade of Discoveries. *Front Immunol* (2021) 12:622064. doi: 10.3389/fimmu.2021.622064
 185. Topalian SL, Taube JM, Anders RA, Pardoll DM. Mechanism-Driven Biomarkers to Guide Immune Checkpoint Blockade in Cancer Therapy. *Nat Rev Cancer* (2016) 16(5):275–87. doi: 10.1038/nrc.2016.36
 186. Doroshow DB, Sanmamed MF, Hastings K, Politi K, Rimm DL, Chen L, et al. Immunotherapy in Non-Small Cell Lung Cancer: Facts and Hopes. *Clin Cancer Res* (2019) 25(15):4592–602. doi: 10.1158/1078-0432.CCR-18-1538
 187. Rimm DL, Han G, Taube JM, Yi ES, Bridge JA, Flieder DB, et al. A Prospective, Multi-Institutional, Pathologist-Based Assessment of 4 Immunohistochemistry Assays for PD-L1 Expression in Non-Small Cell Lung Cancer. *JAMA Oncol* (2017) 3(8):1051–8. doi: 10.1001/jamaoncol.2017.0013
 188. Rizvi NA, Hellmann MD, Snyder A, Kvistborg P, Makarov V, Havel JJ, et al. Cancer Immunology. Mutational Landscape Determines Sensitivity to PD-1 Blockade in Non-Small Cell Lung Cancer. *Science* (2015) 348(6230):124–8. doi: 10.1126/science.aaa1348
 189. Marcus L, Lemery SJ, Keegan P, Pazdur R. FDA Approval Summary: Pembrolizumab for the Treatment of Microsatellite Instability-High Solid Tumors. *Clin Cancer Res* (2019) 25(13):3753–8. doi: 10.1158/1078-0432.CCR-18-4070
 190. Benci JL, Xu B, Qiu Y, Wu TJ, Dada H, Twyman-Saint Victor C, et al. Tumor Interferon Signaling Regulates a Multigenic Resistance Program to Immune Checkpoint Blockade. *Cell* (2016) 167(6):1540–54.e12. doi: 10.1016/j.cell.2016.11.022
 191. Tumeh PC, Harview CL, Yearley JH, Shintaku IP, Taylor EJ, Robert L, et al. PD-1 Blockade Induces Responses by Inhibiting Adaptive Immune Resistance. *Nature* (2014) 515(7528):568–71. doi: 10.1038/nature13954

Conflict of Interest: Authors BLR and LJD were employed by company Buboo (Pty) Ltd.

The remaining authors declare that the research was conducted in the absence of any commercial or financial relationships that could be construed as a potential conflict of interest.

Copyright © 2021 Russell, Sooklal, Malindisa, Daka and Ntwasa. This is an open-access article distributed under the terms of the Creative Commons Attribution License (CC BY). The use, distribution or reproduction in other forums is permitted, provided the original author(s) and the copyright owner(s) are credited and that the original publication in this journal is cited, in accordance with accepted academic practice. No use, distribution or reproduction is permitted which does not comply with these terms.



OPEN ACCESS

Edited by:

Liwu Fu,
Sun Yat-sen University, China

Reviewed by:

Alessandra Ghigo,
University of Turin, Italy
Tianxin Lin,
Sun Yat-sen Memorial Hospital, China

***Correspondence:**

Chen Yang
YangC_Huashan@163.com
Haowen Jiang
haowj_sh@fudan.edu.cn
Na Liu
liuna_sia@shu.edu.cn

†ORCID:

Chen Yang
orcid.org/0000-0001-6011-4067
Siqi Wu
orcid.org/0000-0001-6464-2772

‡These authors have contributed
equally to this work and share first
authorship

Specialty section:

This article was submitted to
Molecular and Cellular Oncology,
a section of the journal
Frontiers in Cell and Developmental
Biology

Received: 22 January 2021

Accepted: 24 May 2021

Published: 07 July 2021

Citation:

Yang C, Wu S, Mou Z, Zhou Q,
Zhang Z, Chen Y, Ou Y, Chen X,
Dai X, Xu C, Liu N and Jiang H (2021)
Transcriptomic Analysis Identified
ARHGAP Family as a Novel Biomarker
Associated With Tumor-Promoting
Immune Infiltration
and Nanomechanical Characteristics
in Bladder Cancer.
Front. Cell Dev. Biol. 9:657219.
doi: 10.3389/fcell.2021.657219

Transcriptomic Analysis Identified ARHGAP Family as a Novel Biomarker Associated With Tumor-Promoting Immune Infiltration and Nanomechanical Characteristics in Bladder Cancer

Chen Yang^{1,2,3*†}, Siqi Wu^{1,2†}, Zezhong Mou^{1,2†}, Quan Zhou^{1,2†}, Zheyu Zhang^{1,2}, Yiling Chen^{1,2}, Yuxi Ou^{1,2}, Xinan Chen^{1,2}, Xiyu Dai^{1,2}, Chenyang Xu^{1,2}, Na Liu^{4*} and Haowen Jiang^{1,2,3*}

¹ Department of Urology, Huashan Hospital, Fudan University, Shanghai, China, ² Fudan Institute of Urology, Huashan Hospital, Fudan University, Shanghai, China, ³ National Clinical Research Center for Aging and Medicine, Fudan University, Shanghai, China, ⁴ School of Mechatronics Engineering and Automation, Shanghai University, Shanghai, China

Bladder cancer (BCa) is a common lethal urinary malignancy worldwide. The role of ARHGAP family genes in BCa and its association with immuno-microenvironment remain largely unknown. ARHGAP family expression and immune infiltration in BCa were analyzed by bioinformatics analysis. Then, we investigated cell proliferation, invasion, and migration *in vivo* and *in vitro* of the ARHGAP family. Furthermore, atomic force microscopy (AFM) was employed in measuring cellular mechanical properties of BCa cells. The results demonstrated that ARHGAP family genes correlate with a tumor-promoting microenvironment with a lower Th1/Th2 cell ratio, higher DC cell infiltration, higher Treg cell infiltration, and T-cell exhaustion phenotype. Silencing ARHGAP5, ARHGAP17, and ARHGAP24 suppressed BCa cell proliferation, migration, and metastasis. Knocking down of ARHGAPs in T24 cells caused a relatively higher Young's modulus and lower adhesive force and cell height. Taken together, ARHGAP family genes promote BCa progressing through establishing a tumor-promoting microenvironment and promoting cancer progression.

Keywords: bladder cancer, ARHGAP, immune infiltration, tumor microenvironment, cellular mechanical properties

Abbreviations: AFM, atomic force microscopy; ARHGAP, Rho GTPase-activating protein; BCa, bladder cancer; BP, biological process; CC, cellular component; CCK8, Cell Counting Kit-8; DC, dendritic cell; DMEM, Dulbecco's modified Eagle's medium; EdU, 5-ethynyl-2'-deoxyuridine; EMT, epithelial-mesenchymal transition; FDR, false discovery rate; FBS, fetal bovine serum; FPKM, fragments per kilobase million; KEGG, Kyoto Encyclopedia of Genes and Genomes; GO, Gene Ontology; GTEX, Genotype-Tissue Expression; GSEA, gene set enrichment analysis; IL-2, interleukin 2; IL-6, interleukin 6; MCODE, Molecular Complex Detection; MF, molecular function; NES, normalized enrichment score; NK, natural killer; PFA, paraformaldehyde; PPI, protein-protein interaction; RhoA, Ras homolog family member A; TAMs, tumor-associated macrophages; TCGA, The Cancer Genome Atlas; TGF- β , transforming growth factor beta; TNF- α , tumor necrosis factor alpha; Th1, type 1 T helper; Th1, type 2 T helper; WB, Western blotting; YM, Young's modulus.

INTRODUCTION

Bladder cancer (BCa) is the ninth leading diagnosed malignancy, which causes 17,980 mortality worldwide in 2020 (Siegel et al., 2020). The majority of BCa cases are classified as non-muscle invasive BCa representing the curable pathological type, while the other 25% are muscle-invasive BCa characterized by rapid progression and high recurrence rate, and eventually progress into metastatic disease (Smith et al., 2012; Nekolla et al., 2019). In recent years, various attempts to detect BCa at an early stage or explore the potential mechanism of lethal BCa have been made (Chen et al., 2020; Xie et al., 2021), so treatment strategies based on underlying molecular mechanisms in the metastasis and progression of BCa is in urgent need (Duggan et al., 2000).

Cancer cells are endowed with unique biological capabilities allowing them for constitutive survival, proliferation, and invasion ability during carcinogenesis (Chaffer and Weinberg, 2011). Adaptive immune response, a key regulator in regulating oncogenesis, has been well studied in the past decades. Several cancer-related hallmarks have been found responsible for the interaction of tumor and immune cells. Some of them can impair the differentiation and maturation of various immune cell subpopulations, which eventually leads to weakened antitumor functions in the tumor microenvironment, helping cancer cells to escape from immune surveillance (Chen and Mellman, 2017). In several tumor types, a better prognosis is mainly associated with infiltration of CD8⁺ T cells, type 1 T helper (Th1) cells, natural killer (NK) cells, and M1 macrophages. Conversely, poor prognosis usually correlates with high infiltration of Treg cells, Th2 cells, MDSCs, and M2 macrophages, and neutrophils (Fridman et al., 2012; Becht et al., 2016). These findings implied a distinctive mechanism of BCa-related immunological regulation, which could bring a radical revolution in BCa treatment other than the classical cisplatin-based chemotherapy.

The Rho GTPase family, a part of the Ras superfamily, consists of some highly conserved genes in regulating biological processes like cytoskeleton organization, vesicle trafficking, cell cycle, cell polarity, cell invasion, and cell migration (Haraguchi et al., 2019). Rho GTPases catalyze the conversion between active form and inactive form of Ras superfamily, henceforth, suppressing Rho GTPase downstream cellular biological processes. GTPase-activating proteins (RhoGAPs), which negatively regulates Rho GTPases are known as ARHGAP family (Post et al., 2013). While the roles of several ARHGAP family members have been identified in several types of cancer (Gen et al., 2009; Wang et al., 2014a,b; Luo et al., 2016; Hashimoto et al., 2018), the function of ARHGAP family in BCa, especially in immunological microenvironment of BCa, has not been elucidated.

Through comprehensive assessment of ARHGAP genes, we found a lower ARHGAP family expression in BCa, of which ARHGAP5, ARHGAP8, ARHGAP11A, ARHGAP17, ARHGAP24, ARHGAP37 (STARD13), and ARHGAP38 (STARD8) were highly related with prognosis. Axon guidance, focal adhesion, and leukocyte transendothelial migration were

associated with the ARHGAP family genes, while focal adhesion, chemokine signaling pathway, and T-cell receptor signaling pathway were enriched in ARHGAP coexpression genes. We demonstrated that the ARHGAP family genes correlate with a tumor-promoting microenvironment. Silencing ARHGAP5, ARHGAP17, and ARHGAP24 suppressed BC cell proliferation, migration, and metastasis. Meanwhile, we validated that knocking down of ARHGAPs in T24 cells caused a relatively higher Young's modulus and lower adhesive force and cell height, suggesting that ARHGAP could maintain a malignant cellular mechanical property of BCa. Our work offers novel insights into a potential mechanism of ARHGAP family genes' correlation with immune microenvironment in BCa.

MATERIALS AND METHODS

cBioPortal Database Analysis

The cBioPortal database¹ offers visualized analysis of cancer genomics based on available high-throughput sequencing data (Cerami et al., 2012). To analyze the mutation of the ARHGAP family genes, a network of the mutation profile of ARHGAP family was generated based on data of 413 samples in The Cancer Genome Atlas database (TCGA, Bladder Cancer, Cell, 2017) (Robertson et al., 2017) in cBioPortal.

Oncomine Database Analysis

The Oncomine database (Rhodes et al., 2004)² compiled 86,733 cancer samples within 715 gene expression into construction of a comprehensive data-mining database. We assessed the ARHGAP family expression in various kinds of tumor types.

TIMER Database Analysis

The TIMER³ database contributes to analyzing immune cell infiltration level in multiple cancers through pathological validation and improved statistical methodology to evaluate tumor immune infiltration (Li et al., 2017). We employed this database to assess differences in expression level of several candidates in the ARHGAP family in BCa to explore the association between ARHGAP family expression and infiltration level of particular immune cell subsets including B cells, CD4⁺ T and CD8⁺ T cells, neutrophils, macrophages, and dendritic cells. The Kaplan–Meier curve is also applied to analyze patient survival of the differential expression of the ARHGAP family gene-associated immune cell infiltration. The correlation between candidate ARHGAP family genes expression and gene markers of immune cells through relevant modules were analyzed.

GEPIA Database Analysis

The GEPIA database (Tang et al., 2017)⁴ facilitates the standardized analysis of RNA-seq data from 9,736

¹<http://www.cbioportal.org>

²<https://www.oncomine.org/resource/login.html>

³<https://cistrome.shinyapps.io/timer/>

⁴<http://gepia.cancer-pku.cn/>

tumors and 8,587 normal samples originating from The Cancer Genome Atlas (TCGA) and the Genotype-Tissue Expression (GTEx) data sets. We therefore assessed the link between the ARHGAP family gene expression and patients' prognoses in BCa.

Gene Set Enrichment Analysis

To further investigate the biological concepts associated with the ARHGAP family genes, we performed Gene Set Enrichment Analysis (GSEA) on the RNA-seq data downloaded from TCGA database. The mRNA expression of BCa was divided into high and low groups according to expression level. The carcinoma-related pathways gene sets (h.all.v6.0.symbols.gmt) were downloaded from the Molecular Signatures Database-MsigDB⁵. Enrichment analysis was performed by randomly repeating 1,000 times. Gene sets with a p -value < 0.05, normalized enrichment score (NES) > 1 or < -1, and false discovery rate (FDR) < 0.25 were considered as significantly enriched.

Correlation and Protein Interaction Analysis

We both performed correlation and protein-protein interaction (PPI) analysis on the ARHGAP family genes. Herein, we generated correlation analysis by using BCa's mRNA expression of the ARHGAP family genes downloaded from TCGA database. The results of correlation and relative p -value were constructed by using "corrplot" package in R (version 4.0.2). Then we applied GeneMANIA⁶ to analyze the ARHGAP family gene interaction and showed the PPI network including coexpression, pathway, predicted, colocalization, and genetic interactions. We also explored 50 most potentially relevant proteins by STRING⁷ database to serve the PPI network and showed the MCODE components identified by Metascape⁸.

Gene Ontology and Kyoto Encyclopedia of Genes and Genomes Functional Enrichment Analysis

To explore the biological functions and novel pathways of the ARHGAP family genes, we applied Gene Ontology (GO) enrichment and Kyoto Encyclopedia of Genes and Genomes database (KEGG) enrichment. All GO and KEGG functional enrichment analysis were carried out by "clusterProfiler" and "enrichplot" package in R (version 4.0.2). Results of GO enrichment analysis including "Biological Process," "Cellular Component," and "Molecular Function" were visualized as a dot plot. Several most representative GO and KEGG analysis were also shown by R (version 4.0.2). A p -value < 0.05 was set as the cutoff criterion and considered as statistically significant.

⁵<https://www.gsea-msigdb.org/gsea/msigdb>

⁶<https://genemania.org/>

⁷<https://string-db.org/>

⁸<https://metascape.org/>

Tumor-Infiltrating Immune Cell Portraying

Two methods, xCell (Aran et al., 2017) and TIMER (Tumor Immune Estimation Resource,⁹ were used to analyze the tissue-infiltrating cell-type abundance from bulk RNA-seq data. Pre-calculated TCGA data by xCell was downloaded from the xCell web tool¹⁰. Cell type enrichment scores of TCGA-BLCA samples were extracted as reflection of certain cell type abundance. Metrics including immune score, stroma score, and microenvironment score were defined according to the source code of xCell on GitHub. Among 64 cell types xCell could output, cell types including CD8+ T cells, NK cells, dendritic cells (DCs), CD4+ T cells, regulatory T cells (Tregs), macrophage M1, macrophage M2, type 2 T-helper cells (Th2 cells), and type 1 T-helper cells (Th1 cells) were chosen to perform further analysis. R package "ggpubr" was used to visualize enrichment scores between groups. Samples with certain gene expression level (FPKM normalized expression level) higher than the median of that of all selected samples were defined as highly expressed, while the remaining samples as lowly expressed. Wilcoxon signed rank test was used to compare means between two groups. "Gene module" of TIMER was used to explore the correlation between gene expression and abundance of immune infiltrates, with BLCA (bladder urothelial carcinoma) selected as cancer types.

Patient Samples

The study protocol was approved by the Ethics Committee of Huashan Hospital (Shanghai, China; approval no. KY2011-009) and conducted in accordance with the tenets of the Declaration of Helsinki. All patients consented to the use of resected tissues for research purposes.

A total of 90 pairs of BC tissues and adjacent tissues were collected for tissue microarray (TMA) construction from BC patients after surgical treatment in Huashan Hospital, Fudan University, between January 2007 and January 2013 including a 5-year follow-up. Two experienced pathologists confirm the pathological diagnoses of BC according to the 7th edition of the TNM classification of the Union for International Cancer Control (Wittekind et al., 2019).

Another seven pairs of high-grade and seven pairs of low-grade bladder cancer with normal samples were obtained from Huashan Urology Tissue Bank under an approval from the Ethics Committee of Huashan Hospital. Samples were harvested and immediately snap frozen in liquid nitrogen. Meanwhile, 20 fresh bladder cancer tumor tissues were obtained for flow cytometry.

Immunohistochemical Staining

Single immunohistochemical staining was performed on TMA slides and 20 FFPE tissues from fresh resected tumors. The immunohistochemical staining procedure is illustrated as below. The slides were deparaffinized

⁹<https://cistrome.shinyapps.io/timer/>

¹⁰<http://xCell.ucsf.edu/>

TABLE 1 | Summary of sub-family in ARHGAP family genes.

	Subfamily	Description	Alias
ARHGAP1		Rho GTPase activating protein 1	CDC42GAP, RHOGAP, RHOGAP1, p50rhoGAP
ARHGAP2	CHN1	chimerin 1	ARHGAP2, CHN, DURS2, NC, RHOGAP2
ARHGAP3	CHN2	chimerin 2	ARHGAP3, BCH, CHN2-3, RHOGAP3
ARHGAP4		Rho GTPase activating protein 4	C1, RGC1, RhoGAP4, SrGAP4, p115
ARHGAP5		Rho GTPase activating protein 5	GFI2, RhoGAP5, p190-B, p190BRhoGAP
ARHGAP6		Rho GTPase activating protein 6	RHOGAP6, RHOGAPX-1
ARHGAP7	DLC1	DLC1 Rho GTPase activating protein	ARHGAP7, HP, STARD12, p122-RhoGAP
ARHGAP8		Rho GTPase activating protein 8	BPGAP1, PP610
ARHGAP9		Rho GTPase activating protein 9	10C, RGL1
ARHGAP10		Rho GTPase activating protein 10	GRAF2, PS-GAP, PSGAP, ARHGAP21
ARHGAP11A		Rho GTPase activating protein 11A	GAP (1-12)
ARHGAP11B		Rho GTPase activating protein 11B	B'-T, FAM7B1
ARHGAP12		Rho GTPase activating protein 12	ARHGAP12
ARHGAP13	SRGAP1	SLIT-ROBO Rho GTPase activating protein 1	ARHGAP13
ARHGAP14	SRGAP3	SLIT-ROBO Rho GTPase activating protein 3	ARHGAP14, MEGAP, SRGAP2, WRP
ARHGAP15		Rho GTPase activating protein 15	BM046
ARHGAP17		Rho GTPase activating protein 17	MST066, MST110, MSTP038, MSTP066, MSTP110, NADRIN, PP367, PP4534, RICH-1, RICH1, WBP15
ARHGAP18		Rho GTPase activating protein 18	MacGAP, SENEX, bA307O14.2
ARHGAP19		Rho GTPase activating protein 19	ARHGAP19
ARHGAP20		Rho GTPase activating protein 20	RARHOGAP
ARHGAP21		Rho GTPase activating protein 21	ARHGAP10
ARHGAP22		Rho GTPase activating protein 22	RhoGAP2, RhoGap22
ARHGAP23		Rho GTPase activating protein 23	ARHGAP23
ARHGAP24		Rho GTPase activating protein 24	FILGAP, RC-GAP72, RCGAP72, p73, p73RhoGAP
ARHGAP25		Rho GTPase activating protein 25	HEL-S-308, KAIA0053
ARHGAP26		Rho GTPase activating protein 26	GRAF, GRAF1, OPHN1L, OPHN1L1
ARHGAP27		Rho GTPase activating protein 27	CAMGAP1, PP905, SH3D20, SH3P20
ARHGAP28		Rho GTPase activating protein 28	ARHGAP28
ARHGAP29		Rho GTPase activating protein 29	PARG1
ARHGAP30		Rho GTPase activating protein 30	ARHGAP30
ARHGAP31		Rho GTPase activating protein 31	AOS1, CDGAP
ARHGAP32		Rho GTPase activating protein 32	GC-GAP, GRIT, PX-RICS, RICS, p200RhoGAP, p250GAP
ARHGAP33		Rho GTPase activating protein 33	NOMA-GAP, SNX26, TCGAP
ARHGAP34	SRGAP2	SLIT-ROBO Rho GTPase activating protein 2	ARHGAP34, FBNP2, SRGAP2A, SRGAP3
ARHGAP35		Rho GTPase activating protein 35	GRF-1, GRLF1, P190-A, P190A, p190ARhoGAP, p190RhoGAP
ARHGAP36		Rho GTPase activating protein 36	ARHGAP36
ARHGAP37	STARD13	StAR-related lipid transfer (START) domain containing 13	ARHGAP37, DLC2, GT650, LINC00464
ARHGAP38	STARD8	StAR-related lipid transfer (START) domain containing 8	ARHGAP38, DLC3, STARTGAP3
ARHGAP39		Rho GTPase activating protein 39	CrGAP, Vilse
ARHGAP40		Rho GTPase activating protein 40	C20orf95, dJ1100H13.4
ARHGAP41	OPHN1	oligophrenin 1	ARHGAP41, MRX60, OPN1
ARHGAP42		Rho GTPase activating protein 42	GRAF3
ARHGAP43	SH3BP1	SH3-domain binding protein 1	ARHGAP43
ARHGAP44		Rho GTPase activating protein 44	NPC-A-10, RICH2
ARHGAP45	HMHA1	histocompatibility (minor) HA-1	ARHGAP45, HA-1, HLA-HA1
ARHGAP46	GMIP	GEM interacting protein	ARHGAP46
ARHGAP47	TAGAP	T-cell activation RhoGTPase activating protein	ARHGAP47, FKSG15, IDDM21, TAGAP1
ARHGAP48	FAM13A	family with sequence similarity 13, member A	ARHGAP48, FAM13A1
ARHGAP49	FAM13B	family with sequence similarity 13, member B	ARHGAP49, C5orf5, FAM13B1, KHCHP, N61

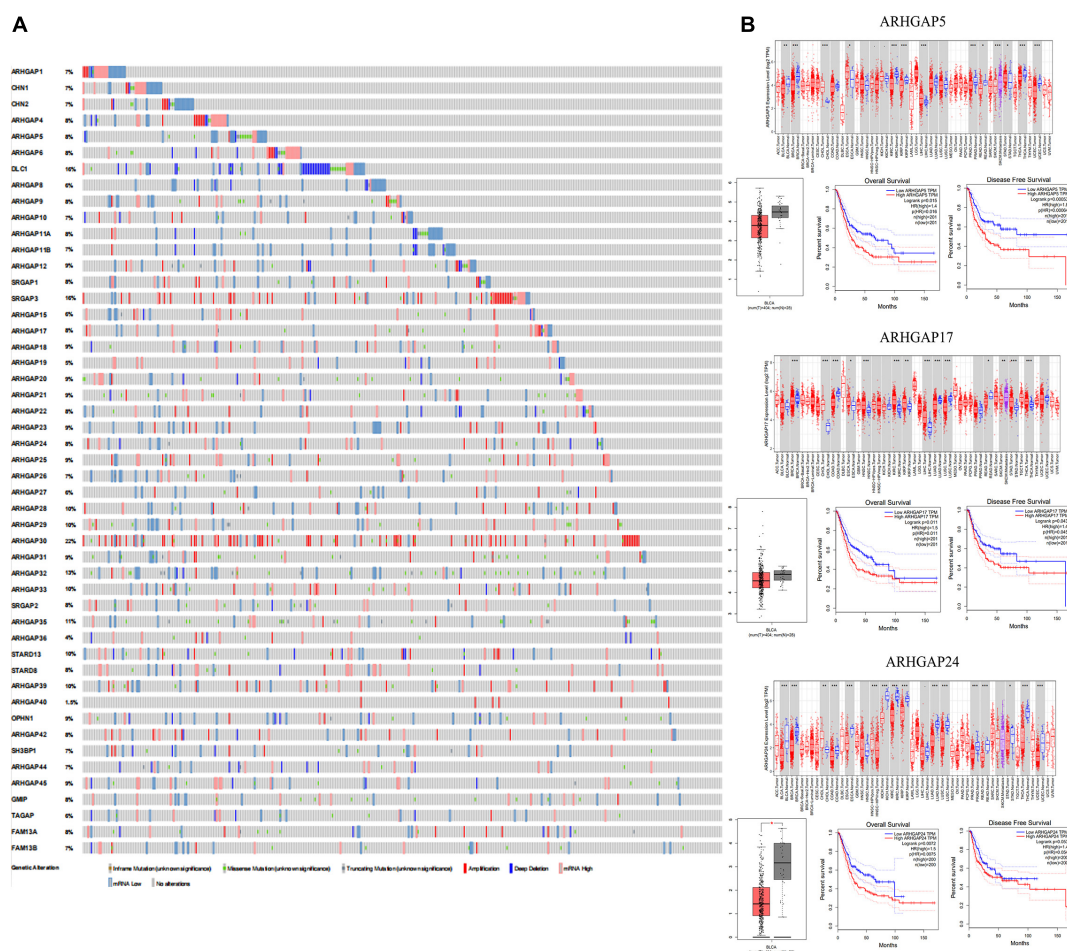


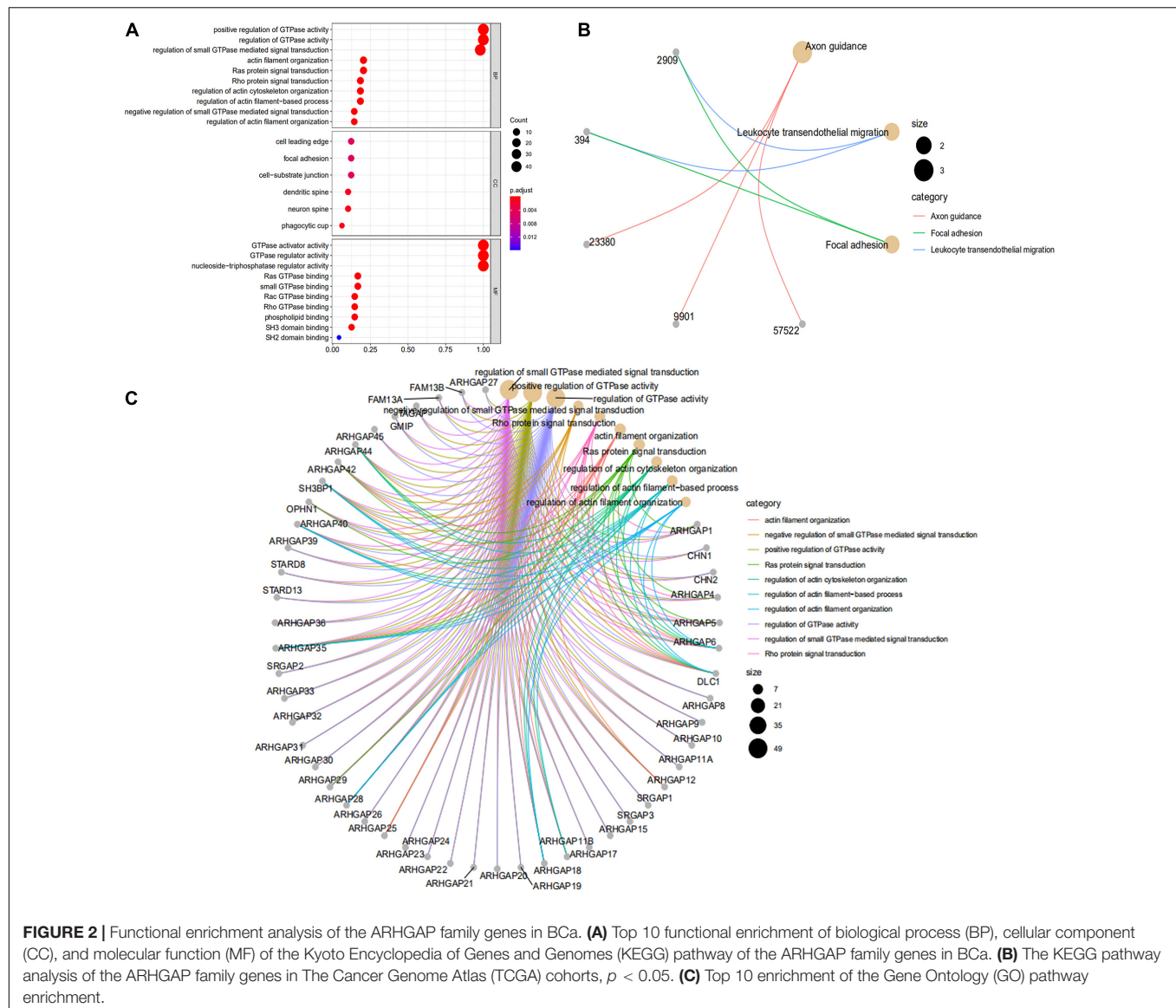
FIGURE 1 | Identification of expression profile and prognosis related to the Rho-GTPase-activating proteins (ARHGAP) family gene in bladder cancer (BCa). **(A)** ARHGAP mutation level in BCa according to the analysis of cBioPortal. **(B)** Expression level of ARHGAP5, ARHGAP17, and ARHGAP24 in several tumor and normal tissues and Expression, OS and DFS of ARHGAP5 in BCa.

and rehydrated in advance with dimethylbenzene and ethanol. Heated sodium citrate buffer (0.01 M, pH = 6) was then applied for the slides for antigen repair. The slides were incubated in normal equine serum for 1 h at 37°C for blocking non-specific binding. The slides were washed and incubated with CD8 (Abcam, ab17147), CD4 (Abcam, ab67001), FOXP3 (Abcam, ab22510), ARHGAP5 (Abcam, ab32328), ARHGAP17 (Abcam, ab229221), and ARHGAP24 (Abcam, ab203874) overnight at 4°C in a wet chamber. The slides were stained with horseradish peroxidase-conjugated secondary antibody for 1 h at room temperature and then developed with DAB and hematoxylin. For the quantification of immunohistochemical staining, three randomized high-power fields of each sample were quantitated for the positive-staining cells, and the mean value was adopted. We quantitated FOXP3+ cells in each whole section since its relatively low infiltration in tumor. The 90 samples of the TMA slides were evenly divided into the ARHGAP family high/low groups according to the median value of ARHGAP5+, ARHGAP17+, and

ARHGAP24+ cells. Then the three cutoff values were applied for the 20 fresh tumor tissues to define the ARHGAP family high/low groups.

Cell Culture and Infection

Bladder transitional cell carcinoma cell lines (RT4, UM-UC-3, T24, 5,637, and J82), immortalized uroepithelium cell line (SV-HUC-1), and human embryonic kidney cells (HEK-293) were received from Shanghai Yuanze Bio-Technology Co. (Shanghai, China). All cells were maintained at 37°C with 5% CO₂ in Dulbecco's modified Eagle's medium (DMEM; Gibco, New York, NY, United States) supplemented with 10% fetal bovine serum (FBS; Gibco, New York, NY, United States). To knock down ARHGAP5, 17, 24, the recombinant plasmid vector or control was purchased from Vigene (Jinan, China). HEK-293T cells were seeded into a 10-cm culture dish 24 h before transfection with PSPAX2 and PMD2G. The medium containing virus particles was collected at 72 h post-transfection. After filtration (0.45-μm filter), the medium was added to T24 and UM-UC-3 for viral



infection with fresh medium replenished 24 h later. After 48 h postinfection, selection was done with 1.0 $\mu\text{g/ml}$ of puromycin (Sangon, China).

Cell Proliferation Assay

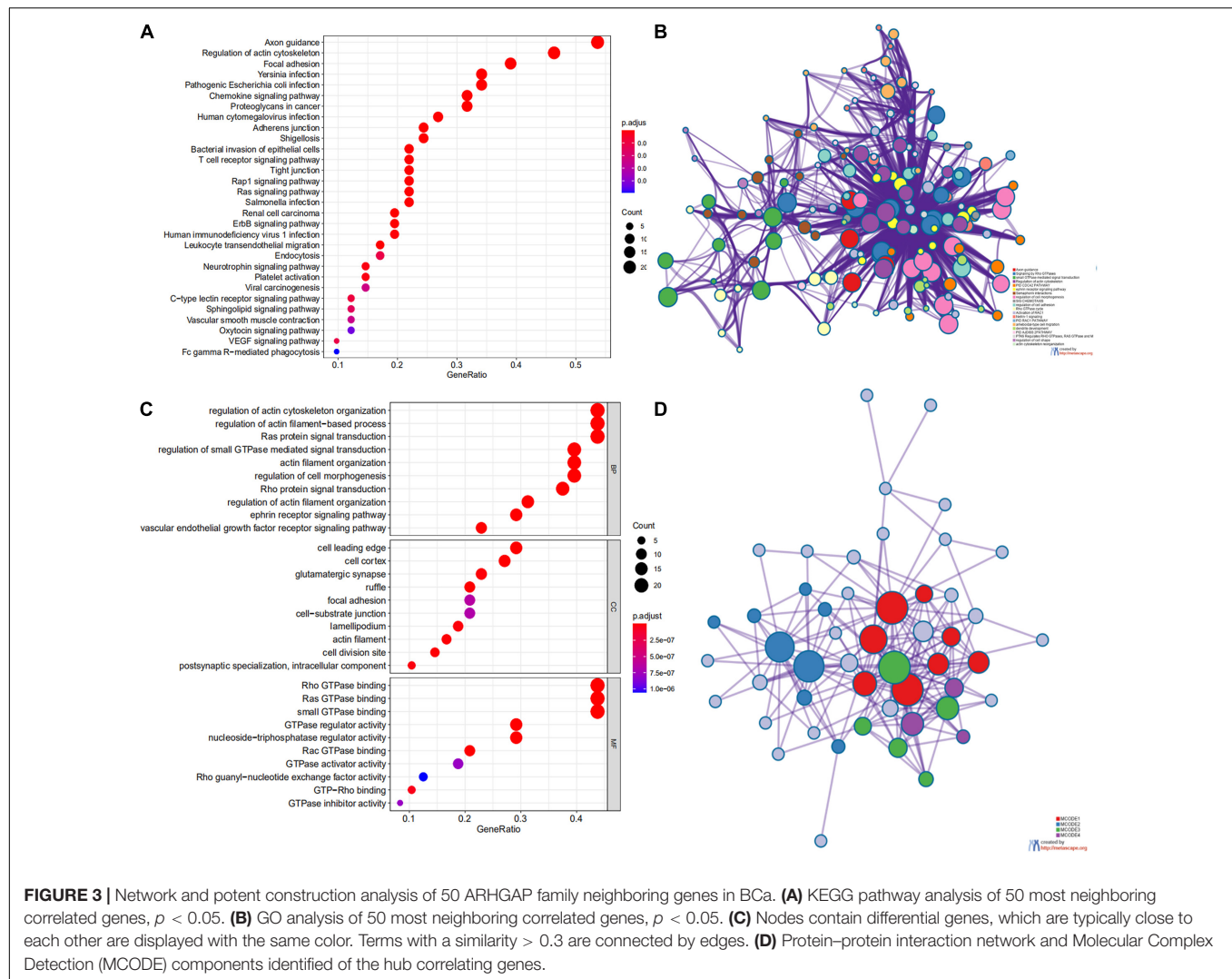
For colony formation assay, cells were seeded into six-well plates at a density of 600 cells per well. After 7–9 days of incubation, cells were fixed with 4% (w/v) paraformaldehyde (PFA) and stained with crystal violet solution.

5-Ethynyl-2'-Deoxyuridine Assay

5-Ethynyl-2'-deoxyuridine (EdU) assay kit (RiboBio, Guangzhou, China) was used to quantitatively investigate cell proliferation through DNA synthesis. A Nikon microscope (Nikon, Tokyo, Japan) was used to measure DNA synthesis reflected by red signals.

Atomic Force Microscopy

The mechanical properties of cells were quantified using a commercial atomic force microscopy (AFM) instrument (BioScope Resolve; Bruker Corporation, Billerica, MA, United States). For characterization, dishes containing cultured primary cells were placed on a stage equipped with a vacuum pump with low noise and drum effects. A PeakForce Quantitative Nanomechanical Mapping—Live Cell probe (Bruker Corporation), with a tip length of 17 μm , tip radius of 65 nm, tip half angle of 18°, and spring constant of 0.076 N/m, was applied to probe the cell surface of the contact model. For characterization, a constant loading force of 1 nN was applied. Deflection images (32 \times 32 pixels) were acquired at a ramp rate of 10 Hz and a ramp area of 5 $\mu\text{m} \times 5 \mu\text{m}$. Automatic gain control was used to improve the feedback for surface tracking. YM and AF signal channels were used to map the cell force. All experiments were completed



within 2 h to ensure cellular health, and the nanomechanical properties were determined from the AFM force map using Nanoscope Analysis software v1.80 (Bruker Nano Surfaces, Goleta, CA, United States).

Transwell Assay

Cell migration was analyzed using Transwell chambers (Corning, New York, NY, United States) in accordance with the manufacturer's protocol. After incubation for 24 h, the cells on the upper surfaces of the Transwell chambers were removed, and the cells located on the lower surfaces were fixed with 4% PFA, followed with crystal violet staining. The stained cells were photographed and counted in five randomly selected fields.

Western Blot Analysis

Lysates from cells and tumor tissues were prepared to determine protein levels using the Bradford assay (Bio-Rad). Proteins were separated by 10% SDS-PAGE and transferred to polyvinylidene difluoride transfer membranes. The blots were blocked with freshly prepared 5% non-fat milk in PBST for 2 h at room

temperature. Then the blots were incubated at 4°C overnight with primary antibodies. After washing with PBST, the blots were incubated with horseradish peroxidase-conjugated (HRP-conjugated) donkey anti-rabbit IgG or sheep anti-mouse IgG (Invitrogen, Shanghai, China) at room temperature for 2 h. ECL substrate (CLiNX, Shanghai, China) was used for detecting HRP-conjugated antibody.

Xenograft Mouse Model and Metastasis Model

Male BALB/c nude mice (5 weeks old) were obtained from SLACOM (Shanghai, China) and used as xenograft hosts. Nude mice were maintained under a specific pathogen-free condition with approval of the Animal Care Committee of Fudan University.

For subcutaneous tumor formation assay, 1×10^7 transfected T24 cells were suspended in 0.2 ml of PBS and subcutaneously injected ($n = 6$ for each group). From day 4 on, tumor size was measured every 5 days by a caliper and was recorded as volume

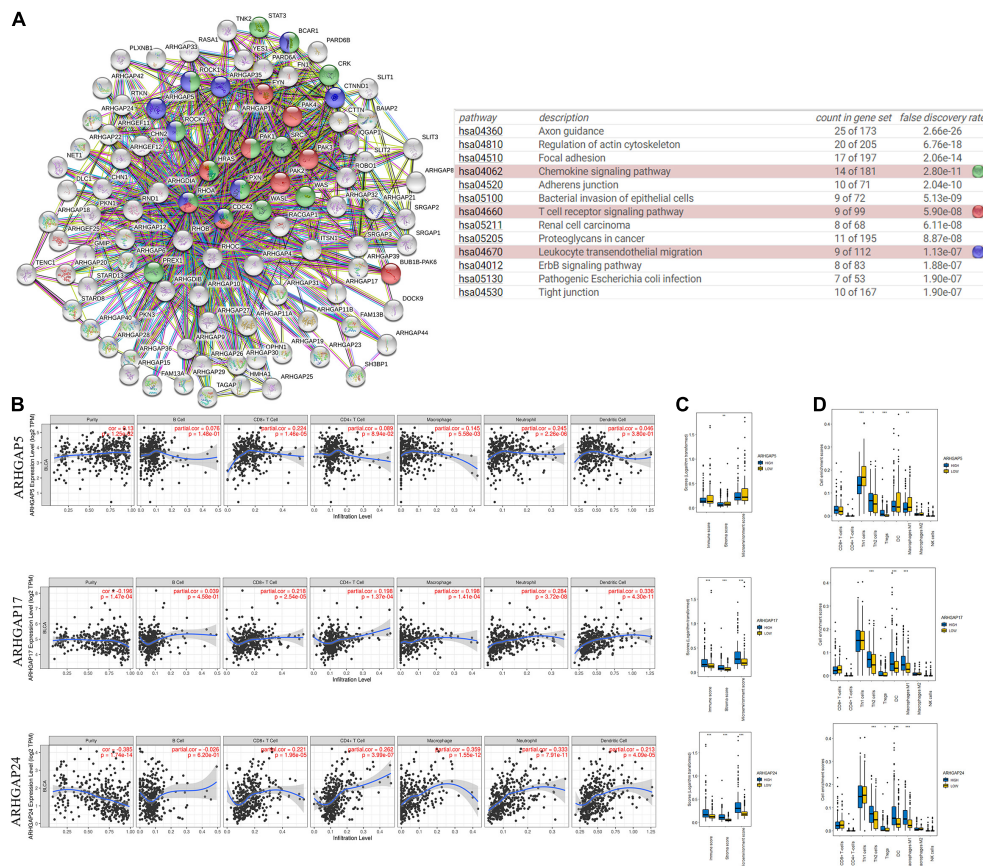


FIGURE 4 | Correlations between prognosis-related ARHGAP family gene-associated immune cell infiltration. **(A)** Immune-related ARHGAP family gene protein-protein interaction (PPI) network was constructed in STRING. **(B)** Immune infiltration correlation with ARHGAP5, ARHGAP17, and ARHGAP24 in TCGA-BCa samples were carried out by TIMER. **(C)** Boxplots were used to visualize ARHGAP family-associated certain cell type enrichment scores and logarithm-transformed immune scores, stroma scores, and microenvironment scores of different groups through xCell-analyzed TCGA samples in BCa. **(D)** ARHGAP family-associated infiltration of CD8+ T cells, CD4+ T cells, type 1 T-helper (Th1) cells, type 2 T-helper (Th2) cells, natural killer (NK) cells, Treg cells, M1 macrophages, M2 macrophages, and dendritic cell were analyzed through xCell-analyzed TCGA samples in BCa. Grouping was done according to the expression level of prognosis-related ARHGAP family gene (* $p < 0.05$; ** $p < 0.01$; *** $p < 0.001$; ns, not statistically significant, Wilcoxon signed rank test).

($1/6 \times \Pi \times L \times W \times H$). The mice were sacrificed for dissection 21 days after injection.

For metastasis analyses, 1×10^5 transfected T24-luc cells were intravenously injected into mice tails ($n = 6$ mice per group). After 28 days, mice were intraperitoneally injected with 150 mg D-luciferin/kg body weight (Beyotime, Shanghai, China), then tumor development was monitored by bioluminescence imaging with the IVIS Spectrum *in vivo* Imaging System and Living Image software (PerkinElmer, Waltham, MA, United States).

Flow Cytometry

Twenty fresh resected bladder cancer tissues were obtained from Huashan Hospital. The flow cytometry procedure is illustrated below. Tumor tissues were digested with 1 mg/ml of collagenase V (Sigma, St. Louis, MO, United States, C9263) and 0.2 mg/ml of DNase I (Sangon Biotech, Shanghai, China, A610099) for 12 h, incubated in RBC lysis buffer for 5 min and then filtered through a 70- μ m strainer to collect single-cell populations. The single cell suspensions

were stained with membrane antibodies including CD45 (BD Biosciences, Franklin Lakes, NJ, United States, 557833), CD3 (BD Biosciences, 552852), CD8 (BD Biosciences, 564526), PD-1 (BD Biosciences, 561272), Tim-3 (BD Bioscience, 565558), and LAG-3 (BD Biosciences, 565616) for 30 min at 4°C after Fc receptor blocking. The single-cell suspensions were then treated with BD Fixation/Permeabilization Solution Kit with BD Golgistop (BD Biosciences, 554715) to stain intracellular proteins including IFN- γ (BD Biosciences, 557643), GZMB (BD Biosciences, 560212), and perforin (BD Biosciences, 556437). Cells were collected and then analyzed on a BD FACSVers Flow Cytometer (BD Biosciences, Franklin Lakes, NJ, United States).

Statistical Analysis

The databases in our research were used for generating survival plots to analyze HR and p -value through log-rank test. Spearman's correlation was used to gauge correlation between particular variables.

TABLE 2 | Correspondence between ARHGAP family gene expression and type of immune infiltration based on immuno-related markers in BCa.

Description	Markers	ARHGAP5				ARHGAP8				ARHGAP11a				ARHGAP17				ARHGAP24				STARD13				STARD8			
		None		Purity		None		Purity		None		Purity		None		Purity		None		Purity		None		Purity		None		Purity	
		Cor	P	Cor	P	Cor	P	Cor	P	Cor	P	Cor	P	Cor	P	Cor	P	Cor	P	Cor	P	Cor	P	Cor	P	Cor	P	Cor	P
B cell	CD19	-0.124	1.23E-02	-0.069	1.86E-01	-0.037	4.58E-01	0.022	6.69E-01	-0.084	8.86E-02	-0.046	3.82E-01	0.248	3.93E-07	0.168	1.25E-03	0.33	8.35E-12	0.178	6.12E-04	0.348	4.61E-13	0.183	4.14E-04	0.435	2.98E-20	0.274	8.94E-08
T cell(general)	CD79A	-0.074	1.38E-01	-0.015	7.80E-01	-0.054	2.75E-01	0.014	7.85E-01	-0.13	8.81E-03	-0.111	3.34E-02	0.188	1.38E-04	0.065	2.11E-01	0.354	1.84E-13	0.182	4.48E-04	0.39	3.11E-16	0.197	1.37E-04	0.471	6.22E-24	0.282	3.53E-08
	CD2	-0.07	8.81E+01	0.088	9.37E-02	-0.193	8.92E-05	-0.137	8.41E-03	0.022	6.52E-01	0.078	1.34E-01	0.248	3.77E-07	0.134	9.90E-03	0.338	2.46E-12	0.133	1.05E-02	0.391	8.84E-18	0.201	1.01E-04	0.485	0.00E+00	0.27	1.49E-07
	CD3D	-0.075	1.31E-01	-0.013	8.05E-01	-0.159	1.23E-03	-0.098	5.92E-02	-0.05	3.11E-01	-0.033	5.31E-01	0.164	8.66E-04	0.031	5.59E-01	0.282	6.63E-09	0.087	9.68E-02	0.345	8.10E-13	0.156	2.71E-03	0.425	2.65E-19	0.206	7.04E-05
CD8+ T cell	CD3E	-0.005	9.20E-01	0.086	1.00E-01	-0.196	6.45E-05	-0.137	8.57E-03	0.007	8.86E-01	0.063	2.29E-01	0.245	5.30E-07	0.121	2.04E-02	0.365	2.87E-14	0.16	2.02E-03	0.418	0.00E+00	0.228	1.02E-05	0.499	0.00E+00	0.277	6.49E-08
	CD8A	0.011	8.21E-01	0.091	7.99E-02	-0.174	4.05E-04	-0.109	3.66E-02	0.15	2.35E-08	0.217	2.58E-05	0.303	4.25E-10	0.214	3.44E-05	0.315	7.70E-11	0.146	5.01E-03	0.354	2.33E-13	0.189	2.69E-04	0.442	0.00E+00	0.246	1.75E-06
	CD8B	0.006	8.97E-01	0.057	2.74E-01	-0.175	3.76E-04	-0.118	2.41E-02	0.118	1.66E-02	0.161	1.92E-03	0.298	8.15E-10	0.234	5.55E-06	0.25	3.00E-07	0.133	1.05E-02	0.283	5.81E-09	0.152	3.45E-03	0.402	2.70E-17	0.275	8.55E-08
Monocyte	CD86	-0.008	8.73E-01	0.084	1.07E-01	-0.302	4.79E-10	-0.267	2.00E-07	0.136	5.96E-03	0.248	1.44E-06	0.344	8.73E-13	0.258	5.35E-07	0.505	8.54E-28	0.355	2.39E-12	0.477	0.00E+00	0.311	1.14E-09	0.562	0.00E+00	0.38	4.04E-14
	CSF1R	-0.011	8.21E-01	0.075	1.52E-01	-0.265	5.22E-08	-0.217	2.57E-05	0.039	4.30E-01	0.11	3.56E-02	0.364	3.34E-14	0.288	1.81E-08	0.533	2.77E-31	0.39	7.73E-15	0.583	0.00E+00	0.462	7.31E-21	0.669	0.00E+00	0.54	3.07E-29
TAM	CCL2	-0.097	5.04E-02	-0.028	5.87E-01	-0.067	1.76E-01	0.013	8.02E-01	-0.009	8.63E-01	0.068	1.96E-01	0.381	1.43E-15	0.31	1.24E-09	0.473	3.89E-24	0.315	6.79E-10	0.526	0.00E+00	0.388	1.20E-14	0.601	0.00E+00	0.445	2.55E-19
	CD68	0.114	2.17E-02	0.17	1.07E-03	-0.419	9.17E-19	-0.392	6.25E-15	0.155	1.72E-03	0.218	2.41E-05	0.185	1.65E-04	0.074	1.55E-01	0.365	2.73E-14	0.232	7.16E-06	0.346	8.28E-13	0.197	1.39E-04	0.421	0.00E+00	0.258	5.19E-07
M1 Macrophage	IL10	-0.064	1.97E+00	-0.004	9.42E-01	-0.137	5.43E-03	-0.06	2.52E-01	0.087	7.82E-02	0.177	6.46E-04	0.362	4.70E-14	0.284	2.81E-08	0.533	2.77E-31	0.39	7.73E-15	0.583	0.00E+00	0.462	7.31E-21	0.669	0.00E+00	0.54	3.07E-29
	INOS(NOS2)	0.132	7.79E-03	0.159	2.16E-03	-0.086	8.12E-02	-0.043	4.06E-01	0.117	1.84E-02	0.151	3.64E-03	0.198	5.59E-05	0.181	4.77E-04	0.224	5.03E-06	0.176	6.94E-04	0.186	1.54E-04	0.157	2.58E-03	0.254	1.97E-07	0.195	1.74E-04
	IRF5	-0.059	2.32E-01	-0.08	1.26E-01	0.273	2.07E-08	0.264	2.72E-07	-0.049	3.25E-01	-0.051	3.25E-01	-0.043	3.83E-01	-0.053	3.14E-01	-0.156	1.56E-03	-0.165	1.47E-03	-0.093	5.99E-02	-0.103	4.73E-02	-0.033	5.06E-01	-0.041	4.33E-01
M2 Macrophage	COX2(PTGS2)	0.258	1.37E-07	0.291	1.37E-08	0.077	1.21E-01	0.116	2.64E-02	0.033	5.09E-01	0.058	2.66E-01	0.098	4.76E-02	0.045	3.90E-01	0.207	2.40E-05	0.149	4.26E-03	0.351	4.11E+13	0.292	1.08E-08	0.125	1.15E-02	0.036	4.86E-01
	CD163	-0.068	1.70E-01	0.006	9.13E-01	-0.229	2.95E-06	-0.169	1.16E-03	0.12	1.55E-02	0.22	2.06E-05	0.385	7.07E-16	0.318	4.13E-10	0.525	2.51E-30	0.38	4.41E-14	0.549	0.00E+00	0.411	2.02E-16	0.677	0.00E+00	0.551	1.36E-30
	VSIG4	-0.065	1.87E-01	0.007	9.00E-01	-0.247	4.58E-07	-0.198	1.32E-04	0.087	8.02E-02	0.175	7.49E-04	0.351	2.96E-13	0.28	4.65E-08	0.52	1.32E-29	0.374	1.12E-13	0.533	0.00E+00	0.396	2.99E-15	0.631	0.00E+00	0.487	2.65E-23
Neutrophils	MS4A4A	-0.072	1.46E-01	0.003	9.52E-01	-0.258	1.31E-07	-0.213	3.67E-05	0.098	4.81E-02	0.199	1.25E-04	0.345	7.74E-13	0.266	2.32E-07	0.545	5.85E-33	0.411	2.13E-16	0.546	0.00E+00	0.416	8.41E-17	0.677	0.00E+00	0.545	7.32E-30
	CD66b(CEACAM8)	0.102	3.93E-02	0.06	2.49E-01	-0.047	3.41E-01	-0.071	1.76E-01	0.091	6.75E-02	0.096	6.51E-02	0.072	1.48E-01	0.081	1.20E-01	0.114	2.17E-02	0.124	1.71E-02	0.057	2.53E-01	0.083	1.13E-01	0.037	4.57E-01	0.049	3.50E-01
	CD11b(ITGAM)	-0.058	2.46E-01	0.007	8.93E-01	-0.164	8.87E-04	-0.088	9.04E-02	0.073	1.39E-01	0.149	4.16E-03	0.395	1.16E-16	0.324	1.86E-10	0.476	1.83E-24	0.327	1.31E-10	0.491	0.00E+00	0.339	2.36E-11	0.618	0.00E+00	0.464	4.76E-21
Natural killer cell	CCR7	-0.184	1.93E-04	-0.146	4.87E-03	0.246	4.70E-07	0.266	2.13E-07	-0.17	5.69E-04	-0.166	1.39E-03	0.005	9.19E-01	-0.046	3.80E-01	0.035	4.78E-01	-0.035	5.07E-01	0.125	1.15E-02	0.031	5.56E-01	0.167	6.98E-04	0.104	4.61E-02
	KIR2DL1	-0.072	1.48E-01	-0.055	2.96E-01	-0.108	2.95E-02	-0.055	2.92E-01	0.068	1.70E-01	0.077	1.39E-01	0.147	3.00E-03	0.063	2.26E-01	0.171	5.36E-04	0.042	4.21E-01	0.153	1.97E-03	0.033	5.30E-01	0.249	3.40E-07	0.108	3.80E-02
	KIR2DL3	-0.049	3.23E-01	0.001	9.87E-01	-0.183	1.99E-04	-0.124	1.73E-02	0.112	2.37E-02	0.137	8.73E-03	0.273	2.15E-08	0.189	2.71E-04	0.198	5.84E-05	0.047	3.65E-01	0.217	9.55E-06	0.078	1.33E-01	0.338	2.44E-12	0.174	7.82E-04
Th1	KIR2DL4	0.038	4.44E-01	0.1	5.46E-02	-0.223	5.67E-06	-0.169	1.13E-03	0.24	9.64E-07	0.295	7.91E-09	0.194	7.68E-05	0.122	1.97E-02	0.225	4.26E-06	0.094	7.19E-02	0.171	5.35E-04	0.033	5.29E-01	0.234	1.81E-06	0.064	2.19E-01
	KIR3DL1	-0.045	3.60E-01	-0.01	8.52E-01	-0.11	2.63E-02	-0.051	3.29E-01	0.043	3.84E-01	0.035	5.05E-01	0.229	3.05E-06	0.173	8.84E-04	0.154	1.78E-03	0.044	4.02E-01	0.21	1.98E-05	0.124	1.74E-02	0.29	2.42E-09	0.191	2.26E-04
	KIR3DL2	-0.046	3.57E-01	-0.009	8.66E-01	-0.125	1.15E-02	-0.068	1.92E-01	0.104	3.51E-02	0.129	1.31E-02	0.143	3.80E-03	0.061	2.46E-01	0.165	8.23E-04	0.028	5.97E-01	0.177	3.25E-04	0.046	3.79E-01	0.263	6.81E-08	0.11	3.42E-02
Dendritic cell	KIR3DL3	0.002	9.69E-01	0.012	8.21E-01	-0.117	1.80E-02	-0.094	7.16E-02	0.121	1.44E-02	0.12	2.10E-02	0.027	5.87E-01	-0.01	8.44E-01	0.044	3.76E-01	-0.01	8.54E-01	0.031	5.26E-01	-0.021	6.94E-01	0.035	4.85E-01	-0.038	4.70E-01
	KIR2DS4	-0.065	1.93E-01	-0.029	5.77E-01	-0.161	1.12E-03	-0.109	3.71E-02	0.13	8.62E-03	0.137	8.29E-03	0.176	3.68E-04	0.094	7.09E-02	0.126	1.08E-02	-0.004	9.39E-01	0.15	2.44E-03	0.032	5.44E-01	0.217	9.83E-06	0.068	1.94E-01
	HLA-DPB1	-0.081	1.01E-01	-0.015	7.70E-01	-0.246	4.62E-07	-0.197	1.38E-04	-0.013	7.93E-01	0.036	4.95E-01	0.306	2.91E-10	0.21	4.81E-05	0.374	5.13E-15	0.177	6.69E-04	0.46	0.00E+00	0.281	4.27E-08	0.556	0.00E+00	0.371	1.80E-13
Th2	HLA-DQB1	-0.011	8.27E-01	0.079	1.29E-01	-0.222	6.15E-06	-0.173	8.41E-04	0.015	7.69E-01	0.063	2.30E-01	0.288	2.98E-09	0.2	1.13E-04	0.33	7.54E-12	0.154	3.07E-03	0.395	1.14E-16	0.231	7.51E-06	0.46	8.45E-23	0.253	8.98E-07
	HLA-DRA	0.022	6.93E-01	0.111	3.33E-02	-0.252	2.51E-07	-0.197	1.42E-04	0.062	2.11E-01	0.067	2.50E-02	0.299	6.93E-10	0.207	6.13E-05	0.351	3.06E-13	0.168	1.22E-02	0.343</							

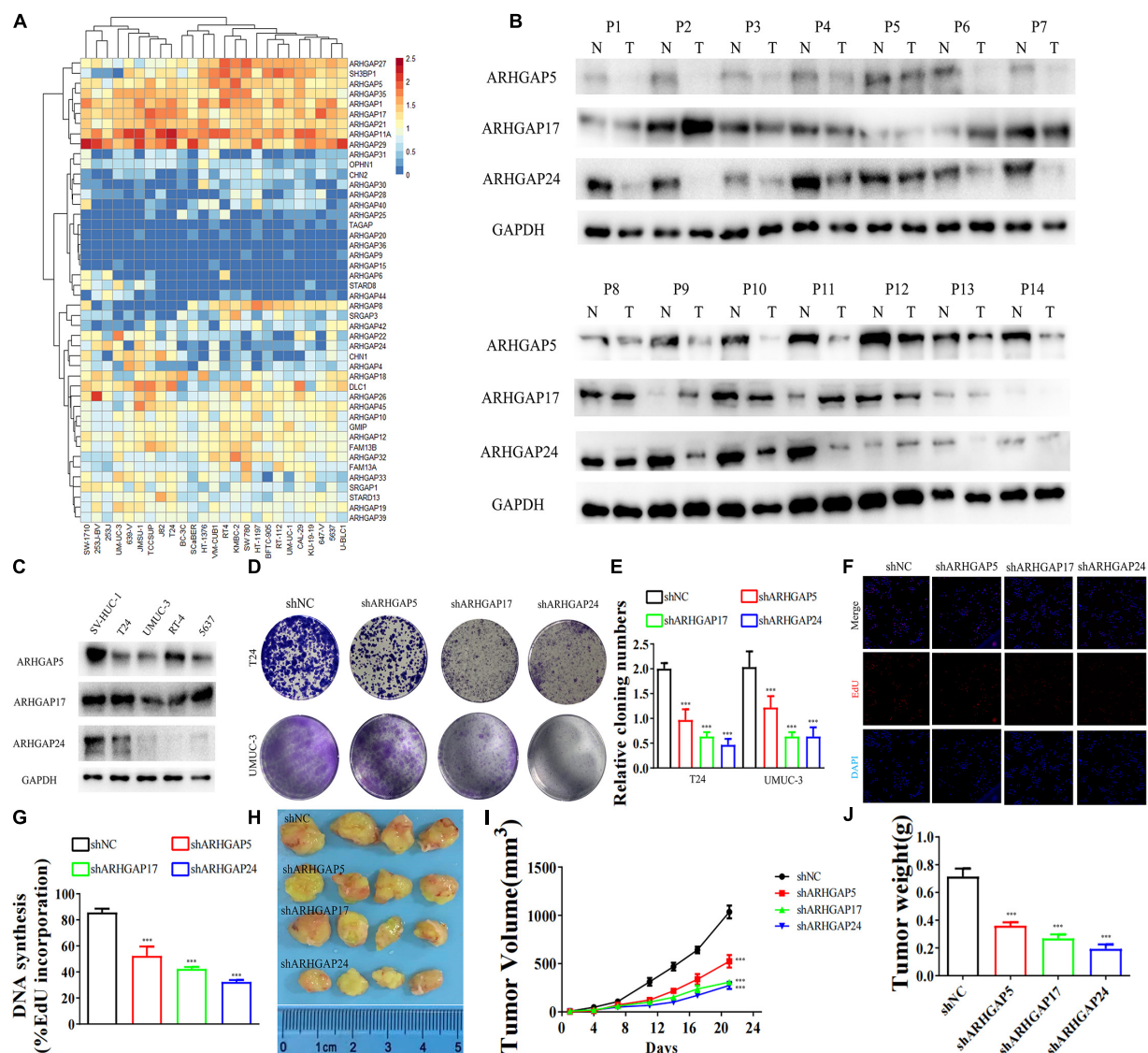


FIGURE 5 | Knockdown of ARHGAP5-, ARHGAP17-, and ARHGAP24-suppressed BC cell proliferation *in vivo* and *in vitro*. **(A)** System analysis of expression of ARHGAP family gene in BCa cancer cell lines in the CCLE database. **(B)** ARHGAP5, ARHGAP17, and ARHGAP24 expression in seven pairs of low-grade BCa and seven pairs of high-grade BCa; GAPDH serves as a loading control. **(C)** ARHGAP5, ARHGAP17, and ARHGAP24 expression in four bladder transitional cell carcinoma cell lines (RT4, UM-UC-3, T24, and 5637) compared with immortalized epithelium cell line (SV-HUC-1). **(D,E)** Cloning formation of T24, UMUC-3, and ARHGAP5, ARHGAP17, and ARHGAP24 knocking down T24, UMUC-3 ($***p < 0.001$ versus shNC). **(F,G)** 5-Ethynyl-2'-deoxyuridine (EdU) assay of T24 and shARHGAP5-, ARHGAP17-, and ARHGAP24-transfected T24 ($***p < 0.001$ versus shNC). **(H)** Tumor growth size of subcutaneous T24 tumors transfected with shNC or shARHGAP5, ARHGAP17, and ARHGAP24 21 days after tumor implantation. **(I)** Tumor growth curve of subcutaneous T24 tumors transfected with shNC or shARHGAP5, ARHGAP17, and ARHGAP24 in 21 days of tumor implantation. **(J)** Average weights of tumors from shNC and shARHGAP5, ARHGAP17, and ARHGAP24 are shown in the histogram. Error bars indicate SD.

RESULTS

Dysregulated Mutation and Expression of Rho-GTPase-Activating Proteins Genes Correlate With RFS and OS in Bladder Cancer Patients

With the discovery and validation of Rho GTPase-activating proteins, we merely included ARHGAP1 to ARHGAP49 in our

work with the summary of subfamily in the ARHGAP family genes (Table 1 and Figure 1A).

Overall, ARHGAP genes harbored a 10% mutation level in BCa according to the analysis of cBioPortal (Figure 1A). The expression of ARHGAP family genes was analyzed in several cancer types in Oncomine, and a relatively lower ARHGAP gene expression was observed in BCa (Supplementary Figure 1A). Moreover, we found that higher expression of ARHGAP mainly predicted unpreferable prognosis in

TABLE 3 | Clinicopathological features in 14 pairs of bladder cancer frozen in liquid nitrogen for analysis of ARHGAP isoforms.

Characteristics	No. (%)
Gender	
Male	10 (71.4)
Female	4 (28.6)
Age	
< 65	9 (64.3)
≥ 65	5 (35.7)
Tumor size	
< 3 cm	6 (42.9)
≥ 3 cm	8 (57.1)
Clinical stage	
Ta-T1	8 (57.1)
T2-T4	6 (42.9)
Grade	
Low	7 (50.0)
High	7 (50.0)
Lymphatic metastasis	
Yes	3 (21.4)
No	11 (78.6)
Muscle invasion	
NMIBC	8 (57.1)
MIBC	6 (42.9)
Total	14

BCa. We further attempted to ascertain the BCa prognosis-related members of ARHGAP family genes and identified that ARHGAP5, ARHGAP8, ARHGAP11A, ARHGAP17, ARHGAP24, ARHGAP37 (STARD13), and ARHGAP38 (STARD8) correlated with either or both RFS and OS in BCa (Figure 1B and Supplementary Figure 1B).

Correlation and Functional Enrichment Analysis Reveals Rho-GTPase-Activating Proteins Family Genes Correlate With Immune-Related Biological Processes in BC Patients

We first identified the correlation of the ARHGAP family genes in BC patients' expression levels. As Supplementary Figure 2A showed, colors in blue or red revealed positive or negative correlation, respectively. For example, ARHGAP37 (STARD13) and coexpression with ARHGAP38 (STARD8), positively correlated with ARHGAP31 and ARHGAP24, meaning these ARHGAP genes may exert a synergism biological effect. Then we explored the coexpression genes of the ARHGAP family genes by GeneMANIA (Supplementary Figure 2B). We also identified 50 relevant altered genes by STRING database and constructed PPI network (Supplementary Figure 2C). GO and KEGG functional enrichment analysis were applied to explore the functional process and novel pathways of the ARHGAP family genes. Figure 2A showed 10 most relevant functional processes of ARHGAP family genes in biological process (BP), cellular component (CC), and molecular function

(MF), respectively, most of which enriched as regulating GTPase activity and downstream actin organization. As shown in Figure 2B, axon guidance, focal adhesion, and leukocyte transendothelial migration were associated with the ARHGAP family genes. Regulation of small GTPase-mediated signal transduction, positive regulation of GTPase activity, regulation of GTPase activity, etc., were the three most according functional processes (Figure 2C). To further distinguish the correlation of reciprocal genes of the ARHGAP family, we applied GO and KEGG analysis of 50 altered neighboring genes identified by STRING (Figures 3A,B). As we expected, focal adhesion, chemokine signaling pathway, and T-cell receptor signaling pathway were enriched. Then the protein-protein interaction enrichment analysis network was constructed by Metascape following the previous manuscript. As shown in Figure 3C, the subsets that contain the close genes of enriched terms have been selected and presented as a network plot. Besides, we applied Molecular Complex Detection (MCODE) algorithm to identify hub genes among the correlating genes. Pathways and functional enrichment analysis were performed by each MCODE component independently. Each three most significant pathways of MCODE are shown in Supplementary Table 1. All results above implied an association between the ARHGAP family genes and tumorigenesis, migration, and tumor-immunologic microenvironment. ARHGAP regulates GTPase-mediated cell cytoskeleton organization including actin or filament-related focal adhesion and cell motility, which is crucial for immune cells, especially tumor-infiltrating cells for transendothelial migration from the bloodstream to participate in the tumor-immunologic microenvironment. As focal adhesion, leukocyte transendothelial migration from the ARHGAP family genes and focal adhesion, the chemokine signaling pathway and T-cell receptor signaling pathway were enriched from the ARHGAP family genes, we made the hypothesis that the ARHGAP genes regulate immune-related tumor microenvironment in BCa (Figure 3D).

Expression of Prognosis-Related Rho-GTPase-Activating Proteins Family Genes Correlated With Immune Cell Infiltration in Bladder Cancer

Ras homolog family member A (RhoA) and CDC42 are key downstream components of ARHGAP correlating with leukocyte transendothelial, chemokine signaling pathway, and T-cell receptor signaling pathway in enriched ARHGAP family genes PPI network, indicating that the ARHGAP family genes are involved in several immune pathways in immune-related tumor microenvironment in BCa (Figure 4A). As such, we next explored the relationship between prognosis-related ARHGAP family gene expression and the degree of immune cell infiltration in BCa using xCell and TIMER to analyze the tissue-infiltrating cell-type abundance from bulk RNA-seq data in TCGA database. First, all prognosis-related ARHGAP family gene correlates with tumor purity (Figure 4B and Supplementary Figure 3A). Interestingly, the ARHGAP family genes correlated with immune cell infiltration in different levels. ARHGAP5 and ARHGAP11A

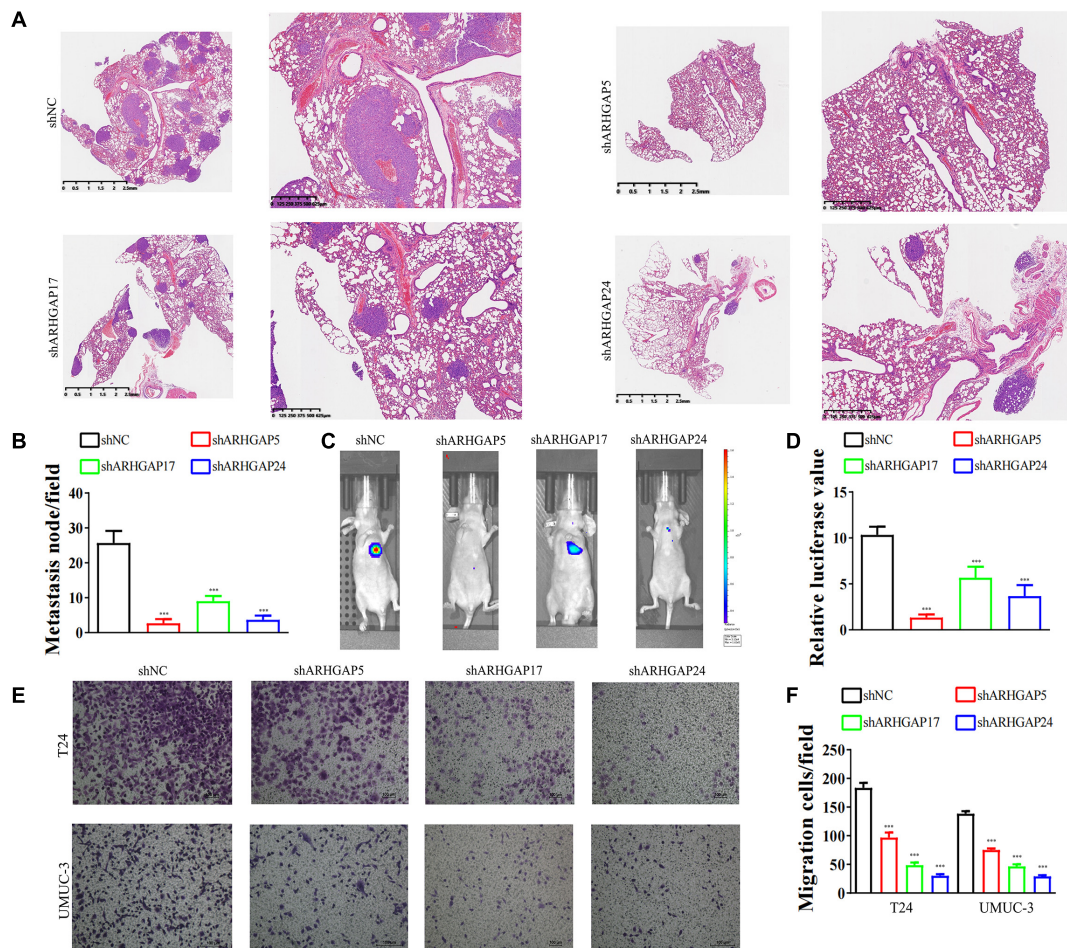


FIGURE 6 | Knockdown of ARHGAP5, ARHGAP17, and ARHGAP24 suppressed the metastasis and migration of BC cell *in vivo* and *in vitro*. **(A,B)** Representative hematoxylin and eosin-stained taken from shNC-T24 and shARHGAP5, ARHGAP17, and ARHGAP24-T24-bearing mice ($***p < 0.001$ versus shNC). **(C,D)** Bioluminescence imaging in mice T24 metastasis model and knockdown ARHGAP5, ARHGAP17, and ARHGAP24 T24 cell metastasis model ($***p < 0.001$ versus shNC). **(E,F)** Transwell assay showed that ARHGAP5, ARHGAP17, and ARHGAP24 knockdown hindered migration of T24 and UM-UC-3 ($***p < 0.001$ versus shNC).

showed no significant correlation with immune infiltration score, while ARHGAP8, ARHGAP17, ARHGAP24, ARHGAP37 (STARD13), and ARHGAP38 (STARD8) significantly correlated with immune infiltration score (Figure 4C and Supplementary Figure 3B). For example, a higher ARHGAP5 correlated with lower Th1/Th2 cell ratio, higher Treg cell, and lower M1 macrophage infiltration, indicating a relatively tumor-promoting microenvironment. A higher ARHGAP8 correlated both with lower Th1/Th2 cell ratio and lower M1 macrophage infiltration, which indicated a tumor-promoting microenvironment and lower DC cell infiltration, which contributed to a tumor suppression microenvironment. Lower Th1/Th2 cell ratio, higher DC cell infiltration, and higher Treg cell infiltration were observed in ARHGAP17, ARHGAP24, and ARHGAP37 (STARD13), indicating a tumor-promoting microenvironment (Figures 4B,D, and Supplementary Figure 3C). We further explored the correspondence between the ARHGAP family gene expression and the type of immune infiltration based on

immuno-related markers in BCa, especially Tfh cells, Th17 cells, and exhausted T cells in addition to our previous analysis. Besides further validation of the infiltration of monocyte, TAM, M1 macrophage, M2 macrophage, neutrophils, NK cell, DC, Th1, and Th2 cell in prognosis-related ARHGAP family genes in BCa, we further found that higher ARHGAP17, ARHGAP24, ARHGAP37 (STARD13), and ARHGAP38 (STARD8) expression positively correlated with T-cell exhaustion markers: PD-1, CTLA4, TIM3, GZMB, and LAG3 (Damo and Joshi, 2019), while ARHGAP5 and ARHGAP8 showed negative or absence of correlation with T-cell exhaustion markers (Table 2). CD8 + T cells exert antitumor activity through regulation of Th1/Th2 cells, Treg cells, DC cells, and macrophages (Xiao et al., 2020) and higher T-cell exhaustion markers indicating a dysfunction state of CD8 + T-cell-related tumor-suppressing microenvironment. In conclusion, through comprehensive analysis of immune cell infiltration in BCa, we identified that the ARHGAP family genes correlate with a tumor-promoting microenvironment.

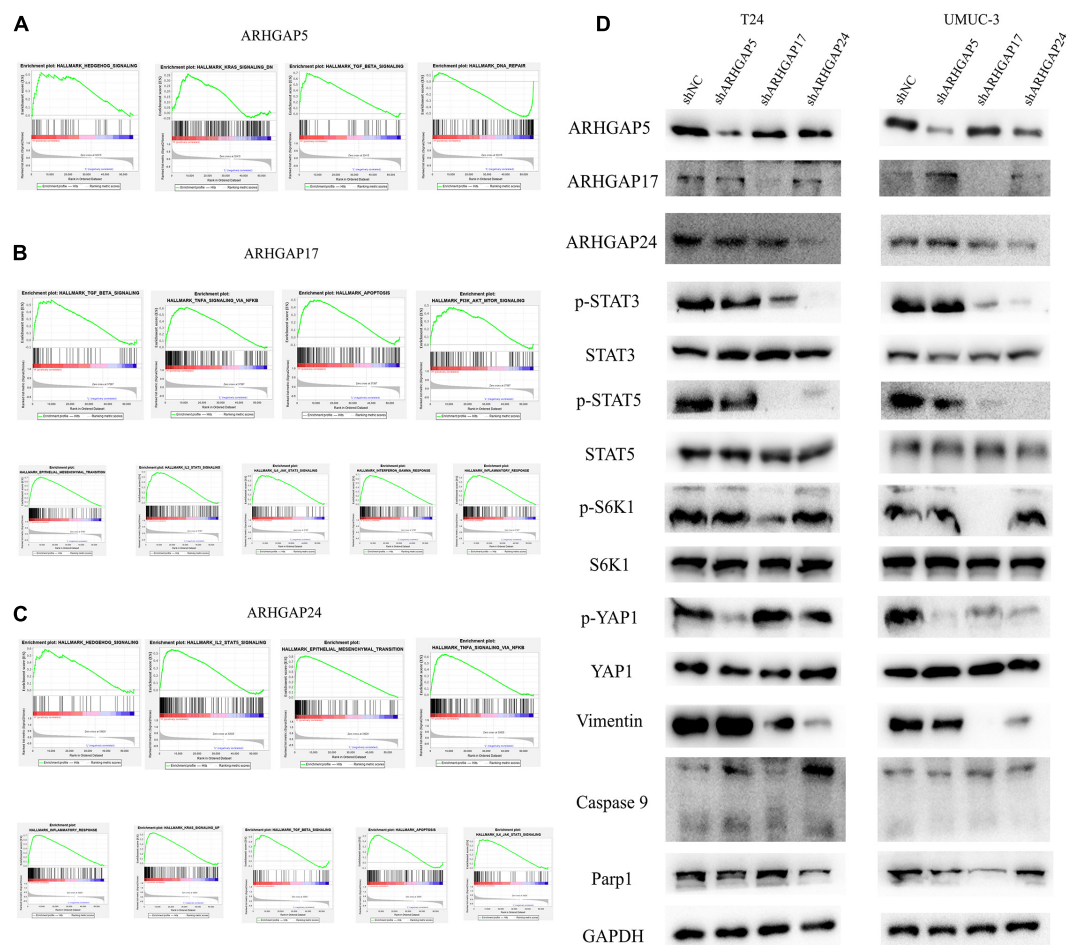


FIGURE 7 | Molecular mechanism of representative ARHGAP family genes in BC biological process. Gene set enrichment analysis (GSEA) plot of **(A)** ARHGAP5, **(B)** ARHGAP17, and **(C)** ARHGAP24, $p < 0.05$. False discovery rate (FDR) < 0.25 . **(D)** Western blot analysis of p-STAT3, STAT3, p-STAT5, STAT5, p-S6K1, S6K1, p-YAP1, YAP1, vimentin, caspase 9, and Parp1 in T24, UMUC-3, and ARHGAP5, ARHGAP17, and ARHGAP24 knocking down T24, UMUC-3.

Knockdown of ARHGAP5, ARHGAP17, and ARHGAP24 Suppressed BC Cell Proliferation, Migration, and Metastasis *in vitro* and *in vivo*

We further began to study the biological role of prognosis-related ARHGAP genes in BCa. Through system analysis of ARHGAP family gene expression in BCa cell lines through CCLE (Barretina et al., 2012; **Figure 5A**), we selected ARHGAP5, ARHGAP17, and ARHGAP24 for further exploration because of their relatively high expression and immuno-related role in BCa. ARHGAP5 and ARHGAP24 were significantly downregulated in BCa cell lines compared with normal SV-HUC-1 cells and BCa tumor compared with adjacent normal tissue, while ARHGAP17 showed no significant difference (**Figures 5B,C** and **Table 3**). We designed three shRNAs targeting ARHGAP5, ARHGAP17, and ARHGAP24, respectively, and the most significant reduction in parental gene expression of shRNA was selected. Cell cloning formation assays showed that knockdown of ARHGAP5, ARHGAP17, and ARHGAP24 significantly

inhibited proliferation of T24 and UM-UC-3 (**Figures 5D,E**). The EdU assay presented similar results based on detecting cellular DNA synthesis (**Figures 5F,G**). T24 cells transfected with scramble shRNA (sh-NC) and shRNA targeting ARHGAP5, ARHGAP17, and ARHGAP24 were injected into nude mice subcutaneously, and knockdown of these genes significantly reduced BC tumor growth (**Figures 5H–J**). To verify the metastasis function of the ARHGAP family *in vivo*, we chose the tail vein injection lung metastasis mouse model. The metastatic foci were significantly visible from mice injected with T24 cells in comparison with sh-T24 cells (**Figure 6A**). Through correspondence with the micropathological results, H&E-stained tissues showed that sh-T24 cells formed up fewer nodule areas in the lungs (**Figures 6A,B**). Bioluminescence imaging revealed that silencing ARHGAP5, ARHGAP17, and ARHGAP24 reduced the metastasis potential of T24 cells (**Figures 6C,D**). Transwell assay suggested that ARHGAP5, ARHGAP17, and ARHGAP24 knockdown inhibited migration of T24 and UM-UC-3 (**Figures 6E,F**). Taken together, our data showed that, in addition to the immuno-related role in BCa,

TABLE 4 | Clinicopathological features in Tissue Microarray of 90 pairs of bladder cancer.

Characteristics	No. (%)
Gender	
Male	81 (90.0)
Female	9 (10.0)
Age	
< 65	56 (62.2)
≥ 65	34 (37.8)
Tumor size	
< 3 cm	38 (42.2)
≥ 3 cm	52 (57.8)
Clinical stage	
Ta-T1	44 (48.9)
T2-T4	46 (51.1)
Grade	
Low	51 (56.7)
High	39 (43.3)
Lymphatic metastasis	
Yes	22 (24.4)
No	68 (75.6)
Muscle invasion	
NMIBC	61 (67.8)
MIBC	29 (32.2)
Total	90

silencing ARHGAP5, ARHGAP17, and ARHGAP24 suppressed BC cell proliferation, migration, and metastasis.

Discovering Underlying Molecular Mechanism of ARHGAP5, ARHGAP17, and ARHGAP24 in Bladder Cancer

We further performed gene set enrichment analysis (GSEA) of ARHGAP5, ARHGAP17, and ARHGAP24 in BCa based on TCGA database to analyze downstream pathway. As for immune-related pathway, ARHGAP5 (Figure 7A and Supplementary Table 2) only correlates with TGF- β signaling, while ARHGAP17 (Figure 7B, Supplementary Table 3) and ARHGAP24 (Figure 7C, Supplementary Table 4) correlate with TGF- β , TNF- α , IL-2/STAT5, IL-6/JAK/STAT3, and the inflammatory response pathway, which, in line with our previous result, showed an immune-related role of ARHGAP17 and ARHGAP24 rather than ARHGAP5 (Figure 4C). Also, we observed that ARHGAP5 correlates with HALLMARK_PI3K_AKT_MTOR_SIGNALING, HALLMARK_KRAS_SIGNALING, and HALLMARK_HEDGEHOG_SIGNALING, while ARHGAP17 correlates with HALLMARK_APOPTOSIS, HALLMARK_EPITHELIAL_MESENCHYMAL_TRANSITION, HALLMARK_PI3K_AKT_MTOR_SIGNALING and HALLMARK_KRAS_SIGNALING, and ARHGAP24 correlates with HALLMARK_KRAS_SIGNALING, HALLMARK_HEDGEHOG_SIGNALING, HALLMARK_EPITHELIAL_MESENCHYMAL_TRANSITION, and HALLMARK_APOPTOSIS. We further validated the key pathway indicator protein *via* particular knocking down of ARHGAP5,

ARHGAP17, and ARHGAP24 in T24 and UMUC-3. Significant downregulation of p-s6k was observed in sh-ARHGAP17-T24 or UMUC-3, not in ARHGAP5 or ARHGAP24 knocking down cells. Inhibition of vimentin was specifically seen after knocking down ARHGAP17 and ARHGAP24, indicating that ARHGAP17 and ARHGAP24 could activate EMT in BCa cells. Activation of YAP was abolished in ARHGAP5 knocking down BCa cells T24 and UMUC-3, while inhibition of YAP was only observed in ARHGAP17, and ARHGAP24 knocked down UMUC-3. No significant cleaved form of PARP1 or caspase 9 was observed in ARHGAP knocked down BCa, indicating little contribution of ARHGAP in cellular apoptosis. Furthermore, significant deficiency of p-STAT3 and p-STAT5 in shARHGAP17 and shARHGAP24 BCa cells were validated according to GSEA enrichment (Figure 7D). GSEA analysis based on TCGA database and validation experiment indicated that ARHGAP5, ARHGAP17, and ARHGAP24, representing the ARHGAP family, showed, to some extent, difference, rather than similarity, in downstream pathway, performing diverse biological activities while serving as the activator of Rho GTPase.

ARHGAP17 and ARHGAP24 Correlated With CD8+ T Cells and Treg Infiltration and T-Cell Exhaustion Markers in Bladder Cancer Microenvironment

We have demonstrated that the ARHGAP family genes correlated with an immuno-related tumor-promoting microenvironment through bioinformatic analysis, and our *in vivo* and *in vitro* experiments validated that ARHGAP5, ARHGAP17, and ARHGAP24 promoted the proliferation, migration, and metastasis phenotype of BCa cells. However, these *in silico* results, which indicated ARHGAP expression, correlating with a tumor-supporting microenvironment, need further validation to elucidate the relative contribution of tumor and leukocyte ARHGAP in BCa. We performed immunohistochemistry staining on 90 tissues of TMA (Table 4) and conducted flow cytometry for the tumor-infiltrating CD8 + T cells to explore the association between ARHGAP family and tumor immune microenvironment. ARHGAP5, ARHGAP17, and ARHGAP24 were detected in bladder cancer tumor sections as well as CD8 + T cells, CD4 + T cells, and Treg cells (Figures 8A,B). We found that decreased CD8 + T cells were infiltrated in ARHGAP17 and ARHGAP24 high groups than the low ones. As in *in silico* analysis, expression of ARHGAP5, ARHGAP17, and ARHGAP24 shows no correlation with CD4 + T-cell infiltration (Figure 8C). Moreover, the Treg cells showed an increased infiltration in the ARHGAP24 high group. The function of CD8 + T cells were detected through flow cytometry (Table 5 and Supplementary Figure 4). Interestingly, less IFN- γ and GZMB were expressed on CD8 + T cells in high vs. low ARHGAP17 and ARHGAP24 groups, and the CD8 + T cells in the high ARHGAP17 group expressed declined perforin, which indicate a dampened antitumor function of CD8 + T cells with high ARHGAP17/24 expression (Figure 8D). Moreover, PD-1 was highly expressed on CD8 + T cells in the high ARHGAP5/17/24 groups, and more CD8 + T cells in the

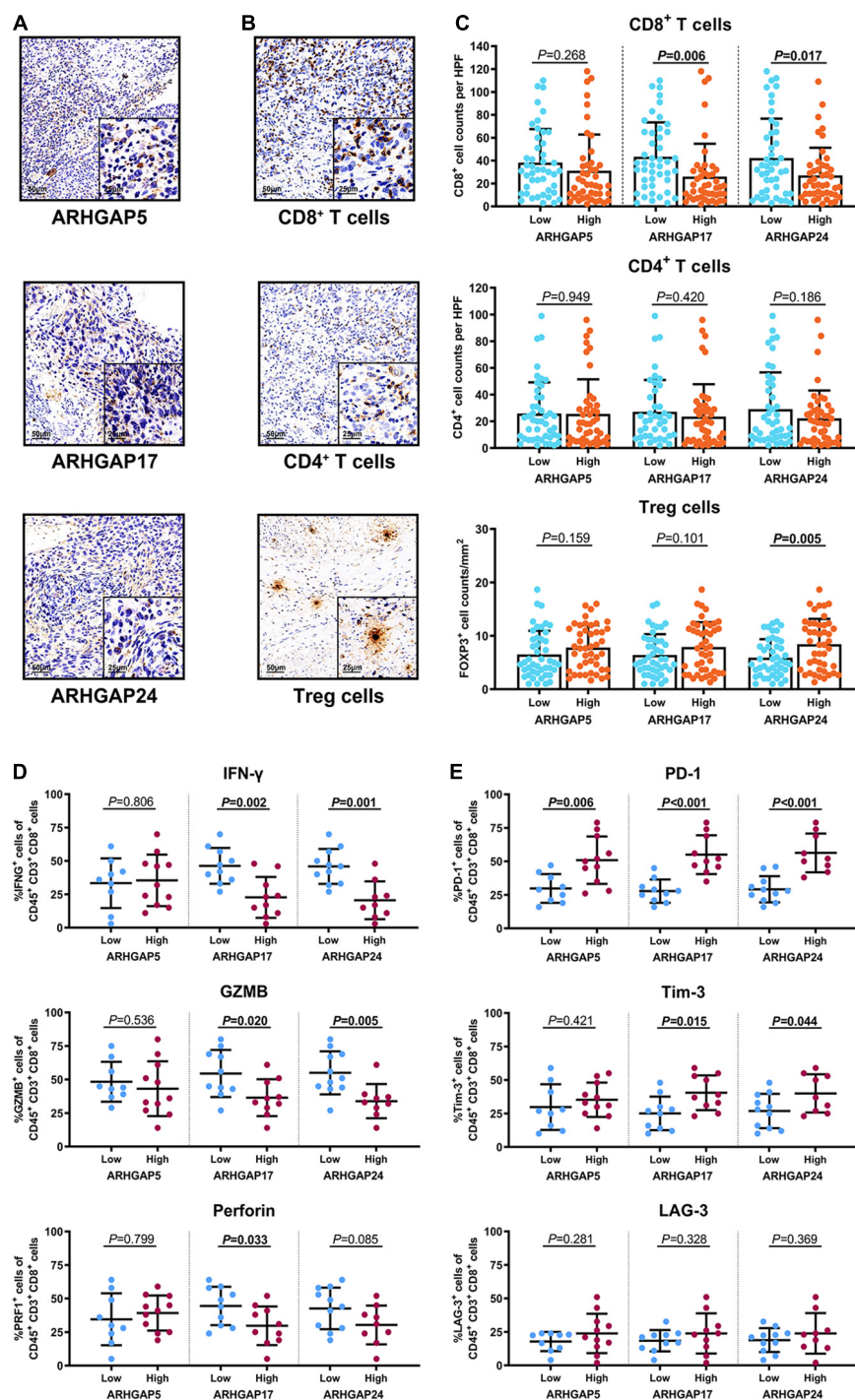


FIGURE 8 | Immunosuppressive tumor microenvironment was associated with ARHGAP family expression. (A,B) Representative immunohistochemistry staining of the ARHGAP family [(A); ARHGAP5, ARHGAP17, and ARHGAP24] and immune cells [(B); CD8⁺ T cells, CD4⁺ T cells, and Treg cells]. (C) Comparison of CD8⁺ T cell, CD4⁺ T cell, and Treg cell infiltration in bladder cancer according to ARHGAP5, ARHGAP17, and ARHGAP24 high/low groups. (D,E) Comparison of effector molecules [(D); IFN-γ, GZMB, and perforin] and immune checkpoint [(E); PD-1, Tim-3, and LAG-3] in bladder cancer according to ARHGAP5, ARHGAP17, and ARHGAP24 high/low groups.

high ARHGAP17/24 groups expressed Tim-3 (Figure 8E). These results demonstrated that ARHGAP17/24 may lead to an immunosuppressive tumor microenvironment and an

impaired antitumor state of CD8⁺ T cells in bladder cancer. Considering that higher T-cell exhaustion markers indicating a CD8⁺ T-cell-related tumor-promoting microenvironment

TABLE 5 | Clinicopathological features of 20 fresh bladder cancer for Flow cytometry analysis.

Characteristics	No. (%)
Gender	
Male	14 (70.0)
Female	6 (20.0)
Age	
< 65	13 (65.0)
≥ 65	7 (35.0)
Tumor size	
< 3 cm	10 (50.0)
≥ 3 cm	10 (50.0)
Clinical stage	
Ta-T1	12 (60.0)
T2-T4	8 (40.0)
Grade	
Low	11 (55.0)
High	9 (45.0)
Lymphatic metastasis	
Yes	4 (20.0)
No	16 (80.0)
Muscle invasion	
NMIBC	12 (60.0)
MIBC	8 (40.0)
Total	20

and CD8 + T cells exert antitumor activity through Treg cell regulation (Xiao et al., 2020), our data demonstrated that ARHGAP17 and ARHGAP24 correlated with CD8 + T cells and Treg cell infiltration and function in BCa microenvironment. We noticed that ARHGAP5 showed less correlation with leukocyte infiltration and function. Interestingly, ARHGAP17 and ARHGAP24 influenced immuno-related IL-2/STAT5 and IL-6/JAK/STAT3 pathways, while ARHGAP5 mainly correlated pathways, which have less interaction with immune related environment. Also, in **Figure 4C**, ARHGAP5 showed no correlation with immuno-microenvironment, while ARHGAP17 and ARHGAP24 correlated with immuno-microenvironment in BCa through xcell analysis. In conclusion, our results indicated that through crosstalk of tumor and leukocyte in BCa, ARHGAP17 and ARHGAP24 correlate with a tumor-promoting microenvironment through regulating CD8 + T cells and Treg infiltration and T cell function.

Rho-GTPase-Activating Proteins Maintain Malignancy-Related Cellular Mechanical Properties of Bladder Cancer

Cell motility, mostly determined by cytoskeleton mediated by ARHGAP-activated Rho GTPase, played a vital role in tumor invasion and metastasis as well as immune cell chemotaxis and infiltration. To further validate ARHGAP-related cell motility, we measured cellular mechanical properties of BCa (Hecht et al., 2012). Generally, cancer cells are typically less “stiff” than normal cells with a trend in a reduced Young’s modulus (YM) value and an increase in adhesive force (AF) *via* AFM

quantifying cellular nanomechanical properties (Plodinec et al., 2012; Chen et al., 2013). Cells with a low YM are more likely to undergo transendothelial migration or translocation into the tissues under bloodstream pressure (Dufrêne and Pelling, 2013; Li et al., 2014). A higher AF contributes to cell adhesion in the microenvironment of targeted tissues (Park and Lee, 2014). Both topography and mechanical properties of T24 and T24-shARHGAP5, ARHGAP17, and ARHGAP24 were measured. T24 cells showed an isotropic well-spread shape, while sh-ARHGAP cells showed a more spindle-like or irregular shape with relative ARHGAP knocking down. As shown in the elastic maps, the cell edge of each cell showed a larger Young’s modulus value than the cell center, which corresponded to the area of cell nucleus. This high Young’s modulus of the cell edge is due to the substrate and is consistent with a previous report (Park and Lee, 2014; Weder et al., 2014; **Figure 9A**). We also measured irregular phalloidin, which indicates dysfunction of cytoskeleton system and reduction in cell motility, in ARHGAP5 and ARHGAP24 knocked down T24 cells. The T24 cells possess the lowest Young’s modulus, the highest adhesive force and cell height, while the T24-shARHGAP cells possess relatively higher Young’s modulus and lower adhesive force and cell height, suggesting that ARHGAP maintained malignancy-related cellular mechanical properties of BCa (**Figure 9B**).

DISCUSSION

Rho-GTPases are GTP-binding cytoskeletal proteins that were thought to construct mechanical support to the cell membrane for preserving biological processes (Kumar and Epstein, 2011). Regulation of Rho-GTPases can be highly related to cancer progression (Li et al., 2020). Rho-GTPase-activating proteins (ARHGAP) serve as negative regulators of Rho-GTPases, and alteration in the genes and transcriptomes of the ARHGAP family can exert a carcinogenesis effect through Rho-like GTPase dysregulation in several cancer types. ARHGAP7 downregulation correlates with unfavorable prognosis in breast cancer patients especially in metastatic lesions (Chen et al., 2019). In contrast, ARHGAP18 upregulation correlates with favorable prognosis in breast cancer (Humphries et al., 2017). ARHGAP15, induced *via* androgen, plays a tumor suppressor role (Takagi et al., 2018). ARHGAP regulates several pathways of cytoskeleton dynamic remodeling and assembling, which may exert an important role in immune cell migration, thus, eventually influencing tumor immune activity and infiltration. However, the role of the ARHGAP family has not been clearly identified in BCa, especially in immune-related BCa microenvironment, which has not been elucidated.

Through integrative analysis of ARHGAP genes in BCa *via* cBioPortal, Oncomine, and Gepia, we found that the ARHGAP family mutates at 10% level in BCa, and a relatively lower ARHGAP gene expression was observed in BCa. ARHGAP5, ARHGAP8, ARHGAP11A, ARHGAP17, ARHGAP24, ARHGAP37 (STARD13), and ARHGAP38 (STARD8) were identified as prognosis-related ARHGAP genes in BCa.

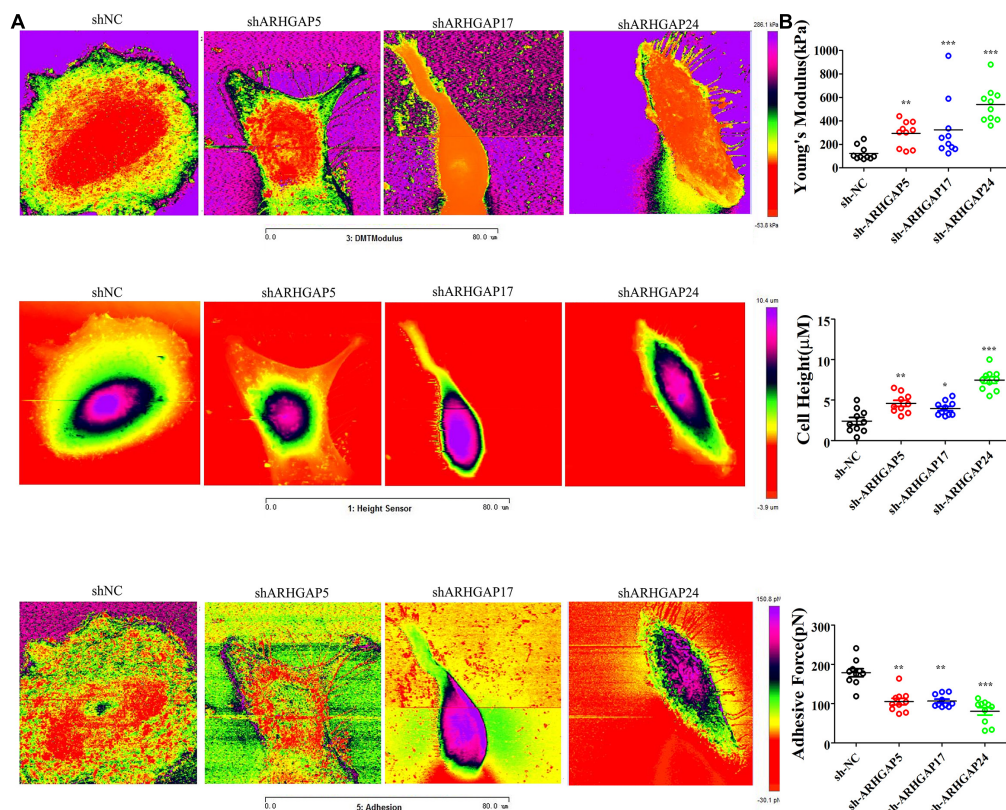


FIGURE 9 | Identification the nanomechanical parameters via knocking down of ARHGAP5, ARHGAP17, and ARHGAP24 in BCa. **(A)** High-magnification images of the distinctive contrast patterns observed for T24 and knocking down ARHGAP5, ARHGAP17, and ARHGAP24 T24 cells. First-row images correspond to Young's modulus (YM) maps. Second-row images correspond to cell height. Third-row images correspond to AF maps. **(B)** All cellular nanomechanical properties were analyzed in GraphPad Prism5 (* $p < 0.05$; ** $p < 0.01$; *** $p < 0.001$; ns, not statistically significant, Wilcoxon signed rank test).

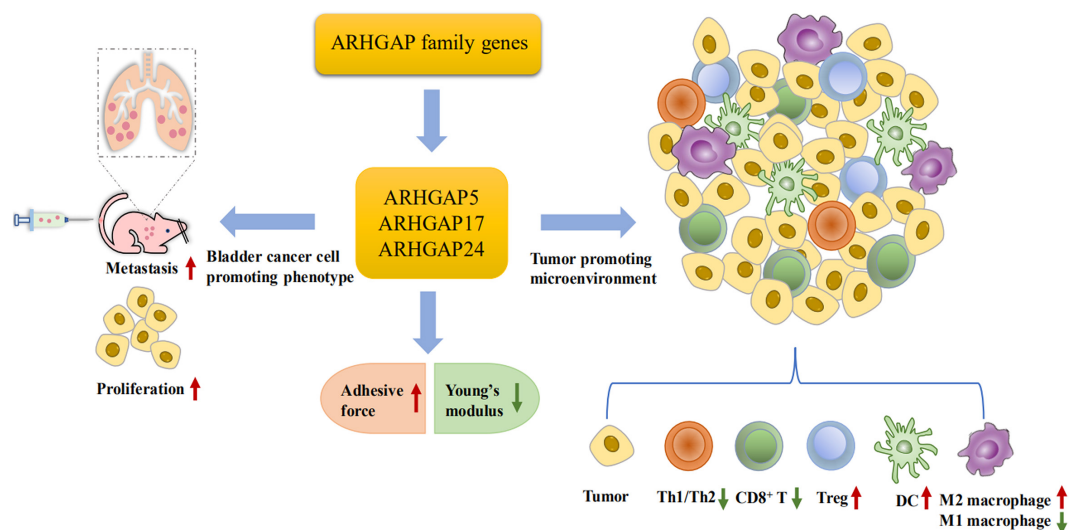


FIGURE 10 | Scheme of ARHGAP family gene promotes BC progressing through establishing a tumor-promoting microenvironment and promotes BC cell proliferation, migration, and metastasis through cellular mechanical property-mediated cell motility.

GeneMANIA, STRING, and MCODE analysis of neighboring and coexpression genes of the ARHGAP family followed by GO and KEGG functional enrichment identified axon guidance, focal adhesion, and leukocyte transendothelial migration to be associated with the ARHGAP family genes, and focal adhesion, chemokine signaling pathway, and T-cell receptor signaling pathways were enriched in ARHGAP coexpression genes. Surprisingly, the ARHGAP family genes and coexpression genes were found to influence several non-cytoskeleton-related pathways including the chemokine signaling pathway and T-cell receptor signaling pathway in the tumor immune microenvironment.

Immune cell infiltration in a cancer-associated immune microenvironment is closely related with prognosis and immunotherapy efficiency in several cancer types. High TILs often relate to a better prognosis than low TILs. Tumor-infiltrating CD4 + T cells, CD8 + T cells, tumor-associated macrophages (TAMs), and neutrophils were associated with patient prognosis and tumor chemosensitivity. We analyzed the correlation between prognosis-related ARHGAP family gene expression and the degree of immune cell infiltration in BCa using xCell and TIMER. Higher ARHGAP5 correlates with lower Th1/Th2 cell ratio, higher Treg cell, and lower M1 macrophage infiltration, which indicates a relative tumor-promoting microenvironment. Lower Th1/Th2 cell ratio, higher DC cell infiltration, and higher Treg cell infiltration were observed in ARHGAP17, ARHGAP24, and ARHGAP37 (STARD13), indicating a tumor-promoting microenvironment. Higher ARHGAP17, ARHGAP24, ARHGAP37 (STARD13), and ARHGAP38 (STARD8) expression positively correlated with T-cell exhaustion markers: PD-1, CTLA4, TIM3, GZMB, and LAG3, while ARHGAP5 and ARHGAP8 shows negative or absence correlation with T-cell exhaustion markers. The CD8 + T cell serves as the most crucial member of the immune-related tumor microenvironment. They mediate tumor cell-specific immune responses through themselves or interaction with other immune cells. High infiltration and low T-cell exhaustion marker of CD8 + T cells predict a higher response to chemotherapy and an overall better prognosis. We also observed a higher DC cell infiltration and a higher Treg cell infiltration in tumor-suppressing ARHGAP microenvironment, which indicates that the ARHGAP family gene is closely linked with tumor DC penetration. DCs increase tumor cell metastasis *via* enhancing Treg cells and suppressing CD8 + T-cell antitumor cytotoxicity. Collectively, we demonstrated that immune cell infiltration in prognosis-related ARHGAP family genes correlates with a tumor-promoting microenvironment.

Furthermore, we validated that silencing ARHGAP5, ARHGAP17, and ARHGAP24 suppressed BC cell proliferation, migration, and metastasis. Immune-related TGF- β , TNF- α , IL-2/STAT5, IL-6/JAK/STAT3, and the inflammatory response pathway and other signal pathways were related in ARHGAP5-, ARHGAP17-, and ARHGAP24-related BC carcinogenesis. Finally, since the different nanomechanical properties between normal and cancerous living cells enable cellular mechanical properties to be efficient markers for grading

malignant-level cancer cells, we validated that T24-shARHGAP cells possess a relatively higher Young's modulus and lower adhesive force and cell height, suggesting that ARHGAP maintains malignancy-related cellular mechanical properties of BCa. We still need to test the nanomechanical properties of immune cell mediated *via* knocking down ARHGAP. Taken together, we found that the ARHGAP family genes promote BC progressing through establishing a tumor-promoting microenvironment and promote BC cell proliferation, migration, and metastasis through cellular mechanical property-mediated cell motility (Figure 10).

DATA AVAILABILITY STATEMENT

The original contributions presented in the study are included in the article/Supplementary Material, further inquiries can be directed to the corresponding author/s.

ETHICS STATEMENT

The animal study was reviewed and approved by Animal Care Committee of Fudan University.

AUTHOR CONTRIBUTIONS

HJ, YC, NL, and ZM were responsible for the conception and design, and study supervision. SW, QZ, and ZZ were responsible for the development of the methodology, analysis, and experiments. XC, YO, CY, CX, and XD performed the statistical and bioinformatic analysis. All authors read and approved the final manuscript.

FUNDING

This work was supported by the National Natural Science Foundation of China (Grant No. 81802569) and Clinical Research and Training Project (SHDC12017X10) provided by Shanghai Shen Kang Hospital Development Center.

SUPPLEMENTARY MATERIAL

The Supplementary Material for this article can be found online at: <https://www.frontiersin.org/articles/10.3389/fcell.2021.657219/full#supplementary-material>

Supplementary Figure 1 | Identification of expression profile and prognosis related ARHGAP family gene in BCa. (A) Expression level of ARHGAP family gene in several tumor and normal tissues in Oncomine. (B) Expression level of ARHGAP8, ARHGAP11A, ARHGAP37, and ARHGAP38 in several tumor and normal tissues and Expression, OS and DFS of ARHGAP8, ARHGAP11A, ARHGAP37, and ARHGAP38 in BCa.

Supplementary Figure 2 | Functional enrichment analysis of ARHGAP family genes in BCa. (A) Correlation analysis of ARHGAP family genes. (B,C) Protein-protein interaction network of ARHGAP family genes and relevant co-expression genes through GeneMANIA and STRING analysis.

Supplementary Figure 3 | Correlations between prognosis related ARHGAP family gene associated immune cell infiltration. **(A)** Immune infiltration correlation with ARHGAP8, ARHGAP11A, ARHGAP37, and ARHGAP38 in TCGA-BCa samples were carried out by TIMER. **(B)** Boxplots were used to visualize ARHGAP family associated certain cell type enrichment scores and logarithm transformed immune scores, stroma scores, microenvironment scores of different groups through xCell analyzed TCGA samples in BCa. **(C)** ARHGAP family associated infiltration of CD8+ T cells, CD4+ T cells, type 1

T helper (Th1) cells, type 2 T helper (Th2) cells, natural killer (NK) cells, Treg cells, M1 macrophages, M2 macrophages and Dendritic cell were analyzed through xCell analyzed TCGA samples in BCa. Grouping was done according to the expression level of prognosis related ARHGAP family gene. (* $p < 0.05$; ** $p < 0.01$; *** $p < 0.001$; ns, not statistically significant, Wilcoxon signed rank test).

Supplementary Figure 4 | Gating strategy for CD8+ T cells.

REFERENCES

- Aran, D., Hu, Z., and Butte, A. J. (2017). xCell: digitally portraying the tissue cellular heterogeneity landscape. *Genome Biol.* 18:220. doi: 10.1186/s13059-017-1349-1
- Barretina, J., Caponigro, G., Stransky, N., Venkatesan, K., Margolin, A. A., Kim, S., et al. (2012). The Cancer Cell Line Encyclopedia enables predictive modelling of anticancer drug sensitivity. *Nature* 483, 603–607. doi: 10.1038/nature11003
- Becht, E., Giraldo, N. A., Germain, C., de Reyniès, A., Laurent-Puig, P., Zucman-Rossi, J., et al. (2016). Immune Contexture, Immunoscore, and Malignant Cell Molecular Subgroups for Prognostic and Theranostic Classifications of Cancers. *Adv. Immunol.* 130, 95–190. doi: 10.1016/bs.ai.2015.12.002
- Cerami, E., Gao, J., Dogrusoz, U., Gross, B. E., Sumer, S. O., Aksoy, B. A., et al. (2012). The cBio cancer genomics portal: an open platform for exploring multidimensional cancer genomics data. *Cancer Discov.* 2, 401–404. doi: 10.1158/2159-8290.cd-12-0095
- Chaffer, C. L., and Weinberg, R. A. (2011). A perspective on cancer cell metastasis. *Science* 331, 1559–1564. doi: 10.1126/science.1203543
- Chen, C.-L., Mahalingam, D., Osmulski, P., Jadhav, R. R., Wang, C.-M., Leach, R. J., et al. (2013). Single-cell analysis of circulating tumor cells identifies cumulative expression patterns of EMT-related genes in metastatic prostate cancer. *Prostate* 73, 813–826. doi: 10.1002/pros.22625
- Chen, D. S., and Mellman, I. (2017). Elements of cancer immunity and the cancer-immune set point. *Nature* 541, 321–330. doi: 10.1038/nature21349
- Chen, W.-X., Lou, M., Cheng, L., Qian, Q., Xu, L.-Y., Sun, L., et al. (2019). Bioinformatics analysis of potential therapeutic targets among ARHGAP genes in breast cancer. *Oncol. Lett.* 18, 6017–6025. doi: 10.3892/ol.2019.10949
- Chen, X., Zhang, J., Ruan, W., Huang, M., Wang, C., Wang, H., et al. (2020). Urine DNA methylation assay enables early detection and recurrence monitoring for bladder cancer. *J. Clin. Invest.* 130, 6278–6289. doi: 10.1172/JCI139597
- Damo, M., and Joshi, N. S. (2019). Treg cell IL-10 and IL-35 exhaust CD8+ T cells in tumors. *Nat. Immunol.* 20, 674–675. doi: 10.1038/s41590-019-0389-y
- Dufrene, Y. F., and Pelling, A. E. (2013). Force nanoscopy of cell mechanics and cell adhesion. *Nanoscale* 5, 4094–4104. doi: 10.1039/c3nr00340j
- Duggan, B., Kelly, J., Keane, P. F., Williamson, K., and Johnston, S. R. (2000). Bcl-2 expression identifies patients with advanced bladder cancer treated by radiotherapy who benefit from neoadjuvant chemotherapy. *BJU Int.* 86:757. doi: 10.1046/j.1464-410x.2000.00895-6.x
- Fridman, W. H., Pagès, F., Sautès-Fridman, C., and Galon, J. (2012). The immune contexture in human tumours: impact on clinical outcome. *Nat. Rev. Cancer* 12, 298–306. doi: 10.1038/nrc3245
- Gen, Y., Yasui, K., Zen, K., Nakajima, T., Tsuji, K., Endo, M., et al. (2009). A novel amplification target, ARHGAP5, promotes cell spreading and migration by negatively regulating RhoA in Huh-7 hepatocellular carcinoma cells. *Cancer Lett.* 275, 27–34. doi: 10.1016/j.canlet.2008.09.036
- Haraguchi, M., Fukushige, T., Kanekura, T., and Ozawa, M. (2019). E-cadherin loss in RMG-1 cells inhibits cell migration and its regulation by Rho GTPases. *Biochem. Biophys. Rep.* 18:100650. doi: 10.1016/j.bbrep.2019.100650
- Hashimoto, K., Ochi, H., Sunamura, S., Kosaka, N., Mabuchi, Y., Fukuda, T., et al. (2018). Cancer-secreted hsa-miR-940 induces an osteoblastic phenotype in the bone metastatic microenvironment via targeting ARHGAP1 and FAM134A. *Proc. Natl. Acad. Sci. U. S. A.* 115, 2204–2209. doi: 10.1073/pnas.1717363115
- Hecht, E., Thompson, K., Frick, M., Wittekindt, O. H., Dietl, P., Mizaikoff, B., et al. (2012). Combined atomic force microscopy-fluorescence microscopy: analyzing exocytosis in alveolar type II cells. *Anal. Chem.* 84, 5716–5722. doi: 10.1021/ac300775j
- Humphries, B., Wang, Z., Li, Y., Jhan, J.-R., Jiang, Y., and Yang, C. (2017). ARHGAP18 Downregulation by miR-200b Suppresses Metastasis of Triple-Negative Breast Cancer by Enhancing Activation of RhoA. *Cancer Res.* 77, 4051–4064. doi: 10.1158/0008-5472.can-16-3141
- Kumar, J., and Epstein, D. L. (2011). Rho GTPase-mediated cytoskeletal organization in Schlemm's canal cells play a critical role in the regulation of aqueous humor outflow facility. *J. Cell Biochem.* 112, 600–606. doi: 10.1002/jcb.22950
- Li, M., Liu, L., Xi, N., and Wang, Y. (2014). Research progress in quantifying the mechanical properties of single living cells using atomic force microscopy. *Chin. Sci. Bull.* 59, 4020–4029. doi: 10.1007/s11434-014-0581-2
- Li, T., Fan, J., Wang, B., Traugh, N., Chen, Q., Liu, J. S., et al. (2017). TIMER: a Web Server for Comprehensive Analysis of Tumor-Infiltrating Immune Cells. *Cancer Res.* 77, e108–e110. doi: 10.1158/0008-5472.CAN-17-0307
- Li, Z., Wang, Q., Peng, S., Yao, K., Chen, J., Tao, Y., et al. (2020). The metastatic promoter DEPDC1B induces epithelial-mesenchymal transition and promotes prostate cancer cell proliferation via Rac1-PAK1 signaling. *Clin. Transl. Med.* 10:e191. doi: 10.1002/ctm2.191
- Luo, N., Guo, J., Chen, L., Yang, W., Qu, X., and Cheng, Z. (2016). ARHGAP10, downregulated in ovarian cancer, suppresses tumorigenicity of ovarian cancer cells. *Cell Death Dis.* 7:e2157. doi: 10.1038/cddis.2015.401
- Nekolla, K., Brieu, N., Gavriel, C. G., Widmaier, M., Budco, A., Medrikova, D., et al. (2019). Prognostic immunoprofiling of muscle invasive bladder cancer (MIBC) patients in a multicentre setting. *Ann. Oncol.* 30, v49–v50. doi: 10.1093/annonc/mdz239.067
- Park, S., and Lee, Y. J. (2014). AFM-based dual nano-mechanical phenotypes for cancer metastasis. *J. Biol. Phys.* 40, 413–419. doi: 10.1007/s10867-014-9353-0
- Plodinec, M., Lopicar, M., Monnier, C. A., Obermann, E. C., Zanetti-Dallenbach, R., Oertle, P., et al. (2012). The nanomechanical signature of breast cancer. *Nat. Nanotechnol.* 7, 757–765.
- Post, A., Pannekoek, W.-J., Ross, S. H., Verlaan, I., Brouwer, P. M., and Bos, J. L. (2013). Rasip1 mediates Rap1 regulation of Rho in endothelial barrier function through ArhGAP29. *Proc. Natl. Acad. Sci. U. S. A.* 110, 11427–11432. doi: 10.1073/pnas.1306595110
- Rhodes, D. R., Yu, J., Shanker, K., Deshpande, N., Varambally, R., Ghosh, D., et al. (2004). ONCOMINE: a Cancer Microarray Database and Integrated Data-Mining Platform. *Neoplasia* 6, 1–6. doi: 10.1016/s1476-5586(04)80047-2
- Robertson, A. G., Kim, J., Al-Ahmadie, H., Bellmunt, J., Guo, G., Cherniack, A. D., et al. (2017). Comprehensive Molecular Characterization of Muscle-Invasive Bladder Cancer. *Cell* 171, 540–556.e25.
- Siegel, R. L., Miller, K. D., and Jemal, A. (2020). Cancer statistics, 2020. *CA Cancer J. Clin.* 70, 7–30. doi: 10.3322/caac.21590
- Smith, A., Nix, J. W., Nielsen, M. E., Wallen, E., and Pruthi, R. (2012). Prospective randomized controlled trial of robotic versus open radical cystectomy for bladder cancer: median 3-year follow-up. *J. Clin. Oncol.* 30:284–284. doi: 10.1200/jco.2012.30.5_suppl.284
- Takagi, K., Miki, Y., Onodera, Y., Ishida, T., Watanabe, M., Sasano, H., et al. (2018). ARHGAP15 in Human Breast Carcinoma: a Potent Tumor Suppressor Regulated by Androgens. *Int. J. Mol. Sci.* 19:804. doi: 10.3390/ijms19030804
- Tang, Z., Li, C., Kang, B., Gao, G., Li, C., and Zhang, Z. (2017). GEPIA: a web server for cancer and normal gene expression profiling and interactive analyses. *Nucleic Acids Res.* 45, W98–W102.
- Wang, J., Qian, J., Hu, Y., Kong, X., Chen, H., Shi, Q., et al. (2014a). ArhGAP30 promotes p53 acetylation and function in colorectal cancer. *Nat. Commun.* 5:4735.
- Wang, J., Tian, X., Han, R., Zhang, X., Wang, X., Shen, H., et al. (2014b). Downregulation of miR-486-5p contributes to tumor progression and metastasis by targeting protumorigenic ARHGAP5 in lung cancer. *Oncogene* 33, 1181–1189. doi: 10.1038/onc.2013.42
- Weder, G., Hendriks-Balk, M. C., Smajda, R., Rimoldi, D., Liley, M., Heinzelmann, H., et al. (2014). Increased plasticity of the stiffness of melanoma cells correlates

- with their acquisition of metastatic properties. *Nanomedicine* 10, 141–148. doi: 10.1016/j.nano.2013.07.007
- Wittekind, C., Asamura, H., and Sobin Leslie, H. (2019). *TNM Atlas*. Hoboken, NJ: Wiley-Blackwell.
- Xiao, Z., Hu, L., Yang, L., Wang, S., Gao, Y., Zhu, Q., et al. (2020). TGF β 2 is a prognostic-related biomarker and correlated with immune infiltrates in gastric cancer. *J. Cell. Mol. Med.* 24, 7151–7162.
- Xie, R., Chen, X., Cheng, L., Huang, M., Zhou, Q., Zhang, J., et al. (2021). NONO Inhibits Lymphatic Metastasis of Bladder Cancer via Alternative Splicing of SETMAR. *Mol. Ther.* 29, 291–307. doi: 10.1016/j.ymthe.2020.08.018

Conflict of Interest: The authors declare that the research was conducted in the absence of any commercial or financial relationships that could be construed as a potential conflict of interest.

Copyright © 2021 Yang, Wu, Mou, Zhou, Zhang, Chen, Ou, Chen, Dai, Xu, Liu and Jiang. This is an open-access article distributed under the terms of the Creative Commons Attribution License (CC BY). The use, distribution or reproduction in other forums is permitted, provided the original author(s) and the copyright owner(s) are credited and that the original publication in this journal is cited, in accordance with accepted academic practice. No use, distribution or reproduction is permitted which does not comply with these terms.



PAK1 Mediates Bone Marrow Stromal Cell-Induced Drug Resistance in Acute Myeloid Leukemia via ERK1/2 Signaling Pathway

Banban Li^{1,2}, Ruinan Jia¹, Wei Li¹, Ying Zhou¹, Dongmei Guo², Qingliang Teng², Shenghong Du^{1,2}, Mingying Li¹, Wēi Li¹, Tao Sun^{1,3}, Daoxin Ma^{1,3}, Min Ji^{1*} and Chunyan Ji¹

¹ Department of Hematology, Qilu Hospital, Cheeloo College of Medicine, Shandong University, Jinan, China, ² Department of Hematology, Taian City Central Hospital, Taian, China, ³ Shandong Key Laboratory of Immunohematology, Qilu Hospital, Shandong University, Jinan, China

OPEN ACCESS

Edited by:

Wei Zhao,
City University of Hong Kong,
Hong Kong

Reviewed by:

Michele Redell,
Baylor College of Medicine,
United States
Bruno Nervi,
Pontificia Universidad Católica
de Chile, Chile

*Correspondence:

Min Ji
jimin@sdu.edu.cn

Specialty section:

This article was submitted to
Molecular and Cellular Oncology,
a section of the journal
Frontiers in Cell and Developmental
Biology

Received: 27 March 2021

Accepted: 03 June 2021

Published: 08 July 2021

Citation:

Li B, Jia R, Li W, Zhou Y, Guo D, Teng Q, Du S, Li M, Li W, Sun T, Ma D, Ji M and Ji C (2021) PAK1 Mediates Bone Marrow Stromal Cell-Induced Drug Resistance in Acute Myeloid Leukemia via ERK1/2 Signaling Pathway. *Front. Cell Dev. Biol.* 9:686695. doi: 10.3389/fcell.2021.686695

Background: Chemoresistance is emerging as a major barrier to successful treatment in acute myeloid leukemia (AML), and bone marrow stromal cells (BMSCs) protect leukemia cells from chemotherapy eventually leading to recurrence. This study was designed to investigate the role of p21-activated kinase 1 (PAK1) in AML progression and chemosensitivity, highlighting the mechanism of stroma-mediated chemoresistance.

Methods: The GEPIA and TCGA datasets were used to analyze the relationship between PAK1 mRNA expression and various clinical parameters of AML patients. Cell proliferation and apoptosis were examined to evaluate the role of PAK1 on chemosensitivity in AML by silencing PAK1 with shRNA or small molecular inhibitor. Human BMSC (HS-5) was utilized to mimic the leukemia bone marrow microenvironment (BMM) *in vitro*, and co-culture model was established to investigate the role of PAK1 in BMSC-mediated drug resistance.

Results: p21-activated kinase 1 high expression was shown to be associated with shorter overall survival in AML patients. The silence of PAK1 could repress cell proliferation, promote apoptosis, and enhance the sensitivity of AML cells to chemotherapeutic agents. More importantly, BMSCs induced PAK1 up-regulation in AML cells, subsequently activating the ERK1/2 signaling pathway. The effect of BMSC-mediated apoptotic-resistance could be partly reversed by knock down of PAK1.

Conclusion: p21-activated kinase 1 is a potential prognostic predictor for AML patients. PAK1 may play a pivotal role in mediating BMM-induced drug resistance, representing a novel therapeutic target in AML.

Keywords: p21-activated kinase 1, acute myeloid leukemia, bone marrow stromal cell, ERK1/2, drug resistance

INTRODUCTION

Acute myeloid leukemia (AML) is a hematological malignancy characterized by proliferation of myeloid precursors with a reduced capacity to differentiate into more mature cellular elements in the bone marrow (BM), and is correlated with genetic and epigenetic alterations. Cytogenetic and molecular genetic abnormalities are responsible for determining the response to chemotherapy and survival outcome (Metzeler et al., 2016; Dohner et al., 2017). Although some improvement during the last decades has been made accompanied by current standard chemotherapy including anthracycline drugs and Cytarabine, the prognosis of AML is generally poor. The drug resistance and recurrence of leukemia are still more difficult issues for current treatment (Dombret and Gardin, 2016; Tallman et al., 2019). Therefore, further identification of drug-resistance relevant genes and signaling pathway provides insights into combinational targeted therapy.

The bone marrow microenvironment (BMM), which consists of soluble factors and supporting tissues, such as bone marrow stromal cells (BMSCs), extracellular matrix (ECM), provides a home for AML cells, and is responsible for disease relapse and treatment resistance (Shafat et al., 2017). BMM plays an important role in leukemia drug resistance by secreting various chemicals and contacting signals (Ayala et al., 2009). Previous studies have shown that many proteins were dramatically up-regulated in BMSC-conditioned AML cell lines, such as Galectin-3, cysteine-rich 61 and autophagy-related E1 ligase 7 (Hu et al., 2015; Long et al., 2015; Piya et al., 2016). However, the mechanisms of BMM-mediated drug resistance have been poorly elucidated.

The p21-activated kinase (PAK) family, belonging to serine/threonine kinases, is classified into group I (PAK1-3) and group II (PAK4-6) based on structural homology and regulatory function (Yao et al., 2020). Recently, the p21-activated kinase 1 (PAK1) has emerged as a potential therapeutic target in cancer, due to its key influence in a variety of oncogenic signaling pathways, including leukemia (Rane and Minden, 2014). Flis et al. (2019) demonstrated that the PAK1 inhibitor combined with BCR-ABL1 tyrosine kinase inhibitor displayed synergistic effect against chronic myeloid leukemia cells. Siekmann et al. (2018) also reported that combined inhibition of PAK1 and receptor tyrosine represented a valuable therapeutic strategy in childhood acute lymphoblastic leukemia (ALL). However, the role of PAK1 in BMSC-mediated drug resistance in AML has not been reported.

In the present study, we characterized PAK1 expression in AML patients using publicly available datasets to determine its association with their clinical and molecular characteristics and clinical outcome. High expression of total and phosphorylated (active) PAK1 in the majority of AML cell lines was observed. Additionally, the inhibition of PAK1 by genetic silencing could enhance the sensitivity of AML cells to chemotherapeutic agents. Moreover, PAK1 was dramatically up-regulated in BMSC-conditioned AML cell lines, accompanied by activation of ERK1/2 signaling. Collectively, our studies support that PAK1 mediates BMM-induced drug resistance via ERK1/2 signaling

pathway in AML, which provides insights for the molecular mechanism of BMM-mediated treatment resistance and targeted or combined treatment.

MATERIALS AND METHODS

TCGA RNA Sequencing and Clinical Data

The publicly available RNA sequencing data of 173 AML patients and complete clinical, molecular and survival data were downloaded from The Cancer Genome Atlas (TCGA) database. This database contains patients with previously untreated AML, all of them had been diagnosed, cytogenetics risk category according to the National Comprehensive Cancer Network (NCCN) guidelines. The RNA-seq and clinical data was analyzed using Gene Expression Profiling Interactive Analysis (GEPIA).

Reagents and Antibodies

Cytarabine (Ara-C), Idarubicin (IDA), and dimethyl sulfoxide (DMSO) were purchased from Actavis (Nerviano, Italy) and Sigma (Merck, Germany), respectively. IPA-3 was obtained from Selleck (Houston, TX, United States). Antibodies of PAK1 and p-PAK1 was purchased from Abcam (MA, Cambridge, United States). GAPDH, ERK1/2, p-ERK1/2, β -actin and PARP, Cleaved-PARP antibodies were obtained from Cell Signaling Technology (Danvers, MA, United States).

AML Cell Lines and Primary Samples

Five human AML cell lines THP1, Kasumi-1, U937, HL60, and KG1, a CML cell line K562, and a T-ALL cell line Jurkat (purchased from the Institute of Hematology and Blood Diseases Hospital, Chinese Academy of Medical Sciences, and Peking Union Medical College, Tianjin, China) were cultured in RPMI 1640 medium containing 10% heat-inactivated fetal calf serum with penicillin and streptomycin (all from Sigma) at 37°C with 5% CO₂ in humidified incubator. The latest authentication of cell lines was conducted by Shanghai Zhong Qiao Xin Zhou Biotechnology Co., Ltd. (August to September, 2019). Bone marrow primary AML samples were collected from patients during routine diagnostic assessments in Qilu Hospital, Shandong University, Jinan, China. Control samples were obtained from healthy donors. Informed consent was obtained in accordance with the Declaration of Helsinki. Mononuclear cells from bone marrow aspirates were separated by Ficoll-Paque Plus (Pharmacia LKB Biotechnology) density gradient centrifugation.

Lentiviral Transduction

The shRNAs against PAK1 in a lentiviral vector with green fluorescent protein, as well as the negative control were designed and synthesized by GeneChem (Shanghai, China). High-titer lentivirus was produced in 293T cells by transfection of the lentiviral expression vector and packaging vectors GV248 using a calcium phosphate cell transfection kit according to the manufacturer's instructions (GeneChem, Shanghai, China). The lentivirus was harvested 48 h later, filtered, enriched using 40% polyethylene glycol, and then used to infect AML cells. After transfection for 72 h, the efficiency was estimated by evaluation of

GFP expression by fluorescence microscopy and flow cytometry. The PAK1 specific shRNA sequence used in our study was 5'-CCAAGAAAGAGCTGATTATTA-3'. We used a flow sorter to sort the transfected cells expressing GFP fluorescence for subsequent experiments.

Cell Viability Assay

Cell viability was determined by Cell Counting Kit-8 (CCK-8). CCK-8 was obtained from BestBio (Shanghai, China). Measurements were taken 24 h after drug exposure at the indicated concentrations. Absorbance was detected at 450/630 nm by a Microplate Reader (Bio-Rad).

Cell Apoptosis Assay

Cell apoptosis was detected using an Annexin V-FITC/PI or Annexin V-FITC/7-AAD double stain apoptosis detection kit (BestBio, Shanghai, China) according to the manufacturer's protocols.

RNA Isolation and Quantitative RT-PCR Analysis

Total RNA was extracted from cells using the TRIzol reagent (Invitrogen, Carlsbad, CA, United States). Reverse transcription was performed with an M-MLV RTase cDNA Synthesis Kit (Takara, Japan). Real-time PCR was performed with the Roche Applied Science LightCycler 480 II Real-Time PCR System using the SYBR Green gene expression assay (Takara, Japan). The following primer sets were used (BioSune, China).

PAK1: 5'-CGCCAGAGCACACAAAATC-3' (forward)
 5'-GTCCCGAGTTGGAGTGACAG-3' (reverse)
 GAPDH: 5'-GCACCGTCAAGGCTGAGAAC-3' (forward)
 5'-TGGTGAAGACGCCAGTGGA-3' (reverse)

Co-culture and Transwell Co-culture Experiments

For co-culture experiments, BMSCs (HS-5 cells) were seeded into 12 or 6-well plates at a density of 1×10^5 /ml overnight. Then, human AML cell lines or primary AML cells were seeded with HS-5 cells for 24 h. Cells were then treated with chemotherapy drugs or inhibitors for 24 h before performing Annexin V apoptosis assays. Co-cultured AML cells were separated from HS-5 monolayer by careful pipetting with ice-cold PBS (repeated twice). After collecting the leukemic cells, HS-5 cells monolayer was observed under microscopy ($\times 100$) to confirm that BMSC monolayer was not damaged and that <10 leukemic cells pervision field remained attached. As a control, AML cells were cultured alone and treated with chemotherapy drugs in parallel. For the transwell co-culture experiments, AML cell lines were plated inside the transwell microporous inserts (0.4 μ m pore size) while underneath the inserts HS-5 cells were seeded into 12 or 6-well plates (ratio of AML cells: stromal cells, 1:1).

Protein Extraction and Western Blot Analysis

Collected cells were lysed in lysis buffer and protease inhibitors. Fifteen to fifty micrograms of protein were separated by 10–12%

sodium dodecyl sulfate-polyacrylamide gel electrophoresis (SDS-PAGE) and electrotransferred onto polyvinylidene fluoride membranes. The membranes were blocked in 5% bovine serum albumin (BSA) at room temperature for 2 h, incubated with primary antibodies overnight at 4°C, and then incubated with a secondary antibody at room temperature for 1 h. Immunoreactive bands were visualized using an infrared imaging system.

Immunofluorescence

The cell lines which were washed with PBS were plated onto cover-slips and fixed with 4% paraformaldehyde solution for 10 min. Permeabilize cells by incubating with 0.1% Triton X-100 for 15 min. All slides were then washed with PBS and blocked with Goat serum at room temperature for 30 min. Cells were incubated with primary antibodies at 4°C overnight in a dark humidity chamber. Washed samples with PBS three times, and then incubated cells with secondary antibodies for 1 h at room temperature. In the dark, dye with DAPI for 10 min. Cells were examined immediately using Evos Fiber Illuminator (Invitrogen, United States) fluorescence microscope.

Statistical Analysis

Statistical analysis were performed using SPSS V20.0. Data were presented as mean \pm standard deviation (SD) from at least three independent experiments. Statistical differences between two groups were evaluated using Student's *t*-test (paired or unpaired, as appropriate), and one-way ANOVA was used to determine the significant differences among multiple groups. Mann-Whitney *U* test was used for cases with unequal variances. Pearson's Chi-square test was used to compare the clinicopathological characteristics between groups. Survival was presented with a Kaplan-Meier survival plot. Spearman correlation test was used to test the correlation between gene expressions. Differences were considered statistically significant at $P < 0.05$.

RESULTS

PAK1 Is Highly Expressed in AML Patients and Cell Lines

The RNA-seq dataset of 173 adult newly diagnosed AML patients and corresponding clinical profiles were obtained from TCGA database. Detailed clinical and molecular characteristics of them are shown in **Table 1**. Using GEPIA, we compared the mRNA expression levels of PAK family members between AML patients ($n = 173$) and normal controls ($n = 70$). The results showed that the expression levels of PAK1 and PAK6 were significantly higher in AML patients than in normal controls ($P < 0.05$, **Figure 1A**). However, the expression levels of other PAK family members, including PAK2, PAK3, and PAK4, were not statistically different between AML patients and normal controls (**Figure 1A**). We further divided AML patients into two groups based on the median expression value of PAK1-6, and the survival of AML patients in different groups were analyzed. The results showed that only PAK1 high expression was associated with poor overall

TABLE 1 | Association of PAK1 expression with clinical characteristics of AML patients.

Characteristics	Overall Cohort (<i>n</i> = 173)		P-Value
	PAK_High	PAK_Low	
	<i>n</i> = 99	<i>n</i> = 74	
Gender (male/female)	58/41	35/39	0.1423
Age: median (range)	61 (18–88)	53 (21–82)	0.0070
Peripheral blast, % median (range)	70 (0–98)	72 (0–100)	0.6416
Bone marrow blast, % median (range)	18 (0–96)	48 (0–98)	0.0020
WBC count (10 ⁹ /L), median (range)	19 (1–224)	14 (1–297)	0.8964
Hemoglobin (g/dL), median (range)	9 (6–13)	10 (6–14)	0.0500
Platelet count (10 ⁹ /L), median (range)	57 (11–351)	37 (8–232)	0.0082
FAB classification (n)			
M0	10	6	0.6544
M1	19	23	0.0712
M2	20	19	0.3940
M3	0	16	<0.0001
M4	32	3	<0.0010
M5	16	2	0.0041
M6	1	1	0.8354
M7	1	2	0.3988
NA	0	2	0.1000
Cytogenetic risk group (n)			<0.0001
Favorable	6	26	<0.0001
Intermediate/normal	67	36	0.0116
Poor	26	10	0.0410
NA	0	2	0.1000
Molecular abnormality			
FLT3 mutation			0.0099
Positive	21	29	
Negative	74	39	
NA	4	6	
IDH1 mutation			0.8678
Positive	17	12	
Negative	80	57	
NA	2	5	
RAS mutation			0.9172
Positive	5	4	
Negative	94	67	
NA	0	3	
NPMc mutation			0.7108
Positive	23	19	
Negative	76	52	
NA	0	3	
Cytogenetic abnormality (n)			
Normal	54	34	0.2630
Complex	17	5	0.0419
Trisomy 8	5	4	0.9172
del (7q)/7q–	5	2	0.4381
Inv. (16)	3	4	0.4328
<i>t</i> (8;21)	1	6	0.0191
<i>t</i> (15;17)	0	11	<0.0010
Others	2	3	0.4295
NA	12	5	0.2409

survival (OS) in AML patients ($P = 0.007$, **Figure 1B**). Moreover, we detected the expression of PAK1 and phosphorylated PAK1 at Ser144 (p-PAK1) in seven leukemia cell lines (THP1, Kasumi-1, U937, HL60, and KG1 are AML cell lines, K562 is a CML cell line, and Jurkat is a T-ALL cell line) by western blot analysis. As illustrated in **Figure 1C**, PAK1 was highly expressed and phosphorylated in the majority of AML cell lines. PAK1 mRNA levels were detected in the bone marrow samples of AML patients ($n = 32$) and control samples (CTR, $n = 8$). PAK1 expression was significantly increased in AML patients compared to control ($P < 0.01$, **Figure 1D**). PAK1 expression was higher in patients with newly diagnosed AML ($n = 20$) and relapsed/refractory AML ($n = 12$) than in patients with complete remission ($n = 9$, $P < 0.05$, **Figure 1E**).

PAK1 High Expression Is Associated With Poor Prognosis of AML Patients

To explore the significance of PAK1 in AML, we first divided AML patients into low and high groups based on PAK1 median expression value. Characteristics of 99 patients with high PAK1 expression and 74 patients with low PAK1 expression were analyzed (**Table 1**). High expression of PAK1 was shown to be closely associated with older age and higher cytogenetic risk. We found that patients in the favorable group had significantly lower PAK1 expression compared with other groups ($P < 0.001$, **Figure 2A**). In addition, patients of M4 and M5 subtypes had relatively higher PAK1 expression, but patients of M3 subtype, which was the best type of AML, had significantly lower PAK1 expression ($P < 0.001$, **Figure 2B**). The significance of PAK1 expression implicated in the prognosis of AML patients with genomic mutations and cytogenetic abnormalities was also analyzed. As shown in **Table 1**, FLT3 mutation was more frequent in patients with low PAK1 expression. However, patients with high PAK1 expression tended to have more complex karyotype ($P = 0.0419$), but less *t* (8;21) and *t* (15;17) cytogenetic abnormalities ($P = 0.0191$, $P < 0.001$). Furthermore, high PAK1 expression was shown to be associated with poorer prognosis in AML patients without FLT3, IDH1, NPMc, or RAS mutation ($P < 0.05$, **Figures 2C–F**). For FLT3 mutation status, there was statistical difference among patients with high or low PAK1 expression ($P = 0.018$). Specifically, patients with FLT3 mutation and high PAK1 expression had the shortest survival time, though this was not statistically different from patients with no FLT3 mutation and high PAK1 expression. COX multi-factor analysis showed that, similar to the age and cytogenetic risk status, PAK1 might be an independent prognostic factor for AML ($P = 0.055$, **Figure 2G**).

PAK1 Suppression Inhibits Cell Growth and Promotes Apoptosis of AML Cells

To explore the functional significance of PAK1 in AML, we firstly downregulated PAK1 expression in THP1 and Kasumi-1 cells by lentivirus with shRNAs that targeted PAK1 (ShPAK1). Transfection efficiency was more than 95% evaluated by fluorescence microscope and flow fluorescence analysis (**Supplementary Figure 1**). RT-qPCR and western blot

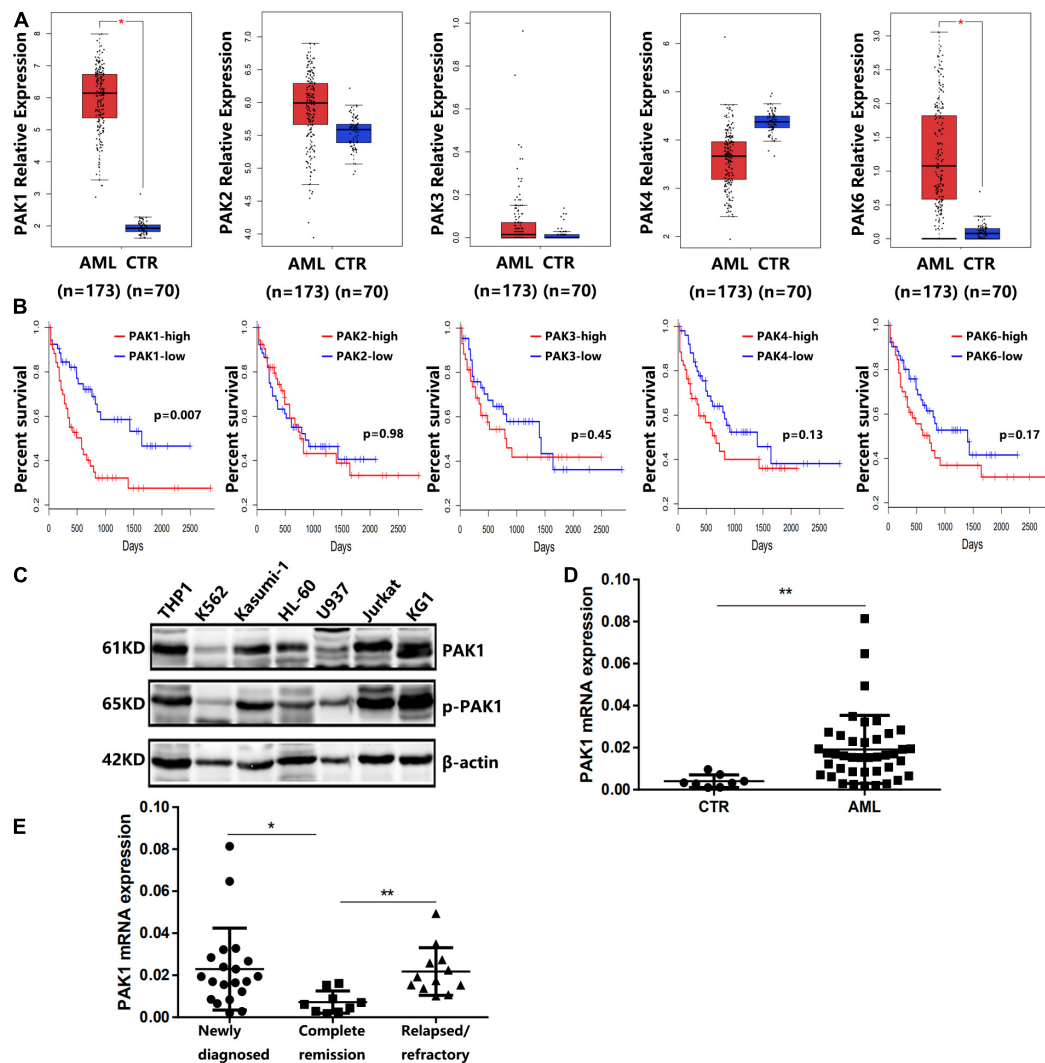


FIGURE 1 | Expression of PAK family members in AML patients and cell lines. **(A)** The expression levels of PAK family members in AML patients ($n = 173$) and normal controls (CTR, $n = 70$) from the TCGA database. **(B)** Overall survival of AML patients from TCGA database. AML patients were divided into low and high groups based on the median expression value of PAK1-6. **(C)** The expression of PAK1 and phosphorylated PAK1 at Ser144 (P-PAK1) in seven leukemia cell lines by western blot analysis. THP1, Kasumi-1, U937, HL60, and KG1 are AML cell lines, K562 is a CML cell line, and Jurkat is a T-ALL cell line. β -actin was used as an internal loading control. **(D)** Quantitative mRNA expression of PAK1 by RT-qPCR in AML patient samples ($n = 32$) and controls (CTR, $n = 8$). **(E)** Quantitative mRNA expression of PAK1 in patients with newly diagnosed AML ($n = 20$), patients with relapsed/refractory AML ($n = 12$) and patients with complete remission ($n = 9$). * $P < 0.05$, ** $P < 0.01$.

showed that PAK1 mRNA and protein levels were significantly downregulated in THP1 and Kasumi-1 cells (Figures 3A,B). We then verified the effects of PAK1 suppression on cell proliferation and apoptosis. The results showed that after PAK1 suppression by shRNA lentivirus, cell growth was inhibited in both THP1 and Kasumi-1 cells, and cell apoptosis was increased (Figures 3C,D).

To better understand the role of PAK1 in AML, a selective non-ATP competitive PAK1 small molecule inhibitor IPA-3 (Rane and Minden, 2014; Yao et al., 2020) was used to suppress PAK1 expression. THP1 and Kasumi-1 cells were treated with IPA-3 (0, 10, and 20 μ M) for 12 and 24 h, respectively. Western blot showed that IPA-3 significantly reduced the expression of p-PAK1 and PAK1 (Figure 3E). Functional assays revealed

that PAK1 silencing by IPA-3 could remarkably suppress cell viability of THP1 cells and increase the apoptosis of THP1 and Kasumi-1 cells (Figures 3E,G). These results suggested that the silence of PAK1 could inhibit cell proliferation and promote apoptosis of AML cells.

PAK1 Suppression Enhances Chemotherapy Drugs Induced Apoptosis of AML Cells

It is well known that resistance to chemotherapy is the main reason for the relapse and refractory of leukemia, which resulted in fast progression of disease. Based on the fact that AML patients

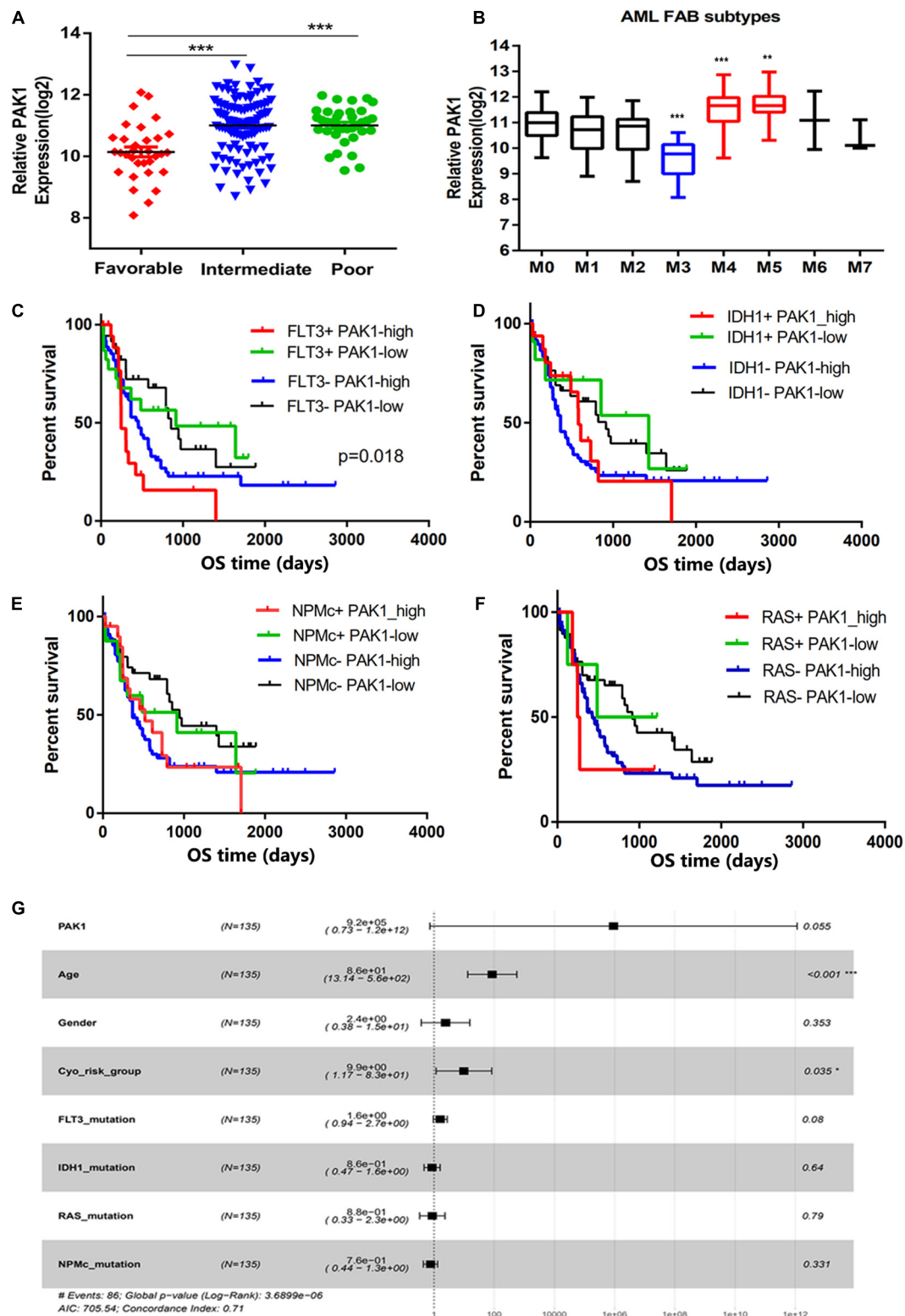


FIGURE 2 | p21-activated kinase 1 (PAK1) high expression is associated with poor prognosis of AML patients. **(A)** The PAK1 expression of AML patients in different cytogenetic risk status from TCGA database. **(B)** The PAK1 relative expression in distinct AML FAB subtypes according to cytomorphological classification. **(C–F)** Significance of PAK1 expression in the prognosis of AML patients with genomic mutations, such as FLT3, IDH1, NPMc, and RAS mutations. AML patients were divided into four groups according to genomic mutation status and PAK1 expression level. **(G)** Forest map of COX multi-factor analysis. * $P < 0.05$, ** $P < 0.01$, *** $P < 0.001$.

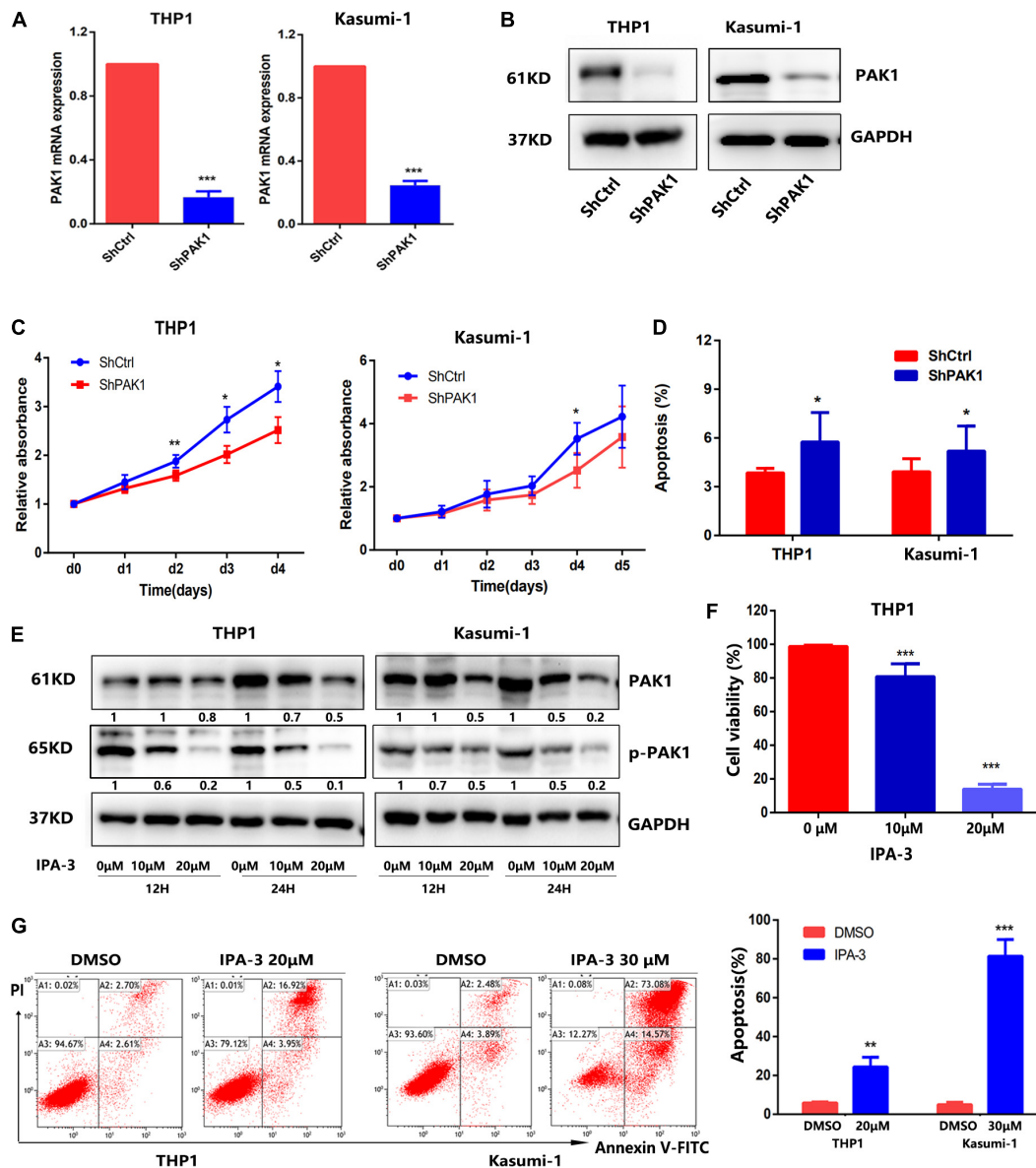


FIGURE 3 | p21-activated kinase 1 (PAK1) suppression inhibits cell growth and promotes apoptosis of AML cells. **(A,B)** THP1 and Kasumi-1 cells were infected with lentiviral particles with specific PAK1 shRNAs (ShPAK1) or scrambled control (ShCtrl) for 48 h. PAK1 mRNA was detected by RT-qPCR **(A)** and the protein of PAK1 was detected by western blot **(B)**. **(C)** After PAK1 suppression, the proliferation of THP1 and Kasumi-1 cells (shPAK1 or shCtrl) was assessed by CCK-8 assays. **(D)** After PAK1 suppression, the apoptosis of THP1 and Kasumi-1 cells (shPAK1 or shCtrl) was detected by flow cytometry. **(E)** THP1 and Kasumi-1 cells were treated with IPA-3 (0, 10, and 20 μM) for 12 and 24 h, respectively. The expression of PAK1 and p-PAK1 was detected by western blot. **(F)** THP1 cells were treated with 10 and 20 μM IPA-3 for 24 h and the cell viability was detected by CCK-8 assay. **(G)** THP1 and Kasumi-1 cells were treated with 20 and 30 μM IPA-3 for 24 h, respectively. Cell apoptosis was evaluated by flow cytometry. All the experiments were repeated for at least three times. * $P < 0.05$, ** $P < 0.01$, *** $P < 0.001$.

with PAK1 overexpression had shorter overall survival, we further explored the effect of PAK1 on drug-induced apoptosis. After PAK1 suppression by lentivirus with shRNA, THP1, and Kasumi-1 cells were treated with different concentrations of Ara-C (THP1: 0, 2, and 4 μM; Kasumi-1: 0, 4, and 8 μM) or IDA (THP1: 0, 10, and 20 μg/L; Kasumi-1: 0, 20, and 40 μg/L) for 24 h, and flow cytometry was performed to determine the apoptosis of AML cells induced by chemotherapy drugs. The results showed that knockdown of PAK1 could markedly increase Ara-C and

IDA induced apoptosis of AML cells in a dose-dependent manner **(Figures 4A–D)**. Our data indicated that downregulation of PAK1 could significantly enhance the sensitivity of AML cells to chemotherapy drugs.

THP1 cells were treated with IPA-3 (10 μM) and Ara-C (1 μM) or IDA (10 μg/L) for 24 h. The cell viability was detected by CCK-8 assay **(Figure 4E)**. Flow cytometry was performed to determine the apoptosis of THP1 cells induced by chemotherapy drugs with or without IPA-3 **(Figure 4F1–2)**. Our data suggest

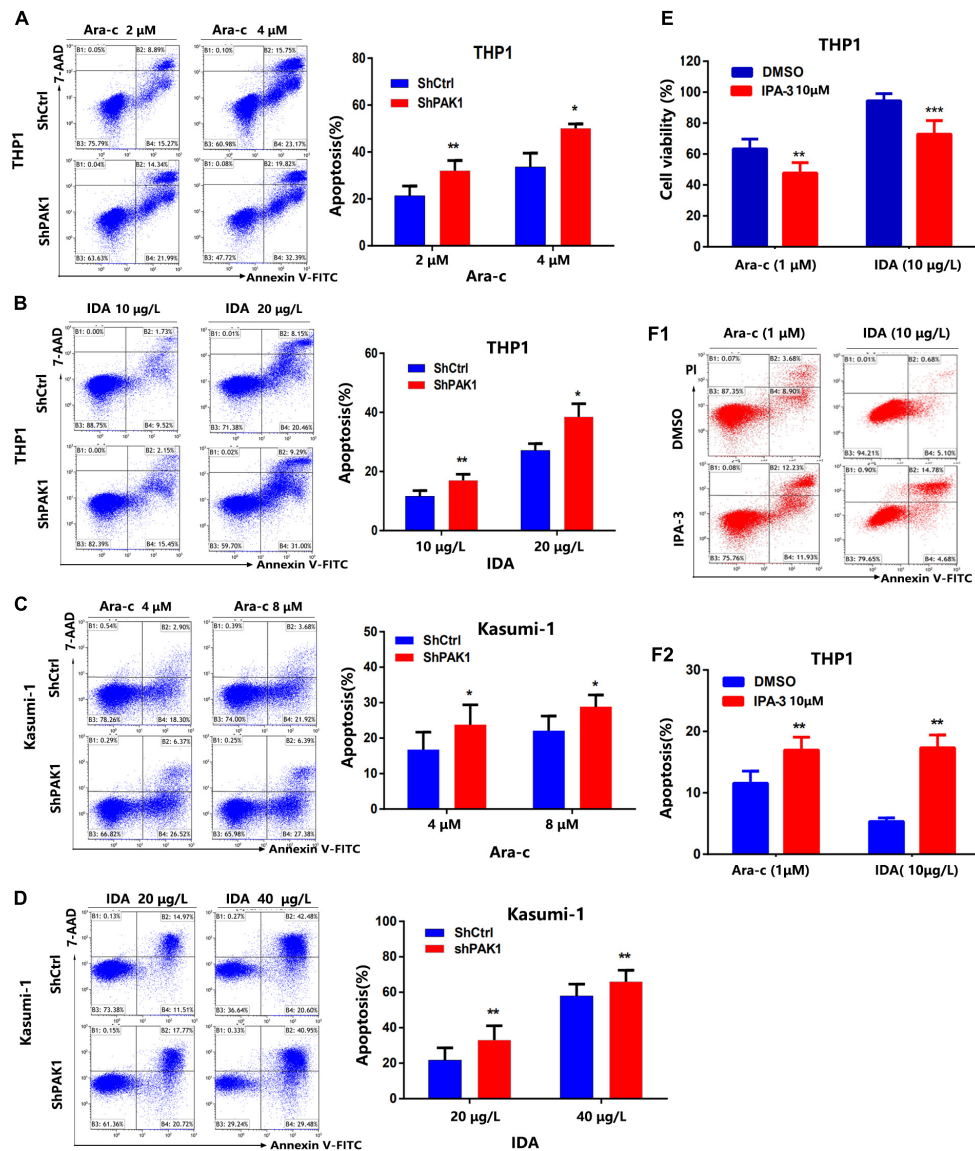


FIGURE 4 | p21-activated kinase 1 (PAK1) suppression enhances chemotherapy drugs induced apoptosis of AML cells. **(A,B)** After PAK1 suppression, THP1 cells (shPAK1 or shCtrl) were treated with different concentrations of Ara-C (0, 2, and 4 μ M) or IDA (0, 10, and 20 μ g/L) for 24 h, and flow cytometry was performed to determine the apoptosis of AML cells induced by chemotherapy drugs. **(C,D)** After PAK1 suppression, Kasumi-1 cells (shPAK1 or shCtrl) were treated with different concentrations of Ara-C (0, 4, and 8 μ M) or IDA (0, 20, and 40 μ g/L) for 24 h, and flow cytometry was performed to determine the apoptosis of AML cells induced by chemotherapy drugs. **(E)** THP1 cells were treated with 10 μ M IPA-3 and Ara-C (1 μ M) or IDA (10 μ g/L) for 24 h. The cell viability was detected by CCK-8 assay. **(F1,F2)** THP1 cells were treated with IPA-3 (10 μ M) and Ara-C (1 μ M) or IDA (10 μ g/L) for 24 h. Flow cytometry was performed to determine the apoptosis of THP1 cells induced by chemotherapy drugs. All the experiments were repeated for three times. * $P < 0.05$, ** $P < 0.01$, *** $P < 0.001$.

that the PAK1 small molecule inhibitor IPA-3 combined with traditional chemotherapy drugs could significantly increase the inhibition rate and apoptosis rate of AML cells.

PAK1 Plays a Critical Role in Stroma-Mediated Protection of AML Cells

Accumulating evidence indicates that the interaction between hematological malignancies and BMM plays an important role

in drug resistance by secreting various chemicals and contacting signals (Mendez-Ferrer et al., 2020). Among the components of the BMM, bone marrow-derived mesenchymal stem cells (BMSCs) are the most important factor, which is involved in tumor survival and drug resistance (Ridge et al., 2017). In this study, we found that the expression of PAK1 in AML cells were significantly increased when AML cells were co-cultured with BMSCs directly or indirectly. As shown in **Figure 5A**, primary AML cells and AML cell lines (THP1, Kasumi-1, and KG1) were cultured with BMSCs HS-5 in a direct contact co-culture

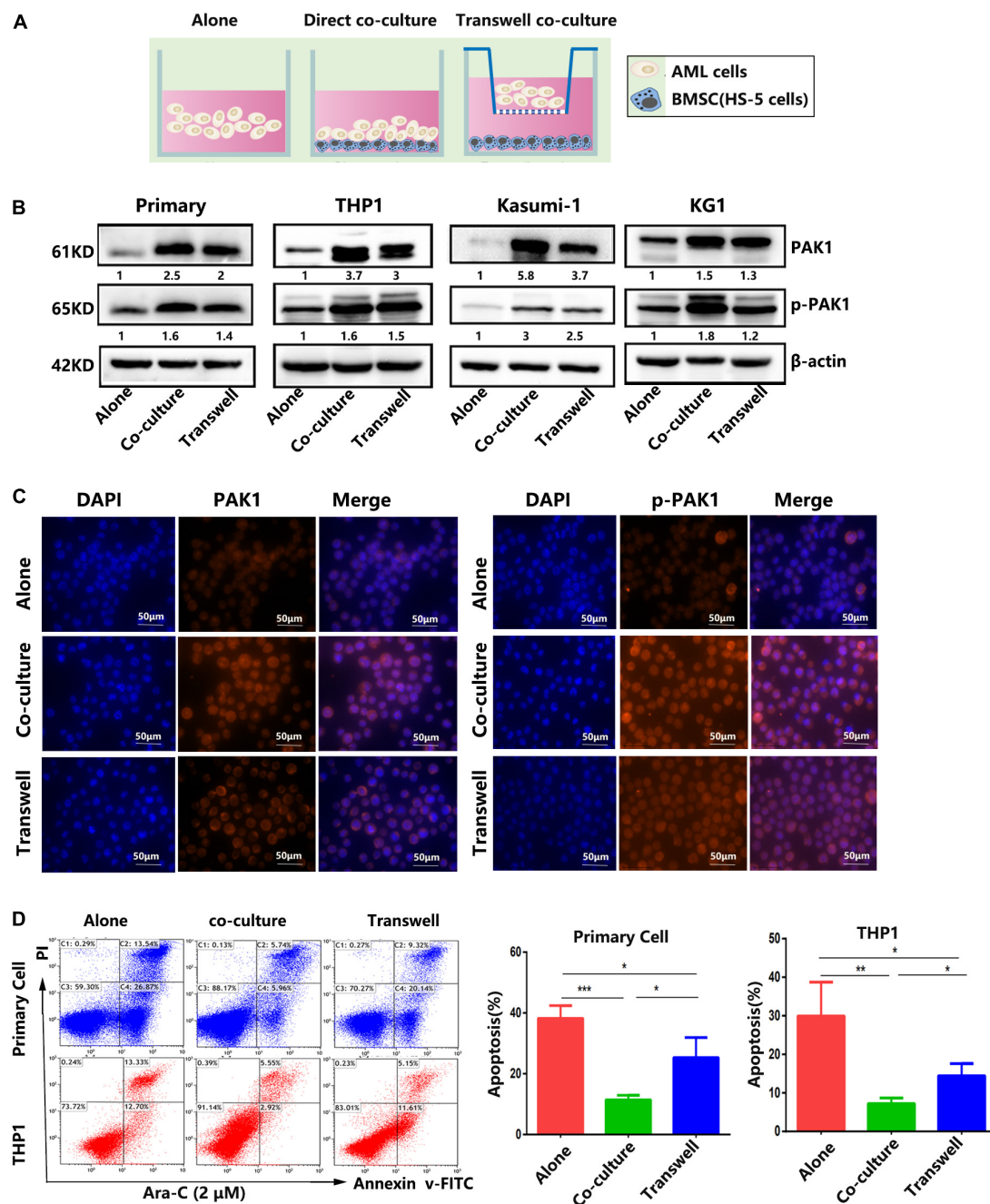


FIGURE 5 | Bone marrow stromal cells confer resistance to Ara-C-induced apoptosis in AML cell lines and primary AML cells. **(A)** AML cells were cultured alone or with bone marrow stromal cells HS-5 (1:1) in a direct contact co-culture system (co-culture) or an indirect transwell co-culture system (transwell). **(B)** Primary AML cells and AML cell lines (THP1, Kasumi-1, and KG1) were cultured alone or with HS-5 for 24 h. Western blot was performed to evaluate the expression levels of PAK1 and p-PAK1 in AML cells. **(C)** THP-1 cells were cultured alone or co-cultured with HS-5 cells for 24 h, and immunofluorescence was utilized to analyze the expression of PAK1 and p-PAK1 protein. Representative images of nucleus, PAK1/p-PAK1 staining and merged images of nucleus and PAK1/p-PAK1 were shown. **(D)** Primary AML cells and THP1 cells were cultured alone or with HS-5 overnight, and then AML cells were treated with 2 μ M Ara-C for 24 h. Flow cytometry was performed to analyze the apoptotic rate. All the experiments were repeated for three times. * P < 0.05, ** P < 0.01, *** P < 0.001.

system or an indirect transwell co-culture system. Western blot showed that PAK1 as well as phosphorylated PAK1 (p-PAK1) of AML cells were overexpressed in co-culture systems compared with AML cell culture alone (Figure 5B). Immunofluorescence

analysis also verified that the fluorescent expression of PAK and p-PAK1 was enhanced when AML cells were co-cultured with BMSCs (Figure 5C). Moreover, the expression levels of PAK1 and p-PAK1 seemed to be even higher in the direct co-culture system

than in the indirect transwell system. Meanwhile, the apoptosis of AML cells induced by Ara-C was significantly inhibited in both co-culture systems compared with AML cell culture alone (Figure 5D). And the apoptotic rate of AML cells was even lower in the direct co-culture system than in the indirect transwell system, which was oppositely consistent with PAK1 expression (Figure 5D). Our results indicate that PAK1 may exert a significant role in BMSC mediated drug resistance in AML cells.

PAK1 Suppression Reverses the Stroma-Induced Drug Resistance in AML Cells

To further elucidate whether the stroma-induced drug resistance of AML cells is due to the activation of PAK1, THP1 and Kasumi-1 cells were transfected with PAK1 shRNAs and then co-cultured with HS-5 cells. After exposure to Ara-C (2 μ M) for 24 h, cell apoptosis of co-cultured cells was examined by flow cytometry. As shown in Figures 6A,B, after knockdown of PAK1 by shRNAs, the apoptosis of co-cultured AML cells induced by Ara-C was dramatically increased. Moreover, the same results were also observed in the co-cultured THP1 cells after cells were treated with PAK small molecule inhibitor IPA-3 (20 μ M) (Figure 6C). These findings suggested that PAK1 played an important role in the protection of BMSCs against AML cells. Inhibition of PAK1 could attenuate the protective effect of BMSCs on AML cells and increase the sensitivity of AML cells to chemotherapeutic agents.

PAK1 Promotes AML Chemoresistance by Activating the ERK Signaling Pathway

We subsequently tried to figure out the mechanism of PAK1 in AML chemoresistance. Previous studies showed that PAK1 was innately associated with ERK pathway in various tumors, such as melanoma, breast cancer, malignant peripheral nerve sheath tumors and Non-small cell lung cancer (Ong et al., 2013; Semenova et al., 2017; Kanumuri et al., 2020; Song et al., 2021). But there is no report on whether ERK signaling pathway is activated in AML. Accordingly, we further explored the regulation of PAK1 on ERK signaling pathway in AML cells. We used GEPIA and TCGA datasets to analyze the relationship between PAK1 and ERK1/2 mRNA expression in AML patients. The results verified that ERK1 and ERK2 expression were positively correlated with PAK1 expression in AML patients ($P < 0.001$, Supplementary Figure 2). We found that the expression of phosphorylated ERK1/2 (Thr202/Tyr204) were remarkably reduced after inhibition of PAK1 by shRNAs or IPA-3 in THP1 and Kasumi-1 cells (Figures 7A,B). When AML cells were co-cultured with BMSCs, the expression level of phosphorylated ERK1/2 was also significantly upregulated compared with cultured alone, which was the same as that of PAK1 and p-PAK1 (Figures 7C,D). Furthermore, p-ERK1/2 expression was also decreased after knockdown of PAK1 in AML cells co-cultured with BMSCs. Additionally, we also evaluated the expression of cleaved-PARP, an important apoptosis molecule. Regardless of whether it was cultured alone or in a co-culture system, the expression of cleaved-PARP was significantly increased

when knocking down the PAK1 expression. Since the ERK pathway is pivotal for regulating cell proliferation, apoptosis and chemoresistance, our results implied that the roles of PAK1 in those process were partially attributed to the activation of ERK signaling pathway.

DISCUSSION

Acute myeloid leukemia is the most common malignant myeloid disorder in adults, and is characterized by clonal heterogeneity of hemopoietic progenitor cells. Front-line induction therapy with cytarabine and anthracycline remains a standard of care in AML (Tallman et al., 2019). With the sequential emergence of gene-targeted drugs and the development of cell therapy and biological immunotherapy, the complete remission rate and survival rate of leukemia patients have markedly improved compared with the past (Dombret and Gardin, 2016). However, there are still considerable patients with treatment failure or disease recurrence, which is closely related to the resistance of chemotherapy drugs. In recent years, the drug resistance-related mutations, especially its interaction with the tumor microenvironment, has gradually become a hot spot in tumor research. For instance, Konopleva et al. (2002) demonstrated that stromal cells prevent apoptosis of AML cells by up-regulation of anti-apoptotic proteins, including BCL2. Additionally, bone marrow stroma can mediate drug resistance to FLT3 inhibitors by persistent activation of extracellular regulated kinase in FLT-ITD AML (Yang et al., 2014).

The PAKs are a family of serine-threonine kinases that consist of six members (PAK1-PAK6), which are overexpressed in variety of cancers. PAK1 and PAK2 are overexpressed in breast and liver cancer, and promote the occurrence and development of tumors (Ong et al., 2015; Rane and Minden, 2019). PAK3 currently has been found to be overexpressed in neuroendocrine tumors (Liu et al., 2010). High expression of PAK4 promotes myeloma cell proliferation through activation of multiple myeloma anti-apoptotic and survival pathways (Fulciniti et al., 2017). By analyzing the data of newly diagnosed AML patients from the TCGA and public GEPIA database, we found that only PAK1 is significantly up-regulated in primary AML patients and confers to poor survival of AML compared with other PAK family members. Our findings were in accordance with the studies of Pandolfi et al. (2015). In addition, PAK1 gene amplification or protein overexpression was also observed in many other kinds of tumors, including breast cancer, colorectal cancer, and hepatocellular carcinoma (Kawahara et al., 2012; Xu et al., 2012; Song et al., 2015). It is well acknowledged that genetic and cytogenetics abnormality were responsible for the progression and prognosis of AML patients (Metzeler et al., 2016; Papaemmanuil et al., 2016; Bullinger et al., 2017). In the present study, our data also revealed that the high expression of PAK1 was intimately linked to higher cytogenetic risk and complex karyotype, serving as one of the risk factors in newly diagnosed AML patients.

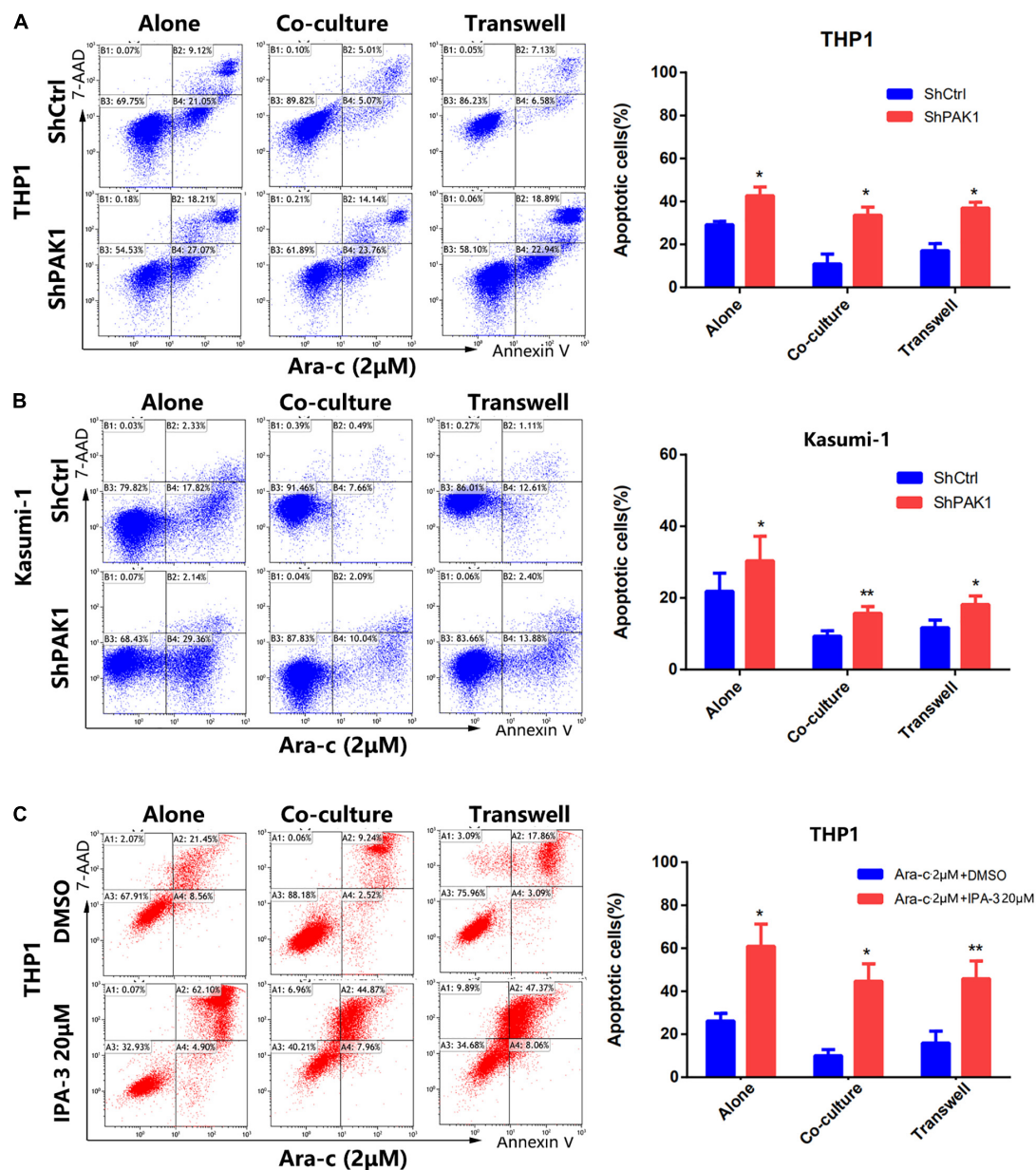


FIGURE 6 | p21-activated kinase 1 (PAK1) suppression reverses the stroma-induced drug resistance in AML cells. **(A,B)** The PAK1 expression in THP1 and Kasumi-1 cells was knocked down by PAK1 shRNAs (ShPAK1). Then cells were cultured alone or co-cultured with HS-5, including direct and indirect transwell contact. Cells were treated with 2 μ M Ara-C for 24 h, and the apoptotic rates of AML cells were detected by flow cytometry. **(C)** The THP1 cells were cultured alone or co-cultured with HS-5, including direct and indirect transwell contact. After exposure to IPA-3 (20 μ M) and Ara-C (2 μ M) for 24 h, the apoptotic rates were detected by flow cytometry. All the experiments were repeated for three times. * $P < 0.05$, ** $P < 0.01$.

And we also found in AML patients without FLT3, IDH1, NPMc, or RAS mutation, high PAK1 expression indicated poor prognosis. Besides, complex karyotype, specific chromosomal aneuploidies (e.g., trisomy 8, -7/7q-) combined with FLT3-ITD mutation are identified as poor prognostic markers. Our study showed that FLT3 mutation positive patients with high PAK1 expression had the shortest survival time, but this was not statistically different from FLT3 mutation negative patients with high PAK1 expression. Previous studies reported that

PAK1 was involved in drug resistance of multiple tumors (Yao et al., 2020). Lu et al. (2017) investigated that PAKs became activated in cells with acquired drug resistance and have a pivotal role in mediating resistance. In BRAFi-resistant cells of metastatic melanoma, PAKs phosphorylated CRAF and MEK to reactivate ERK. Gonzalez et al. (2017) reported that pharmacological inhibition of RAC1-PAK1 axis could enhance tamoxifen sensitivity in human resistant breast cancer cells. PAK1 inhibitor remarkably attenuated tumor growth and metastasis

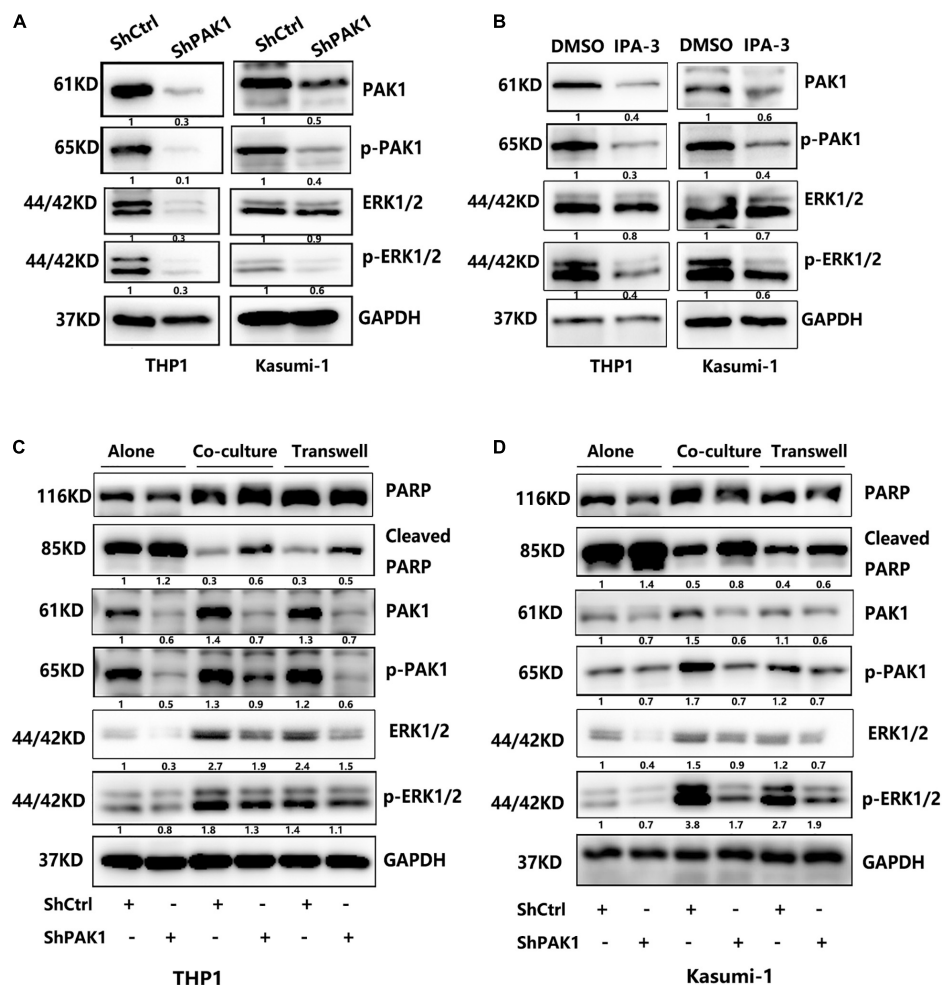


FIGURE 7 | p21-activated kinase 1 (PAK1) works by activating the ERK signaling pathway. **(A)** THP1 and Kasumi-1 cells were transduced with lentivirus containing PAK1 shRNAs (ShPAK1) or scrambled control (ShCtrl). Then, the proteins of ERK1/2 and phosphorylated ERK1/2 (p-ERK1/2) were analyzed by western blot. GAPDH was used as an internal loading control. **(B)** THP1 and Kasumi-1 cells were treated with PAK inhibitor IPA-3 (20 μ M) for 24 h and western blot was performed to evaluate the expression levels of ERK1/2 and p-ERK1/2. **(C,D)** THP1 and Kasumi-1 cells transduced with ShPAK1 or ShCtrl were cultured alone or co-cultured with HS-5, including direct and indirect transwell contact, and western blot was used to detect the expression of PAK1, p-PAK1, ERK1/2, p-ERK1/2, and PARP, cleaved-PARP. GAPDH was used as an internal loading control.

in vivo, and the combined treatment containing synergistic inhibition of PAK1 benefits the tumor therapy. Flis et al. (2019) confirmed that repression of PAK1 displayed synergistic effect with tyrosine kinase inhibitors in chronic myeloid leukemia. In this study, we experimentally validated that knockdown of PAK1 could reduce cell proliferation and promote AML cell apoptosis. Our studies also showed that down-regulation of PAK1 significantly increased the apoptotic effect of the chemotherapy drugs Cytarabine and Idarubicin in AML. The data revealed that the inhibition of PAK1 could enhance chemosensitivity, highlighting the crucial role of PAK1 in drug resistance of AML.

In addition to genetic abnormalities, the BMM also exerts important influences on the chemotherapy resistance of hematological tumors. Previous reports have revealed that bone marrow stroma contributes greatly to the development of drug

resistance to chemotherapy in multiple myeloma, acute, and chronic myelogenous leukemia (Konopleva et al., 2002; Nefedova et al., 2003, 2004). BMSCs can protect leukemia cells against chemotherapy drugs through various cytokines or growth factors (e.g., PDGF, VEGF, EGF, SCF, etc.) or cell-cell surface contact (e.g., SDF1/CXCR4, VLA4/VCAM1, CD44/E-selectin, etc.) (Manabe et al., 1994; Wilson and Trumpp, 2006; Weisberg et al., 2008; Zeng et al., 2009; Sison and Brown, 2011). In our study, the co-culture system of BMSCs HS-5 and acute leukemia cells, including direct co-culture and indirect transwell co-culture to mimic the BMM was established, and the Annexin V-FITC analysis showed that HS-5 obviously suppressed the apoptosis of AML cells induced by Ara-c. Interestingly, the qRT-PCR and western blot results demonstrated that co-culture with BMSCs induced PAK1 expression in AML cells, and knockdown of PAK1 in AML cells partially reversed the BMSCs-induced resistance

to Ara-c by apoptotic analysis. There are also some literatures reports that PAK1 may play a critical role in stroma-mediated protection of solid tumor cells. For example, Yeo et al. (2017) found that knockout of PAK1 in the stroma led to a decrease in PAK1 levels and activity, and subsequent tumor growth inhibition in pancreatic cancer. Additionally, the expression level of PAK1 in tumors was also shown to affect PAK1 levels in the stroma. Thus, PAK1 appears to have a role in signaling from the stroma to the tumor, and from the tumor to the stroma. Our data revealed that the BMSCs-mediated drug resistance may partially depend on the PAK1 activity. But how BMSCs induce the PAK1 expression and thus mediate drug resistance of AML cells requires further study.

It is well known that PI3K/AKT and MEK/ERK signaling pathways play critical roles in the interaction between the BMSCs and tumor cells (Bertrand et al., 2005; Tabe et al., 2007). Previous studies demonstrated that PAK1 could be crucial for PI3K/AKT and MEK/ERK signaling pathways, and blockage of PAK1 alleviates the tumor cells malignant behaviors via inhibiting ERK and AKT signaling activity in multiple malignant tumors (Semenova et al., 2017; Kanumuri et al., 2020; Song et al., 2021). PAK1 makes itself a contribution in this network by activating ERK, MEK, and Raf (Higuchi et al., 2008). In this study, we also found that in the BMSCs co-culture system, downregulation of PAK1 could inhibit the expression of p-ERK by western blot. Moreover, the apoptotic factor cleaved-PARP expression was also markedly increased. These data indicated that BMSCs-mediated chemotherapy-resistance may be ascribed to the PAK1 activated ERK1/2-cleaved-PARP signaling pathways.

In conclusion, in the PAK family, PAK1 overexpression confers to the shorter survival and poor prognosis of AML patients. The knockdown of PAK1 could reverse chemoresistance by induction of apoptosis in AML cells. Additionally, PAK1 plays critical roles in stroma-mediated protection of AML cells, which results in BMSCs-mediated apoptosis tolerance by activating ERK1/2 signaling pathway. Our data support the strategy of targeting PAK1 to overcome chemoresistance in AML, suggesting that the combination of inhibiting PAK1 and traditional chemotherapy drugs represents a potentially novel approach. However, due to the complexity and heterogeneity of the tumor microenvironment, as well as the crosstalk among oncogenic signaling pathways, the PAK1 mediated downstream molecular mechanism need deeply investigated.

DATA AVAILABILITY STATEMENT

Publicly available datasets were analyzed in this study. This data can be found here: The Cancer Genome Atlas

(TCGA) database/Gene Expression Profiling Interactive Analysis (GEPIA).

ETHICS STATEMENT

Informed consent was obtained in accordance with the Declaration of Helsinki. All laboratory experiments with primary samples were reviewed and approved by the Medical Ethics Committee of Qilu Hospital, Shandong University. The patients/participants provided their written informed consent to participate in this study.

AUTHOR CONTRIBUTIONS

MJ and BL conceived and designed the experiments and drafted the manuscript. RJ, WeL, YZ, SD, WëL, and ML performed the *in vitro* experiments. DG and QT took responsibility for statistical analyses and interpretation of data. TS and DM collected specimens and prepared the figures. CJ took responsibility for full-text evaluation and guidance, finally approval of the version to be submitted. All authors have read and approved the final manuscript.

FUNDING

This work was supported by grants from the Distinguished Taishan Scholars in Climbing Plan (tspd20210321), the National Natural Science Foundation of China (81770159 and 81873425), the Natural Science Foundation of Shandong Province (ZR2020MH118 and ZR2020KH016), the Fundamental Research Funds of Shandong University (2018JC003), and the Shandong Province Medical Science and Technology Development Program (2019WS206 and 2019WS207).

SUPPLEMENTARY MATERIAL

The Supplementary Material for this article can be found online at: <https://www.frontiersin.org/articles/10.3389/fcell.2021.686695/full#supplementary-material>

Supplementary Figure 1 | (A) THP1 cells were infected with lentiviral particles with specific PAK1 shRNAs (ShPAK1) or scrambled control (ShCtrl) for 48 h. Transfection efficiency was evaluated by fluorescence microscope. **(B)** THP1 and Kasumi-1 cells were infected with lentiviral particles with ShPAK1 or ShCtrl for 48 h. Transfection efficiency was evaluated by flow cytometer.

Supplementary Figure 2 | The expression of ERK1, ERK2, and PAK1 in AML patients were shown as scatter diagram (from GEPIA and TCGA datasets). ERK1 and ERK2 were positively correlated with PAK1 expression in AML patients.

REFERENCES

Ayala, F., Dewar, R., Kieran, M., and Kalluri, R. (2009). Contribution of bone microenvironment to leukemogenesis and leukemia progression. *Leukemia* 23, 2233–2241. doi: 10.1038/leu.2009.175

Bertrand, F. E., Spengeman, J. D., Shelton, J. G., and McCubrey, J. A. (2005). Inhibition of PI3K, mTOR and MEK signaling pathways promotes rapid apoptosis in B-lineage ALL in the presence of stromal cell support. *Leukemia* 19, 98–102. doi: 10.1038/sj.leu.2403560

- Bullinger, L., Dohner, K., and Dohner, H. (2017). Genomics of acute myeloid leukemia diagnosis and pathways. *J. Clin. Oncol.* 35, 934–946. doi: 10.1200/JCO.2016.71.2208
- Dohner, H., Estey, E., Grimwade, D., Amadori, S., Appelbaum, F. R., Buchner, T., et al. (2017). Diagnosis and management of AML in adults: 2017 ELN recommendations from an international expert panel. *Blood* 129, 424–447. doi: 10.1182/blood-2016-08-733196
- Dombret, H., and Gardin, C. (2016). An update of current treatments for adult acute myeloid leukemia. *Blood* 127, 53–61. doi: 10.1182/blood-2015-08-604520
- Flis, S., Bratek, E., Chojnacki, T., Piskorek, M., and Skorski, T. (2019). Simultaneous inhibition of BCR-ABL1 tyrosine kinase and PAK1/2 serine/threonine kinase exerts synergistic effect against chronic myeloid leukemia cells. *Cancers (Basel)* 11:1544. doi: 10.3390/cancers11101544
- Fulciniti, M., Martinez-Lopez, J., Senapedis, W., Oliva, S., Lakshmi Bandi, R., Amodio, N., et al. (2017). Functional role and therapeutic targeting of p21-activated kinase 4 in multiple myeloma. *Blood* 129, 2233–2245. doi: 10.1182/blood-2016-06-724831
- Gonzalez, N., Cardama, G. A., Comin, M. J., Segatori, V. I., Pifano, M., Alonso, D. F., et al. (2017). Pharmacological inhibition of Rac1-PAK1 axis restores tamoxifen sensitivity in human resistant breast cancer cells. *Cell Signal.* 30, 154–161. doi: 10.1016/j.cellsig.2016.12.002
- Higuchi, M., Onishi, K., Kikuchi, C., and Gotoh, Y. (2008). Scaffolding function of PAK in the PDK1-Akt pathway. *Nat. Cell Biol.* 10, 1356–1364. doi: 10.1038/ncb1795
- Hu, K., Gu, Y., Lou, L., Liu, L., Hu, Y., Wang, B., et al. (2015). Galectin-3 mediates bone marrow microenvironment-induced drug resistance in acute leukemia cells via Wnt/beta-catenin signaling pathway. *J. Hematol. Oncol.* 8:1. doi: 10.1186/s13045-014-0099-8
- Kanumuri, R., Saravanan, R., Pavithra, V., Sundaram, S., Rayala, S. K., and Venkatraman, G. (2020). Current trends and opportunities in targeting p21 activated kinase-1 (PAK1) for therapeutic management of breast cancers. *Gene* 760:144991. doi: 10.1016/j.gene.2020.144991
- Kawahara, M., Pandolfi, A., Bartholdy, B., Barreyro, L., Will, B., Roth, M., et al. (2012). H2O₂-like homeobox regulates early hematopoiesis and promotes acute myeloid leukemia. *Cancer Cell* 22, 194–208. doi: 10.1016/j.ccr.2012.06.027
- Konopleva, M., Konoplev, S., Hu, W., Zaritskey, A. Y., Afanasiev, B. V., and Andreff, M. (2002). Stromal cells prevent apoptosis of AML cells by up-regulation of anti-apoptotic proteins. *Leukemia* 16, 1713–1724. doi: 10.1038/sj.leu.2402608
- Liu, R. X., Wang, W. Q., Ye, L., Bi, Y. F., Fang, H., Cui, B., et al. (2010). p21-activated kinase 3 is overexpressed in thymic neuroendocrine tumors (carcinoids) with ectopic ACTH syndrome and participates in cell migration. *Endocrine* 38, 38–47. doi: 10.1007/s12020-010-9324-6
- Long, X., Yu, Y., Perlaky, L., Man, T. K., and Redell, M. S. (2015). Stromal CYR61 confers resistance to mitoxantrone via spleen tyrosine kinase activation in human acute myeloid leukaemia. *Br. J. Haematol.* 170, 704–718. doi: 10.1111/bjh.13492
- Lu, H., Liu, S., Zhang, G., Bin, W., Zhu, Y., Frederick, D. T., et al. (2017). PAK signalling drives acquired drug resistance to MAPK inhibitors in BRAF-mutant melanomas. *Nature* 550, 133–136. doi: 10.1038/nature24040
- Manabe, A., Murti, K. G., Coustan-Smith, E., Kumagai, M., Behm, F. G., Raimondi, S. C., et al. (1994). Adhesion-dependent survival of normal and leukemic human B lymphoblasts on bone marrow stromal cells. *Blood* 83, 758–766. doi: 10.1182/blood.v83.3.758.bloodjournal833758
- Mendez-Ferrer, S., Bonnet, D., Steensma, D. P., Hasserjian, R. P., Ghobrial, I. M., Gribben, J. G., et al. (2020). Bone marrow niches in haematological malignancies. *Nat. Rev. Cancer* 20, 285–298. doi: 10.1038/s41568-020-0245-2
- Metzeler, K. H., Herold, T., Rothenberg-Thurley, M., Amler, S., Sauerland, M. C., Gorlich, D., et al. (2016). Spectrum and prognostic relevance of driver gene mutations in acute myeloid leukemia. *Blood* 128, 686–698. doi: 10.1182/blood-2016-01-693879
- Nefedova, Y., Cheng, P., Alsina, M., Dalton, W. S., and Gabrilovich, D. I. (2004). Involvement of Notch-1 signaling in bone marrow stroma-mediated de novo drug resistance of myeloma and other malignant lymphoid cell lines. *Blood* 103, 3503–3510. doi: 10.1182/blood-2003-07-2340
- Nefedova, Y., Landowski, T. H., and Dalton, W. S. (2003). Bone marrow stromal-derived soluble factors and direct cell contact contribute to de novo drug resistance of myeloma cells by distinct mechanisms. *Leukemia* 17, 1175–1182. doi: 10.1038/sj.leu.2402924
- Ong, C. C., Gierke, S., Pitt, C., Sagolla, M., Cheng, C. K., Zhou, W., et al. (2015). Small molecule inhibition of group I p21-activated kinases in breast cancer induces apoptosis and potentiates the activity of microtubule stabilizing agents. *Breast Cancer Res.* 17:59. doi: 10.1186/s13058-015-0564-5
- Ong, C. C., Jubbs, A. M., Jakubiak, D., Zhou, W., Rudolph, J., Haverty, P. M., et al. (2013). P21-activated kinase 1 (PAK1) as a therapeutic target in BRAF wild-type melanoma. *J. Natl. Cancer Inst.* 105, 606–607. doi: 10.1093/jnci/djt054
- Pandolfi, A., Stanley, R. F., Yu, Y., Bartholdy, B., Pendurti, G., Gritsman, K., et al. (2015). PAK1 is a therapeutic target in acute myeloid leukemia and myelodysplastic syndrome. *Blood* 126, 1118–1127. doi: 10.1182/blood-2014-12-618801
- Papaemmanuil, E., Gerstung, M., Bullinger, L., Gaidzik, V. I., Paschka, P., Roberts, N. D., et al. (2016). Genomic classification and prognosis in acute myeloid leukemia. *N. Engl. J. Med.* 374, 2209–2221. doi: 10.1056/NEJMoa1516192
- Piya, S., Kornblau, S. M., Ruvolo, V. R., Mu, H., Ruvolo, P. P., McQueen, T., et al. (2016). Atg7 suppression enhances chemotherapeutic agent sensitivity and overcomes stroma-mediated chemoresistance in acute myeloid leukemia. *Blood* 128, 1260–1269. doi: 10.1182/blood-2016-01-692244
- Rane, C. K., and Minden, A. (2014). P21 activated kinases: structure, regulation, and functions. *Small GTPases* 5:e28003. doi: 10.4161/sgtp.28003
- Rane, C. K., and Minden, A. (2019). P21 activated kinase signaling in cancer. *Semin. Cancer Biol.* 54, 40–49. doi: 10.1016/j.semcancer.2018.01.006
- Ridge, S. M., Sullivan, F. J., and Glynn, S. A. (2017). Mesenchymal stem cells: key players in cancer progression. *Mol. Cancer* 16:31. doi: 10.1186/s12943-017-0597-8
- Semenova, G., Stepanova, D. S., Dubyk, C., Handorf, E., Deyev, S. M., Lazar, A. J., et al. (2017). Targeting group I p21-activated kinases to control malignant peripheral nerve sheath tumor growth and metastasis. *Oncogene* 36, 5421–5431. doi: 10.1038/onc.2017.143
- Shafat, M. S., Gnanaswaran, B., Bowles, K. M., and Rushworth, S. A. (2017). The bone marrow microenvironment – home of the leukemic blasts. *Blood Rev.* 31, 277–286. doi: 10.1016/j.blre.2017.03.004
- Siekman, I. K., Dierck, K., Prall, S., Klokow, M., Strauss, J., Buhs, S., et al. (2018). Combined inhibition of receptor tyrosine and p21-activated kinases as a therapeutic strategy in childhood ALL. *Blood Adv.* 2, 2554–2567. doi: 10.1182/bloodadvances.2018020693
- Sison, E. A., and Brown, P. (2011). The bone marrow microenvironment and leukemia: biology and therapeutic targeting. *Expert. Rev. Hematol.* 4, 271–283. doi: 10.1586/ehm.11.30
- Song, B., Wang, W., Zheng, Y., Yang, J., and Xu, Z. (2015). P21-activated kinase 1 and 4 were associated with colorectal cancer metastasis and infiltration. *J. Surg. Res.* 196, 130–135. doi: 10.1016/j.jss.2015.02.035
- Song, P., Song, B., Liu, J., Wang, X., Nan, X., and Wang, J. (2021). Blockage of PAK1 alleviates the proliferation and invasion of NSCLC cells via inhibiting ERK and AKT signaling activity. *Clin. Transl. Oncol.* 23, 892–901. doi: 10.1007/s12094-020-02486-5
- Tabe, Y., Jin, L., Tsutsumi-Ishii, Y., Xu, Y., McQueen, T., Priebe, W., et al. (2007). Activation of integrin-linked kinase is a critical prosurvival pathway induced in leukemic cells by bone marrow-derived stromal cells. *Cancer Res.* 67, 684–694. doi: 10.1158/0008-5472.CAN-06-3166
- Tallman, M. S., Wang, E. S., Altman, J. K., Appelbaum, F. R., Bhatt, V. R., Bixby, D., et al. (2019). Acute myeloid leukemia, version 3.2019, NCCN clinical practice guidelines in oncology. *J. Natl. Compr. Canc. Netw.* 17, 721–749. doi: 10.6004/jnccn.2019.0028
- Weisberg, E., Wright, R. D., McMillin, D. W., Mitsiades, C., Ray, A., Barrett, R., et al. (2008). Stromal-mediated protection of tyrosine kinase inhibitor-treated BCR-ABL-expressing leukemia cells. *Mol. Cancer Ther.* 7, 1121–1129. doi: 10.1158/1535-7163.MCT-07-2331
- Wilson, A., and Trumpp, A. (2006). Bone-marrow haematopoietic-stem-cell niches. *Nat. Rev. Immunol.* 6, 93–106. doi: 10.1038/nri1779
- Xu, J., Liu, H., Chen, L., Wang, S., Zhou, L., Yun, X., et al. (2012). Hepatitis B virus X protein confers resistance of hepatoma cells to anoikis by up-regulating and activating p21-activated kinase 1. *Gastroenterology* 143, 199–212.e4. doi: 10.1053/j.gastro.2012.03.053
- Yang, X., Sexauer, A., and Levis, M. (2014). Bone marrow stroma-mediated resistance to FLT3 inhibitors in FLT3-ITD AML is mediated by persistent

- activation of extracellular regulated kinase. *Br. J. Haematol.* 164, 61–72. doi: 10.1111/bjh.12599
- Yao, D., Li, C., Rajoka, M. S. R., He, Z., Huang, J., Wang, J., et al. (2020). P21-activated kinase 1: emerging biological functions and potential therapeutic targets in cancer. *Theranostics* 10, 9741–9766. doi: 10.7150/thno.46913
- Yeo, D., Phillips, P., Baldwin, G. S., He, H., and Nikfarjam, M. (2017). Inhibition of group 1 p21-activated kinases suppresses pancreatic stellate cell activation and increases survival of mice with pancreatic cancer. *Int. J. Cancer* 140, 2101–2111. doi: 10.1002/ijc.30615
- Zeng, Z., Shi, Y. X., Samudio, I. J., Wang, R. Y., Ling, X., Frolova, O., et al. (2009). Targeting the leukemia microenvironment by CXCR4 inhibition overcomes resistance to kinase inhibitors and chemotherapy in AML. *Blood* 113, 6215–6224. doi: 10.1182/blood-2008-05-158311
- Conflict of Interest:** The authors declare that the research was conducted in the absence of any commercial or financial relationships that could be construed as a potential conflict of interest.

Copyright © 2021 Li, Jia, Li, Zhou, Guo, Teng, Du, Li, Li, Sun, Ma, Ji and Ji. This is an open-access article distributed under the terms of the Creative Commons Attribution License (CC BY). The use, distribution or reproduction in other forums is permitted, provided the original author(s) and the copyright owner(s) are credited and that the original publication in this journal is cited, in accordance with accepted academic practice. No use, distribution or reproduction is permitted which does not comply with these terms.



LINC00261 Suppresses Cisplatin Resistance of Esophageal Squamous Cell Carcinoma Through miR-545-3p/MT1M Axis

Lijun Wang, Xiaojun Wang, Pengwei Yan, Yatian Liu* and Xuesong Jiang*

Department of Radiation Oncology, Jiangsu Cancer Hospital, Jiangsu Institute of Cancer Research, The Affiliated Cancer Hospital of Nanjing Medical University, Nanjing, China

OPEN ACCESS

Edited by:

Wei Zhao,
City University of Hong Kong,
Hong Kong

Reviewed by:

Bingxian Xie,
University of Pittsburgh, United States
Jiang-Jiang Qin,
Institute of Cancer and Basic
Medicine, Chinese Academy
of Sciences (CAS), China

*Correspondence:

Yatian Liu
lyt_84@163.com
Xuesong Jiang
13851700790@126.com

Specialty section:

This article was submitted to
Molecular and Cellular Oncology,
a section of the journal
Frontiers in Cell and Developmental
Biology

Received: 30 March 2021

Accepted: 24 June 2021

Published: 15 July 2021

Citation:

Wang L, Wang X, Yan P, Liu Y and
Jiang X (2021) LINC00261
Suppresses Cisplatin Resistance
of Esophageal Squamous Cell
Carcinoma Through
miR-545-3p/MT1M Axis.
Front. Cell Dev. Biol. 9:687788.
doi: 10.3389/fcell.2021.687788

To improve the survival rate and cure rate of patients, it is necessary to find a new treatment scheme according to the molecular composition of (ESCC) in esophageal squamous cell carcinoma. Long non-coding RNAs (lncRNAs) regulate the progression of ESCC by various pathophysiological pathways. We explored the possible function of the lncRNA LINC00261 (LINC00261) on cisplatin (DDP) resistance of ESCC and its relative molecular mechanisms. In the study, we found that LINC00261 was downregulated in ESCC tissues, cell lines, and DDP-resistant ESCC patients. Besides, overexpression of LINC00261 not only inhibited cell proliferation, and DDP resistance but also promotes cell apoptosis. Further mechanistic research showed that LINC00261 sponged miR-545-3p which was negatively correlated with the expression of LINC00261. In addition, functional experiments revealed that upregulation of miR-766-5p promoted proliferation and enhanced DDP resistance. Subsequently, MT1M was testified to be the downstream target gene of miR-545-3p. Rescue experiments revealed that overexpression of MT1M largely restores miR-545-3p mimics-mediated function on ESCC progression. Our results demonstrate that the LINC00261 suppressed the DDP resistance of ESCC through miR-545-3p/MT1M axis.

Keywords: LINC00261, miR-545-3p, MT1M, DDP resistance, ESCC

INTRODUCTION

Esophageal carcinoma (EC) serves as one of the most common malignant tumors with strong aggressiveness and poor prognosis, and it is the sixth leading cause of cancer-related death worldwide (Adenis et al., 2015). According to the latest cancer epidemiology, the incidence and fatality of esophageal cancer in China ranks fifth and fourth, respectively (Zhang et al., 2016; Zuo et al., 2016). Pathologically, more than 90% of EC in China is esophageal squamous cell carcinoma (ESCC) (Chen et al., 2016; Bray et al., 2018). Despite the great progress in the treatment of EC in recent years, the prognosis of ESCC was still very poor, with a 5-year survival rate of less than 10% (Ohashi et al., 2015). Four reasons contribute to the poor prognosis of EC which are (1) the detection time of ESCC is later than other cancers; (2) the lymph node metastasis is earlier; (3) surgical treatment is difficult to eradicate; (4) often accompanied by recurrence; and (5) metastasis after treatment (Okugawa et al., 2015; Jung et al., 2020). Besides, drug resistance is also

an important reason for the failure of chemotherapy and poor prognosis in patients with ESCC. Clinical data shows that more than 90% of the deaths of patients with malignant tumors are related to chemotherapy resistance (Luqmani, 2005; Vadlapatla et al., 2013). Therefore, understanding the molecular mechanisms of ESCC proliferation, metastasis, and drug resistance has profound scientific significance and value for improving treatment methods and strategies and predicting the clinical prognosis (Lou et al., 2019).

Long non-coding RNA (lncRNA) is a kind of regulatory RNA whose transcriptional length exceeds 200 nucleotides and has no protein coding ability (Geisler and Coller, 2013). lncRNA has been proven to be closely related to the occurrence and development of tumors (Xiao et al., 2019). lncRNA regulates the expression of coding genes in many aspects such as transcriptional regulation, post-transcriptional regulation, and epigenetics, and thus plays a corresponding role in the occurrence, development, proliferation, metastasis, invasion, and drug resistance of tumors (Cheng et al., 2020; Liang et al., 2020). Currently, the role of lncRNA in tumors is a research hotspot, including lung cancer, liver cancer and bladder cancer (Chen et al., 2017, 2020; Gao et al., 2020). In addition, the role of lncRNAs in ESCC has also been extensively reported. For example, lncRNA LOC440173 promotes the progression of ESCC by modulating the miR-30d-5p/HDAC9 axis and the epithelial-mesenchymal transition (EMT) (Wang et al., 2020). In addition, lncRNA FOXD2-AS1 promotes DDP-resistance in ESCC by the miR-195/Akt/mTOR PATH (Liu H. et al., 2020). Lin et al. (2019) proved that LINC00261 is highly expressed in EC. Taken together, these studies imply that LINC00261 is involved in EC, but the specific role of LINC00261 in ESCC is still unclear. This study explored the molecular mechanism of LINC00261 on the biological processes of ESCC proliferation, apoptosis, and DDP-resistance from the cellular and molecular biology level, laying the foundation for ESCC targeted therapy and patient prognosis analysis.

MATERIALS AND METHODS

ESCC Patients and Clinical Samples

Total 30 paired ESCC tumor tissues and adjacent non-tumor tissues were collected from Jiangsu Cancer Hospital. All patients did not get treatment. Patient data and samples are anonymized and obtained in accordance with ethical and legal guidelines. All participants had signed informed consent forms. This study was approved by the Ethics Committee of Jiangsu Cancer Hospital.

Cell Culture and Cell Treatment

Two ESCC cell lines (TE-1 and ECA109) were purchased from the Chinese Academy of Sciences cell bank (Shanghai, China). All cells were cultured in RPMI-1640 containing contained with 10% fetal bovine serum (FBS) and incubated at 5% CO₂ 37°C.

MiR-545-3p mimics and corresponding control NC-mimics, vectors for overexpression of LINC00261, MT1M and their negative control vector were obtained from the RiboBio (Guangzhou, China). These plasmids were transfected into cells

by Lipofectamine 3000 (Thermo Fisher Scientific, United States) according to the protocols.

Establishment of DDP-Resistant Cell Lines

DDP-resistant ESCC cells (TE-1/DDP and ECA109/DDP) were constructed by gradually increasing the concentration of DDP (Macklin, Shanghai, China) according to previous reports (Lin et al., 2019; Liu H. et al., 2020). Briefly, TE-1 and ECA109 were exposed to an initial DDP concentration of 0.2 μmol/L in RPMI-1640 containing 10% FBS for 72 h. After washing three times with PBS, cells were cultured in DDP-free medium. Upon reaching 70–80% confluence, the cells were cultured with a higher concentration (10–20% increase per passage) of DDP. The above treatment was repeated until the concentration reached 10 mol/L.

RT-qPCR

Total RNA was extracted from samples using the Trizol reagents (Takara, Otsu, Shiga, Japan) according to the manuals of manufacturers. The PrimeScriptTMII 1st Strand cDNA Synthesis Kit (Takara, Otsu, Shiga, Japan) was used to induced cDNA. Quantitative real-time quantitative PCR (qPCR) was performed using SYBR green main mixture in a 4800 real-time PCR instrument (Bio-RAD, CA, United States). U6 and β-actin were used as internal references. The $2^{-\Delta\Delta Ct}$ method was used to calculate the relative mRNA expression levels. The primers for RT-qPCR were shown in Table 1.

Western Blotting

Total proteins were extracted with ice-cold RIPA lysis buffer (Solarbio, Beijing, China) plus PMSF (Solarbio) from ESCC cell lines. Then the protein concentrations were detected by a BCA assay kit (Solarbio). The separated proteins were isolated in 10% sodium dodecyl sulfate-polyacrylamide gel electrophoresis (SDS-PAGE), and transferred into PVDF membranes. After blocked by skim milk, these bands were incubated with primary antibodies against Bcl-2, Bax, cleaved caspase-3, cleaved caspase-9, MT1Mβ-actin (all from Abcam, Cambridge, United Kingdom) at 4°C overnights. Next, membranes were washed with PBS followed by incubation with the appropriate secondary antibody for 1 h at 22–23°C. Finally, the enhanced chemiluminescence (ECL, Pierce,

TABLE 1 | Primer sequences used for RT-qPCR.

Genes		Primer sequences (5'–3')
LINC00261	Forward	GTCAGAAGGAAAGGCCGTGA
x	Reverse	TGAGCCGAGATGAACAGGTG
MT1M	Forward	
	Reverse	
β-actin	Forward	AGCGAGCATCCCCAAAGTT
	Reverse	GGGCACGAAGGCTCATCATT
miR-545-3p	Forward	TGCGCTCAGCAACATTATTG
	Reverse	CCAGTGCAGGGTCCGAGGTATT
U6	Forward	CTCGCTTCGGCAGCACATATACTA
	Reverse	ACGAATTTGCGTGTCACTCCTTGCG

Rockford, IL) visualized these membranes. Image J software was used to analyze membranes.

CCK-8 Assay

The proliferation of ESCC cells was detected by CCK-8 assay. In brief, ESCC cells were seeded in the 96-well plate. Next, CCK-8 reagent was added to each well. The optical density (OD) value at 450 nm was measured by an enzyme plate analyzer (Shimadzu, Kyoto, Japan).

Clone Formation Assay

Logarithmic growth cells (1×10^2 cells/well) were inoculated into a 6-well plate and incubated for 7 days at 37°C in a 5% CO₂ incubator. Then, 4% paraformaldehyde was fixed at room temperature for 30 s, and 0.1% crystal violet solution was dyed for 15 min. Finally, the colony formation number and relative colony formation were calculated by randomly selecting 10 fields under the microscope (Optical-SH, Shanghai, China).

Flow Cytometry

The apoptosis of ESCC cells was assessed by flow cytometry assay. In brief, ESCC cells were collected and suspended in 100 µL of buffer solution. The cells were stained with FITC Annexin V and Propidium Iodide (PI) in dark for 10 min. Afterward, 400 µL of binding buffer was added to each tube, and the apoptosis was assessed by flow cytometry (BD Bioscience, CA, United States).

Bioinformatics Analysis

The online prediction tool StarBase¹ was used for the targeted prediction between LINC00261 and miR-545-3p, whereas Targetscan² was used for the targeted prediction between miR-545-3p and MT1M.

Luciferase Reporter Test

LINC00261-WT or LINC00261-Mut were co-transfected with miR-545-3p mimic or miR-NC into TE-1 and ECA109 cells using Lipofectamine 3000 (Thermo Fisher Scientific). MT1M-WT or MT1M-Mut were also co-transfected with miR-545-3p mimic or miR-NC into TE-1 and ECA109 cells using Lipofectamine 3000 (Thermo Fisher Scientific). After 48 h, the relative luciferase activities were detected by the dual Glo Luciferase Assay System (Promega, Shanghai, China) in accordance with the protocols. Renilla signals were used to normalize luciferase activity.

Isolation of Nuclear and Cytoplasmic RNA

Nuclear and cytoplasmic RNA were separated using a Cytoplasmic and Nuclear RNA Purification Kit (Norgen Biotek, Canada) following the manuals of manufacturers. After purification and DNaseI treatment, the isolated nuclear or cytoplasmic RNA fractions were reverse transcribed and used for PCR as described above.

¹<http://starbase.sysu.edu.cn/>

²http://www.targetscan.org/vert_72/

Statistical Analysis

All data were expressed as mean \pm SD. The Student's *t*-test was used to determine the statistical differences between the two groups and ANOVA was used to analyze the statistical differences among the multiple groups. *P* < 0.05 was considered as statistically significant. All experiments were conducted in triplicates.

RESULTS

LINC00261 Expression Is Decreased in ESCC Tissues and ESCC Cells

To determine whether LINC00261 affect ESCC, the expression of LINC00261 in ESCC tissues and adjacent tissue was first detected. The results showed that LINC00261 expression was significantly lower in ESCC tissues than in the normal adjacent tissues (Figure 1A). Interestingly, we found that the expression of LINC00261 was downregulated in DDP-resistant ESCC patients compared with DDP-sensitive ESCC patients (Figure 1B). Moreover, Kaplan-Meier survival analysis revealed that the high expression of LINC00261 was related to a high overall survival rate in ESCC patients (Figure 1C).

Overexpression of LINC00261 Inhibits the Proliferation and Promotes Apoptosis of ESCC Cells

To explore the specific functions of LINC00261 in ESCC progression, pcDNA-LINC00261 and its corresponding control were transfected ESCC cells (TE-1 and ECA109). First, the transfection efficiency was detected by RT-qPCR and the results showed that LINC00261 expression was increased in the pcDNA-LINC00261 group compared to the control group (Figure 2A). CCK-8 and clone formation assay showed that overexpression of LINC00261 inhibited cell viability and reduced the number of colonies in TE-1 and ECA109 cells (Figures 2B,C), indicating that LINC00261 had a negative effect on ESCC cells proliferation. Besides, the apoptotic cells were remarkably increased in the pcDNA-LINC00261 group compared with the control group (Figure 2D). Besides, western blot got similar results, which overexpression of LINC00261 induced Bax, cleaved-caspase 3, cleaved-caspase 9 expression and inhibited Bcl-2 expression in TE-1 and ECA109 cells (Figure 2E).

Overexpression of LINC00261 Suppresses DDP Resistance in ESCC Cells

To gain whether LINC00261 is involved in DDP resistance, we tested LINC00261 expression in TE-1, ECA109 and their corresponding DDP resistant (TE-1/DDP and ECA109/DDP) cell. As shown in Figure 3A, the expression of LINC00261 in TE-1/DDP (ECA109/DDP) cells was dramatically lower than that in TE-1 (ECA109) cells. To assess the functional role of LINC00261 in DDP resistance in ESCC cells, we overexpressed LINC00261 and evaluated its effect on cell proliferation and

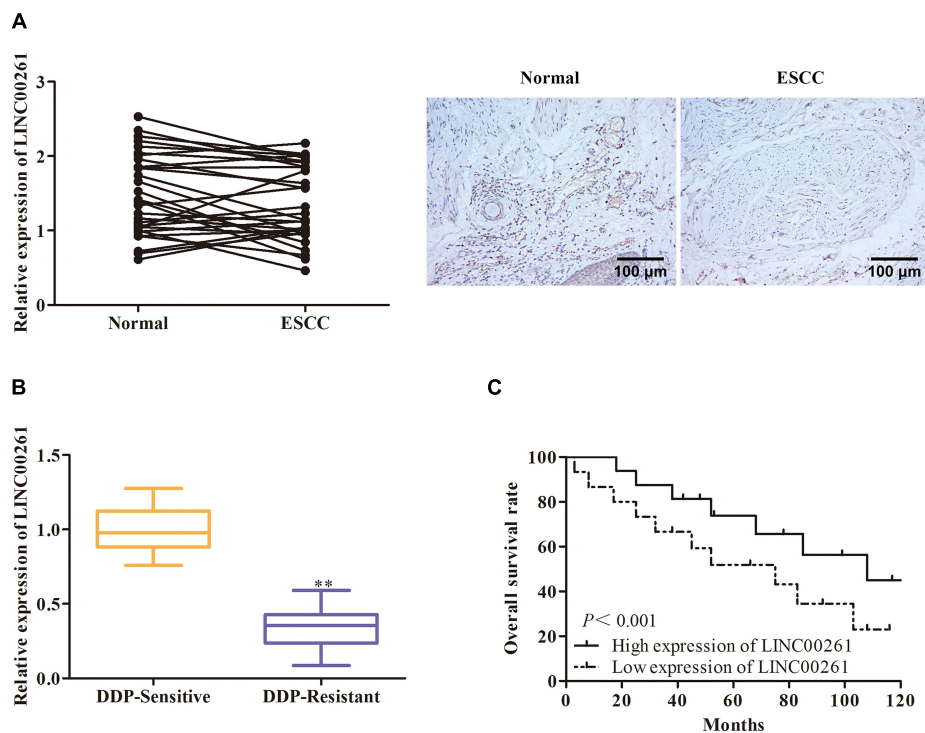


FIGURE 1 | LINC00261 expression is decreased in ESCC tissues and ESCC cells. **(A)** The expression of LINC00261 in ESCC tissues and adjacent tissues. **(B)** The expression of LINC00261 in DDP-sensitive and DDP-resistant ESCC patients. **(C)** Survival analysis based on ESCC patients with high-level or low-level LINC00261. $**P < 0.01$ compared with the corresponding control group.

apoptosis in TE-1/DDP and ECA109/DDP cells. Overexpression of LINC00261 significantly promoted LINC00261 expression in TE-1/DDP and ECA109/DDP cells (**Figure 3B**). CCK-8 assay showed that cell proliferation was dose-dependently inhibited by DDP, overexpression of LINC00261 significantly inhibited the growth of DDP-supplemented cells compared with the control group (**Figure 3C**). Furthermore, flow cytometry assay revealed that overexpression of LINC00261 increased the apoptosis of TE-1/DDP and ECA109/DDP cells as compared with the pcDNA (**Figure 3D**).

LINC00261 Functions as a Molecular Sponge for MiR-545-3p

Then we studied the specific mechanism of LINC00261 in ESCC. Numerous studies have shown that lncRNAs function as a competing endogenous RNA (ceRNA) binding to miRNA, then promote transcription (28281528). We firstly detected the cellular position of LINC00261 and found that LINC00261 was mainly located in the cytoplasm (**Figure 4A**). Bioinformatics prediction indicated that there were specific binding sites between the LINC00261 sequence and the miR-545-3p sequence, hinted that LINC00261 might be a target gene of miR-545-3p (**Figure 4B**). To confirm the relationship between LINC00261 and miR-545-3p, the luciferase reporter vectors LINC00261-WT or LINC00261-MUT, miR-545-3p mimics or NC mimics were constructed to transfect into TE-1 and

ECA109 cells. MiR-545-3p mimic significantly prompted the expression of miR-545-3p (**Figure 4C**), and greatly reduced the luciferase activities of LINC00261-WT but had no effect on LINC00261-MUT (**Figure 4D**). In addition, RT-qPCR showed that overexpression of LINC00261 remarkably downregulated miR-545-3p (**Figure 4E**). Subsequently, we discovered that miR-545-3p expression was notably upregulated in ESCC tissues compared with adjacent tissues (**Figure 4F**), and the expression of miR-545-3p was increased in DDP-resistant ESCC patients compared with DDP-sensitive ESCC patients (**Figure 4G**). Besides, correlational analyses showed that there was a negative relationship between LINC00261 and miR-545-3p (**Figure 4H**). The above data demonstrated that LINC00261 functions as a sponger for the miR-545-3p in ESCC.

MiR-545-3p Promotes the Proliferation and Enhances DDP Resistance in ESCC Cells

Next, we further study the functions of miR-545-3p in the progression of ESCC. As shown in **Figures 5A,B**, CCK-8 and clone formation assay demonstrated that overexpression of miR-545-3p promoted the proliferation in TE-1 and ECA109 cells. Flow cytometry assay showed that the apoptotic rate was significantly reduced in the miR-545-3p mimics group compared with the NC mimics group (**Figure 5C**). On the other hand, we assessed the functional role of miR-545-3p in the DDP

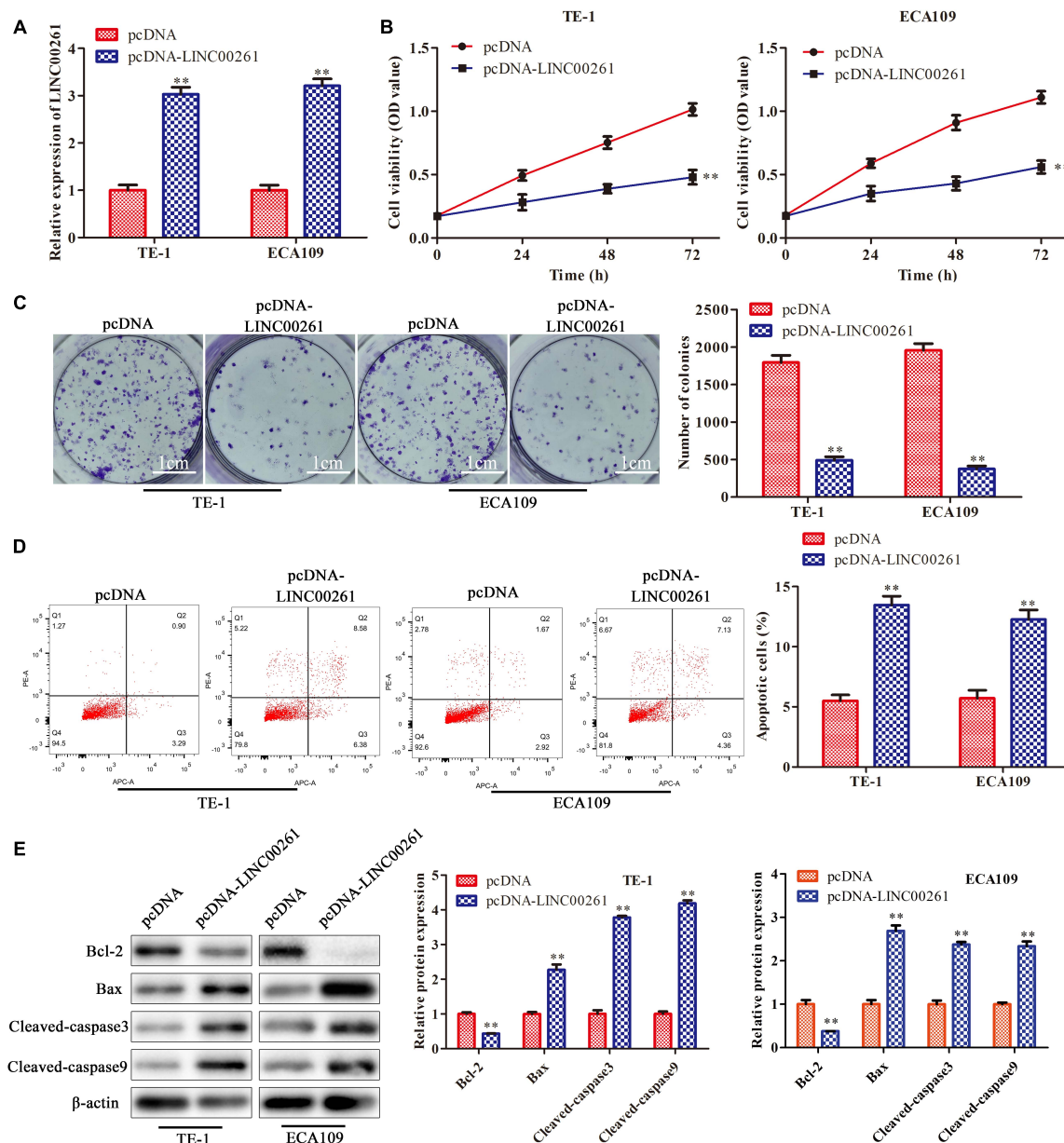


FIGURE 2 | Overexpression of LINC00261 inhibits the proliferation and promotes apoptosis of ESCC cells. TE-1 and ECA109 cells were transfected with pcDNA-LINC00261 and pcDNA. **(A)** The expression of LINC00261 detected by RT-qPCR. **(B)** The proliferation assessed by CCK-8 assay. **(C)** The proliferation measured by clone formation assay. **(D)** The apoptotic cell detected by flow cytometry assay. **(E)** The apoptosis-related protein detected by western blot in TE-1 and ECA109 cells. ** $P < 0.01$ compared with the corresponding control group.

resistance of ESCC cells. RT-qPCR results showed that miR-545-3p expression in TE-1/DDP (ECA109/DDP) cells was vastly higher than that in TE-1 (ECA109) cells (Figure 5D). And miR-545-3p mimic promoted the expression of miR-545-3p whether in TE-1/DDP and ECA109/DDP cells (Figure 5E). Moreover, the CCK-8 assay showed that DDP inhibited cell proliferation in TE-1/DDP and ECA109/DDP cells dose-relatedly, overexpression of miR-545-3p significantly promoted the growth of DDP-supplemented cells compared with the control group (Figure 5F). Furthermore, flow cytometry assay revealed that overexpression

of miR-545-3p decreased the apoptosis of TE-1/DDP and ECA109/DDP cells as compared with the pcDNA (Figure 5G).

MT1M Is a Target Gene of MiR-545-3p

To study the downstream functional genes of miR-545-3p, the Bioinformatics website was used to predict that MT1M might be a target gene of miR-545-3p (Figure 6A), and there was a binding site between the MT1M sequence and miR-545-3p sequence (Figure 6B). Luciferase reporter analysis showed a significant reduction in the luciferase activity of the

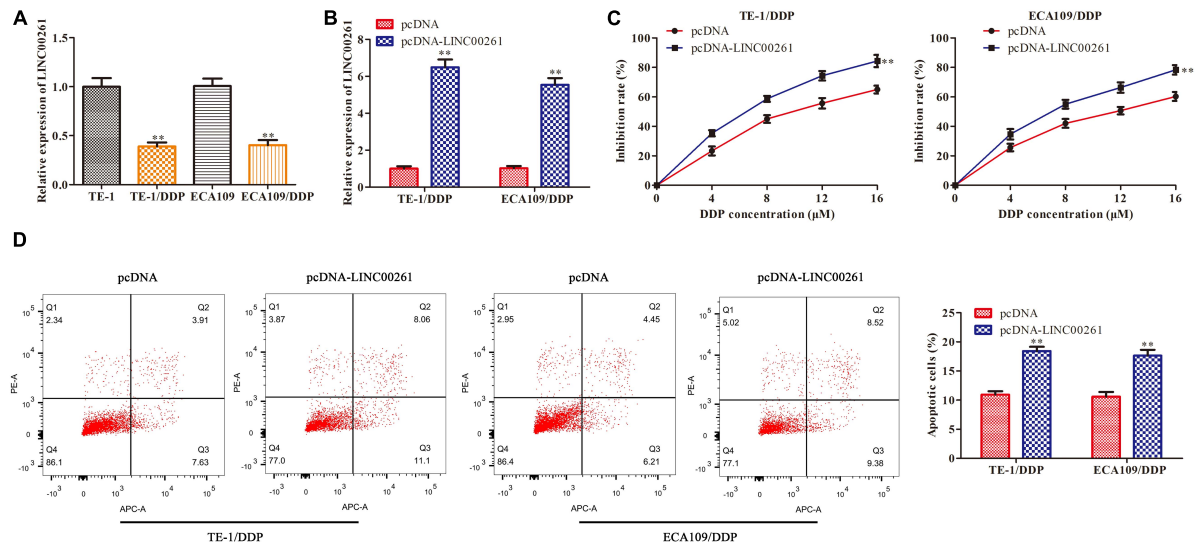


FIGURE 3 | Overexpression of LINC00261 suppresses DDP resistance in ESCC cells. We constructed the DDP-resistant cells line (TE-1/DDP and ECA109/DDP). TE-1/DDP and ECA109/DDP were transfected with pcDNA-LINC00261 and pcDNA. **(A)** The expression of LINC00261 in TE-1, TE-1/DDP, ECA109, and ECA109/DDP cells. **(B)** The expression of LINC00261. **(C)** The proliferation inhibition rate assessed by CCK-8 assay. **(D)** The apoptotic cell detected by flow cytometry assay. ** $P < 0.01$ compared with the corresponding control group.

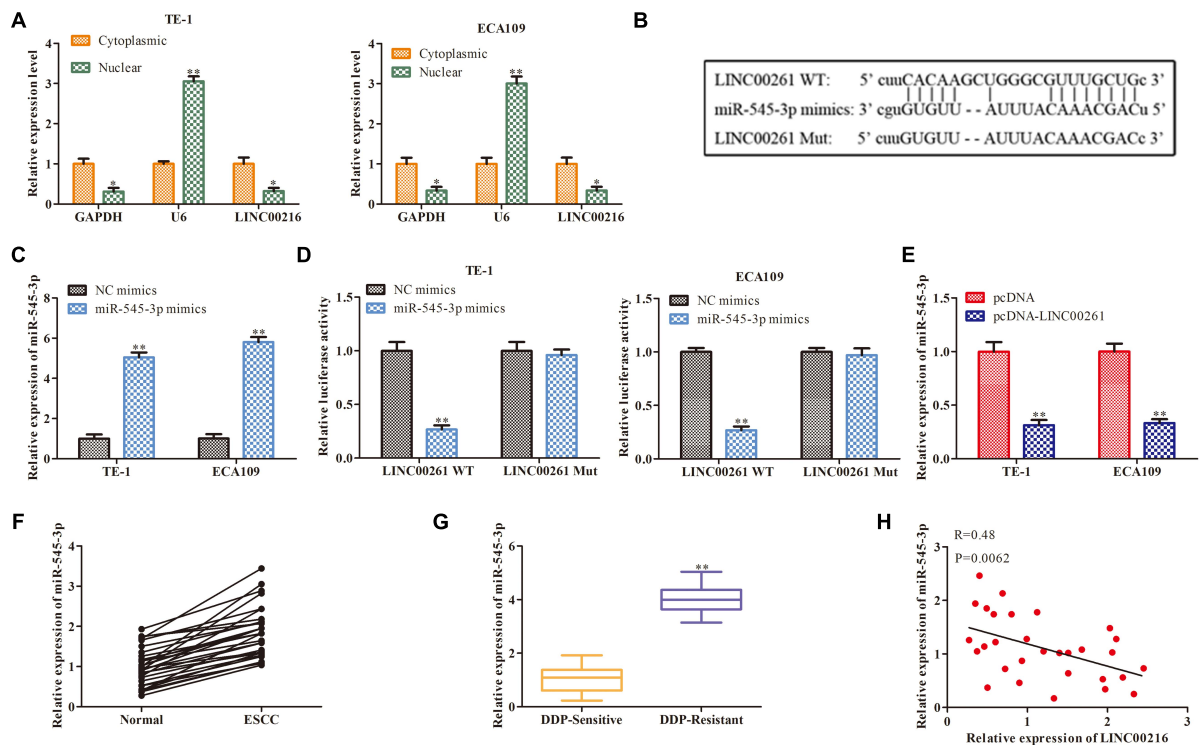
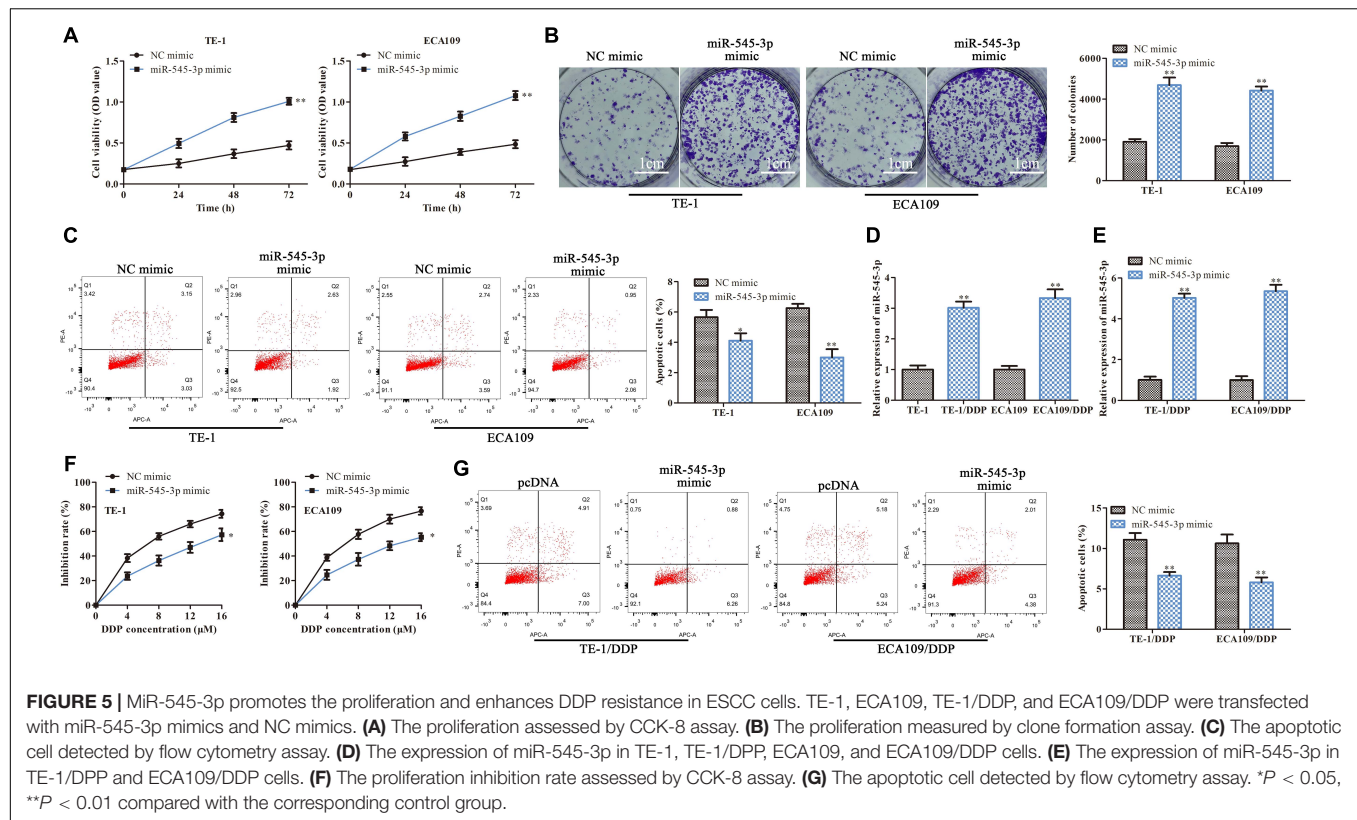


FIGURE 4 | LINC00261 functions as a molecular sponge for miR-545-3p. **(A)** The location of NEAT1. **(B)** The binding sites between LINC00261 and miR-545-3p predicted by Bioinformatics websites. **(C)** The mRNA level of miR-545-3p in NC-mimics group and miR-545-3p mimics group. **(D)** The relationship between LINC00261 and miR-545-3p verified by luciferase reporter assay. **(E)** The mRNA level of miR-545-3p in pcDNA group and pcDNA-LINC00261 group. **(F)** The expression of miR-545-3p in ESCC tissues and adjacent tissues. **(G)** The expression of miR-545-3p in DDP-sensitive and DDP-resistant ESCC patients. **(H)** Pearson's correlation analysis demonstrated the correlation of LINC00261 expression with miR-545-3p. * $P < 0.05$, ** $P < 0.01$ compared with the corresponding control group.



3'UTR region of MT1M when the cells were co-transfected with MT1M WT and miR-545-3p mimics. However, there was no notable difference in luciferase activity of MT1M Mut between the miR-545-3p mimics group and the control group (Figure 6C). In addition, we found that the protein and mRNA levels of MT1M were significantly downregulated in the miR-545-3p mimic group compared with the NC mimics group (Figures 6D,E). Thereafter, we detect the relationship between LINC00261 and MT1M. RT-qPCR and western blot analysis showed that overexpression of LINC00261 upregulated MT1M expression (Figures 6F,G). And MT1M expression was downregulated in ESCC tissues compared to adjacent tissues (Figure 6H). Interestingly, the expression of MT1M was notably downregulated in DDP-resistant ESCC patients compared with DDP-sensitive ESCC patients (Figure 6I). Furthermore, correlation analysis confirmed a positive correlation between LINC00261 and MT1M (Figure 6J), while a negative correlation between miR-545-3p and MT1M (Figure 6K). These results demonstrated that MT1M is a downstream target gene of miR-545-3p.

LINC00261 Inhibits ESCC Progression and DDP Resistance by MiR-545-3p/MT1M Axis

Finally, attempts were made to determine whether LINC00261-mediated effects were indeed through miR-545-3p/MT1M axis, MT1M, miR-545-3p, and their corresponding control were used to transfect the stable overexpression

LINC00261 cell line (ECA109/pcDNA-LINC00261). The transfection efficiency was measured by RT-qPCR and the result was showed in Figure 7A. CCK-8 and clone formation assay suggested that overexpression of MT1M partly reversed the positive effects of miR-545-3p mimics on the proliferation in ECA109/pcDNA-LINC00261 cells (Figures 7B,C). Compared with the miR-545-3p mimics group, increased apoptotic cells were detected in the miR-545-3p mimics + MT1M group (Figure 7D). Additionally, overexpression of MT1M reversed the effects of miR-545-3p mimics on the growth and the apoptosis in DDP-supplemented ECA109/pcDNA-LINC00261 cells (Figures 7E,F).

DISCUSSION

In the current study, LINC00261 expression decreased in ESCC tissues and ESCC cells. It was also found that overexpression of LINC00261 inhibited cell proliferation and promoted cancer cell apoptosis. Further, LINC00261 could suppressed the DDP resistance of ESCC and it participate in regulation through miR-545-3p/MT1M axis. DDP is a common clinical chemotherapy drug, which induces apoptosis of G2 phase cells to achieve the killing effect on malignant tumor cells (Ferreira et al., 2016). It is widely used in the treatment of a variety of tumors including ESCC. However, low-concentration DDP is very easy to cause drug resistance, which limits its wide clinical application. At the same time, DDP-resistant also severely affects the actual curative effect of DDP, and eventually causes

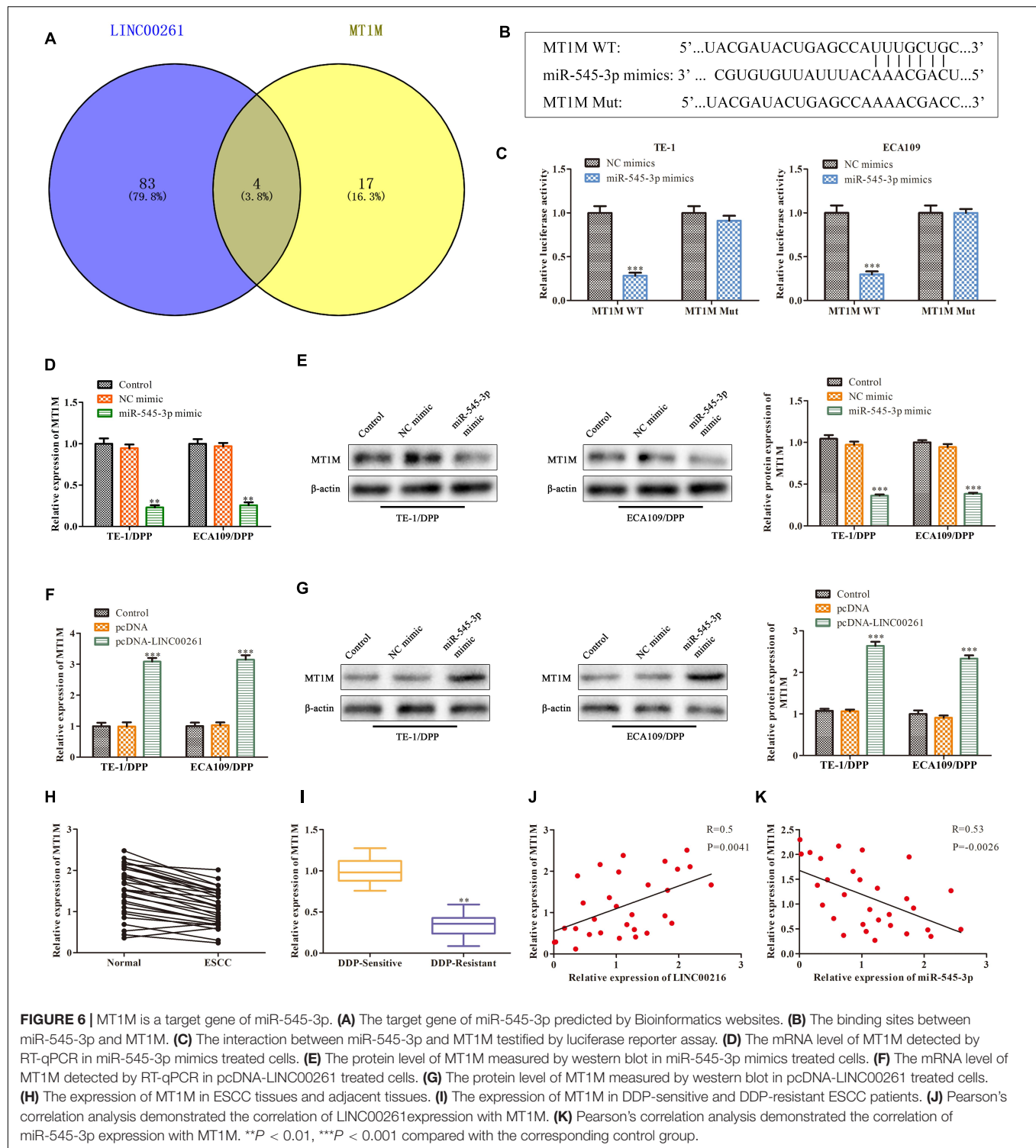
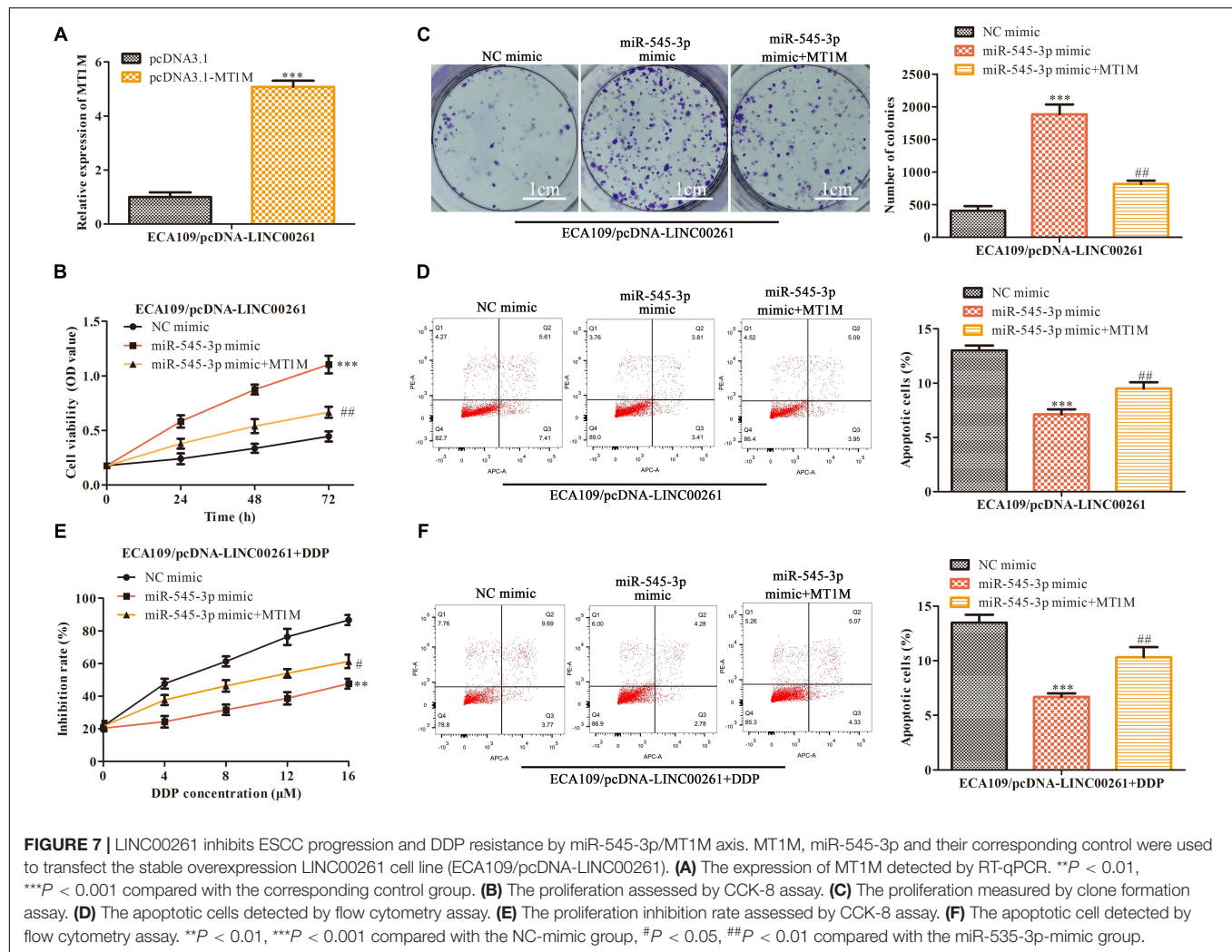


FIGURE 6 | MT1M is a target gene of miR-545-3p. **(A)** The target gene of miR-545-3p predicted by Bioinformatics websites. **(B)** The binding sites between miR-545-3p and MT1M. **(C)** The interaction between miR-545-3p and MT1M testified by luciferase reporter assay. **(D)** The mRNA level of MT1M detected by RT-qPCR in miR-545-3p mimics treated cells. **(E)** The protein level of MT1M measured by western blot in miR-545-3p mimics treated cells. **(F)** The mRNA level of MT1M detected by RT-qPCR in pcDNA-LINC00261 treated cells. **(G)** The protein level of MT1M measured by western blot in pcDNA-LINC00261 treated cells. **(H)** The expression of MT1M in ESCC tissues and adjacent tissues. **(I)** The expression of MT1M in DDP-sensitive and DDP-resistant ESCC patients. **(J)** Pearson's correlation analysis demonstrated the correlation of LINC00261 expression with MT1M. **(K)** Pearson's correlation analysis demonstrated the correlation of miR-545-3p expression with MT1M. ** $P < 0.01$, *** $P < 0.001$ compared with the corresponding control group.

recurrence of ESCC patients after postoperative chemotherapy, leading to chemotherapy failure (Sharma et al., 2012). Therefore, DDP resistance has become an important factor that seriously affects the prognosis of patients with ESCC. At present, the mechanism of DDP-resistance in ESCC has not been fully explored. Hence, a better understanding of the molecular

mechanism of cisplatin resistance in ESCC is needed to improve the prognosis.

Recent studies have revealed that certain lncRNAs are involved in drug resistance (Song et al., 2019; Tian et al., 2019; Wu et al., 2019). Furthermore, the gene LINC00261 was determined by comparing the expression of lncRNAs in ESCC and adjacent



tissues. Interestingly, lower levels of LINC00261 were also observed in DDP-resistant ESCC patients compared with DDP-sensitive ESCC patients. In view of these findings, LINC00261 was first confirmed to exert a major role in the formation of cisplatin resistance.

The previous study has revealed that lncRNAs contribute to transcriptional and posttranscriptional regulation in ESCC. For instance, Yao et al. (2019) found that lncRNA MALAT1 was significantly upregulated in the ESCC cells, and MALAT1 increased the stemness of ESCC by enhancing YAP transcriptional activity. The progression of DDP-resistant in tumors was related to abnormal expression of lncRNA. For example, overexpression of FOXD2-AS1 enhanced DDP-resistance in ESCC tissues and cells, and silencing FOXD2-AS1 improved DDP-resistance in ESCC (Liu H. et al., 2020). LINC00261 acts as a tumor suppressor gene in many cancers, LINC00261 suppresses the growth and metastasis of liver cancer, prostate cancer, and pancreatic cancer (Guo et al., 2020; Li Y. et al., 2020; Liu et al., 2020). It has been stated in the results that LINC00261 is the candidate gene screened in our previous experiments. Furthermore, overexpression of

LINC00261 relieves DDP-resistance of colon cancer cells by increasing cell apoptosis and inhibiting proliferation (Wang et al., 2017). All these reports demonstrated that LINC00261 could be a potential target for the treatment of cancer. Our study showed that LINC00261 was down-regulated in the ESCC tissues and cells, as well as in patients with ESCC that are resistant to DDP. Additionally, patients with higher expression of LINC00261 had a longer overall survival time. Further experiments revealed that overexpression of LINC00261 remarkably inhibited the proliferation, DDP-resistant, and promoted apoptosis of ESCC cells. These results further support the idea of that LINC00261 may be a key therapeutic target for ESCC.

Increasing reports demonstrated that lncRNAs took effects on tumorigenesis by bonding with specific miRNA. In order to dig further and find the combined miRNA, a series of follow-up studies will be carried out. In this study, LINC00261 was mainly located in the cytoplasm of ESCC cells by subcellular separation assay, illustrating that LINC00261 might modulate its downstream gene expression after transcription. Bioinformatics websites predicted the target gene of LINC00261 and identified

miR-545-3p which has been reported to exert major roles in multiples cancers, such as non-small-cell lung cancer cells (Li H. et al., 2020), hepatocellular carcinoma (Changjun et al., 2018), and laryngeal cancer (Cui et al., 2019). Our present study verified that LINC00261 served as a ceRNA for miR-545-3p and negatively regulated miR-545-3p expression. In addition, miR-545-3p expression was greatly increased in ESCC tissues and cells, as well as in patients with ESCC that are resistant to DDP. And miR-545-3p promoted the proliferation and enhanced DDP resistance in ESCC cells. These results are in line with those of previous studies.

Thereafter, we further explored the mechanisms of miR-545-3p on ESCC progression. Bioinformatics websites predicted the target gene of miR-545-3p, identified MT1M. MT1M is a cysteine-enriched small molecule protein, belonging to the metallothionein (MT-1) family. MTs are involved in the regulation of tumor cell growth, angiogenesis, metastasis, and drug resistance, and MTs family members have different anti-cancer or anti-cancer effects in different types of tumors (Si and Lang, 2018). In hepatocellular carcinoma, the low expression of MT1M is positively correlated with poor prognosis, suggesting that MT1M plays a tumor-suppressive role in hepatocellular carcinoma. However, there are few reports on the function of this family of genes in ESCC. In this study, MT1M was downregulated in ESCC tissues and cells, as well as in patients with ESCC that are resistant to DDP, and was positively correlated with LINC00261 whereas was negatively correlated with miR-545-3p. And rescue experiments demonstrated that MT1M overexpression reversed that miR-545-3p mimic-induced positive function on the proliferation and DDP-resistant in ESCC cells. This finding fills the gap in the molecular regulation mechanism of MT1M in ESCC and is helpful to further improve the prognostic treatment of ESCC.

In summary, the findings demonstrated a potential therapeutic target for ESCC and found the molecular mechanism

of action. LINC00261 regulated the proliferation and apoptosis of ESCC, further suppressed the DDP resistance of ESCC by miR-545-3p/MT1M axis.

DATA AVAILABILITY STATEMENT

The raw data supporting the conclusions of this article will be made available by the authors, without undue reservation.

ETHICS STATEMENT

The studies involving human participants were reviewed and approved by the Ethics Committee of Jiangsu Cancer Hospital. The patients/participants provided their written informed consent to participate in this study.

AUTHOR CONTRIBUTIONS

LW, XJ, and YL drafted the manuscript, conceived and designed the study, and accomplished the revision of manuscript for important intellectual content. XW performed the acquisition of data. PY performed the analysis and interpretation of data. LW and YL obtained funding. All authors read and approved the final manuscript.

FUNDING

This work was supported by the grants from Jiangsu Preventive Medicine Association Project (No. Y2018091), Jiangsu Provincial Medical Youth Talent (No. QNRC2016658), Jiangsu Cancer Hospital Project (No. ZQ201107), and Jiangsu Commission of Health Project (No. H2017036).

REFERENCES

- Adenis, A., Robb, W. B., and Mariette, C. (2015). Esophageal carcinoma. *N. Engl. J. Med.* 372:1471.
- Bray, F., Ferlay, J., Soerjomataram, I., Siegel, R. L., Torre, L. A., and Jemal, A. (2018). Global cancer statistics 2018: GLOBOCAN estimates of incidence and mortality worldwide for 36 cancers in 185 countries. *CA Cancer J. Clin.* 68, 394–424. doi: 10.3322/caac.21492
- Changjun, L., Feizhou, H., Dezheng, P., Zhao, L., and Xianhai, M. (2018). MiR-545-3p/MT1M axis regulates cell proliferation, invasion and migration in hepatocellular carcinoma. *Biomed. Pharmacother.* 108, 347–354. doi: 10.1016/j.biopha.2018.09.009
- Chen, D., Chen, T., Guo, Y., Wang, C., Dong, L., and Lu, C. (2020). Platycodin D (PD) regulates LncRNA-XIST/miR-335 axis to slow down bladder cancer progression in vitro and in vivo. *Exp. Cell Res.* 396:112281. doi: 10.1016/j.yexcr.2020.112281
- Chen, W., Zheng, R., Baade, P. D., Zhang, S., Zeng, H., Bray, F., et al. (2016). Cancer statistics in China, 2015. *CA Cancer J. Clin.* 66, 115–132. doi: 10.3322/caac.21338
- Chen, Z., Chen, X., Chen, P., Yu, S., Nie, F., Lu, B., et al. (2017). Long non-coding RNA SNHG20 promotes non-small cell lung cancer cell proliferation and migration by epigenetically silencing of P21 expression. *Cell Death Dis.* 8:e3092. doi: 10.1038/cddis.2017.484
- Cheng, J., Meng, J., Zhu, L., and Peng, Y. (2020). Exosomal noncoding RNAs in Glioma: biological functions and potential clinical applications. *Mol. Cancer* 19:66.
- Cui, X., Xiao, D., Cui, Y., and Wang, X. (2019). Exosomes-derived long non-coding RNA HOTAIR reduces laryngeal cancer radiosensitivity by regulating microRNA-454-3p/E2F2 Axis. *Oncotargets Ther.* 12, 10827–10839. doi: 10.2147/ott.s224881
- Ferreira, J. A., Peixoto, A., Neves, M., Gaiteiro, C., Reis, C. A., Assaraf, Y. G., et al. (2016). Mechanisms of cisplatin resistance and targeting of cancer stem cells: Adding glycosylation to the equation. *Drug Resist. Updat.* 24, 34–54. doi: 10.1016/j.drug.2015.11.003
- Gao, J., Dai, C., Yu, X., Yin, X. B., and Zhou, F. (2020). Long noncoding RNA LINC00324 exerts protumorigenic effects on liver cancer stem cells by upregulating fas ligand via PU box binding protein. *FASEB J.* 34, 5800–5817. doi: 10.1096/fj.201902705rr
- Geisler, S., and Coller, J. (2013). RNA in unexpected places: long non-coding RNA functions in diverse cellular contexts. *Nat. Rev. Mol. Cell Biol.* 14, 699–712. doi: 10.1038/nrm3679

- Guo, C., Shi, H., Shang, Y., Zhang, Y., Cui, J., and Yu, H. (2020). LncRNA LINC00261 overexpression suppresses the growth and metastasis of lung cancer via regulating miR-1269a/FOXO1 axis. *Cancer Cell Int.* 20:275.
- Jung, G., Hernandez-Illan, E., Moreira, L., Balaguer, F., and Goel, A. (2020). Epigenetics of colorectal cancer: biomarker and therapeutic potential. *Nat. Rev. Gastroenterol. Hepatol.* 17, 111–130. doi: 10.1038/s41575-019-0230-y
- Li, H., Liu, F., and Qin, W. (2020). Circ_0072083 interference enhances growth-inhibiting effects of cisplatin in non-small-cell lung cancer cells via miR-545-3p/CBL1 axis. *Cancer Cell Int.* 20:78.
- Li, Y., Li, H., and Wei, X. (2020). Long noncoding RNA LINC00261 suppresses prostate cancer tumorigenesis through upregulation of GATA6-mediated DKK3. *Cancer Cell Int.* 20:474.
- Liang, M., Pan, Z., Yu, F., and Chen, C. (2020). Long noncoding RNA SNHG12 suppresses esophageal squamous cell carcinoma progression through competing endogenous RNA networks. *Clin. Transl. Oncol.* 22, 1786–1795. doi: 10.1007/s12094-020-02317-7
- Lin, K., Jiang, H., Zhuang, S. S., Qin, Y. S., Qiu, G. D., She, Y. Q., et al. (2019). Long noncoding RNA LINC00261 induces chemosensitization to 5-fluorouracil by mediating methylation-dependent repression of DPYD in human esophageal cancer. *FASEB J.* 33, 1972–1988. doi: 10.1096/fj.201800759r
- Liu, H., Zhang, J., Luo, X., Zeng, M., Xu, L., Zhang, Q., et al. (2020). Overexpression of the Long Noncoding RNA FOXD2-AS1 promotes cisplatin resistance in esophageal squamous cell carcinoma through the miR-195/Akt/mTOR Axis. *Oncol. Res.* 28, 65–73. doi: 10.3727/096504019x15656904013079
- Liu, S., Zheng, Y., Zhang, Y., Zhang, J., Xie, F., Guo, S., et al. (2020). Methylation-mediated LINC00261 suppresses pancreatic cancer progression by epigenetically inhibiting c-Myc transcription. *Theranostics* 10, 10634–10651. doi: 10.7150/tno.44278
- Lou, Y., Yu, Y., Xu, X., Zhou, S., Shen, H., Fan, T., et al. (2019). Long non-coding RNA LUCAT1 promotes tumorigenesis by inhibiting ANXA2 phosphorylation in hepatocellular carcinoma. *J. Cell Mol. Med.* 23, 1873–1884. doi: 10.1111/jcmm.14088
- Luqmani, Y. A. (2005). Mechanisms of drug resistance in cancer chemotherapy. *Med. Princ. Pract.* 14, 35–48.
- Ohashi, S., Miyamoto, S., Kikuchi, O., Goto, T., Amanuma, Y., and Muto, M. (2015). Recent advances from basic and clinical studies of Esophageal Squamous Cell Carcinoma. *Gastroenterology* 149, 1700–1715. doi: 10.1053/j.gastro.2015.08.054
- Okugawa, Y., Grady, W. M., and Goel, A. (2015). Epigenetic alterations in colorectal cancer: emerging biomarkers. *Gastroenterology* 149, 1204–1225. doi: 10.1053/j.gastro.2015.07.011
- Sharma, S., Santiskulvong, C., Bentolila, L. A., Rao, J., Dorigo, O., and Gimzewski, J. K. (2012). Correlative nanomechanical profiling with super-resolution F-actin imaging reveals novel insights into mechanisms of cisplatin resistance in ovarian cancer cells. *Nanomedicine* 8, 757–766. doi: 10.1016/j.nano.2011.09.015
- Si, M., and Lang, J. (2018). The roles of metallothioneins in carcinogenesis. *J. Hematol. Oncol.* 11:107.
- Song, L., Zhou, Z., Gan, Y., Li, P., Xu, Y., Zhang, Z., et al. (2019). Long noncoding RNA OIP5-AS1 causes cisplatin resistance in osteosarcoma through inducing the LPAATbeta/PI3K/AKT/mTOR signaling pathway by sponging the miR-340-5p. *J. Cell Biochem.* 120, 9656–9666. doi: 10.1002/jcb.28244
- Tian, L. J., Wu, Y. P., Wang, D., Zhou, Z. H., Xue, S. B., Zhang, D. Y., et al. (2019). Upregulation of Long Noncoding RNA (lncRNA) X-Inactive Specific Transcript (XIST) is associated with Cisplatin resistance in Non-Small Cell Lung Cancer (NSCLC) by downregulating microRNA-144-3p. *Med. Sci. Monit.* 25, 8095–8104. doi: 10.12659/msm.916075
- Vadlapatla, R. K., Vadlapudi, A. D., Pal, D., and Mitra, A. K. (2013). Mechanisms of drug resistance in cancer chemotherapy: coordinated role and regulation of efflux transporters and metabolizing enzymes. *Curr. Pharm. Des.* 19, 7126–7140. doi: 10.2174/13816128113199990493
- Wang, G., Feng, B., Niu, Y., Wu, J., Yang, Y., Shen, S., et al. (2020). A novel long noncoding RNA, LOC440173, promotes the progression of esophageal squamous cell carcinoma by modulating the miR-30d-5p/HDAC9 axis and the epithelial-mesenchymal transition. *Mol. Carcinog* 59, 1392–1408. doi: 10.1002/mc.23264
- Wang, Z. K., Yang, L., Wu, L. L., Mao, H., Zhou, Y. H., Zhang, P. F., et al. (2017). Long non-coding RNA LINC00261 sensitizes human colon cancer cells to cisplatin therapy. *Braz. J. Med. Bio. Res.* 51:e6793.
- Wu, J., Chen, H., Ye, M., Wang, B., Zhang, Y., Sheng, J., et al. (2019). Long noncoding RNA HCP5 contributes to cisplatin resistance in human triple-negative breast cancer via regulation of PTEN expression. *Biomed. Pharmacother.* 115:108869. doi: 10.1016/j.biopha.2019.108869
- Xiao, Y., Su, M., Ou, W., Wang, H., Tian, B., Ma, J., et al. (2019). Involvement of noncoding RNAs in epigenetic modifications of esophageal cancer. *Biomed. Pharmacother.* 117:109192. doi: 10.1016/j.biopha.2019.109192
- Yao, Q., Yang, J., Liu, T., Zhang, J., and Zheng, Y. (2019). Long noncoding RNA MALAT1 promotes the stemness of esophageal squamous cell carcinoma by enhancing YAP transcriptional activity. *FEBS Open Bio.* 9, 1392–1402. doi: 10.1002/2211-5463.12676
- Zhang, S. W., Zheng, R. S., Zuo, T. T., Zeng, H. M., Chen, W. Q., and He, J. (2016). [Mortality and survival analysis of esophageal cancer in China]. *Zhonghua Zhong Liu Za Zhi* 38, 709–715.
- Zuo, T. T., Zheng, R. S., Zeng, H. M., Zhang, S. W., Chen, W. Q., and He, J. (2016). [Incidence and trend analysis of esophageal cancer in China]. *Zhonghua Zhong Liu Za Zhi* 38, 703–708.

Conflict of Interest: The authors declare that the research was conducted in the absence of any commercial or financial relationships that could be construed as a potential conflict of interest.

Copyright © 2021 Wang, Wang, Yan, Liu and Jiang. This is an open-access article distributed under the terms of the Creative Commons Attribution License (CC BY). The use, distribution or reproduction in other forums is permitted, provided the original author(s) and the copyright owner(s) are credited and that the original publication in this journal is cited, in accordance with accepted academic practice. No use, distribution or reproduction is permitted which does not comply with these terms.



Inhibition of miR-185-3p Confers Erlotinib Resistance Through Upregulation of PFKL/MET in Lung Cancers

Ke Li¹, Xinling Zhu² and Conghu Yuan^{3*}

¹ Department of Oncology, Jiangsu Cancer Hospital, Jiangsu Institute of Cancer Research, The Affiliated Cancer Hospital of Nanjing Medical University, Nanjing, China, ² Department of Operating Room, Jiangsu Cancer Hospital, Jiangsu Institute of Cancer Research, The Affiliated Cancer Hospital of Nanjing Medical University, Nanjing, China, ³ Department of Anesthesiology, Yancheng Third People's Hospital, The Yancheng School of Clinical Medicine of Nanjing Medical University, Yancheng, China

OPEN ACCESS

Edited by:

Wei Zhao,
City University of Hong Kong,
Hong Kong

Reviewed by:

Xiaoyun Zhang,
Jiangxi University of Traditional
Chinese Medicine, China
Ling Yu,
The First Affiliated Hospital of Sun
Yat-sen University, China

*Correspondence:

Conghu Yuan
yuanconghura@163.com

Specialty section:

This article was submitted to
Molecular and Cellular Oncology,
a section of the journal
Frontiers in Cell and Developmental
Biology

Received: 08 March 2021

Accepted: 21 June 2021

Published: 21 July 2021

Citation:

Li K, Zhu X and Yuan C (2021)
Inhibition of miR-185-3p Confers
Erlotinib Resistance Through
Upregulation of PFKL/MET in Lung
Cancers.
Front. Cell Dev. Biol. 9:677860.
doi: 10.3389/fcell.2021.677860

Erlotinib (ER), as an epidermal growth factor receptor (EGFR) tyrosine kinase inhibitor (TKI), has a significant therapeutic effect in lung cancers. However, EGFR TKI resistance inevitably occurs after treatment for approximately 12 months, which weakens its antitumor effect. Here, we identified miR-185-3p as a significantly downregulated microRNA responsible for acquired EGFR TKI resistance in cells and patients with lung cancer. qRT-PCR and Western Blot were performed to determine the relative expression of miR-185-3p in ER-resistant tumor tissues and cells. The viability and apoptosis of lung cancer cells were evaluated by Cell Counting Kit-8 (CCK8) assay and flow cytometry, respectively. The binding between miR-185-3p and liver-type phosphofructokinase (PFKL) was verified by dual luciferase assay. It was found that overexpression of miR-185-3p conferred ER sensitivity in lung cancer cell lines. MiR-185-3p was downregulated in ER-resistant lung cancer cells (H1299/ER and A549/ER). MiR-185-3p inhibited proliferation and induced cell apoptosis in ER-resistant cells. Mechanistically, miR-185-3p downregulation contributed to ER resistance through upregulating the PFKL. Moreover, Mesenchymal to epithelial transition (MET) oncoprotein promoted EGFR-TKI resistance by regulating miR-185-3p and PFKL. These findings revealed a novel mechanism in which downregulation of miR-185-3p may induce overexpression of PFKL and MET and confer ER resistance in lung cells. Combination of PFKL/MET inhibitors and EGFR TKIs could be a rational therapeutic approach for lung cancer patients with EGFR mutation.

Keywords: lung cancer, miR-185-3p, PFKL, ER-resistance, tyrosine kinase inhibitor

INTRODUCTION

Lung cancer is a main cause of death worldwide. There are about 2 million newly diagnosed cases of lung cancer and 1.8 million deaths each year (Chen Y. et al., 2020). The 5-years survival rate for patients with non-small-cell lung cancer is no more than 16% (Fu et al., 2020). For lung adenocarcinoma, the median survival period is 4–5 months and the 1-year survival rate is less than 10% (Luo et al., 2019). Clinically, surgery, radiotherapy, and chemotherapy are the main treatments for lung cancers (Pan et al., 2019). Targeted drugs are used in most lung cancer patients who

are diagnosed at advanced stages and infeasible for surgery (Pdq Cancer Information Summaries, 2002; Xia et al., 2018). Erlotinib (ER), an epidermal growth factor receptor (EGFR) tyrosine kinase inhibitor (TKI), is a targeted drug for lung cancer treatment. EGFR TKI has been successfully employed in the clinic, especially in lung cancer patients who have EGFR mutations (Capelletto and Novello, 2012; Suda et al., 2012). However, it is inevitable that the vast majority of patients with ER treatment become resistant within 9–13 months, which weakens its antitumor effect (Camidge et al., 2014; van der Wekken et al., 2016). Therefore, it is necessary to investigate the mechanism of ER resistance in order to elevate the treatment effect of lung cancer patients.

MicroRNAs (miRNAs) play vital roles in lung cancer progression (Hu et al., 2018; Wang et al., 2018). It is well known that miRNAs can affect mRNA level to promote or inhibit tumor progression, such as cell proliferation, apoptosis, epithelial–mesenchymal transition (EMT), and metastasis (Li S. et al., 2018; Lu C. et al., 2018). Abnormal expression of miR-185-3p is found in various tumors. For example, miR-185-3p was suppressed in both colorectal cancer (Zhou C. et al., 2020) and breast cancer (Lu G. et al., 2018). MiR-185-3p inhibited the invasion and metastasis of nasopharyngeal carcinoma *via* WNT2B (Liu et al., 2017). A growing body of evidence showed that miRNAs were associated with ER resistance (Zheng et al., 2020). For example, MiR-124 affects ER resistance in pancreatic cancer by targeting EphA2 (Du et al., 2019). By repressing the level of neurofibromatosis 1, the upregulated expression of miR-641 promotes resistance to ER in non-small-cell lung cancer cells (Chen et al., 2018). Previous studies indicated that miR-185-3p can promote the antitumor effect of other antitumor drugs (Uhr et al., 2019; Zhou C. et al., 2020). However, it is not clear whether miR-185-3p affects the ER resistance in lung cancer. Phosphofructokinase (PFK) is a critical rate-limiting enzyme that promotes the phosphorylation of fructose-6-phosphate to fructose-1,6-bisphosphate, a core step in the pathway of glycolysis (Wegener and Krause, 2002). A recent study found that repression of PFK suppressed cell proliferation and oncogenicity (Yi et al., 2012). There are three subtypes of PFK in human: PFKL (liver), PFKM (muscle), and PFKP (platelet) (Yalcin et al., 2009; Lee et al., 2017). However, the role of PFKL in lung cancer cells is unknown.

Activation of alternative or bypass pathway often causes primary drug resistance. Through activation of bypass pathway, cancer cells can survive and proliferate, even when they are inhibited by the initial driver pathway. The most common bypass pathway is MET amplification, which accounts for 5–10% of cases with acquired resistance to EGFR TKIs (Wu and Shih, 2018). MET gene amplification could activate phosphoinositide 3-kinase (PI3K)–AKT signaling pathway, which is independent of EGFR, through driving Erb-B2 receptor tyrosine kinase 3 (ERBB3) dimerization and signaling. However, the threshold of MET amplification that would induce TKI resistance has not been clarified. Overexpression of hepatocyte growth factor, the ligand of MET oncoprotein, also promotes EGFR TKI resistance. Activation of other alternative pathways, including human epidermal growth factor receptor 2 (HER2) amplification, phosphatidylinositol-4,5-bisphosphate 3-kinase catalytic subunit

alpha (PIK3CA) mutation, v-raf murine sarcoma viral oncogene homolog B1 (BRAF) mutation, and increased expression of the receptor tyrosine kinase AXL, has been reported to promote acquired resistance to EGFR TKIs (Wu and Shih, 2018).

In this study, we aimed to investigate the role of miR-185-3p in lung cancer progression and ER resistance. Lung cancer cell lines were used to evaluate the function of miR-185-3p on lung cancer and the association among miR-185-3p, PFKL, and MET. Our results indicated that PFKL/MET inhibitors in combination with EGFR TKIs could be synergistic in the clinical management of lung cancer.

MATERIALS AND METHODS

Patients

Tumor tissues of ER-resistant ($n = 30$) and ER-sensitive ($n = 30$) lung cancer were obtained from patients who underwent surgery at the Nanjing Medical Hospital. Normal tissues adjacent to cancers were obtained at the same time. All tissues were kept frozen until used. The 5-years overall survival was assessed with ER treatment until death. The collection of clinical samples was approved by the Ethics Committee of Nanjing Medical University. All patients have signed their informed consents.

Cell Culture and Erlotinib Treatment

Human lung cancer cell lines, H1299 and A549, were obtained from Procell Life Science and Technology (Wuhan, China). The cell lines were maintained in RPMI-1640 (Procell Life Science and Technology, Wuhan, China) containing 10% fetal bovine serum (FBS; Procell Life Science and Technology, Wuhan, China), penicillin (100 U/ml), and streptomycin (50 g/ml) in a humidified CO₂ incubator at 37°C. ER-resistant cell lines (H1299/ER, A549/ER) were induced by treatment with ER (HY-50896, MedChemExpress, Shanghai, China) (Wu et al., 2020). Briefly, the ER-resistant cell lines were developed from H1299 and A549 cells by stepwise exposure to increasing concentrations of ER from 2 nM to 10 μ M, and the drug-resistant cell lines H1299/ER and A549/ER were established after 3 months.

Cell Transfection

Si-MET, si-NC, NC mimic, miR-185-3p mimic, Vector, and PFKL plasmid were obtained from RIBOBIO (Guangzhou,

TABLE 1 | Primer sequences for qRT-PCR.

Primer name	(5'–3') Primer sequences
miR-185-3p-Forward	5'-GGGGCTGGCTTTCCTCTG-3'
miR-185-3p-Reverse	5'-GTGGAGTCGGCAATTGCAC-3'
U6-Forward	5'-CTCGCTTCGGCAGCACA-3'
U6-Reverse	5'-AACGCTTCACGAATTTGCGT-3'
PFKL-Forward	5'-GTGGTTGTCCGAGAAAGCTGCGC-3'
PFKL-Reverse	5'-CGGTGCTCGAAATCAGTGTCT-3'
β -actin-Forward	5'-GACCTGACTGACTACCTCATGAAGAT-3'
β -actin-Reverse	5'-GTCACACTTCATGATGGAGTTGAAGG-3'

China). A549/ER and H1299/ER cells were seeded in six-well plates at a density of 6×10^4 and 3.5×10^5 cells/well, respectively. Transfections were performed using Lipofectamine 2000 (Invitrogen, CA, United States) following the manufacturer's instructions.

RNA Extraction and qRT-PCR Assay

Total RNA was extracted from tissues and cell lines using TRIzol reagents (R1030, Applygen, Beijing, China). Reverse transcription was performed by the Applied Biosystems High-Capacity cDNA Reverse Transcription Kit (D1802, Haigene, Harbin, China) for miR-185-3p and Kit (D0401, Haigene, Harbin, China) for PFKL. Quantitative RT-PCR was performed with the ABI PRISM 7500 using TaqMan primers, probes for PFKL, and control gene β -actin (Thermo Fisher) (Zhao et al., 2017). The primers are listed in Table 1. U6 (Zhou C. et al., 2020) and β -actin (Li L. et al., 2018) act as endogenous controls. Samples were analyzed with the comparative CT method, where fold change was calculated from the $\Delta\Delta CT$ value with the formula $2^{-\Delta\Delta CT}$.

Cell Viability

Cell viability was assessed with CCK8 kit (HY-K0301, MedChemExpress, Shanghai, China). A549 and H1299 cells were cultured at a density of 10^4 /well. Followed by incubating with 10 μ l CCK8 for 1–4 h. The light absorbance was measured by GloMax System (Promega, WI, United States) at 450 nm wavelength (Chen C. et al., 2020). The percentage of growth was determined and compared to that of the untreated controls.

Apoptosis Detection

The apoptotic rate of lung cancer cells was evaluated by Annexin V-fluorescein isothiocyanate (FITC)/propidium iodide (PI) Apoptosis Detection Kit (40302ES20, Yeasen, Shanghai, China) via flow cytometry. A549/ER and H1299/ER cells were seeded in six-well plates at a density of 6×10^4 and 3.5×10^5 cells/well, respectively. When cell confluence reached 80%, cells were harvested, followed by staining with 10 μ l of Annexin V-FITC and PI. Then, cells were analyzed by a flow cytometer (BD, New Jersey, United States) (Wang et al., 2020).

Western Blot

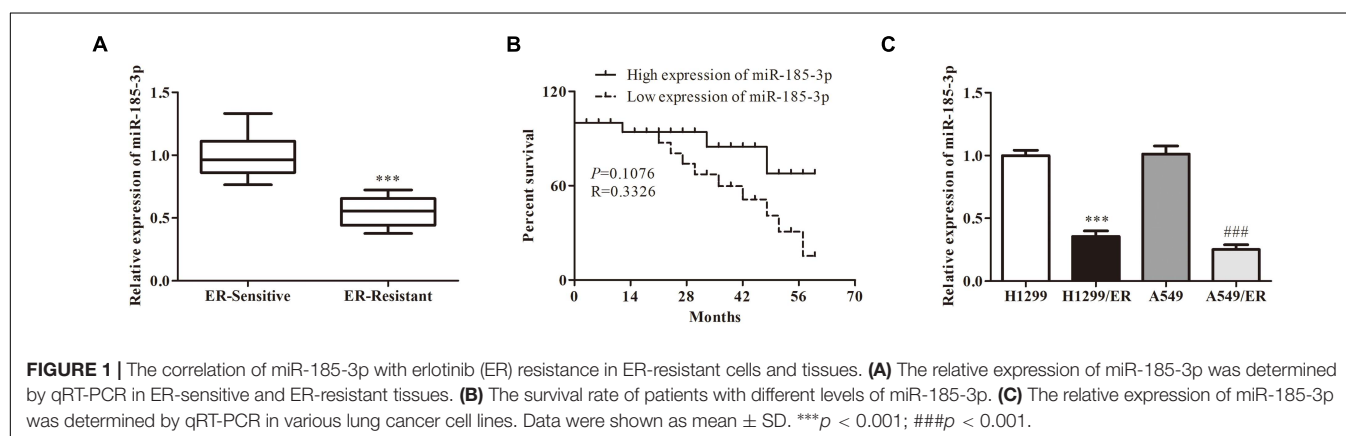
Tissues or cells were washed with phosphate buffered saline (PBS) three times and lysed in radioimmunoprecipitation assay (RIPA) lysis buffer (Cell Signaling Technology, Shanghai, China), containing both protease and phosphatase inhibitors (APExBIO, Houston, United States). Pierce bicinchoninic acid (BCA) protein assays (Thermo Scientific, United States) were used to determine protein concentrations. Protein was resolved on 10% sodium dodecyl sulfate polyacrylamide gel electrophoresis (SDS-PAGE) gels, transferred onto polyvinylidene fluoride (PVDF) membranes, and blocked at 37°C for 1 h, followed by incubation with primary antibodies: rabbit anti-BAX (1:5,000, ab32503), anti-Bcl-2 (1:1,000, ab59348), anti-Cleaved-caspase3 (1:1,000, ab49822), anti-Cleaved-caspase9 (1:1,000, ab2324), anti-PFKL (1:5,000, ab181064), anti-MET, anti-HER2, anti-AXL, anti-ERBB3, anti-PI3K, and rabbit anti- β -actin (1:2,000, ab8227) at 4°C overnight. The membranes were then re-probed with immunoglobulin G (IgG) (1:2,000, ab6721) antibody. The immune reactive bands were visualized by ECL Prime Western Blotting Detecting Reagent and exposed using a Chemiluminescence Western Blot Scanner (CDIGIT). The integrated density of each band was quantified by ImageJ software (ImageJ Software Inc., United States). Antibodies mentioned above were supplied by Abcam (Cambridge, United Kingdom).

Dual Luciferase Reporter Assay

PFKL-WT (containing the binding sites of miR-185-3p at PFKL 3'-UTR) and PFKL-MUT (mutation of binding sites) were cloned into Luciferase Reporter Vector (AM5795, Invitrogen, CA, United States). PFKL-WT or PFKL-MUT was co-transfected with miR-185-3p mimic into H1299/ER or A549/ER cells. After transfection for 48 h, H1299/ER and A549/ER cells were evaluated using the Reporter Vector System (AM5795, Invitrogen, CA, United States) using a GloMax 20/20 Luminometer (Promega, WI, United States) (Zhang et al., 2020).

RNA Pull-Down Assay

The miR-185-3p mimic, miR-185-3p mock, and their control were labeled with different biotins, Bio-miR-185-3p WT, Bio-miR-185-3p MUT, or Bio-NC. A PureBinding™ RNA-Protein Pull down Kit (P0201, Genesee, Guangzhou, China) was



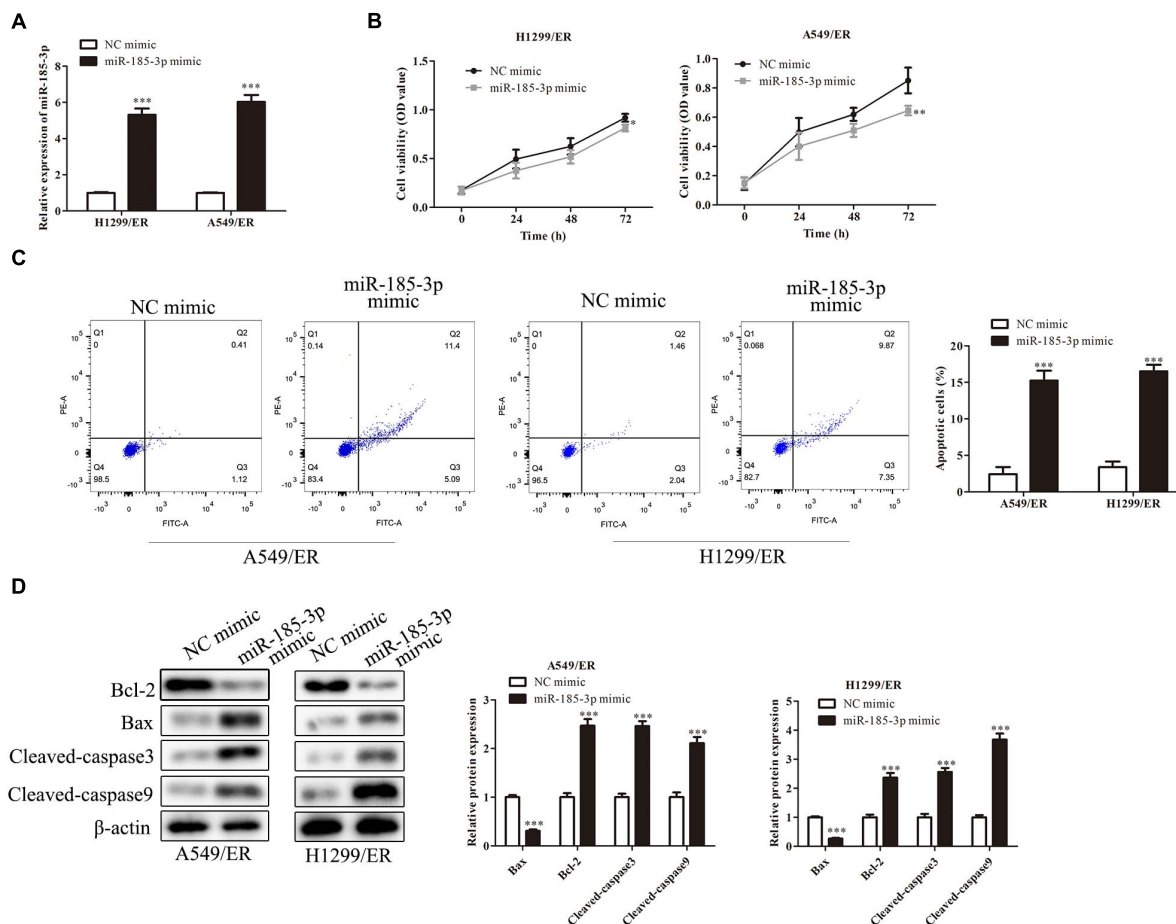


FIGURE 2 | MiR-185-3p suppresses cell proliferation and induces apoptosis. **(A)** The level of miR-185-3p was determined by qRT-PCR in H1299/ER and A549/ER cells. **(B)** Cell viability was determined by Cell Counting Kit-8 (CCK8) assay in H1299/ER and A549/ER cells at 24, 48, and 72 h. **(C)** Cell apoptosis was determined by flow cytometry assay in H1299/ER and A549/ER cells. **(D)** The levels of apoptosis-related proteins Bcl-2, Bax, Cleaved-caspase3, and Cleaved-caspase9 were investigated by Western blot in H1299/ER and A549/ER cells. Data were shown as mean \pm SD. * $p < 0.05$; ** $p < 0.01$; *** $p < 0.001$.

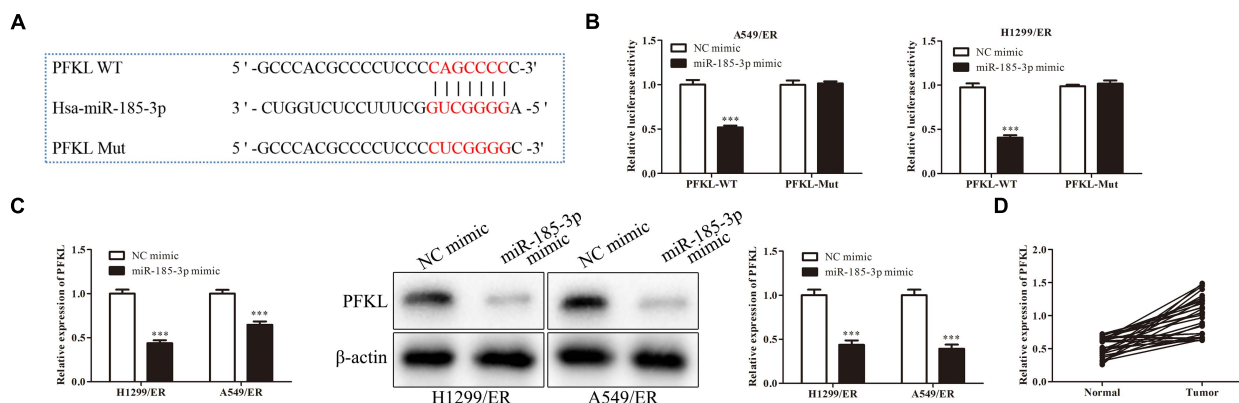
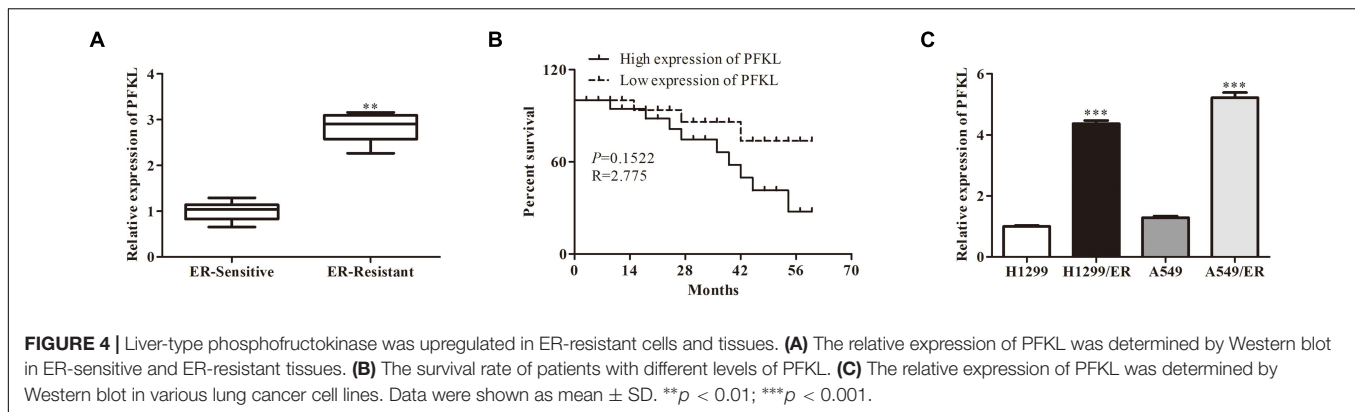


FIGURE 3 | MiR-185-3p targets liver-type phosphofructokinase (PFKL) and downregulates its expression. **(A)** The bioinformatics analysis of miR-185-3p and PFKL. **(B)** MiR-185-3p mimic targeting PFKL was determined by dual luciferase reporter assay. **(C)** The level of PFKL in H1299/ER and A549/ER cells was detected by Western blot. **(D)** Spearman's correlation analysis assessed the PFKL expression in normal and tumor tissues. Data were shown as mean \pm SD. *** $p < 0.001$.



employed to carry out the RNA pull-down assay. Briefly, biotin-labeled miR-185-3p was incubated with streptavidin agarose beads (Invitrogen, CA, United States) for 1 h. Finally, the pulled-down PFKL was detected by qRT-PCR (Wang and Chang, 2020).

Statistical Analysis

The mean \pm SD represents data from three replicates. SPSS version 22.0 software (IBM Corp., NY, United States) was applied for statistical analysis of all data, and Prism version 7.0 (GraphPad) was used to generate graphics. Student's *t*-test was performed for comparison between two groups. One-way ANOVA and Tukey's posttests were used for multiple groups. The level of significance was $p < 0.05$.

RESULTS

The Correlation of miR-185-3p With Erlotinib Resistance in Erlotinib-Resistant Cells and Tissues

To evaluate the role of miR-185-3p in ER-resistant lung cancer patients, the level of miR-185-3p was evaluated by qRT-PCR in ER-resistant and ER-sensitive tissues. The data revealed that miR-185-3p was suppressed in ER-resistant tissues compared with ER-sensitive tissues (Figure 1A). Then, we assessed the relationship between miR-185-3p level in tumor tissues and the survival data. The result demonstrated that the high level of miR-185-3p was associated with a high survival rate (Figure 1B). In the *in vitro* cell models, the level of miR-185-3p in H1299/ER and A549/ER cells was significantly lower than those in H1299 and A549 cells, respectively (Figure 1C). These results suggested that miR-185-3p is downregulated in ER-resistant lung cancer cells and tissues. The level of miR-185-3p is correlated with patients' survival.

MiR-185-3p Suppressed Proliferation and Induced Apoptosis of Lung Cancer Cells

To further verify the role of miR-185-3p on lung cancer cells, we overexpressed miR-185-3p with miR-185-3p mimic in both H1299/ER and A549/ER cells. The level of miR-185-3p increased in both H1299/ER and A549/ER cells treated with miR-185-3p

mimic (Figure 2A). Moreover, the cell viability was significantly suppressed in both H1299/ER and A549/ER cells treated with miR-185-3p mimic for 72 h (Figure 2B). Besides, cell apoptosis was markedly induced by miR-185-3p mimic in H1299/ER and A549/ER cells (Figure 2C). To further verify the level of apoptosis, the level of apoptosis-related proteins was investigated by Western blot. The data demonstrated that Bax was suppressed, whereas Bcl-2, Cleaved-caspase3, and Cleaved-caspase9 were markedly promoted by miR-185-3p mimic (Figure 2D). These results demonstrated that miR-185-3p could suppress cell proliferation and induce cell apoptosis.

MiR-185-3p Targeted Liver-Type Phosphofructokinase and Downregulated Its Expression

Liver-type phosphofructokinase (PFKL) was predicted to be a target of miR-185-3p *via* bioinformatics analysis (Figure 3A) and confirmed by dual luciferase reporter assay. MiR-185-3p mimic and PFKL-WT or PFKL-Mut were co-transfected into H1299 cells. Dual luciferase reporter assay showed that miR-185-3p mimic inhibited the luciferase activity of PFKL-WT in A549 cells (Figure 3B). To further demonstrate the interaction between miR-185-3p and PFKL, the expression of PFKL was examined by qRT-PCR and Western blot. The data revealed that PFKL was markedly inhibited by miR-185-3p mimic in both H1299/ER and A549/ER cells (Figure 3C), demonstrating that miR-185-3p targeted PFKL and downregulated its expression. Next, qRT-PCR was carried out to assess PFKL expression in normal and tumor tissues. An inverse correlation was observed *via* Spearman's correlation analysis, indicating that PFKL level was higher in normal tissues than that in tumor tissues (Figure 3D).

Liver-Type Phosphofructokinase Was Upregulated in Erlotinib-Resistant Cells and Tissues

Analysis with qRT-PCR revealed that PFKL level was higher in ER-resistant tissues than in ER-sensitive tissues (Figure 4A). The low expression of PFKL was associated with high survival rate of patients (Figure 4B). Besides, the levels of PFKL in H1299/ER and A549/ER cells were significantly higher than those in H1299

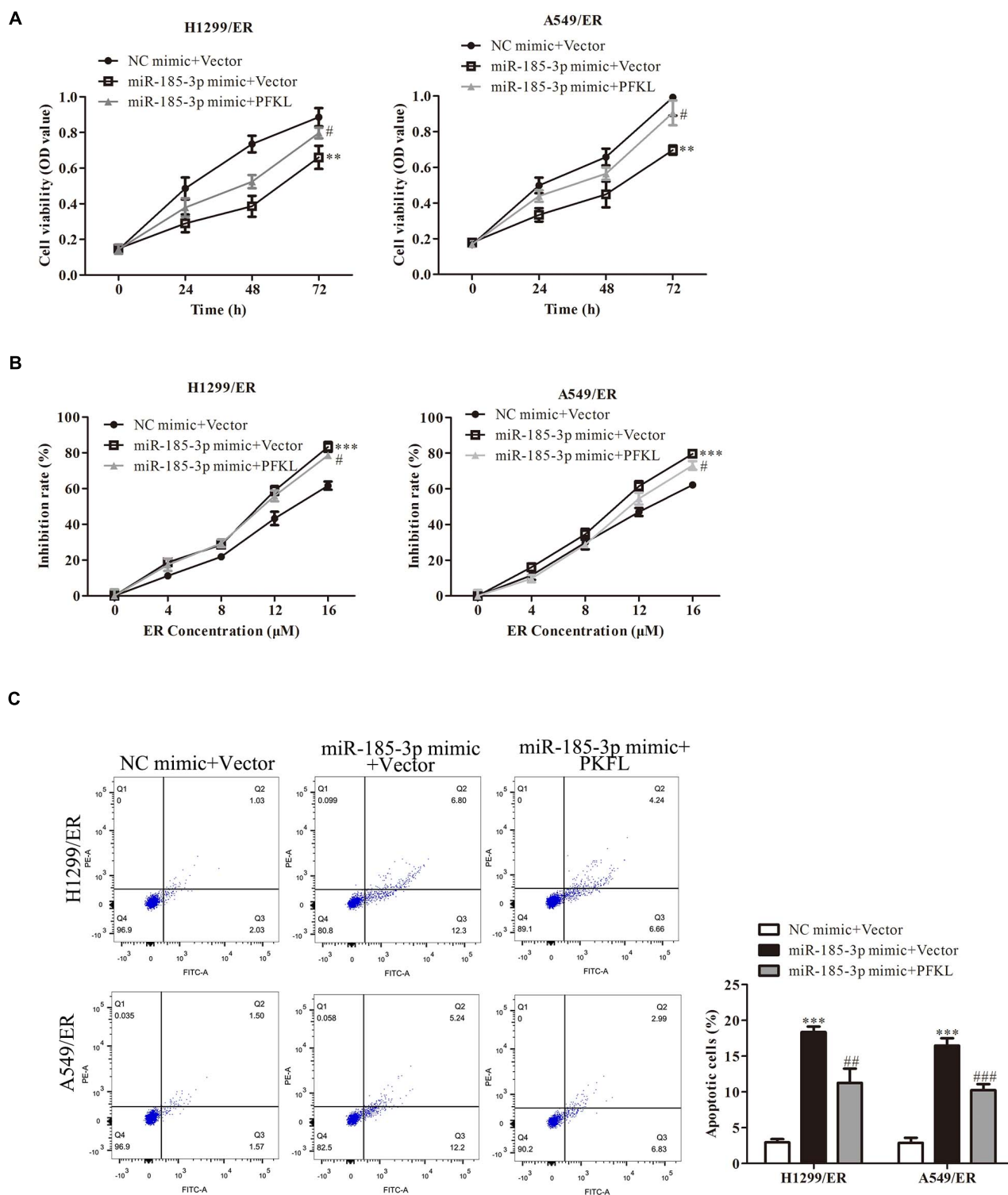


FIGURE 5 | Liver-type phosphofructokinase inhibits tumor cell proliferation and ER resistance. **(A)** Cell viability was determined by CCK8 assay in H1299/ER and A549/ER cells at 24, 48, and 72 h. **(B)** The inhibition rate was determined with various ER concentrations from 0 to 16 μ M in H1299/ER and A549/ER cells. **(C)** Cell apoptosis was determined using flow cytometry assay in H1299/ER and A549/ER cells. Data were shown as mean \pm SD. ** $p < 0.01$; *** $p < 0.001$ vs. NC mimic + Vector, # $p < 0.05$, ### $p < 0.001$ vs. miR-185-3p mimic + Vector.

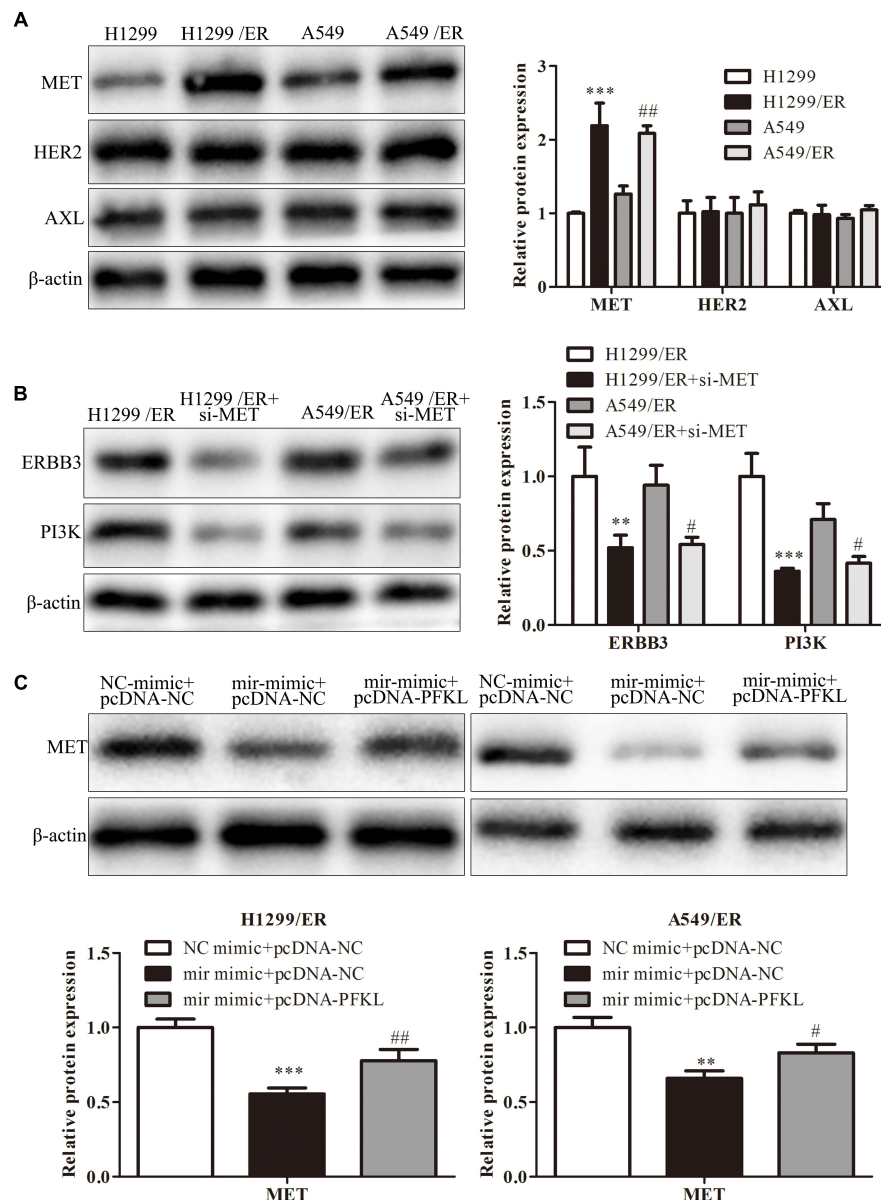


FIGURE 6 | MiR-185-3p/PFKL alleviates ER resistance of lung cancer by inhibiting the epidermal growth factor receptor (EGFR) alternative pathways. **(A)** The levels of MET, human epidermal growth factor receptor 2 (HER2), and AXL were determined by Western blot in H1299, A549, H1299/ER, and A549/ER cells. **(B)** The levels of Erb-B2 receptor tyrosine kinase 3 (ERBB3) and phosphoinositide 3-kinase (PI3K) were determined by Western blot in H1299, A549, H1299/ER, and A549/ER cells with or without si-MET. **(C)** The level of MET was determined by Western blot in H1299/ER and A549/ER cells. Data were shown as mean \pm SD. ** $p < 0.01$; *** $p < 0.001$; # $p < 0.05$; ## $p < 0.01$.

and A549 cells. The above results demonstrated that PFKL was overexpressed in ER-resistant cells (Figure 4C).

MiR-185-3p Downregulated Liver-Type Phosphofructokinase to Inhibit Tumor Cell Proliferation and Erlotinib Resistance

The role of PFKL under miR-185-3p regulation in lung cancer cells was assessed. We co-transfected miR-185-3p mimic and

PFKL plasmids into both H1299/ER and A549/ER cells. The data depicted that cell viability was strikingly suppressed by miR-185-3p mimic, whereas that was reversed by PFKL overexpression (Figure 5A). The cell growth inhibitory rate in both H1299/ER and A549/ER cells increased with increasing ER concentration from 0 to 16 μ M. Moreover, the inhibitory rate of miR-185-3p mimic in both H1299/ER and A549/ER cells was higher than that in cells transfected with NC mimic, whereas that was reversed by PFKL overexpression (Figure 5B). Besides, cell apoptosis was increased by miR-185-3p mimic, whereas it was alleviated

by PFKL overexpression (Figure 5C). These results indicated that miR-185-3p suppressed cell proliferation and induced cell apoptosis by downregulating PFKL.

MiR-185-3p/Liver-Type Phosphofructokinase Alleviates Erlotinib Resistance of Lung Cancer Cells by Inhibiting Epidermal Growth Factor Receptor Alternative Pathway

Erlotinib could stimulate tumor cell to produce resistance by alternative pathways such as MET, HER2, or AXL pathway. Western blot was used to examine the expression of molecules in these pathways. The findings revealed that the level of MET in H1299/ER and A549/ER cells was strikingly higher than that in H1299 and A549 cells, while the level of HER2 and AXL remained unchanged (Figure 6A). These results illuminated that ER resistance might be caused by activation of the MET signaling pathway. Furthermore, the levels of ERBB3 and PI3K were markedly decreased in both H1299/ER and A549/ER cells transfected with si-MET compared with cells transfected with si-NC (Figure 6B), indicating that MET could activate EGFR downstream signaling molecules, such as ERBB3 and PI3K. The MET level of treatment with miR-185-3p mimic in both H1299/ER and A549 cell lines was lower than that of NC mimic, whereas that was reversed by PFKL overexpression. These results demonstrated that miR-185-3p/PFKL could regulate the activation of the MET alternative pathway in ER-resistant lung cancer cells (Figure 6C).

DISCUSSION

The development of lung cancer is a multistep process involved in the accumulation of genetic and epigenetic changes that lead to DNA damage and eventually the conversion of epithelial cells into cancer cells (Asghariazar et al., 2019). Lung cancer has become one of the most common cancers because of lifestyle changes and increased risk factors (Hosseini et al., 2009).

MicroRNAs are short non-coding RNAs that affect the expression of target genes by inhibiting their translation or degrading their messenger RNAs (Yang et al., 2020). There is growing body of evidence indicating that miRNAs play different roles in the progression of lung cancers. MiR-222-3p stimulates the proliferation and represses apoptosis of non-small-cell lung cancer cells *via* repressing p53 upregulated modulator of apoptosis (PUMA) (Chen and Li, 2020). A study conducted by Li and Yuan (2020) revealed that miR-103 was elevated in A549 and H1299 cells and promoted cell growth and EMT and reduced cell apoptosis. On the contrary, miR-330 represses the viability, proliferation, and migration of lung cancer cells (Mohammadi et al., 2020). Another study conducted by Wei et al. (2020) revealed that miR-16 represses the growth and metastasis of lung cancer cells by suppressing Yes-associated protein 1 (YAP1) level. In this study, our data demonstrated that miR-185-3p was

downregulated in lung cancer tissues, repressed cell proliferation, and stimulated cell apoptosis.

Although their definite role in targeted treatment is not yet clear, miRNAs can alter tumor sensitivity to antitumor drugs (Liu et al., 2020). A number of studies have shown that some antitumor drugs exert their antitumor effect *via* affecting miRNAs and their targeted genes. Chikuda et al. (2020) revealed that miR-629-3p is associated with conferring anticancer drug resistance in head and neck cancer. Kaempferol was demonstrated to play an anticancer role, which attenuated oxygen glucose deprivation (OGD)-induced cell damage *via* suppressing miR-15b level stimulated by the PI3K/AKT and Wnt3a/ β -catenin signaling pathways (Li et al., 2020). ER, as an EGFR TKI, was demonstrated to play the anticancer role in cancer treatment. MiR-23a suppression elevated the ER sensitivity of lung cancer stem cells *via* PTEN/PI3K/Akt signaling pathway (Han et al., 2017). miR-223 level was markedly enhanced in HCC827/ER cells, and suppressing miR-223 led to alleviated resistance in HCC827/ER cells (Zhang et al., 2017). On the contrary, our data demonstrated that miR-185-3p was downregulated in ER-resistant lung cancer tissues and cells, and miR-185-3p reduced ER resistance in lung cancer cells.

To investigate the mechanism of miR-185-3p in ER resistance, we identified that PFKL is a putative target of miR-185-3p by bioinformatics analysis and verified by dual luciferase reporter assay. PFKL is one of the subtypes of PFK in human (Lee et al., 2017). In hepatocellular carcinoma (HCC), PFKL was degraded by interaction with A20 and suppressed the progression of HCC (Feng et al., 2020). Iodine-125 irradiation played an anticancer role in HCC by stimulating miR-338/PFKL axis (Zheng et al., 2019). PFKL could be upregulated by TAp73 and then enhance cell proliferation and tumor growth (Li L. et al., 2018). Yang et al. (2016) revealed that PFKL is suppressed by miR-128 and stimulates lung cancer cell growth *in vitro*. Similarly, our data revealed that miR-185-3p targeted PFKL to repress cell proliferation and ER resistance in lung cancer.

In summary, our findings elucidated that miR-185-3p was suppressed and PFKL was elevated in ER-resistant lung cancer tissues and cells. MiR-185-3p repressed the level of PFKL/MET to repress cell proliferation and ER resistance in lung cancer. Therefore, targeting the miR-185-3p/PFKL/MET axis may serve as a potential treatment for ER-resistant lung cancer.

DATA AVAILABILITY STATEMENT

The original contributions presented in the study are included in the article/supplementary material, further inquiries can be directed to the corresponding author.

ETHICS STATEMENT

The studies involving human participants were reviewed and approved by the Ethics Committee of Nanjing Medical

University. The patients/participants provided their written informed consent to participate in this study.

AUTHOR CONTRIBUTIONS

CY conceived the study and obtained the funding. KL and XZ performed the experiments and analyzed the data. All authors

participated in writing and revising the article and approved the final manuscript.

FUNDING

This work was supported by the Six talent peaks in Jiangsu Province (2015-wsw-042).

REFERENCES

- Asghariazar, V., Sakhinia, E., Mansoori, B., Mohammadi, A., and Baradaran, B. (2019). Tumor suppressor microRNAs in lung cancer: an insight to signaling pathways and drug resistance. *J. Cell Biochem.* 120, 19274–19289. doi: 10.1002/jcb.29295
- Camidge, D. R., Pao, W., and Sequist, L. V. (2014). Acquired resistance to TKIs in solid tumours: learning from lung cancer. *Nat. Rev. Clin. Oncol.* 11, 473–481. doi: 10.1038/nrclinonc.2014.104
- Capelletto, E., and Novello, S. (2012). Emerging new agents for the management of patients with non-small cell lung cancer. *Drugs* 72, 37–52. doi: 10.2165/1163028-s0-000000000-00000
- Chen, C., Liu, W. R., Zhang, B., Zhang, L. M., Li, C. G., Liu, C., et al. (2020). LncRNA H19 downregulation confers erlotinib resistance through upregulation of PKM2 and phosphorylation of AKT in EGFR-mutant lung cancers. *Cancer Lett.* 486, 58–70. doi: 10.1016/j.canlet.2020.05.009
- Chen, J., Cui, J. D., Guo, X. T., Cao, X., and Li, Q. (2018). Increased expression of miR-641 contributes to erlotinib resistance in non-small-cell lung cancer cells by targeting NF1. *Cancer Med.* 7, 1394–1403. doi: 10.1002/cam4.1326
- Chen, W., and Li, X. (2020). MiR-222-3p Promotes Cell Proliferation and Inhibits Apoptosis by Targeting PUMA (BBC3) in Non-Small Cell Lung Cancer. *Technol. Cancer Res. Treat.* 19:1533033820922558.
- Chen, Y., Tang, J., Lu, T., and Liu, F. (2020). CAPN1 promotes malignant behavior and erlotinib resistance mediated by phosphorylation of c-Met and PIK3R2 via degrading PTPN1 in lung adenocarcinoma. *Thorac. Cancer* 11, 1848–1860. doi: 10.1111/1759-7714.13465
- Chikuda, J., Otsuka, K., Shimomura, I., Ito, K., Miyazaki, H., Takahashi, R. U., et al. (2020). CD44s Induces miR-629-3p Expression in Association with Cisplatin Resistance in Head and Neck Cancer Cells. *Cancers* 12:856. doi: 10.3390/cancers12040856
- Du, J., He, Y., Wu, W., Li, P., Chen, Y., Hu, Z., et al. (2019). Targeting EphA2 with miR-124 mediates Erlotinib resistance in K-RAS mutated pancreatic cancer. *J. Pharm. Pharmacol.* 71, 196–205. doi: 10.1111/jphp.12941
- Feng, Y., Zhang, Y., Cai, Y., Liu, R., Lu, M., Li, T., et al. (2020). A20 targets PFKL and glycolysis to inhibit the progression of hepatocellular carcinoma. *Cell Death Dis.* 11:89.
- Fu, J., Yuan, J. C., Xiong, R. L., Zhu, T. T., Ni, R., Lou, H. X., et al. (2020). Elevation of FGD5-AS1 contributes to cell progression by improving cisplatin resistance against non-small cell lung cancer cells through regulating miR-140-5p/WEE1 axis. *Gene* 755:144886. doi: 10.1016/j.gene.2020.144886
- Han, Z., Zhou, X., Li, S., Qin, Y., Chen, Y., and Liu, H. (2017). Inhibition of miR-23a increases the sensitivity of lung cancer stem cells to erlotinib through PTEN/PI3K/Akt pathway. *Oncol. Rep.* 38, 3064–3070. doi: 10.3892/or.2017.5938
- Hosseini, M., Naghan, P. A., Karimi, S., SeyedAlinaghi, S., Bahadori, M., Khodadad, K., et al. (2009). Environmental risk factors for lung cancer in Iran: a case-control study. *Int. J. Epidemiol.* 38, 989–996.
- Hu, X., Miao, J., Zhang, M., Wang, X., Wang, Z., Han, J., et al. (2018). miRNA-103a-3p Promotes Human Gastric Cancer Cell Proliferation by Targeting and Suppressing ATF7 *in vitro*. *Mol. Cells* 41, 390–400.
- Lee, J. H., Liu, R., Li, J., Zhang, C., Wang, Y., Cai, Q., et al. (2017). Stabilization of phosphofructokinase 1 platelet isoform by AKT promotes tumorigenesis. *Nat. Commun.* 8:949.
- Li, K., and Yuan, C. (2020). MicroRNA103 modulates tumor progression by targeting KLF7 in non-small cell lung cancer. *Int. J. Mol. Med.* 46, 1013–1028. doi: 10.3892/ijmm.2020.4649
- Li, L., Li, L., Li, W., Chen, T., Zou, B., Zhao, L., et al. (2018). TAp73-induced phosphofructokinase-1 transcription promotes the Warburg effect and enhances cell proliferation. *Nat. Commun.* 9:4683.
- Li, L., Liu, D., Cao, X., Wu, J., Du, G., and Shang, Y. (2020). Kaempferol Regulates miR-15b/Bcl-2/TLR4 to Alleviate OGD-Induced Injury in H9c2 Cells. *Int. Heart J.* 61, 585–594. doi: 10.1536/ihj.19-359
- Li, S., Zhou, J., Wang, Z., Wang, P., Gao, X., and Wang, Y. (2018). Long non-coding RNA GAS5 suppresses triple negative breast cancer progression through inhibition of proliferation and invasion by competitively binding miR-196a-5p. *Biomed. Pharmacother.* 104, 451–457. doi: 10.1016/j.biopha.2018.05.056
- Liu, C., Li, G., Ren, S., Su, Z., Wang, Y., Tian, Y., et al. (2017). miR-185-3p regulates the invasion and metastasis of nasopharyngeal carcinoma by targeting WNT2B *in vitro*. *Oncol. Lett.* 13, 2631–2636. doi: 10.3892/ol.2017.5778
- Liu, Y. R., Wang, P. Y., Xie, N., and Xie, S. Y. (2020). MicroRNAs as Therapeutic Targets for Anticancer Drugs in Lung Cancer Therapy. *Anticancer Agents Med. Chem.* 20, 1883–1894. doi: 10.2174/1871520620666200615133011
- Lu, C., Peng, K., Guo, H., Ren, X., Hu, S., Cai, Y., et al. (2018). miR-18a-5p promotes cell invasion and migration of osteosarcoma by directly targeting IRF2. *Oncol. Lett.* 16, 3150–3156.
- Lu, G., Li, Y., Ma, Y., Lu, J., Chen, Y., Jiang, Q., et al. (2018). Long non-coding RNA LINC00511 contributes to breast cancer tumorigenesis and stemness by inducing the miR-185-3p/E2F1/Nanog axis. *J. Exp. Clin. Cancer Res.* 37:289.
- Luo, Y. H., Luo, L., Wampfler, J. A., Wang, Y., Liu, D., Chen, Y. M., et al. (2019). 5-year overall survival in patients with lung cancer eligible or ineligible for screening according to US Preventive Services Task Force criteria: a prospective, observational cohort study. *Lancet Oncol.* 20, 1098–1108. doi: 10.1016/s1470-2045(19)30329-8
- Mohammadi, A., Mansoori, B., Duijf, P. H. G., Safarzadeh, E., Tebbi, L., Najafi, S., et al. (2020). Restoration of miR-330 expression suppresses lung cancer cell viability, proliferation, and migration. *J. Cell Physiol.* 236, 273–283. doi: 10.1002/jcp.29840
- Pan, X., Chen, Y., Shen, Y., and Tantai, J. (2019). Knockdown of TRIM65 inhibits autophagy and cisplatin resistance in A549/DDP cells by regulating miR-138-5p/ATG7. *Cell Death Dis.* 10:429.
- Pdq Cancer Information Summaries (2002). *Non-Small Cell Lung Cancer Treatment (PDQ(R)): Patient Version*. Bethesda: National Cancer Institute.
- Suda, K., Mizuuchi, H., Maehara, Y., and Mitsudomi, T. (2012). Acquired resistance mechanisms to tyrosine kinase inhibitors in lung cancer with activating epidermal growth factor receptor mutation—diversity, ductility, and destiny. *Cancer Metastasis Rev.* 31, 807–814. doi: 10.1007/s10555-012-9391-7
- Uhr, K., Prager-van der Smitten, W. J. C., Heine, A. A. J., Ozturk, B., van Jaarsveld, M. T. M., Boersma, A. W. M., et al. (2019). MicroRNAs as possible indicators of drug sensitivity in breast cancer cell lines. *PLoS One* 14:e0216400. doi: 10.1371/journal.pone.0216400
- van der Wekken, A. J., Saber, A., Hiltermann, T. J., Kok, K., van den Berg, A., and Groen, H. J. (2016). Resistance mechanisms after tyrosine kinase inhibitors afatinib and crizotinib in non-small cell lung cancer, a review of the literature. *Crit. Rev. Oncol. Hematol.* 100, 107–116. doi: 10.1016/j.critrevonc.2016.01.024
- Wang, X., Gao, X., Tian, J., Zhang, R., Qiao, Y., Hua, X., et al. (2020). LINC00261 inhibits progression of pancreatic cancer by down-regulating miR-23a-3p. *Arch. Biochem. Biophys.* 689:108469. doi: 10.1016/j.abb.2020.108469
- Wang, Y. X., Zhu, H. F., Zhang, Z. Y., Ren, F., and Hu, Y. H. (2018). MiR-384 inhibits the proliferation of colorectal cancer by targeting AKT3. *Cancer Cell Int.* 18:124.
- Wang, Y., and Chang, Q. (2020). MicroRNA miR-212 regulates PDCD4 to attenuate Abeta25-35-induced neurotoxicity via PI3K/AKT signaling pathway

- in Alzheimer's disease. *Biotechnol. Lett.* 42, 1789–1797. doi: 10.1007/s10529-020-02915-z
- Wegener, G., and Krause, U. (2002). Different modes of activating phosphofructokinase, a key regulatory enzyme of glycolysis, in working vertebrate muscle. *Biochem. Soc. Trans.* 30, 264–270. doi: 10.1042/bst0300264
- Wei, J., Jia, A., Ma, L., Wang, Y., Qiu, L., and Xiao, B. (2020). MicroRNA-16 inhibits the proliferation and metastasis of human lung cancer cells by modulating the expression of YAP1. *J. BUON* 25, 862–868.
- Wu, P. F., Gao, W. W., Sun, C. L., Ma, T., and Hao, J. Q. (2020). Suberoylanilide hydroxamic acid overcomes erlotinib-acquired resistance via phosphatase and tensin homolog deleted on chromosome 10-mediated apoptosis in non-small cell lung cancer. *Chin. Med. J.* 133, 1304–1311. doi: 10.1097/cm9.0000000000000823
- Wu, S. G., and Shih, J. Y. (2018). Management of acquired resistance to EGFR TKI-targeted therapy in advanced non-small cell lung cancer. *Mol. Cancer* 17:38.
- Xia, A., Li, H., Li, R., Lu, L., and Wu, X. (2018). Co-treatment with BEZ235 enhances chemosensitivity of A549/DDP cells to cisplatin via inhibition of PI3K/Akt/mTOR signaling and downregulation of ERCC1 expression. *Oncol. Rep.* 40, 2353–2362.
- Yalcin, A., Telang, S., Clem, B., and Chesney, J. (2009). Regulation of glucose metabolism by 6-phosphofructo-2-kinase/fructose-2,6-bisphosphatases in cancer. *Exp. Mol. Pathol.* 86, 174–179. doi: 10.1016/j.yexmp.2009.01.003
- Yang, J., Li, J., Le, Y., Zhou, C., Zhang, S., and Gong, Z. (2016). PFKL/miR-128 axis regulates glycolysis by inhibiting AKT phosphorylation and predicts poor survival in lung cancer. *Am. J. Cancer. Res.* 6, 473–485.
- Yang, X., Wang, B., Chen, W., and Man, X. (2020). MicroRNA-188 inhibits biological activity of lung cancer stem cells through targeting MDK and mediating the Hippo pathway. *Exp. Physiol.* 105, 1360–1372. doi: 10.1113/ep088704
- Yi, W., Clark, P. M., Mason, D. E., Keenan, M. C., Hill, C., Goddard, W. A., et al. (2012). Phosphofructokinase 1 glycosylation regulates cell growth and metabolism. *Science* 337, 975–980. doi: 10.1126/science.1222278
- Zhang, H., Chen, F., He, Y., Yi, L., Ge, C., Shi, X., et al. (2017). Sensitivity of non-small cell lung cancer to erlotinib is regulated by the Notch/miR-223/FBXW7 pathway. *Biosci. Rep.* 37:BSR20160478.
- Zhang, R. L., Aimudula, A., Dai, J. H., and Bao, Y. X. (2020). RASA1 inhibits the progression of renal cell carcinoma by decreasing the expression of miR-223-3p and promoting the expression of FBXW7. *Biosci. Rep.* 40:BSR20194143.
- Zhao, T. F., Jia, H. Z., Zhang, Z. Z., Zhao, X. S., Zou, Y. F., Zhang, W., et al. (2017). LncRNA H19 regulates ID2 expression through competitive binding to hsa-miR-19a/b in acute myelocytic leukemia. *Mol. Med. Rep.* 16, 3687–3693. doi: 10.3892/mmr.2017.7029
- Zheng, J., Luo, J., Zeng, H., Guo, L., and Shao, G. (2019). (125)I suppressed the Warburg effect via regulating miR-338/PFKL axis in hepatocellular carcinoma. *Biomed. Pharmacother.* 119:109402. doi: 10.1016/j.biopha.2019.109402
- Zheng, Y., Song, A., Zhou, Y., Zhong, Y., Zhang, W., Wang, C., et al. (2020). Identification of extracellular vesicles-transported miRNAs in Erlotinib-resistant head and neck squamous cell carcinoma. *J. Cell Commun. Signal* 14, 389–402. doi: 10.1007/s12079-020-00546-7
- Zhou, C., Kong, W., Ju, T., Xie, Q., and Zhai, L. (2020). MiR-185-3p mimic promotes the chemosensitivity of CRC cells via AQP5. *Cancer Biol. Ther.* 21, 790–798. doi: 10.1080/15384047.2020.1761238

Conflict of Interest: The authors declare that the research was conducted in the absence of any commercial or financial relationships that could be construed as a potential conflict of interest.

Copyright © 2021 Li, Zhu and Yuan. This is an open-access article distributed under the terms of the Creative Commons Attribution License (CC BY). The use, distribution or reproduction in other forums is permitted, provided the original author(s) and the copyright owner(s) are credited and that the original publication in this journal is cited, in accordance with accepted academic practice. No use, distribution or reproduction is permitted which does not comply with these terms.



Identification of a Novel Immune Landscape Signature for Predicting Prognosis and Response of Endometrial Carcinoma to Immunotherapy and Chemotherapy

Jinhui Liu^{1†}, Yichun Wang^{2†}, Jie Mei^{3,4†}, Sipei Nie¹ and Yan Zhang^{3*}

OPEN ACCESS

Edited by:

Wei Zhao,
City University of Hong Kong,
Hong Kong

Reviewed by:

Anna Myriam Perrone,
Sant'Orsola-Malpighi Polyclinic, Italy
Danillo G. Augusto,
University of California,
San Francisco, United States
Xiaoli Ma,
Jinan Central Hospital, China

*Correspondence:

Yan Zhang
fuyou2007@126.com

[†]These authors have contributed
equally to this work

Specialty section:

This article was submitted to
Molecular and Cellular Oncology,
a section of the journal
Frontiers in Cell and Developmental
Biology

Received: 24 February 2021

Accepted: 01 July 2021

Published: 23 July 2021

Citation:

Liu J, Wang Y, Mei J, Nie S and
Zhang Y (2021) Identification of a
Novel Immune Landscape Signature
for Predicting Prognosis
and Response of Endometrial
Carcinoma to Immunotherapy
and Chemotherapy.
Front. Cell Dev. Biol. 9:671736.
doi: 10.3389/fcell.2021.671736

¹ Department of Gynecology, The First Affiliated Hospital of Nanjing Medical University, Nanjing, China, ² Department of Urology, The First Affiliated Hospital of Nanjing Medical University, Nanjing, China, ³ Department of Gynecology and Obstetrics, Wuxi Maternal and Child Health Hospital, The Affiliated Hospital to Nanjing Medical University, Wuxi, China, ⁴ Wuxi Clinical Medical College, Nanjing Medical University, Wuxi, China

Uterine Corpus Endometrial Carcinoma (UCEC) is the most common gynecological cancer. Here, we have investigated the significance of immune-related genes in predicting the prognosis and response of UCEC patients to immunotherapy and chemotherapy. Based on the Cancer Genome Atlas (TCGA) database, the single-sample gene-set enrichment analysis (ssGSEA) scores was utilized to obtain enrichment of 29 immune signatures. Univariate, multivariate Cox regression and least absolute shrinkage and selection operator (LASSO) regression analyses were performed to generate an immune-related prognostic signature (IRPS). The biological functions of IRPS-associated genes were evaluated using GSEA, Tumor Immune Estimation Resource (TIMER) Database analysis, Mutation analysis, Immunophenoscore (IPS) analysis, Gene Expression Profiling Interactive Analysis (GEPIA), Genomics of Drug Sensitivity in Cancer (GDSC) and Immune Cell Abundance Identifier (ImmuCellAI). Potential small molecule drugs for UCEC were predicted using the connectivity map (Cmap). The mRNA and protein expression levels of IRPS-associated genes were tested via quantitative real-time PCR (qPCR) and immunohistology. Two immune-related genes (CCL13 and KLRC1) were identified to construct the IRPS. Both genes were related to the prognosis of UCEC patients ($P < 0.05$). The IRPS could distinguish patients with different prognosis and was closely associated with the infiltration of several types of immune cells. Our findings showed that patients with low IRPS benefited more from immunotherapy and developed stronger response to several chemotherapies, which was also confirmed by the results of ImmuCellAI. Finally, we identified three small molecular drugs that might improve the prognosis of patients with high IRPS. IRPS can be utilized to predict the prognosis of UCEC patients and provide valuable information about their therapeutic response to immunotherapy and chemotherapy.

Keywords: endometrial carcinoma, prognosis, tumor immune microenvironment, immunotherapy, chemotherapy

INTRODUCTION

Uterine Corpus Endometrial Carcinoma (UCEC) is the most common gynecological cancer. In 2018, 382,069 new cases and 89,929 deaths were reported worldwide (Bray et al., 2018). Despite the emergence of targeted therapy and immunological therapy, the incidence and mortality of UCEC have shown a consistent increase (Lortet-Tieulent et al., 2018). The overall 5-year survival rate can reach 75–86% (Gottwald et al., 2010), however, the survival time of patients with cancer metastasis or recurrence after treatment may drop below 16 weeks (Chaudhry and Asselin, 2009). Besides, the therapeutic regimens such as immunotherapy and chemotherapy are mainly designed according to the clinical stage of patients and regardless of the patients' varying responses. Therefore, it is an urgent need of the scientific community to build a new prognostic model to identify patients that are at a high risk and suitable for certain regimens.

Surgery is the most preferred route to treat UCEC, commonly supported by radiotherapy and chemotherapy that are designed according to histopathologic parameters of the patients. Surprisingly, chemotherapy may exert different or even opposite effects on patients with identical pathological grade. Furthermore, there is limited evidence regarding the type of patients who can draw benefit from chemotherapy. To further complicate this, immunotherapy can trigger strong response in patients with DNA polymerase ϵ (POLE) mutation, microsatellite instability and high-tumor mutational burden (TMB), however, the difficulty of assessing these factors makes them unsuitable as prognostic markers.

Recently, the tumor immune microenvironment and infiltration of immune cells have been found to be associated with cancer development, prognosis and therapeutic response (Galon et al., 2013; Jain et al., 2016; Pages et al., 2018; Yu et al., 2018). Immune and stromal cells play critical roles in cancer biology. Immune related genes may regulate the infiltration of immune cells, a process that has close correlation with immunotherapeutic response (Binnewies et al., 2018). Therefore, we hypothesized that immune-related genes may be utilized to predict the prognosis and therapeutic response of UCEC patients. In this study, we identified two immune-related genes, their different expression levels have significant prognostic value, and developed a model for predicting the survival and therapeutic response of UCEC patients.

Abbreviations: UCEC, Uterine Corpus Endometrial Carcinoma; LASSO, least absolute shrinkage and selection operator; IRPS, immune-related prognostic signature; GEPIA, Gene Expression Profiling Interactive Analysis; GDSC, Genomics of Drug Sensitivity in Cancer; TMB, tumor mutational burden; TIME, tumor immune microenvironment; TCGA, the Cancer Genome Atlas; GO, gene ontology; KEGG, Kyoto Encyclopedia of Genes and Genomes; FDR, false discovery rate; ROC, receiver operating characteristic; AUC, area under the curve; DCA, decision curve analysis; GSEA, gene set enrichment analysis; TIICs, tumor-infiltrating immune cells; KLRC1, Killer Cell Lectin Like Receptor C1.

MATERIALS AND METHODS

Data Sources and Clustering

Downloaded from the Cancer Genome Atlas (TCGA) database were data about mRNA expression data of 547 UCEC patients and clinical characteristics, including age, tumor grade, histological type and clinical stage from TCGA¹ on Dec 1, 2019. All the mRNA expression data were derived from 552 tumor cases and 23 normal cases. 32 patients without well-annotated clinical information and survival time less than 30 days were excluded. After that, 515 patients were obtained. The tumor purity, infiltration level and stromal content were calculated through the ESTIMATE method (Yoshihara et al., 2013). The single-sample gene-set enrichment analysis (ssGSEA) scores were implemented via invoking the R package "GSEAbase" scores. to obtain the enrichment level of 29 immune signatures in each UCEC tissue by evaluating the mRNA expression level of UCEC patients and perform hierarchical clustering of UCEC using R package "hclust" (Barbie et al., 2009; Hanzelmann et al., 2013).

A total of 15 UCEC specimens and 15 adjacent tissues were obtained from patients at the Wuxi Maternal and Child Health Hospital, the Affiliated Hospital to Nanjing Medical University from 2018 to 2019 and routine written informed consent was obtained from all patients. These tissues were used to validate the mRNA and protein expression of KLRC1 and CCL13 in an external set.

Differentially Expressed Genes and Immune-Related Genes

To identify the differentially expressed genes (DEGs) among all of the three groups, we first compared the DEGs between Immunity_L and Immunity_H, Immunity_L and Immunity_M, and Immunity_M and Immunity_H. After that, we imported the immune gene set from Immport database². Then, the overlapping genes were obtained by Venn analysis.

Gene Ontology and Kyoto Encyclopedia of Genes and Genomes Enrichment Analyses

We performed functional enrichment analyses to investigate the potential mechanisms of different hierarchical clustering based on 29 immune signatures. Gene ontology (GO) and Kyoto Encyclopedia of Genes and Genomes (KEGG) enrichment analyses were utilized to reveal the enriched biological process, cellular component, molecular function and signaling pathway. Terms with a false discovery rate (FDR) < 0.05 were listed using R package "ClusterProfiler".

Establishment of the Immune-Related Prognostic Signature

We divided all the cases into a training set and a testing set with the ratio of 1:1. We used the training set to identify the prognostic immune-related genes and to establish the IRPS. The

¹<http://cancergenome.nih.gov/>

²<https://www.immport.org>

testing set and entire set were used to validate its prognostic capability. First, a univariate Cox regression analysis was used to identify prognosis-related genes in the training set. The inclusion criterion was set at $P < 0.05$ and least absolute shrinkage and selection operator (LASSO) regression was utilized to minimize the overfitting. We then utilized multivariate Cox model to verify the correlation and developed an immune risk score model using the coefficients of multivariate Cox analysis. The risk score for patients in training set, testing set and total set was calculated using the following equation:

$$\begin{aligned} \text{Risk score} = & \text{Expression of the 1}^{\text{st}} \text{ gene} \cdot \text{coefficient} \\ & + \text{Expression of the 2}^{\text{nd}} \text{ gene} \cdot \text{coefficient} \\ & + \text{Expression of the } n^{\text{th}} \text{ gene} \cdot \text{coefficient} \end{aligned}$$

Patients were then divided into high-risk and low-risk groups according the risk score.

Validation of the IRPS

The receiver operating characteristic (ROC) curve was plotted to validate the prognostic value of IRPS. The area under the curve (AUC) was calculated using R package “survivalROC”. The survival analyses were conducted using Kaplan-Meier survival curves and “survival” R package. We also used the decision curve analysis (DCA) curve to obtain the predictive power of the IRPS and other clinical characteristics.

Construction and Validation of a Predictive Nomogram

To fully expand the predictive power of a prognostic model, a nomogram was constructed based on the clinical characteristics of UCEC, including age, stage, grade and histological type. Validation of the nomogram was evaluated using calibration plot.

Gene Set Enrichment Analysis

To identify potential biological mechanism related IRPS, we performed GSEA and GO analysis. KEGG terms with $\text{FDR} \leq 0.05$ were considered enriched. Based on IRPS, patients were divided into different groups, the different expression genes with a fold change (FC) > 1 and an adjusted P -value < 0.05 were identified using R package “limma”. The GO analysis was then performed using the “clusterProfiler” R package.

Estimate of Tumor-Infiltrating Immune Cells

We used the CIBERSORT tool to quantify 22 types of immunocyte fractions based on TCGA RNA-sequencing data. $P < 0.05$ was set as the threshold. $P < 0.05$ was set as the threshold.

TIMER Database Analysis

TIMER is a comprehensive resource for systematical evaluations of the clinical impact of different immune cells on diverse cancer types³. We analyzed the expressions of KLRC1 and

CCL13 in UCEC and evaluated their correlation with the infiltration of immune cells. Besides, correlations of KLRC1 and CCL13 expression with markers of several immune cells were also statistically evaluated using Spearman's correlation and represented via scatterplots.

TISIDB Database Analysis

The TISIDB online platform was used to analyze the correlation of KLRC1 and CCL13 expression with 28 immune infiltrating cells⁴.

Mutation Analysis

We downloaded the mutation data of UCEC patients from the TCGA database⁵ and utilized the maftools to analyze the mutation data. The tumor mutational burden (TMB) score was calculated using following formula:

$$\text{TMB} = \frac{\text{Total mutation}}{\text{Total covered bases}} \cdot (10)^6$$

IPS Analysis

IPS can be generated in an unbiased manner using machine learning based on four major gene categories that determine immunogenicity. The IPS was calculated with z-scores of representative genes associated with immunogenicity. The IPSs of patients were obtained from the Cancer Immunome Atlas (TCIA)⁶.

Immunotherapy Response Prediction

The response to immunotherapy was predicted using an online tool called Immune Cell Abundance Identifier (ImmuCellAI) (Miao et al., 2020), which can estimate the abundance of 24 immune cells from gene expression datasets, including RNA-Seq and microarray data, and predict the patient's response to an existing immune checkpoint blockade therapy.

Verification of Gene Correlation in GEPIA

To further verify the correlation of KLRC1 and CCL13 expression with immune cells markers, the Gene Expression Profiling Interactive Analysis (GEPIA)⁷ database was employed. Statistical analysis was performed using Spearman's correlation.

Chemotherapy Response and Candidate Small Molecule Drugs Prediction

The response of chemotherapy in UCEC patients was determined using a public database called Genomics of Drug Sensitivity in Cancer (GDSC⁸). The half-maximal inhibitory concentration (IC50) was estimated which represented the drug response. The potential small molecule drugs for UCEC were predicted using Connectivity map (CMap)⁹. This database comprises

⁴<http://cis.hku.hk/TISIDB/index.php>

⁵<https://portal.gdc.cancer.gov>

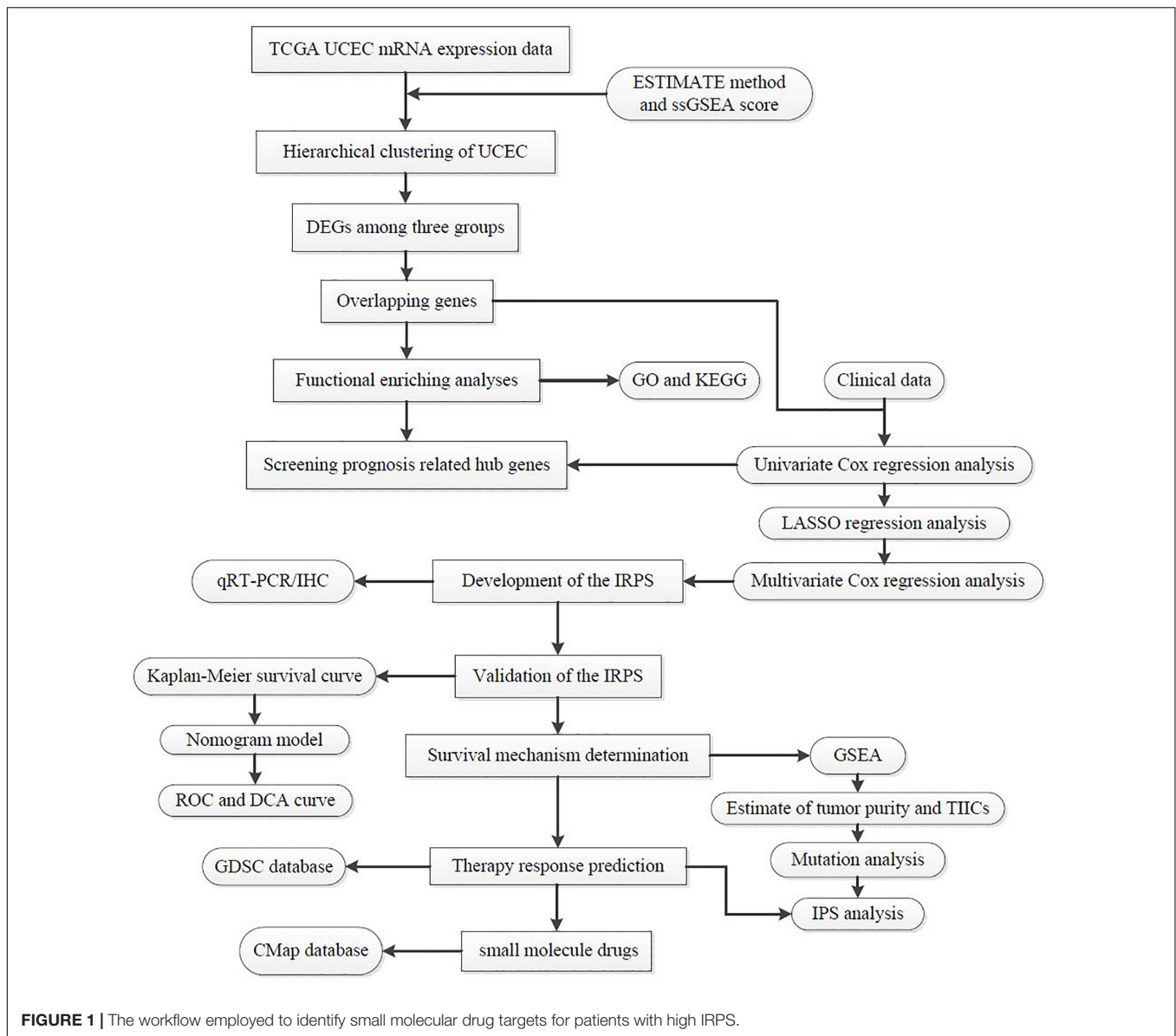
⁶<https://tcia.at/home>

⁷<http://gepia.cancer-pku.cn/index.html>

⁸<https://www.cancerrxgene.org>

⁹<https://www.broadinstitute.org/connectivity-map-cmap>

³<https://cistrome.shinyapps.io/timer>



of genome-wide transcriptional expression data from small molecule drugs, and can discover the connections between drugs, genes and diseases through the variation of gene-expression profiles. These small molecule drugs were predicted based on 382 DEGs between high-risk and low-risk group with $|\log_2\text{fold change (FC)}| > 1$ and $\text{FDR} < 0.05$. The 3D structures of the three most significant drugs were obtained from Pubchem¹⁰.

Quantitative Real-Time RT-PCR

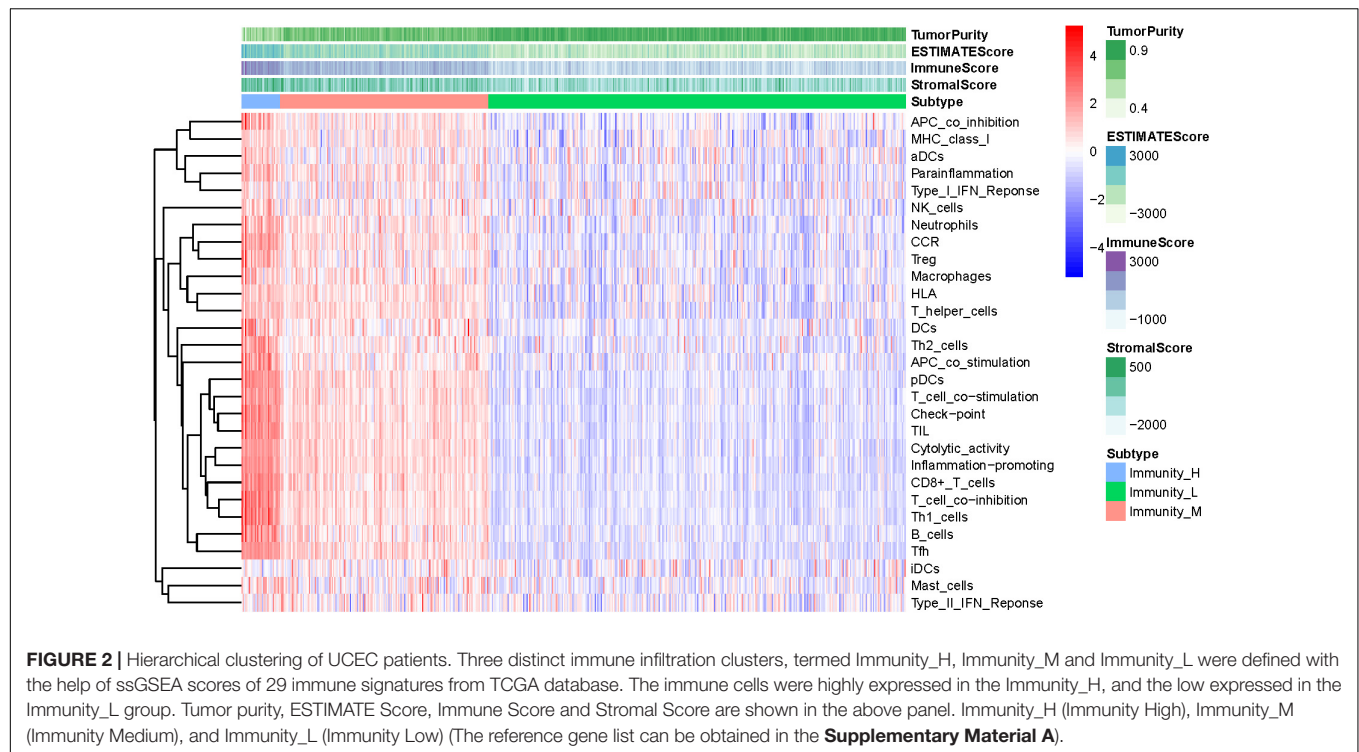
Total RNA from 15 UCEC samples and 15 adjacent tissues was extracted using TRIzol reagent (Invitrogen) and the total RNA integrity were checked by RNA 6000 Nano kit. Before reverse transcription to cDNA, 4 × gDNA wiper Mix (Vazyme

R323-01), DEPC and total RNA (1 μg) were resuspended and reacted at 42°C for 2 min to remove the residual genomic DNA from total RNA. PrimeScript® RT reagent kit was used to synthesize the complementary RNA. The SYBR® Premix Ex Taq™ Kit (TaKaRa DRR041) was utilized to perform real-time quantification. The relative expression levels of target genes were normalized by GAPDH and estimated using the $2^{-\Delta\Delta C_t}$ method. The PCR primers are listed in **Supplementary Table 2**.

Immunohistochemical Staining

The protein expression levels of CCL13 and KLRC1 were estimated via immunohistochemical (IHC) staining. Briefly, the tissues slides were deparaffinized, rehydrated and treated with 3% H₂O₂ for 15 min to eliminate endogenous peroxidase. Then, antigen retrieval was performed by

¹⁰<https://pubchem.ncbi.nlm.nih.gov/>



heating the slides in sodium citrate buffer for 3 min. Next, the slides were incubated with rabbit anti-CCL13 or anti-KLRC1 primary antibodies (Affinity, Biosciences, 1:200) at 4°C overnight. The slides were washed and incubated with HRP-conjugated donkey anti-rabbit secondary antibodies (Abcam) for 15 min. The staining was visualized using DAB solution and samples were counterstained with hematoxylin.

Immunostaining of CCL13 and KLRC1 were analyzed by two pathologists who were blinded to the same information. The staining intensity score was defined on a scale of 0 to 3 in which 0 means no staining, 1 means mild staining, 2 means medium staining and 3 means intense staining. The percentage score of stained cells were also calculated on a scale of 1 to 4 in which 1 represents (0–25%), 2 = (26–50%), 3 = (51–75%) and 4 = (76–100%). In order to obtain the final score, the intensity score and percentage score were multiplied to reach the final score ranging from 0 to 12.

Statistical Analysis

We adopted the R project (version 3.6.2; R Foundation) for all analysis¹¹. The following R packages was adopted in this study (“pheatmap”, “rms”, “ggplot2”, “forest plot”, “limma”, “glmnet”, “preprocessCore”, “GSVA”, “survminer”, “survival ROC”, “beeswarm”, “ggstatsplot”). Two-side statistical analyses were performed and samples with P -value < 0.05 were considered statistically significant.

¹¹<http://www.r-project.org/>

RESULTS

Construction of UCEC Subgrouping

The total workflow is as shown in the following figure (Figure 1). With the help of the ssGSEA scores of 29 immune signatures and R package “hclust”, we divided the patients into three clusters according to immune infiltration: Immunity High (Immunity_H), Immunity Medium (Immunity_M), and Immunity Low (Immunity_L). The three distinct clusters, Immunity_H, Immunity_M, and Immunity_L, showed different immune activities. The hierarchical clustering map was shown in **Supplementary Figure 1**. We found that the patients in the Immunity_H group had higher ESTIMATE Score, Immune Score and Stromal Score and lower Tumor Purity (Figures 2, 3A–C) than other groups. Besides, the expression levels of most HLA genes were significantly higher in Immunity_H group than that in Immunity_L group (Figure 3D). The type of immune cells was different among three groups (Figure 3E). We also compared the expression of several immune regulators, including PD-1, PD-L1, TIM-3, LAG-3, and CTLA4. The expression levels of these immune regulators in Immunity_H group were all higher than those in Immunity_L group (Figures 3F–J). We then conducted Kaplan-Meier survival analysis which highlighted that patients in three groups had distinct clinical outcomes ($P = 0.027$, Figure 3K).

Differentially Expressed Genes and Immune-Related Genes

To identify the differentially expressed genes (DEGs) among all of the three groups, we first compared the DEGs between

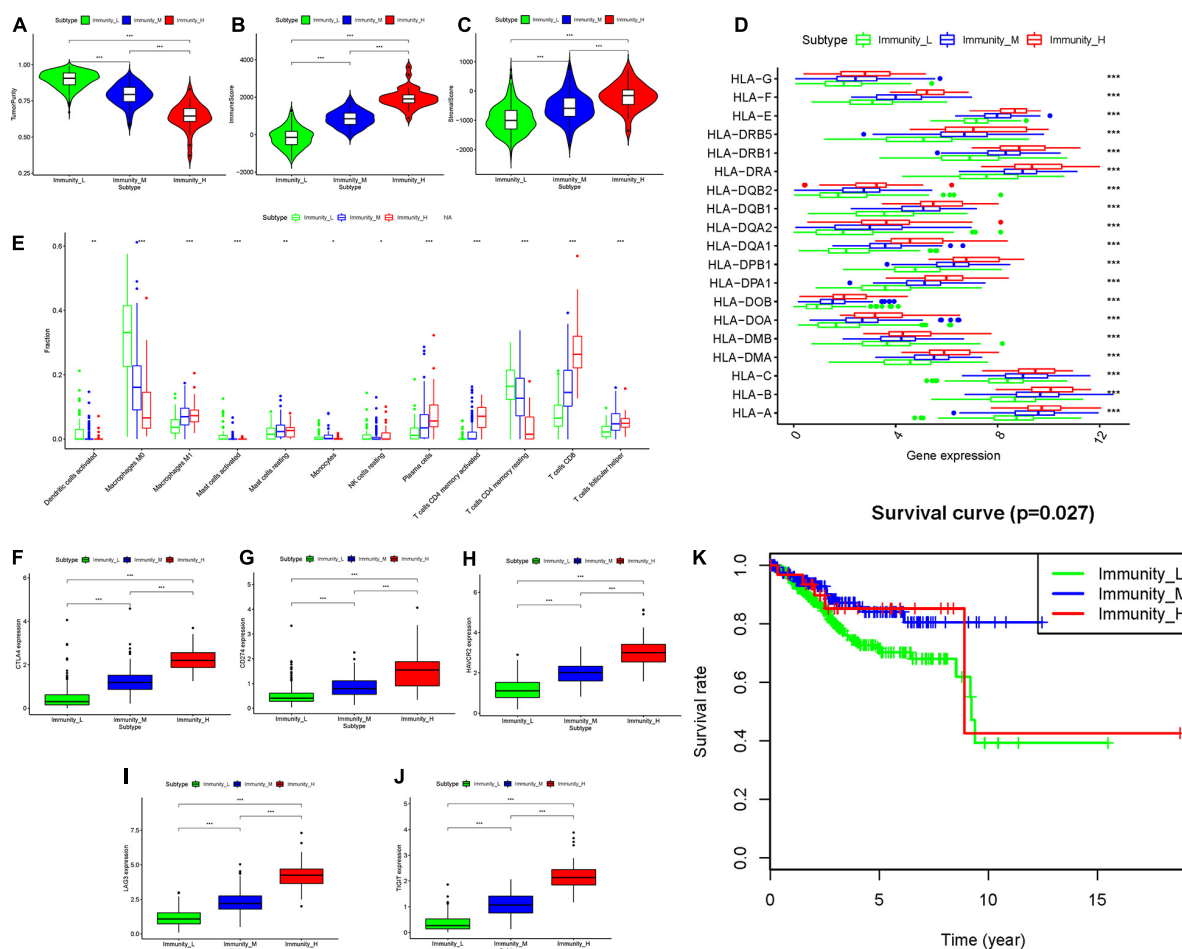


FIGURE 3 | Three UCEC subtypes displayed different phenotypes. **(A–C)** The difference in Tumor Purity, Immune Score and Stromal Score in three UCEC subtypes. **(D)** The mRNA expression of HLA genes among UCEC subtypes. **(E)** The proportion of different immune cells in three UCEC subtypes. **(F–J)** The mRNA expression of 5 immune checkpoint molecules (CTLA4, CD274, HAVCR2, LAG3 and TIGIT) in three UCEC subtypes. **(K)** The survival curve exhibited that the prognosis of patients among UCEC subtypes is different. * $0.01 \leq P < 0.05$; ** $0.001 \leq P < 0.01$; *** $P < 0.001$.

TABLE 1 | Multivariate Cox analyses based on 2 hub genes.

Gene	Coef	HR	95%CI	P-value
CCL13	−0.398	0.672	0.437–1.034	0.0709
KLRC1	−2.163	0.115	0.008–1.645	0.1111

Immunity_L and Immunity_H, Immunity_L and Immunity_M, and Immunity_M and Immunity_H and identified 2314, 411 and 1378 DEGs (**Supplementary Figures 2A–C**). Then, according to the gene set from Immport database (see text footnote 2), we obtained 1811 immune genes (**Supplementary Material B**). Then, the overlapping genes were obtained by Venn analysis. Finally, 89 overlapping genes were found differentially expressed in all four subgroups, which suggested to play a crucial role in immune status of UCEC (**Supplementary Material C**). Thus, the 89 overlapped DEGs were selected as key immune related DEGs for further analysis (**Supplementary Figure 2D**).

Identification of Potential Biological Function-Related Genes

Go and KEGG analyses were performed which highlighted 89 biological function-related key genes in UCEC. We found that biological functions like such as T cell activation, leukocyte cell-cell adhesion, positive regulation of leukocyte activation, etc. were associated with the identified 89 genes. Furthermore, these genes participated in the KEGG pathways including Cytokine-cytokine receptor interaction, Natural killer cell mediated cytotoxicity, and Viral protein interaction with cytokine and cytokine receptor etc. (**Supplementary Figures 3A–D**).

Development and Validation of the IRPS

To construct the IRPS based on 89 identified overlapping genes, the univariate Cox regression analysis was utilized to identify prognosis-related genes (**Supplementary Table 1**). 3 overlapping genes were identified. After that, we used LASSO Cox analysis to decrease overfitting (**Supplementary Figures 4A,B**). After

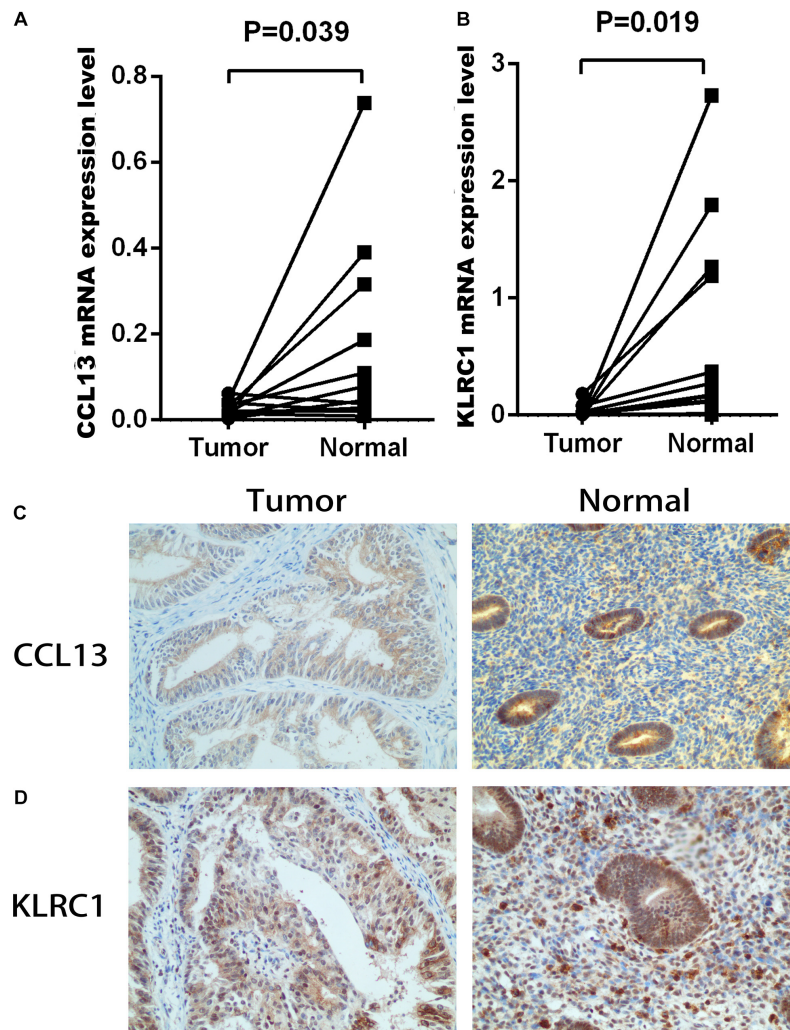


FIGURE 4 | The mRNA and protein expression level of CCL13 and KLRC1 in UCEC tumor and the adjacent tissues. **(A,B)** The mRNA expression of CCL13 and KLRC1 in UCEC tumor and the adjacent tissues. **(C,D)** The protein expression of CCL13 and KLRC1 in UCEC tumor and the adjacent tissues observed using IHC.

analysis, three genes were all reserved, including KLRC1, CCL13 and LTA. All these genes were associated with the overall survival of UCEC patients (**Supplementary Figure 5**). We then performed multivariate Cox proportional hazards regression analysis to build the IRPS (**Table 1**). Two hub genes were reserved. The mRNA and protein expression of these two genes were presented in **Figure 4**. The mRNA expression of CCL13 and KLRC1 in tumor tissues were significantly lower than that in the normal tissues (**Figures 4A,B**). Similarly, the protein expression of CCL13 and KLRC1 was consistent with their mRNA expression (**Figures 4C,D**). The risk score was obtained according to the corresponding coefficients and the expression levels of hub genes. Risk score was calculated using the following formula:

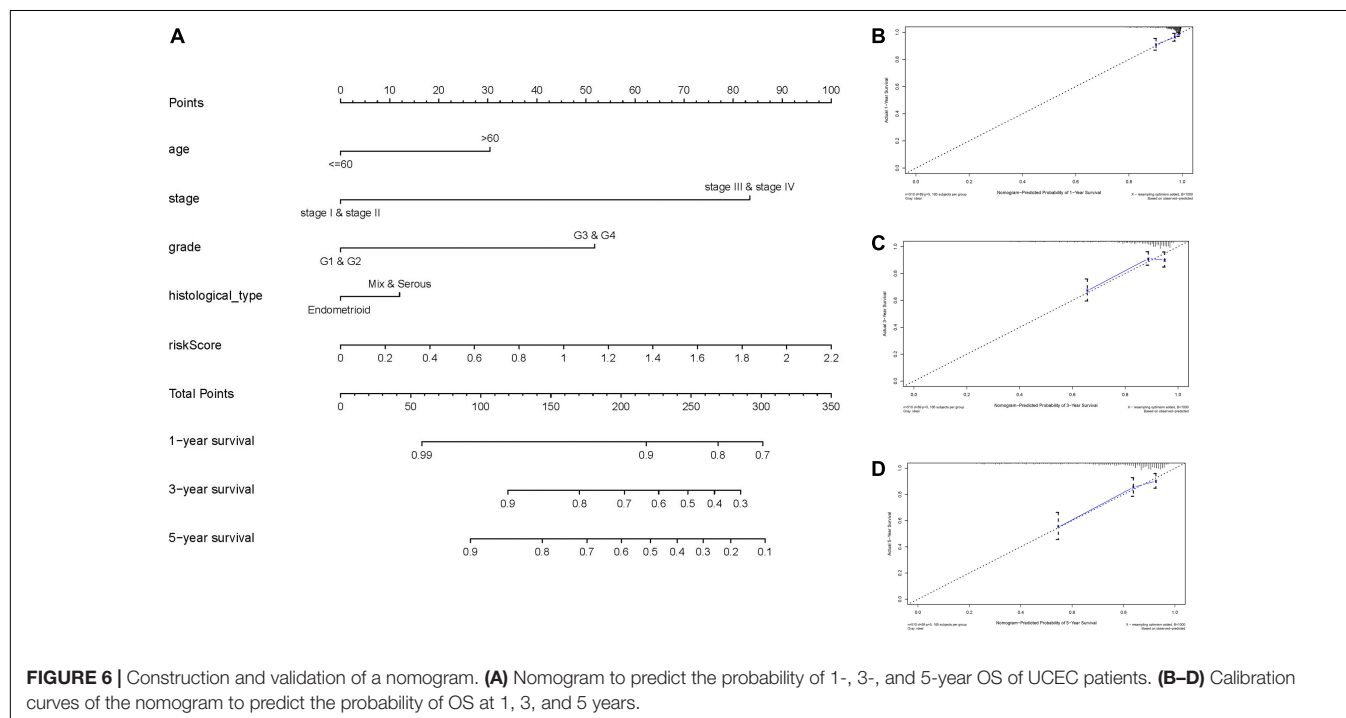
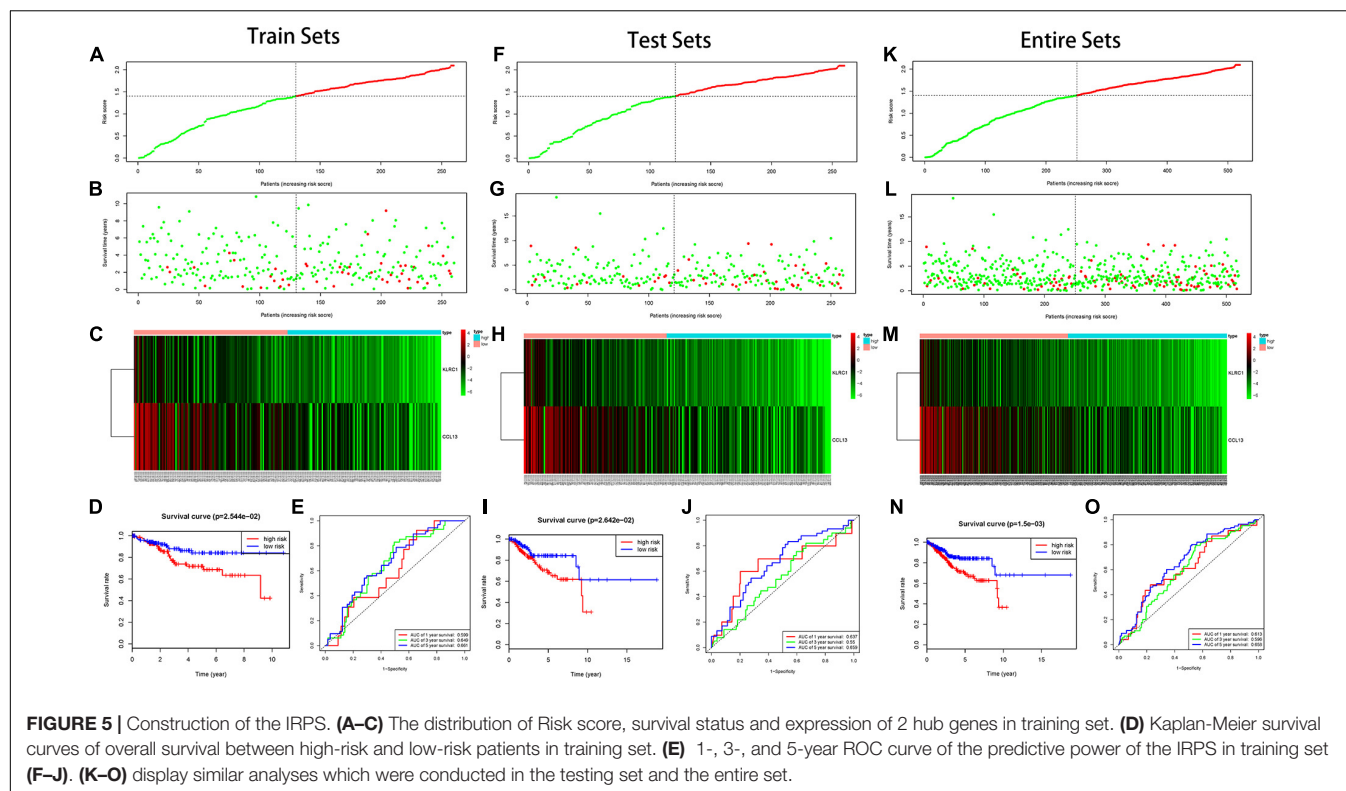
$$\text{Risk factor} = [(-2.163) \cdot \text{KLRC1} + (-0.398) \cdot \text{CCL13}]$$

A cutoff Risk score value of 1.40 was selected based on the median value of the risk score in the training set and used to divide the

patients into low-risk (Risk score ≤ 1.4028) and high-risk (Risk score > 1.4028) groups.

In the training set, we found the IRPS can distinguish risk score, survival status and expression of 2 hub genes as displayed in **Figures 5A–C**. Kaplan-Meier survival analysis showed statistical difference between two groups (**Figure 5D**), and the areas under the ROC curves (AUC) were 0.599, 0.649, and 0.661 for 1-, 3-, and 5-year survival, respectively (**Figure 5E**). The testing set cohort and the entire cohort were used to validate the prognostic power of the IRPS model. The distribution of risk score, survival status and expression of two hub genes in the testing and entire sets are presented in **Figures 5F–H,K–M**. Patients in high-risk group showed worse prognosis than low-risk group in both testing and entire sets (**Figures 5I,N**). ROC analysis revealed the prognostic accuracy of the IRPS in testing and entire sets (**Figures 5J,O**).

Furthermore, we analyzed the prognostic power of the IRPS with different clinical features in the entire set. We first



represented the data in a heatmap to obtain the general distribution of risk score, hub genes and other clinical features (Supplementary Figure 5A) and then utilized subgroup Kaplan-Meier analysis to evaluate the prognostic value of IRPS in some specific conditions (Supplementary

Figures 6B–G). We found the IRPS reached satisfactory prognostic discrimination in patients with age ≤ 60 (Supplementary Figure 6B), grade G1&G2 (Supplementary Figure 6C), grade G3&G4 (Supplementary Figure 6D), histological type endometrial (Supplementary Figure 6E),

stage I&II (Supplementary Figure 6F) and stage III&IV (Supplementary Figure 6G).

Construction and Validation of a Prediction Nomogram

We conducted the univariate and multivariate Cox regression analyses to determine whether the IRPS was an independent prognostic indicator for UCEC. According to univariate Cox regression analysis, the hazard ratio (HR) of risk score and 95% confidence interval (CI) were 2.717 (1.407–5.248), 1.783 (1.013–3.140), and 2.191 (1.425–3.370) in training, testing, and entire sets, respectively (Table 2). When turns to multivariate Cox regression analysis, the HR and 95% CI were 2.224 (1.137–4.350) and 1.949 (1.273–2.983) in training and entire set, respectively. However, in testing sets, the HR of risk score and 95% CI were 1.653 (0.956–2.859) (Table 2). According to the univariate and multivariate Cox regression analyses, the age, stage, histological type, grade and risk score are significant prognostic factors and should be involved in the construction of the prognostic models.

To expand the prognostic power of the IRPS and other clinical characteristics, we constructed a nomogram that integrated age, clinical stage, grade, histological type, and risk score. Each parameter was assigned with a score and their total score was calculated. To validate the performance of the nomogram (Figure 6A), 1, 3, and 5-year calibration curves were constructed (Figures 6B–D), which revealed a close association between the predicted and actual curves. We further compared the AUC of IRPS and other clinical characteristics for 1-, 3-, and 5-year survival (Figures 7A–C) and found that the results were not suitable for clinical usage. However, when these factors were combined, the AUC reached 0.736, 0.746 and 0.796 for 1-, 3-,

and 5-year survival, respectively (Figures 7D–F), suggesting the combination of IRPS and other clinical characteristics was highly reliable. This methodology was further confirmed by the decision curve analysis (DCA) (Figures 7G,H).

Potential Biological Pathways Associated With IRPS

According to the GSEA analysis. We identified that pathways, such as axon guidance, basal cell carcinoma, glycosaminoglycan biosynthesis chondroitin sulfate, were enriched in the high-risk group, whereas autoimmune thyroid disease, B cell receptor signaling pathway, and chemokine signaling pathway were enriched in the low-risk group (Supplementary Figures 7A,B). Besides, we also identified several immune-related GO terms such as T cell activation, regulation of leukocyte activation, regulation of lymphocyte activation, regulation of T cell activation and leukocyte cell-cell adhesion (Supplementary Figures 6C,D).

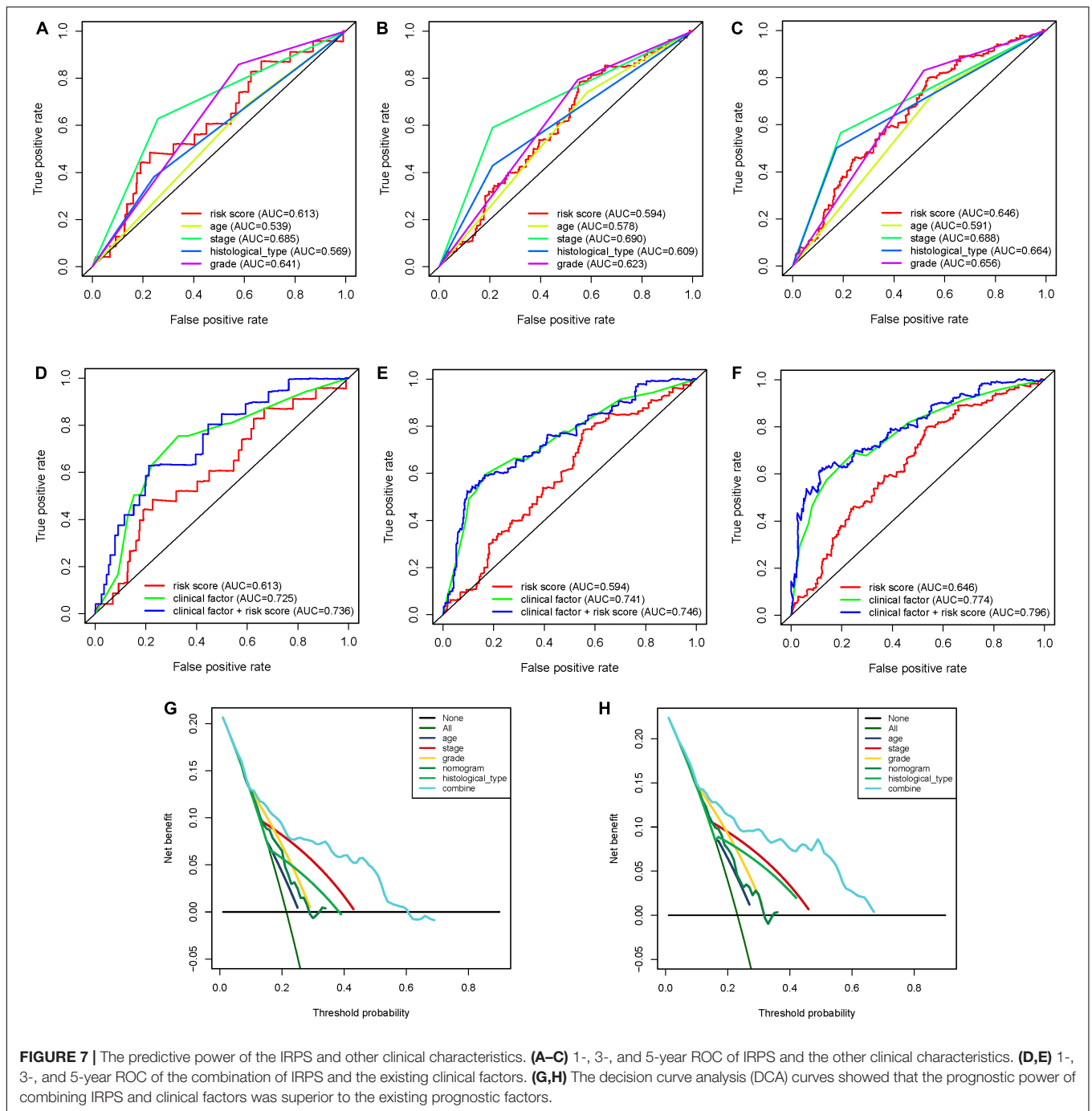
Correlation Between IRPS and Immune Cell Infiltration

We used CIBERSORT to obtain the proportion of the 22 immune cells (Figure 8A) and found that the proportions of several types of immune cells, including plasma cells, CD8+ T cells, CD4+ memory T cell, follicular helper T cells and M1 macrophages, were higher in the low-risk group, but those of immune cells like, CD4+ memory T cells, M0 macrophages and mast cells were lower in the high-risk group. Besides, we also investigated the correlation between IRPS and different types of immune cells. The IRPS showed positive correlation with memory B cells, activated dendritic cells, M0 macrophages, mast cells, CD4+

TABLE 2 | Univariate and multivariate Cox regression analyses of the prognosis-related factors.

Variables	Univariate analysis			Multivariate analysis		
	HR	95%CI	P-value	HR	95%CI	P-value
Training sets						
Age	1.303	0.674–2.517	0.431	1.037	0.505–2.130	0.921
Stage	4.044	2.179–7.506	<0.001	2.902	1.496–5.629	0.002
Histological type	3.443	1.870–6.340	<0.001	1.597	0.729–3.500	0.242
Grade	2.869	1.327–6.202	0.007	1.881	0.774–4.568	0.163
RiskScore	2.717	1.407–5.248	0.003	2.224	1.137–4.350	0.020
Testing sets						
Age	2.465	1.253–4.851	0.009	2.346	1.159–4.751	0.018
Stage	4.126	2.306–7.383	<0.001	3.852	2.030–7.310	<0.001
Histological type	2.682	1.506–4.777	<0.001	0.918	0.462–1.822	0.806
Grade	3.996	1.864–8.565	<0.001	2.521	1.085–5.857	0.032
RiskScore	1.783	1.013–3.140	0.045	1.653	0.956–2.859	0.072
Entire sets						
Age	1.778	1.112–2.843	0.016	1.563	0.952–2.567	0.078
Stage	4.116	2.700–6.275	<0.001	3.400	2.152–5.371	<0.001
Histological type	3.044	2.003–4.624	<0.001	1.193	0.716–1.989	0.498
Grade	3.397	1.976–5.840	<0.001	2.137	1.163–3.928	0.014
RiskScore	2.191	1.425–3.370	<0.001	1.949	1.273–2.983	0.002

HR, hazard ratio; CI, confidence interval.



memory T cells, and negative correlation with M1 macrophages, NK cells, CD4+ memory T cells, CD8+ T cells and follicular helper T cell (Figures 8B,C).

Correlation Analysis Between 2 Hub Genes and Immune Infiltration Level

To investigate the relationship between the two hub genes, tumor purity and the immune infiltrating cells, we used the TIMER database to obtain their relationship. We first analyzed

the correlations between CCL13 expression, tumor purity and immune infiltration level of 6 immune cells. The results showed that CCL13 expression level had negative correlation with tumor purity. Besides, CCL13 expression level had significant positive correlations with infiltrating levels of B cell, CD8+ T cell, CD4+ T cell, Macrophage, Neutrophil and Dendritic cell (Supplementary Figure 8A). Similarly, the KLRC1 expression level had negative correlation with tumor purity and positive correlation with infiltrating levels of B cell, CD8+ T cell, CD4+ T cell, Macrophage, Neutrophil and Dendritic

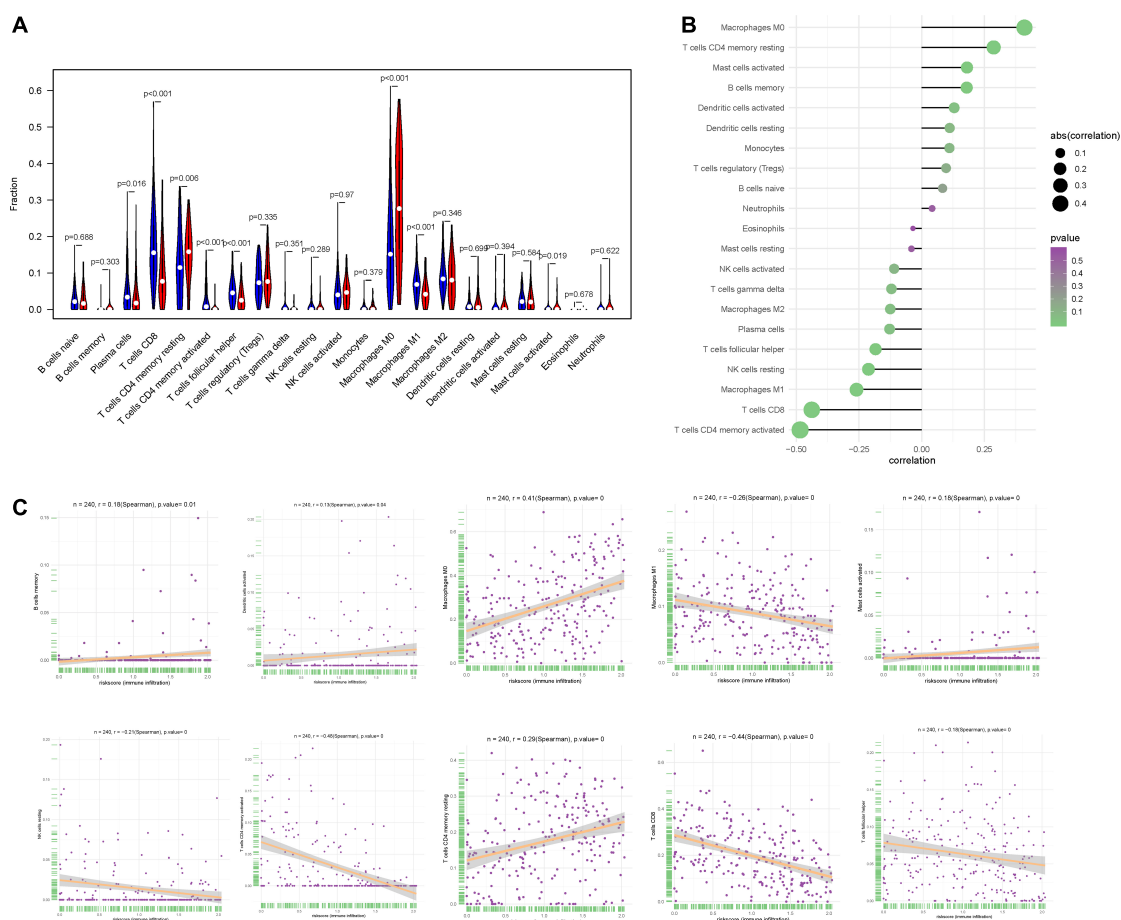


FIGURE 8 | Correlation between IRPS and immune cell infiltration. **(A)** The landscape of immune cell infiltration in low-risk and high-risk groups. The low-risk and high-risk groups are represented via blue and red violin, respectively. **(B)** The association between IRPS and immune cell infiltration. **(C)** The association between IRPS and each type of immune cell.

cell (**Supplementary Figure 8B**). The above results were also validated using the TISIDB dataset (**Supplementary Figures 9A–C**). These results suggest that CCL13 and KLRC1 play a specific role in immune infiltration in UCEC.

We further revealed the relationship between the two hub genes and several immune markers, including CD8+ T cells, T cells (general), B cells, monocytes, TAMs, M1 and M2 macrophages, neutrophils, NK cells, DCs and several functional T cells. After adjustment by purity, the results showed that CCL13 expression level was associated with most immune marker sets of immune cells and different T cells except for the M1 Macrophage and Dendritic cell (**Table 3**). In addition, the KLRC1 expression level was associated with nearly all of the immune cells. These results were also verified using the GEPIA database (**Table 4**). In general, according to the above results, CCL13 and KLRC1 play a remarkable role in immune regulation in UCEC.

In addition, we analyzed the relationships of the mutants of these 2 hub genes with immune infiltrates in UCEC. Compared with the immune infiltration levels in samples with wild type signatures, diverse forms of mutation in two hub genes could inhibit the immune infiltration levels of several immune

cells, including CD8+ T cell, macrophages and dendritic cells (**Supplementary Figures 8C,D**).

Correlation Between IRPS and Mutation Profile

The relationship between IRPS and mutation profile was evaluated in UCEC patients using somatic mutation data. The top 10 mutated genes in high-risk and low-risk group are shown in the **Figures 9A,B**. And the most frequently mutated genes in high-risk and low-risk group are presented in **Figure 9C**. The results revealed that somatic mutation was more frequently observed in the low-risk group. And the TMB scores in low-risk group were significantly higher than that in high-risk group ($P < 0.05$, **Figure 9D**). Further results revealed that TMB score had negative correlation with IROS ($P = 4.015e-09$, **Figure 9E**).

Correlation Between IRPS and Two Therapeutic Regimens

We also analyzed the expression of four immune checkpoint molecules in high-risk and low-risk groups. The results revealed

TABLE 3 | Correlation analysis between two hub genes and immune cells markers in TIMER.

Description	Gene markers	CCL13				KLRC1			
		None		Purity		None		Purity	
		Cor	P	Cor	P	Cor	P	Cor	P
CD8+ T cell	CD8A	0.452	***	0.435	***	0.597	***	0.581	***
	CD8B	0.248	***	0.196	**	0.384	***	0.369	***
T cell (general)	CD3D	0.444	***	0.444	***	0.605	***	0.623	***
	CD3E	0.422	***	0.412	***	0.634	***	0.66	***
	CD2	0.468	***	0.466	***	0.624	***	0.624	***
B cell	CD19	0.157	**	0.119	0.041	0.385	***	0.399	***
	CD79A	0.307	***	0.296	***	0.454	***	0.436	***
Monocyte	CD86	0.343	***	0.301	***	0.542	***	0.543	***
	CD115 (CSF1R)	0.159	**	0.11	0.06	0.443	***	0.47	***
TAM	CCL2	0.303	***	0.272	***	0.282	***	0.253	***
	CD68	0.312	***	0.289	***	0.459	***	0.438	***
	IL10	0.136	*	0.125	0.032	0.236	***	0.199	**
M1 Macrophage	INOS (NOS2)	−0.019	0.659	−0.039	0.502	0.119	*	0.034	0.563
	IRF5	0.027	0.531	0.03	0.605	0.241	***	0.207	**
	COX2(PTGS2)	−0.015	0.732	−0.084	0.154	−0.033	0.446	−0.036	0.535
M2 Macrophage	CD163	0.376	***	0.324	***	0.393	***	0.365	***
	VSIG4	0.26	***	0.195	**	0.409	***	0.388	***
	MS4A4A	0.377	***	0.335	***	0.492	***	0.466	***
Neutrophils	CD66b (CEACAM8)	−0.092	0.031	−0.082	0.162	0.068	0.113	0.09	0.125
	CD11b (ITGAM)	0.228	***	0.158	*	0.441	***	0.466	***
	CCR7	0.33	***	0.344	***	0.482	***	0.518	***
Natural killer cell	KIR2DL1	0.164	**	0.091	0.12	0.445	***	0.423	***
	KIR2DL3	0.2	***	0.165	*	0.514	***	0.514	***
	KIR2DL4	0.29	***	0.322	***	0.693	***	0.696	***
	KIR3DL1	0.241	***	0.24	***	0.525	***	0.577	***
	KIR3DL2	0.193	***	0.21	**	0.485	***	0.493	***
	KIR3DL3	0.154	**	0.126	0.031	0.364	***	0.386	***
	KIR2DS4	0.182	***	0.136	0.02	0.465	***	0.512	***
Dendritic cell	HLA-DPB1	0.208	***	0.11	0.06	0.472	***	0.442	***
	HLA-DQB1	0.152	**	0.071	0.226	0.418	***	0.375	***
	HLA-DRA	0.182	***	0.084	0.152	0.475	***	0.435	***
	HLA-DPA1	0.234	***	0.143	0.014	0.539	***	0.519	***
	BDCA-1(CD1C)	0.027	0.529	0.01	0.868	0.345	***	0.344	***
	BDCA-4(NRP1)	0.081	0.059	0.075	0.203	0.304	***	0.238	***
	CD11c (ITGAX)	0.188	***	0.14	0.016	0.556	***	0.569	***
Th1	T-bet (TBX21)	0.45	***	0.411	***	0.631	***	0.617	***
	STAT4	0.282	***	0.24	***	0.493	***	0.46	***
	STAT1	0.27	***	0.248	***	0.296	***	0.244	***
	IFN- γ (IFNG)	0.495	***	0.489	***	0.498	***	0.481	***
Th2	TNF- α (TNF)	−0.031	0.464	0.009	0.876	0.086	0.044	0.068	0.245
	GATA3	0.195	***	0.164	*	0.237	***	0.19	*
	STAT6	−0.048	0.265	−0.103	0.079	0.065	0.129	−0.03	0.604
	STAT5A	0.119	*	0.053	0.367	0.274	***	0.303	***
	IL13	0.193	***	0.226	***	0.116	*	0.084	0.153
Tfh	BCL6	−0.085	0.046	−0.088	0.132	−0.005	0.902	0.054	0.356
	IL21	0.314	***	0.316	***	0.207	***	0.245	***
Th17	STAT3	0.02	0.643	−0.038	0.52	0.15	**	0.141	0.016
	IL17A	0.279	***	0.288	***	0.14	*	0.168	*

(Continued)

TABLE 3 | Continued

Description	Gene markers	CCL13				KLRC1			
		None		Purity		None		Purity	
		Cor	P	Cor	P	Cor	P	Cor	P
Treg	FOXP3	0.36	***	0.376	***	0.439	***	0.453	***
	CCR8	0.345	***	0.366	***	0.312	***	0.341	***
	STAT5B	0.065	0.129	0.044	0.449	0.107	0.013	0.111	0.058
	TGFβ (TGFB1)	0.103	0.016	0.114	0.052	0.223	***	0.213	**
T cell exhaustion	PD-1 (PDCD1)	0.421	***	0.371	***	0.466	***	0.458	***
	CTLA4	0.445	***	0.412	***	0.523	***	0.5	***
	LAG3	0.462	***	0.447	***	0.476	***	0.448	***
	TIM-3 (HAVCR2)	0.367	***	0.314	***	0.617	***	0.603	***
	GZMB	0.467	***	0.478	***	0.587	***	0.58	***

Cor, R-value of Spearman's correlation; None, correlation without adjustment. Purity, correlation adjusted by purity; *P < 0.01; **P < 0.001; ***P < 0.0001.

that IRPS was negatively correlated with the listed four immune checkpoint molecules (Figure 10A). Besides, we performed IPS analysis to acquire immunogenicity. The results showed that four molecules displayed higher scores in the low-risk group (Figure 10B). Besides, according to the ImmuCellAI, patients in the low-risk group showed higher immunotherapy response rate compared with patients in the high-risk group (Figures 10C,D), which implied that patients in the low-risk group would benefit from immunotherapy.

Chemotherapy is the most common way to treat UCEC cancer, in this research, we used GDSC database to predict the likelihood of response to several common chemotherapy drugs. We estimated the IC50 of each sample and observed a significant difference of IC50 between high-risk and low-risk groups among eight chemo drugs. Patients in the low-risk group were more sensitive to commonly administered chemodrugs ($P = 1.467 \times 10^{-5}$ for cisplatin, $P = 4.412 \times 10^{-6}$ for gemcitabine, $P = 0.039$ for paclitaxel, $P = 0.002$ for bleomycin, $P = 1.458 \times 10^{-6}$ for vinblastine, $P = 0.048$ for vinorelbine, $P = 4.620 \times 10^{-5}$ for vorinostat, $P = 0.005$ for methotrexate) (Figure 11). In contrast, the chemotherapeutic response of Docetaxel and Doxorubicin was not significantly different between both groups.

Potential Small Molecular Drugs for UCEC

In order to explore new therapeutic regimens for UCEC, the Cmap database was employed (Lamb et al., 2006). We found eight associated small molecule drugs that are listed in the Table 5. Among these small molecule drugs, the 3D chemical structures of three most significant small molecule drugs were obtained from PubChem (Figure 12).

DISCUSSION

UCEC is the most common tumor affecting female reproductive system, with a 5-year survival rate of 16% in patients with distant metastasis (Siegel et al., 2019). To date, the therapeutic regimens, such as immunological therapy and chemotherapy, are

mainly designed according to the clinical stages of the tumor. Due to physiological differences, not all the patients can benefit from the current therapeutic regimens (Brooks et al., 2019). To overcome this challenge, in this research, we developed a model for predicting the survival and therapeutic response of UCEC patients using two immune-related genes.

We first estimated the relative levels of 24 immune cells based on the training set online data and used hierarchical clustering analysis to profile the infiltration of immune cells. The results revealed that the infiltration of immune cells varied much among UCEC patients. We found different tumor purities, immune scores, stromal scores, fractions of different immune cells, expression of several HLA genes and expression of five immune checkpoint molecules (CTLA4, CD274, HAVCR2, LAG3 and TIGHT) among UCEC subtypes. These results strongly suggest that tumor immune microenvironment has different landscapes in UCEC patients. Emerging evidence demonstrates that tumor immune microenvironment is closely associated with the prognosis of several cancers¹³ (Liu et al., 2020). In this research, we found the overall survival of three UCEC subtypes differed significantly. The hierarchical clustering analysis is capable of distinguishing patients with different prognosis. However, this method is complicated and produces irrelevant information, making it less clinically applicable.

To overcome the shortcomings, we filtered out two hub genes (CCL13 and KLRC1) closely related to the prognosis of UCEC patients. The mRNA and protein expression levels of both genes were verified via qPCR and IHC. The survival analyses confirmed the ability of IRPS in distinguishing patients with different prognosis. In order to enhance the predictive power of the IRPS, we added other clinical characteristics and built a nomogram model. According to the ROC and DCA curves, this nomogram model exhibited remarkable ability in predicting the prognosis of patients.

We further investigated the potential biological function of IRPS. The GSEA analysis revealed that several immune-related pathways were significantly enriched in the low-risk group. In contrast, the same pathways in the high-risk group were scattered. It is widely acknowledged that innate and

adaptive immune cells play a major role in regulating the cancer growth. Increasing evidence shows that some immune cells (like Neutrophils, Macrophage M2, T regulatory cell) can stimulate, while some (like Macrophage M1, CD8+ T cell and Th1 CD4+ T cell) can inhibit cancer growth (Coussens and Werb, 2002; Disis, 2010). In the present study, low-risk and high-risk groups differed

in the proportion of immune cells in UCEC, including plasma cells, CD8+ T cells, CD4+ memory T cells, CD4+ memory T cells, follicular helper T cells, M0 macrophages, M1 macrophages and activated mast cells. To be specific, M1 Macrophages, CD4+ and CD8+ T cells and plasma cells were activated in the low-risk group, suggesting that they can inhibit cancer growth and improve the prognosis of UCEC patients.

As listed in the methods section, the IRPS was established using the expression profiles of CCL13 and KLRC1. CCL13 is a gene located on chromosome 17q11.2 that encodes monocyte chemoattractant protein 4 (MCP-4), a Cys-Cys (CC) type cytokine characterized by two adjacent cysteines. In the immunoregulatory and inflammatory processes, CCL13 demonstrates chemotaxis to monocytes, lymphocytes, basophils and eosinophils, but not neutrophils, and plays a role in the accumulation of leukocytes during inflammation. Increasing evidence has confirmed that chemokines and their receptors can facilitate the entry of specific immune cells into tumors, thus enhancing anti-tumor response and improving patient prognosis (Rusakiewicz et al., 2013; Jacquelot et al., 2018).

KLRC1 (Killer Cell Lectin Like Receptor C1), also known as NKG2A, is a protein-coding gene associated with Natural killer (NK) cells. NK cells can mediate the lysis of certain tumor cells and virus-infected cells, and specific humoral and cell-mediated immunity. The protein encoded by KLRC1 belongs to the killer cell lectin-like receptor family, also called NKG2 family, which is a group of transmembrane proteins preferentially expressed in NK cells. KLRC1 can form a complex with KLRD1/CD94 and participate in the recognition of the MHC class I HLA-E molecules in NK cells. Researcher has also proved that crystal structure of CD94-NKG2A in complex with HLA-E bound to a peptide derived from the leader sequence of HLA-G. A previous study found KLRC1 expression changed with CD8+ T cell infiltration in 34 types of human cancers (Chen et al., 2019).

It is well known that tumors can escape the immune system via several mechanisms, including expanding T regulatory cells, inducing the production of certain inhibitory cytokines, altering the function of antigen presenting cells (APCs) (Disis, 2010). In this research, we found that the expression of CCL13 and KLRC1 had a positive correlation with the activation of several types of immune cells. Mutations in these two genes can inhibit the infiltration of some immune cells, especially in CD8+ T cells. Thus, IRPS based on both genes can distinguish cellular immunoactivation and immunosuppression.

We also investigated whether IRPS can provide valuable information about the host response to immunotherapy and chemotherapy. Immune checkpoint molecules are traditional biomarkers for evaluating the therapeutic benefit of immunotherapy. In this research, we found that the expression levels of four immune checkpoint molecules (PD-1, PD-L1, PD-L2 and CTLA4) were significantly low in the high-risk group, suggesting that the patients in the high-risk group might not benefit from immunotherapy based on immune checkpoint inhibitors. Apart from immune checkpoint molecules, tumor mutational burden (TMB) has emerged as a promising predictive biomarker for immunotherapy based on immune checkpoint inhibitors in several tumor types

TABLE 4 | Correlation analysis between two hub genes and immune cells markers in GEPIA.

Description	Gene markers	CCL13		KLRC1	
		R	P	R	P
CD8+ T cell	CD8A	0.59	***	0.65	***
	CD8B	0.37	***	0.52	***
T cell (general)	CD3D	0.47	***	0.59	***
	CD3E	0.49	***	0.65	***
B cell	CD2	0.49	***	0.65	***
	CD19	0.13	0.091	0.31	***
Monocyte	CD79A	0.31	***	0.45	***
	CD86	0.41	***	0.62	***
TAM	CD115 (CSF1R)	0.29	**	0.52	***
	CCL2	0.41	***	0.34	***
M2 Macrophage	CD68	0.42	***	0.52	***
	IL10	0.14	0.071	0.3	***
Neutrophils	CD163	0.39	***	0.48	***
	VSIG4	0.35	***	0.52	***
Natural killer cell	MS4A4A	0.42	***	0.57	***
	CD66b (CEACAM8)	-0.13	0.093	0.022	0.77
Dendritic cell	CD11b (ITGAM)	0.3	***	0.56	***
	CCR7	0.38	***	0.51	***
Th1	KIR2DL1	0.12	0.12	0.44	***
	KIR2DL3	0.3	***	0.54	***
T cell exhaustion	KIR2DL4	0.36	***	0.75	***
	KIR3DL1	0.35	***	0.5	***
T cell exhaustion	KIR3DL2	0.21	**	0.56	***
	KIR3DL3	0.25	***	0.39	***
T cell exhaustion	KIR2DS4	0.2	**	0.41	***
	HLA-DPB1	0.3	***	0.56	***
T cell exhaustion	HLA-DQB1	0.22	**	0.36	***
	HLA-DRA	0.28	***	0.53	***
T cell exhaustion	HLA-DPA1	0.36	***	0.6	***
	BDCA-1(CD1C)	0.12	0.13	0.35	***
T cell exhaustion	BDCA-4(NRP1)	0.14	0.057	0.36	***
	CD11c (ITGAX)	0.26	***	0.59	***
T cell exhaustion	T-bet (TBX21)	0.48	***	0.67	***
	STAT4	0.37	***	0.48	***
T cell exhaustion	STAT1	0.24	*	0.37	***
	IFN- γ (IFNG)	0.56	***	0.63	***
T cell exhaustion	TNF- α (TNF)	-0.022	0.77	0.041	0.6
	PD-1 (PDCD1)	0.45	***	0.55	***
T cell exhaustion	CTLA4	0.52	***	0.6	***
	LAG3	0.42	***	0.52	***
T cell exhaustion	TIM-3 (HAVCR2)	0.4	***	0.66	***
	GZMB	0.48	***	0.66	***

* $P < 0.01$; ** $P < 0.001$; *** $P < 0.0001$.

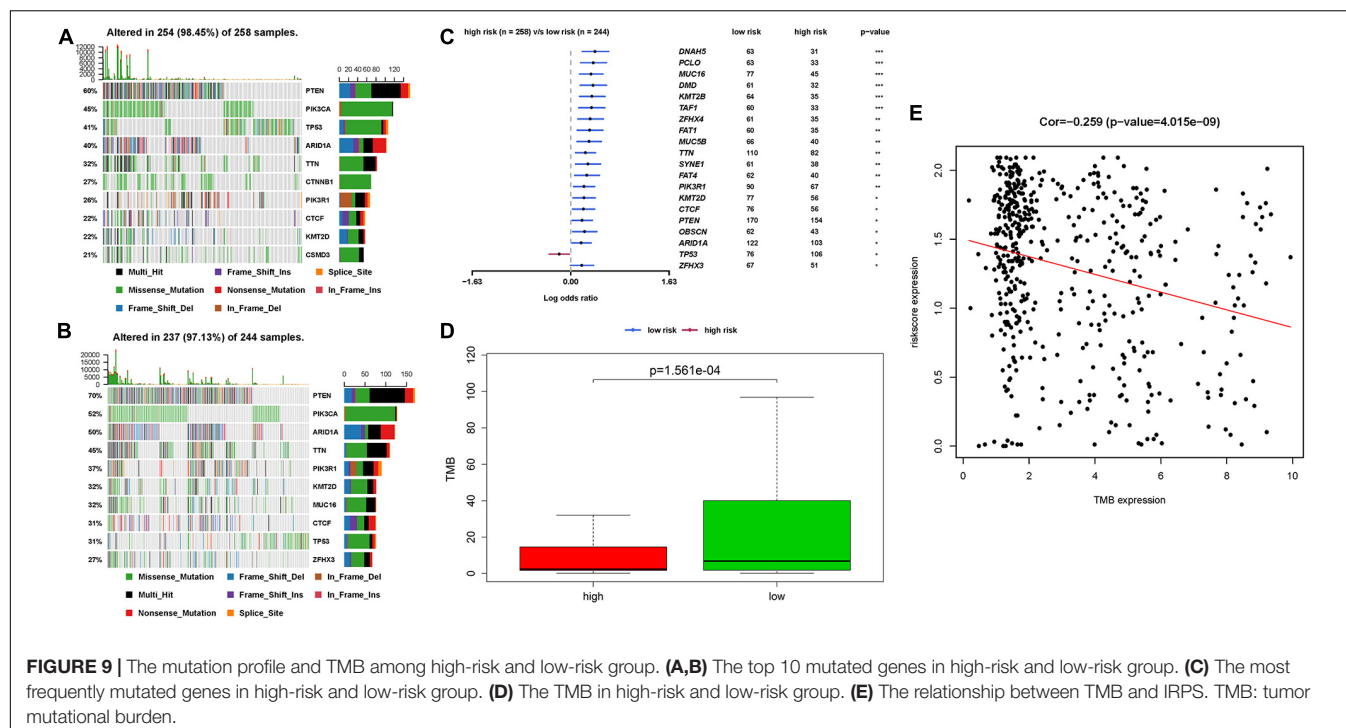


FIGURE 9 | The mutation profile and TMB among high-risk and low-risk group. **(A,B)** The top 10 mutated genes in high-risk and low-risk group. **(C)** The most frequently mutated genes in high-risk and low-risk group. **(D)** The TMB in high-risk and low-risk group. **(E)** The relationship between TMB and IRPS. TMB: tumor mutational burden.

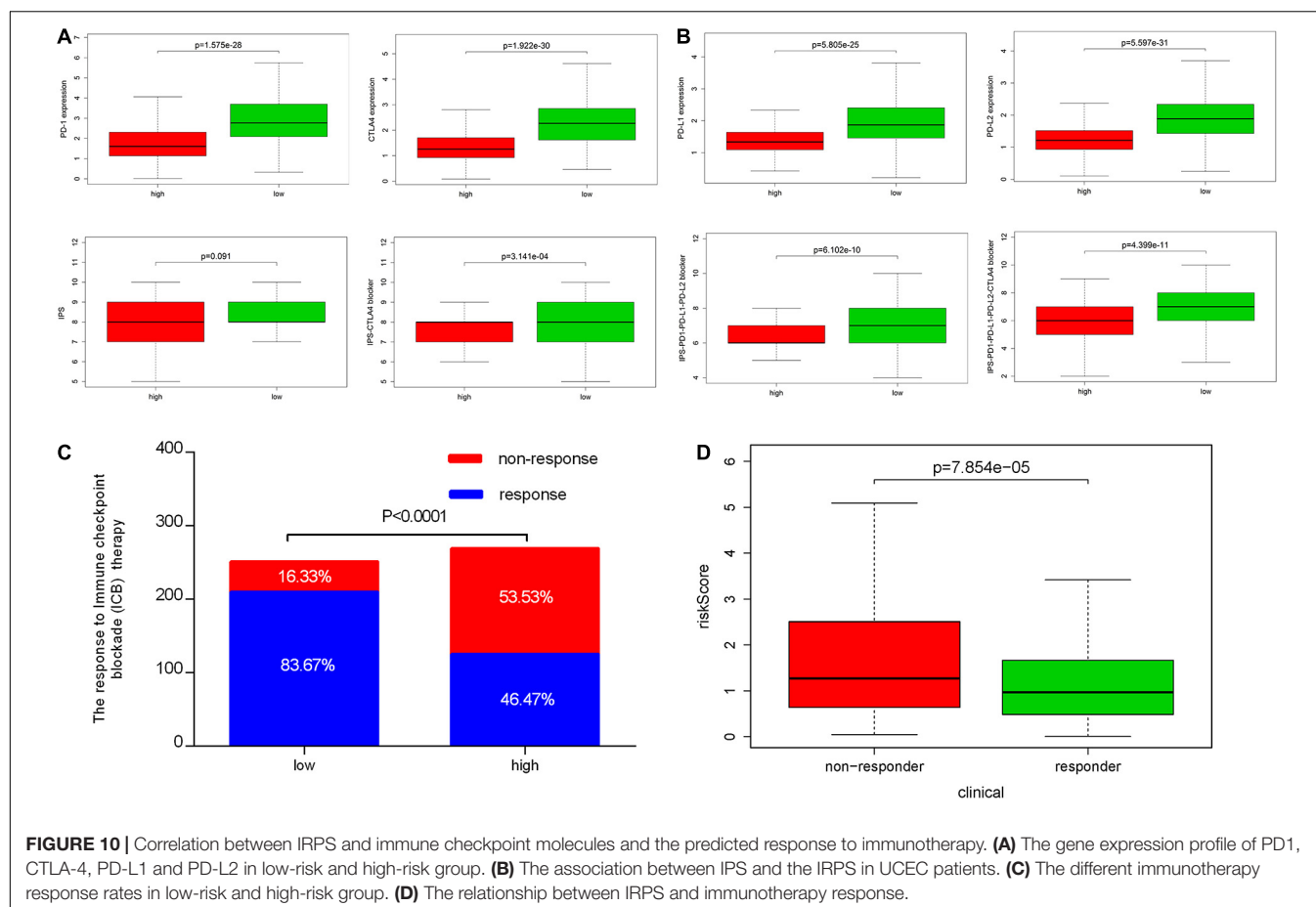


FIGURE 10 | Correlation between IRPS and immune checkpoint molecules and the predicted response to immunotherapy. **(A)** The gene expression profile of PD1, CTLA-4, PD-L1 and PD-L2 in low-risk and high-risk group. **(B)** The association between IPS and the IRPS in UCEC patients. **(C)** The different immunotherapy response rates in low-risk and high-risk group. **(D)** The relationship between IRPS and immunotherapy response.

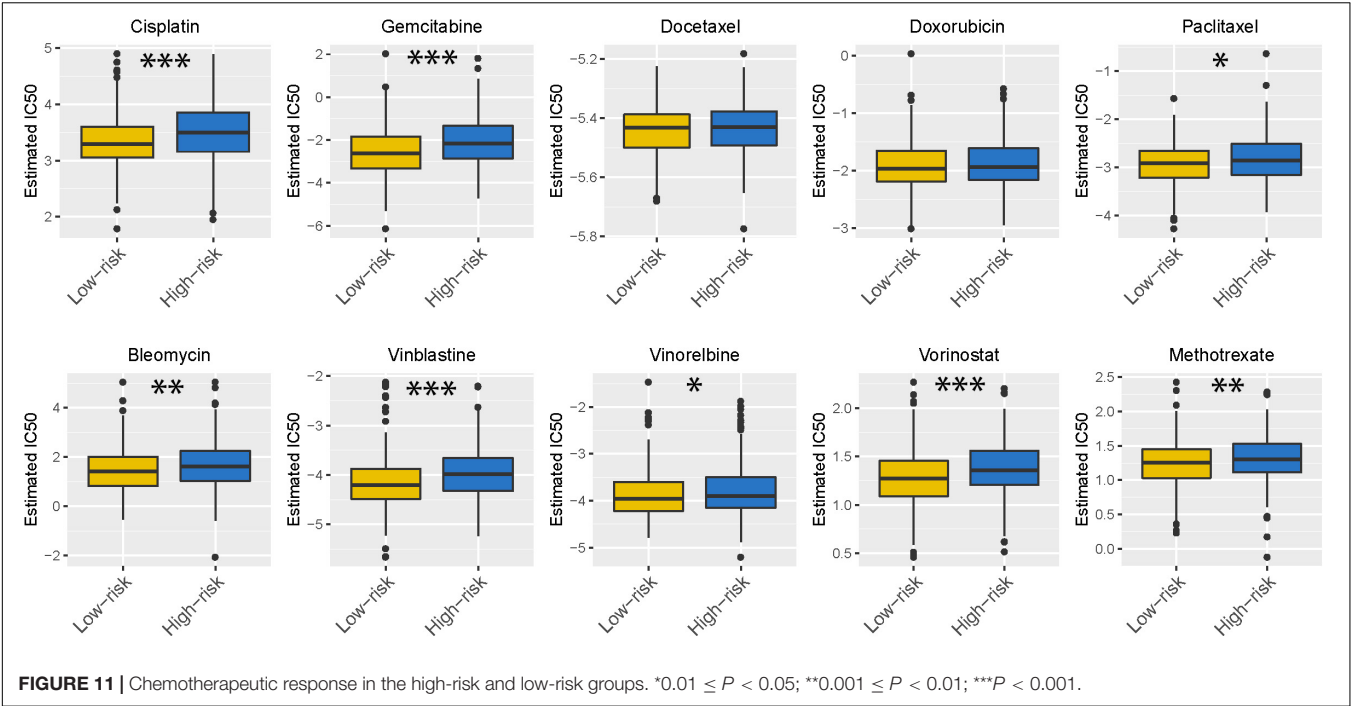
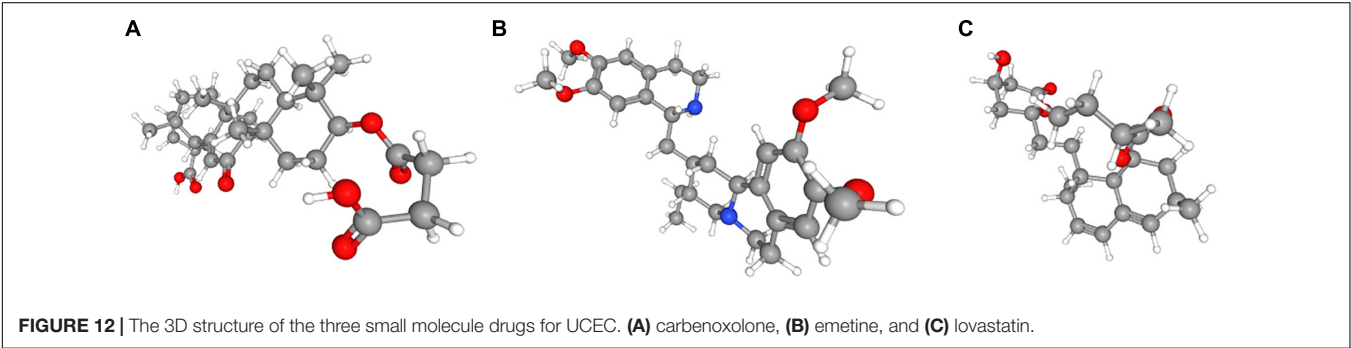


TABLE 5 | Results of CMap analysis.

Cmap name	Mean	<i>n</i>	Enrichment	<i>p</i>	Specificity	Percent non-null
Carbenoxolone	−0.332	4	−0.807	0.00271	0	50
Emetine	−0.6	4	−0.713	0.01369	0.1941	75
Lovastatin	−0.367	4	−0.704	0.01578	0.0233	50
MG-262	−0.567	3	−0.794	0.01787	0.1417	66
Piperlongumine	0.368	2	0.897	0.02181	0.1234	50
Megestrol	−0.406	4	−0.677	0.02425	0.0068	50
Semustine	−0.398	4	−0.653	0.03364	0.1111	50
Trimethoprim	−0.442	5	−0.577	0.04055	0.0449	60



(Chen et al., 2019). High TMB and high neoantigen load have positive correlation with sensitivity to immunotherapy (Hollern et al., 2019). Multiple studies have proved that TMB may be a surrogate for overall neoantigen load²⁰ (Rizvi et al., 2015; Rooney et al., 2015). During the cancer onset, somatic cells mutate and express neoantigens (Gubin et al., 2015). These neoantigens can sometimes induce T-cell-dependent immune responses by activating CD8+ T cells that can recognize those neoantigens and initiate tumor cell lysis (Chen and Flies, 2013).

In this research, when it turns to the evidence regarding immune checkpoint molecules, According to TMB and ImmuCellAI tool, patients in the low-risk group may benefit more from immunotherapy with immune checkpoint inhibitors, but those in the high-risk group may not. Similarly, the patients in the low-risk group were sensitive to chemodrugs such

as cisplatin, gemcitabine, paclitaxel, bleomycin, vinblastine, vinorelbine, vorinostat and methotrexate. However, patients in the high-risk group were resistant to these drugs, which may explain their poor prognosis.

Fortunately, we found that several small molecule drugs, such as carbenoxolone, emetine, lovastatin and MG-262, could provide potential benefits for patients in the high-risk group. There is limited research regarding the effects of these drugs on tumor. Carbenoxolone is widely used as an antiulcer drug, but with unknown effect on tumor. Carbenoxolone can also act as the inhibitor of Pannexin 1 (Panx-1) and suppress the migration and invasion of testicular cancer cells to counter cancer progression and metastasis (Penuela et al., 2012; Furlow et al., 2015; Jankowski et al., 2018; Liu et al., 2019). Emetine, a potent anti-protozoal and emetic drug, recent evidence has verified its anti-malarial, anti-bacterial and anti-amoebic effects (Matthews et al., 2013; Hudson et al., 2016; Khandelwal et al., 2017; Yang et al., 2018). Over the past decades, emetine has been reported to have anti-tumor effects on leukemia, ovarian cancer, bladder cancer and lung cancer by inhibiting tumor growth by regulating multiple mechanisms such as apoptosis and autophagy (Moller and Wink, 2007; Moller et al., 2007; Kim et al., 2015; Sun et al., 2015). Lovastatin, an HMG-CoA reductase inhibitor, can decrease cholesterol biosynthesis and is an ideal medicine for treating coronary heart disease. In 2004, lovastatin was found to be a useful adjuvant drug for breast cancer (Shibata et al., 2004). Besides, lovastatin can reduce cancer-related deaths. MG-262, also known as Z-Leu-Leu-Leu-B(OH)₂, is a proteasome inhibitor that can reversibly and selectively inhibit chymotryptic activity of the proteasome. As we know, proteasome inhibition has emerged as a novel approach to treat cancer. In some studies, MG-262 has exhibited obvious inhibitory effect on the growth of malignant cells.

The above drugs are untraditional anti-tumor drugs and there is limited evidence of their effects on tumors especially UCEC. However, for patients in the high-risk group, all drugs with potential benefits should be tried. For patients who may not benefit from traditional drugs, adjuvant agents should be tried.

Nevertheless, there are still some limitations in this research. First, this study only includes the immune-related genes and did not take other biomarkers into consideration. Another important issue, there are lots of immune cells varies significantly among individuals, it is hard to distinguish if the gene expression level mainly depends on the varieties of immune cells. The variable number of NK cells might be a confounder for KLRC1 expression. We used Timer2.0 to explore the correlation of KLRC1 and NK cells, the result confirmed that the expression of KLRC1 is positively correlated with NK cells. However, according to the results of CIBERSORT analysis, the proportion of NK cells showed no significant difference in high- and low- risk group. Besides, by analyzing the correlation between the RiskScore and different types of immune cells, we found the RiskScore was negatively correlated with NK cells. Thus, we speculated that the expression of KLRC1 might not mainly depend on the number of NK cells varieties among individuals. It was an independent prognosis related factor. Additionally, this research is based on

the online data, and large-sample clinical studies are still needed to validate the predictive value of our IRPS model.

In summary, our study identified two immune-related genes, CCL13 and KLRC1 in the development of UCEC. The IRPS of both genes can predict the prognosis and immune status of UCEC patients and evaluate their therapeutic response to immunotherapy and chemotherapy.

DATA AVAILABILITY STATEMENT

The datasets presented in this study can be found in online repositories. The names of the repository/repositories and accession number(s) can be found in the article/**Supplementary Material**.

ETHICS STATEMENT

The studies involving human participants were reviewed and approved by Clinical Research Ethics Committee, Wuxi Maternal and Child Health Hospital, The Affiliated Hospital to Nanjing Medical University. The patients/participants provided their written informed consent to participate in this study.

AUTHOR CONTRIBUTIONS

YZ conceived the study. JL, YW, and JM participated in the design, analysis, and draft of the study. JL and YW plotted all figures in this manuscript. JM helped in data analysis. All authors approved the final version of this manuscript and agreed to be accountable for all aspects of the work.

FUNDING

This study was financially supported by the Wuxi Science and Technology Bureau Project (No. CSE31N1720), the Jiangsu Province Youth Medical Talent Fund Project (No. QNRC2016166), and the Jiangsu Provincial Six Talent Peaks Project (No. YY-124).

ACKNOWLEDGMENTS

We thank Cao Yongke, Ph.D., from Nanjing KEY Translation Studio for editing the English text of a draft of this manuscript.

SUPPLEMENTARY MATERIAL

The Supplementary Material for this article can be found online at: <https://www.frontiersin.org/articles/10.3389/fcell.2021.671736/full#supplementary-material>

REFERENCES

- Barbie, D. A., Tamayo, P., Boehm, J. S., Kim, S. Y., Moody, S. E., Dunn, I. F., et al. (2009). Systematic RNA interference reveals that oncogenic KRAS-driven cancers require TBK1. *Nature* 462, 108–112. doi: 10.1038/nature08460
- Binnewies, M., Roberts, E. W., Kersten, K., Chan, V., Fearon, D. F., Merad, M., et al. (2018). Understanding the tumor immune microenvironment (TIME) for effective therapy. *Nat. Med.* 24, 541–550. doi: 10.1038/s41591-018-0014-x
- Bray, F., Ferlay, J., Soerjomataram, I., Siegel, R. L., Torre, L. A., and Jemal, A. (2018). Global cancer statistics 2018: GLOBOCAN estimates of incidence and mortality worldwide for 36 cancers in 185 countries. *CA Cancer J. Clin.* 68, 394–424. doi: 10.3322/caac.21492
- Brooks, R. A., Fleming, G. F., Lastra, R. R., Lee, N. K., Moroney, J. W., Son, C. H., et al. (2019). Current recommendations and recent progress in endometrial cancer. *CA Cancer J. Clin.* 69, 258–279. doi: 10.3322/caac.21561
- Chaudhry, P., and Asselin, E. (2009). Resistance to chemotherapy and hormone therapy in endometrial cancer. *Endocr. Relat. Cancer* 16, 363–380. doi: 10.1677/ERC-08-0266
- Chen, L., and Flies, D. B. (2013). Molecular mechanisms of T cell co-stimulation and co-inhibition. *Nat. Rev. Immunol.* 13, 227–242. doi: 10.1038/nri3405
- Chen, Y., Xin, Z., Huang, L., Zhao, L., Wang, S., Cheng, J., et al. (2019). CD8(+) T cells form the predominant subset of NKG2A(+) cells in human lung cancer. *Front. Immunol.* 10:3002. doi: 10.3389/fimmu.2019.03002
- Coussens, L. M., and Werb, Z. (2002). Inflammation and cancer. *Nature* 420, 860–867. doi: 10.1038/nature01322
- Disis, M. L. (2010). Immune regulation of cancer. *J. Clin. Oncol.* 28, 4531–4538. doi: 10.1200/JCO.2009.27.2146
- Furlow, P. W., Zhang, S., Soong, T. D., Halberg, N., Goodarzi, H., Mangrum, C., et al. (2015). Mechanosensitive pannexin-1 channels mediate microvascular metastatic cell survival. *Nat. Cell Biol.* 17, 943–952. doi: 10.1038/ncb3194
- Galon, J., Angell, H. K., Bedognetti, D., and Marincola, F. M. (2013). The continuum of cancer immunosurveillance: prognostic, predictive, and mechanistic signatures. *Immunity* 39, 11–26. doi: 10.1016/j.immuni.2013.07.008
- Gottwald, L., Pluta, P., Piekarski, J., Szych, M., Hendzel, K., Topczewska-Tylinska, K., et al. (2010). Long-term survival of endometrioid endometrial cancer patients. *Arch. Med. Sci.* 6, 937–944. doi: 10.5114/aoms.2010.19305
- Gubin, M. M., Artyomov, M. N., Mardis, E. R., and Schreiber, R. D. (2015). Tumor neoantigens: building a framework for personalized cancer immunotherapy. *J. Clin. Invest.* 125, 3413–3421. doi: 10.1172/JCI80008
- Hanzelmann, S., Castelo, R., and Guinney, J. (2013). GSEA: gene set variation analysis for microarray and RNA-seq data. *BMC Bioinformatics* 14:7. doi: 10.1186/1471-2105-14-7
- Hollern, D. P., Xu, N., Thennavan, A., Glodowski, C., Garcia-Recio, S., Mott, K. R., et al. (2019). B Cells and T follicular helper cells mediate response to checkpoint inhibitors in high mutation burden mouse models of breast cancer. *Cell* 179, 1191–1206.e21. doi: 10.1016/j.cell.2019.10.028
- Hudson, L. K., Dancho, M. E., Li, J., Bruchfeld, J. B., Ragab, A. A., He, M. M., et al. (2016). Emetine Di-HCl attenuates type 1 diabetes mellitus in mice. *Mol. Med.* 22, 585–596. doi: 10.2119/molmed.2016.00082
- Jacquelot, N., Duong, C. P. M., Belz, G. T., and Zitvogel, L. (2018). Targeting chemokines and chemokine receptors in melanoma and other cancers. *Front. Immunol.* 9:2480. doi: 10.3389/fimmu.2018.02480
- Jain, A., Chia, W. K., and Toh, H. C. (2016). Immunotherapy for nasopharyngeal cancer—a review. *Chin. Clin. Oncol.* 5:22. doi: 10.21037/cco.2016.03.08
- Jankowski, J., Perry, H. M., Medina, C. B., Huang, L., Yao, J., Bajwa, A., et al. (2018). Epithelial and endothelial pannexin1 channels mediate AKI. *J. Am. Soc. Nephrol.* 29, 1887–1899. doi: 10.1681/ASN.2017121306
- Khandelwal, N., Chander, Y., Rawat, K. D., Riyesh, T., Nishanth, C., Sharma, S., et al. (2017). Emetine inhibits replication of RNA and DNA viruses without generating drug-resistant virus variants. *Antiviral Res.* 144, 196–204. doi: 10.1016/j.antiviral.2017.06.006
- Kim, J. H., Cho, E. B., Lee, J., Jung, O., Ryu, B. J., Kim, S. H., et al. (2015). Emetine inhibits migration and invasion of human non-small-cell lung cancer cells via regulation of ERK and p38 signaling pathways. *Chem. Biol. Interact.* 242, 25–33. doi: 10.1016/j.cbi.2015.08.014
- Lamb, J., Crawford, E. D., Peck, D., Modell, J. W., Blat, I. C., Wrobel, M. J., et al. (2006). The connectivity map: using gene-expression signatures to connect small molecules, genes, and disease. *Science* 313, 1929–1935. doi: 10.1126/science.1132939
- Liu, H., Yuan, M., Yao, Y., Wu, D., Dong, S., and Tong, X. (2019). In vitro effect of Pannexin 1 channel on the invasion and migration of I-10 testicular cancer cells via ERK1/2 signaling pathway. *Biomed. Pharmacother.* 117:109090. doi: 10.1016/j.biopha.2019.109090
- Liu, S. L., Bian, L. J., Liu, Z. X., Chen, Q. Y., Sun, X. S., Sun, R., et al. (2020). Development and validation of the immune signature to predict distant metastasis in patients with nasopharyngeal carcinoma. *J. Immunother. Cancer* 8:e000205. doi: 10.1136/jitc-2019-000205
- Lortet-Tieulent, J., Ferlay, J., Bray, F., and Jemal, A. (2018). International patterns and trends in endometrial cancer incidence, 1978–2013. *J. Natl. Cancer Inst.* 110, 354–361. doi: 10.1093/jnci/djx214
- Matthews, H., Usman-Idris, M., Khan, F., Read, M., and Nirmalan, N. (2013). Drug repositioning as a route to anti-malarial drug discovery: preliminary investigation of the in vitro anti-malarial efficacy of emetine dihydrochloride hydrate. *Malar J.* 12:359. doi: 10.1186/1475-2875-12-359
- Miao, Y. R., Zhang, Q., Lei, Q., Luo, M., Xie, G. Y., Wang, H., et al. (2020). ImmuCellAI: a unique method for comprehensive T-cell subsets abundance prediction and its application in cancer immunotherapy. *Adv. Sci. (Weinh)* 7:1902880. doi: 10.1002/advs.201902880
- Moller, M., Herzer, K., Wenger, T., Herr, I., and Wink, M. (2007). The alkaloid emetine as a promising agent for the induction and enhancement of drug-induced apoptosis in leukemia cells. *Oncol. Rep.* 18, 737–744.
- Moller, M., and Wink, M. (2007). Characteristics of apoptosis induction by the alkaloid emetine in human tumour cell lines. *Planta Med.* 73, 1389–1396. doi: 10.1055/s-2007-990229
- Pages, F., Mlecnik, B., Marliot, F., Bindea, G., Ou, F. S., Bifulco, C., et al. (2018). International validation of the consensus immunescore for the classification of colon cancer: a prognostic and accuracy study. *Lancet* 391, 2128–2139. doi: 10.1016/S0140-6736(18)30789-X
- Penuela, S., Gyenies, L., Ablack, A., Churko, J. M., Berger, A. C., Litchfield, D. W., et al. (2012). Loss of pannexin 1 attenuates melanoma progression by reversion to a melanocytic phenotype. *J. Biol. Chem.* 287, 29184–29193. doi: 10.1074/jbc.M112.377176
- Rizvi, N. A., Hellmann, M. D., Snyder, A., Kvistborg, P., Makarov, V., Havel, J. J., et al. (2015). Cancer immunology. Mutational landscape determines sensitivity to PD-1 blockade in non-small cell lung cancer. *Science* 348, 124–128. doi: 10.1126/science.aaa1348
- Rooney, M. S., Shukla, S. A., Wu, C. J., Getz, G., and Hacohen, N. (2015). Molecular and genetic properties of tumors associated with local immune cytolytic activity. *Cell* 160, 48–61. doi: 10.1016/j.cell.2014.12.033
- Rusakiewicz, S., Semeraro, M., Sarabi, M., Desbois, M., Locher, C., Mendez, R., et al. (2013). Immune infiltrates are prognostic factors in localized gastrointestinal stromal tumors. *Cancer Res.* 73, 3499–3510. doi: 10.1158/0008-5472.CAN-13-0371
- Shibata, M. A., Ito, Y., Morimoto, J., and Otsuki, Y. (2004). Lovastatin inhibits tumor growth and lung metastasis in mouse mammary carcinoma model: a p53-independent mitochondrial-mediated apoptotic mechanism. *Carcinogenesis* 25, 1887–1898. doi: 10.1093/carcin/bgh201
- Siegel, R. L., Miller, K. D., and Jemal, A. (2019). Cancer statistics, 2019. *CA Cancer J. Clin.* 69, 7–34. doi: 10.3322/caac.21551
- Sun, Q., Yogosawa, S., Iizumi, Y., Sakai, T., and Sowa, Y. (2015). The alkaloid emetine sensitizes ovarian carcinoma cells to cisplatin through downregulation of bcl-xL. *Int. J. Oncol.* 46, 389–394. doi: 10.3892/ijo.2014.2703
- Yang, S., Xu, M., Lee, E. M., Gorshkov, K., Shiryaev, S. A., He, S., et al. (2018). Emetine inhibits Zika and Ebola virus infections through two molecular mechanisms: inhibiting viral replication and decreasing viral entry. *Cell Discov.* 4:31. doi: 10.1038/s41421-018-0034-1

- Yoshihara, K., Shahmoradgoli, M., Martinez, E., Vegesna, R., Kim, H., Torres-Garcia, W., et al. (2013). Inferring tumour purity and stromal and immune cell admixture from expression data. *Nat. Commun.* 4:2612. doi: 10.1038/ncomms3612
- Yu, Y., Ke, L., Lv, X., Ling, Y. H., Lu, J., Liang, H., et al. (2018). The prognostic significance of carcinoma-associated fibroblasts and tumor-associated macrophages in nasopharyngeal carcinoma. *Cancer Manag. Res.* 10, 1935–1946. doi: 10.2147/CMAR.S167071

Conflict of Interest: The authors declare that the research was conducted in the absence of any commercial or financial relationships that could be construed as a potential conflict of interest.

Publisher's Note: All claims expressed in this article are solely those of the authors and do not necessarily represent those of their affiliated organizations, or those of the publisher, the editors and the reviewers. Any product that may be evaluated in this article, or claim that may be made by its manufacturer, is not guaranteed or endorsed by the publisher.

Copyright © 2021 Liu, Wang, Mei, Nie and Zhang. This is an open-access article distributed under the terms of the Creative Commons Attribution License (CC BY). The use, distribution or reproduction in other forums is permitted, provided the original author(s) and the copyright owner(s) are credited and that the original publication in this journal is cited, in accordance with accepted academic practice. No use, distribution or reproduction is permitted which does not comply with these terms.



Surface PEGylated Cancer Cell Membrane-Coated Nanoparticles for Codelivery of Curcumin and Doxorubicin for the Treatment of Multidrug Resistant Esophageal Carcinoma

Yi Gao¹, Yue Zhu¹, Xiaopeng Xu¹, Fangjun Wang¹, Weidong Shen¹, Xia Leng¹, Jiyi Zhao¹, Bingtuan Liu¹, Yangyun Wang² and Pengfei Liu^{1*}

¹ Department of Gastroenterology, The Affiliated Jiangyin Hospital of Xuzhou Medical University, Jiangyin, China, ² State Key Laboratory of Radiation Medicine and Protection, Medical College of Soochow University, Suzhou, China

OPEN ACCESS

Edited by:

Wei Zhao,
City University of Hong Kong,
Hong Kong, SAR China

Reviewed by:

Haishi Qiao,
China Pharmaceutical University,
China
Lingling Liu,
Chengdu Medical College, China

*Correspondence:

Pengfei Liu
pengfeimd@163.com

Specialty section:

This article was submitted to
Molecular and Cellular Oncology,
a section of the journal
Frontiers in Cell and Developmental
Biology

Received: 30 March 2021

Accepted: 23 June 2021

Published: 27 July 2021

Citation:

Gao Y, Zhu Y, Xu X, Wang F,
Shen W, Leng X, Zhao J, Liu B,
Wang Y and Liu P (2021) Surface
PEGylated Cancer Cell
Membrane-Coated Nanoparticles
for Codelivery of Curcumin
and Doxorubicin for the Treatment
of Multidrug Resistant Esophageal
Carcinoma.
Front. Cell Dev. Biol. 9:688070.
doi: 10.3389/fcell.2021.688070

Objective: The emergence of multi-drug resistance (MDR) in esophageal carcinoma has severely affected the effect of chemotherapy and shortened the survival of patients. To this end, we intend to develop a biomimetic nano-targeting drug modified by cancer cell membrane, and investigate its therapeutic effect.

Methods: The degradable poly(lactic-co-glycolic acid) (PLGA) nanoparticles (NPs) co-loaded with doxorubicin (DOX) and curcumin (Cur) were prepared by solvent evaporation method. TE10 cell membrane and Distearoyl phosphatidylethanolamine-polyethylene glycol (DSPE-PEG) were then coated on the PLGA NPs by membrane extrusion to prepare the PEG-TE10@PLGA@DOX-Cur NPs (PMPNs). Size and zeta potential of the PMPNs were analyzed by laser particle analyzer, and the morphology of PMPNs was observed by transmission electron microscope. The TE10 cell membrane protein on PMPNs was analyzed by gel electrophoresis. The DOX-resistant esophageal cancer cell model TE10/DOX was established through high-dose induction. The *In vitro* homologous targeting ability of PMPNs was evaluated by cell uptake assay, and the *in vitro* anti-tumor effect of PMPNs was assessed through CCK-8, clone formation and flow cytometry. A Balb/c mouse model of TE10/DOX xenograft was constructed to evaluate the anti-tumor effect *in vivo* and the bio-safety of PMPNs.

Results: The prepared cell membrane coated PMPNs had a regular spherical structure with an average diameter of 177 nm. PMPNs could directly target TE10 and TE10/DOX cells or TE10/DOX xenografted tumor and effectively inhibit the growth of DOX-resistant esophageal carcinoma. Besides, the PMPNs was confirmed to have high biosafety.

Conclusion: In this study, a targeted biomimetic nano-drug delivery system PMPNs was successfully prepared, which overcome the MDR of esophageal carcinoma by co-delivering DOX and sensitizer curcumin.

Keywords: esophageal carcinoma, multidrug resistant, homologous targeting, doxorubicin, curcumin

INTRODUCTION

Esophageal carcinoma (ESCA) is a common tumor in the digestive system (Alsop and Sharma, 2016). It is insidious, almost asymptomatic in the early stage, and most patients have entered the advanced stage when discovered, which significantly increases the difficulty of treatment and the chance of recurrence (Domper Arnal et al., 2015; Ohashi et al., 2015). In addition to surgical resection, two strategies have been employed to improve the therapeutic effect of ESCA, one is to seek more effective drugs, such as molecular-targeted drugs; the other one is drug combination, through combining one chemotherapy drug with other chemotherapy drugs, molecular-targeted drugs or sensitizers, which assemble different mechanisms to enhance the effect of chemotherapy (Hu et al., 2020; Zhao et al., 2020). However, the MDR of esophageal carcinoma is still a difficult problem to overcome. Therefore, the combination of chemotherapeutics and sensitizers has received widespread attention. DOX is the first-line clinical drug for the treatment of esophageal carcinoma, but its narrow therapeutic window, cardiotoxicity, and other side effects and drug resistance restrict its application (Amjadi et al., 2019). Studies have shown that the combined use of DOX and sensitizers can significantly enhance its antitumor ability (Oh et al., 2015). Cur, an extract of traditional Chinese medicine, was found to be a potential chemotherapeutic sensitizer, which can reverse MDR and reduce the side effects of chemotherapeutic drugs, to achieve the effect of synergistic treatment of tumor (Xu et al., 2020).

In recent years, with the development of nanotechnology, tumor targeting therapy mediated by nanoscale materials has aroused widespread attention. Lee et al. (2020) synthesized PLGA NPs loaded with DOX. Through the interaction between DOX and sialic acid on tumor cells, the targeting capacity of NPs and the permeability of the tumor were simultaneously enhanced, which was beneficial for NPs enter the tumor to exert their efficacy. Drug-loaded nano-system has many advantages. On the one hand, it enhances the solubility and bioavailability of drugs; on the other hand, it has the sustained effect for drug release, which makes the drug concentration in blood stable in a safe and effective range over a period of time, thus extending the efficacy time and reducing the toxicity and side effects of drugs (Li et al., 2017; Ma et al., 2013; Prakash and Dhesingh, 2017; Son and Kim, 2017). The frequently used drug delivery nano-system include liposomes, solid lipid nanoparticles, polymer nanoparticles, dendrimers, nanoemulsions, inorganic porous silicon nanoparticles, magnetic iron oxide nanoparticles, etc. (Rabanel et al., 2012; Carita et al., 2018). PLGA is a biodegradable functional polymer organic compound with good biocompatibility, spheronization, and non-toxicity. It has been widely used in drug delivery and medical materials in recent years (Han et al., 2016; Lagreca et al., 2020).

In the multiple researches of nano-therapeutics, direct targeting of tumors by surface modification of NPS has always been a hot topic. It has been reported that NPs can be enriched in tumor tissues by passive targeting, that is, taking advantage of the

enhanced permeability and retention (EPR) effect (Maeda, 2017). However, the enrichment efficiency of EPR effect is not high, exhibiting obvious diversity and heterogeneity (Danhier, 2016). Therefore, researchers have gradually turned their attention to how to achieve the active targeting function of NPs. The emergence of the cell membrane wrapping technology provides a new modification and camouflage strategy for the development of NPs with high targeting and low immunogenicity. The first report of this technology was Hu et al. (2011), they wrapped NPs with erythrocyte membrane to allow it to evade immune surveillance. Different cell membrane coating endows NPs different functions. For example, NPs wrapped with erythrocyte membrane can evade immune surveillance, NPs wrapped with stem cell membranes show good targeting anti-tumor effects, and macrophage membranes wrapped NPs can reduce the effects of opsonin and prolong circulation time (Wang et al., 2018). Compared to wrapping with other cell membranes, NPs encapsulated with tumor cell membranes have excellent targeting effect (Zhen et al., 2019). In addition to accumulate to the target sites by EPR effect, it can also actively aggregate to tumor sites through homologous recognition mechanism. Research by Fang et al. (2014) showed that the NPs wrapped with tumor cell membrane were 40 and 20 times more efficient to be taken up by tumor cells than erythrocyte membrane-coated NPs and the naked NPs, respectively. Hence, the use of tumor cell membranes to encapsulate drug-loaded NPs is an effective tool to achieve efficient drug delivery and targeted attack on tumors. In addition, NPs are unstable in the body and are easily swallowed by the reticuloendothelial system (RES), resulting in shorter circulation time in the body and reduced drug release, thereby reducing clinical effects. The most common solution to solve this problem is to modify the surface of NPs with PEG. PEG is a non-toxic, non-immunogenic and antigenic, highly water-soluble compound, and has no effect on the release of drugs. PEGylation can enhance the stability of the NPs, prevent the binding of NPs and plasma proteins, thereby reducing the clearance rate of the reticuloendothelial system and prolonging the half-life of the drug, besides, it can reduce the immunogenicity of NPs and enhance drug retention (Yadav and Dewangan, 2021).

Herein, we designed and synthesized PMPNs for targeted therapy of MDR esophageal carcinoma. The PLGA NPs co-loaded anti-cancer drugs DOX and Cur was prepared by solvent volatilization method, thus enhanced the anti-tumor effect through the synergistic effect of the drugs. Then, the extracted TE10 cell membrane and DSPE-PEG were self-assembled to wrap the drug-loaded PLGA NPs, so that the homologous recognition mechanism between tumor cells could be used to achieve tumor targeting. The PMPNs could avoid the rapid clearance of the RES to a certain extent and increase the circulation time in the body. It was confirmed that PMPNs have a good therapeutic effect on MDR esophageal carcinoma, it could not only overcome the side effects of chemotherapy drugs, but also target tumor sites and increase the residence time of drugs in tumor. Our research will become an innovative strategy for treating MDR esophageal carcinoma.

MATERIALS AND METHODS

Materials

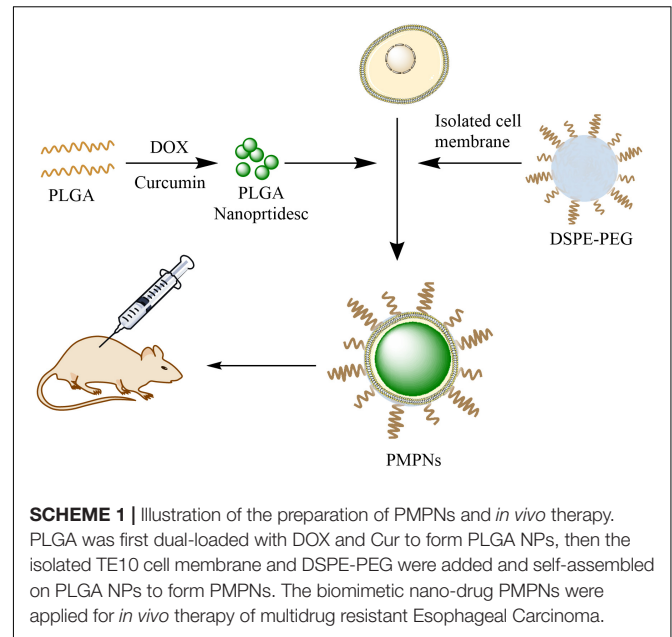
Cell lines were all obtained from American Type Culture Collection (ATCC). DMEM medium, Fetal Bovine Serum (FBS) were purchased from Hyclone (United States). Penicillin and Streptomycin mixture, trypsin ethylenediaminetetraacetic acid (EDTA), Coomassie Brilliant Blue Dye, Bull Serum Albumin (BSA), ECL luminescence reagent, 4',6-diamidino-2-phenylindole (DAPI) reagent, Propidium Iodide (PI) reagent, Cell Counting kit (CCK) - 8, Hematoxylin-Eosin (HE) staining kit, membrane protein extraction kit and TdT-mediated dUTP Nick-End Labeling (TUNEL) apoptosis assay kit were obtained from Sangon Biotech (China). The malondialdehyde (MDA) content detection kit and superoxide dismutase (SOD) activity detection kit was purchased from Solarbio life sciences (China), the Glutathione peroxidase (GSH-Px) detection kit was purchased from Leagene Biotechnology (China). PLGA (Lactic acid: Glycolic acid = 50:50), Polyvinyl alcohol (PVA), DSPE-PEG and tetramethyl rhodamine (TRITC) were purchased from Sigma-Aldrich (United States). DOX and Cur was provided by Meilunbio (China). The polycarbonate membrane (220 nm), polyvinylidene fluoride (PVDF) membrane and Transwell chamber were purchased from Millipore (Germany). The monoclonal antibody against ABCB1 (ab231535), ABCC1 (ab69296), LGR5 (ab75850), CD44 (ab51037), Bax (ab270742), Cyto-C (ab133504), cleaved caspase 3 (ab214430) and β -actin (ab179467) were purchased from Abcam (United Kingdom). The secondary antibodies including Goat anti-mouse IgG (ab205719) and Goat anti-rabbit IgG (ab205718) were obtained from Thermo Fisher Scientific (United States).

Cell Culture

TE10, L02, and A549 cells were used in this study. These cells were first resuscitated with Dulbecco's Modified Eagle Medium (DMEM) complete medium supplemented with 10% fetal bovine serum (FBS), 100 U/mL penicillin and streptomycin, then cultured and passaged in an incubator containing 5% CO₂ at 37°C.

Cell Membrane Extraction

The digested TE10 cells (1×10^8) were collected and centrifuged at 700 g for 5 min. The cells were suspended in pre-cooled phosphate buffer saline (PBS) buffer (pH = 7.4) and then centrifuged at 700 g for 5 min. According to the instruction of Cell membrane protein and cytoplasmic protein extraction kit (Beyotime, China), specifically, TE10 cells were collected and washed 3 times with pre-cooled PBS, and then resuspended with 1 mL reagent A. After ice bathing for 15 min, the cell suspension was placed in liquid nitrogen and room temperature (RT) successively, and then freeze-thaw for twice. After that, it was centrifuged at 700 g, 4°C for 10 min, then the supernatant was centrifuged 14,000 g, 4°C for 30 min. Finally, the collected cell pellets were suspended with membrane protein extraction reagent containing Phenylmethylsulfonyl fluoride (PMSF). The



cells were ice-bathed in this hypotonic lysis buffer for 10–15 min and then lysed with ultrasound. Cell lysate was centrifuged at 700 g for 10 min and the supernatant was then centrifuged at 14,000 g for 30 min. The precipitate was the extracted cell membrane.

Preparation of Drug-Loaded PLGA NPs

To prepare the dual-loaded PLGA NPs, we first dissolved 10 mg Cur and 300 mg PLGA (50:50) in 10 mL of dichloromethane under sonication to prepare the oil phase. Next, 10 mg DOX was dissolved in 1 mL ddH₂O as water phase. The oil and water phase were mixed up with ultrasonic wave (Kunshan KQ-250E Ultrasonic Instrument, China) for 10 min. Then, the mixed emulsion was quickly added to 100 mL PVA (2%) solution under high-speed magnetic stirring to form microspheres. Finally, the microspheres were stirred magnetically at 800 rpm for 8 h in RT to completely evaporate methylene chloride. The sample was frozen for 12 h after washing with ddH₂O for three times and then vacuum dried (Christ Freeze dryer, Germany) for subsequent use (Scheme 1).

Preparation of PMPNs

The TE10 cell membrane and DSPE-PEG15000 at a 5 mg/mL concentration were blended with drug-loaded PLGA NPs under ultrasonic. Then, Avanti Mini-Extruder (Beckman Coulter, United States) was used to squeeze 10 times on a 200 nm polycarbonate porous membrane, and then the solution was centrifuged to remove excess cell membrane (Scheme 1).

Characterization of PMPNs

After preparing the appropriate concentration of PLGA NPs, TE10 vesicles, TE10-PLGA and PEG-TE10-PLGA NPs, the size and zeta potential were measured with laser particle size analyzer (Malvern, United Kingdom). Then, we dropped 10 μ L of them

on a 200-mesh copper mesh with carbon-supported film, after keeping for 5 min at RT, the excess liquid was absorbed with filter paper. After that, 5 μ L of 1% phosphotungstic acid was dropped on the copper mesh and dyed for 2 min, then the structure of the samples was observed with a transmission electron microscope (FEI Talos L120C, United States).

To characterize the cancer cell membrane proteins on the surface of the NPs, we mixed PLGA NPs, TE10 vesicles, TE10@PLGA, and PEG-TE10-PLGA NPs with the loading buffer, and denatured at 95°C for 5 min. Then, samples and the protein marker were slowly added to the wells of two gels and underwent electrophoresis at constant voltage of 100 V (Bio-rad Mini-ProteinTetra, United States). After electrophoresis, the gels were taken out and one gel was stained with Coomassie Brilliant Blue Solution and photographed for analysis. Another gel was performed trans-membrane assay. After the experiment, the membrane was blocked with 1% BSA, then incubated with the primary antibody LGR5 and CD44 (1: 2,000 dilution) at 4°C overnight, followed by secondary antibody (1: 10,000 dilution) at 37°C for 1 h. Finally, the membrane was rinsed with PBST and developed with ECL.

To determine the effect of surface modification of PEG with different molecular weights on the properties of NPs, BSA adsorption experiment was first performed, briefly, PLGA NPs coated with PEG of different molecular weight (MW = 5,000, 10,000, 15,000) were prepared, and then incubated with TRITC-labeled BSA for 10, 30, and 60 min, respectively. After rinsed with PBS, the BSA adsorption capacity of PEGylated NPs was evaluated via the fluorescence intensity of TRITC measured by Fluorescence spectrophotometer (PerkinElmer FL8500, South Korea). Then the uptake of different molecular weight PEG-modified NPs by macrophage was evaluated by flow cytometry (BD FACSCalibur, United States) and Laser scanning confocal microscope (LSCM) (Olympus FV3000, Japan).

Establishment of the Drug-Resistant Cell Line TE10/DOX

High-dose intermittent induction method was used to establish DOX-resistant TE10 cell line (Xiao et al., 2017). ① TE10 cells in the logarithmic growth phase were inoculated in 96-well plates. After 24 h, the cells were treated with DOX at the final concentrations of 0.032, 0.16, 0.8, 4, and 20 μ M, and continued to culture for 48 h. Then, CCK-8 method was applied to detect the IC_{50} value. ② TE10 cells were inoculated in a 6 cm petri dish and grew to logarithmic growth phase, then DOX with a final concentration of 100 μ M was added and incubated for 12 h. After that, the drug-containing medium was discarded and the cells were cultured in DOX-free medium for several generations. After the cells grew well, the above method was repeated until the cells could be cultured in 100 μ M DOX for a long time, thus the drug-resistant human esophageal cancer cell model TE10/DOX was established.

Identification of the prepared DOX-resistant cells: First, the IC_{50} values of TE10 cells and TE10/DOX cells were detected by CCK-8 assay. Next, the expression of resistance proteins ABCB1 and ABCC1 in TE10 cells and TE10/DOX cells was detected

by Western blot (WB). The primary antibody anti-ABCB1 was 1:5,000 diluted, anti-ABCC1 was 1:3,000 diluted, and the secondary antibody goat anti-rabbit IgG and goat anti-mouse IgG were 1:10,000 diluted.

In vitro Drug Release

Low-speed centrifugation was used to detect the *in vitro* drug release of PMPNs. PLGA@DOX, TE10-PLGA@DOX, and PEG-TE10-PLGA@DOX with equal DOX concentration were placed in a centrifuge tube, respectively, and then shaken at 37°C at 100 rpm. Then the tubes were taken out at the preset time point and centrifuged at 1,000 rpm for 5 min. The supernatant was collected and measured at OD_{480nm}, the unloaded NPs under the same conditions were used as the blank reference.

Cell Uptake Experiments in vitro

To evaluate whether the prepared NPs could be uptaken by tumor cells *in vitro*, TE10 cells were first seeded in a 24-well plate containing cell slides. After the cells were completely attached, PLGA@DOX, TE10-PLGA@DOX, and PEG-TE10-PLGA@DOX were added and co-incubated for 4 h. Then, the culture medium was removed, the cells were washed with PBS for three times and then fixed with 4% paraformaldehyde for 15 min. At last, the slides were pasted onto the glass slide with DAPI-containing mounting reagent, then observed and recorded under the LSCM.

Next, flow cytometry was used to analyze the uptake of NPs quantitatively: Firstly, cell culture was conducted according to the above steps and treated with NPs for 4 h. After rinsing with PBS, cells were collected and quantitatively analyzed via flow cytometry.

Tumor Targeting Experiments in vitro

L02, A549, TE10, and TE10/DOX cells were used to determine the tumor targeting function. Cells were incubated with PMPNs. Other operations were carried out as described above.

Determination of Anti-tumor Ability in vitro

CCK-8 assay, clone formation experiment and AnnexinV-PI apoptosis assay were used to investigate the *in vitro* anti-tumor activity of the PMPNs.

CCK-8 assay: TE10/DOX cells were inoculated in a 96-well plate with 200 μ L per well (about 2×10^4 cells). Cells were divided into three groups: PLGA@Cur + DOX, TE10-PLGA@Cur + DOX and PEG-TE10-PLGA@Cur + DOX groups, different concentrations of NPs were added to each group of cells, and the concentrations of loading drug were 3.125, 6.25, 12.5, 25, and 50 μ g/mL, respectively. After incubation for 24 h, 10 μ L of CCK-8 reagent was added to each well, and incubated for another 2 h. The OD_{450nm} was measured by microplate reader (Bio-Tek Epoch, United States).

Clone formation experiment: TE10/DOX cells were first inoculated in a 6-well plate, then the cells were divided into four groups: PBS, PLGA@Cur + DOX, TE10-PLGA@Cur + DOX and PEG-TE10-PLGA@Cur + DOX. After treatment for 24 h, cells were digested into single cells, then inoculated in a dish at a

density of 200 cells/well, and continue cultured for 1–2 weeks. After that, the supernatant was discarded and washed twice with PBS. After immobilization, cells were stained with Giemsa staining solution for 30 min. The number of clones was counted with a microscope.

In addition, flow cytometry was used to detect the apoptotic proportions, and WB method was performed to assess the expression of apoptosis-related proteins. The detected cytochrome C (Cyto-C) is the content of Cyto-C released by mitochondria into the cytoplasm. Briefly, after the cells were lysed, the lysate was centrifuged twice at 4°C for 10 min, and the obtained supernatant was centrifuged at 4°C, 10,000g for 30 min, then the supernatant was centrifuged at 4°C, 100,000 g for 1 h to precipitate organelles including mitochondria, and the final obtained supernatant was used for WB detection. The experiment was performed as described above. Primary antibodies were diluted as follow: anti-Bax (1:1,000), anti-Cyto-C (1:2,000), anti-cleaved cas 3 (1:2,000), and anti-β-actin (1:5,000). The secondary antibodies were all diluted at 1:1,000.

To study the drug synergy of DOX and Cur, we prepared TE10-PLGA@Cur, TE10-PLGA@DOX and TE10-PLGA@Cur + DOX, respectively, and incubated them with TE10/DOX cells. CCK-8 assay, flow cytometry and WB were performed as described above to assess cell viability and cell apoptosis. Then, transwell assay was conducted to assess cell invasion. In brief, cells treated by different NPs were seeded into the upper transwell chamber, after 24 h, cells in lower chamber were immobilized with aldehyde fixative for 30 min and stained with 0.1% crystal violet for 20 min, the results were recorded with the microscope.

Biodistribution of PMPNs *in vivo*

We chose 6–8 weeks old female Balb/c nude mice as animal model. The animal experiment had been approved by the Ethics Committee of Jiangyin People's Hospital, the Jiangyin Clinical College of Xuzhou Medical University. To investigate the biodistribution of PEG-TE10-PLGA NPs *in vivo*, we injected 100 μL PBS containing 5×10^6 TE10/DOX cells into the subcutaneous breast. When the tumor grew to nearly 300 mm³, PLGA@DiR, TE10-PLGA@DiR, and PEG-TE10-PLGA@DiR (5 mg/kg) were injected through the tail vein, and the control group was injected with equal volume of saline. After 0, 8, 24, and 48 h, tail vein blood (200 μL) was taken and the serum was collected by centrifugation. The drug concentration in blood was evaluated through the fluorescence intensity of DiR. The fluorescence intensity at the tumor site was measured with a live animal imager (Perkin Elmer PE IVIS SPECTRUM, United States). After 48 h of intravenous injection, the mice were dissected, heart, liver, spleen, lung, kidney and tumor were taken out and the fluorescence intensity in each organ and tumor tissue was measured.

Determination of the Anti-tumor Ability and Biological Safety *in vivo*

The mice were first inoculated with TE10/DOX cells, when the tumors grew to about 100 mm³, the mice were randomly

divided into four groups: saline, PLGA@Cur + DOX, TE10-PLGA@Cur + DOX and PEG-TE10-PLGA@Cur + DOX, with 5 mice in each group. Then we injected Cur/DOX into the tail vein at a dose of 5 mg/kg or corresponding volume of saline. The drug was administered every 3 days, and the tumor volume and body weight were measured at the same time. On the day 16, the mice were sacrificed, then the tumor tissues were stripped and weighed (Scheme 1).

Next, the obtained tumor tissues were soaked in formalin solution, then embed in paraffin and sliced. HE staining kit and the TUNEL apoptosis detection kit were applied to detect the degree of tumor necrosis and apoptosis. For HE staining, paraffin sections were first dewaxed with xylene and hydrated with low to high concentrations of alcohol, then stained with hematoxylin and eosin successively. After washing off the excess dye with water, the slices were dehydrated using graded alcohol and vitrification by xylene. Finally, the slices were sealed with resin and observed under microscope. As for TUNEL method to detect apoptosis, the samples were first deparaffinized and hydrated, then adding the proteinase K for permeabilization. After rinsing with PBS, adding TdT enzyme working solution for labeling. Finally, observing the green fluorescence with the LSCM. At the same time, the heart, liver, spleen, lung and kidney were sectioned and the damage degree of the main organs was evaluated by HE staining.

For the purpose of evaluating the effect of different surface-modified NPs on the oxidative stress level of mouse cardiomyocytes, we cut off mouse myocardium and rinsed with pre-cooled PBS. Then the homogenate was prepared and centrifuged at 2,500 rpm at 4°C for 10 min. The content of MDA, GSH-Px, and SOD in cardiomyocytes was detected by kit. Ultraviolet spectrophotometry was applied to detect the content of MDA, GSH-Px, and SOD in mouse cardiomyocytes. The prepared tissue homogenate was mixed with working reagents in the kit, and then the concentration was detected and calculated under the corresponding absorbance.

In addition, the blood was collected for biochemical analysis (Cobas c311, United States) to detect the concentration of alanine aminotransferase (ALT), aspartate aminotransferase (AST), white blood cells (WBC), red blood cells (RBC) and platelets (PLT) in serum.

Moreover, to evaluate the survival of mice in each group, we took the same number of mice, repeated tumor transplantation and drug treatment according to the above operation, and administered the drug every 3 days. The mice of each group were fed until the 40th day, and the survival time of each group was recorded.

Statistical Analysis

Three parallel experiments were performed for each experiment, and the results were expressed as mean ± standard deviation. One-way analysis of variance was used to compare the differences between the two sets of data. $P < 0.05$ was considered statistically significant.

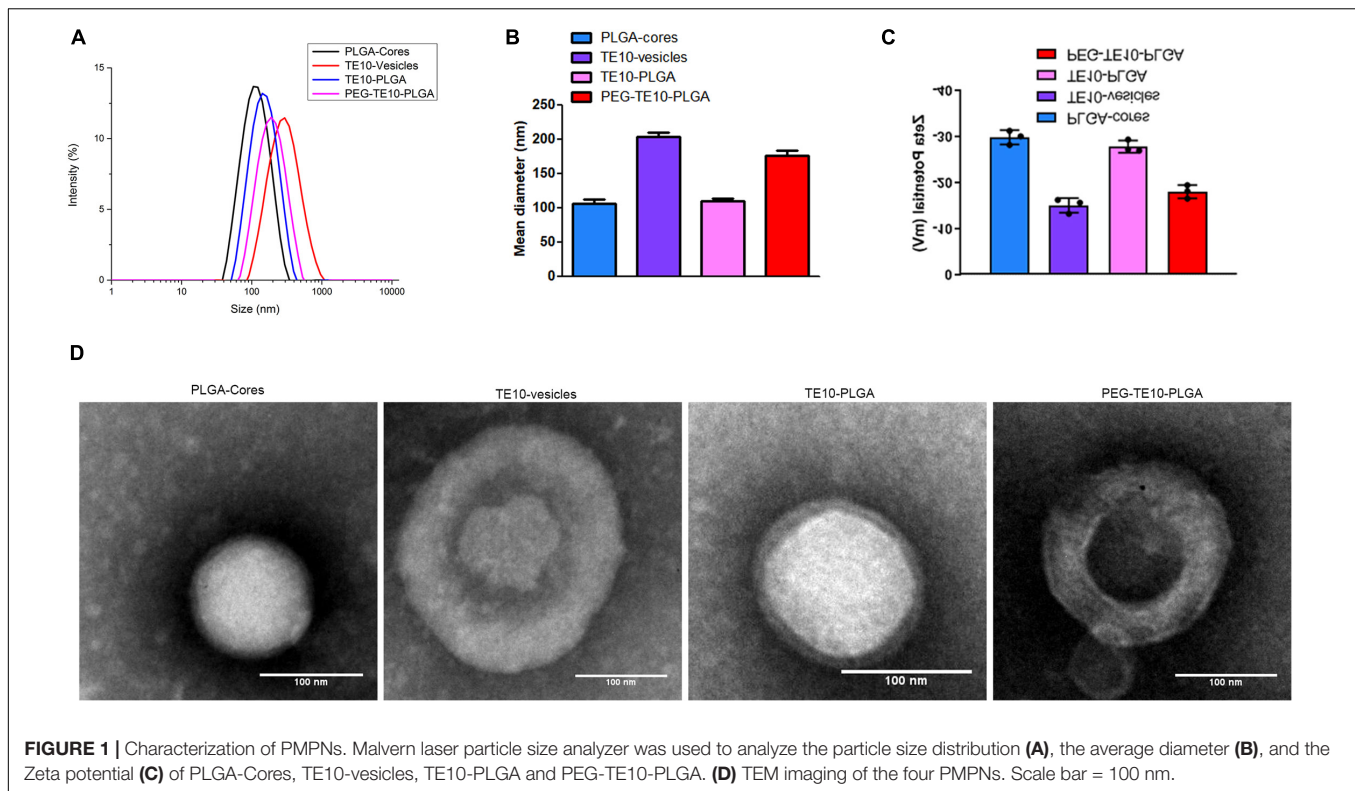


FIGURE 1 | Characterization of PMPNs. Malvern laser particle size analyzer was used to analyze the particle size distribution (A), the average diameter (B), and the Zeta potential (C) of PLGA-Cores, TE10-vesicles, TE10-PLGA and PEG-TE10-PLGA. (D) TEM imaging of the four PMPNs. Scale bar = 100 nm.

RESULTS

Preparation and Characterization of PMPNs

In this research, we first prepared PLGA NPs loaded with anti-tumor drugs DOX and Cur. It was shown in **Figures 1A–C** that the hydrodynamic diameter of the PLGA core was about 106 nm and the hydrodynamic diameter of the extracted TE10 cell membrane was about 204 nm. We mixed the extracted TE10 cell membrane with the PLGA core to prepare TE10-PLGA NPs, and the hydrodynamic diameter increased to 109 nm. These indicated that TE10 cell membrane had been successfully coated on the surface of PLGA core. Next, we mixed the PLGA core with equal concentration of the extracted TE10 cell membrane and DSPE-PEG, it was found that the hydrodynamic diameter of the obtained PEG-TE10-PLGA NPs increased to 177 nm, indicating that PEG was also successfully inserted into the surface of the NPs. Here, we evaluated the effect of PEG modification with different molecular weights on NPs. DSPE-PEG5000, DSPE-PEG10000 and DSPE-PEG15000 were modified on the surface of PLGA NPs, respectively, it was confirmed that DSPE-PEG15000 has the least adsorption of BSA, which allowing NPs to escape macrophages' uptake (**Supplementary Figure 1**). Transmission Electron Microscopy (TEM) images in **Figure 1D** proved that both of TE10-PLGA and PEG-TE10-PLGA displayed a core-shell structure and the hydrodynamic diameter of the NPs was consistent with the Dynamic Light Scattering (DLS) results.

Homologous Targeting of PMPNs to Tumor Cells *in vitro*

First, SDS-PAGE electrophoresis assay and WB assay were used to further verify whether TE10 cell membrane was successfully encapsulated on PLGA NPs. The results were shown in **Figures 2A,B**. Uncoated NPs (PLGA-core) had no protein bands and specific surface markers (LGR5 and CD44) of TE10 cells, while NPs coated with TE10 membrane (TE10-PLGA and PEG-TE10-PLGA) had protein bands similar to TE10 vesicles, and the protein markers were also possessed. These results certified that the cell membrane had been successfully coated on the surface of the NPs, and the membrane protein was well retained during the preparation process.

Next, in order to verify the homologous targeting effect of the PMPNs, we used LSCM and flow cytometry to detect the uptake of PLGA@DOX, TE10-PLGA@DOX and PEG-TE10-PLGA@DOX NPs by TE10 cells and the intracellular drug distribution. As shown in **Figures 2C,D**, the fluorescence intensity of the TE10 cell membrane-coated NPs in TE10 cells was significantly higher than that of the uncoated PLGA@DOX NPs.

In addition, we established and identified DOX-resistant TE10 cell model, as shown in **Supplementary Figure 2**, the IC_{50} of TE10 cells was 12.61 μ M, while the IC_{50} of TE10/DOX cells was 45.01 μ M. Besides, the resistance proteins ABCB1 and ABCC1 were found high-expressed in TE10/DOX cells. Then we evaluated the targeting specificity of PEG-TE10-PLGA@DOX NPs to different cells (L02, A549, TE10 and TE10/DOX cells). It was found that the fluorescence intensity in TE10 and TE10/DOX

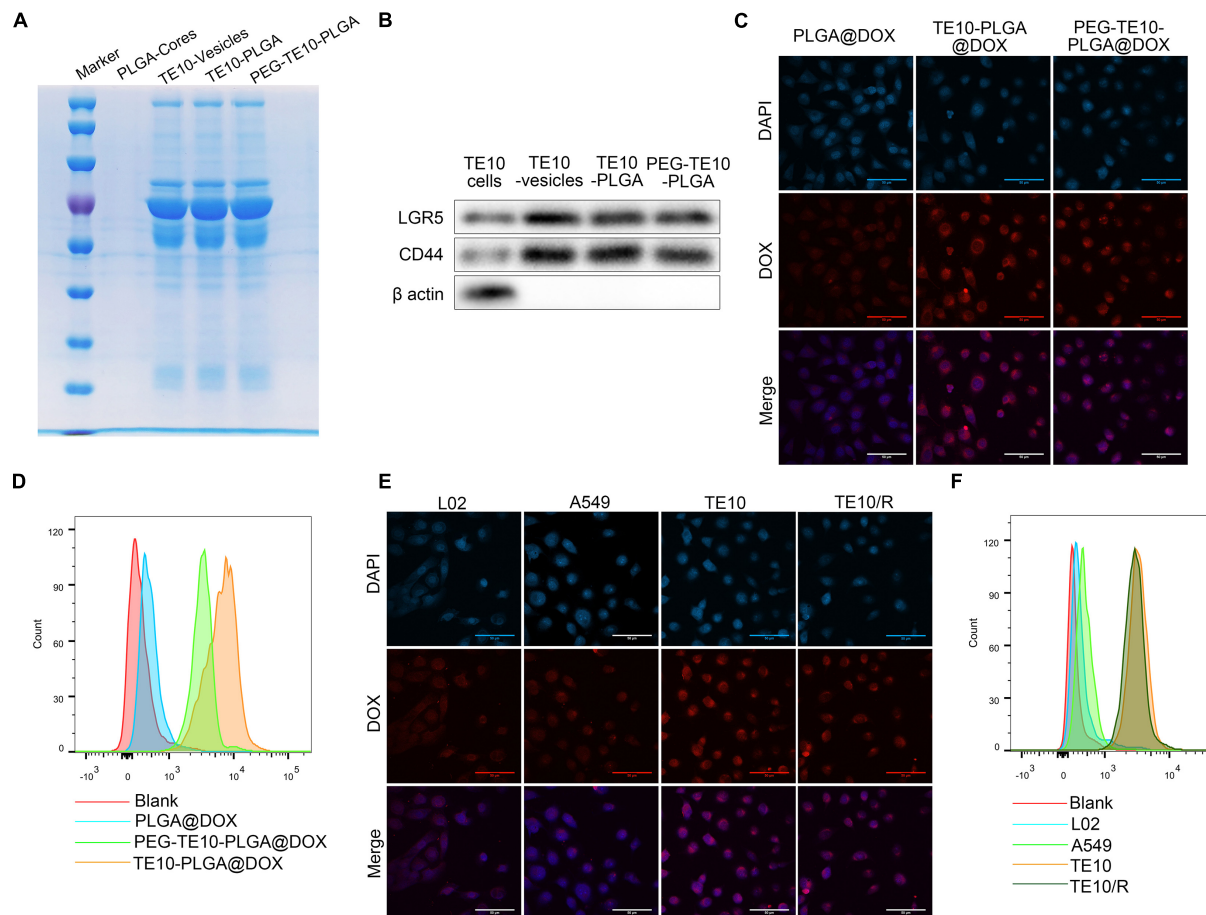


FIGURE 2 | Specific uptake of PMPNs by homologous tumor cells. **(A)** SDS-PAGE analysis of PLGA-Cores, TE10-vesicles, TE10-PLGA and PEG-TE10-PLGA. **(B)** Western blot analysis of biomarkers of TE10 cell membrane on PLGA-Cores, TE10-vesicles, TE10-PLGA and PEG-TE10-PLGA. **(C,D)** Evaluating the uptake of PLGA@DOX, TE10-PLGA@DOX, and PEG-TE10-PLGA@DOX into TE10 cells by laser confocal microscopy **(C)** and flow cytometry **(D)**. **(E,F)** L02, A549 and TE10/DOX cells were used to evaluate the tumor targeting capacity of PEG-TE10-PLGA@DOX by laser confocal microscopy **(E)** and flow cytometry **(F)**.

cells was significantly higher than that in A549 and L02 cells (Figures 2E,F).

Evaluation of the *in vitro* Anti-tumor Activity

In order to evaluate the anti-tumor effect of the synthesized NPs *in vitro*, CCK-8 assay and clone formation assay were performed to evaluate the toxic effects of PLGA@Cur + DOX, TE10@Cur + DOX and PEG-TE10-PLGA@Cur + DOX on TE10/DOX cells. We found that when the drug concentration was over 25 μ g/mL, TE10-PLGA@Cur + DOX and PEG-TE10-PLGA@Cur + DOX had significantly enhanced toxic effects on TE10/DOX cells, while PLGA@Cur + DOX had no obvious toxic effects (Figure 3A). In the clone formation assay, the number of clones in the cells treated with TE10-PLGA@Cur + DOX and PEG-TE10-PLGA@Cur + DOX was significantly less than that treated with PBS and PLGA@Cur + DOX (Figure 3B). The above results indicated that the drug carrier PLGA NPs had good biocompatibility and could well controlled the drug release.

After that, we further investigated the *in vitro* anti-tumor effect of PLGA@Cur + DOX, TE10-PLGA@Cur + DOX and PEG-TE10-PLGA@Cur + DOX using apoptosis analysis. As shown in Figure 3C, TE10-PLGA@Cur + DOX treated cells had the highest apoptosis ratio, while the apoptosis ratio of PBS and PLGA@Cur + DOX treated cells was much lower. Several apoptosis-related proteins were detected by WB and the expression of the Cyto-C released into cytoplasm, Bax and Cleaved caspase 3 in the cells treated with TE10-PLGA@Cur + DOX and PEG-TE10-PLGA@Cur + DOX was significantly higher than that in the other two groups (Figure 3D). This result confirmed that the combination of Cur and DOX had a strong anti-tumor effect *in vitro*, and the encapsulation of PLGA effectively avoided rapid leakage of the drug. Furthermore, we confirmed that there was a synergistic anti-tumor effect between Cur and DOX through CCK-8 assay, apoptosis analysis, and transwell assay. The anti-tumor effect of combination DOX and Cur was much better than DOX or Cur alone (Supplementary Figure 3).

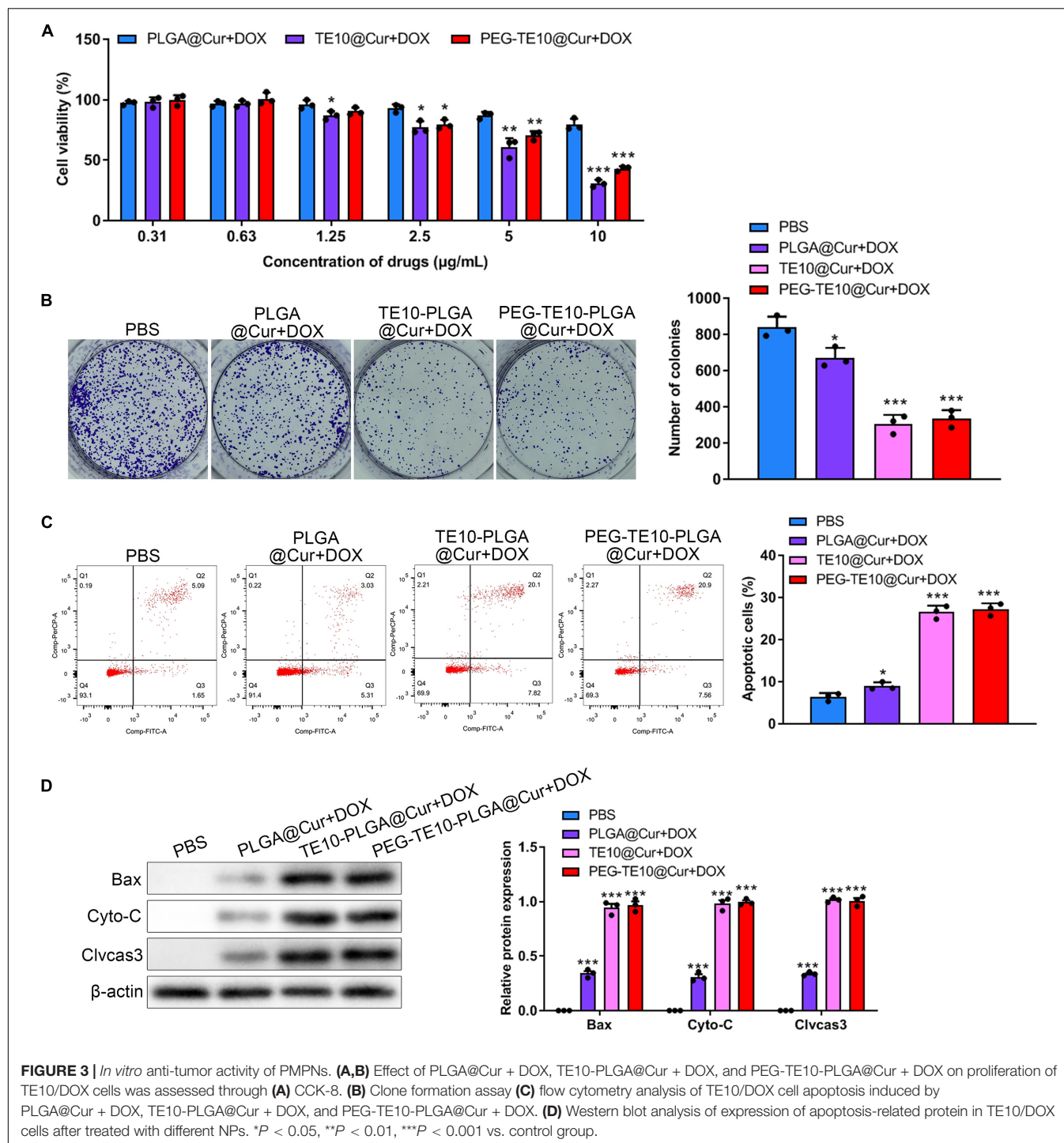
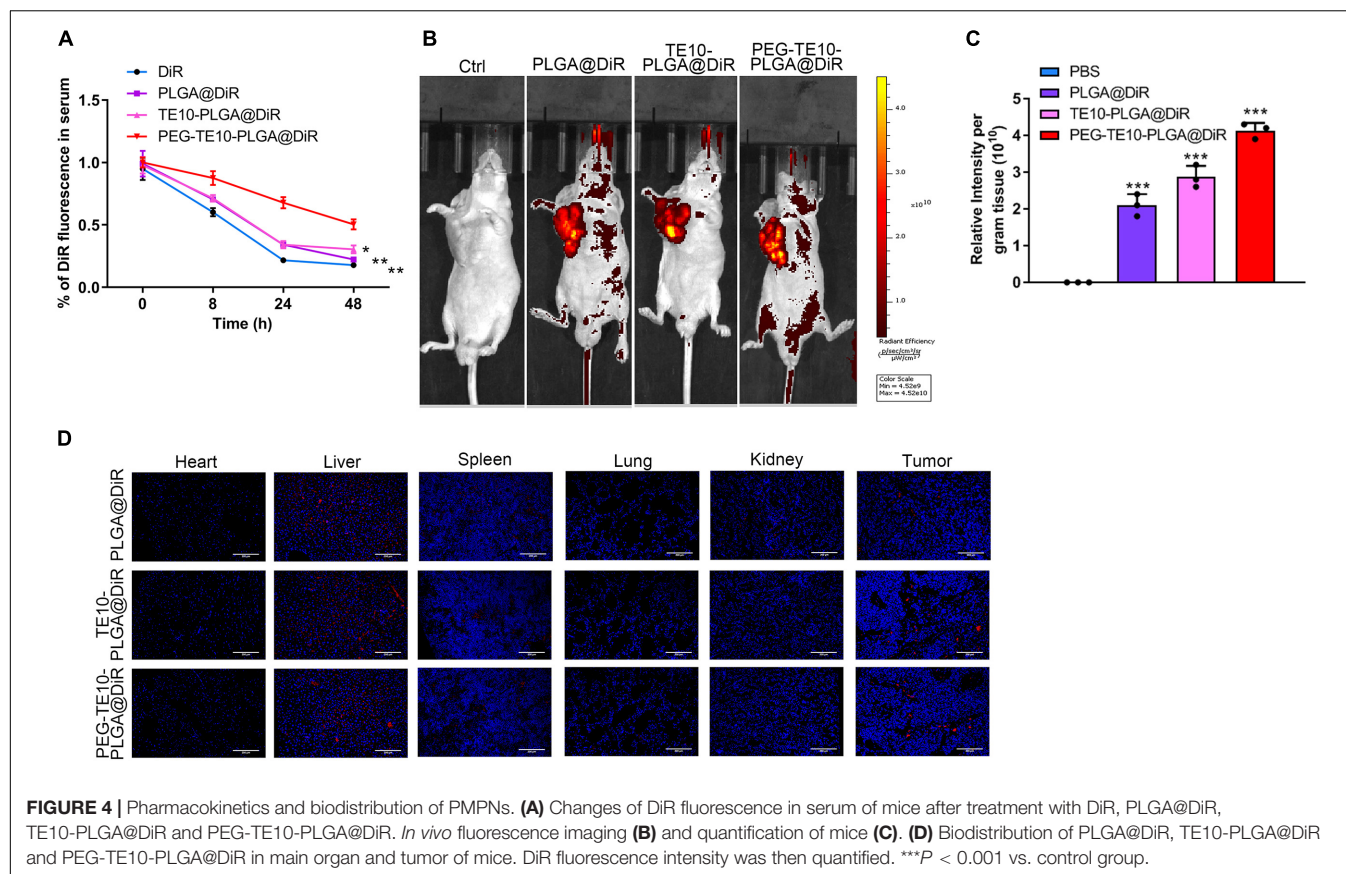


FIGURE 3 | *In vitro* anti-tumor activity of PMPNs. **(A,B)** Effect of PLGA@Cur + DOX, TE10-PLGA@Cur + DOX, and PEG-TE10-PLGA@Cur + DOX on proliferation of TE10/DOX cells was assessed through **(A)** CCK-8. **(B)** Clone formation assay **(C)** flow cytometry analysis of TE10/DOX cell apoptosis induced by PLGA@Cur + DOX, TE10-PLGA@Cur + DOX, and PEG-TE10-PLGA@Cur + DOX. **(D)** Western blot analysis of expression of apoptosis-related protein in TE10/DOX cells after treated with different NPs. * $P < 0.05$, ** $P < 0.01$, *** $P < 0.001$ vs. control group.

Biodistribution of PMPNs *in vivo*

By means of DiR, a cell membrane probe, we successfully monitored the drug metabolism and biodistribution of the prepared NPs in mice. DiR, PLGA@DiR, TE10-PLGA@DiR and PEG-TE10-PLGA@DiR were injected into the tail vein of nude mice, and the fluorescence intensity of DiR in serum was detected at 0, 8, 24, and 48 h to evaluate the metabolism of NPs in mice. Mice in the PEG-TE10-PLGA@DiR group

maintained a higher blood drug concentration 48h after injection (Figure 4A). Supplementary Figure 4 showed the *in vitro* drug release curves of three NPs, PEG-TE10-PLGA@DOX had the slowest drug release. Using the small animal live imaging device, we clearly observed the fluorescence of the xenografted tumor of each mouse and quantitatively analyzed the intensity (Figures 4B,C). In addition, the fluorescence imaging and quantitative analysis of mouse heart, liver, spleen, lung, kidney



and tumor tissues showed that the fluorescence intensity of these three kinds of NPs was strongest in liver, followed by the tumor, indicating that the NPs were metabolized via the liver (Figure 4D).

Evaluation of the *in vivo* Anti-tumor Capacity of PMPNs

We attempted to explore the anti-tumor capacity of the synthesized PMPNs *in vivo*, to this end, we xenografted TE10/DOX cells to nude mice. PLGA@Cur + DOX or TE10-PLGA@Cur + DOX or PEG-TE10-PLGA@Cur + DOX was injected into each group of mice after tumor formation. Changes in the tumor volume were measured and compared (Figure 5A). The tumor growth rate of mice treated with PEG-TE10-PLGA@Cur + DOX or TE10-PLGA@Cur + DOX was prolonged compared with the control group ($P < 0.01$). The effect of PEG-TE10@PLGA@Cur + DOX treatment was slightly better than that of TE10@PLGA@Cur + DOX, indicating that the modification with PEG increased the circulation time of NPs in the blood and prevented them from being cleaned up, thus the encapsulated drug could be released continuously and killed the tumor. The therapeutic effect of the PLGA@Cur + DOX group was only better than that of the control group ($P < 0.05$), indicating that although PLGA could sustained-released the drug, it is quickly eliminated by immune system due to the absence of targeting of homologous cell membrane and stealth of PEG.

The monitoring of the overall survival of mice in each group was consistent with the above results (Figure 5B). The tumor tissue sections of each group of mice were stained with H&E and TUNEL to evaluate necrosis and apoptosis. Figure 5C showed that the tumor cells in mice treated with PEG-TE10-PLGA@Cur + DOX had the most severe necrosis and apoptosis, and the most significant antitumor effect in these four groups.

Biosafety Assessment of PMPNs

It has been confirmed that the synthesized PMPNs have certain anti-tumor effect *in vivo* and *in vitro*, and we want to further investigate its biosafety in normal organs and tissues. First, we assessed the weight changes of mice after xenograft and treatment with the PMPNs. The weight gain of mice treated with PEG-TE10-PLGA@Cur + DOX was much higher than that of PLGA@Cur + DOX group ($P < 0.01$) (Figure 6A). Then, we evaluated the oxidative stress level of the cardiomyocytes of the mice in each group. The concentrations of MDA, GSH-Px and SOD in the cardiomyocytes of the mice treated with PEG-TE10-PLGA@Cur + DOX were almost the same as those of the control group, indicating that the treatment of PEG-TE10-PLGA@Cur + DOX did not cause oxidative stress damage to the cardiomyocytes (Figure 6B). Next, we performed H&E staining on the main organs of the mice. There was little tissue damage in the PEG-TE10-PLGA@Cur + DOX and TE10-PLGA@Cur + DOX treatment group, while the heart, liver

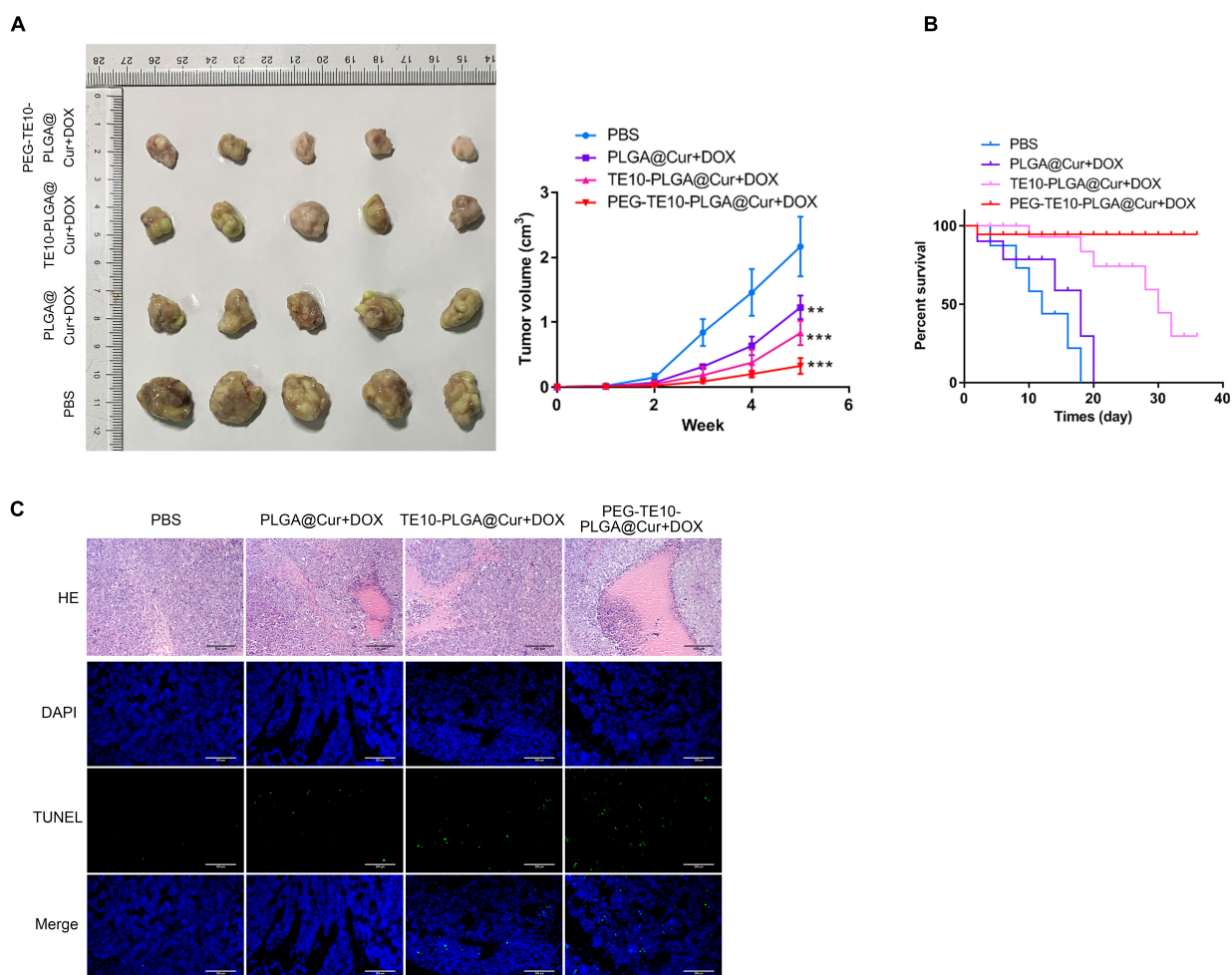


FIGURE 5 | *In vivo* anti-tumor activity of PMPNs. **(A)** Changes of tumor volume during the 16 days treatment of PMPNs. **(B)** The survival percent of mice treated with saline, PLGA@Cur + DOX, TE10-PLGA@Cur + DOX and PEG-TE10-PLGA@Cur + DOX during 40 days. **(C)** H&E and TUNEL staining of tumor tissue section of mice in the four groups. ** $P < 0.01$, *** $P < 0.001$ vs. control group.

and kidney of mice in the PLGA@Cur + DOX group showed a certain degree of damage (**Figure 6C**). Moreover, the biochemical analysis of serum showed that ALT, AST, WBC, RBC, and PLT levels of the mice in the PEG-TE10-PLGA@Cur + DOX treatment group had no significant difference compared with the saline group, while the levels of ALT and AST in the serum of mice in the PLGA@Cur + DOX and TE10-PLGA@Cur + DOX treatment group increased, and the levels of WBC, RBC and PLT decreased significantly (**Figure 6D**). The above results implied that PEG-TE10-PLGA@Cur + DOX had high biological safety and almost no damage to normal tissues and organs.

DISCUSSION

DOX is a broad-spectrum anti-tumor drug that can be used to treat various cancers, including esophageal carcinoma, hepatocellular carcinoma, and ovarian carcinoma (Rivankar, 2014). However, its clinical application is restricted by side effects

such as cardiotoxicity and susceptible to drug resistance (Chen et al., 2018). Cur is a natural active substance extracted from traditional Chinese medicine Turmeric. Studies have shown that Cur has many functions, such as anti-inflammatory, anti-oxidant, and anti-fibrosis (Kocaadam and Şanlıer, 2017). Besides, Cur has also been found to have anti-tumor properties. Liu et al. (2018) found that Cur induced the apoptosis of esophageal squamous cell carcinoma by inhibiting the phosphorylation of STAT3 and blocking its downstream signal pathway. Xiang et al. (2020) pointed out that Cur inhibited human colorectal cancer. They considered that Cur exerted anti-tumor effect through regulating the NF- κ B pathway, thus inhibiting the metastasis of tumor cells and promoting the apoptosis of colorectal cancer cells. In addition, studies have found that Cur regulates the level of ROS in tumors, reverses tumor MDR, and reduces the side effects of chemotherapeutic drugs (Larasati et al., 2018; Momtazi-Borojeni et al., 2019). Cur can be used as a sensitizer for a variety of chemotherapeutic drugs including DOX, which can significantly improve the therapeutic effect (Batra et al., 2019). Although

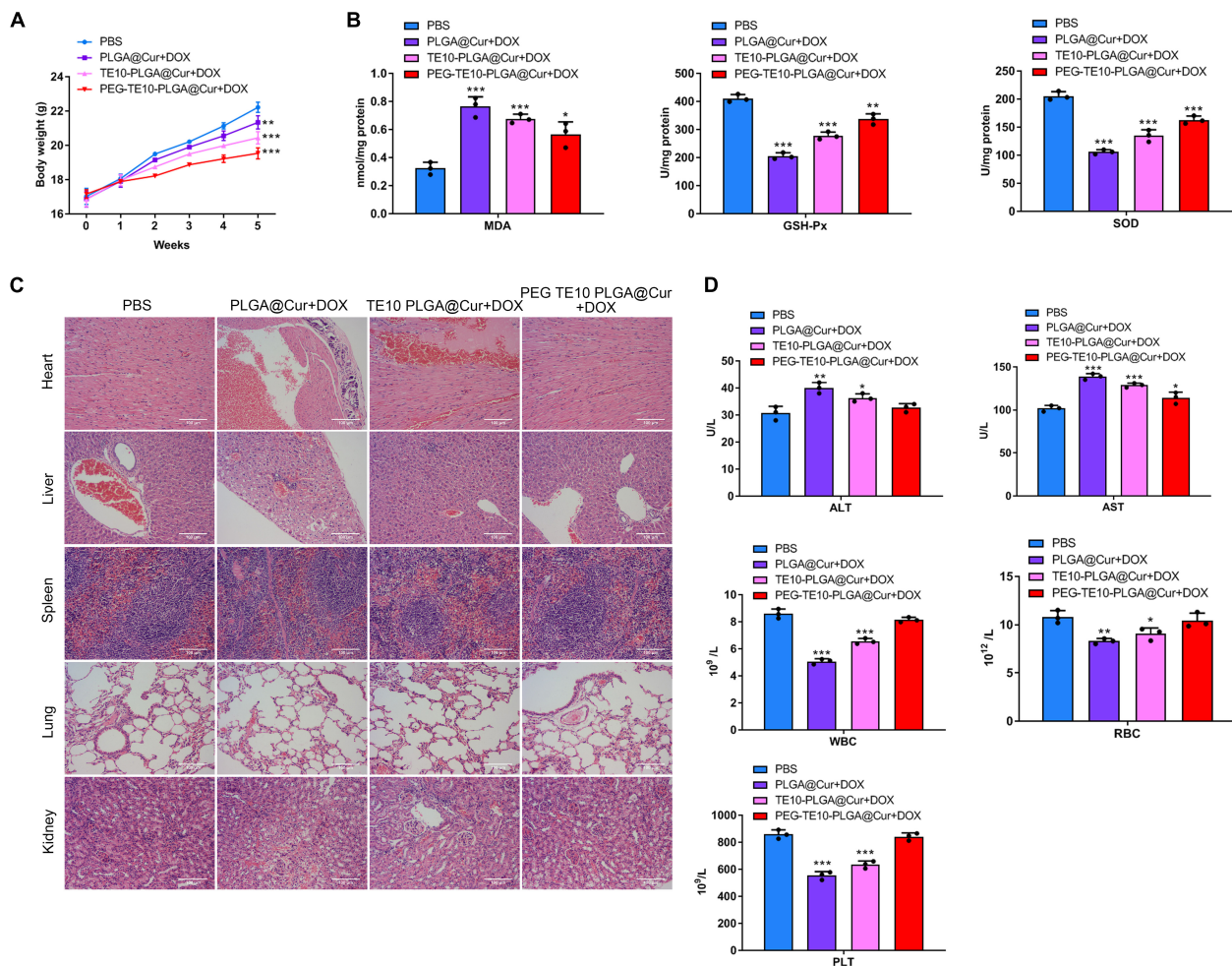


FIGURE 6 | System safety assessment. **(A)** Body weight changes of mice treated with saline, PLGA@Cur + DOX, TE10-PLGA@Cur + DOX and PEG-TE10-PLGA@Cur + DOX. **(B)** Detection of the oxidative stress in mouse cardiomyocytes. **(C)** H&E staining of five major tissue sections of mice. **(D)** Detection of the concentration of ALT, AST, WBC, RBC, and PLT in the serum of mice. * $P < 0.05$, ** $P < 0.01$, *** $P < 0.001$ vs. control group.

Cur has many advantages, it still has the characteristics of poor water solubility, fast clearance and high clearance rate *in vivo*, which limit its clinical application (Anand et al., 2007). For the sake of overcoming the deficiency of DOX and Cur, we adopted the biodegradable nano-carrier PLGA to co-load DOX and Cur, which can not only sustained drug release, but also improve the bioavailability of the drugs and maximize the advantages of the combination of DOX and Cur. In this paper, we found that DOX and CUR had a significant synergistic therapeutic effect, and the tumor killing effect on MDR esophageal carcinoma was significantly better than using DOX alone.

In recent years, the research on biomimetic nanomedicine using cell membrane has become a hot topic. Hu et al. (2011) modified PLGA with erythrocyte membranes to achieve long-cycle characteristics. This independent original research provides a unique method to functionalize nanoparticles. The cell membrane wrapping technology makes full use of the natural characteristics of cell membrane and the principle of bionics.

It transfers the cell membrane and various surface molecules carried by the membrane to the encapsulated NPs and endows them with different biological functions. NPs wrapped by tumor cell membranes have active targeting effects compared to NPs wrapped by other cell membranes. In addition to EPR effect, tumor cell membrane-coated NPs can also actively aggregate to the target sites using homologous recognition mechanism. Chen et al. (2016) loaded the photosensitizer indocyanine green (ICG) with PLGA and coated it with the cell membrane of MCF-7 cells to prepare the ICNP with homologous targeting function. *In vivo* and *in vitro* experiments have confirmed that ICNP can target human breast cancer cells for imaging and photothermal therapy. Liu et al. (2019) coated MCF-7 cell membrane on copper/manganese silicate nanospheres (CMSN), which entered tumor cells through homologous targeting, and killed tumor cells through the synergy of photodynamic and chemodynamic therapy. In this manuscript, we used the cell membrane of TE10 to coat the drug-loaded PLGA NPs, thus

enabling the drug carrier to have homologous targeting function, and significantly increasing the drug concentration at the target site. In addition, we also modified the cell membrane with PEG, which could not only further extend the circulation time of the drug carrier in the blood, but also reduce the non-specific binding between NPs and serum proteins. Besides, PEGylated modification prevents NPs from being eliminated by the immune system (Ochyl et al., 2018). In this study, we also found that the systemic toxicity of the nanomedicine was significantly reduced after PEG modification (**Figure 6**), which may be related to the charge blocking effect of PEG layer on NPs. In the process of blood circulation, the surface charge of NPs may cause the aggregation or hemolysis of red blood cells, thus causing systemic toxicity. In addition, the release of hemoglobin and cell debris caused by hemolysis will adsorb to the surface of NPs, which makes NPs easily recognized and cleared by immune cells.

In summary, we synthesized PMPNs for tumor targeting and efficient loading of anti-cancer drugs DOX and Cur. By establishing TE10/DOX cell line, a drug-resistant cell model of esophageal carcinoma, we confirmed that PMPNs could be specifically taken up by TE10/DOX cells, and exhibited good anti-tumor effect *in vitro*. In addition, we also used TE10/DOX to xenograft mice to study the targeting and anti-tumor activity of PMPNs to TE10/DOX *in vivo*. The results showed that PMPNs had excellent targeting and therapeutic effect on TE10/DOX *in vivo*. At the same time, PMPNs had good biological safety, which effectively avoid the side effects of chemotherapy drugs. Our research provides a new strategy for nanomedicine treatment of multidrug resistant esophageal cancer.

DATA AVAILABILITY STATEMENT

The raw data supporting the conclusions of this article will be made available by the authors, without undue reservation.

REFERENCES

- Alsop, B. R., and Sharma, P. (2016). Esophageal Cancer. *Gastroenterol. Clin North Am.* 45, 399–412.
- Amjadi, I., Mohajeri, M., Borisov, A., and Hosseini, M. S. (2019). Antiproliferative Effects of Free and Encapsulated Hypericum Perforatum L. Extract and Its Potential Interaction with Doxorubicin for Esophageal Squamous Cell Carcinoma. *J. Pharm.* 22, 102–108.
- Anand, P., Kunnumakkara, A. B., Newman, R. A., and Aggarwal, B. B. (2007). Bioavailability of curcumin: problems and promises. *Mole. Pharm.* 4, 807–818. doi: 10.1021/mp700113r
- Batra, H., Pawar, S., and Bahl, D. (2019). Curcumin in combination with anti-cancer drugs: A nanomedicine review. *Pharm. Res.* 139, 91–105. doi: 10.1016/j.phrs.2018.11.005
- Carita, A. C., Eloy, J. O., Chorilli, M., Lee, R. J., and Leonardi, G. R. (2018). Recent Advances and Perspectives in Liposomes for Cutaneous Drug Delivery. *Curr. Med. Chem.* 25, 606–635. doi: 10.2174/0929867324666171009120154
- Chen, C., Lu, L., Yan, S., Yi, H., Yao, H., Wu, D., et al. (2018). Autophagy and doxorubicin resistance in cancer. *Anti-Cancer Drugs* 29, 1–9. doi: 10.1097/cad.0000000000000572

ETHICS STATEMENT

The animal study was reviewed and approved by the Ethics Committee of Jiangyin People's Hospital, the Jiangyin Clinical College of Xuzhou Medical University.

AUTHOR CONTRIBUTIONS

YG designed and developed the study. YZ, XX, FW, WS, XL, JZ, BL, and YW performed the experiments. YG and PL analyzed the data and wrote the manuscript. All authors contributed to the article and approved the submitted version.

FUNDING

This work was supported by the Key Research and Development Program of Jiangsu Province (BE2020637), the Program for Innovative Research of Xuzhou Medical University (XYFC2020002), the Program for Innovative Research of Wuxi (BJ2020102), the Open Project of Jiangsu Key Laboratory of Immunology and Metabolism (XZSYSKF2020020), and the Open Project of State Key Laboratory of Radiation Medicine and Protection (GZK1201911).

ACKNOWLEDGMENTS

We would like to give our sincere gratitude to the reviewers for their constructive comments.

SUPPLEMENTARY MATERIAL

The Supplementary Material for this article can be found online at: <https://www.frontiersin.org/articles/10.3389/fcell.2021.688070/full#supplementary-material>

- Chen, Z., Zhao, P., Luo, Z., Zheng, M., Tian, H., Gong, P., et al. (2016). Cancer Cell Membrane-Biomimetic Nanoparticles for Homologous-Targeting Dual-Modal Imaging and Photothermal Therapy. *ACS Nano* 10, 10049–10057. doi: 10.1021/acsnano.6b04695
- Danhier, F. (2016). To exploit the tumor microenvironment: Since the EPR effect fails in the clinic, what is the future of nanomedicine? *J. Control. Release* 244(Pt A), 108–121. doi: 10.1016/j.jconrel.2016.11.015
- Domper Arnal, M. J., Ferrández Arenas, Á., and Lanás Arbeloa, Á. (2015). Esophageal cancer: Risk factors, screening and endoscopic treatment in Western and Eastern countries. *World J. Gastroenterol.* 21, 7933–7943. doi: 10.3748/wjg.v21.i26.7933
- Fang, R. H., Hu, C. M., Luk, B. T., Gao, W., Copp, J. A., Tai, Y., et al. (2014). Cancer cell membrane-coated nanoparticles for anticancer vaccination and drug delivery. *Nano Lett.* 14, 2181–2188. doi: 10.1021/nl500618u
- Han, S., Zhang, X., and Li, M. (2016). Progress in research and application of PLGA embolic microspheres. *Front. Biosci.* 21:931–940. doi: 10.2741/4430
- Hu, C. M., Zhang, L., Aryal, S., Cheung, C., Fang, R. H., and Zhang, L. (2011). Erythrocyte membrane-camouflaged polymeric nanoparticles as a biomimetic

- delivery platform. *Proc. Natl. Acad. Sci USA* 108, 10980–10985. doi: 10.1073/pnas.1106634108
- Hu, L., Kong, Z., Meng, Q., Wang, J., Zhou, M., Yu, J., et al. (2020). The Safety and Efficacy of Apatinib Treatment in Addition to Concurrent Chemoradiotherapy in Patients with Nonoperative Locally Advanced Esophageal Squamous Cell Carcinoma. *Med. Sci. Monitor* 26:e927221.
- Kocaadam, B., and Şanlıer, N. (2017). Curcumin, an active component of turmeric (*Curcuma longa*), and its effects on health. *Crit. Rev. Food Sci. Nutr.* 57, 2889–2895. doi: 10.1080/10408398.2015.1077195
- Lagrecia, E., Onesto, V., Di Natale, C., La Manna, S., Netti, P. A., and Vecchione, R. (2020). Recent advances in the formulation of PLGA microparticles for controlled drug delivery. *Prog. Biomat.* 9, 153–157. doi: 10.1007/s40204-020-00139-y
- Larasati, Y. A., Yoneda-Kato, N., Nakamae, I., Yokoyama, T., Meiyanto, E., and Kato, J. Y. (2018). Curcumin targets multiple enzymes involved in the ROS metabolic pathway to suppress tumor cell growth. *Sci. Rep.* 8: 2039.
- Lee, S. Y., Nam, S., Koo, J. S., Kim, S., Yang, M., Jeong, D. I., et al. (2020). Possible contribution of sialic acid to the enhanced tumor targeting efficiency of nanoparticles engineered with doxorubicin. *Sci. Rep.* 10:19738.
- Li, B., Li, Q., Mo, J., and Dai, H. (2017). Drug-Loaded Polymeric Nanoparticles for Cancer Stem Cell Targeting. *Front. Pharm.* 8:51.
- Liu, C., Wang, D., Zhang, S., Cheng, Y., Yang, F., Xing, Y., et al. (2019). Biodegradable Biomimetic Copper/Manganese Silicate Nanospheres for Chemodynamic/Photodynamic Synergistic Therapy with Simultaneous Glutathione Depletion and Hypoxia Relief. *ACS Nano* 13, 4267–4277. doi: 10.1021/acsnano.8b09387
- Liu, Y., Wang, X., Zeng, S., Zhang, X., Zhao, J., Zhang, X., et al. (2018). The natural polyphenol curcumin induces apoptosis by suppressing STAT3 signaling in esophageal squamous cell carcinoma. *J. Exp. Clin. Can. Res.* 37:303.
- Ma, J., Du, L. F., Chen, M., Wang, H. H., Xing, L. X., Jing, L. F., et al. (2013). Drug-loaded nano-microcapsules delivery system mediated by ultrasound-targeted microbubble destruction: A promising therapy method. *Biomed. Rep.* 1, 506–510. doi: 10.3892/br.2013.110
- Maeda, H. (2017). Polymer therapeutics and the EPR effect. *J. Drug Target.* 25, 781–785. doi: 10.1080/1061186x.2017.1365878
- Momtazi-Borojeni, A. A., Mosafer, J., Nikfar, B., Ekhlesi-Hundrieser, M., Chaichian, S., Mehdizadehkashi, A., et al. (2019). Curcumin in Advancing Treatment for Gynecological Cancers with Developed Drug- and Radiotherapy-Associated Resistance. *Rev. Physiol. Biochem. Pharm.* 176, 107–129. doi: 10.1007/112_2018_11
- Ochyl, L. J., Bazzill, J. D., Park, C., Xu, Y., Kuai, R., and Moon, J. J. (2018). PEGylated tumor cell membrane vesicles as a new vaccine platform for cancer immunotherapy. *Biomaterials* 182, 157–166. doi: 10.1016/j.biomaterials.2018.08.016
- Oh, Y., Swierczewska, M., Kim, T. H., Lim, S. M., Eom, H. N., Park, J. H., et al. (2015). Delivery of tumor-homing TRAIL sensitizer with long-acting TRAIL as a therapy for TRAIL-resistant tumors. *J. Control. Release* 220(Pt B), 671–681. doi: 10.1016/j.jconrel.2015.09.014
- Ohashi, S., Miyamoto, S., Kikuchi, O., Goto, T., Amanuma, Y., and Muto, M. (2015). Recent Advances From Basic and Clinical Studies of Esophageal Squamous Cell Carcinoma. *Gastroenterology* 149, 1700–1715. doi: 10.1053/j.gastro.2015.08.054
- Prakash, M., and Dhesingh, R. S. (2017). Nanoparticle Modified Drug Loaded Biodegradable Polymeric Contact Lenses for Sustainable Ocular Drug Delivery. *Curr. Drug Del.* 14, 555–565.
- Rabanel, J. M., Aoun, V., Elkin, I., Mokhtar, M., and Hildgen, P. (2012). Drug-loaded nanocarriers: passive targeting and crossing of biological barriers. *Curr. Med. Chem.* 19, 3070–3102. doi: 10.2174/092986712800784702
- Rivankar, S. (2014). An overview of doxorubicin formulations in cancer therapy. *J. Cancer Res. Therapeut.* 10, 853–858. doi: 10.4103/0973-1482.139267
- Son, K. D., and Kim, Y. J. (2017). Anticancer activity of drug-loaded calcium phosphate nanocomposites against human osteosarcoma. *Biomater. Res.* 21:13.
- Wang, D., Dong, H., Li, M., Cao, Y., Yang, F., Zhang, K., et al. (2018). Erythrocyte-Cancer Hybrid Membrane Camouflaged Hollow Copper Sulfide Nanoparticles for Prolonged Circulation Life and Homotypic-Targeting Photothermal/Chemotherapy of Melanoma. *ACS Nano* 12, 5241–5252. doi: 10.1021/acsnano.7b08355
- Xiang, L., He, B., Liu, Q., Hu, D., Liao, W., Li, R., et al. (2020). Antitumor effects of curcumin on the proliferation, migration and apoptosis of human colorectal carcinoma HCT-116 cells. *Oncol. Rep.* 44, 1997–2008.
- Xiao, C. R., Hong, X. L., Hu, J. S., Chen, Y. M., and Lu, Q. Y. (2017). Targeting miR155 restores chemotherapy sensitivity in drug-resistant myeloma cell-line RPMI8226/DOX cells. *Zhonghua Xue Ye Xue Za Zhi = Zhonghua Xueyexue Zazhi* 38, 55–59. doi: 10.1159/000077803
- Xu, T., Guo, P., He, Y., Pi, C., Wang, Y., Feng, X., et al. (2020). Application of curcumin and its derivatives in tumor multidrug resistance. *Phytother. Res.* 34, 2438–2458. doi: 10.1002/ptr.6694
- Yadav, D., and Dewangan, H. K. (2021). PEGYLATION: an important approach for novel drug delivery system. *J. Biomat. Sci. Poly. Edn.* 32, 266–280. doi: 10.1080/09205063.2020.1825304
- Zhao, J., Lei, T., Zhang, T., Chen, X., Dong, J., Guan, Y., et al. (2020). The efficacy and safety of simultaneous integrated dose reduction in clinical target volume with intensity-modulated radiotherapy for patients with locally advanced esophageal squamous cell carcinoma. *Ann. Translat. Med.* 8:1160. doi: 10.21037/atm-20-4366
- Zhen, X., Cheng, P., and Pu, K. (2019). Recent Advances in Cell Membrane-Camouflaged Nanoparticles for Cancer Phototherapy. *Small* 15:e1804105.

Conflict of Interest: The authors declare that the research was conducted in the absence of any commercial or financial relationships that could be construed as a potential conflict of interest.

Publisher's Note: All claims expressed in this article are solely those of the authors and do not necessarily represent those of their affiliated organizations, or those of the publisher, the editors and the reviewers. Any product that may be evaluated in this article, or claim that may be made by its manufacturer, is not guaranteed or endorsed by the publisher.

Copyright © 2021 Gao, Zhu, Xu, Wang, Shen, Leng, Zhao, Liu, Wang and Liu. This is an open-access article distributed under the terms of the Creative Commons Attribution License (CC BY). The use, distribution or reproduction in other forums is permitted, provided the original author(s) and the copyright owner(s) are credited and that the original publication in this journal is cited, in accordance with accepted academic practice. No use, distribution or reproduction is permitted which does not comply with these terms.



Long Non-coding RNA MAFG-AS1 Promotes Cell Proliferation, Migration, and EMT by miR-3196/STRN4 in Drug-Resistant Cells of Liver Cancer

Tianming Chen^{1†}, Bin Huang^{2†} and Yaozhen Pan^{3*}

¹ Department of Surgery, Drum Tower Hospital Affiliated to Nanjing University Medical School, Nanjing, China, ² The Comprehensive Cancer Center of Nanjing Drum Tower Hospital, The Affiliated Hospital of Nanjing University Medical School & Clinical Cancer Institute of Nanjing University, Nanjing, China, ³ Department of Hepatobiliary Surgery, The Affiliated Hospital of Guizhou Medical University, Guiyang, China

OPEN ACCESS

Edited by:

Wei Zhao,
City University of Hong Kong,
Hong Kong

Reviewed by:

Peng Shen,
Nanjing Medical University, China
Xiancheng Liu,
Affiliated Hospital of Nantong
University, China

*Correspondence:

Yaozhen Pan
panyaozhen112@163.com

[†] These authors have contributed
equally to this work

Specialty section:

This article was submitted to
Molecular and Cellular Oncology,
a section of the journal
Frontiers in Cell and Developmental
Biology

Received: 31 March 2021

Accepted: 21 June 2021

Published: 27 July 2021

Citation:

Chen T, Huang B and Pan Y
(2021) Long Non-coding RNA
MAFG-AS1 Promotes Cell
Proliferation, Migration, and EMT by
miR-3196/STRN4 in Drug-Resistant
Cells of Liver Cancer.
Front. Cell Dev. Biol. 9:688603.
doi: 10.3389/fcell.2021.688603

Long non-coding RNAs (lncRNAs) have been shown to participate in the development and progression of several different types of cancer. Past studies indicated that lncRNA MAFG-antisense 1 (AS1) promotes colorectal cancer. However, the role of MAFG-AS1 in hepatocellular carcinoma (HCC) remains unclear. The aim of the present study is to examine the effect of lncRNA MAFG-AS1 on drug resistance HCC. The results indicated that MAFG-AS1 is upregulated in drug-resistant cells. Further, MAFG-AS1 promotes growth and migration of HCC by upregulating STRN4 through absorbing miR-3196. Thus, lncRNA MAFG-AS1 may become a novel target to treat HCC patients.

Keywords: long non-coding RNA, MAFG-AS1, miR-3196, STRN4, liver cancer

INTRODUCTION

Liver cancer is the sixth most ordinary cancer and the third main cause of death of cancer (Altekruse et al., 2014). Liver cancer could be induced by many factors, including hepatitis B virus, alcohol abuse, aflatoxin, and hepatitis C virus infection; non-alcoholic fatty liver disease could also increase the risk of liver cancer specifically (Duan et al., 2014). Although many advances have been achieved in the treatment of liver cancer, the survival rate is still low. Hepatocellular carcinoma (HCC) is proved to be the most common form of liver cancer, taking up 90% of all liver cancers (Feng and Ho, 2014). HCC is featured by rapid growth and invasive tumor and has a tendency for a high probability of metastasis and recurrence (Dika and Abou-Alfa, 2017; Liu et al., 2017). Traditional therapeutic methods for HCC, including surgical resection and chemoradiotherapy, are hard to completely inhibit the tumor growth (Innes et al., 2018). Fundamentally, the molecular mechanisms for HCC metastasis need to be sequentially explored.

Long non-coding RNAs (lncRNAs) are classes of RNAs which are over 200 nt in length without protein-coding ability. lncRNAs can regulate important tumor biological functions, such as epithelial-mesenchymal transition (EMT), invasion-metastasis cascade, proliferation, and drug resistance (Yuan et al., 2014; Li et al., 2016; Tan et al., 2017; Xu et al., 2017). For instance, lncRNA-ATB facilitated cell proliferation in gastric cancer by miR-141-3p/TGFβ2 signaling (Lei et al., 2017). Another study indicated that lncRNA Igf2 was upregulated in HCC cells and tissues and

controlled HCC progression through the ERK/MAPK signaling pathway (Bao et al., 2017). Another example is that MAFB ZIP transcription factor G antisense RNA 1 (MAFG-AS1) can expedite cell proliferation and invasion in colorectal cancer by targeting miR-147b/NDUFA4 (Cui et al., 2018). Besides, it is reported that LINC00511 boosted the progression of breast cancer by targeting miR-185-3p/E2F1/Nanog (Lu et al., 2018). MAFG-AS1 is a novel clinical biomarker for clinical progression and unfavorable prognosis in gastric cancer (Li et al., 2020). Downregulation of MAFG-AS1 represses tumorigenesis of colorectal cancer cells through the microRNA-149-3p-dependent inhibition of HOXB8 (Ruan et al., 2020).

However, few studies have provided quantitative evidence of the effects of MAFG-AS1 on HCC progression. Here, we studied the biological functions of MAFG-AS1 in HCC. The impacts of MAFG-AS1 on the regulation of cell invasion, migration, and EMT were also studied. These results provide important evidence that MAFG-AS1 may be a novel therapeutic target and a biomarker for predicting response to sorafenib treatment of HCC.

MATERIALS AND METHODS

HCC Cell Lines

Human HCC cell lines (Huh7, HepG2) and normal liver cell lines (Lo-2) were provided by the Chinese Academy of Sciences Cell Bank (Shanghai, China). In a humidified atmosphere with 5% CO₂, HCC cells were cultured in Dulbecco's modified Eagle's medium (DMEM, Gibco, Grand Island, NY, United States) with 10% fetal bovine serum (FBS, Gibco, Grand Island, NY, United States) at 37°C. The related sorafenib-resistant cell line (HepG2/SF) was generated by exposing cells to increasing concentrations ($\leq 2 \mu\text{M}$) of sorafenib.

Chemicals

The media and antibiotics for cell culture were purchased from HiMedia (Chandigarh, India), Sigma-Aldrich (St. Louis, MO, United States), and Thermo Fisher Scientific China (Shanghai, China). Sorafenib was procured from Santa Cruz Biotechnology, Inc. (Dallas, TX, United States). Sorafenib was dissolved in dimethyl sulfoxide (DMSO) to prepare 1- and 20-mM stocks, respectively, for further use in cell lines.

Western Blotting

Western blotting was performed according to a standard protocol. Total protein extracts from HCC cells transfected with miR-3196 mimics or miR-3196 inhibitor were loaded on SDS-PAGE gels and transferred into PVDF membranes. After being blocked by skimmed milk, these bands were incubated with primary antibodies at 4°C overnights. Next, membranes were washed with PBS followed by incubation with the appropriate secondary antibody for 1 h at 22–23°C. Finally, enhanced chemiluminescence (ECL, Pierce, Rockford, IL, United States) was added to visualize these membranes. The mouse anti-E cadherin, vimentin, and α -SMA antibodies (R&D Systems Europe Ltd.) were diluted 500 times. Quantification

of Western blotting was performed by densitometry using the Storm 820 Phosphor Imager (Molecular Dynamics, Sunnyvale, CA, United States).

Real-Time Quantitative Polymerase Chain Reaction (qRT-PCR)

qRT-PCR was performed as previously reported (Zhang et al., 2011). Total RNA was extracted with TRIzol. The primers used for gene amplification from the cDNA templates were as follows: α -SMA: 5'-CTGACAGAGGCACCACTGAA-3', 5'-CATCTCCAGAGTCCAGCACA-3'; MAFG-AS1: 5'-CGT TCT TAG TTG GTG GAG CG-3' and reverse, 5'-CCG GAC ATC TAA GGG CAT CA-3'; GAPDH: 5'-AATGG ATTTGGACGCATTGGT-3', 5'-TTTGCACTGGTACGTGTTG AT-3'. For miRNA, 800 ng RNA was transcribed for cDNA with a reverse transcription kit and miRNA-specific primers supplied by Clontech (Mir-XTM miRNA First-Strand Synthesis, San Francisco Bay, CA, United States). qRT-PCR was performed with miScript SYBR Green PCR Kit, and U6 was used as a normalized control. mouse-miR-3196 mimics, mouse-miR-3196 inhibitors, and their corresponding negative controls were purchased from Qiagen (Dusseldorf, Germany).

Cell Counting Kit-8 (CCK-8) Assay

Cell proliferation assay was performed according to the instruction of the CCK-8 kit (Solarbio, Beijing, China). Cells at the logarithmic phase were made into single-cell suspension and seeded to 96-well plates with 5×10^3 cells. After seeding, 10 μl of CCK-8 solution mixed with 90 μl of DMEM was added into each well. After 2 h of incubation, absorbance was measured at 450 nm. The 50% growth inhibition (IC₅₀) was measured according to a previous paper (Ma et al., 2017).

Transwell Invasion and Migration Assay

Transwell assays were performed as described previously (Wang et al., 2017). Briefly, Huh7/R and HepG2/R cells were seeded in Matrigel-coated upper chambers with a pore (50 IL Matrigel, BD Bioscience, United States). Medium without serum and 10% FBS was added into the upper chamber, and medium with 10% FBS was added into the lower chambers. After being incubated for 24 h, the migrated and invaded cells on the lower membrane surface were fixed and then stained with 20% Giemsa solution. Five random fields were counted per chamber by an inverted microscope (Olympus, Japan). Each experiment was repeated three times.

Wound Healing Assay

Wound healing tests were used to evaluate cell migration in HCCs. Cells were transfected with 80 nmol/l miR-3196 mimics, or 80 nmol/l miR-3196 inhibitors, respectively. Cells are inoculated to produce confluent monolayers in a six-well plate. The fused cells were scraped with a 200- μl sterile pipette. After 48 h of cultivation, the wounds were evaluated using a microscope.

Immunohistochemistry Staining Analysis

α -Smooth muscle actin (α -SMA) was determined by immunohistochemistry staining. Briefly, sections were dewaxed and endogenous peroxidase activity was quenched by 3% hydrogen peroxide for 15 min. Then, the mixture was blocked with normal goat serum for 30 min to eliminate non-specific binding and incubated overnight at 4°C with primary antibodies against α -SMA (1:100; Abcam). The next day, the specific sections of the sample were treated with a PV6000 Histostain™ kit (ZSGB, Beijing, China) and stained with diaminobenzidine (ZSGB, Beijing, China). Finally, the sections were counterstained by hematoxylin and images acquired with FSX100 (Olympus, Tokyo, Japan).

Luciferase Reporter Assay

The 3' untranslated region (UTR) fragments of STRN4 containing the miR-binding sites were amplified by PCR using the cDNA template obtained from the RNA sample of macrophages. The wild-type 3' UTRs of STRN4 as well as mutant 3' UTRs with nucleotide substitutions in the putative binding sites corresponding to the seed sequence of miR-3196 were cloned downstream of the firefly luciferase gene in the pGL3 vector (Promega, Madison, WI, United States). Cells were co-transfected with miR-3196 or a control microRNA. Forty-eight hours later, cells were washed in PBS and luciferase

activity was measured by a luminometer (Promega, Madison, WI, United States), using a dual-luciferase reporter assay system.

RNA Immunoprecipitation (RIP)

RIP was performed using the Magna RIP RNA-Binding Protein Immunoprecipitation Kit (Sigma, CA, United States). HepG2 was transfected with miR-3196-biotin or non-sense control (NC)-biotin. Cells were lysed in RIP lysis buffer. A/G magnetic beads with anti-biotin ligation were used to pull down the miR-3196-biotin immunoprecipitation. After the antibody was recovered by protein beads, qRT-PCR was performed to detect STRN4 and miR-3196 in the precipitates.

RNA Fluorescence *in situ* Hybridization

Fluorescence *in situ* Hybridization (FISH) assay was conducted, referring to the protocol of the kit from GenePharma (Shanghai, China).

Statistical Analysis

All data were analyzed using SPSS 17.0 software (IBM, Armonk, NY, United States); every experiment was repeated in triplicate, and the data were presented as mean \pm standard error (SE) of the mean. Statistical analysis was performed by Student's *t*-tests. Differences in more than three groups were determined by one-way analysis of variance (ANOVA) test followed by

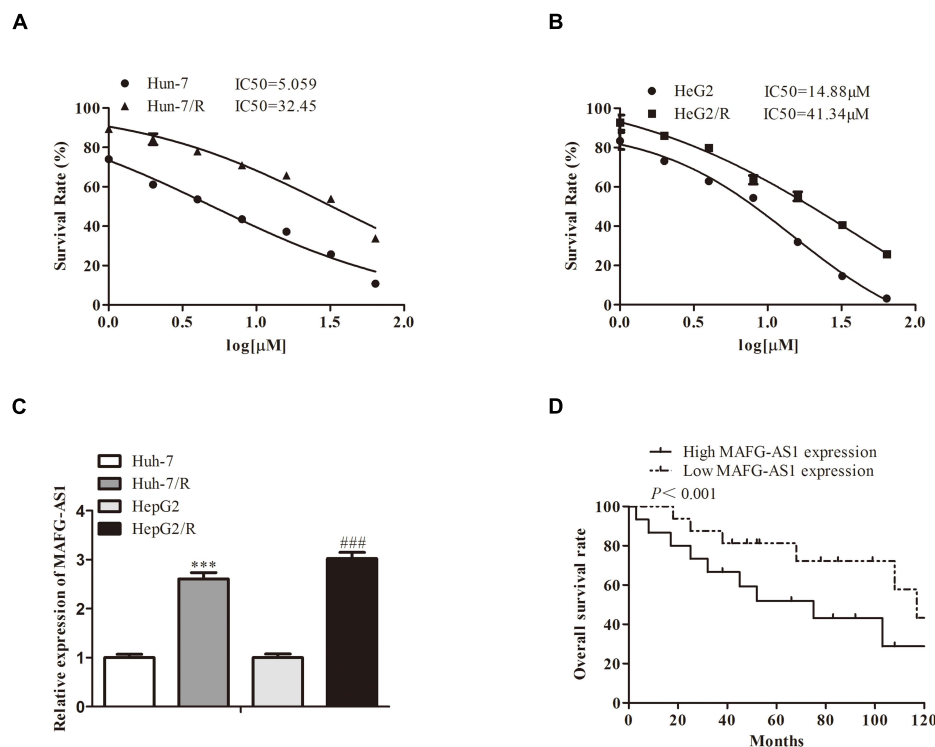


FIGURE 1 | A high expression of MAFG-AS1 is found in drug-resistant cells of liver cancer. **(A,B)** The half-maximal inhibitory concentration (IC50) values of two liver cancer cell lines. **(C)** RT-PCR showed that MAFG-AS1 was upregulated in drug-resistant HCC cell lines (Huh7/R, HepG2/R) compared with parental cell lines. **(D)** The line chart showed the overall survival rate of HCC cell lines with different MAFG-AS1 expression levels.

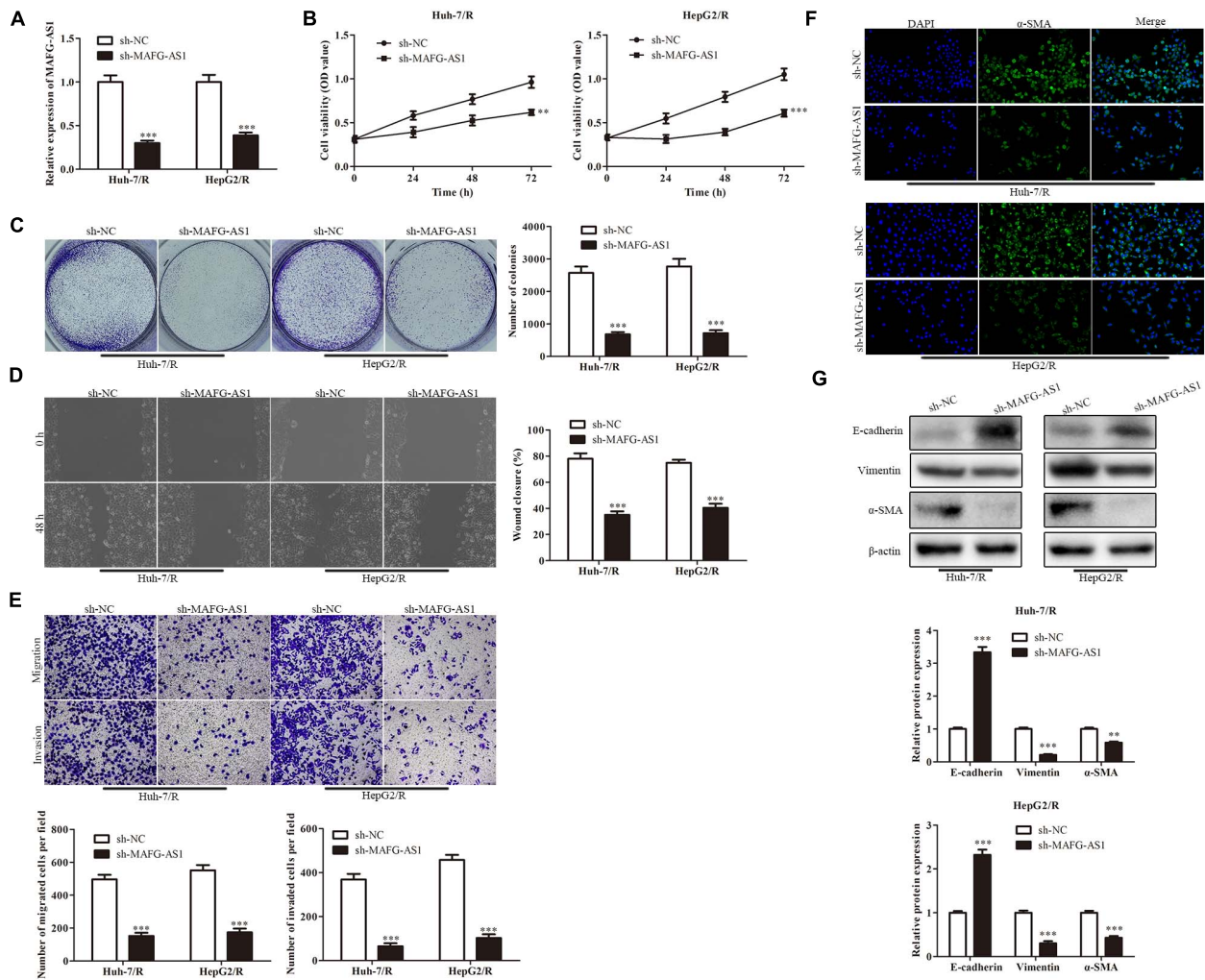


FIGURE 2 | MAFG-AS1 knockdown inhibits proliferation, invasion, migration, and EMT of HCC cells. **(A)** RT-PCR analysis was used to verify the interfering efficiency. **(B)** CCK-8 assay indicated the cell viability in the sh-MAFG-AS1 group compared with the sh-NC group. **(C)** The clone formation abilities of the Huh7/R and HepG2/R cells. **(D,E)** Wound healing assay **(D)** and transwell analysis **(E)** to test the effect on the invasion and migration of HCC cells. **(F,G)** Immunostaining **(F)** and western blotting **(G)** detected the EMT of Huh7/R and HepG2/R cells. Scale bars: 50 μ m. ** $P < 0.01$, *** $P < 0.001$ vs sh-NC group.

Tukey's multiple comparison test. $p < 0.05$ was considered statistically significant.

RESULTS

High Expression of MAFG-AS1 Is Found in Drug-Resistant Cells of Liver Cancer

To investigate the resistance of induced drug-resistant cells, we investigated the cytotoxicity by 3-(4,5-dimethylthiazol-2-yl)-2,5-diphenyl tetrazolium bromide (MTT) assay. After a 48-h treatment with drugs, the growth of HCC cells was markedly inhibited in a concentration-dependent manner. The half-maximal inhibitory concentration (IC₅₀) values of the drug ranged from 5 to 40 μ M for two liver cancer cell lines, respectively (Figures 1A,B). Meanwhile, expressions of

MAFG-AS1 in drug-resistant cell lines HepG2/R and Huh7/R and parent strain cells HepG2 and Huh7 were detected by RT-qPCR. The results showed that MAFG-AS1 expression in drug-resistant cell lines was obviously higher than that in normal strain cells (Figure 1C). Additionally, the HCC cells showed a longer overall survival rate with a low MAFG-AS1 expression (Figure 1D).

MAFG-AS1 Knockdown Inhibits Proliferation, Invasion, Migration, and EMT of HCC Cells

To further explore the effect of MAFG-AS1 on drug-resistant liver cancer cell lines, two low-expression MAFG-AS1-resistant cell lines were constructed, and the efficiency was detected by qRT-PCR (Figure 2A). CCK-8 assay was used to detect the viability of cells in each group. The results showed that in

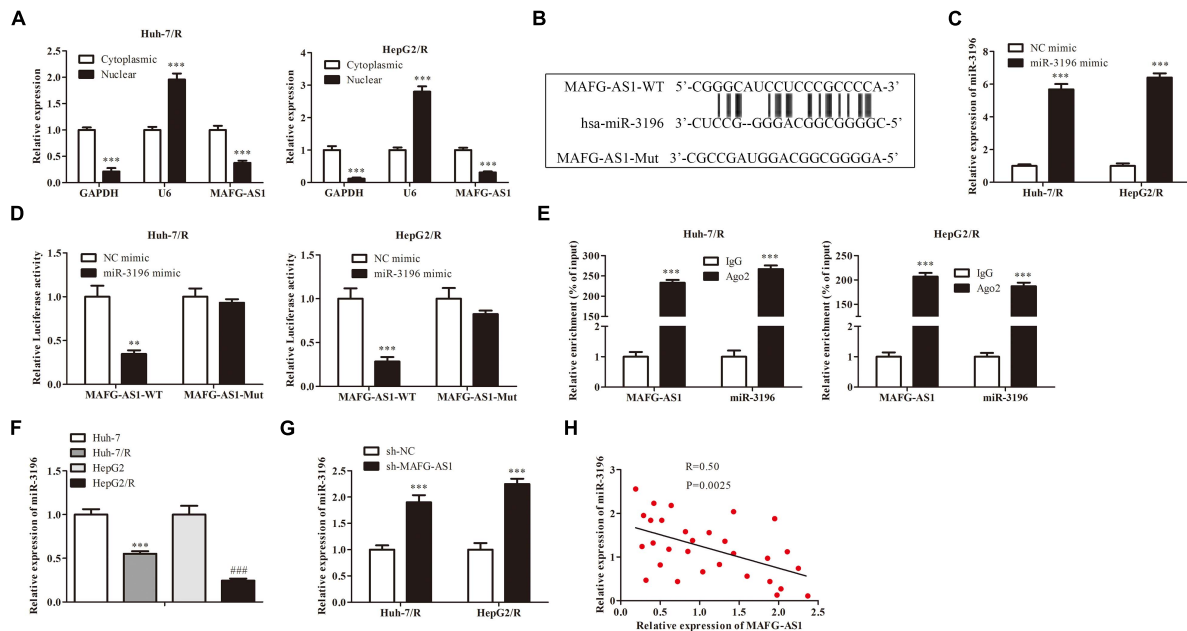


FIGURE 3 | miR-3196 bound with MAFG-AS1. **(A)** RNA-FISH assay implied the location of MAFG-AS1. *** $P < 0.001$ vs cytoplasmic group. **(B)** Schematic diagram demonstrated the complementary binding within miR-3196 and MAFG-AS1 3'-UTR with binding sites predicted by bioinformatics programs (StarBase V 2.0, <http://starbase.sysu.edu.cn/mirLncRNA>). **(C)** RT-PCR analysis was used to verify the efficiency. *** $P < 0.001$ vs NC-mimic group. **(D)** Luciferase reporter gene assay was performed in Huh7/R and HepG2/R cells transfected with MAFG-AS1 wild/mutant type and miR-3196 mimics/control. ** $P < 0.01$, *** $P < 0.001$ vs NC-mimic group. **(E)** The relationship between MAFG-AS1 and Ago2 was detected by RIP assay. *** $P < 0.001$ vs IgG group. **(F)** miR-3196 expression levels were measured in drug-resistant cell lines and parental cell lines using RT-PCR. *** $P < 0.001$, ### $P < 0.001$ vs Corresponding control group. **(G)** RT-PCR showed the miR-3196 expression levels in Huh7/R and HepG2/R cells transfected with MAFG-AS1 shRNA or empty vector. *** $P < 0.001$ vs sh-NC group. **(H)** Pearson's correlation analysis of the correlation between miR-3196 and MAFG-AS1.

contrast to the sh-NC group, the viability of Huh7/R cells in the sh-MAFG-AS1 group was dramatically decreased. Meanwhile, the cell viability was greatly decreased in the sh-MAFG-AS1 group of HepG2/R cell lines (Figure 2B). To further confirm the inhibition of cell proliferation by sh-MAFG-AS1 in liver cancer cells, the colony formation assay and soft agar colony formation assay were conducted on Huh7/R and HepG2/R cells. As shown in Figure 2C, the clone formation abilities of the cells were clearly suppressed by incubation of MAFG-AS1. Next, we performed wound healing analysis to test the effect of MAFG-AS1 on the invasion and migration of HCC cells. The results showed that MAFG-AS1 knockdown significantly reversed liver cancer cell migration (Figure 2D). Moreover, transwell assay showed that in Huh7/R and HepG2/R cells, MAFG-AS1 knockdown decreased the migrated and invasive cell number compared to empty vector-transfected cells (Figure 2E). It has been reported in a previous study that EMT is a critical step of HCC metastasis (Ke et al., 2011). Next, we investigated whether MAFG-AS1 could induce EMT in HCC cells. The results showed that knockdown of MAFG-AS1 could significantly increase the expression of E-cadherin but decrease the expression of vimentin and α -SMA in Huh7/R and HepG2/R cells, as demonstrated by IF or Western blotting (Figures 2F,G). Overall, these results concluded that MAFG-AS1 knockdown inhibited the proliferation, migration, invasion, and tumor growth of drug-resistant HCC cells *in vitro*, suggesting the

potential tumor-promoting role of MAFG-AS1 in drug resistance of HCC.

miR-3196 Bounds With MAFG-AS1

To explore the mechanism of MAFG-AS1, RNA-FISH assay results were collected and analyzed, which implied that MAFG-AS1 was indeed concentrated in the cytoplasm, indicating that MAFG-AS1 might play a role in the cytoplasm (Figure 3A). To investigate the potential molecular mechanism of MAFG-AS1, bioinformatics prediction tools (StarBase V 2.0)¹ were used. Results revealed that miR-3196 shared a complementary binding of MAFG-AS1 by binding sites (Figure 3B). To further explore the effect of miR-3196 on drug-resistant liver cancer cell lines, two miR-3196 mimic cell lines were constructed, and the efficiency was detected by qRT-PCR (Figure 3C). Furthermore, luciferase reporter gene assay showed that the luciferase activity was decreased in the combination of MAFG-AS1 wild-type and miR-3196 mimics of Huh7/R and HepG2/R cells (Figure 3D). The relationship between MAFG-AS1 and Ago2 was detected by RIP assay. The results revealed that the specific adsorption level of MAFG-AS1 on Ago2 increased obviously compared to the IgG group of Huh7/R and HepG2/R cell lines (Figure 3E). We also performed RT-PCR analysis for the expression of miR-3196 in Huh7/R and HepG2/R cell lines

¹<http://starbase.sysu.edu.cn/mirLncRNA>

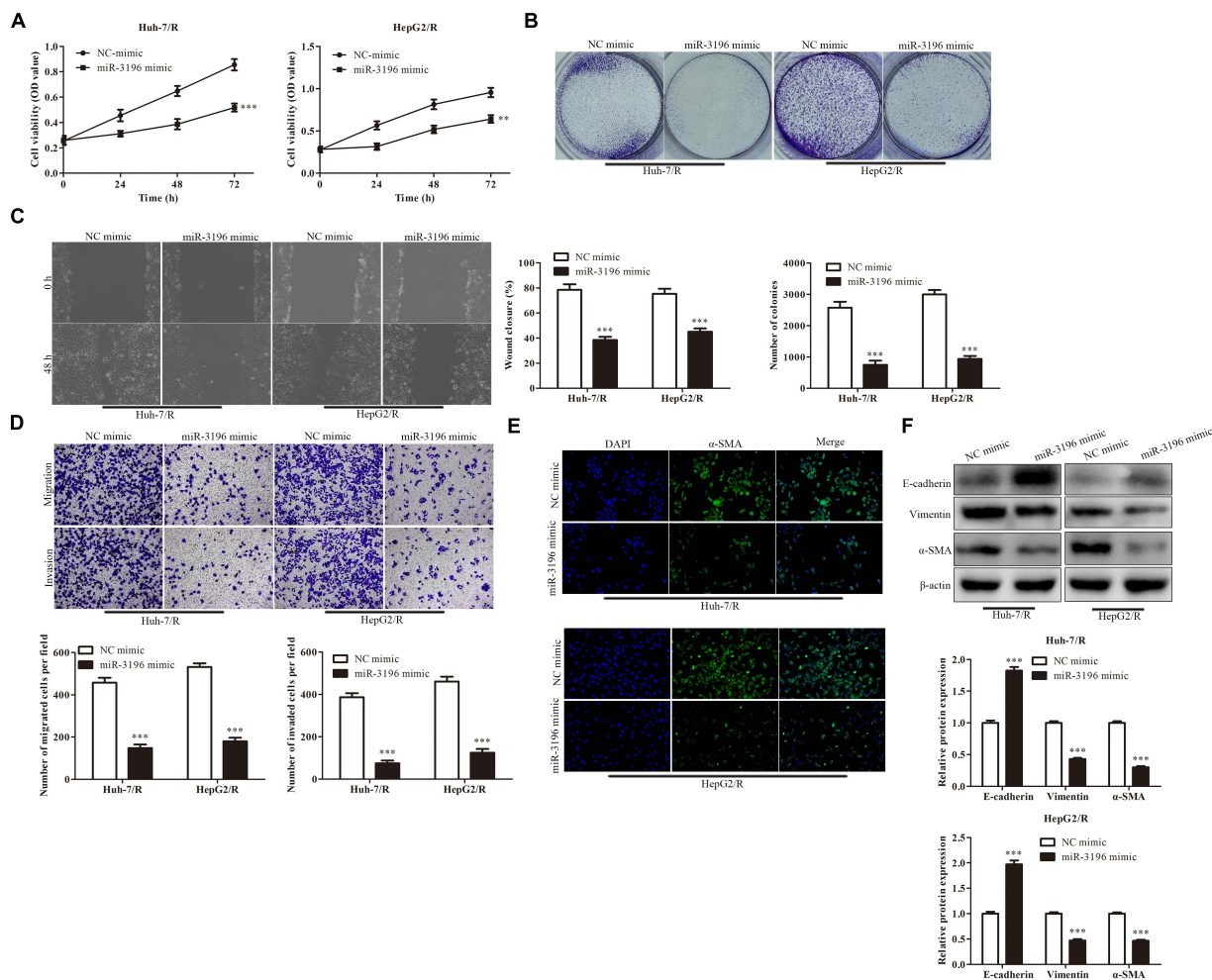


FIGURE 4 | miR-3196 overexpression inhibits proliferation, invasion, migration, and EMT of HCC cells. **(A)** CCK-8 assay indicated the cell viability in Huh7/R and HepG2/R cells transfected with miR-3196 mimic compared to a negative control. **(B)** The colony formation abilities of the Huh7/R and HepG2/R cells in miR-3196 mimic compared to the negative control. **(C,D)** Wound healing assay **(C)** and transwell analysis **(D)** to test the effect on the invasion and migration of HCC cells. **(E,F)** Immunostaining **(E)** and western blotting **(F)** detected the EMT of Huh7/R and HepG2/R cells transfected with miR-3196 mimic compared to a negative control. Scale bars: 50 μ m. $^{**}P < 0.01$, $^{***}P < 0.001$ vs NC-mimic group.

and parent lines, which indicated that a lower expression was detected in drug-resistant cell lines (Figure 3F). Additionally, the expression of miR-3196 was increased with MAFG-AS1 knockdown (Figure 3G). Afterward, using correlation analysis, we found a negative association between the expressions of miR-3196 and MAFG-AS1 in liver cancer cells (Figure 3H). The above results demonstrate that MAFG-AS1 targets and negatively regulates miR-3196.

miR-3196 Overexpression Inhibits Proliferation, Invasion, Migration, and EMT of HCC Cells

We further explore the effect of miR-3196 on drug-resistant liver cancer cell lines. CCK-8 assay was used to detect the viability of cells in each group. The results showed that in contrast to the NC mimic group, the viability of Huh7/R

cells in the miR-3196 mimic group was dramatically decreased. Besides, the cell viability was greatly decreased in the miR-3196 mimic group of HepG2/R cell lines (Figure 4A). To further confirm the inhibition of cell proliferation by miR-3196 in liver cancer cells, the colony formation assay and soft agar colony formation assay were conducted on Huh7/R and HepG2/R cells. As shown in Figure 4B, the colony formation abilities of the cells were clearly suppressed by incubation of miR-3196 mimic. Next, we performed wound healing analysis to test the effects of miR-3196 on the invasion and migration of HCC cells. The results showed that miR-3196 mimic significantly reversed liver cancer cell migration (Figure 4C). Transwell assay showed that in Huh7/R and HepG2/R cells, miR-3196 overexpression decreased the invasive cell number compared to empty vector-transfected cells (Figure 4D). Next, we investigated the induction capacity of miR-3196 to EMT in HCC cells. The results showed that overexpression of miR-3196 could

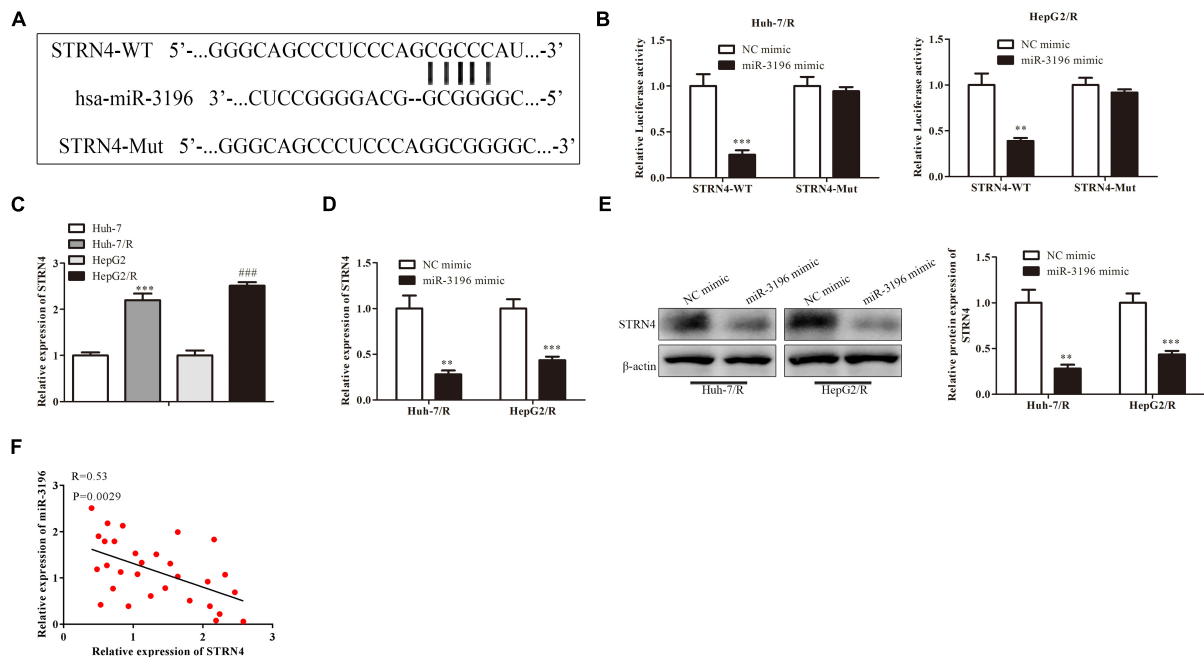


FIGURE 5 | MAFG-AS1 modulates STRN4 protein expression through targeting miR-3196 in liver cancer cells. **(A)** Schematic diagram shows the binding sites within miR-3196 and STRN4 mRNA 3'-UTR. **(B)** Luciferase reporter assay shows the molecular bond within miR-3196 and STRN4 mRNA 3'-UTR. **(C,D)** RT-PCR shows the STRN4 mRNA expression levels in Huh7/R and HepG2/R cells **(C)** or transfected with miR-3196 mimic **(D)**. **(E)** Western blot analysis quantified STRN4 protein expression in Huh7/R and HepG2/R cells transfected with miR-3196 mimic and negative control mimic. **(F)** Correlation analysis found a negative association between the expressions of miR-3196 and STRN4 in liver cancer cells. ** $P < 0.01$, *** $P < 0.001$, ### $P < 0.001$ vs Corresponding control group.

significantly increase the expression of E-cadherin but decrease the expression of vimentin and α -SMA in Huh7/R and HepG2/R cells (Figures 4E,F). Overall, results concluded that miR-3196 overexpression inhibited the migration, invasion, and tumor growth of drug-resistant HCC cells, suggesting the potential tumor-promoting role of miR-3196 in drug resistance of HCC.

MAFG-AS1 Modulates STRN4 Protein Expression Through Targeting miR-3196 in Liver Cancer Cells

Next, bioinformatics results showed that miR-3196 shared complementary binding sites with STRN4 mRNA 3'-UTR (Figure 5A). Luciferase reporter assay showed that the luciferase activity was decreased when co-transfected with miR-3196 mimics and the STRN4 mild type, suggesting the molecular bond within miR-3196 and STRN4 mRNA 3'-UTR (Figure 5B). We also performed RT-PCR analysis for the expression of STRN4 in Huh7/R and HepG2/R cell lines and parent lines, which indicated a lower expression in drug-resistant cell lines (Figure 5C). In Huh7/R and HepG2/R cells, the STRN4 mRNA expression level decreased when transfected with miR-3196 mimic. Additionally, Western blot revealed that miR-3196 mimic transfection decreased the STRN4 protein expression (Figures 5D,E). Additionally, correlation analysis found a negative association between the expressions of miR-3196 and STRN4 in liver cancer cells (Figure 5F). Overall, results indicated that STRN4 acted as the target protein of miR-3196,

suggesting the regulation of MAFG-AS1 on STRN4 through targeting miR-3196.

The Mechanism of MAFG-AS1 Modulating STRN4 Protein Expression Through Targeting miR-3196 in Liver Cancer Cells

In order to investigate whether MAFG-AS1 affects the drug-resistant liver cancer cell lines by regulating the miR-3196/STRN4 pathway, we manipulated the expression of miR-3196 and STRN4 with miR-3196 inhibitor and sh-STRN4, respectively. The knockdown efficiency of miR-3196 inhibitor and STRN4 shRNA-transfected HCC cells was detected by RT-qPCR. Next, CCK-8 analysis showed that sh-STRN4 decreased the activation of Huh7/R cell proliferation induced by a miR-3196 inhibitor (Figure 6A). Meanwhile, colony formation assay analysis showed that the miR-3196 inhibitor reversed Huh7/R cell proliferation by knockdown of MAFG-AS1 (Figure 6B). In addition, wound healing analysis was conducted to test the effect on the invasion and migration of HCC cells. The results showed that the miR-3196 inhibitor significantly reversed liver cancer cell migration, while STRN4 knockdown enhanced this effect (Figure 6C). Next, transwell analysis showed that the migration and invasion ability of Huh7/R and HepG2/R cells increased when these cells were co-transfected with the miR-3196 inhibitor compared with the sh-MAFG-AS1 group. Sh-STRN4 enhanced the reduction in migration and invasion induced by miR-3196

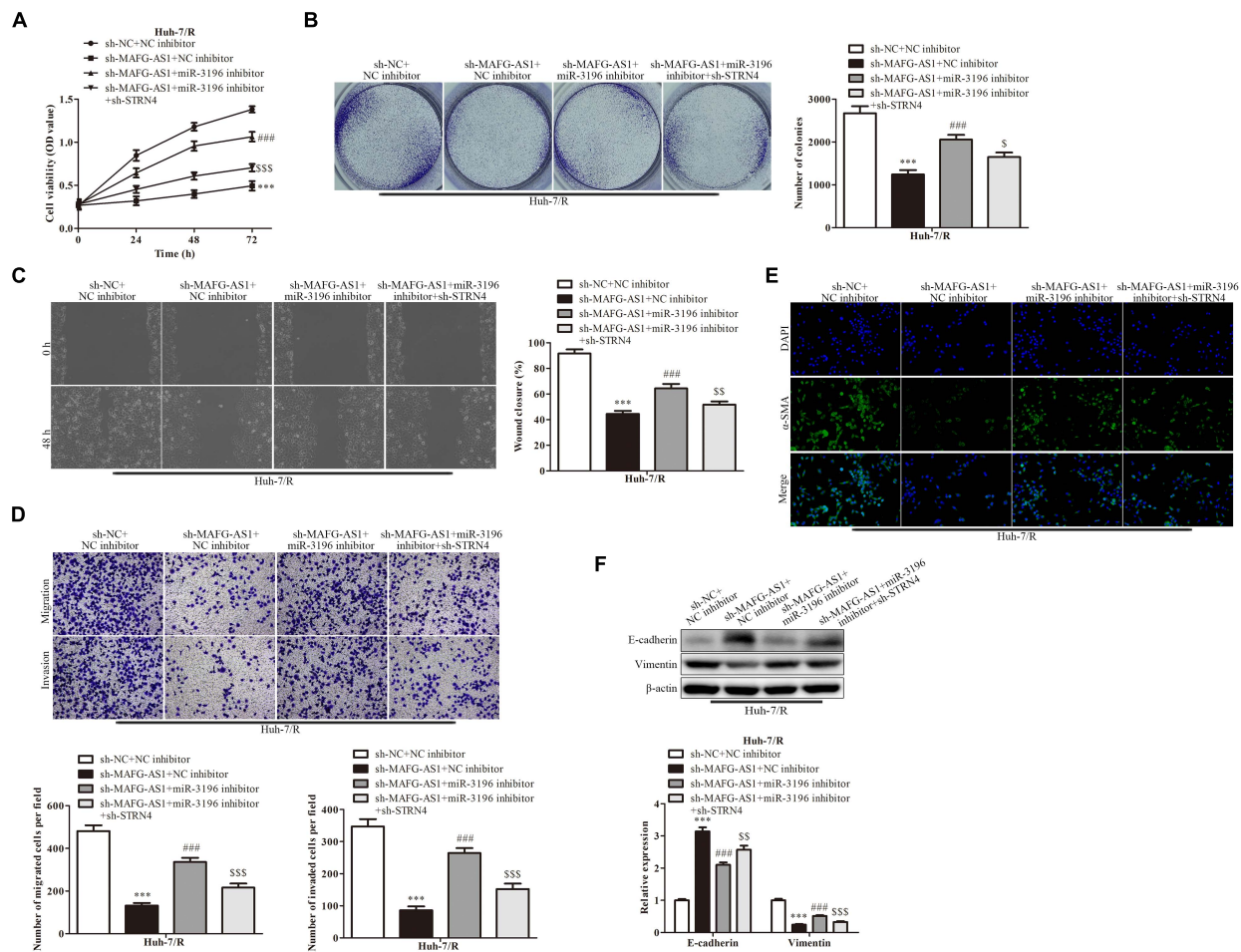


FIGURE 6 | The mechanism for MAFG-AS1 modulating STRN4 protein expression through targeting miR-3196 in liver cancer cells. **(A)** CCK-8 assay indicated the cell viability in Huh7/R and HepG2/R cells transfected with sh-MAFG-AS1, miR-3196 inhibitor, or sh-STRN4 compared to their negative controls. **(B)** The clone formation abilities of the Huh7/R and HepG2/R cells in different groups. **(C)** Wound healing assay **(D)** and transwell analysis to test the effect on the invasion and migration of HCC cells. **(E)** Immunostaining and **(F)** western blotting detected the EMT of Huh7/R and HepG2/R cells transfected with sh-MAFG-AS1, miR-3196 inhibitor, or sh-STRN4 compared to their negative controls. Scale bars: 50 μ m. *** P < 0.001 vs sh-NC + NC inhibitor group, ### P < 0.001 vs sh-MAFG-AS1 + NC inhibitor group, \$ P < 0.05, \$\$ P < 0.01, \$\$\$ P < 0.001 vs sh-MAFG-AS1 + miR-3196 inhibitor group.

inhibitors (Figure 6D). In addition, our results showed that decreased α -SMA proteins were induced by sh-MAFG-AS1 in Huh7/R cells, while the miR-3196 inhibitor reversed this effect (Figure 6E). The results showed that knockdown of MAFG-AS1 could significantly increase the expression of E-cadherin but decrease the expression of vimentin and α -SMA in Huh7/R and HepG2/R cells as demonstrated by IF or western blotting (Figure 6F). Based on the results, we concluded that MAFG-AS1 regulates the progression of liver cancer cells through the miR-3196/STRN4 axis.

DISCUSSION

Numerous lncRNAs are aberrantly expressed in HCC, regulating various miRNAs and genes and modulating a variety of biological processes (Chen et al., 2016; She et al., 2016;

Han et al., 2017). Therefore, one or more of these lncRNAs may serve as a potential therapeutic target for treating patients with HCC. In the present study, the functional effects and potential underlying mechanism of lncRNA MAFG-AS1 in HCC were examined. Based on the RT-qPCR results, lncRNA MAFG-AS1 was highly expressed in HCC cell lines. After knockdown of lncRNA MAFG-AS1, the proliferation, migration, and invasion of HCC cell lines were significantly decreased. Interestingly, lncRNA MAFG-AS1 and miR-3196 were demonstrated to exhibit a reciprocally negative regulatory association with each other. By inhibiting the expression of miR-3196, MAFG-AS1 promoted the proliferation, migration, and invasion of HCC cells.

Zhang et al. (2018) processed a regulatory network analysis of lncRNAs in colorectal cancer and showed that lncRNA MAFG-AS1 was upregulated in this disease. In addition, high-throughput data analysis and *in vitro* experiments confirmed that lncRNA

MAFG-AS1 was highly expressed and affects the proliferation of osteosarcoma cells. Similarly, lncRNA MAFG-AS1 expression was also upregulated in HCC cell lines and primarily distributed in the cytoplasm of HCC cells in the present study. After knockdown of lncRNA MAFG-AS1, the proliferation, migration, and invasion of HCC cell lines were significantly inhibited. Therefore, lncRNA MAFG-AS1 may serve a critical role in the pathogenesis of HCC. This study showed similar results.

Previous studies confirmed the influence of MiRNA in tumor development. Wang et al. suggested that miR-183 promoted MDR in HCC cells by regulating the miR-183-IDH2/SOCS6-HIF-1 α feedback loop. Both miR-183 knockdown and SOCS6 overexpression sensitized BEL-7402/5-FU cells to 5-FU (Wang et al., 2016). In this study, we found that miR-3196 could bind with MAFG-AS1. MiR-3196 was lowly expressed in HCC cell lines, and the upregulation of miR-3196 repressed HCC cell proliferative and migratory capacities. Moreover, many studies proved that miRNAs can bind to the 3' UTR of mRNAs to silence these mRNAs (Tomimaru et al., 2010; Wang et al., 2016). In this research, we confirmed that STRN4 was the downstream target of miR-3196 and demonstrated that STRN4 expression was positively regulated by MAFG-AS1 and negatively regulated by miR-3196.

REFERENCES

- Altekruse, S. F., Henley, S. J., Cucinelli, J. E., and McGlynn, K. A. (2014). Changing hepatocellular carcinoma incidence and liver cancer mortality rates in the United States. *Am. J. Gastroenterol.* 109, 542–553. doi: 10.1038/ajg.2014.11
- Bao, H., Guo, C. G., Qiu, P. C., Zhang, X. L., Dong, Q., and Wang, Y. K. (2017). Long non-coding RNA lgf2as controls hepatocellular carcinoma progression through the ERK/MAPK signaling pathway. *Oncol. Lett.* 14, 2831–2837. doi: 10.3892/ol.2017.6492
- Chen, Z., Yu, C., Zhan, L., Pan, Y., Chen, L., Sun, C., et al. (2016). LncRNA CRNDE promotes hepatic carcinoma cell proliferation, migration and invasion by suppressing miR-384. *Am. J. Cancer Res.* 6, 2299–2309.
- Cui, S., Yang, X., Zhang, L., Zhao, Y., and Yan, W. (2018). LncRNA MAFG-AS1 promotes the progression of colorectal cancer by sponging miR-147b and activation of NDUFA4. *Biochem. Biophys. Res. Commun.* 506, 251–258. doi: 10.1016/j.bbrc.2018.10.112
- Dika, I. E., and Abou-Alfa, G. K. (2017). Treatment options after sorafenib failure in patients with hepatocellular carcinoma. *Clin. Mol. Hepatol.* 23, 273–279. doi: 10.3350/cmh.2017.0108
- Duan, X. Y., Zhang, L., Fan, J. G., and Qiao, L. (2014). NAFLD leads to liver cancer: do we have sufficient evidence? *Cancer Lett.* 345, 230–234. doi: 10.1016/j.canlet.2013.07.033
- Feng, M., and Ho, M. (2014). Glypican-3 antibodies: a new therapeutic target for liver cancer. *FEBS Lett.* 588, 377–382. doi: 10.1016/j.febslet.2013.10.002
- Han, F., Wang, C., Wang, Y., and Zhang, L. (2017). Long noncoding RNA ATB promotes osteosarcoma cell proliferation, migration and invasion by suppressing miR-200s. *Am. J. Cancer Res.* 7, 770–783.
- Innes, H., Barclay, S. T., Hayes, P. C., Fraser, A., Dillon, J. F., Stanley, A., et al. (2018). The risk of hepatocellular carcinoma in cirrhotic patients with hepatitis C and sustained viral response: role of the treatment regimen. *J. Hepatol.* 68, 646–654. doi: 10.1016/j.jhep.2017.10.033
- Ke, A. W., Shi, G. M., Zhou, J., Huang, X. Y., Shi, Y. H., Ding, Z. B., et al. (2011). CD151 amplifies signaling by integrin $\alpha 6 \beta 1$ to PI3K and induces the epithelial-mesenchymal transition in HCC cells. *Gastroenterology* 140, 1629–1641.e15.

CONCLUSION

In conclusion, MAFG-AS1 was upregulated in HCC cell lines and could bind with miR-3196. Our data hinted that MAFG-AS1 regulated HCC cell growth and migration through the miR-3196/STRN4 axis, exposing a potential neo-biomarker for diagnosis or treatment for liver cancer patients. These results provide important evidence that MAFG-AS1 may be a novel therapeutic target and a biomarker for predicting response to sorafenib treatment of HCC.

DATA AVAILABILITY STATEMENT

The raw data supporting the conclusions of this article will be made available by the authors, without undue reservation, to any qualified researcher.

AUTHOR CONTRIBUTIONS

TC conceived and designed the study and data extraction. BH performed the literature search. YP drafted the manuscript. All authors read and approved the final manuscript.

- Lei, K., Liang, X., Gao, Y., Xu, B., Xu, Y., Li, Y., et al. (2017). Lnc-ATB contributes to gastric cancer growth through a MiR-141-3p/TGFBeta2 feedback loop. *Biochem. Biophys. Res. Commun.* 484, 514–521. doi: 10.1016/j.bbrc.2017.01.094
- Li, C., Wu, R., and Xing, Y. (2020). MAFG-AS1 is a novel clinical biomarker for clinical progression and unfavorable prognosis in gastric cancer[J]. *Cell Cycle* 19, 601–609. doi: 10.1080/15384101.2020.1728017
- Li, T., Xie, J., Shen, C., Cheng, D., Shi, Y., Wu, Z., et al. (2016). Upregulation of long noncoding RNA ZEB1-AS1 promotes tumor metastasis and predicts poor prognosis in hepatocellular carcinoma. *Oncogene* 35, 1575–1584. doi: 10.1038/onc.2015.223
- Liu, K., Wu, X., Zang, X., Huang, Z., Lin, Z., Tan, W., et al. (2017). TRAF4 regulates migration, invasion, and epithelial-mesenchymal transition via PI3K/AKT signaling in hepatocellular carcinoma. *Oncol. Res.* 25, 1329–1340. doi: 10.3727/096504017x14876227286564
- Lu, G., Li, Y., Ma, Y., Lu, J., Chen, Y., and Jiang, Q. (2018). Long noncoding RNA LINC00511 contributes to breast cancer tumorigenesis and stemness by inducing the miR-185-3p/E2F1/Nanog axis. *J. Exp. Clin. Cancer Res.* 37:289.
- Ma, J., Zeng, S., Zhang, Y., Deng, G., Qu, Y., Guo, C., et al. (2017). BMP4 promotes oxaliplatin resistance by an induction of epithelial-mesenchymal transition via MEK1/ERK/ELK1 signaling in hepatocellular carcinoma. *Cancer Lett.* 411, 117–129. doi: 10.1016/j.canlet.2017.09.041
- Ruan, Z., Deng, H., Liang, M., Xu, Z., Lai, M., Ren, H., et al. (2020). Downregulation of long non-coding RNA MAFG-AS1 represses tumorigenesis of colorectal cancer cells through the microRNA-149-3p-dependent inhibition of HOXB8[J]. *Cancer Cell Int.* 20:511.
- She, K., Huang, J., Zhou, H., Huang, T., Chen, G., and He, J. (2016). LncRNA-SNHG7 promotes the proliferation, migration and invasion and inhibits apoptosis of lung cancer cells by enhancing the FAIM2 expression. *Oncol. Rep.* 36, 2673–2680. doi: 10.3892/or.2016.5105
- Tan, D. S. W., Chong, F. T., Leong, H. S., Toh, S. Y., Lau, D. P., Kwang, X. L., et al. (2017). Long noncoding RNA EGFR-AS1 mediates epidermal growth factor receptor addiction and modulates treatment response in squamous cell carcinoma. *Nat. Med.* 23, 1167–1175. doi: 10.1038/nm.4401
- Tomimaru, Y., Eguchi, H., Nagano, H., Wada, H., Tomokuni, A., Kobayashi, S., et al. (2010). MicroRNA-21 induces resistance to the anti-tumour effect of

- interferon-alpha/5-fluorouracil in hepatocellular carcinoma cells. *Br. J. Cancer* 103, 1617–1626. doi: 10.1038/sj.bjc.6605958
- Wang, X. J., Zhang, D.-L., Fu, C., Wei, B.-Z., and Li, G.-J. (2016). MiR-183 modulates multi-drug resistance in hepatocellular cancer (HCC) cells via miR-183-IDH2/SOCS6-HIF-1alpha feedback loop. *Eur. Rev. Med. Pharmacol. Sci.* 20, 2020–2027.
- Wang, Y., Zhang, Y., Yang, T., Zhao, W., Wang, N., Li, P., et al. (2017). Long non-coding RNA MALAT1 for promoting metastasis and proliferation by acting as a ceRNA of miR-144-3p in osteosarcoma cells. *Oncotarget* 8, 59417–59434. doi: 10.18632/oncotarget.19727
- Xu, Y., Ge, Z., Zhang, E., Zuo, Q., Huang, S., Yang, N., et al. (2017). The lncRNA TUG1 modulates proliferation in trophoblast cells via epigenetic suppression of RND3. *Cell Death Dis.* 8:e3104. doi: 10.1038/cddis.2017.503
- Yuan, J. H., Yang, F., Wang, F., Ma, J., Guo, Y., Tao, Q., et al. (2014). A long noncoding RNA activated by TGF-beta promotes the invasion-metastasis cascade in hepatocellular carcinoma. *Cancer Cell* 25, 666–681. doi: 10.1016/j.ccr.2014.03.010
- Zhang, Y., Tao, Y., Li, Y., Zhao, J., Zhang, L., and Zhang, X. (2018). The regulatory network analysis of long noncoding RNAs in human colorectal cancer. *Funct. Integr. Genomics* 18, 261–275. doi: 10.1007/s10142-017-0588-2
- Zhang, Z. F., Zhang, Y., Hu, D., Shi, J., Liu, J., Zhao, Z., et al. (2011). Smad interacting protein 1 as a regulator of skin fibrosis in pathological scars. *Burns* 37, 665–672. doi: 10.1016/j.burns.2010.12.001
- Conflict of Interest:** The authors declare that the research was conducted in the absence of any commercial or financial relationships that could be construed as a potential conflict of interest.
- Publisher's Note:** All claims expressed in this article are solely those of the authors and do not necessarily represent those of their affiliated organizations, or those of the publisher, the editors and the reviewers. Any product that may be evaluated in this article, or claim that may be made by its manufacturer, is not guaranteed or endorsed by the publisher.

Copyright © 2021 Chen, Huang and Pan. This is an open-access article distributed under the terms of the Creative Commons Attribution License (CC BY). The use, distribution or reproduction in other forums is permitted, provided the original author(s) and the copyright owner(s) are credited and that the original publication in this journal is cited, in accordance with accepted academic practice. No use, distribution or reproduction is permitted which does not comply with these terms.

Advantages of publishing in Frontiers



OPEN ACCESS

Articles are free to read
for greatest visibility
and readership



FAST PUBLICATION

Around 90 days
from submission
to decision



HIGH QUALITY PEER-REVIEW

Rigorous, collaborative,
and constructive
peer-review



TRANSPARENT PEER-REVIEW

Editors and reviewers
acknowledged by name
on published articles

Frontiers

Avenue du Tribunal-Fédéral 34
1005 Lausanne | Switzerland

Visit us: www.frontiersin.org

Contact us: frontiersin.org/about/contact



REPRODUCIBILITY OF RESEARCH

Support open data
and methods to enhance
research reproducibility



DIGITAL PUBLISHING

Articles designed
for optimal readership
across devices



FOLLOW US

@frontiersin



IMPACT METRICS

Advanced article metrics
track visibility across
digital media



EXTENSIVE PROMOTION

Marketing
and promotion
of impactful research



LOOP RESEARCH NETWORK

Our network
increases your
article's readership